UNITED STATES
DEPARTMENT OF THE INTERIOR
GEOLOGICAL SURVEY

SHORT PAPERS OF THE FOURTH INTERNATIONAL CONFERENCE, GEOCHRONOLOGY, COSMOCHRONOLOGY, ISOTOPE GEOLOGY

1978

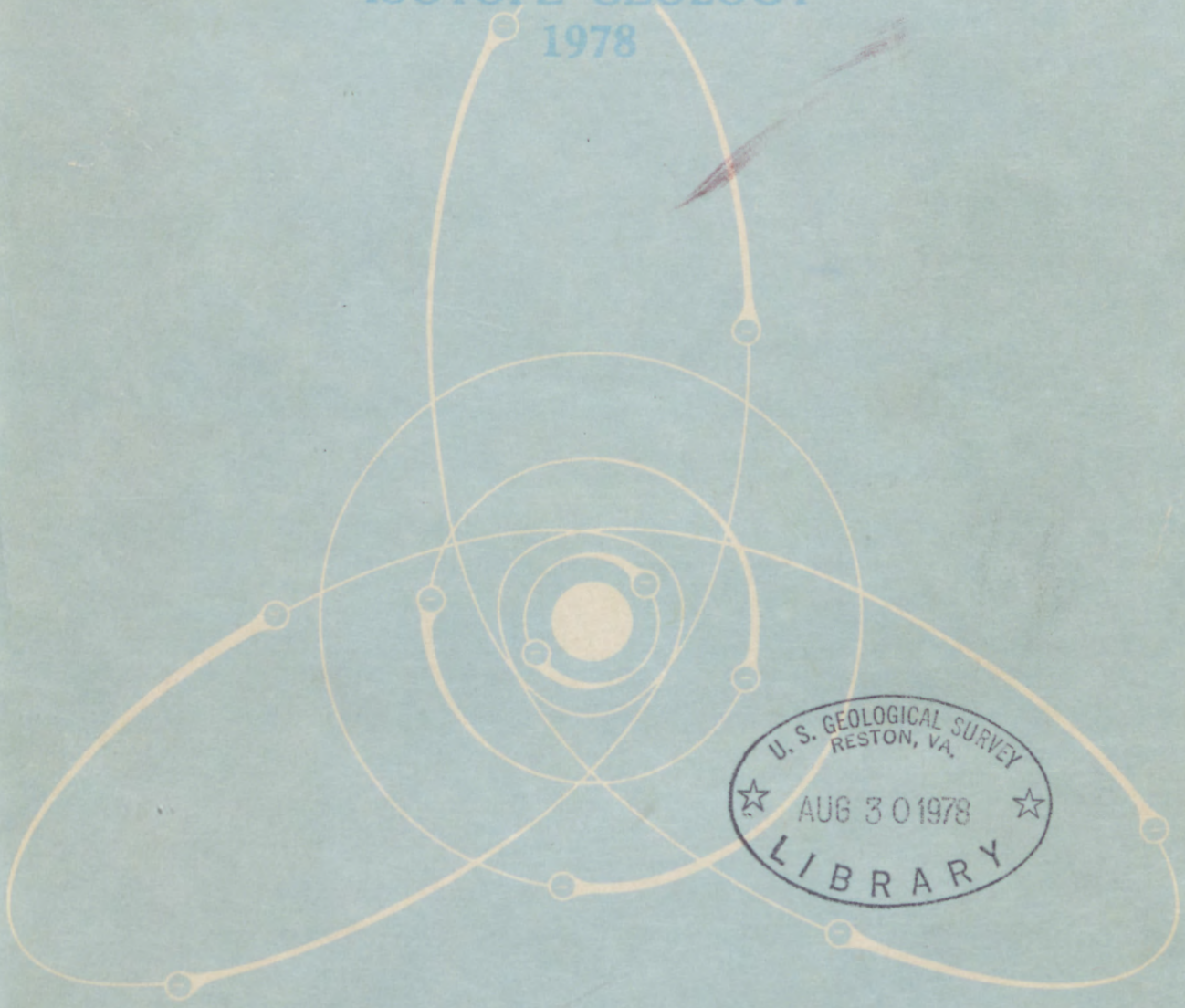

Geological Survey Open-File Report 78-701

UNITED STATES
DEPARTMENT OF THE INTERIOR
GEOLOGICAL SURVEY

SHORT PAPERS OF THE FOURTH INTERNATIONAL CONFERENCE, GEOCHRONOLOGY, COSMOCHRONOLOGY, ISOTOPE GEOLOGY 1978

Edited by Robert E. Zartman, 1936-

Geological Survey Open-File Report 78-701

CONFERENCE HELD AUGUST 20–25, 1978
IN SNOWMASS-AT-ASPEN, COLORADO
UNITED STATES OF AMERICA

PREFACE

The first International Conference on Geochronology, Cosmochronology, and Isotope Geology was held in Edmonton, Alberta, Canada, in 1967; the second was in Bern-Zurich, Switzerland, in 1969; and the third took place in Paris, France, in 1974. The meeting attendance has doubled at each successive meeting, which attests to the increasing interest in these subjects.

Sponsors of the Fourth International Conference in Snowmass-at-Aspen, Colorado, U.S.A., are Carnegie Institution of Washington, Department of Terrestrial Magnetism; Geochemical Society; IUGS Subcommission Of Geochronology; Lunar Science Institute; and National Committee on Geology, National Academy of Sciences. As a major sponsor of the conference, the U.S. Geological Survey has published this volume of short papers submitted for the meeting. The original estimate for the number of papers expected was 125; the final volume is almost double that number and triple the number of pages originally planned for. A great amount of effort has been expended by personnel of the U.S. Geological Survey in Denver in order to review and edit the manuscripts, prepare camera-ready copy, and organize this publication within the limited period of time available.

The members of the Organizing Committee wish to extend their deepest gratitude for a job well done to all those individuals who made it possible for this publication to be prepared in time for distribution prior to the meeting. We also wish to thank all of the authors for their contributions to the conference and to this publication.

EDITOR'S PREFACE

This publication assembles 228 short papers on the subject of isotopic research in the earth and space sciences, contributed by authors from thirty countries to the Fourth International Conference on Geochronology, Cosmochronology, and Isotope Geology. The abstracts presented a wide variety of format and writing and illustrating styles, and they have been edited for these matters as well as for technical content. References in reference lists were completed where necessary, if time allowed. Any use of trade names and trademarks in this publication is for descriptive purposes only and does not constitute endorsement by the U.S. Geological Survey.

CONTENTS

AGE OF METAMORPHISM AND PLUTONISM IN THE JURASSIC-CRETACEOUS RANGITATA OROGENIC BELT, SOUTH ISLAND, NEW ZEALAND

By C. J. D. Adams
Institute of Nuclear Sciences, DSIR,
Lower Hutt, New Zealand

Permian-Jurassic geosynclinal sedimentation in New Zealand culminated in the widespread deformation, metamorphism, and plutonism of the Rangitata orogeny (Jurassic-Cretaceous) (see review by Fleming, 1970). The main elements of the orogenic belt have been disrupted by 480-km right-lateral (Wellman and Cooper, 1971) and 9 - 16 km vertical movement (Sheppard and others, 1975) along the Alpine Fault (fig. 1, inset) and are shown with horizontal movement restored in figure 1. A fault zone, the Median Tectonic Line separates paired metamorphic belts (Landis and Coombs, 1967). To the east, the Wakatipu Metamorphic Belt comprises a northwest-southeast zone of medium-rank metasediments, the Haast Schists, which are flanked to the northeast and southwest by lower-rank metasediments, the Hokinui (Permian-Jurassic) and Torlesse Facies (Carboniferous-Jurassic), respectively. Here metamorphism is charterized by low temperature-pressure (T-P) ratios, in contrast to the western belt, the Tasman Metamorphic Belt, which has high T-P ratios. Major Rangitata orogenic plutonism is confined to this zone in several north-south trending batholiths, which intrude Devonian-Carboniferous granites and gneisses and Precambrian-Paleozoic metasediments. This paper reviews the age data in an east-west sector of the orogenic belt (fig. 1) extending through the Paparoa Range (PG), Karamea (K), Victoria Range (VR), and Separation Point (SP) granite batholiths into the Haast Schist-Torlesse Terrane at Haast Pass (HP), Lakes Wanaka (W) and Hawea (LH), Dansey Pass (DP), Dunedin (D), and equivalent schists in the Chatham Islands (400 km east of the South Island (Mason, 1962; Harper and Landis, 1967; Aronson, 1968; Hulston and McCabe, 1972; Adams, 1974; Sheppard and others, 1975; Adams and Robinson, 1977; Adams and Nathan, 1978; Adams, Eggers, and Tulloch, unpub. data). Data from the Haast Schists in the Lewis Pass (LP)-Hanmer (H) region are also shown (Sheppard and others, 1975).

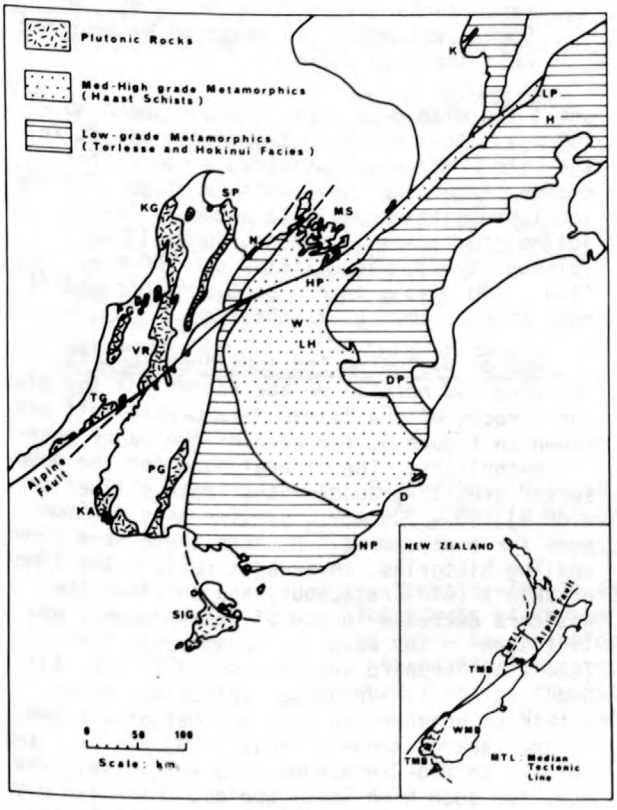

Figure 1.--Main elements of the Rangitata Orogenic Belt, South Island, New Zealand, with 480 km right-lateral Alpine Fault displacement restored, and showing areas of detailed K-Ar dating. For explanation of abbreviations, see text. Inset: Present configuration of Alpine Fault, Median Tectonic Line (MTL), and Wakatipu and Tasman Metamorphic Belts (WMB, TMB) in New Zealand.

Age of metamorphism and subsequent uplift: K-Ar total-rock and mica ages of the Haast Schists (mostly mica-schists) and pre-Jurassic metasediments (mostly slates) of the Torlesse Group in relation to their metamorphic rank are shown in figure 2. Data for the "chlorite" zone is subdivided into textural zones 1 - 4 (Bishop, 1972). Younger age patterns, particularly in garnet and oligoclase (= staurolite-amphibolite facies) zone schists in the Alpine zone (fig. 2), are complicated by great Pliocene-Halocene uplift on the Alpine Fault (Gabites and Adams, this conference). The remaining age data in figure 2 show a significant inverse correlation of age with metamorphic rank, from about 80 m.y. at the biotite isograd (350 - 450°C) to about 190 m.y in textural zones 1 - 2, prehnite-pumpellyite facies

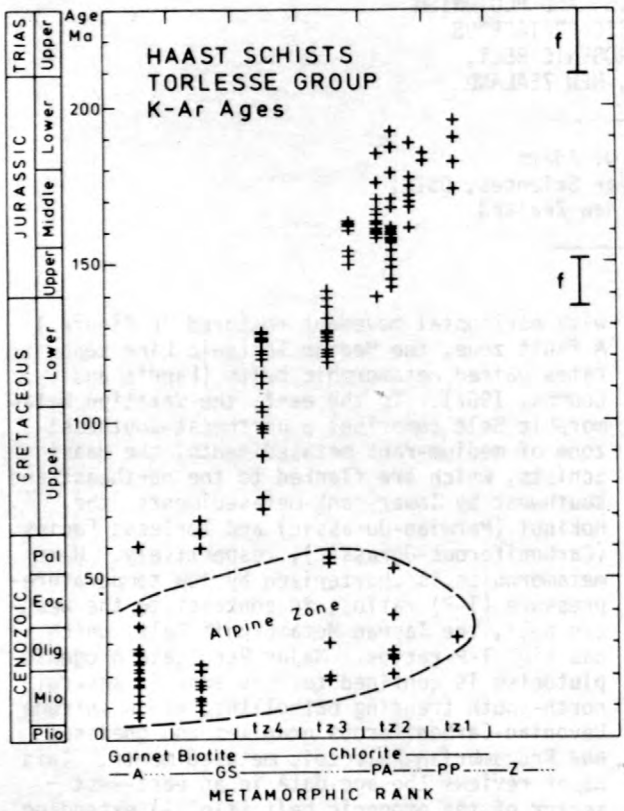

Figure 2.--Variation of total-rock and mineral K-Ar ages of Haast Schists and Torlesse Group in the Wakatipu Metamorphic Belt, along traverse in figure 1. f, range of fossils recorded in Torlesse Group; A, amphibolite facies; GS, greenschist facies; PA, pumpellyite-actinolite facies; PP, prehnite-pumpellyite facies; Z, zeolite facies; tz, textural zone.

(200 - 250°C). All the ages are regarded as metamorphic (rather than diagenetic or "detrital") in character, because pumpellyite-actinolite facies rocks and above show completely recrystallized textures and prehnite-pumpellyite facies rocks, principally slates, contain very low contents of K-bearing detrital phases in proportion to metamorphic micas. In the latter case, all the slates dated were formed close to, but above their argon retention threshold temperature, about 200°C, and, thus, the maximum total-rock ages, 175 - 195 m.y., provide a minimum but close approximation to the time of metamorphism itself--mid-Early Jurassic. Although older than the previous Early Cretaceous age estimate for the metamorphism (Fleming, 1970), this, nonetheless, coincides with an important break in the Torlesse Group fossil record (see f, fig. 2). The younger ages, 80 - 180 m.y., are related to post-metamorphic uplift which interrupted Torlesse sedimentation until the Late Jurassic, about 140 m.y. ago (see fig. 2), and locally

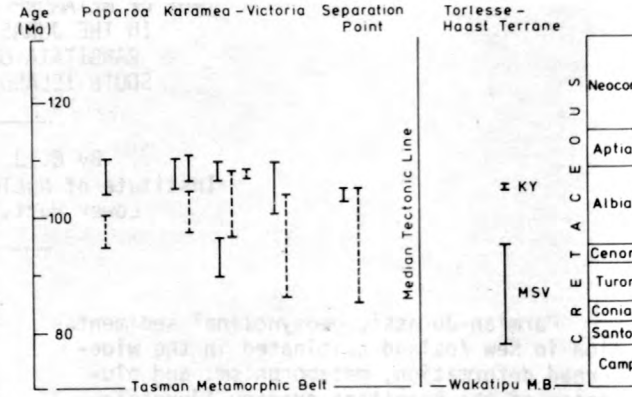

Figure 3.--Ranges of K-Ar mineral ages of Rangitata igneous rocks in major batholiths in the Tasman Metamorphic Belt, along traverse in figure 1. Solid lines, plutonics; dashed lines, hypabyssal and volcanic rocks. Ages of equivalent volcanic rocks (KY, Kyeburn Tuff; MSV, Mt. Somers Volcanics) in Wakatipu Metamorphic Belt are also shown.

until the Middle-Late Cretaceous, about 80 - 100 m.y. ago. Rapid post-orogenic uplift in the Late Cretaceous, provided a source for coarse terrestrial sediments in Otago. If the total prehnite-pumpellyite-pumpellyite-actinolite facies thickness, about 13 km (Bishop, 1972), was uplifted over 50 m.y. (140 - 190 m.y.), then a post-orogenic uplift rate of 0.26 km/m.y. is obtained.

Age of plutonism and subsequent uplift: The mica and hornblende age ranges for the plutonic rocks of the Tasman Metamorphic Belt are shown in figure 3, for each of the major granite batholiths. The mineral ages for the deep-seated granite-granodiorites (dashed lines in fig. 3), 80 - 105 m.y., provide only minimum ages for emplacement. Because these have slow cooling histories, their ages reflect the time of uplift (mid-Cretaceous) and continue the westward decrease in age of post-orogenic uplift seen in the Wakatipu Metamorphic Belt (see also Sheppard and others, 1975, fig. 5). Small satellite hypabyssal intrusives occur within or adjacent to the main batholiths and, in the Paparoa Range at least (PG, fig. 1), are related to mid-Cretaceous acid volcanism. The ages for such high-level bodies, 105 - 110 m.y. (solid lines in fig. 3) are, thus, likely to represent the time of intrusion. This phase is particularly consistent across the Tasman Metamorphic Belt and interestingly, correlates with the biotite age of tuffs (KY, fig. 3) in post-metamorphic Cretaceous terrestrial sediments in Otago (DP, fig. 1). In general, the main granite batholiths are older than the hypabyssal suite and are, thus, at least 110 m.y. old. A few Rb-Sr total-rock ages (Aronson, 1968) suggest emplacement occurred about 120 m.y. ago.

Because pebbles of similar granites occur in mid-Cretaceous terrestrial sediments in the Paparoa Range (PG, fig. 1), then rapid uplift, probably 25 km in 25 m.y.; that is, 1 km m.y., must have followed. In the Wakatipu Metamorphic Belt, igneous activity is rare and confined to the Mt. Somers Volcanics of Canterbury (MSV, fig. 3), which yield 85 - 95 m.y. ages (Late Cretaceous) and correlate with post-orogenic uplift rather than with a plutonic phase.

In summary, the conventional timespan for the Rangitata orogeny, latest Jurassic-Early Cretaceous, must now be considerably extended. A major metamorphic phase in the Wakatipu Metamorphic Belt occurred in the Early Jurassic followed by substantial uplift in the period, Middle Jurassic to Late Cretaceous. Plutonism in the western Tasman Metamorphic Belt appears to be entirely younger, 100 - 120 m.y. (mid-Cretaceous) and post-orogenic uplift followed into the Late Cretaceous. The separation of these major events in both time and space may necessitate some revision of the major tectonic history of the Rangitata orogeny in New Zealand.

Adams, C. J. D., 1974, New Zealand potassium-argon age list-2: New Zealand Journal of Geology and Geophysics, v. 18, p. 443-467.

Adams, C. J. D., and Nathan, S., (in press), Cretaceous chronology of the Lower Buller Valley, South Island, New Zealand: New Zealand Journal of Geology and Geophysics.

Adams, C. J. D., and Robinson, P., 1977, Potassium-argon ages of schists from Chatham Island, New Zealand Plateau, Southwest Pacific: New Zealand Journal of Geology and Geophysics, v. 20, p. 287-301.

Aronson, J. L., 1968, Regional geochronology of New Zealand: Geochimica Cosmochimica Acta, v. 32, p. 669-697.

Bishop, D. G., 1972, Progressive metamorphism from prehnite-pumpellyite to greenschist in the Dansey Pass area, Otago, New Zealand: Geological Society of America Bulletin, v. 83, p. 3177-3179.

Fleming, C. A., 1970, The Mesozoic of New Zealand; chapters in the history of the Circum-Pacific Mobile Belt: Quarterly Journal of the Geological Society of London, v. 125, p. 125-170.

Harper, C. T., and Landis, C. A., 1967, K-Ar ages from regionally metamorphosed rocks, South Island, New Zealand: Earth and Planetary Science Letters, v. 2, p. 419-429.

Hulston, J. R., and McCabe, W. J., 1972, New Zealand potassium-argon age list-1: New Zealand Journal of Geology and Geophysics, v. 15, p. 406-422.

Landis, C. A., and Coombs, D. S., 1967, Metamorphic belts and orogenesis in southern New Zealand: Tectonophysics, v. 4, p. 501-518.

Mason, B., 1962, Metamorphism in the Southern Alps of New Zealand: American Museum of Natural History Bulletin, v. 123, p. 211.

Sheppard, D. S., Adams, C. J., and Bird, G. W., 1975, Age of metamorphism and uplift in the Alpine Schist Belt, New Zealand: Geological Society of America Bulletin, v. 86, p. 1147-1153.

Wellman, P., and Cooper, A., 1971, Potassium-argon ages of some New Zealand lamprophyre dykes near the Alpine Fault: New Zealand Journal of Geology and Geophysics, v. 14, p. 341-350.

DETERMINATION OF THE ISOTOPIC ABUNDANCE OF BORON IN METEORITES AND TEKTITES

By E. K. Agyei[1] and C. C. McMullen[2]
[1]Department of Physics, University of Ghana
Geochronology Laboratory
Ghana Atomic Energy Commission, Ghana
[2]Department of Physics, McMaster University
Hamilton, Canada

There is a controversy over the isotopic composition of boron in meteorites. Deductions from theories by Burbidge and others (1957), Fowler and others (1962), and Burnett and others (1965) on the nucleosynthesis of the L-nuclei seem to suggest that the meteoritic $^{11}B/^{10}B$ ratio should be smaller than the average terrestrial value. A theoretical model by Bernas and others (1967) predicted that meteoritic and terrestrial $^{11}B/^{10}B$ ratios should be equal. Mass spectrometric measurements of spallation yields for the L-nuclei with energetic protons on CNO targets by Yiou and others (1967) support Bernas' theory.

The experimental work of Shima (1962) indicated that the $^{11}B/^{10}B$ ratio is lower in meteorites than in terrestrial samples and the elemental content of boron in both stony and iron meteorites is about the same. Because some theories on tektites suggest meteoritic origin, it was thought useful to analyze some tektites as well in the present work. After careful

blank runs using repurified analytical grade reagents and all-quartz apparatus, it was found that the conventional chemical technique of methly borate distillation still gave blanks up to 2.5 μg B, while the expected B from the samples was about 5 μg. A search for a cleaner method resulted in the following: figure 1

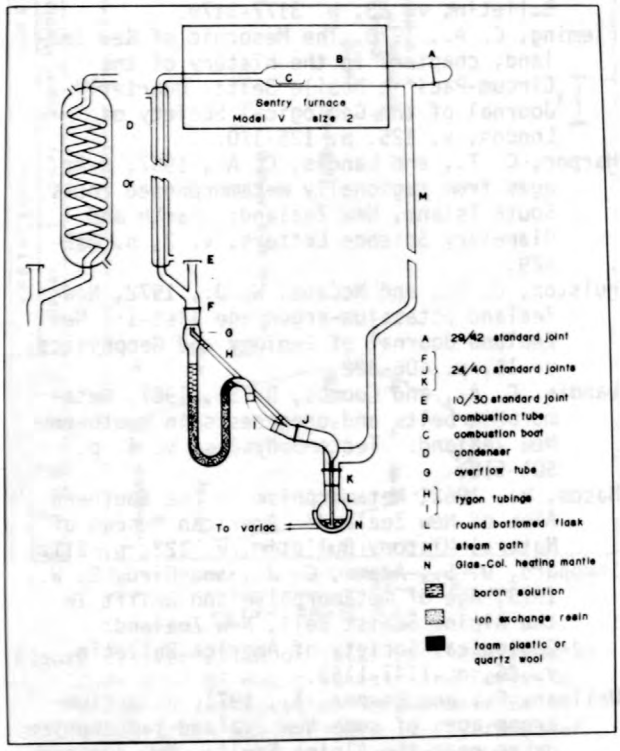

Figure 1.--Diagram of cyclic pyrohydrolysis apparatus.

shows the apparatus used for the separation of boron. Full description of it was given by Agyei (1968). The main apparatus, which is all quartz except the connecting tygon tubes, incorporates an ion-exchange column and a pyrohydrolysis unit in which water is recycled. The ion-exchange resin used is about a 1:1 (dry weight) mixture of Dowex 50 AG, X8, 50-100 mesh and Amberlite IR-45, 20-50 mesh, all of which are analytical grade.

The sample placed in a platinum boat was introduced into the combustion tube through the entrance, A, and heated to temperatures of about 1330°C (maximum operating temperature of the furnace was 1400°C) while steam was passed through the tube. The extracted boron passed through the ion-exchange column, and then into the flask where it remained during the recycling of the water. Steel samples were heated slightly below 1200°C to prevent them from reacting with the platinum boat.

It was necessary to use uranium oxide as catalyst for silicate samples but not for steel samples. The catalyst was purified by pyrohydrolysis as a temperature slightly above that used for the test samples and with the ion-exchange column disconnected. After the entire system had been flushed for about 12 hours under extraction conditions, a 24-hour blank run yielded on the average a value of about 0.05 μg or less. A weighed amount of powdered silicate was mixed thoroughly with about 25 g of the catalyst, which had been pyrohydrolyzed and thus purified. The amount of sample was chosen in such a way that the expected total boron was not less than about 5 μg and the sample size not more than 10 g. Because very small amounts of NBS 1163 and 1164 steel samples were required, they were pyrohydrolyzed as turnings, whereas NBS 1165 and 465 were analyzed as small pieces, similar to the iron meteorites.

Sea-water sample diluted with redistilled water was put directly on top of the ion-exchange resin and elution carried out by recycling of steam, keeping the furnace hot to help the circulation of steam. It was found that even in the silicate meteorites where extraction was slowest, 80 percent of the boron was extracted in the first three hours. For the iron meteorites and the steel standards, almost 100-percent extraction was possible after the first two hours or so. The total boric acid removed from the flask was then made up to a known volume in a quartz volumetric flask. The boron content was determined by the curcumin colorimeter method on an aliquot of this. A sufficient aliquot was then neutralized with a stoichiometric amount of analytical-grade sodium hydroxide to form borax, evaporated to dryness, and analyzed on a 10-inch solid-source mass spectrometer by measuring the $Na_2BO_2^+$ ions.

Table 1 shows both the boron content and the $^{11}B/^{10}B$ ratios of all the samples analyzed except the iron meteorites, for which the extracted boron was not enough for mass spectrometric analysis. The average statistical error associated with the boron contents is about 6 percent and with $^{11}B/^{10}B$ ratios 0.15 percent, both at the 95 percent confidence limits.

Figure 2 is a frequency distribution of the $^{11}B/^{10}B$ ratios of all the independent samples analyzed. The δ-values indicated in the figure are defined as follows:

$$\delta \text{ (permil)} = \left[\frac{(^{11}B/^{10}B)}{4.000} \text{ sample} - 1 \right] \times 1000$$

where $(^{11}B/^{10}B)$ sample is the absolute ratio and 4.000 the reference level. The question marks correspond to the badly weathered samples.

Within experimental errors, the boron content of 10.6 ppm for W-1 obtained in this work agrees with the values of 11.1, 12, and 10 ppm reported by Mills (1966), Lerman (1966), Clark and Swaine (1962), respectively, and others. For the steel standards, the NBS values are 50, 12, 10, and 10 ppm for nos. 1164, 1163, 1165, and 465, respectively, as against the values of 57, 10.4, 0.4, and 0.83 ppm, respectively, ob-

Sample	Boron content (ppm)	Absolute $^{11}B/^{10}B$
Standards:		
W-1 diabase rock---	10.6	4.074
NBS 1164, steel----	57.0	4.042
NBS 1163, steel----	10.4	4.064
NBS 1165, steel----	0.78	4.156
NBS 465, steel----	0.87	4.129
Chondritic meteorites:		
Brudeheim----------	0.74	4.053
Abee----------	0.87	4.027
Peace River--------	0.62	4.029
Vulcan----------	0.49	4.031
**Gladstone	0.47	4.011
Dimmitt	0.57	4.024
Iron meteorites:		
Madoc----------	0.03	-----
Skookum----------	0.02	-----
Toluca (Xiquipilco)	0.02	-----
Odessa----------	0.07	-----
Canyon Diablo	0.03	-----
Canyon Diablo (silicate phase)---	0.63	4.064
Stony-iron meteorites[1]:		
Bondoc----------	0.11	4.074
Dalgaranga----------	0.90	4.158
Tektites:		
Indochinite (Dalat, South Vietnam)-----	19.5	4.024
Indochinite (northeast Thailand)	26.0	4.019
Bediasite (Somerville, Texas)	10.0	4.025
Rizalite (Bugad, Luzon)-----	35.8	4.024
Terrestrial:		
Beryl----------	7.0	4.032
Basalt (Hawaiian)---	1.8	4.031
Porcelain----------	40.0	4.034
Slate (shale)-------	10.5	4.044
Kimberlite----------	4.0	4.041
Tourmaline (Finland)	3.27×10^4	4.001
Sea water:		
Pacific Ocean------	4.33	4.220
Arctic Ocean-------	4.10	4.236
Atlantic Ocean-----	4.10	4.214

[1]These samples were badly weathered.

tained in this work. The average boron content for all the chondrites analyzed is about 0.67 ppm (0.47 - 0.97 ppm), whereas for irons it is 0.03 ppm (0.02 - 0.07 ppm) in agreement with the geochemical fact that boron is lithophile and that it will tend to concentrate in the stony meteorites along with Li, as reported by Fireman and Schwarzer (1957). The results also agree with those obtained by Wasson (1965) and Quijano-Rico and Wanke (1969). The results for the irons, however, are in disagreement with Shima's (1962) report that boron content for Toluca iron meteorite is 0.45 ppm. The four tektites studied have boron contents ranging from 10 ppm to 35.8 ppm, as compared to 3 ppm to 22 ppm reported by Preuss (1935), and 10 ppm reported by Taylor and Sachs (1960) for other kinds of tektites. Sea water has a very narrow range of boron content from 4.10 ppm to 4.40 ppm (mean 4.22 ppm), which also agrees with the currently accepted value of 4.5 ppm.

The average $^{11}B/^{10}B$ ratio 4.045 (4.008 - 4.095) for chondrites is only 0.45 percent different from the average value 4.027 (3.977 - 4.074) for terrestrial rocks and minerals, and only 0.1 percent different from the value 4.023 (4.019 - 4.027) for tektites. These results disagree with those reported by Shima (1962), but agree with those of Krankowsky and Miiller (1967), and others, who find that the terrestrial lithium isotope ratio is essentially the same as the meteoritic lithium isotope ratio. Although tektitic and meteoritic $^{11}B/^{10}B$ are similar, they could not have been produced by fusion of chondritic meteorites or igneous rocks because of the larger boron contents of tektites. Sea water is enriched in ^{11}B. This has been shown by Schwarcz and others (1966) to be due to adsorption of sea water on clay minerals.

Agyei, E. K., 1968, Isotopic and elemental composition of boron in meteorites, tektites, and terrestrial materials: Hamilton, Canada, McMaster University, Ph.D. thesis.

Bernas, R., Gradsztajn, E., Reeves, H., and Schatzman, E., 1967, On the nucleosynthesis of lithium, beryllium, and boron: Annals of Physics, v. 44, p. 426-478.

Burbidge, E. M., Burbidge, G. R., Fowler, W. A., and Hoyle, F., 1957, Synthesis of the elements in Stars: Revue of Modern Physics, v. 29, no. 4, p. 547-650.

Burnett, D. S., Fowler, W. A., and Hoyle, F., 1965, Nucleosynthesis in the early history of the solar system: Geochimica Cosmochimica Acta, v. 29, p. 1200-1241.

Clark, M. C., and Swaine, D. J., 1962, The content of several trace elements in the standard rocks G-1 and W-1: Geochimica Cosmochimica Acta, v. 26, p. 511-517.

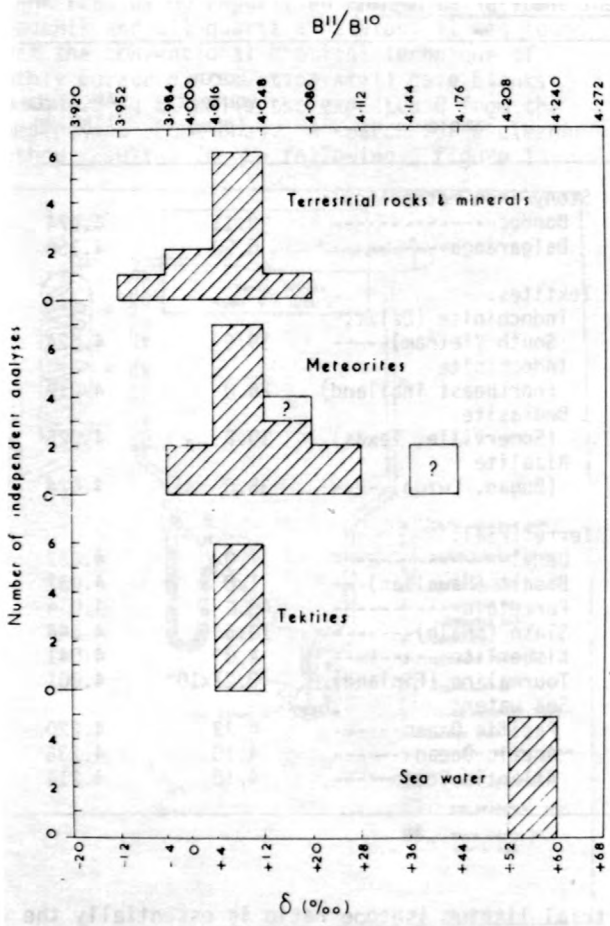

Figure 2.--Distribution of the boron isotopes in nature.

Fireman, E. L., and Schwarzer, D., 1957, Measurement of Li^6, He^3, and H^3 in meteorites in relation to cosmic radiation: Geochimica Cosmochimica Acta, v. 11, p. 252-262.

Fowler, W. A., Greenstein, J. L., and Hoyle, F., 1962, Nucleosynthesis during the early history of the solar system: Geophysical Journal, v. 6, p. 148-220.

Krankowsky, D., and Miiller, O., 1967, Isotopic composition and abundance of lithium in meteoritic matter: Geochimica Cosmochimica Acta, v. 31, p. 1833-1842.

Lerman, A., 1966, Boron in clays and estimation of paleosalinities: Sedimentology, v. 6, p. 267-286.

Mills, A. A., 1966, The separation and determination of boron in meteorites and tektites: Analytical Chemistry Society Proceedings, v. 3, p. 161-162.

Preuss, D., 1935, Specktralanalytische untersuchung der Tektite: Chem Erde, v. 9, p. 365-418.

Quijano-Rico and Wanke, H., 1969, Meteorite Research, Millman, P. M., ed.,: International Atomic Energy Agency, p. 132-145.

Schwarcz, H. P., Agyei, E. K., and McMullen, C. C., 1969, Boron isotopic fractionation during clay absorption from sea-water: Earth and Planetary Science Letters, v. 6, p. 1-5.

Shima, M., 1962, Boron in meteorites: Journal of Geophysical Research, v. 67, no. 11, p. 4521-4523.

Taylor, S. R., and Sachs, M., 1960, Trace elements in australites: Nature, v. 188, p. 387-388.

Wasson, J. T., 1965, Boron in meteorites: Journal of Geophysical Research, v. 70, p. 4443-4445.

Yiou and others, 1967.

MMhb-1: A NEW ^{40}Ar-^{39}Ar DATING STANDARD

By E. C. Alexander, Jr.[1],
G. M. Mickelson[1], and M. A. Lanphere[2]
[1]Department of Geology and Geophysics
University of Minnesota
Minneapolis, Minnesota 55455
[2]U. S. Geological Survey
Menlo Park, California 94025

In the ^{40}Ar-^{39}Ar technique, the age of a sample is calculated by comparing the $^{40}*Ar/^{39}*Ar$ ratio measured in the sample with the same ratio measured in "standard" or "monitor" materials, which have been subjected to the same dose of neutrons as the sample. As the ^{40}Ar-^{39}Ar technique developed over the past decade, each new laboratory adopted its own working standard. Each laboratory's choice of standard, while constrained to some degree by the age of the samples routinely dated by that laboratory (Turner, 1971), was often a matter of using whatever appropriate material happened to be available in that laboratory when its first ^{40}Ar-

^{39}Ar irradiation was prepared. The resulting multiplicity of working standards introduces an unnecessary error into the interlaboratory comparison of ^{40}Ar-^{39}Ar ages. In an attempt to alleviate this problem, we have prepared approximately 1.3 kg of a high purity hornblende separate, MMhb-1, for use as a ^{40}Ar-^{39}Ar age standard.

Our goal was to obtain a reasonable quantity of a hornblende separate which: (1) is rich in potassium, (2) has a well-defined $^{40}*Ar/^{40}K$ ratio, and (3) is about 500 m.y. old. The latter constraint was imposed so that a single standard could be used to date samples ranging in age from 4500 m.y. to less than 10 m.y. Rocks from the Cambrian alkalic igneous intrusions of south-central Colorado proved to be the most accessible candidates.

The standard was prepared from a syenite from the McClure Mountain Complex (Parker and Hildebrand, 1963; Shawe and Parker, 1967; Olsen and others, 1977), which is located in Fremont County, Colorado. The sample was collected in Copper Gulch, approximately 0.3 miles north of the N.E. corner of sec. 1, T20S, R73W along the west side of a gravel road (approximately lat 38°21'N; long 105°29'W). About 250 kg of individual, 10- to 30-kg boulders were collected. The material was not direct outcrop.

The following description of the rock has been selected from a petrographic description supplied by Dr. J. F. Olmsted, Department of Earth Sciences, State University of New York, College at Plattsburgh (written commun., 1977). Major minerals are plagioclase, perthitic K-feldspar, biotite, and hornblende. Accessory minerals include sphene, apatite, oxides, and minor amounts of alteration products. The size distribution of the minerals is bimodal with ~ 80 percent of the rock composed of phenocrysts and the remainder being finer grained material. Large alkali feldspars range from 1 to 3 mm in length while smaller grains are on the order of 0.2 to 0.5 mm. The micas and amphiboles are also found in both size ranges. Two representative modal analyses are shown in table 1. The hornblende is zoned in color from olive green to greenish brown in the γ direction and is light yellowish green in the α direction. Zoning is apparent in most grains but probably involves very minor compositional changes. Most of the hornblende occurs as large composite grains or clusters of crystals. The hornblende has $2V = 60°$ and is optically negative. The extinction angle ($Z \wedge c$) is between 10° and 14° and the dispersion is moderate.

Hornblende made up less than 10 percent of the rock and a large amount of rock was processed to recover the hornblende separate. The large rocks were broken into centimeter-size fragments. Those pieces showing alteration stains were discarded. The selected pieces were washed in warm water, air dried, and then crushed in jaw and roller crushers. The crushers were carefully cleaned, conditioned by crushing a few kilograms of the rock (which was then discarded), and then cleaned again. After each pass through the crushers, that portion of the material which passed a 20-mesh nylon screen was isolated and further sieved in new stainless steel screens into -40+60, -60+80, -80+100, and -100 mesh fractions. The sized fractions were then magnetically separated crudely into a "light" fraction (plagioclase plus K-feldspar) and a "dark" fraction (biotite, hornblende, plus accessory minerals). This process discarded about three-fourths of the material. The "dark" fractions were: (1) ultrasonically cleaned in distilled water and acetone; (2) run through the magnetic separator several times; and then (3) split into crude biotite and hornblende fractions using a methylene iodide and tetrabromoethane mixture adjusted to $\rho = 3.215$. The crude hornblende fractions were then purified by repeated batch processing in heavy liquids adjusted to $\rho = 3.286$, with any floating material being discarded. The -40+60 mesh fraction was then gently crushed and added to the finer fractions and the -60+80 fraction was carefully resized. This -60+80 fraction was then run through the magnetic and heavy liquid separations several more times. The hornblende separate was then ultrasonically cleaned in dilute sulfuric acid once, rinsed in distilled water ultrasonically several times, and finally rinsed ultrasonically in reagent-grade acetone several times and air dried. MMhb-1 is the resulting -60+80 mesh hornblende separate.

Table 1.--Modal mineralogy of the parent rock of the MMhb-1 standard[1]

Mineral	Section A	Section C
Plagioclase	48.0	48.1
K-feldspar	29.7	33.7
Biotite	9.1	7.1
Hornblende	8.8	7.1
Sphene	1.1	1.7
Apatite	0.7	0.9
Oxides	0.6	0.5
Alteration	1.8	0.9

[1]Based on 2000 points in each thin section. Values are in percent of the total.

The initial analyses of the standard indicate that it is homogeneous. F. Flanagan of the U. S. Geological Survey in Reston has made five XRF chemical analyses of material taken from three randomly selected splits of MMhb-1. The data are summarized in table 2. Flanagan (written commun., 1977) reported that the variance between bottles is not significantly greater than the analytical error of the XRF technique. The K_2O and $^{40}Ar_{rad}$ analyses available to date are shown in table 3. A group of 12 K_2O

Table 2.--XRF chemical analysis of MMhb-1 standard

[Analysis by F. Flanagan, USGS, Reston. All values in weight percent. The errors are the 1σ variation of five analyses taken from three different splits.]

SiO_2	37.16±0.44	TiO_2	3.68 ±0.08
FeO	20.56±0.26	Na_2O	2.88 ±0.28
Al_2O_3	12.92±0.31	K_2O	1.90 ±0.07
CaO	10.18±0.16	MnO	0.746±0.011
MgO	6.42±0.11	P_2O_5	0.054±0.015

Sum = 96.50

Table 3.--K and Ar data for the MMhb-1 standard

Method	K_2O (percent)	$^{40}Ar_{rad}$ (in units of 10^{-9} mol/g)	Age[1] (m.y.)
U. S. Geological Survey laboratory, Menlo Park			
Flame photometer	1.867	1.874	1.629
Do	1.881	1.872	1.611
Do	1.876	1.869	1.622
Do	1.877	1.873	1.632
Do	1.875	1.867	
Do	1.881	1.872	
Mean	1.874 ±0.004$_7$	1.624 ±0.009$_3$	519.5 ±2.5
Mineralogical-Geological Museum laboratory, Oslo			
XRF	1.91		
Flame photometer	1.92		
Do	1.93		
Mean	1.92 ±0.01		
Department of Geology and Mineralogy laboratory, Ohio State University			
Flame photometer	1.876		
Do	1.880		
Do	1.878		
Mean	1.878 ±0.002		
U. S. Geological Survey laboratory, Reston			
XRF	1.9	1.9	
Do	1.8	1.9	
Do	2.0		
Mean	1.90 ±0.07		

[1]Using the constants recommended by Steiger and Jäger (1977).

analyses by the U. S. Geological Survey in Menlo Park yielded a standard deviation of 0.25 percent, and four $^{40}Ar_{rad}$ analyses by the same group shows a standard deviation of 0.57 percent. Both results are close to the precision of the analytical method used. Using only the Menlo Park data, the K/Ar age of the standard is 519.5 ± 2.5 m.y. (using Steiger and Jäger's, 1977, constants). Olsen and others (1977) report an average K/Ar age of 520 m.y. (which corresponds to an age of 529 m.y. with the new constants) for the hornblendes from the biotite-hornblende syenites and nepheline-bearing rocks of the McClure Mountain Complex.

E. C. Alexander, Jr., will be responsible for the distribution of the standard. The distribution will be upon request and will be in one of two modes. Splits of ∿ 5 grams will be distributed to workers wanting to use it as a K-Ar interlaboratory calibration standard. Splits of 30 to 40 grams will be distributed to a limited number of ^{40}Ar-^{39}Ar laboratories that want to adopt it as a standard. The goal is to reserve the bulk of the standard for those uses where high-precision, interlaboratory comparisons are important--for example, experiments aimed at fine-scale calibration of the Geologic Time Scale, age determinations of lunar samples, and so forth. The splits will be distributed with the understanding that the recipients will supply their analytical results for compilations similar to those published for P-207 (Lanphere and Dalrymple, 1967).

Lanphere, M. A., and Dalrymple, G. B., 1967, K-Ar and Rb-Sr measurements on P-207, the U. S. Geological Survey interlaboratory standard muscovite: Geochimica Cosmochimica Acta, v. 31, p. 1091-1094.

Olsen, J. C., Marvin, R. F., Parker, R. L., and Mehnert, H. H., 1977, Age and tectonic setting of lower Paleozoic alkalic and mafic rocks, carbonatites, and thorium veins in south-central Colorado: U. S. Geological Survey, Journal of Research, v. 5, p. 673-687.

Parker, R. L., and Hildebrand, F. A., 1963, Preliminary report on alkalic intrusive rocks in the northern Wet Mountains, Colorado, in Geological Survey Research 1962: U. S. Geological Survey, Professional Paper 450-E, p. E8-E10.

Shawe, D. R., and Parker, R. L., 1967, Mafic-ultramafic layered intrusion at Iron Mountain, Fremont County, Colorado: U. S. Geological Survey, Bulletin 1251-A, p. A1-A29.

Steiger, R. H., and Jäger, E., 1977, Subcommission on geochronology; convention on the use of decay constants in geo- and cosmochronology: Earth and Planetary Science Letters, v. 36, p. 359-362.

Turner, G., 1971, Argon 40-Argon 39 dating; the optimization of irradiation parameters: Earth and Planetary Science Letters, v. 10, p. 227-234.

EARLY HISTORY OF THE SOLAR SYSTEM USING METEORITE RADIOCHRONOLOGIES

By C. J. Allegre, J. L. Birck, J. C. Lorin,
G. Manhes, and J. F. Minster
Laboratoire de Géochimie et
Cosmochimie - L.A. 196
Institut de Physique du Globe et Department
des Sciences de la Terre
Universités de Paris VI et VII
4, Place Jussieu - 75230 PARIS CEDEX 05 - France

In this paper we synthethize all the results we have obtained during the last four years on meteorites by ^{87}Rb-^{87}Sr, U-Pb, ^{26}Al-^{26}Mg isotope chronometers. We also include a new discussion of ^{129}I-^{129}Xe chronology (C. J. Allegre, unpublished data).

^{87}Rb-^{87}Sr CHRONOLOGY

Differentiated Objects

We have studied basaltic achondrites, diogenites, pallasites, and iron meteorites. Generally, the ^{87}Rb-^{87}Sr system in these groups of meteorites has been disturbed by secondary events. We interpret these events as probable bombardments during their lifetime. Some objects are considered as undisturbed, because their study yields an internal isochron. These have a common ^{87}Rb-^{87}Sr age of 4.45 ± 0.13 b.y. ($\lambda^{87}Rb = 1.42^{-11}$ yr^{-1}) and an $^{87}Sr/^{86}Sr$ initial ratio = 0.69800 ± 0.00005.

Chondrites

H chondrites have been analyzed by whole-rock and internal mineral study. Tieschietz (H_3) whole rocks and minerals give a well-defined isochron yielding an age of 4.53 ± 0.02 b.y. and $^{87}Sr/^{86}Sr$ initial ratio of 0.69881 ± 0.00016. This isochron is reasonably interpreted as a "primitive isochron" of condensation from the solar nebula. In this model, condensation has occurred within a short interval of time (< 10 m.y. as deduced from the $^{87}Sr/^{86}Sr$ initial ratio). Other equilibrated chondrites are later reequilibrated.

The same approach has been applied to L chondrites. However, no whole-rock isochron was obtained. It appears that whole rocks that are internally disturbed plot above the primitive isochron, whereas those which are undisturbed plot on this line. This fact, and some values on LL chondrites, indicate that the primitive isochron gives the age of all ordinary chondrites. Some enstatite chondrites and achondrites have been studied for internal isochrons (Indarch, Cumerland Falls, Norton County). They have been altered some 100 m.y. after the formation of ordinary chondrites.

The main result of these investigations is that the old perturbations occur frequently. When unperturbed objects are considered, a common age is obtained within an internal age of < 20 m.y.

U-Pb CHRONOLOGY

U-Pb ages from the literature show some discrepancies, and are usually the discordant. We have shown that concordant ages can be obtained when contamination is carefully controlled; the main source of pollution generally occurs before the laboratory procedure.

Some chondrites (Saint Severin, Elenovka) and achondrites (Juvinas) have been found to be concordant, within an internal age of 20 m.y. Minerals from these meteorites have been found to present discordant ages.

^{129}I-^{129}Xe CHRONOLOGY

Taking into account the fact that most objects have been disturbed by secondary events, the ^{129}I-^{129}Xe chronology of meteorites has been reexamined. When possibly perturbed meteorites are discarded, a very small time interval of 2 to 3 m.y. is obtained. The correlations between trapped $^{129}Xe/^{132}Xe$ ratios and ^{129}I-^{129}Xe ages might indicate the existence of premeteorite reservoirs. Cooling time intervals of about 20 m.y. can be estimated for the parent bodies. This is in fair agreement with the ^{87}Rb-^{87}Sr and ^{39}Ar-^{40}Ar time intervals if differences in retention temperatures are considered.

^{26}Al-^{26}Mg CHRONOLOGY

A relative ^{26}Al-^{26}Mg chronology has been obtained for the two carbonaceous chrondrites, Leoville and Allende. The time difference between condensation-accretion of plagioclase and primary hibonite is similar for the two meteorites, but absolute ages are slightly shifted. The time intervals are of some 100,000 years.

CONCLUSION

We believe that:

1. Meteorites have formed in a short time interval of 1.5 m.y. or less.
2. A condensation-accretion time delay of around 100,000 years occurred in a given part of the solar nebula.
3. Meteorite parent bodies generally cool within a few tens of millions of years.

4. Most meteorites have been perturbed by secondary events. Contrary to common belief, the probability of finding unperturbed objects is quite low. We think that most of the broadening of the "sharp isochronism" model is created by these secondary events.

5. Information contained in whole rocks is different from that contained in internal minerals, and appears crucial to the estimation of formation ages.

SYSTEMATICS OF Sr, Nd AND Pb ISOTOPES IN GARNET LHERZOLITE NODULES IN KIMBERLITES

By C. J. Allègre, G. Manhes, P. Richard, D. Rousseau and N. Shimizu
Laboratoire de Géochimie et Cosmochimie(LA 196)
Institut de Physique du Globe,
Universitie, Paris 6
France

Systematics of Sr, Nd, and Pb isotopic composition of major minerals in garnet lherzolite nodules from kimberlites have been studied to test whether the minerals were in isotopic equilibrium when the nodules were finally incorporated in the host kimberlites and were brought up to the surface. The previous studies on spinel lherzolite nodules in basalts (Stueber and Ikramuddin, 1974; Dasch and Green, 1975; Basu and Murthy, 1977) suggest that minerals in some nodules had not been in isotopic equilibrium for a long time (a Rb-Sr mineral isochron age given by Basu and Murthy, 1977, is 3.4 b.y.). However, the recent experimental data on diffusion of Sr in diopside ($D \sim 2 \times 10^{-12}$ cm^2 sec^{-1} at 1250°C; Sneeringer and Hart, 1978) are much higher than the Ca-Mg diffusion in pyroxenes (an upper limit value given by Huebner and others, 1975 is 4×10^{-15} cm^2 sec^{-1} at 1266°C), and strongly suggest an isotopic equilibrium among mantle minerals as long as the major elements are in equilibrium. This further suggests that the isotopic equilibrium among minerals at the time of kimberlite intrusion should be carefully studied before the pressure and temperature conditions estimated from the major element compositions of minerals are used for studying paleogeotherms.

We separated the major minerals (clinopyroxene, garnet, orthopyroxene, and olivine) from various types of garnet lherzolites by hand-picking and analyzed them for Sr, Nd, and Pb isotopic composition and for Rb, Sr, Sm, Nd, U, and Pb concentrations.

An example of isotopic equilibria a garnet lherzolite nodule (W397) from the Premier kimberlite pipe (South Africa) is: Rb-Sr internal isochron gives the age of 1.40 ± 0.03 b.y. with $(^{87}Sr/^{86}Sr)_I = 0.70241$; Sm-Nd gives 1.41 b.y. with $(^{143}Nd/^{144}Nd)_I = 0.51015$; Pb-Pb isochron drawn for garnet and diopside gives 1.35 b.y. These ages agree with one another and also with the age of the Premier kimberlite (1.25 - 1.40 b.y.), given by Barrett and Allsop (1973). The $^{87}Sr/^{86}Sr$ and $^{143}Nd/^{144}Nd$ initial ratios are accounted for by a model of single-stage closed-system evolution of a system with chondritic relative REE abundances between 4.55 and 1.4 b.y. The Pb-Pb isochron provides a μ_o value for this particular piece of the closed-system mantle of 8.01 ± 0.02.

Among the nodules in the Cretaceous kimberlites from South Africa and Lesotho, we have observed that garnet lherzolites with sheared structure (higher T-higher P representing the "inflected" part of the pyroxene geotherm of Boyd, 1973) yield Rb-Sr isochron ages much older than the host kimberlites with low $(^{87}Sr/^{86}Sr)_I$, indicating that they had been in isotopic disequilibrium before they were incorporated in the host kimberlites; those with granular texture (lower T-lower P part of the pyroxene geotherm) yield Rb-Sr isochron ages close to the host kimberlites with elevated $(^{87}Sr/^{86}Sr)_I$, indicating continuous isotopic re-equilibration.

The results strongly caution against the use of the inflected part of the pyroxene geotherm as implying any geodynamic process in the Cretaceous Period. Possible explanations for the apparent contradiction of the present results (isotopic disequilibrium for samples with higher T in contrast to continuous equilibration for samples with lower T), include a model which assumes that the 'granular' garnet lherzolites were originally at a greater depth than the 'sheared' ones, and when the part of the mantle was uplifted around 1.7 - 2.0 b.y. ago, the P, T and Rb-Sr systematics of the former were quenched, whereas the latter remained at high enough temperature to get continuously re-equilibrated.

Barrett, D. R., and Allsopp, H. L., 1973,

Rubidium-strontium age determinations on South African kimberlite pipes: 1st. Kimberlite Conference Extended Abstracts, p. 23.

Basu, A. R., and Murthy, V. R., 1977, Ancient lithospheric lherzolite xenolith in alkali basalt from Baja, California: Earth and Planetary Science Letters, v. 35, p. 239.

Boyd, F. R., 1973, A pyroxene geotherm: Geochimica Cosmochimica Acta, v. 37, p. 2533.

Dasch, E. J., and Green, D. H., 1975, Strontium isotope geochemistry of lherzolite inclusion and host basaltic rocks: American Journal of Science, v. 275, p. 461.

Huebner, J. S., Ross, M., and Hickling, N., 1975, Significance of exsolved pyroxenes from lunar breccia 77215: Geochimica Cosmochimica Acta, Supplement, 6, v. 1, p. 529.

Sneeringer, M., and Hart, S. R., 1978, Sr diffusion in diopside: EOS, v. 59, p. 402

Stueber, A. M., and Ikramuddin, M., 1974, Rubidium, strontium and the isotopic composition of strontium in ultramafic nodule minerals and host basalts: Geochimica Cosmochimica Acta, v. 38, p. 207.

THE EVOLUTION OF ENHANCED $^{234}U/^{238}U$ ACTIVITY RATIOS FOR DISSOLVED URANIUM AND GROUND-WATER DATING

By John N. Andrews and R. Linden F. Kay
University of Bath
Bath, United Kingdom

The use of variations in the $^{234}U/^{238}U$ activity ratio of dissolved U for ground-water dating (Osmond and others, 1974; Kronfeld and others, 1975) is complicated by the fact that U in solution does not form a closed system. Further solution or deposition and ^{234}U ingrowth due to ^{234}Th recoil may take place as ground-water migrates in an aquifer. The effects of variables on the $^{234}U/^{238}U$ activity ratio are examined below and discussed in relation to the (Triassic) Bunter Sandstone aquifer in England.

The isotopes ^{234}U and ^{238}U are present in secular equilibrium in the bulk of a rock matrix, as required by the decay sequence:

$$^{238}U \xrightarrow[4.5 \times 10^9 \text{ yr}]{\alpha} {}^{234}Th \xrightarrow[24.1 \text{ d}]{\beta} {}^{234m}Pa \xrightarrow[1.18 \text{ min}]{\beta} {}^{234}U \xrightarrow[2.5 \times 10^5 \text{ yr}]{\alpha}$$

The ^{234}U activity, $^{234}A_t$, in isotopically pure ^{238}U increases with time, t, according to the equation:

$$^{234}A_t = {}^{238}\lambda \; {}^{238}N_o \; (1 - e^{-{}^{234}\lambda t})$$

where $^{238}N_o$ is the number of ^{238}U atoms initially present and $^{234}\lambda$ and $^{238}\lambda$ are the respective decay constants for ^{234}U and ^{238}U. This growth to equilibrium is complete after 1.25 m.y.; during this growth time the decrease in $^{238}N_o$ is insignificant.

A combination of differential chemical etch of ^{234}U and ^{238}U and α-recoil induced enhancement of ^{234}U in solution, may lead to activity disequilibrium between these isotopes in solution. The rates of solution of ^{234}U and ^{238}U by chemical etch processes may differ due to lattice damage in the neighborhood of ^{234}U atoms caused by the decay processes involved in their formation. The ^{238}U decay product, ^{234}Th, may enter solution by an α-recoil process (Kigoshi, 1971) and dissolved ^{234}Th will reach a maximum equilibrium activity after about 100 days of rock/water contact. If the ^{234}Th activity in solution remains constant due to the α-recoil process continuing at a constant rate, decay of ^{234}Th will produce ^{234}U in solution and the activity of the latter will reach equilibrium with the ^{234}Th activity solution after 1.25 m.y. The change in the ^{234}Th recoil rate in this time is negligible, 100 m.y. being required to reduce it by one percent. Only ^{234}Th atoms formed by ^{238}U decay within the ^{234}Th recoil range, R, of a mineral surface can escape that surface as a result of α-recoil. It may be shown that only 23.5% of all recoil atoms generated within a surface layer of thickness R can enter solution (Andrews and Wood, 1972).

Uranium is also dissolved by chemical etch processes which are of zero order kinetics, that is, the linear surface etch rate is constant and independent of the U content of the rock. If the ^{234}U and ^{238}U etch rates are controlled by rate constants ^{234}k and ^{238}k respectively, the $^{234}U/^{238}U$ isotopic ratio for dissolved uranium is given by:

$$^{234}U/^{238}U = \frac{^{234}U \text{ from recoil process} + {}^{234}U \text{ from chemical etch}}{^{238}U \text{ from chemical etch}}$$

$$= \frac{0.235 \; {}^{238}N_s \; (1 - e^{-{}^{234}\lambda t}) + {}^{234}k \; {}^{238}N_c t}{{}^{238}k \; {}^{238}N_c t} \qquad (1)$$

where t is the reaction time, $^{238}N_S$ = number of ^{238}U atoms cm^{-2} within the recoil range, R, of the surface and $^{234}N_C$; $^{238}N_C$ are the contents of the uranium isotopes in 1 g of rock. Substituting $^{238}N_S = {}^{238}N_C\rho.R$ atoms cm^{-2} (ρ = rock density) and multiplying by the appropriate decay constants gives the $^{234}U/^{238}U$ activity ratio, A.R.:

$$A.R. = \frac{0.235\ {}^{238}\lambda\ {}^{238}N_C\rho.R\ (1 - e^{-{}^{234}\lambda t}) + {}^{234}k\ {}^{234}\lambda\ {}^{234}N_C t}{{}^{238}k\ {}^{238}\lambda\ {}^{238}N_C t} \quad (2)$$

$$= \frac{0.235\ \rho.R\ (1 - e^{-{}^{234}\lambda t})}{{}^{238}k\ t} + \frac{{}^{234}k}{{}^{238}k} \quad (3)$$

provided that $^{234}\lambda\ {}^{234}N = {}^{238}\lambda\ {}^{238}N$, which requires that the rock surface is in equilibrium. This will necessarily be so for high etch rates since new surface in equilibrium is then being continuously exposed. Even for very low etch rates, when recoil predominates, disequilibrium in the surface can never produce a $^{234}U/^{238}U$ activity ratio of less than 0.75.

Activity ratios may be calculated from equation (3) if estimates of the ^{234}Th recoil range and chemical etch rates in aquifers can be made. The recoil range of the 85 KeV ^{222}Rn atom in glass is 0.036 μm (Heckter, 1934) and when scaled to the 71 KeV recoil ^{234}Th atom yields a recoil range of 0.030 μm. This compares with the 0.055 μm range estimate by Kigoshi (1971) and observed α-recoil track lengths of 0.01 μm in micas (Huang and others, 1967). Chemical etch rates have been estimated for the Bunter Sandstone aquifer in Nottinghamshire and range from 10^{-11} cm yr^{-1} in the confined aquifer to about 3.5 X 10^{-10} cm yr^{-1} at recharge. Activity ratios calculated from equation (3) using etch rates around this range for various ground-water residence times are plotted in figure 1. The influence of various relative ^{234}U etch rates is also shown for residence times $\leq$ 1000 years.

For etch rate constants $< 10^{-10}$ cm yr^{-1}, recoil acquires a very significant role in activity ratio enhancement. The highest ratios are acquired at recharge and these decrease with ground-water age, evolving along a path such as A (fig. 1) if etch rate remains constant, or A' (fig. 1) if etch rate decreases as residence time increases. A ground-water which has acquired a high activity ratio due to the recoil effect, necessarily had a low initial chemical etch rate and consequently a low dissolved U content which increases with age whilst activity ratio decreases.

High chemical etch rate constants resulting in above average ground-water U contents and enhanced activity ratios can only be generated if $^{234}k > {}^{238}k$. Enhanced ^{234}U etch rates, however, cannot maintain high activity ratios for dissolved uranium under high etch-rate conditions except in the initial stages of surface etch. As surface erosion progresses, uranium isotopes in equilibrium are released and this effect predominates as the dissolved U content increases, the activity ratio evolving along path C (fig. 1) and the ground-water age being indeterminate.

A ground-water with a high activity ratio due primarily to an enhanced ^{234}U etch rate, evolves along a path similar to B (fig. 1). The activity ratio falls and the ground-water U content increases as etch proceeds in the initial stages of recharge. As the ground-water encounters reducing conditions etch rate falls, excess ^{234}U partially decays, and evolution towards recoil-dominated conditions takes place. Subsequent activity ratio change is very slow as indicated in figure 1.

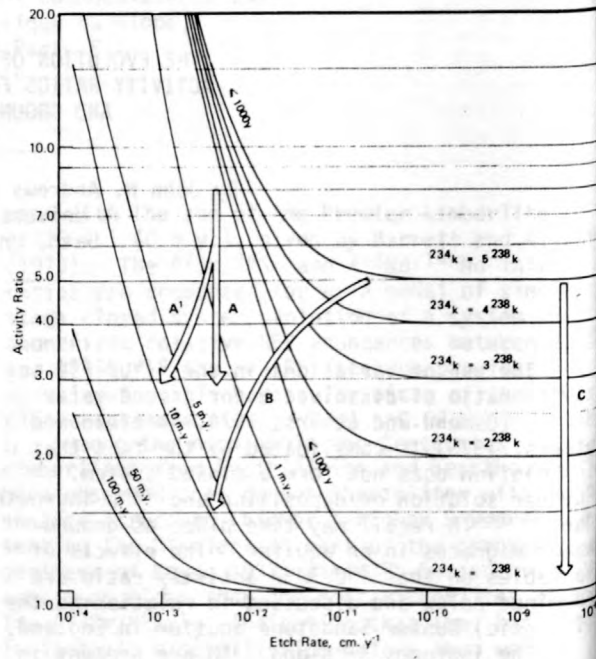

Figure 1.--Activity ratios ($^{234}U/^{238}U$) calculated for various etch rates and ground-water ages.

A consequence of the evolutionary trends described is the frequently observed trend of increasing activity ratio with decreasing U content (Osmond and Cowart, 1976). Activity ratios for dissolved uranium in the Bunter Sandstone ground-waters of Nottinghamshire generally follow such a trend (fig. 2). These ground-waters are from pumped wells as much as 320 m deep in a confined aquifer and are about 15 km from the recharge area. Their residence times are as long as 35,000 years (A. H. Bath, written commun., 1978). The activity ratios and estimated etch rates indicate that ^{234}k is initially greater than ^{238}k. The same formation is overlain by 2300 m of Mesozoic sediments in Dorset where the nearest recharge is 75 km distant. Drill-stem samples of the Bunter Sandstone, obtained from an exploration well at this location, have activity ratios ar

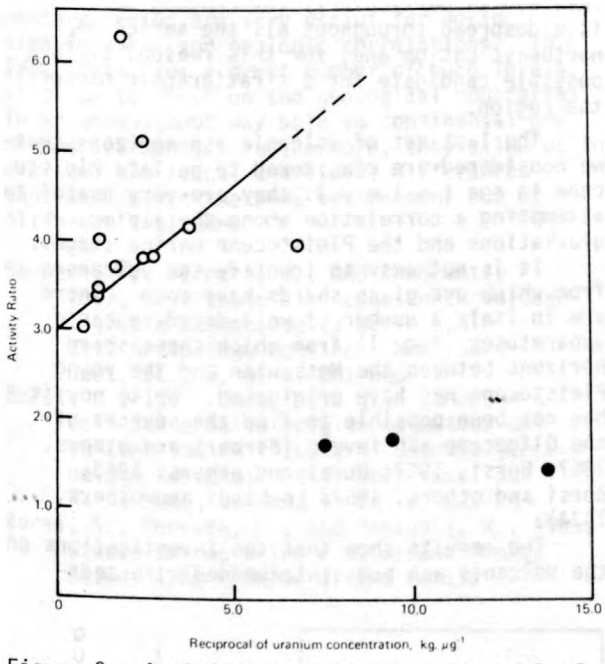

Figure 2.--Activity ratio versus reciprocal of uranium concentration for ground-waters from the Bunter Sandstone. (Open circles are samples from Nottinghamshire, full circles are deep borehole samples from Dorset.)

U contents much lower than those for the more recently recharged sources in Nottinghamshire. Assuming that these deep ground-waters have evolved from high activity ratio ground-waters similar to those of Nottinghamshire, they have a minimum age of 300,000 years if the excess ^{234}U acquired at recharge simply decays to that amount observed at depth. However, if etch processes continue at reduced rates at depth and are accompanied by recoil processes, the activity ratio would evolve along a path similar to B (fig. 1) and several million years would be required for the activity ratio to fall to its observed value. Very high ^{4}He contents and enhanced $^{40}Ar/^{36}Ar$ ratios for the dissolved Ar also indicate that these deep ground-waters have ages of this order (Andrews and Lee, in preparation).

This work was supported by the Natural Environment Research Council.

Andrews, J. N. and Wood, D. F., 1972, Mechanisms of radon release in rock matrices and entry into ground-waters: Institution of Mining and Metallurgy, Transactions, Section B, v. 81, no. 792, p. B198-B209.

Heckter, M., 1934, Radiochemische Oberflachenbestimmung an Glas: Glastechnische Berichte, v. 12, p. 156-72.

Huang, W. H., Maurette, M., and Walker, R. M., 1967, Observation of fossil α-particle recoil tracks and their implications for dating measurements: in Radioactive dating and methods of low level counting, International Atomic Energy Agency, Vienna, p. 415-429.

Kigoshi, K., 1971, Alpha-recoil ^{234}Th: dissolution into water and the $^{234}U/^{238}U$ disequilibrium in nature: Science, v. 173, p. 47-48.

Kronfeld, J., Gradoztajn, E., Muller, H. W., Radin, J., Yamir, A., and Zach, R., 1975, Excess ^{234}U: an aging effect in confined waters: Earth and Planetary Science Letters, v. 27, p. 342-345.

Osmond, J. K., and Cowart, J. B., 1976, The theory and use of natural uranium isotopic variations in hydrology: Atomic Energy Review, v. 14, p. 621-679.

Osmond, J. K., Kaufman, M. I., and Cowart, J. B., 1974, Mixing volume calculations, sources and aging trends of Floridan aquifer water by uranium isotopic methods: Geochimica Cosmochimica Acta, v. 38, p. 1083-1100.

TERTIARY-QUATERNARY CHRONOSTRATIGRAPHY BY RADIOMETRIC MEASUREMENTS ON VOLCANICS INTERBEDDED IN SEDIMENTARY SERIES

By Claudio Arias [1,2], Giulio Bigazzi[2], Francescopaolo Bonadonna [1,2], and Osvaldo Giuliani[2]
[1]Laboratorio di Geologia Nucleare dell'Universitá
[2]Laboratorio di Geocronologia e Geochimica Isotopica del C.N.R., Pisa, Italy

Ash shard horizons interbedded with marine and continental strata are frequently found in the Mediterranean basin. For some time we have carried on the study of these horizons with the

following aims in mind: dating of glass shards by fission tracks and K-Ar methods, construction of a palaeomagnetic stratigraphy based on the ash horizons, dating of volcanoes in order to identify the sources of these horizons, and a chemical study of the glasses and volcanics. Our investigations are being carried out in collaboration with paleontologists and field geologists to obtain all possible information on the rocks being studied and to allow us to more correctly interpret the chronological and biostratigraphical setting of the sediments interlayered with volcanic ashes. In this way we are trying to identify some marker beds for use in correlations between the chronostratigraphy and biostratigraphy of Tertiary and Quaternary sediments; we are also trying to find some correlations between continental and marine stages.

Figure 1 is a stratigraphic scheme of the ash levels as inferred by biostratigraphy. On those parts of the series with interlayered volcanic horizons, detailed micropaleontological studies were carried on; furthermore, on some series, the paleomagnetic stratigraphy has been worked out by other researchers and ourselves.

The results now on hand allow us to place the volcanic ash levels within some defined time intervals. The oldest horizons among those considered are late Oligocene in age. The radiometric ages range between about 20 and 24 m.y. These ash beds have variable thickness and are within the marine Marche and Emilia series of the northeast Apennines (Mezzetti, 1969). Although sometimes it is possible to distinguish various ash levels within the same series having similar radiometric ages the time interval of the volcanic activity that produced these ashes cannot be clearly defined because the experimental error overlaps with the life span of the volcanism.

In Italy, at present, no volcanic horizons are known to exist in the upper Oligocene-upper Tortonian interval. We have made some radiometric measurements in the Mediterranean Morocco (Melilla basin) and in Italy near the Tortonian-Messinian boundary. For this period another radiometric age in southern Spain obtained by Curtis and Van Couvering (Van Couvering, 1976) is available. All these measurements confirm an age of about 6.5 m.y. for the Tortonian-Messinian boundary.

The next volcanic horizons are found in the Calabrian sediments of northeast Latium, which are assigned to the middle Pliocene by biostratigraphy. Their radiometric age is about 4 m.y. In the upper part of these sediments are other younger volcanic ash beds ($\sim$ 2 m.y.), one of which occurs in the Vrica-Calabria series and marks the Neogene-Quaternary boundary, according to the opinion of some researchers. This horizon lies between the beginning of Matuyama reversed epoch and the Oldway normal event. In the same position and with the same age ($\sim$ 2 m.y.) another volcanic ash bed in the marine Fornace Tini series near Rome has been dated. This ash is particularly interesting because it is widespread throughout all the series of northeast Latium and, for this reason, it is a possible candidate for a stratigraphic marker in the region.

The last set of volcanic ash horizons that we considered are considered to be late Pleistocene in age ($\sim$ 1 m.y.); they are very useful in attempting a correlation among the alpine glaciations and the Pleistocene marine stages.

It is not easy to identify the volcanoes from which our glass shards have come. There are in Italy a number of well-dated volcanic apparatuses (fig. 1) from which these shard horizons between the Messinian and the young Pleistocene may have originated. Up to now it has not been possible to find the sources of the Oligocene ash levels (Barberi and others, 1967; Borsi, 1967; Borsi and others, 1965; Borsi and others, 1967; Lombardi and others, 1974).

The results show that the investigations on the volcanic ash beds interbedded with sedi-

Figure 1.--Geographical Location and Stratigraphy of Acid Volcanics in Italy. Volcanoes are marked on the left of the stratigraphical column at levels corresponding to their age. Volcanic ashes interbedded with sedimentary series are marked in the stratigraphical column.

Volcanoes - 1) Capraia Isle (Toscana): latite; 2) San Vincenzo (Toscana): Rhyodacite; 3) Montecatini Val Di Cecina (Toscana): selagite; 4) Roccastrada (Toscana): rhyolite overlying Pliocene sediments; 5) Monte Amiata (Toscana): rhyodacite; 6) Monte Cimino (Lazio): ignimbrite; 7) Tolfa (Lazio): rhyolite; 8) Cerite and Manziate (Lazio): Tiparites, rhyolites and latites; 9) Ponza Isle (Lazio): rhyolite.

Volcanic Ashes Interbedded with Sedimentary Series - 10) Trino Vercellese (Piemonte): volcanic ashes scattered in a middle-up per Pleistocene series; 11) Apennines at Parma (Emilia); 12) Mon Tearligo (Emilia); 13) Fossombrone (Marche); 14) Tarugo Creek (Marche): Volcanic ashes interbedded with Oligo-Miocene series; 15) Montopoli (Toscana): Two levels interbedded with a Plio-quaternary serie; 16) Ascoli Piceno (Marche): Volcanic ash interbedded with a Mio-Pliocene serie; 17) Corchiano (Lazio): volcanic ash interbedded with a Pliocene serie; 18) Fornace Tini (Lazio): volcanic ash interbedded with a Plio-quarternary serie; 19) Marco Simone (Lazio): volcanic ash interbedded with a Pliocene serie; 20) Sanfili (Calabria): volcanic ash interbedded with a Miocene serie; 21) and 22) Vrica (Calabria): volcanic ashes levels interbedded with a Plio-Pleistocene serie; 23) Spirito Santo-Terreti (Calabria): volcanic ash interbedded with a Plio-Pleistocene serie.

mentary series are very useful for world stratigraphic and geologic correlations. In fact, data from a great number of such levels allow us to focus on the geological boundaries in an unambiguous way both in continental and marine sediments. Furthermore, they allow us to overcome the faunal and floral differences that we find in the same environment but at different latitudes.

Barberi, F., Ferrara, G., and Innocenti, F., 1967, Contributo alla conoscenza vulcanologica e magmatologica delle isole dell'Arcipelago Pontino: Mem. Soc. Geol. It., v. 6, p. 581-606.

Borsi, S., 1967, Contributo alla conoscenza dell'età e della origine magmatica del vulcanesimo dell'Isola di Capraia (Arcipelago Toscano): Atti Soc. Tosc. Sc. Nat., Mem., ser. A, v. 74, p. 232-243.

Borsi, S., Ferrara, G., and Mazzuoli, R., 1965, Studio petrografico e datazione con i metodi K/Ar e Rb/Sr di una roccia granitica presso Roccastrada (Grosseto): Atti Soc. Tosc. Sc. Nat., Mem., ser. A, v. 72, p. 1-25.

Borsi, S., Ferrara, G., and Tongiorgi, E., 1967, Datazione con il metodo del K/Ar delle eta delle rocce magmatiche: Boll. Soc. Geol. It., v. 86, p. 403-410.

Lombardi, G., Nicoletti, M., and Petrucciani, C., 1974, Eta delle vulcaniti acide dei complessi Tolfetano, Cerite e Manziate (Lazio Nord-Occidentale): Periodico Mineral., v. 43, p. 351-375.

Mezzetti, R., 1969, Studio petrografico di ceneri vulcaniche appenniniche. I) Le intercalazioni langhiane dell'Emilia e delle Marche: Miner. Petrogr. Acta, v. 15, p. 9-34.

Van Couvering, J. A., 1976, Andalusian correlation and Messinian circulation; a modified deep-basin model: Messinian Seminar n. 2, Gargnano, Sept. 5-12 (Italy), Proceedings, p. 28-29, Cita, M. B., ed., University of Milano.

THE CLIMATIC RESPONSE IN THE $\delta^{13}C$ VALUES OF JUNIPER TREES FROM THE AMERICAN SOUTHWEST

By L. David Arnold
Laboratory of Isotope Geochemistry
Department of Geosciences
University of Arizona
Tucson, Arizona 85721

The $\delta^{13}C$ values of cellulose from four species of juniper trees show substantial correlation with the temperature and precipitation of the sampling locations. Juniper trees (Juniperus osteosperma, J. monosperma, J. scopulorum and J. deppeana) grow under widely varying climatic and edaphic conditions throughout the American Southwest. In order to test for a climatic response in the $\delta^{13}C$ values of such trees, a total of 17 trees were sampled in the immediate vicinity of 7 meteorological stations scattered across the State of Arizona. Care was taken to insure that each tree obtained water from only natural precipitation and that none were located adjacent to concentrated water supplies such as streams or ponds. As a cross-check, artificially watered trees and one located on a stream bank were also included in the survey. Each tree was sampled in four places, at each cardinal direction, and all samples were taken approximately 2 meters above the ground. Each sample consisted of a mixture of one to four year old twigs and leaves totalling approximately 20 grams.

The $\delta^{13}C$ value for each location was derived from an average of three trees per location, the value for each tree being the mean of its four samples. The one sigma variation between trees at any one location was found to be ± 0.5 permil and within a single tree, ± 0.4 permil. All samples were reduced to cellulose (holocellulose) before combustion and analysis for the $\delta^{13}C$ values.

The $\delta^{13}C$ values determined for the juniper sites were regressed against the mean annual as well as selected mean seasonal values (four year averages) of temperature, precipitation and their ratio (T/P). The correlation coefficients for these regressions (fig. 1) show considerable variation with precipitation but are rather stable for temperature over the months considered. The regression using a temperature to precipitation ratio averaged from March, April, and May combined (TPR 345) clearly shows the strongest correlation of all with a coefficient of 0.99 at the 99.9 percent confidence level (fig. 2). This finding adds further support to evidence that tree rings in junipers also show strong climatic correlation with the March, April, and May growing period

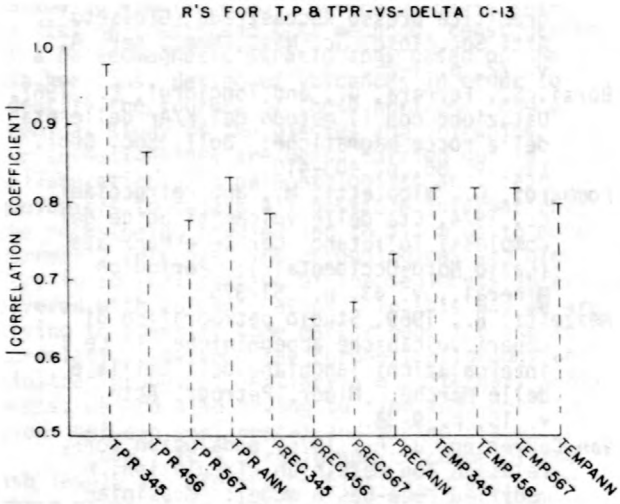

Figure 1.--Correlation coefficients (in absolute values) for juniper cellulose $\delta^{13}C$ values at 7 Arizona locations regressed (R) against mean annual and the averages of monthly combinations of temperature (TEMP), precipitation (PREC) and their ratios (TPR). Precipitation (PREC) regressions have negative coefficients, all others are positive. Note: 345 = March, April, May; 456 = April, May, June; 567 = May, June, July; ANN = annual.

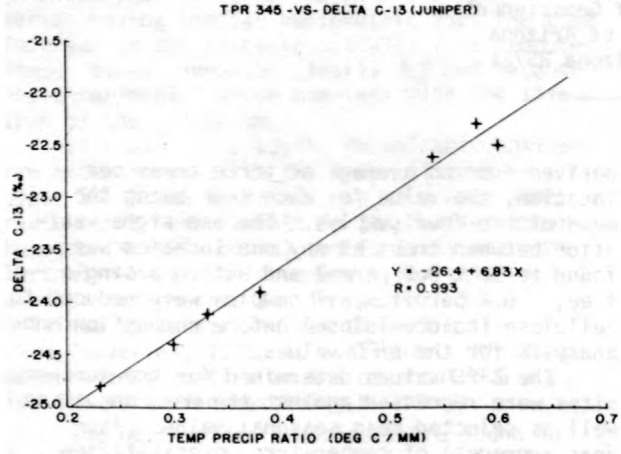

Figure 2.--Regression of juniper cellulose $\delta^{13}C$ values (+) for 7 Arizona locations against the respective temperature to precipitation ratios averaged from March, April, and May combined (TPR 345).

(Fritts and others, 1965). The weaker regressions using temperature (fig. 3) and precipitation (fig. 4) separately for the same three-month average shows not only the interdependence of the two climatic parameters but also the opposite effect of each on the $\delta^{13}C$ values.

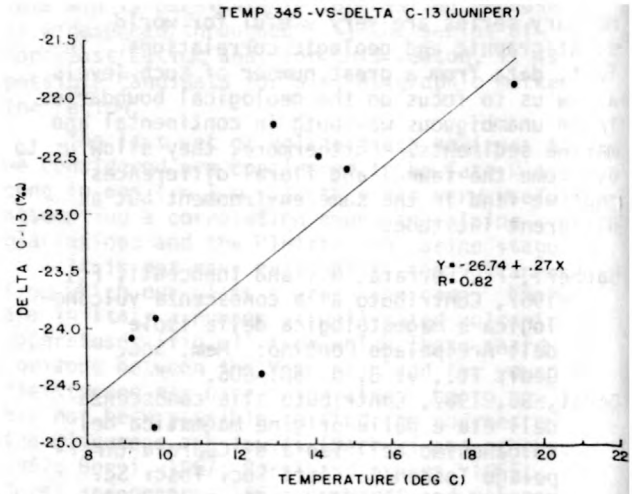

Figure 3.--Regression of juniper cellulose $\delta^{13}C$ values (solid circles) for 8 Arizona locations against the respective temperatures averaged from March, April, and May combined (TEMP 345).

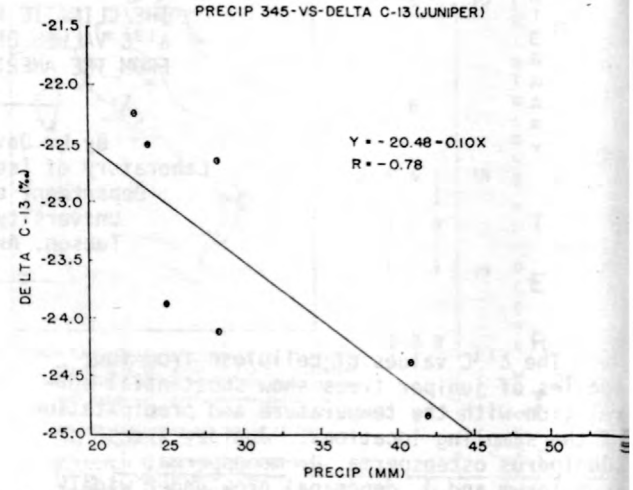

Figure 4.--Regression of juniper cellulose $\delta^{13}C$ values (solid circles) for 7 Arizona locations against the respective precipitation totals averaged from March, April and May combined (PRECIP 345).

This opposite effect appears to support similar indications from work in New Zealand on Pinus longaeva (Grinsted, 1977). In addition, the 0.27 permil/°C temperature coefficient for juniper (the slope in fig. 3) agrees reasonably well, for example, with the 0.22 permil/°C for Pseudotsuga menziesii (Grinsted, 1977) and a value for Pinus radiata of at least 0.2 permil/ C (Wilson and Grinsted, 1977).

The variation of $\delta^{13}C$ around a given tree (± 0.4 permil) generally follows what might be

a differential heating effect with the south-facing side having the heaviest value and the north-facing side often the lightest value. This is a pattern similar to that obtained for different radii of trees from Chaco Canyon (Mazany and others, 1978).

The artificially watered trees, as well as the one sampled from a stream bank, clearly show the influence of having water in excess of the site's natural precipitation. The $\delta^{13}C$ values for these samples (not illustrated) were about 1.5-2.5 permil more negative than the naturally watered trees, a direction expected from the relationship shown in figure 4.

The most immediate application for these findings appears to be an investigation of paleoclimate using the juniper twigs so abundant in most of the fossil packrat nests now under study at the University of Arizona (Van Devender, 1977). Many of the juniper samples from these nests have been radiocarbon-dated as earlier than the Holocene-Pleistocene boundary.

I would like to thank Dr. Austin Long and Dr. Juan Carlos Lerman of the Laboratory of Isotope Geochemistry, Department of Geosciences, University of Arizona for their kind support and advice during this research. This work was supported in part by N.S.F. Grant ATM77-06790 and in part by the State of Arizona.

Fritts, H. C., Smith, D. G., and Stokes, M. A., 1965, The biological model for paleoclimatic interpretation of Mesa Verde tree ring series: American Antiquity, v. 31, no. 2, p. 101-121.

Grinsted, M. J., 1977, A study of the relationship between climate and stable isotope ratios in tree rings: Ph.D. thesis dissertation, Waikato Univ., New Zealand.

Mazany, T., Lerman, J. C., and Long, A., 1978, Climatic sensitivity in $^{13}C/^{12}C$ values in tree rings from Chaco Canyon [abs.]: American Association for the Advancement of Science Poster Session, Feb. 12-17, 1978, Washington D.C.

Van Devender, T. R., 1977, Holocene woodlands in the Southwest desert: Science, v. 198, p. 189-192.

Wilson, A. T., and Grinsted, M. J., 1977, $^{12}C/^{13}C$ in cellulose and lignin as paleothermometers: Nature, v. 265, p. 133-135.

GEOCHRONOLOGY AND MAGNETOSTRATIGRAPHY OF FLUVIAL-DELTAIC SEDIMENTS EMBRACING THE CRETACEOUS-TERTIARY BOUNDARY, RED DEER VALLEY, ALBERTA, CANADA

By H. Baadsgaard[1], J. F. Lerbekmo[1], and M. E. Evans[2]
[1]Department of Geology
and [2]Department of Physics
University of Alberta, Edmonton, Canada

Detailed magnetostratigraphy and K-Ar radiometric ages have been compiled for a sequence of fluvial-deltaic coal and bentonite-bearing sediments defined as embracing the Cretaceous-Tertiary boundary on the basis of their palynofloral and dinosaur remains.

A notable floral extinction occurred in North America from Colorado to Alberta at a horizon which coincides with the Hell Creek-Fort Union formational boundary and is a few meters above the highest occurrence of dinosaur bones, which are not reworked. This extinction includes the disappearance of all but one species of Aquilapollenites and numerous other species (including Wodehouseia spinata) which are replaced by such species as Wodehouseia fimbrata (Leffingwell, 1971; Tschudy, 1971; Tschudy and Leopold, 1971). The same floral crisis occurs at the top of the Nevis Coal in the Red Deer Valley of Alberta and is about four meters above the highest known local occurrence of dinosaur remains (Snead, 1969; Srivastava, 1970; C. Singh, written commun., 1976). This floral extinction is widely held to be the best choice for the Cretaceous-Tertiary boundary in continental sediments of western North America.

Eleven high-purity sanidine separates were obtained from four bentonite horizons located 17.5, 17, and 11 meters above the palynological boundary and 1 meter below. Table 1 gives the analytical results of conventional argon and isotope-dilution K determinations. If the minimum rate of sedimentation in this basin for the Late Cretaceous is taken to be 50 meters per million years (Folinsbee and others, 1961), the total vertical age variation should be about 0.4 m.y. This variation is smaller than the expected precision of a single measurement, and the eleven values are averaged to give a mean value of 63.1 ± 0.5 (2σ) m.y. Considering the major known sources of error, the K-Ar date for the Red Deer Valley Cretaceous-Tertiary boundary is placed at 63 ± 2 m.y.

able 1.--Analytical results from K-Ar dating of bentonite sanidine; tabulated in stratigraphic order

Sample, elevation, mesh size	^{40}K (ppm)[1]	$\frac{^{40}Ar\ rad}{^{40}Ar\ total} \times 100$	$\frac{^{40}Ar}{^{40}K}$	Date (m.y.)[1]
3-1 (17.5) +150	10.97	97.6	0.003726	63.0
3-1 (17.5) -150	9.68	96.3	0.003723	63.0
5-102 (17.5) -80+120	11.03	96.5	0.003745	63.3
5-100 (17) -80+120	10.82	94.8	0.003740	63.2
5-100 (17) -120+170	9.88	95.7	0.003710	62.8
5-104A (11) -80+120	11.44	96.1	0.003725	63.0
5-104A (11) -120+170	11.24	98.2	0.003704	62.7
Assumed Cretaceous-Tertiary boundary				
4-1 (-1) -80+120	11.46	97.8	0.003726	63.0
4-1 (-1) -120+170	11.54	97.5	0.003744	63.3
5-400 (-1) -80+120	11.57	96.7	0.003753	63.5
5-400 (-1) -120+170	11.34	96.0	0.003753	63.5

[1]Constants used: λ_β=4.962x10^{-10}yr^{-1}, λ_ε=0.581x10^{-10}yr^{-1}, ^{39}K=93.2581 atom-percent, ^{40}K=0.01167 atom-percent, ^{41}K=6.7302 atom-percent.

Recently published magnetic-polarity time scales and paleomagnetic studies for this part of the geologic column correlate the Cretaceous-Tertiary boundary with some position within sea-floor magnetic anomaly 29, or in the reversed zones above or below it (Tarling and Mitchell, 1976; Van Hinte, 1976; Labrecque and others, 1977; Butler and others, 1977; Lowrie and Alvarez, 1977). Magnetic-polarity measurements have been made on approximately 500 samples from 100 horizons encompassing 85 meters of section above the Kneehills Tuff datum in the Red Deer Valley. The 18.5 meter section incorporating the K-Ar-dated bentonites covers the lower half of a normal-polarity zone which is tentatively correlated with sea-floor anomaly 29. A zone of alternating, but dominantly reversed, polarity begins one meter below the Cretaceous-Tertiary palynological boundary and continues downward for 25 meters to the top of another major normal-polarity zone. This mixed-polarity zone is correlated with the sea floor reversed-polarity zone between anomalies 29 and 30.

Butler, R. F., Lindsay, E. H., Jacobs, L. L., and Johnson, N. M., 1977, Magnetostratigraphy of the Cretaceous-Tertiary boundary in the San Juan Basin, New Mexico: Nature, v. 267, p. 318-323.

Folinsbee, R. E., Baadsgaard, H., and Lipson, J., 1961, Potassium-argon dates of Upper Cretaceous ash falls, Alberta, Canada: New York Academy of Sciences Annals, v. 91, p. 352-363.

La Brecque, J. L., Kent, D. V., and Cande, S. C., 1977, Revised magnetic polarity time scale for late Cretaceous and Cenozoic time: Geology, v. 5, p. 330-335.

Leffingwell, H. A., 1971, Palynology of the Lance (Late Cretaceous) and Fort Union (Paleocene) Formations of the type Lance area, in Symposium on palynology of the Late Cretaceous and Early Tertiary, eds., Kosanke, R. M., and Cross, A. T.: Geological Society of America Special Paper 127, p. 1-64.

Lowrie, W., and Alvarez, W., 1977, Late Cretaceous geomagnetic polarity sequence - detailed rock and paleomagnetic studies of the Scaglia Rossa Limestone at Gubbio, Italy: Geophysical Journal of the Royal Astronomical Society, London, v. 51, p. 561-582.

Snead, R. G., 1969, Microfloral diagnosis of the Cretaceous-Tertiary boundary, central Alberta: Research Council of Alberta Bulletin, v. 25, 148 p.

Srivastava, S. K., 1970, Pollen biostratigraphy and paleoecology of the Edmonton Formation (Maestrichtian), Alberta, Canada: Palaeogeography, Palaeoclimatology, Palaeoecology, v. 7, p. 221-276.

Tarling, D. H., and Mitchell, J. F., 1976, Revised Cenozoic polarity time scale: Geology, v. 4, p. 133-136.

Tschudy, R. H., 1971, Palynology of the Cretaceous-Tertiary boundary in the northern Rocky Mountain and Mississippi Embayment regions, in Symposium on palynology of the Late Cretaceous and Early Tertiary, eds., Kosanke, R. M., and Cross, A. T.: Geological Society of America Special Paper 127, p. 65-111.

Tschudy, B. D., and Leopold, E. B., 1971, Aquilapollenites (Rouse) Funkhouser - selected Rocky Mountain taxa and their stratigraphic ranges, in Symposium on palynology of the Late Cretaceous and Early Tertiary, eds., Kosanke, R. M., and Cross, A. T.: Geological Society of America Special Paper 127, p. 113-167.

Van Hinte, J. E., 1976, A Cretaceous time scale: American Association of Petroleum Geologists Bulletin, v. 60, no. 4, p. 498-516.

K-Ar AGES OF A SUITE OF LOWER PALAEOZOIC POSTTECTONIC GRANITES, SOUTHERN INDIA

By M. N. Balasubrahmanyan and A. Sarkar
Geological Survey of India
Calcutta, India

A posttectonic suite of intrusive granitic rocks with dominant pegmatitic facies characteristically mark the close of igneous activity in the Precambrian terrains of India. The intrusion of such granitic rocks generally resulted in (1) widespread migmatization of pre-existing rocks, chiefly in the form of K-feldspathization and (2) a strong thermal overprint on isotopic ages of the invaded rocks. The present contribution deals with the K-Ar ages of one such suite of posttectonic granitic rocks of the Southern Indian Shield.

In the Kadavur (10°36':78°12') - Manapparai (10°36'30":78°25'30") belt, Tiruchirapalle dt., Tamilnadu, located at the southern margin of the Eastern Ghats belt, a wide variety of granitic rocks occur as an anastomosing network of sills and dikes intruding high-grade metamorphics (represented by sillimanite-bearing quartzites and quartz-schists, calc-silicate rocks, amphibolites, charnockitis and migmatitic gneisses) and older basic intrusions. The tectonomagmatic evolution has been worked out in detail during investigations on the gabbro-anorthositic rocks of the area (A. Sarkar, unpub. data). The area, having a polyphase deformation (A. Sarkar and M. K. Bose, oral commun., 1978) and metamorphic history (Balasubrahmanyan, 1976), witnessed repeated pulses of basic magmatism to give rise to the Kadavur gabbro-anorthosite complex (including related minor intrusion near Manapparai)--a composite igneous intrusion of dominantly layered affinity (A. Sarkar and M. K. Bose, oral commun., 1978).

The granitic rocks, posttectonic with respect to the last major folding event (F_3-open, asymmetric cross-folds with approximately east-west trending axial traces) have the following emplacement sequence: Trondhjemite-granodiorite-adamellite-alkali granite (alaskites). Of the variants, alaskites are the most abundant. The rocks, in general, represent a medium- to coarse-grained quartz-rich granitoid suite composed of quartz, microcline ($Or_{84.6-87.5}$), sodic plagioclase ($An_{17.0-34.9}$), muscovite, and biotite. Apatite and garnet occur as accessories.

Four mica separates from this granitic suite and one hornblende separate from the invaded gabbroic rocks have been dated by the ^{40}K-^{40}Ar method. The age date are detailed in table 1.

Each sample has been analyzed in duplicate for argon using a VG Micromass 600 Gas Source Mass Spectrometer (90° sector, 62 mm radius, magnetic deflection type) operated under static mode and using pure ^{38}Ar as tracer. Sample fusion was done by the step-heating technique using an all-metal sample fusion system with an all-metal on-line ^{38}Ar spike system.

Table 1.--^{40}K-^{40}Ar ages of minerals, Kadavur, Southern India

[Ar analyses, A. Sarkar; K analyses by AAS, N. R. Sengupta]

No. [1]	Sample No.	Vol. Rad. Ar (nl/gm)	Atmospheric Ar (percent)	K (percent)	$^{40}Ar/^{40}K$	Age (m.y.)
1.	AS/Kd/352	199.45	1.1	8.39 8.39	0.03556	527±11
2.	AS/Kd/4	197.41	3.8	8.62 8.60	0.03430	510±11
3.	AS/Kd/53	194.18	8.9	8.94 8.96	0.03246	486±10
4.	AS/Kd/145B	177.33	7.1	8.37 8.43	0.00316	475±10
5.	AS/Kd/34	7.48	18.1	0.33 0.35	0.03292	492±10

[1] 1. Coarse muscovite from trondhjemite-pegmatite; 2. Muscovite (medium grained) from quartz-rich granodiorite; 3. Coarse muscovite from alaskitic granite; 4. Medium- to fine-grained biotite from alaskitic granite; 5. Medium-grained hornblende from cumulate hornblende leuco-gabbro, Unit III, Kadavur complex.

The K-Ar mineral ages of micas (table 1, nos. 1 - 4) from the granitic rocks range from 475-527 m.y. with a mean of ∿ 500 m.y. This mean age of 500 m.y. can be assumed to closely approximate the age of intrusion for the following reasons: (1) the minerals are from posttectonic, undeformed and unmetamorphosed rocks, and (2) there is a close agreement in mica ages between variants of the granite and between differing size fractions (see table 1).

It is curious to note that muscovite from the trondhjemitic rocks give relatively older ages--a fact in accordance with the emplacement sequence observed in the field. A cumulate hornblende separate from a sample of leuco-gabbro of the Kadavur complex (A. Sarkar and M. K. Bose, oral commun., 1978), located very close to the granitic rocks, gives an age of 492 ± 10 m.y. (table 1, No. 5)--obviously a thermally reset age.

The posttectonic granitic and pegmatitic activity appears to reflect an episode of reheating. Available age data on the Indian Precambrian do indicate a pronounced event at 600 ± 200 m.y. (see review by Sarkar, 1968; Balsundaram and Balasubrahmanyan, 1973) with a maximum at ∿ 500 m.y. This episode, generally referred to as the Indian Ocean Cycle, is now recognized as a period of worldwide crustal instability (Hurley, 1974). The closing of this cycle around 450 - 550 m.y. ago is marked by

posttectonic granitic intrusions in many segments of the Indian Precambrian, as testified by yet another example emerging from the present study.

The periodicity of events in the Indian Precambrian is closely comparable to that of Africa (as outlined by Clifford, 1968, p. 303), events ∿ 1400 m.y. ago having been subsequently discovered (Balsundaram and Balasubrahmanyan, 1973; Sarkar and others, 1977). The models of crustal evolution proposed for Africa in recent years (Kroner, 1977; Gass, 1977) have attached considerable importance to the impressive late Precambrian/early Palaeozoic episode of the continent. In India, with increasing availability of data, the widespread imprint of the Indian Ocean Cycle is becoming obvious. Review of the available data vis-a-vis their distribution shows that segments with an imprint of ∿ 500 m.y. event (and, for that matter, the 600 ± 200 m.y. cycle) represent activity in linear zones fully encircling or partially cratonized blocks that generally yield much older isotopic ages.

Balasubrahmanyan, M. N., 1976, Significance of sapphirine and kornerupine-bearing cordierite rocks from around Kiranur, Tiruchirapalle dt., Tamilnadu [abs.]: Journal of the Geochemical Society of India, v. 17, no. 1, p. 158.

Balsundaram, M. S., and Balasubrahmanyan, M. N., 1973, Geochronology of the Indian Precambrian: Geological Society of Malaysia Bull. 6, p. 213-226.

Clifford, T. N., 1968, Radiometric dating and Pre-Silurian geology of Africa, in Radiometric dating for geologists, Hamilton, E. I., and Farquhar, R. M., eds.: London, Interscience Pub., p. 299-416.

Gass, I. G., 1977, The evolution of Pan-African crystalline basement in NE Africa and Arabia: Journal of the Geological Society of London, v. 134, p. 129-138.

Hurley, P. M., 1974, Pangaeic orogenic system: Geology, v. 2, p. 373-376.

Kroner, A., 1977, The Precambrian geotectonic evolution of Africa; plate accretion versus plate destruction: Precambrian Research, v. 4, p. 163-213.

Sarkar, A., Bhanumathi, L., and Balasubrahmanyan, M. N., 1977, Petrology, geochemistry and geochronology of the Chilka Lake Igneous Complex, Orissa state, India--an appraisal: Volume of abstracts, IUGS-UNESCO-IGCP Symposium on Archean geochemistry, Hyderabad, India, p. 71-73.

Sarkar, S. N., 1968, Precambrian stratigraphy and geochronology on peninsular India: India, Dhanbad Publishers, p. 1-33.

ISOTOPICALLY ANOMALOUS TELLURIUM ACCOMPANIES ISOTOPIC ANOMALOUS COMPONENTS OF HEAVY NOBLE GASES IN ALLENDE

By Robert V. Ballad, Lawrence L. Oliver, R. Greg Downing, and Oliver K. Manuel
Chemistry Department
University of Missouri
Rolla, Missouri 65401

Abundances of the even mass isotopes of tellurium--^{120}Te, ^{122}Te, ^{124}Te, ^{126}Te, ^{128}Te, and ^{130}Te--have been determined in acid-resistant residues of the Allende meteorite by neutron activation and γ-ray spectrometry. The results of our analyses reveal the existence of large isotopic anomalies in Te (as much as 20 percent) and the anomaly pattern is similar to that observed in Xe: the most neutron-rich isotope, ^{130}Te, and the most neutron-poor isotope, ^{120}Te, are highly enriched and the largest enrichment is at ^{130}Te.

The sample was etched with HCl and HF acids, as developed at Chicago (Srinivasan and others, 1975), and then etched with concentrated HNO_3 to remove the phases containing isotopically normal Ar, Kr, and Xe. The residues were irradiated in late January 1978 for 95 hours at a flux of 6 x 10^{14} neutrons cm^{-2} sec^{-1} with monitors of Os, Ru, U, and Te. The irradiated residues were then etched in a 3:8 mixture of concentrated H_3PO_4:H_2SO_4 to dissolve Phase I, which has been tentatively identified as chromite at Chicago (Lewis and others, 1975). Phase II, which is believed to consist mainly of carbon (Lewis and others, 1975), was dissolved in the same 3:8 mixture of concentrated acids plus CrO_3. Carriers of Os, Ru, I, and Te were used in the post irradiation chemistry to isolate osmium as $Os(NH_2\text{-}CS\cdot NH_2)_6CR(SCN)_6$, ruthenium as $Ru(NH_2\text{-}CS\cdot NH_2)_6Cr(SCN)_6$, iodine as PdI_2, and tellurium as the free metal. We made no detailed attempt to characterize the phases, except to compare activities of ^{59}Fe and ^{51}Cr in the solutions of Phases I and II. The ratio of iron in Phase I:Phase II is 1.000:0.006

and the ratio of chromium is 1.000:0.062. The ratio of iron activities may better reflect the removal of chromite, because iron would be complexed as a phosphate in the dissolving solution.

The Os and Ru were highly enriched in the residues, apparently as a result of their insolubility in the etching acids. No isotopic anomalies were observed in these two elements: Takaheshi and others (1976) earlier reported normal values of $^{184}Os/^{190}Os$ in similar residues of Allende.

The activity of ^{133}I in the PdI_2 precipitates from Phase I, Phase II, and the uranium monitors was used to correct for the production of ^{131}Te by neutron-induced fission of ^{235}U during the irradiation.

We interpret the results of our analyses on Te, previous analyses on elemental and isotopic abundances of noble gases (Lewis and others, 1975; 1977; Frick and Moniot, 1976; Srinivasan and others, 1977), and the recent report on isotopically anomalous uranium (Arden, 1977) in residues of Allende and other meteorites as evidence of local element synthesis in a precursor star approximately concentric with the present Sun (Manuel and Sabu, 1975, 1977; Hennecke and Manuel, 1977). The isotopically anomalous components of uranium, tellurium, and heavy noble gases are accompanied by high concentrations of isotopically normal He and Ne, as shown in figure 1 for xenon in the residues of Allende (Lewis and others, 1975) and Murchison (Srinivasan and others, 1977). Takahashi and others (1976) also note that the carbon and oxygen in these residues have isotopic compositions within 1 percent of their mean terrestrial values. These results and the correlations shown in figure 1 suggest that the primitive nebula was chemically and isotopically very heterogeneous, with isotopically anomalous components of the high Z elements associated with isotopically normal components of the low Z elements. Interstellar dust grains (Clayton, 1976) or injection of freshly synthesized material from a nearby supernova (Cameron and Truran, 1977) cannot explain the correlations observed between isotopically anomalous components of high Z elements and chemical abundances of isotopically normal low Z elements.

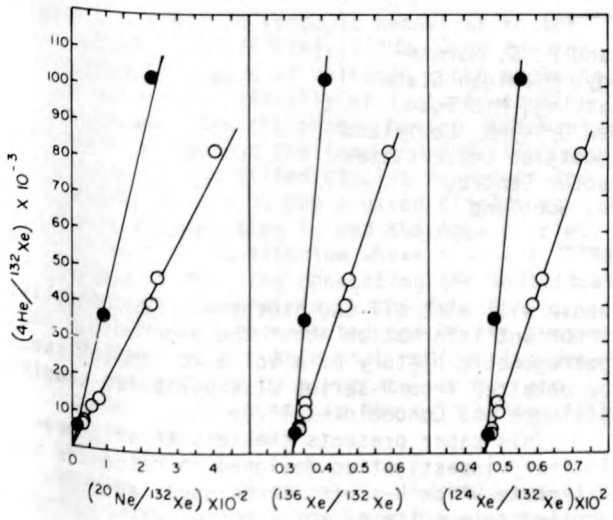

Figure 1.--Variations in isotopic composition of Xe in acid-resistant residues of Allende (open circles, Lewis and others, 1975) and Murchison (solid circles, Srinivasan and others, 1977) chondrites correlate linearly with elemental abundances of isotopically normal He and Ne. Correlations indicate a primitive noble gas component with zero values of He and Ne and $^{136}Xe/^{132}Xe \lesssim 0.32$, $^{124}Xe/^{132}Xe \lesssim 0.0045$. Differences in trapping efficiencies for light and heavy noble gases by minerals of Allende and Murchison may explain differences in slopes of correlation lines for elemental and isotopic ratios of noble gases in these two meteorites. Additional evidence for a primitive noble gas component devoid of He and Ne was presented by Wilkening and Marti (1976). They report that the Kenna ureilite contains high concentrations of heavy noble gases, including $^{136}Xe/^{132}Xe = 0.312$ and $^{124}Xe/^{132}Xe = 0.0047$, but they found no evidence of trapped He or Ne.

Arden, John W., 1977, Isotopic composition of uranium in chondritic meteorites: Nature, v. 269, p. 788-789.

Cameron, A. G. W., and Truran, J. W., 1977, The supernova trigger for formation of the solar system: Icarus, v. 30, p. 447-461.

Clayton, Donald D., 1976, Spectrum of carbonaceous-chondrite fission xenon: Geochimica Cosmochimica Acta, v. 40, p. 563-565.

Frick, U., and Moniot, R. K., 1976, Noble gases in carbonaceous residues from the Orgueil and Murray meteorites: Meteoritics, v. 11, p. 281-283.

Hennecke, E. W., and Manuel, O. K., 1977, Argon, krypton, and xenon in iron meteorites: Earth and Planetary Science Letters, v. 36, p. 29-43.

Lewis, R. S., Gros, J., and Anders, E. A., 1977, Isotopic anomalies of noble gases in meteorites and their origins, 2; Separated minerals from Allende: Journal of Geophysical Research, v. 82, p. 779-792.

Lewis, R. S., Srinvasan, B., and Anders, E., 1975, Host phase of a strange xenon component in Allende: Science, v. 190, p. 1251-1262.

Manuel, O. K., and Sabu, D. D., 1975, Elemental and isotopic inhomogeneities in noble gases--The case for local synthesis of the chemical elements: Transactions of the Missouri Academy of Science, v. 9, p. 104-122.

Manuel, O. K., and Sabu, D. D., 1977, Strange xenon, extinct superheavy elements, and the solar neutrino puzzle: Science, v. 195, p. 208-209.

Srinivasan, B., Gros, Jacques, and Anders, Edwards, 1977, Noble gases in separated meteoritic minerals; Murchison (C2), Orns (C3), Karoonda (C5), and Abee (E4): Journal of Geophysical Research, v. 82, p. 762-778.

Srinivasan, B., Lewis, R. S., and Anders, E., 1975, Origin of noble gases in Allende, 1; Host phases of fission xenon and other gases: Meteoritics, v. 10, p. 491-492.

Takahashi, H., Higuchi, H., Gros, Jacques, Morgan, John W., and Anders, Edward, 1976, Allende meteorite; Isotopically anomalous xenon is accompanied by normal osmium: Proceedings of the National Academy of Science, v. 73, p. 4253-4256.

Wilkening, L. L., and Marti, K., 1976, Rare gases and fossil particle tracks in the Kenna ureilite: Geochimica Cosmochimica Acta, v. 40, p. 1465-1473.

U-SERIES CHRONOLOGY OF TWO RHYOLITES OF LATE PLEISTOCENE AGE FROM LONG VALLEY, CALIFORNIA

By J. Baranowski[1] and R. S. Harmon[2]
Department of Geology, Michigan State University, East Lansing, Michigan
[1]Chevron Oil Company, New Orleans, Louisiana
[2]Isotope Geology Unit, Scottish Universities Research and Reactor Centre, East Kilbride, Scotland

The application of U-series techniques to volcanic rocks of late Pleistocene age is feasible because chemical fractionations occur during magmatic processes in such a way that a disequilibrium is commonly observed between uranium parents and their daughter nuclides (Somayajulu and others, 1966; Cherdynstev and others, 1967; Oversby and Gast, 1968; Condomines and others, 1976). Given an initial state of disequilibrium, decay products within the ^{238}U-series will exhibit a progressive change, with time, toward a state of secular equilibrium. Thus, the systematic growth of ^{230}Th ($t_{1/2}$ = 75,200 yr) into equilibrium with its parent ^{238}U can, through an analogy with the Rb-Sr method, be used to determine the crystallization age of a young volcanic rock. In such a case, the individual $(^{230}Th/^{232}Th)$-$(^{238}U/^{232}Th)$ activity ratios for the constituent phases will define an internal isochron whose slope varies as a function of time according to the relationship:

$$(^{230}Th/^{232}Th)_t = (^{230}Th/^{232}Th)_0 (e^{-\lambda_{230}t}) + (^{238}U/^{232}Th)(1 - e^{-\lambda_{230}t}) \quad (1)$$

In order for an accurate age to be obtained, the phases must have identical $(^{230}Th/^{232}Th)$ ratios at the time of formation, the phases must have formed at essentially the same time, and the system must have remained closed with respect to isotope migration. Provided this is the case, Eq.1 will define an isochron whose slope, given by the function $(1-e^{-\lambda 230^t})$, will change from zero to unity with increasing age (fig. 1). Phases that do not satisfy the conditions stated above will plot off the isochron. Additionally, important information about the geochemical and petrogenetic history of a volcanic complex can be obtained from U-series disequilibrium studies (Allegre and Condomines, 1976).

This paper presents the results of a preliminary investigation designed to determine the extent to which U-series techniques can be applied to a suite of volcanics of late Pleistocene age from Long Valley, California. The geology and K-Ar geochronology of the area have recently been described in detail by Bailey and others (1976). Briefly, the Long Valley Caldera (37°40'N, 118°50'W) is a 17 x 32 km elliptical depression that is located on the east side of the Sierra Nevada Mountains and formed some 700,000 years ago during the eruption of the Bishop Tuff. Volcanism continued within the caldera for the next 100,000 years, in the form of aphyric rhyolite domes, flows, and tuffs, in conjunction with resurgent doming. This was followed by eruption of three groups of porphyritic rhyolites from vent sites peripheral to the dome at approximately 500,000, 300,000, and 100,000 years B.P. Contemporaneous with the eruption of the last group of moat rhyolites was the eruption of porphyritic rhyolites from ring fractures on the caldera rim and basalts and trachy andesites along an intercaldera fracture zone from 200,000 to 50,000 years B.P. Finally, eruption of rhyolite and rhyodacite lava occurred within the caldera as recently as 450 years B.P.

The two samples analyzed, 76A003 and

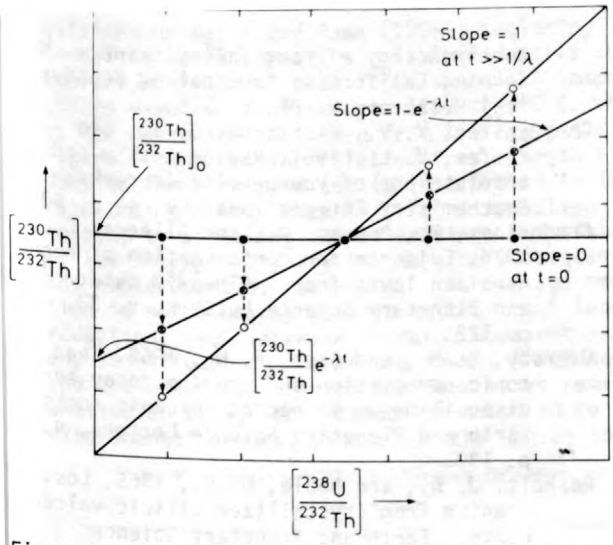

Figure 1.--U and Th isotopic behaviour in the system $(^{230}Th/^{232}Th)$-$(^{238}U/^{232}Th)$ for the separate phases of volcanic rocks evolving from a melt initially at isotopic equilibrium and with the phases having different U/Th ratios but the same $(^{230}Th/^{232}Th)$ ratios. The filled circles represent the system at t = 0, the crossed circles at some elapsed time t, and the open circles at secular equilibrium where $t >> 1/\lambda$. The slope of the line connecting the individual phases is determined by the function $(1-e^{-\lambda t})$ and defines the age of the system at any time t. Note that radioactive decay is represented by a vertical vector and chemical change within the U-Th system by a horizontal vector.

76A004, are white, vitrophyric, hornblende-biotite rhyolites of the youngest moat-rhyolite sequence. They were collected on a knoll north of Mammoth Lakes and correspond to samples 726009 and 726008 of Bailey and others (1976). After removal of any weathered surfaces, 5-10 kg of each sample were crushed and powdered to between 100-200 mesh. Standard heavy-liquid and magnetic techniques were then used to separate the constituent phases. Whole-rock and mineral splits of about 5 to 10 gm each were dissolved, spiked with a $^{228}Th/^{232}U$ tracer, and a combination of coprecipitation, ion-exchange, and solvent-extraction techniques were used to isolate pure uranium and thorium for thin-source alpha counting. ^{238}U, ^{234}U, ^{232}U, ^{232}Th, ^{230}Th and ^{228}Th, activities were measured for each sample immediately after preparation, using a silicon surface-barrier detector/low-noise amplifier system coupled to a multi-channel analyzer.

Both samples show similar U and Th abundances (6.8/18.1 and 5.8/14.2 ppm respectively). ^{234}U is close to or at equilibrium with ^{238}U in sanidine and quartz, slightly enriched in the glass, and very much enriched in the mafic phases. Internal $(^{230}Th/^{232}Th)$-$(^{238}U/^{232}Th)$ isochrons derived from the observed disequilibrium are presented in figure 2. The calculated ages of 87,000 ± 20,000 years B.P. for sample 76A003 and 127,000 ± 16,000 for sample 76A004 are in general agreement with the late Pleistocene K-Ar ages of 103,000 ± 3,000 years B.P. and 94,000 ± 10,000 years B.P. reported by Bailey and others (1976) for the same samples. The anomalous behaviour of the glass phase in both samples is of interest. Rosholt and Noble (1969) have observed U-leaching of altered glass within Tertiary silicic ash flows and lavas in the western United States. It is doubtful that such a process is responsible for the U-depletion observed in the rhyolites of Long Valley. In both samples the glass was vitric, showed no petrographic evidence of alteration, and had equivalent U abundances and $(^{234}U/^{238}U)$ ratios. A more likely cause is some process

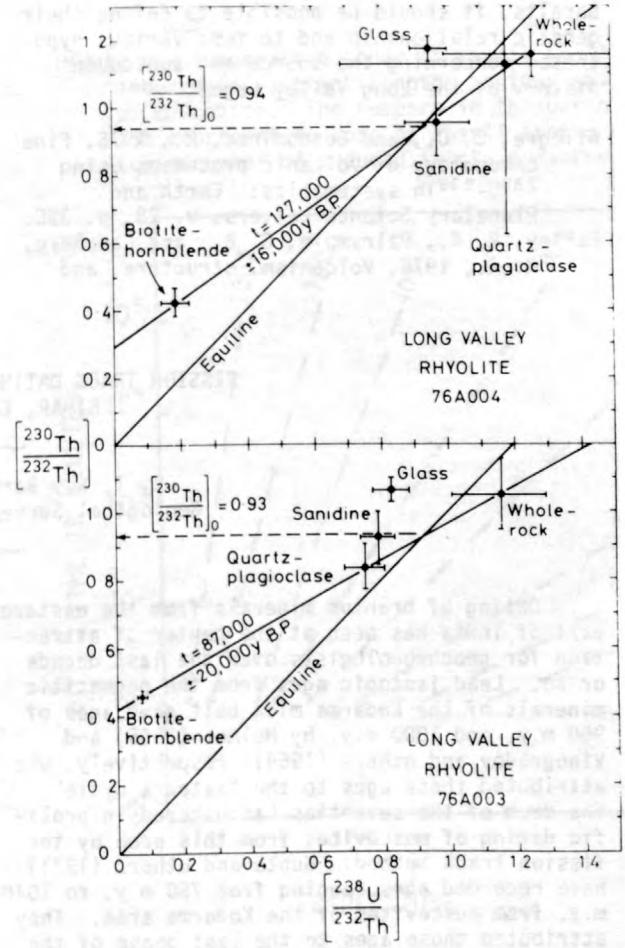

Figure 2.--Internal isochron plots for Long Valley moat-rhyolite samples 76A003 and 76A004. The slope and intercept of the isochrons were calculated by linear regression using a least-squares technique. In both cases the glass phase was not considered in construction of the isochron.

which would have depleted the U in the melt some time shortly after crustal formation but before eruption. For example, there might be a loss of U to a gas phase that was subsequently separated from the melt through fumarolic activity. In any case, such anomalous behaviour of the glass casts doubts on the use of glass-hornblende pairs as age estimators as suggested by Taddeucci and others (1968).

Finally, it should be noted that additional study of the volcanics of Long Valley by U-series techniques holds the promise of further understanding the geochemical history and petrogenesis of the younger moat rhyolites and inter-caldera basalts. That both rhyolites have equivalent initial ($^{230}Th/^{232}Th$) and Th/U ratios (.93 and 3.3, respectively) suggests a common origin and history. Through the use of such data for a suite of younger rhyolites and basalts, it should be possible to define their genetic relationship and to test various hypotheses concerning the source and subsequent history of the Long Valley magma.

Allegre, C. J., and Condomines, M., 1976, Fine chronology of volcanic processes using ^{238}U-^{230}Th systematics: Earth and Planetary Science Letters, v. 28, p. 395.

Bailey, R. A., Dalrymple, G. B., and Lanphere, M. A., 1976, Volcanism, structure, and geochronology of Long Valley Caldera, Mo County, California: Journal of Geophysical Research, v. 81, p. 725.

Cherdynstev, V. V., Kishtsina, G. I., and Zverev, V. L., 1967, Radioactivity and absolute age of young volcanic rocks: Geochemistry International, v. 4, p. 639

Condomines, M., Bernat, M., and Allegre, C. J 1976, Evidence for contamination of rece Hawaiian lavas from ^{230}Th-^{238}U data: Ea and Planetary Science Letters, v. 33, p. 122.

Oversby, V. M., and Gast, P. W., 1968, Lead i topic composition and uranium decay seri disequilibrium in recent volcanic rocks: Earth and Planetary Science Letters, v. p. 199.

Rosholt, J. N., and Noble, D. C., 1969, Loss uranium from crystallized silicic volca rocks: Earth and Planetary Science Letters, v. 6, p. 268-270.

Somayajula, B. L. K., Tatsumoto, M., Rosholt, J. N., and Knight, R. J., 1966, Disequilibrium of the ^{238}U series in basalt: Earth and Planetary Science Letters, v. p. 387.

Taddeucci, A., Broecker, W. S., and Thurber, D. L., 1968, ^{230}Th dating of volcanic rocks: Earth and Planetary Science Letters, v. 3, p. 338.

FISSION TRACK DATING OF MICA FROM KODARMA, BIHAR, EASTERN INDIA

By T. Roy Barman and K. Nandi
Geological Survey of India, Calcutta

Dating of uranium minerals from the eastern part of India has been at the center of attraction for geochronologists over the last decade or so. Lead isotopic ages from the pegmatitic minerals of the Kodarma mica belt gave ages of 950 m.y. and 1000 m.y. by Holmes (1955) and Vinogradov and others (1964), respectively, who attributed these ages to the "Satpura Cycle". The dawn of the seventies has ushered in prolific dating of muscovites from this area by the fission track method. Gupta and others (1971) have recorded ages ranging from 750 m.y. to 1040 m.y. from muscovites of the Kodarma area. They attributed those ages to the last phase of the "Satpura Cycle". Mehta and Nagpaul (1971) have recorded fission track ages from the Bandarchua and Sugi mines of the Kodarma area as 828 ± 107 m.y. and 869 ± 169 m.y., respectively. Gupta and others (1970), however, dated the biotites from the Kodarma area, which gave ages ranging from 760 m.y. to 890 m.y. According to those authors, the ages of biotite from pegmatite appear to mark the last phase of the "Satpura Cycle of Orogeny" (850 m.y., 1100 m.y., and m.y.) of this region.

Earlier workers considered fission trac dating of muscovite to be fairly accurate fo determining the thermal history of an area. study of micas from the Bihar mica belt, ea India, by the present authors have indicate anomalies in ages from layer to layer and, a such, the mica fission track ages are consi unreliable for any logical interpretation. are thought to be related to the introducti leaching of uranium (Miller, 1968; Miller a Jäger, 1968) and, also, to conditions of tr annealing in muscovite under water pressure a result of lowering of surface energy by n tralization of ionic charge and its replace by weak hydrogen bond in the muscovite laye water molecules coordinated with K-ions (La and Miller, 1970).

Muscovite samples from Bendro, Bandar and Sasi and coexisting biotite from the D Sugi mica mine of the Kodarma area, Bihar, studied according to the fission track met

outlined by Mehta and Rama (1969), including annealing characteristics. Table 1 details the age and analytic al data. The annealing temperatures used for biotite were 150° to 400°C, whereas for muscovite they were from 150° to 550°C. Figure 1 compares the relative track length reduction for each mine and is interpreted to indicate that the less than 15 percent reduction is related to annealing characteristics pertaining to low thermal activity in the area subsequent to the emplacement of pegmatites. As the age correction is not linearly related to the track length reduction, such decrease in range does not make any significant change in the fossil track density and the muscovite ages of the four mines remain unaffected by age corrections as compared to the experimental errors, except for the Debaur Sugi

Table 1.--Age and analytical data for muscovite samples

[$\phi = 1.82 \times 10^{17}$nvt]

ρ_s	ρ_i	ρ_s/ρ_i	Cu	Age (m.y.)
		Bendro mine, Kodarma		
5.373×10^{3}	3.835×10^{4}	0.1401	5.253×10^{-10}	1392±120
5.517×10^{3}	4.443×10^{4}	.1241	6.082×10^{-10}	1247±120
		Bandarchua mine, Kodarma		
3.663×10^{3}	3.645×10^{4}	.1004	4.993×10^{-10}	1026±140
4.973×10^{3}	4.308×10^{4}	.1154	5.901×10^{-10}	1159±120
		Sashi mine, Kodarma		
5.023×10^{3}	4.852×10^{4}	.1035	6.647×10^{-10}	1079±120
5.500×10^{3}	4.768×10^{4}	.1153	6.532×10^{-10}	1162±120
5.346×10^{3}	4.329×10^{4}	.1234	5.930×10^{-10}	1241±120
5.079×10^{3}	4.643×10^{4}	.1093	6.360×10^{-10}	1111±120
		Debaur Sugi, Kodarma		
2.957×10^{3}	1.248×10^{5}	.0236	1.709×10^{-9}	257±46
2.768×10^{3}	1.616×10^{5}	.0171	2.213×10^{-9}	187±49
2.989×10^{3}	1.415×10^{5}	.0211	1.938×10^{-9}	228±45
2.699×10^{3}	1.301×10^{5}	.0207	1.782×10^{-9}	225±50
		Biotite		
2.497×10^{3}	1.460×10^{5}	.0171	2.566×10^{-9}	187±20
2.442×10^{3}	1.324×10^{5}	.0184	2.327×10^{-9}	199±20
2.265×10^{3}	6.783×10^{4}	.0333	11.924×10^{-10}	347±24
2.471×10^{3}	7.783×10^{4}	.0317	13.682×10^{-10}	317±23
1.237×10^{3}	8.326×10^{4}	.0148	14.637×10^{-10}	1467±80
1.217×10^{3}	9.613×10^{4}	.0126	16.899×10^{-10}	1270±80

area. This shortening may be due either to existing water pressure or to rising temperature or to the combined effect of both. As the fission-track age of muscovite agrees well with the absolute age determined by other methods, the rock temperature must have remained to the right of 0 percent track-loss line of the Arrehnius plot shown on figure 2, except for the Debaur Sugi mine, which gave low fission track age.

The evolution of the pegmatites in the area have been described by Mahadevan and Maithani (1967). They have envisaged a three-phase hydrothermal activity related to (1) an early phase with siliceous solutions with varying amounts of K, (2) followed by an intermediate phase rich in Na and K, and (3) a soda-dominant final phase. This is indicative of the fact that

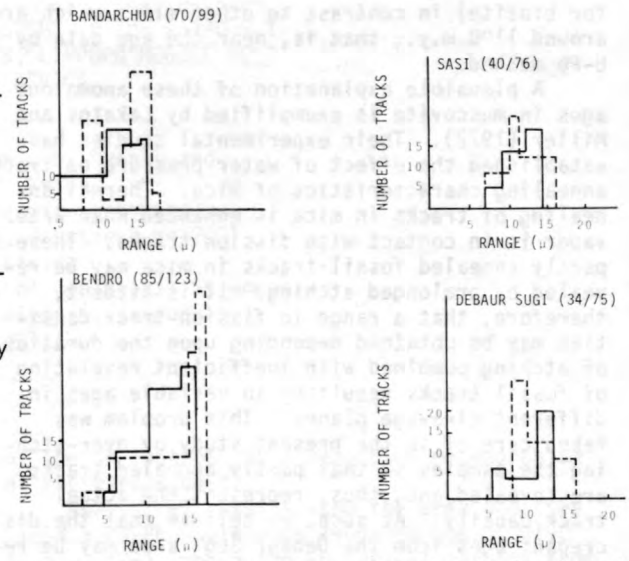

Figure 1.--Comparative study of fossil (——) and induced (---) track lengths in four samples of muscovite. The numbers in the parenthesis represent (number of fossil tracks measured/number of induced tracks measured).

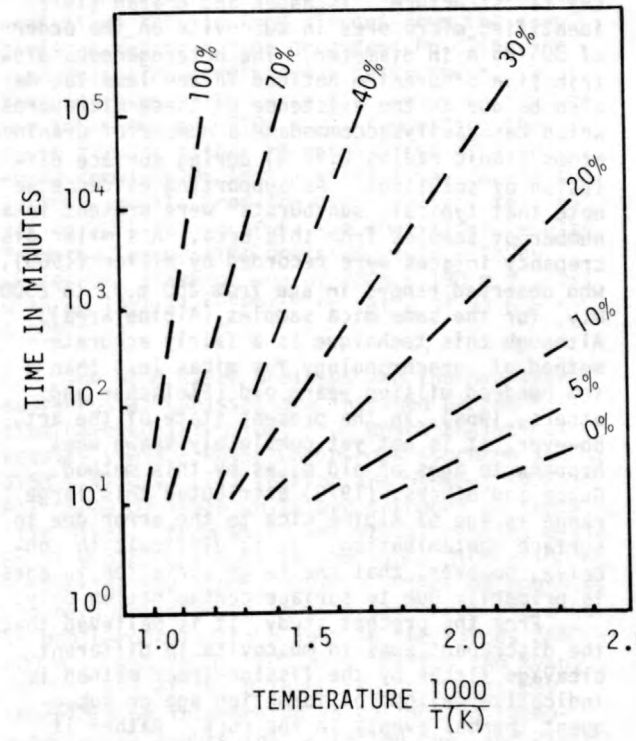

Figure 2.--Arrehnius plot of fission-track annealing in muscovite.

the system was not a closed one. This appears to be reflected in the fission-track age data for the Debaur Sugi mine at least. Muscovite from this locality shows unusually low age values (187-257 m.y. for muscovite) and (187-1467 m.y.

for biotite) in contrast to other mines which are around 1100 m.y.; that is, near the age data by U-Pb method.

A plausible explanation of these anomalous ages in muscovite is exemplified by Lakatos and Miller (1972). Their experimental studies have established the effect of water pressure on track annealing characteristics of mica. Thermal annealing of tracks in mica is enhanced when water vapor is in contact with fission tracks. These partly annealed fossil tracks in mica may be revealed by prolonged etching. It is evident, therefore, that a range in fission-track densities may be obtained depending upon the duration of etching combined with inefficient revelation of fossil tracks resulting in variable ages in different cleavage planes. This problem was taken care of in the present study by over-etching the samples so that partly annealed tracks are revealed and, thus, represent the actual track density. As such, we believe that the discrepant ages from the Debaur Sugi area may be related to the addition or loss of uranium along the cleavages subsequent to its fixation in the lattice by the complex hydrothermal activity as described by Mahadevan and Maithani (1967). In addition, the existing micropores in muscovite may facilitate penetration of water into the crystal structure. Tschapek and Grazan (1972) identified micropores in muscovite on the order of 305-95 Å in diameter. The heterogeneous distribution of uranium noticed in the lamellae may also be due to the existence of these micropores, which can easily accommodate a number of uranium atoms (ionic radius 0.94 Å) during surface diffusion of solutions. As supporting evidence we note that typical "sun bursts" were present in a number of samples from this area. A similar discrepancy in ages were recorded by Miller (1968), who observed ranges in age from 250 m.y. to 2500 m.y. for the same mica samples (Alpine area). Although this technique is a fairly accurate method of geochronology for micas less than a few hundred million years old (Fleischer and others, 1964), in the present state of the art, however, it is not yet completely known what happens to ages of old micas by this method. Gupta and others, (1970) attributed this large range in age of Alpine mica to the error due to surface contamination. It is difficult to conceive, however, that the large variation in ages is primarily due to surface contamination only.

From the present study, it is believed that the discrepant ages in muscovite in different cleavage flakes by the fission-track method is indicative neither of formation age or subsequent thermal events in the rock. Rather it appears to be evidence for subsequent activity of solutions responsible for redistribution of uranium in the muscovite. The discrepancy in ages may also apply to the biotites or possibly to the mica group as a whole.

The help and encouragement received from Dr. M. N. Balasubrahmanyan, Director, Geochronology and Isotope Geology Division, G.S.I., is gratefully acknowledged.

Fleischer, R. L., Price, P. B., Syemes, E. M., and Miller, D. S., 1964, Fission track ages and track annealing behaviour of some micas: Science, v. 143, p. 349-351.

Gupta, M. L., Mehta, P. P., and Nagpaul, K. K., 1970, Fission track ages of some Indian biotites: Indian Journal of Pure and Applied Physics, v. 9, p. 466-469.

Gupta, M. L., Nagpaul, K. K., and Mehta, P. P., 1971, Fission track ages of some Indian muscovites, Candaian Journal of Earth Sciences, v. 8, p. 1491-1495.

Holmes, A., 1955, Dating the Precambrian of peninsular India and Ceylon: Geological Association of Canada Proceedings, v. 7, no. 2, p. 81-106.

Lakatos, S., and Miller, D. S., 1970, Water pressure effect on fission track annealing in an Alpine muscovite: Earth and Planetary Science Letters, v. 9, p. 77-81.

Lakatos, S., and Miller, D. S., 1972, Problems of dating mica by F.T. method: Canadian Journal of Earth Sciences, v. 10, p. 403-407.

Mahadevan, T. M., and Maithani, J. B. P., 1967, Mem. G.S.I. v. 93, 113 p.

Mehta, P. P., and Nagpaul, K. K., 1971, Fission track ages of mica belts and some other pr cambrian muscovites of India: Pure and Applied Geophysics, v. 87, p. 174-191.

Mehta, P. P., and Rama, 1969, Annealing effects in muscovite and their influence on dating by fission track method: Earth and Planetary Science Letters, v. 7, p. 82-86.

Miller, D. S., 1968, Fission track ages on 250 and 2500 Ma micas: Earth and Planetary Science Letters, v. 4, p. 379-383.

Miller, D. S., and Jäger, E., 1968, Fission track ages of some alpine micas: Earth and Planetary Science Letters, v. 4, p. 375-378.

Tschapek, M., and Grazan, A. M., 1972, Microporosity of muscovite sheets: American Mineralogist, v. 57, p. 986-988.

Vinogradov, A., Tugarinov, A., Zhykov, C., and others, 1964, Geochronology of Indian Precambrian: Int. Geol. Cong. Rep. 22nd Session. pt X. P. 553-567.

THE RELATIONSHIP BETWEEN Rb-Sr AND U-Th-Pb WHOLE-ROCK AND ZIRCON SYSTEMS IN THE >3790 M.Y. OLD SAND RIVER GNEISSES, LIMPOPO MOBILE BELT SOUTHERN AFRICA

By J. M. Barton Jr., B. Ryan[1], and R. E. P. Fripp
University of The Witwatersrand
1 Jan Smuts Avenue, Johannesburg 2001
South Africa
[1]Present address: Dept. of Geological Sciences
Univ. of British Columbia, Vancouver
Canada V6T 1W5

The Sand River Gneisses form a basement to the metamorphosed supracrustal rocks exposed in the Central Zone of the Limpopo Mobile Belt near Messina, South Africa. In an approximately 100 km^2 area immediately southeast of Messina, these gneisses are composed of a grey-quartz-dioritic facies and a leucocratic granodioritic facies. Contact relationships between these facies have been obscured by polyphase folding and by associated deformations. However, the overall outcrop pattern indicates that the grey gneisses are probably xenoliths in the leucocratic gneisses. Analytical results from tholeiitic dikes intruding the Sand River Gneisses yield a Rb-Sr whole-rock isochron age of 3566 ± 100 m.y. (2σ; $\lambda\ ^{87}Rb = 1.42 \times 10^{-11}\ yr^{-1}$), establishing a minimum age for these gneisses (Barton and others, 1977).

Detailed Rb-Sr and U-Th-Pb isotopic studies of the Sand River Gneisses have been undertaken in an exposure of approximately 2 km^2 in area in the bed of the Sand River and its tributaries 7 km southeast of Messina. Here, over the period from ∿3800 m.y. ago until ∿1900 m.y. ago, the Sand River Gneisses have been subjected to at least six periods of penetrative deformation and have been intruded by at least five generations of felsic dikes and veins and by at least three generations of tholeiitic dikes. Nevertheless, apparently meaningful isotopic age patterns have been preserved in these gneisses.

Analytical results from the grey gneiss facies of the Sand River Gneisses yield a Rb-Sr whole-rock isochron age of 3727 ± 57 m.y. (2σ) with an initial $^{87}Sr/^{86}Sr$ ratio of 0.7015 ± 0.0008 (2σ), and analytical results from the leucocratic gneiss facies yield a Rb-Sr whole-rock isochron age of 3776 ± 97 m.y. (2σ) with an initial $^{87}Sr/^{86}Sr$ ratio of 0.7014 ± 0.0010 (2σ). These two isochrons are essentially identical and combining the data yields a Rb-Sr whole-rock isochron age of 3786 ± 61 m.y. (2σ) with an initial $^{87}Sr/^{86}Sr$ ratio of 0.70122 ± 0.00016 (2σ). Because the leucocratic gneisses are believed to be younger than the grey gneisses, this age is interpreted to be a minimum age for the Sand River Gneisses and to reflect a homogenization of the Sr isotopes as a result of metamorphism of these rock units.

Analytical results from the grey gneisses yield a Pb-Pb whole-rock isochron age of 3190^{29}_{34} m.y. (2σ), while the analytical results from the leucocratic gneisses do not yield an isochron but do not scatter about a line of a slope corresponding to an age of ∿2800 m.y. On U-Pb isochron diagrams these data scatter, but suggest that both the grey gneisses and the leucocratic gneisses have experienced recent U loss. Analytical results from zircons from the grey gneisses define a time dependent Pb-diffusion cord to the concordia curve (Wasserburg, 1963), that intersects the curve at a point corresponding to an age of ∿3100 m.y., suggesting that these zircons either recrystallized or experienced complete Pb loss at this time. While analytical results from the grey gneisses fail to define a Th-Pb isochron, the analytical results from the leucocratic gneisses yield a Th-Pb whole-rock isochron age of 2848 ± 190 m.y. (2σ) with an initial $^{208}Pb/^{204}Pb$ ratio of 34.635 ± 0.009 (2σ).

The Sand River Gneisses and the overlying supracrustal gneisses are intruded by the Messina Layered Intrusion, from which analytical results yield a Rb-Sr whole-rock isochron age of 3153 ± 47 m.y. (2σ) (Barton and others, 1978). All three of these units are intruded by tholeiitic dikes, from which analytical results yield Rb-Sr whole-rock ages in the range 3100 ± 100 m.y. (Barton and others, 1977). Other orthogneiss and paragneiss units in this same area yield Rb-Sr whole-rock isochron ages in the ranges 2800 ± 100 m.y. and 2550 ± 100 m.y. (Barton and Ryan, 1978). All of the U-Th-Pb isotopic ages may therefore be interpreted as reflecting igneo-metamorphic events that affected the Sand River Gneisses and the Limpopo Mobile Belt.

In the Sand River Gneisses, the Rb-Sr whole-rock systematics have been more resistant to changes than the U-Th-Pb whole-rock and zircon systematics have been. In addition, U-Th-Pb isotopes have behaved differently in the grey gneisses than they have in the leucocratic

gneisses. This same pattern occurs elsewhere within the Limpopo Mobile Belt, in the Singelele Gneiss. It is, however, in marked contrast to the pattern found in many other old polymetamorphic terrains such as in Labrador and West Greenland where the U-Th-Pb systematics are either more resistant to resetting than are the Rb-Sr systematics or equally so (Barton, 1978). The exact reasons for this differential behavior are unknown but no doubt they are involved with some fundamental differences in metamorphic conditions within the Limpopo Mobile Belt compared with those in most other polymetamorphic terrains. Furthermore, these results point out the fallacy in being too dogmatic concerning the relative merits of Rb-Sr whole-rock systems and U-Th-Pb whole-rock and zircon systems as age indicators.

Barton, J. M., Jr., (in press), Total-rock U-Th-Pb studies of the Hebron Gneiss, Labrador: Earth Planetary Science Letters.

Barton, J. M., Jr., Fripp, R. E. P., Horrocks, P., and McLean, N., (in press), The geology, age and tectonic setting of the Messin Layered Intrusion, Limpopo Mobile Belt, Southern Africa: American Journal of Science.

Barton, J. M., Jr., Fripp, R. E. P., and Ryan, B., 1977, Rb/Sr ages and geological settin of ancient dykes in the Sand River area, Limpopo Mobile Belt, South Africa: Nature v. 267, p. 487-490.

Barton, J. M., Jr., and Ryan, B., (in press) A review of the geochronologic framework of the Limpopo Mobile Belt: Geological Surve of Botswana Bulletin 9.

Wasserburg, G. J., 1963, Diffusion processes i lead-uranium systems: Journal of Geophysical Research, v. 68, p. 4823-4845.

Nd ISOTOPES IN MANTLE-DERIVED ROCKS AND MINERALS AND THE EVOLUTION OF THE EARTH'S MANTLE

By Asish R. Basu and Mitsunobu Tatsumoto
U.S. Geological Survey, Denver, Colorado 80225

Introduction: Garnet lherzolite inclusions in kimberlites from southern Africa can be grouped into two types, based on texture and bulk composition (Boyd, 1973; MacGregor and Basu, 1974). The first group is thought to have originated at depths of from 100 to 150 kms, based on the application of experimental phase equilibria studies to natural mineral assemblages of the lherzolites. The second group, called the sheared lherzolites, is believed to have originated at a depth of from 150 to 200 kms and shows varying degrees of deformation and recrystallization textures, in contrast to the first group, which shows coarse granular texture. A significant mineralogical difference between the two groups is the absence of phlogopite in the sheared rocks (that is, in the deeper seated rocks). Because the kimberlites enclose these two groups of xenoliths, along with various other types of inclusions, they must be derived from depths of at least 200 kms--the site of the deepest sheared lherzolite. Thus, kimberlites are the only rock type known to have come to the Earth's surface from such great depths in the mantle. It is generally believed by petrologists that kimberlites are produced by a small degree of partial melting of a mantle peridotite (olivine + orthopyroxene + clinopyroxene + garnet) containing CO_2 and H_2O and that they ascend explosively to the Earth's surface.

Samples: We have analyzed the Sm-Nd contents and the $^{143}Nd/^{144}Nd$ ratios of coexisting garnet, clinopyroxene, and phlogopite of a gra ular garnet lherzolite and of a garnet from a sheared xenolith, as well as the host kimberli from the Bultfontein pipe in South Africa. Th data also include five other kimberlites from North America, India, and South Africa that range in age from 90 to 1300 m.y.

The minerals of the xenoliths were hand-picked under a binocular microscope. Clear grains, free of inclusions and any surface con tamination, were chosen for analysis. The kim berlites were selected preferentially and contain few phenocrysts and xenocrysts; the fine-grained, blue-gray, carbonate-silicate matrix material of the kimberlites was picked for analysis. The Benfontein sample essentially represents the differentiated carbonatitic layer of the kimberlitic sill.

Age of eruption of the kimberlite pipes: precise knowledge of the time of emplacement o the kimberlite pipes analyzed is essential to this study. Zircons from the kimberlites of Kimberley area in South Africa are all nearly the same age (90 m.y.), as determined by the U-Pb method (Davis, 1977). The Premier pipe the only kimberlite from South Africa that sh an Rb-Sr age of from 1.2 to 1.4 b.y. (Barrett and Allsopp, 1973). We have chosen to assign average age of 1.3 b.y. for this pipe. The k berlite pipes in southern India, near Latta-varam, are reported to range in age from 840 956 m.y. (Paul and others, 1975) as determine by the K-Ar method. Harald Mehnert of the U.

Geological Survey, Denver, determined the K-Ar ages of the two samples that we analyzed to be 933 ± 37 m.y. and 962 ± 38 m.y. for L-1 and L-2, respectively. We chose an average age of 940 m.y. for these two pipes in southern India. The last sample, Nix-2, has not been dated; but the adjoining Schaffer pipe, near the Colorado-Wyoming stateline about 9 km north of the Nix-2 pipe, has been dated by the fission track method to be 377 m.y. ± 9 m.y. old (Naesar and McCallum, 1977). We have assigned an age of 370 m.y. to the Nix-2 pipe.

Results: The results of the present study are shown in figures 1 and 2. Figure 2 shows our high precision measurements of the Sm and Nd contents of the six kimberlites compared with the complete REE patterns of kimberlites from the Premier and Wesselton pipes taken from the literature. The REE pattern of the basaltic achondrite, Jivinas, is also shown in figure 1 for comparison.

Our data show that, in the garnet lherzolite, Sm and Nd contents are highest in the clinopyroxene, intermediate in the garnet, and lowest in the phlogopite. The initial

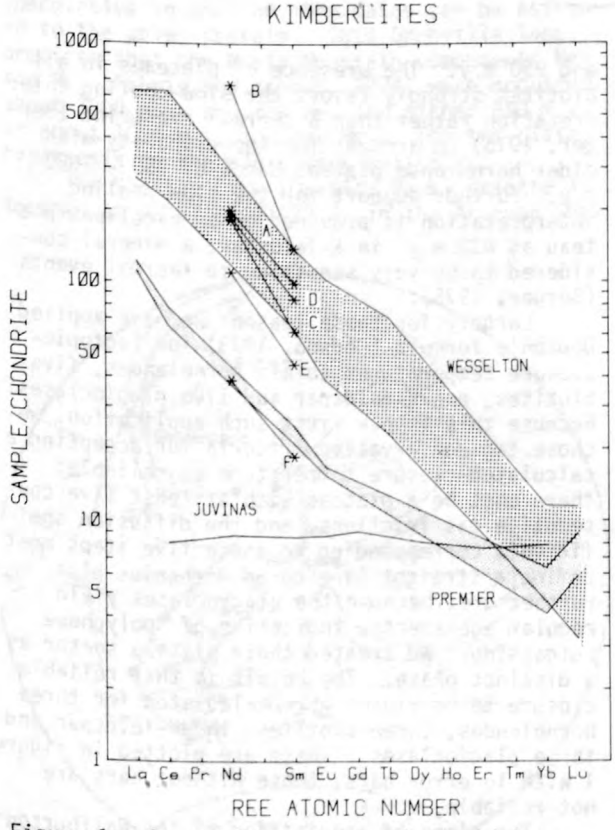

Figure 1.--Sm and Nd contents of six kimberlites: A, Bultfontein; B, Benfontein; C, Nix-2; D and E, southern India kimberlites; F, Premier. Shaded area REE patterns of several analyses (taken from the literature) of kimberlites from the Wesselton and the Premier pipes of South Africa.

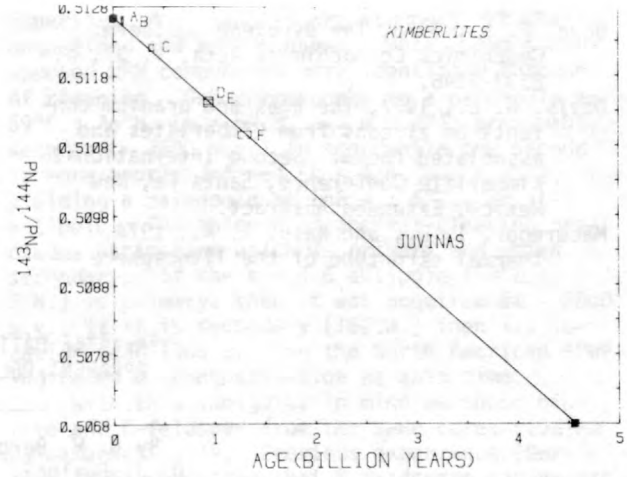

Figure 2.--Initial $^{143}Nd/^{144}Nd$ ratios of the six kimberlites compared with the $^{143}Nd/^{144}Nd$ growth curve of the basaltic achondrite, Juvinas. A, Bultfontein; B, Benfontein; C, Nix-2; D and E, southern India kimberlites; F, Premier.

$^{143}Nd/^{144}Nd$ ratios in the garnets and in the clinopyroxene are identical within the precision of the analyses, but differ from the same ratios in phlogopite and in the host kimberlite. The Nd-isotopic composition of the phlogopite is intermediate between that of the host kimberlite and of the pyroxene and garnets.

Figure 1 shows that the kimberlites have variable, light REE enriched patterns, but have low and constant Sm/Nd ratios. The carbonatitic kimberlite from the Benfontein pipe shows the highest light REE enrichment among the kimberlites.

Conclusion and discussion: The Nd-isotopic compositions of the xenolithic minerals and of their host kimberlite reflect local homogenites(?) of the subcontinental mantle beneath South Africa. The fact that both garnet and clinopyroxene are in isotopic equilibrium in the same xenolith lends credibility to the fundamental assumption in the estimation of temperature and pressure of equilibration of the xenoliths on the basis of major element partitioning. We regard the different Nd-isotopic composition of the phlogopite from the coexisting garnet and clinopyroxene of the xenolith as due to contamination from the host kimberlite.

The most singular conclusion that emerges from the data of the six kimberlites is that kimberlites are derived, in space and time, from relatively undifferentiated, primitive, and unique mantle reservoirs, having an identical chondritic signature in Sm/Nd and $^{143}Nd/^{144}Nd$ ratios.

Barrett, D. R., and Allsopp, H. L., 1973, Rubidium-strontium age determinations on South African kimberlite pipes: First International Kimberlite Conference,

University of Cape Town, Extended Abstract, p. 23-25.
Boyd, F. R., 1973, The pyroxene geotherm: Geochimica Cosmochimica Acta, v. 37, p. 2533-2546.
Davis, G. L., 1977, The ages and uranium contents of zircons from kimberlites and associated rocks: Second International Kimberlite Conference, Santa Fe, New Mexico, Extended Abstract.
MacGregor, I. D., and Basu, A. R., 1974, Thermal structure of the lithosphere - A petrologic model: Science, v. 185, p. 1007-1011.
Naeser, C. W., and McCallum, M. E., 1977, Fission track dating of kimberlitic zircons: Second International Kimberlite Conference, Santa Fe, New Mexico, Extended Abstract.
Paul, D. K., Rex, D. C., and Harris, P. G., 1975, Chemical characteristics and K-Ar ages of Indian kimberlites: Geological Society of America Bulletin, v. 86, p. 364-366.

$^{40}Ar/^{39}Ar$ DATING OF PRECAMBRIAN APPARENT-POLAR-WANDER PATHS

By G. W. Berger[1], D. York[1], D. J. Dunlop[1], and K. L. Buchan[2]
[1]Department of Physics
University of Toronto
Toronto, Canada
[2]Geological Survey of Canada
601 Booth Street
Ottawa, Canada

Most Precambrian rocks have been heated to a few hundred degrees over long periods of time since their crystallization, so that their original magnetization may have been totally or partially reset. Because of this polyphase magnetization, a rock unit may contain a magnetic record for several points in time over hundreds of millions of years. To establish apparent-polar-wander paths (APWP) for Precambrian time we must show that one or more components is of thermal origin (Buchan and others, 1977) before we can determine the absolute age of each component. For this latter purpose we have applied the $^{40}Ar/^{39}Ar$ dating technique to two areas--Haliburton in the Grenville of southern Ontario and Shelley Lake in the Superior of northwestern Ontario.

Paleopoles for Grenville rocks are displaced from those of the rest of the North American Precambrian. The proposed explanations have invoked either the "one-plate" or the "two-plate" tectonic hypothesis. The choice depends upon the absolute ages, previously undated, of the magnetization components. In this detailed dating study of the problem, we selected various minerals from the three Haliburton basic intrusives for which the paleomagnetics have been carefully documented (Buchan and Dunlop, 1976). The advantage of using these samples is that two TRM components occur in the same rock, and these manifest spot readings of the magnetic field at widely different times because their paleopoles diverge by about 60°.

Detailed incremental heating (15 steps) of five biotites yields excellent plateaus with significantly different ages between 900 m.y. and 950 m.y. The presence of plateaus in all biotites strongly favors the slow-cooling interpretation rather than a thermal overprint (Berger, 1975) to account for the disparity with older hornblende plateau dates of 950 - 1020 m.y. Further support for the slow-cooling interpretation is provided by an excellent plateau at 830 m.y. in K-feldspar, a mineral considered to be very sensitive to thermal events (Berger, 1975).

Largely for these reasons we have applied Dodson's formula (Dodson, 1973) for isotopic-closure temperatures to six hornblendes, five biotites, one K-feldspar and five plagioclases. Because this is our first such application, we chose two conservative criteria for accepting a calculated-closure temperature as reliable: there must be a plateau with at least five consecutive gas fractions, and the diffusion coefficients corresponding to these five steps must define a straight line on an Arrhenius plot. Furthermore, because the plagioclases yield irregular age spectra indicative of "polyphase outgassing," we treated their plateau sector as a distinct phase. The result is that reliable closure temperatures were calculated for three hornblendes, three biotites, the K-feldspar and three plagioclases. These are plotted in figure 1 with 1σ error bars; those without bars are not reliable.

The times of acquisition of the Haliburton TRM components are read from this "calibrated" cooling curve. Specifically, magnetizations Hb_1 and Hb_2, which probably represent temperatures near 580°C and near 200°C (Buchan and others, 1977), were acquired near 970 m.y. and 830 m.y.

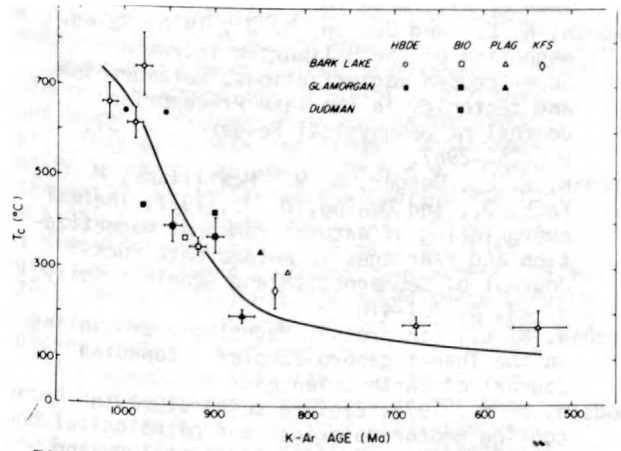

Figure 1.--A cooling curve for the Haliburton area using decay constants of Steiger and Jäger (1977). A cooling rate of 5°/m.y. was assumed for all but the two rightmost points for which 0.5°/m.y. was chosen.

respectively. The consequent APWP is shown in solid lines in figure 2. The dashed path is speculative in that no firm dates can be assigned to the poles therein. This Grenville loop predicts that the Mealy Mountain components Me_1 and Me_2 (Fahrig and others, 1974) were acquired about 1000 m.y. ago for Me_1 and either 850 m.y. or about 1050 m.y. ago for Me_2. The two-plate hypothesis is therefore very unlikely.

The Shelley Lake (Quetico Park) Granite is located at 48°27'N.; 91°22'W. in the Archean Shebandowan volcanic-plutonic belt, west of Lake Superior. Most samples are strongly but softly magnetized and most behaved stably. Two superimposed NRM components were identified through AF cleaning. One corresponds to a paleopole at 69°E.; 76°N. ($k = 69.8$, $\alpha_{95} = 5.2°$), presumably Kenoran (~ 2500 m.y.) in age, while the second is more poorly defined ($k = 4.6$, $\alpha_{95} = 25°$), yielding a paleopole at 162°W.; 5°S., or its antipole. The absence of thermal cleaning precludes estimating which is primary and which secondary. If the $k = 4.6$ antipole (18°E.; 5°N.) is primary, then it was acquired at ~ 2800 m.y.; if it is secondary (162°W.) then its location near 1300 m.y. on the North American APWP indicates a remagnetization at this time.

With this ambiguity in mind we chose biotite and K-feldspar from the same cores studied paleomagnetically. Previous experience (Berger, 1975) suggested that K-feldspars can permit the dating of secondary thermal events even though other minerals have not been affected. Figure 3 shows the age spectrum plots for three separate sites. The excellent plateau after the first step in the biotite implies that this rock cooled below the argon-closure temperature of 278 ± 35° (1σ, 5°/m.y.) at 2590 ± 15 m.y. (1σ). The remarkable agreement at 1050 - 1100 m.y. of the minima from the microclines suggests a thermal event at this time.

At this time we interpret figure 3 to indicate initial cooling of the Shelley Lake Granite below 280°C at 2600 m.y., followed by a secondary, weak thermal event at 1100 m.y. This event has apparently not reset the secondary magnetization completely because it lies near

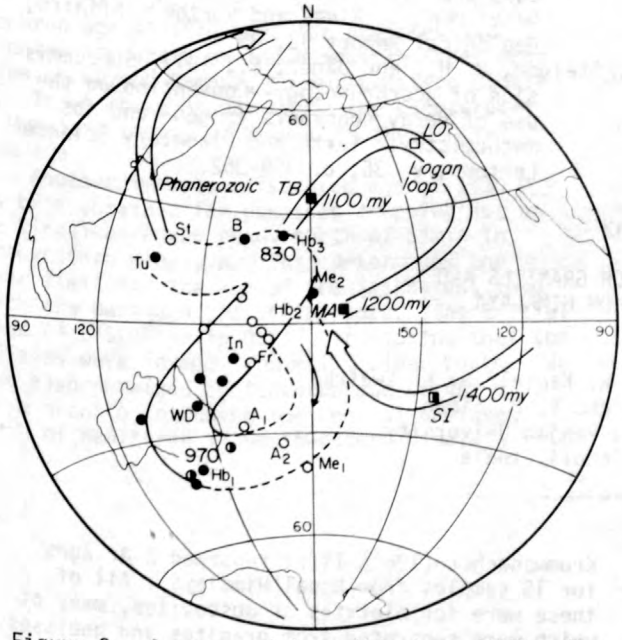

Figure 2.--A proposed Grenville Loop APWP. The calibrated paths (solid lines) correspond to an average drift rate of 4 cm yr^{-1}. The symbols are defined in Buchan (1978).

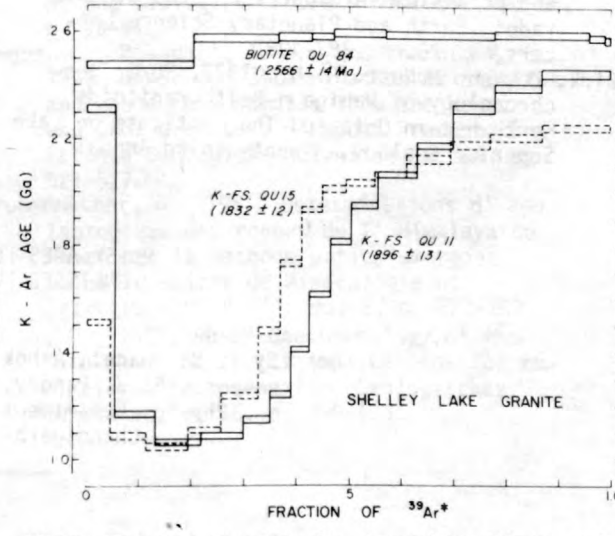

Figure 3.--Age spectra for two microclines and a biotite from a northwestern Ontario granite. Step intervals are 40 - 60° between ~600° and 1200°C. Bar heights are ±1σ. Dates in parentheses are integrated. Small (< 1 percent) fluence-gradient corrections have not yet been made.

1300 m.y. on the APWP. Support for this interpretation comes from independent conventional K-Ar dating of biotites from the nearby Poohbah Lake alkaline complex (Mitchell, 1976), where a thermal event after 2600 m.y. is suspected. Supporting the biotite plateau date are Rb-Sr whole-rock isochron dates of about 2620 ± 40 m.y. for various plutons within the Wabagoon Belt to the north (Birk and McNutt, 1977) and U-Pb zircon dates at 2660 ± 20 m.y. for emplacement of granites in the English River Gneiss Belt further north (Krogh and others, 1976). Unpublished paleomagnetic studies have isolated essentially the same secondary component from rocks of the Shebandowan, Quetico, and Wabigoon Belts. This indicates a widespread remagnetization event. Finally, it has been speculated (Shklanka, 1972) that the fault system in the Steep Rock Lake area just 25 km to the north may have been active with lamprophyre-dike emplacement about 1000 - 1200 m.y. ago. The partially mapped Shelley Lake Granite is itself within 10 km of the Olifaunt Lake fault.

In conclusion, we have assigned absolute dates to the Grenvillian paleopoles from Haliburton on the basis of a slow-cooling model and we have detected a thermal event at 1100 m.y. in the 2600 m.y. old Shelley Lake Granite. The $^{40}Ar/^{39}Ar$ technique thus reveals its power to date Precambrian paleopoles through its application to common minerals. In particular, we find that primary magnetite TRM will have been acquired just after the closing of hornblende to argon loss.

Berger, G. W., 1975, $^{40}Ar/^{39}Ar$ step heating of thermally overprinted biotite, hornblende and potassium feldspar from Eldora, Colorado: Earth and Planetary Science Letters, v. 26, p. 387-408.

Birk, D., and McNutt, R. H., 1977, Rb/Sr geochronology of Wabigoon Belt granitoids, northwestern Ontario, The Institute on Lake Superior Geology, Twenty-third Annual Meeting Proceedings: Lakehead University, Thunder Bay, Ontario.

Buchan, K. L., and Dunlop, D. J., 1976, Paleomagnetism of the Haliburton intrusions--Superimposed magnetizations, metamorphism, and tectonics in the late Precambrian: Journal of Geophysical Research, v. 81, p. 2951-2967.

Buchan, K. L., Berger, G. W., McWilliams, M. O., York, D., and Dunlop, D. J., 1977, Thermal overprinting of natural remanent magnetization and K/Ar ages in metamorphic rocks: Journal of Geomagnetism and Geoelectricity, v. 29, p. 401-410.

Buchan, K. L., (in press), Magnetic overprinting in the Thanet gabbro complex: Canadian Journal of Earth Sciences.

Dodson, M. H., 1973, Closure temperature in cooling geochronological and petrological systems: Contributions to Mineralogy and Petrology, v. 40, p. 259-274.

Fahrig, W. F., Christie, K. W., and Schwarz, E. J., 1974, Paleomagnetism of the Mealy Mountain anorthosite suite and of the Shabogamo gabbro, Labrador, Canada: Canadian Journal of Earth Sciences, v. 11, p. 18-29.

Krogh, T. E., Harris, N. B. W., and Davis, G. L., 1976, Archean rocks for the eastern Lac Seul region of the English River Gneiss Belt, northwestern Ontario, part 2, Geochronology: Canadian Journal of Earth Sciences, v. 13, p. 1212-1215.

Mitchell, R. H., 1976, Potassium-argon geochronology of the Poohbah Lake alkaline complex, northwestern Ontario: Canadian Journal of Earth Sciences, v. 13, p. 1456-1459.

Shklanka, R., 1972, Geology of the Steep Rock Lake area District of Rainy River: Ontario Department of Mines and Northern Affairs, Geological Report 93, 39 p.

Steiger, R. H., and Jäger, E., 1977, Subcommission of geochronology--Convention on the use of decay constants in geo- and cosmochemistry: Earth and Planetary Science Letters, v. 36, p. 359-362.

Rb-Sr AGES FOR GRANITES AND GNEISSES FROM HIMALAYA

By V. B. Bhanot, Ashok K. Kansal, S. K. Kwatra, B. K. Pandey, and V. P. Singh
Physics Department, Panjab University
Chandigarh-160014, India

Only a small amount of data has been reported so far for the isotopic and geochronological studies for the Himalayan Mountains. This paper presents a brief review of the earlier data and reports several new Rb-Sr ages for outcrops in northwestern and central Himalaya.

Krummenacher (1961) first reported K-Ar ages for 15 samples from Nepal Himalaya. All of these were for biotites or muscovites, many of which were separated from granites and gneisses. Except for one sample, all ages were less than 18 m.y. This led to an erroneous idea among

many geologists working in Himalaya that most of the granites, including those in the lesser Himalaya, were of Tertiary age.

Jäger and others (1971), published an Rb-Sr whole-rock isochron age of 500 m.y. for the Mandi Granite of lower Himalaya in the northwest. They also obtained, from a whole-rock biotite isochron, an age of 20.5 m.y. They interpreted the latter as the cooling age for the biotite, which was recrystallized during the Himalayan orogeny. More data for this region was published by Bhanot and others (1974, 1975). Mehta (1977) has supported these results with many precise determinations on granites and gneisses from the same region.

A Precambrian age (1263 m.y.), was reported by Bhanot and others (1976) for the Bandal granite exposed in the Larji-Rampur Window in northwestern Himalaya, on the basis of Rb-Sr whole-rock data. The quartzites into which this granite intrude had been considered to be of Devonian age and were correlated with the Muth quartzites. Bhanot and others (1977) have recently reported the oldest radiometric age found for a Himalayan rock. They determined an age of 1895 m.y. for a gneiss at Munsiari ($30^{\circ}3'$;$80^{\circ}12'$) in the Central Crystallines.

Rb-Sr isotopic data is obtained in our laboratory using a sector-type mass-spectrometer with a 90°-deflection analyzer of 27 cm radius, fitted with an ion source for solid samples. This was fabricated and provided to us at Chandigarh by the Bhabha Atomic Research Centre of Bombay. Conventional mass spectrometric and isotopic dilution techniques are employed. The decay constant for Rb is now taken as 1.42×10^{-11} yr^{-1}, with $^{87}Rb = 2.591$ and $^{88}Sr/^{86}Sr = 8.375$. New Rb-Sr data includes a whole-rock isochron age of 1840 m.y. for gneisses outcropping at Wangtu on the Hindustan-Tibet road, a few km beyond Rampur, in northwestern Himalaya. These rocks appear to be the counterpart of Munsiari Gneiss of Kumaon in the central Himalaya.

Another important isochron age of 1430 m.y. has been obtained for gneisses cropping out on the Kingal-Baragaon road, north of Simla in northwestern Himalaya. This determines the lower limit for the age of the Salkhalas, into which the Baragaon Gneiss intrudes. The initial value of $^{87}Sr/^{86}Sr$ is 0.745, indicating that the gneisses were formed from still older rocks. We have also obtained an isochron age of 467 m.y. for a granite intruding the Central Gneisses north of Manikaran in northwestern Himalaya ($32^{\circ}26'$;$77^{\circ}25'$). The cooling-age of the recrystallized biotite is found to be 8.8 m.y.

In the Kumaon region of central Himalaya, we have confirmed the age of the Munsiari Gneiss, which was based earlier on data for only two samples. We have obtained an Rb-Sr age of 1900 m.y. for the Askot crystallines ($29^{\circ}46'$; $80^{\circ}12'$), which had been considered by geologists as a nappe of the Central Crystallines. As well as confirming the occurrance of such very old gneisses in Himalaya, our data supports the hypothesis that Askot is a nappe of Central Crystallines rather than of some other autochthonous rock. We have obtained an isochron age of 1215 m.y. for the Ramgarh Porphyries in the lower Himalaya of Kumaon. We believe that the very old Central Crystallines formed the basement of a geosyncline in which the Tethyan sedimentation took place.

Bhanot, V. B., Bhandari, A. K., Singh, U. P., and Kansal, A. K., (in press), Proceedings of Conference on Himalayan Geology, Delhi, India.

Bhanot, V. B., Gill, J. S., Arora, R. P., and Bhalla, J. K., 1974, Radiometric dating of the Dalhousie Granite: Current Science, v. 43, p. 208.

Bhanot, V. B., Goel, A. K., Singh, V. P., and Kwatra, S. K., 1975, Rb-Sr radiometric studies for the Dalhousie and Rohtang Areas, Himachal Pradesh: Current Science, v. 44, p. 219-220.

Bhanot, V. B., Singh, V. P., Kansal, Ashok, K., and Thakur, V. C., 1977, Early Proterozoic Rb-Sr whole-rock age for central crystalline gneiss of higher Himalaya, Kumaun, Journal of the Geological Society of India, v. 18, p. 90-91.

Jäger, E., Bhandari, A. K., and Bhanot, V. B., 1971, Rb-Sr age determination of biotites and whole rock samples from the Mandi and Chor-Granites, Himachal Pradesh, India: Eclogae Geologicae Helvetiae, v. 64, p. 521-527.

Krummenacher, D., 1961, Determinations d' age isotopique des roches de I' Himalaya du Nepal par la methode potassiumargon: Bulletin Suisse de Mineralogie et Petrographie, v. 41, no. 2, p. 273-283.

Mehta, P., 1977, Rb-Sr Geochronology of the Kulu-Mandi Belt -its implications for the Himalayan tectogenesis: Geologisches Rundschau, v. 66, p. 156-175.

CORRELATION OF ISOTOPE CHEMISTRY WITH MOLECULAR STRUCTURE BY SECOND MOMENT PERTURBATION THEORY

By Jacob Bigeleisen[1], Myung W. Lee[1], and Takanobu Ishida[2]
[1]Department of Chemistry
University of Rochester
Rochester, New York 14627
[2]Department of Chemistry
Brooklyn College
Brooklyn, New York 11210

Chemical and phase equilibrium isotope fractionation factors are directly related to the respective isotopic reduced partition function ratios of the chemical species (Bigeleisen and Mayer, 1947) and of the phases (Bigeleisen, 1961) through which isotope fractionation takes place. The reduced partition function ratios of gaseous molecules are simple functions of the molecular vibrations and their shifts on isotopic substitution. In the case of fractionation involving condensed phases, one must consider the mean square force, the mean square torque, shifts in the internal vibrations in the condensed phase, as well as coupling between translation, rotation, and vibration (Bigeleisen, 1964; Yato and others, 1975). Extensive tabulations of reduced partition function ratios calculated from spectroscopic determination of molecular structure parameters now appear in the literature of isotope chemistry. For simple molecules, such as H_2, H_2O, CO_2, NH_3, and so forth, where there is sufficient structural data to evaluate the anharmonic terms (Wolfsberg, 1969; Hulston, 1969) and where one can calculate a priori the small corrections to the Born-Oppenheimer approximation (Wolfsberg and Kleinman, 1975), one finds quantitative agreement between measured isotope fractionation factors and those calculated theoretically from molecular structural parameters (Bron and others, 1973; Bardo and Wolfsberg, 1976). The latter have been greatly facilitated by the development of computer codes (Wolfsberg and Stern, 1964) which have been widely distributed.

Expansion of the isotopic reduced partition function ratio in terms of a number of arguments has led to greater insight into the relationship between isotopic fractionation factors and molecular structure than can be obtained even from a critical analysis of each of the terms that contribute to the isotopic reduced partition function ratio. The two most significant of these expansion methods are: (1) expansion of ln(s/s')f, logarithm of the isotopic reduced partition function ratio, in terms of the even moments of the vibrational frequencies (Ishida and others, 1969); and (2) expansion of either (s/s')f or ln(s/s')f around a reference molecule which has no off-diagonal elements in the G (kinetic energy) and F (force constant) matrices whose solution yield the molecular vibrations. In one case, the corrections from the reference molecule to the real molecule have been made through second order statistical mechanical perturbation theory (Singh and Wolfsberg, 1975), while in an independent development the method of moments has been used to evaluate the perturbation (Bigeleisen and others, 1978). The latter two methods yield results of comparable accuracy.

The method of moments has led to the formulation of the first order rules of isotope chemistry (Bigeleisen, 1975). They are: Bigeleisen

1. Isotope effects, ln(s/s')f, depend only on the masses of the isotopic atoms and the force constants bonding the atom at the site of isotopic substitution with other atoms in the molecule.

2. Isotope effects between different compounds occur only when there are force constant changes at the site of isotopic substitution.

3. Isotope effects are additive.

A. Isotopic additivity

$$\ln(s/s')f(D_2{}^{18}O/H_2{}^{16}O) = \ln(s/s')f(D_2{}^{16}O/H_2{}^{16}O) + \ln(s/s')f(H_2{}^{18}O/H_2{}^{16}O)$$

B. Substituent additivity

$$\ln(s/s')f(CHDFCl/CH_2FCl) = \ln(s/s')f(CH_2DF/CH_3F) + \ln(s/s')f(CH_2DCl/CH_3Cl) - \ln(s/s')f(CH_3D/CH_4)$$

4. Isotope effects are cumulative (first rule of the geometric mean).

$$\ln(s/s')f(CH_2D_2/CH_4) = 2\ln(s/s')f(CH_3D/CH_4)$$

5. Equivalent isomers have the same isotope chemistry.

$$\ln(s/s')f(C_6H_5D_2(o)/C_6H_6) = \ln(s/s')f(C_6H_4D_{2(m)}/C_6H_6) = \ln(s/s')f(C_6H_4D_2(p)/C_6H_6)$$

The first order rules of isotopic chemistry follow directly from the first order term in the moment expansion

$$\ln(s/s')f = \sum_i \sum_j (W_1/24)\,(\hbar/kT)^2 (g'_{ij} - g_{ij}) f_{ij} \qquad (1a)$$

$$\ln(s/s')f = \sum_i (W_1/24)\,(\hbar/kT)^2\,(\mu_i - \mu_i) f_{ij} \qquad (1b)$$

where g'_{ij} and g_{ij} are respectively the G matrix elements of the light and heavy isotopic molecules, f_{ij} is an F matrix element, and the optimum W values are the WINIMAX coefficients (Lee

and Bigeleisen, 1978). Typical results obtained by the WINIMAX methods are given in tables 1 and 2 for deuterium and heavy atom isotopic substitution, respectively.

Table 1.--Approximation of isotopic reduced partition function ratios (300° K) by WINIMAX polynomials

	Deuterium substitution		
Molecule	Exact	WINIMAX (1)	WINIMAX (2)
HDO/H_2O	2.5829	2.595	2.585
D_2O/H_2O	5.2025	5.189	5.178
CH_3D/CH_4	2.4561	2.321	2.401 (JM)[1]
CH_3D/CH_4	2.3117	2.170	2.262 (HS)[2]
$HDCO/H_2CO$	2.1997	2.021	2.144
C_2H_3D/C_2H_4	2.3177	2.125	2.218
C_2H_5D/C_2H_6	2.3645	2.159	2.281
RMS Deviation (in percent)		6.31	2.60

[1]Calculated with force constants of Jones and McDowell (1959).

[2]Calculated with force constants of Hartshorn and Shimer (1972).

The WIMPER perturbation method (Bigeleisen and others, 1978) permits one to develop $\ln(s/s')f$ in terms of a basis moelcule with a finite number of correction terms which can be exactly evaluated in terms of the isotopic moments.

$$\ln(s/s')f = \ln(s/s')f_o + \sum_j W_j A_j \sum_t [\delta(\underset{\sim}{H}^j)_{tt} - \delta(\underset{\sim}{H})^j_{tt}] \quad (2)$$

$\ln(s/s')f_o$ is the logarithm of the isotopic reduced partition function for the reference molecules which has eigenvalues defined by $\lambda_{io} = f_{ii}g_{ij}$. The diagonal matrix elements, f_{ii} and g_{ij}, are those of the real molecule. The reference molecule differs from the real molecule by replacement of all off-diagonal elements in the $\underset{\sim}{F}$ and $\underset{\sim}{G}$ matrices of the real molecule by zeros. It corresponds to a set of uncoupled oscillators.

The diagonal element approximation, $\ln(s/s')f_o$, gives very good results for hydrogen isotope substitution. The latter is a consequence of the fact that the off-diagonal G matrix elements involving the mass of hydrogen are either zero, or negligible, and the relatively light mass of hydrogen compared to other elements. Typical results are given in table 3.

Table 2.--Approximation of isotopic reduced partition function ratios (300° K) by WINIMAX polynomials

	Heavy Atom Effects			
Molecule	Exact	WINIMAX (1)	WINIMAX (2)	WINIMAX (3)
$H_2{}^{18}O/H_2{}^{16}O$	0.0643	0.0710	0.0600	0.0644
$^{13}CH_4/^{12}CH_4$	0.1113	0.1105	0.1029 (JM)[1]	0.1108
$^{13}CH_4/^{12}CH_4$	0.1148	0.1183	0.1071 (HS)[2]	0.1146
$H_2{}^{13}CO/H_2{}^{12}CO$	0.1369	0.1240	0.1324	0.1377
$H_2C^{18}O/H_2C^{16}O$	0.0904	0.0710	0.0880	0.0914
$^{13}CO_2/^{12}CO_2$	0.1728	0.1774	0.1620	0.1699
$C^{18}O/C^{16}O$	0.1090	0.0970	0.1042	0.1089
$^{13}CCH_4/^{12}C_2H_4$	0.1273	0.1090	0.1169	0.1255
$^{13}CCH_6/^{12}C_2H_6$	0.1283	0.1146	0.1162	0.1256
RMS Deviation (in percent)		11.1	6.5	1.1

[1]Calculated with force constants of Jones and McDowell (1959).

[2]Calculated with force constants of Hartshorn and Shimer (1972).

The off-diagonal element corrections to $\ln(s/s')f_o$ are of the order of 10 - 20 percent of the latter for carbon and oxygen isotope substitutions. These are easily evaluated by the WINIMAX polynomials. The correction terms, through second order $(\hbar/kT)^4$, added to $\ln(s/s')f_o$ provide an analytical formulation for the direct evaluation of $\ln(s/s')f$ for any molecule in terms of the F and G matrix elements. Through

Table 3.--Contributions of bending and stretching forces to $\ln(s/s')f$ for deuterium substitution at 25° C

[Numbers in parentheses indicate degrees of freedom]

	Stretch		Bend		Total	
Molecule	(Exact)	(GoFo)	(Exact)	(GoFo)	(Exact)	(GoFo)
HDO/H_2O	0.1129	0				
	2.1127	2.2200				
	2.2256	2.2200	0.3573	0.3611	2.5829	2.5812
D_2O/H_2O	2.2129	2.2200				
	2.2353	2.2200				
	4.4512	4.4400	0.7514	0.7577	5.2025	5.1978
CH_3D/CH_4	1.6978	1.7093				
	0.0239	0	0.2594(2)			
	0.0008(2)	0	0.1070(2)	0.2565(3)		
	1.7219	1.7093	0.7328	0.7695	2.4561	2.4780

this method it is now possible to analyze ln(s/s')f in terms of the stretching, bending, and interaction force constants in a molecule. Typical results for $^{13}C/^{12}C$ substitution in methane are given in table 4.

Table 4.--Contributions of stretching and bending forces to ln(s/s')f for carbon isotope substitution in methane at 300° K

[Numbers in parentheses indicate degrees of freedom]

Coordinate	ln(s/s')f Exact	ln(s/s')fo GoFo	$(h/kT)^2$ Correction	$(h/kT)^4$ Correction	ln(s/s')f WIMPER (2)
Stretch-------"0.0687(3)"		0.0788(4)		0.0035	0.0823
Bend----------"0.0426(3)"		0.0516(6)		-0.0013	0.0503
Stretch-stretch-----			-0.0032	0.0014	-0.0018
Stretch-bend--------			-0.0221	0.0062	-0.0159
Bend-bend--------			-0.0016	0.0002	-0.0014
Total---------	0.1113	0.1304	-0.0268	+0.0100	0.1135

Research supported in part by the Division of Basic Energy Sciences of the U. S. Department of Energy, Contracts EY76-S-02-3498 and -3127.

Bardo, R., and Wolfsberg, M., 1976, A theoretical calculation of the equilibrium constant for the isotopic exchange reaction between H_2O and HD: Journal of Physical Chemistry, v. 80, p. 1068.

Bigeleisen, J., 1961, Statistical mechanics of isotope effects on the thermodynamic properties of condensed systems: Journal of Chemical Physics, v. 34, p. 1485.

_____1964, Isotope effects in phase equilibria--a new tool for the study of intermolecular forces: Journal of Chemical Physics, v. 61, p. 87.

_____1975, Quantum mechanical foundations of isotope chemistry: American Chemical Society Symposium Series, v. 11, p. 1.

Bigeleisen, J., and Goeppert-Mayer, M., 1947, Calculation of equilibrium constants for isotopic exchange reactions: Journal of Chemical Physics, v. 15, p. 261.

Bigeleisen, J., Lee, M. W., Ishida, T., and Bigeleisen, P. E., (in press), Approximation of isotopic reduced partition function ratios by the WINIMAX polynomial perturbation method (WIMPER): Journal of Chemical Physics.

Bron, J., Chang, C. F., and Wolfsberg, M., 1973, Isotope partition function ratios involving hydrogen, water, hydrogen sulfide, hydrogen selenide, and ammonia: Zeitschrift Pur Naturforschung, v. A28, p. 129.

Hartshorn, S. R., and Shiner, V. J., Jr., 1972, Calculation of H/D, $^{12}C/^{13}C$, and $^{12}C/^{14}C$ fractionation factors from valence force fields derived for a series of simple organic molecules: Journal of the American Chemical Society, v. 94, p. 9002-9012.

Hulston, J. R., 1969, Revised zero-point energy calculation for $H_2O + D_2O \rightleftarrows 2HDO$ isotopic equilibrium: Journal of Chemical Physics, v. 50, p. 1483.

Ishida, T., Spindel, W., and Bigeleisen, J., 1969, Theoretical analysis of chemical isotope fractionation by orthogonal polynomial methods, in Advances in chemistry: American Chemical Society Monograph 89, p. 192-247.

Jones, Llewellyn, H., and McDowell, R. S., 1959, Force constants of methane; infrared spectra and thermodynamic functions of isotope methanes: Journal of Molecular Spectroscopy, v. 3, p. 632-653.

Lee, M. W., and Bigeleisen, J., (in press), Generalized finite polynomial approximation (WINIMAX) to the reduced partition function of isotopic molecules: Journal of Chemical Physics.

Singh, G., and Wolfsberg, M., 1975, The calculation of isotopic partition function ratios by a perturbation theory technique: Journal of Chemical Physics, v. 62, p. 4165.

Wolfsberg, M., 1969, Correction to the effect of anharmonicity on isotopic exchange equibria-application to polyatomic molecules: Journal of Chemical Physics, v. 50, p. 1484.

Wolfsberg, M., and Kleinman, L., 1975, Corrections to the Born-Oppenheimer approximation in the calculation of isotope effects on equilibrium constants: Isotopes and Chemical Principles, American Chemical Society Symposium Series, v. 11, p. 64.

Wolfsberg, M., and Stern, M. J., 1964, Validity of some approximation procedures used in the theoretical calculation of isotope effects: Pure and Applied Chemistry, v. 8, p. 225.

Yato, Y., Lee, M. W., and Bigeleisen, J., 1975, Phase equilibrium isotope effects in molecular solids and liquids--vapor pressures of the isotopic nitrous oxide molecules: Journal of Chemical Physics, v. 63, p. 1555.

GEOCHRONOLOGY OF THE TIN GRANITES OF SOUTHEAST ASIA

By J. D. Bignell[1], N. J. Snelling[2], and D. E. Teggin[3]
[1]Warren Spring Laboratory, Stevenage, Herts, United Kingdom
[2]Institute of Geological Sciences, London SW7, United Kingdom
[3]Instituto de Quimica, Universidad Central de Venezuela, Caracas, Venezuela

Rubidium-strontium and potassium-argon age dating of the granitic rocks of the Malay Peninsula shows that important episodes of granite intrusion occurred during Late Carboniferous (about 280 m.y.), Late Permian/Early Triassic (about 250 m.y.), and Late Triassic (230 m.y. to 200 m.y.) times. Granites of these ages constitute the Main Range batholith, the East Coast batholiths, and the Gunong Benom granite in central Malaya. Small granite plutons of Late Cretaceous age occur in Johore, Malacca and northern Kelantan.

The granites of the East Coast region were intruded in two episodes at 250 m.y. and 220 m.y. (Rb-Sr isochrons). K-Ar ages on micas are generally concordant with the appropriate Rb-Sr isochron age. In southern Malaya and Singapore, granite intrusion appears to be restricted to a 220 m.y. event. Mica K-Ar ages are generally concordant with the isochron age.

The Main Range batholith is composed of granites of Late Carboniferous (about 280 m.y.) and Late Triassic (about 230 m.y. and 200 m.y.) age. Potassium-argon ages on micas from the southern part of the batholith often show evidence of considerable argon loss. Evidence of the 280 m.y. intrusive event has been completely erased and most K-Ar apparent ages fall in the range 80 m.y. to 200 m.y. This argon loss appears to be related to major wrench faults which traverse this segment of the batholith and which caused extensive cataclasis.

A similar fault-related disturbance has affected the K-Ar mineral ages in the northern part of the batholith, and in adjacent stocks in Kedah and Langkawi Island.

Micas from the granitic rocks of Perak, including granites of the Main Range, Kledang Range and Bintang Range and those of southern Kedah and Penang, show less evidence of argon loss and are concentrated in the range 180 m.y. to 200 m.y. However K-Ar evidence of the 280 m.y. intrusive event, known to be represented in this area, has been completely erased, presumably by the thermal effects of the Late Triassic intrusions.

A Devonian intrusive event (about 360 m.y.) has been tenatively inferred from an isochron based on the analysis of widely dispersed samples from the Main Range batholith in Perak and Kedah.

Emplacement of the G Benom batholith in central Malaya occurred at 200 m.y. Mica K-Ar ages are generally concordant with the isochron age.

Samples of the Kamahang and similar foliated granites from northern Malaya give apparent Rb-Sr ages indicating intrusion in early Palaeozoic time. Micas from the Taku Schist and the Benta Migmatite give Late Triassic K-Ar ages, which we interpret as cooling or resetting ages and which throw no light on the age of their main metamorphism. Micas from the Stong Complex give Late Cretaceous K-Ar ages believed to reflect resetting by the postulated Upper Cretaceous granites of northern Kelantan.

The initial $^{87}Sr/^{86}Sr$ ratios of the Malayan granites range from 0.7074 to 0.7165. The Upper Carboniferous granites of the Main Range batholith give a weighted mean of 0.7111 ± 0.0008, which does not differ significantly from the weighted mean of the Upper Triassic granites from the same batholith of 0.7098 ± 0.0005. The Upper Permian to Lower Triassic granites of the East Coast Province also give a similar initial ratio--0.7102 ± 0.0004. These values are significantly higher than those of the East Coast Upper Triassic granites, and of the contemporaneous granites from Singapore and Johore, which, taken together, give a weighted mean of 0.7075 ± 0.0003, and of the G Benom granite which has an initial $^{87}Sr/^{86}Sr$ ratio of 0.7080 ± 0.0009. The Upper Cretaceous granites of southern Malaya give an initial $^{87}Sr/^{86}Sr$ ratio of 0.7079 ± 0.0005, while the postulated Devonian granite gives 0.7074 ± 0.0013.

Two small stocks on the western margin of the Main Range batholith give relatively high initial $^{87}Sr/^{86}Sr$ ratios; the Gunong Bujang Melaka granite, 0.7165 ± 0.0009, and the Kulim granite, 0.714 ± 0.002.

Consideration of various geochemical parameters all indicate that the Upper Triassic granites of the Main Range batholith are highly differentiated, the Upper Carboniferous granite less differentiated, and the Upper Triassic granites of the East Coast, the south Johore and

Singapore intrusives and the Upper Cretaceous granites of southern Malaya the least differentiated. It is suggested that the higher initial ratios (about 0.710) of the components of the Main Range batholith and of the granites of the East Coast Province intruded at about 250 m.y.--compared with those of the Triassic (about 220 m.y.) granites of the East Coast region (about 0.708)--reflect relatively prolonged differentiation within a crustal environment during which time contamination by more radiogenic strontium occurred. The granites with lower initial ratios (about 0.708) are less differentiated, reflecting relatively rapid emplacement.

The G Bujang Melaka and Kulim granites, which exhibit the highest initial $^{87}Sr/^{86}Sr$ ratios, are believed to reflect partial palingenesis of existing sialic basement, which on sedimentalogical grounds is inferred to exist immediately west of the batholith.

The petrographically similar granites of northern Thailand also give Late Triassic ages: Mae Sariang, 213 m.y.; Samoeng, 195 m.y.; Khuntan, 206 m.y.; Tak (white), 208 m.y.; and Tak (pink), 212 m.y. In contrast to the situation in Malaya, the K-Ar ages of micas and hornblendes from the Khuntan and Mae Sariang granites are reasonably concordant with the Rb-Sr ages. Micas from the Samoeng granite give K-Ar ages ranging from 43 m.y. to 71 m.y. These discordant ages relate in a regular way to a small body of younger lencogranite with associated tungsten mineralization.

The most striking feature of these granites is their high initial $^{87}Sr/^{86}Sr$ ratios as follows: Samoeng, 0.7337 ± 0.0008; Khuntan, 0.7248 ± 0.0009; Tak (white), 0.7162 ± 0.0007; and Tak (pink), 0.7110 ± 0.0007. It is difficult to avoid the conclusion that the Samoeng and Khuntan granites are the result of refusion of continental crust and that such palingenesis has played a major part in the evolution of the Tak granites, particularly the white variety.

Attention is drawn to the contrast between the Cordilleran batholiths of North and South America, characterized by metaluminous (hornblendic) rocks ranging from gabbro to granite but dominated by tonalites, and associated with copper-dominated base-metal sulphide mineralization on the one hand, and the stanniferous granites of south east Asia characterized by highly differentiated peraluminous rocks predominantly granitic in composition and associated with tin mineralization with subsidary amounts of niobium, tantalum, and tungsten on the other. The significance of this contrast in relation to the geochemical and isotopic data is discussed.

K-Ar MINERAL DATES, AND THE MAGNETIC REVERSAL WITHIN THE TATOOSH PLUTON, WASHINGTON, U.S.A.

By Michael Bikerman and Mary S. Robison[1]
Department of Earth and Planetary Sciences
University of Pittsburgh
Pittsburgh, Pennsylvania 15260
[1]Now at: Teledyne-Isotopes Inc.
Westwood, New Jersey 07675

Introduction: The Tatoosh pluton, which underlies the Mount Rainier volcano, is exposed in several places in Mount Rainer National Park, Washington (fig. 1). An excellent geological study of the park (Fiske and others, 1963) is available and is used as background here.

A magnetic reversal (R→N) was discovered in the Nisqually Valley, south of Mount Rainier, in the Tatoosh intrusion by Dunn and others (1971) and studied intensively for its paleomagnetic record by that group (Dodson and others, in press). The age of the intrusion has previously been determined by K-Ar on biotite by Folinsbee (Fiske and others, 1963) as 14.7 ± 1 m.y. on a sample from the Nisqually Valley, and 13. ± 1 m.y. on a sample from the White River Valley northeast of the volcano. Also, Mattinson (1977) reported U-Pb dates on zircons from the same two localities as 17.5 m.y. and 14.1 m.y., respectively. He considered the White River Valley dates to represent a younger phase of the Tatoosh, which had reset the K-Ar biotite date of the Nisqually Valley portion of the intrusion.

Data and results: Our study, to determine the K-Ar dates on coexisting hornblende and biotite separated from the same rock, was carried out on three large hand samples collected for paleomagnetic study. These samples from the Nisqually Valley (lat 45°50'N; long 121°45'W) were found to be reversed, intermediate, and

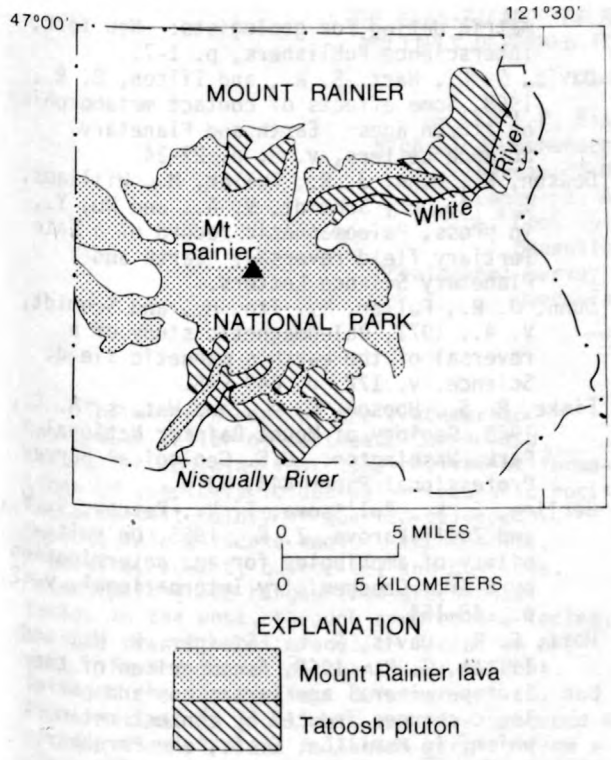

Figure 1.--Simplified geologic sketch map of Mount Rainier National Park showing location of major intrusions. Modified from Fiske, Hopson, and Waters (1963, fig. 31).

normal in paleopole orientation.

Analytical techniques used were conventional. Argon was done by isotope dilution (Zurich spike, metal-valved gas pipette modeled after Lanphere and Dalrymple, 1966) on an AEI MS-10 operated statically. The results are shown in table 1. With one exception, noted in the table, all samples were baked at 300 to 315°C. overnight prior to fusion. The constants used are $^{40}K = 1.2 \times 10^{-4}$ g/g K, $\lambda_{ec} = .585 \times 10^{-10}$ yr^{-1}, and $\lambda_{\beta} = 4.78 \times 10^{-10}$ yr^{-1} (Damon, 1968). Use of the newer constants (Steiger and Jäger, 1977) would raise the tabulated values by a bit more than 2 percent, and affect the correlation with the current paleomagnetic reversal time scale, which is based on the older constants, by the same amount.

The results show no correlation with the R→N movement of the cooling front. Since magnetic reversals are estimated to take 10^4 to 10^5 years, or less than our experimental error, this lack of correlation is no surprise. In the table we average all the determinations for hornblendes, treating them as variations of a single date, and do the same for the biotites. The resulting values, 18.0 m.y. and 16.2 m.y., respectively, are outside of statistical spread, and require explanation. Incidentally, we do not know why our biotite dates are different

Table 1.--K-Ar dates on hornblende and biotite separates from the Nisqually Valley exposure of the Tatoosh intrusion

Lab No.	Sample[1]	K[2] (percent)	^{40}Ar (x 10^{-10} moles/gm)	Atmos. Ar (percent)	Date (m.y.)
F-R		Reversed polarity			
	Hornblende	2.55	0.815	22.0	17.9
	Biotite	7.45	2.162	8.3	16.2
	Biotite (unbaked).	7.45	2.149	63.6	16.1
F-I		Intermediate polarity			
	Hornblende	1.15	.357	42.0	17.4
	Biotite	7.03	2.059	16.4	16.4
F-N		Normal polarity			
	Hornblende	0.99	.325	28.2	18.3
	Hornblende (duplicate run).	.99	.330	44.7	18.6
	Biotite	6.98	2.008	12.5	16.1

[1]All samples baked overnight in fusion system at ~ 300°C. except as marked.
[2]Heinz Dehn, analyst.
Average values: hornblendes--18.04±.53 (S.D.)
biotites (baked)--16.24±.16 (S.D.)
biotites (all)--16.2 ±.14 (S.D.)

from that of Folinsbee. To check on the possibility that the younger dates on the biotites were induced by argon loss during the bakeout step, we reran one unbaked, and aside from the expected increase in atmospheric argon (and, hence, uncertainty) found no difference.

Discussion: Possible reasons for the apparent age difference between the hornblendes and biotites in our determinations could be:

1. Slow cooling of the Tatoosh intrusion with some 2 m.y. elapsing between the closure temperature of the hornblende, estimated to be in the range 570° to 500°C. (Gerling and others, 1965; Hart and others, 1968; Damon, 1968; Dallmeyer and others, 1975) to that of biotite, normally considered (Jäger and others, 1967; Hart and others, 1968; Dallmeyer and others, 1975) to be 350° to 300°C., though sometimes put (Damon, 1968; Brewer, 1969) as low as 200°C. or less.

2. An initial emplacement at 18 m.y., followed by a later reheating and partial resetting of the biotite K-Ar clock.

The zircon dates of Mattinson bear on both of these models. If the zircons closed at about 500°C. (Davis and others, 1968; Hart and others, 1968), then the Nisqually Valley zircon at 17.5 m.y. corroborates the hornblende date. If the 14.1 m.y. zircon from the White River exposure reflects the tongue of a younger pluton underlying the Nisqually Valley region, then a partial degassing could have occurred.

Dodson and others (in press) have used a blocking temperature of 580° to 560°C. for their cooling rate models. Their analyses suggest that simple conductive models require too much time and would spread the reversal over much more than the few tens of meters involved in the mapped reversal. Using a two-stage model with rapid initial convective cooling by interaction with groundwater (Taylor, 1971), followed by a longer and slower conductive cooling, they got more suitable times.

We suggest that if the rapid initial stage lasted only to approximately 500°C., and the slow conductive down-and-inward migration of the isotherms was responsible for the rest of the cooling, then our data could be explained without the necessity for a reheating episode, for which no other evidence exists.

Timing of the reversal: Using the 580° to 560°C. blocking temperature range would place the age of this reversal at about 18 m.y., though a higher zircon closure temperature than given above could lower the date towards 17.5 m.y. Table 2 shows three models of the sea floor reversal time scale from the literature. Our dated reversal could correlate with either of the two in column 1, and, less closely, with 5C of column 2 or the lower 5D of column 3.

Table 2.--Some normal polarity intervals in the age range of the Tatoosh pluton, ages in m.y.

1	2		3	
17.33-17.80	17.27-17.47	5C	17.11-17.45	5D
17.83-18.02	18.12-18.49	5D	17.67-17.69	5D
			18.13-18.67	5E

1. From Heitzler and others (1968).
2. From Blakeley (1974).
3. From LaBrecque, Kent, and Cande (1977).

Blakeley, R. J., 1974, Geomagnetic reversals and crustal spreading rates during the Miocene: Journal of Geophysical Research, v. 77, p. 7065-7072.

Brewer, M. S., 1969, Excess radiogenic argon in metamorphic micas from the Eastern Alps, Austria: Earth and Planetary Science Letters, v. 6, p. 321-331.

Dallmeyer, R. D., Sutter, J. F., and Baker, D. J., 1975, Incremental $^{40}Ar/^{39}Ar$ ages of biotite and hornblende from the northeastern Reading Prong; their bearing on late Proterozoic thermal and tectonic history: Geological Society of America Bulletin, v. 86, p. 1435-1443.

Damon, P. E., 1968, Potassium-argon dating of igneous and metamorphic rocks, in Hamilton, E. I., and Farquhar, R. M., eds., Radiometric dating for geologists: New York, Interscience Publishers, p. 1-71.

Davis, G. L., Hart, S. R., and Tilton, G. R., 1968, Some effects of contact metamorphism on zircon ages: Earth and Planetary Science Letters, v. 5, p. 27-34.

Dodson, R., Dunn, J. R., Fuller, M., Williams, I., Ito, H., Schmidt, V. A., and Wu, Y., in press, Paleomagnetic record of a Late Tertiary field reversal: Earth and Planetary Science Letters.

Dunn, J. R., Fuller, M., Ito, H., and Schmidt, V. A., 1971, Paleomagnetic study of a reversal of the earth's magnetic field: Science, v. 172, p. 849-945.

Fiske, R. S., Hopson, C. A., and Waters, A. C., 1963, Geology of Mount Rainier National Park, Washington: U.S. Geological Survey Professional Paper 444, 93 p.

Gerling, E. K., Kol'tsova, T. V., Petrov, B. V., and Zul'fikarova, Z. K., 1965, On suitability of amphiboles for age determination by K-Ar: Geochemistry International, v. 2, p. 148-154.

Hart, S. R., Davis, G. L., Steiger, R. H., and Tilton, G. R., 1968, A comparison of the isotope mineral age variations and petrologic changes induced by contact metamorphism, in Hamilton, E. I., and Farquhar, R. M., eds., Radiometric dating for geologists: New York, Interscience Publishers, p. 73-110.

Heitzler, J. R., Dickson, G. O., Herron, E. M., Pittman, W. C., III, and LePichon, X., 1968, Marine magnetic anomalies, geomagnetic field reversals, and motions of the ocean floor and continents: Journal of Geophysical Research, v. 73, p. 2119-2136.

Jäger, E., Niggli, E., and Wenke, E., 1967, Rb-Sr Alterbestimmungen and Glimmern der Zentralalpen: Beitrage zur Geologischen Karte der Schweiz, N.F., 134, Liefg., Bern.

LaBrecque, J. L., Kent, D. V., and Cande, S. C., 1977, Revised magnetic polarity time scale for late Cretaceous and Cenozoic time: Geology, v. 5, p. 330-335.

Lanphere, M. A., and Dalrymple, G. B., 1966, Simplified bulb tracer system for argon analyses: Nature, v. 209, p. 902-903.

Mattinson, J. M., 1977, Emplacement history of the Tatoosh volcanic-plutonic complex, Washington: Age of zircons: Geological Society of America Bulletin, v. 88, p. 1509-1514.

Steiger, R. H., and Jäger, E., 1977, Convention on the use of decay constants in geo- and cosmochronology: Earth and Planetary Science Letters, v. 35, p. 359-362.

Taylor, W. P., 1971, Oxygen isotope evidence for large scale interaction between meteoric groundwaters and Tertiary granodiorite intrusions, Western Cascade Range, Oregon: Journal of Geophysical Research, v. 76, p. 7855-7874.

THE SIGNIFICANCE OF Rb-Sr TOTAL-ROCK AGES IN A MULTIPLY DEFORMED AND POLYMETAMORPHIC TERRAIN

By Lance P. Black[1], Tim H. Bell[2], Michael J. Rubenach[2], and Ian W. Withnall[3]
[1]Bureau of Mineral Resources, Canberra, A.C.T., Australia
[2]James Cook University, Townsville, Queensland, Australia
[3]Geological Survey of Queensland, Brisbane, Queensland, Australia

The western part of the Precambrian Georgetown Inlier of northeast Queensland, Australia, contains four time-equivalent formations of complexly folded polymetamorphic rocks. These consist mainly of quartzo-feldspathic gneiss, calc-silicate gneiss, amphibolite, migmatite, schist, quartzite, and phyllite. Metamorphic grade ranges from greenschist facies in the west, through amphibolite facies, to some transitional granulite facies in the west. Five deformation events are evident. Folds of the two earliest deformations (D_1 and D_2) are tight to isoclinal, and have produced a pervasive axial-plane foliation ranging from a slaty cleavage to a schistosity for D_1, and from a crenulation cleavage to a schistosity for D_2. The subsequent deformations (D_3, D_4, and D_5) were less intense and produced generally open folds with weak to nonexistent axial-plane foliations. D_1 and D_2 were accompanied by prograde metamorphism; D_3, D_4, and D_5 were associated with retrogressive metamorphism.

Suites of approximately 1 kg samples were selected from $1m^3$ of rock at localities where a particular deformation was dominant, and the effects of subsequent deformations were minimal. The resultant Rb-Sr total-rock isochrons produced ages for the most intense structural metamorphic events (D_1, D_2, and D_3). D_1 is defined by the isochrons of figures 1, 2, and 3; they yield a pooled mean age of 1570 ± 20 m.y. D_2 is best defined (figs. 4, 5, and 6) by a pooled mean age of 1470 ± 20 m.y. A mean age of 970 ± 30 m.y. is obtained for D_3 from the isochrons of figures 7 and 8.

The isotopic and structural data suggest that the development of tight or isoclinal folds does not necessarily produce resetting of total-rock Rb-Sr isotopic systems over these distances ($1m^3$). The critical structural requisite appears to be the development of a penetrative schistosity. As no penetrative schistosity has yet been found associated with D_4 and D_5 events, these events remain undated by this technique. A detailed account of this study is being published elsewhere (Black and others, in press).

L. P. Black and I. W. Withnall publish with the permission of the Director, Bureau of Mineral Resources and the Chief Government Geologist, Queensland, respectively.

Black, L. P., Bell, T. H., Rubenach, M. J., and Withnall, I. W., (in press), Geochronology of discrete structural-metamorphic events in a multiply deformed Precambrian terrain: Tectonophysics.

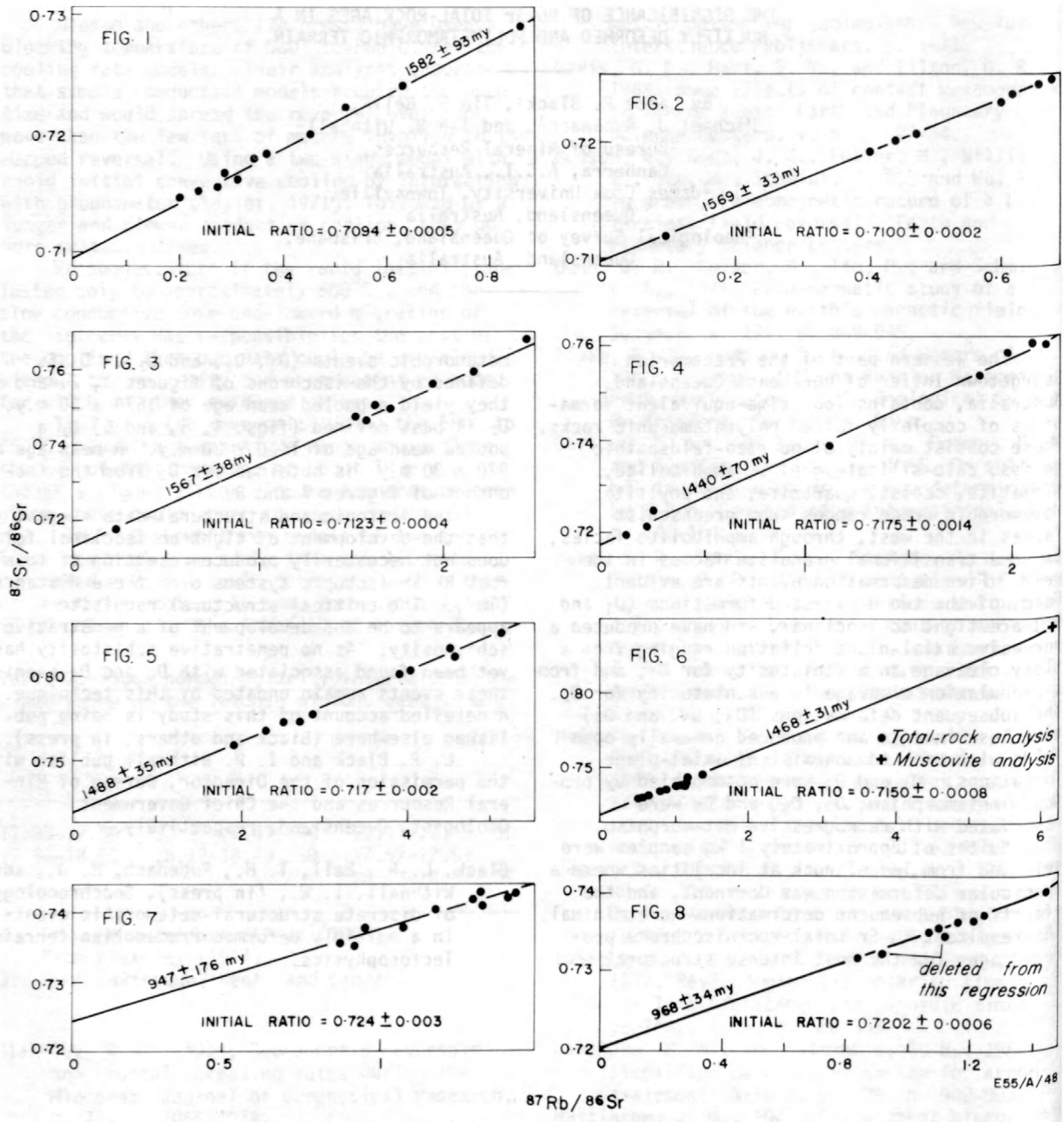

Figures 1-8.--Rb-Sr isochron diagrams for metamorphic rocks of the Georgetown Inlier. The age of the earliest structural-metamorphic event (D_1) is derived from the isochrons of figures 1, 2, and 3, D_2 from those of figures 4, 5, and 6, and D_3 from the isochrons of figures 7 and 8.

^{40}Ar-^{39}Ar DATING OF SHOCK EVENTS IN THE SHERGOTTY ACHONDRITE AND THE PLAINVIEW CHONDRITE

By D. D. Bogard[1] and Liaquat Husain[2]
[1]NASA Johnson Space Center
Houston, Texas 77058
[2]State Department of Health
Albany, New York 12201

Shergotty: The Shergotty achondrite is unusual in that its plagioclase (∿ 20 volume percent) has been entirely converted to maskelynite by strong shock metamorphism while at relatively low temperature (for example, Duke, 1968). Such obvious effects of intense shock, although common in chondrites, have rarely been reported in achondrites. Shergotty has been classified by some as a eucrite, but differs from typical eucrites in its higher abundances of alkali elements, augite and magnetite and the fact that it is not brecciated (Duke, 1968). Because many achondrites are believed to result from magma differentiation on asteroidal bodies which are different from the parent bodies of shocked chondrites, it is informative to compare shock histories of the two meteorite groups. We have made ^{40}Ar-^{39}Ar analyses of Shergotty to investigate the chronology of the shock event. L. Nyquist and coworkers (1978) at the Johnson Space Center have also investigated the ^{87}Rb-^{87}Sr and ^{147}Sm-^{143}Nd chronologies of Shergotty. All these data present a unique opportunity to compare the effects of strong shock, using the results of these three major dating techniques.

We analyzed a 0.32-g whole-rock sample and a 0.060-g plagioclase sample which had been magnetically separated from a 74-149 μm size fraction of the whole rock and which was estimated to be > 99 percent feldspar. The apparent $^{40}Ar/^{39}Ar$ ages and K/Ca ratios for stepwise Ar releases are shown in figure 1 as a function of the cumulative fraction of ^{39}Ar. All gas fractions gave ages less than 0.7 b.y., indicating that Shergotty was extensively degassed by a recent event. The plagioclase shows a good plateau age of 0.25 ± .01 b.y. for from 15 percent to 83 percent of the total ^{39}Ar released. There is no good evidence in the plagioclase release of an age appreciably older or younger than 0.25 b.y. The Ar isotopic ratios for the gas release of 83 - 93 percent ^{39}Ar suggest that the slightly higher age for this release was caused by atmospheric Ar. This gas fraction was taken after the sample had lain unheated in the extraction furnace for two days, and a higher-than-normal blank might be expected. The Ar isotopic ratios also suggest that the 6 - 15 percent ^{39}Ar fraction contained atmospheric Ar adsorbed on the sample.

The Shergotty whole-rock sample shows a complex release with apparent $^{40}Ar/^{39}Ar$ ages varying between 0.24 b.y. and 0.64 b.y. We interpret this complex release as due to variable mixtures between Ar released from plagioclase with an apparent age of 0.25 b.y. and Ar released from pyroxene and other phases with considerably older apparent ages. Evidence that K in our whole-rock sample residues in several phases comes from the observation that the K/Ca ratio for the plagioclase changes only from ∿ 0.06 to ∿ 0.02, whereas the K/Ca for the whole rock changes by the much larger factor of ∿ 0.6 to ∿ 0.01. Alternatively, the variation in K/Ca in the uncrushed whole-rock sample may reflect zoning of some maskelynite grains with higher orthoclase contents on the rims than in the interior (McSween and Stolper, 1978). We have concluded from heavily-shocked chondrites (Bogard and others, 1976) that the feldspar had lost radiogenic Ar more readily than the pyroxene. The feldspar in the Shergotty achondrite has also been more affected by the shock event than has the pyroxene (Duke, 1968), which is consistent with the known susceptibilities of these minerals to shock (Stöffler, 1972).

One straightforward interpretation of the data is that the $^{40}Ar/^{39}Ar$ age plateau for Shergotty plagioclase defines the time of the shock event at 0.25 b.y. ago, and that ages of nonplagioclase phases were not totally reset. However, $^{87}Rb/^{87}Sr$ and $^{147}Sm/^{143}Nd$ data (Nyquist and others, 1978) indicate ages somewhat different from 0.25 b.y. $^{87}Rb/^{87}Sr$ data from plagioclase, pyroxene, and whole rock from two samples of the Shergotty showed some scatter about an isochron but appear most consistent with an age of 0.167 ± .014 b.y. On a scale of 0-4.5 b.y. the $^{40}Ar/^{39}Ar$ and $^{87}Rb/^{87}Sr$ ages are similar, but they do differ outside their respective uncertainties. $^{147}Sm/^{143}Nd$-data on two pyroxenes and a whole-rock sample gave an age of ∿ 1.1 b.y., which may reflect incomplete resetting by the shock event or an actual igneous crystallization age (Nyquist and others, 1978). One possible interpretation of the differences in K-Ar and Rb-Sr ages is that the time of the shock event was ∿ 0.17 b.y. ago and that radiogenic ^{40}Ar was not completely degassed. By this explanation ∿ 6.5 percent of the total ^{40}Ar present in the plagioclase would have been retained after the shock event if the solidification age of the sample were the same as the Nd-Sm age (∿ 1.1 b.y.), and only ∿ 0.5

percent of the total ^{40}Ar present in the plagioclase would have been retained if the solidification age were ∿ 4.5 b.y. We do not interpret the $^{40}Ar/^{39}Ar$ of the plagioclase as representing an igneous crystallization age for the Shergotty sample because of the presence of obvious shock features, the older $^{40}Ar/^{39}Ar$ age for the whole-rock sample, and the considerably older $^{147}Sm/^{143}Nd$ age.

The inferred shock age for the Shergotty achondrite of 0.16 to 0.25 b.y. is considerably older than the cosmic ray exposure age of ∿ 2 m.y. (Heymann and others, 1968), but it is similar to shock degassing ages of ∿ 0.04-0.7 b.y., which have been inferred for several

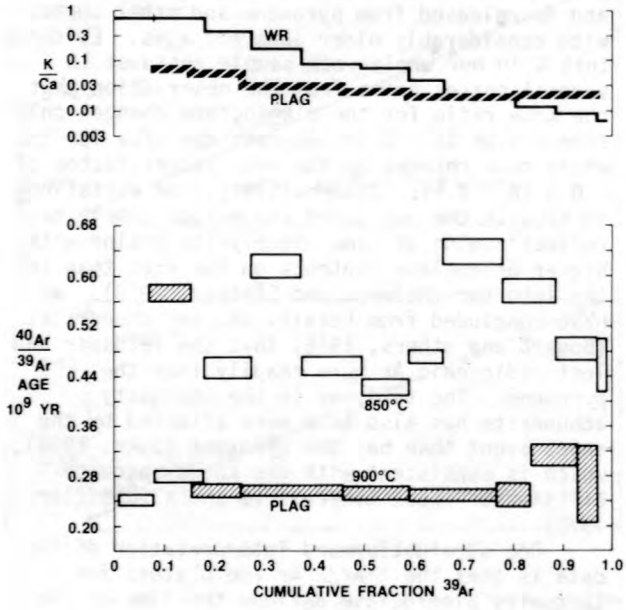

Figure 1.--Apparent $^{40}Ar/^{39}Ar$ ages and K/Ca ratios for Shergotty achondrite (open symbol, whole-rock; crosshatched symbol, plagioclase).

chondrites (Turner, 1969; Bogard and others, 1976). The most likely explanation for shock ages in the Shergotty and in shocked chondrites is that they represent the times of major disruptions of the main-belt asteroidal parent bodies (for example, Bogard and others, 1976). Relatively large fragments probably were ejected and perturbed by gravitational interactions into Earth-crossing orbits. Cosmic-ray exposure was initiated by more recent and less severe collisions, which reduced these meteorites to sizes of $\lesssim$ 1 meter. A course of such events possibly gains support from the observation that some iron meteorites have received multi-stage irradiation by cosmic rays in the time period of ∿ 0.01-1 b.y. ago (for example, Wanke, 1967).

Plainview: ^{40}Ar-^{39}Ar analyses have been performed on two clasts and the host material of the Plainview H-5 chondrite. These analyses are part of a cooperative study of the Plainview by several laboratories and include petrology, chemical composition, and chronology (Keil and others, 1978). The Plainview is a brecciated chondrite, which contains solar wind-implanted gases and clasts of carbonaceous and noncarbonaceous material (Wilkening and Clayton, 1974; Fodor and Keil, 1976). The light-colored lithic clasts may represent shock-melted chondritic material, which were formed near the surface of the Plainview parent object (Fodor and Keil, 1976; Keil and others, 1978). Those portions of the meteorite that contain solar and carbonaceous gases could not have been heated appreciably, or else these gases would have been driven off. Thus, formation of the clasts must have occurred prior to the assembly of the Plainview meteorite. Dating of the clasts would give the maximum age of the meteorite breccia.

The ^{40}Ar-^{39}Ar data for one light chondritic clast from the Plainview define a nearly constant age of 3.57 to 3.67 b.y. for from 21 percent to 87 percent of the ^{39}Ar released. We interpret the plateau age of 3.63 ± .06 b.y. to be the last time of major degassing of this clast. Argon data for a second, similar clast showed evidence of appreciable diffusive loss of ^{40}Ar and did not yield a plateau. Its highest apparent ^{40}Ar-^{39}Ar age was 3.3 b.y. This second clast could have an ^{40}Ar-^{39}Ar age older than 3.3 b.y. and could have experienced major degassing contemporaneously with the first clast. The host chondrite showed a complex release with apparent ^{40}Ar-^{39}Ar ages varying between 3.8 and 4.4 b.y. The bulk of the chondrite is considerably older than the clasts and probably contains material as old as 4.4 b.y.

We conclude that the Plainview brecciated chondrite was assembled near the surface of its parent object, probably by a major impact, at a time more recent than 3.63 b.y. ago. Such an age is similar to ages of 3.48 - 3.89 b.y. obtained on various clasts from the Kapoeta howardite (Huneke and others, 1977), but is considerably older than the conventional K-Ar age of 1.36 b.y. reported for a clast in the St. Mesmin LL-chondrite (Schultz and Signer, 1977). Thus, evidence exists that meteorite breccia formation has occurred over an extensive time period on several parent objects.

Bogard, D. D., Husain, L., and Wright, R. J., 1976, ^{40}Ar-^{39}Ar dating of collisional events in chondrite parent bodies: Journal of Geophysical Research, v. 81, p. 5664-5678.

Duke, M. B., 1968, The Shergotty meteorite; Magmatic and shock metamorphic features, in Shock Metamorphism of Natural Materials: Baltimore, Mono Book Corp., p. 613-621.

Fodor, R. V., and Keil, K., 1976, Carbonaceous and noncarbonaceous lithic fragments in the Plainview, Texas, chondrite: Origin and history: Geochimica Cosmochimica Acta, v. 40, p. 177-190.

Heyman, D., Mazor, E., and Anders, E., 1968, Ages of calcium-rich achondrites--I. Eucrites: Geochimica Cosmochimica Acta, v. 32, p. 1241-1268.
Huneke, J. C., Smith, S. P., Rajan, R. S., Papanastassiou, D. A., and Wasserburg, G. J., 1977, Comparison of the chronology of the Kapoeta parent planet and the Moon: Lunar Science VIII (abstracts), The Lunar Science Institute, p. 484-486.
Keil, K., Fodor, R. V., Schmitt, R. A., Bogard, D. D., and Husain, L., 1978, (in preparation.
McSween, H. Y., and Stolper, E., 1978, Shergottite meteorites, I; Mineralogy and petrography [abs.] : Lunar and Planetary Science IX, Lunar and Planetary Institute, Houston, p. 732-734.
Nyquist, L. E., Shih, C. Y., Bansal, B. M., Wooden, J., Wiesmann, H., and McKay, G., 1978, Rb-Sr and Sm-Nd chronology of the Shergotty achondrite: (this conference).
Schultz, L., and Signer, P., 1977, Noble gases in the St. Mesmin chondrite; Implications to the irradiation history of a brecciated meteorite: Earth and Planetary Science Letters, v. 36, p. 363-371.
Stöffler, D., 1972, Deformation and transformation of rock-forming minerals by natural and experimental shock processes, 1; Behavior of minerals under shock compression: Fortschrittle der Mineralogie, v. 49, p. 50-113.
Turner, G., 1969, Thermal histories of meteorites by the ^{40}Ar-^{39}Ar method; in Meteorite Research: Dordrecht, Netherlands, D. Reidel, Publishing Co., p. 407.
Wanke, H., 1967, Meteoritenalter und verwandte probleme der kosmochemie: Fortschritte der Chemischen Forschung 7, p. 322-408.
Wilkening, L. L., and Clayton, R. N., 1974, Foreign inclusions in stony meteorites - II. Rare gases and oxygen isotopes in a carbonaceous xenolith in the Plainview gas-rich chondrite: Geochimica Cosmochimica Acta, v. 38, p. 937-945.

FIRST ISOTOPIC DATING OF UPPER PRECAMBRIAN SEDIMENTS IN THE PROVINCE OF BUENOS AIRES, ARGENTINA

By Michel G. Bonhomme[1]
and Carlos A. Cingolani[2]
[1]Institut de Géologie, Université Louis Pasteur
Centre de Sédimentologie et
Géochimie de la Surface, Strasbourg, France
[2]Facultad de Ciencias Naturales y Museo
Universidad Nacional de la Plata
La Plata, Rép. Argentina

The "La Tinta" series lies 300 km south of Buenos Aires. Its age is not well defined and it has been proposed to be either Paleozoic or upper Precambrian. It rests on a basement in which mineral ages have been determined to be between one and two billion years. The series is cut by basic intrusives dated by one of us (C.C.) as Ordovician.

SEDIMENTOLOGY

An attempt has been made to carry out direct isotopic dating on the clay fractions, which are found at various levels in the "La Tinta" series. To select suitable samples for isotopic work, a general clay mineralogical study was made. Three different clay assemblages can be distinguished:

1. In Olavarria the sediments contain mainly illite with some mixed-layer clay and chlorite. The illite crystallinity index is typical for sediments free of inherited fine-grained micas or subsequent slight metamorphism.

2. In Barker the same minerals are observed, but the clay fraction also contains kaolinite and pyrophyllite. The latter mineral and the illite crystallinity index indicate the possibility of either detrital clays or slight metamorphism. The field evidence better supports the inheritance hypothesis owing to the recurrence of lateritic horizons indicating meteoric alteration, and the kaolinitic and illitic horizons showing the short distance transportation of residues of weathering.

3. Near Mar del Plata, the sequence contains mainly kaolinite and detrital illite appearing as lenses of clay inside a massive sandstone formation.

The first two assemblages were chosed for the isotopic study. The sediments of Olavarria seem to be more likely to give a sedimentary age. The sediments in Barker were studied to test the two hypotheses--inheritance or subsequent metamorphism. The kaolinites of Mar del Plata were rejected in this first study.

ISOTOPIC RESULTS AND DISCUSSION

a) Olavarria Region

The samples collected in the AUST quarry show two isotopic Rb-Sr lines with the following ages. ($\lambda^{87}Rb = 1.42\ 10^{-11} yr^{-1}$)

- 797 ± 18 m.y. with an initial ratio of 0.707 ± 0.005
- 756 ± 22 m.y. with an initial ratio of 0.712 ± 0.005

The samples collected at CERRO NEGRO and L.O.S.A. show an isotopic Rb-Sr line with an age of

- 709 ± 24 m.y. with an intercept at 0.718 ± 0.003.

These isotopic evolution lines are not mathematically distinguishable, except for the two extremes.

The corresponding K-Ar ages cannot be used to more precisely define the chronological order, because the results are dispersed between 760 and 697 m.y. (new constants) without any relation to the level from which the samples came.

The stratigraphy of the "La Tinta" sediments sets the AUST quarry below the L.O.S.A. outcrop. The Rb-Sr results confirm that succession. In the AUST quarry two events seem to appear. Even if the isotopic evidence by the ages and intercepts is not convincing, the isotopic composition of the strontium contained in a limestone bed (0.714 for $^{87}Rb/^{86}Sr = 0.178$) shows that an isotopic mobility existed for the strontium after deposition. Furthermore, the clay fractions are not perfectly aligned. This suggests two hypotheses: (1) the 797 m.y. age represents that of inherited clays and the 756 m.y. age that of early diagenesis; (2) the 797 m.y. age represents the early diagenesis and the 756 m.y. age represents a late diagenesis. The second hypothesis is supported by the potassium-argon results, because the influence of isotopic inheritance is often very strong on K-Ar results.

b) Barker Region

The Rb-Sr results for the Barker sediments show a scatter of points for which it is impossible to determine any isotopic line. This is typical for detrital material as well as for clay fractions with very low Rb/Sr ratios.

The K-Ar results of 632 and 374 m.y. support this interpretation and also suggest an actual effect of meteoric water on the sample rich in kaolinite and pyrophyllite.

CONCLUSION

The age of the "LaTinta" series was confirmed as late Precambrian. A preliminary form of numerical chronostratigraphy for these sediments was established. The results must be compared with other age determinations on Precambrian sediments in Brazil and Southern Africa.

ARGON ISOTOPIC GEOCHEMISTRY IN CLAYS-- THE INFLUENCE OF AN INHERITED FRACTION

By Michel G. Bonhomme[1], Francoise Elsass[2], and Christine Mosser[1]
[1]Institut de Geologie,
Universite Louis Pasteur,
Centre de Sedimentologie et Geochimie de la Surface,
Strasbourg, France
[2]Labatoire de Chimie Minerale,
Universite Paris VI, Paris, France

INTRODUCTION

Potassium-argon studies have been performed on fine-grained fractions of shale and sandstone constituted by various assemblages of clay minerals, and collected in the Autunian at Autun, in the Toarcian in Lorraine, and in the Bartonian at Cassel (all these localities in France).

In the Autunian, the lithostratigraphic sequence contains recurrent successions of sandstone, siltstone, and bituminous shale. The studied level of the Toarcian is also a bituminous shale. At Cassel, the Bartonian is represented by glauconitic shelly sandstone. In the three instances, potassium-argon data were obtained on the > 2 μm fraction, and for some samples of the Autunian and Toarcian shales granulometric separations were done within the 2 μm fraction.

POTASSIUM-ARGON ISOTOPIC RESULTS (Calculated with the new constants)

The Autunian

The 0.4 - 1 μm and 1 - 2 μm fractions of the three analyzed samples define an isotopic line showing an age of 298 ± 6 m.y. (±2σ) with $(^{40}Ar/^{36}Ar)_{initial} = 189 \pm 71$ (±2σ). On the other hand, the three fractions smaller than 0.4 micron define another line. Yielding an age of 261 ± 15 m.y. with $(^{40}Ar/^{36}Ar)_{initial} = 307 \pm 100$, which is the correct age for that stage.

The Toarcian

In the case of the Toarcian, the K-Ar isotopic data points do not define any isotopic

line. The apparent age is of the order of 300 m.y. for the 2-micrometer fractions, and the ages indicated by two 1-2 μ samples are 382 and 373 m.y. On the other hand, the finest fractions of the same samples give respectively 207 and 228 m.y., which are near the presumed age, that is nearly 180 m.y.

The Bartonian

Among the ten analyzed samples, the five richest in potassium define an isotopic line showing an age of 4.38 ± 3.2 m.y. with $(^{40}Ar/^{36}Ar)_{initial} = 283 \pm 61$, which is the correct age for that stage. All the other samples, situated at a lower position in the stratigraphic sequence and generally poorly crystallized and lower in potassium give greater ages.

DISCUSSION

Before making any attempt to interpret these data, it is necessary to review some observations:

A--the coarse or poorly crystallized clay fractions give apparent ages greater than the stratigraphically correct ones;

B--on the contrary, the finest, or well-crystallized, or richest in potassium generally give either the correct age or values close to it;

C--in the case of the too high ages, the isochron plot shows an initial ratio generally lower than 295.5;

D--in all three instances 1) the mineralogical evolution from detrital material, such as smectite, kaolinite, illite, and mixed-layer clays to new illite and glauconite, 2) the increase in potassium content, and 3) the tendency to approach the correct age are strongly positively correlated.

Microscopic and mineralogic examination has demonstrated that all these observations are effects of the diagenesis, which affected these formations. When the diagenesis is strong enough, it leads to potassium-argon isochrons showing the age of the diagenesis and a normal intercept. A lower intercept could indicate an uncomplete recrystallization and the addition of potassium without complete outgassing of inherited radiogenic argon.

The influence of excess argon related to inherited clay fragments seems to be general. It must be carefully analyzed by means of granulometric separations within the clay fraction. It might also explain the difficulties encountered ten years ago by various authors in applying the K-Ar method to clays actually deposited in oceans and rivers.

FRANCEVILLIAN REVISITED. RADIOCHRONOLOGY OF A FOSSIL NUCLEAR REACTOR ENVIRONMENT

By Michel G. Bonhomme and Francis Weber
Institut de Géologie,
Université Louis Pasteur,
Centre de Sédimentologie et
Géochimie de la Surface,
Strasbourg, France

Introduction: The sedimentary rocks of the Francevillian basin, in Gabon, were the first typical Precambrian strata to be dated by means of the Rb-Sr method on clays. Since then, some fossil nuclear reactors were discovered at Oklo, which has generated a new interest in those rocks. From the radiochronological point of view, a contradiction appeared between the results of dating by the Rb-Sr and K-Ar methods and by the U-Pb and fission products methods.

Geological Setting: The stratigraphic sequence of the Francevillian basin is thought to have had a total thickness of nearly 4000-5000 m. The tectonic aspect of the sediments confirms that idea. The illite crystallinity index is representative of a strong diagenesis, but not of an anchimetamorphic level. The petrography and fluid inclusion studies suggest that the Francevillian suffered two diagenetic episodes. The first one--corresponding to a burial of nearly 4000 m--is mainly siliceous. The second one, at a depth of 3000 m is related to the emplacement of carbonates in the sandstones of the lowest sedimentary member F_A.

The fossil reactors lie at the contact between F_A and the overlying F_B member, consisting mainly by shales. Field and fluid inclusion evidence show that the nuclear reaction took place between the two diagenetic episodes. The high temperature and the desilicification related to the nuclear reaction generated 2M illites inside a distance of nearly 1-2 m from the reactors. These 2M illites were then retrograded to 1M illites due to intense radioactive damage in the cores of the reactors.

Rb-Sr and K-Ar Results: The normal illites away from the reactors define two isotopic lines whose characteristics are as following: 1917 ± 13 m.y. ($\pm 2\sigma$, $\lambda^{87}Rb = 1.42\ 10^{-11}\ yr^{-1}$) with $(^{87}Sr/^{86}Sr)_o = 0.7079 \pm 0.0013$; 1865 ± 15 m.y.

with $(^{87}Sr/^{86}Sr)_o = 0.7072 \pm 0.0007$.

The 2M illites of the reactors define an isotopic line yielding an age of 1695 ± 24 m.y. with $(^{87}Sr/^{86}Sr)_o = 0.7045 \pm 0.0024$ or lie between the 1865 and 1695 m.y. lines.

Fine-grained fractions smaller than 0.2 m and between 0.2 and 0.4 μm from the zone of carbonate diagenesis also lie between the 1865 and 1695 m.y. lines, as does the smaller than 0.4 μm fraction of a normal F_A clay sample.

K-Ar analyses of normal illites give ages between 1870 and 1800 m.y.; K-Ar analyses of 2M reactor illites give ages between 1860 and 1700 m.y.

Discussion and Interpretation: Two geologic events have been defined and the isotopic results give three ages. Under these conditions, we might propose two hypotheses:

1. 1917 m.y. is the date of the siliceous diagenesis and 1865 the date of the carbonate diagenesis. In that case, 1695 m.y. represents a slight alteration episode only visible on illites weakened by radioactivity near the uranium ore or by their smaller size.

2. 1865 m.y. is the date of the siliceous diagenesis and 1695 m.y. the date of the carbonate diagenesis. In that case, 1917 m.y. might be an artifact produced by the mixing line of detrital illites.

Rb-Sr dating of a syenitic massif at N-Goutou showed that the real age of the F_B member might be nearly 1925 m.y. The siliceous diagenesis affects all the Francevillian sequence. It might be rather difficult to understand how the general burial effect could affect the total sequence only a few million years after the deposition of the two lowest of five members. So, it is easier to suggest that 1865 m.y. represents the age of the siliceous diagenesis.

On the other hand, a time gap of 170 m.y. between the two types of diagenesis appears to be rather long. But there is evidence in the region of any other event near 1700 m.y. Also, this latter age is not yet firmly established because the very fine fractions of the clays collected in the carbonate diagenetic zone are not perfectly aligned at 1695 m.y.

In conclusion, it is not yet possible to choose between the two hypotheses and the age of the Oklo natural fossil reactors might be either close to 1917 m.y. or 1865 m.y. The difference between the Rb-Sr and K-Ar results and the U-Pb and fission products would be smaller if the first hypothesis were adopted.

INTRA- AND INTER-CRYSTALLINE VARIATIONS OF Pb ISOTOPIC COMPOSITION IN GALENA FROM THE MISSISSIPPI VALLEY TYPE ORES: AN ION-MICROPROBE STUDY

By O. Brevard, N. Shimizu, and C. J. Allègre
Laboratoire de Géochimie et Cosmochimie(LA 196)
Institut de Physique du Globe
University of Paris 6

Local as well as regional variations of Pb isotopic composition in galena samples have been well known for the Mississippi Valley type ores since Nier's (1938) first Pb isotope analysis, and have an important bearing on the origin of this type of ores. Cannon and others (1963) described a galena crystal showing an isotopic zonation, with the Pb isotope ratios becoming monotonically more radiogenic toward the rim of the crystal. It was suggested that the isotopic variation could be explained by a mixing of common lead and radiogenic lead, with the latter having changed with time due to radioactive decay of U and Th in the source area during the crystal growth.

Using an ion-microprobe technique (Shimizu and others, 1978), with a Cameca IMS 300 instrument, Pb isotopic composition was analyzed on spots with an area of approximately 200 X 200 µm. With a primary beam of O_2^+ ions at a current ranging from 400 to 700 nA with net energy of 5.5 KeV, secondary ion intensity in excess of 10^{-11}A was obtained for Pb in galena samples. The intensity variation within the 'flat' part of a peak was much less than 1 percent and the intensities were measured as amplified analog signals on the peak tops with a computer control peak-switching device. The results on a galena from Manitouwadge show that a precision of analysis of about 0.1 percent(2σ) was obtained for both $^{207}Pb/^{206}Pb$ and $^{208}Pb/^{206}Pb$ ratios; accuracy was better than 0.5 percent relative to the values given by Stacey and others (1969) with a triple-filament technique.

Our results on Pb isotope ratios of a galena crystal from Picher, Oklahoma, agree with those of Cannon and others (1963) but show an oscillatory variation of Pb isotopic ratios with crystal-growth zones instead of a monotonic variation as originally suggested. A tenative interpretation is that there were at least two sources of Pb distinct in isotopic composition due to different U/Pb and Th/Pb ratios, and Pb from these two sources was transported to the place of deposition by different ground water systems. During the growth of the crystal, dominance of one of the sources over the other changed with time, resulting in an oscillatory variation.

The results on galena crystals from the Buick Mine, Missouri, include isotopically homogeneous crystals and those showing a step-wise zoning. The relationships between the isotopic composition and the crystal forms (cubic mineralization versus octahedral mineralization) will also be discussed.

Cannon, R. S., Jr., Pierce, A. P., and Delevaux, M. H., 1963, Lead isotope variation with growth zoning in a galena crystal: Science, v. 142, p. 574.

Nier, A. O., 1938, Variations in the relative abundances of the isotopes of common lead from various sources: Journal of the American Chemical Society, v. 60, p. 1571.

Shimizu, N., Semet, M. P., and Allegre, C. J., (in press), Geochemical applications of quantitative ion-microprobe analysis: Geochimica Cosmochimica Acta.

Stacey, J. S., Delevaux, M. H., and Ulrych, T. J., 1969, Some triple-filament lead ratio measurements and an absolute growth curve for single-stage leads: Earth and Planetary Science Letters, v. 6, p. 15.

A CONTRIBUTION TO THE PLEISTOCENE GEOCHRONOLOGY OF ALASKA AND THE YUKON TERRITORY: FISSION-TRACK AGE OF DISTAL TEPHRA UNITS

By Nancy D. Briggs and John A. Westgate
Department of Geology, University of Toronto
Toronto, Ontario, Canada, M5S 1A1

The Yukon Territory and Alaska underwent repeated glaciation from several different sources during the Pleistocene. Laurentide and Cordilleran ice sheets invaded the Yukon from

the east and south and several areas were affected by mountain and piedmont glaciers. However, large parts of Alaska and the central and northern Yukon remained ice-free throughout the Pleistocene. This diversity of depositional environments has greatly inhibited long distance correlation of the sedimentary sequences, the chronology of which remains largely unknown, except for those sediments within the range of the ^{14}C dating technique.

Tephra layers, which are widespread in this region in both an areal and a stratigraphic sense, can be used to solve problems of correlation and chronology, but this potential has not been fully exploited. In this paper we present fission-track data on the age of four felsic tephra beds from the unglaciated parts of Alaska and the Yukon Territory.

In our recent tephro-chronological studies we used the fission-track dating method outlined by Naeser (1976). Glass shards were concentrated by standard heavy-liquid separation techniques. The 250 to 125 μm fraction was used wherever possible, but in many samples the fine grain-size or concentration of pumiceous glass in the coarser fraction made it necessary to use material as fine as 125 to 63 μm. Part of each glass separate was irradiated at McMaster Nuclear Reactor in Hamilton, Ontario. Glass dosimeters (N.B.S. glass standard SRM 962: 37.38 ± 0.08 ppm U) were placed at the top and bottom of each irradiation can and the thermal neutron dose was calibrated against a mean of the values obtained from Cu and Au foils, which were included with the standard glasses during irradiation at N.B.S. (Carpenter and Reimer, 1974). The dose for each tephra sample was calculated by extrapolating between the values determined for the standards.

Splits of the irradiated and nonirradiated samples were mounted in clear epoxy resin on separate glass slides, ground to expose an internal surface, polished, and etched together in 24 percent HF until tracks of a suitable size for counting were obtained. Tracks were counted in transmitted light at x500 magnification. The conventional method of determining glass area by use of an eyepiece grid proved impractical because the glass shards were either too fine-grained, thin-walled, or coarsely pumiceous. Instead, we used a modified version of the point-counting technique developed by Seward and Kohn (Seward, 1974).

Glasses of a known age were dated in order to provide a check on the reliability of the ages obtained for the Alaskan and Yukon tephras. The extent of agreement is shown in table 1. Dates obtained on several other glasses, not reported in table 1, likewise agree closely with unpublished fission-track ages determined by Naeser and Izett of the United States Geological Survey (C. Naeser and G. Izett, written commun., 1977).

Although glass is more susceptible to track fading than minerals such as zircon and apatite (Fleischer and others, 1975), it had to be used in this study because of the small size of our samples; suitable minerals were not present in sufficient quantity. However, we feel the problem of track fading in glass is greatly minimized in the Yukon Territory and Alaska where Pleistocene tephras have been in a permafrost environment throughout much of their history. This belief is corroborated by the lack of any noticeable difference in the size of the spontaneous and induced tracks. Nonetheless, larger bulk samples of the older tephras should be collected so that sufficient zircon can be isolated and dated to provide an independent check on the veracity of the glass ages.

Mosquito Gulch tephra (UT 19) occurs in alluvium on a high terrace of Bonanza Creek in the unglaciated uplands south of Dawson (M. Milner, personal commun., 1977; fig. 1). The oldest and topographically highest deposit of late Cenozoic age along southern (upstream) Bonanza Creek is the White Channel gravels. The upper part of these gravels in the downstream part of the valley interfinger with and are overlain by the Klondike gravels, thought to represent part of the "pre-Reid" outwash and to be of early Pleistocene age (Hughes and others, 1972). Because the Mosquito Gulch tephra lies on a terrace that formed subsequent to extensive dissection of the White Channel gravels, its age of 1.25 ± 0.25 m.y. (table 1) provides a minimum date for the Klondike gravels and therefore for the old "pre-Reid" glaciations of the central Yukon.

Exposures of the Old Crow tephra (UT 1) can be seen in several stratigraphic sections along the Porcupine and Old Crow Rivers in northwestern Yukon Territory. The tephra occurs in the upper part of a fluviatile sequence, which is capped by lacustrine silts and clays that accumulated in the Old Crow Basin when eastward drainage was last blocked by westward advance of the Laurentide ice sheet against the Richardson Mountains (Hughes, 1972). It forms an important marker bed in this area, because of its relationship to fluctuations of the Laurentide ice sheet and because it occurs just below sediments that contain possible bone artifacts (Morlan and Matthews, 1978). Peat about 5 m above the Old Crow tephra has a ^{14}C age of 35,500 ± 1050 years (GSC-2507). The fission-track age data (table 1) confirm a young age; no spontaneous tracks were detected in the glass. An age between 80,000 and 35,000 years seems likely.

Lost Chicken tephra (UA 771) occurs about 15 m below the top of a 30 m section of organic silts at Lost Chicken Mine, close to the Taylor Highway in east-central Alaska (fig. 1). It immediately overlies peat beds with *Pinus*, *Picea*, and *Betula* pollen, which Matthews (1970) suggests accumulated under forested conditions during an interglacial climate. The fission-track age of the tephra indicates that the

Table 1.--Glass fission-track age of tephra beds from the Yukon Territory and Alaska

Sample	Neutron dose ($\times 10^{14}$ ncm^{-2})	Spontaneous tracks		Induced tracks		Age[2] (m.y.)
		counted	cm^{-2}	counted	cm^{-2} ($\times 10^3$) [1]	
Yukon and Alaskan tephra						
UT 1	25.55	0	<42	1485	>163	<0.04±0.04
UT 19	25.67	26	324	635	40	1.25±0.25
UA 743	21.80	40	332	3291	96	0.45±0.07
UA 771	21.65	130	1671	4167	128	1.70±0.15
Reference samples						
Wascana Creek Ash, Saskatchewan.	25.71	27	871	2745	214	0.63±0.12
	-----	---	----	----	---	0.60±0.04[3]
Moldavite, Czechoslovakia.	25.88	341	12.3 x 10^3	2067	129	14.8 ±0.9
	21.57	559	12.4 x 10^3	1298	109	14.7 ±0.8
	-----	---	----	----	---	14.7 ±0.7 [4]

[1]Measured density minus spontaneous tracks.
[2]Calculated from the fission-track age equation (Fleischer and others, 1965; Naeser, 1967), using the following values: $\lambda_D = 1.551 \times 10^{-10}$yr^{-1}; $\lambda_F = 7.03 \times 10^{-17}$yr^{-1} (Roberts and others, 1968); $\sigma = 580 \times 10^{-24}$cm^2; I=7.252x10-3
[3]Westgate and others, 1977; average of 5 glass fission-track dates.
[4]Gentner and others, 1967; K-Ar age.

interglacial peats were deposited about 1.7 m.y. ago.

Ester Ash Bed (UA 743) occurs within the basal part of the Gold Hill Loess, the oldest loess recognized in central Alaska (Péwé, 1975; fig. 1). This loess lies between two interglacial forest beds and represents a long period of rigorous glacial climate. As the upper forest bed is > 57,000 years old, Péwé (1975) interprets the Gold Hill Loess as "Illinoian" in age and the Ester Ash Bed as early "Illinoian". The Ester Ash Bed, at its type locality near Fairbanks (fig. 1), is 0.45 ± 0.07 m.y. old (table 1), which is consistent with an early Illinoian age, as defined in the mid-continent region of the United States.

The Dome Ash Bed crops out near the top of the Gold Hill Loess but its glass is too pumiceous to be dated by the fission-track method.

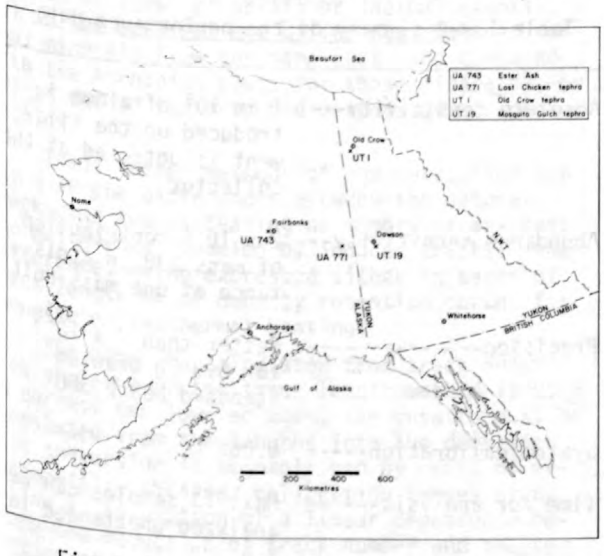

Figure 1.--Location of dated separates.

Contribution number 11, Northern Yukon Research Programme

Carpenter, B. S., and Reimer, G. M., 1974, Standard reference materials - calibrated glass standards for fission track use: National Bureau of Standards, Special Publication 260-40, 16 p.

Fleischer, R. L., Price, P. B., and Walker, R. M., 1965, Tracks of charged particles in solids: Science, v. 149, p. 383-393.

_____1975, Nuclear tracks in solids - principles and applications: Berkeley, University of California Press, 605 p.

Gentner, W., Kleinmann, B., and Wagner, G. A., 1967, New K-Ar and fission track ages of impact glasses and tektites: Earth and Planetary Science Letters, v. 2, p. 83-86.

Hughes, O. L., 1972, Surficial geology of the northern Yukon Territory and northwestern District of Mackenzie, Northwest Terri-

tories: Geological Survey of Canada Paper 69-36, 11 p.
Hughes, O. L., Rampton, V. N., and Rutter, N. W., 1972, Quaternary geology and geomorphology, southern and central Yukon (northern Canada): International Geological Congress Guidebook, No. 24, Part A11, 59 p.
Matthews, J. V. Jr., 1970, Quaternary environmental history of interior Alaska - pollen samples from organic colluvium and peats: Arctic and Alpine Research, v. 2, p. 241-251.
Morlan, R. E., and Matthews, J. V. Jr., 1978, New dates for early man: GEOS, winter, 1978, p. 2-5.
Naeser, C. W., 1967, The use of apatite and sphene for fission track age determinations: Geological Society of America Bulletin, v. 78, p. 1523-1526.
_____1976, Fission track dating: U.S. Geological Survey Open-File Report 76-190, 71 p.
Péwé, T. L., 1975, Quaternary stratigraphic nomenclature in unglaciated central Alaska: U.S. Geological Survey Professional Paper 862, 32 p.
Roberts, J. H., Gold, R., and Armani, R. J., 1968, Spontaneous-fission decay constant of ^{238}U: Physical Review, v. 174, p. 1482-1484.
Seward, D., 1974, Age of New Zealand Pleistocene substages by fission-track dating of glass shards from tephra horizons: Earth and planetary Science Letters, v. 24, p. 242-248.
Westgate, J. A., Christiansen, E. A., and Boellstorff, J. D., 1977, Wascana Creek Ash (Middle Pleistocene) in southern Saskatchewan - characterization, source, fission track age, palaeomagnetism, and stratigraphic significance: Canadian Journal of Earth Sciences, v. 14, p. 357-374.

ISOTOPE RATIO STUDIES USING A MASS SPECTROMETER WITH SPECIAL GEOMETRY AND COMPUTER CONTROL

By C. Brunnee, G. Kappus, H. Rache, and W. A. Wolstenholme
Varian MAT, Barkhausenstr 2
Bremen, West Germany

The basic criteria involved in high-precision isotope-ratio measurements have been considered in detail. As a result, and bearing in mind the utmost importance of obtaining the maximum ion current from a given sample, and of reproducible operation and procedures, an isotope-ratio mass spectrometer has been designed and built, and its performance evaluated. In order to maximize the ion current from a given sample, ion-source sensitivity and ion transmission through the analyzer were maximized by use of a special ion optical system providing stigmatic focusing. This results in almost 100 percent ion transmission through the analyzer and a dispersion equivalent to a conventional system with twice the analyzer radius. In addition, very high abundance sensitivity is obtained. Using two versions of the instrument, measurements on both solid and gaseous samples have been made with the same analyzer system, employing an appropriate ion source, inlet system, and collector geometry.

A factor of great importance in isotope-ratio experimental techniques is the reproducibility of the analytical procedure. In order to ensure good reproducibility while maintaining ease of operation, the instrument has been designed with full computer control As a solid source mass spectrometer using thermal ionization, for example, the precision, accuracy, and sample throughput depend to a great extent on the precise and reproducible control of all instrumental parameters. The effect of ionization parameters, a very important factor, was studied by de Bievre (1977). He obtained dramatically improved results by employing careful control of the thermal ionization conditions. Without such

Table 1.--A summary of the performance data

Absolute sensitivity---	1 in 10^3 of atoms introduced on the filament is detected at the collector
Abundance sensitivity--	2×10^{-6} contribution of mass 238 in a distance of one mass unit
Precision----------	Better than 7×10^{-5} for 0.3 µg Uranium standard NBS U 500
System calibration-----	0.06%
Time for analysis------	Max. 13 samples can be analyzed unattended in 8 h.

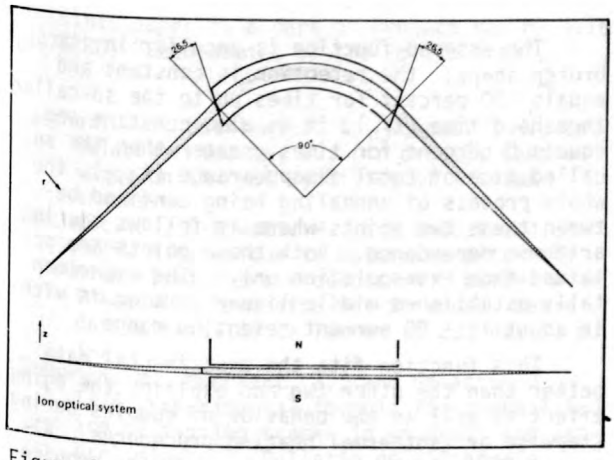

Figure 1.--A schematic diagram of the ion optical system used in the instruments.

control, isotopic fractionation effects occurring during evaporation of the sample are a major cause of irreproducible results (Kanno, 1971). Such effects are minimized by the use of automatic control and when used in conjunction

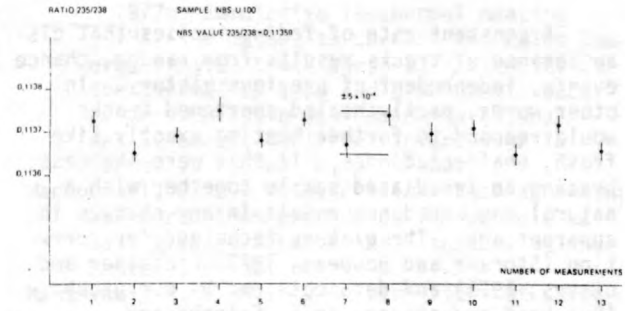

Figure 2.--Some results of uranium isotope-ratio measurements obtained on 13 simultaneously loaded and automatically run samples.

with the automatic control of a multi-sample turret with automatic pre-heat and ionizing conditions, allowing routine high-precision analyses to be obtained.

De Bievre, P., 1977, Advances in Mass Spectrometry, ed. Daly, N. R., Heyden, London, 7.
Kanno, H., 1971, Bulletin of the Chemical Society of Japan, v. 44, p. 1808

RATE OF TRACK FADING IN CRYSTALS AS AN INDICATOR OF THERMAL HISTORY OF ROCKS

By Jan Burchart[1], and
Jolanta Galazka-Friedman[2]
[1]Polish Academy of Sciences, Warsaw, Poland
[2]Technical University, Warsaw, Poland

Geological interpretations of thermally lowered fission track ages are based either (1) on the spatial distribution of the apparent ages relative to a supposed heat source (and explained in terms of uplift or thermal events), (2) on the apparent age differences between various minerals from the same rock (and compared with the Arrhenius plots for these minerals), or (3) on one of the proposed methods of age correction.

These latter methods of age correction are based on the differences between the natural tracks and tracks bearing no memory of any past thermal events (modeled by induced tracks)--the differences being expressed either in terms of track length or of density retention curves for stepwise or isothermal heating.

The ages are calculated from track densities and even if the track length method is used to correct the lowered ages, the results must be translated from the lengths into the densities. This conversion is accomplished by means of experimentally obtained calibration curves or by making an assumption of a linear dependence between the reduction of track number and the reduction of track lengths.

Behavior of track density during heating is a key to understanding the process of partial or complete resetting of the fission track clocks, but it may also validate the methods of age correction.

Let us discuss a case of isothermal heating, which gives much better control of the experimental errors than stepwise temperature rise. The crude results of annealing experiments are usually shown in the retention versus heating-time graphs. Tracks do fade when heated, but in spite of numerous experiments the shape of the function describing the process has not been agreed upon by all the workers in the field. In a recently prepared paper (Burchart and others, 1978) we made a statistical reevaluation of the goodness of fit of various functions proposed for the experimental data on apatite. Let us introduce a notion of the "rate of track fading" defined as $[|d(\rho/\rho_0)|/dt]/(\rho/\rho_0)$, which is a logarithmic derivative of the function that describes the fading (ρ/ρ_0), track retention; t, total time of isothermal heating). If the damage repair is imagined as involving a single mechanism, one may expect the rate to be constant or monotonously changing as the process develops.

A constant rate of fading implies that disappearance of tracks results from random, chance events, independent of previous history. In other words, partly healed shortened tracks would respond to further heating exactly like fresh, unaffected ones. If this were the case, heating an irradiated sample together with a natural one would not result in any changes in apparent age. The plateau technique for correction (Storzer and Poupeau, 1973; Fleischer and others, 1975) and data obtained by our group (Burchart and others, 1975; Galazka and Burchart, 1977a, b) disprove such a possibility.

An increasing rate of the process implies that on heating, a partly annealed sample would anneal faster than an irradiated one, hence the apparent age would be decreasing, which is exactly opposite to the plateau technique and CIH (cumulative isothermal heating) results.

A decreasing rate means that on heating a partly annealed sample anneals more slowly than an irradiated one, the amount of lag being a measure of the degree of annealing prior to the experiment, that is, in nature. As a consequence, there is an apparent age increase on heating (up to a maximum). Such a differential annealing has been demonstrated both by the plateau and by the CIH methods. Moreover, this also explains the "aging" effect observed by Macdougall (1976), which would be hard to understand if the rate were constant or increasing.

If one goes back from the derivatives to the original functions (retention versus time), one notes that a constant rate would be obtained if the retention is assumed to decrease linearly with exp t (or log ρ/ρ_0 with t), and an increasing rate if the retention is assumed to decrease linearly with t. The former possibility was claimed by Märk and others (1973), the latter by Mantovani (1974).

As shown by Burchart and others (1978) the experimental points to which these functions have been fitted, fit even better to a logarithmic function; that is, $\rho/\rho_0 \sim \log t$, first introduced by Naeser and Faul (1969) and corroborated by much data. Such a shape of the function has been assumed in the mathematical proof of the CIH method (Galazka and Burchart, 1977a).

It should be added that, as noticed by Dakowski and others (1974), the logarithmic function can be applied to crystals only. The function for glasses is concave in the ρ/ρ_0 versus log t coordinates and therefore the differential annealing, "aging", and memory may be even more strongly expressed than in the case of crystals. The mathematics involved is more complex.

However, even the simple logarithmic function should be looked upon with caution: not as a description of a real physical process, but rather as a crude generalization of the experimental data which, unfortunately, are subject to high and usually underestimated errors, and which are particularly ambiguous for the final steps of annealing.

The assumed function is peculiar in its broken shape: the retention is constant and equals 100 percent for times up to the so-called threshold time (t_{th}), it is also constant and equals 0 percent for times greater than the so-called time of total disappearance (t_{dis}), the whole process of annealing being confined between these two points where it follows the logarithmic dependence. Both these points are obtained from extrapolation only. The experimentally established middle linear portion is within about 10 - 90 percent retention range.

This function fits the experimental data better than the other two and explains the aging effect as well as the behavior of samples during stepwise or isothermal heating procedures. Also, at first look, it seems to meet the requirement of a decreasing rate of annealing. However, its first derivative is not continuous at t_{th} and t_{dis}, which seems unnatural for a physical process. Moreover, the theoretically calculated rate of fading decreases with time of isothermal heating, but only to a certain value, and then it starts to increase, first very slowly, and at the very end--rapidly. The distance between t_1 (time of isothermal annealing at which the rate reaches its minimum) and t_{dis} is constant [$\ln t_1 = (\ln t_{dis})-1$] and therefore t_1 occurs at very low value of retention (relatively close to the end of the annealing process) if t_{dis} is long; that is, if the annealing is carried out at relatively low temperatures. At higher temperatures, when t_{dis} is shorter, t_1 would occur much earlier in the t_{th}-t_{dis} interval; that is, at higher retention.

Intuitively we look with suspicion at the portion of the logarithmic function for which the rate increases and we regard it as an indication that though the function discussed is the best one of the three functions so far proposed, it is still not good enough. It may serve as a practically useful approximation for low-temperature annealing, but for higher temperatures the simplification introduced may be already inadmissible.

In view of experimental errors we believe that, with available techniques one can hardly expect the annealing experiments alone to produce data accurate enough to yield a true description of the track fading process in its entire range. It may prove possible but not without developing a theory of damage repair in minerals, which we expect from solid-state physicists.

As long as nothing better is proposed, we may use the logarithmic function as a tentative working hypothesis for crystals only, which, in the interval up to ($\ln t_{dis}$)-1 meets the requirement of a decreasing rate, fits fairly well to the experimental data, explains the phenomenon of differential annealing and "aging", shows that tracks have memory for thermal events, and creates a basis for decoding the record of such memory.

This paper is a part of Project no. MR.1.16 (1976/80) "Geodynamics of the Polish area".

Burchart, J., Butkiewicz, T., Dakowski, M., and Galazka-Friedman, J., (in press), Controversy on thermal stability of fission tracks.

Burchart, J., Dakowski, M., and Galazka, J., 1975, A technique to determine extremely high fission track densities: Bulletin de l'Academie Polonaise des Sciences, Serie des Sciences de la Terre, v. 23, no. 1, p. 1-7.

Dakowski, M., Burchart, J., and Galazka, J., 1974, Experimental formula for thermal fading of fission tracks in minerals and natural glasses: Bulletin de l'Academie Polonaise des Sciences, Serie des Sciences de la Terre, v. 22, no. 1, p. 11-17.

Fleischer, R. L., Price, P. B., and Walker, R. M., 1975, Nuclear tracks in solids: Berkeley, University of California Press, 605 p.

Galazka, J., and Burchart, J., 1977a, Cumulative isothermal heating (CIH) as a method to correct thermally lowered fission track ages, I--Mathematical models: Bulletin de l'Academie Polonaise des Sciences, Serie des Sciences de la Terre, v. 25, no. 1, p. 1-7.

_____1977b, Cumulative isothermal heating (CIH) as a method to correct thermally lowered fission track ages, II--Intensity of the thermal episode and time of its occurrence: Bulletin de l'Academie Polonaise des Sciences, Serie des Sciences de la Terre, v. 25, no. 2, p. 57-65.

Macdougall, J. D., 1976, Fission track annealing and correction procedures for oceanic basalt glasses: Earth and Planetary Science Letters, v. 30, no. 1, p. 19-26.

Mantovani, M. S. M., 1974, Variations of characteristics of fission tracks in muscovites by thermal effects: Earth and Planetary Science Letters, v. 24, p. 311-316.

Märk, E., Pahl, M., Purtscheller, F., and Märk, T. D., 1973, Thermische Ausheilung von Uran-Spaltspuren in Apatiten, Alterskorrekturen und Beiträge zur Geothermochronologie: Tschermaks Mineralogische und Petrographische Mitteilungen, v. 20, p. 131-154.

Naeser, C. W., and Faul, H., 1969, Fission track annealing in apatite and sphene: Journal of Geophysical Research, v. 74, no. 2, p. 705-710.

Storzer, D., and Poupeau, G., 1973, Ages-plateaux de minéraux et verres par la méthode des traces de fission: Paris, Académie des Sciences, Comptes rendus, ser. D, v. 276, p. 137-139.

GEOCHRONOLOGY OF PALEOZOIC MAGMATISM IN THE MASSIF CENTRAL (FRANCE); ITS CONNECTIONS WITH TECTONISM AND METAMORPHISM

By Jean Marie Cantagrel[1], Jean Louis Duthou[1], and Jean Bernard-Griffiths[2]

[1]Laboratoire Associé n°10, CNRS et Université, 5 rue Kessler, 63038 Clermont-Ferrand Cedex, France

[2]Centre Armoricain d'Etude des Socles, avenue du Général Leclerc, 35031 Rennes Cedex, France

GEOLOGICAL SETTING

The Massif Central is classically described as a part of the middle European Variscan (Hercynian) belt, this orogeny being the last to have affected the region. More than 60 percent of the surface is constituted by magmatic rocks--basic and acid orthogneisses, metavolcanics, granites, and others. Except for some unusual low-grade metamorphic rocks, the age of the various metamorphic series remains stratigraphically unknown. In the south (Montagne Noire), a younger Visean metamorphic series is present; likewise, in the Lyonnais area, the sediments and the spilite-keratophyre lavas (Brevenne group) of likely Devonian to Dinantian age were weakly metamorphosed during an Hercynian event. This group has been described as discordantly overlying older metamorphic basement. Further west, the youngest paleontologically dated sediments are of Late Silurian age, whereas the lower metapelitic schists are probably of late Precambrian or Early Cambrian age. In the northeast, non-metamorphic upper Visean volcanics overlie a locally eroded basement.

In a general way, the Massif Central is a polymetamorphic region. The first tectonometamorphic event is of a high- to intermediate-pressure type with staurolite, kyanite, and sillimanite paragenesis (locally, eclogitic and granulitic rocks have been recognized). In contrast, the second event, of low-pressure type, is well developed in the south and southeast. Until now, older events have never been clearly proved. This paper is devoted only to geochronological results measured on magmatic rocks

and the recorded ages are reported on the map (fig. 1).

PRETECTONIC MAGMATISM

We will first examine the main results from the western part of the massif (Limousin). Here the first magmatic episode is of Cambrian age, including fine- to medium-grained mesocratic orthogneisses (quartz dioritic and trondhjemiti to dacitic in composition), another alkalic augen orthogneiss, numerous metabasalt or meta-

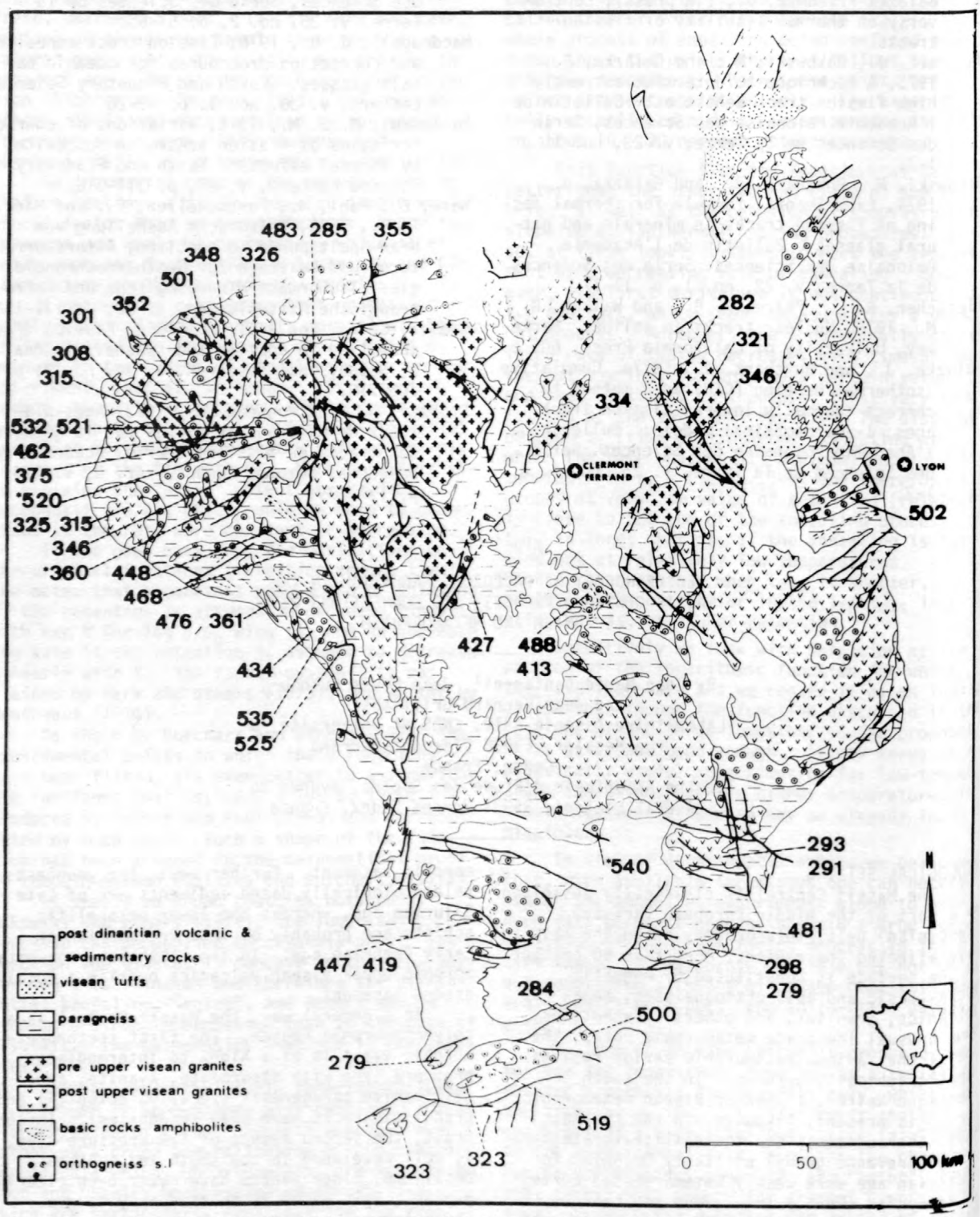

Figure 1.--Geochronological map of Paleozoic magmatism of the Massif Central, France.

gabbro dikes, and small basic to ultrabasic bodies of tholeiitic composition (Coffrant and others, 1975). Some of these igneous-derived materials, in particular the volcanics, seem to have been partly reworked soon after their deposition. Calc-alkalic metagranites give, for example, the following ages and initial $^{87}Sr/^{86}Sr$ ratios ($\lambda Rb = 1.42 \times 10^{-11}$ yr^{-1}): Fine-grained Mulatet granite, 535 ± 21 m.y. (0.7088); Thaurion augen gneisses, 532 ± 20 m.y. (0.7036); isogranular Thaurion gneisses, 521 ± 12 m.y. (0.7065); Chameyrat augen gneisses, 525 ± 12 m.y. (0.7033). Basic rocks give similar results--metagabbroic rocks of Sauviat, 520 m.y. (U/Pb by Gebauer and Bernard-Griffiths, 1978). Younger ages (Ordovician and Silurian) have been measured on fine-grained metagranites or metavolcanics--St. Yrieix, 468 ± 8 m.y. (0.7075); Meuzac, 448 ± 9 m.y. (0.7098); fine-grained Thaurion granite (with lepidomelane and hastingsite), 462 ± 12 m.y. (0.7072). The youngest age has been measured on strongly alkalic feldspar-rich gneisses from Aubazine--434 ± 8 m.y. (0.714). All of the above results are interpreted as times of intrusion. Although the chronology of tectonic and metamorphic episodes might be different in other areas, similar early Paleozoic ages have been measured--Mendic granite from Montagne Noire, 500 ± 20 m.y. (0.7065) (Hamet and others, 1976); metaquartz diorite from Lot, 540 ± 15 m.y. (U/Pb by Pin and Lancelot, in press); Yseron ortho-gneiss from Lyonnais 502 ± 7 m.y. (0.7073); porphyritic Tauve alkalic metagranite from Dordogne 427 ± 5 m.y. (0.7098).

Again, in Limousin, the peak of the first metamorphic phase (Barrovian-type) is dated by diatexites from Thaurion metagranites at 375 m.y. (0.7152) during an intra-Devonian event (Acadian orogeny) (Bernard-Griffiths and others, 1977). That this Acadian event is a general one throughout the Massif Central remains to be proved. In the south, the major phase of metamorphism is younger--anatectic granites of the central Montagne Noire give a Carboniferous age of 323 m.y. (Hamet and Allegre, 1976) reflecting an Hercynian event. In the southeast, the broad anatectic area of the Velay, related to the second low-pressure metamorphic phase, is not yet geochronologically dated, but its age most likely is also Hercynian.

POST-TECTONIC MAGMATISM

Classically, in the Massif Central, the numerous post-tectonic granites are divided into two main groups, in relation to the widespread upper Visean calc-alkaline rhyodacitic volcanic tuffs and ignimbrites.

Pre-late Visean Magmatism

The oldest granites have been dated at 335 to 345 m.y.; for example: cordierite-bearing granite of Guéret, 355 ± 10 m.y. (0.7098); monzonitic Aureil granite, 346 ± 14 m.y. (0.7114); Bois Noir granite, 346 ± 8 m.y. (0.704); leucocratic Chateauponsac two-mica granite, 348 ± 6 m.y. Quartz diorites or tonalitic rocks from Limousin have recently been dated at about 360 m.y. (U/Pb by Gebauer and Bernard-Griffiths, this conference). Until now, no pre-upper Visean granites have been dated in the southern part of the Massif Central.

Post-late Visean Magmatism

This group is broadly distributed throughout the massif; it includes various calc-alkaline granodiorites, monzonitic granites, and two-mica leucogranites. Their ages are between 330 and 280 m.y. old. In the Limousin, two-mica leucogranites of probable crustal anatectic origin give, for example: St. Sylvestre, 326 ± 18 m.y.; Blond, 301 ± 5 m.y.; Esse monzonitic granite, 315 ± 10 m.y. From the Cevennes area, we may include the Mt. Lozère biotite granite of 293 ± 15 m.y. and two-mica granite of 291 ± 11 m.y. The relatively low initial $^{87}Sr/^{86}Sr$ (0.706 - 0.711) from the granites probably reflects a short history for the underlying sialic crust. The youngest presently dated igneous rock is the Chateau Montgilbert granite, whose age is 282 ± 8 m.y. (late Stephanian to Early Permian). This period corresponds with the final cratonization for all of this region, which, afterwards was subjected only to late Hercynian faulting and intense erosion to form molassic detrital basins of Permian age.

CONCLUSION

During the lower Paleozoic (Cambrian to Silurian), an important basic to acidic magmatic episode seems to have occurred in the Massif Central. These results are not peculiar to this region; similar dates have already been measured elsewhere in the Hercynian orogenic belt. More detailed petrographic and geochemical work is necessary to identify possible magmatic polarity and to understand more clearly its geodynamic meaning. In the western part of the maffic, tholeiitic and late alkaline magmatism seems to be characteristic and related to movements at a continental margin under extension; no typical ophiolitic association may be found in the Massif Central. Subduction, which occurs during Late Silurian and Early Devonian time (400 - 340 m.y.) could account for the high-pressure phase (370 m.y.) of blue schist metamorphism found mostly in the west (South Britany Vendée), and for the calc-alkaline quartz diorite to granodiorite intrusions (360 - 345 m.y.). Hercynian history could be explained by continental collision processes, as proposed by various authors, with great thrusting phases of the Himalayan type, low-pressure metamorphism well-developed in the south and southeast, and leucogranitic plutonic intrusions. During Devonian to Dinantian time, the northeast was affected by intense volcanic activity--basic, spilitic pillow lavas in the Brevenne, and rhyodacitic subaerial volcanic tuffs of possible island arc type. Between the different parts of the Massif Central, some differences appear--Early Carboniferous (pre-Visean) post-orogenic magmatism is mainly located in the northern half of the Massif. In contrast, the post-Visean

group of plutons are well represented throughout the Massif Central. Uplift and erosion began earlier in the north. If the two metamorphic episodes are well divided in Lyonnais, they are more continuous in Limousin, where the rocks are less affected by Hercynian phases. This is emphasized by K-Ar hornblende ages of 350 to 300 m.y., related to post-metamorphic cooling and uplift, although these dates show a complex pattern owing to thermal domes associated with the numerous Upper Carboniferous plutons. Finally, all these geochronological results for magmatic rocks and metamorphic events during the Paleozoic reveal the history of the Massif Central, the orogenic phases of which occur in a broad Acadian-Hercynian cycle.

Bernard-Griffiths, J., Cantagre, J. M., and Duthou, J. L., 1977, Contributions to Petrology and Mineralogy, v. 61, p. 199-212.

Bernard-Griffiths, J., 1975, Ann. Scient. Univ. Clermont, 55, n°27.

Cantagrel, J. M., 1973, Ann. Scient. Univ. Clermont, 50, n°24.

Coffrant, D., and Piboule, M., 1975, Bulletin de la Societe Géologique de France, 7, XVIII n°4, 620-628.

Duthou, J. L., 1977, Ann. Scient. Univ. Clermont, 63, n°30.

Gebauer, D., and Bernard-Griffiths, J., 1978: (this conference).

Hamet, J., and Allegre, C. J., 1976, Geological Society of America Bulletin, v. 87, p. 1429-1442.

_____1976, Hercynian orogeny in the Montagne Noire (France); application of Rb^{87}-Sr^{87} systematics: Geological Society of America Bulletin, v. 87, p. 1429-1442.

Pin, C., and Lancelot, J., (in press), Bulletin de la Societe Géologique de France.

IMPLICATIONS FOR THE STRUCTURE OF CHEMICAL HETEROGENEITY IN THE MANTLE FROM Nd AND Sr ISOTOPIC VARIATIONS

By R. W. Carlson[1], J. D. Macdougall[1], and G. W. Lugmair[2]

[1]Scripps Institution of Oceanography
University of California, San Diego
La Jolla, California 92093

[2]Department of Chemistry
University of California, San Diego
La Jolla, California 92093

The isotopic composition of Sr and Nd in basaltic rocks provides important information on the composition and history of their source materials in the upper mantle. However, a thorough understanding of the processes which can lead to differences between the isotopic composition of a basalt and that of its source is critical to the correct interpretation of the isotopic data. Of the basalts present on the earth, oceanic-ridge basalts appear to have been the least modified isotopically by the materials with which they interacted on their way to the surface. Extensive Sr isotopic data on oceanic-ridge tholeiites show, to a first order, a remarkably narrow range of initial $^{87}Sr/^{86}Sr$ composition, which is also the least radiogenic Sr found on the earth today. The Nd isotopic data available for oceanic tholeiites also indicate a rather homogeneous source for these basalts. Our measurements of oceanic tholeiites (table 1) from the three major ocean basins show a range of $^{143}Nd/^{144}Nd$ from about 0.51310 to 0.51323, with no resolvable differences between ridge basalts from the Pacific, Atlantic, and Indian Oceans. This range is comparable to that measured by DePaolo and Wasserburg (1976a,b) and O'Nions and others (1977). Presumably this narrow range represents the derivation of ocean-ridge basalts from a relatively homogeneous mantle reservoir which underlies all of the world's ocean basins.

On the other hand, ocean-island basalts commonly display a rather large variation in both chemical and isotopic composition. This variation is not restricted to oceanic islands but has been found to exist in basalts erupted in close proximity along oceanic ridges (Batiza and others, 1977). In the area of the Siqueiros fracture zone (East Pacific Rise) studied by Batiza and others (1977), nepheline normative basalts and rather high Mg abyssal tholeiites were recovered within a few kilometers of one another. The Nd isotopic data for these basalts reflect the compositional difference, as a nepheline normative basalt (SD 8-5) has a significantly lower $^{143}Nd/^{144}Nd$ than a tholeiite (SD 8-3) (table 1). One explanation of this type of chemical and isotopic variation found on a small geographic scale, is the variable influence of trace quantities of incompatible element-rich phases. It is difficult to evaluate the importance of these trace phases in

Table 1.--Nd isotopic composition of some oceanic tholeiites

Sample	Sm (ppm)	Nd (ppm)	$^{147}Sm/^{144}Nd$ [1]	$^{143}Nd/^{144}Nd$ [2]	JUV(T)
Pacific Ocean					
SD 8-3, tholeiite-----	2.16	5.75	0.226	0.513177±26	+10.6±5
SD 8-5, alkali basalt-	6.47	28.12	0.139	0.512993±34	+ 7.0±7
Atlantic Ocean					
DSDP 3-14, tholeiite--	1.62	3.60	0.273	0.513241±30	+11.5±6
DSDP 3-18, tholeiite--	1.40	3.17	0.267	0.513122±18	+ 9.3±4
TR 123-4g, tholeiite--	1.59	3.88	0.247	0.513109±17	+ 9.2±4
Indian Ocean					
D 113, tholeiite------	3.41	9.71	0.213	0.513181±39	+10.6±8
D 114, tholeiite------	3.22	9.76	0.200	0.513119±25	+ 9.4±5

[1]Uncertainty = 0.1 percent.
[2]Nd measured as NdO^+, fractionation corrected to $^{148}NdO/^{144}NdO = 0.242436$ ($^{148}Nd/^{144}Nd = 0.241572$). Data accurate to 95 percent confidence level.

determining the trace-element character of a basalt. However, a strong argument against the disequilibrium melting of such phases as a method of producing isotopic variation, is the fact that individual islands commonly exhibit nearly constant isotopic composition despite wide variations in the chemistry of the basalts.

An alternative explanation of the difference in isotopic composition of abyssal tholeiites and island basalts is the presence of chemically distinct basalt source reservoirs within the mantle. The distribution of these reservoirs is not well constrained. Models of a vertically stratified upper mantle generally place a layer of "depleted" mantle above an "undepleted" deep mantle, although a recent model (Tatsumoto, 1978) reverses this stratification. In a two-reservoir model, the diversity of isotopic composition of island basalts can easily be explained by invoking various degrees of mixing between depleted and undepleted materials. This mixing is seemingly well displayed in the region around Iceland (Schilling, 1971). The isotopic data on Hawaii, however, does not fit a simple mixing model between two reservoirs. The data of O'Nions and others (1977) on a wide spectrum of Hawaiian basalts suggest that $^{143}Nd/^{144}Nd$ increases with decreasing Sm/Nd. This apparent trend between $^{143}Nd/^{144}Nd$ and Sm/Nd ratio is difficult to explain but could conceivably be the result of the interaction of liquid with a low $^{143}Nd/^{144}Nd$, with materials of the high $^{143}Nd/^{144}Nd$ oceanic mantle. However, the positive correlation of $^{143}Nd/^{144}Nd$ with Nd concentration, which would be expected for various mechanisms of incompatible element transfer, is lacking in the Hawaiian samples.

While models of a vertically stratified mantle can provide an adequate explanation for much of the island isotopic data, we have shown recently (Carlson and others, 1978) that small but significant deviations in Nd isotopic composition can occur even along "normal" ridge segments. This observation is apparent in the Siqueiros data and also in the results for basalts from Leg 3 of the Deep Sea Drilling Project. DSDP basalt samples 3-14 and 3-18 (table 1) are both high-Mg tholeiites (MgO/MgO + FeO* = 0.54 and 0.56, respectively) with similar major and trace-element compositions (Frey and others, 1974). The difference in $^{143}Nd/^{144}Nd$ of these two basalts can only be the result of subtle differences in the Sm/Nd ratio of their sources. The magnitude of the isotopic difference requires $\sim 10^9$ yr of separation of their respective source materials. The result and the variance displayed on a small geographic scale near the Siqueiros fracture zone seem to indicate the existence of heterogeneities within the mantle source of oceanic tholeiites. The magnitude of the measured heterogeneity is small compared to the variation found among oceanic islands. However, the concept of a mantle with isolated heterogeneous areas, as opposed to a vertically stratified mantle, leads to two fundamentally different interpretations of the history of the Earth's mantle.

If a heterogeneous mantle is to be a favored interpretation for the isotopic variation found in oceanic rocks, then it becomes necessary to determine the nature of the heterogeneity (that is, vertically stratified versus corpuscular segregation) before meaningful models of the evolution of the Earth's mantle can be derived. Isotopic data on continental basalts can possibly provide information on the structure of chemical variation in the mantle. Continental basalts consistently have higher $^{87}Sr/^{86}Sr$ than that considered to be a characteristic of "oceanic" mantle (~ 0.7026). Also, the work of DePaolo and Wasserburg (1976a,b) has shown that a lower value for $^{143}Nd/^{144}Nd$ exists in continental basalts compared to the values found for oceanic tholeiites. The distinct difference between oceanic and continental basalt trace-element and isotopic characteristics suggests that mantle with oceanic (depleted) character may not exist under the continental platforms. However, the available Sr isotopic data on the most extensively studied of the continental flood-basalt provinces, the Columbia River province (McDougall, 1976), indicate a very wide range in $^{87}Sr/^{86}Sr$ within the basalts. This variance is also apparent in the limited Nd isotopic measurements (DePaolo and Wasserburg, 1976b). It is not yet apparent whether this range is indicative of multiple mantle sources or reflects varying degrees of interaction with the materials that the magma came in contact with prior to eruption.

We are currently undertaking a study of the Nd and Sr isotopic composition of the variety of basalt sequences found in the Columbia River province. The relative behavior of the Sr and Nd isotopic systems can potentially provide an indication of the process(es) which lead to this chemical and isotopic variation. The evaluation of the isotopic modifications, which these magmas incurred in the interval between the separa-

tion from their source material and the time of their eruption, is critical to any meaningful model of the isotopic composition of the mantle underlying the Columbia Plateau.

Batiza, R., Rosendahl, B. R., and Fisher, R. L., 1977, Evolution of the oceanic crust 3. Petrology and chemistry of basalts from the East Pacific Rise and the Siqueiros Transform Fault: Journal of Geophysical Research, v. 82, p. 265-276.

Carlson, R. W., Macdougall, J. D., and Lugmair, G. W., 1978, Differential Sm/Nd evolution in oceanic basalts: Geophysical Research Letters, v. 5, p. 229-232.

DePaolo, D. J., and Wasserburg, G. J., 1976a, Nd isotopic variations and petrogenetic models: Geophysical Research Letters, v. 3, p. 249-252.

_____1976b, Inferences about magma sources and mantle structure from variations of $^{143}Nd/^{144}Nd$: Geophysical Research Letters, v. 3, p. 743-746.

Frey, F. A., Bryan, W. B., and Thompson, G., 1974, Atlantic Ocean floor - Geochemistry and petrology of basalts from legs 2 and 3 of the Deep Sea Drilling Project: Journal of Geophysical Research, v. 79, p. 5507-5527.

McDougall, I., 1976, Geochemistry and origin of basalt of the Columbia River Group, Oregon and Washington: Geological Society of America Bulletin, v. 87, p. 777-792.

O'Nions, R. K., Hamilton, P. J., and Evensen, N. M., 1977, Variations in $^{143}Nd/^{144}Nd$ and $^{87}Sr/^{86}Sr$ ratios in oceanic basalts: Earth and Planetary Science Letters, v. 34, p. 13-22.

Schilling, J. G., 1971, Iceland mantle plume - geochemical study of the Reykjanes Ridge: Nature, v. 242, p. 565.

Tatsumoto, M., 1978, Isotopic composition of lead in oceanic basalt and its implication to mantle evolution: Earth and Planetary Science Letters, v. 38, p. 63-87.

DETERMINATION OF THERMAL NEUTRON FLUX FOR FISSION TRACK GEOCHRONOLOGY

By B. Stephen Carpenter
Inorganic Analytical Research Division
Center for Analytical Chemistry
National Bureau of Standards
Washington, D.C. 20234

The nuclear track technique (NTT) has been applied in geology since Price and Walker (1962) found that natural mica contained a number of fission tracks from the spontaneous fission decay of ^{238}U. With this discovery and the simplified age equation suggested by Price and Walker (1963), the geologist had a new tool for determining ages of various minerals. The age determination from the following equation:

$$A = \frac{\rho_s}{\rho_i} \cdot \frac{I(\Phi t)\hat{\sigma}}{\lambda_f^{238}}$$

where,

A = Age of sample (yr)
ρ_s = Spontaneous fission track density (tracks cm^{-2})
ρ_i = Induced fission track density (tracks cm^{-2})
I = Isotopic ratio of $^{235}U/^{238}U$
(Φt) = Total neutron fluence component ($n\ cm^{-2}$)
$\hat{\sigma}$ = Effective cross-section for the ^{235}U (n,f) reaction (cm^2)
λ_f^{238} = Spontaneous fission decay rate of $^{238}U(yr^{-1})$,

was based on the simple theory that the absolute rate at which spontaneous fission events or tracks from ^{238}U accumulate in minerals is proportional to the uranium content and, therefore, the measurement of both the spontaneous track abundance and the uranium content is necessary. The uranium content is determined simply by inducing fission in a measurable portion of the uranium. This measurement utilizes the fact that thermal neutrons cause fission of ^{235}U. The final step in measuring the age is to count the spontaneous tracks. The sample is then exposed to a known thermal neutron fluence in a nuclear reactor and the newly induced tracks are counted. The age is then calculated from the ratio of these two track densities together with the thermal neutron fluence.

The simplicity of both the technique and the theory has caused difficulties and problems in the determination of ages. One of the problems arose in selecting the best decay constant because several values exist. To a large extent, this problem has been resolved by reporting the value used in the determination. However, the neutron fluence value cannot be as easily resolved, because each nuclear reactor is unique and their neutron spectra will vary.

The neutron flux, Φ(n cm^{-2} s^{-1}), is comprised of two components and is defined as:

$$\Phi = \phi_{th} + \int_{0.5ev}^{\infty} \phi_{epi}(E)dE$$

where ϕ_{th} is the thermal neutron flux, ϕ_{epi} is the epithermal neutron flux per unit of energy, and dE is the energy interval. The contribution from each of these components to the total neutron flux is a function of sample position relative to the core during irradiation and the type of moderation used. As the neutron flux changes with energy, so does the effective cross-section, $\hat{\sigma}$, for the ^{235}U (n,f) reaction which is defined as:

$$\hat{\sigma} = \sigma_o \left(1 + \frac{\phi_{epi} \cdot I_o}{\phi_{th} \cdot \sigma_o}\right)$$

where σ_o = 582 x 10^{-24} cm^2 is the cross-section of ^{235}U for 2200 m sec^{-1} neutrons, and I_o is the resonance integral for the ^{235}U (n,f) reaction at infinite dilution.

$$I_o = \int_{0.5ev}^{\infty} \frac{\sigma(E)}{E} dE = 280 \times 10^{-24} \text{ cm}^2.$$

If the flux is not highly thermalized, a large fraction of fissions will be induced from ^{235}U, as well as ^{238}U and ^{232}Th, by epithermal neutrons.

There are several ways by which either the total neutron flux or the thermal neutron flux can be determined. One method of determining the neutron flux, as suggested by Fleischer and others (1975), Carpenter and Reimer (1974), and Kleeman and Lovering (1970), is to use glasses with known uranium content that are then irradiated with metal foils. The radioactivity produced from the metals during the irradiation is used to determine the neutron flux. The neutron flux observed by the metal foil is related to the track density produced in the glass.

In order to determine the thermal activity, A_{th}, induced from the total activity, A_{tot}, in the foil monitor, it is necessary to know the cadmium ratio R_{cd} of the metal foil for the irradiation position used. If the absorption of part of the epithermal neutrons in the cadmium shield is neglected, then $A_{th} = A_{tot}(1-1/R_{cd})$. Finally, the thermal neutron flux is calculated from the activation equation:

$$\phi_{th} = \frac{A_{th}}{N\sigma_m} (1-e^{-\lambda_m t})^{-1}$$

where N is the number of target atoms present in the metal foil; σ_m is the thermal cross section of the atoms in the metal foil, cm^2; λ_m is the decay constant of the product nuclide; and t is the irradiation time.

Carpenter, B. S., and Reimer, G. M., 1974, Calibrated glass standards for fission track use: National Bureau of Standards Special Publication 260-4.

Fleischer, R. L., Price, P. B., and Walker, R. M., 1975, Nuclear tracks in solids, principles and applications, Berkeley, University of California Press, p. 159-214.

Kleeman, J. D., and Lovering, J. F., 1970, The evaluation of the spatial parameters K and α in equations for fission track uranium analysis: Radiation Effects, v. 5, p. 233-237.

Price, P. B., and Walker, R. M., 1962, Observation of fossil particle tracks in natural micas: Nature, v. 196, p. 732-734.

_____1963, Fossil tracks of charged particles in mica and the age of minerals: Journal of Geophysical Research, v. 68, p. 4847-4862.

CORRELATION OF REWORKED ASH DEPOSITS; THE KBS TUFF, NORTHERN KENYA

By T. E. Cerling[1], B. W. Cerling[2], G. H. Curtis[2], R. E. Drake[2], and F. H. Brown[3]

[1]Oak Ridge National Laboratory
Oak Ridge, Tennessee 37830

[2]Department of Geology and Geophysics
University of California
Berkeley, California 94720

[3]Department of Geology
University of Utah
Salt Lake City, Utah 77016

Reworked ash deposits present unique correlation problems not encountered in airfall deposits. Rapid downcutting by vigorous streams in a newly-blanketed ash terrain may incorporate ash and pumice from other volcanic deposits, and detrital minerals from older

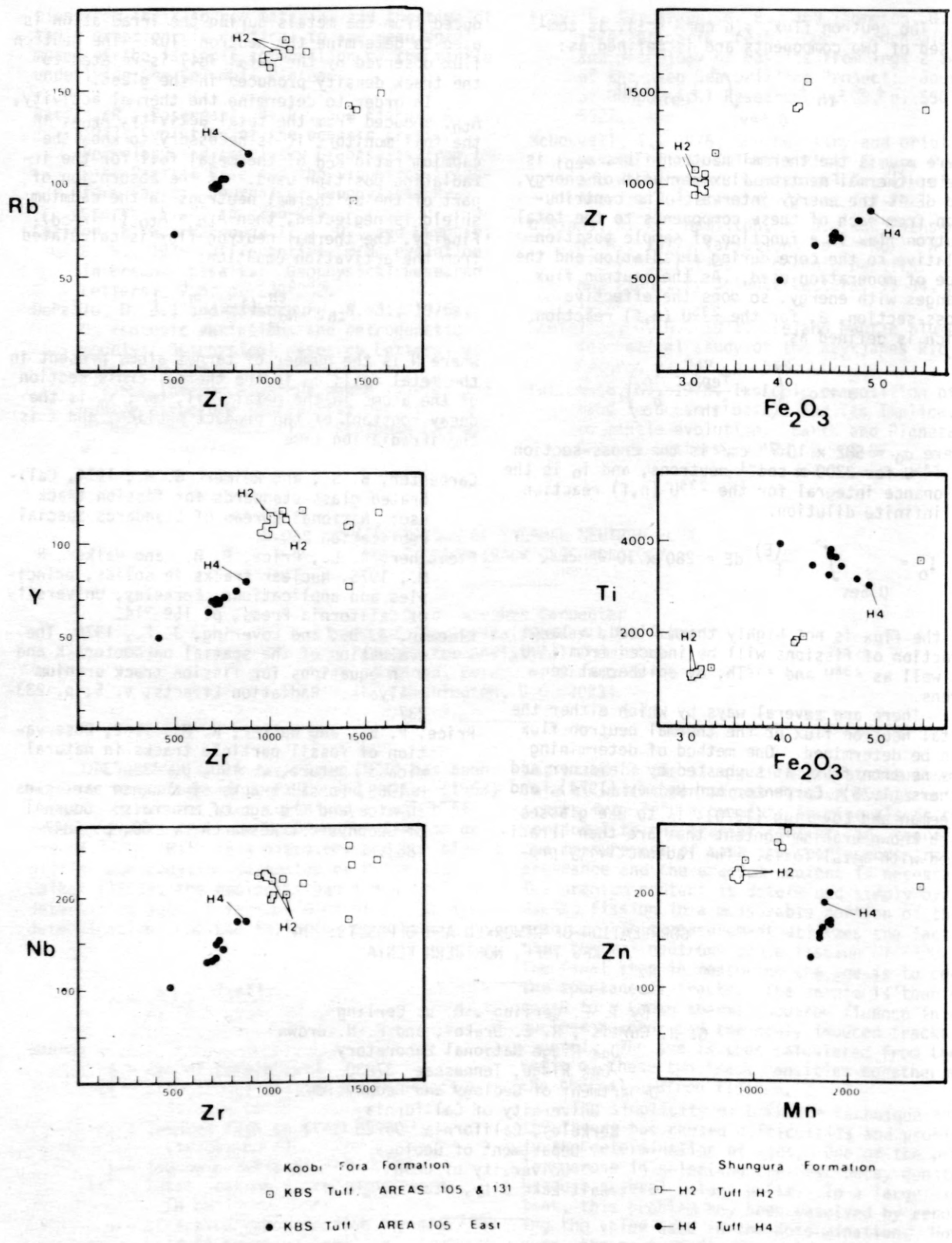

Figure 1.--Trace-element trends in pumice collected from the Koobi Fora and Shungura Formations.

sediments. Abrasion of the distinctive glass mantles on primary crystals and their dilution by detrital minerals may remove the possibility of using distinctive mineral suites for correlation. When ash deposits with differing glass compositions are mixed together, trace-element comparisons on whole-rock or pure glass separates are of dubious value; incorporation of older pumice may result in erroneous dates of ash deposits.

Fluvial tuffs in the Koobi Fora and Shungura Formations of northern Kenya and southern Ethiopia are important marker horizons in these hominid-rich Pliocene-Pleistocene sediments. Correlation and chronology of the KBS Tuff in the Koobi Fora Formation is controversial: Curtis and others, (1975) propose that more than one tuff is presently mapped as the KBS Tuff and has at least two age components of about 1.8 and 1.6 m.y. Other workers believe only one tuff is represented and is 2.4 to 2.6 m.y. old (Fitch and others, 1976; Hurford and others, 1976). Electron microprobe studies of glass shards in other tuffs within this stratigraphic succession show that some ash units contain several populations of glass shards with differing compositions. This may indicate mixing of several different ash units. Because pumice is more likely than tuffs to be homogeneous, glass separates were made from pumice collected from four outcrops of the KBS Tuff and from Tuffs H2 and H4 of the Shungura Formation, 100 kilometers north. KBS outcrops are in fossil-collecting localities known as Area 105, Area 105-East, and Area 131.

Analyzed glass separates from eight pumice localities in Area 131 fall into three distinctive compositional groups (fig. 1) that are low, intermediate, and high in iron content (3 percent, 4 percent, and 5.5 percent Fe_2O_3, respectively). Two pumice samples from the KBS Tuff in Area 105 have compositions that also fall in the low iron group. Two pumice samples in Area 105-East show a distinctly different compositional trend that resembles a comendite-pantellerite differentiation series (Weaver and others, 1972). Conventional K-Ar dating was carried out on all compositional groups in the event that older pumice were incorporated into the ash deposit; no evidence for this type of reworking was found. Trace-element and K-Ar data indicate a probable correlation of Tuff H2 of the Shungura Formation with one of these tuffs and a possible correlation of Tuff H4 with the other (fig. 1). These dates indicate ages of about 1.80 and 1.75 m.y. for these two tuffs; several dates averaging about 1.6 m.y. ago were obtained on sanidine concentrates from extremely leached pumice collected in several other outcrops. Thus, at least two and possibly three separate "KBS" Tuffs have been identified.

Curtis, G. H., Drake, R. E., Cerling, T. E., Cerling, B. W., and Hampel, J. H., 1975, Age of KBS Tuff in Koobi Fora Formation, northern Kenya: Nature, v. 258, p. 395-398.

Fitch, F. J., Hooker, P. J., and Miller, J. A., 1976, $^{40}Ar/^{39}Ar$ dating of the KBS Tuff in Koobi Fora Formation, East Rudolf, Kenya: Nature, v. 263, p. 740-744.

Hurford, A. J., Gleadow, A J. W., and Naeser, C. W., 1976, Fission-tract dating of pumice from the KBS Tuff, East Rudolf, Kenya: Nature, v. 263, p. 738-740.

Weaver, S. D., Sceal, G. S. C., and Gibson, I. L., 1972, Trace-element data relevant to the origin of trachytic and pantelleritic lavas in the East African Rift System: Contributions to Mineralogy and Petrology, v. 36, p. 181-194.

ISOTOPIC, GEOCHEMICAL, AND FAUNAL EVIDENCE FOR PLEISTOCENE CLIMATIC CHANGE IN EAST AFRICA

By T. E. Cerling[1], R. L. Hay[2], and J. R. O'Neil[3]

[1]Oak Ridge National Laboratory, Oak Ridge, Tennessee

[2]Department of Geology and Geophysics, University of California, Berkeley, California

[3]U. S. Geological Survey, Menlo Park, California

Terrestrial evidence for climatic trends through the Pliocene and Pleistocene is rare because few terrestrial deposits that span this period are accessible and contain suitable material for dating. However, active volcanism and deposition accompanied by faulting in the Rift Valleys of East Africa has resulted in good exposures of eolian, fluvial, deltaic, and lacustrine deposits. Excellent sections ranging from more than 4 m.y. to 1.3 m.y. ago are found

at Lake Turkana in northern Kenya; Olduvai Gorge in northern Tanzania has sediments ranging in age from 2.0 m.y. to the present. Geochemical evidence for climatic change includes isotopic studies of carbonates and modern water, as well as changes in authigenic mineral assemblage; physical evidence includes the extent of eolian and deltaic deposits versus lacustrine deposits; faunal evidence includes both invertebrate and vertebrate fossils.

Lake Turkana, Northern Kenya: The isotopic record at Lake Turkana is preserved in lacustrine nodules formed in lake and lake margin sediments. Samples from the Lower Member (> 1.8 m.y.) of the Koobi Fora Formation are depleted in ^{18}O whereas those in the Upper Member (< 1.8 m.y.) are enriched in ^{18}O (fig. 1A). Extrapolation of sedimentation rates between dated horizons places this "event" between 2.0 and 1.7 m.y. ago. This coincides with changes in authigenic mineral assemblages and faunal remains. The only occurrence of clinoptilolite, the oldest zeolite in this sedimentary succession, is found in the KBS Tuff (1.8 m.y., Curtis and others, 1975). Analcime and chabazite are common between 1.5 and 1.3 m.y.; dolomite first occurs at about 1.7 m.y., and is common to about 1.3 m.y. Faunal changes also document this transition. Several molluscan forms become extinct at about the KBS level (P. Williamson, oral comm.). Mammals also indicate drier climates starting about 1.8 m.y. ago--a fauna dominated by forest and bush forms gave way to one with dominantly open plains elements (Gentry, 1976; Harris, 1976). Increased deltaic deposits and an unstable shoreline after 1.8 m.y. suggest that the lake changed from a permanently open basin to one that was periodically closed. The abrupt disappearance of all deposits after the Chari Tuff (1.3 m.y.) indicates that either another major climatic change took place or that a major tectonic event occurred. The climate today is probably drier than most periods of the Upper Member as evidenced by the complete disappearance of many bovids and primates.

Olduvai Gorge, Northern Tanzania: Sediments of Olduvai Gorge contain an almost complete record of the Pleistocene. Caliches show major deviations in $\delta^{18}O$ at 1.65 m.y., 1.2 m.y., and 0.55 m.y. ago (fig. 1B). This coincides with changes in authigenic mineralogy; it is most clear in the eolian tuff lithofacies. Unaltered glass, montmorillonite, and rare zeolites occur in Bed I (2.0 to 1.7 m.y.); extensive zeolites (principally phillipsite) and dolomite occur in the Lemuta Member (1.6 to 1.7 m.y.); Upper Bed II, Bed III, and Bed IV do not have eolian tuffs but montmorillonite in claystones is extremely altered to illite. For rocks deposited from Masek time (0.55 m.y.) to the present, montmorillonite is altered to illite in claystones, and authigenic zeolites, analcime, dolomite, and dawsonite ($NaAl(OH)_2CO_3$) are common in eolian tuffs. Extensive eolian

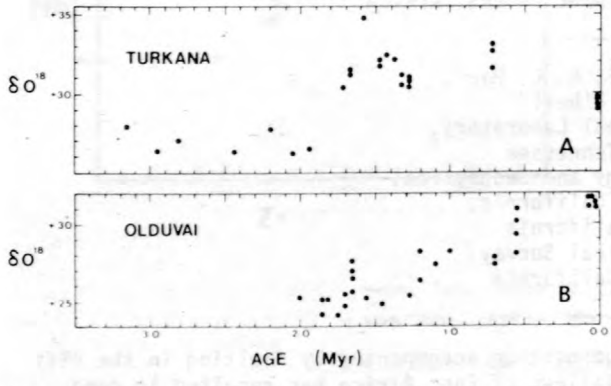

Figure 1.--Relationship between time and $\delta^{18}O$ of carbonates: A, Lake Turkana; B, Olduvai Gorge.

ORNL-DWG 78-6163

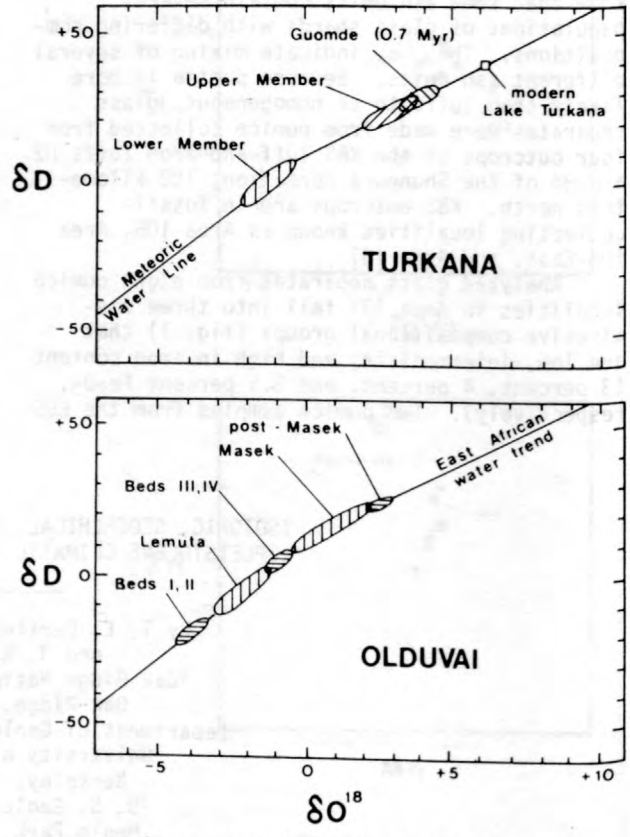

Figure 2.--Estimated isotopic compositions of paleo-ground waters from Lake Turkana and Olduvai Gorge. This assumes isotopic equilibrium of calcite and water at 25°C and that the waters lie along the meteoric water line or the evaporation line of Craig (1961).

activity occurs in the Lemuta Member and rocks deposited from Masek time to the present. Urocyclid slugs in Bed I indicate swampy conditions; the land snail Limicolaria first appears in the Masek Beds (Hay, 1976). An abrupt change in mammals occurs at the Lemuta Member--below this swamp-dwelling forms predominate; above it plains-animals occur (Hay, 1976).

Changes in isotopic composition of carbonates in these terrestrial sediments are most likely due to changes in the isotopic composition of water. East African lakes lie close to the evaporation line of Craig (1961; $\delta D = 5\ \delta^{18}O + 10$). Changes in temperature only would require that the later deposits formed under cooler conditions; however, authigenic minerals, fauna, and flora all indicate that the more recent deposits formed under more arid conditions. Olduvai Gorge presently has a mean annual soil temperature of 25.6°C and a mean annual air temperature of about 23°C (Hay, 1976); presence of mammals requiring abundant water and foliage in Bed I precludes temperatures significantly warmer than today. Therefore, it is most likely that the isotopic changes observed are due to changes in the isotopic composition of water because of increasing aridity. A preliminary estimate of the paleoisotopic composition of ground water is shown in figure 2. This estimate is based on the assumption that isotopic changes in carbonates are due only to changes in the isotopic composition of water. Lower temperatures during the earlier, more moist periods would result in an increased spread in these values.

Correspondence in timing between the two areas is only suggestive. At Lake Turkana the change in isotopic composition of carbonates occurs between 2.0 and 1.7 m.y. ago; faunal changes occur about 1.8 m.y. ago; the first zeolite at 1.8 m.y., and the first dolomite at 1.7 m.y. At Olduvai Gorge, isotopic, geochemical, faunal, and sedimentologic evidence for drier conditions occur at 1.65 m.y. From 1.65 to 1.2 m.y., isotopic values return to previous lower values whereas at Lake Turkana they do not. The second major change in isotopic compositions occurs at 1.2 m.y. at Olduvai Gorge; at Lake Turkana this corresponds to the end of sedimentation for either climatic or tectonic reasons. The third change at Olduvai occurs at about 0.55 m.y.; no sediments of this age are found at Lake Turkana. These data suggest progressively drier conditions at about 1.65 to 1.8 m.y., 1.2 m.y., and 0.55 m.y.

Craig, H., 1961, Isotopic variations in meteoric waters: Science, v. 133, p. 1702-1703.

Curtis, G. H., Drake, R. E., Cerling, T. E., Cerling, B. W., and Hampel, J. H., 1975, Age of KBS Tuff in Koobi Fora Formation, northern Kenya: Nature, v. 258, p. 395-398.

Harris, J. M., 1976, Bovidae from the East Rudolf succession, in Coppens, Y., and others (eds.), Earliest man and environments in the Lake Rudolf Basin, University of Chicago Press, p. 293-301.

Hay, R. L., 1976, Geology of the Olduvai Gorge, University of California Press, 203 p.

Gentry, A. W., 1976, Bovidae from the Omo Group deposits, in Coppens, Y., and others (eds.), Earliest man and environments in the Lake Rudolf Basin, University of Chicago Press, p. 275-292.

AGE AND ORIGIN OF THE SIERRA NEVADA BATHOLITH, CALIFORNIA

By J. H. Chen
Department of Geological Sciences,
University of California, Santa Barbara
California 93106

The volcanic-plutonic activity in the Sierra Nevada magmatic province records a segment of the tectonic history of the Cordilleran orogenesis from late Paleozoic to late Mesozoic. This study provides new information on the timing and geochemical nature of granitic rocks in the southern portion of the Sierra Nevada complex.

Eighty zircon and six sphene U-Pb ages have been determined from 26 plutons along a more or less continuous belt across the Sierra Nevada batholith between latitude 37°N and 36°15'N. Granitic plutonic rocks in this area range in age from 165 to 85 m.y. The Mesozoic magmatism was virtually continuous from about 134 to 85 m.y. ago. In this segment of the Sierra Nevada batholith, the U-Pb ages of plutons show an essentially symmetrical pattern with the youngest ones in the high part of the range--High Sierra Nevada Crest--and the older plutons on each side.

Initial $^{87}Sr/^{86}Sr$ values (r_o) and initial lead isotopic ratios have been determined for all 26 plutons in this region. From west to

east, the r_o values increase gradually from 0.7036 to 0.7075. On the other hand, the initial $^{206}Pb/^{204}Pb$ ratios (α_o) show a similar west to east increase in radiogenic nature (from 18.52 to 19.74) on the western part of the batholith. However, the α_o value decreases to 18.59 and then increases slightly to about 19.0 on the eastern margin. Both Pb and Sr isotopic data show a source region for the batholith that is laterally variable in composition. A low r_o value ($r_o < 0.704$) for plutonic rocks in the western margin of the batholith suggests mantle-derived source material, while a high r_o value ($r_o > 0.707$) for plutonic rocks in the central and eastern parts of the batholith suggests continental-crust derived source material.

In a r_o versus α_o diagram, a good correlation between Pb and Sr isotopes exists for granitic rocks emplaced 146, 110, and 100 m.y. ago, reflecting properties of the source rocks of the magma, rather than simple mixing of two components or natural contamination. Samples from the plutons emplaced in the central belt 83 to 103 m.y. ago have highly radiogenic Sr ($r_o \sim 0.7075$) and less radiogenic Pb ($\alpha_o \sim 18.6$) values. A possible source material for these plutons is a K-feldspar rich rock, probably an augen gneiss. In fact, these granitic rocks do contain K-feldspar phenocrysts.

In a $^{207}Pb/^{204}Pb$ versus $^{206}Pb/^{204}Pb$ diagram, all samples from the Sierran granitic rocks lie above the ocean regression line defined by the oceanic basalts, suggesting that there is at most only a small component of oceanic mantle lead in the Sierra Nevada batholith plutons. A secondary isochron age of 1.97 b.y. can be calculated from the slope of a regression line through the granitoid lead data. This age is within the range of the oldest Precambrian basement rocks in the Western Coast states. Lead and Sr data suggest an origin of the batholith from a source that might be at least in part Precambrian in age and different from the oceanic upper mantle.

CARBON ISOTOPE EFFECTS DURING THE PYROLYTIC FORMATION OF METHANE FROM COAL

By H. Moses Chung and William M. Sackett
Texas A & M University
College Station, Texas 77843

Stable carbon isotope compositions have provided important information on the origin and transformation of many naturally occurring carbonaceous substances. However, measurements on coal have not been particularly helpful with Craig (1953) reporting no temporal or spatial correlations between isotopic compositions and coal ages from the Tertiary to the Late Paleozoic and with Compston (1960) and Wickman (1956) reporting no correlation of isotopic compositions with percentages of carbon or hydrogen. In one study, Wickman (1953), did show a unidirectional trend in compositions of coals from the Late Carboniferous to the Pliocene in three different basins.

Pyrolysis of coals has been used with some trepidation by geochemists for many years (beginning with Mott in 1942) as a simulation of natural coalification processes. Mott described coalification as a series of gasification steps. Regardless of whether or not the laboratory pyrolysis experiments duplicate natural processes, these types of experiments have helped in understanding the structure of coal (Bhattacharyya and others, 1964: Friedrich and Juntgen, 1972). Consequently the study described below was based on the premise that if coals of different ranks are broken down by converting some functional groups into methane, the kinetics and stable carbon isotope effects associated with methane generation should give new insights into the characteristics of coalification processes.

A description of our experimental procedures is as follows: About ten weighted aliquots of homogenized samples are evacuated while being heated to about 100°C, effectively eliminating water, and are sealed in pyrex glass breakseals. The samples are placed in a furnace, usually at 500°C, and are withdrawn individually, at times determined by preliminary experiments, over a period of from one-half hour to several days. The gases generated in the breakseals are expanded into a vacuum system and the methane and any carbon monoxide are separated by fractional distillation at liquid-nitrogen temperature. This procedure quantitatively excludes any carbon dioxide also generated during pyrolysis. The carbon monoxide is selectively oxidized at 200°C to carbon dioxide which is separated from the methane by condensation at liquid-nitrogen temperature. The methane is then oxidized at 850°C, both oxidations taking place over cupric oxide. The carbon dioxide is measured manometrically and then transferred to an isotope ratio mass spectrometer for isotopic analysis. The amounts of methane are normalyzed to the sample weight and plotted versus time, as in figure 1, and their

isotopic compositions relative to their parent compositions versus the mole ratio of methane to the carbon in the parent are plotted, as in figure 2. For the purposes of this short paper, data are reported for a suite of coal samples obtained from the U.S. Geological Survey in Denver, Colorado. These samples from a variety of locations, listed in table 1, range in rank from lignite to anthracite.

As can be seen in figure 1, the generation of methane by pyrolysis at 500°C essentially stops after about 20 hours. The bituminous coal exhibits the greatest capacity for producing methane, anthracite the least. The solid lines in figure 2 show the changes in the isotopic compositions of methane relative to the compositions of the parent as a function of the amount of methane formed, expressed as the mole ratio of methane to that of carbon in the parent. Although the slopes of the lines change systematically from 30 permil per mole CH_4/mole carbon for lignite to 1900 permil for anthracite, isotopic fractionations (the extrapolations to zero amounts of methane formed) do not, when treated in this manner. However, by plotting the isotopic composition of the methane relative to the isotopic composition of the total accumulated methane as shown by the dashed lines in figure 2, fractionations of -1.8, -8.8, -10.4, and -12.1 are obtained for the lignite, sub-bituminous, bituminous and anthracite samples, respectively. Thus, both the slopes and isotope fractionations determined from our experimental curves are proportional to the ranking supplied by the U.S. Geological Survey. Other lignite and anthracite samples from other locations show the same trends as their representatives in the suite described here. Bituminous coals lie between the lignite and anthracite trends but uncertainties in the rank classifications assigned by other organizations make comparisons somewhat difficult.

Vitrinite reflectance has become the accepted parameter for the determination of coal

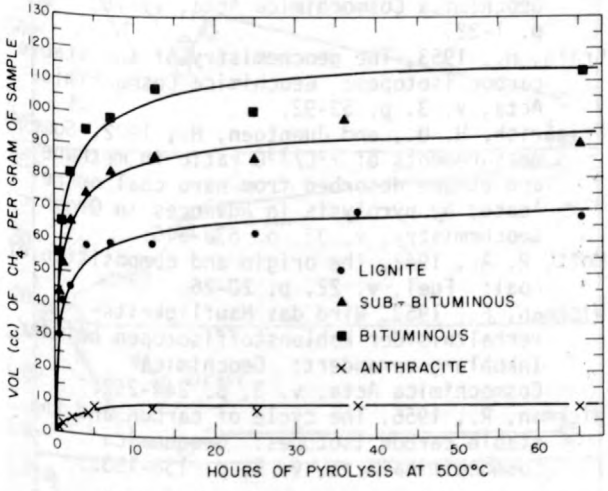

Figure 1.--Methane generation as a function of time.

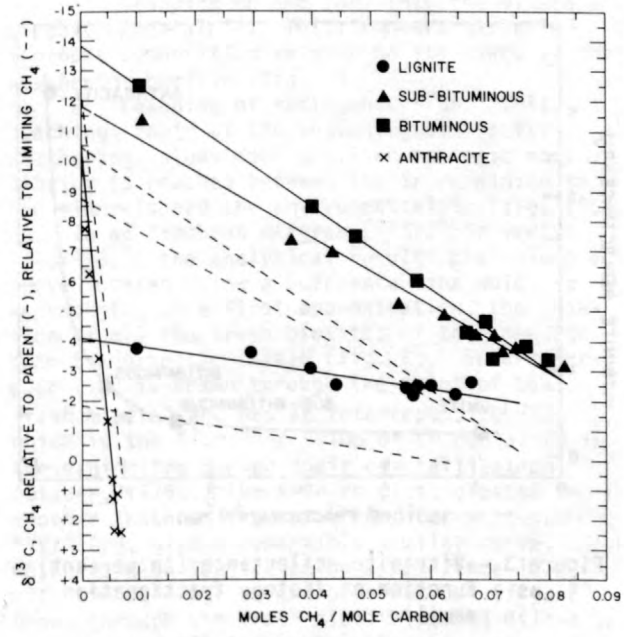

Figure 2.--$\delta^{13}C$ as a function of methane generated.

Table 1.--Descriptions and composition data for coals and their pyrolysis products

Rank[1]	Source[1]	Total Carbon		Limiting Methane	Isotope Fractionation (permil)	
		percent	$\delta^{13}C$ (permil vs PDB)	$\delta^{13}C$ (permil vs PDB)	vs Bulk Carbon	vs Limiting Methane
Lignite	Ward, N. Dak.	56	-23.2	-25.4	- 4.0	- 1.8
Sub-bitum.	Big Horn, Mont.	64	-23.9	-27.6	-11.9	- 8.2
Bituminous	Dickenson, Va.	75	-24.1	-27.5	-13.8	-10.4
Anthracite	Schuykill, Pa.	82	-23.4	-21.1	- 9.8	-12.1

[1]Samples and information provided by Vernon E. Swanson, U.S. Geological Survey.

rank. However, we feel that this parameter is less definitive than the method described above for ranking low-rank lignite to sub-bituminous coals. For example, figure 3, gives a plot of vitrinite reflectance versus experimentally determined isotope fractionations between initial and limiting methane for the same suite of coals. A large range in fractionations exists between lignite and bituminous coals, which allows for detailed rank classification.

To readers familiar with isotopic processes, carbon isotope exchange between methane and carbon monoxide and between methane and carbon dioxide to give anomalous compositions would seem to be a strong possibility. However, equilibration experiments at 500°C for the two systems, CH_4-CO_2-H_2O and CH_4-CO-H_2O, indicate that measurable carbon isotope exchange does not occur between methane and carbon dioxide and methane and carbon monoxide over the time periods used in our experiments.

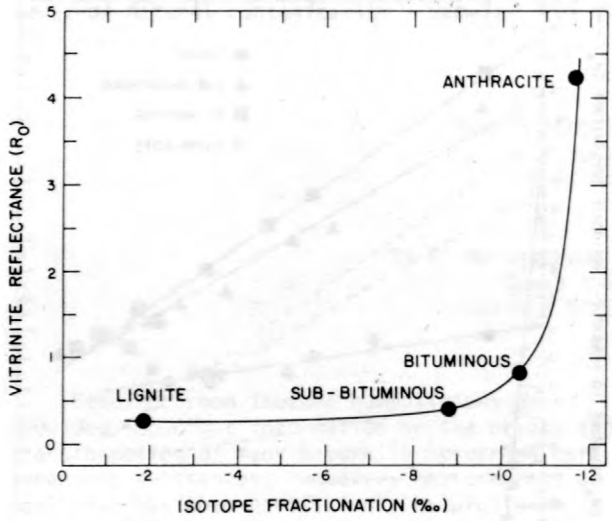

Figure 3.--Vitrinite reflectance (in percent) as a function of isotope fractionation (in permil).

A by-product of these studies is the experimental observation that oxygen-containing functional groups and methane-precursor functional groups in anthracites, as measured by the isotopic composition of the limiting methane, are enriched in carbon-13 as compared to the total carbon in coals. These are examples of the intramolecular heterogenous distribution of stable carbon isotopes, a phenomenon which provides important additional information on the formation, structure, and maturation of naturally occurring carbonaceous substances.

This work was supported by grants from the Robert A. Welch Foundation and the National Science Foundation.

Bhattacharyya, A. C., Mazumdar, A. D., and Lahiri, A., 1964, Studies on reduced coal I. Mechanism of coal pyrolysis: Fuel, v. 43, p. 181-202.

Compston, W., 1960, The carbon isotopic composition of certain marine invertebrates and coals from the Australian Permian: Geochimica Cosmochimica Acta, v. 18, p. 1-22.

Craig, H., 1953, The geochemistry of the stable carbon isotopes: Geochimica Cosmochimica Acta, v. 3, p. 53-92.

Friedrich, H. U., and Juentgen, H., 1972, Some measurements of $^{12}C/^{13}C$ ratio in methane and ethane desorbed from hard coal or released by pyrolysis in Advances in Organic Geochemistry, v. 33, p. 639-646.

Mott, R. A., 1942, The origin and composition of coal: Fuel, v. 22, p. 20-26.

Wickman, F., 1953, Wird das Haufligkeitsverhaltnis der Kohlenstoffisotopen bei der Inkohlung verandert: Geochimica Cosmochimica Acta, v. 3, p. 244-252.

Wickman, R., 1956, The cycle of carbon and the stable carbon isotopes: Geochemica Cosmochimica Acta, v. 9, p. 136-153.

BEHAVIOUR OF STRONTIUM AND ARGON ISOTOPES IN BIOTITES DURING A PROGRESSIVE NATURAL WEATHERING

By Norbert Clauer[1]
Centre de Sédimentologie et Géochimie de la Surface, Institut de Géologie, Université Louis Pasteur, 1 rue Blessig, 67084 - Strasbourg - Cedex, France
[1]Temporarily at the Department of Geology and Mineralogy, Ohio State University, 125 South Oval Mall, Columbus, Ohio 43210 (U.S.A.)

During the 4th European Colloquim of Geochronology in Amsterdam, the mineralogical, geochemical, and preliminary Rb-Sr isotopical results of progressively weathered biotites were presented (Clauer and Tardy, 1976). The study is now completed with additional Rb-Sr and new

K-Ar measurements, which will be compared to the behaviour of the Rb-Sr system.

The biotites come from a weathering profile located on the Guera granitic shield (Chad Republic in central Africa, fig. 1). They were extracted from one fresh and several weathered migmatitic rocks underlying kaolinitic and smectitic soils. The climate, characterized by a four-month humid season succeeded by a long dry period (annual rainfall is 850 mm with a mean annual temperature of 29°C), favors an intensive weathering of the exposed rocks.

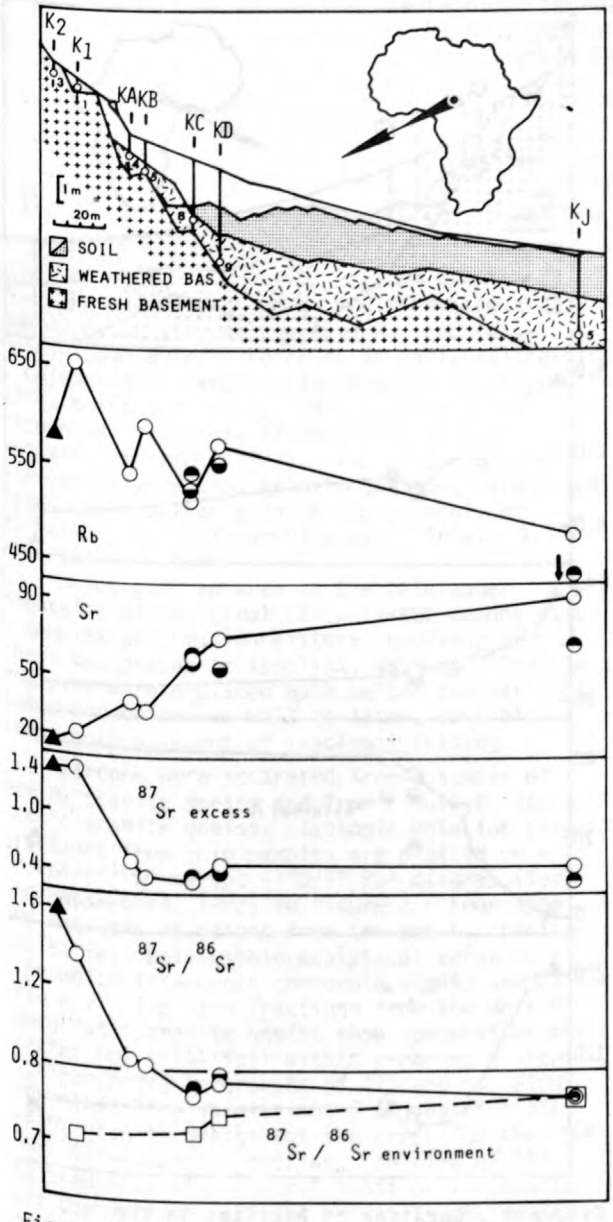

Figure 1.--Location of biotites in the weathering profile of Kossélili, Guera massif, Chad Republic, central Africa. Rb, Sr, ^{87}Sr excess contents in µg/g, $^{87}Sr/^{86}Sr$ of environmental Sr. Fresh biotite, ▲ . Weathered biotites: size fraction 200 - 400 µ, ○ ; 100 - 200 µ, ◓ ; 100 - 50 µ, ◒ .

The previous X-ray and chemical studies showed that the weathering product of these micas is mostly kaolinite (as much as 40 percent) with some smectite (less than 10 percent) and that their constitutive elements are affected in the following way: K, Mg, Mn, and Ti are leached, the amounts of Si, Al, and Fe^{3+} increase relatively, while Ca and H_2O increase absolutely. The enrichment of Fe is due to quick oxidation of Fe^{2+} into Fe^{3+}. The data relevant to the Rb-Sr method allowed the following observations:

1. Leaching of Rb out of the minerals (fig. 1). The decrease in the K/Rb ratio (fig. 3) shows that the K, which is considered the most sensitive element in the biotites during weathering, is leached faster than the Rb.

2. Trapping on and (or) into the minerals of environmental Sr. This Sr has a variable isotopic composition related to its place in the weathering profile (fig. 1).

3. Leaching of radiogenic ^{87}Sr. This leaching, rapid at the beginning of biotite weathering, slows down until an isotopic equilibrium is reached between the Sr remaining in the minerals and the environmental Sr (fig. 1).

In an isochron diagram [$^{87}Sr/^{86}Sr$ versus $^{87}Rb/^{86}Sr$], the analytical results plot along a curve located below a reference line which represents, to a first approximation, the location of all the fresh biotites of the same age from the granitic shield (fig. 2). This reference line is drawn through the point of the fresh mineral and has an intercept of 0.712, which is the $^{87}Sr/^{86}Sr$ value of Sr contained in these biotites during their crystallization (Clauer, 1976). The K-Ar results, plotted in another isochron diagram [$^{40}Ar/^{36}Ar$ versus $^{40}K/^{36}Ar$], give a remarkably similar curve, which is also located below a reference line with the same age as the previous one (fig. 2). Drawn through the fresh biotite point, it has an intercept of 295.5 for the $^{40}Ar/^{36}Ar$ ratio of the trapped argon during mineral crystallization. This K-Ar curve is the result of K-leaching, radiogenic ^{40}Ar diffusion out of the minerals, and also adsorption of external Ar on and (or) into the minerals (fig. 3).

In summary, the geochemical and isotopical behaviour of the Rb-Sr and K-Ar systems from biotites are affected during progressive natural weathering by differential leaching of Rb, K, and radiogenic ^{87}Sr, diffusion of radiogenic ^{40}Ar, and also by adsorption of external Sr and Ar. In most of the samples, the K-Ar system mimics remarkably the behaviour of the Rb-Sr system. This similarity requires consideration of the behaviour of the two radiogenic isotopes and of the origin of the external adsorbed Sr and Ar. The Rb-Sr system is, nevertheless, more sensitive than the K-Ar system at the beginning of weathering. This has been shown previously

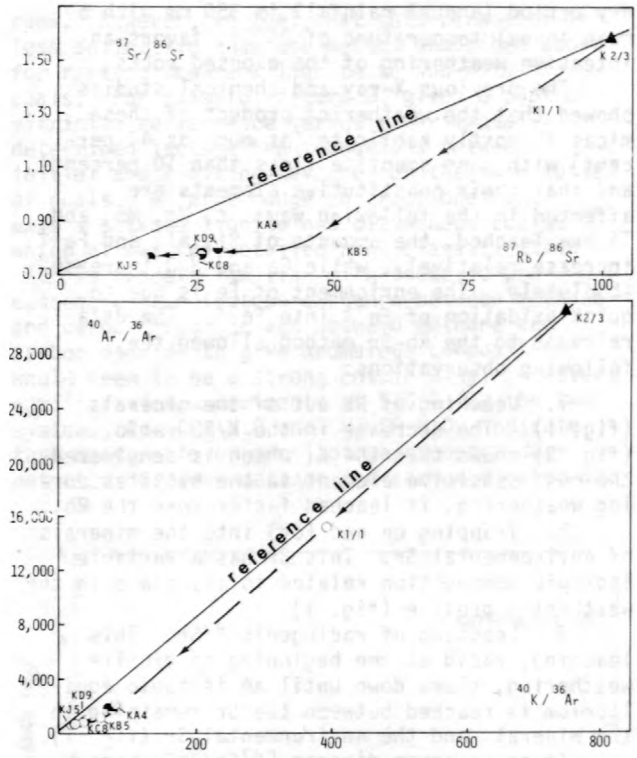

Figure 2.--Progressive natural weathering of biotites from weathering profile of Kossélili, Guera massif, Chad Republic, central Africa. Isochron diagrams [$^{87}Sr/^{86}Sr$ versus $^{87}Rb/^{86}Sr$] and [$^{40}Ar/^{36}Ar$ versus $^{40}K/^{36}Ar$]. Fresh biotite, ▲ . Weathered biotites: size fraction 200 - 400 μ, ○ ; 100 - 200 μ, ◓ ; 100 - 50 μ, ◓ .

on slightly weathered glauconites (Odin and others, 1974), where K and radiogenic ^{40}Ar are lost concomitantly if the loss of K is less than 10 percent, while the radiogenic ^{87}Sr is already leached preferentially. Moreover, when an isotopic equilibrium between the $^{87}Sr/^{86}Sr$ ratio of the external Sr and the Sr still contained in the weathered minerals is reached, the extraction of radiogenic ^{87}Sr out of the lattices is stopped, while the diffusion of radiogenic ^{40}Ar continues.

In conclusion, the low ages related to natural weathering obtained on biotites by both the Rb-Sr and K-Ar methods cannot any longer be explained only by a preferential leaching of radiogenic ^{87}Sr with regard to Rb, or by a simple diffusion of radiogenic ^{40}Ar preferentially to the loss of K. The effects of weathering on the Rb-Sr and K-Ar systems from biotites are, in fact, much more complicated, especially with additional trapping of variable external Sr and Ar. From a strict geochemical and isotopical point of view, the most important result of this study is that, between the initial weathering stage (less than 3 percent K loss) and the intensive weathering stage (more than 32 percent K loss), the K-Ar system mimics perfectly the Rb-Sr system.

Clauer, N., 1976, Géochimie isotopique du strontium des milieux sédimentaires. Application à la géochronologie de la couverture du craton ouest-africain: Mémoires de la Société Géologique, Strasbourg, v. 45, 256 p.

Clauer, N., and Tardy, Y., 1976, Effects of natural weathering on the mineralogical, chemical and isotopical composition of

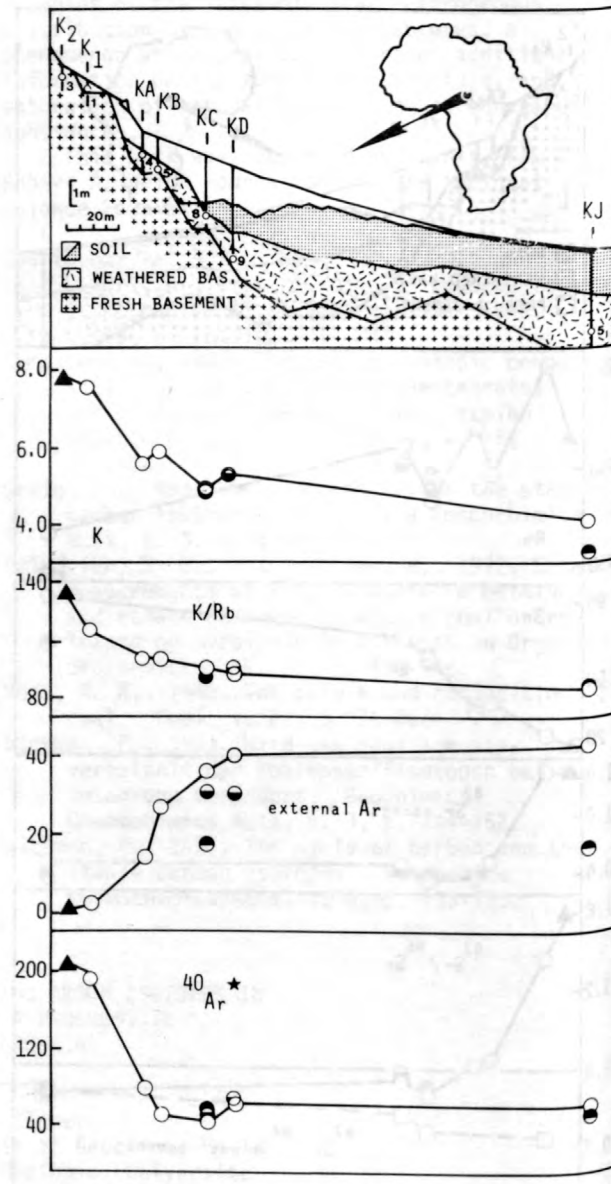

Figure 3.--Location of biotites in the weathering profile of Kossélili, Guera massif, Chad Republic, central Africa. K content in percent; K/Rb and external Ar in percent; radiogenic ^{40}Ar in 10^{-6} cm^3 g^{-1} S.T.P. of these biotites. Fresh biotite, ▲ . Weathered biotites: size fraction 200 - 400 μ, ○ ; 100 - 200 μ, ◓ ; 100 - 50 μ, ◓ .

biotites: European Colloquium of Geochronology, 4th, Amsterdam, April 5-10, p. 23.
Odin, G., Clauer, N., Hunziker, J. C., Keppens, E., and Pasteels, P., 1974, Influence of natural and artificial weathering on glauconite K-Ar and Rb-Sr apparent ages: International Meeting for Geochronology, Cosmochronology, and Isotope Geology, Paris, August 26-31, 2 p.

ZIRCON U/Pb ISOTOPIC EVIDENCE FOR EARLY PALAEOZOIC TECTONIC ACTIVITY IN THE AUSTROALPINE NAPPE, THE EASTERN ALPS

By R. A. Cliff
Department of Earth Sciences
University of Leeds
United Kingdom

The nature and age of pre-Hercynian tectonic activity in the Alps has been disputed--some authors refer to an early Palaeozoic ("Caledonian") orogeny (for example Grauert, 1966; Borsi and others, 1973), while others recognize only early Palaeozoic magmatic activity (Schmidt, 1977). The zircon data on structurally defined granite gneisses, presented here, confirm that granite emplacement, deformation, and metamorphism were closely associated in time.

Mapping of an area in the Deferegger Mountains of Ost-tirol (fig. 1) has demonstrated a complex deformation history involving at least two phases of isoclinal folding. Granite gneisses were emplaced both before the earliest folds recognized as well as later, possibly after both episodes of isoclinal folding.

Zircons were separated from a sample of pre-D_1 granite gneiss and from a post-D_1 leucocratic granite gneiss. Isotopic data for zircon fractions from both samples are plotted on a $^{207}Pb^*/^{206}Pb^*$ versus $^{238}U/^{206}Pb^*$ diagram (Tera and Wasserburg, 1972) in figure 2. Four size and magnetic fractions from the pre-D_1 granite gneiss fall well within analytical error on a line which intercepts concordia at 443 and ca. 1750 m.y. The five fractions from the post-D_1 leucocratic granite gneiss show somewhat greater scatter but still fall within error on a line with concordia intercepts of 427 and ca. 2400 m.y. This line is distinct from that for the pre-D_1 granite gneiss but the errors on the lower intercepts do overlap. In view of (1) the predominantly euhedral habit of zircons in both populations, (2) the proximity of the data points to the lower intercept with concordia, and (3) the occasional occurrence of euhedral crystals with rounded cores, the ages indicated by the lower intercepts are interpreted as the age of crystallization of the host rocks. The upper intercepts are not well defined but are clearly different for the two suites analyzed; they are thought to reflect incorporation of Precambrian zircons either from the source rocks or from the country rocks by assimilation. The apparent ages of these Precambrian components do not necessarily have any geological significance because these components may themselves be mixtures.

The structural data on the dated rocks, plus the measured ages, indicate that the D_1 deformation of this part of the Austroalpine Nappe took place ca. 435 m.y. ago. Because the structural relationship of the younger leucocratic gneiss to the D_2 deformation is ambiguous, this deformation may also be bracketed by the measured ages, although it may be younger. In either case a Late Ordovician or Silurian episode of deformation is established. The inferred age of crystallization of the granite gneisses studied here is in good agreement with Rb-Sr whole-rock ages measured on similar rocks from other parts of the Austroalpine Nappe Complex by Grauert (1966), by Borsi and others (1973), and by Satir (1976).

Several recent studies have investigated the response of the U-Pb isotopic system in zircon to different degrees of metamorphism at various times after their crystallization. The susceptibility of old, radiation-damaged zircons or "hot spots" within zircons to lead loss during the lowest grades of metamorphism was recently emphasized by Gebauer and Grunenfelder (1977). On the other hand, recently annealed zircons may also undergo limited lead loss even in the presence of a granitic melt. The transition between these extremes will depend on the concentration and distribution of uranium in the zircons and on the time elapsed since annealing occurred. In the present study both granite gneisses were subject to Hercynian metamorphism: biotite in the pre-D_1 granite gneiss gave a K-Ar age of 257 m.y. while muscovite and biotite from the post-D_1 leucocratic granite gneiss gave 297 and 224 m.y., respectively (Cliff and Rex, 1977). The pre-D_1 granite gneiss, which has a rather low uranium

concentration, gives no indication of any lead loss during Hercynian metamorphism. The post-D_2 leucocratic granite gneiss has as much as ten times more uranium and the scatter of data points, although within error on a straight line, would be consistent with small degrees of increasing lead loss correlated with increasing uranium content. The amount of lead loss must be small, however, because of the field relations of the two granite gneisses and the agreement of the zircon ages with Rb-Sr whole-rock data from similar rocks noted above. Taken together, the data suggest that up to 150 m.y. after annealing, even uranium-rich zircons may be only slightly affected by a metamorphism that was sufficient to reset muscovite K-Ar ages. Information on the distribution of uranium within the analyzed zircon fractions is required before these conclusions can be related to other situations.

Borsi, D., Del Moro, A., Sassi, F. P., and Zirpoli, G., 1973, Metamorphic evolution of the Austridic rocks to the South of the Tauern Window (Eastern Alps); Radiometric and geopetrologic data: Geological Society of Italy Memoir 12, p. 549-71.

Cliff, R. A., and Rex, D. C., 1977, Mineral ages from the Austroalpine Nappe in the Deferegger Mountains, East Tyrol, Austria: 20th Annual Report of the Research Institute for African Geology, University of Leeds 1976, p. 78-79.

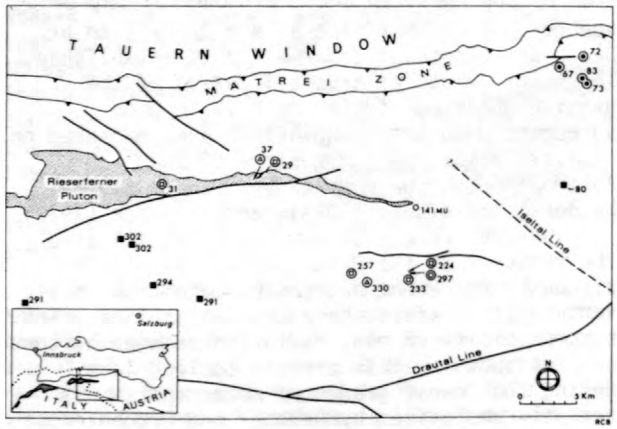

Figure 1.--Tectonic sketch map of part of the Austroalpine Nappe Complex south of the Tauern Window. Numbers refer to K-Ar and Rb-Sr mineral ages from the literature. The zircon data reported here relate to the samples ~ 10 km north of the Drautal Line, giving biotite K-Ar ages of 224 and 257 m.y.

Gebauer, D., and Grunenfelder, M., 1977, U-Pb systematics of detrital zircons from some unmetamorphosed sediments of Central Europe: Contributions to Mineralogy and Petrology, v. 65, p. 29-38.

Grauert, B., 1966, Rb-Sr age determination on orthogneisses of the Silvretta (Switzerland): Earth and Planetary Science Letters, v. 1, p. 139-147.

Satir, M., 1976, Rb-Sr und K-Ar Altersbestimmungen an Gesteinen und Mineralien des südlichen Ötztalkristallins und der westlichen Hohen Tauern: Geologisches Rundschau, v. 65, p. 394-410.

Schmidt, K., 1977, Der Altpalaeozoische Magmatismus und seine Stellung in der tektonischen Geschichte Mittel-und Süd Westeuropas: Zeitschrift deutscher geologischer Geschichte, v. 128, p. 121-141.

Tera, F., and Wasserburg, G. J., 1972, U-Th-Pb systematics in three apollo 14 basalts and the problem of initial lead in lunar rocks. Earth and Planetary Science Letters, v. 14, p. 281-304.

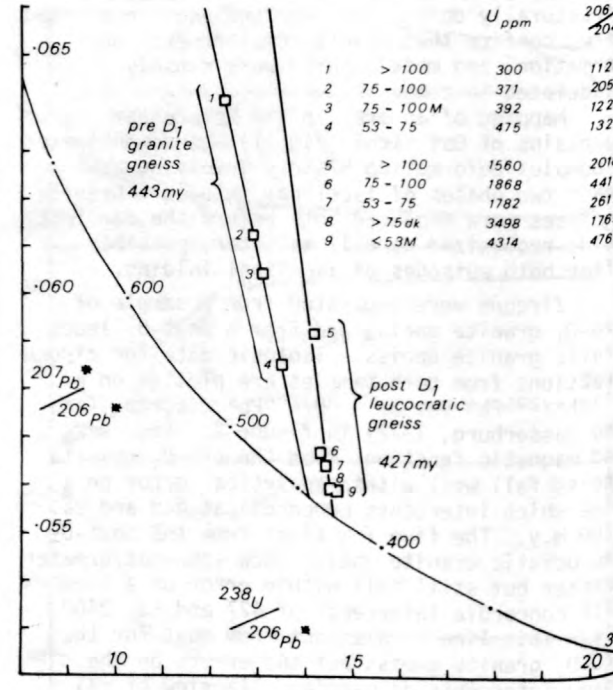

Figure 2.--U-Pb isotopic data for zircons from two granite gneiss samples. $^{207}Pb^*$ and $^{206}Pb^*$ are radiogenic lead abundances. Error boxes indicate estimated 2σ errors.

CHEMICAL AND ISOTOPIC COMPOSITION OF NATURAL GASES FROM PALEOZOIC ROCKS IN ILLINOIS

By Dennis D. Coleman and Wayne P. Meents
Illinois State Geological Survey
Urbana, Illinois 61801

In an attempt to learn more about the origin of natural gas in Illinois, gas samples were collected from 47 gas wells in sedimentary rocks ranging from Ordovician to Pennsylvanian in age. Most of these gas deposits are relatively small and are found at depths ranging from 20 to 720 meters. The chemical compositions of the samples were determined by gas chromatography, and carbon isotopic compositions of methane were determined by mass spectrometry. The analytical results for the gas well samples and for 6 samples collected from oil wells are shown in table 1.

Figure 1 shows the isotopic composition of the samples from wells listed in table 1 and the isotopic compositions of 28 samples from gas wells in glacial drift. Carbon-14 analysis shows that the glacial-drift gas formed during bacterial decomposition of organic materials within the glacial drift (Coleman, 1976). Most of the samples from bedrock have $\delta^{13}C$ values ranging from -46 to -64 permil, whereas most of the samples from wells in glacial drift have $\delta^{13}C$ values from -68 to -84 permil. Bedrock samples having $\delta^{13}C$ values lighter than approximately -62 permil are mostly from very shallow wells and are believed to be at least partially of bacterial origin. Radiocarbon analysis of one of these light bedrock gas samples (table 1, no. 2) verified that some of the CH_4 had formed from materials in the glacial drift. This sample also contained ethane and propane, indicating that it was a mixture of thermally produced and bacterially produced gas. Coleman (1976) has demonstrated that soil gas and glacial-drift gas can be carried downward with ground water to become mixed with older gas.

Figure 2 shows the locations of the wells that were sampled and their relationship to the location of the oil-producing areas of the state. Although the wells samples do not include all gas-producing areas, they are fairly representative. Gas wells in or near the areas of oil production are frequently closely associated with oil accumulations, and the isotopic compositions of methane from these gas wells is similar to that of methane from solution gas collected from nearby oil wells. Although there are no known gas fields in the central part of the oil-producing area, gas caps were originally present over many of the oil accumulations but the gas has now been depleted. Future sampling will involve collection of solution gas from this area. For those wells located away from the oil-producing areas, nearly all are from localities in which minor shows of oil have been reported.

The close association between gas and oil strongly suggests that the gas was thermally produced during formation of oil. These samples are geochemically significant, because the concentration of hydrocarbons heavier than methane is very low when compared to most petroleum gases. Although gas produced during coalification is frequently low in heavy hydrocarbons, it is also generally much heavier isotopically than the gases observed in these samples. There does not appear to be any correlation between the isotopic composition of the methane and the occurrence of coal. There is, however, a general trend of increasing $\delta^{13}C$ in a southward direction, which is also the direction of increased metamorphism as identified by coal rank (Damberger, 1971).

The association between gas and oil and the comparison of the data to the models of Stahl (1974, 1977) suggests that most of the gas wells in bedrock in Illinois produce gas that is of low-grade thermal origin. Research is underway to determine whether the relatively low concentrations of hydrocarbons heavier than methane may have been caused by chemical fractionation during migration.

Coleman, D. D., 1976, The origin of drift-gas deposits as determined by radiocarbon dating of methane, in Proceedings of the Ninth

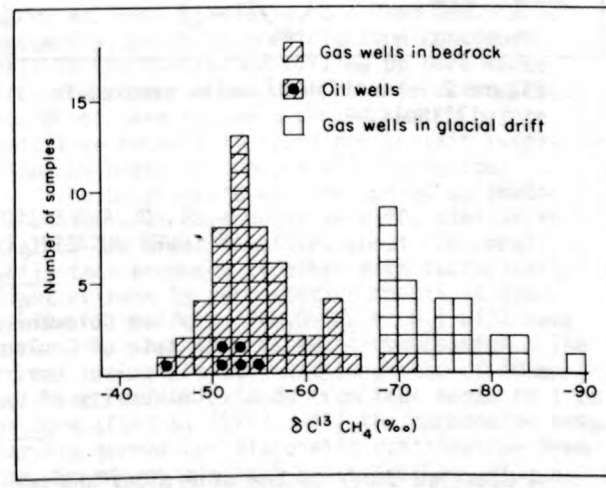

Figure 1.--Histogram of isotopic compositions.

International Radiocarbon Conference: Los Angeles and San Diego, June 20-26, 1976, in press.

Damberger, H. H., 1971, Coalification pattern of the Illinois Basin: Economic Geology, v. 66, p. 488-494.

Stahl, W. J., 1974, Carbon isotope fractionations in natural gases: Nature, v. 251, p. 134-135.

Stahl, W. J., 1977, Carbon and nitrogen isotopes in hydrocarbon research and exploration: Chemical Geology, v. 20, p. 121-149.

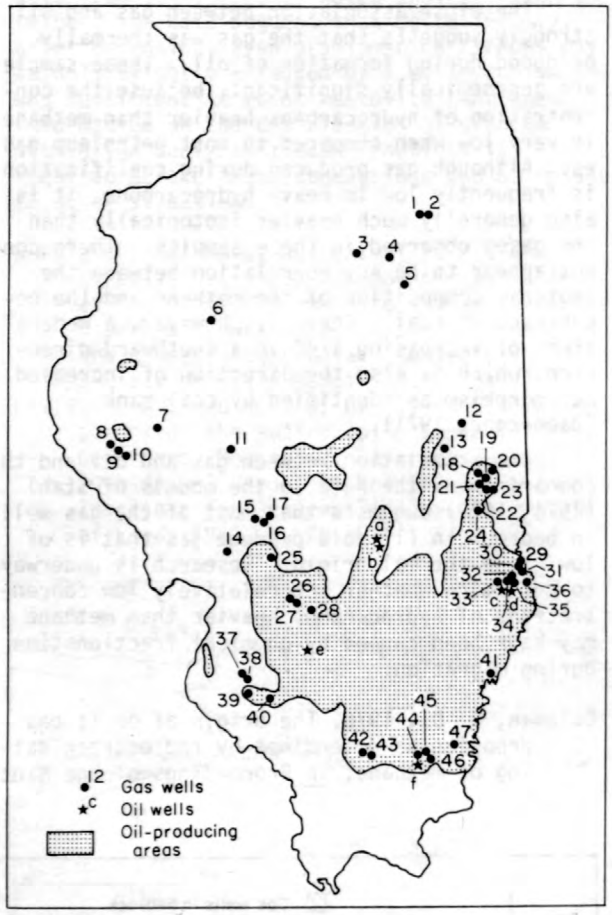

Figure 2.--Location of wells sampled in Illinois.

Table 1.--Chemical and isotopic composition of natural gas samples

No.	Depth[a] (m)	Res[b]	CH_4 (%)	C_2H_6 (%)	C_3H_8 (%)	$C_{n\geq3}$ (%)	N_2 (%)	CO_2 (%)	O_2+ Ar (%)	$\delta^{13}C$[d] CH_4 (‰)
Gas Wells										
1	12-28	Penn	94.7	--	--	--	4.2	1.0	0.1	-59.8
2	11-49	Penn	94.4	0.1	tr	--	5.2	.2	0.1	-64.2
3	?-76	Ord	96.9	0.1	0.3	0.4	1.7	0.5	0.2	-60.1
4	?-94	Penn	96.9	--	--	--	2.7	0.4	--	-56.1
5	?-21	Penn	81.4	0.1	--	--	17.9	0.4	0.3	-62.5
6	92-94	Penn	78.1	0.1	--	--	21.4	0.1	0.4	-69.3
7	155-157	Sil	90.6	tr	--	--	8.9	0.5	--	-56.8
8	149-152	Sil	90.6	--	--	--	8.7	0.6	0.1	-56.6
9	148-153	Sil	96.0	--	--	--	3.5	0.5	0.1	-55.0
10	146-148	Sil	97.1	tr	--	--	2.9	tr	tr	-55.7
11	84-89	Penn	96.2	--	--	--	0.3	3.5	--	-49.4
12	102-107	Penn	98.7	--	--	--	0.8	0.5	--	-51.9
13	28-34	Dev	90.5	--	--	--	7.3	2.0	0.3	-62.4
14	110-114	Penn	63.7	--	--	--	27.7	2.0	6.7	-62.5
15	49-55	Penn	60.1	--	--	--	25.5	0.4	6.0	-70.0
16	169-172	Penn	86.0	0.1	tr	--	13.8	--	0.1	-56.2
17	160-173	Penn	90.5	0.1	--	--	9.4	tr	--	-53.0
18	109-111	Penn	97.8	--	--	--	0.9	1.3	--	-53.3
19	116-121	Penn	95.2	tr	--	--	4.0	0.7	--	-52.8
20	83-101	Penn	93.9	0.1	0.3	0.7	4.0	0.4	0.7	-52.1
21	125-129	Penn	94.8	0.1	--	--	2.7	2.4	--	-53.3
22	117-133	Penn	96.1	0.3	0.3	0.2	0.5	2.6	--	-52.1
23	128-160	Penn	97.7	0.1	--	--	0.8	1.4	--	-54.1
24	?-66	Penn	95.8	0.2	--	--	3.2	0.3	0.6	-60.2
25	184-185	Penn	88.0	0.1	--	--	11.5	0.4	--	-58.8
26	278-284	Miss	93.0	0.2	--	--	6.6	0.3	--	-53.4
27	172-178	Penn	78.2	0.1	--	--	21.7	--	--	-62.4
28	314-315	Miss	91.4	--	--	--	8.6	--	--	-51.2
29	159-162	Penn	97.2	tr			2.2	0.4	0.1	-53.5
30	182-184	Penn	96.8	tr			3.0	0.1	--	-54.7
31	180-181	Penn	96.9	0.1	--	--	2.1	1.0	--	-52.8
32	240-241	Penn	96.3	tr			3.5	0.2	0.1	-52.2
33	67-296	Penn	83.2	2.5	0.1	0.1	13.6	0.4	--	-53.1
34	229-307	Penn	92.5	0.2	tr	tr	5.4	1.9	--	-54.2
35	166-167	Penn	95.3	0.1	--	--	4.5	0.1	--	-55.9
36	234-237	Penn	96.4	tr			3.5	0.1	--	-51.6
37	78-88	Miss	97.9	--	--	--	0.3	1.8	--	-50.6
38	76-82	Miss	98.2	--	--	--	0.4	1.4	--	-50.5
39	70-76	Miss	78.0	--	--	--	0.7	21.1	0.2	-50.9
40	249-250	Miss	94.4	tr	--	--	5.6	--	--	-54.1
41	233-237	Penn	92.3	tr	--	--	7.6	tr	0.1	-56.8
42	591-595	Miss	97.0	0.8	0.2	0.2	1.8	tr	--	-49.9
43	592-595	Miss	96.81	0.9	0.1	--	1.7	0.5	--	-49.9
44	592-594	Miss	90.5	2.8	1.1	1.5	4.1	--	--	-47.7
45	717-718	Miss	80.5	4.0	2.0	0.3	13.1	--	0.1	-46.8
46	587-591	Miss	89.9	0.8	0.1	0.1	9.1	--	--	-48.5
47	196-198	Penn	95.2	0.1	--	--	4.5	--	0.2	-57.1
Oil Wells										
a	?	Dev	84.1	3.0	2.8	5.0	4.3	0.8	--	-51.6
b	?	Dev	76.8	4.0	4.8	4.2	9.4	0.8	--	-53.3
c	395-397	Penn	94.4	0.5	0.1	--	4.2	--	--	-55.8
d	279-289	Penn	89.1	0.1	0.1	--	10.3	0.4	--	-53.7
e	?	Sil	49.2	13.8	13.3	7.1	16.0	0.6		-50.6
f	644-646	Miss	69.8	5.6	1.5	1.3	21.5	0.3	--	-45.8

[a]Depth of producing zone.
[b]Geologic age of reservoir rock.
[c]Concentrations between 0.01 and 0.05% are indicated as "trace" (tr).
[d]Relative to PDB.

C, O, AND S ISOTOPE INVESTIGATION OF LOWER JURASSIC CARBONATE CONCRETIONS

By Max Coleman[1] and Rob Raiswell[2]
[1]Institute of Geological Sciences, London
[2]School of Environmental Sciences
University of East Anglia, Norwich

A detailed study of the mineralogy and geochemistry of carbonate concretions from organic rich shales suggested a microbiological origin in which growth was maintained by influx of dis-

solved organic material (Raiswell, 1976). In order to refine the genetic model, it was decided to measure isotopic ratios of carbonate oxygen and carbon, organic carbon, and pyritic sulphur. The samples used were some of those analyzed by Raiswell (1976) and come from the Falcifer Zone (the Jet Rock), Upper Lias at Port Mulgrave, 11 km northwest of Whitby, Yorkshire, England. A concretion was taken from each of two horizons: one of these beds (samples UA) relative to the other (samples UB) has a lower concentration of concretions and of organic matter. Each concretion had cut from it an equatorial slice (parallel to the bedding plane). For analysis a continuous series of samples was taken along a diameter of the slice from one edge through the center to the other: nine were taken from concretion UA and eleven from UB. The samples are numbered successively, thus sample UA5 is from the center and 1 and 9 are from opposite outside edges. (For further details of samples, see Raiswell, 1976). Three samples of host rock associated with each concretion were analyzed also.

Two aliquots were taken from each sample, one for carbonate analysis and the other for organic carbon and sulphide. The former was treated with a 1-percent solution of sodium hypochlorite to destroy organic matter.

The other samples were washed with cold 10-percent hydrochloric acid to dissolve the carbonate fraction. After treatment both sets were washed three times with water and dried. Carbon dioxide was prepared from the carbonates by reaction with 100-percent phosphoric acid using a method similar to that described by McCrea (1950). The carbonate-free samples were oxidized with cuprous oxide at 1070°C and the resultant CO_2 and SO_2 were separated by fractional sublimation (Oana and Ishikawa, 1966). The gas samples were analyzed isotopically using two Micromass 602-C mass spectrometers, one of which had been modified by the incorporation of a heated inlet system to permit its use with SO_2. The raw data were corrected for instrumental and isotopic effects in the usual way (Craig, 1957).

The results are presented in table 1 relative to PDB and Canon Diablo troilite. The approximate analytical uncertainty (2 x standard error of the mean) for $\delta^{13}C$ carbonate, $\delta^{18}O$ carbonate, $\delta^{13}C$ organic, and $\delta^{34}S$ are, respectively, 0.02 permil, 0.03 permil, 0.1 permil, and 0.05 permil. Together with the isotopic data in table 1 are included the data on carbonate and pyrite concentrations from Raiswell (1976).

It is apparent from the mineralogical data shown in table 1 that pyrite is an important component of both concretions at the outer rim. As suggested by Raiswell (1976), microbiological reduction of sulphate would provide the sulphide, and consequently some of the carbonate, by oxidation of organic matter (in general terms $2CH_2O + SO_4^{2-} \rightarrow H_2S + 2HCO_3^-$). Bacterial reduction can produce a large and variable negative isotopic fractionation in the resulting sulphide (for example, Nakai and Jensen, 1964). Successively precipitated sulphides will be enriched progressively in the heavier isotope as the finite reservoir of light isotope is exhausted. However, in a closed system the total sulphide produced will have an isotopic composition identical to that of the original sulphate if the reduction goes to completion. It is estimated that Lias seawater sulphate had an isotopic composition of about +17 permil, and it is obvious from the data that because the heaviest $\delta^{34}S$ value is -2.56 permil (sample UA1) the system was not a completely closed one. For both UA and UB the framboidal pyrites of the host rock show fairly uniform values slightly more than 40 permil lighter than the sea water--typical values for open system reduction (Schwarcz and Burnie, 1973). Both concretions show an increase in pyrite concentration and $\delta^{34}S$ towards the rim. This suggests progressive precipitation from the center outwards. Although the isotopic data suggests a system closed to ingress, for the reasons outlined above, the reduction did not go to completion.

It is interesting to note that the inside parts of both concretions have a lower concentration of pyrite than the host rock but that the former have isotopically much heavier sulphur suggesting later precipitation. The high concentration of pyrite at the rim is the heaviest (and latest) and is sufficient to raise the sulphide content of the entire concretion to, or above, the average of that of the bed as a whole (UB or UA, respectively). This is evidence for the sequence of formation of the concretion. At a fairly early diagenetic stage a small amount of framboidal pyrite had been precipitated throughout the bed, and at this stage the concretion came into existence. The inner parts became different from the host rock generally, in that no more open-system pyrite was precipitated. The host rock (and maybe the rim of the concretion) continued to accumulate isotopically light pyrite until the system became, at least partially, a closed one. Subsequently, sulphide precipitation continued only in the concretion filling up pore space from the center outward. The concretion itself could not have become a closed system before this time because it could not contain sufficient sulphate to produce all the pyrite.

The bicarbonate evolved during sulphate reduction will have negative $\delta^{13}C$, similar to that of the organic matter, about -28 permil; while that produced together with isotopically light methane by fermentation reactions (generally of the form, $2CH_2O \rightarrow CH_4 + CO_2$) will have a much more positive isotopic composition. The former process is dominant to depths of 10 m while the latter extends from that depth to 1 km or more (Curtis, 1977). All the carbonates have varying amounts of diagenetic contribution from the two microbiological processes, as well as an original component precipitated in equilib-

rium with seawater (about 0 permil). Both concretions have $\delta^{13}C$ values compatible with a considerable input from sulphate reduction. In fact, UB has more light carbon than can be accounted for by its sulphide contents, which is at a lower concentration than in the host rock which has a relatively heavy average $\delta^{13}C$, -6.98 permil. This implies that either the concretion concentrated some of the isotopically light carbon produced throughout the system or that some of the sulphur is no longer in the concretion as we see it now.

In greater detail, concretion UA, which has a very low pyrite concentration in the center that increases radially outward, shows a corresponding trend in $\delta^{13}C$. Thus, it appears that as sulphate reduction proceeded in the system, carbonate was precipitated in the concretion while a proportion of the sulphide was lost. Concretion UB has a somewhat higher internal pyrite content and slightly lighter and more uniform $\delta^{13}C$. Both concretions show a marked change to $\delta^{13}C$ enrichment at the margins, which is to be expected as these parts would be most accessible for precipitation of heavy carbon produced by fermentation later and at greater depth.

The isotope ratios of the residual organic carbon are difficult to interpret, particularly the sudden change in UB to very light values at the rim. As in the case of carbonate carbon, this might be the result of bacterial fermentation in which certain organic molecules are attacked preferentially. This is in accord with

Table 1.--Isotopic and mineralogical data

Sample No.	$CaCO_3$ (percent)	$\delta^{13}C_{CaCO_3}$	$\delta^{18}O$	$\delta^{13}C_{org}$	Pyrite (percent)	$\delta^{34}S$
Edge - UA1	26.3	-13.32	-9.90	-32.5	56.1	-2.56
UA2	85.7	-14.17	-9.55	-33.9	1.95	-10.06
UA3	85.9	-14.39	-9.46	-33.2	1.02	-20.39
UA4	87.6	-14.30	-9.24	-32.8	0.90	-24.28
Center-UA5	87.5	-13.77	-9.12	-33.5	0.79	-24.01
UA6	87.1	-13.73	-8.94	-33.5	0.81	-16.84
UA7	86.5	-13.90	-9.23	-33.4	0.90	-17.86
UA8	86.5	-14.15	-9.34	-32.3	1.53	-11.27
Edge - UA9	25.6	-12.90	-9.51	-32.1	57.6	-3.04
UA Total----	73.0	-14.20	-9.39	-	13.4	-7.06
UA Host 1	5.6	-7.46	-10.19	-33.8	7.1	-26.00
UA Host 2	6.0	-6.31	-8.43	-34.5	9.8	-26.02
UA Host 3	5.7	-6.70	-10.75	-31.2	5.3	-25.27
Edge - UB1	53.6	-13.68	-4.77	-35.6	27.1	-4.99
UB2	74.1	-14.99	-2.73	-32.6	6.47	-7.12
UB3	87.4	-15.05	-2.36	-29.9	2.34	-13.42
UB4	84.7	-15.22	-2.35	-30.9	1.95	-14.46
UB5	81.4	-15.26	-2.97	-30.0	2.00	-13.32
Center-UB6	84.2	-15.27	-2.40	-29.3	3.70	-8.05
UB7	85.4	-15.19	-2.26	-28.7	2.06	-11.25
UB8	85.0	-15.44	-2.40	-29.4	2.13	-13.05
UB9	84.7	-15.29	-2.35	-26.1	2.38	-12.20
UB10	81.2	-15.26	-2.56	-29.9	5.41	-8.93
Edge - UB11	53.5	-13.60	-4.70	-37.0	23.8	-5.50
UB Total----	77.4	-14.01	-2.32	-	7.5	-7.42
UB Host 1	17.1	-6.67	-7.70	-30.4	9.8	-21.97
UB Host 2	23.4	-7.11	-7.75	-30.4	11.1	-24.78
UB Host 3	21.3	-7.15	-8.07	-30.3	9.5	-25.66

ideas on the origin of petroleum where residual components are lipids which are 4 to 8 permil lighter than the total carbon.

At first glance, the oxygen isotope composition seems to present an unresolvable paradox. It is usually considered that carbonates formed in equilibrium with Jurassic seawater will have an isotopic composition of about 0 permil at about 14°C (Craig, 1965; Shackleton and Kennett, 1975) and either a more positive or negative value at lower or higher temperatures, respectively. The effect of interaction with meteoric water will give much lighter values. In conflict with the evidence for formation near the sediment surface in a marine environment, the oxygen data imply either a meteoric water influence or a high temperature (concretion UA approximately 60°C compared with 21°C at the center to 34°C at the rim of UB). Even a high estimate of the geothermal gradient will place the formation of UA at an unrealistic depth, particularly in comparison with UB.

There are two possible arguments that can reconcile this paradox. First, although the value of carbon in a carbonate may reflect sensitively the various sources of its components because the bicarbonate ion will be buffered constantly at a low level by precipitation, there is a large reservoir of oxygen in the water and, at least partial, isotopic exchange may occur. Thus, the oxygen isotopic composition of the carbonate may be related to that of the water at the stage when the carbonate cement had filled most of the pore space and reduced free access of water.

The second argument is concerned with the fact that the system may have been a partially closed one. In the same way as the sulphur isotope values can change, so can the oxygen. In this case, successive precipitation of carbonates will deplete the oxygen reservoir of the heavier isotope because the oxygen in calcite is about 30 permil heavier than the associated water. Thus, concretions forming in porous organic-rich shales may have limited access to the water above and may evolve isotopically in an essentially closed system: this effect will be accentuated by the reduction of volume caused by expression of pore water (possibly laterally) and by cement filling pores. A similar isotopic evolution on a more limited scale is seen in deep sea sediments (Lawrence and others, 1975).

The oxygen data is now capable of a more probable interpretation--concretion UA retained its porosity to a greater depth than UB and consequently has a larger component of fermentation-produced carbon (heavier values). It is interesting to note that UB was cemented much earlier than its host (and UA), reflecting the higher organic content of the bed and the greater production of carbonate by sulphate reduction.

With certain modifications the model for concretionary growth proposed by Raiswell (1976) is a valid one. Early in the diagenetic history of the rock, after the precipitation of the first framboidal pyrite, the concretions came into existence. Their form at this time is problematical. One conjectural possibility is that if the organic content is sufficiently high, the dispersed population of sulphate-reducing bacteria forms local concentrations at randomly placed sites. Instead of normal framboidal pyrite being precipitated, it may be that the sulphide was produced too fast for available iron to react with it, and the outward diffusion of dissolved reduced sulphur was balanced at some distance by inward diffusion of iron. This "shell" of precipitated iron sulphide surrounded a protected volume in which no further sulphide was formed. The number of such centers would be controlled by the amount of organic nutrient in the system, which is borne out by the greater concentration of concretions in the more organic-rich bed from which UB was taken.

The change in pyrite concentration on passing from the host to concretion also gives support for this idea: the bed of UA, in which the organic content and, thus, sulphide concentration would be lower, shows a much sharper gradient as would be expected of more dilute solutions. The greater amount of sulphate reduction in bed UB also explains why the $\delta^{13}C$ for its carbonates is lighter than those of bed UA. Further sulphate reduction continued in the concretion and the bed as a whole, the bicarbonate produced being precipitated as calcite. At some stage while this was occurring, the system effectively became closed to influx of sulphate; the isotopic result of this was accentuated by expression of pore fluids. Sulphate continued to be reduced within the concretions, the pore spaces being filled from the center outwards, until expression and reduction had removed a large part of the sulphate.

Again, due to the higher organic content of bed UB, the large amount of diagenetic bicarbonate had cemented up the concretion by a fairly early stage and only a small amount of fermentation-produced bicarbonate filled the pore space left in the rim. However, there was space for further cementation in the host sediments. In comparison, precipitation of calcite in UA and its host continued to a greater depth. The residual organic material present in both beds shows that further diagenetic carbonate might have been produced had any more pore space been available.

Craig, H., 1957, Isotopic standards for carbon and oxygen and correction factors for mass spectrometer analysis of CO_2: Geochimica Cosmochimica Acta, v. 12, p. 133-149.

_____1965, Measurement of oxygen isotope palaeotemperatures: Spoleto Conference Proceedings on Stable isotopes in oceano-

graphic studies and palaeotemperatures, v. 3, p. 7.
Curtis, C. D., 1977, Sedimentary geochemistry; environments and processes dominated by involvement of an aqueous phase: Philosophical Transactions of the Royal Society of London, ser. A, v. 286, p. 353-372.
Lawrence, J. R., Gieskes, J. M., and Broecker, W. S., 1975, Oxygen isotope and cation composition of DSDP pore waters and the alteration of layer II basalts: Earth and Planetary Science Letters, v. 27, p. 1-10.
McCrea, J. M., 1950, The isotopic chemistry of carbonates and a palaeotemperature scale: Journal of Chemical Physics, v. 18, p. 849-857.
Nakai, N., and Jensen, M. L., 1964, The kinetic isotope effect in the bacterial reduction of oxidation of sulfur: Geochimica Cosmochimica Acta, v. 28, p. 1893-1912.
Oana, S., and Ishikawa, H., 1966, Sulphur isotopic fractionation between sulfur and sulfuric acid in the hydrothermal solution of sulfur dioxide: Geochemical Journal (Japan), v. 1, p. 45-50.
Raiswell, R., 1976, The microbiological formation of carbonate concretions in the Upper Lias of NE England: Chemical Geology, v. 18, no. 3, p. 227-244.
Schwarcz, H. P., and Burnie, S. W., 1973, Influence of sedimentary environments of sulfur isotope ratios in clastic rocks--a review: Mineralium Deposita, v. 8, p. 264-277.
Shackleton, N. J., and Kennett, J. P., 1975, Palaeotemperature history of the Cenozoic and the initiation of Antarctic glaciation; O and C isotope analysis in Deep Sea Drilling Project sites 277 and 281: Initial Report Deep Sea Drilling Project, v. 29, p. 743-755.

VOLCANIC PROCESSES STUDIED BY URANIUM - IONIUM SYSTEMATICS

By M. Condomines, P. Morand and C. J. Allegre
Laboratoire de Géochimie et Cosmochimie - L.A. 196
Institut de Physique du Globe et Departement des Sciences de la Terre
Universités de Paris VI et VII
4, Place Jussieu - 75230 Paris Cedex 05 - France

^{230}Th (ionium) is a decay product of the ^{238}U desintegration chain. Radioactive disequilibrium created in this chain by chemical fractionation can be used as a chronometer. The chronological equations can be written:

$$^{230}Th/^{232}Th = (^{230}Th/^{232}Th)_0 e^{-} t + ^{238}U/^{232}Th (1 - e^{-t})$$

Cogenetic systems of variable U/Th ratios, can then be used to determine ages and initial ratios as in the ^{87}Rb-^{87}Sr systematics.

Using this uranium-ionium chronometer, as described by Allegre (1968) and Allegre and Concomines (1976), we have studied several different magmatic systems--a volcanic chain (Costa Rica), a shield volcano (Etna), an oceanic ridge (Iceland), a submarine flow (Famous area), a continental volcano (Chaîne des Puys - France), and an oceanic island (Hawaii).

In nonmarine environments, internal isochron chronologies can be achieved, and meaningful ages, as well as initial $^{230}Th/^{232}Th$ ratios, can be obtained. This chronology shows that the life time of a volcano lies between 10,000 and 200,000 years. Each volcano seems to have a magma chamber. For some of them (Costa Rica), each cone seems to correspond to a given magma injection; in some others (Etna), several successive injections may have occurred. This information is obtained from the study of the evolution of the $^{230}Th/^{232}Th$ initial ratio in the magma chamber. When this ratio grows regularly and its evolution can be described by a closed system model, it can be reasonably deduced that there is a single magma chamber. When the evolution of this ratio shows several discontinuous variations, it can be shown that this is related to magma injections (figure 1). In marine environments (Famous area and Hawaiian Islands), strong contamination effects by a component with a high $^{230}Th/^{232}Th$ ratio might occur. Determinations of ages and initial $^{230}Th/^{232}Th$ ratios become very difficult. However, models of the

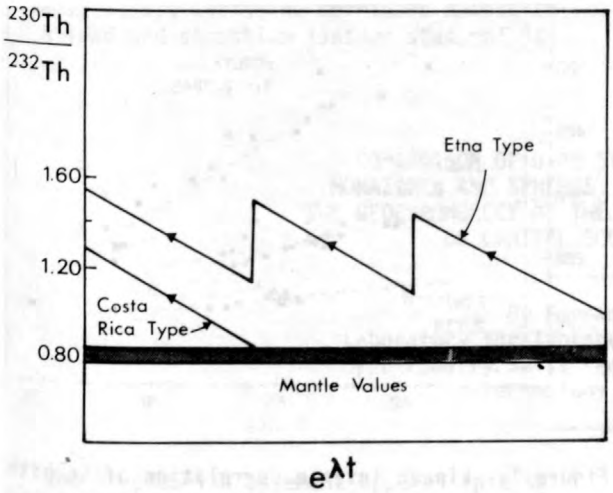

Figure 1.--Initial ($^{230}Th/^{232}Th$) ratio evolution as a function of $e^{\lambda t}$ for different volcanoes. In one case (Icaru-Costa Rica) a single magma chamber evolving as a closed system can be imagined. In the other (Etna) several injections with a given chamber must be envisioned. Mantle values correspond to radioactive equilibrium.

contamination processes can be deduced from the ionium-uranium system. We have shown that the ionium-uranium ratio is an extremely sensitive indication of sea water interactions. It has been modeled in the case of Hawaiian lavas by a contamination of ascending magma by upper crust.

For continental volcanoes (Massif Central, France) evidence for an important interaction between continental crust and magmas can be given. This contamination seems to occur within the magma chamber.

In the case of Iceland the results can be either described by complex contamination processes, or an extremely heterogeneous mantle source. In all cases, $^{230}Th/^{232}Th$ ratios from upper mantle sources are discussed. Evidences for variations of the U/Th ratio are given. In some cases (ridges), a reasonable model evokes radioactive disequilibrium in the mantle source.

Allegre, C. J., 1968, ^{230}Th dating of volcanic rocks - a comment: Earth and Planetary Science Letters, v. 3, p. 209-210.

Allegre, C. J., and Condomines, M., 1976, Fine chronology of volcanic processes using ^{238}U -^{230}Th systematics: Earth and Planetary Science Letters, v. 28, p. 395-406.

ESTIMATION OF SOURCE Rb/Sr FOR INDIVIDUAL IGNEOUS-DERIVED GRANITOIDS AND THE INFERRED AGE OF THE LOWER CRUST IN SOUTHEAST AUSTRALIA

By W. Compston and B. W. Chappell
Australian National University,
Canberra, Australia

The geochemical variation within many granitoids from southeast Australia shows evidence of restite-control; they exhibit well-fitted linear variation lines (fig. 1) that can be hypothesized as the physical unmixing of a felsic melt from the refractory residue after melting (termed the restite). Using this hypothesis, the average chemistry of the source rocks must also lie on the variation lines, and this can be specified for each granitoid magma in terms of the chemistry of the individual melt and restite end-members, plus a parameter, the fractional amount of minimum-melt component in the particular source (F). Thus, if Rb and Sr can be estimated for the melt and restite and if the possible range in F of the source can be sufficiently constrained, we can calculate the approximate Rb/Sr for the particular rocks that were partially melted to form a given granitoid. As the initial $^{87}Sr/^{86}Sr$ of the granitoid measures the mean $^{87}Sr/^{86}Sr$ of the source at the time of melting, we therefore obtain one point per granitoid source towards the construction of a source Rb-Sr isochron.

The Rb and Sr contents of the melt end-members are generally well-determined empirically by the analytical data. We have combined published distribution coefficients for Rb and Sr with their abundance in the granitoid in order to estimate their concentrations in the model restite, taking the latter as a pyroxene + plagioclase ± K-feldspar assemblage and taking the SiO_2 content of the restite from the disappearance of normative quartz when the variation lines for the major elements are extrapolated towards lower SiO_2. We have estimated Rb/Sr for the source rocks of seventeen different Palaeozoic granitoids in southeast Australia, as functions of F. The granitoids have been restricted to those believed to be derived from pre-existing igneous rocks (I-types), without any significant contribution from metasediments.

The parameter F may be constrained as greater than about 15 percent in all cases, adapting a published analysis of melt extraction for basalts and employing published data for rhyolite viscosity. We believe that granitic

melts from source rocks having smaller F are not widespread because such melts would be almost completely retained within the source region. For granitoids that contain nonminimum melts, F appears to average ∿ 19 percent according to the empirically-observed SiO_2 contents of ∿ 70 percent for their melt end-members, combined with the argument that magmas will deform and move rapidly when the degree of melting reaches ∿ 25 percent. Thus, for the source rocks of nonminimum melts, F will lie between the limits of ∿ 15 percent and ∿ 25 percent, and may be taken to a first approximation as equal to 19 percent for all such rocks. We have calculated the source Rb/Sr for nine nonminimum melt-bearing granitoids on this basis and find that their initial $^{87}Sr/^{86}Sr$ correlates strongly and positively with the source Rb/Sr (fig. 2). The slope of this "source isochron" corresponds to a primary source age of ∿ 1.1 x 10^9 yr. If the source rocks are modelled as a Precambrian island arc, their initial $^{87}Sr/^{86}Sr$ will be ∿ 0.7035 when first formed in the arc, and their age estimate increases to ∿ 1.2 x 10^9 yr. Uncertainties in source age due to the possible range in F will be ∿ ± 0.3 x 10^9 yr.

For granitoids containing minimum melts, F may range upwards from 25 percent and can be constrained further only by modelling the source rocks. We have used the published chemical data for Fijian, Lau, and Tongan Islands to model the possible range in SiO_2 of large volumes of "normal" island arc volcanics, and believe that 65 percent SiO_2 would be the highest value expected on a regionally averaged basis. This is equivalent to ∿ 60 percent for F. The eight minimum-melt granitoids studies do not define a source isochron for any equal values of F. In addition, even though their source rocks usually have higher F and, therefore, higher Rb/Sr than those of the nonminimum melts, the initial $^{87}Sr/^{86}Sr$ of the minimum-melt granitoids is lower. We conclude that their source rocks were substantially younger than those of the nonminimum melts. A source isochron of ∿ 0.75 x 10^9 yr. can be fitted to all the minimum-melt sources within the 25 percent to 60 percent limits for F.

These results show that Precambrian continental material was present on the lower crust in southeast Australia during the early Palaeozoic, so that the crust in this region did not originate solely as new oceanic crust in the early Palaeozoic. Instead, sizeable continental blocks remained, containing both middle and upper Precambrian metaigneous rocks and presumably also contemporary metasediments. Precambrian material at least 800 m.y. old has been independently detected from inherited zircons in one of the minimum-melt granitoids by Williams (1977), who has found still older zircons in a number of sedimentary-derived granitoids not considered here.

The derivation of specific values of source Rb/Sr for particular granitoids greatly strengthens the use of initial $^{87}Sr/^{86}Sr$ in tracing the origin of igneous rocks.

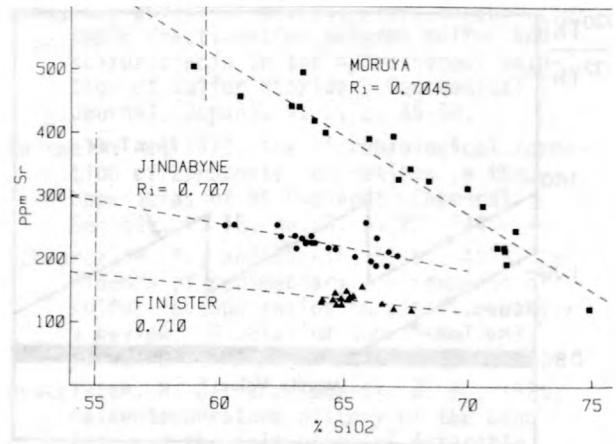

Figure 1.--Linear inverse correlation of Sr with SiO_2 for three I-type igneous suites, interpreted as the unmixing of felsic melt from refractory source residue. The broken vertical lines indicate our estimates for the mean source SiO_2. For most estimates for source SiO_2, the order in source Sr contents will be Finister < Jindabyne < Moruya, which correlates inversely with the initial $^{87}Sr/^{86}Sr$ and is indicative of aging in the source rocks.

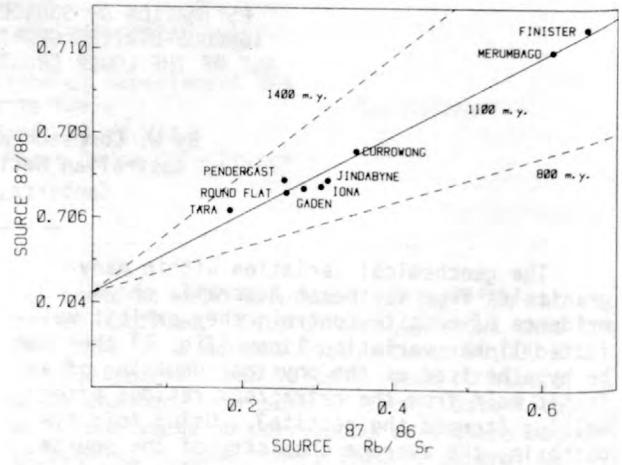

Figure 2.--Source isochron for the nonminimum melt bearing granitoids as registered 420 m.y. ago. The isochron slope is $e^{\lambda\tau_o}-e^{\lambda\tau}$, where τ_o is 1100 m.y. and τ is 420 m.y. The age of 1100 m.y. is associated with values for source $^{87}Rb/^{86}Sr$ calculated for 19 percent as the minimum melt fraction F of the source rocks. The upper and lower age limits correspond to the limiting values for F of 15 percent and 25 percent.

Williams, I. S., 1977, The Berridale Batholith--A lead and strontium isotope study of its origin: Australian National University Ph. D. Thesis.

COMPARISON OF U-Pb SYSTEMS IN ZIRCONS, MONAZITES AND SPHENES. A CONTRIBUTION TO THE GEOCHRONOLOGY OF THE PRECAMBRIAN BASEMENT OF CENTRAL SOUTH NORWAY

By Fernando Corfu
Laboratory for Isotope Geology and Mass Spectrometry, Swiss Federal Institute of Technology, Zurich

The Precambrian basement appears in a series of windows beneath the Jotun nappe-complex (Heim and others, 1978) (fig. 1). It can be subdivided into two main rock groups--an old high-grade metamorphic complex and younger granitic intrusives.

Based on field evidence, the age of both rock groups is Precambrian. The purpose of this study was to obtain more precise ages and to study the age relationships.

From the old high-grade metamorphic complex three rocks were investigated (fig. 1 and 2): A quartz-plagioclase rock (BV-1), a biotite-plagioclase-clinopyroxene-orthopyroxene rock (BV-5), and a calcite-sericite-epidote-biotite gneiss (BB-2).

Zircon fractions from a felsic rock (BV-1) yield strongly discordant data points, which on a Concordia diagram, define a chord intercepting the Concordia curve at 1506 ± 45 m.y. The zircon population appears to be very heterogeneous. The opaque zircons vary in color from white to black and are rich in uranium (3000-4000 ppm). They are strongly metamict. The translucent to transparent pink zircons contain less U (< 2000 ppm), are less metamict and finer grained than the first group. They also occur as overgrowths on metamict zircons. Within the single groups, we note the usual correlation between grain size, magnetic properties, U content, and degree of discordancy. These features indicate a two-stage development. First, a magmatic crystallization of U-rich zircons and, secondly, a metamorphic event during which the U-poor overgrowths and the pink zircons crystallized. Data points from two monazite fractions (fig. 1) plot slightly discordant near the upper intersection of the chord through the zircon data points, suggesting metamorphic crystallization of the monazites at the same time as the zircons of the second group. It is interesting to note that the monazite contains comparatively little U (1300 ppm).

In order to support this interpretation, two zircon fractions and one sphene fraction from a mafic gneiss (BV-5) collected in the same locality were analyzed. The fine magnetic zircon fraction (fig. 2) is strongly enriched in gray and milky-white crystals with a short prismatic subhedral habit and an U content of about 1400 ppm (analogous to the BV-1 zircons). The non-magnetic fraction (fig. 2) is enriched in purple zircons, which are frequently coarse grained, transparent, short prismatic to isometric with a low U content of about 460 ppm. The two data points plot on the BV-1 discordia-line. The sphene fraction gives a slightly discordant age of about 1520 m.y., which agrees well with the two monazite data points of BV-1.

A characteristic feature of the zircons of both rocks and also of the monazites is the very low radiogenic ^{208}Pb-content of less than 0.1 percent in the BV-1 zircons, of about 6 percent in the BV-5 zircons, and of only 8 percent of the total radiogenic lead in the monazites. This uncommonly low value of ^{208}Pb, in addition to the zircon features discussed above, points to a common origin of these rocks as magmatic differentiates from the same melt.

The third sample investigated is a coarse-grained biotite-gneiss (BB-2). The zircons from this rock are predominantly clear and transparent, light pink, sometimes with cracks and older cores. They are euhedral or oval shaped. The low U-content of the zircons (170-340 ppm), in addition to their morphology and to the mineralogical composition of the rock, suggests a detrital origin. The data points of the analyzed zircon fractions (fig. 2) lie on or above the discordia-line defined by the BV-1 and BV-5 zircons. The scatter seems to be due to the primary heterogeneity of the detrital zircons, although a minor lead loss during the intrusion of the Sveconorwegian Øye-granite, which crops out at a distance of 5 km cannot be excluded. This assumption is supported by the "younger" upper intercept age of the best-fit line through the six data points of 1467 ± 20 m.y. The zircons of BB-2 nevertheless confirm the major metamorphic event indicated by the data points of the two igneous samples at about 1520 m.y.

Two samples from the second main group of rocks recognized in the area, the young granitic intrusives, were investigated. BH-1 was col-

lected in the western basal gneiss region (fig.1) for the purpose of comparing it with a basement zone involved in greater Sveconorwegian and Caledonian tectonic disturbances. Both granites are mineralogically and texturally very similar. The zircons (inset in fig. 3) are mainly euhedral and prismatic, they are pink and transparent, frequently with fluid inclusions. Often they consist of a central subhedral core rimmed either by clear or by radially fractured zones. The U content ranges between 200 and 800 ppm. The data points of the BO-1 zircons (fig. 3) plot on a best-fit line which intersects the Concordia curve at 963 ± 24 m.y. and at 339 ± 39 m.y.; those of the BH-1 zircons on a chord intersecting the Concordia curve at 1014 ± 30 m.y. and 354 ± 44 m.y.

These features suggest that the granites presumably originated from the same anatectic melt. The differences in the upper apparent ages of BO-1 and BH-1 could be explained as reflecting a different content of old inherited lead in the zircon cores. Accordingly, the true age of crystallization may be younger than the upper intercept ages. Three sphene fractions yielded slightly discordant ages which plot on the upper continuation of the extrapolated best-fit line of the zircon data. As sphenes are not known to contain inherited radiogenic lead, it appears that also the zircons are virtually free of inherited lead. Therefore, the age of the intrusion is about 1000 m.y. A Rb-Sr whole-rock age of ca. 1000 m.y. obtained by Priem and others (1973) from the Hestbrepiggan granite (fig. 1), which is apparently similar to the Øye and Hafslo granites, seem to support the second interpretation.

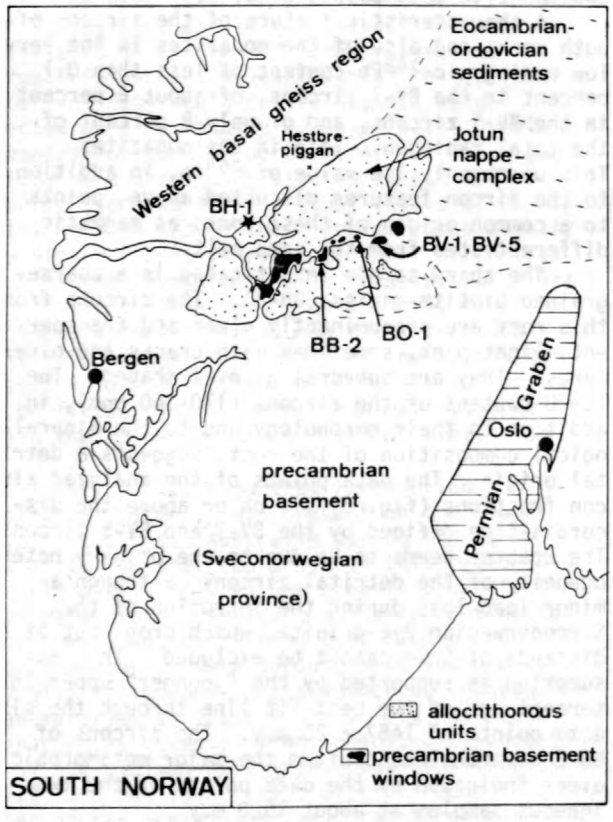

Figure 1.--Simplified tectonic sketch map of South-Norway with sample locations and numbers.

CONCLUSIONS

In the investigated Precambrian region three main events of varying degree of intensity are recorded by the U-Pb systems: (1) A regional high-grade metamorphism at approximately 1520 m.y., (2) a period of anatectic granitic melt intrusions around 1000 m.y., and, (3) a low-grade metamorphism in late Caledonian time.

The age of the first event agrees well with ages of 1520 ± 30 m.y. and 1520 ± 10 m.y. reported by Råheim and Berg (1977) and Lappin and others (1978) from the western basal gneiss region. There the event is thought to represent the time of gneissification of the basement and of magmatic crystallization of mangeritic rocks. The good alignment of zircon data points from ortho- and paragneisses around a discordia line pointing to 1500 m.y. is remarkable considering that zircons from paragneisses usually trend to higher ages than the equivalent orthogneisses. The second event at 1000 m.y. falls within the Sveconorwegian orogenic period. At that time granitic melts intruded a metamorphic complex without significantly disturbing the U-Pb systems in the surrounding rocks. Thus, we must

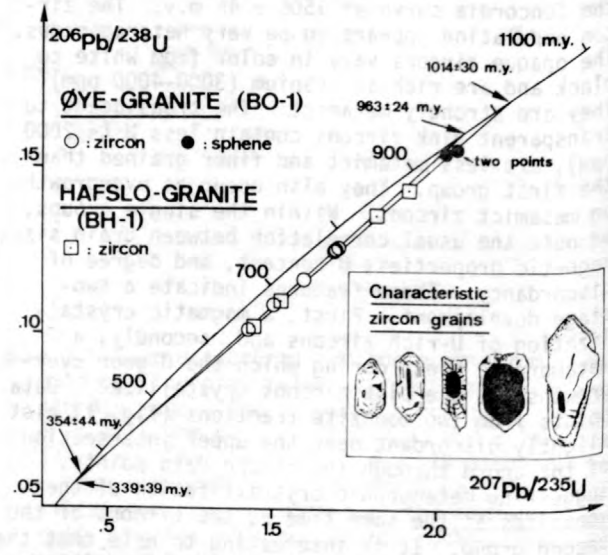

Figure 2.--Concordia diagram with zircon, monazite and sphene data points from rocks of the metamorphic basement. Discordia line is drawn through BV-1 zircon and monazite data points. Inset shows types of zircons in sample BV-1.

interpret this area as marking the north-eastern boundary of the Sveconorwegian province (Pasteels and Michot, 1975).

The Caledonian metamorphism is the third event registered by the U-Pb systems. The lower intercept ages scatter around 350-370 m.y. An interpretation in terms of an episodic lead loss would imply that the climax of the metamorphism occurred between 350 and 370 m.y. This contrasts, however, with Rb-Sr and K-Ar ages, mostly between 380 and 420 m.y., from minerals and whole rocks reported by a number of authors in south Norway, and with concordant sphene ages and lower intercept ages around 400 m.y. reported by Schärer (1978) from the Jotun nappe-complex.

So we must assume either that some other mechanism connected with an episodic lead loss is responsible for the low ages or that a metamorphism really occurred at this time. This would correspond to the Acadian (or Svalbardian) phase of the Caledonian cycle which involved gentle folding, thrusting, and some overthrusting of the Middle Devonian sediments in western Norway (Kvale, 1976). However, no metamorphism is known to be coupled to this tectonic phase.

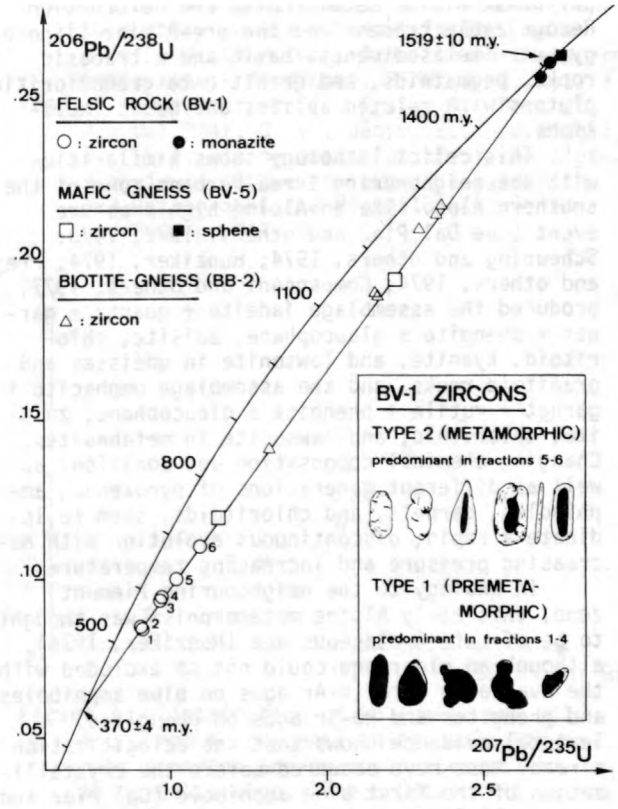

Figure 3.--Concordia diagram with zircon and sphene data points from two Sveconorwegian granites.

Heim, M., Schärer, U., and Milnes, A. G., 1977, The nappe complex in the Tyin-Bygdin-Vang region, central southern Norway. Norsk Geologisk Tidsskrift, v. 57, p. 171-178.

Kvale, A., 1976, Major features of the European Caledonides and their development, in, Ager, D. V., and Brooks, M., eds., Europe from crust to core: London, John Wiley, p. 81-115.

Lappin, M. A., Pidgeon, R. T., and van Breeman, O., 1978, Geochronology of basal gneisses and mangerite syenites of Stadlandet, south west Norway: Norsk Geologisk Tidsskrift, (in press).

Pasteels, P., and Michot, J., 1975, Geochronologic investigation of the metamorphic terrain of southwestern Norway: Norsk Geologisk Tidsskrift, v. 55, p. 111-134.

Priem, H. N. A., Boelrijk, N. A. I. M., Hebeda, E. H., Verdurmen, E. A. Th., and Verschure, R. H., 1973, A note on the geochronology of the Hestbreppigan granite in west Jotunheimen: Norges Geologiske Undersoekelse, v. 289, p. 31-35.

Råheim, A., and Berg, Ø., 1977, Open Rb-Sr systems behaviour of total rock samples; examples from Norway and Tasmania: European Colloquium of Geochronology, Pisa.

Schärer, U., 1978, Rock deformation and zircon-sphene U/Pb dating: (This conference).

THE SESIA-LANZO ZONE, A SLICE OF SUBDUCTED CONTINENTAL CRUST?

By G. V. Dal Piaz[1], J. C. Hunziker[2], and W. B. Stern[3]

[1]Padova, Italy

[2]Universität Bern, Bern, Switzerland

[3]Basel, Switzerland

The Sesia-Lanzo zone, a tectonic unit of the western Alps, southeast of the Piemont zone, is regarded by the authors as the root zone of the Monte Emilius-Arolla nappe, the lower unit of the Dent Blanche System. The pre-Alpine lithology has been changed to a great extent by

polyphase Alpine metamorphism and deformation. Recognizable traces from the pre-Alpine lithology are: metasediments, basic and ultrabasic rocks, pegmatoids, and granitic to granodioritic plutons with related aplites and basic inclusions.

This relict lithology shows similarities with the neighbouring Ivrea-Verbano zone of the southern Alps. The eo-Alpine high pressure event (see Dal Piaz and others, 1972, 1973; Scheuring and others, 1974; Hunziker, 1974; Frey and others, 1974; Compagnoni and others, 1977) produced the assemblage jadeite + quartz + garnet + phengite ± glaucophane, zoisite, chloritoid, kyanite, and lawsonite in gneisses and granitoid rocks, and the assemblage omphacite + garnet + rutile + phengite ± glaucophane, zoisite, chloritoid, and lawsonite in metabasites. Changing chemical composition and zonation, as well as different generations of pyroxenes, amphiboles, garnets, and chloritoids, seem to indicate a rapid, discontinuous evolution with decreasing pressure and increasing temperature.

In analogy to the neighbouring Piemont zone, this early Alpine metamorphism was thought to be of Late Cretaceous age (Hunziker, 1974), although an older age could not be excluded with the available data (K-Ar ages on blue amphiboles and phengites and Rb-Sr ages on phengites). Textural evidence shows that the eclogitization already must have occurred before the crystallization of the first blue amphibole (Dal Piaz and others, 1972).

In the Sesia-Lanzo zone the widespread granodioritic to granitic rocks in eclogite facies provide an excellent opportunity for the Rb-Sr dating of this eo-Alpine event. These rocks exist in all stages of transition between the still recognizable pre-eclogitic mineralogy (biotite + k-feldspar + plagioclase as relicts) and the complete transformation into a rock containing jadeite + quartz + garnet + phengite ± glaucophane + zoisite.

Accordingly, 25 granitoids from the Sesia-Lanzo zone were sampled, 15 of them from one pluton at Monte Mucrone near Biella over an area of 500 x 500 m, the rest from more distant localities of the Aosta-valley. Each sample consists of more than 20 kg of rock. Main-element and trace-element analyses--as well as Rb-Sr analysis of the whole rocks and K-Ar and Rb-Sr analysis of some minerals--have been performed so far. U-Pb work on the zircon populations is in progress.

The Rb-Sr data show clearly that when sampled in a small area also eclogites may yield an isochron, whereas samples from a bigger area tend to scatter beyond experimental error. The samples from the Monte Mucrone area define a preliminary isochron of 129 ± 22 m.y. with an initial ratio of 0.7133 ± 0.0006 (fig. 1). This result most likely has to be interpreted as the eo-Alpine age of eclogitization and is linked directly to the problem of the generation of eclogite-facies conditions in a crustal rock.

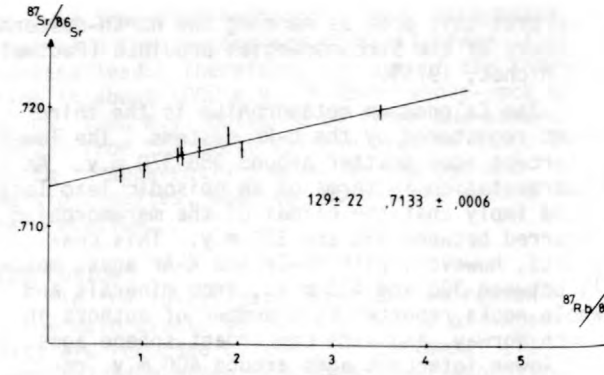

Figure 1.--Rb-Sr isochron of whole-rock eclogite facies granitoid samples defining an age of 129 ± 22 m.y. with an initial ratio of 0.7133 ± 0.0006 calculated with the λ^{87}Rb decay constant of 1.42×10^{-11} yr^{-1}.

Here the problem arises as to whether this metamorphism was isochemical or allochemical. First of all, we have to take into consideration the previous history of our granitoids. In the neighbouring Ivrea Verbano zone, the well known Baveno granite suite shows a late Hercynian age of around 280 m.y. (Jäger and Faul, 1960). These granites are the closest possible correlatives to the metagranitoids of the Sesia-Lanzo zone. Both are characterized by rather high Ba values, as documented for the Sesia-Lanzo granitoids on figure 2.

Furthermore, the mechanism that led to the transformation of these granitoid rocks into "eclogites" has to be considered. The paragenesis of jadeite + quartz of these metagranitoids, together with the temperature estimations between 350 and 550°C (Dal Piaz and others, 1972; Velde and Kienast, 1973), leads to pressures between 10 and 15 kb equivalent to depths of between 35 and 50 km. Stable isotope determinations of Desmons and O'Neil (1977) strongly favor the higher temperature. Paleogeographically speaking, we can only account for an overburden of 5 to a maximum of 10 km. These facts have lead various authors to propose subduction models for the western Alps. The question arising from such an interpretation is, what happened in these depths under such pressures at relatively elevated temperatures with respect to the chemistry of the rocks?

The K/Rb ratio of the Sesia-Lanzo metagranitoids (fig. 3) shows crustal values of between 200 and 280. The K/Rb ratio for aplitic rocks is around 200, while the coarse-grained granites and granodiorites tend toward the higher values. Also, the relatively constant Mn/Fe ratio of 0.016 - 0.014 is in favor of a rather stable chemical behaviour during the eo-Alpine metamorphism.

The same conclusion can be documented in the QLM diagram (fig. 4) showing that, for both partially and completely transformed metagranitoids, the points cluster around the original

eutectic point for alkali feldspar + quartz. No trend of the jadeite-rich eclogites towards the jadeite-pyroxene line can be distinguished.

Both the Rb-Sr and K-Ar mineral ages show that the eclogitization was followed first by a rise in temperature and then by a subsequent cooling that led to K-Ar phengite ages around 60 m.y.

Conclusions: The Hercynian granitoids of the Sesia-Lanzo zone underwent an eo-Alpine eclogitization around 130 m.y. This transformation was more or less isochemical. The delayed rise in temperature brought the rocks up to around 550°C at pressures of around 15 kb. A subduction model is the simplest explanation as no adequate geologic overburden can be found. By 60 m.y. ago this subducted crustal segment had already cooled to below 300°C.

Compagnoni, R., Dal Piaz, G. V., Hunziker, J. C., Gosso, G., Lombardo, B., and Williams, P. F., 1977, The Sesia-Lanzo zone a slice of continental crust with Alpine high-pressure low-temperature assemblages in the Western Italian Alps: Rendiconti SIMP, v. 33, pt. 1.

Dal Piaz, G. V., Hunziker, J. C., and Martinotti, G., 1972, La zona Sesia-Lanzo e l'evoluzione tettonico metamorphica delle Alpi Nordoccidentali interni: Mem. Soc. Geol. Ital., v. 11.

1973, Excursion to the Sesia zone of the Schweiz. Mineralogische und Petrographische Gesellschaft: Schweizerische Mineralogische und Petrographische Mitteilungen, v. 53, no. 3, p. 477-490.

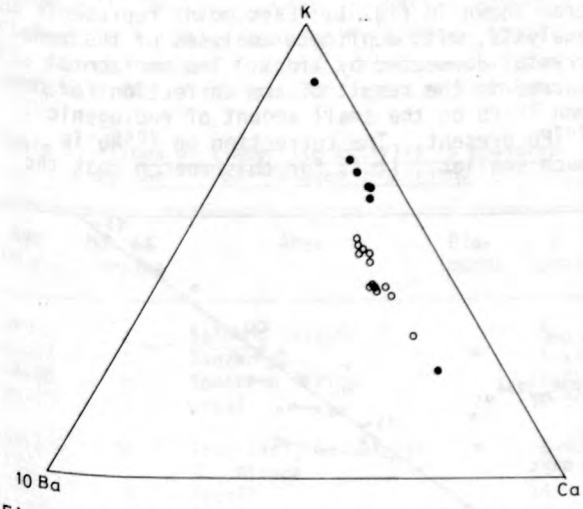

Figure 2.--K, Ca, 10 x Ba diagram showing the homogeneous distribution and high barium content in the granitoid rocks of the Sesia-Lanzo zone (corresponding to Ba/Ca and Ba/K ratios of 0.015 and 0.005, respectively). Open circles, metagranitoids; solid circles, metaaplites.

Desmons, J., and O'Neil, R., 1977, Stable isotope measurements on minerals from eclogites and other rocks from the northeastern Sesia zone: Rendiconti SIMP, v. 33, pt. 1.

Frey, M., Hunziker, J. C., Frank, W., Bocquet, J., Dal Piaz, G. V., Jäger, E., and Niggli, E., 1974, Alpine metamorphism of the Alps--A review: Schweizerische Mineralogische und Petrographische Mitteilungen, v. 54, no. 2-3, p. 247-290.

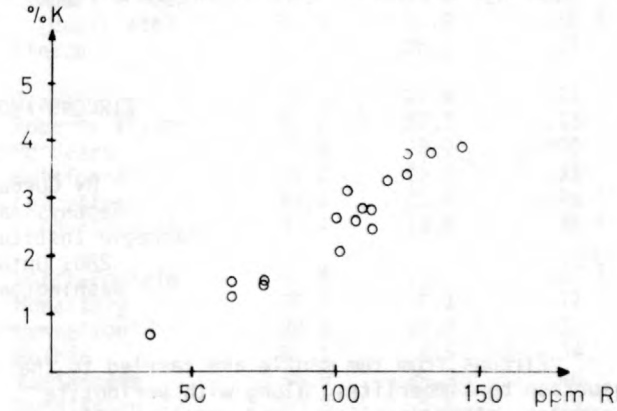

Figure 3.--Distribution of Rb (parts per million) and K (percent) in the eclogite-facies granites and granodiorites of the Sesia-Lanzo zone. The crustal K/Rb ratios of 200 - 280 show that no great changes occurred during eclogitization.

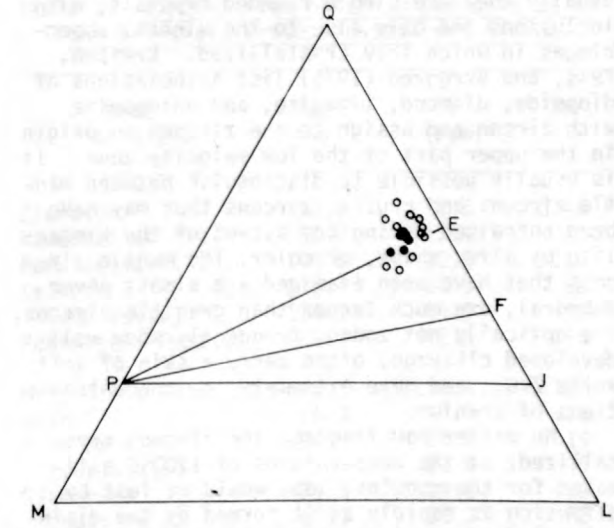

Figure 4.--QLM diagram with data of Sesia-Lanzo metagranitoids. Solid circles, rocks with the pre-eclogitic mineralogy still recognizable (biotite, plagioclase, k-feldspar); open circles, completely transformed rocks with jadeite + quartz + garnet + phengite ± glaucophane, zoisite, lawsonite; E, eutectic point for alkali feldspar + quartz; J, jadeite, F, Ab + Or + An; P, pyroxene.

Hunziker, J. C., 1974, Rb-Sr and K-Ar age determination and the Alpine tectonic history of the western Alps: Memorie Inst. Geol. Mineral Univ., Padova, v. 31.

Jäger, E., and Faul, H., 1960, Altersbestimmungen an einigen Schweizer Gesteinen und dem Granit von Baveno: Schweizerische Mineralogische und Petrographische Mitteilungen, v. 40, no. 1, p. 10-12.

Scheuring, B., Ahrendt, H., Hunziker, J. C., and Zingg, A., 1974, Palaeobotanical and geochronological evidence for the Alpine age of the metamorphism in the Sesia zone: Geologisches Rundschau, v. 63, no. 1, p. 305-326.

Velde, B., and Kienast, J. R., 1973, Zonéographie du métamorphisme de la zone Sesia-Lanzo (Alpes piémontaises); étude des omphacites et grenats des micaschistes éclogitiques à la microsonde électronique: Paris, Académie des Sciences, Comptes rendus, series D, p. 1801-1804.

ZIRCONS FROM THE MANTLE

By Gordon L. Davis
Geophysical Laboratory
Carnegie Institution of Washington
2801 Upton St., N.W.
Washington, D. C. 20008

Zircons from the mantle are carried to the surface by kimberlites, along with peridotite nodules, other xenoliths, and sometimes diamonds. The zircon content of kimberlites is so low that samples are recovered only where commercial mining and separating processes are used, or where large volumes of kimberlite are assayed in a prospecting operation. Some pipes appear to carry no zircons. In a few cases zircons are found in place in the nodules but usually they are single rounded crystals, with inclusions the only clue to the mineral assemblages in which they crystallized. Kresten, Fels, and Berggren (1975) list associations of diopside, diamond, ilmenite, and phlogopite with zircon and assign to the zircons an origin in the upper part of the low-velocity zone. It is usually possible to distinguish between mantle zircons and crustal zircons that may have been entrained during the ascent of the kimberlite by size, shape, or color. The mantle zircons that have been examined are almost never euhedral, are much larger than granitic zircons, are optically not zoned, frequently show well developed cleavage, often carry a skin of soft white ZrO_2, and have extremely low concentrations of uranium.

No matter how long ago the zircons crystallized, at the temperatures of 1100°C estimated for the nodules, lead would be lost by diffusion as rapidly as it formed by the disintegration of uranium. Lead did not begin to accumulate in the zircons until the temperature dropped at the time of eruption.

In 1976, Davis, Krogh, and Erlank (1976) published the first analyses by isotope dilution and age measurements for kimberlite zircons. These results were made possible by the development of a hydrothermal method of decomposition and the use of ultra-pure reagents (Krogh, 1973; Mattinson, 1972). Additional analyses can be found in the extended abstracts of the Second International Kimberlite Conference as well as in the Carnegie Institution of Washington Yearbook 76. New determinations are indicated in the tables below.

The analyses require a lot of care: decomposition is slow and the utmost precautions against contamination by lead must be taken. Blanks must be low in order to determine accurately and correct for the small amount of common lead present. A mixed tracer of ^{205}Pb and ^{235}U was used. Some idea of the quality of the results can be obtained from the concordia diagram shown in fig. 1. Each point represents an analysis, with duplicate analyses of the same crystal connected by lines. The horizontal spread is the result of the correction for common ^{207}Pb on the small amount of radiogenic ^{207}Pb present. The correction on ^{206}Pb is much smaller. It is for this reason that the

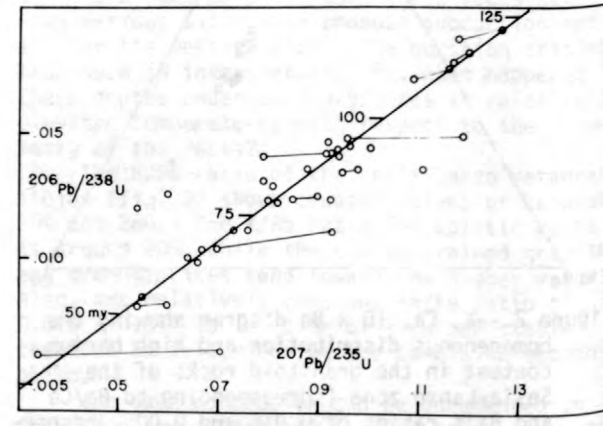

Figure 1.--U-Pb concordia diagram for zircons from kimberlites. Points from duplicate analyses are connected.

ages in the tables have been calculated from the $^{206}Pb/^{238}U$ ratio. The results of this study of zircons from 40 kimberlites are summarized below in tables 1, 2, and 3.

Table 1 gives the times of kimberlite activity as indicated by the zircon ages. The range of concentrations of uranium is also given, along with an indication of whether or not the pipes contain diamonds. The kimberlites from southern Africa and Brazil date from about the time of opening of the South Atlantic ocean and continue throughout Cretaceous, Paleocene, and Eocene time. Whether there was other than a chronological relationship is speculative at this time.

The ages, concentrations of uranium, and Th-U ratios are given in table 2 and table 3 for zircons from southern Africa. Thorium was not determined, the Th-U ratio being calculated from the measured ^{206}Pb-^{208}Pb ratios and the ^{206}Pb-^{238}U ages. The kimberlites listed in table 2 are all from the Transvaal Craton, notable for the diamond pipes near Kimberley. With the exception of Orapa, the pipes occur within an area about 800 km in diameter. The kimberlites were emplaced during the interval between 84 and 110 m.y., with the peak of activity at 92 m.y. The zircons comprise a closely related group with the average Th/U of 0.34, the same as the average value given for three kimberlite zircons by Ahrens, Cherry, and Erlank (1967). The average concentration of uranium is 24 ppm, a little higher than the average of 16.5 ppm given by Kresten, Fels, and Berggren (1975) who used fission-track analysis.

The low uranium contents provide a clue as to the tenor of the mantle with respect to this element if the U_{zircon}/U_{liquid} partition coefficient is $\geq$ 100 as deduced by Kresten (1974). The source regions for the zircons would then contain 0.06 - 0.85 ppm, or less, or uranium.

Table 1.--Times of kimberlite activity as measured by the $^{206}Pb/^{238}U$ ages of zircons

Age (m.y.)	No. of samples	Area	Diamonds	U (ppm)
34	1	Solomon Islands		5
40-53	2	Tanzania	+	6-13
54-80	9	Southern Africa		12-450
80-93	5	Brazil	?	17-50
84-110	14	Transvaal, So. Africa	+	6-40
115	1	So. Africa		85
120	1	Brazil	?	14
133	1	Angola	+	3
150	2	So. Africa		12-18
157	2	Yakutia, USSR	+	8-18
194	1	So. Africa		7
344	1	Yakutia, USSR	+	8
412-443	2	Yakutia, USSR	+	7

Table 2.--Zircons from the diamond pipes of the Transvaal Craton, South Africa

Name of pipe	Age (m.y.)	U (ppm)	Th/U
Last Hope (1)	111.6	35.1	0.27 [1]
(duplicate)	111.5	37.6	.28 [1]
Last Hope (2)	108.9	37.7	.22 [1]
Kimberley Rock	95.4	39.9	.65
(duplicate)	94.9	40.9	.58 [1]
Finsch	94.1	26.1	.37
Orapa	93.1	14.4	.21
Roberts Victor	92.2	27.7	.43
De Beers	92.0	28.2	.30
Bultfontein	91.2	13.1	.33
Leicester	92.4	21.6	.28 [1]
(duplicate)	90.4	18.5	.46 [1]
Koffiefontein	90.4	19.9	.27 [1]
Monastery	90.4	6.1	.17
Wesselton	90.3	18.4	.35
Mothae	87.1	8.6	.34
Kamfersdam	86.9	29.8	.40
Dutoitspan	83.8	5.6	.15

[1]New determinations.

Table 3.--Zircons from barren pipes outside of the Transvaal Craton in southern Africa

Name of pipe	Age (m.y.)	U (ppm)	Th/U
Clarkton	193.9	6.5	0.48 [1]
Ramatseliso (1)	150.8	17.9	.65
Ramatseliso (2)	148.6	12.0	.28
Kalkput	116.4	84.3	.58 [1]
(duplicate)	114.1	84.9	.53 [1]
McKenzie's Post (1)	80.3	12.4	.30
McKenzie's Post (2)	79.7	129.4	.90
Lushof	78.3	64.9	.66
Rietfontein	71.9	25.2	.19
(duplicate)	71.7	23.4	.19
Riembreek	71.6	34.3	.27 [1]
(duplicate)	67.1	35.1	.85 [1]
Platbakkies	66.7	440.5	1.46
Bokputs	64.2	200.8	1.26 [1]
(duplicate)	64.1	185.9	1.26 [1]
Melkfontein	63.4	109.4	1.59
Brakfontein	54.1	338.1	.41

[1]New determinations.

Conditions in the mantle underneath the Transvaal Craton during or before the interval from 84 m.y. to 110 m.y. were favorable for the crystallization of diamonds and for their preservation during the ascent and eruption of the kimberlites. (There are barren pipes in this area but no zircon samples from them were available.) The same favorable conditions did not exist in the regions from which the zircons in table 3 came. Two zircons with the lowest uranium concentrations came from peridotite nodules (Monastery and Dutoitspan). Some of the zircons with high concentrations of uranium and high Th-U ratios (Platbakkies and Bokputs) may have come from melilite-bearing pipes (Cornelissen and Verwoerd, 1975).

Zircon samples were provided by F. R. Boyd, J. B. Hawthorn, P. H. Nixon, N. V. Sobolev, and A. J. Erlank.

Ahrens, L. H., Cherry, R. D., and Erlank, A. J., 1967, Observations on the Th-U relationship in zircons from granitic rocks and from kimberlites: Geochim Cosmochimica Acta, v. 31, p. 2379-2387.

Cornelissen, A. K., and Verwoerd, W. J., 1975, The Bushmanland kimberlites and related rocks: Physics and Chemistry of the Earth, v. 9, p. 71-80.

Davis, G. L., Krogh, T. E., and Erlank, A. J., 1976, The ages of zircons from kimberlites from South Africa: Carnegie Institution of Washington Year Book 75, p. 821-824.

Kresten, P., 1974, Uranium in kimberlites and associated rocks, with special reference to Lesotho occurrences: Lithos, v. 7, p. 171-180.

Kresten, P., Fels, P., and Berggren, G., 1975, Kimberlitic zircons--a possible aid in prospecting for kimberlites: Mineralium Deposita, v. 10, p. 47-56.

Krogh, T. E., 1973, A low-contamination method for hydrothermal decomposition of zircon and extraction of U and Pb for isotopic age determination: Geochimica Cosmochimica Acta, v. 37, p. 485-494.

Mattinson, J. M., 1972, Preparation of hydrofluoric, hydrochloric and nitric acids at ultra-low lead levels: Analytical Chemistry, v. 44, p. 1715-1716.

THE ORIGIN OF ANORTHOSITES; GEOCHEMICAL AND ISOTOPIC CONSTRAINTS

By D. Demaiffe
Departement de Géologie,
Musée Royal de l'Afrique Centrale,
Tervuren and Laboratoire de Minéralogie-Pétrologie, Université Libre de Bruxelles

One of the main problems in anorthosite petrogenesis is the nature and origin of the parental magma. This paper is restricted to the Proterozoïc massif-type anorthosites. The anorthositic layers in stratiform intrusions and the Archean An-rich anorthosites are not considered. Two rock types, both from the Rogaland complex of Southern Norway (Michot and Michot, 1969), have been investigated in the present study:

1. Plagioclasic cumulates (anorthosite, leuconorite, norite).
2. Fine-grained rocks of intermediate composition (jotunite, according to Streckeisen, 1974) occurring as border rocks to some anorthositic bodies or as dikes crosscutting the whole complex.

Data on charnockitic rocks spatially related to anorthosites have been presented elsewhere (Demaiffe and others, 1978). Before discussing the nature of the parental magma, isotopic (Sr and O) and petrological data, which are able to fix some limitations on the source-region of the anorthosites, are reviewed.

The $^{87}Sr/^{86}Sr$ initial ratios are generally low but variable from massif to massif; the range of values for the whole complex (≃ 1500 km^2) is 0.7035 - 0.7065. These low values point to a mantle or deep crustal origin.

The measured ratio has been corrected taking into account the in situ decay of ^{87}Rb, assuming an age of 1 b.y. The Sr isotopic composition has been measured on the VARIAN TH5 mass-spectrometer of the Belgian Centre for Geochronology, which gives: for the E. and A. Sr standard, 0.70807 ± 7 ($1\sigma_M$) (10 measurements); for the NBS 987 Sr standard, 0.71015 ± 4 ($1\sigma_M$) (7 measurements).

The intermassif differences in the isotopic composition cannot be explained by a supracrustal contamination process because rocks with the highest ratios (jotunitic dikes) have very low LIL elements content (Rb, < 25 ppm; Th, < 3.5 ppm; U, < 1 ppm). It seems unreasonable to appeal to a disequilibrium melting process (O'Nions and Pankhurst, 1974) on the basis of the Sr diffusion velocity at mantle temperatures

in the presence of a melted phase (Hofmann and Hart, 1978). Mantle heterogeneity, on the scale of the Rogaland province, is thus the only plausible mechanism to explain the Sr isotopic variations.

The oxygen isotopic composition of the anorthosites is in agreement with Taylor's data (1969); the $\delta^{18}O$ values are in the range of 5.2 to 6.6 permil, which is nearly identical to the values reported for unaltered basaltic material of mantle origin. Two other petrological arguments point to a mantle origin for the anorthosites.

1. The temperature of crystallization of the plagioclase in porphyritic jotunites has been estimated at 1050° to 1150°C with the Kudo-Weill geothermometer, by considering the fine-grained jotunite as a glassy matrix. As Wyllie (1971) has already mentioned for rocks of intermediate composition (like andesite), these temperatures are so high that it seems improbable that the parental liquids could be generated in the crust.

2. The anorthosite massifs contain very Al rich orthopyroxene megacrysts (as much as 9 percent Al_2O_3) and, following the experimental work of Emslie (1975), should have crystallized at a pressure of about 15 kb, which is definitively unrealistic for crustal rocks.

Recent fieldwork (Demaiffe and others, 1973) has shown the existence of a fine-grained (400 μm), locally porphyritic, jotunitic rock at the border of the Hidra and Garsaknatt bodies. This jotunite grades progressively toward the central anorthosite by enrichment in plagioclase phenocrysts and has been interpreted as a magmatic liquid equivalent to the chilled margins of shallower intrusions.

The REE geochemistry (Duchesne and Demaiffe, 1978) has demonstrated that this jotunite characterized by a smooth REE distribution pattern without any Eu anomaly cannot be considered as a residual liquid left over after the crystallization of the anorthositic cumulate with a large positive Eu anomaly (Eu/EU ≃ 8). This jotunite may thus be considered as the parental magma of the anorthositic suite.

The main geochemical features of the jotunites are the following (Duchesne and Demaiffe, 1978):

1. High TiO_2 (4.5 percent) and P_2O_5 (1.5 percent) contents
2. High total REE content (Σ REE ≃ 130 ppm) with a fractionated distribution trend (La/Yb = 7 - 10)
3. Transition-elements geochemistry comparable to that of the andesitic rocks with Ni and Cr depletions.

Only a qualitative approach of the partial melting process is presented below.

The high REE content of the jotunite implies a small to moderate degree of partial melting of peridotitic mantle material (= lherzolitic) composition.

The relative heavy REE depletion suggest that garnet is a residual mineral of the melting process.

In a plot of two trace elements (P_2O_5-Ce; La-Ce; Nd-Ce; ...), the data are co-linear with the origin. This means, as Sun and Hanson (1975) and Hanson (1978) have shown, that in the classical equation of batch partial melting (Gast, 1968)

$$C_l/C_o = 1/[Do + (1 - P) F],$$

rewritten using the bulk partition coefficient of the residual solid (D_{RS}), the numerical value of D_{RS} for both elements is much less than the extent of partial melting F. Thus, the ratio C_l/C_o is inversely proportional to F; i.e., $C_l/C_o = 1/F$.

The co-linearity P_2O_5-Ce suggests that apatite melts completely and is not a residual phase in the mantle.

Conclusion: The anorthosites are the products of the fractional crystallization of jotunitic liquids generated in the upper mantle by a small to moderate degree of partial melting, probably involving the complete melting of apatite while garnet and olivine are present in the residue.

Demaiffe, D., Duchesne, J. C., Michot, J., and Pasteels, P., 1973, Le massif anorthositique d'Hidra et son faciès de bordure: Paris, Académie des Science, Comptes Rendus, Sereís D, v. 17, p. 277.

Demaiffe, D., Duchesne, J. C., and Hertogen, J., (in press), Trace element variations and isotopic composition of charnockitic acidic rocks related to anorthosites (Rogaland, S. Norway): Symposium on Origin and distribution of the elements, 2nd, Proc.

Duchesne, J. C., and Demaiffe, D., 1978, Trace elements and anorthosite genesis: Earth and Planetary Science Letters, v. 38, p. 249.

Emslie, R., 1975, Pyroxene megacrysts from anorthositic rocks; new clues to the sources and evolution of parent magmas: Canadian Mineralogist, v. 13, p. 138.

Gast, P. W., 1968, Trace-element fractionation and the origin of tholeiitic and alkaline magma types: Geochimica Cosmochimica Acta, v. 32, p. 1057.

Hanson, G. N., 1978, The application of trace elements to the petrogenesis of igneous rocks of granitic composition: Earth and Planetary Science Letters, v. 38, p. 26.

Hofmann, A., and Hart, S. R., 1978, An assessment of local and regional isotopic equilibrium in the mantle: Earth and Planetary Science Letters, v. 38, p. 44.

Michot, J., and Michot, P., 1969, The problem of the anorthosites of the south Rogaland igneous complex, in Isachsen, Y., ed., Origin of anorthosites and related rocks: New York State Museum and Science Service, Memoir 18, p. 399.

D'Nions, R. K., and Pankhurst, R. J., 1974, Petrogenetic significance of isotope and trace-element variations in volcanic rocks from the mid-Atlantic: Journal of Petrology, v. 15, p. 603.

Streckeisen, A., 1974, How should charnockitic rocks be named?, in Geologie des domaines cristallins: Liege, Societe Geologique de Belgique, p. 349-360.

Sun, S. S., and Hanson, G. N., 1975, Origin of Ross Island basanitoids and limitations upon the heterogeneity of mantle sources for alkali basalts and nephelinites: Contributions to Mineralogy and Petrology, v. 52, p. 77.

Taylor, S. R., 1969, Trace-element chemistry of andesites and associated calc-alkaline rocks, in Andesite conference, Eugene and Bend, Oregon, 1968, Proc.: Oregon Department of Geology and Mineral Industries Bulletin 65, p. 43.

Wyllie, P. J., 1971, The dynamic earth: New York, John Wiley, 416 p.

DIETARY ANALYSIS FROM $^{13}C/^{12}C$ RATIOS OF CARBONATE AND COLLAGEN FRACTIONS OF BONE

By Michael J. DeNiro and Samuel Epstein
Division of Geological and Planetary Sciences
California Institute of Technology
Pasadena, California 91125

The isotopic composition of animal carbon records information about the diet of the animal. The $\delta^{13}C$ value of the diet can be determined from the $\delta^{13}C$ value of some component of the animal by taking into account the specific isotopic fractionation which occurs during the synthesis of that component from diet carbon. For the studies to be reported here, the relevant fractionation factors have been determined using mice raised on diets of known and constant $\delta^{13}C$ value. The $\delta^{13}C$ value of the diet is 3.2 ± 0.4 permil more negative than that of the bone collagen fraction and 9.6 ± 0.1 permil more negative than that of the bone carbonate fraction. The $\delta^{13}C$ value of the diet as estimated from the $\delta^{13}C$ value of one or both of these carbon-containing bone fractions can then be used to determine the relative consumption of dietary sources whose $\delta^{13}C$ values are known or can be inferred. The precision of the method generally limits its application to situations in which the diet sources come from groups with large differences in their $\delta^{13}C$ values, such as C_3 versus C_4 plants or aquatic versus terrestrial organisms.

Differences in feeding habits of recent species can, in some cases, be analyzed from the $\delta^{13}C$ values of bone carbon. Procavia johnstoni and Heterohyrax brucei are sympatric hyrax species which live on and around rocky outcrops in the Serengeti National Park of Tanzania. The former species is primarily a grazer while the latter is almost exclusively a browser. Most of the grasses available to these animals are C_4 plants, while most of the browse materials are C_3 plants. The difference in the $\delta^{13}C$ values of the diets of the two species as estimated from the $\delta^{13}C$ values of both the carbonate and collagen fractions of bone reflects the 10 - 15 permil difference in the $\delta^{13}C$ values of the two classes of diet materials.

Analysis of the $\delta^{13}C$ values of the carbon from bones of American Indians whose diets are known from anthropological data illustrates other types of dietary analysis which can be made using this method. The $\delta^{13}C$ values for bone carbon of tribes whose diets were largely based on land mammals (caribou or buffalo) are more negative than the values for tribes whose diets were based primarily on marine animals (seal or fish). Differences among tribes in the utilization of corn, a C_4 plant, as a dietary component in regions where most other diet sources were derived from C_3 plants, correlate with differences in the $\delta^{13}C$ values of the bone carbon.

Dietary analysis from the $\delta^{13}C$ values of carbon contained in fossil bone is possible if the original isotopic imprint has not been altered during diagenesis. The carbonate fraction of bone is subject to exchange with atmospheric CO_2 and (or) CO_2 dissolved in groundwater, and, consequently, is unlikely to retain its original isotopic composition. The bone collagen fraction is not subject to such exchange with postmortem carbon sources and is likely to retain isotopic information relating to diet. These points are illustrated by the carbon isotopic analysis of the collagen and carbonate fractions of bone from extant and fossil domesticated llamas from Peru, which are thought to have eaten similar diets. The $\delta^{13}C$ values of the diets as estimated from the bone collagen fractions agree to within 2 permil, while the diet values as estimated from the bone carbonate fractions differ by 8 permil. It must still be determined if the small difference in diet $\delta^{13}C$ values as estimated from the collagen

fractions represents a real difference in the diets of the recent and fossil animals, or if changes in the concentration and amino acid composition of collagen in bone, which are known to occur during diagenesis, account for some of the difference.

Changes in the $\delta^{13}C$ values of bone carbon through a stratigraphic column provide information about the evolution of dietary habits. This is demonstrated by the analysis of human skeletal remains from the Viru Valley of Peru. $\delta^{13}C$ values for bone collagen at the base of the column are consistent with archeological evidence which suggests that the diet at this time was based primarily on seafood. A shift towards more positive $\delta^{13}C$ values higher in the column can be related to the introduction of corn from the Peruvian highlands; the isotopic evidence permits this event to be dated at least several hundred years earlier than do the earliest remains of corn. A further shift to even more positive $\delta^{13}C$ values of bone collagen near the top of the column correlates with archeological evidence for increased sophistication in agricultural methods, which presumably resulted in an increased utilization of cultivated crops, including corn.

In summary, the $\delta^{13}C$ values of the carbonate and collagen fractions of bone, if unaltered by diagenetic processes, coupled with ecological, paleontological, archeological, or anthropological evidence about possible diet sources, provide a qualitative and, in some cases, a quantitative estimate of diet.

The bones reported on here were provided by H. N. Hoeck (hyrax), L. Angel (American Indian), E. Wing (llama), and J. Ericson (Viru Valley). The assistance of R. S. MacNeish in directing us to some of these specimens and discussions with him are gratefully acknowledged.

Nd AND Sr ISOTOPE SYSTEMATICS OF YOUNG CONTINENTAL IGNEOUS ROCKS

By Donald J. DePaolo
Department of Earth and Space Sciences
University of California
Los Angeles, California 90024

Recent studies of Nd isotope variations in igneous rocks have suggested that a striking chemical difference may exist between the mantle in oceanic and continental areas (DePaolo and Wasserburg, 1976a, b). Furthermore, some data suggest that major portions of the subcontinental mantle may be undifferentiated, having retained a chondritic relative rare-earth element (REE) pattern since the formation of the Earth. Because of the implications of these possibilities for models of crustal growth and mantle structure, a suite of young continental volcanic and plutonic rocks from a variety of geologic settings have been analyzed for $^{143}Nd/^{144}Nd$ and $^{87}Sr/^{86}Sr$ in an attempt to better define the patterns of isotopic variations in continental areas, and thereby provide a further test of these hypotheses.

The samples analyzed are listed in table 1. For each sample is given the initial $^{143}Nd/^{144}Nd$ and $^{87}Sr/^{86}Sr$ expressed in terms of the parameters ε_{Nd} and ε_{Sr} (DePaolo and Wasserburg, 1976a, 1977). The initial ratios have been calculated from the measured ratios using the known age of each rock and the measured Sm/Nd and Rb/Sr. $\varepsilon_{Nd}(T) = 0$ is characteristic of a reservoir which has a chondritic relative REE pattern for all time (T). Reservoirs which have REE patterns fractionated with respect to chondritic for more than about 10^8 yr have ε_{Nd} different from zero. Reservoirs with light REE-depleted patterns (high Sm/Nd) have $\varepsilon_{Nd} > 0$, and reservoirs with light REE-enriched patterns (low Sm/Nd) have $\varepsilon_{Nd} < 0$. The absolute value of ε_{Nd} is proportional to the degree of fractionation of Sm/Nd and the time since the fractionation occurred. ε_{Nd} of igneous rocks, therefore, give information about the age and chemistry of the reservoirs from which the magmas were melted. For Rb-Sr, the analogous parameter $\varepsilon_{Sr}(T) = 0$ characterizes a reservoir which has Rb/Sr = 0.029 for all time. This Rb/Sr was chosen because it may be characteristic of unfractionated material in the earth's mantle (DePaolo and Wasserburg, 1976b, 1977; O'Nions and others, 1977). The Nd data for the samples from table 1, plus other data from the literature, are shown in figure 1. Nd and Sr data from table 1, plus data on continental rocks from DePaolo and Wasserburg (1976a, b, 1977), are shown on figure 2. Additional data on continental rocks have been given by Carter and others (1978).

Figure 1 shows that all of the continental rocks have ε_{Nd} less than about +7. This contrasts with MOR and island arc rocks which have $\varepsilon_{Nd} > +7$, as well as with some intraplate oceanic island basalts which also have $\varepsilon_{Nd} > +7$. The data confirm the existence of a profound difference between magma sources in oceanic and continental regions as suggested by DePaolo and

Wasserburg (1976b). However, the suggestion that continental magma sources are, in general, unfractionated is not supported by the data. The new data on rocks from continental margin magmatic arcs and continental alkaline basalts show that these rocks may, in general, have ε_{Nd} displaced from zero in the direction of the oceanic rocks. Thus, some continental magma sources appear to be fractionated with respect to REE, and therefore do not appear to be undifferentiated primordial material. The data suggest that the subcontinental mantle is less depleted in "crustal components" than is the suboceanic mantle.

Figure 2 shows the data on continental rocks plotted on a graph of ε_{Nd} versus ε_{Sr}. The solid line in this figure represents the ε_{Nd}-ε_{Sr} correlation trend defined by MOR basalts and ocean island basalts (DePaolo and Wasserburg, 1976b; O'Nions and others, 1977). The dashed lines enclose the field of present-day Nd and Sr isotopic compositions of continental crustal rocks. The young continental igneous rocks which have $\varepsilon_{Nd} > -4$ and $\varepsilon_{Sr} < +15$ generally conform to the oceanic trend. This indicates that the Nd-Sr systematics found in oceanic areas also apply to continental magma sources and suggests that the process responsible for the ε_{Nd}-ε_{Sr} correlation is operative in both regions, despite the fact that the subcontinental mantle may have considerably different physical properties than the suboceanic mantle and may be isolated from the convective mixing with the suboceanic mantle. The remainder of the samples can be separated into two groups. Some continental flood basalts form a trend which parallels the upper dashed curve and extends from $\varepsilon_{Nd} = 0$, $\varepsilon_{Sr} = 0$ to about $\varepsilon_{Nd} = -19$, $\varepsilon_{Sr} = +300$. This trend has a slope distinctly different from that discussed above (solid line on fig. 2) and corresponds to that expected if basaltic magma with $\varepsilon_{Nd} = 0$, $\varepsilon_{Sr} = 0$ is contaminated to varying degrees with Rb-rich granitic material from the upper crust. This explanation is plausible because the basalts involved show evidence of having differentiated in magma chambers at crustal depths. However, this trend could instead indicate subcontinental magma sources with unique histories of Rb-Sr and Sm-Nd fractionation. The second group of samples scatter within the field enclosed by the dashed lines (see also Carter and others, 1978). These variations are not understood, but could result from crustal melting or contamination.

Table 1.--Nd and Sr isotopic parameters for young continental igneous rocks
[All samples have ages less than about 15 million years except as noted.]

Sample	ε_{Nd}	ε_{Sr}
Flood basalts		
PAR-1 (Parana basin, Brazil)[1]	-1.5±0.4	+6.6± 2.0
PAR-2 (Parana basin, Brazil)[1]	-4.2±0.5	+15.7± 0.7
ADT-1 (Red Hill, Tasmania)[2]	-4.5±0.5	+98.0±10.0
AF-133 (Afar depression)	+4.9±0.5	-14.2± 0.2
AF-134 (Afar depression)	+6.1±0.5	-11.1± 0.6
DTY-18 (Yakima Basalt Subgroup, Oregon)	+1.0±0.5	+7.4± 0.7
Alkaline basalts		
CSQ-3 (basanite, Baja, California)	+6.7±0.5	-21.1± 0.7
CHA-2 (basalt, Patagonia)	+3.9±0.3	-4.1± 0.9
V-9 (basalt, Patagonia)	+2.3±0.3	-5.1± 0.7
ANB2128 (newer basalt, Australia)	+4.0±0.2	-10.4± 0.7
ANB2120Q (newer basalt, Australia)	+4.5±0.3	-13.8± 1.0
WBK-1 (Golan Heights)	+5.1±0.4	-11.6± 0.6
DU-111 (Ugandite, Uganda)	-2.3±0.4	+13.1± 1.6
Continental margin arcs		
CAS-1 (basalt, Mt. Shasta, California)	+4.6±0.3	-11.9± 0.9
WMG-1 (granodiorite, southern California)[1]	+3.6±0.6	-13.4± 2.0
RL-1 (granite, southern California)[1]	+1.3±0.5	-18.0± 7.0
MEX-1 (andesite, Arenal, Costa Rica)	+7.4±0.4	-10.4± 1.4
Kimberlites and carbonatites		
AK-1 (kimberlite, DeBeers, South Africa)[3]	+3.6±0.5	-15.2± 0.9
AK-2 (kimberlite, Kao Mine, Lesotho)[4]	-11.0±0.5	+44.4± 1.6
OLC-1 (carbonatite, Tanzania)	+0.1±0.9	-4.8± 1.0

[1] 120 m.y.
[2] 165 m.y.
[3] 90 m.y.
[4] 127 m.y.

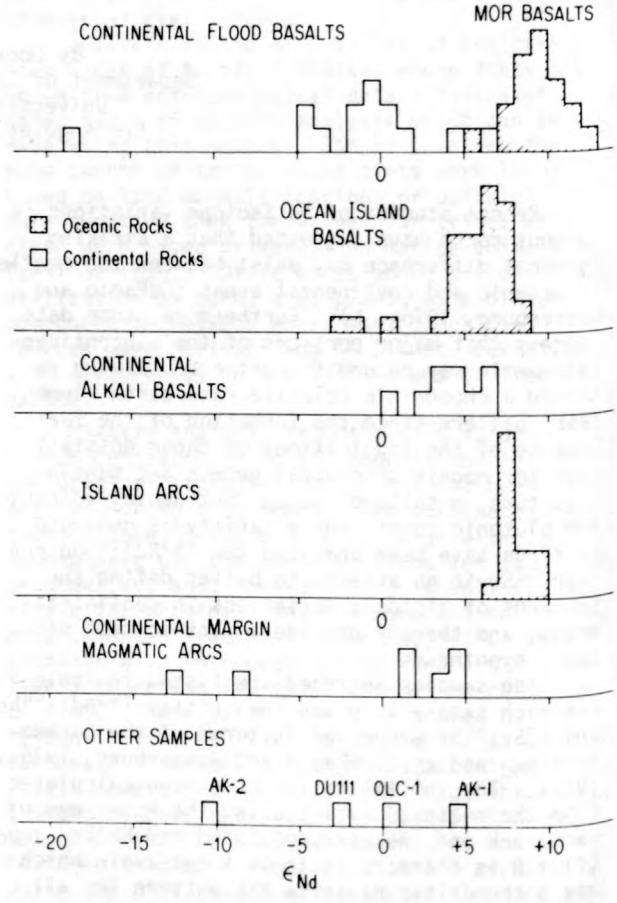

Figure 1.--Histogram of ε_{Nd} values of young igneous rocks. Sources of data from DePaolo (1978).

New analyses of continental flood basalts from the Parana basin and Columbia River province confirm that ε_{Nd} of these rocks cluster near zero, and, thus, that they may be derived from previously undifferentiated reservoirs which have retained a chondritic REE pattern. Two flood basalts from the Afar region, a continental equivalent of a spreading ridge, have also been measured. The ε_{Nd} values of these basalts are intermediate between other continental flood basalts and MOR basalts.

The continental alkaline basalts generally have ε_{Nd} displaced from zero and overlapping the range of ocean island basalts. On figure 2 they follow closely the oceanic trend. The limited data suggest that the mafic lavas erupted closest to continental margins have ε_{Nd} most similar to ocean island lavas, while those found farther into the interior of the continents have lower ε_{Nd}. This geographic pattern suggests large-scale chemical structure in the subcontinental mantle, and, for the western United States appears to be broadly consistent with structure deduced from Pb isotope studies (Zartman, 1974).

Samples from magmatic arcs along the western margin of North and South America show a wide range of ε_{Nd}. An andesite from Costa Rica has ε_{Nd} identical to island arc rocks, whereas a Cascade basalt and plutonic rocks from southern California have lower ε_{Nd} clearly displaced from the island arcs. Two Andean lavas have large negative ε_{Nd}, drastically lower than the other samples. ε_{Nd} of all magmatic arc samples appear to be correlated with the age of the underlying continental crust, with the lowest ε_{Nd} values occurring in regions underlain by the oldest crust (Andes), and the highest ε_{Nd} value, identical to island arcs, occurring where there is no older crust. This correlation must be tested with additional data, but appears to indicate that a substantial portion of the magmas emplaced above subduction zones at continental margins may result from melting or pre-existing crust.

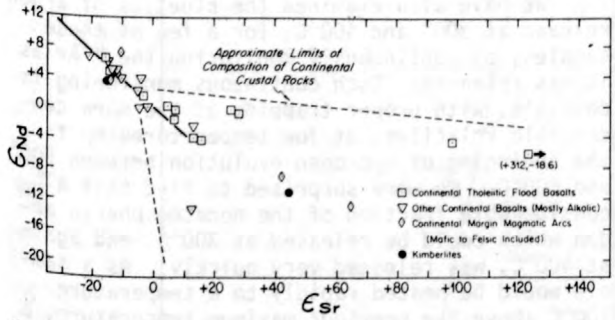

Figure 2.--ε_{Nd} versus ε_{Sr} for young continental igneous rocks analyzed in this study and from DePaolo and Wasserburg (1976a, b, 1977).

Two South African kimberlite samples display grossly different ε_{Nd}. One sample (highly serpentinized) has ε_{Nd} and ε_{Sr} similar to other alkaline basalts, while the other sample (slightly serpentinized) has large negative ε_{Nd} and positive ε_{Sr}. The latter rock may have been melted from a special mantle reservoir which has been enriched in light REE (low Sm/Nd) for at least 1 b.y. This could explain the highly fractionated REE pattern (Sm/Nd = 0.100) and extreme abundance of light REE (Nd = 550X chondrites) measured on this sample.

Carter, S. R., Evensen, N. M., Hamilton, P. J., and O'Nions, R. K., 1978, Continental volcanics derived from enriched and depleted source regions; Nd- and Sr-isotope evidence: Earth and Planetary Science Letters, v. 37, p. 401-409.

DePaolo, D. J., 1978, Study of magma sources, mantle structure and the differentiation of the earth using variations of $^{143}Nd/^{144}Nd$ in igneous rocks: California Institute of Technology, Ph.D. thesis, 360 p.

DePaolo, D. J., and Wasserburg, G. J., 1976a, Nd isotopic variations and petrogenic models: Geophysical Research Letters, v. 3, p. 249-252.

_____1976b, Inferences about magma sources and mantle structure from variations of $^{143}Nd/^{144}Nd$: Geophysical Research Letters, v. 3, p. 743-746.

_____1977, The sources of island arcs as indicated by Nd and Sr isotopic studies: Geophysical Research Letters, v. 4, p. 465-468.

O'Nions, R. K., Hamilton, P. J., and Evensen, N. M., 1977, Variations in $^{143}Nd/^{144}Nd$ and $^{87}Sr/^{86}Sr$ ratios in oceanic basalts: Earth and Planetary Science Letters, v. 34, p. 13-22.

Zartman, R. E., 1974, Lead isotopic provinces in the Cordillera of the western United States and their geologic significance: Economic Geology, v. 69, p. 792-805.

LOW TEMPERATURE RELEASE OF EXCESS ^{40}Ar FROM GEORGIA DOLERITES

By Robert E. Dooley[1] and J. M. Wampler[2]
[1]The Geologic and Water Resources Division
Department of Natural Resources of
Georgia, Atlanta
[2]Georgia Institute of Technology
Atlanta, Georgia

Excess ^{40}Ar is present in many of the Mesozoic dolerites which intrude the Piedmont Province of Georgia (Dooley, 1977). Calculated ages much in excess of 200 m.y. were obtained for most of the dikes in this earlier study. A histogram of K-Ar apparent ages shows a pattern similar to the one for K-Ar apparent ages of Liberian dolerite dikes (Dalrymple and others, 1975). The amount of excess argon is highly variable from dike to dike and within single dikes, even one as thin as 15 cm. Dikes intruding the northwestern portion of the Piedmont tend to contain larger amounts of excess ^{40}Ar than those further to the southeast. A number of the latter have K-Ar apparent ages less than 200 m.y., and may not contain excess ^{40}Ar. A preliminary $^{40}Ar/^{39}Ar$ incremental release spectrum for one of these samples showed a nearly constant $^{40}Ar/^{39}Ar$ ratio for all increments. Another $^{40}Ar/^{39}Ar$ spectrum from a dike that contains considerable excess ^{40}Ar shows the trough shape which Lanphere and Dalrymple (1977) have identified as characteristic of samples with excess ^{40}Ar. In Georgia there is no large difference in age or character of the country rocks intruded by dikes with much excess ^{40}Ar and those which have little or no excess argon. Most of the dikes intrude metamorphic rocks which, in terms of K-Ar cooling age, were quite young at the time of intrusion in the early Mesozoic. Thus, unlike Dalrymple, Grommé, and White (1975), we see no clear relationship between the character of the country rock and the presence or absence of excess argon. Therefore, we must keep open the possibility that excess argon arrives at the site of emplacement as a part of the magma, either by preferential incorporation into silicate liquids upon partial melting of the asthenosphere (Dymond and Hogan, 1978) or through crustal contamination at much greater depths than the site of emplacement.

We have carried out two types of experiment that have a bearing on the location of argon components in dolerites. The first involves the release of argon at low temperatures (100 - 400° C), from crushed samples and block samples within a quartz glass tube heated by a Lindberg furnace. The samples were heated for specific time intervals (1 hour or more) at successively higher temperatures to 400°C. The argon released at low temperatures was analyzed on a MS 10 mass spectrometer after cleaning the gas sample of its reactive volatiles. Two quite different types of argon release pattern were observed. These patterns are reflected in the $^{40}Ar/^{36}Ar$ ratios of the argon released, as a function of temperature (fig. 1). Sample ME 13 shows $^{40}Ar/^{36}Ar$ ratios which are atmospheric for 100° and 200°C increments and only slightly higher than atmospheric at 300°C. At 400°C the $^{40}Ar/^{36}Ar$ ratio is 899, showing a larger fraction of non-atmospheric argon evolving at this temperature. Sample C3 shows a dramatic increase in the $^{40}Ar/^{36}Ar$ ratio of the argon released at successively higher temperatures. At 100°C the $^{40}Ar/^{36}Ar$ ratio is atmospheric, but non-atmospheric argon was released in increasing proportion at 200°, 300°, and 400°C. The amount of argon released increased with temperature, and by 400°C about 10 percent of the total excess argon in the sample had been released. Similar work on other dolerite samples has shown such low-temperature release of non-atmospheric argon to be characteristic of Georgia dolerites which contain excess argon, and has been suggested as a useful criterion for recognizing the presence of excess argon in dolerites (Dooley and Wampler, 1977).

We have also examined the kinetics of argon release at 300° and 400°C, for a few of these samples, by continuously monitoring the ^{40}Ar as it was released. Such continuous monitoring is possible, with proper trapping of the more condensible volatiles, at low temperatures up to the beginning of hydrogen evolution between 500° and 600°C. We were surprised to find that a considerable fraction of the nonatmospheric argon which could be released at 300°C, and again at 400°C, was released very quickly. As a sample would be heated rapidly to a temperature 100°C above the previous maximum temperature, a pulse of argon would be released within the first ten minutes. Figure 2 shows the pulse of argon (98 percent nonatmospheric) released from a block of sample C3 at 400°C. Such pulses were followed by a much lower, and gradually decreasing, rate of argon release. After 300 hours at 400°C the rate of release of argon from the block sample of C3 was only about 30 0.03 picoliters per gram-per minute, less than 0.03 percent of the rate at the peak of the initial pulse. We attribute the low-temperature release on nonatmospheric argon to trapped argon which is released by the mechanical effects of thermal expansion. Argon might be trapped in sites such

as microfractures, microtubes, or simply the zones of irregularity at crystal boundaries, and then be released abruptly as these open because of differential expansion.

A second line of experimentation to determine the distribution of excess ^{40}Ar involves a favorable geologic setting coupled with low-temperature release observations and conventional K-Ar whole-rock dating. A 1.2-m-wide dike intruding a granitic gneiss (freshly exposed in a Gwinnett County quarry) has two small (15-cm wide) dikes, parallel to and well away (greater than 10 m) from it. Table 1 shows conventional K-Ar analytical data for a set of small whole-rock samples across 12 cm of the chilled margin of the large dike (samples RDV1-1AC through RDV1-6AC) and across 10 cm of one of the small dikes (samples RDV14-1AC through RDV14-4AC), and for a sample from the center of the large dike (sample RDV4-1AC). Disregarding the results from the two samples nearest the contact, which contain alteration products, the margin of the large dike appears to have a rather constant amount of excess ^{40}Ar, which is roughly one-third of the total nonradiogenic argon. The concentration of excess argon in the middle of the dike is about ten times greater. The small dike contains excess argon, and there is a pronounced increase in the concentration of excess argon from the margin to the center of the small dike. The concentrations of excess argon in the small dike are of similar magnitude to those in the large dike.

We observed the low-temperature release of argon from a set of block samples taken across the width of the same small dike and found that little nonatmospheric argon was released, less

Table 1.--K-Ar analytical data for two dikes from a quarry in Gwinnett County, Georgia

Sample No.	K (in weight percent)	Atmospheric ^{40}Ar (percent)	Nonatmospheric ^{40}Ar (nl g^{-1})	Apparent K-Ar age[1]	Approx. excess[2] ^{40}Ar (nl g^{-1})
RDV1-1AC	0.163	91.1	0.99	150	----
RDV1-2AC	.135	94.3	1.14	204	----
RDV1-3AC	.143	64.5	1.80	297	0.74
RDV1-4AC	.171	66.5	1.91	268	0.64
RDV1-5AC	.164	72.2	1.99	288	0.78
RDV1-6AC	.153	78.5	1.92	297	0.79
RDV4-1AC	.142	17.5	10.16	1269	9.1
RDV14-1AC	.177	67.6	1.79	242	0.47
RDV14-2AC	.210	44.6	2.99	334	1.43
RDV14-3AC	.421	42.2	7.14	391	4.0
RDV14-4AC	.491	42.1	7.43	353	3.8

[1]Calculated using the following constants: $\lambda(^{40}K_{B-}) = 4.962 \times 10^{-10}$ yr^{-1}; $\lambda(^{40}K_{\varepsilon}) + \lambda'(^{40}K_{\varepsilon}) = 0.581 \times 10^{-10}$ yr^{-1}; $^{40}K = 0.01167$ atom percent.

[2]Calculated using an assumed age of 180 m.y. for the Georgia dolerites.

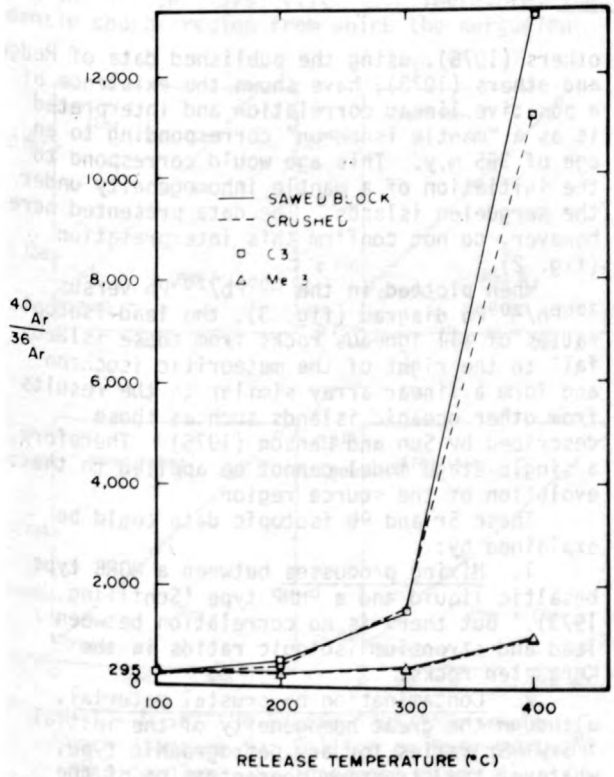

Figure 1.--$^{40}Ar/^{36}Ar$ ratios as a function of temperature for low temperatures. C3 and Me 13 are sample numbers.

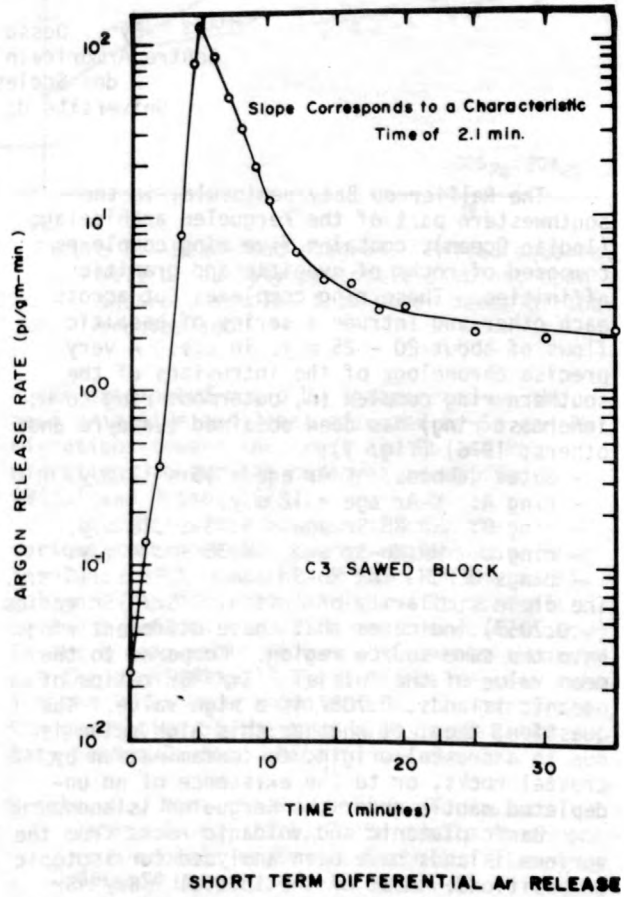

Figure 2.--Argon release rate at 400°C for block sample C3.

than one-tenth that expected on the basis of similar experiments on samples of large dikes with a comparable content of excess ^{40}Ar.

We interpret the observation that the excess argon content of the small dike is comparable to that of the large dike as an indication that the excess argon arrived with the magma. We attribute the low-temperature release of non-atmospheric argon from large dikes to the concentration of argon in structural irregularities by diffusion out of crystals during slow cooling. Rapid cooling of the small dike would have left the initial argon more generally distributed throughout the crystals in which it was dissolved during crystallization, with little time for exsolution at intermediate temperatures.

Dalrymple, G. B., Gromme, C. S., and White, R. W., 1975, Potassium-argon age and paleomagnetism of diabase dikes in Liberia; Initiation of central Atlantic rifting: Geological Society of America Bulletin, v. 86, p. 399-411.

Dooley, Robert E., 1977, K-Ar relationships in dolerite dikes of the Georgia Piedmont: Georgia Institute of Technology, masters thesis, 186 p.

Dooley, Robert E., and Wampler, J. M., 1977, Location of environmental excess ^{40}Ar in dolerites (abs.): Georgia Journal of Science, v. 35, no. 2, p. 88.

Dymond, J., and Hogan, L., 1978, Factors controlling the Noble gas abundance patterns of deep-sea basalts: Earth and Planetary Science Letters, v. 38, p. 117-125.

Lanphere, M. A., and Dalrymple, G. B., 1977, Identification of excess ^{40}Ar by the $^{40}Ar/^{39}Ar$ age spectrum technique: Earth and Planetary Science Letters, v. 32, p. 141-148.

THE ISOTOPIC GEOCHEMISTRY OF Pb AND Sr OF ROCKS FROM THE KERGUELEN ISLANDS

By L. Dosso and P. Vidal
Centre Armoricain d'Etude Structurale
des Socles (C.N.R.S.)
Universite de Rennes, France

The Rallier du Baty peninsula, in the southwestern part of the Kerguelen archipelago (Indian Ocean), contains five ring complexes composed of rocks of syenitic and granitic affinities. These ring complexes cut across each other and intrude a series of basaltic flows of about 20 - 25 m.y. in age. A very precise chronology of the intrusions of the southern ring complex (A, outermost ring to H, innermost ring) has been obtained (Lameyre and others, 1976) (fig. 1):

- outer gabbros: K-Ar age = 15 - 13 m.y.
- ring A: K-Ar age = 12 m.y.
- ring B: WR Rb-Sr age = 9.73 ± .18 m.y.
- ring C: WR Rb-Sr age = 8.38 ± .14 m.y.
- rings DEFGH: WR Rb-Sr age = 7.88 ± .10 m.y.

The close similarity of initial $^{87}Sr/^{86}Sr$ ratios ($\sim$ 0.7057) indicates that these different rings have the same source region. Compared to the mean value of the initial $^{87}Sr/^{86}Sr$ ratios of oceanic islands, 0.7057 is a high value. The question, then, is whether this high value is due to a crustal origin, to contamination by crustal rocks, or to the existence of an undepleted mantle under the Kerguelen islands.

Basic plutonic and volcanic rocks from the various islands have been analyzed for isotopic compositions. Most of the initial $^{87}Sr/^{86}Sr$ ratios are about 0.7057, although some local variations do exist. These values do not correlate with their Rb/Sr ratios. Brooks and others (1976), using the published data of Hedge and others (1973), have shown the existence of a positive linear correlation and interpreted it as a "mantle isochron" corresponding to an age of 355 m.y. This age would correspond to the initiation of a mantle inhomogeneity under the Kerguelen islands. The data presented here, however, do not confirm this interpretation (fig. 2).

When plotted in the $^{207}Pb/^{204}Pb$ versus $^{206}Pb/^{204}Pb$ diagram (fig. 3), the lead-isotopic ratios of all igneous rocks from these islands fall to the right of the meteoritic isochron and form a linear array similar to the results from other oceanic islands such as those described by Sun and Hanson (1975). Therefore, a single-stage model cannot be applied to the evolution of the source region.

These Sr and Pb isotopic data could be explained by:

1. Mixing processes between a MORB type basaltic liquid and a PHMP type (Schilling, 1973). But there is no correlation between lead and strontium isotopic ratios in the Kerguelen rocks.

2. Contamination by crustal material, although the great homogeneity of the initial $^{87}Sr/^{86}Sr$ ratios for any petrographic type, whatever the strontium concentration of the rocks, does not favor this hypothesis. However, although the $^{206}Pb/^{204}Pb$ ratios are typical of

oceanic islands, the scatter of $^{207}Pb/^{204}Pb$ ratios cannot exclude the possibility of slight sialic contamination.

3. A two stage evolution model. In this model, the lead isochron age would be 2.2 b.y. The source region would have evolved since the earth's formation to 2 b.y. ago with a $\mu = {}^{238}U/{}^{204}Pb$ of 7.9. Then following differentiation, μ values would have increased--ranging from 9 to 11. The $^{207}Pb/^{204}Pb$ scatter could be explained by a differentiation of the mantle source region, which would have taken at least 200 m.y.

4. A fundamental mantle heterogeneity. The Sr data appear relatively homogeneous (0.3 percent heterogeneity) whereas the lead data reveal the presence of an heterogeneity (1 percent for $^{207}Pb/^{204}Pb$ and 4 percent for $^{206}Pb/^{204}Pb$). This contradiction is only apparent because a fractionation of similar percentage in both Rb/Sr and μ ratios in the mantle 2 b.y. ago will cause present-day variations, which are much more important for lead-isotopic ratios than for strontium. However, isotopic homogenization is very difficult to accomplish in the mantle (Hofmann, 1975) and the origin of the small variations in initial $^{87}Sr/^{86}Sr$ ratios must be looked for in the heterogeneous characteristics of the mantle.

5. An origin in a primitive mantle source. On an initial $^{87}Sr/^{86}Sr$ versus $^{206}Pb/^{204}Pb$ plot, the Kerguelen data follow the trend shown by Sun and Hanson (1975) (fig. 4). Therefore, the mantle source region from which the Kerguelen

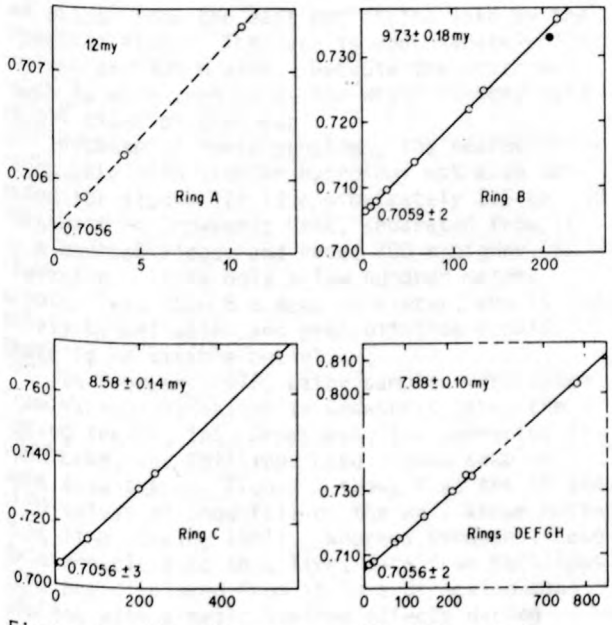

Figure 1.--$^{87}Sr/^{86}Sr$ versus $^{87}Rb/^{86}Sr$ whole-rock diagrams for Rallier du Baty southern ring complex. A, innermost ring; H, outermost ring; solid circle, pegmatitic sample.

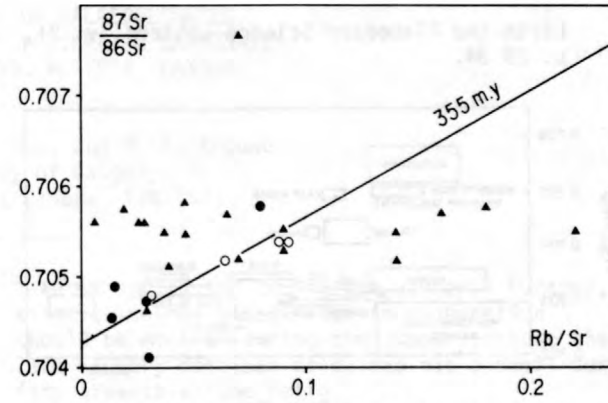

Figure 2.--Isochron plot data for Kerguelen samples (after Brooks and others, 1976). Circles (solid-tholeiitic basalts; open-alkalic basalts), Hedge and others (1973) data; triangles, this publication data.

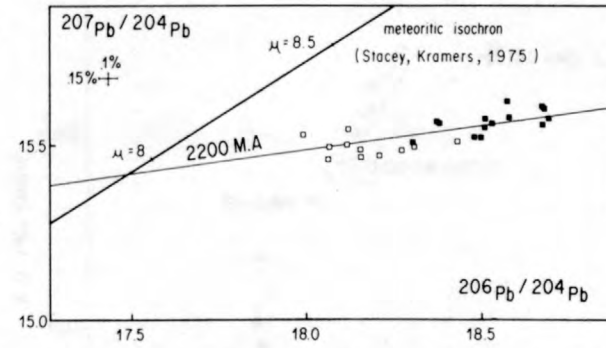

Figure 3.--Lead-lead diagram. Filled squares, Rallier du Baty peninsula samples; open squares, samples from other parts of the archipelago.

rocks originated could be interpreted as the most primitive and least affected by Sr and Rb migrations toward the crust and Rb and Pb migrations toward the core yet identified (Vidal and Dosso, 1978).

In conclusion, it seems likely that various heterogeneous source regions have been involved in the magmatic history of the archipelago. The coherence of Sr and Pb isotopic patterns between the different source regions favors a comparable sequence of events throughout the archipelago. These source regions are located in an undepleted mantle. In particular, the generation of the acid plutons of Rallier du Baty peninsula took place in the mantle.

Brooks, C., Hart, S. R., Hofman, A. W., and James, D. E., 1976, Rb-Sr mantle isochrons from oceanic regions: Earth and Planetary Science Letters, v. 32, p. 51-61.

Hedge, C. E., Watkins, N. D., Hildreth, R. A., Doering, W. P., 1973, $^{87}Sr/^{86}Sr$ ratios in basalts from islands in the Indian Ocean:

Earth and Planetary Science Letters, v. 21, p. 29-34.

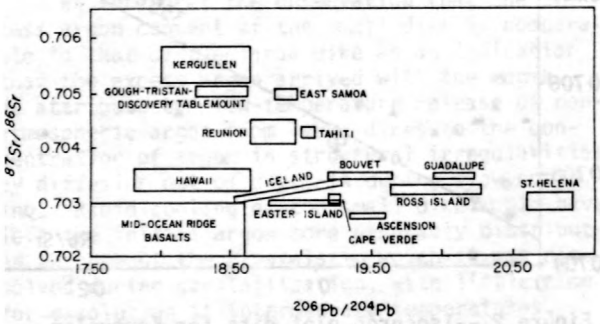

Figure 4.--$^{87}Sr/^{86}Sr$ versus $^{206}Pb/^{204}Pb$ for oceanic islands (after Sun and others, 1975).

Hofmann, A. W., 1975, Diffusion of Ca and Sr in a basalt melt: Carnegie Institution of Washington Yearbook, no. 74, p. 183-189.

Lameyre, J., Marot, A., Zimine, S., Cantagrel, J. M., Dosso, L., and Vidal P., 1976, Chronological evolution of the Kerguelen Islands syenite-granite ring complex: Nature, v. 263, p. 306-307.

Schilling, J. G., 1973, Iceland mantle plume-geochemical study of the Reykjanes Ridge: Nature, v. 242, p. 565-571.

Sun, S. S., and Hanson, G. N., 1975, Evolution of the mantle-geochemical evidence from alkali basalt: Geology, v. 3, no. 6, p. 297-302.

Vidal, P., and Dosso, L., 1978, Core formation-catastrophic or continuous? Sr and Pb isotopic constraints: Geophysical Research Letters, v. 5, no. 3, p. 169-172.

PROBLEMS IN THE STUDY OF PALAEOCLIMATES BY ISOTOPIC ANALYSES OF FRESHWATER CARBONATES NEAR CROWSNEST PASS, ALBERTA, CANADA

By J. Driver, H. M. Brown, and H. R. Krouse
The University of Calgary
Calgary, Alberta, Canada T2N 1N4

Crowsnest Lake, in the Rocky Mountains of Alberta (49°37'N, 114°38'W), was cored to obtain a palynological record from Holocene lake bed sediments. Samples of the freshwater pelecypod Pisidium were extracted from the core with the view of obtaining a temperature record of the lake through $^{18}O/^{16}O$ analyses. The aim of the study was to correlate temperature changes with palynological changes over the last 10,000 years. Analysis of pollen showed climatic fluctuations but $^{18}O/^{16}O$ ratios apparently bore little relationship to climatic trends. In particular, the warm dry Altithermal climatic period (7500 to 6000 years before the present in Crowsnest) did not correlate with more positive $\delta^{18}O$ values.

When the hydrology of the lake was examined, it was realized that the lake was not a simple system, and that a variety of factors could have influenced the $^{18}O/^{16}O$ ratio. Sources feeding Crowsnest Lake include meltwater from snow and rain entering through creeks, either directly or via the connected Island Lake to the west, and a large spring, which feeds directly into the lake on its northern shore. Water exists from the east end of the lake by the Crowsnest River. The lake is approximately 3.5 km long and 800 m wide. Because the depth may reach to more than 70 m, the water is very cold at all times of the year.

Because of these problems, the nearby Phillipps Lake with simpler hydrology was also selected for study. It is approximately 2.5 km northwest of Crowsnest Lake, separated from it by a bedrock ridge, and about 200 m higher in elevation. It is only a few hundred meters across, less than 8 m deep in winter, and is fed solely by meltwater and precipitation runoff. There is no visible outlet.

In February 1978, water samples were taken from various locations in Crowsnest Lake, the spring feeding into Crowsnest, the connected Island Lake, and Phillipps Lake. Snow samples were also taken. Figure 1 shows that the δD and $\delta^{18}O$ values of snow fall on the well-known meteoric line (Craig, 1961). Whereas Crowsnest Lake data are close to this line, data from Phillipps Lake are displaced from it in a direction consistent with kinetic isotope effects during evaporation. It must be noted that the Phillipps Lake data represent water remaining in the lake prior to freeze-up and therefore display the effects of summer and fall evaporation from a small shallow lake. In contrast, Crowsnest Lake is spring fed during the winter. Further, kinetic isotope effects due to evaporation should be minimal during the summer because the lake is very deep and cold, and has a small surface area-to-volume ratio.

The difference in $\delta^{18}O$ values of modern water in the two lakes is also found in shells

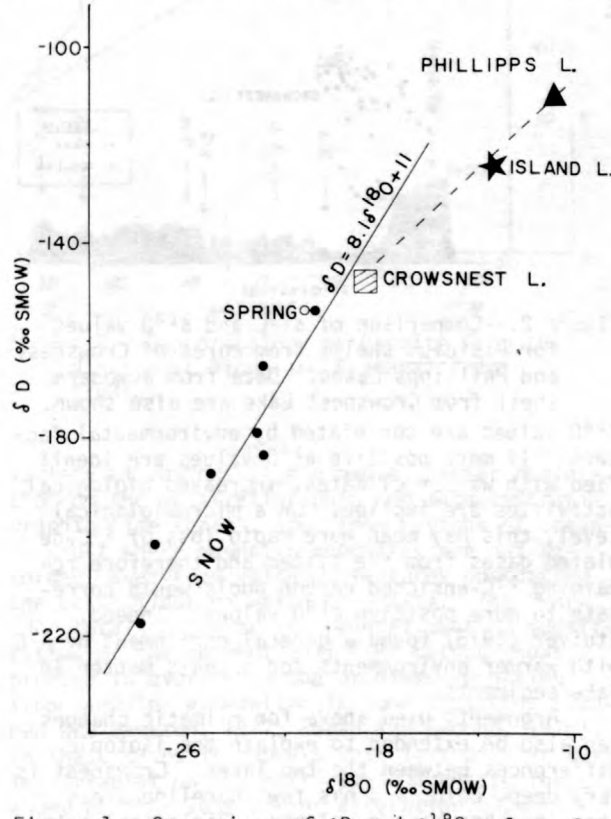

Figure 1.--Comparison of δD and $\delta^{18}O$ values for snow and water samples collected near Crowsnest Lake, February, 1978.

from their cores (fig. 2). The considerable range of $\delta^{18}O$ values at each location would seem to reflect the varying hydrology of the systems during the Holocene and, therefore, paleotemperature interpretation is difficult. For example, in a warmer period of time, the mean $\delta^{18}O$ value of precipitation should be more positive and, in addition, further ^{18}O enrichments in lake water would occur due to increased evaporation. Therefore, the combination of these effects create $\delta^{18}O$ variations, which over-estimate the temperature fluctuations.

The $\delta^{13}C$ values for shell carbonate from the core of Phillipps Lake are on the average 6 permil higher than those of Crowsnest Lake with a scatter at each location comparable to that found with the oxygen isotope data. On a $\delta^{13}C$ versus $\delta^{18}O$ diagram, these data sets trend along a line of unity slope. Similar trends were noted by Stuiver (1970) and Fritz and Poplawski (1974). This suggests that the $\delta^{13}C$ and $\delta^{18}O$ values are correlated by environmental factors. If more positive $\delta^{18}O$ values are identified with warmer climates, increased biological activities are implied. On a microbiological level, this may mean more rapid loss of ^{13}C-depleted gases from the system and therefore remaining ^{13}C-enriched carbon pools would correlate to more positive $\delta^{18}O$ values. Indeed, Stuiver (1975) found a general enrichment of ^{13}C with warmer environments for organic matter in lake sediments.

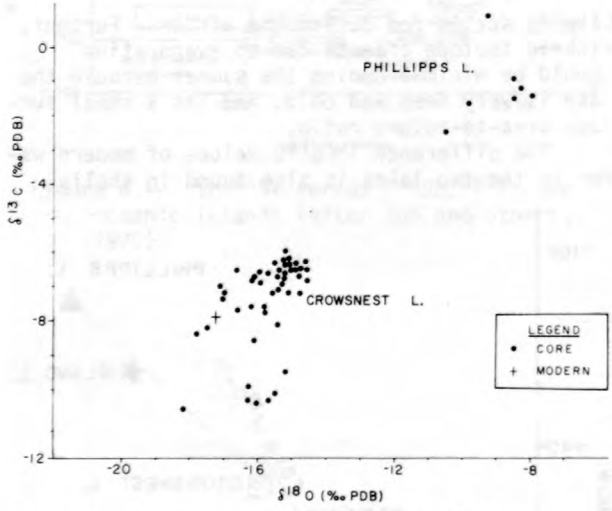

Figure 2.--Comparison of $\delta^{13}C$ and $\delta^{18}O$ values for Pisidium shells from cores of Crowsnest and Phillipps Lakes. Data from a modern shell from Crowsnest Lake are also shown.

Arguments used above for climatic changes can also be extended to explain the isotopic differences between the two lakes. Crowsnest is very deep, cold, and has few shoreline areas where marshes have developed. Biological activity in deep water is likely limited. The lake can thus be described as oligotrophic. In contrast, the warmer Phillipps Lake is biologically productive. Consequently bicarbonate of the lake water may become more enriched in ^{13}C during photosynthesis because aquatic plants preferentially utilize ^{12}C. It can also be argued that the shallower, smaller Phillipps Lake might exchange its dissolved bicarbonate with atmospheric CO_2 more readily, thereby increasing its $\delta^{13}C$ value. A number of other factors considered by Stuiver (1970) and Fritz and Poplawski (1974) can be invoked in comparing these two lakes.

One should not dismiss the possibility that the water systems have interacted with carbonate strata in the vicinity. The ranges of $\delta^{13}C$ and $\delta^{18}O$ values for Phillipps Lake are close to those identified with marine environments (Hudson, 1977). However, we believe that this influence is minimal because field observations suggest that Crowsnest Lake is more likely to have interacted with the carbonate strata than Phillipps Lake but the isotopic data suggest the reverse.

In summary, we believe that the variations in $\delta^{13}C$ and $\delta^{18}O$ values which we have found resulted from temperature changes. However an assessment of these temperature changes is complicated because both the hydrologic cycle and the biosphere are involved. The fact that the data are so different from two lakes so close together serves to emphasize the problems.

Craig, H., 1961, Isotopic variations in meteoric waters: Science, v. 133, p. 1702-3.

Fritz, P., and Poplawski, S., 1974, ^{18}O and ^{13}C in the shells of freshwater molluscs and their environments: Earth and Planetary Science Letters, v. 24, p. 91-98,

Hudson, J. D., 1977, Stable isotopes and limestone lithification: Journal of the Geological Society of London, v. 133, p. 637-660.

Stuiver, M., 1970, Oxygen and carbon isotope ratios of fresh-water carbonates as climatic indicators: Journal of Geophysical Research, v. 75, p. 5247-5257.

Stuiver, M., 1975, Climate versus changes in ^{13}C content of the organic components of lake sediments during the late Quaternary: Quaternary Research, v. 5, p. 251-262.

^{40}Ar-^{39}Ar GEOCHRONOLOGY OF BASALTS FROM OCEAN BASINS--SOME SUCCESSES WITH SAMPLES FROM ASEISMIC RIDGES

By R. A. Duncan
School of Oceanography
Oregon State University
Corvallis, Oregon 97331

Determination of reliable absolute ages for basaltic samples from the ocean basins has been frustrated by alteration effects, which disrupt the important assumptions of the conventional

K-Ar method. Lavas erupted under abyssal hydrostatic pressures may not totally degas a mantle argon composition prior to crystallization. Later chemical exchange with seawater may contribute potassium to the rock, while radiogenic argon may diffuse out of the rock from a glass phase or as primary crystallization phases convert to clay minerals. Because of these effects, conventional K-Ar ages from seafloor basalts are suspect and often are incompatible with indirect age estimates such as those derived from identified magnetic anomalies and the paleontology of basal sediments overlying the basalts.

Nevertheless, absolute ages of crustal rocks from the ocean basins are important for a

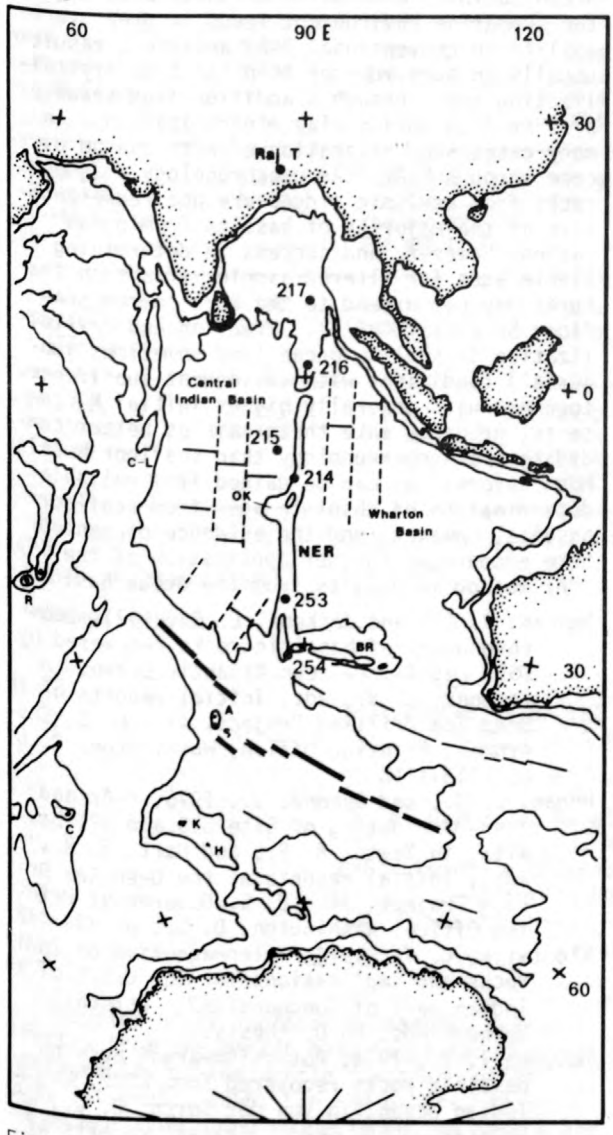

Figure 1.--Tectonic features of the eastern Indian Ocean, including DSDP sites along the Ninetyeast Ridge.

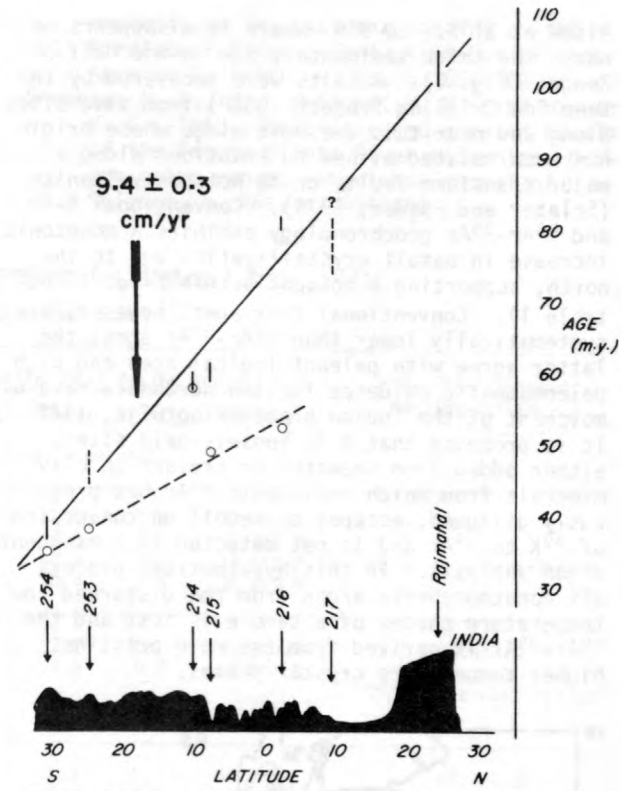

Figure 2.--Geochronology of basalts from the Ninetyeast Ridge and Rajmahal Traps (India).

variety of reasons (for example, better definition of the biostratigraphic and magnetostratigraphic time scales, ages from regions of oceanic crust where magnetic anomalies are not recorded, ages from volcanic features postdating the ocean floor on which they sit). The ^{40}Ar-^{39}Ar total fusion or incremental heating modification of the conventional K-Ar method shows promise in overcoming the problems resulting from seawater alteration in some instances (Duncan and Jackson, 1977; Hogan and Dymond, 1976). In these cases it appears that loss of ^{39}Ar during irradiation may partially compensate for K added or ^{40}Ar lost during alteration. This study reports age determinations for two aseismic ridges formed in ocean basins--the Ninetyeast Ridge located in the eastern Indian Ocean and the Coast Range basalts, erupted in the eastern Pacific Ocean, but not outcropping along the western margin of North America. Conventional K-Ar ages from these volcanic provinces are scattered and are often at variance with paleontological age estimates. ^{40}Ar-^{39}Ar total fusion and incremental heating ages show much less variability and are more compatible with the stratigraphy.

The Ninetyeast Ridge is a 4500-km volcanic lineament extending along the 90°E. meridian from just south of its junction with the Broken

Ridge at 31°S., to 9°N. where it disappears beneath the thick sedimentary fan in the Gulf of Bengal (fig. 1). Basalts were recovered by the Deep Sea Drilling Project (DSDP) from five sites along and near this aseismic ridge whose origin has been related either to eruptions along a major transform fault, or to hotspot volcanism (Sclater and Fisher, 1974). Conventional K-Ar and ^{40}Ar-^{39}Ar geochronology exhibits a monotonic increase in basalt crystallization age to the north, supporting a hotspot origin (fig. 2 and table 1). Conventional K-Ar ages, however, are systematically lower than ^{40}Ar-^{39}Ar ages; the latter agree with paleontological ages and with paleomagnetic evidence for the northward rate of movement of the Indian plate (Klootwijk, 1974). It is proposed that K in loosely-held sites, either added from seawater or present in clay minerals from which radiogenic ^{40}Ar has previously diffused, escapes by recoil on conversion of ^{39}K to ^{39}Ar and is not detected in subsequent argon analysis. In this hypothetical process all nonatmospheric argon from the disturbed low temperature phases of a sample is lost and the ^{40}Ar-^{39}Ar is derived from the more pristine, higher temperature crystal phases.

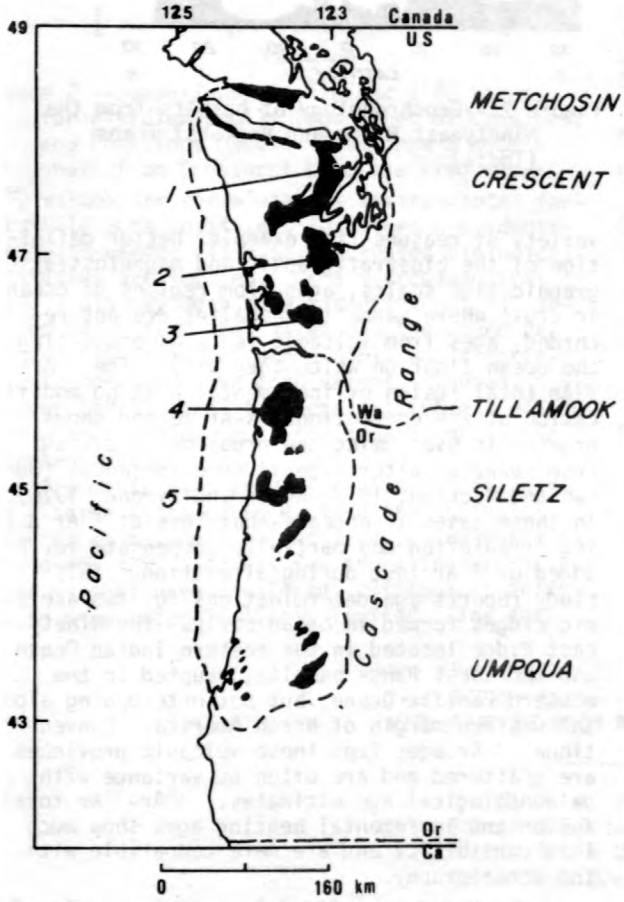

Figure 3.--Outcrop and inferred extent of the lower Eocene basalts of the Coast Range, Oregon and Washington.

On the basis of geometry and major-element chemistry, basalts found in the Coast Range Province of western Oregon and Washington (fig. 3) have been compared to those forming oceanic aseismic ridges such as the Hawaiian Islands (Snavely and others, 1968). Submarine volcanism (at separate centers) followed by restricted subaerial eruptions produced this volcanic lineament, which volumetrically exceeds the Columbia River basalts. Again, conventional K-Ar ages are variable and are usually significantly lower than the paleontological age of interfingering and overlying sediments (lower Eocene). ^{40}Ar-^{39}Ar ages are less scattered and confirm the paleontological age assignment.

These two examples show that reliable absolute ages can be derived from basalts from the ocean basins. Alteration of these basalts in the submarine environment leads to great variability in conventional K-Ar analyses, resulting usually in ages younger than the true crystallization age, through K addition from seawater or ^{40}Ar loss during clay mineralization. In many cases such alteration effects can be overcome through ^{40}Ar-^{39}Ar geochronology. Igneous rocks from aseismic ridges are not representative of the majority of basalts from ocean basins, however, and success in determining reliable ages for altered samples from such features may not extend to the more common seafloor basalts (MORB's). Eruption and crystallization in shallow ocean (and sometimes subaerial) conditions with subsequent subsidence, together with generally higher initial K contents, probably make these samples better candidates for geochronology than seafloor basalts. Much information can be gained from reliable determination of absolute ages from seafloor basalts, however, and the evidence presented here encourages further application of the ^{40}Ar-^{39}Ar method to basalts from the ocean basins.

Duncan, R. A., and Jackson, E. D., 1977, Geochronology of basaltic rocks recovered by DSDP Leg 41, eastern Atlantic Ocean, in Gardner, J. V., ed., Initial reports of the Deep Sea Drilling Project, 41: U. S. Government Printing Office, Washington, D. C., p. 1113-1118.

Hogan, L. G., and Dymond, J., 1976, K-Ar and ^{40}Ar-^{39}Ar dating of Site 319 and 321 basalts, in Yeats, R. S., and Hart, S. R., eds., Initial reports of the Deep Sea Drilling Project, 34: U. S. Government Printing Office, Washington, D. C., p. 439-442.

Klootwijk, C. T., 1974, Paleomagnetism of Indian rocks and implications for the drift of the Indian part of Gondwanaland: Utrecht, Netherlands, Ph.D. thesis.

McDougall, I., 1974, Potassium-argon ages on basaltic rocks recovered from DSDP, Leg 22, Indian Ocean, in von der Borch, C. C., and Sclater, J. G., eds., Initial reports of the Deep Sea Drilling Project, 22: U. S. Government Printing Office, Washington, D. C., p. 377-380.

Rundle, C. C., Brook, M., Snelling, N. J., Reynolds, P. H., and Barr, S. M., 1974, Radiometric age determinations, in Davies, T. A., and Luyendyk, B. P., eds., Initial reports of the Deep Sea Drilling Project, 26: U. S. Government Printing Office, Washington, D. C., p. 513-516.

Sclater, J. G., and Fisher, R. L., 1974, Evolution of the east central Indian Ocean with emphasis on the tectonic setting of the Ninetyeast Ridge: Geological Society of America Bulletin, v. 85, p. 683-702.

Snavely, P. D., Jr., McCleod, N. S., and Wagner, H. C., 1968, Tholeiitic and alkalic basalts of the Eocene Siletz River volcanics, Oregon coast range: American Journal of Science, v. 266, p. 454-481.

Table 1.--K-Ar and ^{40}Ar-^{39}Ar geochronology for Ninetyeast Ridge basalts

[s.d. = standard deviation]

DSDP site and sample no.	K (percent)	K-Ar age (m.y.)±1 s.d.	^{40}Ar-^{39}Ar total fusion analysis				^{40}Ar-^{39}Ar incremental heating age (m.y.) ±1 s.d.
			$^{40}Ar_{rad}$	$^{36}Ar_{Ca}$	$^{39}Ar_{Ca}$	Age(m.y.) ±1 s.d.	
			(analyses in percent)				
Site 254	0.175	(49.0±5) [1]	37.8	17.5	1.0	37.2±1.1	36.0±2.5
26-254-35-2,	0.174	(18.0±0.5) [1]	38.3	17.5	1.0	36.3±1.7	
39-42 cm.			40.4	17.6	1.0	41.0±1.2	40/36 intercept=265±10
			8.6	0.0	0.0	36.6±1.9	
Site 214	1.620	58.0±0.4	79.9	7.3	0.1	59.3±0.9	60.9±1.3
22-214-48-1,	1.630	58.5±0.4	76.7	7.0	0.1	58.0±1.0	
147-150 cm.		(53.9±0.8) [2]					40/36 intercept=262±22
		(52.9±0.8) [2]					
Site 215	0.896	49.1±0.8	50.9	6.3	0.3	60.9±1.2	62.1±1.3
22-215-19-2,	0.896	49.8±0.7	38.8	6.3	0.5	58.5±1.5	
112-115 cm.							40/36 intercept=302±8
Site 216	0.753	(62.9±1.2) [2]	73.5	19.7	0.5	79.8±1.1	72.9±9.5
22-216-38-1,	0.750	(64.9±2.0) [2]	70.3	18.9	0.6	82.0±1.2	
93-96 cm.		(64.4±1.4) [2]	76.2	19.8	0.5	79.9±1.2	40/36 intercept=134±84
			84.1	14.7	0.2	83.2±1.1	

$\lambda_\varepsilon = 0.585 \times 10^{-10}yr^{-1}$; $\lambda_\beta = 4.72 \times 10^{-10}yr^{-1}$; $^{40}K/K = 1.19 \times 10^{-4}$ mol/mol

[1]Rundle and others (1974).

[2]McDougall (1974).

HETEROGENEITY OF THE MANTLE FROM ARCHEAN TO PRESENT: A Pb ISOTOPE STUDY

By B. Dupré, B. Hamelin, C. J. Allegre, and G. Manhes
Laboratoire de Geochimie et Cosmochimie (LA196)
Institut de Physique du Globe
4, Place Jussieu - 75230, Paris, Cedex 05
France

Studies of Pb isotopes in samples derived directly from the mantle have suggested chemical heterogeneity of the mantle (Gast and others, 1964; Tatsumoto, 1966; Sun and others, 1975), and we are attempting to decipher the nature and origin of the heterogeneity (Manhes and others, in press). Progress in the analytical techniques has allowed us to analyze samples with low-Pb concentrations. The study of the ultrabasic nodules in basalts and kimberlites, considered as samples of the mantle, has thus been developed. In the last three years, we have been studying this problem of the mantle heterogeneity in two different ways: (1) a detailed study of two selected areas from the North Atlantic--the FAMOUS area and the Azores Islands;

and (2) a study of continental basalts, particularly the layered igneous complexes of various ages (Archean to Tertiary).

The Azores Islands are characterized by the absence of any single trend in a $^{206}Pb/^{204}Pb$ vs $^{207}Pb/^{204}Pb$ diagram (Dupré and Allegre, in preparation). One can recognize the three following domains: one consisting of Corvo and Flores Islands on the America plate, one for the central islands of Terceira, Saint Jorges, Pico and Graciosa, and one for Sao-Miguel and Santa Maria Islands. The isotopic variations in each island could be explained in part by contamination of the magma by host rocks. The absence of linear relationships among islands precludes an application of a simple two-stage model to the Azores mantle as a whole.

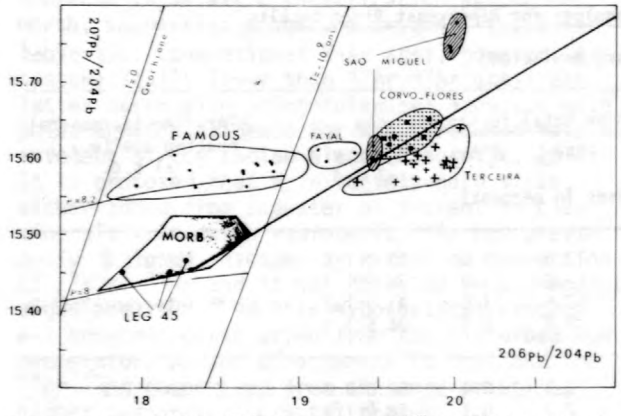

Figure 1.--$^{206}Pb/^{204}Pb$ versus $^{207}Pb/^{204}Pb$ diagram for volcanic rocks of the Azores Islands and the FAMOUS area.

Our results on the tholeiites from the Deep Sea Drilling Project Leg 45 suggest that the FAMOUS area is not the mixture of the typical ridge-basalt magma, such as the Leg 45 MORB samples, and nearby Azores mantle. The data could reflect continuous variations of Pb isotopic composition in the mantle source due to continuous U-Pb fractionation derived from convection in the mantle.

Our results on the layered igneous complexes show that direct Pb-Pb dating is feasible because the ages obtained are in agreement with other methods: Stillwater (Montana) = 2.66 ± 0.01 b.y.; Kemi (Finland) = 2.44 ± 0.04 b.y.; Kola (USSR) = 2.13 ± 0.04 b.y.; Duluth (Minnesota) = 1.24 ± 0.04 b.y.; Porttivaara = 0.90 ± 0.8 b.y. The Porttivaara data show a scatter that is possibly related to secondary events.

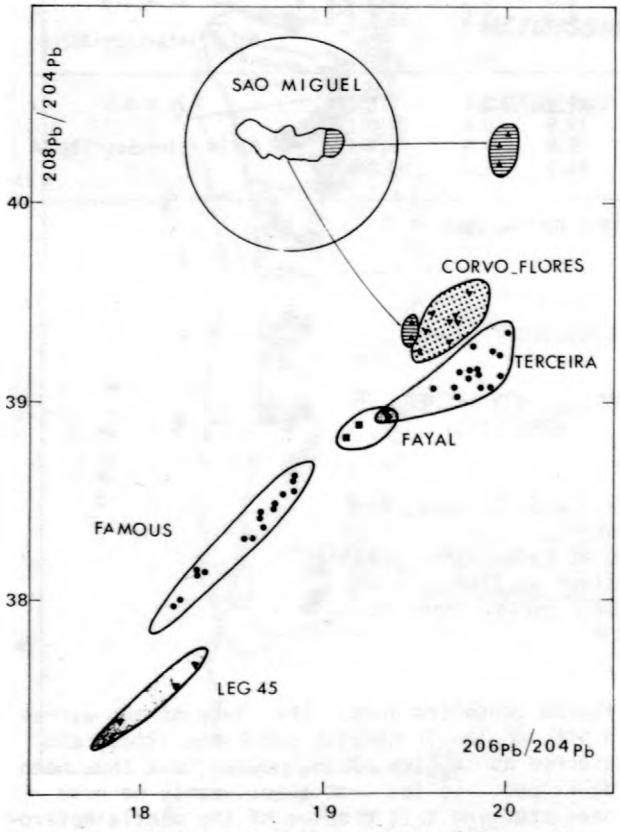

Figure 2.--$^{206}Pb/^{204}Pb$ versus $^{208}Pb/^{204}Pb$ diagram for volcanic rocks of the Azores Islands and the FAMOUS area.

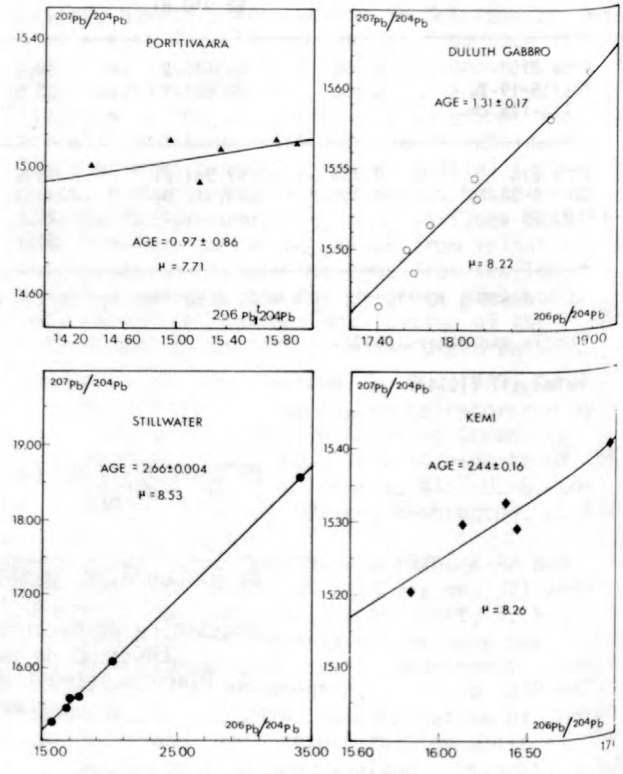

Figure 3.--$^{206}Pb/^{204}Pb$ versus $^{207}Pb/^{204}Pb$ diagram for some suites of rocks from layered igneous complexes (ages in b.y.).

Gast, P. W., Tilton, G. R., and Hedge, C. E., 1964, Isotopic composition of lead and strontium from Ascension and Gough Islands: Science, v. 145, p. 1181-1185.

Manhes, G. Dupré, B., Hamelin, B., and Allègre, C. J., (in press), Composition isotopique du plomb des roches basaltiques et heterogeneites du manteau a diverse échelles: Société Géologique de France.
Sun, S. S., Tatsumoto, M., Schilling, J. G., 1975, Mantle plume mixing along the Reykjanes ridge axis: lead isotopic evidence: Nature, p. 190.
Tatsumoto, M., 1966, Genetic relations of oceanic basalts as indicated by lead isotopes: Science v. 153, p. 1094-1101.

HEAVY NOBLE GASES IN THE ORGUEIL NEON-E RICH PHASE

By P. Eberhardt
Physikalisches Institut, University of Bern,
Sidlerstr. 5, 3012 Bern, Switzerland, and
Enrico Fermi Institute, University of Chicago,
Chicago, Illinois, U.S.A.

The Ne-E in Orgueil is located in a distinct, separable phase (Eberhardt, 1974). Results of He and Ne measurements on such an Ne-E rich phase, G4j, have been published (Eberhardt, 1974, 1975, 1978). In table 1 the Ar, Kr, and Xe concentrations in G4j and in the bulk silicate phase, CD00, are given. Within experimental errors, the Kr and Xe isotopic composition is the same in G4j and in CD00.

The Ne-E rich phase G4j is depleted in the heavy noble gases. The depletion factor is identical for all three noble gases. This observation and the similarity of the isotopic compositions strongly suggest that the presence of Ar, Kr, and Xe in G4j is due to a 27 percent contamination with CD00 material. This conclusion is supported by the observed Ne temperature release pattern. Between 700° and 900°C G4j gives off planetary type Ne. In this temperature interval CD00 releases most of its trapped Ne (see Eberhardt, 1978).

The Ne-E rich phase G4j also contains a magnetite contamination. This is evident from the separation procedure, from X-ray diffraction pictures, and from the He isotopic composition in G4j (Eberhardt, 1974, 1978). Ar, Kr, and Xe concentrations in magnetite are < 10 percent of those in the silicate (Jeffery and Anders, 1970). Furthermore, the magnetite contamination is only $\sim$ 12 percent and, therefore, the contribution from the magnetite to the Ar, Kr, and Xe in G4j can be neglected.

For further discussion we will assume that: G4j contains a 27 percent CD00 contamination; the remaining ^{4}He is due to the incomplete separation of magnetite from G4j; and Glα, the magnetite separated from G4j (see Eberhardt, 1974), represents the remaining magnetite contamination of G4j.

In table 2 the corrections are compiled and the resulting gas concentrations in the "contamination free Ne-E phase," designated as G4j*, are given. It is important to point out that G4j* is not necessarily the pure carrier phase of Ne-E. G4j* could still contain a (very large) contamination with meteorite grains free of trapped gases. The Ne-E concentrations given in table 2 are thus only lower limits for the Ne-E carrier phase.

The ^{21}Ne/^{22}Ne ratio in G4j* is considerably higher than the upper limit obtained for Ne-E from the stepwise heating experiments. G4j* must contain spallation ^{21}Ne. Using the high-temperature Ne correlation (Eberhardt, 1978), a spallation ^{21}Ne content of 0.5 x 10^{-8} cm^3 STP ^{21}Ne g^{-1} is calculated. The ^{3}He/^{21}Ne$_c$ ratio in G4j* is 3, suggesting that the ^{3}He in G4j* is spallation-produced. ^{21}Ne$_c$ is about a factor of two lower in G4j* than in G4j or in the bulk silicates CD00. This could be due to contamination with gas-free terrestrial material prior to or during the mineral separation (see Anders and others, 1964).

Conclusions:

1. The observed noble gas abundance pattern in G4j can best be explained if no other noble gases are associated with Ne-E.

2. The isotopic abundances in Ne-E would then be

$$^{20}\text{Ne} : {}^{21}\text{Ne} : {}^{22}\text{Ne} = 1 : 0.011 : 1.$$

3. Ne-E could then not be a mixture of pure ^{22}Ne from the decay of ^{22}Na and solar-, atmospheric-, A-, B-, or C-type Ne (^{21}Ne abundance too high).

This work was supported by NASA Grant NGL-14-001-010 and by the Swiss National Science Foundation.

Anders, E., DuFresne, E. R., Hayatsu, R., Cavaillé, A., DuFresne, A., and Fitch, F. W., 1964, Contaminated meteorite: Science, v. 146, p. 1157-1161.
Eberhardt, P., 1974, A neon-E rich phase in the Orgueil carbonaceous chondrite: Earth and Planetary Science Letters, v. 24, p. 182-187.

_____1975, Ne-E rich phase in Orgueil: EOS, Transactions of the American Geophysical Union, v. 56, p. 392; Meteoritics, v. 10, p. 401.
_____(in press), A neon-E rich phase in Orgueil; results of stepwise heating experiments: Lunar and Planetary Science Conference, 9th, Proceedings.
Jeffery, P. M., and Anders, E., 1970, Primordial noble gases in separated meteoritic minerals-I: Geochimica Cosmochimica Acta, v. 34, p. 1175-1198.

Table 1.--^{36}Ar, ^{84}Kr, and ^{132}Xe concentrations in the bulk silicates and a Ne-E rich phase of Orgueil

Phase	^{36}Ar	^{84}Kr	^{132}Xe
CD00 (bulk silicates)[1] --	150	1.65	2.15
G4j (Ne-E rich phase)[1] --	39	0.46	0.59
Concentration in G4j relative to CD00 (in percent) ----------	26.0	27.9	27.4

[1]Concentrations in units of 10^{-8} cm^3 STP g^{-1}.

Table 2.--Orgueil Ne-E rich phase--correction of He and Ne results for contamination with bulk silicates and magnetite

[All concentrations in units of 10^{-8} cm^3 STP g^{-1}. G4j* is the "contamination free Ne-E phase" obtained by assuming that G4j contains 27 weight percent of CD00 and 12.3 weight percent of Gla.]

	^{3}He	^{4}He	^{20}Ne	^{21}Ne	^{22}Ne	^{36}Ar	^{84}Kr	^{132}Xe
Measured conc. in G4j -------	8.54	20,500	37.5	0.980	8.99	39	0.46	0.59
Concentration in G4j* -------	1.7	([1])	8.73	.622	8.89	[2]-1.5	[2].01	[2].01
Spallation gas in G4j* ------	1.7	-	.49	.531	.58	-	-	-
Trapped gas (Ne-E) in G4j* --	-	-	8.24	.091	8.31	-	-	-

[1]Gla contamination adjusted to give $^{4}He \equiv 0$.
[2]These residual concentrations are identical to zero within the experimental uncertainties.

Cl: THE CASE OF MISSING ^{26}Al

By Tezer M. Esat, Typhoon Lee,
D. A. Papanastassiou, and G. J. Wasserburg
The Lunatic Asylum, Division of Geology and
Planetary Sciences, Caltech, Pasadena,
California 91125

A wide range of isotopic anomalies have been discovered in two, so far unique, Ca-Al rich Allende inclusions Cl and EK1-4-1. The anomalies range from low-Z elements O (Clayton and Mayeda, 1977) and Mg (Wasserburg and others, 1977), to the heavier elements Ca (Lee and others, 1978), Sr (Papanastassiou and others, 1978), Ba and Nd (McCulloch and Wasserburg, 1978a) and Sm (Lugmair and others, 1978; McCulloch and Wasserburg, 1978b). A qualitative comparison can be made between the pattern of anomalies in the two inclusions; namely, the absolute magnitude of the nuclear anomalies in EK1-4-1 is 2 to 6 times larger than those found in Cl. Thus, Cl seems to be a "poor relative" of EK1-4-1. At present, the data can best be explained by generic models involving an onion-shell supernova explosion followed by injection into the solar nebula (see, for example, Cameron and Truran, 1977). Indeed, a supernova source may be essential to account for the presence of live ^{26}Al at the time of condensation of the Allende inclusions (Lee and others, 1977a). Establishing the presence of excess ^{26}Mg ($^{26}Mg^*$) correlated with the $^{27}Al/^{24}Mg$ ratio in Cl and EK1-4-1 mineral phases would lend support to the association of the nuclear anomalies with a nearby supernova and provide a time scale for the event.

In this paper we report the Mg isotopic composition of the major mineral phases in the inclusion Cl. The Mg isotopic composition of several phases in Cl was previously reported by Wasserburg and others (1977). The effects were designated as FUN anomalies (F, fractionation; UN, unknown nuclear anomalies). Briefly, Mg

analyses of Cl showed large fractionation (30 permil per mass unit) and negative $\delta^{26}Mg$ of up to -2 permil after correcting for fractionation.

Procedures for sample preparation, handling, and various characterization techniques have been described in detail in previous publications (Lee and others, 1977b). The Mg isotopic composition of Cl samples, except for plagioclase, are shown in table 1. It is evident that spinel, pyroxene, and melilite have a homogeneous Mg isotopic composition. This observation is in agreement with the homogeneous Mg isotopic composition found in EK1-4-1 (Wasserburg and others, 1977). Therefore, the O isotopic heterogeneity in the FUN samples, particularly for melilite, may not reflect a primary isotopic heterogeneity but must be due to a secondary process such as back-reaction with a cool solar nebula with normal oxygen composition (Wasserburg and others, 1977; Clayton and Mayeda, 1977). Fine-grained alteration products ("fuzz") rich in Cl, Na, Fe, and Mg permeate the inclusion Cl and, in particular, are associated with melilite and plagioclase. The alteration products are believed to be due to this back-reaction with volatile-rich material in the solar nebula. The Mg isotopic composition of the "fuzz" is the same as the rest of the Cl minerals (table 1). Therefore, the back-reaction did not introduce additional Mg of different isotopic composition to that found in Cl. The simplest assumption is that the interaction occurred in an environment depleted in Mg.

Table 1.--Mg isotopic composition of Cl samples except for plagioclase

Sample	Weight[1] (mg)	Fractionation (permil)[2] (25/24)	(26/24)	$\delta^{26}Mg$ (permil)	$^{27}Al/^{24}Mg$
Pyroxene-A (bulk)	15	29.6-30.8	58.2-60.6	-1.6±0.2	2
Pyroxene-A (residue)	0.2	30.0-31.8	58.9-62.4	-2.0±0.2	2
Pyroxene-B (200 crystals)	0.3	29.3-30.6	57.4-59.4	-2.0±0.2	2
Pyroxene-C[3] (single crystal)	0.002	27.8-30.4	53.8-57.5	-1.3±0.6	1.9
Melilite-A (bulk)	0.5	29.4-30.8	58.8-60.4	-1.5±0.2	1-2
Melilite-B (28 crystals)	0.01	31.2-32.6	62.3-64.1	-1.6±0.2	1-2
Melilite-C[3] (single crystal)	0.0015	27.8-30.0	54.1-56.9	-1.2±0.6	1.1
Fuzz-A (bulk; ρ<2.5 gm/cm^3)	0.1	29.6-31.0	58.6-60.5	-1.9±0.3	-

[1]For ug-size samples, weight estimated from crystal volume.
[2]Fractionation relative to the values obtained for normal Mg: $^{26}Mg/^{24}Mg$ = 0.12475, $^{26}Mg/^{25}Mg$ = 0.13569.
[3]Directly loaded crystal.

In addition to Mg, it has been established that the isotopic compositions of Ca, Sr, Ba, Nd, and Sm are anomalous but uniform in pyroxene and melilite. This isotopic uniformity indicates that the inclusions were condensed from a locally homogeneous parcel of the solar nebula or have been isotopically equilibrated after the condensation process. The possibility that these inclusions are composed of a conglomerate of interstellar dust particles preserved with their original isotopic compositions intact is untenable.

Table 2 presents the results of a series of experiments with handpicked plagioclase grains. The surfaces of most of these grains were coated with fine-grained alteration products. Examination with an electron microprobe showed that the "fuzz" material was Mg rich (< 8 percent).

Table 2.--Mg isotopic composition of plagioclase samples in Cl

Sample	Weight[1] (ug)	Fractionation (permil)[2] (25/24)	(26/24)	$\delta^{26}Mg$ (permil)	$^{27}Al/^{24}Mg$[3]	Mg^4 (ng)
A --------	2.1	18.5-24.6	40.7-49.4	3.0±1.8	165	3
B --------	2.4	26.0-29.1	55.0-52.7	0.1±1	21	27
C --------	-	24.0-29.2	50.8-57.0	2.4±1.4	-	-
D --------	2.4	18.0-25.3	40.5-46.4	2.1±1.5	78	8
E --------	-	13.2-19.0	32.1-38.0	3.0±1.2	-	-
F[5] -------	8.5	29.4-31.5	60.1-63.3	-0.6±0.3	20	90
G --------	1.9	5.1-10.6	11.2-17.9	0.9±1.1	63	6
Moore County Plagioclase --	2.3	(-0.5)-(-4.3)	(-4.0)-(-8.5)	0.0±1.0	300	2

[1]Weight of anorthite crystals determined from the Ca content.
[2]Fractionation relative to the values obtained for normal Mg: (25/26) = 0.12475; (26/24) = 0.13569.)
[3]Mg and Ca concentrations measured by isotope dilution on a small aliquot of the sample; Al obtained by using Al/Ca ratio from electron microprobe analysis.
[4]Mg amount in sample.
[5]Sample processed through chemistry; all other samples analyzed by direct loading. A bias of +1.5 permil has been added to $\delta^{26}Mg$ for directly loaded samples.

Because plagioclase grains with very high $^{27}Al/^{24}Mg$ ratios are required in order to best demonstrate any effects due to ^{26}Al decay, microsurgical cleaning techniques, using sharp tungsten needles and fine pointed tungsten tweezers, were used to scrape the contaminant material from individual crystals. As shown in table 2, these efforts did not always produce crystals with high $^{27}Al/^{24}Mg$ ratios. This is, in part, due to the low abundance of plagioclase in Cl and its smaller crystal size as compared to inclusion WA (Lee and others, 1977a) in which these techniques were previously applied.

The most striking feature of the results on plagioclase in Cl is the presence of only small excesses of $^{26}Mg^*$ in phases highly enriched in $^{27}Al/^{24}Mg$. For example, for the initial $(^{26}Al/^{27}Al)_o = 5 \times 10^{-6}$ as determined in inclusion WA (Lee and others, 1977a) the corresponding $\delta^{26}Mg$ for plagioclase-A in Cl ($^{27}Al/^{24}Mg$ = 165, see table 2) should have been 59 permil in contrast with the measured value of 3.0 ± 1.8 permil which is a factor of nine lower. A possibly more reliable limit can be derived from the "bulk" sample plagioclase-F. In order to avoid any possible bias in the data obtained by the direct loading technique (Lee and others, 1977b) Mg was chemically separated from this sample. Data on plagioclase-F indicate that $^{26}Al/^{27}Al$ in Cl must be lower than in WA by a factor of at least 6. These conclusions are independent of possible contamination of the samples with normal or fractionated Mg. The above limits were determined by assuming that in the absence of ^{26}Al effects, $\delta^{26}Mg$ in plagioclase is -1.5 permil (as found for melilite, table 1). However, the precise interpretation of the data is complicated by the existence of plagioclase analyses which show Mg with distinctly lower mass fractionation than the 30 permil per mass unit observed for all the other mineral phases in Cl. Given the Mg isotopic composition of the fine-grained fuzz, this material would not be expected to reduce the Mg isotopic fractionation. At present, the situation with regard to

variable fractionation effects in plagioclase remains unresolved and further experiments are in progress.

As mentioned previously, Cl appears to be a "poor relative" of EK1-4-1 in that anomalies in EK1-4-1 are much more extensive both in the range of anomalous isotopes and magnitude of effects. Following the same pattern, it is possible that Cl did not receive its full complement of ^{26}Al. This conclusion implies that ^{26}Al-^{27}Al mixtures in the solar nebula were heterogeneous and that differences in $^{26}Al/^{27}Al$ may not be used as a chronometer. Alternative postulates are (1) Cl condensed at a somewhat later time than WA ($\Delta T \simeq 2.5 \times 10^6$ yr); or (2) Mg in Cl was isotopically equilibrated by the remelting of the inclusion such that most of the $^{26}Mg^*$ was incorporated into and diluted beyond recognition in Mg rich phases.

The present data show that a small ^{26}Mg excess does exist in Cl and that it is roughly correlated with the $^{27}Al/^{24}Mg$ ratio. This indicates that some ^{26}Al was present in Cl, together with the more general nuclear anomalies. It is possible that study of EK1-4-1 will better clarify the relationship between ^{26}Al and the FUN anomalies. The absence of nuclear anomalies in Ca, Sr, and Ba in inclusion WA, which shows a high initial $^{26}Al/^{27}Al$ ratio indicates that the correlation of ^{26}Al with the FUN anomalies is not a simple matter. The observation of both positive and negative nuclear anomalies (Lee and others, 1978; McCulloch and Wasserburg, 1978a) has necessitated the presence of at least two components with distinct isotopic compositions. The association of ^{26}Al with either or both of these components remains an open question.

Cameron, A. G. W., and Truran, J. W., 1977, The supernova trigger for the formation of the solar system: Icarus, v. 30, p. 447.

Clayton, R. N., and Mayeda, T. K., 1977, Correlated oxygen and magnesium isotopic anomalies in Allende inclusions I; oxygen: Geophysical Research Letters, v. 4, p. 295.

Lee, T., Papanastassiou, D. A., and Wasserburg, G. J., 1977a, Aluminum-26 in the early solar system; fossil or fuel?: Astrophysical Journal Letters, v. 211, p. 107.

_____1977b, Mg and Ca isotopic study of individual microscopic crystals from the Allende meteorite by the direct loading technique: Geochimica Cosmochimica Acta, v. 41, p. 1473.

_____1978, Calcium isotopic anomalies in the Allende meteorite: Astrophysical Journal Letters, v. 220, p. 21.

Lugmair, G. W., Marti, K., and Scheinin, N. B., 1978, Incomplete mixing of products from r-, p-, and s-process nucleosynthesis; Sm-Nd systematics in Allende inclusion EK1-4-1: Lunar Science, IX; The Lunar Science Institute, p. 672.

McCulloch, M. T., and Wasserburg, G. J., 1978a, Barium and neodymium isotopic anomalies in the Allende meteorite: Astrophysical Journal Letters, v. 220, p. 15.

_____1978b, More mysteries from Pandora's box: (this conference).

Papanastassiou, D. A., Huneke, J. C., Esat, T. M., and Wasserburg, G. J., 1978, Pandora's box of the nuclides: Lunar Science, IX; The Lunar Science Institute, p. 859.

Wasserburg, G. J., Lee, T., and Papanastassiou, D. A., 1977, Correlated oxygen and magnesium isotopic anomalies in Allende inclusions, II; magnesium: Geophysical Research Letters, v. 4, p. 299.

THE ORGANIC GEOCHEMISTRY OF THE STABLE HYDROGEN ISOTOPES

By Marilyn F. Estep and Thomas C. Hoering
Geophysical Laboratory
Carnegie Institution of Washington
Washington, D. C. 20008

Biochemical reactions are selective towards hydrogen isotopes and naturally occurring organic matter is, in general, depleted in deuterium relative to coexisting waters. Experiments have been carried out with micro-organisms cultured under controlled conditions in an attempt to learn some of the processes governing hydrogen isotope fractionation. A survey has been made of the isotope ratio in lipids of naturally growing plants. Measurements have been made on classes of organic matter in recent marine and non-marine sediments. Hydrogen isotope ratios have been measured on fractions from selected petroleums, including some of Precambrian age.

Algal cultures were grown axenically at constant temperatures in defined inorganic media with one percent carbon dioxide. When the cells reached a density of from 0.2 to 0.4 milligrams dry weight per milliliter, they were centrifuged, freeze-dried, and stored in a dessicator until constant weight was reached. The dried cells were quantitatively combusted to water, and the water was converted to hydrogen by reac-

The coccoid, green alga Chlorella sorokiniana and the filamentous, blue-green alga Nostoc muscorum had a δD that averaged 115 permil lower than the water in the medium. The differences in hydrogen-isotope fractionation between marine and fresh-water organisms may reflect differences in the transport of water across cellular membranes.

Chlorella sorokiniana was adapted to grow heterotrophically in the dark on glucose in water of varying isotopic composition. The isotope ratio in the cells was the same, within experimental error, as the isotope ratio of the glucose and did not change appreciably when the δD of the water in the culture media was varied tion with uranium metal at 700°C.

The marine, coccoid, blue-green alga, Agmenellum quadruplicatum, had a δD that was 147.9 permil lower than the water in the culture medium. The units are defined as follows:

$$\delta D = \left\{ \frac{(D/H)_x - (D/H)_s}{(D/H)_s} - 1 \right\} \times 1000$$

where the subscript x refers to the unknown sample and the subscript s refers to the standard reference material (Standard Mean Ocean Water from the International Atomic Energy Agency, Vienna). The measurements had a standard deviation of 5.4 permil for six independent cultures. Similar results were obtained for the marine, pennate diatoms, Cylindrotheca sp. and Amphora sp. The observed isotope effect in A. quadruplicatum did not vary with changing concentration of sodium chloride in the medium over the range from 0.31M. to 0.043M. There was no effect from changing the temperature in the range from 27 to 39°C. Mixed phytoplankton, mainly diatoms, collected in the Chesapeake Bay had a δD that was 132 permil lower than the surface waters.

Cultures of fresh-water algae showed significantly less hydrogen isotope fractionation. 42 permil. A significant amount of the hydrogen in the cells was inherited directly from the glucose without appreciable isotope fractionation. These results imply that cellular respiration has little hydrogen isotope effect and that a major factor governing the deuterium content of plants is associated with the conversion of carbon dioxide to carbohydrates during photosynthesis.

Lipids were extracted from tree leaves and macroscopic marine algae. After saponification, the lipids were fractionated by column chromatography on silicic acid and their isotopic composition was measured. Lipids are significantly depleted (greater than 50 permil) in the heavy isotope as compared to carbohydrates plus protiens, and fall into two groups. Sterols, phytol and carotene pigments, which are synthesized by the isoprenoid pathway, have a D/H ratio that is as much as 150 permil lower than the fatty acids and hydrocarbons, which are synthesized by the acetate pathway.

A suite of sediment samples were collected in the Atchafalaya River of Louisiana and adjacent continental shelf in the Gulf of Mexico. A humic-acid and fatty-acid fraction were isolated from each and analyzed for carbon and hydrogen isotopes. The fatty acids showed a consistent depletion of the heavy isotopes for both elements, similar to that found in living organisms. The δD of the fatty acids are in the range expected for fresh water and marine plankton.

A series of crude oils and shale extracts of varying age was fractionated by silica gel chromotography into a hexane, benzene and methanol eluates and their δD measured. Younger, immature petroleums showed a wide range of deuterium content in the three fractions. Older material, including some of Precambrian age was much more homogeneous. There was no systematic change in isotopic composition with age. The results indicate that a large-scale transfer of hydrogen occurs during diagenesis of sedimentary organic matter.

TERRESTRIAL URANIUM, HEAT FLOW, AND COSMOCHEMISTRY

By David E. Fisher
Rosenstiel School of Marine and Atmospheric Science,
University of Miami,
Miami, Florida 33149

The U abundance of the earth's interior, and particularly of the upper mantle, is of basic importance in terrestrial heat-flow models (Rybach, 1977; MacDonald, 1964). The U content of the whole-earth has been used as one of the four basic parameters by which the abundance of all 83 naturally occurring elements is estimated and planetary models are formulated (Ganapathy and Anders, 1974; Anders and Owen, 1977). In this paper I discuss the U content of the

oceanic crust and its implications for deep-earth abundances, heat-flow calculations, and cosmochemistry.

The uranium content of 50 fresh oceanic basalts was measured by fission-track analysis. Measurements on several weathered basalts were also carried out; the results indicate that the effect of such weathering is to drastically increase the uranium concentrations, in agreement with Aumento (1971), and MacDougall (1977), and in contrast to Gray and others (1977). These results indicate that the U enrichment previously observed (Fisher and Bostrom, 1969), in metalliferous sediments is not due to sea water leaching of erupting basalts at the ocean ridges.

Including the results of previous data on fresh, unweathered oceanic basalts (defined by $H_2O^+ < 1$ percent and $Fe_2O_3/FeO < 1$) the average uranium concentration is 78 ± 48 ppb for 77 samples; limiting the samples to glasses, the concentration is 65 ± 40 ppb for 40 samples (table 1).

Basaltic magmas erupted above postulated mantle plumes are treated separately from the above samples since previous work has shown them to have distinct chemical compositions, including large concentrations of radiogenic lead and the large-ion-lithophile elements (Schilling, 1973, 1975a, b; Bonatti and others, 1977). A series of samples from the Easter Volcanic Chain show an average uranium concentration of 1600 ± 1000 ppb, more than an order of magnitude increase over the ridge and intraplate basalts. These uranium concentrations vary coherently with other LIL elements, and plot in distinctly different sections of correlation diagrams from the ridge and intraplate basalts.

An oceanic mantle pyrolite defined according to Clark and Ringwood (1964), with the U abundances of ridge and intra-plate basalts, leads to an estimated U concentration of ~20 ppb in the upper mantle. Such an upper mantle, together with the oceanic crust, will generate $\lesssim$0.2 Heat Flow Units (for any reasonable K/U and Th/U ratios); the heat loss flowing through the oceanic crust is over 2.2 HFU (Williams and von Herzen, 1974). Even if the average U content of the entire mantle is ~20 ppb, the heat generated is still <1 HFU. If the U content of the mantle plume areas is characteristic of large portions of the mantle, the difficulty is removed. The large U and K abundances measured in the Easter Volcanic Chain would lead to a mantle-heat generation of 2.6 HFU for the upper 400 km, or 18 HFU for the entire mantle. If such magmas do not provide a significant contribution to the overall mantle composition, then it is necessary to consider a deep-seated source of heat; perhaps heat flow from the core should be considered.

The absolute abundance of U in the whole-earth (U_e) has been taken as 18 ppb (Ganapathy and Anders, 1974; Anders and Owen, 1977). A detailed examination reveals severe deficiences in the derivation of this number. A realistic upper limit can be set by considering the amount of U necessary to generate the observed heat flow through the earth's surface, with $K/U > 10^3$ and Th/U>2.5, U_e<35 ppb. A lower limit can be set by noting that $\gtrsim$85 ppb K is necessary to provide the ^{40}Ar content of the atmosphere, with $K/U \lesssim 10^4$, $U_e \gtrsim 8.5$ ppb. Justification of these choices will be discussed.

Table 1.--U abundances in deep sea basalts

Reference	Location	Number of samples	U(ppb)
MacDougall (1977)	DSDP	12	63±35
Mitchell and Aumento (1977)	DSDP-37	6	43±25
Tatsumoto (1978)	MAR, Galapagos	9	103±27
This work	MAR, EPR	50	77±48

Anders, E., and Owen, T., 1977, Mars and earth--origin and abundance of volatiles: Science, v. 198, p. 453-465.

Aumento, F., 1971, Uranium content of mid-oceanic basalts: Earth and Planetary Science Letters, v. 11, p. 89.

Bonatti, E., Harrison, C. G. A., Fisher, D. E., Honnorez, J., Schilling, J.-G., Stipp, J. M., and Zentille, M., 1977, Easter Volcanic Chain (Southeast Pacific)--A mantle hot line: Journal of Geophysical Research, v. 82, no. 17, p. 2457-2478.

Clark, S. P., and Ringwood, A. E., 1964, Density distribution and constitution of the mantle: Reviews of Geophysics, v. 2, p. 1.

Fisher, D. E., and Bostrom, K., 1969, Uranium rich sediments on the East Pacific Rise: Nature, v. 224, p. 64-65.

Ganapathy, R., and Anders, E., 1974, Bulk compositions of the moon and earth, estimated from meteorites: Geochimica Cosmochimica Acta, Supplement 5, p. 1181.

Gray, J., Cumming, G. L., and Lambert, R. St J., 1977, Oxygen and strontium isotopic compositions and thorium and uranium contents of basalts from DSDP 37 cores: Initial Reports of the Deep Sea Drilling Project 37, p. 607-611.

MacDonald, G. J. F., 1964, Dependence of the surface heat flow on the radioactivity of the earth: Journal of Geophysical Research, v. 69, no. 14, p. 2933.

MacDougall, J. D., 1977, Uranium in marine basalts--concentration, distribution, and implications: Earth and Planetary Science Letters, v. 35, p. 6770.
Mitchell, W. S., and Aumento, Fabrizio, 1977, Uranium in oceanic rocks: DSDP Leg 37: Canadian Journal of Earth Sciences, v. 14, p. 794-808.
Rybach, L., 1977, Radioactive heat production--a physical property determined by the chemistry of rocks, in Strens, R. G. J., ed., The Physics and Chemistry of Minerals and Rocks: London, p. 309-318.
Schilling, J.-G., 1973, Iceland mantle plume--geochemical evidence along Reykjanes ridge: Nature, v. 242, p. 565-571.
_____1975a, Rare-earth variations across "normal segments" of the Reykjanes ridge, 60°-53°N, mid-Atlantic ridge, 29°S and east Pacific rise, 2°-19°S, and evidence on the composition of the underlying low-velocity layer: Journal of Geophysical Research, v. 80, p. 1459-1473.
_____1975b, Azores mantle blob--rare earth evidence: Earth and Planetary Science Letters, v. 25, p. 103-115.
Tatsumoto, Mitsunobu, 1978, Isotopic composition of lead in oceanic basalt and its implication to mantle evolution: Earth and Planetary Science Letters, v. 38, p. 63-87.
Williams, D. L., and von Herzen, R. P., 1974, Heat loss from the earth--new estimate: Geology, v. 2, p. 327-328.

AGE OF THE THANET BEDS (PALAEOCENE) OF EAST KENT, ENGLAND

By Frank J. Fitch[1], Paul J. Hooker[2], and John A. Miller[2]
[1]Birkbeck College, London, England
[2]University of Cambridge, Cambridge, England

Great changes in the geography of northern Europe were initiated early in the Palaeocene. The Chalk Sea withdrew from much of the present-day land area of Britain and the nearby continent. In northwestern Britain, regional uplift and rifting were accompanied by several major episodes of basaltic volcanism heralding the final break with Greenland and North America. In the central North Sea Basin, reactivation of Jurassic rifts resulted in the formation of fault-scarps marked by oligostromes of chalk fragments in a clastic matrix of early Palaeocene age. Rapid subsidence of the North Sea Basin continued throughout the lower Tertiary, with the accumulation of a thick complex of Palaeogene sands in a central depression. During this rather unstable period, the North Sea alternately advanced and retreated in a southwestern gulf covering much of what is now the Paris, Hampshire, and London Basins. In southeastern England, several sedimentary cycles resulting from this instability can be recognized in the Palaeogene deposits. The oldest of these rocks are seen resting upon an emergent platform of eroded chalk in East Kent and are known as the Thanet Beds. They were deposited by a short-lived, restricted marine transgression that penetrated into the London Basin from the east, in middle and late Palaeocene times.

The Thanet Beds in East Kent are particularly rich in glauconite. They have not been deeply buried since deposition nor did they suffer more than gentle warping during mid-Tertiary movements. Thus, they should provide ideal samples for glauconite dating by the K-Ar method. It is not surprising, therefore, that a sample from the uppermost Thanet Beds from the seacliff at Bishopstone Glen (often mistakenly called the Oldhaven Gap), East Kent, was included in the classic paper on glauconite dating by Evernden and others (1961). Their results from this sample, a glauconite concentrate from a glauconitic sandstone, were as follows: KA274 - K_2O = 6.05 percent; V/M = 0.011675 mm^3g^{-1}; atmospheric correction = 29 percent; t = 57 m.y. Evernden and others (1961) regarded this as an excellent result. Recalculated using the new IUGS standard constants (all ages subsequently quoted in this paper are based on these new constants), this date for the uppermost Thanet Beds becomes 58.4 m.y. By chance it happens that it was on this sample that Evernden and his colleagues carried out an experiment illustrating the effect of bakeout temperatures on glauconite samples. Sample KA 274 was held at a bakeout temperature of 85°C overnight before the argon analysis; two further samples of the same concentrate were held at 190°C and 260°C overnight, respectively. The result of these higher temperature bakeouts was to reduce the apparent ages obtained by 14 percent and 40 percent without changing the atmospheric correction required.

The results of conventional K-Ar dating of six glauconite samples extracted from two horizons in the Thanet Beds, one from close to the base, the other near the top, are shown in table 1. The total thickness of the Thanet

Table 1.--Results of conventional K-Ar dating of glauconites from East Kent
[Bakeout temperature in sample holder; room temperature.
Constants used; IUGS.]

Location	Sample	Mesh size	K_2O (percent)	Atmos. contam. (percent)	V/M (mm /g)	Apparent age and error (m.y.)
0.3 m above base of basal Thanet Beds, Pegwell Bay, Kent.	1A	70/100	5.51	31.40	$1.1109 \times 10^{-}$	61.4
	1B	120/140	5.73	27.40	$1.1294 \times 10^{-}$	60.1
	1C	100/120	5.61	35.40	$1.1243 \times 10^{-}$	61.1
			Mean conventional apparent age---			60.9
			Error by Peter's formula---------			0.9
4.57 m below top of Reculver Sands, Bishopstone Glen., Herne Bay, Kent.	7A	22/30	6.50	35.90	$1.2497 \times 10^{-}$	58.7
	7B	40/50	6.13	45.90	$1.1585 \times 10^{-}$	57.7
	7C	50/70	6.10	36.70	$1.1607 \times 10^{-}$	58.1
			Mean conventional apparent age---			58.2
			Error by Peter's formula---------			0.6

Beds in East Kent is close to 25 m. The three samples, Kent 1A, 1B, and 1C, were collected from the middle of the glauconite-rich Thanet Base Bed, 0.3 m above the unconformity with the Chalk, at Pegwell Bay, East Kent. Samples Kent 7A, 7B, and 7C were collected from the glauconite sandstones of the Reculver Sands, 4.57 m below the top of Thanet Beds in the seacliff immediately east of Bishopstone Glen, Herne Bay, East Kent. The junction between the Thanet Beds and the overlying Woolwich Beds at this locality was taken to be 6 m below the outcrop of the easily identifiable Blackheath Pebble Bed at the base of the Oldhaven Beds. It is assumed that sample KA 274 was collected in the same seacliff close to a band of tabular sandy concretions that was formerly regarded as marking the top of the Thanet Beds in this locality. Thus, in the usage of this paper, this sample was most probably collected 7.62 m below the top of the Thanet Beds, some 3.05 m below the Kent 7 site. The average conventional K-Ar apparent ages of glauconites from these three horizons (58.2 m.y., 58.4 m.y., and 60.9 m.y., respectively) are consistent with their relative positions within the Thanet Beds and justify an estimated total age range of 60.95 to 57.6 m.y. for the East Kent outcrops. Stratigraphically, the Thanet Beds of East Kent are of late middle to early late Palaeocene age. They most probably include part of the nannoplankton zone 6 and all of zones 7 and 8 of Martini (1971) and are approximately equivalent to planktonic foraminiferal zone 4 of Berggren (D. Curry, oral commun.). Thus, the age span of 60.95 m.y. to 57.6 m.y. for the Thanet Beds of East Kent suggested by our work with glauconite is consistent with the ages of 61.4 m.y. and 54.8 m.y. preferred for the top and bottom of the Thanetian Stage as a whole by Hardenbol and Berggren (in press). A Rb-Sr glauconite model age of 56.8 m.y. has recently been obtained from a horizon in the Beaufort Formation outcrop in North Carolina, some 1.5 m below the top of the Thanetian (Harris and Baum, 1977).

Further confirmation of these glauconite K-Ar ages can be obtained by a consideration of the timing of events that were happening far to the northwest of East Kent. Before and during the final disruption of the former North Atlantic continent by sea floor spreading, an extensive plateau of flood basalts was erupted from East Greenland to the Faeroe Islands. Paleontological evidence from East Greenland suggests that this important volcanic episode occurred in late Thanetian (Sparnacian) to earliest Ypresian times and is equivalent in age to the 15 m of strata, comprising the Woolwich and Oldhaven Beds and lowermost London Clay, which directly overlies the Thanet Beds in East Kent (Soper, Downie, and others, 1976; Soper, Higgins, and others, 1976). A very extensive tuff horizon of Sparnacian age is known throughout the North Sea Basin (Jacqué and Thouvenin, 1975). Conventional K-Ar ages of the volcanic rocks of the Blosseville Group of East Greenland and from the Faeroe Islands (Beckinsale and others, 1970; Tarling and Gale, 1968) were scattered and appear rather inconclusive until the analyses are plotted in various combinations on argon-40/argon-36 versus potassium-40/argon-36 correlation diagrams. Figure 1 is one such plot in which all available data from the basalts of the Faeroe Islands have been used. Regression analyses of these datum points suggest an average apparent age of 55.7 ± 1.3 m.y. for these lavas. Similarly, correlation diagram regression analyses of K-Ar data from a lava at Kap Brewster, high in the Blosseville Group succession suggest an apparent age of 55.8 ± 1.0 m.y. The lowest value obtained by this approach was that of 52.2 ± 3 m.y. obtained when all available data (that is, unselected) from lavas of the Blosseville Group were plotted. Selected data from the Faeroe basalts gave apparent ages of 55.2 ± 1.0 m.y. and 54.6 ± 1.2 m.y. for the base of the lower and the top of the middle parts of the Faeroe basalts, respectively. Thus, it would be reasonable to ascribe a maximum age range of $\sim$ 56 m.y. to $>$ 52 m.y. to this Sparnacian volcanic episode. From this and other evidence we have suggested an age range of 57.4 m.y. to 54.3 m.y. for the Sparnacian (Fitch and others, 1978), which is completely consistent with the glauconite dates obtained from the slightly older Thanet Beds of East Kent. It would appear from this, and from an examination of the dates obtained from Palaeocene igneous rocks generally, that samples KA 274, Kent 1A-C, and Kent 7A-C were "ideal" glauconite dating samples. In fact, the six Kent samples were selected as "ideal" dating samples from a considerably larger collection of glauconite samples from East Kent on the basis of, among other things, an examination of the characteristics of their argon-40/argon-36 versus argon-39/argon-36 correlation diagram plots. It has been shown that glauconite cannot be dated satisfactorily by the argon-40/argon-39 stepwise degassing method because of serial errors resulting from argon-39 recoil diffusion phenomena during irradiation (Brereton and others, 1976), but it appears that the characteristic shapes of the age spectra and correlation plots are preserved, thus still al-

lowing evaluation of the dating promise of a sample. Figure 2 illustrates this point in respect to sample Kent 1A. The work we report here would appear to confirm that carefully selected glauconite can be satisfactory material for K-Ar dating. This conclusion has not been universally acceptable (Hurley and others, 1960), and the discrepancy between our glauconite dates for the Thanet Beds of East Kent and those obtained by Odin and his associates (Odin and others, 1969; Odin, 1975), who quote much lower ages, in the range 56 - 53 m.y. from the same horizon, needs to be resolved. We believe that for successful glauconite dating of the age of deposition, samples must be collected from sediments that have not been deeply buried or subjected to prolonged diagenetic change and have not been involved in any significant earth movements or excessive groundwater migration or mineralization effects; in fact, samples in which the glauconite pellets are as close to their original sedimentation state as is geologically possible. It is unlikely that these conditions will be met by very ancient glauconites. We do not believe that a high potassium content is necessarily an indication that the sample is to be preferred, because, although it is likely that such pellets are more stable and more resistant to subsequent argon loss, it is also likely that time zero for their internal K-Ar "clocks" is closer to that of the cessation of diagnetic change than to the moment of sedimentation. Additionally, it is clear that absence of contamination by older detrital glauconite pellets, protection from any violent treatment that might cause argon loss during collection and preparation and from excessive heat treatment of the sample, either during washing and drying or during the preheat sequence in the argon line of the mass spectrometer, are all important factors in glauconite dating.

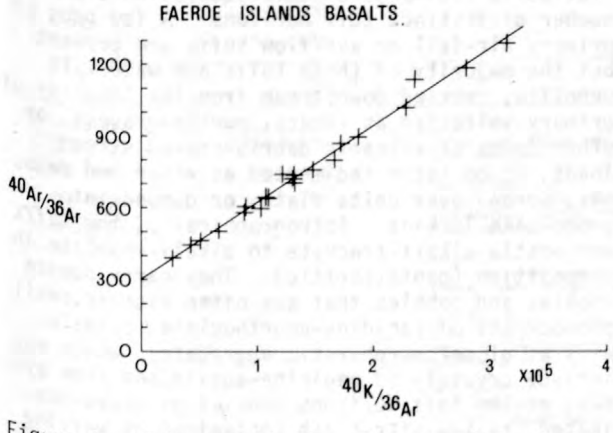

Figure 1.--K-Ar correlation diagram plot of the conventional K-Ar data obtained from basalt lavas of the Faeroe Islands by Tarling and Gale (1968). Some scatter and, therefore discrepancy is present but the regression line apparent age of 55.7 ± 1.3 m.y. (intercept value 301 ± 32) appears to be a close estimate of the true average age of volcanism.

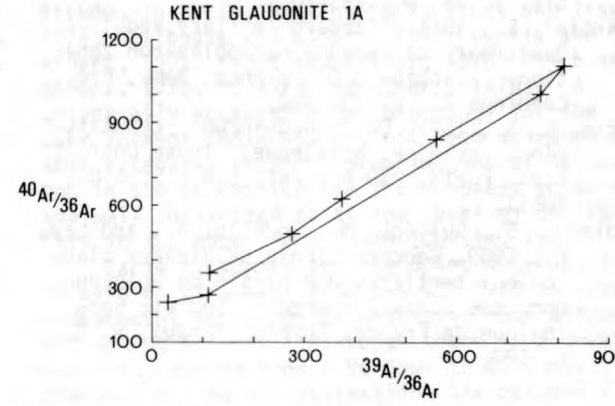

Figure 2.--Isotope correlation diagram plot of the data obtained from $^{40}Ar/^{39}Ar$ age spectrum analysis of glauconite sample Kent 1A from the basal Thanet Beds, Pegwell Bay, East Kent. A single isochronous major component dominates the argon isotope release pattern.

Beckinsale, R. D., Brooks, C. K., and Rex, D. C., 1970, K-Ar ages for the Tertiary of East Greenland: Geological Society of Denmark Bulletin, v. 20, p. 27-37.

Brereton, N. R., Hooker, P. J., and Miller, J. A., 1976, Some conventional K-Ar and $^{40}Ar/^{39}Ar$ age studies of glauconite: Geological Magazine, v. 113, p. 329-40.

Evernden, J. F., Curtis, G. H., Obradovich, J., and Kistler, R., 1961, On the evaluation of glauconite and illite for dating sedimentary rocks by the potassium-argon method: Geochimica Cosmochimica Acta, v. 23, p. 78-99.

Fitch, F. J., Hooker, P. J., Miller, J. A., and Brereton, N. R., 1978, Glauconite dating of Palaeocene-Eocene rocks from East Kent and the time-scale of Palaeogene volcanism in the North Atlantic region: Geological Society of London Journal, (in press).

Hardenbol, J., and Berggren, W. A., (in press). A new Palaeogene numerical time-scale: International Geologic Congress, 25th, Sydney, Australia, August 1976.

Harris, W. B., and Baum, G. R., 1977, Foraminifera and Rb-Sr glauconite ages of a Paleocene Beaufort Formation outcrop in North Carolina: Geological Soceity of America Bulletin, v. 88, p. 69-872.

Jacqué, M., and Thouvenin, J., 1975, Lower Tertiary tuffs and volcanic activity in the North Sea, in Woodland, A. W., ed., Petroleum continental shelf of northwest Europe, v. 1, Geology: London, Applied Science Publishers.

Hurley, P. M., Cormier, R. F., Howe, J., Fairbairn, H. W., and Pinson, W. H., 1960,

Reliability of glauconite for age measurement by K-Ar and Rb-Sr methods: American Association of Petroleum Geologists Bulletin, v. 44, p. 1793-1808.

Martini, E., 1971, Standard Tertiary and Quaternary calcareous nannoplankton zonation: Planktonic Conference, Rome, Proceedings II, p. 739-788.

Odin, G. S., 1975, De Glauconiorum: constitutione, origine, aetateque: These Doct. Etat. Paris, 250 p., ref. C.N.R.S. A.O. 10611.

Odin, G. S., Gulinck, M., Bodelle, J., and Lay, C., 1969, Géochronologie de niveaux glauconieux tertiares due bassin de Belgique (methode potassium-argon): Société Geologique de France, Comptes rendus, v. 6, p. 198.

Soper, N. J., Downie, C., Higgins, A. C., and Costa, L. I., 1976, Biostratigraphic ages of Tertiary basalts on the East Greenland continental margin and their relationship to plate separation in the northeast Atlantic: Earth and Planetary Science Letters, v. 32, p. 49-57.

Soper, N. J., Higgins, A. C., Downie, C., Mathews, D. W., and Brown, P. E., 1976, Late Cretaceous-early Tertiary stratigraphy of the Kangerlugssuak area, east Greenland, and the age of the opening of the northeast Atlantic: Geological Society of London Journal, v. 132, p. 85-104.

Tarling, D. H., and Gale, N. H., 1968, Isotopic dating and palaeomagnetic polarity in the Faeroe Islands: Nature, v. 218, p. 1043-1044.

THE KBS TUFF PROBLEM

By Frank J. Fitch[1], Anthony J. Hurford[1], Paul J. Hooker[2], and John A. Miller[2]
[1]Birkbeck College
University of London, U.K.
[2]University of Cambridge, U.K.

Superficially, the KBS Tuff problem is an unresolved controversy regarding the age of a locally important tuff horizon in northern Kenya. Different K-Ar dates for this tuff have been proposed by the Birkbeck/Cambridge (UK) and Berkeley (USA) dating groups. Fission track dating by three independent laboratories (London (UK), Denver (USA), and Melbourne (Australia) has produced internally consistent results that agree with the Birkbeck/Cambridge group age for the KBS Tuff. It has been suggested that the divergence between the conventional K-Ar results from Berkeley and the conventional K-Ar and $^{40}Ar/^{39}Ar$ age spectrum results from Birkbeck/Cambridge group arises either from contamination or from other discrepancies inherent in the analytical procedures adopted. It is difficult to accept this explanation. Our contention is that geochronometric error is not a major problem in this controversy and, thus, it is highly unlikely that replicate analyses undertaken by other laboratories will provide a solution. The KBS Tuff problem appears rather to be one of interpretation, the resolution of which should be sought in a reexamination of the basic geology, volcanology, petrography, geochemistry, and paragenesis of the KBS Tuff (and the dating samples collected from it) and in a more rigorous evaluation of the geochronometric meaning of the analytical data derived from routine dating experiments. It is this latter aspect that makes the controversy of more general geochronological interest.

The Pliocene-Pleistocene sediments around Lake Turkana (formerly Lake Rudolf) in east Africa was particularly rich in fossil mammals, especially in the remains of early man and his artifacts (see Coppens and others, 1975). Interbedded with the mainly lacustrine, deltaic, and fluviatile sediments of this succession are a number of distinct tuff horizons. A few beds of primary air-fall or ash-flow tuffs are present but the majority of these tuffs are waterlain deposits, carried downstream from the locality of primary volcanism as lahars, pumice-gravels, or other forms of volcanic debris-choked stream loads, to be later sedimented as river bed deposits, spread over delta flats, or dumped into proto-Lake Turkana. Petrographically, the tuffs are mostly alkali-trachyte to alkali-rhyolite in composition (pantelleritic). They carry pumice cobbles and pebbles that are often rich in small phenocrysts of sanidine-anorthoclase, occasionally as glomeroporphyritic aggregates, which may include crystals of aegirine-augite and iron ore. Most of the tuff horizons consist of glass-dominated crystal-vitric ash contamined by varying amounts of typical Turkana Basin sedimentary detritus. Because the principal source of this sediment is either the high-grade metamorphic rocks and granites of the Precambrian to Palaeozoic Mozambique Complex and (or) an overlying sheet of Miocene/Pliocene basic to acid volcanics, ancient feldspars and zircons are common detrital contaminants within the tuffs. Thus, although some layers within each tuff may

approach purity, few are composed completely of juvenile ash: most are mixed volcanic-epiclastic rocks more properly called tuffites. A variety of geological arguments suggest, however, that apart from a few which are present as two or more sedimentary leaves, each of these tuff or tuffite beds in the Pliocene-Pleistocene succession around Lake Turkana represents a single volcanic event. Therefore, the radiometric dating of their juvenile volcanic components (in particular, feldspar and zircon separated from pumice), should provide an accurate geochronological framework for the fossiliferous succession (Fitch and others in Bishop, in press).

The geochronology of the Pliocene-Pleistocene succession around Lake Turkana has been studied in detail in a variety of different ways: Kenyan, French, American, and British teams have mapped the rocks and proposed local and regional stratigraphies; palaeontological zonation has been attempted using the vertebrate and invertebrate faunas; the magnetic reversal stratigraphy has been examined and the tuffs have been dated by conventional K-Ar, $^{40}Ar/^{39}Ar$, and fission track methods in several different laboratories (see Coppens and others, 1975; Bishop, in press; Maglio, 1972; Brock and Issac, 1974; Hillhouse and others, 1977; Curtis and others, 1975; Fitch and Miller, 1970; Fitch and others, 1976; Hurford and others, 1976). A universally acceptable geochronology for the Lake Turkana sediments has not been achieved by this extensive research program, and at no horizon in the succession are the problems so acute and well publicized as at the level of the KBS Tuff in the Koobi Fora Basin (Curtis, 1972).

Table 1.--Summary of dates obtained from the KBS Tuff (m.y.)

[K-Ar dates recalculated to the new IUGS standard constants]

Total fusion K-Ar	Total fusion $^{40}Ar/^{39}Ar$	$^{40}Ar/^{39}Ar$ age spectrum
Area 105		
3.72±2.1 (FM)[1] p	3.19±1.1 (FM)[1] p	2.48±0.01 (FM) f (Regression analysis; four datum points).
2.46±1.0 (FM) p	2.31±0.5 (FM) p	
2.44±0.3 (FM) f	2.45±0.3 (FM) f	1.96±0.11 (FM) f (Full regression analysis; complex overprint spectrum).
2.42±0.3 (FM) f		
2.01±0.03 (B)[1] f	0.53±0.33 (FM) f	
2.40±0.03 (B)[1] f	1.60±0.19 (FM) f	
1.56±0.02 (B) f	1.87±0.19 (FM) f	
1.65±0.02 (B) f		
1.61±0.02 (B) f	2.11±0.19 (FM) f	
1.68±0.01 (B) g	1.09±0.29 (FM) f	
2.53±0.02 (B)[1] f	1.58±0.12 (FM) f	
1.50±0.02 (B) f	1.39±0.14 (FM) f	
1.62±0.02 (B) f		
1.65±0.02 (B) f	2.17±0.10 (FM) f	
Area 131		
2.16±0.03 (B)[1] f	0.93±0.54 (FM) f	1.57±1.0 (FM) f ("Peak" age; complex overprint spectrum).
1.83±0.02 (B) f	0.93±0.54 (FM) f	
1.84±0.07 (B) g		
1.81±0.02 (B) f	2.15±0.19 (FM) f	
1.85±0.03 (B) f	0.70±0.17 (FM) f	1.78±0.03 (FM) f (Average double line regression analysis; complex overprint spectrum).
1.73±0.03 (B) f		
1.83±0.03 (B) f		
		1.10±0.32 (FM) f (Full regression analysis, complex overprint spectrum).
		1.79±0.02 (FM) f (Four datum point regression analysis; complex overprint spectrum).
		1.96±0.03 (FM) f (Six datum points regression analysis; complex overprint spectrum).
Area 10		
6.90±0.05 (B)[1] f		2.47±0.02 (FM) f (Average double line regression analysis).
1.54±0.02 (B) f		
1.60±0.01 (B) f		

[1]Authors of original papers suggest possible detrital contamination. p = pumice sample, whole rock; f = sanidine-anorthoclase; g = glass. Bracketed dates are from a single sample. FM = Fitch and Miller (1970, 1975); Fitch, Hooker, and Miller (1976, 1978). B = Curtis and others (1975). Fission track date on zircon from Area 131 is 2.44±0.08 m.y., obtained by Hurford, Gleadow, and Naeser (1976).

Table 1, summarizes the dates obtained from 30 samples of pumice from the KBS Tuff in five independent laboratories utilizing four different dating methods. Although there is a great scatter, ranging from 6.90 down to 0.53 m.y., the bulk of the age estimations lie between 2.5 and 1.5 m.y. The preferred ages of 2.4 to 2.5 m.y. (Birkbeck/Cambridge dating group and fission track workers), and 1.82 and 1.60 m.y. (Berkeley dating group), appear as three of four "peaks" on a simple unweighted frequency distribution diagram on the data (fig. 1), the fourth, smaller peak lying at 2.15 m.y. Several possible causes have been suggested for this scatter of ages and the apparent discrepancy between the results from different laboratories:

1. The contamination of the tuff by pumice blocks of different age either in the volcanic source area, or at the site of deposition by the incorporation of eroded pumice.
2. The inadvertent inclusion of detrital feldspar in those dated feldspar concentrates which give apparent ages > 1.82 m.y.
3. Simple or complex K-Ar overprinting of the KBS Tuff during its subsequent geological history.
4. The use of sample and analytical preparation procedures (including the preheating routine in the argon line) that have adversely affected the atmospheric correction factor.
5. Various supposed deficiences inherent in the $^{40}Ar/^{39}Ar$ dating technique.
6. The use in the fission track method of the wrong uranium spontaneous fission decay constant.
7. The erroneous field correlation of more than one tuff horizon as a single KBS Tuff unit.

Contamination of the pumice population of the KBS Tuff by reworked older pumice is thought to be unlikely because of the virtual absence of cobble-sized pumice in the adjacent basin sediments.

Detrital contamination is undoubtedly present in some of the dating samples. In most mineral concentrates from clean, matrix-free KBS pumice lumps, numerous rounded, clearly detrital feldspar and zircon grains can be recognized. In fission track dating it is possible to isolate visually the results from these older grains and avoid any age discrepancy that they might otherwise cause. In K-Ar and $^{40}Ar/^{39}Ar$ dating

this is not possible, and every effort must be made to physically remove any possibly older grains from the sample before analysis. In performing the K-Ar and $^{40}Ar/^{39}Ar$ analyses quoted in table 1 (excepting those marked with an asterisk) an attempt was made to avoid detrital contamination by carefully hand-picking the feldspar samples. Petrographic examination of core and crust samples taken from single large pumice lumps from Koobi Fora tuffs usually show a concentration of obvious detrital grains in the outermost layers, but one surprising byproduct of the fission track work has been the frequent discovery of older crystals of zircon within the cores of these lumps. Connecting vesicles are not found in most Koobi Fora pumices and thus the zircons are in positions to which they could not have penetrated after the consolidation of the lava froth. By analogy, the unidentifiable presence of older feldspar must be accepted as a possible cause of discrepancy, for example, contamination of KBS feldspar concentrates by a small number of much older feldspars. The source of these older contaminating crystals is at present unknown: they must have been derived from older rocks, ashes, or detritus during the eruptive process.

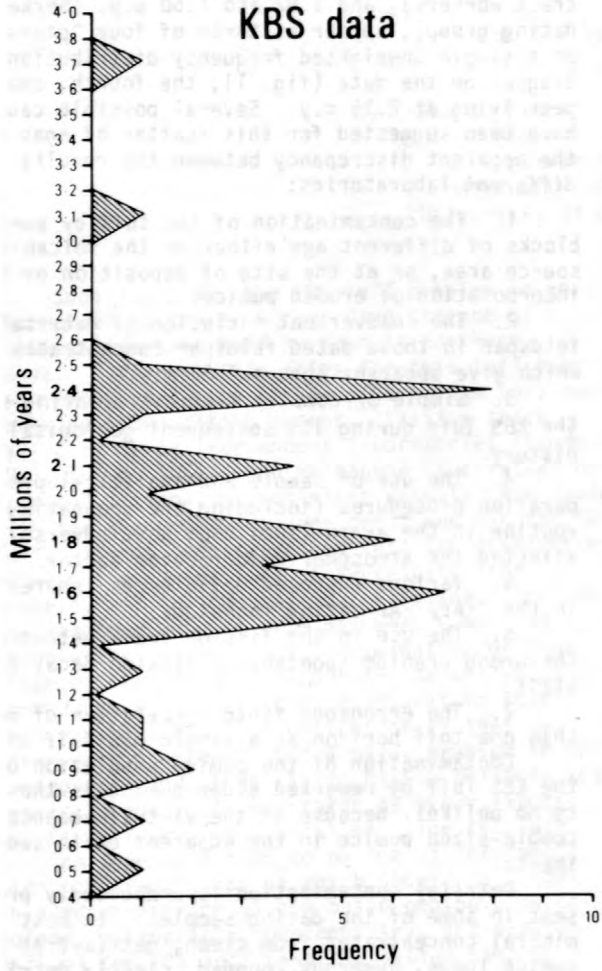

Figure 1.--Unweighted frequency distribution diagram of published dates from the KBS Tuff.

The KBS Tuff occurs near the top of an older section of the sedimentary sequence in the Koobi Fora basin. It was followed by a sedimentary hiatus during which extensive erosion occurred. Thus there was an appreciable time-lag before what remained of this particular tuff became buried beneath any thickness of overlying sediment. Geological events and (or) groundwater activity during this period may have caused partial overprinting disturbance to KBS feldspars.

Different sample preparation procedures (acid treatment, ultrasonic cleaning, preheating) in use in the Berkeley and Cambridge K-Ar dating laboratories, and the difference between conventional total fusion K-Ar, total fusion $^{40}Ar/^{38}Ar$ and $^{40}Ar/^{39}Ar$ incremental heating dating techniques may be responsible for some minor variation in the published results from the KBS Tuff, but neither of these factors, nor any supposed difference between the K-Ar and fission track time-scales can be responsible for the scatter of the K-Ar dates or the major interlaboratory discrepancy in the dating of the KBS Tuff because they do not result in a similar discrepancy in the dating of the other horizons at Koobi Fora or elsewhere. Dates obtained by the Birbeck/Cambridge group, the Berkeley group, and fission track workers for the Chari/Karari horizon at Koobi Fora, for example, are concordant, as are numerous other K-Ar, $^{40}Ar/^{39}Ar$, and fission track dates for horizons throughout Phanerozoic time (for example, Hurford and Gleadow, 1977).

The type locality of the KBS Tuff is in Area 105 of the Koobi Fora Basin. Today, this part of the East African Rift is a semi-arid region of low hills, ridges, and lag-gravel covered plateaus dissected by the gulleys, wadis, and ravines of numerous intermittent rivers. Between the low upland areas the faulted Pliocene-Pleistocene outcrop is covered by more recent deposits. Basic lithological outcrop mapping of the basin sediments awaits completion and the correlations across certain areas of unexposed ground and across some faults is still controversial. An essential pre-requisite to any satisfactory interpretation of the geochronology of the area is a categorical confirmation from the field geologists that the tuffite horizon at present known as the "KBS Tuff" in Areas 105, 131 and 10 is of the same geological age throughout.

Bishop, W. W., ed., (in press), Geological background to Fossil Man: Edinburgh, Scottish Academy Press.

Brock, A., and Isaac, G. Ll., 1974, Palaeomagnetic stratigraphy and chronology of hominid bearing sediments east of Lake Rudolf, Kenya: Nature, v. 247, p. 344-348.

Coppens, Y., Howell, F. C., Isaac, G. Ll., and Leakey, R. E. F., eds., 1975, Earliest man

and environments in the East Rudolf Basin; Stratigraphy, Palaeoecology and Evolution: Chicago, University of Chicago Press.
Curtis, G. H., 1975, Improvement of K-Ar dating, 1962-1975: World Archaeology, v. 7, p. 198-209.
Curtis, G. H., Drake, R. F., Cerling, T. E., Cerling, B. L., and Hampel, J. H, 1975, Age of KBS Tuff in Koobi Fora Formation, East Rudolf, Kenya: Nature, v. 258, p. 395-398.
Fitch, F. J., and Miller, J. A., 1970, Radioisotopic age determinations of Lake Rudolf Artifact site: Nature, v. 226, p. 225-228.
Fitch and Miller, 1975.
Fitch, F. J., Hooker, P. J., and Miller, J. A., 1976, $^{40}Ar/^{39}Ar$ dating of the KBS Tuff in the Koobi Fora Formation, East Rudolf, Kenya: Nature, v. 263, p. 740-744.
Fitch, Hooker, and Miller, 1978.
Hillhouse, J. W., Ndombi, J. W. M., Cox, A., and Brock, A., 1977, Additional results on palaeomagnetic stratigraphy of the Koobi Fora Formation, east of Lake Turkana (Lake Rudolf), Kenya: Nature, v. 265, p. 411-415.
Hurford, A. J., and Gleadow, A. J. W., 1977, Calibration of fission track dating parameters: Nuclear Track Detection, v. 1, p. 41-48.
Hurford, A. J., Gleadow, A. J. W., and Naeser, C. W., 1976, Fission track dating from the KBS Tuff, East Rudolf, Kenya: Nature, v. 263, p. 738-740.
Maglio, V. J., 1972, Vertebrate faunas and chronology of hominid bearing sediments east of Lake Rudolf, Kenya: Nature, v. 239, p. 379-385.

LEAD ISOTOPE EVIDENCE FOR THE EXISTENCE AND POSSIBLE ORIGIN OF SOME MISSISSIPPI VALLEY TYPE DEPOSITS IN SOUTHEASTERN ONTARIO

By Ian R. Fletcher, R. M. Farquhar, and P. R. Kuybida
Geophysics Laboratory, Physics Department, University of Toronto, Toronto, Canada

Within the southern part of the Grenville province in southeastern Ontario and adjacent New York State (fig. 1) there are fissure vein deposits, which we believe to be analogous to the deposits found in the better-known Mississippi Valley type base-metal mining districts (fig. 2). The Precambrian crystalline basement rocks of the Grenville Series are well exposed in this region and include a variety of Precambrian Pb-Zn sulphide deposits. The region, therefore, provides a good opportunity

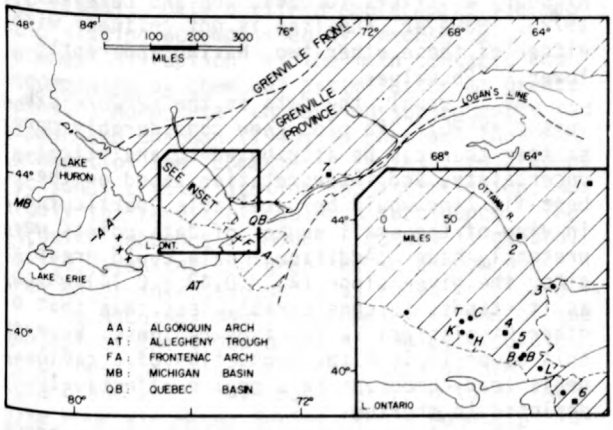

Figure 1.--The Grenville province in Ontario, Quebec, and New York State, bounded to the south by overlying relatively undeformed sediments. Solid circles are Mississippi Valley type fissure vein deposits; see table 1 for key to lettered sites. Unlabelled sites show known extent of isotopically similar veins. Solid squares are Grenville Pb-Zn deposits of differing types. Numbers are referred to in text. X indicates galena showing in the Niagara escarpment.

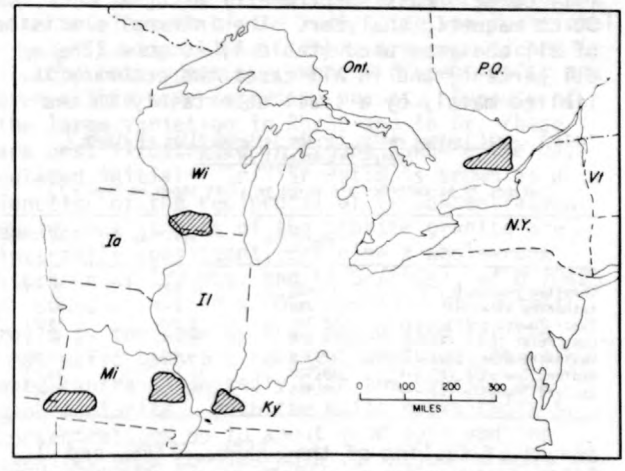

Figure 2.--Spatial relationship of the Ontario deposits to other Mississippi Valley type regions.

to determine whether the underlying basement, or the sulphide mineralization within the basement, is a source of any major component of the lead in the Mississippi Valley type deposits.

The calcite-barite-galena veins we have sampled are part of a more diverse and extensive set of veins, which center on the Frontenac Arch in southeast Ontario. The veins are known to be post-Ordovician because some cut surrounding (overlying) Ordovician strata. They are probably genetically related to the Ottawa-Bonnechere graben. The samples analyzed to date are confined to the axis and southwest flank of the Frontenac Arch (fig. 1), but previously published preliminary analyses (Fletcher and Farquhar, 1977) suggest that deposits belonging to the same Pb isotope system may extend eastwards beyond the Frontenac Arch (for example, the Kingdon mine, point 3 in fig. 1) and westward and stratigraphically up to the Silurian exposures of the Niagara escarpment (crosses in fig. 1).

The Frontenac Arch formed a basement high throughout the Palaeozoic, but was submerged during the major post-Lower Ordovician Palaeozoic oceanic transgressions. During the periods of sedimentation our sample area probably formed a sedimentary extension of the eastern margin of the Michigan Basin and a northern margin of the Appalachian Basin. The general form of the stratigraphic sequence (locally almost entirely removed by erosion) is the same as that in the Wisconsin-Illinois-Iowa base metal region to the west of the Michigan Basin. In particular, it includes, below the main Ordovician dolomitic members, basal beds which could have acted as aquifers for mineralizing solutions.

Samples were analyzed by solid source (silica gel) mass spectrometry using a 90°, 30-cm magnetic analyzer. The internal precision of all analyses used (table 1) is good ($2\sigma_{\bar{x}}$ < 0.1 percent) and in all cases the accuracy is limited mainly by a small uncertainty in the amount of tailing of the ^{206}Pb, ^{207}Pb, and ^{208}Pb peaks under the ^{204}Pb peak. All the data in table 1 are believed to be accurate to < 0.15 percent (normalized to SRM-981) and, in determining the slopes of the best-fit lines, 1σ values of 0.075 percent and error correlation coefficients of 1.0 were used.

Table 1.--Lead isotope ratios for the lettered sites of figure 1. Analytical details in text

[Letters in parentheses are keyed to sites shown on figure 1]

	$^{206}Pb/^{204}Pb$	$^{207}Pb/^{204}Pb$	$^{208}Pb/^{204}Pb$
Chrysler prospect (C) --	18.404	15.537	39.27
Katherine mine (K) -----	20.248	15.696	40.07
Tudor Township (T) -----	18.723	15.556	39.27
Long Point (L) ---------	19.078	15.602	39.15
Hollandia mine (H) -----	18.325	15.536	38.99
Bedford Township (B) ---	18.988	15.590	39.17
Bedford Township (B) ---	18.925	15.582	39.03

By comparing the lower part of figure 3 with data from other Mississippi Valley type

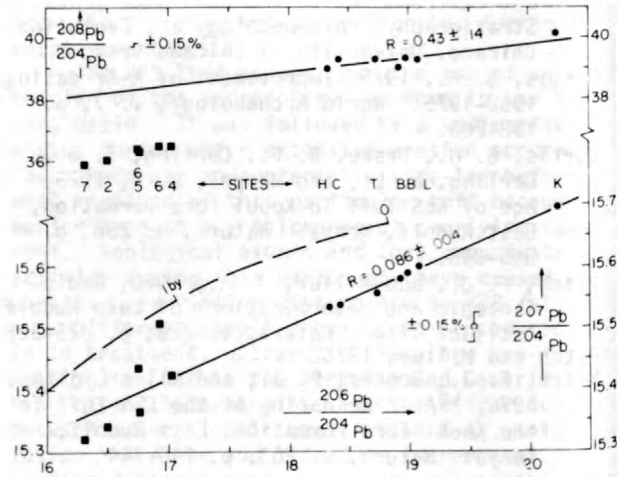

Figure 3.--Data from table 1 with their best-fit lines, plus points for Grenville Pb-Zn deposits and part of the "average-earth" growth curve. Note that the most diverse ratios (H and K) correspond to geographically close sample sites.

base metal regions, it is obvious that the lead in the calcite-barite-galena vein deposits within the Grenville display characteristics common to leads from the other regions. Most of our samples, particularly K (Katherine mine) show distinct, though relatively small, J-type anomalies (negative apparent ages). The slope (R = 0.086 ± 0.004) of the $^{207}Pb/^{204}Pb$ versus $^{206}Pb/^{204}Pb$ best-fit line is virtually identical to those for the upper Mississippi (0.088 ± 0.009, Heyl and others, 1966) and southeast Missouri districts (0.0864, Doe and Delevaux, 1972). However, the line is not colinear with either of these other two, having apparently lower ^{207}Pb values.

As is usual, the data on the $^{208}Pb/^{204}Pb$ versus $^{206}Pb/^{204}Pb$ plot show considerably more scatter than can be attributed to analytical uncertainty, and interpretation based on the best-fit line would be unreliable, particularly in view of the small number of data points we presently have. Additional data could greatly alter the given slope (R' = 0.43 ± 0.14) which, as it stands, is considerably less than that of other Mississippi Valley type regions. However, this slope implies the production of a radiogenic lead component in a region effectively depleted in thorium.

Extrapolation of the best-fit lines through the field of presently known Grenville sulphide data is also interesting. The $^{207}Pb/^{206}Pb$ line does not pass, as was previously thought by Fletcher and Farquhar (1977), through the points for the major deposits of single-stage(?) leads (Tetrault, point 7; New Calumet, point 2), nor does it pass through either of the values for the large metasedimentary(?) Pb-Zn deposits at Balmat (point 6) or the Balmat-like Long Lake deposit (point 5). The colinearity with the small Ore Chimney quartz vein deposit (point 4) is undoubtedly coincidental.

The fact that the $^{207}Pb/^{206}Pb$ best-fit line passes fairly centrally through the field of Grenville sulphide data-points suggest that some sedimentary average of these deposits could provide a major proportion of the "nonradiogenic" component of the lead in the veins, but the lack of a similar correspondence for the $^{208}Pb/^{206}Pb$ line (as presently determined) makes even this seem unlikely.

At the very least, it is now obvious that there is no simple genetic connection between the major premetamorphic and metamorphic sulphide deposits in the Grenville and the Grenville-hosted Mississippi Valley type fissure vein deposits.

Doe, B. R., and Delevaux, M. H., 1972, Source of lead in south-east Missouri galena ores: Economic Geology, v. 67, p. 409-425.

Fletcher, I. R., and Farquhar, R. M., 1977, Lead isotopes in the Grenville and adjacent Palaeozoic formations: Canadian Journal of Earth Science, v. 14, p. 56-66.

Heyl, A. V., Delevaux, M. H., Zartman, R. E., and Brock, M. R., 1966, Isotopic study of galenas from the upper Mississippi Valley, the Illinois-Kentucky, and some Appalachian Valley mineral districts: Economic Geology, v. 61, p. 933-961.

Sr ISOTOPE RELATIONS AMONG COGENETIC INTRUSIONS AND INCLUSIONS OF THE ASCUTNEY MOUNTAIN COMPLEX, VERMONT

By K. A. Foland and R. P. Lesser, Jr.
Department of Geology
University of Pennsylvania
Philadelphia, Pennsylvania 19104

The subject of this paper is the Sr isotope relations of various intrusives and inclusions as applied to petrogenesis of the Ascutney Mountain Complex. The Mesozoic intrusive rocks of Ascutney Mountain in eastern Vermont were first comprehensively described in a classic paper by Daly (1903). Daly outlined emplacement via magmatic stoping accomplished by "mechanical, piecemeal disruption" at the main contacts and "accompanied by chemical assimilation at greater depths." More detailed mapping subsequently led Chapman and Chapman (1940) to conclude that emplacement of the "comagmatic series", related by fractional crystallization and assimilation, was largely the result of cauldron subsidence. The intrusive sequence at Mount Ascutney is gabbro, diorite, syenite, and granite, which compose three major intrusive units as shown in figure 1.

The Ascutney Mountain Complex is one of the youngest of the group of nonorogenic, Mesozoic intrusions that occur in north-central New England and which have been referred to as the White Mountain Magma Series (White Mountain Plutonic-Volcanic Series of same authors). The complex was emplaced into Paleozoic schists and gneisses; the entire Ascutney sequence was apparently emplaced within less than a few million years. Five separate K-Ar biotite determinations ranged only from 122 to 118 m.y. and averaged 120 m.y. (Foland and Faul, 1977).

One of the most striking features to be noted is the abundance of inclusions, particularly in the main syenite unit. These inclusions are mostly sub-rounded, dark gray to green, porphyritic masses. Daly (1903) called the features "basic segregations" but Chapman and Chapman (1940) recognized them as xenoliths of basic rock, probably "greatly reworked by the magma." The mineralogic and normative compositions of the inclusions lead us to believe that they may be cognate xenoliths of the earlier, more mafic intrusions.

We have examined the main intrusive units and several basic inclusions from the main syenite and find that the Sr isotopes are not consistent with development of the rock suite via fractional crystallization alone. There are significant Sr isotope heterogeneities among different units and even within some intrusive phases. Because of the large variation in Rb/Sr and in Sr, these are best illustrated in figure 2 where the calculated initial $^{87}Sr/^{86}Sr$ ratio is shown as a function of the reciprocal of Sr concentration. Whole-rock samples of the biotite granite are internally consistent, defining a whole-rock isochron of 122 m.y. and $(^{87}Sr/^{86}Sr)_0$ of 0.70425 ± .00010 ($\lambda = 1.42 \times 10^{-11}$ yr^{-1}). While this ratio is the same as that calculated for the most mafic gabbroic rock yet analyzed, the granite contrasts markedly with the syenite and gabbro-diorite. Both the mafic rocks (with Sr concentrations up to about 1000 ppm) and the syenites show considerable variation in initial ratio. The initial ratios (fig. 2) appear to reflect primary isotopic heterogeneities. The Ascutney rocks have ^{18}O contents, which are "normal" for such compositions.

Noting the Sr isotope variations, it is natural to question the role of the basic inclusions, which are so abundant in some areas.

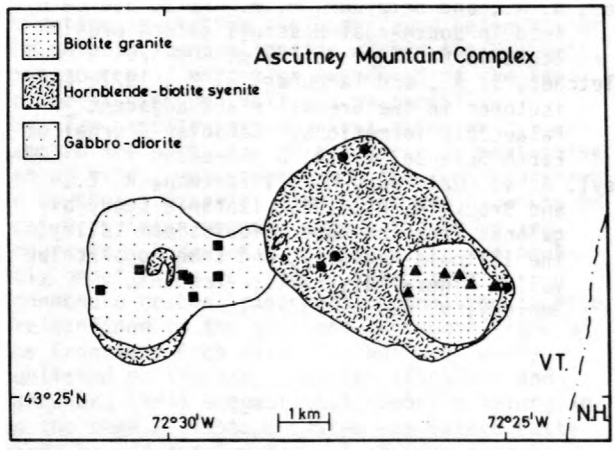

Figure 1.--Simplified geologic map of the Ascutney Mountain Complex modified from Chapman and Chapman, 1940, showing sample localities.

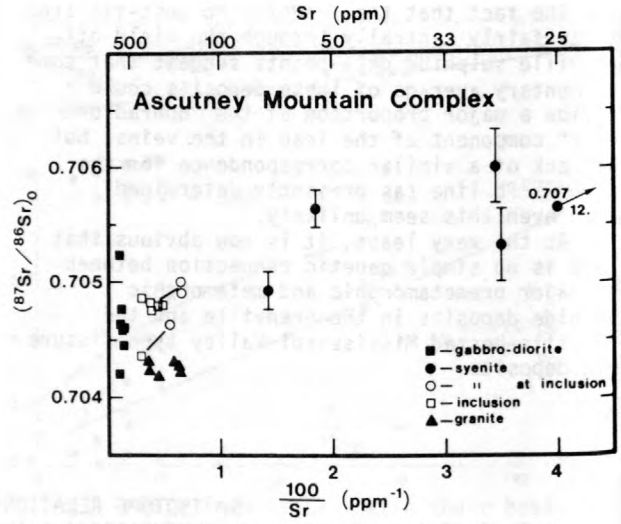

Figure 2.--Calculated $^{87}Sr/^{86}Sr$ initial ratios for whole-rock samples and inclusions as a function of inverse Sr concentration. The initial ratio is calculated using the 122 m.y. whole-rock age given by the granites. Total one-sigma uncertainties in initial ratio are within the symbols except where significantly larger, as noted for high Rb/Sr samples. Two inclusions are shown connected with the immediately adjacent syenite host.

The syenites that were analyzed (fig. 2) were from areas without any observed inclusions and have higher initial ratios. Our analyses of two inclusions suggest that these cannot be caused by assimilation of the most common xenolithic material. In fact, the inclusions have lower $^{87}Sr/^{86}Sr$ ratios, similar to the mafic intrusives. One large inclusion (approximately 11 x 13 x 16 cm) was sectioned in radial fashion and the analyses indicate uniform $(^{87}Sr/^{86}Sr)_0$ ratios across the entire mass at the time of emplacement. However, the syenite immediately adjacent to this inclusion, and a smaller inclusion, give somewhat higher initial ratios indicating that the inclusions were not fully equilibrated with the surrounding magma. The observed $^{87}Sr/^{86}Sr$ relations for the syenites and the inclusions could be explained by mixing, presumably via mechanical and chemical assimilation. On a large scale, such a process would have important influence on the Sr concentrations and isotopic compositions of the evolved rock types.

The large variations in $^{87}Sr/^{86}Sr$ among different units must be explained by either contamination and (or) isotopically heterogeneous primary magma. This further demonstrates that simple models of fractional crystallization cannot adequately describe the evolution of such magmatic complexes.

Chapman, R. W., and Chapman, C. A., 1940, Cauldron subsidence at Ascutney Mountain Vermont: Geological Society of America Bulletin, v. 51, p. 191-212.

Daly, R. A., 1903, Geology of Ascutney Mountain, Vermont: U.S. Geological Survey Bulletin, v. 209, p. 1-122.

Foland, K. A., and Faul, Henry, 1977, Ages of the White Mountain Intrusives--New Hampshire, Vermont, and Maine, USA: American Journal of Science, v. 277, p. 888-904.

K/Ar AGES OF PALEOGENE BASALTS FROM THE VICENZA'S ALPS

By F. Frascari, E. Lipparini, and C. Savelli
CNR, Laboratorio Geologia Marina,
Bologna

Whole-rock samples of basalt flows interbedded in Paleogene sediments from the typical areas of Vicenza's Alps have been dated by the K-Ar method. For basalt grains 1-1/4 mm, argon isotopic composition has been analyzed by isotope dilution with an AEI MS20 metal mass spectrometer. The standard Bern 4M muscovite and G.S. LP-6 biotite, with radiogenic argon contents of 43.0 and 6.28 x 10^{-6} ccSTP g^{-1} respectively, have been used for tracer calibration.

Potassium analyses have been made in duplicate by means of atomic absorption spectrophotometry. K/Ar ages are given with a precision of 3.5 percent (1σ; table 1).

Table 1.--K/Ar data

[M, Marosticano; L, Lessini (fig. 1)]

Sample no. and area	Point of sampling (fig. 2)	K_2O (percent)	$^{40}Arrad$ (scc/g)	$\frac{^{40}Arrad}{^{40}Artotal}$	Radiometric age[1]
Conco 465 - M----	IV	0.79	0.81×10^{-6}	0.276	31.4±1.1
			0.81×10^{-6}	0.339	31.4±1.1
Malo 219 - L----	V	1.13	1.08×10^{-6}	0.500	29.1±1.1
VL 18 - M----	IV	1.32	1.18×10^{-6}	0.329	27.4±1.0
VL 20 - L----	V	1.71	1.41×10^{-6}	0.534	25.3±1.0
VL 24 - L----	V	1.54	1.18×10^{-6}	0.534	23.5±0.9
Conco 463 - M----	III	0.68	0.68×10^{-6}	0.260	30.3±1.1
			0.67×10^{-6}	0.285	29.7±0.9
Conco 464 - M----	III	0.96	0.95×10^{-6}	0.442	30.1±1.1
			0.91×10^{-6}	0.512	29.1±1.1
Conco 467 - M----	III	1.04	1.00×10^{-6}	0.172	30.6±1.1
VL 32 - M----	III	1.34	1.31×10^{-6}	0.764	29.7±1.1
Conco 460 - M----	II	1.11	1.22×10^{-6}	0.235	33.7±1.2
Malo 218 - L----	I	1.21	1.62×10^{-6}	0.656	40.0±1.4
Malo 218bis - L----	I	1.24	1.63×10^{-6}	0.495	39.7±1.4
VL 21 - L----	I	1.57	1.99×10^{-6}	0.564	38.7±1.4
			2.06×10^{-6}	0.573	39.9±1.2

[1]Decay constants: $\lambda_e = 4.963 \times 10^{-10} xa^{-1}$, $\lambda_\beta = 0.581 \times 10^{-10} xa^{-1}$, $^{40}K/K_{tot} = 1.194 \times 10^{-4}$ (weight ratio), $^{40}Ar/^{36}Ar(atm.) = 295.5$ (Steiger and Jaeger, 1977).

[2]Radiogenic argon determinations from Bern laboratory (J. C. Hunziker, oral commun.): Conco 463, 0.66-0.65-0.70 μcc/g; VL21, 2.05-2.07 μcc/g.

The sedimentary rocks have been dated using various typical macroforams (Nummulites, Discocyclina, Asterocyclina, Lepidocyclina, Miogypsina) in correlation with the planktonic foraminiferal zones (Blow, 1969). The ages of the lavas in question are: (1) middle-late Eocene, (2) middle Oligocene, and (3) the interval between middle Oligocene and Aquitanian. The lavas outcrop in the nearby areas of Marosticano and the Eastern Lessini Mountains (fig. 1).

1. Two Eocene lava flows have been sampled at a site located a few kms from the type section of Priabona, at a stratigraphic horizon lying between carbonate sediments of upper Lutetian (Biarritzian) and transgressive sediments of Priabonian Age (fig. 2, sample I). K-Ar ages of 40.0, 39.7, and 38.7 m.y. were obtained for this horizon. The radiogenic argon content of the last sample (38.7 m.y.) has also been determined by the Hunziker of the Bern laboratory (written commun.) to be 39.9 m.y.

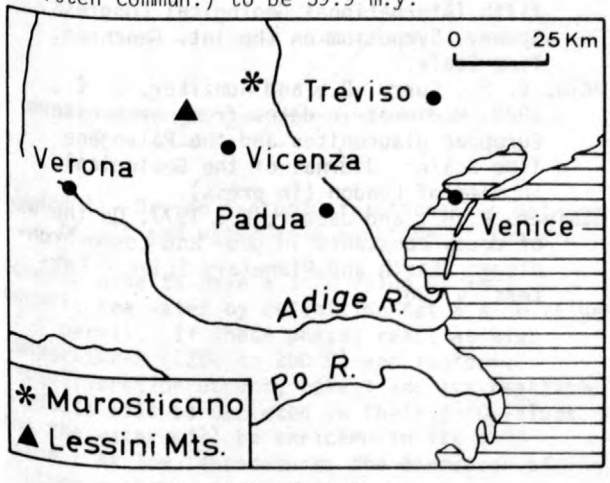

Figure 1.--Location map.

These radiometric ages can be compared with those obtained on glauconite pellets for the Bartonian strata (England, 38.9 and 39.6 m.y.; Odin and others, 1978). The biostratigraphic zones of the two type sections are P15, P16, and P17 for the Priabonian (Cita, M. B., 1969) and P13 pp, P14, and P15 pp for the Bartonian (Odin and others, 1978). These facts indicate that the sampled lavas have about the same age as the lower part of the Bartonian strata, which, on the whole, are older than Priabonian strata. The Priabonian transgression, however, is probably coeval with the more recent levels of Bartonian strata. Other authors have already indicated that the Priabonian Stage is younger than the Bartonian (Hardenbol and Berggren, 1976).

2. Two levels of middle Oligocene lavas outcrop in Marosticano (Frascari, 1972; Frascari and Bassani, 1973). The older level, dated as the early-middle Oligocene boundary, is 33.7 m.y. old (K-Ar age of one sample only);

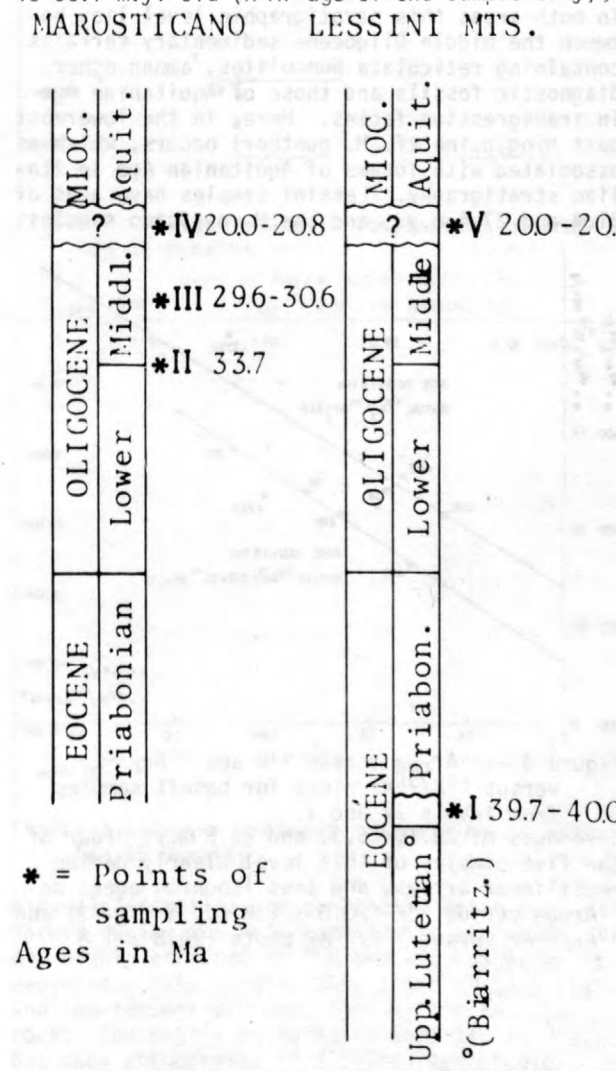

Figure 2.--Stratigraphic columns for the Marosticano and Lessini Mountain areas showing position of dated samples.

the other, belonging to the middle Oligocene s.s., is about 30 m.y. old. (K-Ar ages of four samples are 29.7, 30.6, 29.6, and 30.3 m.y.; fig. 2, samples II and III). The radiogenic argon content of the last sample (30.3 m.y.) has also been determined in the Bern laboratory (Hunziker, written commun.; 29.7 m.y.). The four flows examined from level III yield concordant ages. The range of potassium contents in these samples (0.69 - 1.34 percent K_2O; table 1) precludes loss or gain of radiogenic argon in measurable amounts. Correct atmospheric argon determinations are indicated by concordant ages obtained on samples with widely scattered radiogenic to total argon ratios (0.260 - 0.764, table 1). The radiometric age of the level III lava should be the best defined according to presented analytical data.

3. Lavas from the uppermost levels have been sampled in Marosticano as well as in the Lessini Mountains (fig. 2, samples IV and V). In both areas this stratigraphic level lies between the middle Oligocene sedimentary terrains containing reticulata Nummulites, among other diagnostic fossils and those of Aquitanian Age in transgressive facies. Here, in the lowermost part Miogypsina cf. M. guntheri occurs, which is associated with forams of Aquitanian Age in Italian stratigraphy. Lessini samples have ages of 31.4 and 27.4 m.y., and the Marosticano samples

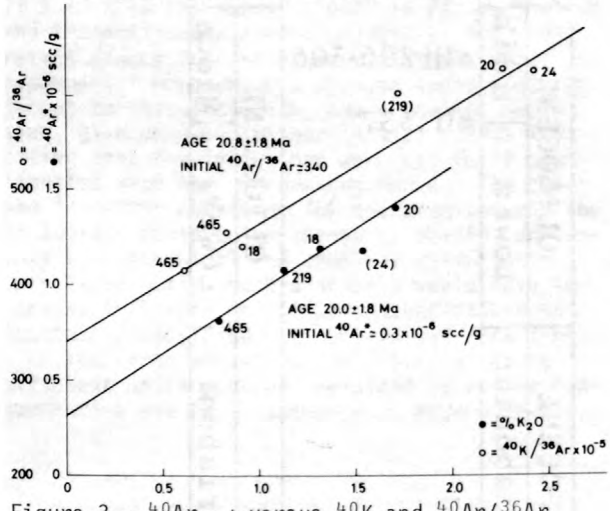

Figure 3.--$^{40}Ar_{rad}$ versus ^{40}K and $^{40}Ar/^{36}Ar$ versus $^{40}K/^{36}Ar$ plots for basalt samples from levels IV and V.

have ages of 29.1, 25.3, and 23.5 m.y. Four of the five samples of this level clearly define rectilinear arrays, and thus isochron ages, on $^{40}Ar_{rad}$ versus ^{40}K (20.0 ± 1.8 m.y.; fig. 3) and $^{40}Ar/^{36}Ar$ versus $^{40}K/^{36}Ar$ plots (20.8 ± 1.8 m.y.). The Y intercept in the first plot indicates ca. 0.3 x 10^{-6} ccSTP gm^{-1} of excess radiogenic argon in the samples in question and in the second an initial or "atmospheric" 40/36 argon ratio of ca. 340 instead of the usual 296 value.

The range of K_2O percentages in the examined basalts is fairly wide (0.79 - 1.71), but smaller than the range of some mineral separates. Different contents of atmospheric argon ranging from 1.03 to 2.12 x 10^{-6} ccSTP gm^{-1} (Samples 24 and 465, respectively) are responsible for the greater length of the upper line as compared to the lower line (fig. 3). The age of 20 to 20.8 m.y. for the lavas from levels IV and V indicates an early Miocene rather than Oligocene age as formerly assumed. The Miocene age of the overlying transgression (Frascari and Bassani, 1973) would thus be confirmed by radiometric evidence. This transgression is widespread in the area in question as well as in various areas of Italy.

Other K-Ar studies are foreseen aimed at further defining the Paleogene chronostratigraphy in northeastern Italy.

Blow, W. H., 1969, Late middle Eocene to recent planktonic foraminiferal biostratigraphy: Proceedings of the First International Conference on Plank. Microfoss. Geneve 1967, 1, p. 199-421.

Cita, M. B., 1969, Le Paléocene et l'Eocène de l'Italie du nord. Colloque sur l'Eocène, Paris 1968: Mém. B.R.G.M., 69, p. 417-430.

Frascari, F., 1972, Evolution des grands forminifères Paléogènes; contribution statistique: Twenty-fourth International Geological Congress, 1972, Section 7, p. 149-154.

Frascari, F., and Bassani, P., 1973, Ricerche geologiche nei dintorni di Bassano del Grappa (Vicenza): Mem. Mus. Trid. Sc. Nat., v. 19, p. 65-112.

Hardenbol, J., and Berggren, W. A., 1976, A new Paleogene numerical time scale: Twenty-fifth International Geological Congress, Sydney, Symposium on the Int. Geochron. Time Scale.

Odin, G. S., Curry, D., and Hunziker, J. C., 1978, Radiometric dates from northwestern European glauconites and the Paleogene Time Scale: Journal of the Geological Society of London (in press).

Steiger, R. H., and Jaeger, E., 1977, On the use of decay constants in geo- and cosmochronology: Earth and Planetary Science Letters, v. 36.

STABLE ISOTOPE EXCHANGE BETWEEN OCEANIC CRUST AND OCEAN WATER

By Hans Friedrichsen and Stephan Hoernes
Tübingen, West Germany

$\delta^{18}O$ analyses of 380 samples and δD analyses of 127 samples from oceanic crust cores of different ages show that almost all rocks recovered during the Deep Sea Drilling Project (DSDP) cruises of Glomar Challenger have interacted with sea water and have exchanged isotopes, trace elements, and major elements. The oceanic basalts investigated in this study were drilled during the DSDP cruises of leg 37, 45, 46, 51, 52, and 53 into the Atlantic Ocean during 1974 to 1976. The basalts are of different ages; leg 37 was drilled near the Mid-Atlantic Ridge into basalts, peridotites, and gabbros with an age of 0 to 3 m.y.; leg 45 and leg 46 are situated east and west of the Mid-Atlantic Ridge where the basalts had an age of about 10 m.y. The oldest rocks were recovered from 100 m.y. old oceanic crust during leg 51, 52, and 53 south of the Bermuda Rise. The purpose of this investigation was to get a detailed understanding of the exchange reactions between the basement and the ocean water and to estimate how the rates of exchange vary with depth and age of the basalts.

Oceanic basalts and sea water are in disequilibrium. Any reaction towards equilibrium will be accompanied by a transfer of either isotopes or solutions. The extent of this exchange can be assessed by measuring the O-isotopic composition of the basalts which reacted with the water (fig. 1). Unaltered

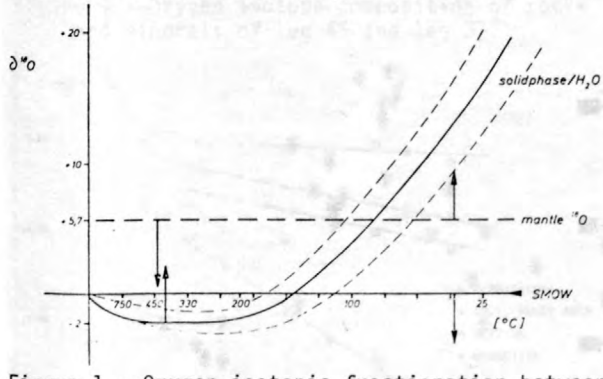

Figure 1.--Oxygen isotopic fractionation between basalt and water as a function of temperature.

oceanic basalts have a $\delta^{18}O$ value of +5.7 permil; sea water by definition has a $\delta^{18}O$ value of 0 permil. If these phases react at high temperatures (1200 to 200°C) and isotopic reequilibration occurs, basalt and its reaction products will be depleted in their $\delta^{18}O$ values and the water will be enriched in its $\delta^{18}O$ value. At low temperatures the direction of isotope exchange is opposite. Low-temperature

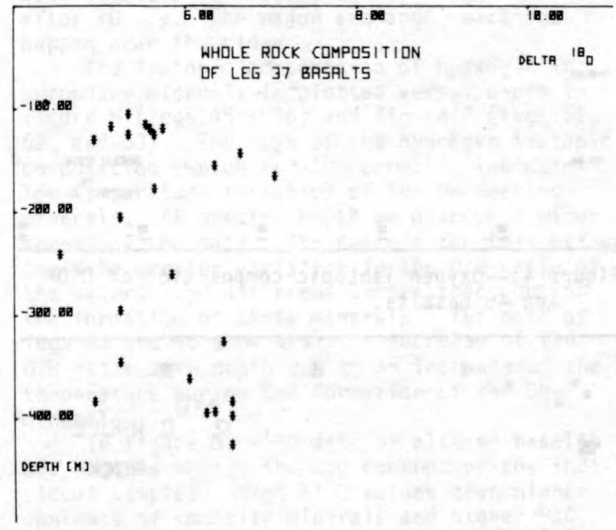

Figure 2.--Oxygen isotopic composition of DSDP leg 37 basalts.

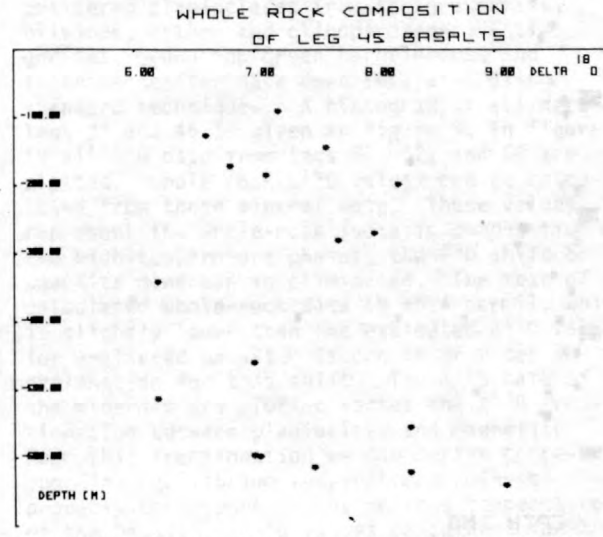

Figure 3.--Oxygen isotopic composition of DSDP leg 45 basalts.

minerals (smectite and zeolites), which are formed during the interaction with sea water, are highly enriched in ^{18}O and the sea water is depleted. Many samples show signs of both high- and low-temperature reactions within the same rock. The matrix is normally enriched in ^{18}O, but many phenocrysts of olivines and plagioclases are depleted in their oxygen isotopic composition. Both whole rock samples and separated minerals were analyzed.

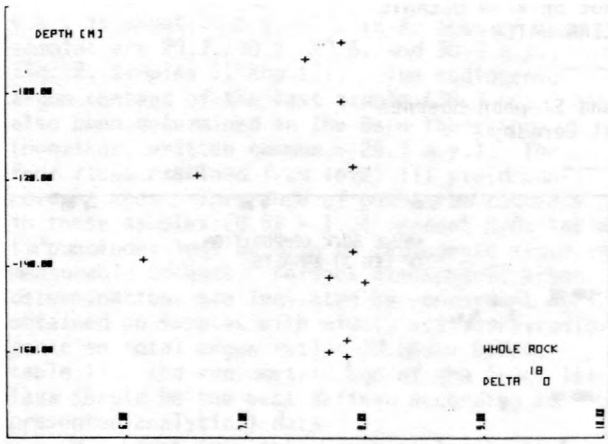

Figure 4.--Oxygen isotopic composition of DSDP leg 46 basalts.

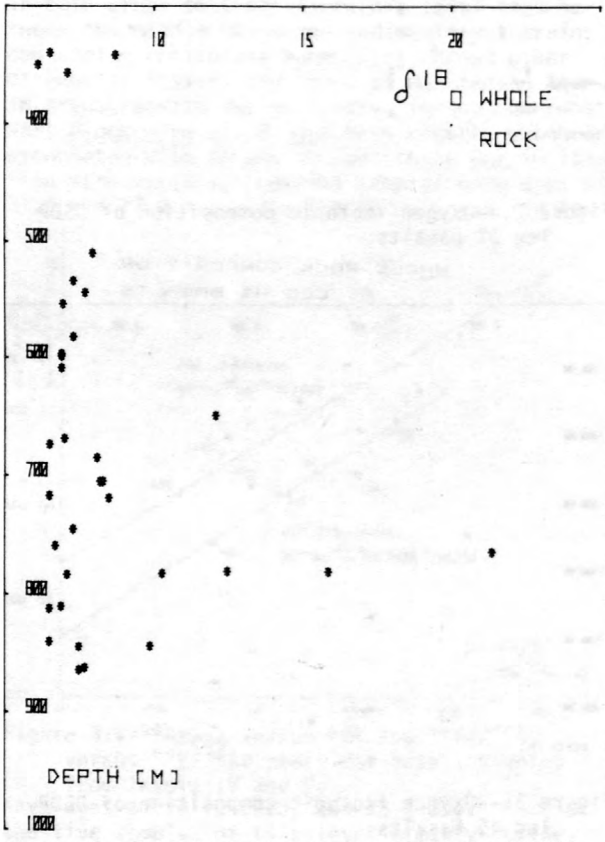

Figure 5.--Oxygen isotopic composition of DSDP legs 51 and 52 basalts.

Whole-rock data: Figures 2 to 5 show the whole-rock $\delta^{18}O$ values of leg 37-332b, leg 45, leg 46, and legs 51 and 52. Very few samples have retained the original $\delta^{18}O$ value of the unaltered basalt. More than 80 percent of all basalts have been enriched in their $\delta^{18}O$ value due to pronounced low-temperature alteration. The mean of all $\delta^{18}O$ data is +7.7 permil, which means an enrichment of +2 permil for the upper

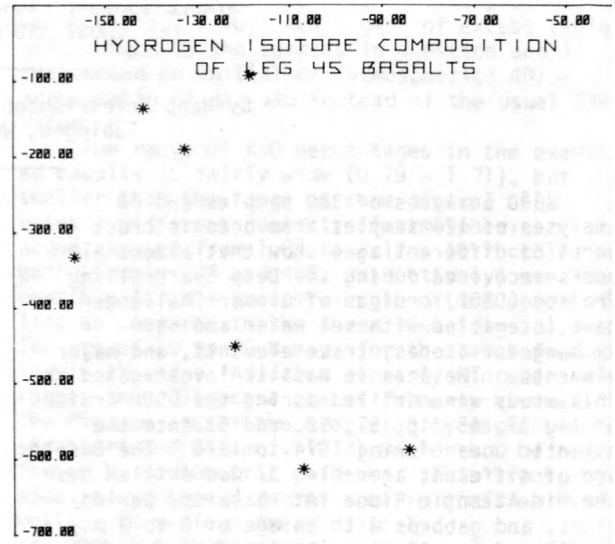

Figure 6.--Hydrogen isotopic composition of DSDP legs 45 and 46 basalts.

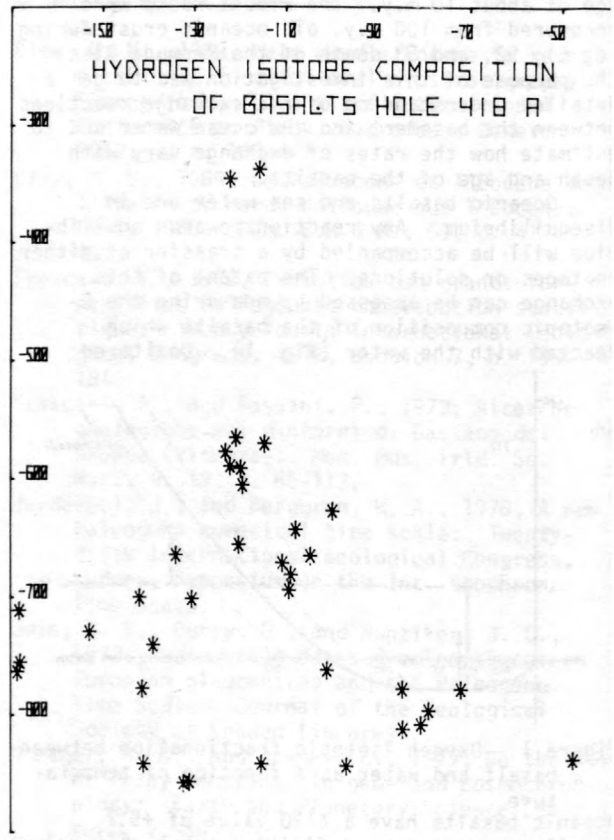

Figure 7.--Hydrogen isotopic composition of DSDP legs 51, 52, and 53 basalts.

600 m of the basement. High $^{18}O/^{16}O$ ratios have been observed at the margins of two different flows or different lithologic units. High values of up to +22 permil mean that more than 70 percent of the oxygen in these basalts is ocean water oxygen.

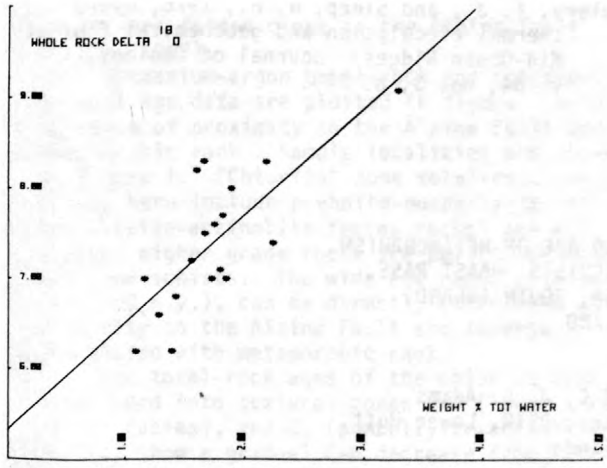

Figure 8.--Oxygen isotopic composition of some altered basalts as a function of their H_2O content.

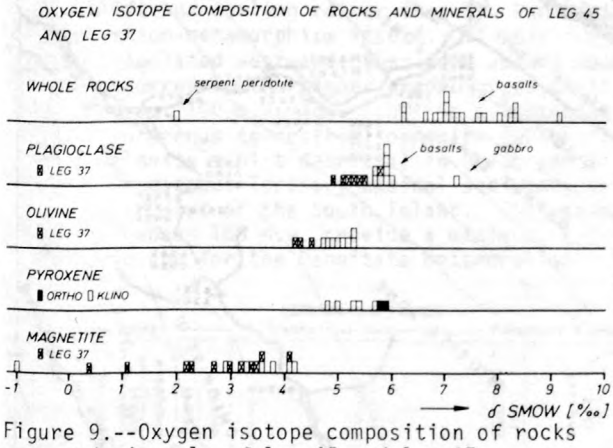

Figure 9.--Oxygen isotope composition of rocks and minerals of leg 45 and leg 37.

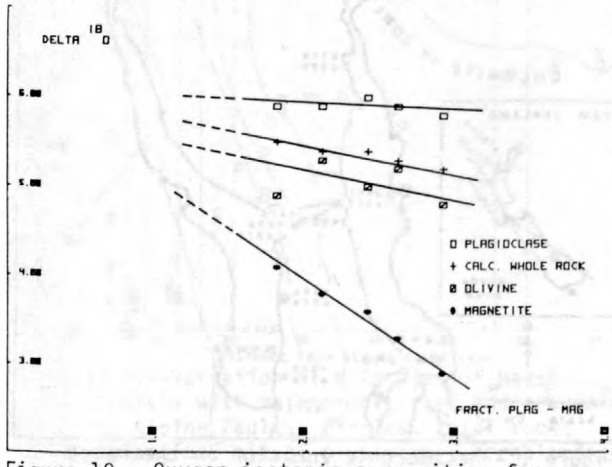

Figure 10.--Oxygen isotopic composition for minerals from DSDP legs 51, 52, and 53 as a function of the $\delta^{18}O$ fractionation between plagioclase and magnetite.

If we compare the average ^{18}O shift of legs 45 and 46, and legs 51, 52, and 53, we have to conclude that there is no significant difference between 10 m.y. old rocks and 100 m.y. old rocks as far as the secondary (low-temperature) alteration is concerned. Wolery and Sleep (1976) have shown from heat-flow data that sea water circulation ceased in the oceanic crust after 10 m.y. The major exchange reactions happen near the ridge.

The isotopic composition of hydrogen in secondary minerals is plotted versus depth in figure 6 (legs 45 + 46) and figure 7 (legs 51, 52, and 53). The mean of the hydrogen isotopic composition (which is -100 permil), indicates low-temperature formation of the OH-bearing minerals. At greater depth we observe a wider spread of the data. The reasons for this effect could be greater variation in the D/H-ratio of the waters, and different temperatures during the formation of these minerals. The data of legs 45 and 46 show a slight increase of the D/H-ratio with depth due to an increase of the temperature during the formation of the OH-minerals.

In figure 8, $\delta^{18}O$ data of altered basalts are plotted versus the H_2O content of the individual samples. High $\delta^{18}O$ values mean higher contents of smectite minerals and higher H_2O content of the sample.

Mineral data: Plagioclase phenocrysts, unaltered plagioclases from the groundmass, olivines, ortho- and clinopyroxenes, antigorites, brown and green hornblendes, and titanomagnetites have been separated using standard techniques. A histogram of all data of legs 37 and 45 is given in figure 9; in figure 10 all ^{18}O data from legs 51, 52, and 53 are plotted. Whole-rock $\delta^{18}O$ values can be calculated from these mineral data. These values represent the whole-rock isotopic composition of the high-temperature phases; the ^{18}O shift by smectite minerals is eliminated. The mean of calculated whole-rock data is +5.4 permil, which is slightly lower than the estimated $\delta^{18}O$ value for unaltered basalt. Figure 10 provides an explanation for this shift. The $\delta^{18}O$ data of the minerals are plotted versus the $\delta^{18}O$ fractionation between plagioclase and magnetite. From this fractionation we can derive corresponding equilibrium temperatures. These probably correspond to the solidus temperature of the basalts. $\delta^{18}O$ values calculated for the whole-rock samples are lower for those that have the lowest formation temperatures. A shift of 0.4 permil means that these samples have interacted with 2.5 weight percent of water. We conclude that sea water has interacted with the basaltic magma and the solidus temperature has been reduced due to the sea water content.

Gabbro slabs, which were cored during the leg 37 cruise and might be part of the layer III, show pronounced depletion of the $\delta^{18}O$

values of the primary minerals. $\delta^{18}O$ (plagioclase-magnetite) and $\delta^{18}O$ (pyroxene-magnetite) fractionations yield solidus temperatures near 840°C.

Wolery, T. J., and Sleep, N. H., 1976, Hydrothermal circulation and geochemical flux at Mid-Ocean Ridges: Journal of Geology, v. 84, no. 3, p. 249.

EXCESS RADIOGENIC ARGON AND AGE OF METAMORPHISM AND UPLIFT IN THE HAAST SCHISTS, HAAST PASS, LAKES WANAKA AND HAWEA, SOUTH ISLAND, NEW ZEALAND

By J. E. Gabites and C. J. D. Adams
Institute of Nuclear Sciences, DSIR, Lower Hutt, New Zealand

Permian-Jurassic geosynclinal sediments, which form a large part of the South Island of New Zealand, were deformed and regionally metamorphosed during the Jurassic-Cretaceous Rangitata orogeny (Fleming, 1970). Within this orogenic belt a curved, medium-grade metamorphic Haast Schist terrane is flanked by low-grade metasediments, the Hokinui and Torlesse facies to the south and northeast, respectively (Suggate, 1961). The Haast Schists are subdivided into the Otago Schists (greenschist) in the E-W sector and Alpine Schists (greenschist-amphibolite) in the N-S sector, where they lie parallel to the Alpine Fault (fig. 1, inset). This fault is a major transcurrent break with about 480 km right lateral and 9 - 15 km vertical displacement (Wellman, 1952; Mason, 1962; Suggate, 1963) and forms the boundary between the Indian and Pacific plates. The present disposition of the Haast Schists in the Southern Alps is a consequence of the extremely rapid uplift at the Alpine Fault during the Miocene-Holocene Kaikoura orogeny. Several geochronological studies of the Haast Schists (Hurley and others, 1962; Harper and Landis, 1967; Sheppard and others, 1975) have attempted to separate Rangitata and Kaikoura orogenic phases of metamorphism and/or deformation and, hence, allow calculation of uplift and cooling rates in the region. This present study is part of a detailed survey of the Alpine Schist sector to investigate the K-Ar and Rb-Sr isotopic systematics in a very young (Pliocene) high-grade metamorphic belt (Adams and Gabites, unpublished data).

The area chosen lies adjacent to the Alpine Fault and extends across a steep metamorphic gradient eastward along the Haast River to the Haast Pass and then south to Lakes Wanaka and Hawea (fig. 1). The rocks comprise a fairly uniform succession of quartzo-feldspathic and pelitic schists, slates, and occasional basic greenschist horizons. The metamorphic gradient extends from oligoclase (= staurolite) zone amphibolite facies in the west to prehnite-pumpellyite facies metagreywackes in the southeast (fig. 1). The area is complexly deformed and the metamorphic isograds, in parti-

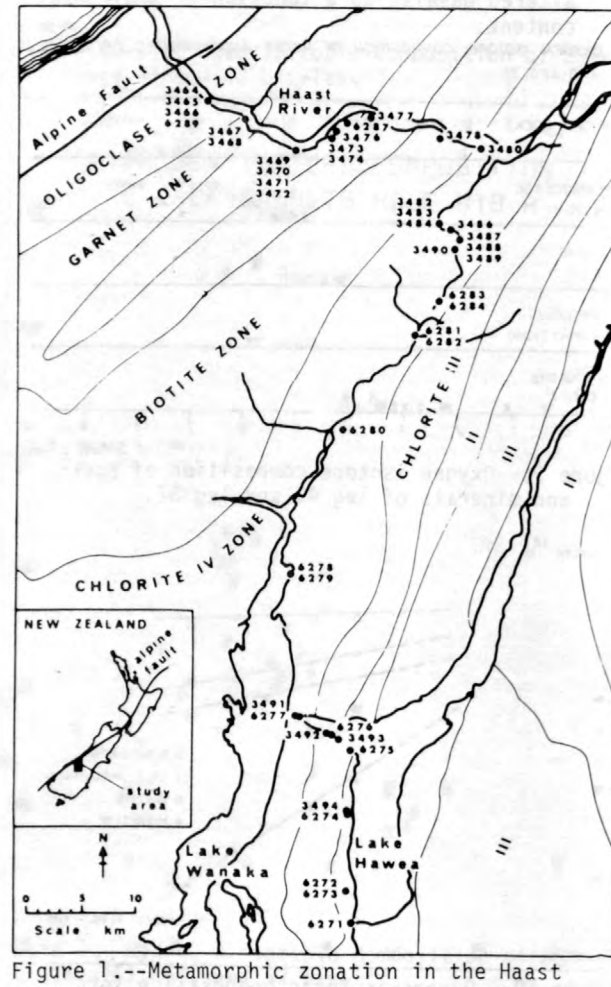

Figure 1.--Metamorphic zonation in the Haast Schists adjacent to the Alpine Fault. Sample localities shown.

cular, are folded close to the Alpine Fault (Mason, 1962).

Potassium-argon total-rock and component-mineral age data are plotted in figure 2 as a function of proximity to the Alpine Fault and metamorphic rank. Sample localities are shown in figure 1. "Chlorite" zone total-rock samples (which here include prehnite-pumpellyite and pumpellyite-actinolite facies rocks) are all slates; higher grade rocks are pelitic schists and greenschists. The wide age range obtained (8 - 160 m.y.), can be directly correlated with proximity to the Alpine Fault and inversely correlated with metamorphic rank.

The total-rock ages of the chlorite zone, subdivided into textural zones 3-4 (lower greenschist facies), and 2, (pumpellyite-actinolite facies) show a gradual E-W decrease from 160 - 120 m.y. (Late Jurassic-Early Cretaceous) until 25 km of the Alpine Fault. In metamorphic terranes of this type, these ages reflect the time of uplift and cooling rather than the Rangitata deformation-metamorphism itself. If this trend is extrapolated westward, then some uplift must have occurred in the higher grade (greenschist) zones about 100 m.y. ago. This is synchronous with Cretaceous terrestrial deposits (which contain chlorite schist detritus) in Otago and Upper Cretaceous-Tertiary basinal sediments on the West Coast of the South Island. The maximum ages of about 160 m.y. provide a minimum, mid-Jurassic age for the Rangitata metamorphism itself.

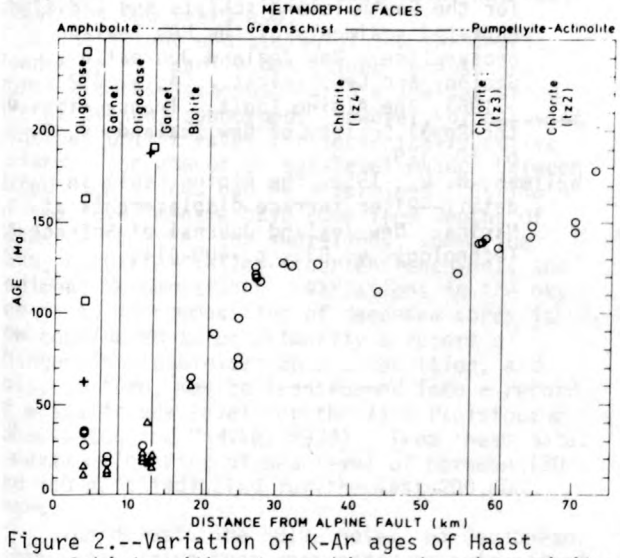

Figure 2.--Variation of K-Ar ages of Haast Schists with metamorphic rank and proximity to Alpine Fault. Circles, total rock; triangles, micas; plus signs, hornblende; squares, plagioclase; tz, textural zone.

Samples within 25 km of the Alpine Fault from chlorite 4, biotite, garnet, and oligoclase zones show a steeper E-W decreasing age trend from about 100 to 8 m.y. (fig. 2). In this case, an "uplift/cooling" interpretation, from the mid-Cretaceous to the Pliocene, does not agree with the stratigraphic history (Fleming, 1962). The age trend seems unaffected by the folding of the isograds and, thus, the recorded isotopic event must postdate isograd folding. In addition, the hornblende and plagioclase ages are highly discordant (60 - 330 m.y.), and do not follow the total-rock and mica age patterns, suggesting the presence of excess argon. To explore this possibility the K-Ar data are shown graphically (in a manner analogous to the Rb-Sr isochron method), subdivided by mineral type and metamorphic rank (fig. 3). It can be seen that,

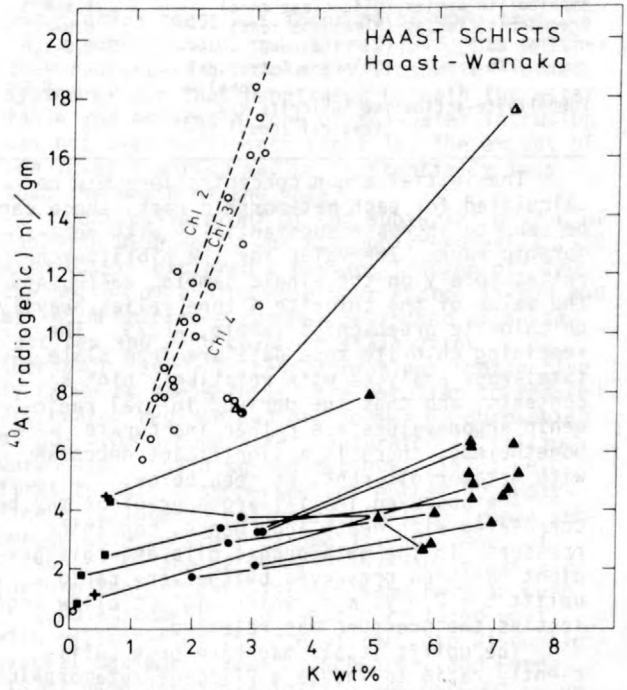

Figure 3.--K-Ar isochron diagram of Haast Schists. Circles, total rock; triangles, micas; plus signs, hornblende; squares, plagioclase. Solid symbols, garnet-oligoclase zones; half-solid symbols, biotite zone; open symbols, chlorite zone (textural zones 2-4). Tielines link coexisting mineral/total-rock data.

with one exception, the coexisting total-rock and component-mineral data (joined by tielines in fig. 3) form consistent isochrons with slopes corresponding to ages of 5 ± 2 m.y. (Miocene and Pliocene). These metamorphic rocks have thus remained closed systems with respect to K and Ar after an isotopic event in the Pliocene when radiogenic argon was redistributed between mineral phases under high pressure conditions, and conventional, complete argon degassing was inhibited. Because the total-rock points do not lie on separate isochrons themselves, there has been no closed-system behaviour at this level. One sample, R3465, which is closest to the Alpine Fault, provides the exception to the above pattern because the plagioclase-total-rock-muscovite-biotite isochron yields a nega-

tive slope. Judging by the age data of its neighbors, the anomaly arises from the feldspar component, which might contain a minor contaminant that is particularly rich in excess argon.

Table 1.--Initial radiogenic argon concentrations in Haast Schists

Metamorphic rank	(Initial ^{40}Ar) (radiogenic) nl/g
Amphibolite facies (Oligoclase zone) ---	1.5-4.0
Greenschist facies (Almandine zone) ----	0.8-2.0
Do (Biotite zone) ------	0.5-1.0
Do (Chlorite 4 textural zone) --	0 -0.5
Pumpellyite-actinolite (Chlorite 2/3 textural zones) ----	0

The initial argon concentrations may be calculated for each metamorphic rank; these can be seen to increase substantially with metamorphic rank. The value for the biotite zone relies solely on the single sample, R3478, and the value of the chlorite 4 zone relies heavily on chlorite greenschist sample, R6279. The remaining chlorite zone data are from slate total-rock analyses with relatively high K contents, and thus the derived initial radiogenic argon values are rather inaccurate. Nonetheless, there is a significant decrease with metamorphic rank, as seen below.

The observed initial-argon gradient may be correlated with depth and, hence, confining pressure, in the metamorphic pile and this gradient has been preserved by the very rapid uplift 5 ± 2 m.y. ago, which did not allow argon loss as the pressure was released.

The uplift itself may have been sufficiently rapid to induce a Pliocene metamorphic effect by frictional heating sufficient to outgas the high-grade rocks adjacent to the fault at that time (Sheppard and others, 1975) or they may have been held at depth after the Jurassic metamorphism, above the argon diffusion threshold temperature, until the Pliocene uplift phase.

Fleming, C. A., 1962, New Zealand biogeography--a palaeontologist's approach: Tuatara, v. 10, p. 53-108.

_____1970, The Mesozoic of New Zealand--chapters in the history of the Circum-Pacific Mobile Belt: Quarterly Journal of the Geological Society of London, v. 125, p. 125-170.

Harper, C. T., and Landis, C. A., 1967, K-Ar ages from regionally metamorphosed rocks, South Island, New Zealand: Earth and Planetary Science Letters, v. 2, p. 419-429.

Hurley, P. M., Hughes, H., Pinson, W. H., Jr., and Fairbairn, H. W., 1962, Radiogenic argon and strontium diffusion parameters in biotite at low temperatures obtained from Alpine Fault uplift in New Zealand: Geochimica Cosmochimica Acta, v. 26, p. 67-80.

Mason, B., 1962, Metamorphism in the Southern Alps of New Zealand: Bulletin of the American Museum of Natural History, v. 123, p. 211-247.

Sheppard, D. S., Adams, C. J., and Bird, G. W., 1975, Age of metamorphism and uplift in the Alpine Schist Belt, New Zealand: Geological Society of America Bulletin, v. 86, p. 1147-1153.

Suggate, R. P., 1961, Rock stratigraphic names for the South Island schists and undifferentiated sediments of the New Zealand geosyncline: New Zealand Journal of Geology and Geophysics, v. 4, p. 392.

_____1963, The Alpine Fault: Transactions of the Royal Society of New Zealand, v. 2, p. 105-129.

Wellman, H. W., 1952, The Alpine Fault in detail--River terrace displacements at Mariua: New Zealand Journal of Science and Technology, v. B33, p. 409-414.

URANIUM SERIES DATING OF SUBMERGED SPELEOTHEM; EVIDENCE OF ILLINOIAN LOW SEA STAND

By M. Gascoyne and H. P. Schwarcz
Department of Geology
McMaster University
Hamilton, Ontario, Canada L8S 4M1

Introduction: Previous work on uranium-series dating of marine carbonates has concentrated mainly on coral-reef terraces. The association has been drawn between these features and high sea stands, which indicate past warm climatic periods. For these deposits to be found above mean sea level today indicates either platform emergence due to tectonic activity or higher sea level sometime in the past. On tectonically active islands, such as Barbados (Mesolella and others, 1969) and New Guinea (Bloom and others, 1974), an excellent record of glacio-eustatic fluctuations is preserved in the form of tiered coral-reef terraces, the oldest generally being at the highest elevation. Islands known to be tectonically stable or slowly subsiding, such as Oahu, Hawaii (Ku and others, 1974), the Bahamas and the Florida Keys (Broecker and Thurber, 1965), only show deposits 5 to 10 m above present sea level, and are associated with the last interglacial maximum, about 125,000 years ago.

The extent and timing of low sea levels cannot be as readily determined because any coral growths associated with a low sea stand are at present submerged. However, by assuming constant uplift rates for tectonically-active islands, the amount of sea-level change between dated high stands can be determined. Estimates of sea level minima have come from depths of submerged beaches and shorelines, submarine fans, estuarine valley-floor entrenchment, and sediment accumulations. Variations in the oxygen isotopic composition of deep-sea cores is now considered to be primarily a record of changes in oceanic isotopic composition, and this, in turn, may be transformed into a record of eustatic sea level for the late Pleistocene (Shackleton and Opdyke, 1973). From these data, a maximum lowering of sea level of between 120 and 150 m is indicated for the last 200,000 years.

Blue Holes: The "Blue Holes" of Caribbean islands have also been recognized as evidence of sea-level lowering because they are comparable to cave and pothole systems found in continental karst regions today. The Blue Holes were probably formed by subaerial weathering processes during glacial periods when sea level fell due to ice accumulation on the continents. They were subsequently inundated by sea water when the ice melted. Recently, a Blue Hole 40 km off the Florida coast was found to be more than 145 m deep (Kohout and others, 1975) but whether this represents a completely freshwater-formed system or one that penetrated beneath the water table and entered a zone of sea-water intrusion has not been determined (that is, the amount of sea-level lowering may be substantially less than the depth of the hole).

Conclusive proof of the subaerial origin of Bahamian Blue Holes was not published until 1970 when divers explored a passage leading off from the bottom of a Blue Hole near Andros Island and at -45 m entered a chamber festooned with stalactites and long columnar stalagmites (Benjamin, 1970). These formations (collectively known as speleothems) are peculiar to vadose freshwater regimes and are formed by outgassing of CO_2 from ground waters saturated in calcium carbonate. Spalding and Matthews (1972) were first to date a submerged speleothem by analyzing a stalagmite collected at -12 m from a submerged cave on Grand Bahama Island. Ages of 21,900 (^{14}C) and 22,000 ($^{230}Th/^{234}U$) years B.P. (before the present) for the same portion were in good agreement, and these correlated well with estimates of the age of the late Wisconsin glacial maximum. Harmon, Schwarcz, and Ford (1978) have dated six in-situ speleothems recovered from depths of -11 m to -5.7 m in Crystal Cave, Bermuda. The results suggest periods of emergence of 195,000 to 150,000, 120,000 to 100,000, and 40,000 to <10,000 years B.P.

Previous work on submerged speleothem deposits is limited to samples recovered from a maximum of 12 m below modern sea level. This depth represents less than 10 percent of maximum estimated sea-level lowering during the late Pleistocene and, therefore, may not correspond to maximum glacial periods. This study presents results of dating speleothems recovered from much greater depths in a Blue Hole near Andros Island by Dr. G. J. Benjamin. Three samples of two in-situ stalagmite columns at -45 m have been dated by the $^{230}Th/^{234}U$ method.

Sample Description: The stalagmite sections measure approximately 20 cm long by 12 cm in diameter. Each contains a central core of original calcite varying from 0 to 8 cm thick, surrounded by an outer aragonitic matrix of cemented shells and a number of encrusting and boring organisms including serpulid and eunicid polychaetes, bryozoa, and siliceous sponges

Table 1.--Results of dating six samples of central calcite core and one sample of outer crust of three Bahama Blue Holes speleothems

Sample No.	Description	U (ppm)	$\frac{^{234}U}{^{238}U}$	$\left[\frac{^{234}U}{^{238}U}\right]_o$ [2]	$\frac{^{230}Th}{^{232}Th}$	Age (X 1000) yrs. B.P., ±1σ error
BH-M	Central portion of 20-cm long stalagmite.	0.26	0.943	0.910	49	$161.6^{23.2}_{19.0}$
BH-L	Lower portion of same.	0.35	0.987	0.981	54	$127.8^{9.2}_{8.5}$
76015-1	Base of upper portion of stalagmite column.	0.29	0.993	0.990	155	$123.1^{9.5}_{8.7}$
76015-2	Replicate split of 76015-1.	0.28	1.016	1.023	61	$118.5^{9.7}_{8.9}$
76015-3	Top of upper portion of stalagmite column.	0.32	1.019	1.026	26	$104.1^{10.6}_{9.7}$
76016-3	Base of lower portion (approx. 2 m below top) of stalagmite column.	0.28	1.019	1.025	>1000	$101.1^{7.7}_{7.2}$
76015-7	Sample of outer aragonitic deposits.	1.30	1.143	1.148	>1000	11.1±1.1 [1]

[1]5 percent Th yield.

[2]Initial value of ratio.

(Dr. M. J. Risk, oral comm.). The inner calcite core is preserved as a single homoaxial crystalline mass, but is contaminated by sponge and polychaete borings.

Results: Samples of the calcite core were chipped out by pneumatic drill and analyzed according to the procedure developed by Thompson (1973), and modified by Gascoyne (1977). Seven analyses of the three speleothem samples showed ages ranging between 162,000 ± 21,000 and 101,000 ± 8,000 (table 1). The lack of stratigraphic ordering of ages for these samples is thought to be due to incorporation of minor amounts of aragonitic deposits present as worm tubes that pass through the calcite. In support of this, a portion of the outer crust, sample 76015-7, was dated and found to be much younger than the core. Subsequently, an experiment was set up to leach a sample of crushed calcite core with dilute acid, the softer aragonitic deposits tending to be dissolved in the earlier fractions. Each fraction was isotopically spiked and dated. Results are shown in table 2. The age obtained for the final "cleanest" fraction (157,000 ± 11,000) is in good agreement with the oldest date from earlier analyses (162,000 ± 20,000).

Further work is continuing in an attempt to reproduce these results and also to use trace elements (Mg, Sr) as indicators of purity of the dated calcite core.

Table 2.--Results of dating portions of a successively leached sample of crushed calcite core of a Bahama Blue Holes speleothem

Sample No.	Description	U (ppm)	$\frac{^{234}U}{^{238}U}$	$\left[\frac{^{234}U}{^{238}U}\right]$	$\frac{^{230}Th}{^{232}Th}$	Age (X 1000) yrs. B.P., ±1σ error
76016-5A	First fraction-------	0.17 [1]	0.978	0.977	6	15.0±2.0
76016-5B	Second fraction------	0.20	0.961	0.958	13	31.9±2.6
76016-5C	Final fraction-------	0.36	1.023	1.035	49	$156.5^{11.5}_{10.4}$

[1]Uranium concentrations are only approximate (±50 percent) as sample was not re-weighed between dissolutions.

Conclusion: These preliminary results suggest that eustatic sea level was at least 45 m below modern sea level approximately 160,000 years ago. This correlates well with stage 6 of the $\delta^{18}O$ curve from core V28-238 (Shackleton and Opdyke, 1973) and is consistent with a maximum glacial condition having occurred about 155,000 years ago.

Benjamin, G. J., 1970, Diving into the Blue Holes of the Bahamas: National Geographic, v. 138, p. 347-363.

Bloom, A. L., Broecker, W. S., Chappell, J. M. A., Matthews, R. K., and Mesolella, K. J., 1974, Quaternary sea level fluctuations on a tectonic coast; new $^{230}Th/^{234}U$ dates from the Huon Peninsula, New Guinea: Quaternary Research, v. 4, p. 185-205.

Broecker, W. S., and Thurber, D. L., 1965, Uranium series dating of corals and oolites from Bahamian and Florida Key limestones: Science, v. 149, p. 58-60.

Gascoyne, M., 1977, Uranium series dating of speleothem; an investigation of technique, data processing and precision: Hamilton, Ontario, McMaster University, Department of Geology, Tech. Memo. 77-4.

Harmon, R. S., Schwarcz, H. P., and Ford, D. C., 1978, Late Pleistocene sea level history of Bermuda: Quaternary Research, v. 9, p. 205-218.

Kohout, F. A., Leve, G. W., and Smith, F. T., 1975, Red Snapper Sink and groundwater flow, offshore northeastern Florida: International Congress of the International Association of Hydrogeologists, 12th, Huntsville, Alabama.

Ku, T. L., Kimmel, M. A., Easton, W. H., and O'Neill, T. J., 1974, Eustatic sea level 120,000 years ago on Oahu, Hawaii: Science, v. 183, p. 959-962.

Mesolella, K. J., Matthews, R. K., Broecker, W. S., and Thurber, D. L., 1969, The astronomical theory of climate change: Barbados data: Journal of Geology, v. 77, p. 250-274.

Shackleton, N. J., and Opdyke, N. D., 1973, Oxygen isotope and palaeomagnetic stratigraphy of equatorial Pacific core V28-238; oxygen isotope temperatures and ice volumes on a 10^5 year and 10^6 year scale: Quaternary Research, v. 3, p. 39-55.

Spalding, R. F., and Matthews, T. D., 1972, Stalagmites from caves in the Bahamas; Indicators of low sea level stand: Quaternary Reserach, v. 2, p. 470-472.

Thompson, P., 1973, Procedures for extraction and isotopic analysis of uranium and thorium from speleothem: Hamilton, Ontario, McMaster University, Department of Geology, Tech. Memo. 73-9.

U-Pb SYSTEMATICS OF ZIRCONS AND MONAZITES FROM A MAFIC TO ULTRAMAFIC COMPLEX AND ITS COUNTRY ROCKS (SAUVIAT-SUR-VIGE, FRENCH CENTRAL MASSIF)

By Dieter Gebauer[1], Jean Bernard-Griffiths[2], Otto Krebs[1], and Marc Grünenfelder[1]
[1]Laboratory for Isotope Geology and Mass Spectrometry, Swiss Federal Institute of Technology, Zurich
[2]Present address: Institut de Géologie, Université de Rennes, France

The western part of the French Central Massif consists mainly of medium-grade, semipelitic metasediments, which are intruded by numerous pre-, syn-, and postmetamorphic felsic to mafic igneous rocks. The upper stratigraphic part of this series, being least metamorphosed, contains fossils indicating a depositional age at the Silurian-Devonian boundary.

The largest mafic to ultramafic body of the French Central Massif (approximately 6 km x 2 km) outcrops in the lower part of this relatively monotonous stratigraphic unit. According to Coffrant (1971) the primary magmatic mineral assemblage was troctolitic, gabbroic, and peridotitic. Depending on the chemical composition, grain-size, and tectonism these rocks are variably transformed into metagabbros, eclogites, and garnet peridotites. In a following syntectonic stage most of these rocks were amphibolitized at lower total but higher H_2O-pressures. Taking into account various experimental data on the stability fields of minerals and rocks, both mafics/ultramafics and their country rocks have formed at temperatures around 600°C and at pressures of about 7 - 8 kb. Thus, a simultaneous formation of all rock types within the crust is probable and is also supported by field evidence.

The geologic and petrologic situation, as described above, was chosen in an attempt to solve the following problems: (1) Can the primary rock age of the various mafic to ultramafic differentiates and (or) the age(s) of metamorphism be deciphered using the U-Pb zircon suite method? (2) Is there a genetic relationship between mafic/ultramafic rocks and the felsic metaigneous country rocks? (3) Can a difference in the age of metamorphism be detected between the mafic/ultramafic complex and their present country rocks in case of a tectonic emplacement from the mantle? (4) Is there a correlation between the degree of discordance of zircons and the recrystallization of the host rocks as was found for similar rock types by Gebauer and Grünenfelder (1978a,b)? (5) Would the zircon data support the field evidence; that is, that the garnet peridotites are also formed within the crust at about 600°C and 7 - 8 kb or would they favor a metamorphic origin within the mantle? A mantle origin is usually inferred by petrologists and was confirmed by the first U-Pb data on zircon from such rocks (Gebauer and Grünenfelder, 1978a).

The data points of zircon fractions from an eclogitized metagabbro, a weakly and a strongly amphibolitized metagabbro, and two garnet peridotites plot on a single discordia trajectory. The extrapolated intercept ages lie within the range of the Cambrian-Ordovician boundary (ca. 500 m.y.) and within the Hercynian orogeny (ca. 325 m.y.). Thus, the primary rock age of the mafic/ultramafic differentiates falls towards the beginning of the Caledonian period while their eclogite-facies metamorphism, including amphibolitization, took place in the course of the Hercynian. As in the case of metagabbros and eclogites of the Münchberg Gneiss Massif in northeastern Bavaria (Gebauer and Grünenfelder, 1978a,b), the maximum data spread for extreme size and magnetic fractions from one rock is only several percent. In addition, there is neither a correlation between U content (17 - 1130 ppm) and degree of discordance within a single population nor for all four analyzed populations. Instead, metamorphic recrystallization of the host rocks seems to play the major role in determining the degree of discordance. In contrast to zircon fractions from the mafic differentiates which are only as much as 15 percent discordant, zircons from the two more strongly recyrstallized ultramafic rock samples plot close to the middle of the discordia trajectory. Surprisingly, the U contents in zircons from these strongly recrystallized rocks are not systematically lower than those within the mafic differentiates. In contrast to concordant (or 100 percent discordant) zircons from garnet peridotites equilibrated under mantle conditions (Gebauer and Grünenfelder, 1978c), zircons from garnet peridotites analyzed in the course of this study still contain large amounts of lead produced since the magmatic formation of the rock. In fact, they contain more primary lead than zircons from crustal eclogites of the Münchberg Gneiss Massif in northeastern Bavaria (Gebauer and Grünenfelder, 1978a,b), which are similarly old and formed under similar P-T conditions. Thus, one can take this as strong indication that some garnet peridotites also can form under crustal P-T conditions; that is, there is no need to claim a tectonic emplacement as it is usually done for such rocks.

The primary age of the rocks discussed so far agrees with the Rb-Sr whole-rock age of 514 ± 24 m.y. (Duthou, 1977) obtained on metaigneous augen gneisses occurring to the north and west of the mafic/ultramafic complex. As these rocks had $^{87}Sr/^{86}Sr$ ratios of 0.704 at the time of intrusion, they might well be comagmatic with the protoliths of the metagabbroic to peridotitic rocks. Consequently, they suffered the same metamorphic history as has been predicted before by field evidence and petrological constraints.

In contrast to most monazite ages obtained on Central European basement rocks (for example, see Köppel and Grünenfelder, 1971, 1975; Gebauer and Grünenfelder, 1974; Grauert and others, 1974; Hänny and others, 1975), monazites from metaigneous augen gneisses are variably discordant (ca. 10 - 80 percent). They define a trajectory which cannot be distinguished statistically from that defined by zircons from the mafics and ultramafics. Thus, these monazite data are also in agreement with the geological and petrological results (Coffrant, 1971).

It is interesting to note that monazites from variably disintegrated augen gneisses were not open for U and (or) Pb during strong weathering of the host rock. This conforms with similar results obtained on monazites from completely weathered granodioritic orthogneisses of the Montagne Noire at the southern rim of the French Central Massif. Additionally, detrital monazite from unmetamorphosed to very low-grade Ordovician and Cambrian sedimentary rocks from the Montagne Noire indicate that monazites--similar to detrital zircons--not only remained closed systems for U and Pb during weathering but also during transport, diagenesis, and very low-grade metamorphism.

Surprisingly, neither the monazite nor the zircon data indicate open U-Pb systems during an Acadian event around 360 m.y. This event is detected at various localities in the western part of the French Central Massif by a number of mineral and whole-rock ages on metasediments and metaigneous rocks (for example, Bernard-Griffiths, 1975; Bernard-Griffiths and others, 1977; Duthou, 1977). At the present stage of investigation we can only state that monazites from paragneisses taken several kilometers northwest and southwest of the mafic/ultramafic complex might have been affected and (or) formed during an Acadian event. However, the present data are more in favor of a Caledonian formation of monazite in the course of a first metamorphic event. Such Caledonian ages are also known from Rb-Sr whole-rock isochrons and errorchrons obtained on metasediments of this area (Bernard-Griffiths, 1975). Thus, zircons from the mafic and ultramafic rocks as well as monazite from orthogneisses of the immediate country rocks obviously survived two metamorphic events, assuming these events actually affected the studied rocks. From Rb-Sr data of metasedimentary and metaigneous rocks of the Münchberg Gneiss Massif in northeastern Bavaria--which seems to have a very similar history as the western part of the French Central Massif--we know (Söllner, 1978) that Caledonian, Acadian and Hercynian mineral and whole-rock ages occur in an area not larger than 25 km x 15 km. Thus, it is suggested that the geological and petrological development in the western part of the French Central Massif is much more complex than previously thought; that is, that not only one, but at least two if not three distinct metamorphic events took place at various times and (or) in various zones within this region.

Additionally, tectonic activities might have resulted in a juxtaposition of different old rocks causing abrupt change of ages on a small scale.

Bernard-Griffiths, J., 1975, Essai sur la signification des âges au strontium dans une série métamorphique; le Bas Limousin (Massif Central Francais): Thèse. Ann. Sci. Univ. Clermont. Fd. 55, 243 p.

Bernard-Griffiths, J., Cantagrel, J. M., and Duthou, J. L., 1977, Radiometric evidence for an acadian tectono-metamorphic event in Western Massif Central Francais. Contributions to Mineralogy and Petrology, v. 61, p. 199-212.

Coffrant, D., 1971, Les éclogites et les roches basiques et ultrabasiques associées du massif de Sauviat-sur-Vige (Haute Vienne); Etude pétrographique et géochimique: Thèse 3ème Cycle. Univ. Claude Bernard, Lyon.

Duthou, J. L., 1977, Chronologie Rb-Sr et géochimie des granitoïdes d'un segment de la chaîne varisque; Relations avec le métamorphisme, Le Nord Limousin (Massif Central Francais): Thèse, Université de Clermont. Fd. II, p. 275.

Gebauer, D., and Grünenfelder, M., 1974, Comparative studies of U-Pb systems in zircons and monazites as well as Rb-Sr systematics in minerals and whole-rocks during the anatexis of a polymetamorphic paragneiss (crystalline basement of northeast Bavaria): International meeting for geochronology, cosmochronology and isotope geology, Paris, abstracts.

_____1978a, U-Pb zircon dating of eclogites. Example: Münchberg Gneiss Massif (northeast Bavaria): (this conference).

_____1978b, U-Pb zircon and Rb-Sr mineral dating of eclogites and their country rocks. Example: Münchberg Gneiss Massif, northeast Bavaria: Earth and Planetary Science Letters, (in press).

_____1978c, U-Pb zircon dating of alpine-type peridotites. Example: Val Ultimo (Northern Italy), (in preparation).

Grauert, B., Hänny, R., Soptrajanova, G., 1974, Geochronology of a polymetamorphic and anatectic gneiss region; the Moldanubicum of the area Lam-Deggendorf, Eastern Bavaria, Germany: Contributions to Mineralogy and Petrology, v. 45, p. 37-63.

Hänny, R., Grauert, B., and Soptrajanova, G., 1975, Palaeozoic migmatites affected by high-grade Tertiary matamorphism in the Central Alps (Valle Bodengo, Italy): Contributions to Mineralogy and Petrology, v. 51, p. 173-196.

Köppel, V., and Grünenfelder, M., 1971, A study of inherited and newly formed zircons from paragneisses and granitised sediments of the Strona-Ceneri zone (Southern Alps): Schweizerische Mineralogische und Petrographische Mitteilungen, v. 51, p. 387-411.

_____1975, Concordant U-Pb ages of monazites from the Central Alps and the timing of the high temperature Alpine metamorphism, a preliminary report: Schweizerische Mineralogische und Petrographische Mitteilungen, v. 55, p. 129-131.

Söllner, F., 1978, Rb-Sr Altersbestimmungen an Mineralen und Gesteinen der Münchberger Gneismasse: Munich University, Ph.D. Thesis.

LOW TEMPERATURE RECRYSTALLIZATION OF ZIRCON AS A CAUSE OF DISCORDANT U-Pb DATA

By Dieter Gebauer and Marc Grünenfelder
Laboratory for Isotope Geology
and Mass Spectrometry
Swiss Federal Institute of Technology
Zurich, Switzerland

Since the first U-Pb ages on minerals were published more than 20 years ago, a large number of models has been created to explain the generally observed discordant age patterns. Almost all of them are based on zircon data. Today, episodic lead loss due to recrystallization of zircon in the course of a metamorphic cycle is probably the most frequently applied model to explain the observed data patterns. However, mainly in Precambrian terranes, there are numerous data indicating open U-Pb zircon systems after metamorphic and (or) magmatic (re)crystallization of the corresponding host rocks. Unfortunately, it is not known at what minimum temperatures recrystallization of strongly metamict zircons commences in a natural rock system. Therefore, the goal of this study was to find out if elevated temperatures during burial and (or) a weak thermal pulse--not necessarily detected by other dating techniques--are able to anneal metamict zircon structures. If such a process is found to exist, secondary ages (= lower intercept ages) apparently unrelated to a geological event might be explained. The most promising approach seemed to be to take samples from a metamorphic profile ranging from rocks as little metamorphosed as possible to their high-grade equivalents. Thus, it should be possible to compare the U-Pb zircon data obtained on the low- and medium-grade rocks with those of the high-grade equivalents. The latter are known to give reliable results provided the U-Pb systems were open during not more than one metamorphic event. Also, Rb-Sr data were expected to serve as an additional control over the U-Pb zircon results of the low- and medium-grade rocks.

Three detrital zircon populations of staurolite-, biotite-, and chlorite-grade metasediments from a metamorphic profile associated with the gneiss dome of the Montagne Noire at the southern rim of the French Central Massif were analyzed using the classical zircon-suite method introduced by Silver and Deutsch (1963). The data points of all three populations are on the average 85 percent discordant and plot on three closely parallel discordia trajectories intersecting the Concordia between 1936 m.y. and 2162 m.y., and between 417 m.y. and 445 m.y., respectively. This indicates drastic lead loss of about 2 b.y.-old detrital zircons during a Caledonian metamorphism of the corresponding host rocks. Rb-Sr whole-rock errorchrons of schists, gneisses, and migmatites from the same area (Vachette, 1967; Roques and others, 1971; Gebauer and Grünenfelder, 1976) are in agreement with the U-Pb zircon results.

As to the well-known Hercynian event in this region (Vachette, 1967; Roques and others, 1971; Gebauer and Grünenfelder, 1974a; Hamet, 1974), we must conclude that the U-Pb systems of the analyzed fractions remained unaffected about 300 m.y. ago. Obviously, not enough radiation damage was produced in the time span of about 130 m.y. between Caledonian and Hercynian metamorphism to reopen the U-Pb zircon systems during the Hercynian event.

From experimental work on metamict zircons (Mumpton and Roy, 1961; Pidgeon and others, 1973) we propose that the main causes for the observed open-system behavior must lie in the strong radiation damage produced over more than 1.5 b.y. Under these conditions recrystallization, as reflected by the present unit-cell dimensions of these zircons, took place. In fact, the measured c_o and a_o values fall into the same range as was found for zircons formed

or recrystallized during a Caledonian event and having also U-contents between 500 and 1000 ppm (Köppel and Grünenfelder, 1971). In an α-dosage versus unit-cell dimension plot (Holland and Gottfried, 1955) the cell parameters can easily be distinguished from those found in zircons that did not recrystallize after about 2 b.y. ago (an age corresponding to the upper intercepts of the three zircon suites with the Concordia). Here, much higher values quite different than the observed ones must be expected.

Polished sections of the studied zircons did not reveal any macroscopically visible zones or regions which are leached (Krogh and Davis, 1973; Sommerauer, 1974). Thus, the high resistancy of the analyzed fractions to HF-etching is another factor supporting their recrystallization during chlorite- and higher-grade metamorphism of the host rock.

The results strongly suggest that the conditions for open U-Pb systems in zircons can exist at temperatures as low as about 350 - 400°C. Furthermore, this low-temperature recrystallization and lead loss suggests that zircons from amphibolite facies metasediments already act as closed systems for U and Pb before the thermal maximum of the corresponding metamorphism is reached. The proof that recrystallized zircons behave as closed systems for U and Pb at temperatures well above 350 - 400°C is given by many zircons of the Central European basement, that crystallized or recrystallized during the Caledonian and were not affected isotopically about 150 m.y. later during amphibolite facies Hercynian metamorphism (Grauert and Arnold, 1968; Pidgeon and others, 1970; Gebauer and Grünenfelder, 1974b).

In general, under these circumstances, zircon ages from highly metamorphosed gneisses would give maximum ages for the thermal peak of metamorphism because of recrystallization, thus the closing of U-Pb systems is completed in an early stage of metamorphism. Naturally, dating of an early stage of metamorphism, as derived by the present study, will only be valid if there was no new growth of zircon during metamorphism. Such a new growth, however, is generally observed only in rocks undergoing anatexis (Eckelmann and Poldervaart, 1957; Gastil and others, 1967; Gebauer and Grünenfelder, 1974b).

From the data presented so far, we cannot give minimum temperatures necessary for the beginning of recrystallization of metamict zircons as the Precambrian metasediments of the Montagne Noire do not exist at less than chlorite-grade metamorphism. However, U-Pb data on zircons from zeolite facies siltstones in the Innerbohemian Algonkian in the CSSR indicate Gebauer and Grünenfelder, 1977) that temperatures at or even below 300°C are sufficient to cause recrystallization and thus open U-Pb systems. Assuming this minimum temperature range to be 200°C and 300°C, a burial of about 6 - 10 km--assuming a normal geothermal gradient of about 30°C km^{-1}--would be enough to start annealing at least the most disordered regions or domains within the single zircon grains. Of course, it is very hard to find out by independent evidence whether or not temperatures of that order were reached in the late stages of the history of ancient-shield areas. Very probably, both conditions are possible. However, from the very few published papers reporting geologically unsupported secondary ages as well as the corresponding unit-cell parameters, (Fairbairn and Hurley, 1957; Kouvo, 1958; Silver and Deutsch, 1963, or Pidgeon and Hopgood, 1975) it can be seen that most zircons are better crystallized than one would expect from their radiation dosage. Mainly for this reason, radiation-damage ages obtained on these zircons are generally too low, when compared with the time of the last known magmatic or metamorphic event, which can be derived from the corresponding upper intercept ages. Thus, low-temperature annealing, and with it open U-Pb systems, in other words lead loss, occurring in the late stages of the history of zircon, can readily explain both the relatively well ordered crystal lattices and the low secondary ages of Proterozoic or Archaean zircons.

Eckelmann, F. D., and Poldervaart, A., 1957, Geologic evolution of the Beartooth Mountains, Montana and Wyoming: Geological Society of America Bulletin, v. 68, p. 1225-1261.

Fairbairn, H. W., and Hurley, P. M., 1957, Radiation damage in zircon and its relation to ages of Palaeozoic igneous rocks in northern New England and adjacent Canada: American Geophysical Union Transactions, v. 38, p. 99-107.

Gastil, G. R., Delisle, M., and Morgan, J. R., 1967, Some effects of progressive metamorphism on zircons: Geological Society of America Bulletin, v. 78, p. 879-906.

Gebauer, D., and Grünenfelder, M., 1974a, Rb-Sr whole-rock dating of late diagenetic to anchimetamorphic, Palaeozoic sediments in Southern France (Montagne Noire): Contributions to Mineralogy and Petrology, v. 47, p. 113-130.

_____1974b, Comparative studies of U-Pb systems in zircons and monazites as well as Rb-Sr systematics in minerals and whole-rocks during the anatexis of a polymetamorphic paragneiss (crystalline basement of NE-Bavaria: Paris, International meeting for geochronology, cosmochronology and isotope geology, abstracts.

_____1976, U-Pb zircon and Rb-Sr whole-rock dating of low-grade metasediments. Example - Montagne Noire (Southern France): Contributions to Mineralogy and Petrology, v. 59, p. 13-32.

_____1977, U-Pb systematics of detrital zircons from some unmetamorphosed to slightly metamorphosed sediments of Central Europe:

Contributions to Mineralogy and Petrology, v. 65, p. 29-37.
Grauert, B., and Arnold, A., 1968, Deutung diskordanter Zirkonalter der Silvrettadecke und des Gotthardmassivs (Schweizer Alpen): Contributions to Mineralogy and Petrology, v. 20, p. 34-56.
Hamet, J., 1974, Montagne Noire - résultats geochronologiques: Paris, International meeting for geochronology, cosmochronology and isotope geology. Excursion géologique, Montagne Noire and Pyrénées.
Holland, H. D., and Gottfried, D., 1955, The effect of nuclear radiation on the structure of zircon: Acta Crystallographica, v. 8, p. 291-300.
Köppel, V., and Grünenfelder, M., 1971, A study of inherited and newly formed zircons from paragneisses and granitized sediments of the Strona-Ceneri zone (Southern Alps): Schweizerische Mineralogische und Petrographische Mitteilungen, v. 51, p. 387-411.
Kouvo, O., 1958, Radioactive age of some Finnish pre-Cambrian minerals: Finnlande Commission Géologique Bulletin, v. 182, p. 1-70.
Krogh, T. E., and Davis, G. L., 1973, Alteration in zircons and differential dissolution of altered and metamict zircon: Carnegie Institution of Washington, Year-Book 1974-1975, p. 619-625.
Mumpton, F. A., and Roy, R., 1961, Hydrothermal stability studies on the zircon-thorite group: Geochimica Cosmochimica Acta, v. 21, p. 217-238.
Pidgeon, R. T., Köppel, V., and Grünenfelder, M., 1970, U-Pb isotopic relationship in zircon suites from a para- and orthogneiss from the Ceneri zone, Southern Switzerland: Contributions to Mineralogy and Petrology, v. 26, p. 1-11.
Pidgeon, R. T., O'Neil, R. J., and Silver, L. T., 1973, Observations on the crystallinity and the U-Pb system of a metamict Ceylon zircon under experimental hydrothermal conditions: Fortschritte der Mineralogie, v. 50, p. 118.
Pidgeon, R. T., and Hopgood, A. M., 1975, Geochronology of Archaean gneisses and tonalites from north of the Frederishabs isblink, S.W. Greenland: Geochimica Cosmochimica Acta, v. 39, p. 1333-1346.
Roques, M., Vachette, M., Vialette, Y., Bernard-Griffiths, J., Cantagrel, J. -M., and Duthou, J. -L., 1971, Géochronologie du socle due Massif Central: Brussels, European Colloquium of Geochronology, abstracts.
Silver, L. T., and Deutsch, S., 1963, U-Pb isotopic variations in zircons, a case study: Journal of Geology, v. 71, p. 721-758.
Sommerauer, J., 1974, Trace element distribution patterns and the mineralogical stability of zircon - an application for combined electron microprobe techniques: Elektronenmikroskopie-vereniging van Suidelike Afrika, Johannisburg.
Vachette, M., 1967, Etude géochronologique de la Montagne Noire dans le Massif Central français: Annales Fac. Sci. Universite de Clermont 36.

U-Pb ZIRCON DATING OF ALPINE-TYPE GARNET-PERIDOTITES EXAMPLE: VAL ULTIMO (EASTERN ALPS, NORTHERN ITALY)

By Dieter Gebauer and Marc Grünenfelder
Laboratory for Isotope Geology
and Mass Spectrometry,
Swiss Federal Institute of Technology, Zurich

The purpose of this study is: (1) to determine whether zircons occurring in garnet-peridotites and various garnet-pyroxenites are of primary magmatic and/or metamorphic origin; (2) to test--in case zircons were found to be magmatic--whether primary ages can still be deduced; and (3) to compare the zircon-ages of the ultramafics with Rb-Sr and U-Pb monazite ages obtained on the country rocks. The last point is of significance for the petrogenetic and tectonic development of such rocks because there is considerable petrological uncertainty of the stability field of garnet-peridotites. Although there is general agreement on their tectonic emplacement, there are different opinions about the tectonic level in which the metamorphic mineral assemblages were formed. Geological considerations frequently suggest a formation of garnet-peridotites together with their country rocks in the crust (Rost and Grigel, 1969; Brenneis, 1971; Coffrant, 1971) whereas many petrological studies demand P-T conditions reached only in the mantle (Wood and Banno, 1973; MacGregor, 1974). It was therefore hoped that U-Pb zircon studies on the ultramafics, as well as on their immediate country rocks, would shed light on this problem. If both rock types are of a crustal origin both rock types should give identical ages of metamorphism.

Samples were taken from an approximately 100 m thick lense of garnet-peridotite occurring with numerous other ultramafic lenses of similar

size, in high-grade gneisses of the southern part of the pre-Alpine Otztal crystalline complex (Eastern Alps, Northern Italy). All peridotite lenses lie within the schistose zone of the country rock and follow the Insubric Line to the southeast, a distance of about 2 km (Brenneis, 1971). Because the Insubric Line, separating the Southern Alps from the Western; Central and Eastern Alps, is a major geotectonic suture, a direct relationship might exist between this fault zone and the tectonic emplacement of the peridotites of the Val Ultimo.

The peridotites frequently show compositional layering which is tightly folded. The mineral paragenesis of a sample taken for zircon analysis is olivine-orthopyroxene-clinopyroxene-garnet and spinel. There is only weak kelyphitization of garnet and little serpentinization of olivine. A second sample was taken from a prefolded garnet-rich pyroxenite boudin about 1 m long and 40 cm thick. Such relatively inhomogeneous rocks occur as mm-thin, strongly folded layers to boudins of up to 1.5 m thickness within the peridotites. A third sample was taken from a late-tectonic garnet-pyroxenite occurring as an unfolded but nevertheless slightly deformed 10 - 20 cm thick dike within the strongly folded peridotites.

The analyzed zircons are colorless to pink in the garnet-peridotite and the weakly deformed garnet-pyroxenite, and reddish in the prefolded garnet-rich pyroxenite. They appear very homogeneous and are frequently fractured, which seems to be typical for many zircons crystallized under very high pressures. Under the binocular microscope no free-grown crystal faces are visible. Instead, indentations due to limited-growth conditions are frequently observed.

The analytical results obtained on zircons from all three rock types gave concordant age patterns falling into the Hercynian. One data point of a zircon fraction (75 - 100μ; U: 216 ppm) from the garnet-peridotite and data points from two size fractions (-53μ and +250μ; U: 967 ppm and 111 ppm) of the garnet-rich, prefolded pyroxenite agree within limits of analytical error at 336 m.y. In contrast, two zircon fractions from the weakly deformed garnet-pyroxenite dike gave identical but very slightly younger ages at 332 m.y. At the present stage of investigation the significance of this age difference has not been proven.

The 336 m.y. age of zircons from the garnet-peridotite and the garnet-rich pyroxenite probably reflect an age related to a mantle metamorphism of the host rock at temperatures possibly exceeding 1000°C. At this time probably both new formation and complete isotopic resetting during recrystallization of zircon occurred. The primary magmatic occurrence of zircon can be deduced by the presence of zircons within the garnet-rich pyroxenites, showing an oscillating change of concentrations of heavy elements over as many as 30 euhedral zones within one crystal. Obviously, there were strong physico-chemical changes during intrusion of the protolith of this rock into the peridotite. It is interesting to note that such strongly varying conditions are not reflected by the heavy-element distribution in zircons from the weakly deformed garnet-pyroxenites, which show, as do zircons of the peridotite--a relatively uniform cathode luminescence pattern. Therefore, at the present stage of investigation, it seems most plausible that the primary magmatic zircons in the protolith of the garnet-rich pyroxenite, and possibly also of the peridotite, recrystallized completely and may actually have newly formed during the metamorphic transformation of the host rock(s) within the mantle. Thus, no primary lead can be expected to be still present in the zircon. Also, this metamorphism was probably accompanied by strong folding.

The intrusion of the source rock of the weakly deformed garnet-pyroxenite falls into a later stage of the history of the peridotite and garnet-rich pyroxenite. The exsolution of garnet in orthopyroxene in this younger rock and the strong folding must have occurred in the stability field of garnet-peridotite (the mantle). Consequently, the protolith of this rock did not intrude the crust as a melt.

In case the slightly younger zircon age of this rock turns out to be significant, there would be strong evidence that zircons once formed in a pyroxenitic melt, remain closed U-Pb systems for U and Pb during cooling of the rock. The solidus of such melts probably lies at around 1350°C, assuming pressures of about 20 kb (Ringwood, 1975).

Preliminary U-Pb data on monazite and Rb-Sr data on muscovites of the host rocks of the peridotite lenses yielded younger ages for the metamorphism of the crustal country rocks. Thus, it will be possible to determine the time that the peridotite intruded the crust over a vertical distance of about 40 km or even more.

Brenneis, R. P., 1971, Zur Geochemie und Genese der Ultramafite im Bergzug südlich des Ultentals, Südtirol: University Saarbrücken (FRG), Ph.D. Thesis, 129 p.

Coffrant, D., 1971, Les éclogites et les roches basiques et ultrabasiques associées du massif de Sauviat-sur-Vige (Haute-Vienne): Thèse 3ème Cycle, Université Claude Bernard de Lyon, 89 p.

MacGregor, I. D., 1974, The system MgO - Al_2O_3-SiO_2-solubility of Al_2O_3 in enstatite for spinel and garnet peridotite compositions: American Mineralogist, v. 59, p. 110.

Ringwood, A. E., 1975, Composition and petrology of the earth's mantle: New York, McGraw-

Hill Book Company, 618 p.
Rost, F., and Grigel, W., 1969, Zur Geochemie und Genese granatführender Ultramafite des mitteleuropäischen Grundgebirges: Chemie der Erde, v. 28, p. 91.
Wood, B. J., and Banno, S., 1973, Garnet-orthopyroxene and orthopyroxene-clinopyroxene relationships in simple and complex systems: Contributions to Mineralogy and Petrology, v. 42, p. 109.

U-Pb ZIRCON DATING OF ECLOGITES: EXAMPLE, MÜNCHBERG GNEISS MASSIF (NORTHEASTERN-BAVARIA)

Bu Dieter Gebauer and Marc Grünenfelder
Laboratory for Isotope Geology and Mass Spectrometry
Swiss Federal Institute of Technology, Zürich

Eclogites are undoubtedly of great importance in dating the geological, petrological, and tectonic development of orogenic belts. Nevertheless, geochronological data are scarce mainly due to analytical difficulties and (or) uncertainties with the interpretation of the results. Although zircons are generally thought to not occur in eclogites, this does not hold true for at least some central European eclogites. Thus, the main purpose of this study is to test the U-Pb zircon-suite method for its reliability in dating such rocks.

From a number of studies (Poldervaart, 1956; Nunes and Tilton, 1971; Gebauer and Grünenfelder, 1973; Pupin, 1976) we know that zircon can be of primary magmatic origin in gabbroic rocks. Therefore, it might become possible to date--in addition to the time of eclogite-formation--the age of the corresponding protolith. For a better understanding of the U-Pb zircon data, Rb-Sr analyses have been carried out on minerals of the eclogites as well as of the felsic country rocks. There are so far no Rb-Sr whole-rock data indicating primary rock ages. However, such primary ages might also be obtained using the new Sm-Nd dating technique.

Samples were taken from the Münchberg Gneiss Massif (northeastern Bavaria) which forms an oval shaped complex 25 km in length and 15 km in width. It is surrounded by very low-grade, stratigraphically controlled, old Palaeozoic metasediments which were deformed and metamorphosed during the Hercynian orogeny. Eclogites and metagabbros occur as tectonic lenses but sometimes in situ in quartz-plagioclase-muscovite-biotite-garnet-staurolite-kyanite rocks of sedimentary origin (Schüller, 1947; Stettner, 1960; Matthes and others, 1975). Two eclogite samples were taken from the top of the Weissenstein; that is, from the largest eclogite body within the nonalpine part of central Europe. One sample of a metagabbro was taken from another lense separated by about 300 m from the eclogites.

Petrographically, the analyzed eclogites consist of omphacite, garnet, quartz, and rutile. Synkinematic hornblende and phengite belong to the posteclogitic mineral assemblage. The mineral paragenesis of a metagabbro sample is plagioclase, hornblende, garnet, quartz, saussurite, rutile, sphene, biotite, and opaques. Its chemical composition, including H_2O, deviates slightly from the eclogites. Its composition, larger grain-size, and tectonic setting are probably the main reasons why it was not transformed into an eclogite. Pressure-temperature estimates for the formation of the country rocks yield temperatures of around 600°C and pressures at or above 5 - 7 kb.

The data points of seven grain-size and magnetic zircon fractions extracted from two eclogite samples and the data points of two extreme size and magnetic fractions from a metagabbro plot within analytical error on a single discordia trajectory. The intersection ages are 525 m.y. and 380 m.y., respectively indicating a Cambrian age for the tholeiitic protolith and an Early to Middle Devonian age for the eclogite facies metamorphism. In contrast to the two zircon populations of the eclogites, the two zircon fractions of the metagabbro are only slightly (ca. 20 percent) discordant--although their U content (300 and 475 ppm, respectively) is two to four times higher than that of the eclogites. This can best be explained by the significant differences in the mineralogical and structural transformation of the two rock types. Zircons of the metagabbro appear typically magmatic and much less disturbed by metamorphic recrystallization, overgrowth and (or) possible new growth than zircons from the eclogites. The weak discordancy of the zircons of the metagabbro clearly demonstrates that zircons only little damaged by radiation can survive metamorphic temperatures of around 600°C without losing significant amounts of radiogenic lead if the host rock remained simultaneously undeformed.

The most striking difference from many other zircon suites of granitic host rocks is that the usually observed correlation of grain

size, magnetic susceptibility, and U content versus degree of discordance was not found for the eclogite zircons. One can take this as further evidence for a probable overgrowth and (or) complete new growth of zircon in a solid state during eclogite facies metamorphism. This is all the more striking in that the magmatic-looking zircons of the metagabbro show the usually observed correlation.

In conclusion, the results obtained prove the possibility of dating eclogites and their magmatic source rocks using the U-Pb zircon suite method. In contrast to many other zircon populations of felsic rocks, the zircon population of only one sample does not supply a great enough data spread to define a reliable internal discordia trajectory. Similar observations have been made for zircon populations of mafic rocks from other regions within Central Europe (Gebauer and Grünenfelder, unpublished data). However, due to complete lack of comparable data from older terranes this statement must be restricted at the moment to Phanerozoic rocks only.

Knowing the primary age of the tholeiitic source rock and the age of eclogite facies metamorphism, it would be interesting to find out also whether the so-called retrograde formation of hornblende and phengite took place immediately after formation of the eclogite mineral assemblage. From the stratigraphical, structural, and metamorphic state of the Palaeozoic sediments surrounding the Münchberg Gneiss Massif, a Hercynian tectonism and very low grade metamorphism about 320 m.y. ago is well known. This metamorphism may possibly extend into the Münchberg Gneiss complex with increasing strength. Thus, the retrograde mineral assemblage within the eclogites could well be of Hercynian age. In order to solve this problem, Rb-Sr analyses were carried out on hornblende and phengite from an eclogite previously separated for its zircon population. Additionally, muscovite of the regionally overprinted contact-metamorphosed country rock of the protolith of the eclogites was analyzed together with its corresponding whole-rock system. The results indicate that the retrograde formation of hornblende and phengite within the eclogites took place immediately after the eclogite facies metamorphism and not during a possible later Hercynian event.

The initial Sr isotopic composition of the hornblende-phengite pair ($^{87}Sr/^{86}Sr$ = 0.704) is in accordance with a mantle origin of the source rock. However, the corresponding initial value of the whole-rock-muscovite pair of the immediate country rock of the eclogite ($^{87}Sr/^{86}Sr$ of ca. 706) might have been lowered during intrusion and (or) metamorphism of the protolith of the eclogite.

Gebauer, D., and Grünenfelder, M., 1973, Vergleichende U/Pb-und Rb/Sr-Altersbestimmungen im bayerischen Teil des Moldanubikums: Fortschritte der Mineralogie, v. 50, p. 4.

Matthes, S., Richter, P., and Schmidt, K., 1975, Die Eklogitvorkommen des kristallinen Grundgebirges in NE-Bayern, IX. Petrographie, Geochemie und Petrogenese der Eklogite des Münchberger Gneisgebietes: Neus Jahrbuch fur Mineralogie Abhandlungen, v. 126, p. 45-86.

Nunes, P. D., and Tilton, G. R., 1971, Uranium-lead ages of minerals from the Stillwater complex and associated rocks, Montana: Geological Society of America Bulletin, v. 82, p. 2231-2250.

Poldervaart, A., 1956, Zircon in rocks; 2, Igneous rocks: American Journal of Science, v. 254, p. 521-554.

Pupin, J., 1976, Signification des caractères morphologiques du zircon commun des roches en pétrologie. Base de la méthode typologique. Applications: Thèse de Doctorat ès-Sciences 1976, Université de Nice, Laboratoire de Pétrologie-Minéralogie.

Schüller, A., 1947, Zur tektonischen Analyse der Münchberger Gneismasse: Zeitschrift deutsche geologische Gesellschaft, v. 97, p. 66-94.

Stettner, G., 1960, Ueber Bau und Entwicklung der Münchberger Gneismasse: Geologisches Rundschau, v. 49, p. 350-375.

OXYGEN DIFFUSION IN MINERALS AND MODELS FOR ^{18}O EXCHANGE BETWEEN A GABBROIC INTRUSION AND CIRCULATING METEORIC WATERS

By Bruno J. Giletti and E. M. Parmentier
Department of Geological Sciences
Brown University
Providence, Rhode Island 02912

The determination of oxygen diffusion rates in minerals in wet systems has now been reported for the Ca, Na, and K feldspars (Giletti and others, 1978), phlogopite (Giletti and Anderson, 1975), and magnetite (Castle and Surman, 1969). In addition, preliminary

data are in hand for olivine (Fo_{100}) and quartz, and some maximal values of the diffusivity in garnet and a pyroxene (fig. 1). In addition, the dependence of the diffusivity of O on total water pressure has been measured for K-feldspar (Yund and Anderson, 1978).

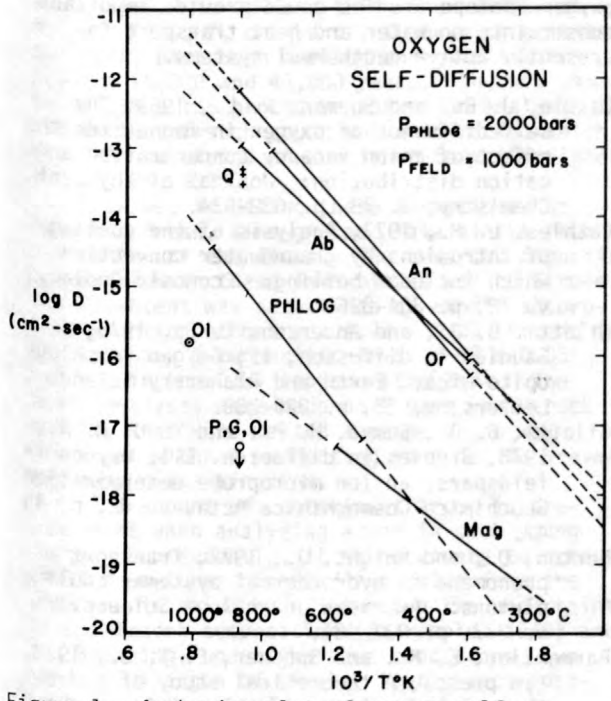

Figure 1.--Arrhenius plot of oxygen self-diffusion in hydrothermal experiments for: feldspars (Ab, An, Or); quartz (Q); phlogopite mica (PHLOG); magnetite (Mag); diopside (P); grossular garnet (G); and olivine (ol).

The depletion of ^{18}O reported for some intrusions results from oxygen exchange between hot permeable rock and meteoric water circulated by natural convection. This depletion has been modeled with the basic assumption that exchange occurs by diffusion. Because of the large differences in diffusional behavior between the mafic minerals and plagioclase, a gabbroic rock exchanging its oxygen may be treated as plagioclase in an inert matrix. The cooling rock system is hypothetical, but is similar to those described by Taylor and Forester (1971).

As can been seen from figure 6 of Giletti and others (1978), this exchange of oxygen isotopes in feldspars can occur readily on time scales of $\leq 10^6$ years for minerals in rocks with normal igneous textures at temperatures as low as 350°C. The measurements extend down to 350°C. In contrast to this, the measurements on magnetite, olivine, diopside, and grossular garnet are all between two and four orders of magnitude lower in D. For a rock with an assemblage of plagioclase, pyroxene, olivine, and magnetite, we would thus predict extensive exchange of feldspar oxygens long before the mafics had undergone appreciable exchange.

Models describing the thermal history of intrusions cooled by circulating water have been formulated by Cathles (1977) and by Norton and Knight (1977). Assuming that the cracks and fractures through which water moves are closely spaced, these models are based on mathematical descriptions of water circulation and thermal energy transport in a permeable medium. The models considered here are similar, but simultaneously describe fluid phase transport of ^{18}O and the exchange between rock and water.

In the models to be discussed, diffusion is considered to be the sole mechanism of exchange. These are clearly minimum models in that reaction or solution-precipitation may also occur, thus increasing the overall exchange rate. The models also assume that flow through intergranular pores and (or) diffusion along grain boundaries keeps the surface of depleting feldspar grains in isotopic equilibrium with water in nearby through-going cracks and fractures. This assumption will maximize the amount of exchange that occurs by diffusion.

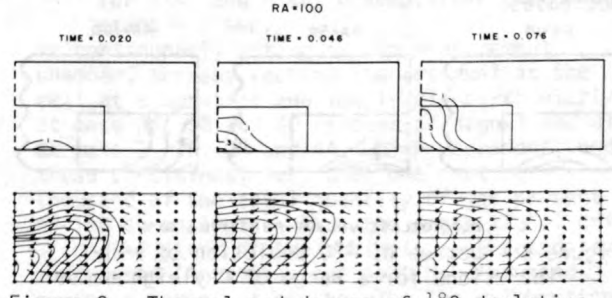

Figure 2.--Thermal and degree of ^{18}O depletion history for a model intrusion with Rayleigh number (RA) = 100. Temperature increases from lowest, 100°C (on reader's right) to highest (on reader's left), time is non-dimensional.

The thermal and depletion history of a model intrusion is shown in figure 2. The intrusion is modeled as a block of initially hot (1000°C), permeable rock instantaneously emplaced into country rock of the same permeability. The water circulation is generated only by the heat of the intrusion with no heat being supplied at the bottom of the layer of permeable country rock. At each of three nondimensional times, the temperatures are shown by isotherms, and the direction and relative magnitude of water movement by flow vectors. The depletion is represented by contours indicating the fractional approach to equilibrium of feldspar oxygen with that of meteoric water. The thermal history presented is for a particular value of the dimensionless Rayleigh number, RA, (see Parmentier and Spooner, 1978) which governs the magnitude of water movement. RA depends on the thermodynamic and transport properties of the water and is proportional to the rock permeability, the

initial temperature difference between intrusive and country rock, and the half-width of the intrusion (3 km). The physical parameters governing the depletion, in addition to the diffusion coefficient, include the volume fraction of feldspar in the rock (30 percent) and the radii of feldspar grains, all of which are the same (1 mm) in this simple model.

Depletion occurs mainly in the hot interior of the intrusion and, for the conditions considered, is limited primarily by fluid phase transport rather than by diffusional exchange. The outer portions of the intrusion cool quickly so that slow diffusion at temperatures less than about 400°C does not allow significant exchange. Temperatures in the country rock above the intrusion are high enough for exchange to occur, but water flowing through the intrusion has already equilibrated with intrusive rock. The transport-limited nature of exchange in the interior of the intrusion is indicated by the results of figure 3, which show the final depletions for a range of RA. Other results show that depletion increases as the plagioclase volume fraction decreases.

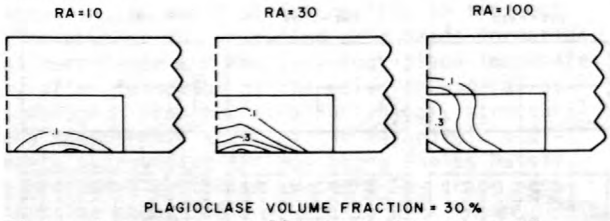

Figure 3.--Degree of ^{18}O depletion of model intrusions for a range of Rayleigh number (RA).

These simple models are presently being extended to include: (1) textural differences between intrusive and host rocks, because host volcanics are much finer grained than intrusive rock and will exchange more readily; (2) heat supplied to the permeable host rock from deeper levels of the intrusion; and (3) meteoric water addition at the ground surface, which will reduce the amount of recycling of water and increase the amount of deletion which occurs.

The results of the present models, if confirmed by more refined models and by field testing in exposed intrusions, suggest that ^{18}O depletion within intrusions is limited by fluid phase transport rather than isotope exchange kinetics. Therefore, if properly interpreted, oxygen isotope studies could provide important constraints on water and heat transport in presently active geothermal systems.

Castle, J. E., and Surman, P. L., 1969, The self-diffusion of oxygen in magnetite; the effect of anion vacancy concentration and cation distribution: Journal of Physical Chemistry, v. 73, p. 632-634.

Cathles, L. M., 1977, Analysis of the cooling of intrusions by groundwater convection which includes boiling: Economic Geology, v. 72, p. 804-826.

Giletti, B. J., and Anderson, T. F., 1975, Studies in diffusion, II; Oxygen in phlogopite mica: Earth and Planetary Science Letters, v. 28, p. 225-233.

Giletti, B. J., Semet, M. P., and Yund, R. A., 1978, Studies in diffusion, III; Oxygen in feldspars, an ion microprobe determination: Geochimica Cosmochimica Acta, v. 42, p. 45-47.

Norton, D., and Knight, J., 1977, Transport phenomena in hydrothermal systems; cooling plutons: American Journal of Science, v. 277, p. 937-981.

Parmentier, E. M., and Spooner, E. T. C., 1978, (in press), A theoretical study of hydrothermal convection and the origin of the ophiolitic sulphide ore deposits of Cyprus: Earth and Planetary Science Letters.

Taylor, H. P., Jr., and Forester, R. W., 1971, Low-O^{18} igneous rocks from the intrusive complexes of Skye, Mull, and Ardnamurchan, western Scotland: Journal of Petrology, v. 12, p. 465-497.

Yund, R. A., and Anderson, T. F., 1978, The effect of fluid pressure on oxygen isotope exchange between feldspar and water: Geochimica Cosmochimica Acta, v. 42, p. 235-239.

K - Ar DATING OF THE LASCHAMP MAGNETIC EXCURSION: A METHOD FOR DATING YOUNG VOLCANIC ROCKS

By Pierre-Yves Gillot
Centre des Faibles Radioactivites
Laboratoire mixte CNRS-CEA
91190-Gif-sur-Yvette, France

Two lava flows at Olby and Laschamp (Chaine des Puys, Massif Central, France), showing a reversed remanent magnetization, have been described by Bonhommet and Babkine (1967). Bonhommet and Zähringer (1969), from their K-Ar measurements and from ^{14}C data, set limits

between 20,000 years and 8700 years for the end of this Laschamp polarity event. However, the occurrence of such a magnetic event in the same range of ages was not confirmed (Denham and Cox, 1971; Verosub, 1977). We have therefore improved the age determinations of these two lava flows. To achieve this, four different methods (^{14}C, TL on quartz, TL on plagioclases, and K-Ar) have been applied and give limits between 25,000 and 45,000 years. In this paper, we describe the procedure for argon analysis for the dating of such young volcanic rocks, which has been developed at our laboratory (Cassignol and others, 1978).

For use in dating these formations, we selected fresh, fine-grained lava blocks from the center of the flows. The reversed magnetic orientation in these lava blocks was confirmed. The K content was determined by atomic absorption spectrophotometry : 1.77 ± 0.03 percent in the Laschamp K-mugearitic lava, 1.67 ± 0.03 percent in the Olby labradoritic lava. The argon analyses were made on 7 gram whole-rock samples that were melted and the argon was extracted without preheating in order to prevent any mass discrimination.

The amount of contaminant argon is preponderant when analyzing argon in such young rocks. Consequently, it is necessary to detect small departures of $^{40}Ar/^{36}Ar$ ratio from the atmospheric value by eliminating the uncertainty in the tracer composition (Dalrymple, 1969) and by comparing, under the same conditions, two amounts of argon of similar isotopic composition: the atmospheric argon and the sample argon. For this purpose, instead of using the technique of isotopic dilution with ^{38}Ar as a tracer, we determined the quantity of argon from the mass spectrometer ion beam intensity. We have already established that, under certain conditions, the ion beam intensity is representative of the amount of argon introduced with an accuracy of better than one part per thousand (Cassignol and others, 1978). The conditions necessary for this relationship are as follows: (1) to measure all of the argon contained in the sample; (2) to eliminate the helium which penetrates through the silica wall when the extracted gases are purified on titanium sponge; and (3) to keep the level of the chemically active components in the cell constant during the measurements, and as low as possible.

The first two conditions are easily fulfilled. After extraction and purification, the argon is concentrated by trapping it on charcoal (liquid N_2 cooled) in a chamber near the cell, after which helium is eliminated by pumping. The chamber is isolated from the line, the argon released, and then the mass spectrometer cell is opened. The ion beam reaches its equilibrium value within a few seconds (fig. 1); its stability and its reliability with respect to other measurements made in the same way then depend on the third condition. To achieve the best results, a zirconium aluminium getten pump

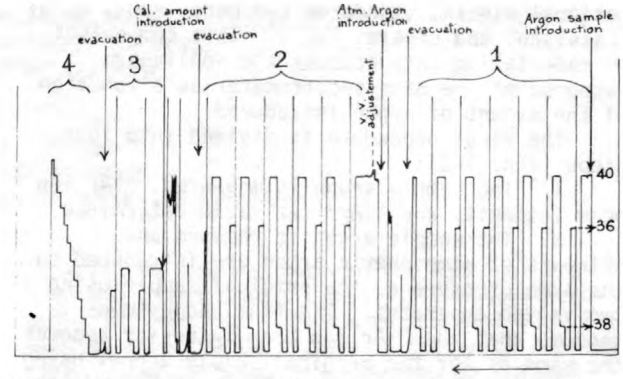

Figure 1.--Recording of Argon measurements of Laschamp sample M706, obtained using a cyclic process instead of a voltage scanning. The accelerating voltage is successively switched to the values corresponding to 36, 38 and 40 mass collection (David, 1974). The duration of 1 cycle is 3 minutes. Measurement conditions: sensitivity = 30 mV; input resistor of the electrometer = 5.10^8 Ω for the ^{40}Ar, and 10^{11} Ω for ^{36}Ar and ^{38}Ar; preamplifier time constant = 2 sec.

is continuously acting in the measurement chamber, thereby keeping the residual in the cell at a constant and low level--particularly at mass 36, 38 and 40 (isobar of argon) and also at mass 2, 16, 28 and 44, which represent, under these conditions, less than one part per thousand of the total quantity of gas present during an analysis. Thus the argon signal drift after the start of the analysis is practically suppressed (less than one part per thousand during a period of one hour). The calibration is made by comparing this ^{40}Ar signal with the signal of a given amount of atmospheric argon measured under the same conditions. This latter amount has itself been compared with inter-

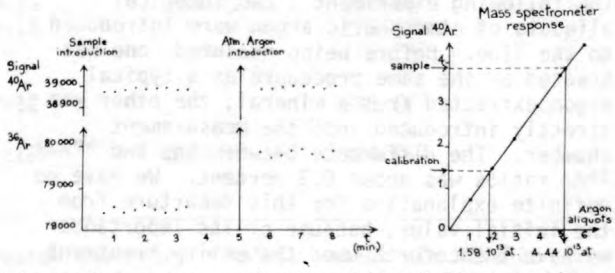

Figure 2.--Argon analysis of the M 791 Laschamp sample, obtained using simultaneous collection of the 40 and 36 masses (Cassignol, 1977). The values plotted against time are the summation of the currents during a period of 10 sec. each 20 sec. (one per sec. for the 40 and 2 per sec. for the 36). Measurement conditions: ^{40}Ar channel = sensitivity 1V, input resistor 10^{10} Ω; ^{36}Ar channel = sensitivity 30 mV, input resistor 10^{11} Ω; preamplifiers time constant: 2 sec.

national mineral standards (4M Bern, P207, GL 0) (Cassignol and others, 1977). This comparison is made taking into account the nonlinear response of the mass spectrometer as a function of the amount of argon introduced.

The final procedure is divided into four steps (fig. 1-2):

1. The sample argon is measured, ^{40}Ar ion beam intensity and $^{40}Ar/^{36}Ar$ ratio determined.

2. The sample argon is removed and aliquots of atmospheric argon are introduced to the same pressure as the original sample using a two valved apparatus. The final adjustment is made so that the ^{40}Ar ion beam intensity becomes the same as for the original sample argon, using a variable chamber volume. Thus, the $^{40}Ar/^{36}Ar$ ratio in atmospheric argon is measured under the same conditions as the sample argon, the ion source parameters being kept constant. From a comparison of each ratio, the radiogenic ^{40}Ar level in the sample argon can be obtained.

3. The mass spectrometer is evacuated, the calibrated amount of argon is introduced, and its ^{40}Ar ion beam intensity measured under the same conditions.

4. After evacuating the cell once more, the mass spectrometer response diagram is established by measuring the ^{40}Ar signals as successive atmospheric argon aliquots are added to the cell.

Using this procedure, we can measure a 1 percent radiogenic ^{40}Ar enrichment with an accuracy of 15 percent.

It has not been demonstrated that the inherited argon is negligible within such a high accuracy. To check this, we have analyzed volcanic lavas of zero age (Mount Etna, Lipari Island). Most of them exhibited a constant radiogenic ^{40}Ar level of 2 to 4 parts per thousand. Because of the constancy of this level, we doubt that it was inherited argon from these rocks. Consequently, we have done the following experiment : two identical aliquots of atmospheric argon were introduced to the line. Before being measured, one was treated by the same procedure as a typical argon extracted from a mineral; the other was directly introduced into the measurement chamber. The difference between the two $^{40}Ar/^{36}Ar$ ratios was about 0.3 percent. We have no definite explanation for this departure from the initial value, because of its importance we have thenceforth used the entire treatment for atmospheric argon as well. For previously analyzed argon samples, we believe that the radiogenic ^{40}Ar percentage can be corrected for this effect by substracting 0.30 ± 0.15 percent.

For the Laschamp and Olby lava flows we have obtained ages of 37,500 ± 7500 (2σ on 5 samples) and 38,000 ± 10,000 years (2σ on 6 samples) respectively, using the method described. These values are comparable to those obtained from TL measurements on quartz baked by the flows, while ^{14}C data on a paleosoil overlain by the Olby flow reveals a minimum age value of 25,000 years.

Bonhommet, N., and Babkine, J., 1967, Sur la présence d'aimantations inversées dans la Chaine des Puys: Centre de Recherches, Academie de Science, Paris, v. 264B, p. 92-94.

Bonhommet, N., and Zähringer, J., 1969, Paleomagnetism and Potassium Argon age determinations of the Laschamp geomagnetic polarity event: Earth and Planetary Science Letters, v. 6, p. 43-46.

Cassignol, C., 1977, Simultaneous collection of ^{40}Ar and ^{36}Ar isotopes for potassium argon datation purposes: Pisa, Italy, ECOG V.

Cassignol, C., Cornette, Y., David, B., and Gillot, P. Y., 1978, Technologie potassium-argon: CEN Saclay, Rept CEA R-4908, 35 p.

Cassignol, C., David, B., and Gillot, P. Y., 1977, Contribution au dosage de l'Argon dans l'échantillon de glauconite GL-0: Geostandard News-letters, v. 1, p. 105-106.

Dalrymple, G. B., 1969, $^{40}Ar/^{36}Ar$ analyses on historic lava flows: Earth and Planetary Science Letters, v. 6, p. 47-55.

David, B., 1974, Accurate Argon measurements: 3rd International Conference on Geochronology, Cosmochronology, and Isotope Geology, Paris, France.

Denham, C. R., and Cox, A., 1971, Evidence that the Laschamp polarity event did not occur 13,300 - 30,400 years ago: Earth and Planetary Science Letters, v. 13, p. 181-190.

Verosub, K. L., 1977, The absence of the mono lake geomagnetic excursion from the paleomagnetic record of Clear Lake, California: Earth and Planetary Science Letters, v. 36, p. 219-230.

COMPARISON OF FISSION-TRACK DATING METHODS: EFFECTS OF ANISOTROPIC ETCHING AND ACCUMULATED α-DAMAGE

By A. J. W. Gleadow
School of Earth Sciences
University of Melbourne, Melbourne, Australia

Fission-track dating essentially involves measuring etched tracks before and after a neutron irradiation and a number of alternative laboratory procedures are possible to achieve this. In this paper the results obtained by different fission-track dating methods are compared for the minerals apatite, sphene, and zircon.

In a previous study (Gleadow, 1978) it was shown that the etching characteristics of tracks in sphene are significantly different before and after thermal annealing due to a progressive modification of the etching properties of spontaneous tracks by α-damage accumulating over the lifetime of the mineral. The most obvious change occurs in the track etching rate. These changes are reversed by thermal annealing, but at a slightly lower temperature than that required for track annealing. The etching properties of undamaged sphene are markedly anisotropic with two important consequences. First, the general etching rate, V_G, and hence the track etching efficiency, varies with crystallographic orientation. Only sur-

Table 1.--Comparison of ages from different fission-track dating methods[1]

Rock	Mineral	PM	SM	EDM	K-Ar[2]
Nepheline syenite of Magnet Cove Complex.	Sphene	106±7[3]	96±6	94±6	96±5
	Apatite	-	-	94±4	
Fish Canyon Tuff (70L-126).	Sphene	44.6±3.5	26.9±1.6	28.3±1.1	-
	"	34.4±2.0[3]	-	-	-
	Apatite	28.4±1.2	-	-	-
	Zircon	41.7±1.2	-	27.1±1.2[4]	27.2±0.7
Fish Canyon Tuff (72N8).	Apatite	26.5±2.0	-	27.7±1.8	-
	Zircon	-	-	27.4±1.3	-
	"	-	-	27.7±1.3	-
	"	-	-	27.5±1.3	-
Mud Tank carbonatite.	Apatite	259±14	-	245±12	-
	Zircon	385±21	254±21	265±14	-
	"	334±18	-	273±13[4]	-
	"	-	-	272±13[5]	-
Mt. Korong Granite.	Apatite	282±12	-	282±11	-
Mt. Painter Amphibolite dike.	Sphene	497±18[6]	353±16[6]	354±16[6]	-

[1]All ages in m.y. ± 1σ, $\lambda f = 6.9 \times 10^{-17}$ yr^{-1}, Neutron dosimetry = NBS Cu values via SRM962. PM = Population method, SM = subtraction method, EDM = external detector method. Apatites etched in 5N HNO_3, zircons in eutectic NaOH:KOH, sphenes in 50N NaOH, unless otherwise indicated.

[2]Independent ages from Zartman and others, (1967) and Steven and others, (1967).

[3]Only low V_G grains counted. All other PM determinations used a random selection of grains.

[4]100N NaOH etchant.

[5]H_2SO_4 : HF etchant.

[6]1HF : 2HNO_3 : 3HCl : 6H_2O etchant.

faces with very low V_G, identified by the presence of sharp polishing scratches after etching, have a high etching efficiency approaching 100 percent. Second, even on these low V_G surfaces, tracks lying in certain orientations are only poorly revealed during normal etching and the track density is likely to be underestimated. The disparity between the strongly and weakly etched tracks in a fresh sphene is markedly decreased as the level of α-damage increases and the etching behaviour becomes more isotropic. Zircon and probably other U-bearing minerals show behaviour similar to sphene. These observations have important implications for the various different fission-track dating methods investigated here.

Most fission-track dating methods are variants of the techniques commonly described as the 'population method' (PM) and the 'external detector method' (EDM). PM ages are obtained by measuring the average spontaneous-track density (ρ_s) over a large number of mineral grains and comparing this with the average induced-track density (ρ_i) in a second set of the mineral grains. This second set of grains is annealed prior to neutron irradiation to remove spontaneous tracks so that the induced tracks can be counted alone. An alternative approach, which may be called the 'subtraction method' (SM), is to leave out the annealing step so that the second set of grains record both spontaneous and induced tracks from which ρ_i is obtained by subtraction of ρ_s.

In the external detector method ρ_s is measured in the mineral grains themselves and ρ_i is measured in an adjacent mica track detector. With this technique only grains with low V_G (sharp polishing scratches) must be counted, as others have a low etching efficiency compared to that of the mica. Also, the track density ratio must be corrected for the different track registration geometries of the spontaneous (4π) and induced (2π) tracks. The ideal value of the geometry factor is 0.5 (i.e., $2\pi/4\pi$) and this has been confirmed experimentally by Gleadow and Lovering (1977).

Results obtained by these three different fission-track dating methods are summarized in table 1 for apatite, sphene, and zircon from five different rocks. Mean K-Ar ages are also shown for two of the rocks.

On table 1 the following observations can be made:

1. Results obtained by the SM and EDM are concordant with each other in every case and also with the independent K-Ar ages, where these are available.

2. For apatites the PM results are also concordant with those from other methods.

3. For sphene and zircon the PM ages are too high by as much as 50 percent, compared with other methods and independent ages. This is explained by the modified etching properties in the annealed mineral grains used to record induced tracks. The thermal annealing produces two important changes which are relevant here. First, the etching rate is reduced so that in a PM determination induced tracks may be under-etched relative to the spontaneous tracks. Second, the induced tracks etch anisotropically so that a fraction of them are only weakly revealed, if at all, during etching, again leading to an underestimate of ρ_i.

4. PM measurements on two spheres (Magnet Cove and Fish Canyon) were made by counting only low V_G grains. These are much closer to the other ages but are still too high.

These findings suggest that the following two alternative approaches may improve the performance of the population method: prolonged etching of the induced tracks and pre-annealing of the α-damage associated with ρ_s at a temperature just below that required for track fading. These proposals were tested using two series of PM measurements on the Mt. Painter sphene. In the first, the ρ_s and ρ_i grains were etched for progressively longer times and the apparent age calculated after each step. This is essentially the procedure proposed by Reimer (1974) for a different situation where the spontaneous track etching is impaired by partial annealing. In the second series, the ρ_s and ρ_i pairs were annealed together at various temperatures for 1 hour before proceeding with a PM measurement on each pair. This is essentially the plateau annealing method (PAM) of Storzer and Poupeau (1973), again originally proposed as a correction procedure for partial annealing. The results of these measurements are shown in figure 1, together with SM and EDM results for comparison.

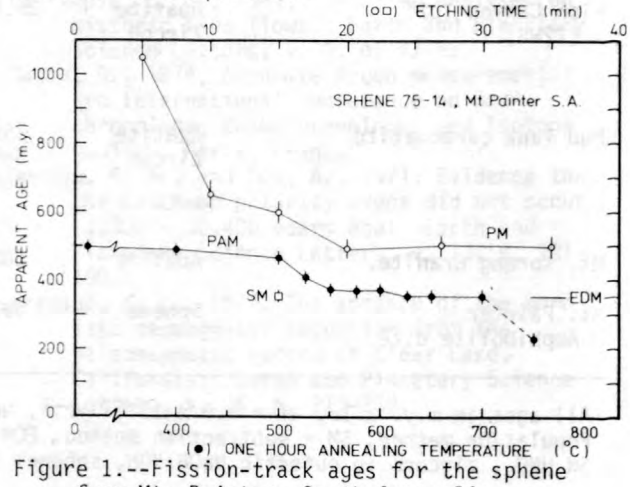

Figure 1.--Fission-track ages for the sphene from Mt. Painter, South Australia, obtained by the population method (PM) with increasing etching time and by the plateau annealing method (PAM). Ages determined by the external detector (EDM) and subtraction methods (SM) are also shown for comparison.

It is obvious from figure 1 that with continued etching the PM results reach a low plateau value which is still aberrantly high com-

pared to the SM and EDM results. Thus, the principal reason for the high PM ages must be the anisotropic etching of the induced tracks rather than their reduced etching rate relative to spontaneous tracks. On the other hand, the ages obtained after pre-annealing do reach a high-temperature plateau closely concordant with the SM and EDM ages. The low age for the 750°C step is not regarded as reliable because the track densities had been reduced to only about 10 percent of their former values. The plateau age obtained after removal of the α-damage by annealing strongly supports the above explanation for the high PM ages.

The consistent agreement of apatite PM ages with the ages from other methods requires some explanation, since this is not observed with the other minerals. This behaviour indicates that the etching properties of apatite are not significantly modified by α-damage. The suggested reason for this is that α-damage is not stable in apatite over long periods of time, even at ambient surface temperatures, and therefore does not accumulate.

The principal conclusion of this study is that the population method is inappropriate for sphene, zircon, and probably other minerals, with the notable exception of apatite, for which any of the methods discussed here seem satisfactory. The external detector method and subtraction method give reliable results in most cases. The EDM is usually more convenient although it will probably underestimate the age when ρ_s is very low ($< 5 \times 10^5$ cm^{-2}). Only in such cases of low ρ_s, and hence little radiation damage, might the PM be applicable to sphene and zircon.

Gleadow, A. J. W., 1978, Anisotropic and variable track etching characteristics in natural sphenes: Nuclear Track Detecting, v. 2, in press.

Gleadow, A. J. W. and Lovering, J. F., 1977, Geometry factor for external detectors in fission track dating: Nuclear Track Detecting, v. 1, p. 99-106.

Reimer, G. M., 1974, Effects of progressive etching on fission track ages: Transactions American Nuclear Society, v. 18, p. 87.

Steven, T. A., Mehnert, H. H., and Obradovich, J. D., 1967, Age of volcanic activity in the San Juan Mountains, Colorado: U.S. Geological Survey Professional Paper 575-D, p. D47-D55.

Storzer, D. and Poupeau, G., 1973, Ages-plateaux de mineraux et verres par la methode des traces de fission: Comptes rendus Academy Science, Paris, v. 276, p. 137-139.

Zartman, M. E., Brock, M. R., Heyl, A. V., and Thomas, H. H., 1967, K-Ar and Rb-Sr ages of some alkalic intrusive rocks from central and eastern United States: American Journal of Science, v. 265, p. 848-870.

FISSION-TRACK EVIDENCE FOR THE EVOLUTION OF RIFTED CONTINENTAL MARGINS

By A. J. W. Gleadow
School of Earth Sciences
University of Melbourne, Melbourne, Australia

Gleadow and Lovering (1978) have suggested that Mesozoic apatite fission-track ages in Precambrian and Palaeozoic granites from King Island in Southeastern Australia relate directly to a period of accelerated uplift and erosion during continental breakup between Australia and Antarctica. To test whether this relationship between apatite ages and continental rifting is a widespread phenomenon, results are presented here for two other areas adjacent to rifted continental margins. These are the Godthaab area of West Greenland and Ireland, both in the North Atlantic region.

The rocks from West Greenland belong to the Archaean Amitsoq (samples numbered 155XXX) and Nûk gneisses which were formed about 3700 and 3050 m.y. ago, respectively, according to Rb-Sr whole-rock evidence (Moorbath and others, 1972). Fission-track ages for four different minerals are given in table 1 and the distribution of apatite ages is shown in figure 1.

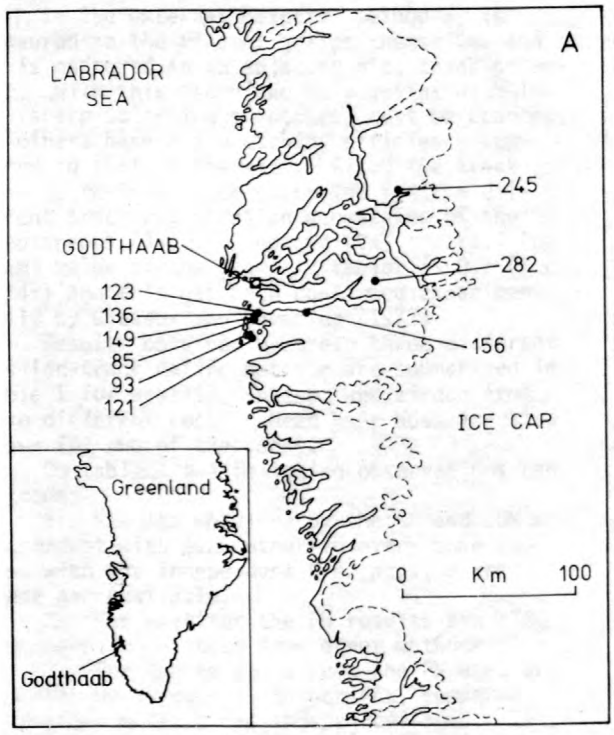

Figure 1.--Distribution of apatite fission-track ages in West Greenland. Location numbers refer to apatite ages on table 1.

The sphene, zircon, and allanite ages all occur in the relatively narrow range of 1085 ± 95 m.y. This is substantially younger than the last metamorphic event (1600 m.y.) recorded in these rocks by Rb-Sr mica ages (Pankhurst and others, 1973, Baadsgaard and others, 1976). It appears that under the extremely slow cooling conditions encountered in these rocks the effective annealing temperatures for sphene, zircon, and allanite are similar to each other though significantly lower than the Rb-Sr biotite-blocking temperature. The significance of these fission-track ages is not clear but it is possible that they reflect a mild uplift event in this area, associated with the 1200 to 1000 m.y. Gadar activity to the south. Apatite ages are all very much younger, ranging down to Late Cretaceous, and figure 1 shows that they increase inland away from the coast.

Results for sphene and apatite from various Caledonian granitic intrusions in Ireland are shown in table 2. The rocks studied occur in three groups around the periphery of the Irish landmass, the first five samples in table 2 being from the various intrusions of the Donegal granite complex. Scattered K-Ar and Rb-Sr mineral ages for the Irish Caledonian granites are virtually all in the range of from 370 to 400 m.y. showing a close correspondence to the sphene ages in table 2. Once again, the apatite ages are substantially younger, ranging in age from 214 m.y. (Late Triassic) to 128 m.y. (Early Cretaceous).

Table 1.--Fission-track ages (m.y.) of Archaean gneisses, West Greenland

Sample No.	Apatite	Other minerals[1]
155704	149±8	Z 1178±64
155711	-	Z 1112±60
155715	85±4	S 1066±51
155720	123±6, 136±7	Z 990±58
155734	-	Z 1060±54
155736	121±6	-
155737	93±5	-
155758	156±8	-
155819	-	S 1101±107, A 1088±114
131502	245±11	-
JHA204331	282±16	-

[1]Z = zircon, S = sphene, A = allanite, $\lambda_f = 6.9 \times 10^{-17}$ yr^{-1}

Table 2.--Fission-track ages (m.y.) in granitic rocks from Ireland

Sample No.	Intrusion	Sphene	Apatite
AG 7526	Thorr	377±18	197±13
AG 7527	"	372±18	183±14
AG 7529	Rosses	-	199±11
AG 7530	Trewenagh	-	187±13
AG 7534	Andara	-	181±20
AG 7535	Corvock	-	128±10
AG 7536	Inish	-	181± 9
AG 7538	Roundtone	394±21	155±10
AG 7539	"	378±26	155±10
AG 7541	Galwey	378±20	178±11
AG 7542	Omey	-	173± 9
AG 7543	Leinster	-	199±10
AG 7544	"	-	214±14

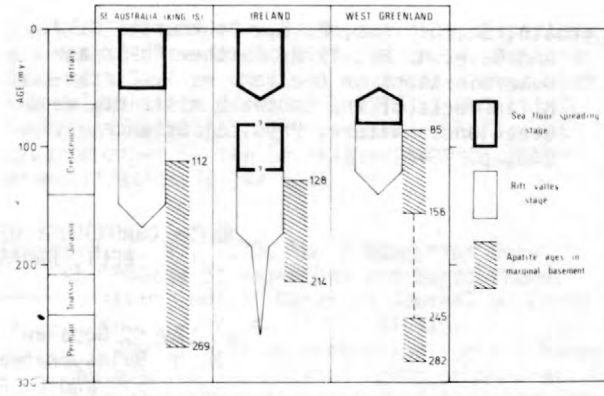

Figure 2.--Comparison of the history of continental breakup with apatite fission-track ages for three rifted continental margins.

The general sequence of events in the evolution of rifted continental margins is now well established, although many variations are known to occur. In the first, or rift valley, stage domal uplift and extensional faulting of the continental crust is thought to occur accompanied by volcanism, dyke injection, and formation of a central graben. Rapid erosion of the uplifted areas occurs with associated deposition of non-marine sediments. In the second stage sea-floor spreading begins and extensional faulting ceases. Sedimentation becomes marine and extensive subsidence of the continental margins occurs. These generalized stages of rifted-margin development are summarized in figure 2 for the two areas reported here, together with comparative data from Southeastern Australia.

All three areas shown in figure 2 have developed at the rift-valley stage for many tens of millions of years prior to the onset of sea-floor spreading. The North Atlantic region has had a particularly complex evolution. The earliest precursors of rift development in this area probably include troughs of Permian and Triassic sedimentation but the main rifting stage began in the Middle Jurassic. The earliest sea-floor spreading occurred in the Rockall Trough to the west of Ireland in the Early Cretaceous, followed by opening of the Bay of Biscay to the south in Middle to Late Cretaceous times. Subsequent spreading occurred for a limited period (80 to 60 m.y.) in the Labrador Sea between Greenland and North America before the main phase of spreading between Greenland and northern Europe began in the early Tertiary.

As shown in figure 2, there is a clear association of the younger apatite ages with the rift-valley stage of continental-margin development in all three areas. The older, apatite ages are probably mixed ages containing some tracks which predate the period of continental breakup. Several lines of evidence show that this association is not fortuitous. First, apatite ages in tectonically undisturbed areas remote from rifted margins are much greater than those found near the margins. For example, Precambrian rocks from the Australian interior have apatite ages of around 500 m.y. (Errey and Gleadow, unpublished data) compared to only 110 to 270 m.y. for King Island. Second, in West Greenland apatite ages progressively increase inland from the coast as predicted for a rifted margin by Gleadow and Lovering (1978). Ireland and King Island are more complex, as they are surrounded by areas of subsidence on all sides. Third, there is no observable relationship between the apatite ages and other fission-track or independent ages for the same areas. This argues against any explanation of the apatite age patterns by simple slow cooling following the last metamorphic or intrusive event.

The results of this study strongly support the proposed relationship between apatite ages in marginal basement rocks and the processes of continental rifting. Detailed studies of the distribution of apatite ages in critical areas should provide important new information on the erosional and tectonic history of rifted margins and enable alternative models for the mechanism of continental breakup to be tested.

Baadsgaard, H., Lambert, R. St. J., and Krupicka, J., 1976, Mineral isotopic age relationships in the polymetamorphic Amîtsoq gneisses, Godthaab District, West Greenland: Geochimica Cosmochima Acta, v. 40, p. 513-527.

Gleadow, A. J. W. and Lovering, J. F., 1978, Fission track geochronology of King Island, Bass Strait, Australia: relationship to continental rifting: Earth and Planetary Science Letters, v. 37, p. 429-437.

Moorbath, S., O'Nions, R. K., Pankhurst, R. J., and Gale, N. H., 1972, Further Rb-Sr age determinations on the very early Precambrian rocks of the Godthaab district, West Greenland: Nature, Physical Science, v. 240, p. 78-81.

Pankhurst, R. J., Moorbath, S., Rex, D. C., and Turner, G., 1973, Mineral age patterns in ca.3700 m.y. old rocks from West Greenland: Earth and Planetary Science Letters, v. 20, p. 157-170.

Rb-Sr CHRONOLOGY OF THE KHETRI COPPER BELT, RAJASTHAN, INDIA

By K. Gopalan[1], J. R. Trivedi[1], M. N. Balasubrahmanyan[2], S. K. Ray[2], and C. A. Sastry[2]
[1]Physical Research Laboratory
Ahmedabad, India
[2]Geological Survey of India
Calcutta, India

The Khetri copper belt is a northeast-trending linear metallogenic province in northern Rajasthan, India (Roy Choudhury and Das Gupta, 1965; Das Gupta, 1968). Only the Precambrian Delhi Group of rocks comprising the older Alwar Formation and the younger Ajabgarh Formation are exposed in the belt. These rocks have been folded into a series of vertical to steeply dipping, high-amplitude folds (F_1-folds) that trend north-northeast to south-southwest. An axial-plane foliation developed concurrent with this folding. Axial planes and limbs of the F_1-folds have been refolded coaxially into vertical and tight F_2-folds. The F_1- and F_2-folds show axial culminations and depressions because of superposition of a set of open round-hinged vertical folds (F_3-folds). Trends of the earlier folds show little variation because of the vertical nature of the F_3-folds and their high-angle relation with the F_1-F_2 fold axes (Ray, 1974; 1976).

Individual granitic bodies in the Khetri belt vary greatly in size but do not reach batholithic dimensions. All these granitic plutons have been referred to by earlier workers as intrusive within the Delhi metasediments and have been correlated with the Erinpura suite of granitic intrusives exposed in the type locality of southern Rajasthan (Pascoe, 1965). Das Gupta (1968) assigned a post-Delhi age to these granites, without specifically correlating them with the Erinpura granites.

Preliminary Rb-Sr analyses have been carried out on four whole-rock samples from two different granitic plutons--the Udaipur granite and the Saladipura granite. Analytical results for these four rocks and biotite-separates from three of them are shown in table 1. The whole-rock samples define a satisfactory isochron (fig. 1) corresponding to an age of 1480 ± 40 m.y. (λ = 1.39 X 10^{-11} yr^{-1}) and an initial Sr composition of 0.7131 ± .006. The two biotites from samples SRD-18 and SRD-14 give a concordant younger age of about 700 m.y., while the biotite from sample SRD-13 gives an even younger age of 550 m.y. Rb-Sr chronology is shown in figure 1.

Table 1.--Analytical results of samples from the Udaipur granite and the Saladipura granite, India

Sample No.	^{87}Rb (ppm)	^{86}Sr (ppm)	$^{87}Rb/^{86}Sr$	$^{87}Sr/^{86}Sr$
SRD-18-WR	71.53	9.98	7.08	0.8580±.002
SRD-18-BIO	268.9	.77	342.9	4.259 ±.006
SRD-14-WRA	29.41	2.97	9.79	.9204±.002
SRD-14-BIO	140.90	1.03	135.2	2.134 ±.004
SRD-13-WR	85.41	2.52	33.5	1.397 ±.003
SRD-13-BIO	451.4	2.14	208.5	2.745 ±.004
SRD-12-WR	66.80	3.33	19.83	1.133 ±.003

The whole-rock age of 1490 m.y. is interpreted as the emplacement time of this suite of rocks and, therefore, its correlation with the Erinpura granites, as suggested by earlier workers, is not tenable. The latter has been dated

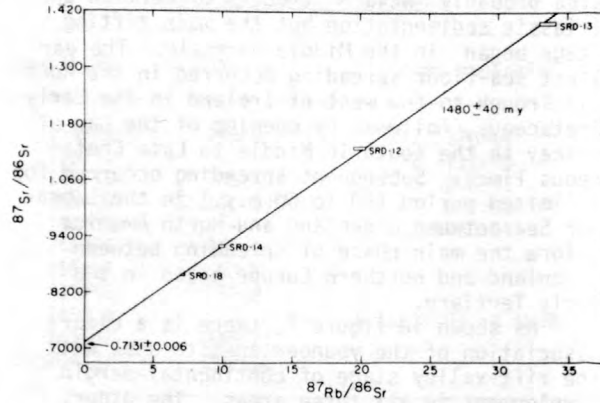

Figure 1.--Rb-Sr chronology of the Khetri copper belt, Rajasthan, India.

at 735 m.y. (Crawford, 1975). It may be significant that the Khetri granites have almost the same age as the nearby nepheline syenites of Kishangarh and associated pegmatites (Crawford, 1970).

The occurrence of the Khetri granites in well-defined structural locales, and their complete structural conformity with the surrounding Delhi metasediments, indicate their intrusive relationship to the Dehli rocks. This implies that the age of the Delhi rocks is older than 1500 m.y. Such an old age for the Delhi rocks has not been proved, but has been inferred by Crawford (1970), based on the 1660 m.y. age of intrusion of Bairat granite into the Alwar series of Delhi rocks south of the Khetri belt.

The younger ages obtained on biotites indicate re-equilibration of strontium isotopes subsequent to their emplacement, presumably during a thermal metamorphism. However, the discordance, even among the three mineral ages, precludes an unambiguous determination of the time of this secondary event. Considering that the two biotites from samples SRD-18 and SRD-14 are nearly concordant in age at 700 m.y., despite wide difference in their radiogenic strongium contents and the fact that the discordant biotite from sample SRD-13 could have been disturbed because of its proximity to a dolorite dike and two major fault zones, the time of the metamorphic resetting is probably close to 700 m.y. This interpretation is supported by the K-Ar ages of 643 and 621 m.y. for phillite and biotite, respectively, from Alwar schists in the belt (Sarkar and others, 1964).

This metamorphic event recorded by the Khetri granites at about 700 m.y. appears to be significant because granites of nearly the same age occur extensively in the Precambrian tracts of Rajasthan. The Malani rhyolites and the associated high-level peralkaline granites of Siwana and Jalor in northwestern Rajasthan have been dated at 745 m.y. (Crawford and Compston, 1970). The granite massifs of Mount Abu west of the Aravalli Mountains and the Idar granites at the southern end of these mountains have also been shown to be contemporaneous with the Malani suite (Crawford, 1975). While this event was geographically widespread, it is not clear whether it can be related to the copper mineralization in the belt.

Crawford, A. R., 1970, The Precambrian geochronology of Rajasthan and Bundelkhand, northern India: Canadian Journal of Earth Science, v. 7, no. 1, p. 91-110.

_____ 1975, Rb-Sr determination for the Mount Abu granite and related rocks of Gujarat: Journal Geological Society of India, v. 16, no. 1, p. 20-28.

Crawford, A. R., and Compston, W., 1970, The age of the Vindhyan System of peninsular India: Quarterly Journal Geological Society of Longon, v. 125, p. 351-372.

Das Gupta, S. P., 1968, The structural history of the Khetri cooper belt, Rajasthan: Geological Survey of India Memoirs, v. 83, p. 110.

Pascoe, E. H., 1965, A manual of geology of India and Burma, Vol. 1: Delhi Geological Survey of India, p. 485.

Ray, S. K., 1974, Structural history of the Saladipura pyrite-pyrrhotite deposit and associated rocks, Khetri copper belt, Rajasthan: Geological Society of India Journal, v. 15, no. 3, p. 227-238.

_____ 1976, Tectonic styles in the Delhi Group of rocks, western India: Miscellaneous Publications Geological Survey India v. 31, pt. 1, p. 239-246.

Roy Choudhury, M. K., and Das Gupta, S. P., 1965, Ore localization in the Khetri copper belt, Rajasthan, India: Economic Geology, v. 60, no. 1, p. 68-88.

Sarkar, S. N., Polkanov, A. A., Gerling, E. K., and Chukrov, F. V., 1964, Geochronology of the Precambrian of peninsular India--a synopsis: Science and Culture, v. 30, p. 527-537.

Rb-Sr AGE OF GODHRA AND RELATED GRANITES, GUJARAT, INDIA

By K. Gopalan[1], J. R. Trivedi[1], S. S. Merh[2], P. P. Patel[2], and S. G. Patel[2]

[1]Physical Research Laboratory, Ahmedabad, India

[2]Department of Geology, M. S. University Baroda, India

The Precambrian rocks exposed in Gujarat State, India, consist of metasediments, gneisses, and granites. These rocks are supposed to be the southern extension of the Precambrian rocks of Rajasthan State to the north. The geological sequence established in the area is therefore analogous to the well documented sequence of rock formations in

Rajasthan (Middlemiss, 1921; Hobson, 1926; Heron, 1953; and Gupta and Mukherjee, 1938). Aravalli metasediments of Rajasthan extend over a wide area in central Gujarat. Another geographically separate metasedimentary series in central Gujarat, called the Champaner Series, has been correlated with the Aravalli System of Rajasthan (Heron, 1953). However, the post-depositional deformation history of these two rock series appears to be different. While the Champaner Series shows a single prominent east-west folding, the Aravalli metasediments carry the imprints of at least two episodes of folding superposed on each other (Merh and Patel, 1968; Naha and Halyburton, 1974).

The metasedimentary rocks are intruded by masses of Precambrian granites. These granites have been subdivided into at least two age groups by previous workers, although there has not been complete agreement in the identity of these age groups. Those occurring in association with the Champaner Series in the areas south of Baria (Panchmahals) and around Chota-Udaipur are supposed to be intrusive into the Champaner and of post-Champaner and pre-Delhi age (Hobson, 1926), whereas the granites around Godhra in central Gujarat have been correlated with the post-Delhi Erinpura granite exposed in the axial zone of the Aravalli Mountains in western Rajasthan (Heron and Ghosh, 1938). Crawford (1975) showed that the Mount Abu-Idar suite of the so-called Erinpura granites and the Malani Rhyolites with the associated granites of Siwana and Jalor in northwest Rajasthan are essentially contemporaneous at 735 m.y. He also postulated that all granites of Gujarat, including those around Godhra, are of this age.

Considering the differing deformation history of the metasediments in Rajasthan and Gujarat and the well-established occurrences of intrusive rocks with distinctly different ages in the Rajasthan Precambrian (Crawford, 1970), the granites of central Gujarat need to be dated separately. Sixteen granite samples from locations around Godhra, Baria, and Chota-Udaipur have been analyzed for Rb and Sr isotopic abundances. The analytical data for these samples, including five biotite separates, are given in table 1.

The samples show only moderate amounts of radiogenic strontium and conform within experimental error to a single isochron (fig. 1) corresponding to an age of 955 ± 20 m.y. (λ = 1.39 x 10^{-11} yr^{-1}) and initial Sr composition of 0.7130 ± .001. The small scatter of some of the data points may be due to incipient weathering effects. All the five biotites are concordant within experimental error at about 900 m.y. This is not significantly different from the whole-rock age and shows that this granite suite has not been thermally disturbed by events subsequent to its emplacement 950 m.y. ago.

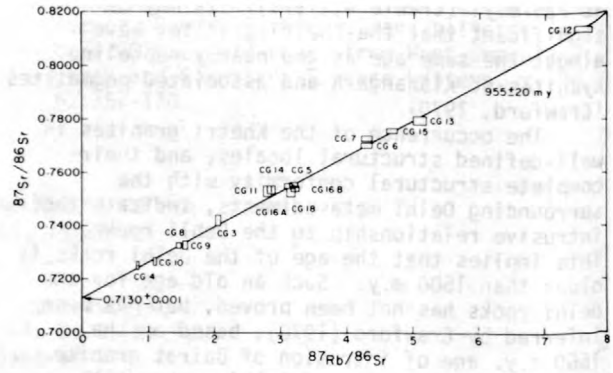

Figure 1.--Rb-Sr age of Godhra and related granites, Gujarat, India.

The main conclusion from the present data is that Crawford's (1975) correlation of the Malani-Mount Abu-Idar suite with granites of central Gujarat is not valid. The former suite has a distinctly younger age of 735 m.y. It may be significant that the 950 m.y. age is within the range of ages measured for Ajmer (935 m.y.), Untala (955 m.y.), and Chhapoli (1010 m.y.) granites in northern Rajasthan (Crawford, 1970). While the Godhra granites are definitely of post-Delhi age, the associated gneisses may be older--being either pre-Delhi or pre-Aravalli. But the single analysis of a schist in the Champaner Series (Craw-

Table 1.--Analytical results

Sample No.	^{87}Rb (ppm)	^{86}Sr (ppm)	$^{87}Rb/^{86}Sr$	$^{87}Sr/^{86}Sr$
CG-3-WR	57.58	27.61	2.06	.7421±.0015
CG-4-WR	45.28	53.32	0.84	.7251±.0015
CG-4-BIO	158.5	7.30	21.45	.9808±.002
CG-5-WR	58.40	18.05	3.20	.7556±.001
CG-5-BIO	231.1	5.03	45.42	1.283 ±.002
CG-6-WR	63.65	14.65	4.29	.7707±.001
CG-7-WR	62.10	14.27	4.30	.7730±.0015
CG-8-WR	54.24	36.69	1.46	.7327±.0015
CG-8-BIO	234.7	2.75	84.36	1.756 ±.002
CG-9-WR	53.24	36.75	1.55	.7325±.002
CG-10-WR	58.01	52.50	1.09	.7265±.0015
CG-11-WR	50.50	17.69	2.82	.7529±.002
CG-12-WR	81.07	10.56	7.59	.8144±.0015
CG-13-WR	67.82	13.12	5.11	.7800±.0015
CG-14-WR	67.75	21.41	3.13	.7551±.0010
CG-15-WR	65.79	13.89	4.68	.7757±.0015
CG-16A-WR	60.05	20.76	2.86	.7534±.002
CG-16A-BIO	204.3	1.12	180.30	2.928 ±.004
CG-16B-WR	57.49	17.63	3.22	.7537±.0015
CG-18-WR	69.39	21.66	3.17	.7524±.0015
CG-18-BIO	257.90	0.571	446.2	6.370 ±.004

ford, 1975) gives an age of about 950 m.y., and hence suggests the possibility that all or part of the Champaner Series rocks have been metamorphosed since their deposition at about the same time the granites were intruded. The present data is not sufficient to test the hypothesis that the granites of central Gujarat are products of palingenetic mobilization of the pre-Champaner basement (Merh, 1975).

Crawford, A. R., 1970, The Precambrian geochronology of Rajasthan and Bundelkhand, northern India: Canadian Journal of Earth Science, v. 7, no. 1, p. 91-110.

_____1975, Rb-Sr age determinations for the Mount Abu granite and related rocks of Gujarat: Journal of the Geological Society of India, v. 16, no. 1, p. 20-28.

Gupta, B. C., and Mukherjee, P. N., 1938, The geology of Gujarat and Southern Rajputana: Geological Survey of India Records, v. 73, p. 163-208.

Heron, A. M., 1953, The geology of central Rajputana: Geological Survey of India Memoirs, v. 79, p. 389.

Heron, A. M., and Ghosh, P. K. 1938, The geology of Palanpur, Danta and parts of Idar State: Geological Survey of India Records, v. 72, p. 367-412.

Hobson, G. V., 1926, The metamorphic rocks and intrusive granite of Chhotaudepur State: Geological Survey of India Records, v. 59, p. 340-357.

Merh, S. S., 1975, Some problems connected with Precambrian geology of central and north Gujarat: Seminar on the recent advances in Precambrian geology of Rajasthan, Udaipur.

Merh, S. S., and Patel, M. P., 1968, On the nature of the Aravalli rocks of Bhiloda-Shemlaji area of Sabarkantha district: Abstracts of the Indian Science Congress, Varanasi.

Middlemiss, C. S., 1921, The geology of Idar State: Geological Survey of India Memoirs, v. 44, p. 115-147.

Naha, K., and Halyburton, R. V., 1974, Precambrian stratigraphy of central and southern Rajasthan: Precambrian Research, v. 1, no. 1, p. 55-73.

Rb-Sr GEOCHRONOLOGY OF PRECAMBRIAN ROCKS OF THE OVRUCH BURIED MOUNTAIN RANGE, NORTHWEST UKRAINE

By Igor M. Gorokhov, Elvina S. Varshavskaya, and Eduard P. Kutyavin
Institute of Precambrian Geology and Geochronology,
Leningrad, USSR

The youngest Precambrian terrains of the Ukrainian Shield are exposed on its northwest margin, within the Ovruch buried mountain range (fig. 1). Recently, the succession and relationships of these terrains were recognized by a geological survey and by extensive drilling (table 1).

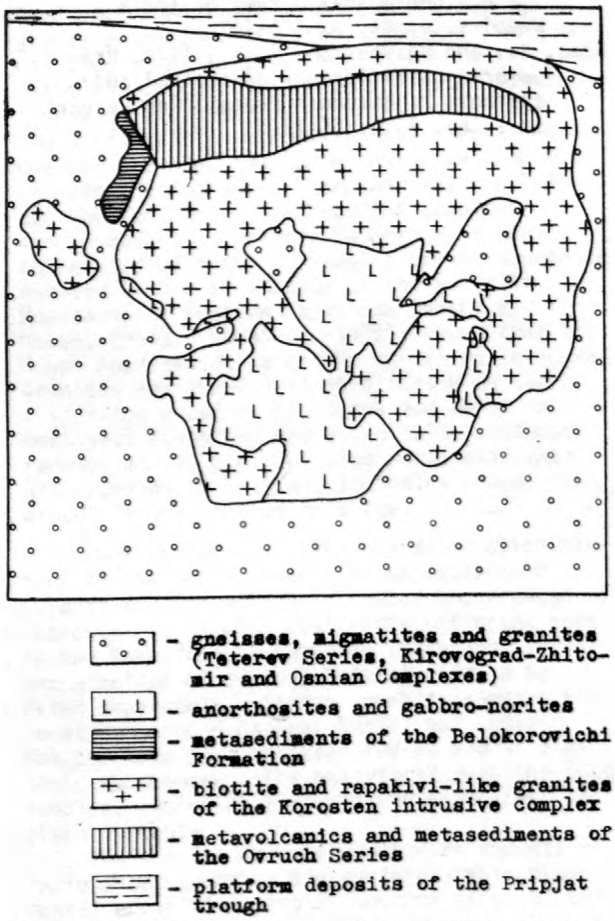

Figure 1.--Simplified geologic map of the Ovruch buried mountain range.

The crystalline basement of the region consists of granites of the Kirovograd-Zhitomir Complex, which intrude gneisses of the Teterev Series and are cut in turn by gabbro-diabase dikes of the Osnian Complex. The basement rocks are unconformably overlain by supercrustal rocks of the Pugachevian Series intersected by granite veins which Lunko and others (1971) considered as belonging to the Korosten Complex. The Korosten granites underlie the Ovruch Series (Drannik and Bogatskaya, 1967) composed mainly of sandstones and acid volcanics. The supercrustal rocks of the Ovruch buried mountain range have been metamorphosed up to greenschist facies (Usenko and others, 1971).

Table 1.--Stratigraphic succession of the Precambrian rocks of the Ovruch buried mountain range (from Drannik and Bogatskaya, 1967)

Series	Formation	Rock type
Ovruch	Tolkachevian	Quartzite-like sandstones, pyrophyllitic slates.
	Zbranki	Sandstones, slates, diabases, quartz-porphyries.
Unconformity		
The Korosten intrusive complex		
Pugachevian	Ozeryany	Metasediments, diabase-porphyrites.
	Belokorovichi	Metasediments, conglomerates, diabases.
Unconformity		
Osnian Complex		

Rb-Sr total-rock analyses were made on metasedimentary rocks of the Belokorovichi Formation (Pugachevian Series) and the Zbranki Formation (Ovruch Series) using samples of about 5 kg. The analysed samples of sericite-quartz schists of the Belokorovichi Formation are composed of fine-flake sericite with minor amounts of chlorite, clay minerals, and lepidocrocite. Grains of quartz have both angular and rounded form. Table 2 lists the analytical data, and Rb-Sr evolution diagram is shown in figure 2. Parameters of the linear regression agree with Model 3 of McIntyre and others (1966). The slope of the errorchron corresponds to an age of 1585 ± 35 m.y. ($\lambda = 1.42 \cdot 10^{-11} yr^{-1}$) with an $^{87}Sr/^{86}Sr$ initial ratio of 0.724 ± 0.011. The uncertainties quoted are the standard deviations (1σ).

Table 2.--Rubidium-strontium data

Sample No.	Rb (ppm)	Sr (total) (ppm)	$^{87}Rb/^{86}Sr$	$^{87}Sr/^{86}Sr$
Metasediments of the Pugachevian Series (the Belokorovichi Formation)				
25-UB	219	37.7	17.46	1.1143
26-UB	223	23.5	29.22	1.3910
27-UB	230	32.4	21.58	1.2206
36-UB	209	48.0	12.95	1.0281
38-UB	266	26.9	30.60	1.4235
39-UB	179	34.9	15.41	1.0671
Metasediments of the Ovruch Series (Zbranki Formation)				
28-UZ	221	87.5	7.435	0.8769
31-UZ	276	127	6.407	0.8567
32-UZ	214	163	3.844	0.8049
34-UZ	226	151	4.378	0.8174

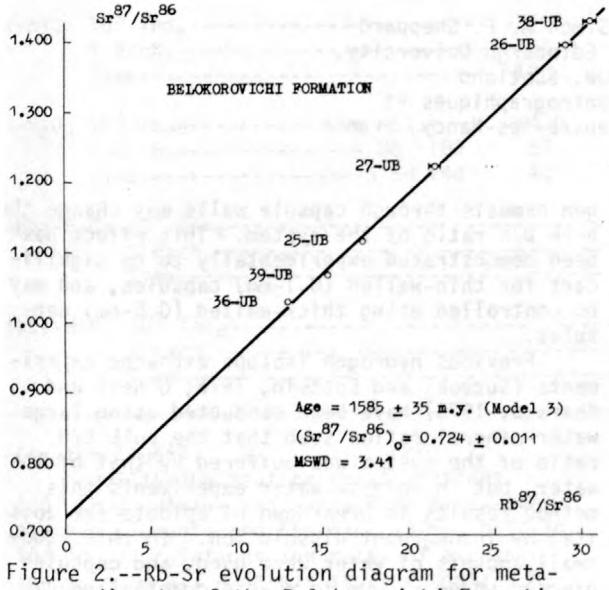

Figure 2.--Rb-Sr evolution diagram for metasediments of the Belokorovichi Formation. Model 3 of McIntyre and others (1966).

The analyzed samples of black phyllite-like slates of the Zbranki Formation are composed of fine clay minerals, among which accumulations of sericite flakes and angular grains of quartz occur. The results are presented in table 2 and plotted on a Rb-Sr evolution diagram (fig. 3). The slope of the isochron (Model 1 of McIntyre and others, 1966) corresponds to an age of 1385 ± 55 m.y. with an $^{87}Sr/^{86}Sr$ initial ratio of 0.729 ± 0.005.

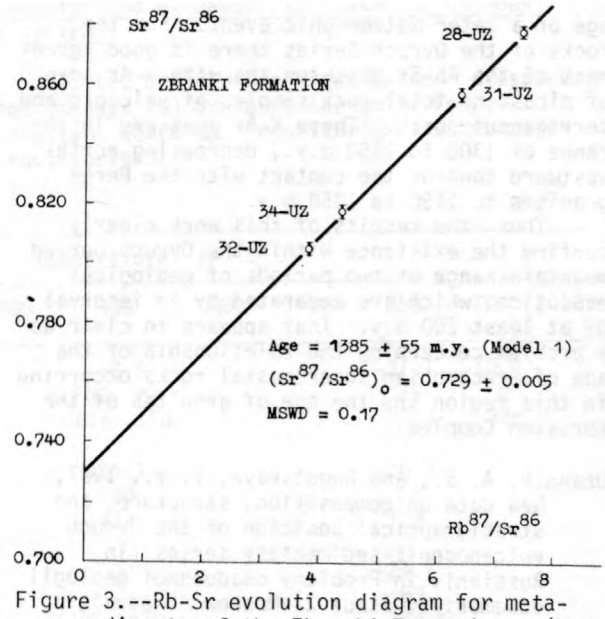

Figure 3.--Rb-Sr evolution diagram for metasediments of the Zbranki Formation. (Model 1 of McIntyre and others (1966).

The age of the schists of the Belokorovichi Formation, 1585 ± 35 m.y., does not exceed the value of 1680 ± 12 m.y. obtained by the Rb-Sr total-rock method for rapakivi-like and biotite granites of the Korosten Complex (Gorokhov, 1964). The latter value agrees with formerly published Rb-Sr and K-Ar ages of micas and individual $^{207}Pb/^{206}PB$ ages of zircons for the Korosten granites.

It follows from the age comparison of the granites and of the Belokorovichi schists intruded by these granites that one cannot consider the value of 1585 ± 35 m.y. as an age of sedimentation. It seems to correspond to the later greenschist facies metamorphic event. Migration of Rb and Sr, on a scale which was larger than the size of the samples analyzed, was earlier discovered at our laboratory for some metasedimentary rocks of the Baltic Shield progressively metamorphosed under similar conditions.

The published K-Ar results for the Belokorovichi Formation were obtained mainly on total-rock samples. In comparison with the time of the metamorphic event, all these values are too low, evidently due to the loss of Ar^{40} by some rock-forming minerals.

The Rb-Sr age of slates of the Ovruch Series is 1385 ± 55 m.y. An occurrence of pyrophyllitic slates, formed by metamorphism of kaolinite beds, among the rocks of this series allows us to estimate the temperature of the metamorphic transformation as 300 to 350°C. This temperature is certainly sufficient to produce Sr isotopic equilibration in water-rich sediments. Therefore, the value of 1385 ± 55 m.y., just like that for the rocks of the Pugachevian Series, does not correspond to the time of sedimentation of the Ovruch rocks, but gives the

age of a later metamorphic event. For the rocks of the Ovruch Series there is good agreement of the Rb-Sr isochron age with K-Ar ages of micas and total-rock samples of volcanic and terrigenous rocks. These K-Ar ages are in the range of 1300 to 1450 m.y., decreasing northwestward towards the contact with the Perga granites to 1150 to 1250 m.y.

Thus, the results of this work clearly confirm the existence within the Ovruch buried mountain range of two periods of geological evolution, which are separated by an interval of at least 200 m.y. That appears to clear up a problem concerning the relationship of the age of Precambrian supercrustal rocks occurring in this region and the age of granites of the Korosten Complex.

Drannik, A. S., and Bogatskaya, I. V., 1967, New data on composition, structure, and stratigraphical position of the Ovruch volcanogenic-sedimentary series [in Russian], in Problemy osadochnoi geologii dokembriya, issue 2, Moscow, "Nedra", p. 169-176.

Gorokhov, I. M., 1964, Rb-Sr total-rock age determination of the Korosten granites and the Dnieper migmatites and metabasites, the Ukraine [in Russian]: Geokhimiya, no. 8, p. 744-753.

Lunko, V. F., Drannik, A. S., Rolik, A. G., and Metalidi, S. V., 1971, The principal features of geological structure and metallogeny of the north-west part of the Ukrainian Shield [in Russian], in Voprosy petrologii i rudonosnosti kristallicheskogo fundamenta BSSR i smezhnykh regionov. Minsk, "Nauka i tekhnika", p. 286-313.

McIntrye, G. A., Brooks, C., Compston, W., and Turek, A., 1966, The statistical assessment of Rb-Sr isochrons: Journal of Geophysical Research, v. 71, no. 22, p. 5459-5468.

Usenko, I. S., Siroshtan, R. I., Shcherbakov, I. B., and Khmaruk, T. G., 1971, Metamorphism of the Ukrainian Shield [in Russian]: Geological Journal, v. 31, no. 2, p. 3-16.

EXPERIMENTAL STUDY OF HYDROGEN ISOTOPE FRACTIONATION IN THE SYSTEMS EPIDOTE-H_2O, ZOISITE-H_2O, AND AlO(OH)-H_2O

By Colin M. Graham[1] and Simon M. F. Sheppard[2]

[1]Department of Geology, Edinburgh University, Edinburgh EH9 3JW, Scotland

[2]Centre de Recherches Petrographiques et Geochemiques, 54500 Vandoeuvre-les-Nancy, France

The nature and origin of hydrothermal and metamorphic fluids involved in water-rock interactions are amenable to investigation through isotopic analysis of coexisting hydrous minerals if mineral-water hydrogen (and oxygen) isotope fractionation factors are known. Equilibrium hydrogen isotope fractionation factors and rates of exchange may only be reliably known from direct experimental investigation. Previous studies (Suzuoki and Epstein, 1976) have concentrated largely on the sheet silicates. In this study, hydrogen isotope fractionations between epidote-group minerals and water have been measured experimentally because (1) they are stable over a wide range of pressure and temperature; (2) they are widespread minerals in many metamorphic, hydrothermal, and geothermal systems; (3) they differ in structure from sheet silicates; (4) hydrogen isotope data on natural epidotes (for example, Heaton and Sheppard, 1977) suggest that epidote concentrates D relative to coexisting hydrous silicates. Boehmite and diaspore (AlO(OH)) have also been studied because they are possible structural analogs of the epidotes and their structures are well understood.

During high P-T isotope exchange experiments with mineral-water systems, preferential loss of ^1H relative to ^2D resulting from hydrogen osmosis through capsule walls may change the bulk D/H ratio of the system. This effect has been demonstrated experimentally to be significant for thin-walled (0.1-mm) capsules, and may be controlled using thick-walled (0.5-mm) capsules.

Previous hydrogen isotope exchange experiments (Suzuoki and Epstein, 1976; O'Neil and Kharaka, 1976) have been conducted using large water-mineral ratios such that the bulk D/H ratio of the system was buffered by that of the water, but in epidote-water experiments this method results in breakdown of epidote (or zoisite) by incongruent dissolution. In this study, small amounts of water were used, and capsules pierced under vacuum to enable quantiative extraction and analysis of the water. This method allows direct measurement of mineral-water fractionations, improves experimental control, and permits mass balance calculations as a check on analyses and on absence of hydrogen osmosis effects.

Results are presented in table 1. Equilibrium fractionations have been measured over the range 650°-1500°C, and equilibrium fractionations in partially exchanged systems interpolated using the method of Suzuoki and Epstein (1976) modified after Northrop and

Table 1.--Experimental hydrogen isotope fractionation and exchange rate data for hydrous mineral-water systems.

[Ep = epidote (Ps 29); Cz = clinozoisite (Ps 9); Zo = zoisite; Boehm = boehmite; Diasp = diaspore; M = molarity; % exch. = percent exchange; time in days (d) or hours (hr); $10^3 \ln\alpha_e$ = $1000 \ln\alpha_{mineral\text{-}water}$ at equilibrium $\approx \delta D_{mineral} - \delta D_{water}$, where α_e = equilibrium fractionation factor = $\frac{D/H \text{ mineral}}{D/H \text{ water}}$ at equilibrium.]

System	Temperature, in °C									
T°C	650	550	450	380	350	300	280	250	200	150
Ep-H_2O: $10^3 \ln\alpha_e$	-37.5	-36.6	-37.4		-33.4			-31.1	-10.1	
% exch.	100	100	100		100 82			76	30	
Time	4.5d	12hr-14d	12hr-14d		77d 15d			77d	37d	
Ep-1M NaCl: $10^3 \ln\alpha_e$		-37.1	-32.2		-29.1			-26.9		
% exch.		100	100		100			54		
Time		14d	9d		77d			15d		
Ep-4M NaCl: $10^3 \ln\alpha_e$		-34.5	-29.4					-24.7		
% exch.		100	100					63		
Time		14d	8d					25d		
Ep-1M $CaCl_2$: $10^3 \ln\alpha_e$		-34.5	-32.0		-26.9					
% exch.		100	100		100					
Time		14d	14d 28d		77d					
Cz-H_2O: $10^3 \ln\alpha_e$			-37.2			-37.8				
% exch.			100			60				
Time			12d			23d				
Zo-H_2O: $10^3 \ln\alpha_e$		-51.1	-64.0		-65.5		-77.0			
% exch.		86 100	87		65		35			
Time		3.5d 14d	4d		34d		38d			
Boehm-H_2O: $10^3 \ln\alpha_e$				-49.9			-53.5		-36.2	-37.4
% exch.				100			100		100	77
Time				26d			34d		48d	37d
Diasp-H_2O: $10^3 \ln\alpha_e$				-75						
% exch.				?						
Time				14d						

Clayton (1966).

Equilibrium isotope fractionations ($10^3 \ln\alpha_e$) differ radically from mica-water systems (Suzuoki and Epstein, 1976), both in $10^3 \ln\alpha_e/T$ relations and rates of exchange. Inasmuch as all minerals studied contain hydrogen-bonded hydrogen, these differences must reflect the primary control of the OH-structure on the isotope exchange properties.

The rate of isotope exchange in the system epidote-H_2O is orders of magnitude faster than in mica-H_2O systems, being complete within 12 hours at 450°C. While D/H data on natural epidotes suggest around 0 permil fractionation between epidote and water at 400 - 550°C (for example, Taylor and O'Neil, 1977; Graham and Sheppard, unpublished data), this study shows that the fractionation is essentially independent of temperature at around -35 permil except at temperatures below 250°C, where it changes towards 0 permil and exchange rates become extremely sluggish. Natural epidotes are likely to have acquired their measured δD values at temperatures of 200°C or less.

Hydrothermal, geothermal, and metamorphic fluids are commonly brines rich in dissolved salts, notably NaCl. At low temperatures, where aqueous salt solutions are more nearly ionic, epidote-brine (NaCl solution) fractionations differ from epidote-H_2O fractionations by 6 permil or more, according to the concentration (and species) of dissolved salts.

The similarity of clinozoisite-H_2O and epidote-H_2O fractionations indicates that Fe^{3+}-Al^{3+} substitution on the epidote M(3)

site does not measurably influence the hydrogen isotope exchange properties.

Zoisite-H_2O fractionations are temperature-dependent and become more negative with decreasing temperature, similar to mica-H_2O fractionation. Rates of exchange are significantly slower than between epidote and water.

The differences between the exchange properties of zoisite and epidote-clinzoisite can largely be accounted for in terms of the degree of symmetry of their O-H---O hydrogen bond, using boehmite and diaspore as structural analogues. Boehmite, with a symmetrical, linear hydrogen bond (Stegmann and others, 1973), shows the fastest exchange of all minerals studied (table 1); exchange in relatively fast even at 150°C. Fractionation is essentially independent of temperature (at around -50 permil) down to 280°C or below, and decreases towards -35 permil at 200°C and below. At the other extreme, diaspore, with an asymmetrical, nonlinear hydrogen bond (Busing and Levy, 1958), showed minimal exchange and probably very large fractionations at 380°C. While the OH-structure of zoisite and epidote are not well known, infra-red studies and structural refinements (Dollase, 1968 and oral commun.; Langer and Raith, 1974) may be interpreted as indicating significantly greater asymmetry in the O-H---O bond in zoisite than in the epidote-clinozoisite series, consistent with their contrasted isotope-exchange properties.

Hydrous mineral-water hydrogen isotope exchange may thus occur over a wide range of temperature, particularly in hydrous minerals containing hydrogen bonding. Measured D-H fractionations between natural coexisting hydrous minerals need not reflect hydrogen isotope exchange equilibrium between the minerals and water at or near the temperature of formation of the mineral assemblage. Isotope exchange will continue as long as the mineral and water coexist and kinetics of exchange are favorable. Inasmuch as D/H ratios of minerals tend to be more diagnostic of the origin of waters than $^{18}O/^{16}O$ ratios, a good understanding of the equilibrium fractionations and varying effective closure temperatures of mineral-water hydrogen isotope exchange equilibria in different hydrous mineral-water systems should provide a useful basis for interpreting the temporal evolution of the hydrous fluid phase during water-rock interactions. Specifically, D/H data on natural epidotes may provide an insight into the nature of retrograde metamorphism.

Busing, W. R., and Levy, H. A., 1958, A single crystal neutron diffraction study of diaspore, AlO(OH): Acta Crystallographica, v. 11, p. 798-803.

Dollase, W. A., 1968, Refinement and comparison of the structures of zoisite and clinozoisite: American Mineralogist, v. 53, p. 1882-1898.

Heaton, T. H. E., and Sheppard, S. M. F., 1977, Hydrogen and oxygen isotope evidence for sea-water - hydrothermal alteration and ore deposition, Troodos complex, Cyprus, in Volcanic processes in ore genesis: London, Institute Mining Metallurgy and Geology Society, p. 42-57.

Langer, K. and Raith, M., 1974, Infrared spectra of Al-Fe(III)-epidotes and zoisites, $Ca_2(Al_{1-p}Fe_p^{3+})Al_2O(OH)(Si_2O_7)(SiO_4)$: American Mineralogist, v. 59, p. 1249-1258.

Northrop, D. A., and Clayton, R. N., 1966, Oxygen isotope fractionation in systems containing dolomite: Journal of Geology, v. 74, p. 174-196.

O'Neil, J. R., and Kharaka, Y. K., 1976, Hydrogen and oxygen isotope exchange reactions between clay minerals and water: Geochmica et Cosmochimica Acta, v. 40, p. 241-246.

Stegmann, M. C., Vivien, D., and Mazieres, C., 1973, Etude des modes de vibration infrarouge dans les oxyhydroxides d'aluminium boehmite et diaspore: Spectrochima Acta, v. 29A, p. 1653-1663.

Suzuoki, T., and Epstein, S., 1976, Hydrogen isotope fractionation between OH-bearing minerals and water: Geochmica Cosmochimica Acta, v. 40, p. 1229-1240.

Taylor, B., and O'Neil, J. R., 1977, Stable isotope studies of metasomatic Ca-Fe-Al-Si skarns and associated metamorphic and igneous rocks, Osgood Mountains, Nevada: Contributions to Mineralogy and Petrology, v. 63, p. 1-49.

APPLICATION OF LEAD ISOTOPES TO EXPLORATION: GOSSAN ASSESSMENT

By Brian L. Gulson
Commonwealth Scientific and Industrial Research Organization Division of Mineralogy,
North Ryde, New South Wales, Australia

In arid and semi-arid terrains, such as Australia, the 'first-line' exploration targets for base-metal sulfides are gossans (or iron-stones). These are usually hydrated iron oxides

that are derived from sulfides by complex oxidation processes and contain anomalous base-metal concentrations. In Australia, the terminology for gossans is as follows: gossans are outcrops which overlie economically viable base-metal mineralization; barren gossans are those which have been derived from dominantly iron-sulfide mineralization with little or no base-metal content; and false gossans are those which are not underlain by sulfide mineralization.

The problem facing exploration companies is to decide whether an ironstone is a true gossan, or is barren, or false without resorting to the expense of drilling. Lead isotopes, in association with other data, offer a relatively rapid, low-cost method to asses the potential of gossans overlying viable mineralization of the stratiform Pb-Zn-(Cu) type. The method makes use of the substantial uniformity of Pb-isotopic data from so-called stratiform deposits (such as Sullivan, Broken Hill, and Captains Flat) and their close fit to the growth curve. If a gossan is derived from such sulfides, its Pb isotopic data should be homogeneous and plot on, or close to, the growth curve. In a false gossan, the Pb and other metals originate by scavenging from the surrounding rocks and the Pb isotopic data should be heterogeneous and scatter abou the growth curve. In an inter mediate situation (barren gossan), where iron-sulfide mineralization without significant base-metal concentrations is the progenitor, or where the samples come from a less favourable part of the gossan outcrop, the isotope ratios in the gossan should reflect a mixture of ore and rock Pb, or the data may cluster slightly off the growth curve.

Research designed to test the theory outlines above involved gossans overlying known ore bodies, false gossans, and barren gossans included in a recent company exploration program. Analyses of gossans overlying known ore bodies were performed in areas where detailed isotopic investigations were either completed or in progress. These included Woodlawn (Pb-Zn-Cu), located in Middle-Upper Silurian felsic volcanics; Currawang (Zn-Cu-Pb), located in basaltic rocks of Middle-Late Silurian age; and Broken Hill (Pb-Zn) and Dugald River (Zn-Pb), both of middle Proterozoic age. The samples analyzed were from gossans of different ages, geological environments, ore types, and vertical depths to primary sulfide. In all cases, the gossan data were identical to the primary sulfide data, indicating that the isotopic ratios were preserved during oxidation.

Examples of false gossans (those not underlain by sulfide), were more difficult to obtain. The Corona ironstone north of Broken Hill, extends for ≈28 km and contains anomalous Zn and Cu (low Pb). Drilling confirmed the absence of sulfides. The Pb isotopes show a large scatter and do not plot near the growth curve. A supposed false gossan near the Woodlawn orebody had high Pb values and identical isotopic ratios with the Woodlawn ore suggesting it was a true gossan. This was confirmed by drilling.

The most important part of the investigation was the evaluation of a recent exploration program in northwest Queensland. Here the time span between primary sulfide and/or host rock and the gossan is on the order of ≈1.5 b.y. Ironstone samples were obtained from five localities, four of which were determined by drilling to be underlain by varying amounts of sulfides. Of the five ironstones examined, three could have been rejected before drilling, on the basis of Pb isotopes one showed particularly high potential, and one showed high potential but a comparison of gossan and sulfide data after drilling, suggested that the hole was drilled on the fringes of economic mineralization.

Future research using Pb isotopes in gossan assessment will center on gossans from southern New South Wales (where the time difference between primary sulfide and gossan is short compared with northwest Queensland) and in gossans overlying major stratiform Cu orebodies.

ISOTOPIC STUDIES RELATIVE TO THE OKLO NATURAL FISSION REACTORS

By Robert Hagemann
CEN/SACLAY, B.P. n°2, GIF-sur-YVETTE 91190
FRANCE

It has been clearly demonstrated that natural fission reactors operated about 2×10^9 years ago in high-grade uranium ore deposits of the Oklo mine in the Republique of Gabon (West Africa)(Bodu and others, 1972; Neuilly and others, 1847; International Atomic Energy Agency, 1975).

Six reaction zones have been identified in which approximately six tons of ^{235}U were consumed and the same amount of fission products deposited in the ground. These fission products, their filiation isotopes, and nuclei formed from

neutron capture are valuable tracers, which can be analyzed to obtain information on the stability of such elements in soil and on the nuclear parameters and characteristics of the nuclear reactors.

The studies which have been developed at Saclay concern several aspects of this phenomenon--the migrations of fission products, the age of the nuclear reaction and the uranium deposit, and the temperature of the reaction zones during the operation of the reactors.

Migration of uranium and rare earths: Rare earths, particularly neodymium, are the fission products which have been studied most extensively. Their abundances relative to uranium and their isotopic compositions give important information for determining parameters of the nuclear reaction. These parameters can be determined well only if the reactor zones have preserved their initial geometries and their initial chemical characteristics. The results of chemical and isotopic analyses of uranium, neodymium, samarium, europium, and dysprosium--performed on 14 samples distributed along the core SC36 passing through reaction zone 2--confirm the remarkable state of preservation of this reaction zone (Ruffenach, 1977). Thus, at 80 cm from the center of the zone the fission rare earths are not detectable. At 40 cm the excess of fission neodymium represents less than 5 percent of the quantity formed in the center of the zone. The corresponding values for samarium and gadolinium are respectively 12 percent and 15 percent. Results were also obtained on dysprosium, which is not a fission product. They confirm the stability of the natural rare earths that were present in the ore before the beginning of the nuclear reaction.

Date of the nuclear reaction: The above detailed study demonstrates that it is possible to use the ratio of uranium to neodymium for the determination of the age of the reaction with a good precision. The equation,

$$d = \frac{1}{\lambda 5} \text{ Ln } (A \frac{Nf5}{U} \cdot \frac{1}{\tau}),$$

permits us to calculate the age of the reaction, d, knowing τ, the fluence; Nf5/U is the ratio of the number of fissions of ^{235}U to the number of atoms of uranium now present in the sample. Nf5 is directly deduced from the ratio Nd/U measured on the samples. The ages obtained from measurements of uranium and neodymium in 8 samples give an average value of $(1.98 \pm 0.05) \times 10^9$ years. (Ruffenach, 1977).

Age of the uranium deposit: The above method, based on the balance of fission neodymium formed to uranium consumed, gives an older age for the nuclear reaction than the obtained age of 1.8×10^9 years for the Franceville basin, according to the concordant results obtained by K-Ar and Rb-Sr methods. To obtain information on the age of the uranium deposit, new measurements of uranium and lead were performed on rich uranium ore samples, which are supposed to represent the higher grade ore of the Oklo uranium deposit (Devillers and Menes, 1977). This study confirms the complex history of the lead whereby it is difficult to separate the effects of inherited lead from those of episodic losses. According to a new interpretation to the uranium deposit may be older than 1900 million years.

Temperature of the reaction zones: Isotopes with neutron-capture cross sections having resonance peaks close to the thermal energy range may be used to obtain information on the equilibrium temperature between the neutrons and the moderating water (Hollinger and others). Two isotopes, ^{176}Lu and ^{155}Gd, have been selected for this purpose. Using a simplified model to represent the neutron energy spectrum, it is possible to calculate the variations of the neutron-capture cross sections of ^{176}Lu and ^{155}Gd with temperature and spectrum index. The comparison between measured isotopic ratios $^{176}Lu/^{175}Lu$ and $^{156}Gd/^{155}Gd$ and ratios derived from the above calculated neutron cross sections, fluence, and index spectrum permits us to obtain the equilibrium neutron temperature. Four samples from zones 2 and 3 were analyzed and gave the same temperature of $280^{\circ}C \pm 20^{\circ}C$. This temperature is indeed a mean temperature over the duration of the nuclear reaction. The fact that the same temperature is found on samples having very different nuclear parameters shows that this temperature is primarily due to the burying of the reactors. The geothermal gradient of 40 to $50^{\circ}C\ km^{-1}$ indicates that the reactors operated at a depth of from about 4000 to 5000 meters.

Bodu, R., Bouzigues, H., Morin, N., and Pfiffelman, J. P., 1972, Isotopic anomalies in the uranium of Gabon: Academie des Sciences, Comptes Rendus, ser. D, v. 275, no. 16, p. 1731-1732.

Neuilly, M., Bussac, J., Frejacques, C., Nief, G., Vendryes, G., and Yvon, J., 1847-1849.

International Atomic Energy Agency (IAEA), 1975, The Oklo Phenomenon, IAEA Symposium, Libreville, Gabon, June 23-27, 1975, Proc.: IAEA-SM-204, 650 p.

Ruffenach, J. C., (in press), in Natural fission reactors: International Atomic Energy Agency Technical Committee Meeting, Dec. 19-21, 1977.

Devillers, C., Menes, J., (in press), (A paper), in Natural fission reactors: International Atomic Energy Agency Technical Committee Meeting, Dec. 19-21, 1977.

Hollinger, P., Devillers, C., Menes, J., (in press), (A paper), in Natural fission reactors: International Atomic Energy Committee Meeting, Dec. 19-21, 1977.

A CONSISTENT AGE FOR THE UNIVERSE

By Kem Hainebach[1], Demosthenes Kazanas[2], and David N. Schramm[2]
[1]Lawrence Livermore Laboratory
Livermore, California 94550
[2]University of Chicago, Chicago 60601

The age of the universe is one of the most interesting cosmological parameters. The fact that the age is finite has intriguing philosophical as well as physical implications. An accurate age, when compared to the present expansion rate parameter (the Hubble constant H_0), can, in the standard Big Bang model, determine the large-scale structure of the universe, and therefore determine whether the universe is open or closed.

Three independent methods (Schramm, 1974) have traditionally been used to determine the age of the universe (T_u). These are:

1. Using the dynamics of the Friedmann universe (Weinberg, 1972), in particular, estimates of H_0, and the limits on the deceleration parameter q_0; given that published values for H_0 range from 40 to 100 km sec^{-1} Mpc^{-1}, and limits on q_0 range up to $\sim$1, the most restrictive age range on which everyone will agree, from this method, is $5 \times 10^9 \lesssim T_u \lesssim 25 \times 10^9$ yr.

2. Using the ages of the oldest stars, in particular, the ages of globular clusters. Assuming that the time from the Big Bang to star formation is $<< 10^9$ yr, globular cluster ages (Iben, 1974) then give $8 \times 10^9 \lesssim T_u \lesssim 18 \times 10^9$ yr where the main uncertainty is in the helium abundance.

3. Using nucleochronology, i.e. direct dating of the nucleosynthesis of radioactive nuclei from their observed or implied abundances. Model independently one obtains the mean age of the elements (Schramm, 1970), which is a lower limit to the age of the universe. This gives (Hainebach and Schramm, 1977) $T_u \gtrsim 6 \times 10^9$ yr for the absolute lower limit, with mean ages ranging from 6 to 10 $\times 10^9$ yr. By coupling the mean age to a galactic evolution model one is able to get a total age for the heavy elements which should be approximately the age of the universe. Most models of galactic evolution which do give the correct mean age (which is known model-independently), have a total age which implies that $T_u \lesssim 20 \times 10^9$ yr (Hainebach and Schramm, 1977).

It is truly amazing that three such diverse methods give roughly the same range. However, it is unfortunate that the uncertainty in the age by each of these methods is large. An interesting point, which is not always appreciated, is that by combining two or more of the methods and inserting constraints from related observations, it is possible to make a much more restrictive determination of the concordant age. This method was used in part by Gott and others (1974) who determined that the age must lie in the range $13 \lesssim T_u \lesssim 20 \times 10^9$ yr. The lower limit on this range was determined by the need for concordance between the deuterium-limited density $\rho \simeq 5 \times 10^{-31}$ g cm^{-3}, the lower limit on the density parameter $\Omega = \rho/\rho_c \simeq 0.06$ (where $\rho_c = 3H_0/8\pi G$ is the critical density), implied from dynamics of galaxy groups and clusters, and by the fact that the age from the dynamical method is totally specified for the standard Big Bang model in which the cosmological constant $\Lambda = 0$ if ρ and Ω are given, since the simultaneous knowledge of each determines H_0 and q_0. The upper limit by Gott and others (1974) comes from either the ages of globular clusters or from nucleochronology plus galactic evolution.

Another method of obtaining a concordant age is to use the fact that the ages of globular clusters depend on the primordial helium abundance. Since the origin of this helium was presumably Big Bang nucleosynthesis, and since the amount of helium produced in the Big Bang is sensitive to the baryon density, ρ, one can use this density to constrain q_0 which, coupled with H_0, determines the age from dynamics. This constrained age must also be concordant with the globular cluster age. This method gives concordant ages near 15×10^9 yr (Gunn, 1976; Schramm and Wagoner, 1977).

The purpose of the present note is to combine the various constraints mentioned above in the context of the standard cosmological model to see what ages are capable of simultaneously satisfying them all. We will see that this simultaneous solution is much more restrictive than the previous ranges on the age.

The prime assumption made in the analysis will be that the universe is described by one of the Friedmann models (Weinberg, 1972). It will be assumed that on large scales it is homogenous, isotropic, and presently matter-dominated with negligible pressure. All these assumptions are supported by observations and hence do not appear to introduce any serious ambiguity. If one then considers the simplest of these models, namely those with zero cosmological constant Λ (an assumption whose consistency must eventually be checked with observations), two parameters are sufficient to completely specify a particular model. These are:

a. The Hubble constant

$$H_0 = \frac{\dot{R}_0}{R_0} \qquad (1)$$

where R = R(t) is the scale factor of the universe and R_o is its present value.

b. The density parameter, $\Omega \equiv \rho/\rho_c$ which is related to the deceleration parameter

$$q_o = - \frac{(\dot{R}_o)^2}{R_o \ddot{R}_o} \qquad (2)$$

by

$$\Omega = 2q_o \qquad (3)$$

For the $\Lambda = 0$ models, the value of Ω determines whether the universe is open ($\Omega < 1$) or closed ($\Omega > 1$). With the above assumptions the age of the universe can be given in terms of the observable quantities Ω and H_o by

$$T_u = \frac{F(\Omega)}{H_o} \qquad (4)$$

where $F(\Omega)$ is given by Weinberg (1972) and Gott and others (1974). The age of the universe, therefore, is constrained within the $\Lambda = 0$ Friedmann models by the measurements of Ω and H_o. Consequently, accurate determination of any two of these parameters will set limits on the third, which will have to be consistent with observations.

Once the above model for the universe has been assumed, one is forced to conclude that at an earlier era its temperature (T) was high enough for nucleosynthesis to occur. Such a scenario for nucleosynthesis has been explored in detail by Wagoner, Fowler, and Hoyle (1967; Schramm and Wagoner, 1977). The strongest conclusion obtained from Big Bang nucleosynthesis is that the predicted ^{4}He abundance agrees well with observations and the yields of both ^{4}He and D depend on the entropy per baryon, $h_o = \rho/T^3$, in the universe and hence on Ω. Using equation (4) and the results of Big Bang nucleosynthesis, each model of the universe can, therefore, be alternatively specified by T_u and Y, the primordially produced ^{4}He abundance. The different models spanning the T_u, Y space are shown in figure 1 (Gunn, 1976; Schramm and Wagoner, 1977). The different curves correspond to models of the same H_o, which ranges between $40 \lesssim H_o \lesssim 100$ km sec^{-1} Mpc^{-1} (Vancouleurs, 1977; Branch and Patchett, 1973), thus, excluding all models with H_o outside this range.

The class of allowed models can be further restricted by estimates of the contribution of matter associated with galaxies to the density parameter (whose values run along the H_o = const. lines in fig. 1). The best values of Ω determined from the dynamics of galaxies, give values in the range $0.06 \lesssim \Omega \lesssim 0.3$ (Gott and others, 1974; Gott and Turner, 1976; Gott and Turner, 1977). One should note that these values give a lower limit of Ω because they do not take into account any contribution from intergalactic matter, the existence of which has not been conclusively shown (Gott and others, 1974). These values of Ω, and the observed deuterium abundance, X_D, can now be used as a consistency check with observations, since X_D depends strongly on the value of baryon density, ρ, and hence on Ω. The most recent values of the deuterium abundance are those of Dupree and others (1977) obtained with the Copernicus satellite. They are D/H = 3.9 (+5.7, -1.7) x 10^{-5} and 0.24 (+0.12, -0.07) x 10^{-5} in the directions of α Aur and α Cen A, respectively. If other sources have not contributed to the deuterium abundance (Epstein and others, 1976) and since deuterium has certainly been destroyed in stars, the primordial deuterium abundance should be greater than the largest of the observed lower bounds, or $D/H \gtrsim 2.2 \times 10^{-5}$, or $X_D \gtrsim 3.4 \times 10^{-5}$, assuming $X_H = 0.768$. The corresponding limit on Ω is then given (Schramm and Wagoner, 1977) by

$$\Omega \lesssim 0.085 \left(\frac{50}{H_o}\right)^2 \qquad (5)$$

Since Ω ranges between 0.06 and 0.03, the corresponding limit on H_o is then $H_o \lesssim 60$ km sec^{-1} Mpc^{-1}. This value of H_o is in concordance with those observed, thus again showing the model to be compatible with observations. (However it disagrees with speculations by Lynden-Bell (1977) on a large value of H_o.)

If it is assumed that the time from the Big Bang to star formation is much less than 10^9 yr, then the ages of the oldest stars would set limits on the age of the universe. Estimates of the globular cluster ages can be made, and are based on detailed stellar-evolution models. Such an analysis concluded that their ages are strongly dependent on the helium abundance Y, and more weakly dependent on the heavy-element mass fraction Z, of the gas out of which they have been formed (Iben, 1974; Iben and Rood, 1970). Since globular clusters are very old, their helium abundance at birth must not be too different from that of helium synthesized in the Big Bang. Their ages (in units of 10^{10} yr) are then given in terms of Y and Z (Iben, 1974)

$$\log_{10} t_c = 0.035 + 2.085\,(0.3 - Y) - 0.034\,(\log_{10} Z + 3) \qquad (6)$$

with $10^{-3} \gtrsim Z \gtrsim 10^{-4}$. The most metal-poor globular clusters appear to have $Z \simeq 10^{-2}\, Z_\odot$, or 1.7×10^{-4} (Kukarkin, 1974), while those with $Z \gtrsim 10^{-3}$ all have young "turnoff" ages (Gunn, 1976) and are therefore not the old objects we seek. The value of the cluster age, t_c, has been plotted in the T_u, Y plane, as a function of the helium abundance Y, with $10^{-3} \gtrsim Z \gtrsim 10^{-4}$. This constraint further restricts the concordant models of the universe. In a recent work, Demarque and McClure (1977) have calculated ages of globular clusters in a way that appears to be almost independent of Y. (However, this is done only by building into their ages an implicit determination of Y from the fitting of the ratio of the number of red giants to horizontal branch stars, which has several uncertainties built into it.) The ages they find range between 15 and 18 x 10^9 yr, which are within the range allowed by Iben (1974).

As already mentioned, another completely

independent way for setting limits to the age of the universe is by nucleochronology plus galactic evolution. These limits, discussed in the beginning of this paper are not very stringent at the present time owing to uncertainties in galactic evolution models. Even with the uncertainties in galactic evolution, the mean age of the elements is a firm lower bound on T_u. In addition, there are uncertainties in the model-independent mean age because of uncertainties in various nuclear parameters. In particular, more accurate measurements of the half-life of ^{187}Re will significantly restrict the range of values deduced by nucleochronology and provide a very important consistency test of the various models.

By incorporating all the above-discussed constraints on the T_u, Y diagram (fig. 1), the allowed age of the universe completely consistent with them is quite restricted. It ranges from 13.5 to 15.5 x 10^9 yr, determined by the limits $0.06 \lesssim \Omega \lesssim 0.3$ and $10^{-4} \lesssim Z_{g.c.} \lesssim 10^{-3}$. These limits are more restrictive than those obtained from the individual constraints and, as argued earlier, are consistent with the independent measurements of H_0, and those of q_0. The limits on H_0 along with the deduced age, T_u, appear to favor an open model of the universe (Schramm and Wasserburg, 1970).

If the age of the universe were eventually found to lie outside this narrow range, then one would be forced to question the standard cosmological model and/or standard globular cluster models, both of which are frequently taken as illustrations of the success of modern astrophysics.

We acknowledge valuable discussions with Dave Dearborn, Jim Gunn, Icko Iben, and R. V. Wagoner. This work was supported in part by the U.S. National Science Foundation and by the U.S. Department of Energy.

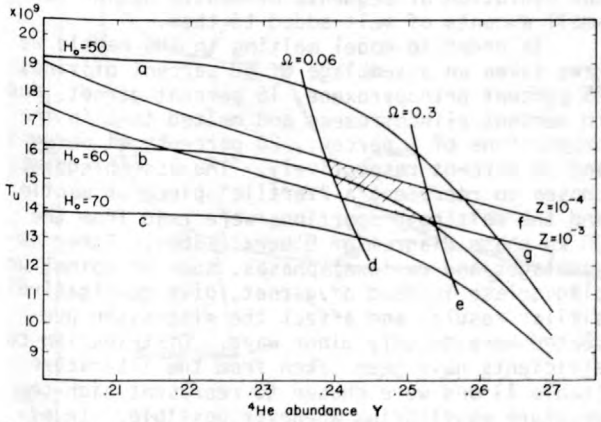

Figure 1.--Constraints on the age of the universe, T_u, and the primordially produced ^4He abundance: Curves of constant age H_0 (a, b, c), and of constant density parameter (d, e), according to the standard Big Bang nucleosynthesis model. Ages of the globular clusters (f, g), for different primordial heavy element abundances Z.

Branch D., 1977, Supernovae and the value of the Hubble Constant, in Schramm, D. N., ed., Supernovae: Dordrecht, Reidel Publishing Co., p. 21-28.

Demarque, P., and McClure, R. D., 1977, The significance of the Star clusters NGC 2420 and 47 Tucanae for galactic evolution: Astrophysical Journal, v. 213, p. 716-722.

de Vaucouleurs, G., 1977, Distances of the Virgo, Fornax and Hydra Clusters of galaxies and the local value of the Hubble Ratio: Nature, v. 266, p. 126-129.

Dupree, A. K., Baliunas, S. L., and Shipman, H. L., 1977, Deuterium and hydrogen in the local interstellar medium: Astrophysical Journal, v. 218, p. 361-369.

Epstein, R. I., Lattimer, J. M., and Schramm, D. N., 1976, The origin of deuterium: Nature, v. 263, p. 198-202.

Gott, J. R., Gunn, J. E., Schramm, D. N., and Tinsley, B. M., 1974, An unbound Universe?: Astrophysical Journal, v. 194, p. 543-553.

Gott, J. R., and Turner, E. L., 1976, The mean luminosity and mass densities in the Universe: Astrophysical Journal, v. 209, p. 1-5.

Gott, J. R., and Turner, E. L., 1977, Groups of Galaxies; III, Mass-to-light ratios and crossing times: Astrophysical Journal, v. 213, p. 309-322.

Gunn, J. E., 1976, Observational tests in cosmology: California Institute of Technology, Orange Aid Preprint 464, p. 1-24.

Hainebach, K. L., and Schramm, D. N., 1977, Comments on galactic evolution and nucleo-cosmochronology: Astrophysical Journal, v. 212, p. 347-359.

Hartwick, F. D. A., and Van den Bergh, D. A., 1973, Theoretical isochrones for metal-rich globular clusters: Astrophysical Journal, v. 185, p. 887-897.

Iben, I., 1974, Post main sequence evolution of single Stars: Annual Review of Astronomy and Astrophysics, v. 12, p. 215-256.

Iben, I., and Rood, R. T., 1970, Metal-poor Stars; I, Evolution from the main sequence to the giant branch: Astrophysical Journal, v. 159, p. 605-617.

Kukarkin, B. V., 1974, The globular Star clusters: Moscow, Nauka, p. 124-129.

Lynden-Bell, D., 1977, Hubble's Constant determined from super-liminal radio sources: Nature, v. 270, p. 396-399.

Schramm, D. N., 1974, Nucleo-cosmochronology: Annual Review of Astronomy and Astrophysics, v. 12, p. 383-406.

Schramm, D. N., and Wagoner, R. V., 1977, element production in the early Universe: Annual Review of Nuclear Science, v. 27, p. 37-74.

Schramm, D. N., and Wasserburg, G. J., 1970, Nucleochronologies and the mean age of the elements: Astrophysical Journal, v. 162,

p. 57-69.
Wagoner, R. V., Fowler, W. A., and Hoyle, F., 1967, On the synthesis of elements at very high temperatures: Astrophysical Journal, v. 148, p. 3-49.
Weinberg, S., 1972, Gravitation and Cosmology, New York, John Wiley.

THE SIGNIFICANCE OF TRACE ELEMENT MODELING CALCULATIONS FOR THE EVOLUTION OF Sr AND Nd ISOTOPES IN THE MANTLE

By C. J. Hawksworth, M. J. Norry, J. C. Roddick and R. Vollmer
Department of Earth Sciences,
The University Leeds LS2 9JT,
England

Recent publications have stated that an inverse correlation exists between Sr and Nd isotope ratios in tholeiitic and alkaline lavas (O'Nions and others, 1977; De Paulo and Wasserburg, 1976). Here we present isotopic data from Patagonian and Kenyan lavas (fig. 1), which fall along the correlation trend derived from published data for Atlantic Ocean samples. We also present data from the Azores, which fall to the high Sr isotope side of the main correlation trend and define a line of lower slope.

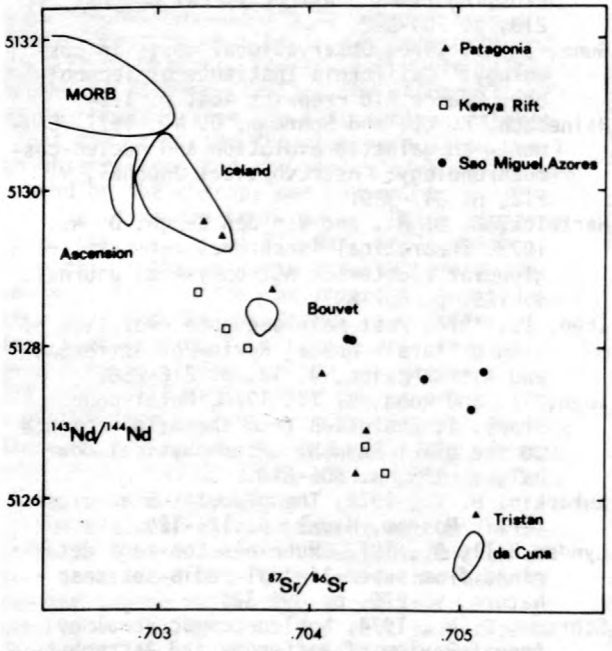

Figure 1.--Isotope data presented in this paper compared with that of O'Nions and others, (1977).

The five lavas from Patagonia are from between latitude 45° and 47°S and range in composition from quartz tholeiite to alkali basalt and leucite basanite. The five Kenyan lavas comprise four alkali basalts and one phonolite from the Rift Valley between Lakes Hannington and Turkana. The five lavas from the Azores come from the volcano Agua de Pau and are alkali olivine basalts. Nd isotope ratios were normalized to a $^{146}Nd/^{144}Nd$ ratio of 0.7216.

The hypothesis that the extraction of basic magmas from the mantle is a major cause of its differentiation would seem attractive in light of the ubiquitous occurrence of basic lavas throughout the geological record. Although for reasonable amounts of melting (about 5 percent) Sm/Nd and Rb/Sr ratios in the derived liquid are similar to those in the original source material, the ratios in the residual material left after melting may be very different. Given time, such residual material would evolve to high Nd and low Sr isotope ratios. In the remainder of this paper we will consider the evolution of segments of the mantle melted to various degrees at various times in the past. We will also speculate on the evolution of segments of mantle having had small amounts of melt added to them.

In order to model melting in the mantle we have taken an assemblage of 50 percent olivine, 25 percent orthopyroxene, 15 percent garnet, and 10 percent clinopyroxene and melted them in the proportions of 6 percent, 20 percent, 44 percent, and 30 percent respectively. The assemblage was chosen to represent a "fertile" piece of mantle and the melting proportions were read from the 30 kb phase diagram of O'Hara (1968). Other assemblages and residual phases, such as spinel or plagioclase instead of garnet, give qualitatively similar results and affect the discussion presented here in only minor ways. Distribution coefficients have been taken from the literature (table 1) and were chosen to represent high-temperature equilibrium whenever possible. In effect, this means that the values are slightly lower than those derived from many experiments that have been performed at temperatures below those characteristic of primitive basalts. The equation of Shaw (1970) was used to model equilibrium batch melting and more sophisticated melting regimes, such as incremental melting, were not considered for reasons that are given

later in the paper.

Table 1.--Distribution coefficients used in melting calculations

	Rb	Sr	Sm	Nd
$D^{ol/Liq}$	2.5×10^{-5}	6×10^{-5}	6.7×10^{-4}	5.1×10^{-4}
$D^{opx/Liq}$	3.2×10^{-4}	7×10^{-4}	3.1×10^{-3}	2.2×10^{-3}
$D^{cpx/Liq}$	1.6×10^{-3}	6.6×10^{-2}	9.0×10^{-2}	6.5×10^{-2}
$D^{gt/Liq}$	2.3×10^{-3}	2.3×10^{-3}	5.1×10^{-2}	1.5×10^{-2}

The results of the equilibrium batch-melting calculations are shown in figure 2, where they are compared with published and unpublished Sm/Nd and Rb/Sr ratios for basic lavas. The Sm/Nd and Rb/Sr ratios derived for the whole (O'Nions et al, 1978) earth have been used for the calculations. It is apparent that the data from basic lavas do not pass through the bulk earth composition as might have been anticipated if the mantle had a simple history of depletion or enrichment. In order to produce compositions in the bottom left quadrant of figure 2, such as the Patagonian data, it would be necessary to first deplete a portion of the mantle by extraction of 0.5 percent or more of the liquid and then partially melt about 0.1 percent to form a second liquid, which could either be extracted and erupted or mixed with other depleted portions of the mantle. Such small amounts of liquid may not, however, be capable of separating from their melting residue. If garnet were not a residual phase during melting, or if the proportion of olivine and orthopyroxene were larger, the problem would be more difficult, as less fractionation would then be achieved for the same amount of melting. Similar problems are encountered in the production of the Italian and Western Rift potassic lavas.

In figure 3 we present the results of calculations concerning the evolution of segments of the mantle that underwent partial melting one billion and two billion years ago. The form of the residue curves does not indicate that the main correlation is due to variable amounts of melt extraction in the past. A more promising explanation would be to postulate that two billion years ago or more about 0.5 percent of the melt was removed from part of the mantle and the residue later mixed with undifferentiated material. As the Sr/Nd ratio is little changed by melting, the resulting mixing line would be practically straight, thus forming the main correlation. For assemblages with less garnet and clinopyroxene, more fractionation would be achieved between the residue and the original material and less liquid could then be extracted to produce a point on the main correlation trend at the present time.

Also shown in figure 3 is the field defined

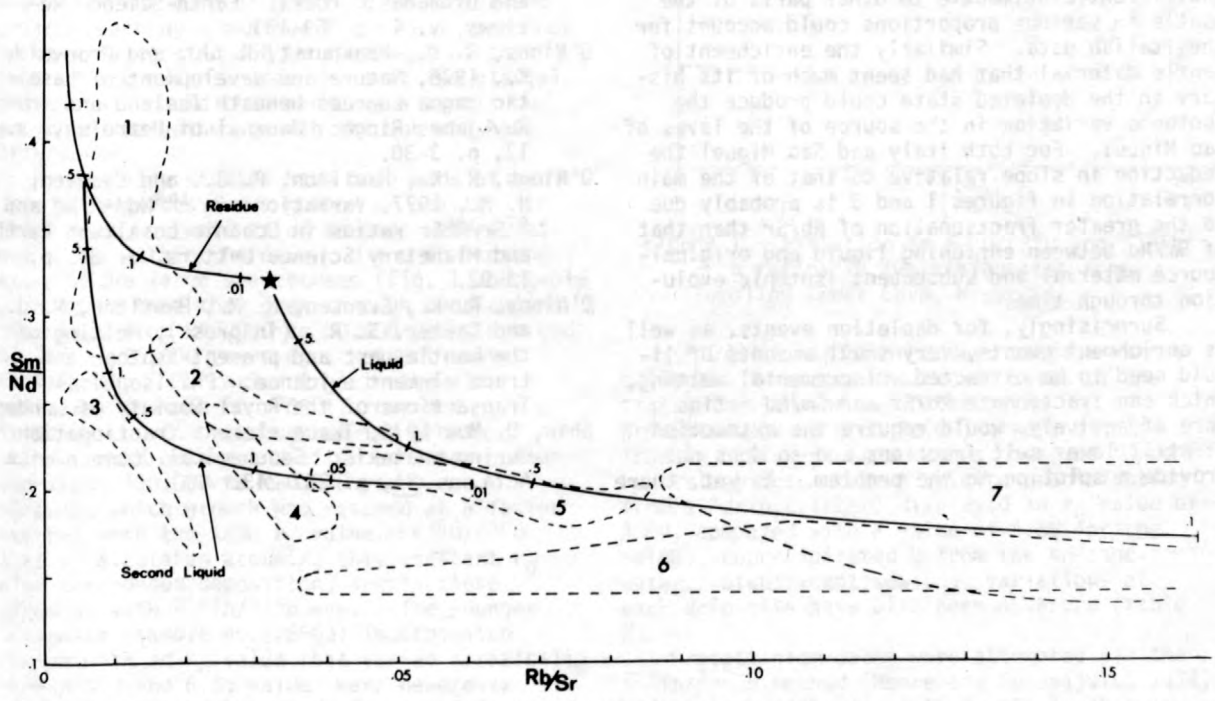

Figure 2.--Batch-melting calculation results with melt fractions in percent. The star represents the bulk earth composition of O'Nions and others, (1978. Data from basic lavas: 1, tholeiites from Iceland (O'Nions and others, 1976); 2, Hawaii (O'Nions and others, 1977); 3, Etna (Carter and others, 1977); 4, Patagonia (Leeds, unpublished data); 5, Sao Miguel (Gibson and Marriner, unpublished data); 6, Western Rift potassic lavas (Mitchell and Bell, 1976); Italian lavas (Hawksworth and Vollmer, unpublished data).

by our data from the Italian potassic lavas (Hawksworth and Vollmer unpublished data). The addition of a liquid derived one billion years ago by somewhat less than 0.1 percent melting of

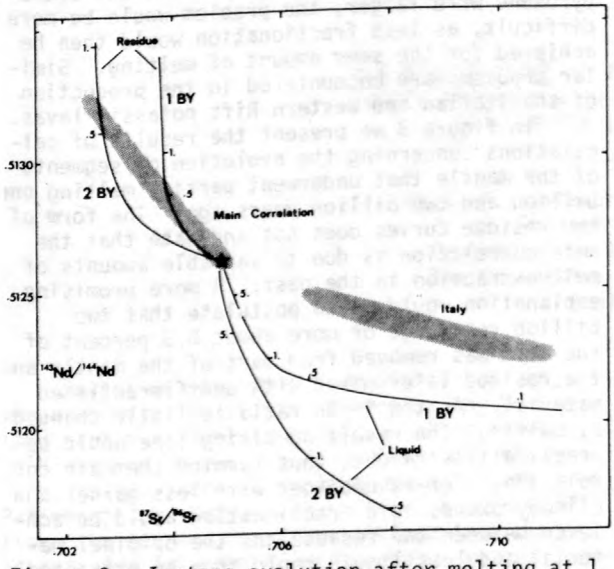

Figure 3.--Isotope evolution after melting at 1 b.y. and 2 b.y. Melt proportions in percent. The star represents the bulk earth composition of O'Nions and others, (1978).

undifferentiated mantle to other parts of the mantle in various proportions could account for the Italian data. Similarly the enrichment of mantle material that had spent much of its history in the depleted state could produce the isotopic variation in the source of the lavas of Sao Miguel. For both Italy and Sao Miguel the reduction in slope relative to that of the main correlation in figures 1 and 3 is probably due to the greater fractionation of Rb/Sr than that of Sm/Nd between enriching liquid and original-source material and subsequent isotopic evolution through time.

Surprisingly, for depletion events, as well as enrichment events, very small amounts of liquid need to be extracted. Incremental melting, which can fractionate Rb/Sr and Sm/Nd ratios more effectively, would require the extraction of still lower melt fractions and so does not provide a solution to the problem. As yet, there is no agreement as to what the smallest extractable melt proportion might be; however, in the future, if it is shown that melts of less than 1 percent cannot separate from their residue, Nd/Sr isotope studies, together with an improved knowledge of distribution coefficients, may show that the agent responsible for the creation of heterogeneous Sm/Nd and Rb/Sr ratios in the mantle is not a basic silicate melt. If other types of fluids are responsible, then they dissolve Rb in preference to Sr, and Nd in preference to Sm.

Carter, S. R., Evensen, N. M., Hamilton, P. J., and O'Nions, R. K., 1977, Derivation of continental volcanics from enriched and depleted source regions-Nd and Sr isotope evidence: Earth and Planetary Science Letters, v. 37, p. 401-408.

De Paolo, D. J., and Wasserburg, G. J., 1976, Nd isotope variations and Petrogenic models: Geophysical Research Letters 3, p. 249-252.

Mitchell, R. H., and Bell, K., 1976, Rare earth element geochemistry of potassic lavas from the Birunga and Toro-Ankole Regions of Uganda, Africa: Contributions to Mineralogy and Petrology, v. 58, p. 293-303.

O'Hara, M. J., 1968, The bearing of phase equilibria studies in synthetic and natural systems on the origin and evolution of basic and ultrabasic rocks: Earth-Science Reviews, v. 4, p. 69-133.

O'Nions, R. K., Pankhurst, R. J., and Gronvold, K., 1976, Nature and development of basaltic magma sources beneath Iceland and the Reykjanes Ridge: Journal of Petrology, v. 17, p. 3-30.

O'Nions, R. K., Hamilton, P. J., and Evensen, N. M., 1977, Variations in $^{143}Nd/^{144}Nd$ and $^{87}Sr/^{86}Sr$ ratios in Oceanic basalts: Earth and Planetary Science Letters, v. 34, p. 13-22.

O'Nions, R. K., Evensen, N. M., Hamilton, P. J., and Carter, S. R., (in press), Melting of the mantle past and present-isotope and trace element evidence: Philisophical Transactions of the Royal Society of London.

Shaw, D. M., 1970, Trace element fractionation during anatexis: Geochemical Cosmochimica Acta, v. 34, p. 237-243.

ISOTOPIC STUDIES OF SPELEOTHEMS FROM A CAVE IN SOUTHERN MISSOURI, U.S.A.

By R. S. Harmon[1], H. P. Schwarcz[2], and T. Aley[3]
[1] Isotope Geology
United Scottish Universities Research and
Reactor Centre
East Kilbride, Scotland
[2] Department of Geology
McMaster University
Hamilton, Ontario, Canada
[3] Ozark Underground Laboratory
Protem, Missouri

The Ozark Underground Laboratory at Tumbling Creek Cave, Protem, Missouri, furnishes a rare opportunity to study modern speleothem deposition under carefully monitored conditions and to obtain a continuous isotopic record of speleothem material formed within the past 350,000 years. The cave is formed within the Ordovician Cotter Formation, a dolostone containing chert nodules and lenses, and thin sandstone and shale interlayers. Mean annual precipitation on the ground surface above the cave is 112 cm, of which about 10 percent is snowfall. Mean annual surface temperature is 14.5°C (July: 26°C; January: 1.7°C); the cave temperature is 15 ± .5°C. Seepage of water into the cave is greatest in winter and spring, reaching a minimum level in late summer. The cave is located 250 km southwest of the limit of ice advance over the last two glacial cycles, and should thus preserve a continuous record of speleothem growth through the late Pleistocene.

Preliminary studies have been made of two large stalagmites and a number of smaller speleothems, as well as of seepage waters, at four sites within the cave. U and Th isotope data for the large speleothems (fig. 1 and table 1) indicate that they grew through overlapping intervals, from 240,000 to 50,000 years ago and 150,000 to 25,000 years ago, respectively. Initial $^{234}U/^{238}U$ ratios (r_o) in the older speleothem (sample no. 76501) remained virtually constant throughout its growth history, both before and after an interruption from about 190,000 to 120,000 years ago following which growth was resumed at a faster rate but with the same r_o value. $^{234}U/^{238}U$ "ages", calculated assuming this constant r_o value throughout deposition, are in close agreement with $^{238}Th/^{234}U$ ages. The younger stalagmite (sample no. 76503) incorporated uranium with an r_o value that varied erratically between 5.3 and 6.3; values were generally higher in the growth period after a hiatus in growth from approximately 90,000 to 70,000 years ago. Depositional histuses in both specimens are marked by textural breaks in the stalagmites, changes in color of the speleothem calcite, and a dusty, slightly corroded interface between pre- and posthiatus material.

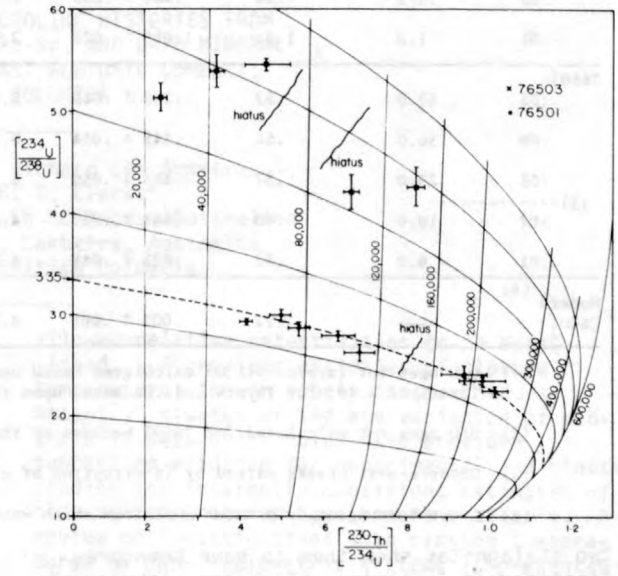

Figure 1.--Variation in $^{234}U/^{238}U$ and $^{230}Th/^{234}U$ ratios in two stalagmites from Tumbling Creek Cave, Missouri.

$^{234}U/^{238}U$ ratios in modern seepage waters collected from near the growth sites of the stalagmites and at two other sites, by coprecipitation of U on $Fe(OH)_3$, were significantly different from values observed in nearby stalagmites. Modern calcite precipitating from a "drip catcher" displayed an r_o value of 4.00, compared with a value of 4.68 for the $Fe(OH)_3$-coprecipitated U from the seepage water. Significant seasonal variations at each drip site have also been observed (table 2).

Protactinium dates were attempted via the $^{227}Th/^{230}Th$ method (Moore and Somayajulu, 1974) and by the $^{227}Th/^{235}U$ method. Speleothem 76503 yielded spurious values, presumably due to its low U content and consequent low count rates; the two dates on 76501 were consistent with $^{230}Th/^{234}U$ dates.

Oxygen and carbon isotopic analyses of the

Table 1.--U Concentrations, Isotope Activity Ratios, and Calculated Ages for Stalagmites 76501, 76503, and Modern $CaCO_3$.

Sample Number	Dist. above base (cm)	U conc. (ppm)	$\frac{230Th}{234U}_t$	$\frac{234U}{238U}_t$	$\frac{234U}{238U}_o$	$\frac{230Th}{232Th}_t$	Th/U age (ka)	U/U age (ka)
76501								
:09	82.0	5.07	.416 ± .017	2.93 ± .03	3.25 ± .04	>1000	55 ± 3	63 ± 6 (1)
:08	64.5	1.22	.407 ± .026	2.99 ± .06	3.40 ± .10	70	68 ± 5	52 ± 11
:07	48.5	.74	.543 ± .024	2.86 ± .07	3.30 ± .12	>1000	77 ± 5	76 ± 13
:06	38.0	1.37	.636 ± .039	2.79 ± .04	3.34 ± .14	>1000	96 ± 12	90 ± 7
:05	23.5	.55	.689 ± .034	2.62 ± .08	3.20 ± .17	>1000	109 ± 8	125 ± 18
(3)----------								
:04	20.5	.21	.936 ± .055	2.40 ± .09	3.38 ± .33	506	190 ± 25	193 ± 24
:03	15.5	.28	.986 ± .055	2.34 ± .05	3.44 ± .33	>1000	216 ± 30	209 ± 16
:01	1.0	1.22	1.016 ± .029	2.24 ± .05	3.39 ± .22	141	236 ± 18	30 ± 15
76503								
:06	43.0	.52	.209 ± .015	5.12 ± .15	5.42 ± .17	>1000	25 ± 1	------- (2)
:09	36.0	.56	.345 ± .014	5.39 ± .16	5.95 ± 21	>1000	43 ± 2	-------
:08	25.0	.37	.463 ± .059	5.45 ± .06	6.29 ± .83	>1000	62 ± 10	-------
(3)----------								
:02	10.0	.60	.668 ± .032	4.21 ± .17	5.26 ± .31	>1000	101 ± 7	-------
:01	6.0	.52	.823 ± .048	4.26 ± .21	5.81 ± .50	>1000	140 ± 14	-------
Modern $CaCO_3$ (4)	----	2.72	.003 ± .001	4.00 ± .06	4.00 ± .06	>1000	-----	-------

(1) U/U ages for layers :01-:03 calculated based upon the mean initial $^{234}U/^{238}U$ ratio for these layers of 3.40; for layers :-4-:09 based upon the mean initial $^{234}U/^{238}U$ ratio of 3.30

(2) U/U ages not calculated for 76503 because of the variable initial $^{234}U/^{238}U$ ratios.

(3) Depositional breaks marked by interruption of growth layers.

(4) Crust forming on drip-water pool from which water no. 2 was collected.

two stalagmites show them to have been precipitated in isotopic equilibrium with parent drip waters. D/H ratios of fluid inclusions (f. i.) were studied to evaluate their temperatures of deposition (Schwarcz and others, 1976). However, if $\delta^{18}O$ of f.i.'s are inferred from normal relationship for meteoric waters: $\delta D = 8\delta O + D_o$, $D_o = 10$ permil (Craig, 1961; Dansgaard, 1964), then unreasonably low temperatures (down to -8°C) result. This can be interpreted as indicating a shift in the δD intercept to a D_o value of ≃ -7 permil during previous glacial periods, although at least part of these data appear to be from the last interglacial. Modern waters from this site lie on the normal meteoric water line (D_o = 10).

Table 2.--$^{234}U/^{238}U$ ratios in modern drip waters

Site	Date of Collection of Sample	
	5/5/77	11/16/77
2	4.68±.06 [1]	1.50±.13
3	2.78±.09	2.01±.15
4	4.81±.06	5.47±.02
6	4.36±.08	3.86±.03

[1] Modern $CaCO_3$ of table 1 formed as crust on pool of this water.

Note: All waters contained 0.10 ± .02 ppb uranium and < .1 ppb Th.

Throughout the last glacial, $\delta^{18}O$ values of speleothem calcite varied by less than 0.7 permil although cave temperature presumably decreased significantly in response to lowered surface temperatures. If we assume that D_o was equal to -7 permil throughout the last glacial period, then cave temperatures calculated from the isotope relationships between the fluid inclusions and their associated calcites vary from near 0°C (assumed) to about 13°C, and indicate warm periods at about 50,000, 80,000, and 125,000 years ago and cold intervals at about 70,000 and 100,000 years ago. However, if D_o varied at all in the past, then true paleotemperatures cannot be obtained using D/H measurements of fluid inclusions alone. Similar variation in D_o appears to have occurred during the Wisconsin, at a site in

Iowa although no such variation is suggested by data from other continental sites. Uniform $\delta^{18}O$ values of calcite growth layers argue against D/H fractionation. Direct oxygen isotopic analysis of fluid-inclusion water may permit resolution of this dilemma.

Thin, modern soda-straw stalactites growing in parts of the cave overlain by different floral elements (cultivated fields versus forest) show identical average carbon isotopic compositions, and show parallel profiles of decreasing $\delta^{13}C$ toward the present, possibly in response to increasing rates of decomposition of humic materials.

Craig, H., 1961, Isotopic variations in meteoric waters: Science, v. 133, p. 1702-1703.

Dansgaard, W., 1964, Stable isotopes in precipitation: Tellus, v. 4, p. 436-468.

Moore, W. S., and Somayajulu, B. L. K., 1974, Age determinations of fossil corals using $^{230}Th/^{234}Th$ and $^{230}Th/^{227}Th$: Journal of Geophysical Research, v. 79, p. 5065-5068.

Schwarcz, H. P., Harmon, R., Thompson, P., and Ford, D., 1976, Stable isotope studies of fluid inclusions in speleothems and their paleoclimatic significance: Geochimica Cosmochimica Acta, v. 40, p. 657-665.

THERMAL MODELS AND COOLING HISTORIES FROM FISSION-TRACK, K-Ar, Rb-Sr, AND U-Pb MINERAL DATES, NORTHERN COAST PLUTONIC COMPLEX, BRITISH COLUMBIA

By T. Mark Harrison[1], Richard Lee Armstrong[2], and Garry K. C. Clarke[2]

[1]Research School of Earth Sciences, Australian National University, Canberra, Australia

[2]University of British Columbia

Isotopic and fission-track dates were determined on coexisting minerals from samples of the Ecstall and Quottoon plutons in the northern part of the Coast Plutonic Complex, near Prince Rupert, B.C. (fig. 1), to resolve the very different cooling histories indicated by Rb-Sr whole-rock isochrons (Armstrong and Runkle, 1978). The previously accepted age of the Ecstall pluton of 75 m.y. based on K-Ar dates for hornblende (Symons, 1974), was extended to 177 m.y. by the Rb-Sr whole-rock method, but the 49 m.y. age of emplacement for the Quottoon pluton indicated by K-Ar dates on biotite and hornblende was not significantly increased (Rb-Sr whole-rock isochron of 51 ± 2 m.y.).

Using previously assigned values for closure temperatures for each type of date that was measured, cooling curves for individual samples of each pluton were constructed (Harrison and others, 1978). These curves were then used to quantitatively test theoretical models for emplacement and cooling history (Harrison and Clarke, 1978).

As the effective closure temperature (ideally, the temperature at the time when the daughter product ceased to escape or disappear from the system) varies with cooling rate, data generated by laboratory experiment must be extrapolated over many orders of magnitude to provide temperature estimates, for geological time, of the thermal stability of the daughter product. Kinetic studies of the thermal effects of intrusion on host-rock mineral dates have allowed relative retentivities to be established, and provided estimates of closure temperature, though poorly constrained. Recently, studies of the age variation of minerals in deep drill holes have provided supporting evidence for experimental and kinetic studies and internally consistent estimates of closure temperatures have become available. A review of investigations into closing temperatures of many radiometric systems is presented in Harrison and others (1978). Estimates of closure temperature ranges for minerals cooling at a rate of $\sim 10°C$ m.y.$^{-1}$ are compiled in table 1.

Quottoon pluton: The Quottoon pluton is a dike-shaped body emplaced into the core of a high grade metamorphic complex (fig. 1). Depth of sample during emplacement is estimated to be between 9 and 15 km. Zircons dated by the U-Pb method from the host-rock granulites suggest that culmination of metamorphism occurred about 68 m.y. ago. The cooling curve for the Quottoon pluton generated by the mineral dates is shown in figure 2. Although orthoclase and plagioclase K-Ar dates were not used in constructing the curve due to lack of pre-existing estimates of closure temperatures, an estimate of these values can be made from the time intercepts with the cooling curve (fig. 2). The apparent effective closure temperatures are 160°C and 250°C for orthoclase and plagioclase, respectively.

As the present-day relief of the Coast Mountains post-dates the late Miocene (Monger and others, 1972), the apatite date of 7.3 m.y.

indicates the end of a pause in uplift during which the sample lay at a temperature of greater than about 100°C (8 m.y. x 0.5 km m.y.$^{-1}$ (late Cenozoic uplift rate from neighboring Kasiks pluton) x 26°C km^{-1} (Mathews, 1972) = 104°C).

Table 1.--Estimates of closure temperatures in chronometric systems cooling ∿10°C m.y.$^{-1}$

Chronometer	Effective closure temperature (°C)
Fission track:	
Apatite	100±20
Zircon	175±25
Sphene	250±50
Potassium-argon:	
Biotite	220±40
Hornblende	500±75
Microperthite	∿160
Plagioclase	∿250
Rubidium-strontium:	
Biotite	300±25
Whole-rock	On crystallization

A geologic model compatible with the chronologic and petrologic constraints has been constructed. Culmination of metamorphism of the host rocks occurred ∿ 68 m.y. ago. Regional uplift at "Alpine" rates brought these rocks to a depth of between 9 and 15 km by ∿ 51 m.y. ago. At this time the pluton, formed in part by partial melting of rocks still undergoing high-grade metamorphism at greater depth, was emplaced diapirically. The region continued to be uplifted; the rocks presently exposed reaching a depth of ∿ 4 km by 45 m.y. ago. Regional uplift then ceased allowing the sample site to cool asymptotically towards the ambient temperature of ∿ 100°C. A period of 35 m.y of isostatic stability followed, terminated by a regional uplift that began ∿ 10 to 15 m.y. ago producing the relief now seen in the Coast Mountains.

Ecstall pluton: The Ecstall pluton (fig. 1) is a composite, zoned, granitic, "tadpole"-shaped body containing concentric phases from diorite on the periphery to quartz monzonite in the core. The pluton has steeply dipping contacts and appears to have domed metasediments to the north on emplacement.

As already mentioned, Rb-Sr whole-rock isochrons for the Ecstall pluton indicate an age of emplacement of 177 m.y. However, the 16 mineral dates determined lie between 36 and 75 m.y. Of these dates, only the K-Ar biotite does not show the relative retentivity of table 1. The mineral dates plotted against their effective closure temperatures are shown in figure 3. Two interpretations of the Ecstall pluton's cooling history are possible, and both involve invoking the presence of excess ^{40}Ar in biotite. A slow-cooling, regional uplift will produce a convex curve passing through all points except K-Ar biotite. The other extreme possibility is of quick cooling in the same fashion as the Quottoon pluton followed by a heating event some 60 to 75 m.y. ago that reset the mineral dates, with the possible exception of only partially resetting the hornblende. As both these interpretations involve ∿ 100 m.y. of ^{40}Ar generation in a pluton at ∿ 2 percent K before the dates

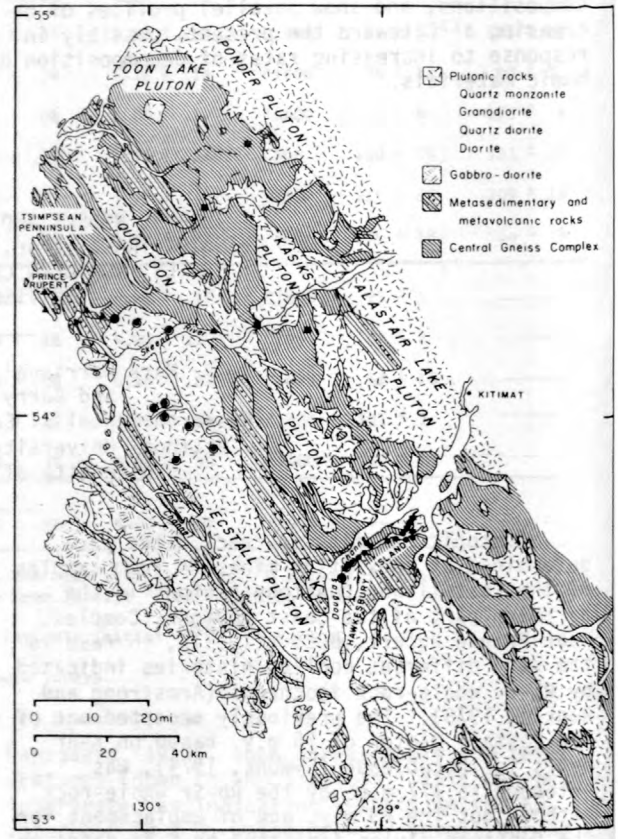

Figure 1.--Generalized geologic map (from Armstrong and Runkle, 1978) of the Prince Rupert-Douglas Channel region showing sample localities for Sr isotopic analyses. Samples of Jurassic plutons are shown as concentric circles and Quottoon pluton sample localities as stars.

are permanently set, there is no difficulty in assuming a fairly high intergranular partial-pressure of Ar.

The favored hypothesis is of rapid cooling following emplacement 177 m.y. ago, followed by a thermal pulse resetting the mineral dates 60 to 75 m.y. ago. This situation is known in the Cordillera and another example is shown by Evernden and Kistler (1970) in the Sierra Nevada. The resetting may be a peripheral effect of metamorphism in the Central Gneiss Complex that culminated about 68 m.y. ago.

Kasiks pluton: Two samples of foliated quartz diorite from the Kaskiks pluton (fig. 1) 6 km apart and with 1.7 km relief between them

were dated by apatite and zircon fission track and biotite K-Ar in the hope of resolving age difference due to uplift. Although no statistical difference existed for the zircons and biotites, a separation of dates for the two apatites was found. Assuming a constant temperature-versus-depth relation during uplift, the difference in elevation divided by the age difference gives a value for the uplift rate of 1.7 km/3.5 m.y. = 0.049 cm yr^{-1}. The maximum and minimum uplift rate at 1σ error are 0.089 and 0.033 cm yr^{-1}, respectively. This rate multiplied by the present day geothermal gradient of 26°C km^{-1} gives a post-Miocene cooling rate of 13°C $m.y.^{-1}$. The slope of this rate is shown in figure 2 and is clearly identical to that final portion of the Quottoon cooling curve.

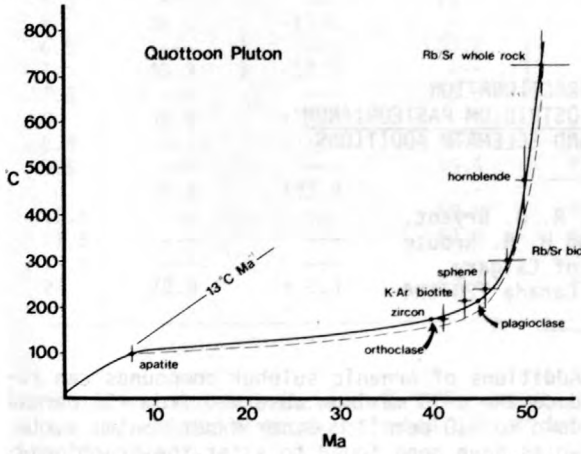

Figure 2.--Cooling history of sample 20-2G from the Quottoon pluton on Loretta Channel. Individual K-Ar, Rb-Sr, and fission-track mineral dates are plotted against independent estimates of closure temperature discussed in text. The 13°C $m.y.^{-1}$ cooling rate shown was calculated from neighboring Kasiks pluton. Errors in time dimension are 1σ for each date. Range shown for temperature is the 10 percent and 90 percent retention temperatures for the appropriate cooling rate. No crosses are shown for the orthoclase and plagioclase. Arrows indicate their position on the cooling curve as inferred from their respective K-Ar dates. Orthoclase and plagioclase dates are consistent with Limited closure temperature information for these minerals. Dashed line is cooling curve generated by the calculations of Harrison and Clarke (1978).

Thermal models: As conventional thermal models (for example, Larsen, 1945; Jaeger, 1964) of closed solution are only applicable to the extreme geological cases of regional uplift and static intrusion into an isothermal medium, they are not able to test the mixed thermal histories described. Consequently, a numerical simulation was constructed to allow the geological models proposed to be tested quantitatively. Our simulation is a time-dependent mathematical model of the two-dimensional cooling of a pluton having rectangular cross section. The model differs from earlier contributions in that the dike is intruded into a medium which is at equilibrium with a geothermal flux and evenly distributed radioactive heat sources. Further, a complicated history of regional uplift can be assumed. This model and a review of the conventional limiting cases is presented in Harrison and Clarke (1978).

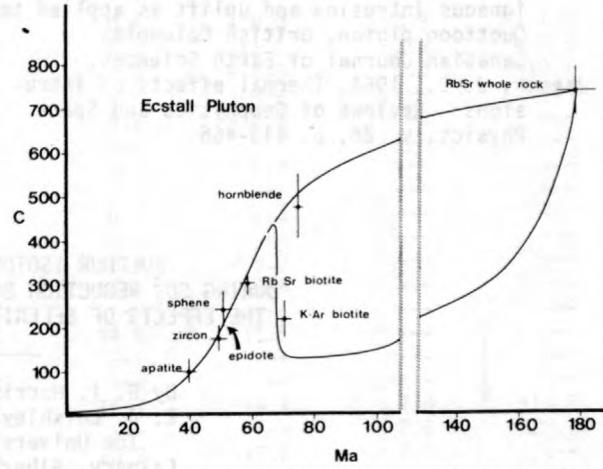

Figure 3.--Cooling history of sample PR 3 from the Ecstall pluton. These data are consistent with either a slow and delayed regional uplift or a distinctly post-initial-cooling mineral resetting event. Other factors discussed in text point to a mineral resetting event.

For the Quottoon pluton, model-input parameters constraining dimensions, thermal properties, thermal flux from mantle, heat production, uplift rates, and initial temperature of the pluton were either measured or estimated independent of the numerical simulation. The theoretical cooling curve for the Quottoon pluton is shown in figure 2 as a dashed line. This curve agrees closely with the experimental curve and we conclude that our geologic model is physically sound.

Further, this model shows that within ∿ 4 km of the earth's surface an uplift rate of 0.05 cm yr^{-1} will produce nearly stationary isotherms, justifying that assumption used when calculating the Kasiks uplift rate. Another implication of the model is that high-grade metamorphism in the Central Gneiss Complex could generate the temperatures needed to reset the mineral dates in the Ecstall pluton.

Armstrong, R. L., and Runkle, D. E., (in press), Rb-Sr geochronometry of the Ecstall, Kitkiata, and Quottoon plutons and their country rocks, Prince Rupert region, Coast Plutonic Complex, British Columbia: Canadian Journal of Earth Sciences.

Evernden, J. F., and Kistler, R. W., 1970,

Chronology of emplacement of Mesozoic batholithic complexes in California and Western Nevada: U.S. Geological Survey Professional Paper, v. 623, 42 p.

Harrison, T. M., Armstrong, R. L., Naeser, C. W., and Harakal, J. E., (in press), Geochronology and thermal history of the Coast Plutonic Complex, near Prince Rupert, B.C.: Canadian Journal of Earth Sciences.

Harrison, T. M., and Clarke, G. K. C., (in press), A model of the thermal effects of igneous intrusion and uplift as applied to Quottoon pluton, British Columbia: Canadian Journal of Earth Sciences.

Jaeger, J. C., 1964, Thermal effects of intrusions: Reviews of Geophysics and Space Physics, v. 26, p. 443-466.

Larsen, E. S., 1945, Time required for the crystallization of the great batholith of southern and lower California: American Journal of Science, v. 243a, p. 399-416.

Mathews, W. H., 1972, Geothermal data from the Granduc area, northern Coast Mountains of British Columbia: Canadian Journal of Earth Sciences, v. 9, p. 1333-1337.

Monger, J. W. H., Souther, J. G., and Gabrielse, H., 1972, Evolution of the Canadian Cordillera; a plate tectonic model: American Journal of Science, v. 272, p. 577-602.

Symons, D. T. A., 1974, Age and tectonic implications of palaeomagnetic results from plutons near Prince Rupert, British Columbia: Journal of Geophysical Research, v. 79, p. 2693-2696.

SULPHUR ISOTOPE FRACTIONATION DURING $SO_3^=$ REDUCTION BY CLOSTRIDIUM PASTEURIANUM: THE EFFECTS OF SELENITE AND SELENATE ADDITIONS

By G. I. Harrison, R. D. Bryant, E. J. Laishley, and H. R. Krouse
The University of Calgary,
Calgary, Alberta, Canada T2N 1N4

McCready and others (1975) reported large inverse isotope effects during $SO_3^=$ reduction by Clostridium pasteurianum, an abundant soil microorganism. In early stages of a typical laboratory reduction experiment, this organism evolves H_2S which is depleted in ^{34}S by about 15 permil. In this paper, $\delta^{34}S$ is defined in terms of the initial composition of the reactant $SO_3^=$

$$\delta^{34}S \text{ in permil} = \left\{ \frac{[^{34}S/^{32}S]_{\text{evolved } H_2S}}{[^{34}S/^{32}S]_{\text{initial } SO_3^=}} - 1 \right\} \times 10^3$$

As the conversion proceeds, the $\delta^{34}S$ value of the H_2S increases reaching values as high as +50 permil. This corresponds to an inverse isotope effect because the H_2S is more enriched in ^{34}S than the unreacted $SO_3^=$ and intermediates in the culture medium. After the $\delta^{34}S$ maximum, the H_2S becomes isotopically lighter again and may achieve negative values. Several hundred $SO_3^=$ reduction experiments have been carried out under a variety of conditions and the inverse isotope effect has always been evident. Possible biogeochemical implications in interpreting sulphur isotope fractionation in environments populated by this organism were discussed by McCready and others (1976). More recently, Laishley and Krouse (1978) have examined the regulation of sulphite reductases by sulphur amino acids with this organism. This work provided evidence for an inductible reductase, considered to be dissimilatory, in addition to the previously reported assimilatory reductase. Additions of organic sulphur compounds can reduce the $\delta^{34}S$ maximum observed from +50 permil down to +10 permil. Other experimental variables have been found to alter the fractionation pattern (Laishley and others, 1976).

Selenium, which is in the same chemical family as sulphur, is required in trace amounts (μM concentration) by bacteria for growth. At mM concentrations, it can be incorporated into many cell constituents. Where enzyme systems are unable to distinguish selenium from sulphur, the cell may encounter metabolic problems due to the greater reactivity and lower stability of selenium compounds. Because of the abundance of Clostridium pasteurianum in nature, it seemed desirable to examine how the addition of selenium compounds affected the metabolism and sulphur isotope fractionation capabilities of this organism. The growing cell experiments of this report were carried out with 1 mM $SO_3^=$, 1 percent sucrose--synthetic salts medium at 37°C. Additions of selenium compounds were made after 3.5 hours. The culturing techniques are described by Laishley and Krouse (1978).

The addition of 1 mM $SeO_4^=$ had no effect on the growth rate but reduced the H_2S production by 30 percent. When 1 mM $SeO_3^=$ was added, H_2S evolution ceased; changes in cell morphology occurred; the growth rate was reduced. The addition of 0.25 mM $SeO_3^=$ stopped H_2S production, but it started again after 1.5 hours at a much reduced rate in comparison to experiments with $SO_3^=$ alone. Morphological changes to the cells

Table 1.--Effects of $SeO_4^=$ and $SeO_3^=$ additions on sulphur isotope fractionation during $SO^=$ reduction by *Clostridium pasteurianum*

[Growth conditions 1 mM $SO_3^=$; 1 percent sucrose; 37°C; selenium compounds added at 3.5 hr. Downward arrows depict change from log to stationary growth phase.]

	Control		+1 mM $SeO_4^=$		+0.25 mM $SeO_3^=$		+1 mM $SeO_3^=$	
Time (hr.)	H_2S produced (percent)	$\delta^{34}S$	H_2S produced (percent)	$\delta^{34}S$	H_2S produced (percent)	$\delta^{34}S$	H_2S produced (percent)	$\delta^{34}S$
2	---	---	0.5	- 6.5	0.6	- 8.0	0.9	- 7.8
3	5.0	-10.2	2.1	- 9.4	2.2	-11.0	3.9	- 9.3
3.5	---	---	4.3	-10.7	4.3	-11.0	5.3	-10.7
4	11.6	-15.4	---	---	---	---	---	---
4.5	---	---	11.7	-12.2	4.9	- 8.8	---	---
5	24.3	-17.3	---	---	---	---	---	---
5.5	---	---	23.0	-12.1	5.2	- 5.8	---	---
6	34.5	-15.6	---	---	---	---	---	---
6.5	---	---	33.2	- 5.1	6.3	- 7.3	---	---
7	40.3	-12.9	---	---	---	---	---	---
7.5	---	---	43.6	+20.5	8.4	- 5.0	---	---
8	62.9	+ 7.7	---	---	---	---	---	---
8.5	---	---	47.1	+20.3	---	---	---	---
9.5	---	---	49.4	+15.8	14.5	+15.6	---	---
10	70.4	+33.8	---	---	---	---	---	---
10.5	---	---	50.8	+12.4	---	---	---	---
11.5	---	---	51.6	+11.5	16.7	+44.7	7.0	+18.2
14.5	---	---	---	---	---	---	7.6	+20.1
24	72.9	+ 8.9	52.6	+ 4.4	20.2	-12.7	7.6	---

were not evident but the growth rate was reduced and partially recovered when H_2S production resumed.

Figure 1 shows how the sulphur isotope composition of the evolved H_2S varied in these experiments. It is interesting that the same general shape for the isotopic fractionation pattern was found in all experiments but it was noticeably compressed along the percentage conversion axis when selenium compounds were added. In specific terms, while the maximum $\delta^{34}S$ value occurred near 60 percent conversion with $SO_3^=$ alone, 1 mM $SeO_4^=$ shifted the maximum $\delta^{34}S$ value down to 40 percent conversion. With $SeO_3^=$, the $\delta^{34}S$ maximum occurred at even lower percentages of conversion and it appears that the shift depends upon the $SeO_3^=$ concentration.

Another interesting aspect of these experiments is seen in table 1. The downward pointing arrows represent the end of log growth in the experiments. The end occurs after longer times in progressing from 1 mM $SeO_4^=$ to 0.25 mM $SeO_3^=$ to 1 mM $SeO_3^=$. This also corresponds to the point in the experiment where the evolved H_2S undergoes a large swing from negative to positive $\delta^{34}S$ values.

Thus, it is seen that the isotopic fractionation pattern depends upon the growth phases, that is, a log versus stationary growth. The extent to which the sulphur isotope behavior is altered by the addition of selenium compounds would then seem to be related to how these additions affect metabolic processes and consequently cell growth.

These observations are not only interesting from the viewpoint of understanding the biochemical pathways in this organism, but they can potentially assist in interpreting natural isotope abundance data in ecosystems where both the selenium and sulphur cycles function; for example in well-known seleniferous soil occurrences.

This research was supported by the National Research Council of Canada [Grants A-5058 (EJL) and A-8176 (HRK)] and The University of Calgary Interdisciplinary Sulphur Research Group (UNISUL).

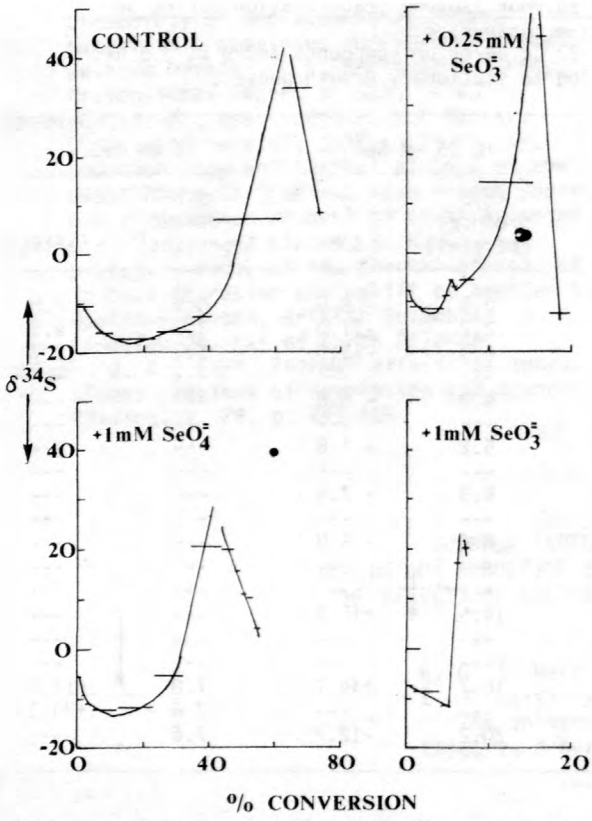

Figure 1.--Effects of $SeO_4^=$ and $SeO_3^=$ on the sulphur isotopic composition of evolved H_2S during $SO_3^=$ reduction by Clostridium pasteurianum. Growth conditions 1 mM $SO_3^=$, 1 percent sucrose--synthetic salts medium at 37°C. The selenium compounds were added after 3.5 hr. The lengths of the horizontal bars correspond to the fractions of H_2S collected during the experiments.

Laishley, E. J., and Krouse, H. R., 1978, Stable isotope fractionation by Clostridium pasteurianum; 2. Regulation of sulfite reductases by sulfur amino acids and their influence on sulfur isotope fractionation during $SO_3^=$ and $SO_4^=$ reduction: Canadian Journal of Microbiology, (in press).

Laishley, E. J., McCready, R. G. L., Bryant, R., and Krouse, H. R., 1976, Stable isotope fractionation by Clostridium pasteurianum, in, Nriagu, J. O., ed., Environmental biogeochemistry, v. 1, Carbon, Nitrogen, Phosphorus, Sulfur and Selenium Cycles: Ann Arbor, Ann Arbor Science, p. 327-349.

McCready, R. G. L., Laishley, E. J., and Krouse, H. R., 1975, Stable isotope fractionation by Clostridium pasteurianum; 1. $^{34}S/^{32}S$; inverse isotope effects during SO_4^{2-} and SO_3^{2-} reduction: Canadian Journal of Microbiology, v. 31, p. 325-344.

_____ 1976, Biogeochemical implications of inverse sulfur isotope effects during reduction of sulfur compounds by Clostridium pasteurianum: Geochimica Cosmochimica Acta, v. 40, p. 979-981.

THE ARGON ISOTOPIC COMPOSITION OF THE OCEANIC CRUST AND A MODEL FOR FORMATION OF THE SIALIC CRUST--ATMOSPHERE FROM THE UPPER MANTLE

By Roger Hart and Jack Dymond
School of Oceanography
Oregon State University
Corvallis, Oregon 97331

The concentration and isotopic composition of argon in the mantle constrain the permissable potassium content and degassing history of the earth. An indication of the mantle argon content may be provided by the noble gas compositions of rapidly quenched seafloor basalts. Measured values of the ^{40}Ar contents in submarine basalts are variable; however, 65 percent of the measurements lie between 0.9 to 3.0 X 10^{-6} cm^3 g^{-1} of ^{40}Ar (fig. 1). The ^{36}Ar contents of deep sea basalts varies from 0.1 to 9.0 X 10^{-9} cm^3 g^{-1}, the $^{40}Ar/^{36}Ar$ values range between 295 and 15,000, and apparent K-Ar ages range from 7 to 1900 X 10^6 yr (fig. 2). Much of this variability can be attributed to degassing and atmospheric contamination (Dymond

and Hogan, 1978).

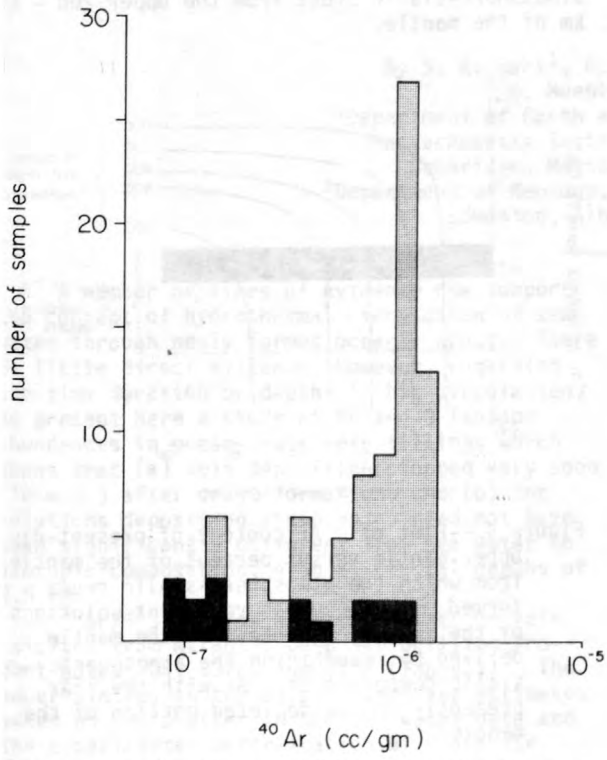

Figure 1.--Histogram of ^{40}Ar concentrations measured in submarine basalts. Black squares, samples from "plume" areas. Data from: Dalrymple and Moore (1968); Funkhouser, Fisher, and Bonatti (1968); Dymond and Hogan (1973, 1978); Fisher (1975); Takaoka and Nagao (in press); and Dymond (unpublished data).

As shown in figure 2, degassing lowers the concentration of Ar and the apparent K-Ar age, but does not greatly affect the $^{40}Ar/^{36}Ar$ ratio. The samples with the highest K-Ar ages (1.5-1.9 X 10^9 years) were dredged from the Juan de Fuca ridge and compositionally appear to be normal mid-ocean ridge basalts. Samples with the lowest K-Ar ages are exclusively from "plume" areas, suggesting that basalts from island platforms have degassed more than samples dredged from deeper portions of the ocean.

Atmospheric contamination raises the concentration of ^{36}Ar, slightly raises the K-Ar age, and greatly lowers the $^{40}Ar/^{36}Ar$ ratio. Atmospheric contamination can occur through low-temperature weathering, by basalt-seawater reaction at the time of cooling, and possibly by seawater contamination of magma. A series of very fresh glassy basalts from the Juan de Fuca Ridge exhibit an inverse correlation between $^{40}Ar/^{36}Ar$ values and their water contents (fig. 3), suggesting that the range in $^{40}Ar/^{36}Ar$ values in these samples results from contamination of the magma by seawater. Plume-area samples also have $^{40}Ar/^{36}Ar$ values which are relatively low and similar to the atmospheric value (295.5), suggesting possible atmospheric contamination.

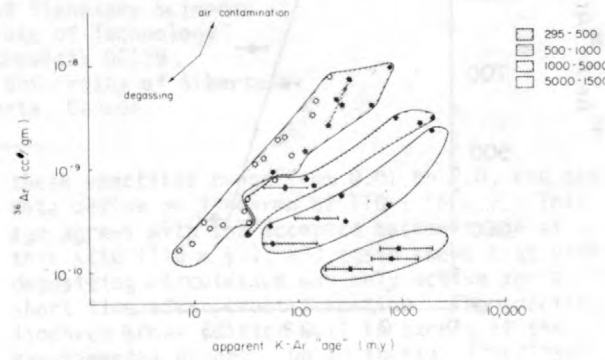

Figure 2.--Plot of ^{36}Ar versus apparent K-Ar age in submarine basalts. K-Ar age calculated from total ^{40}Ar. Data from: Dalrymple and Moore (1968); Funkhouser, Fisher, and Bonatti (1968); Dymond and Hogan (1973, 1978); Fisher (1975); Takaoka and Nagao (in press); and Dymond (unpublished data). Open circles, samples from "plume" areas; solid circles, all other samples. Error bars, samples in which K was estimated from analysis of different portions of the same sample. Patterned areas enclose samples of similar $^{40}Ar/^{36}Ar$ ratio. Dashed line and small arrow connect analysis made on glassy margin of a pillow basalt with analysis made on a holocrystalline; demonstrates effect of atmospheric contamination.

Partial melting and crystal fractionation effects will also cause the argon contents of submarine basalts to be greater than that of the mantle. It can be shown, however, that these processes will not result in marked enrichments in the ^{40}Ar contents (Dymond and Hogan, 1978).

Although we can not be certain at present, of the importance of atmospheric contamination and degassing, the relatively narrow range in ^{40}Ar contents in the majority of submarine basalts (fig. 1) suggests that 3 X 10^{-6} cm^3 g^{-1} may be an upper limit for the argon content of the mantle. By accepting this value, it can be shown that the ^{40}Ar in the atmosphere may have degassed from the upper mantle rather than from the entire mantle. Furthermore, based on the compatibility of the ^{40}Ar content of the atmosphere with the likely K contents of the sialic crust, the ^{40}Ar probably degassed coherently with removal of K from the upper mantle to the sialic crust. We hypothesize that this process has resulted in an upper mantle depleted in LIL elements as well as argon.

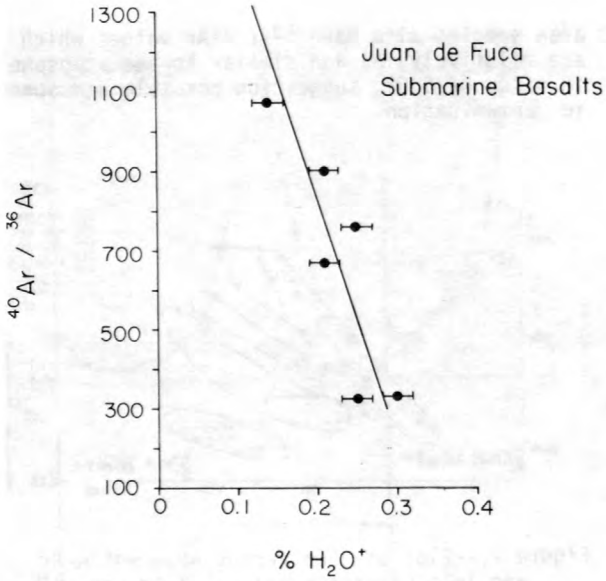

Figure 3.--Plot of $^{40}Ar/^{36}Ar$ versus H_2O^+ of submarine basalts dredged from the Juan de Fuca Ridge.

Many theories of earth degassing assume that atmospheric ^{40}Ar degassed from the entire mantle. The initial potassium content of the mantle can be derived by recombing the ^{40}Ar from the atmosphere and sialic crust with the ^{40}Ar of the present-day mantle and using 4.5 b. y. as the age of the mantle. We suggest that the ^{40}Ar of the atmosphere and sialic crust may not have degassed from the entire mantle, and point out that the permissible initial K content of the mantle is inversely proportional to the portion of the mantle outgassed. This concept is presented graphically in figure 4, a plot of the ^{40}Ar of the depleted portion of the mantle versus the percent of the mantle from which the atmosphere and sialic crust differentiated. This figure also shows that the calculated K content of the nondepleted mantle is directly proportional to the ^{40}Ar content of the present-day depleted mantle.

Figure 4 suggests that if the upper mantle has an ^{40}Ar content of less than 3×10^{-6} cm^3 g^{-1}, the K content of the mantle must be less than 200 ppm in order for the atmosphere-sialic crust to have degassed from the total mantle. In order for the ^{40}Ar in the atmosphere-sialic crust to degas from the entire mantle and the K-content of the upper mantle to be greater than 400 ppm, as stipulated by many heat-flow models, the ^{40}Ar content of the upper mantle must be 10 times greater than that observed in submarine basalts. The observed ^{40}Ar contents of submarine basalts are compatible with an initial K content of 400-1000 ppm and formation of the atmosphere-sialic crust from the upper 200 - 600 km of the mantle.

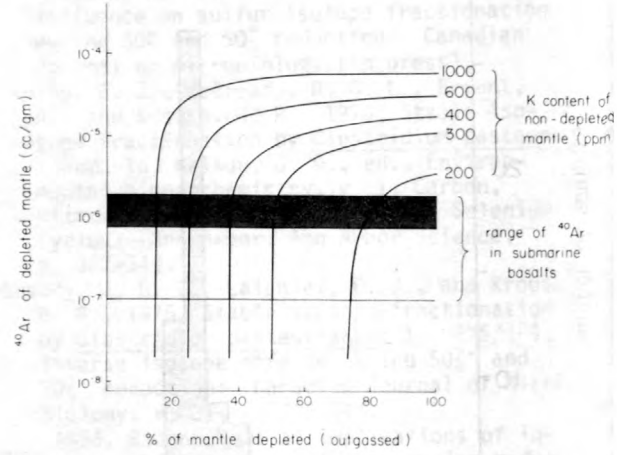

Figure 4.--Plot of ^{40}Ar content of present-day upper mantle versus percent of the mantle from which the atmosphere-sialic crust formed. Iso-K curves represent solutions of the initial K content of the mantle derived by recombining the atmospheric-sialic component of ^{40}Ar with the ^{40}Ar presently in the depleted portion of the mantle.

Dalrymple, G. B., and Moore, J. G., 1968, Argon-40; Excess in submarine pillow basalts from Kilauea Volcano, Hawaii: Science, v. 161, p. 1132.

Dymond, J., and Hogan, L., 1973, Noble gas abundance patterns in deep-sea basalts--Primordial gases from the mantle: Earth and Planetary Science Letters, v. 20, no. 1, p. 131-139.

Dymond, J., and Hogan, L., 1978, Factors controlling the noble gas abundance patterns of deep sea basalts: Earth and Planetary Science Letters, v. 38, p. 117-128.

Fisher, D. E., 1975, Trapped helium and argon and the formation of the atmosphere by degassing: Nature, v. 256, p. 113-114.

Funkhouser, J. F., Fisher, D. E., and Bonatti, E., 1968, Excess argon in deep sea rocks: Earth and Planetary Science Letters, v. 5, p. 95-100.

Takaoka, N., and Nagao, K., in press, Rare-gas studies of Cretaceous deep-sea basalts, in Initial reports of the Deep Sea Drilling Project, v. 51: U.S. Government Printing Office, Washington.

OCEANIC CRUST: AGE OF ALTERATION

By S. R. Hart[1], H. Staudigel[1], and
K. Muehlenbachs[2]
[1]Department of Earth and Planetary Sciences
Massachusetts Institute of Technology
Cambridge, Massachusetts 02139
[2]Department of Geology, University of Alberta
Edmonton, Alberta, Canada

A number of lines of evidence now support the concept of hydrothermal circulation of sea water through newly formed oceanic crust. There is little direct evidence, however, regarding the time duration or depth of this circulation. We present here a study of Sr and O isotope abundances in ocean-crust vein fillings which shows that (a) vein deposition stopped very soon (10 m.y.) after crust formation, and (b) the solutions depositing these veins need not have been significantly different from sea water in isotopic composition, even at crustal depths of 0.5 km.

$^{87}Sr/^{86}Sr$ ratios were determined on vein calcites from Atlantic Deep Sea Drilling Project holes 105, 332B, and 418A (Table 1). The uncertainties in the calcite ages are estimates based on the scatter in the sea water data and the experimental determination of $^{87}Sr/^{86}Sr$. The calcite data agree with the sea water curve within errors. Because of the relatively rapid increase of sea water $^{87}Sr/^{86}Sr$ during the past 200 m.y., the time of deposition of the calcites can be specified fairly precisely; the data show that these vein calcites were deposited within 10 - 20 m.y. after the formation of the crust.

Table 1.--$^{87}Sr/^{86}Sr$ ratios of vein calcites from Atlantic DSDP holes 105, 332A, and 418A

Hole	Basement Age (m.y.)	Calcite $^{87}Sr/^{86}Sr$	Calcite Age (m.y.)[1]
332B	3.5	0.70901·5	3±2
418A	110	0.70734·6	117·8
105	155	0.70691·5	168·10

[1]Determined from sea water data of Peterman, Hedge and Tourtelot, 1970; Dasch and Biscaye, 1971; Veizer and Compston, 1974; Brass, 1976.

In addition to the calcites, eight samples of vein smectite from hole 418A (from depths ranging from 70 - 530 m) were analyzed for Rb, Sr and Sr isotope ratios. The Rb/Sr ratios of these smectites range from 0.01 to 2.0, and the data define an isochron of 110 ± 16 m.y. This age agrees with the accepted basement age at this site (110 m.y.), and again shows that vein-depositing circulation was only active for a short time after crust formation. The smectite isochron shows scatter well in excess of the experimental errors. On an initial $^{87}Sr/^{86}Sr$ versus 1/Sr plot, the data for individual smectites lie on a mixing line, with fresh basalt as one possible end member. Also, the initial ratio of the isochron (0.7063 ± .0002) is lower than that for five calcites from the same hole, suggesting incomplete exchange with sea water during the basalt-smectite reaction. There is a crude trend of smectite initial ratio with depth, suggesting the shallow samples (0.707) were more completely exchanged with 110 m.y. sea water, and the deeper samples (.705) less exchanged (in other words, more "basaltic").

The five calcites from this same hole show a slight variation in $^{87}Sr/^{86}Sr$ (.7070 - .7076) which also appears related to a mixing phenomenon, or lack of complete equilibrium with sea water.

Oxygen isotope ratios were measured on these same calcite and smectite samples from hole 418A. $\delta^{18}O$ ranges from +22 - +30 permil for the calcites and from +15 - +20 permil for the smectites (relative to SMOW). Both the calcite and smectite samples show a decrease of $\delta^{18}O$ with depth. If the depositing solutions were of sea water isotopic composition then the calcite oxygen would correspond to temperatures of deposition (or of final exchange) ranging from 18°C (shallow samples) to 75°C (deepest sample). The decrease of $\delta^{18}O$ in the smectites with depth could also suggest increasing temperature with depth; more likely, it is a combination of an increase of temperature and an increasing admixture of "basalt" oxygen (as indicated by the Sr isotopic data on the smectites).

PETROGENETIC IMPLICATIONS OF Sr-ISOTOPE AND TRACE-ELEMENT DATA IN ALKALINE LAVAS FROM CAPE VERDE ISLANDS AND CANARY ISLANDS

By J. Hertogen[1], S. Deutsch[2], P. De Paepe[1], and J. Klerkx[3]
[1]Rijksuniversiteit Gent
[2]Université Libre de Bruxelles
[3]Musée Royal de l'Afrique Centrale - Tervuren, Belgium

A suite of incompatible (REE, Hf, Ta, Th, U) and compatible (Sc, Co, Cr, V) trace elements have been determined by instrumental neutron activation analysis in 43 volcanic rock samples from the Cape Verde Islands (CVI) and in 23 samples from Fuerteventura, Canary Islands (FU). The Sr-isotopic composition was measured in selected samples.

Cenozoic volcanic activity on CVI is characterized by four main alkaline rock types (fig. 1), (melilite) nephelinites being far less abundant than are commonly assumed. The alkaline magmatism is in strong contrast with the composition of pre-Tertiary basement, which consists of pillow basalts with all the geochemical traits of ocean floor basalts (De Paepe and others, 1974). Volcanic rocks on FU (fig. 2) range from basanitoids to olivine basalts with tholeiitic affinities; strongly undersaturated nephelinites are still less common than on CVI. The subaerial volcanism on FU belongs to four main series (I to IV), Miocene(?) to Subhistoric times). Two well-developed low-pressure crystal differentiation trends are apparent on CVI. The highly evolved nepheling phonolites and syenites are separated from the basaltic rocks by a clear-cut silica gap (48-54 percent SiO_2). Low-pressure differentiation was a rare phenomenon on FU; the alkali olivine basalt-hawaiite-mugearite lineage is entirely confined to lavas of Series I.

Earlier measurements of the Sr-isotopic composition (fig. 1) of CVI lavas and associated plutonic rocks (Klerkx and others, 1974) gave isotopic ratios within a narrow range (0.7029 - 0.7033), typical for alkaline lavas from Atlantic Ocean islands. Recent measurements of basanites from Maio show that they are isotopically distinct (0.7035 - 0.7038) from the other analyzed CVI samples. Preliminary Sr-isotopic data for 12 samples from Fuerteventura yield a range of 0.7030 - 0.7035, with no evidence for a correlation between isotopic ratio and rock type.

The trace-element characteristics (figs. 3 and 4) of the samples that are not part of a low-pressure differentiation lineage, generally follow the trends of "primary" basalts from other oceanic and continental alkaline provinces (for example, Sun and Hanson, 1975). The trace-element variations are most readily explained by assuming that the samples represent primary magmas generated by partial melting of upper mantle material. That is not to say that they did not undergo limited fractionation during ascent to the surface. The appreciably differentiated samples could be readily distinguished from the primary ones, based on Cr, Co, Sc, and Mg contents (figs. 1 and 2).

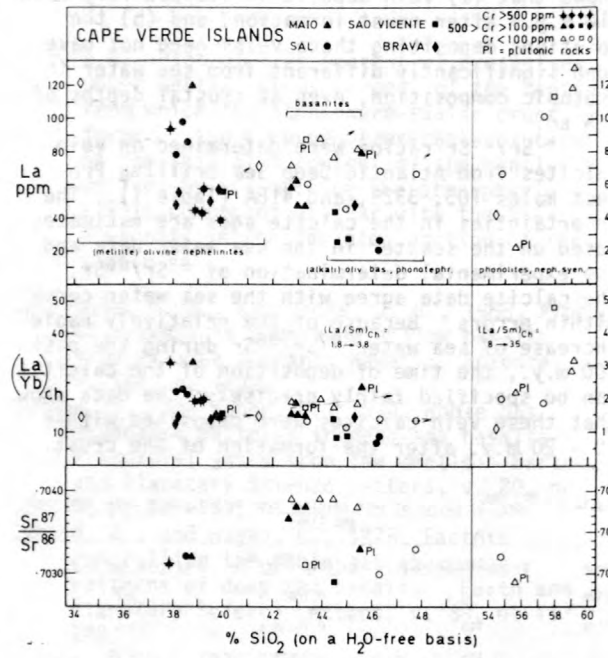

Figure 1.--La content, La/Yb ratio, and $^{87}Sr/^{86}Sr$ ratio versus SiO_2 content for some alkaline lavas from the Cape Verde Islands.

The incompatible trace-element trends of the CVI lavas are not entirely consistent with the notion that (melilite) olivine nephelinites, basanites, and alkali olivine basalts are clearly distinguished by degree of partial melting of the upper mantle (at different depths, but with otherwise similar trace-element composition). For this to be true, all primary basalts samples should lie on a single La versus SiO_2 or La/Yb versus SiO_2 trend. As shown in figure 1, there is a significant offset in these trends, separating basanites and alkali basalts from the nephelinites. Admittedly, crystal accumulation could have partly blurred such a trend; but this

offers no ready explanation for all the nephelinites and the offset in the La/Yb trend. It is thus feasible that 7 - 10 percent partial melting might give rise to either olivine nephelinites or basanites, depending on the H_2O-CO_2 pressure-temperature conditions in the source region (see, for example, Wyllie, 1977). Separation of a REE-rich carbonatite phase by liquid immiscibility could also, in part, be responsible for the rapid decline of incompatible elements in the olivine nephelinites. The REE evolution in the basanite (basanitoid)-(alkali) olivine basalt sequence for both CVI and FU is consistent with increasing degrees of partial melting. However, this does not necessarily imply that all magmas were derived from the same source region, as highlighted by the different isotopic composition of the Maio basanites (fig. 1).

Clearly, the steep REE patterns in (melilite) olivine nephelinites are most readily explained by assuming that the source regions were light REE enriched to start with. Sm-Nd isotopic studies (De Paola and Wasserburg, 1976), however, preclude the source regions being light REE enriched for a long time. Thus, the light REE enrichment must have been a geologically recent event, and was, perhaps, the prelude to major volcanic activity. The alternative; that is, chondritic relative REE source abundances, requires that either exceedingly small fractions of melt can make it to the surface without

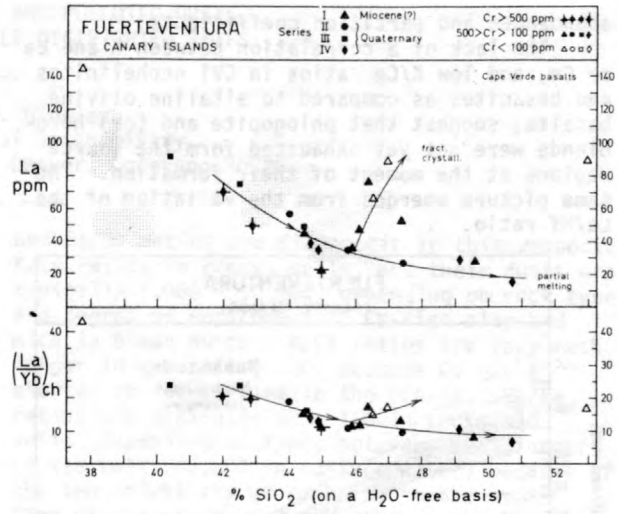

Figure 2.--La content and La/Yb ratio versus SiO_2 content for some alkaline lavas from Fuerteventura, Canary Islands.

large-scale crystal differentiation, or that garnet was very effective in fractionating the REE. Although garnet is most probably present in the source regions of undersaturated rocks, its role in fractionating the REE was probably minor. Otherwise, the near-constancy of the Yb and Lu contents in alkaline rocks from all over the World would require extremely uniform garnet

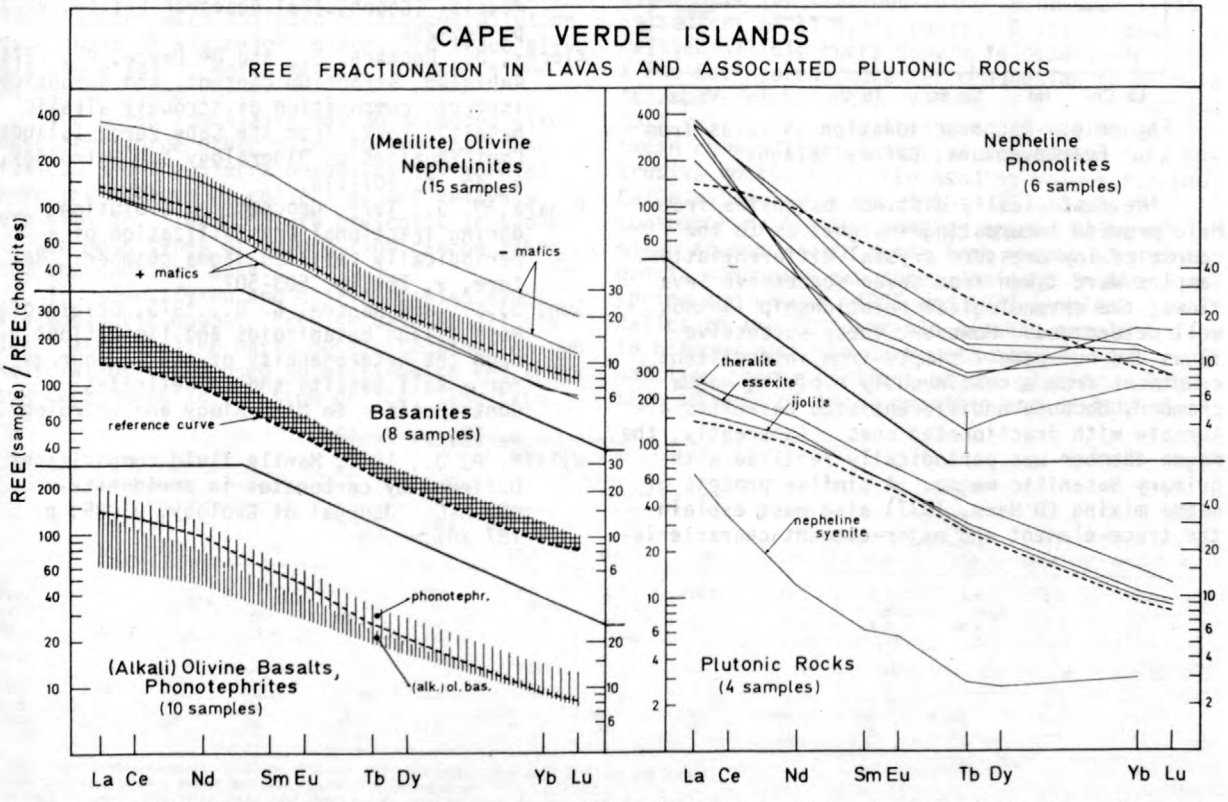

Figure 3.--REE fractionation in lavas and associated plutonic rocks from the Cape Verde Islands.

abundances and partition coefficients.

The lack of a correlation between K and La or Ce, and low K/Ce ratios in CVI nephelinites and basanites as compared to alkaline olivine basalts, suggest that phlogopite and (or) hornblende were not yet exhausted form the source regions at the moment of their formation. The same picture emerges from the variation of the La/Hf ratio.

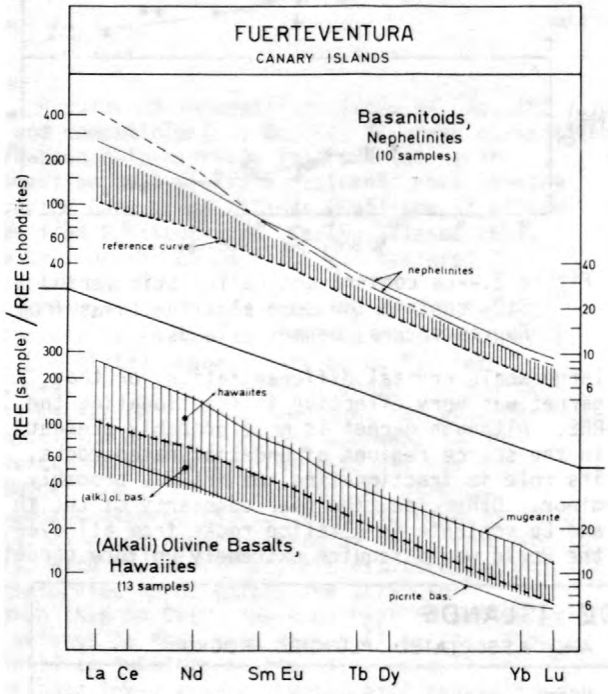

Figure 4.--REE fractionation in lavas from Fuerteventura, Canary Islands.

The isotopically distinct basanites from Maio provide interesting insights as to the course of low-pressure crystal differentiation. Samples were taken from seven successive lava flows; the chronological relationship is thus well determined. However, these successive flows did not result simple from intermittent eruptions from a continuously evolving magma chamber, because undifferentiated basanites alternate with fractionated ones. Apparently, the magma chamber was periodically refilled with primary basanitic magma. A similar process of magma mixing (O'Hara, 1977) also must explain the trace-element and major-element characteristics of the alkali-olivine-basalt-hawaiite lineage in Series I from Fuerteventura.

Judging from trace-element and Sr-isotopic data, the CVI nepheline phonolites and syenites are most probably derived by fractionation from basaltic magmas, despite the silica-gap. Trace-element data alone does not indicate whether the phonolites are linked with the basanitic or the phonotephritic magmas, but Sr-isotopic data favor the latter interpretation; for example, the nepheline syenite from Maio cannot be derived from Maio basanitic magmas ($^{87}Sr/^{86}Sr$ 0.7029 versus 0.7038). The depletion of middle REE and the absence of an overall REE-enrichment in the phonolites and syenites must be attributed to crystallization of amphibole and accessory minerals such as apatite (P_2O_5 is very low in the phonolites). The role of accessory minerals is emphasized by the strong fractionation among the incompatible elements (REE, Hf, Ta, Th). The plutonic rocks do not differ much from their effusive analoges, insofar as Sr-isotopic composition and major and trace elements are concerned.

De Paepe, P., Klerkx, J., Hertogen, J., and Plinke, P., 1974, Oceanic tholeiites on the Cape Verde Islands; Petrochemical and geochemical evidence: Earth and Planetary Science Letters, v. 22, p. 347-354.

De Paolo, D. J., and Wasserburg, G. J., 1976, Nd isotopic variations and petrogenetic models: Geophysical Research Letter, v. 3, p. 249-252.

Klerkx, J., Deutsch, S., and De Paepe, P., 1974, Rubidium, strontium content, and strontium isotopic composition of strongly alkalic basaltic rocks from the Cape Verde Islands: Contributions to Mineralogy and Petrology, v. 45, p. 107-118.

O'Hara, M. J., 1977, Geochemical evolution during fractional crystallization of a periodically refilled magma chamber: Nature, v. 266, p. 503-507.

Sun, S. S., and Hanson, G. N., 1975, Origin of Ross Island basanitoids and limitations upon the heterogeneity of mantle sources for alkali basalts and nephelinites: Contributions to Mineralogy and Petrology, v. 52, p. 77-106.

Wyllie, P. J., 1977, Mantle fluid compositions buffered by carbonates in peridotite--CO_2-H_2O: Journal of Geology, v. 85, p. 187-207.

IDENTITY OF NATURAL AND POLLUTED DUSTS IN SNOWPACKS AT WIDELY DISTRIBUTED SITES

By Todd K. Hinkley
Branch of Regional Geochemistry
U.S. Geological Survey, Denver, Colorado 80225

Measurement of a suite of both rock-forming and suspected-pollutant metals preserved in a succession of annual snow strata may yield information on the sources and the spatial and temporal variability of natural atmospheric dusts, and may also supply a basis for judgment about the extent to which the suspected-pollutant metals are enriched in the dusts compared to crustal rock. The very small amounts of total dust in many ice and snow samples, and the need for reliable values of ratios among metals requires both accurate and precise determinations. The stable isotope dilution method of analysis is the best for such work.

A suite of five samples, each representing total snowfall of a single year, was taken from the accumulation zone of the Kahiltna glacier about 10 km southwest of Mt. McKinley in Alaska. These samples represent years 1950, 1951, 1963, 1965, and 1972. Two more samples represent late-season (spring and summer) accumulation for 1975 and 1977. An eighth sample, from the zone of wastage of the nearby Ruth glacier, represents ice probably 400 plus-or-minus 100 years old. Samples were analyzed by isotope dilution for a suite of six major, minor, and trace alkali and alkaline earth metals (K, Rb, Cs and Ca, Sr, Ba), and for Pb.

The data from Alaska may be compared with those from three other sites (Greenland, Antarctica, and the Sierra Nevada of California), where the methods of collection and analysis were similar. The data are presented in table 1. Two main types of information can be taken from the combined data.

1. Identifying and distinguishing types of atmospheric dusts: Precise data on all six alkali and alkaline earth metals together allows their ratios to be used to distinguish sea salts from rock dusts in the snow or ice. The K/Cs and Ca/Ba ratios are diagnostic in this respect. K/Cs ratios in rocks, soils, and their dusts are typically 1,000 - 10,000, depending on rock type and degree of enrichment of Cs-rich clay and mica in blown dusts. K/Cs ratios are very much larger in sea salt (> 10) because Cs has a shorter residence time in the oceans. Ca/Ba ratios are typically 20 - 150 in rocks and soils, depending on type, but very much larger in sea salt (50,000 in surface water) because of the low solubility of Ba salts in the oceans. From values of these two ratios in the Sierra Nevada and Alaska samples (1,200 - 2,600 for K/Cs and 20 - 80 for Ca/Ba), the source of dusts at these sites appears to be dominantly silicate material. Because K and Ca were the only alkali and alkaline earth metals determined in the samples from Greenland and Antarctica, additional analyses for standard rock-forming elements and Cl were used to assess the relation between rock and sea salt in those samples (Murozumi and others, 1969).

The Ca/K and Ca/Ba ratios are the most diagnostic for distinguishing major rock types as sources of silicate dusts. Granites and related silicic rocks supply feldspars rich in K and Ba, whereas more ferromagnesian rocks have feldspars rich in Ca. Values of 1 - 1.5 for the Ca/K ratio may be in the boundary region between common light intrusive and common dark extrusive rocks; the corresponding values for the Ca/Ba ratio may be about 50 - 75. Dusts in contemporary Alaskan samples appear to be of mixed sources, with dusts from nearby snow-free quartz monzonite exposures dominant in the spring and summer (1975 and 1977 samples). Ratios in the 400-year-old Alaskan sample are in harmony with the dark metavolcanic rock mantling nearby portions of the glacier. Relative amounts of local granitic and distant fer-

Table 1.--Metals in accumulated snowpacks at widely distributed sites
[---, Leaders indicate no data available.]

	Sierra Nevada, California[1]			Alaskan glaciers[2]								
	1973	1974	1975	Summer surface 1977	Top one-third 1975	1972	1965	1963	1951	1950	400 years old	Greenland[3]	Antarctica[4]
K	9.7	35.0	13.0	46.0	---	5.6	5.2	14.5	19.1	3.8	6.0	2.7	1.5
Cs	.0048	.023	.0056	.022	---	.0044	.0021	.0057	.010	.0032	.0023	---	---
Ca	18	62	29	32	17.0	4.3	3.3	12.7	23.5	9.0	16.4	6.3	1.1
Ba	.22	1.0	1.4	1.8	1.2	.11	.086	.37	.72	.13	.27	---	---
Pb	.40	---	.87	.19	.53	.11	.11	---	.29	.19	.12	.18	.02
Ca/K	1.84	1.76	2.27	.69	---	.77	.65	.88	1.23	2.35	2.73	2.3	.73
K/Cs	1,670	1,520	2,290	2,100	---	1,290	2,460	2,550	1,880	1,190	2,560	---	---
Ca/Ba	82	62	20	17.7	13.5	39	39	35	33	70	61	---	---

[1] Accumulated winter snowpack; Hinkley, 1974 and 1975, and unpublished data of Elias and Hirao.
[2] From Kahiltna glacier, except 400-year sample from Ruth glacier.
[3] Average of years 1952, 1955, 1958, 1960, 1963 for Pb; earlier years for K and Ca; Murozumi and others, 1969.
[4] Years 1940-1965; Murozumi and others, 1969.

romagnesian dust sources in Sierra Nevada snow are discussed in detail elsewhere (Hinkley, 1974 and 1975).

Other ratios among the six metals (Rb and Sr data are omitted from this paper for brevity) may be equally useful for distinguishing dust sources where the composition of specific possible source materials have been analyzed. It is anticipated that in the future the ratios may be used as a tool to identify specific sources of dusts preserved in datable snow and ice strata (world deserts and steppes, loess fields, individual volcanic ash eruptions; see Wood, 1977), and to obtain information about directional-transport patterns of the material and changes with time in the pathways and amounts of atmospheric dusts.

2. Differences among sites in amounts of Pb, a suspected pollutant: Among the four localities, for the past two decades, least Pb is present in Antarctica (0.02 ug/kg), most Pb is present in the California Sierra Nevada (0.4 - 0.9). Alaska and Greenland have intermediate concentrations (0.1 - 0.2 in most annual strata). If the amounts of Pb are normalized to the amounts of silicate dusts plus sea salt, based on alkali and alkaline earth metals, Greenland receives perhaps 2 times more Pb than Alaska. This Pb relationship among the three northern hemisphere sites is consistent with the intensity of industrial activity lying to the southwest (source direction at these latitudes) of each site. Strong summer season melting at the low-elevation site of collection of the 400-year-old Alaska sample is consistent with the possibility of contamination of this sample with modern snow and rain rich in industrial Pb.

Alaskan samples were collected with the support of the Central Laboratory for Radiological Protection, Warsaw, Poland. The analyses were done in the laboratory of C. Patterson at the California Institute of Technology.

Hinkley, Todd, 1974, Alkali and alkaline earth metals - Distribution and loss in a high Sierra Nevada watershed: Geological Society of America Bulletin, v. 85, p. 1333-1338.

_____1975, Weathering mechanisms and mass balance in a high Sierra Nevada watershed--distribution of alkali and alkaline earth metals: Ph.D. thesis, Calif. Inst. of Tech.

Murozumi, M., Chow, Tsaihwa J., and Patterson, C., 1969, Chemical concentrations of pollutant lead aerosols, terrestrial dusts, and sea salts in Greenland and Antarctica snow strata: Geochemica Cosmochimica Acta, v. 33, p. 1247-1294.

Wood, Spencer H., 1977, Distribution, correlation and radiocarbon dating of late Holocene tephra, Mono and Inyo craters, eastern California: Geological Society of America Bulletin, v. 88, p. 89-195.

OXYGEN-ISOTOPE COMPOSITIONS IN ARCHAEAN ROCKS FROM WESTERN AUSTRALIA, WITH SPECIAL REFERENCE TO KOMATIITES

By J. Hoefs[1] and R. A. Binns[2]
[1]Geochemisches Institut
Goldschmidstr 1, 3400 Göttingen, Germany
[2]CSIRO, Minerals Research Laboratory
P. O. Box 136, North Ryde, Australia

Recent discoveries of exceptionally magnesian lavas (komatiites) have focused much attention on Archaean volcanic sequences in granite-greenstone belt terrains. Attempts to characterize komatiites and their associates, or to evaluate their genetic interrelationships, must take careful account of the widespread metamorphism to which they were subjected. Even those Archaean volcanic rocks with abundant relic igneous phases usually carry substantial amounts of secondary minerals, and they occur in otherwise extensively recrystallized environments. Archaean metamorphic processes are themselves of considerable interest. Field and petrographic evidence from Western Australia suggests that the volcanic piles in greenstone belts underwent a major but short-lived thermal event associated with reactivation of the sialic basement on which the greenstone sequences were laid down (Binns and others, 1976). Much water was required to hydrate the volcanic rocks during the metamorphic event, and its source is unknown. The same is true of the source for CO_2 in localized carbonate-rich metamorphics.

In applying oxygen-isotope studies to the above problems, our approach has been to examine and compare the freshest available igneous samples, with their variously metamorphosed counterparts, for a range of bulk MgO contents. Also, we have obtained some data on separated igneous and metamorphic minerals to help interpret bulk-rock data. All samples were obtained from the Eastern Goldfields Province of the

Yilgarn Block, Western Australia, a typical "granite-greenstone belt" Archaean terrain developed around 2.6 - 2.7 b.y. (Windley, 1976). We have concentrated on the mafic-ultramafic volcanic sequences, and one kind of dunitic intrusive associated with them. The "fresh igneous" samples come mostly from the lowest grade metamorphic domains. A small suite of granitoid rocks from between greenstone belts was also studied. To avoid weathering problems, drill core or underground samples were used with few exceptions. The samples are divided according to the scheme given in table 1.

Table 1.--Characterization of the rock types analyzed

Group	Rock type	Metamorphic grade	Characteristic minerals
A	Coarse dunite	--	Relic igneous olivine
B	Metamorphosed dunite	Low Medium High	Lizardite Antigorite Olivine-talc
C	Peridotitic komatiite	--	Relic igneous olivine + clinopyroxene
D	Metamorphosed peridotitic komatiite	Low-high	Actinolite + chlorite
E	Basaltic komatiite	--	Relic igneous pyroxene + plagioclase
F	Metamorphosed basaltic komatiite	Low Medium-high	Actinolite-chlorite-epidote/clinozoisite-albite-quartz Hornblende-plagioclase-quartz
G	Tholeiite	--	Relic igneous pyroxene + plagioclase
H	Metamorphosed tholeiite	Low Medium-high	Actinolite-chlorite-epidote/clinozoisite-albite-quartz Hornblende-plagioclase-quartz
J	Carbonate-rich metamorphics	Low-high	Magnesite/calcite/dolomite
K	Granitoid rocks	--	

Whole-rock data (fig. 1) show the fresh igneous rocks to display relatively narrow scatter in $\delta^{18}O$ when grouped according to composition, as follows:

Group A: dunites, range 5.1 - 6.4; mean 5.6

Group C: peridotitic komatiites, range 4.8 - 7.0, mean 5.9

Group E: basaltic komatiites, range 6.1 - 6.9; mean 6.2. Two surface samples (8.0, 8.2) possibly influenced by low-temperature weathering, and an albite rich keratophyre (7.4) are plotted with this group on figure 1, but are not included in the range and average.

Group G: tholeiites, range 6.7 - 7.5, mean 7.1

The steady increase in average $\delta^{18}O$, from 5.6 to 7.1, reflects a systematic decrease in MgO contents, and a change in primary mineralogy from olivine-dominant to clinopyroxene-plagioclase assemblages. If actual or latent plagioclase is taken into account, the whole-rock values are consistent with data for relic igneous olivines and clinopyroxenes cited in table 2. A significant difference between igneous olivine relics and metamorphic olivine outgrowths in one dunite sample suggests limited or negligible exchange between the relics and pervasive metamorphic fluids. Taken together, these observations lend confidence to an interpretation that mean values for the group A - C - E - G sequence genuinely reflect isotopic ratios in the original Archaean igneous rocks, with magmatic fractionation the prime control for the trend. The data are not sufficient to clarify possible relationships between komatiites and tholeiites.

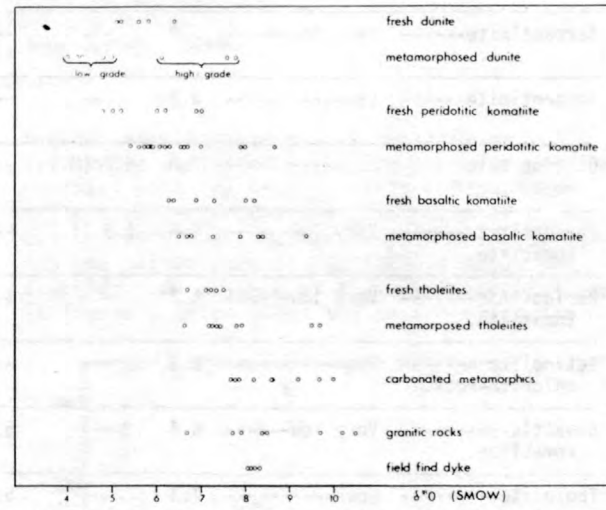

Figure 1.--$\delta^{18}O$-values of the analyzed whole-rock samples.

Mean $\delta^{18}O$ values for the fresh igneous rock groups and their relic mineral phases suggest no significant differences between Archaean magmas and their modern equivalents. Neither is secular variation evident from the Yilgarn granitoids, whose $\delta^{18}O$ values between 6 and 10 (mean 8.5) fall in the range of "normal" Phanerozoic granitic rocks (Taylor, 1978).

The metamorphosed equivalents of the dunites, komatiites and tholeiites show a broader scatter in $\delta^{18}O$ compared to their parents, ranging from 4.0 to 10.0. Recrystallized dunites (Group B) show a most striking dependence on metamorphic grade. Those dunites metamorphosed to olivine-talc rocks in high temperature environments show higher δ-values than their "fresh" parents, while those altered to serpentinite at lower temperatures have lower δ-values. In the other compositional groups (D, F, H), there is no comparable distinction between low- and high-temperature metamorphic products, but in these groups a slight ^{18}O-enrichment relative to fresh equivalents is apparent. Data for metamorphic phases cited in table 2 suggest a pronounced mineralogical control on within-group scatter, despite which it is still a remarkable observation that the spread in isotopic composition is not very large, pointing towards a relatively uniform composition of the fluid phase during metamorphism.

Table 2.--$\delta^{18}O$-values of separated minerals
[I., igneous; M., metamorphic]

Rock type	Metamorphic grade	Whole Rock	Olivine	Clino-pyroxene	Serpentine	Magnetite	Amphibole (hornblende)	Other minerals
Dunite----------	Low-Medium----	5.8	5.4 (I.)	---	---	---	---	---
Dunite----------	High----------	5.1	5.1 (I.) 6.5 (M.)	---	---	---	---	---
Serpentinite------	Very low------	5.0	---	---	Lizardite 5.6	-5.6	---	---
Serpentinite------	Low-----------	4.2	---	---	Antigorite 4.5	0.3	---	---
Olivine talc------ rock.	High----------	7.8	6.7 (M.)	---	---	4.1	---	Talc 8.5
Peridotitic------- komatiite.	Very low------	4.8	4.5 (I.)	---	---	---	---	---
Peridotitic------- komatiite.	Very low-low--	6.2	---	5.9	---	---	---	---
Actinolite-------- chlorite-rock.	High----------	5.5	---	---	---	---	5.5	Chlorite 5.3
Basaltic---------- komatiite.	Very low------	6.4	---	5.6	---	---	---	---
Tholeiite---------	Low-----------	7.3	---	5.3	---	---	---	---
Tholeiite---------	Very low------	6.7	---	5.4	---	---	---	---
Amphibolite-------	---	7.4	---	---	---	---	6.9	Plagioclase[1] 8.1

[1] 30 percent quartz.

The carbonate-rich metamorphics (Group J), ranging from dunitic to tholeiitic in composition, all show relatively high $\delta^{18}O$-values, clearly a consequence of ^{18}O partition towards the respective carbonate phase (table 3). The carbon in the carbonates has $\delta^{13}C$-values between -3.7 and -6.5, which could be tentatively interpreted as suggesting a magmatic origin.

Table 3.--$\delta^{18}O$ and $\delta^{13}C$-values (relative PDB) of the carbonate-rich metamorphic rocks

No.	Percent carbonate	Whole rock	Carbonate $\delta^{18}O$	Carbonate $\delta^{13}C$
224	12.5	7.8	9.9	-3.7
618	~10.0	10.0	13.3	-3.9
909	~10.0	8.2	10.4	-4.5
86	13.7	7.8	10.8	-4.5
910	~ 6.0	9.2	12.0	-4.3
139	6.3	9.7	11.6	-5.0
911	~ 6.0	8.6	10.3	-4.0
912	~ 6.0	7.7	10.7	-6.5

Until hydrogen isotope data become available, it is not possible to draw definite conclusions concerning origin of the water added to the Yilgarn volcanic sequences during their metamorphism. However, the relatively uniform oxygen isotopic compositions of the metamorphosed samples, and their similarity to fresh equivalents, suggest a uniform isotopic composition also for the fluid phase during metamorphism, and probably a deep-seated origin. Data for the granitoids are consistent with a variety of models relating metamorphism to granitic activity. Ocean water may have played a major role in the formation of some low-temperature serpentinites, but this is not evident in low-grade metavolcanic rocks in other compositional groups.

Binns, R. A., Gunthorpe, R. J., and Groves, D. I., 1976, Metamorphic patterns and development of greenstone belts in the Eastern Yilgarn Block, Western Australia, in Windley, B. F., ed., The early history of the earth: London, Wiley and Sons.

Taylor, H. P., 1978, Oxygen and hydrogen isotope studies of plutonic granitic rocks: Earth and Planetary Science Letters, v. 38, p. 177.

Windley, B. F., 1976, The Early History of the Earth: London, Wiley and Sons.

TRACE ELEMENT AND Sr ISOTOPE ABUNDANCES IN RECENT LAVAS FROM KILAUEA, HAWAII

By Albrecht W. Hofmann[1], Thomas L. Wright[2], and Mark Feigenson[3]

[1]Department of Terrestrial Magnestism, Carnegie Institution of Washington, 5241 Broad Branch Road, N. W., Washington, D. C. 20015

[2]U. S. Geological Survey, MS 959, Reston, Virginia 22092

[3]Present Address: Princeton University, Department of Geological and Geophysical Sciences, Princeton, New Jersey 08540

The frequent eruptions of Kilauea offer an unusual opportunity to study the chemical evolution of basaltic magma. Wright, Swanson, and Duffield (1975, hereafter referred to as WSD) have sampled and analyzed in detail a long-lived eruption on the east rift of Kilauea (Mauna Ulu eruption). Using samples collected during 1969 to 1971, WSD showed that the major variations in composition can be explained by olivine fractionation, but that when the effect of olivine control is removed by normalizing all the compositions to an MgO concentration of 7 percent, there remain small but significant variations in composition. WSD recognized five variants, the first two of which are nearly indistinguishable from the composition of the 1967-68 summit eruption in Halemaumau. Subsequent variants showed small differences in SiO_2 (0.25 percent), Al_2O_3 (0.27 percent), and, in particular, small but systematic decreases in K_2O, TiO_2, and P_2O_5. These variations have been modeled by methods given by Wright and Doherty (1970) and by Wright and Helz (1976) and cannot be explained by fractional crystallization at either low or high pressure. In this paper we address the question of whether they can be explained by a partial melting process. We consider two simple models: 1) varying degree of melting of the same source material, or 2) several source batches of differing incompatible element content. Isotopic and trace-element data are useful in this context because new source batches may be recognized by their distinct isotopic composition and abundances of incompatible elements.

We analyzed K, Rb, Cs, Sr, and Ba abundances by isotope dilution and the isotopic composition of Sr on 15 samples of a suite of dated eruptions. Twelve of these samples are from the Mauna Ulu eruption of 1969-1971. The measured $^{87}Sr/^{86}Sr$ ratios were corrected for fractionation, using $^{86}Sr/^{88}Sr = 0.11940$ as an internal standard, and for mass spectrometer bias, using the Eimer and Amend $SrCO_3$ with $^{87}Sr/^{86}Sr = 0.70800$ as a standard of comparison (our measured value was 0.70790). The average value of $^{87}Sr/^{86}Sr = 0.70351$ (with a range of 0.70344 to 0.70360) is very similar to the four values ranging from 0.70357 to 0.70364 found by Hart (1973) on submarine basalts collected from the Kilauea east rift zone. We detected no systematic variation with time of eruption. In contrast with the nearly constant $^{87}Sr/^{86}Sr$ ratios, we found that the abundances of K, Rb, Cs, Sr, and Ba all decrease systematically during the latter part of the 1969-71 Mauna Ulu eruption. An example of this decrease is shown in figure 1 which gives the Sr concentration

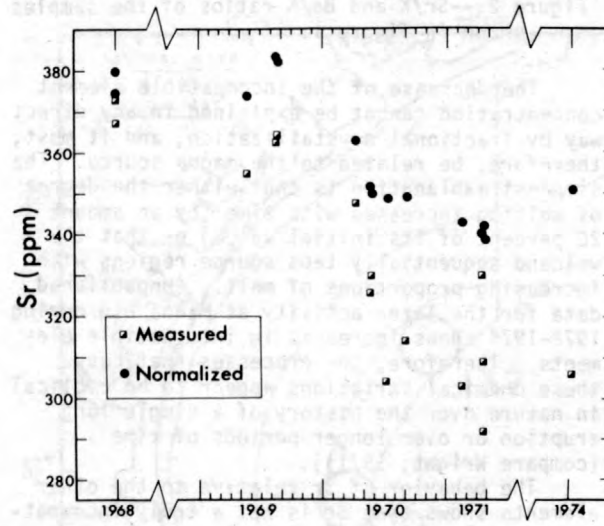

Figure 1.--Sr concentration of basalt versus date of eruption. The continuous sequence dated from 1968 to 1971 are samples from the Mauna Ulu eruption. Samples erupted in 1968 and 1974 are shown for comparison. Squares are measured Sr concentrations; solid circles are normalized to MgO = 7 percent to remove the effect of olivine control.

after normalization to an MgO concentration of 7.0 percent (to remove the effect of olivine fractionation, see WSD). Another method of removing the effects of fractionation is to focus attention on ratios of incompatible elements. Two examples of this are shown in figure 2. The Ba/K ratios remain essentially constant but the Sr/K ratios increase systematically with time during the Mauna Ulu eruption. Using analogous plots for the other trace ele-

ments analyzed, we find that all ratios involving only K, Rb, Cs, and Ba do not show any systematic variation (although they do show varying degrees of scatter), whereas all the ratios involving Sr in the numerator show a systematic increase with time.

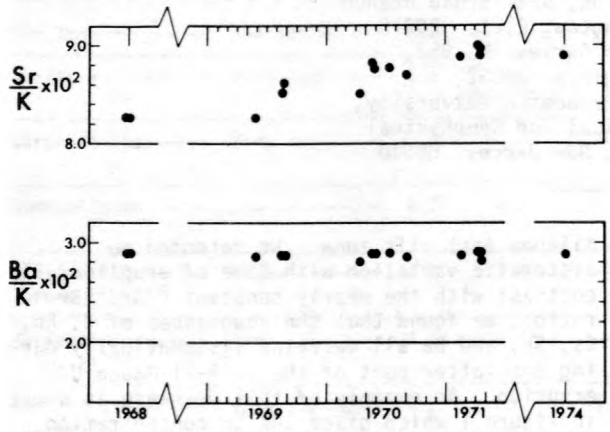

Figure 2.--Sr/K and Ba/K ratios of the samples shown in figure 1.

The decrease of the incompatible element concentration cannot be explained in any direct way by fractional crystallization, and it must, therefore, be related to the magma source. The simplest explanation is that either the degree of melting increases with time (by an amount 20 percent of its initial value) or that the volcano sequentially taps source regions with increasing proportions of melt. (Unpublished data for the later activity at Mauna Ulu during 1972-1974 shows increases in incompatible elements. Therefore, the processes that cause these chemical variations appear to be cyclical in nature over the history of a single long eruption or over longer periods of time (compare Wright, 1971)).

The behavior of Sr relative to the other elements shows that Sr is not a truly incompatible element. Significant amounts of Sr must be retained in a residual solid phase such as clinopyroxene, which has a crystal-liquid partition coefficient for Sr of about 0.1 to 0.3 (Shimizu, 1974; Sun and others, 1974). The major-element differences for CaO, Al_2O_3, and SiO_2 also are compatible with clinopyroxene residue in addition to olivine. We prefer clinopyroxene as the relevant residual phase by arguments of elimination, which exclude feldspar, amphibole, and phlogopite, all of which could potentially retain the appropriate amount of Sr but would affect the concentrations of other trace and (or) major elements in ways that are not compatible with our results.

Hart, S. R., 1973, Submarine basalts from Kilauea rift, Hawaii; nondependence of trace element composition on extrusion depth: Earth and Planetary Science Letters, v. 20, p. 201-203.

Shimizu, N., 1974, An experimental study of the partitioning of K, Rb, Cs, Sr, and Ba between clinopyroxene and liquid at high pressures: Geochimica and Cosmochimica Acta, v. 38, p. 1789-1798.

Sun, C. O., Williams, R. J., and Sun, S. S., 1974, Distribution coefficients of Eu and Sr for plagioclase - liquid and clinopyroxene - liquid equilibria in oceanic ridge basalt: an experimental study: Geochimica and Cosmochimica Acta, v. 38, p. 1415-1433.

Wright, T. L., 1971, Chemistry of Kilauea and Mauna Loa lava in space and time: U. S. Geological Survey Professional Paper 735, p. 1-40.

Wright, T. L., and Doherty, P. C., 1970, A linear programming and least squares computer method for solving petrologic mixing problems: Geological Society of America Bulletin, v. 81, p. 1995-2008.

Wright, T. L., and Helz, R. T., 1976, Use of mass balance equations to evaluate models of magma genesis: Geological Society of America Abstracts with Programs, v. 8, no. 6, p. 1176.

Wright, T. L., Swanson, D. A., and Duffield, W. A., 1975, Chemical compositions of Kilauea east-rift lava, 1968-1971: Journal of Petrology, v. 16, p. 110-133.

^{226}RADIUM CHRONOLOGY OF GULF OF MEXICO SLOPE SEDIMENTS

By Charles W. Holmes and E. Ann Martin
U.S. Geological Survey, Corpus Christi, Texas 78411

To understand the physical and chemical processes in nature necessitates the determination of the duration over which these processes act. Determination of the rates requires methods to measure absolute time. During the past three decades, many age-determining methods

suitable for investigating sediments have been advanced; these range from the ^{210}Pb method with a determinative range of 1 to 200 years to the ^{40}K-^{40}Ar method with an operational span on the order of 10^9 years. For marine sediments, the ^{210}Pb method measures accumulation rates on the order of a millimeter to a centimeter per year while the ^{230}Th-methods measure accumulation rates on the order of millimeters to centimeters per thousand years. Thus, a method that could measure rates on the order of a millimeter to a centimeter per 100 years is desirable. Koide and others (1976) have proposed using unsupported ^{226}Ra (1/2t = 1622 yr) as such a chronological tool. ^{14}C- and ^{32}Si-methods also compete in this range, but these methods require great abundances of carbonaceous or siliceous material. The object of this report is to assess the feasibility of the ^{226}Ra method on the slope sediments of the Gulf of Mexico.

Radium in waters entering the Gulf of Mexico are approximately 15 percent out of equilibrium with its ancestor uranium (table 1). This initial disequilibrium, coupled with the fact that ^{226}radium's immediate parent, ^{230}Th, forms a hydrate and is immediately adsorbed by particulate material, creates a condition of unsupported ^{226}Ra in the water. This excess radium is then available for concentration by marine plankton. Concentrations of 1.8×10^{-12} g/gram have been measured in some species of zooplankton, with an average enrichment factor relative to seawater of 860 (Shannon and Cherry, 1971). The chemical similarity between radium and barium, with barium being shown to be concentrated by plankton (Martin and Knauer, 1973), is added evidence that plankton acts as a carrier of radium, transferring substantial quantities of the isotope to the sediments. This sedimentation process produces an excess of radium in these sediments. This was demonstrated by Koide, Bruland, and Goldberg (1976) in sediments off southern California where they found a ratio of $^{226}Ra/^{230}Th$ greater than one with a maximum of 2.91. There has been no known ^{230}Th activity data determined in the sediments in the northern Gulf; however, Shokes (1976) does present data which shows that radium activity decreases with depth in the sediment column--indirect evidence of such disequilibrium in the sediments.

Table 1.--Contribution of major rivers, western Gulf of Mexico, water year, 1960-1961

[Uranium and radium data from Mallory, Johnson, and Scott (1969).]

River	Uranium		Radium		
	kg	percent	10^{-5} kg	percent	$[^{226}Ra/^{238}U]$[1]
Mississippi --	315,244	(94.5)	11,353	(89.3)	1.05
Sabine -------	2,232	(0.7)	175	(1.3)	2.29
Neches -------	1,860	(0.5)	81	(0.6)	1.27
Trinity ------	4,050	(1.2)	170	(1.3)	1.23
Brazos -------	6,441	(2.0)	848	(6.6)	3.84
Guadalupe ----	2,604	(0.8)	76	(0.5)	0.89
Rio Grande ---	997	(0.3)	12	(0.1)	0.36
Total ---	333,428		12,715		1.14

[1]Activity ratio.

As with other radioisotope dating methods, the isotope used for estimation of time must be relatively immobile for a time interval comparable to the dating interval. Goldberg and Koide (1963) reported some migration of radium in sediments accumulating extremely slowly in the Indian Ocean. However, there is no such evidence of migration in the more rapidly accumulating sediments of continental slopes.

Sediment description: Two cores were obtained from the upper slope east of the coastal bend of Texas (fig. 1). The northernmost core (137) was composed of fine silts and clay-size material with (< 10 percent) foraminiferal tests scattered throughout. X-radiography of this core showed undisturbed laminae with only very few structures which could be attributed to bioturbation. Core 10 was also composed of fine silt and clay. Core 137 was taken with a hydraulically dampened corer whereas core 10 was taken with a modified box corer. There was no physical evidence for surface disturbance of the sediment in either method of coring.

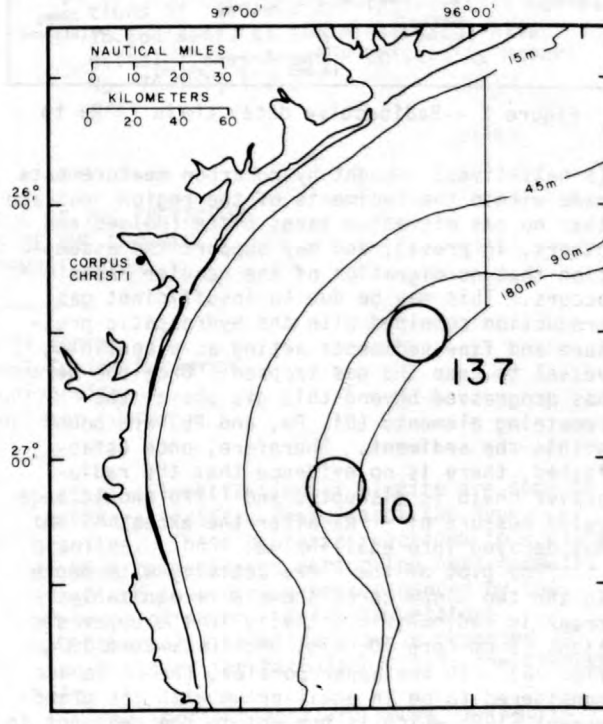

Figure 1.--Map showing locality of cores 10 and 137.

Methods: The only isotope measured was ^{210}Po, the isotope most commonly measured using the ^{210}Pb technique. For the use of this isotope in the measurement of ^{226}Ra, secular equilibrium between ^{226}Ra and ^{210}Pb must be assumed within the sediment section below 10 cm. The ^{210}Po content was measured using the method of Holmes and Martin (1978). In addition to ^{210}Po determinations, calcium was also deter-

mined by atomic absorption as a measure of the total carbonate (% foraminifera material).

Discussions: As mentioned above, the use of ^{210}Po as a measure of ^{226}Ra requires the assumption that secular equilibrium has been reached and maintained over the time interval dated. The decay path from ^{226}Ra to ^{210}Po (fig. 2) passes through the noble gas isotope, ^{222}Rn. If a break in the equilibrium chain were to occur, it is at this juncture that it is most likely to take place. This isotope has a 3.8 day half-life and for a significant break in equilibrium to take place, migration of the gas from the sediment should occur within 20 days

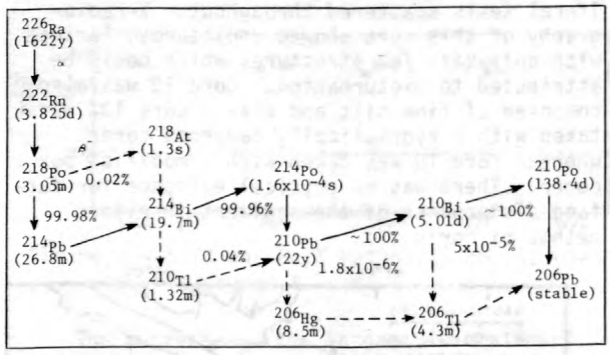

Figure 2.--Radioactive decay chain ^{226}Ra to ^{206}Pb.

(5 half-lives). Light hydrocarbon measurements made within the sediments of the region indicate that no gas migration takes place (Holmes and others, in press), and may support the assumption that no migration of the heavier radon occurs. This may be due to insufficient gas production combined with the hydrostatic pressure and fine sediments acting as a confining vessel to keep the gas trapped. Once the decay has progressed beyond this gas phase, the remaining elements (Bi, Po, and Pb) are bound within the sediment. Therefore, once established, there is no evidence that the radioactive chain is disrupted and ^{210}Po should be a valid measure of ^{226}Ra after the excess ^{210}Pb has decayed into equilibrium.

The plot of the ^{210}Po activity with depth in the two slope cores shows a recognizable break in radiometric activity in the upper sections (8 cm-core 10, fig. 3A; 10 cm-core 137, fig. 3B). In the upper portion, the ^{210}Po is considered to be in equilibrium with its grandparent ^{210}Pb which is present in the sediment in excess of its ancestor ^{226}Ra. Below the break, ^{210}Po is considered to be in equilibrium with ^{226}Ra. By projecting the best-fit lines through the data to zero depth and subtracting the estimated ^{226}Ra activity from the measured ^{210}Po (= equivalent ^{210}Pb) activity, the excess ^{210}Pb is estimated. From this data the rate of sedimentation was calculated and found to be 0.64 mm yr^{-1} and 0.71 mm yr^{-1} for core 137 and core 10, respectively.

In the lower sections, the curves are con-

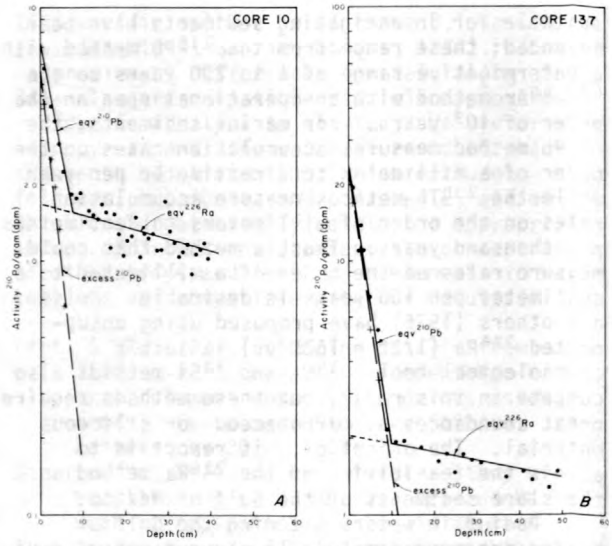

Figure 3.--A, ^{210}Po activity in disintegration per gram of dried sample versus depth in centimeters in core 10. Solid dots represent raw data; plus signs represent interpreted ^{210}Pb excess. B, ^{310}Po activity in disintegration per gram of dried sample versus depth in centimeters in core 137. Solid dots represent the raw data; plus signs represent interpreted ^{210}Pb excess.

sidered to be equivalent to the ^{226}Ra activity and the rates of sedimentation were calculated on the projected best-fit line. These calculations yielded rates of 0.51 mm yr^{-1} for core 137 and 0.37 mm yr^{-1} for core 10. The rates calculated by the ^{210}Pb and ^{226}Ra methods agree very well for core 137; however, for core 10 they differ by a factor or two. The difference in the core 10 core may be the result of data scatter considering the "r" value for the best fit was 0.62 for core 10 as compared to 0.85 for core 137. Both cores are samples of the sediment section from the upper slope in which conditions have remained the same since the sea level came to near its present position about 3000 years ago (Curray, 1960). The oldest measured sediment in the cores was calculated to be about 1000 years. Thus, the fairly good agreement is to be expected if the methods are valid, as the sediment represented by both sections of the cores was deposited under the same sedimentary regime.

The process by which radium is introduced into the sediment is through the zooplankton sedimentological cycle, which, in the Gulf, is predominantly composed of foraminiferal material. As a measure of this material, calcium was measured in the sediment at the same horizon where the ^{210}Po activity was determined. In core 137, the calcium (carbonate) content was found to be twice that of core 10 and was also found to be more homogeneous. The higher calcium (carbonate) content in core 137 is thus responsible for the higher radium activity in

this core. The calcium data, although fluctuating somewhat in core 10, shows no systematic increase or decrease with depth in either core indicating that carbonate is being lost due to leaching within the sediment column. Thus, there is no visible evidence that any radium is undergoing migration due to dissolution.

In conclusion, our data yielded reasonable and consistent results and the ^{226}Ra method may be used to extend measured sediment rates beyond the 200 years permitted by ^{210}Pb methods.

Curray, J. R., 1960, Sediments and history of Holocene transgression, continental shelf, northwest Gulf of Mexico, in, Shepard, F. P., and others, ed., Recent sediments, northwest Gulf of Mexico: American Association of Petroleum Geologists, Oklahoma City, 394 p.

Goldberg, E. D., and Koide, M., 1963, Rates of accumulation in the Indian Ocean, in, Geiss, I., and Goldberg, E. D., compilers, Earth sciences and meteorites: Amsterdam, North-Holland Publishing Company, p. 90-102.

Holmes, C. W., Bernard, B., and Martin, E. Ann, (in press), Gas seeps and trace metal concentrations, in, Berryhill, H. L., ed., Environmental Studies, South Texas Continental Shelf: National Technical Information Service, Springfield, Virginia 22151.

Holmes, C. W., and Martin, E. Ann, (in press), Rates of sedimentation, in, Berryhill, H. L., ed., Environmental Studies, South Texas Continental Shelf, 1976: National Technical Information Service, Springfield, Virginia 22151.

Koide, M., Bruland, K., and Goldberg, E. D., 1976, ^{226}Ra chronology of a coastal sediment: Earth and Planetary Science Letters, v. 31, p. 31-36.

Mallory, E. C., Johnson, J. O., and Scott, R. C., 1969, Water load of uranium, radium, and gross beta activity at selected gauging stations, water year 1960-1961: U.S. Geological Survey Water Supply Paper 1535-O, p. 1-31.

Martin, J. H., and Knauer, G. A., 1973, The elemental composition of plankton: Geochimica Cosmochimica Acta, v. 37, p. 1639.

Shannon, L. V., and Cherry, R. D., 1971, Radium-226 in marine phytoplankton: Earth and Planetary Science Letters, v. 11, p. 339.

Shokes, Robert F., 1976, Rate-dependent distritions of lead-210 and interstitial sulfate in sediments of the Mississippi River delta: Texas A and M University Report No. 76-1-T, 122 p.

$^{18}O/^{16}O$ AND D/H RATIOS OF THE CRETACEOUS GRANITIC ROCKS OF THE CHUGOKU BELT, SOUTHWEST JAPAN

By Hiroji Honma
Institute for Thermal Spring Research
Okayama University
Misasa, Tottori-ken, Japan

D/H ratios of biotite and chlorite from epizonal granites of the Chugoku belt have been obtained and correlated with their $^{18}O/^{16}O$ ratios. Geological, petrological and geochemical differences between the Upper Cretaceous granites (in a broad sense) of the Ryoke metamorphic and Chugoku non-metamorphic belts were discussed in terms of the geological situation of the former belt (Honma and Sakai, 1976; Honma and Kagami, 1977). One of the differences between the belts is in the depth of emplacement of magmas. The granites of the Chugoku belt occur in epizonal batholiths intimately associated with ignimbritic volcanics, while synkinematic Ryoke granites occur in mesozonal plutons accompanied by intense regional thermal metamorphism of the andalusite-sillimanite type. Reaction rims between biotite and K-feldspar, thin reaction band of plagioclase at the boundary between K-feldspar grains, patchy zoning of plagioclase, and partial chloritization of biotite are some of the characteristic features of the Ryoke granites. These deuteric reactions took place at high temperatures during the post-magmatic stage and should have been enhanced by the presence of water. A low-temperature hydrothermal alteration also is observed in some parts of the batholith within the Chugoku belt.

The isotopic data are shown in figures 1 to 3. We see several systematic patterns among the oxygen isotopic characteristics of the rock, and four rock types can be distinguished from the isotopic data as illustrated in figure 4.

Type-O: The oxygen isotopic fractionation among coexisting minerals is nearly constant in most of rocks of the Hiroshima batholith (fig. 1) indicating near isotopic equilibrium at a magmatic temperature (500-600°C after the scale by Bottinga and Javoy, 1974). Many rocks of the Tottori batholith (figs. 2, 3) have similar $\delta^{18}O$

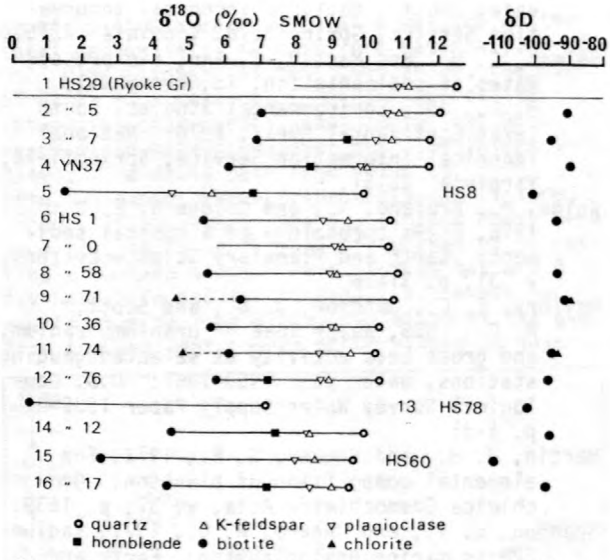

Figure 1.--Oxygen and hydrogen isotope ratios of minerals from rocks of the Hiroshima batholith. Rocks are arranged (1-16) in order of increasing distance from the southern boundary of the batholith. This batholith lies largely within the non-metamorphic Chugoku belt, but the southern part extends into the Ryoke belt. The regional oxygen isotopic variation in this batholith is caused by ^{18}O enrichment of the magma at depth in and around the Ryoke belt (Honma and Sakai, 1976).

quartz values ranging from 8.5 to 9.0 permil. The δD values of biotite from these rocks vary only from -89 to -96 permil, averaging -92 permil. Assuming that the primary D/H ratios of these biotites have been preserved, the δD value of water in the magma existing just before its solidification can be estimated by the δD value and chemistry of these biotites and the fractionation factors determined by Suzuoki and Epstein (1976) (fig. 4). Coexisting minerals in some of rocks, which include a number of minute basic clots (such as the Ningyo-toge granite and NA 3 in fig. 3), are oxygen isotopically not in equilibrium and many of them have relatively high $^{18}O/^{16}O$ and D/H ratios (type-O', fig. 4).

Type-I. HS71, 36,74, 76 (fig. 1): These biotites have especially high $\delta^{18}O$ and, thus, their Δquartz-biotite values are much smaller than equilibrium values. As was mentioned above, the biotites from granites of the Chugoku belt have experienced chloritization to a certain degree. Among then, the type-I biotites are most significantly chloritized (about a half in volume) and their high $\delta^{18}O$ values may be a result of this alteration. The bulk $^{18}O/^{16}O$ ratios of biotite and chlorite are close to estimated values of primary biotite and their δD values are well within the range for other biotites (type-O) which experienced the chloritization to a less significant degree.

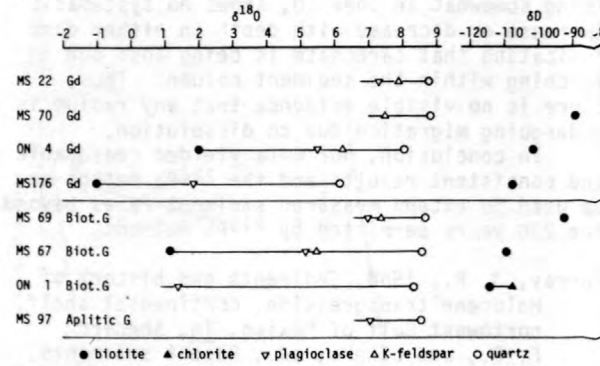

Figure 2.--Oxygen and hydrogen isotope ratios of minerals from the small Okutsu zoned pluton of the Tottori batholith, which lies far away from the Ryoke belt in the northern Chugoku belt.

Type-II. HS8, 78 (fig.1), ON4, MS176 (fig. 2): All mineral species from this type of rocks are distinctly depleted in ^{18}O. Quartz is not in isotopic equilibrium with other minerals but Δfeldspar-biotite values give approximate isotopic temperatures of around 500°C (after the scale by Bottinga and Javoy, 1974). δD values of biotite also are distinctly low. These features resulted from deuteric isotope exchange between the rock or magma and meteoric water (Taylor, 1971). The isotopic trend for biotites shown by the dashed lines in figure 4 can be interpreted in terms of the $\delta^{18}O$ values of meteoric water added, the water/feldspar and water/biotite ratios for oxygen, the water/biotite ratio for hydrogen, and the temperature of equilibrium.

No low-temperature hydrothermal products, such as clay minerals, other than small amounts of chlorite are found in these rocks and petrographically we cannot distinguish them from type-O rocks. This indicates that the

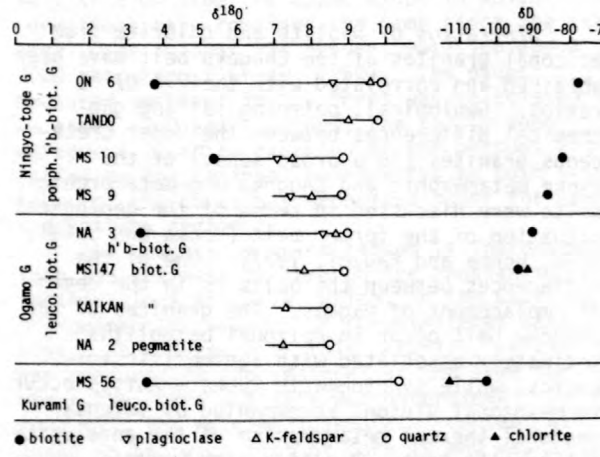

Figure 3.--Oxygen and hydrogen isotope ratios of minerals from the Ningyo-toge, Ogamo, and Kurami granites of the Tottori batholith.

infiltration of meteoric water and isotope exchange reaction took place at considerably high temperatures.

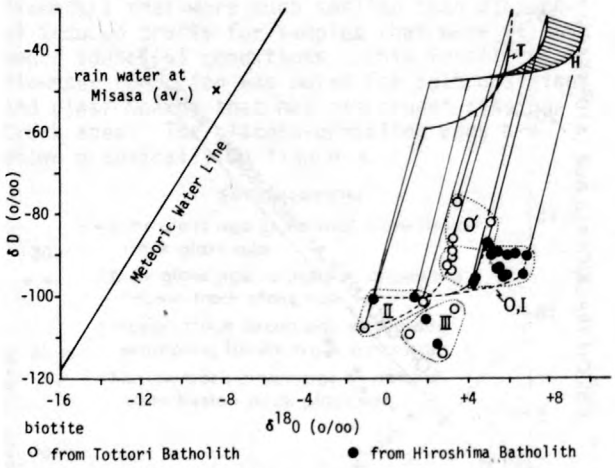

Figure 4.--Plot of δD versus $\delta^{18}O$ for biotites from rocks of the Hiroshima (H) and Tottori (T) batholiths. Also shown are roughly estimated isotopic compositions of water in equilibrium with these biotites at 500°C using biotite-water fractionations of -2.9 permil for $^{18}O/^{16}O$ of both batholiths, -53 permil for D/H of the Hiroshima batholith and -47 permil for D/H of the Tottori batholith. Average for rain water, (X), from Matsubaya (unpub. data); meteoric water line from Craig (1961).

Type-III. HS60 (fig. 1), MS67, ON1, (fig. 2), MS56 (fig. 3): Biotites of this type contain 3.5-4.0 weight percent water and belong to the group of hydromica. Except for MS56, the oxygen in quartz in this rock type is isotopically comparable to that in type-O rocks, while biotites and some of feldspars are much depleted in ^{18}O. Biotites also have very low D/H ratios and plot on the lower part of the D/H-$^{18}O/^{16}O$ diagram (fig. 4). These features can also be interpreted as due to deuteric isotope exchange with meteoric water, but at significantly lower temperatures.

Bottinga, Y., and Javoy, M., 1974, Oxygen isotope geothermometry of igneous and metamorphic rocks [abs.]: American Geophysical Union, Transactions, v. 55, p. 477-478.

Craig, H., 1961, Isotopic variations in meteoric waters: Science, v. 133, p. 1702-1703.

Honma, H., and Kagami, H., 1977, Zonal distribution of oxygen and strontium isotope ratios in the Cretaceous granitic rocks of the Chugoku province, Southwest Japan, in Plutonism in relation to volcanism and metamorphism: [papers presented at the 7th Meeting, U.S.S.R.], pp. 170-183.

Honma, H., and Sakai, H., 1976, Zonal distribution of oxygen isotope ratios in the Hiroshima granite complex, Southwest Japan: Lithos, v. 9, p. 173-178.

Suzuoki, T., and Epstein, S., 1976, Hydrogen isotope fractionation between OH-bearing silicate minerals and water: Geochimica Cosmochimica Acta, v. 40, p. 1229-1240.

Taylor, H. P., 1971, Oxygen isotope evidence for large scale interaction between meteoric ground water and Tertiary granodiorite intrusions, Western Cascade Range, Oregon: Journal of Geophysical Research, v. 76, p. 7855-7874.

AGES OF NATURAL GLASSES BY THE FISSION-TRACK AND K-Ar METHODS

By G. A. Izett, C. W. Naeser, and J. D. Obradovich
U.S. Geological Survey, Denver, Colorado

Introduction: Considerable evidence indicates that fission-track ages of many nonhydrated natural glasses are either equal to or less than K-Ar ages of the same material. This evidence is well known among most fission-track geochronologists; however, many potential users of fission-track glass ages may not be aware of this problem. The first purpose of this paper is to present additional evidence that many nonhydrated glasses, including obsidians and tektites, yield fission-track ages that are significantly younger than K-Ar ages of the same material. Furthermore, fission-track ages of nearly all samples of hydrated glass shards of upper Cenozoic ash beds are markedly younger than fission-track ages of zircon microphenocrysts separated from the ash beds. The anomalously young fission-track ages of the hydrated glass shards results from the well-documented effect of track fading or annealing under ambient conditions during geologic time. A secondary purpose of this paper is to show that some naturally annealed glasses give corrected fission-track ages using the plateau-annealing technique of Storzer

and Poupeau (1973). A third purpose is to briefly review a few of the critical factors that affect the fission-track dating of zircon.

Ages of Nonhydrated Natural Glasses: We dated 24 samples of nonhydrated natural glass by the fission-track method. The samples were chosen because they appeared very fresh and because they were essentially free of microlites. Many obsidians are crowded with microlites and these form fission-track-like etch pits following etching of the obsidians with hydrofluoric acid. The microlite etch pits are difficult to separate from fission tracks formed from the spontaneous decay of ^{238}U and therefore, calculated ages based on counts including microlite etch pits are not reliable.

The ages of the natural glasses, here dated, range from about 30 m.y. to about 0.1 m.y. and include obsidians from 21 widely scattered localities in western North America, as well as a vitrophyre of a welded tuff from Wyoming, an obsidian from South American, and a tektite (moldavite) from Czechoslovakia. Of the 24 nonhydrated natural glasses, 12 have fission-track ages that are significantly younger than K-Ar ages of the same material. The results are shown on figure 1.

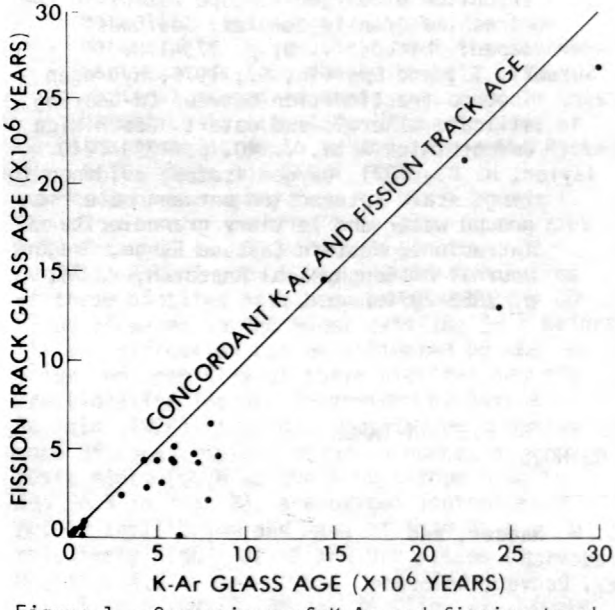

Figure 1.--Comparison of K-Ar and fission track ages of nonhydrated glasses (obsidian and molclavite).

Ages of Hydrated Glass Shards: Fission-track ages of 13 samples of hydrated glass shards were determined. The samples were collected from volcanic ash beds of late Cenozoic age in the western United States. A greater percentage of the samples of hydrated glass shards showed annealing effects than did the nonhydrated obsidians (compare fig. 1 with fig. 2). Over 90 percent (12 of 13) of the volcanic ash samples studied have fission-track glass

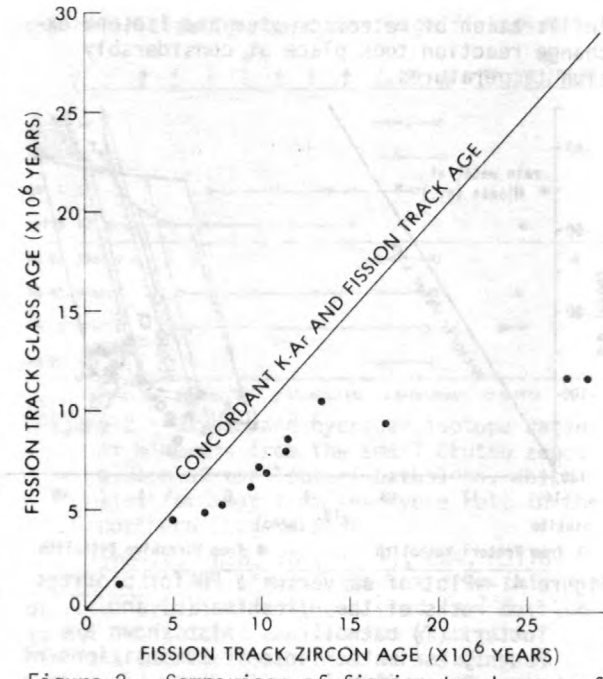

Figure 2.--Comparison of fission track ages of hydrated glass shard and coexisting zircon microphenocrysts.

ages younger than fission-track ages of coexisting zircon microphenocrysts. The fission-track ages of the 13 samples are shown on figure 2. The anomalously young fission-track ages of the shards are not surprising in light of the studies by Lakatos and Miller (1972a, 1972b). They showed that obsidian that was artificially hydrated in the laboratory had annealing temperatures markedly lower than nonhydrated glass. Most glass shards from upper Cenozoic ash beds have water contents in excess of 4 percent, which indicates that some annealing should be expected.

Plateau Annealing: Partially annealed glasses can be treated for track annealing by two techniques in order to correct apparent fission-track ages. One technique is to measure a large number of diameters of fossil and induced tracks of a glass sample and, by relating the average track diameters of the fossil and induced tracks, correct the apparent age. It is critical that the fission tracks in a glass sample be etched under identical conditions (temperature, time, and acid concentration).

A second technique is the so-called plateau-annealing method developed by Storzer and Poupeau (1973). Because the plateau-annealing technique is less time consuming and less tedious than measuring many track diameters, we selected 12 samples to date by the plateau-annealing technique. Two of the samples had statistically concordant (although slightly younger) fission-track glass and K-Ar ages at the 2 sigma level, and the other 10 had fission-track glass ages that were markedly discordant with

either K-Ar or fission-track zircon ages. The samples that had discordant fission-track glass ages were characterized by having fossil-track diameters that were much smaller than diameters of induced tracks for samples that were etched under identical conditions. This fossil-track diameter reduction was noted for both obsidians and glass shards that had discordant fission-track ages. The plateau-annealing ages are shown graphically on figure 3.

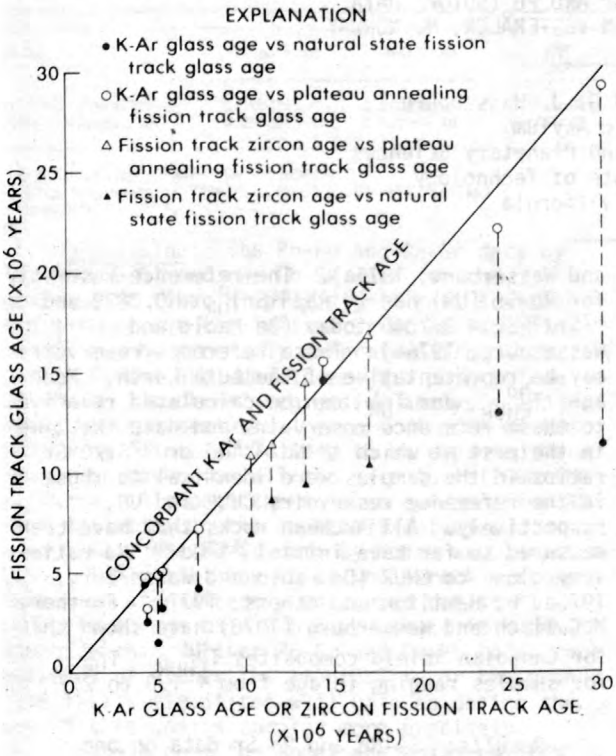

Figure 3.--The correction of glass fission track ages using the plateau annealing procedure of Storzer and Poupeau (1973).

Of the 10 samples studied that had discordant natural-state fission-track glass ages, all but 1 had plateau-annealing ages concordant with K-Ar or fission-track zircon ages at the 2 sigma level. Two natural glasses (molclavite, $\approx$ 15 m.y.; macusanite, $\approx$ 5 m.y.) that had concordant fission-track and K-Ar ages had plateau fission-track ages equal to the K-Ar age, although the fossil- and induced-track densities in both natural glasses were 50 percent lower than the natural-state material after the highest temperature heating step (about 250°C). These results indicate the natural-state material in the two samples was not annealed.

Zircon Geometry Factor: A possible source of error which can affect the accuracy of a zircon fission-track age is the so-called "geometry factor". Fossil fission tracks are counted on an internal surface of a zircon grain and the induced tracks on the cleavage surface of a low-uranium muscovite (< 10 ppb U) that covers the zircon during neutron irradiation. A basic assumption is that there are half as many tracks recorded from the fission of ^{235}U in the muscovite detector as are recorded within a zircon crystal.

In order to determine the geometry factor we used zircon from the Mud Tank Carbonatite (Australia); the zircons were large (2 cm long) and had a uniform uranium concentration of about 20 ppm. The zircon was annealed by heating and placed next to a piece of muscovite for irradiation. After irradiation, the muscovite was etched and the zircon was polished (to expose an internal surface) and etched. Results of this zircon geometry-factor study are as follows:

Internal track density zircon	External track density muscovite	Geometry factor
5.22×10^6 t/cm^2	2.63×10^6 t/cm^2	0.504±0.01
4834 tracks counted	2438 tracks counted	

The measured geometry factor of 0.504 ± 0.01 is very close to the theoritical value of 0.5.

Another approach is to determine the fission-track age of the zircon in two ways--by the population method (Naeser, 1967) and by the external-detector method (Naeser, 1969). If the resulting ages are the same, the geometry factor of 0.5 should be valid. The fission-track ages of zircon from the Mud Tank Carbonatite, as determined by the population and external-detector methods, are equal by the two methods and are given below:

Population method	External-detector method
273±14 m.y.	262±20 m.y. 262±24 m.y.
$\lambda_f = 7.03 \times 10^{-17} yr^{-1}$	

Analytical precision ± is 2 standard deviations about the mean.

The geometry factor of 0.5 determined in this study is in agreement with the results of Gleadow and Lovering (1977).

We are using the value of 7.03×10^{-17} yr^{-1} for the spontaneous decay constant of ^{238}U. We are also using the UBS glass standards for neutron dosimetry and averaging the Cu and Au values in order to determine our neutron dose. The combination of these two factors gives us the best agreement with K-Ar ages on coexisting minerals.

Gleadow, A. J. W., and Lovering, J. F., 1977, Geometry factor of external detectors in fission track dating: Nuclear Track Detection, v. 1, no. 2, p. 99-109.

Lakatos, Stephen, and Miller, D. S., 1972a, Evidence for the effect of water content on fission-track annealing in volcanic glass: Earth and Planetary Science Letters, v. 14, no. 1, p. 128-130.

_____1972b, Fission-track stability in volcanic glass of different water contents: Journal of Geophysical Research, v. 77, p.

6990-6993.
Naeser, C. W., 1967, The use of apatite and sphene for fission-track age determinations: Geological Society of America Bulletin, v. 78, p. 1523-1526.
_____1969, Etching fission tracks in zircon: Science, v. 165, p. 388.
Storzer, D., and Poupeau, G., 1973, Ages--Plateaux de mineraux et verres par la methode des traces de fission: Academy of Science, Paris, Comptes rendus, v. 26, series D., p. 137-139.

INTERPRETATION OF Nd, Sr AND Pb ISOTOPE DATA FROM ARCHEAN MIGMATITES IN VESTERÅLEN, N. NORWAY

By S. B. Jacobsen and G. J. Wasserburg
The Lunatic Asylum
Division of Geological and Planetary Sciences
California Institute of Technology
Pasadena, California

In this report we discuss constraints on the time of crust formation in Vesterålen, northern Norway, and parent-daughter fractionation of Sm-Nd, Rb-Sr and U-Pb during the subsequent granulite facies metamorphism. The rocks collected at Vikan, Langøy, are heterogeneous migmatitic granulite facies gneisses with granitic neosome grading into tonalitic to dioritic palaeosome. A Rb-Sr whole-rock study by Heier and Compston (1969) demonstrated a complex thermal history with events at $\sim$ 2.8 b.y. and $\sim$ 1.8 b.y. Green and others (1972) showed that adjacent amphibolite facies gneisses have REE distribution patterns similar to the granulite facies gneisses, whereas Heier and Thoresen (1971) demonstrated that the granulite facies rocks have been depleted in Rb, U, and Th relative to the amphibolite facies rocks. Taylor (1975) reported a Pb-Pb whole-rock "isochron" age of 3.41 $\pm$ 0.07 b.y. and a Rb-Sr whole-rock "isochron" of 2.30 $\pm$ 0.15 b.y. with a high initial $^{87}Sr/^{86}Sr$ of 0.7126 for the migmatites at Vikan. He interpreted the Pb-Pb age as the time of migmatite formation and the Rb-Sr age as the time of a granulite facies metamorphism resulting in Rb-depletion and argued that the U-Pb system was not disturbed during granulite facies metamorphism. In an attempt to solve this conflict, we analyzed these rocks for Sm and Nd isotopes because the limited available data indicated that the REE did not fractionate during the granulite facies metamorphism. From previous studies, however (Heier and Compston, 1969; Griffin and others, 1978), it seems firmly established that a period of granulite facies metamorphism took place $\sim$ 1.8 b.y. ago.

Approach: We assume that the major REE-fractionation for crustal rocks occurs during their derivation from a mantle reservoir. The mantle reservoir used as a reference for the Sm-Nd system (CHUR) has a chondritic Sm/Nd ratio with $(^{147}Sm/^{144}Nd)^{\circ}_{CHUR} = 0.1936$ and $^{143}Nd/^{144}Nd$ ratio of 0.511836 today (De Paolo and Wasserburg, 1976a). The reference reservoir for Rb-Sr (UR) has $(^{87}Rb/^{86}Sr)^{\circ}_{UR} = 0.0839$ and $^{87}Sr/^{86}Sr = 0.7045$ today (De Paolo and Wasserburg, 1976b). These reference reservoirs may be representative of the bulk Earth. Model ages T^{Nd}_{CHUR} and T^{Sr}_{UR} can be calculated relative to these reference reservoirs and date the time in the past at which $^{143}Nd/^{144}Nd$ or $^{87}Sr/^{86}Sr$ ratios in the samples were identical to those in the reference reservoirs CHUR and UR, respectively. All Archean rocks that have been measured so far have initial $^{143}Nd/^{144}Nd$ ratios very close to CHUR (De Paolo and Wasserburg, 1976a, b; Hamilton and others, 1977). Further, McCulloch and Wasserburg (1978) have shown that for Canadian Shield composites $T^{Nd}_{CHUR} \simeq T^{Sr}_{UR}$ for samples ranging in age from $\sim$ 1.0 to 2.7 b.y.

Results: Sm-Nd and Rb-Sr data on one dioritic and one granitic gneiss sample from Vikan are given in table 1. Their $^{147}Sm/^{144}Nd$ ratios are much lower than chondritic and also lower than the average crustal ratio of 0.11. The T^{Nd}_{CHUR} model ages of both rocks are identical at 2.6 b.y. within analytical error although their Sm/Nd ratios are different by $\sim$ 20 percent. This suggests that Sm-Nd did not fractionate during the much later granulite facies metamorphism. These model ages provide the best estimate for the time of formation of the protoliths of the migmatites. We will use the more precise model age of the granitic sample ($T^{Nd}_{CHUR} = 2.64 \pm 0.02$ b.y.) in the following model calculations for the Rb-Sr and U-Pb systems.

Taylor (1975) obtained a fairly good linear array of data points in a Rb-Sr evolution diagram for these rocks; some scatter about the best-fit line, however, suggests a disturbed Rb-Sr system. We present two additional analyses from the same locality in table 1. Both of these plot far from Taylor's Rb-Sr isochron. Further, all points plot to the left

of a T_{UR}^{Sr} = 2.64 b.y. reference isochron which suggests Rb-depletion significantly later than the time of formation of the protoliths of the migmatites.

Table 1.--Analytical results and model ages

Rb-Sr	$^{87}Rb/^{86}Sr$	$^{87}Sr/^{86}Sr$	T_{UR}^{Sr} [2]
Dioritic granulite---	0.0368±3	0.70890±8	-7.06±0.18
Granitic granulite---	2.01 ±1	0.79026±6	3.13±0.02

Sm-Nd	$^{147}Sm/^{144}Nd$	$^{143}Nd/^{144}Nd$ [1]	T_{CHUR}^{Nd} [2]
Dioritic granulite---	0.10332±5	0.510316±46	2.55±0.08
Granitic granulite---	0.08602±3	0.509961±16	2.64±0.02

[1]Normalized to $^{146}Nd/^{142}Nd$ = 0.636151.
[2]Decay constants $\lambda(^{147}Sm) = 0.00654 \times 10^{9}\ yr^{-1}$; $\lambda(^{87}Rb) = 0.0139 \times 10^{9}\ yr^{-1}$.

Discussion: The Pb-Pb and Rb-Sr data by Taylor (1975) and our Rb-Sr data for the gneisses at Vikan display significant scatter and neither age nor initial Sr or Pb isotopic ratios can be precisely determined from these data. Taylor excluded three data points from the Pb-Pb "isochron" regression analysis and even then the analytical errors of some of the remaining points would have to be expanded by a factor of seven for all the data to fall on the isochron. Although there is no evidence for Rb or U depletion in the amphibolite-facies migmatites, the Rb-Sr data by Heier and Compston (1969) imply that the Rb-Sr whole-rock systems have been significantly disturbed but still indicate an age of ∿ 2.5 b.y. Thus, it seems doubtful that further Rb-Sr and Pb-Pb total rock analyses of either the amphibolite or the granulite facies migmatites will help to define the age of this gneiss complex more precisely.

If we accept the model age obtained from the Sm-Nd data, then the Pb and Sr isotope data can be well explained in terms of a two-stage model with the time of formation of these crustal rocks at T_X = 2.64 b.y. and the time of granulite facies metamorphism at T_M = 1.8 b.y. Choosing α_I = 13.896 and β_I = 14.836 as initial lead from the normal growth curve of Gancarz and Wasserburg (1977)--essentially that of Doe and Stacey (1974)--at 2.64 b.y., we can then calculate a μ_1 value for the time interval from T_X to T_M (stage 1) and a μ_2 value for the time interval T_M to 0 (stage 2). The U/Pb fractionation factor at T_M is then given by $F_{U/Pb} = \mu_2/\mu_1$ and from the data of Taylor (1975) we calculate an average $F_{U/Pb}$ ∿ 0.25, which compares well with the average $(U/Pb)_G/(U/Pb)_A$ of ∿ 0.36 (G = granulite facies, A = amphibolite facies) calculated from the U-Pb data of Heier and Thoresen (1971) for these migmatites. Similarly, by using the $^{87}Sr/^{86}Sr$ value in UR at 2.64 b.y. of 0.70136 we can calculate an average Rb-Sr fractionation factor $F_{Rb/Sr} = (Rb/Sr)_2/(Rb/Sr)_1$ at T_M of ∿ 0.46. From the concentration data of Heier and Thoresen (1971) we obtain $(K/Rb)_A/(K/Rb)_G$ ∿ 0.47. It thus appears that both concentration data and isotopic data are well explained by assuming a bulk loss of U and Rb from the granulite facies gneisses. If this two-stage model is approximately correct, then the isotopic data require this loss to have occurred at ∿ 1.8 b.y. This is one of the rare cases where granulite facies metamorphism postdates rock formation by as much as 0.8 b.y.

We further note that the average $F_{U/Pb}$ and $F_{Rb/Sr}$ vary systematically with the mineralogy or major-element composition of the gneisses at Vikan.

	$F_{U/Pb}$	$F_{Rb/Sr}$
Granitic granulites----------	0.15	0.7
Granodioritic-tonalitic granulites----------	0.4	0.25
Dioritic granulites----------	0.5	0.15

Taylor (1975) obtained the apparently erroneous old Pb-Pb age (3.41 b.y.) by forcing his data into a model with a first stage covering the time between the origin of the earth and 3.41 b.y. and a second stage extending from this age to the present. The very low μ-values of the granulite facies gneisses today (mainly in the range ∿ 1 to 3) imply that their Pb isotope composition has changed much less since 1.8 b.y. than in the time interval from 2.64 to 1.8 b.y. when the μ-values averaged ∿13. Thus, the isochron that was produced in the time interval from 2.64 to 1.8 b.y. has mainly been preserved and only been slightly shifted to the right in a α-β diagram.

Our results strongly suggest that total-rock Rb-Sr and Pb-Pb data have to be interpreted with great care for granulite facies gneisses. Complex Rb-Sr and U-Pb systematics displayed by granulite facies gneisses may, however, be resolved by ages obtained with independent methods and can be used to trace U/Pb and Rb/Sr fractionations during high-grade metamorphism. For migmatite complexes T_{CHUR}^{Nd} model ages appear to provide the best time constraints for the formation of the protoliths as the dominating REE-fractionation will be associated with this event rather than with subsequent metamorphic events. If a granulite facies metamorphism occurred long after the time of crust formation, then in general we may expect $T_{UR}^{Sr} > T_{CHUR}^{Nd}$.

We conclude that the interpretation presented by Taylor (1975) for a very ancient crustal component in the Archean terrane of Vesterålen is not valid. Instead this terrane appears to be part of the worldwide crustal-forming event at 2.6 b.y. The possibility that very ancient crustal segments may really be present in other areas of the Fennoscandian Shield must remain the subject of future investigations.

De Paolo, D. J., and Wasserburg, G. J., 1976a, Nd isotopic variations and petrogenetic models: Geophysical Research Letters, v. 3, p. 249-252.

_____ 1976b, Inferences about magma sources and mantle structure from variations of $^{143}Nd/^{144}Nd$: Geophysical Research Letters, v. 3, p. 743-746.

Doe, B. R., and Stacey, J. S., 1974, The application of lead isotopes to the problem of ore genesis and ore prospect evaluation; a review: Economic Geology, v. 69, p. 757-776.

Gancarz, A. J., and Wasserburg, G. J., 1977, Initial Pb of the Amitsoq gneiss, West Greenland, and implications for the age of the earth: Geochimica Cosmochimica Acta, v. 41, p. 1283-1301.

Green, T. H., Brunfelt, A. O., and Heier, K. S., 1972, Rare-earth element distribution and K/Rb ratios in granulites, mangerites and anorthosites, Lofoten-Vesterålen, Norway: Geochimica Cosmochimica Acta, v. 36, p. 241-257.

Griffin, W. L., Taylor, P. N., Hakkinen, J. W., Heier, K. S., Iden, I. K., Krogh, E. J., Malm, O., Olsen, K. I., Ormassen, D. E., and Tveten, E., (in press), Crustal evolution in Lofoten-Vesterålen, Norway; 3500-400 m.y. B.P.: Journal of the Geological Society of London.

Hamilton, P. J., O'Nions, R. K., and Evensen, N. M., 1977, Sm-Nd dating of Archean basic and ultrabasic volcanics: Earth and Planetary Science Letters, v. 36, p. 263-268.

Heier, K. S., and Compston, W., 1969, Interpretation of Rb-Sr age patterns in high-grade metamorphic rocks, North Norway: Norsk Geologisk Tidsskrift, v. 49, p. 257-283.

Heier, K. S. and Thoresen, K., 1971, Geochemistry of high grade metamorphic rocks, Lofoten-Vesterålen, North Norway: Geochimica Cosmochimica Acta, v. 35, p. 89-99.

McCulloch, M. T., and Wasserburg, G. J., (in press), Sm-Nd and Rb-Sr chronology of continental crust formation: Science.

Taylor, P. N., 1975, An early Precambrian age for migmatitic gneisses from Vikan: Bø, Vesterålen, North Norway: Earth and Planetary Science Letters, v. 27, p. 35-42.

Nd AND Sr ISOTOPIC STUDY OF THE PERMIAN OSLO RIFT

By S. B. Jacobsen and G. J. Wasserburg
The Lunatic Asylum
Division of Geological and Planetary Sciences
Caltech, Pasadena, California 91125

We report measurements of initial $^{143}Nd/^{144}Nd$ and $^{87}Sr/^{86}Sr$ on volcanic and plutonic rocks from the Permian Oslo Rift to evaluate models of magma genesis in this continental riftzone. In addition we report data on the local Precambrian basement in order to decide whether this could be the source for any of the Oslo igneous rocks and to evaluate effects of crustal contamination or mixing with anatectic melts.

A likely source for the magmatic rocks in the rift is a body of dense material extending along the entire length of the Oslo Rift at the base of the crust (Ramberg 1976). While the major part of this lower crustal body may be gabbro, the block probably also includes significant amounts of ultramafic rocks. The presence of a large gabbroic magma chamber would probably also cause significant melting of the lower crust. Ramberg has interpreted this deep crustal magma chamber to be due to the rapid development and rise of a hot asthenospheric diapir and to discharge of basaltic material into the base of a gradually thinned crust.

Previous workers that have studied the variation of initial Sr in the volcanic and plutonic rocks of the Oslo Rift (Heier and Compston, 1969; Sundvoll, 1977) have concluded that these can be explained without postulating any contamination by country rock, and that an observed increase in initial $^{87}Ar/^{86}Sr$ in the more differentiated products can be accounted for by an increase in Rb/Sr ratio with time in a fractionating magma chamber. They further conclude that the magma source is restricted to the upper mantle or the lower crust.

Sm-Nd and Rb-Sr systematics: Initial $^{143}Nd/^{144}Nd$ and $^{87}Sr/^{86}Sr$ of a rock of age T are expressed as fractional deviations in parts in 10^4 from the values in a uniform reference reservoir at time T and denoted ε_{Nd} and ε_{Sr} respectively. The reference reservoir used for Nd (CHUR) has a chondritic Sm/Nd ratio with $(^{147}Sm/^{144}Nd)^0_{CHUR}$ = 0.1936 and $^{143}Nd/^{144}Nd$ = 0.511836 today (DePaolo and Wasserburg, 1976a). The reference reservoir for Sr (UR) has $(^{87}Rb/^{86}Sr)^0_{UR}$ = 0.0839 (Rb/Sr = 0.029) and $^{87}Sr/^{86}Sr$ = 0.7045 today (DePaolo and Wasserburg, 1976b). These reference reservoirs for Nd and Sr are thought to be close approximations to the bulk earth values. A major problem in the interpretation of variations in initial Sr, Pb, and Nd data has been to decide whether

the variations are due to longterm heterogeneities in the mantle sources or to recent mixing of crustal and mantle material. Measurements of young basaltic rocks from oceanic and continental regions have shown that ε_{Nd} and ε_{Sr} are strongly correlated for samples with $\varepsilon_{Sr} < +10$ (DePaolo and Wasserburg, 1976b; O'Nions and others, 1977). This correlation appears to be characteristic of mantle reservoirs and may provide a reference line against which effects due to crust-mantle mixing processes can be evaluated and separated from the variations due to longterm mantle heterogeneity.

Results: Nd isotopic data on twelve Oslo Rift samples are shown in figure 1. All samples have ε_{Nd} lying in the relatively narrow range from -1 to +4. These values are distinct from the bulk of the MOR basalts, ocean island basalts, and island arc rocks but overlap with the bulk of continental flood basalts and fill in the gap between ocean island basalts and continental flood basalts. The Oslo Rift is a mildly alkaline province with sodic alkaline rocks. The ε_{Nd} values are very different from those of potassic alkaline rocks (fig. 1). The ε_{Sr} values on the same samples show a much larger range from -15 to +33. The data plot on both sides of the ε_{Nd} - ε_{Sr} correlation line and show no immediate relation to it. From the ε_{Nd} data we conclude that the source materials of these rocks must have time-integrated REE patterns that range from approximately chondritic to slightly light REE-depleted. The strong light REE-enrichment observed in these alkaline rocks by Neumann and others (1977) must, therefore, result from fractionation during recent magmatic processes. It is clear from the ε_{Nd} data that none of the rocks could have formed by anatexis of either upper or lower continental crustal materials. This includes such felsic rocks as syenite, trachyte, biotite granite, and peralkaline granite.

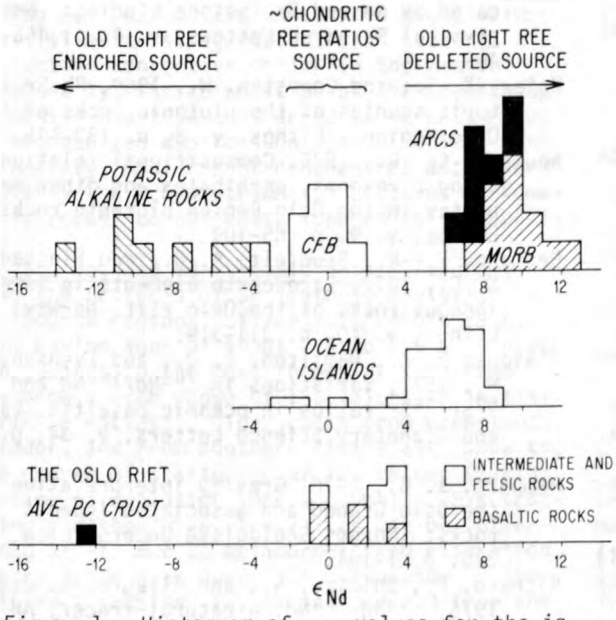

Figure 1.--Histogram of ε_{Nd} values for the igneous rocks in the Oslo Rift compared with histograms of ε_{Nd} values for young basalt samples and inferred REE pattern of their parental reservoirs. Also shown in the ε_{Nd} value measured today of a composite sample of the Precambrian basement in the Oslo Rift. Data on continental flood basalts (CFB), oceanic island basalts, mid-ocean ridge basalts (MORB), island arcs (ARCS) and continental potassic alkaline rocks from DePaolo and Wasserburg (1976a, b, 1977), O'Nions and others (1977), Richard Shimizu, and Allegre (1976), and Carter and others (1978).

Two samples from the Skien basalt series of ankaramites, nephelinites, and basanites that represent the earliest volcanism in the rift have $\varepsilon_{Nd} = +1.5$ and $\varepsilon_{Sr} \sim -15$. They plot further to the left of the ε_{Nd} - ε_{Sr} correlation line than any other terrestrial rocks that have been measured so far.

One explanation for this may be interaction with old lower crustal materials, as low-SiO_2 magmas seem to have a very strong tendency to interact with the quartz-bearing crustal rocks (Turi and Taylor, 1976). However, this would require an extremely Rb-depleted lower crust with a low Sr/Nd ratio. Alternatively they may have been derived from some special mantle reservoir.

One ankaramite from the subsequent alkali-olivine basalt volcanism further north (Holmestrand basalt series) had $\varepsilon_{Nd} = +3$ and $\varepsilon_{Sr} = +20$. This was followed by tholeiitic volcanism in the northern part of the rift (Kolsås basalt member) and two samples give $\varepsilon_{Nd} = -0.7$ and $\varepsilon_{Sr} \sim +18$. They thus plot on a trend typical for continental tholeiitic flood basalts. This trend extrapolates back to the correlation lines at $\varepsilon_{Nd} \approx 0$ and $\varepsilon_{Sr} \approx 0$ and thus indicates a chondritic source with respect to the REE elements. This trend has been interpreted by DePaolo and Wasserburg (1977) to be due to contamination of tholeiitic magmas to varying degree at shallow levels in the crust.

Intermediate volcanic and plutonic rocks have $\varepsilon_{Nd} \sim +3$ to +4 and $\varepsilon_{Sr} \simeq -8$ to -5 and the felsic members have $\varepsilon_{Nd} \sim +3$ to -1 and $\varepsilon_{Sr} \sim 0$ to +33. They all plot to the right of the ε_{Nd} - ε_{Sr} correlation line and suggest that small amounts of crustal contamination may be important in the genesis of these rocks. The composition of the local Precambrian basement in Permian time was $\varepsilon_{Nd} \sim -10$ and $\varepsilon_{Sr} \sim +160$. The dashed line in figure 2 shows the shape of a mixing curve with the monzonitic magmas and the Precambrian basement as end members. The curve was calculated from the Sr and Nd isotopic compositions and concentrations measured for the end members. Variable contamination could probably in part account for the great variety of differentiation trends observed from major- and

trace-element studies of these rocks (Neumann, 1976; Neumann and others, 1977). If crustal contamination is the reason for the variability in the Sr and Nd isotopic composition for the intermediate and felsic rocks, then the uncontaminated parent magmas must have had $\varepsilon_{Nd} > +4$ and $\varepsilon_{Sr} < -10$.

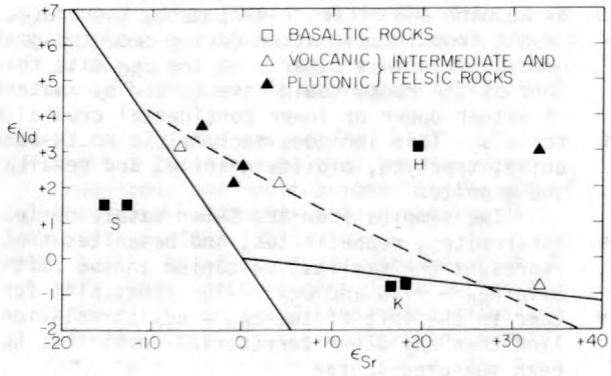

Figure 2.--ε_{Nd} versus ε_{Sr} for rocks from the Oslo Rift. The ε_{Nd} - ε_{Sr} correlation line for young oceanic and continental basalts with $\varepsilon_{Sr} < +10$ is shown. Also shown is a trend with a different slope defined by some continental tholeiitic flood basalts with $\varepsilon_{Sr} > 0$ (DePaolo and Wasserburg, 1977). Dashed curve is a mixing curve with monzonitic magmas and local Precambrian basement as end members. S = nephelinite and ankaramite from the Skien basalt series; H = ankaramite from the Holmestrand basalt series; K = two tholeiite samples from the Kolsås basalt member.

Discussion: The data presented here show that current magma models for this rift zone are oversimplifications. It seems clear that most of the igneous rocks in the Oslo Rift must have been derived from a mantle source with $\varepsilon_{Nd} > +4$. The possibility of crustal contamination makes it difficult to use the isotopic data to put detailed constraints on the mantle sources of these rocks. However, the data suggest that three different sources should be considered: 1) one that is the source of alkali-olivine basalts and intermediate to felsic magmas, 2) one that is the source of nephelinites and ankaramites in the Skien area, and 3) one that is the source of the tholeiitic basalts. The fact that tholeiitic and alkalic rocks alternate in the volcanic series indicates that both tholeiitic and alkalic basaltic magma chambers occurred within the lower crust at the same time. The alkalic magmas are, however, volumetrically the most important.

In this study of ε_{Nd} and ε_{Sr} variations in a continental rift zone, we have attempted to sort out effects due to crustal contamination and thus obtain information about the mantle sources. This was done by using previously established rules for variations of ε_{Nd} and ε_{Sr} in mantle sources. The data base for ε_{Nd} - ε_{Sr} systematics is, however, still small and our understanding of the principles governing these rules is at present inadequate.

Carter, S. R., Evensen, N. M., Hamilton, P. J., and O'Nions, R. K., 1978, Continental volcanics derived from enriched and depleted source regions; Nd- and Sr-isotope evidence: Earth and Planetary Science Letters, v. 37, p. 401-408.

DePaolo, D. J., and Wasserburg, G. J., 1976a, Nd isotopic variations and petrogenetic models: Geophysical Research Letters, v. 3, p. 249-252.

_____1976b, Inferences about magma sources and mantle structure from variations of $^{143}Nd/^{144}Nd$: Geophysical Research Letters, v. 3, p. 743-746.

_____1977, The sources of island arcs as indicated by Nd and Sr isotope studies: Geophysical Research Letters, v. 4, p. 465-468.

Heier, K. S., and Compston, W., 1969, Rb-Sr isotopic studies of the plutonic rocks of the Oslo Region: Lithos, v. 2, p. 133-145.

Neumann, E. -R., 1976, Compositional relations among pyroxenes, amphiboles and other mafic phases in the Oslo Region plutonic rocks: Lithos, v. 9, p. 85-109.

Neumann, E. -R., Brunfelt, A. O., and Finstad, K. G., 1977, Rare earth elements in some igneous rocks of the Oslo rift, Norway: Lithos, v. 10, p. 311-319.

O'Nions, R. K., Hamilton, P. J., and Evensen, N. M., 1977, Variations in $^{143}Nd/^{144}Nd$ and $^{87}Sr/^{86}Sr$ ratios in oceanic basalts: Earth and Planetary Science Letters, v. 34, p. 13-22.

Ramberg, I. B., 1976, Gravity interpretation of the Oslo Graben and associated igneous rocks: Norges Geologiske Undersokelse, v. 325, p. 1-194.

Richard, P., Shimizu, N., and Allegre, C. J., 1976, $^{143}Nd/^{146}Nd$, a natural tracer; An application to oceanic basalts: Earth and Planetary Science Letters, v. 31, p. 269-278.

Sundvoll, B., 1977, Rb-Sr-relationships in the Oslo igneous rocks: News from the Oslo region research group, v. 6, p. 60.

Turi, B., and Raylor, H. P., 1976, Oxygen isotope studies of potassic volcanic rocks of the Roman province, central Italy: Contributions to Mineralogy and Petrology, v. 55, p. 1-31.

COMPOSITIONAL HETEROGENEITY IN THE ARCHEAN MANTLE--EVIDENCE FROM FINNISH GREENSTONE BELTS

By Bor-ming Jahn
Universite de Rennes, Institut de Geologie
35042 Rennes Cedex, France

The chemical and isotopic heterogeneity of the modern upper mantle is well known; however, that of the Archean mantle is not so well documented. It is generally believed that the geothermal gradient was substantially higher in the Archean than in modern times. The experimental study of Green (1975) suggested that the extrusive temperature of many peridotitic komatiites is higher than 1600°C and that the diapirs producing these magmas would have deep origins (> 200 km). Whichever geotherm model of Green is chosen, the sublithospheric convective cell would be deeper in the Archean than today. The rapid ascent of mantle diapirs, which is required to generate a high degree of partial melting for peridotitic komatiitic magma before a partial melt is segregated, also suggests a more active convective motion in the mantle. Consequently, the composition of the Archean upper mantle might be considered to be well mixed and homogenized due to such active motion. Unfortunately, many recent geochemical data, particularly the REE-distribution patterns in komatiitic rocks, do not quite support this supposition.

Sr, Pb, and Nd Isotopic Data: Figure 1 shows the patterns of Sr isotopic evolution in the "source regions" of various Archean rocks. Rocks having ages of about 2.6 to 2.8 m.y. have been subject to the most intensive study and they show a wide range of I_{Sr} values (= initial $^{87}Sr/^{86}Sr$ ratios). Older rocks from Greenland, Labrador, and from southern Africa also show the same degree of scattering of I_{Sr} values (taking the time of evolution into account). This scattering and the "high" I_{Sr} values can be interpreted as (1) due to metamorphic and alteration effects leading to open-system behavior of the whole-rock samples, (2) having derived from anatexis of long-lived sources with high Rb/Sr ratios, particularly for granitic rocks--although the felsic and mafic rock data are not distinguishable in figure 1--or, (3) truly indicating mantle heterogeneity in terms of Rb/Sr abundance ratios. Initial Pb isotopic ratios, and, thereby, calculated μ_1 values from whole-rock secondary isochrons or K-feldspars of many Archean rocks also suggest significant compositional heterogeneity (for example, Moorbath, 1977; Oversby, 1978).

On the other hand, the limited available data on I_{Nd} values (initial $^{143}Nd/^{144}Nd$ ratios) of Archean rocks suggest that these rocks have evolved in a rather uniform reservoir characterized by the chondritic Sm/Nd ratio (= 0.322 by weight) (DePaolo and Wasserburg, 1976; Hamilton and others, 1978). This further implies that: (1) the Archean upper mantle was quite homogeneous in terms of Sm/Nd ratio and thus the REE abundances in general, (2) the compositional heterogeneity is not yet revealed by the limited data, or, (3) the heterogeneity is a short-term phenomenon.

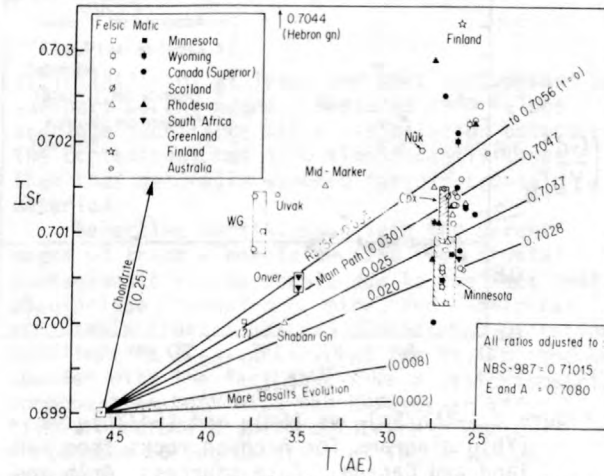

Figure 1.--I_{Sr}-T evolution diagram for Archean rocks. Data sources: Jahn and Nyquist (1976); Hart and Brooks (1977); Cooper and others (1976); Roddick and others (1976); Moorbath and others (1977); Duthou (1977).

Age and REE data for Finnish rocks: The problem of chemical heterogeneity of the Archean mantle was recently discussed by Sun and Nesbitt (1977). New data of REE distribution from Munro Township and Noranda, Canada, and from Finland further substantiate the existence of important heterogeneity in the Archean mantle. The greenstone belts of Finland contain komatiites, tholeiites, and minor amounts of calc-alkaline volcanics. The age was determined indirectly by analyzing some intrusive granites within the belts and surrounding basement gneisses. A Rb-Sr whole-rock isochron yields an age of 2.61 ± 0.06 m.y. and I_{Sr} = 0.7033 ± 7 (2σ) ($\lambda_{^{87}Rb}$ = 1.42 x 10^{-9} yr^{-1}). A common Pb whole-rock secondary isochron yields an age of 2.635 m.y. ($\lambda_{^{238}U}$ = 0.155125 x 10^{-9}; $\lambda_{^{235}U}$ = 0.98485 x 10^{-9} yr^{-1}) (Vidal and Tilton, 1978). Peridotiitic and basaltic komatiites, as well as tholeiitic rocks, have been analyzed for major and trace elements. Figure 2 illustrates the characteristics of REE distribution patterns for rocks from

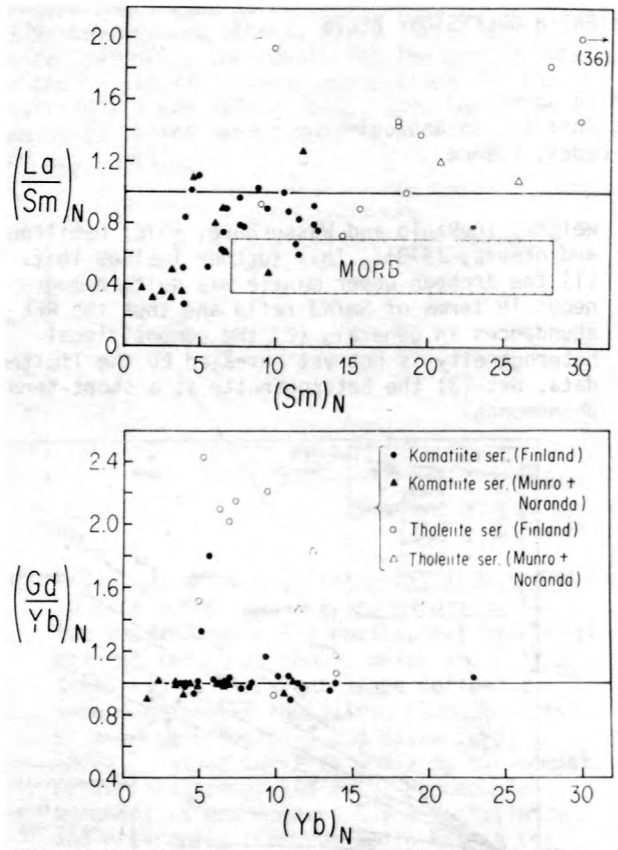

Figure 2.--$(La/Sm)_N$ vs $(Sm)_N$ and $(Gd/Yb)_N$ vs $(Yb)_N$ diagrams for Archean rocks from Finland and Canada. Data sources: Arth and others (1977); Jahn and others (1978) and Jahn (unpub. data).

Finland and Canada. Note that many komatiites are characterized by having remarkably flat heavy REE and depleted light REE. Some typical examples of strongly depleted REE-patterns are shown in figure 3. Due to the residual nature (dominantly of olivine and orthopyroxene) after a large degree of partial melting, the REE-patterns in the peridotitic komatiites must reflect the REE-source characteristics. In rocks from Canada and Finland, the observed REE-patterns suggest that the Archean upper mantle was as heterogeneous as is the upper mantle; that is, its composition had not been homogenized by more vigorous convective motion in Archean time. Although the heterogeneity is well demonstrated by the La/Sm ratios, the degree of heterogeneity becomes less pronounced in terms of Sm/Nd ratios and, thus, the isotopic composition of Nd, particularly if the heterogeneity was created not long before the rock was generated. We suppose that long-lived heterogeneity might have existed in the Archean, but this will have to be proved by future I_{Nd}-data.

So far, very light REE-depleted rocks occur in Finland, Canada, west Australia, and Rhodesia. If the light REE depletion is found to be more widespread than the known occurrences, the causal effect and the complementary parts might be related to: (1) the production of some contemporaneous light REE-enriched tholeiitic rocks, (2) enrichment of light REE and LIL by adding some undersaturated melt to higher level mantle-source regions, which later produced light REE-enriched rocks, or to, (3) the contemporaneous or previous continent-forming events. Because of the heterogeneity of the Archean mantle, the common practice of identifying tectonic settings for Archean greenstone belts by comparing their trace-element abundances (even the refractory REE) with those of modern volcanic rocks should be subject to a more cautious examination.

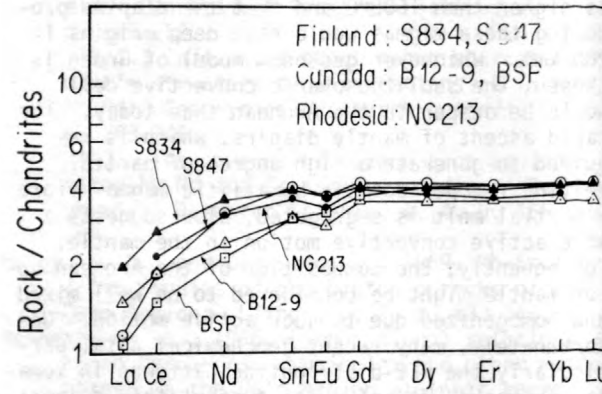

Figure 3.--Some typical examples of peridotitic komatiites with strong depletion in light REE. Data sources: NG213 from Hawkesworth and O'Nions (1977); others from Jahn and others (1978).

Arth, J. G., Arndt, N. T., and Naldrett, A. J., 1977, Geology, v. 5, p. 590-594.

Cooper, J. A., Nesbitt, R. W., Platt, J. P., and Mortimer G., 1976, 25th Int. Geol. Congress, Vol. 1, Sect. 1, 7.

DePaolo, D. J., and Wasserburg, G. J., 1976, Geophysical Research Letters, v. 3, p. 249-252.

Duthou, J. L., 1977, Abstract, European Colloquium of Geochronology V, Pisa.

Green, D. H., 1975, Geology, v. 3, p. 15-18.

Hamilton, P. J., O'Nions, R. K., Evensen, N. M., Bridgwater, D., and Allaart, J. H., 1978, Nature, v. 272, p. 41-43.

Hart, S. R., and Brooks, C., 1977, Contributions to Mineralogy and Petrology, v. 61, p. 109-128.

Hawkesworth, C. J., and O'Nions, R. K., 1977, Journal of Petrology, v. 18, p. 487-520.

Jahn, B. M., and Nyquist, L. E., 1976, in, B. F. Windley, ed., The early history of the Earth, London, John Wiley, p. 55-76.

Jahn, B. M., Auvray, B., Blais, S., Capdevila, R., Cornichet, J., Vidal, F., and Hameurt, J., (in press), Contributions to Mineralogy and Petrology.

Moorbath, S., 1977, Chemical Geology, v. 20, p. 151-187.
Moorbath, S., Wilson, J. F., Goodwin, R., and Humm, M., 1977, Precambrian Research, v. 5, p. 229-239.
Oversby, V., 1978, Earth and Planetary Science Letters, v. 38, p. 237-248.
Roddick and others, 1976.
Sun, S. S., and Nesbitt, R. W., 1977, Earth and Planetary Science Letters, v. 35, p. 429-448.
Vidal and Tilton, 1978: (this conference).

ORIGIN OF HIGH $^{87}Sr/^{86}Sr$ RATIOS IN CENTRAL ANDEAN CALC-ALKALINE LAVAS

By David E. James
Carnegie Institution of Washington
Department of Terrestrial Magnetism
Washington, D.C. 20015

Calc-alkaline lavas of late Cenozoic age of the central Andean volcanic arc are characterized by high $^{87}Sr/^{86}Sr$ ratios (0.705 to 0.708) and high K, Rb, Sr, Ba, light REE, and Ni concentrations relative to island arc volcanics of comparable SiO_2 content and depth to underlying Benioff zone. Conflicting interpretations of these "anomalous" isotopic and trace-element compositions include: (1) sialic contamination of a mantle derived magma of low $^{87}Sr/^{86}Sr$ (for example, Klerkx and others, 1977), and (2) melting of enriched continental lithospheric mantle (James and others, 1976).

Oxygen isotope determinations for more than 30 plagioclase mineral separates from central Andean volcanic samples, for which Sr-isotopic and trace-element compositions are known, demonstrate that neither interpretation can be wholly correct. $\delta^{18}O$ values lie almost entirely in the range +7.0 to +7.5 permil (SMOW), slightly higher than accepted mantle values of +5.5 to +6.5 permil (SMOW), but too low to permit the large degree of crustal contamination that would be required to alter the $^{87}Sr/^{86}Sr$ ratios of a mantle-derived magma to the extent observed. Moreover, the $\delta^{18}O$ values tend to decrease slightly with increasing $^{87}Sr/^{86}Sr$.

Low $\delta^{18}O$ values, coupled with Sr concentrations and other trace-element abundances, provide convincing evidence against crustal contamination as a primary cause of the high $^{87}Sr/^{86}Sr$ ratios observed. High Sr concentrations (500 to 900 ppm) in the lavas require that if the parent magma had low $^{87}Sr/^{86}Sr$ then either very large amounts of contaminant were assimilated or the contaminant had a high $^{87}Sr/^{86}Sr$ ratio (probably > .73). However, plots of other trace elements such as Rb, Ba, and light REE versus $^{87}Sr/^{86}Sr$ ratios reveal systematic variations that would require implausibly high trace-element concentrations in any contaminant with $^{87}Sr/^{86}Sr$ higher than about 0.715. As crustal rocks rarely contain more than a few hundred ppm Sr, even a contaminant with $^{87}Sr/^{86}Sr$ ratio as high as 0.715 implies bulk assimilation of at least one part contaminant to one part parent magma. Measured $\delta^{18}O$ values preclude such large scale assimilation unless the contaminant has $\delta^{18}O$ significantly lower than that generally assumed for old crustal material.

Selective partitioning into the parent magma of trace elements derived from crustal contaminants is improbable due to the fact that plagioclase, hornblende, mica, and K-feldspar are stable crustal phases. Their high partition coefficients (C_{solid}/C_{liquid}) for Sr, Rb, and Ba coupled with the fact that K is a stoichiometric component in both mica and K-feldspar effectively preclude significant trace-element enrichment during partial melting of crustal material.

Finally, though trace-element variations in the central Andean lavas are systematic, they correlate strongly with $^{87}Sr/^{86}Sr$ (see fig. 1). That correlation demonstrates that the trace-element variations cannot be due to fractionation, although small fractionation effects may be superimposed.

Despite compelling arguments against crustal contamination as a cause of high $^{87}Sr/^{86}Sr$ ratios, the $\delta^{18}O$ values require some sialic participation in the magmatic process. If such participation does not occur in the crust, it may occur in the subduction zone. It is the purpose of this study to show that melting of continental sedimentary material in the subduction zone provides a plausible explanation for the high $^{87}Sr/^{86}Sr$ ratios and trace-element concentrations observed. It may also account for observed chemical differences between continental arc and island arc volcanics.

A first important observation is that the volume of continental sediments in the trench and on the continental slope and shelf is inadequate to account for the vast quantities of sedimentary detritus that must have been shed over the past 200 m.y. from the constantly evolving and deeply eroded Andean orogen. Gilluly (1971) noted that offshore sediment

accumulations are at least six times greater on the Atlantic margin of North America than on the Pacific margin despite the fact that the two areas have comparable drainage. He concluded that large volumes of continentally derived sediments have been swept down the subduction zone. The same conclusion appears inescapable for the central Andes.

Subducted material of continental origin (graywacke) will likely include volcanic and plutonic detritus of the evolving arc as well as an admixture of mature sialic material of relatively high $^{87}Sr/^{86}Sr$ ratio (> .71). The bulk composition of the graywacke will thus be of higher $^{87}Sr/^{86}Sr$ and higher K, Rb, Ba, Sr, and probably $\delta^{18}O$ than subducted oceanic crust. Though some ocean floor basalt could be involved in Andean subduction zone melting, observed $^{87}Sr/^{86}Sr$ ratios of altered basalt are not high enough to account for ratios measured in the eruptives.

If graywacke is subducted to 150 km depth and subsequently involved in magma genesis, it will influence isotopic and trace-element compositions in fundamentally different ways than will sialic material involved in crustal contamination of a mantle-derived magma. This can be shown by considering a model similar to that proposed by Nicholls and Ringwood (1973) in which slab-derived magma (in this case, of graywacke rather than oceanic basalt parentage) rises into and equilibrates with overlying mantle material. The modified mantle material then yields andesitic magma that rises to the surface. By that model, the following processes are important in determining the isotopic and trace-element composition of the magma.

1. Preconcentration of trace elements. Major crustal phases that tend to hold trace elements (that is, plagioclase, hornblende, and biotite) are unstable at subduction zone depths. Sanidine may be stable but would be the first phase to melt (Stern and Wyllie, 1973). Thus, residual phases in material of graywacke composition would likely be clinopyroxene, garnet, and possibly coesite, all of which have relatively low partition coefficients for K, Rb, Sr, Ba, and light REE. Partial melting products of metamorphosed graywacke should, therefore, be enriched in K, Rb, Sr, Ba, light REE, H_2O, and probably SiO_2. Similar enrichment will occur during melting of subducted oceanic crust but trace-element abundances for comparable degrees of partial melting will generally be lower, although this may not always be the case, depending upon the mineral assemblages involved.

2. Mixing and equilibration of a slab-derived melt is with bulk-mantle material, not with a mantle-derived melt. Trace-element concentrations in the unmodified mantle are so low that the trace-element abundances and, in particular, the $^{87}Sr/^{86}Sr$ ratios of the modified mantle will be dominated by the slab-derived melt even if the weight proportion of melt is small relative to the mantle material with which it equilibrates. Thus, relatively small weight proportions of sialic contaminant will have greatly disproportionate effects on the isotopic composition of trace elements such as Sr and Nd. For example, if a slab-derived melt of 500 ppm Sr and $^{87}Sr/^{86}Sr$ of 0.708 equilibrates with mantle material of 25 ppm Sr and $^{87}Sr/^{86}Sr$ of 0.703 in the weight proportion .25 parts melt to 1 part mantle material, the modified mantle will have a $^{87}Sr/^{86}Sr$ ratio of 0.7072. Regardless of the way in which the modified mantle undergoes subsequent melting, the melting product will have that $^{87}Sr/^{86}Sr$ ratio.

3. Oxygen isotopic composition will be approximately a simple linear function of the bulk proportion of slab-derived melt to total mantle material with which it equilibrates and of the $\delta^{18}O$ of the two materials. If graywacke retains a $\delta^{18}O$ of about +12 permil (SMOW) at depth (Magaritz and Taylor, 1976) and mantle material is +6 permil (SMOW), the measured $\delta^{18}O$ of +7.2 permil in the lavas requires about 1 part slab melt to 4 parts mantle material. Thus, although the trace-element abundances and Sr-isotopic composition of partial melting products of the modified mantle are dominated by the slab-derived material, the O-isotope and bulk chemical composition of the melt is dominated by material of mantle composition.

4. Partial melting of mantle material modified by uprising slab melt will result in trace-element abundances that are dependent primarily on the phase proportions, melting relations, and partition coefficients of the modified mantle. Mantle material, even highly modified by the influx of slab-derived melt, will strongly partition trace elements into the magma, so that the degree of enrichment of trace elements in the modified mantle will be reflected in trace-element concentrations of the derivative magma.

To judge the plausibility of the process described above, it is necessary to determine whether it can explain the systematic geochemical variations, both regional and local, exhibited by the calc-alkaline volcanics of southern Peru. The calc-alkaline volcanics of the area form several distinct groups--the Barroso volcanics form the most southeasterly group, the Arequipa volcanics the most northwesterly (James and others, 1976). The volcanics follow a southeast to northwest regional trend along the arc of increasing $^{87}Sr/^{86}Sr$, Sr, Ba, K/Rb, and Ni(?) and decreasing Rb, K/Ba, $K_2O/(K_2O + Na_2O)$, Rb/Sr, and $\delta^{18}O(?)$. Potash, SiO_2, and REE abundances do not vary systematically. Local systematic variations are represented by idealized average end-member compositions summarized in figure 1. Of particular interest is the fact that when plotted against $^{87}Sr/^{86}Sr$ many local trace-element variations are in the opposite sense to the regional variation.

Melting model calculations, which include the assumptions implicit in the petrogenetic model described above, indicate that both the regional and local variations in trace-element

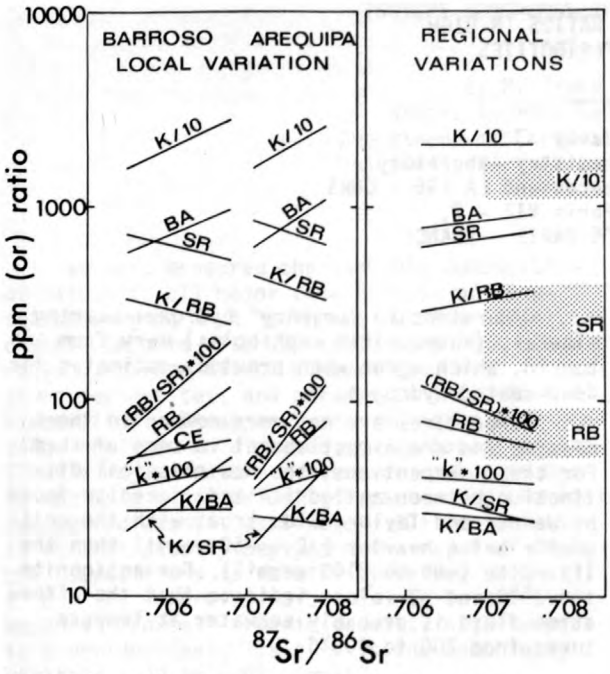

Figure 1.--Abundances and ratios of trace elements plotted against $^{87}Sr/^{86}Sr$. Left diagram shows average trend lines connecting end-member compositions of Barroso and Arequipa volcanics, respectively. Right diagram shows approximate regional trends assuming average Barroso and Arequipa compositions as end-member compositions. "k" = $K_2O/(K_2O + Na_2O)$. Stippled areas on right diagram indicate approximate range of K, Rb, and Sr compositions of Franciscan graywacke and metagraywacke (Bailey and others, 1964; Peterman and others, 1967).

abundances and Sr- and O-isotopic compositions can be interpreted as due to subduction-zone melting of graywacke of average Franciscan composition with $^{87}Sr/^{86}Sr$ ratios less than 0.710. The range of graywacke elemental and isotopic compositions used in the modeling calculations are shown in figure 1 as stippled areas. Model calculations show that the regional variation may reflect a slight increase south to north in the bulk $^{87}Sr/^{86}Sr$ ratio of the subducted material, probably coupled with progressively smaller degrees of partial melting of the modified mantle. Local variations may be modeled in at least two ways: (1) progressive melting of the slab whereby successive batches of melt are tapped from the same slab source region and equilibrated in each stage with previously unmodified mantle material which, in turn, undergoes progressively smaller degrees of partial melting; or (2) variation in the relative proportion of graywacke to oceanic basalt involved in the production of slab-derived melt.

If the petrogenetic model proposed in this paper is correct at least in principle, it follows that subduction and subsequent melting of continental sedimentary detritus can account for the isotopic and trace-element differences observed between certain Andean volcanics and those of island arcs. The model may also explain the progressive increase through time of $^{87}Sr/^{86}Sr$ ratios in Andean eruptives as due to recycling of "aged" sialic material.

Bailey, E. H., Irwin, W. P., and Jones, D. C., 1964, Franciscan and related rocks, and their significance in the geology of western California: California Division of Mines and Geology Bulletin, v. 183, 177 p.

Gilluly, J., 1971, Plate tectonics and magmatic evolution: Geological Society of America Bulletin, v. 82, p. 2383-2396.

James, D. E., Brooks, C., and Cuyubamba, A., 1976, Andean Cenozoic volcanism; magma genesis in the light of strontium isotopic composition and trace-element geochemistry: Geological Society of America Bulletin, v. 87, p. 592-600.

Klerkx, J., Deutsch, S., Pichler, H., and Zeil, W., 1977, Strontium isotopic composition and trace element data bearing on the origin of Cenozoic volcanic rocks of the central and southern Andes: Journal of Volcanology and Geothermal Research, v. 2, p. 49-71.

Magaritz, M., and Taylor, H. P., Jr., 1976, Oxygen, hydrogen, and carbon isotope studies of the Franciscan formation, Coast Ranges, California: Geochimica Cosmochimica Acta, v. 40, p. 215-234.

Nicholls, I. A., and Ringwood, A. E., 1973, Effect of water on olivine stability in tholeiites and the production of silica-saturated magmas in the island arc environment: Journal of Geology, v. 81, p. 285-300.

Peterman, Z. E., Hedge, C. E., Coleman, R. B., and Snavely, P. D., Jr., 1967, $^{87}Sr/^{86}Sr$ ratios in some eugeosynclinal sedimentary rocks and their bearing on the origin of granitic magma in orogenic belts: Earth and Planetary Science Letters, v. 2, p. 433-439.

Stern, C. R., and Wyllie, P. J., 1973, Melting relations of basalt-andesite-rhyolite-H_2O and a pelagic red clay at 30 kilobars: Contributions to Mineralogy and Petrology, v. 42, p. 313-323.

$^{18}O/^{16}O$ AND D/H RATIOS IN HIGH TEMPERATURE PERIDOTITES

By M. Javoy
Stable Isotope Geochemistry Laboratory
Department of Earth Sciences and LA 196 - CNRS
University of Paris VII - 2,
Place Jussieu 75005 PARIS - FRANCE

$^{18}O/^{16}O$ ratios measured in high-temperature peridotite rocks and minerals of Beni Bousera, Lherz, Caussou and Lanzo display a very small range of variation ($+4.5 < \delta^{18}O < +8$). Except for about 5 percent of the samples, the whole-rock $\delta^{18}O$ values correspond to a smaller range ($\delta^{18}O = 5.56 \pm 0.05$), indistinguishable from those of fresh submarine tholeites. The mineral fractionations are consistent with medium (700°C) to very high (> 1200°C) equilibration temperatures. However, many rocks display small disequilibrium features, which together with the abnormal whole-rock values, are explained by fusion-crystallization processes in open systems.

D/H ratios in "primary" hydroxyl-bearing minerals (kaersutitic amphiboles) vary from -88 to -48, which agree with previous estimates for deep-seated hydrogen.

Serpentines are not very common in these massifs and are almost absent in some of them. For these serpentines, the now classical distinction between antigorite and lizardite found by Wenner and Taylor holds true, with the antigorite being heavier ($\delta D \sim -50$ permil than the lizardite (-80 to -100 permil). For antigorite the $\delta^{18}O$ and δD values indicate that the alteration fluid is probably seawater at temperatures from 200 to 400°C.

STABLE ISOTOPE RATIOS IN DSDP LEG 51 BASALTS

By M. Javoy and A. M. Fouillac
Stable Isotope Geochemistry Laboratory
Department of Earth Sciences and LA 196 - CNRS
University Paris VII, 2, Place Jussieu 75005
Paris, France

$^{18}O/^{16}O$ and D/H ratios have been measured on whole-rock samples from holes 417 A and 417 D at depths between 200 m and 400 m below the sea floor. $^{13}C/^{12}C$ and $^{18}O/^{16}O$ ratios have been measured on the carbonate fraction of these rocks and $^{18}O/^{16}O$ and D/H on some smectite vein samples. The carbonate isotopic compositions vary from +25.4 to 29.6 for $\delta^{18}O$ (relative to SMOW) and -4.9 to +2.1 for $\delta^{13}C$ (relative to PDB) and are fairly comparable for both sites. The $\delta^{18}O$ values correspond to equilibrium temperatures of 17°C to 38°C with seawater. The $\delta^{13}C$ may be explained as a mixture of various proportions of primary carbonates of $\delta^{13}C$ around -8 permil with low-temperature precipitated marine carbonate with $\delta^{13}C$ between +2 and +4 permil.

The $\delta^{18}O$ of whole rocks vary from +6.5 to +9.1 permil for hole 417 D and from +6.7 to +20.9 permil for hole 417 A. This observation agrees well with the petrology of these samples, whose degree of alteration is strikingly different despite their very close proximity and comparable situation on the oceanic floor. The correlation of $\delta^{18}O$ with H_2O content indicates that virtually all the ^{18}O variation may be explained by mixtures of fresh basalts with increasing amounts of hydrated minerals (smectites) formed at low temperatures with $\delta^{18}O$ between +25 and +27.5 permil.

The δD values vary from -80 to -47 permil for hole 417 A and from -81 to -64 permil for hole 417 D with respective mean values of -55 and -73 permil and are, thus, strikingly different. These values could be explained by the different chemical composition of clay minerals in both holes, which vary from Al-rich smectites to Fe-Mg-rich saponites and Fe-rich protoceladonites. This would correspond to respective fractionations of about -30 to -70 permil with water at low temperature. The hypothesis that this water is unmodified seawater is roughly verified by the δD results, except that there is too much celadonite in 417 A and too much saponite in 417 D. This could be due either to small variations in the isotopic composition of circulating seawater or to higher temperature of formation in 414 A hole.

ISOTOPE GEOCHEMISTRY OF DEEP SEATED CARBON

By M. Javoy and F. Pineau
Stable Isotope Geochemistry Laboratory
Department of Earth Sciences and LA 196 - CNRS
University Paris VII - 2, Place Jussieu 75005
Paris, France

We have measured the isotopic composition of carbon in all major rock species of deep-seated origin; that is, normal oceanic basalts, oceanic basalts with CO_2 inclusions ("popping-rocks"), carbonatites, kimberlites, high temperature peridotjtes, and peridotite inclusions in kimberlites. These analyses, together with previous analyses on diamonds and carbonatites, reflect a major feature. Wherever carbon is contained in a major or well-characterized chemical species (diamonds, carbonates, CO_2 inclusions), it is isotopically heavy and the range of isotopic compositions is relatively narrow $-8.5 < \delta^{13}C < -4$. Wherever carbon exists in trace amounts ("normal" oceanic basalts, high-temperature peridotites), its $\delta^{13}C$ is low and highly variable (-10 to -30° permil).

In deep-seated systems the overwhelmingly dominant gaseous-carbon species is probably CO_2. Thus, the carbon-isotopic variations are governed by the following limited number of fractionation coefficients: CO_2-carbonates, CO_2-graphite or diamond, and CO_2-carbon dissolved in silicates. The first two coefficients have already been measured or calculated. At temperatures around 1200°C, they should be about +1 permil for CO_2-carbonates and +4 permil for CO_2-graphite and diamond. We have now measured the third coefficient in the range 1100 - 1300°C and find it to vary between 4 and 4.6 permil.

These fractionations make it possible to explain essentially the entire range of terrestrial deep-seated carbon from a very restricted range of primary compositions (-8 permil $< \delta^{13}C < -5$) by varying losses of carbon in the form of ^{13}C enriched CO_2. From this point of view, deep-seated materials behave in various degrees as open and acceptor systems. Peridotite nodules in kimberlites represent the less open and basalts the more open systems. Evolved CO_2 or carbonates concentrate in carbonatites, kimberlites, and the lower crust, with very similar isotopic compositions. Some of this CO_2 is also retained in CO_2-rich oceanic rocks.

THE CLAYTON PLOT

By J. Jordan and T. Kirsten
Max-Planck-Institut F. Kernphysik
Heidelberg, Germany

Inspired by the prediction that large $^{36}Ar/^{38}Ar$ ratios found in some meteorites may owe, in part, their existence to the presence of $^{36}Ar^*$ from decay of supernova synthesized ^{36}Cl (half life of 3×10^5 yr) in presolar grains, Clayton (1977a) has described a Jeffery-Reynolds-type experiment (Jeffery and Reynolds, 1961) whereby one demonstrates the origin of excess ^{36}Ar from extinct ^{36}Cl by showing in a stepwise heating experiment the existence of a correlation of the ^{36}Ar excess with $^{38}Ar^*$ produced by $(n,\gamma\beta)$ reactions on ^{37}Cl. Although a correlation of excess ^{36}Ar with Cl-sites would not unambiguously prove that it owed its existence to supernova synthesized ^{36}Cl, because $^{35}Cl(n,\gamma)$ reactions from in situ neutron capture would also give rise to Cl-correlated excess ^{36}Ar, a quantitative prediction of the amounts of ^{36}Ar from neutron capture could be made from simultaneous measurements of Kr-isotopes produced from (n,γ) reactions on Ba and Se.

In the Jeffery-Reynolds-type experiment, excess $^{129}Xe^*$ is shown to have been produced from decay of ^{129}I by demonstration of a correlation of $^{129}Xe^*$ excess with $^{128}Xe^*$ from ^{127}I $(n,\gamma\beta)$ reactions in the reactor. The relationship is seen by plotting $^{129}Xe/^{132}Xe$ against $^{128}Xe/^{132}Xe$ (or $^{129}Xe/^{130}Xe$ versus $^{128}Xe/^{130}Xe$) in a stepwise heating experiment. A two-component system of trapped ambient gas plus I-correlated gas is expected if all isotopes (but, primarily the reference isotopes ^{132}Xe or ^{130}Xe) are corrected for other components (for example, spallation, reactor produced fission, and natural fission). Shown in figure 1 is such a correlation diagram; the slope is the correlated ratio $(^{129}Xe^*/^{128}Xe^*)$. The trapped component (not indicated), $(^{129}Xe/^{132}Xe)_T = 1.026$, is determined from the trapped ratio, $(^{128}Xe/^{132}Xe)_T = 0.08$, in the unirradiated meteorite. The I-correlated component plots at infinity, because there is no ^{132}Xe in the I-component. Lower temperature points, such as the 1100°C point in the diagram, do not generally correlate due to preferential gas losses from lower temperature sites or slow cooling. The 1600°C point is generally an "empty" fraction and may contain a substantial blank contribution. The corrections for the other components are usually so small that ^{130}Xe and ^{132}Xe are suitable reference isotopes. However, the large corrections for radiogenic $^{40}Ar_R$ prohibit ^{40}Ar from being a suitable reference isotope for demonstrating in a two-component model the correlation of excess ^{36}Ar with reactor-produced $^{38}Ar^*$. Because no other suitable reference isotope exists in the argon systematics, Clayton (1977a) devised a scheme whereby the correlation could be demonstrated with only two isotopes, ^{36}Ar and ^{38}Ar. In the described experiment a meteorite sample is divided into two aliquots labelled 1 and 2. Aliquot 2 is n-irradiated producing $^{38}Ar^*$ via $^{37}Cl\ (n,\gamma)^{38}Cl(\beta^-,\ 37.2\ min)^{38}Ar^*$. After corrections for spallation components, the argon systematics should be composed of a mixture of Cl-correlated gas and uncorrelated ambient trapped gas. Denoting Cl-correlated components by (*) and trapped components by (t), the $^{38}Ar/^{36}Ar$ ratio in the two aliquots may be summarized as follows:

$$\left(\frac{^{38}Ar}{^{36}Ar}\right)_1 = \frac{^{38}Ar_t}{^{36}Ar_t + ^{36}Ar^*}$$

$$\left(\frac{^{38}Ar}{^{36}Ar}\right)_2 = \frac{^{38}Ar_t + ^{38}Ar^*}{^{36}Ar_t + ^{36}Ar^*}$$

For each temperature fraction (T_i) the quantities

$$\Delta(T_i) \equiv \left(\frac{^{38}Ar}{^{36}Ar}\right)_2 - \left(\frac{^{38}Ar}{^{36}Ar}\right)_1$$

and

$$\gamma(T_i) \equiv \left(^{38}Ar/^{36}Ar\right)_2 \,/\, \left(^{38}Ar/^{36}Ar\right)_1$$

are defined. In this two-component model it can be shown that the quantities $[\Delta(T)]^{-1}$ and $[\gamma(T)-1]^{-1}$ correlate and that the temperature steps should fall along a straight line with an intercept which measures the Cl-correlated ratio $(^{36}Ar^*/^{38}Ar^*)_{Cl}$ and a slope measuring the trapped ratio

$$1/\Delta(T) = \left(\frac{^{36}Ar^*}{^{38}Ar^*}\right)_{Cl} + \frac{(^{36}Ar/^{38}Ar)_t}{\gamma(T)-1}\,.$$

Critical for the success of such an experiment is that the release patterns of the uncorrelated trapped gas and the Cl-correlated gas reproduce one another from aliquot to aliquot within the resolvable temperature steps. Indeed, if this criteria is satisfied, the uncorrelated gas need not necessarily be reduced to trapped gas by subtraction of the spallation component; instead, one would have

$$1/\Delta(T) = (^{36}Ar^*/^{38}Ar^*)_{Cl} + \frac{(^{36}Ar/^{38}Ar)_{UNC}}{\gamma(T)-1}$$

where UNC = TRAPPED + SPALLATION.

Although $^{129}Xe^*$ - I systematics should not be expected to be directly comparable to $^{36}Ar^*$-^{36}Cl systematics due to mass differences and the geochemical properties of the now extinct progenitors, it seemed worthwhile to pursue the suggestion of Clayton (1977b) that the outlined method could be tested by attempting to reproduce a $^{129}Xe^*$-^{127}I correlation established by the usual method of plotting. The slope ($^{129}Xe^*/^{128}Xe^*$) of the usual method should appear as the intercept in the Clayton plot. By analogy to the Ar case, after spallation corrections on ^{128}Xe and ^{129}Xe (usually neglibly small) one has the following:

$$\left(\frac{^{128}Xe}{^{129}Xe}\right)_1 = \frac{^{128}Xe_t}{^{129}Xe_t + ^{129}Xe^*}$$

$$\left(\frac{^{128}Xe}{^{129}Xe}\right)_2 = \frac{^{128}Xe_t + ^{128}Xe^*}{^{129}Xe_t + ^{129}Xe^*}.$$

The values for $(^{128}Xe/^{129}Xe)_1$, $(^{128}Xe/^{129}Xe)_2$, $[\Delta(T_i)]^{-1}$ and $[\gamma(T_i)-1]^{-1}$ for Bjurböle standards in separate ampoules of the same irradiation are listed in table 1 and the York fits of the data points are shown in figure 2. The intercept values agree within the errors with the slope values from the usual method (in parentheses). The slopes, although having large errors due to the narrow spread of the points, also agree within these errors with the trapped value calculated from the usual method, $(^{129}Xe/^{128}Xe)_t$ = 12.8. This agreement suggests that this scheme may be useful in determining Cl-correlated $^{36}Ar^*$ in meteorites, independent of the problem of whether Cl-correlated $^{36}Ar^*$ comes from in situ n-irradiation or from decay of extinct ^{36}Cl.

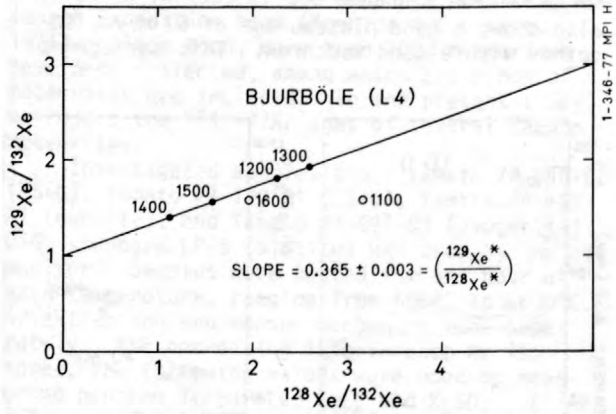

Figure 1.--High temperature two-component correlation diagram used in I-Xe dating. Slope is the I-correlated ratio $(^{129}Xe^*/^{128}Xe^*)_I$.

Clayton, D. D., 1977a, Interstellar potassium and argon: Earth and Planetary Science Letters, v. 36, no. 2, p. 381-390.

_____1977b, Dusty but personal communication.

Jeffery, P. M., and Reynolds, J. H., 1961, Origin of excess ^{129}Xe in stone meteorites: Journal of Geophysical Research, v. 66, no. 10, p. 3582-3583.

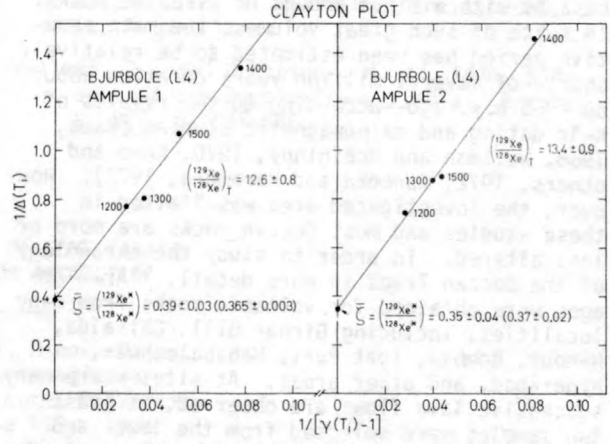

Figure 2.--Clayton two-component diagram applied to I-Xe systematics avoiding use of reference isotope ^{132}Xe. Intercept is the I-correlated ratio $(^{129}Xe^*/^{128}Xe^*)_I$.

Table 1.--Release pattern of $(^{128}Xe/^{129}Xe)$ in Bjurböle (L4) before (1), and after (2), thermal neutron irradiation

[Measurements performed by H. Richter]

T(°C)	$(^{128}Xe/^{129}Xe)_1$	$(^{128}Xe/^{129}Xe)_2$	$^1[\Delta(T_i)]^{-1}$	$^2[\gamma(T_i)-1]^{-1}$
		Ampoule 1		
1200	0.04498±0.00025	1.3365±0.0038	0.7701±0.0023	0.02924±0.00023
1300	0.03797±0.00026	1.2428±0.0049	0.8349±0.0034	0.03755±0.00027
1400	0.05621±0.00025	0.8003±0.0027	1.3439±0.0049	0.07554±0.00045
1500	0.04925±0.00031	0.9979±0.0052	1.0551±0.0058	0.05197±0.00045
		Ampoule 2		
1200	0.04498±0.00025	1.3818±0.0039	0.7441±0.0022	0.02826±0.00022
1300	0.03797±0.00026	1.1835±0.0033	0.8783±0.0025	0.03950±0.00026
1400	0.05621±0.00025	0.7402±0.0020	1.4620±0.0020	0.08218±0.00046
1500	0.04925±0.00031	1.1798±0.0046	0.8846±0.0036	0.04536±0.00034

$^1\Delta(T_i) \equiv (^{128}Xe/^{129}Xe)_2 - (^{128}Xe/^{129}Xe)_1$

$^2\gamma(T_i) \equiv (^{128}Xe/^{129}Xe)_2 / (^{128}Xe/^{129}Xe)_1$

^{40}Ar-^{39}Ar AGES OF THE DECCAN TRAPS, INDIA

By Ichiro Kaneoka
Geophysical Institute
University of Tokyo
Tokyo 113, Japan

The Deccan Traps, covering an area of more than 5 X 10^5 square kilometers in western and central India, form the largest lava plateau in the world with a volume of about (0.5 - 1) X 10^6 km^3. They are composed mainly of tholeiitic basalts with a minor amount of alkaline rocks. In spite of such great volumes, the main eruptive period has been estimated to be relatively short--of several million years duration about 60 - 65 m.y. ago--according to the results of K-Ar dating and paleomagnetic studies (Rama, 1968, Wellman and McElhinny, 1970, Kono and others, 1972, Kaneoka and Haramura, 1973). However, the investigated area was limited in these studies and most Deccan rocks are more or less altered. In order to study the chronology of the Deccan Traps in more detail, ^{40}Ar-^{39}Ar ages were obtained for volcanic rocks from many localities, including Girnar Hill, Chikalda, Nagpur, Bombay, Igat Puri, Mahabaleshwar, Hyderabad, and other areas. At sites where many successive lava flows are observed, at least two samples were selected from the lower and the upper parts of the lava flows. Several of them show good plateau ages.

Figure 1 shows an example of an olivine-augite basalt (IG 15) from the uppermost flow at Igat Puri. For this sample, a good plateau age of 62 m.y. was obtained, together with a good isochron age with the same value. The intercept shows an atmospheric $^{40}Ar/^{36}Ar$ ratio within the experimental error. Hence, this age probably indicates the eruption age for the sample. This value agrees well with the estimated age of the main activity in the Deccan Traps. On the other hand, sample IG 02, from the lower part of the lava flow succession from Igat Puri, shows an older age of about 80 m.y. (fig. 2). For this sample, the plateau is not as good as that of sample IG 15. However, about 62 percent of the ^{39}Ar was released in the 800°C and 900°C fractions, which correspond to a plateau age of about 80 m.y. The total K-Ar age is 82 m.y., and the isochron age indicates a similar value. This evidence suggests that the lower part of the lava flows at Igat Puri erupted about 80 m.y. ago, which is definitely older than the uppermost flow. Although several gaps are observed geologically in the intermediate lava flows at Igat Puri, we cannot identify which boundary corresponds to the large age gap.

Similar older total K-Ar ages are observed for samples from Bombay. Their age patterns, however, are of the inverse staircase type and the isochrons roughly correspond to an age of about 70 m.y. The obsidian from Girnar Hill also shows a good plateau age of 67 m.y., together with a good isochron. This age agrees

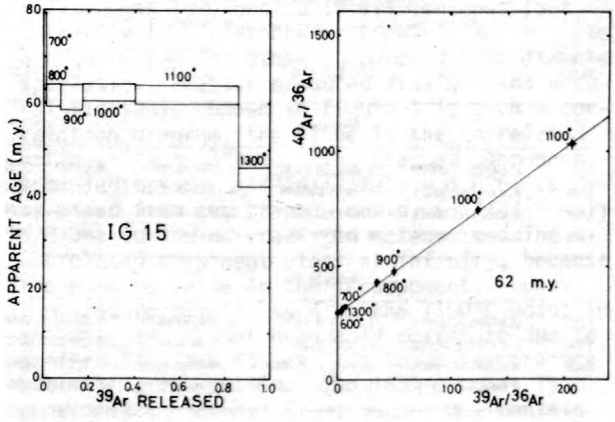

Figure 1.--^{40}Ar-^{39}Ar for the sample Ig 15 (olivine-augite basalt), which was taken from the uppermost flow of the successive lava flows from Igat Puri.
The uncertainties correspond to 1σ. The numbers in the figure indicate the degassing temperatures in degrees Centigrade.

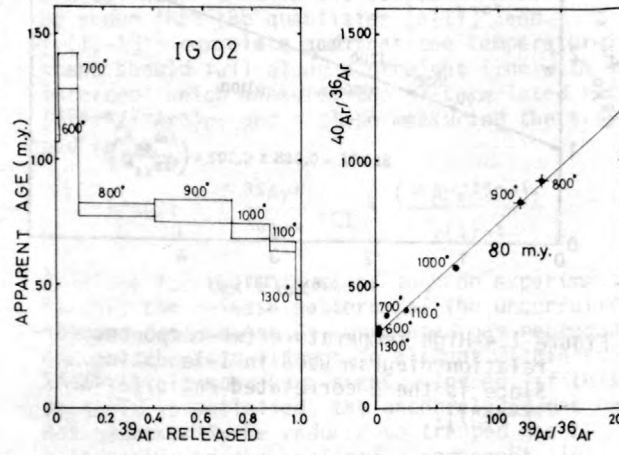

Figure 2.--^{40}Ar-^{39}Ar ages for the sample IG 02 (olivine-augite basalt), which was taken from almost the lowest flow of the successive lava flows from Igat Puri.

well with the K-Ar age of a diorite from Girnar Hill (Kaneoka and Haramura, 1973).

^{40}Ar-^{39}Ar ages for samples from the other areas do not show good isochron ages and are somewhat scattered. However, their total K-Ar ages are mostly concentrated around 60 m.y. This situation is similar to that observed for some Columbia Plateau basalts (Bottomley and York, 1976). Radiogenic ^{40}Ar may have been secondarily redistributed in nature or during neutron irradiation without significant loss from the samples.

In summary, the present study has revealed that an older volcanic activity occurred around 80 m.y. ago in the Deccan Traps. Nevertheless, we confirm earlier studies showing that many volcanic rocks were erupted about 60-65 m.y. ago. Such an age distribution may suggest that the formation mechanism of the Deccan Traps is not a simple one.

Bottomley, R. J., and York, D., 1976, ^{40}Ar-^{39}Ar age determinations on the Owyhee basalt of the Columbia Plateau: Earth and Planetary Science Letters, v. 31, p. 75-84.

Kaneoka, I., and Haramura, H., 1973, K/Ar ages of successive lava flows from the Deccan Traps, India: Earth and Planetary Science Letters, v. 18, p. 229-236.

Kono, M., Kinoshita, H., and Aoki, Y., 1972, Paleomagnetism of the Deccan Trap basalts in India: Journal of Geomagnetism and Geoelectricity, v. 24, p. 49-67.

Rama, S. N. I., 1968, International Geological Congress, 22nd, New Delhi, India, 1964, pt. 7, p. 139.

Wellman, P., and McElhinny, M. W., 1970, K-Ar ages of the Deccan Traps, India: Nature, v. 227, p. 595-596.

^{40}Ar-^{39}Ar AGES OF SOME YAMATO METEORITES FROM ANTARCTICA

By Ichiro Kaneoka, Minoru Ozima, and Masahisa Yanagisawa
Geophysical Institute, University of Tokyo, Tokyo 113, Japan

Yamato meteorites were first found in East Antarctica in 1969 by the Japanese Antarctic Research Expedition team (Yoshida and others, 1971). Since then, more than 1000 meteorites have been collected, among which all kinds of meteorites are included. In the present study, we report the ^{40}Ar-^{39}Ar ages of several Yamato meteorites.

Investigated samples are: Yamato 74-640-02 (H5-6), Yamato 74-190-01 (L5-6), Yamato 74-159-01 (eucrite), and Yamato 74-097-03 (diogenite). USGS standard LP-6 (biotite) was used as the age monitor. Samples were heated for one hour at each temperature, ranging from 600°C to 1500°C. Ar extraction and measurement were made separately. For correcting interference Ar isotopes, the following values were used by measuring neutron irradiated CaF_2 and K_2SO_4: $(^{39}Ar/^{37}Ar)_{Ca} = 7.0 \times 10^{-4}$; $(^{38}Ar/^{37}Ar)_{Ca} = 3.9 \times 10^{-3}$; $(^{36}Ar/^{37}Ar)_{Ca} = 5.5 \times 10^{-4}$; $(^{40}Ar/^{39}Ar)_K = 7.0 \times 10^{-2}$; and $(^{38}Ar/^{39}Ar)_K = 6.7 \times 10^{-2}$. After necessary corrections were made, $^{40}Ar/^{39}Ar$ ages were calculated by using the newly recommended decay constants for ^{40}K (Steiger and Jäger, 1977), which give younger ages by about 0.1 b.y. for the samples of about 4.5 b.y. compared to the older decay constants.

Figure 1 shows the result for Yamato 74-640-02. Although the lower temperature fractions show younger ages than the higher temperature fractions, the apparent ^{40}Ar-^{39}Ar ages increase to a plateau age of 4.41 ± 0.07 (1σ) b.y., which is represented by 1000° - 1350°C

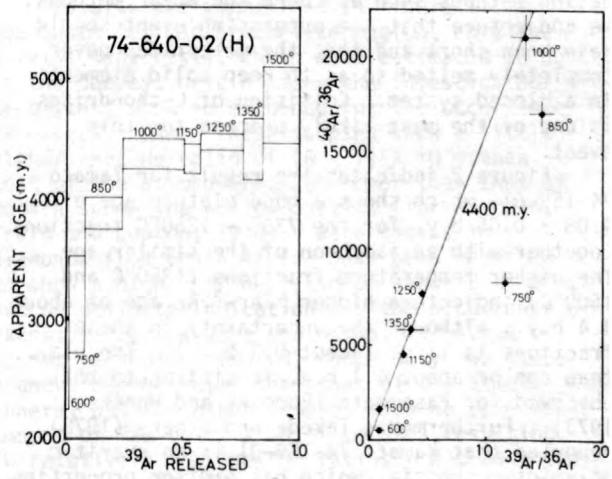

Figure 1.--^{40}Ar-^{39}Ar age diagram and $^{40}Ar/^{36}Ar$ - $^{39}Ar/^{36}Ar$ diagram for Yamato 74-640-02 (H5-6). The uncertainties correspond to 1σ. The numbers in the figure indicate the degassing temperatures in degrees Centigrade.

fractions, accounting for about 61 percent of the released ^{39}Ar. Although the 1500°C-fraction apparently shows a higher ^{40}Ar-^{39}Ar age, we cannot give much weight to this value due to its large uncertainty. In the $^{40}Ar/^{36}Ar$ - $^{39}Ar/^{36}Ar$ diagram, the higher temperature fractions form a good isochron corresponding to 4.4 b.y., which goes through the zero point. Considering that the age of 4.4 b.y. corresponds to the age of 4.5 b.y. calculated by the old decay constants, we conjecture that the plateau age of 4.41 b.y. probably represents the time of formation for this sample. This value agrees well with those of other H-chondrites determined by ^{40}Ar-^{39}Ar method.

On the other hand, Yamato 74-190-01 shows a completely different ^{40}Ar-^{39}Ar age pattern. In the 600° - 880°C temperature fractions, which account for about 46 percent of the ^{39}Ar released, a lower plateau age of 0.36 ± 0.02 b.y. is indicated. The apparent ^{40}Ar-^{39}Ar age increases gradually up to 1.3 b.y. in the highest temperature (1450°C) fraction. However, the 920°C- and 1050°C-fractions still show relatively young ^{40}Ar-^{39}Ar ages of 0.44 and 0.47 b.y., respectively. About 90 percent of the ^{39}Ar was released through the 1050°C-fraction. Such a pattern is quite similar to those observed in many L-chondrites (Turner, 1969), which implies at least one major outgassing event for these L-chondrites about 0.3 - 0.5 b.y. ago. For the present sample, the outgassing event may be dated as about 0.36 b.y. ago from the lower plateau age. Considering that such a young event has not been observed for L-chondrites by other dating methods such as Pb-Pb and Rb-Sr methods, we conjecture that the outgassing event should have been short and that the meteorites never completely melted so as to keep solid elements in a closed system. Collision of L-chondrites is one of the most likely process for this event.

Figure 2 indicates the result for Yamato 74-159-01, which shows a good plateau age of 4.08 ± 0.05 b.y. for the 730° - 1250°C fractions together with an isochron of the similar age. The higher temperature fractions (1350°C and 1500°C) indicate a higher ^{40}Ar-^{39}Ar age of about 4.4 b.y., although the uncertainty in these fractions is large (about 0.3 b.y.). The plateau age of about 4.1 b.y. is similar to that observed for Pasamonte (Podosek and Huneke, 1973). Furthermore, Takeda and others (1978) reported that Yamato 74-159-01 is an eucritic polymictic breccia, which has similar properties to Pasamonte with regards to the texture and pyroxene chemical trend. The ^{40}Ar-^{39}Ar dating result is in accordance with this observation. Although the intermediate plateau ^{40}Ar-^{39}Ar age for Pasamonte agrees well with that of Yamato 74-159-01, Pasamonte shows definitely older Sm-Nd and Pb-Pb ages of about 4.5 b.y. (Unruh and others, 1977). Hence, the age of about 4.1 b.y. probably represents an outgassing event on the achondrite parent body, such as the impact of

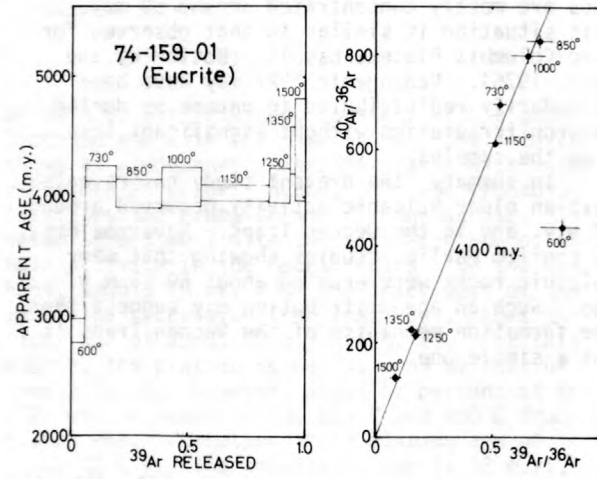

Figure 2.--^{40}Ar-^{39}Ar age diagram and $^{40}Ar/^{36}Ar$ - $^{39}Ar/^{36}Ar$ diagram for Yamato 74-159-01 (eucrite).

meteoroids, which did not disturb the Sm-Nd and Pb-Pb systematics.

Yamato 74-097-03 shows an inverse staircase ^{40}Ar-^{39}Ar age pattern, ranging from 0.96 to 1.3 b.y., whose ages are much younger than those of common achondrites and similar to that of Nakhlites (Podosek, 1973). Because the estimated K-content in this diogenite from the integrated ^{39}Ar amount is less than 50 ppm, however, the calculated ages for this sample have larger uncertainties than the other meteorites.

Podosek, F. A., 1973, Thermal history of the Nakhlites by the ^{40}Ar-^{39}Ar methods: Earth and Planetary Science Letters, v. 19, p. 135-144.

Podosek, F. A., and Huneke, J. C., 1973, Argon 40-Argon 39 chronology of four calcium-rich achondrites: Geochimica Cosmochimica Acta, v. 37, p. 667-684.

Steiger, R. H., and Jäger, E., 1977, Subcommission on geochronology; convention on the use of decay constants in geo- and cosmochronology: Earth and Planetary Science Letters, v. 36, p. 359-362.

Takeda, H., Miyamoto, M., Yanai, K., and Haramura, H., 1978, A preliminary mineralogical examination of the Yamato-74 achondrites: National Institute of Polar Research Memoirs, v. 8, p. 170-184.

Turner, G., 1969, Thermal histories of meteorites by the ^{39}Ar-^{40}Ar method: in, Millman, P., ed., Meteorite Research: Reidel Publishing, p. 407-417.

Unruh, D. M., Nakamura, N., and Tatsumoto, M., 1977, History of the Pasamonte achondrite; relative susceptibility of the Sm-Nd, Rb-Sr, and U-Pb systems to metamorphic event: Earth and Planetary Science Letters, v. 37, p. 1-12.

Yoshida, M., Ando, H., Omoto, K., Naruse, R., and Ageta, Y., 1971, Discovery of meteorites near Yamato mountains, East Antarctica: Antarctic Record, v. 39, p. 62-65.

RARE GAS STATE IN THE LITHOSPHERE ESTIMATED FROM MANTLE-DERIVED ROCKS AND MINERALS

By Ichiro Kaneoka[1], Nobuo Takaoka[2], and Ken-Ichiro Aoki[3]

[1]Geophysical Institute
University of Tokyo
Tokyo 113, Japan

[2]Department of Physics
Osaka University
Toyonaka 560, Japan

[3]Institute of Petrology, Mineralogy and Economic Geology
Tohoku University
Sendai 980, Japan

In order to investigate the rare gas state of the Earth's interior, mantle-derived rocks and minerals, such as ultramafic nodules in alkali basalts, are suitable for the following reasons. Because these materials solidified in the upper mantle, they will trap in-situ rare gases without any atmospheric contamination; the adsorbed atmospheric contamination that may occur after emplacement on the surface can be removed by stepwise degassing techniques; from the mineralogical composition and (or) the occurrence of rocks or minerals, we can infer the derived depth. Thus, by analyzing such samples, which are derived from different depths, we can examine the vertical difference in the rare gas state of the Earth's interior. The regional difference of the rare gas state can also be examined by analyzing similar rocks from different regions. In the present study, the rare gas state includes the $^{40}Ar/^{36}Ar$ ratio in the Earth's interior and the occurrence of some isotopic anomalies, such as higher $^{3}He/^{4}He$ ratio than that of the atmosphere and excess ^{129}Xe. Because most samples were transported as xenoliths, they probably reflect the condition of the lithosphere.

Samples were selected from three different regions: the South African kimberlite region, the Hawaii Islands, and Oki-Dōgo Island, southwest of Japan. They represent continental, oceanic, and ocean-continent margin regions, respectively. In particular, samples from the South African kimberlite region were selected to represent different depths in order to examine the vertical difference of the rare gas state in this region. Rare gasses were analyzed with a Nier-type mass spectrometer with the resolving power of about 600, which makes it possible to completely separate ^{3}He from $HD + H_3$.

Results are summarized in figure 1. In the South African kimberlite region, only the olivine megacrysts, which were estimated to be of the deepest origin among the investigated xenoliths, show an evidence for the occurrence of excess ^{129}Xe. These samples show a little higher $^{3}He/^{4}He$ ratio of $(6 - 7) \times 10^{-6}$ than that of the atmosphere, but lower than that of modern submarine pillow basalts (for example, Craig and Lupton, 1976). Rare gasses in diamonds from South Africa have been reported to show a high $^{3}He/^{4}He$ ratio of about 2×10^{-5}, but no definite indication for the occurrence of excess ^{129}Xe (Takaoka and Ozima, 1978). A Garnet peridotite (MO-43) shows only two times higher $^{3}He/^{4}He$ ratio than that of the atmosphere, but the other samples show no observable amount of ^{3}He ($< 1 \times 10^{-12}$ cm^3STP) resulting in relatively low $^{3}He/^{4}He$ ratios. Although the apparent low $^{3}He/^{4}He$ ratios are partly due to the production and (or) incorporation of radiogenic ^{4}He in these samples, the relatively low amount of ^{3}He in these samples may reflect the depletion of ^{3}He in this region. The $^{40}Ar/^{36}Ar$ ratio is also variable. The shallower samples, such as a phlogopite nodule (DU-02) and a phlogopite-bearing peridotite (BE-03), show relatively high $^{40}Ar/^{36}Ar$ ratios of more than 3000 even after the correction for radiogenic ^{40}Ar after the emplacement of the samples on the

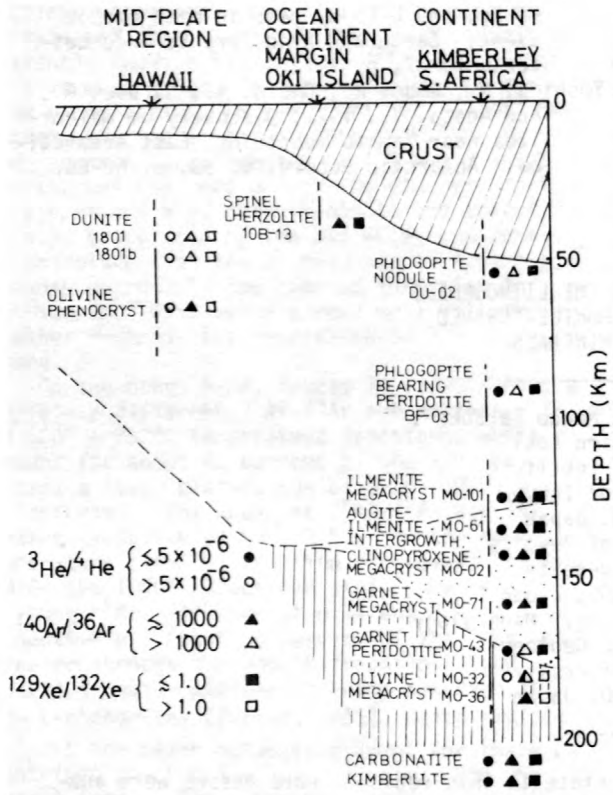

Figure 1.--Schematic diagram of rare gas state in the Earth's deep interior. Structure modified from MacGregor and Basu (1974). Crust; Spinel lherzolites; Spinel and garnet peridotites; garnet peridotites.

surface, whereas the samples derived from the deeper part often show lower $^{40}Ar/^{36}Ar$ ratios of less than 1000. No other definite isotopic anomalies from the atmospheric values were found in these samples. These results suggest that the rare gas state in South African kimberlite region is probably heterogeneous vertically. Only the very limited deep part of the lithosphere may still retain the relatively primitive state of the rare gasses, whereas the shallower region might have been changed from the primitive mantle by a process such as admixture of crustal materials (Kaneoka and others, 1977).

On the other hand, two xenolithic dunites from Hualalai in the Hawaii Islands show excess ^{129}Xe and high $^3He/^4He$ ratios, which are similar to that observed in modern submarine pillow basalts. These dunites also show relatively high $^{40}Ar/^{36}Ar$ ratios of about 1500, though the values are lower than those observed in similar Hualalai samples by Hennecke and Manuel (1975). The olivine phenocrysts separated form Kapuho lava, Kilauea, also show the occurrence of excess ^{129}Xe, whereas its $^3He/^4He$ ratio is 2.5×10^{-5}, higher than that of Hualalai dunites. It is noteworthy that the $^3He/^4He$ ratio in Kilauea fumaroles also has a high value of about 2×10^{-5} (Craig and Lupton, (1976). If the higher $^3He/^4He$ ratio for the Kilauea samples is real, we should also expect a vertical difference in the $^3He/^4He$ ratio under the Hawaii Islands, The $^{40}Ar/^{36}Ar$ ratio in the olivine phenocrysts is about 700. Such isotopic differences probably relate to the different magma sources from which they were formed. The Kilauea samples may reflect the rare gas state of a deeper part of the mantle under the Hawaii Islands.

Spinel lherzolite from Oki-Dōgo Island shows no definite evidence for the occurrence of excess ^{129}Xe. The $^{40}Ar/^{36}Ar$ ratio is about 350. No accurate $^3He/^4He$ ratio could be obtained due to the relatively low amount of He in this sample. Compared to the Hawaiian samples, it has similar contents of heavy rare gasses (Ar, Kr, Xe), but is depleted in lighter rare gasses, especially He. This may reflect a different degassing history for this sample from that of the Hawaiian samples.

These results suggest that the rare gas state in the Earth's interior is inhomogeneous both horizontally and vertically, at least in the lithosphere.

Craig, H., and Lupton, J. E., 1976, Primordial neon, helium, and hydrogen in oceanic basalts: Earth and Planetary Science Letters, v. 31, p. 369-385.

Hennecke, E. W., and Manuel, O. K., 1975, Noble gasses in an Hawaiian xenolith: Nature, v. 257, p. 778-780.

Kaneoka, I., Takaoka, N., and Aoki, K., 1977, Rare gasses in a phlotopite nodule and a phlogopite-bearing peridotite in South African kimberlites: Earth and Planetary Science Letters, v. 36, p. 181-186.

MacGregor, I. D., and Basu, A. R., 1974, Thermal structure of the lithosphere; a petrologic model: Science, v. 185, p. 1007-1011.

Takaoka, N., and Ozima, M., 1978, Rare gas isotopic compositions in diamonds, in, Alexander, E. C., and Ozima, M., eds., terrestrial rare gasses: Tokyo Japan Scientific Society Press.

IODINE-XENON CHRONOLOGY OF ENSTATITE METEORITES

By B. M. Kennedy and F. A. Podosek
Department of Earth and Planetary Sciences
Washington University, St. Louis, Missouri 63130

The enstatite chondrites are a very unusual group of meteorites, characterized by a high degree of reduction and a correspondingly unique mineral assemblage. Within this class, two groups, designated types I and II, are recognized (Anders, 1964; Keil, 1968); two meteorites are considered intermediate cases. Type II differs from type I in having lower Fe and S contents, lower Mg/Si ratios, coarser enstatite crystals, and an absence of chondrules. Keil (1968) argues that the relation between these types is unlikely to be parental, at least in the sense of closed system metamorphism, and that chemical distinctions between these types were established before the assembly of the meteorites. Larimer and Anders (1970) favor the view that type II condensed and accreted before type I, and Baedecker and Wasson (1975) advocate the opposite.

The only class of solar-system materials as reduced as the enstatite chondrites is the enstatite achondrites (aubrites). Wasson and Wai (1970) argue that the chemical and petrographic trends found in the aubrites continue the trends seen in the type I - intermediate - type II sequence and they propose a model in which both the aubrite and enstatite chondrite groups originate in the same parent body, with the sequence reflecting position within and order of accretion to this body (type I first and inside, aubrites last and outside).

Here we consider the relevance of I-Xe chronology to the problem of the history of the enstatite meteorites and possible genetic relationships among them. The methodology of I-Xe dating produces two important parameters relating to the thermal history of a meteorite: a formation age and the $^{129}Xe/^{132}Xe$ ratio in ambient ("trapped") Xe at the time of formation (Podosek, 1970). Both are obtained through observation of a high-temperature (in stepwise heating) linear correlation between radiogenic ^{129}Xe and ^{128}Xe produced from ^{127}I by neutron irradiation.

In an environment in which ^{129}Xe from decay of ^{129}I can be homogenized with ambient gas, the $^{129}Xe/^{132}Xe$ ratio in ambient Xe grows in proportion to the I/Xe ratio in this environment. The time of "formation" is the time at which homogenization of daughter ^{129}Xe with ambient Xe is no longer possible (because of condensation or relaxation of metamorphic conditions). Subsequently produced radiogenic ^{129}Xe is identified as having been produced in situ and remains in association with I; the ratio of in situ ^{129}Xe to ^{127}I is the $^{129}I/^{127}I$ ratio, defining the time of formation relative to other meteorites. The loss of isotopic mobility also "traps" a sample of ambient Xe, so that the trapped $^{129}Xe/^{132}Xe$ ratio is analogous to initial Sr or Pb composition.

Available I-Xe data for enstatite meteorites are summarized in table 1 and illustrated in figure 1. Because the trapped composition is obtained from the intercept of the correlation line (at the AVCC value for $^{128}Xe/^{132}Xe$) and the age from its slope, the uncertainties in these two quantities are anticorrelated and the error fields in figure 1 are slanted. In figure 1 the abscissa is linear in $^{129}I/^{127}I$ (lower scale) so that the corresponding time of formation (upper scale) is logarithmic. With this construction, the evolution of a closed system (constant $^{127}I/^{132}Xe$) is a straight line (fig. 1), with a slope proportional to the I/Xe

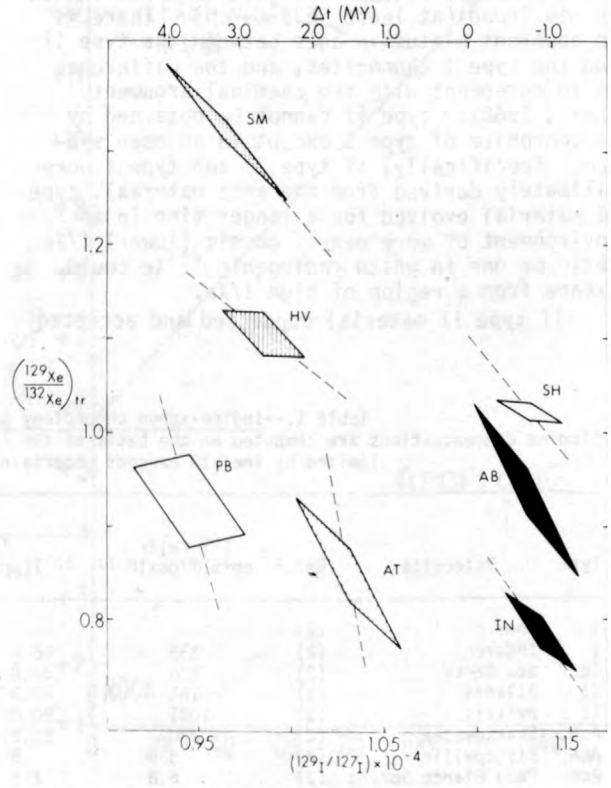

Figure 1.--Relationship between trapped (initial) $^{129}Xe/^{132}Xe$ ratio and ^{129}I - ^{129}Xe gas-retention age in enstatite meteorites. All data from table 1.

ratio. The dashed lines for each meteorite indicate the evolutionary trajectory which would be obtained in a closed system with the I/Xe ratio observed in its high-temperature correlation.

I-Xe ages for enstatite chondrites fall near the center of the span of ages found in other classes of chondrites, but form a cluster of much smaller range. For so narrow an age range, however, the range in trapped composition is large, indicating evolution in a high I/Xe environment. Although I-Xe analyses are available for eight enstatite meteorites, the number of any of the specific types described above is still small and generalizations based on small numbers of samples must be considered tentative. Nevertheless, some interesting trends are observed.

We would expect a closed-system metamorphic family to define a straight evolutionary trajectory on figure 1. The two type II chondrites are consistent with this idea. It is possible to form Hvittis by closed-system metamorphism of the same material from which Atlanta was formed somewhat earlier, and the necessary I/Xe ratio is plausible because it is similar to the ratios actually observed in these meteorites. The equivalent scenario for the two type I chondrites seems less plausible, since it would require a higher I/Xe ratio than is now found (at least in Indarch). There is an apparent hiatus in ages between the type II and the type I chondrites, and the difference is in agreement with the chemical argument (Keil, 1968): type II cannot be obtained by metamorphism of type I except in an open system. Specifically, if type II and type I were ultimately derived from the same material, type II material evolved for a longer time in an environment of more nearly cosmic (lower) I/Xe ratio or one in which radiogenic ^{129}Xe could excape from a region of high I/Xe.

If type II material condensed and accreted before type I, and type II texture is a result of slow cooling and metamorphism in a planetary body environment (Keil, 1968), the duration of the metamorphism (ending at "formation" in the sense of Xe retention) must have been at least 2 to 3 million years in an environment permitting loss of Xe. If type I material condensed first and type II texture is mostly primary (not a result of metamorphic recrystallization in a planetary body) (Baedecker and Wasson, 1975), the difference in condensation time must similarly be about 2 to 3 million years (and up to about 10 million years after condensation of the other classes of meteorites). With current ideas about timescales for condensation and formation of meteorite material, this is an uncomfortably long time. The most plausible viewpoint is that I-Xe ages reflect cooling rather than condensation and it is not clear that the I-Xe age of any meteorite records its condensation.

Without further data the position of St. Marks (intermediate type) is ambiguous. It is evident that St. Marks did not "form" (retain Xe) until after a few million years of evolution in a high I/Xe environment. Since the intermediate chondrites are chemically closer to type I than to type II, the suggestion is that St. Marks is a metamorphic product of primitive material more like type I than type II.

The I-Xe data for the aubrites do not easily support any simple models for their genetic relationships with the chondrites, or with each other. While Pena Blanca Springs could be considered a continuation of the type I-type II trend, Shallowater formed as early as the type I chondrites and Bishopville did not form until much later (at least a few tens of millions of years). Even independent of comparisons with the chondrites, the I-Xe ages of the aubrites are not ordered in the sequence suggested by Wasson and Wai (1970).

Table 1.--Iodine-xenon chronology parameters for enstatite meteorites

[Iodine concentrations are computed on the basis of the ^{128}Xe and ^{129}Xe in excess of trapped gas. Accuracy is limited by the ±10 percent uncertainty in measured gas concentrations.]

Type	Meteorite	Ref.[1]	$[^{132}Xe]tr$ $cm^3STP/gmx10^{-12}$	Iodine concentration: Total ^{127}I(ppb)	Total ^{129}I(ppt)	High-temperature ^{127}I(ppb)	High-temperature ^{129}I(ppt)	Age[2] (10^6yr)	$\left(\frac{^{129}Xe}{^{132}Xe}\right)_{tr}$
I	Abee	(2)						-0.7±0.7	.940±.097
I	Indarch	(2)	339	68.4	5.2	36.0	3.8	-0.9±0.5	.786±.048
Int.	St. Marks	(2)	236	34.8	3.2	27.4	3.0	3.2±0.9	1.322±.078
II	Atlanta	(1)	165	62.3	5.1	39.4	3.9	1.5±0.7	.849±.086
II	Hvittis	(1)	1081	90.0	9.2	85.8	8.7	2.7±0.6	1.106±.023
Ach.	Shallowater	(2)	230	21.2	2.0	17.2	2.0	-0.7±0.5	1.023±.016
Ach.	Bishopville	(2)	3.6	.5					.92 ±.04
Ach.	Pena Blance Spring	(2)	6.8	1.5	0.1	0.9	0.1	3.7±0.8	.928±.063

[1]Data references: (1) Unpublished data from this laboratory (manuscript in preparation); (2) From data tabulated in Podosek (1970).

[2]All ages are relative to Bjurbole≡0.

Anders, E., 1964, Origin age and composition of meteorites: Space Science Reviews, v. 3, p. 583-714.

Baedecker, P. A., and Wasson, J. T., 1975, Elemental fractionations among enstatite chondrites: Geochimica Cosmochimica Acta, v. 39, p. 735-765.

Keil, K., 1968, Mineralogical and chemical relationships among enstatite chondrites: Journal of Geophysical Research, v. 73, no. 22, p. 6945-6976.

Larimer, J. W., and Anders, E., 1970, Chemical fractionations in meteorites - III. Major element fractionation in chondrites: Geochimica Cosmochimica Acta, v. 34, p. 367-387.

Podosek, F. A., 1970, Dating of meteorites by the high-temperature release of iodine-correlated ^{129}Xe: Geochimica Cosmochimica Acta, v. 34, p. 341-365.

Wasson, J. T., and Wai, C. M., 1970, Composition of the metal, schreibersite and perryite of enstatite achondrites and the origin of enstatite chondrites and achondrites: Geochimica Cosmochimica Acta, v. 34, p. 169-184.

ISOTOPIC FRACTIONATION ON THE LUNAR SURFACE

By John F. Kerridge
Institute of Geophysics
University of California
Los Angeles, California 90024

Several elements in the lunar regolith exhibit isotopic variations which are not of nuclear (spallogenic or radiogenic) origin. Study of these isotope systematics can give insights into processes that are active upon the lunar surface. These processes appear to involve mainly physical separation of isotopes, such as mass-dependent differences in diffusion rates. Chemical fractionations, common on earth, appear to play a minor role at most. Observed variations generally fall into three categories, based upon their relationships to various lunar evolutionary time scales.

Category I is characterized by isotopic fractionations which involve systematic enrichment of the heavier isotope(s) with increasing exposure of a soil upon the lunar surface. This exposure may be monitored using the content of solar wind-implanted N. Figure 1 illustrates the strong correlation between $\delta^{34}S$ and N content for bulk analyses of a suite of Apollo 16 soils (Kerridge and others, 1975). The variation in S isotopic composition was shown by Rees and Thode (1972) to be due to a mass-dependent fractionation, and analysis of grain-size fractions by Rees and Thode (1974) revealed maximum surficial enrichments in $\delta^{34}S$ of about 20 permil. Similar surficial enrichments have been observed for $\delta^{18}O$ (50 permil) and $\delta^{30}Si$ (25 permil) during partial fluorination experiments (Taylor and Epstein, 1973). These enrichments also correlate with surface exposure and are mass-dependent (Taylor and Epstein, 1973; Clayton and others, 1974). An element which may fall into category I is K, for which bulk enrichments up to about 8 permil in $^{41}K/^{39}K$, apparently correlated with exposure, have been reported (Garner and others, 1975).

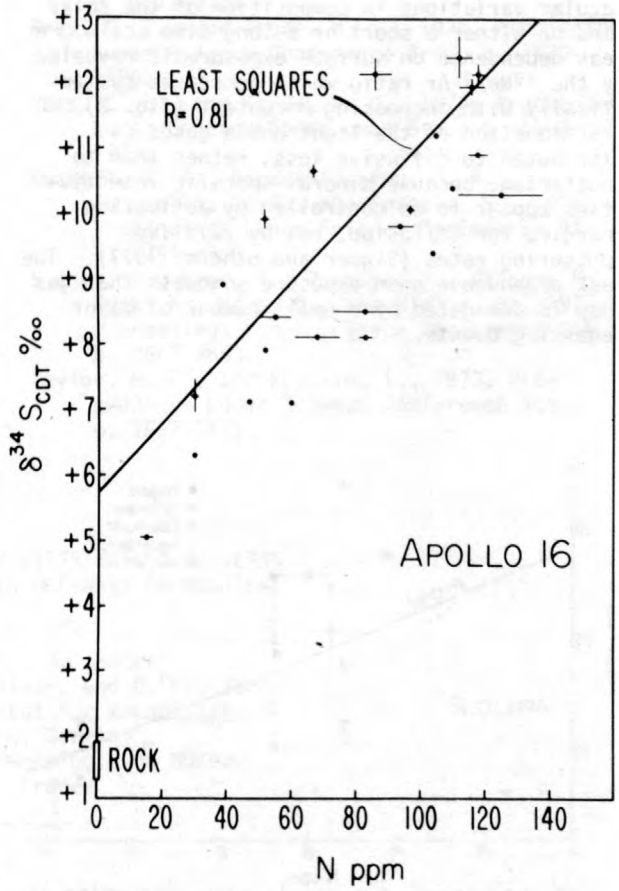

Figure 1.--Correlation between $\delta^{34}S$ and N content.

Observed enrichments in $\delta^{34}S$, $\delta^{18}O$, and $\delta^{30}Si$ agree with predictions by Haff and others (1971) for the effects of sputtering by the solar wind. Sputtering theory and results of simulation experiments (Griffith and others, 1978) predict similar fractionation in Ca, but measurements have so far revealed enrichments of only about 3 permil in $^{44}Ca/^{40}Ca$ (Russell and others, 1977). Proton stripping by the solar wind could, as an alternative, be responsible for fractionation of S, O, and Si but not of K or Ca. These two latter elements, therefore, constitute a test between these processes.

Category II comprises the light noble gases implanted by the solar wind. These show fractionations in the lunar regolith which are large but which correlate weakly, if at all, with surface exposure. The $^{20}Ne/^{22}Ne$ ratio for bulk soils is not obviously related to N content, although the observed values are enriched by up to about 20 percent in ^{22}Ne relative to the solar wind composition (Geiss and others, 1972). Variations in $^{3}He/^{4}He$ are similar. For both systems, possible lunar-fractionation trends may be masked by experimental uncertainties, presence of other components and possible secular variations in composition of the solar wind on either a short or a long time scale. A weak dependence on surface exposure is revealed by the $^{20}Ne/^{36}Ar$ ratio which decreases systematically with increasing N content (fig. 2). Fractionation of the light noble gases is attributed to diffusive loss, rather than to sputtering, because mineral-specific retentivities appear to be controlled by activation energies for diffusion, not by relative sputtering rates (Signer and others, 1977). The weak dependence upon exposure suggests that gas loss is dominated by a small number of major degassing events.

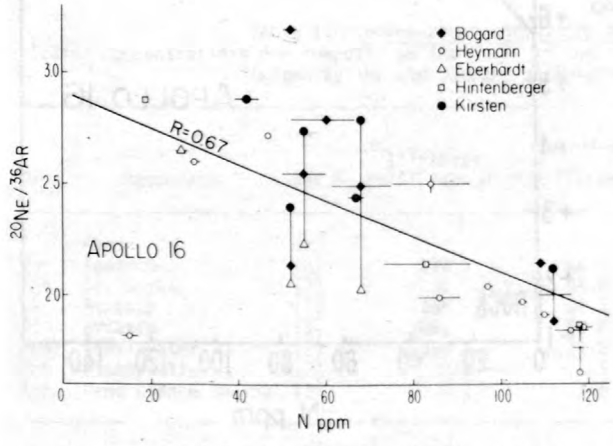

Figure 2.--Correlation between $^{20}Ne/^{36}Ar$ and N content.

Category III consists of trapped solar-wind species whose isotopic composition appears to have varied systematically over the lifetime of the regolith. These species include He (Geiss, 1973) and N (Kerridge, 1975; Becker and Clayton, 1975). The latter has shown an increase of at least 25 percent in $\delta^{15}N$ over a period of about 4 b.y., caused by a currently unknown process, probably in the sun (Kerridge and others, 1977). Nitrogen reveals no evidence for exposure-related fractionation on the lunar surface, using either total data (fig. 3), or data corrected for the secular variation.

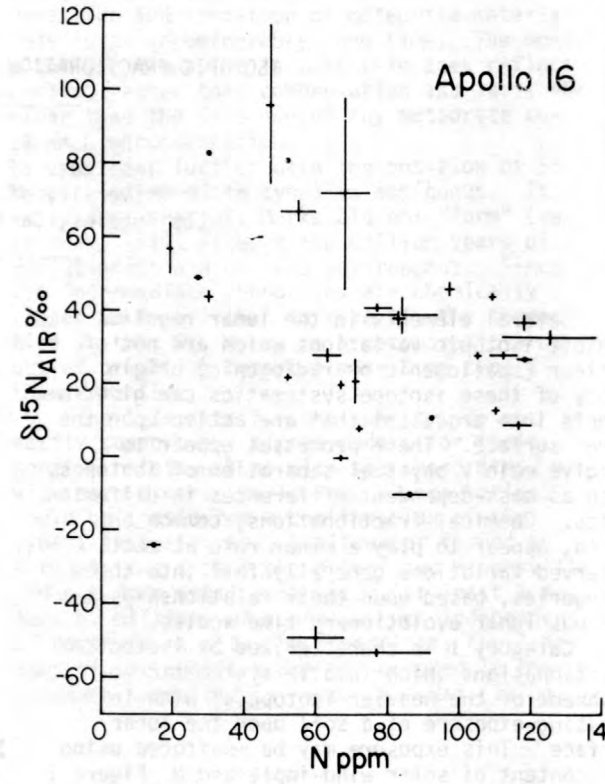

Figure 3.--Relationship between $\delta^{15}N$ and total N.

Isotopic data for C do not fit into any of these categories. Figure 4 shows the relationship between $\delta^{13}C$ and total C, which is equivalent to N content, because the two abundances correlate very closely. No systematic variation of $\delta^{13}C$ with exposure is observed, nor is $\delta^{13}C$ systematically related to the noble gas fractionation pattern--for example $^{20}Ne/^{36}Ar$ ratio--or to $\delta^{15}N$. Combinations of the three types of patterns also fail to generate a systematic trend. The cause of isotopic variation in C is therefore unknown, but it is significant that there is currently no evidence for fractionation of $^{13}C/^{12}C$ on the lunar surface.

The absence of category I effects in the elements of categories II and III, all of which are of wholly or predominately solar-wind origin, indicates that sputtering is not affecting solar wind-implanted species, which means it is not penetrating to their depth within soil grains, about 200 Å. This suggests that sputter-erosion is being impeded by a process such as deposition of material from vapor produced by meteorite impact.

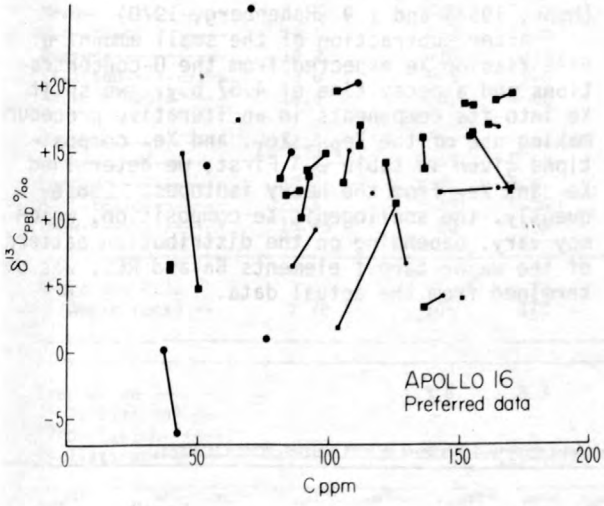

Figure 4.--Relationship between $\delta^{13}C$ and total C.

Becker, R. H., and Clayton, R. N., 1975, Proceedings Lunar Science Conference 6th., p. 2131-2149.

Clayton, R. N., Mayeda, T. K., and Hurd, J. M., 1974, Proceedings Lunar Science Conference 5th., p. 1801-1808.

Garner, E. L., Machlan, L. A., and Barnes, I. L., 1975, Proceedings Lunar Science Conference 6th., p. 1845-1855.

Geiss, J., 1973, International Cosmic Ray Conference Proceedings 13th., p. 3375-3398.

Geiss, J., Buehler, F., Cerutti, H., Eberhardt, P., and Filleux, Ch., 1972, Apollo 16 Preliminary Science Report 14-1: National Aeronautics and Space Administration, SP 315.

Griffith, J. E., Papanastassiou, D. A., Russell, W. A., Tombrello, T. A., and Weller, R. A., 1978, Lunar Science IX, Houston Lunar Science Institute, p. 419-421.

Haff, P. K., Switkowski, Z. E., Burnett, D. S., and Tombrello, T. A., 1977, Proceedings Lunar Science Conference 8th., p. 3807-3815.

Kerridge, J. F., 1975, Science, v. 188, p. 162-164.

Kerridge, J. F., Kaplan, I. R., and Petrowski, C., 1975, Proceedings Lunar Science Conference 6th., p. 2151-2162.

Kerridge, J. F., Kaplan, I. R., Lingenfelter, R. E., and Boynton, W. V., 1977, Proceedings Lunar Science Conference 8th., p. 3773-3789.

Rees, C. E., and Thode, H. G., 1972, Proceedings Lunar Science Conference 3rd., p. 1479-1485.

Rees, C. E., and Thode, H. G., 1974, Proceedings Lunar Science Conference 5th., p. 1963-1973.

Russell, W. A., Papanastassiou, D. A., Tombrello, T. A., and Epstein, S., 1977, Proceedings Lunar Science Conference 8th., p. 3791-3805.

Signer, P., Baur, H., Derksen, U., Etique, P., Funk, H., Horn, P., and Wieler, R., 1977, Proceedings Lunar Science Conference 8th., p. 3657-3683.

Taylor, H. P., and Epstein, S., 1973, Proceedings Lunar Science Conference 4th., p. 1657-1679.

PLUTONIUM AND URANIUM DISTRIBUTION PATTERNS IN PHOSPHATES FROM TEN ORDINARY CHONDRITES

By T. Kirsten[1], J. Jordan[1]
H. Richter[1], P. Pellas[2], and D. Storzer[2]
[1]Max-Planck-Institut fur Kernphysik
Heidelberg, Germany
[2]Laboratoire de Mineralogie du Museum
Paris, France

Extinct ^{244}Pu($T_{1/2}$ = 82 m.y.) plays a key role in the determination of the age of the elements that comprise the Solar System and could, in principle, also serve as a chronometer for the early evolution of the Solar System. Unfortunately, the lack of a stable reference isotope

prevents such a straightforward application because ^{244}Pu concentration differences may be due either to time differences or to chemical fractionations. Consequently, further progress depends on a thorough knowledge of the geochemical behavior of ^{244}Pu during meteorite formation, but at present, ^{244}Pu data are still very limited. In chondrites, it is known that ^{244}Pu (and U and Th) are mainly concentrated in the accessory phosphate minerals whitlockite and apatite. We have therefore determined ^{244}Pu and U concentrations in phosphast separates from 10 ordinary chondrites of type H4, H5, H6, L6, and L7.

^{244}Pu is measured via its fission product xenon because it is retained in the meteoritic minerals. It must be distinguished from trapped Xe_T, cosmogenic Xe_C, and fission xenon from ^{238}U on the basis of its distinct and known isotopic composition. The mass spectrometric analysis of the phosphates was performed in three consecutive extractions at 700°C, 1500°C, and 1650°C. Sample weights are given in table 1. The major gas release always occurred in the 1500°C fraction. The results given in table 2 are the sum of all extractions after correction for blanks and mass discrimination. The absolute calibration was performed by means of atmospheric Xe standards. As indicated from interlaboratory comparisons, Xe calibration still seems to be a problem and 10 percent deviations are generally considered to reflect "good" agreement. For this reason, we have also analyzed a whole-rock sample of the Angra dos Reis Achondrite to compare our fission-^{136}Xe contents with those obtained by other investigators. Our result, 2.09 ± 0.06 (in units of 10^{-11}cc $^{136}Xe_F$ g^{-1}), is to be compared with 2.1 (Munk, 1967) and 1.9 (Hohenberg, 1970).

After subtraction of the small amount of ^{238}U-fission Xe expected from the U-concentrations and a decay time of 4.57 b.y., we split Xe into its components in an iterative procedure making use of the Xe_{Pu}, Xe_T, and Xe_C compositions given in table 2. First, we determined Xe_T and Xe_F from the heavy isotopes. Subsequently, the spallogenic Xe composition, which may vary, depending on the distribution pattern of the major target elements Ba and REE, was determined from the actual data.

Table 1.--Analytical results for 10 phosphate separates and whole rock Angra dos Reis; U data based on track analysis, error ∿ 10 percent

Type	Meteorite	Sample weight (mg)	Phosphate purity (percent)	Whitlockite[2] (percent)	U_{Ph} (ppm)	U_{Wh} (ppm)	U_{Ap} (ppm)	$^{244}Pu_{Ph}$[6] (ppb)	$^{136}Xe_F$	$^{136}Xe_{Pu-F}$[8]	$^{132}Xe_T$	$^{129}Xe_{Ex}$[10]	$^{126}Xe_C$	^{21}Ne Exp age[14] (m.y.)	$^{126}Xe_{C/T}$ (10^{-14}cc/g-m.y.)
									(10^{-11}ccSTP/g mineral separate)[7]						
H4	Menow----------	6.75	97	88.7	[4](0.41)	[4](0.15)	[4](2.5)	22.8	14.0	13.91	38.3	2.7	[c]1.34	[15]9.8±1.4	137
H5	Nadiabondi-----	4.07	95	99	0.086	0.08	2.07	20.8	12.47	12.44	7.02	3.6	1.51	[16]39 ±5	39
H6	Guarena--------	2.0	99	69.6	1.22	0.21	3.47	12.6	8.23	7.86	11.07	[13]3.1	<0.15	[17] 4 ±0.5	<38
H6	Estacado-------	6.87	92	74.9	0.96	0.19	3.26	14.0	8.39	8.11	6.22	[c]0.3	∿0.08	[18]3.4±0.5	23.5
[1]H6	Ambap. Nagla---	6.34	96	[3]69.2	[4](1.15)	[4](0.20)	[4](3.35)	19.8	12.3	11.95	3.25	[13]1.77	[c]0.46	[19]7.7±1	60
L6	Peetz----------	4.95	96.5	[3]62.1	[3]0.81	0.27	1.7	23.1	14.3	14.02	118.8	0	[c]1.1	[20]22.5±3	49
L6	Mocs[5]--------	11.29	94	41.9	1.52	0.13	2.54	12.4	7.85	7.36	0.63	1.5	[c]0.47	[21]12 ±2	39
L6	Leedey[5]------	4.59	94	52.3	1.38	0.14	2.75	20.9	12.8	12.3	18.56	2.6	[d,11]≤0.7	[22]5.5±1	<130
L6	Alfianello[5]---	21.74	99	43.9	1.44	0.18	2.42	27.8	17.8	17.27	3.87	6.0	[c]1.0	[16]17 ±1	59
L7	Shaw-----------	5.14	87	45.5	1.07	0.51	1.55	8.77	5.1	4.80	13.62	[c]1.2	<0.5	[23]0.45±0.05	(<1000)
An	Angra dos Reis whole rock---------525.6		--	--	[5]0.20	(whole rock)		3.23	2.09	2.03	0.569	0.186	[12]0.471	[24]69 ±8	6.8

[1]New classification (feldspar!).

[2]Weight percent whitlockite in phosphate deduced from track analysis. Remainder is apatite.

[3]Preliminary estimate, statistics to be improved.

[4]Educated guess. Evaluation pending.

[5]Tatsumoto and others (1973).

[6]^{244}Pu in pure phosphate from $^{136}Xe_{Pu-F}$; y_{136} = 5.5 percent; λ_F/λ_α = 1.25 x 10^{-3}.

[7]Based on component split using compositions given in table 2. Errors estimated < 5 percent unless marked c (5-30 percent) or d (limit only).

[8]After subtraction of ^{238}U-fission Xe accumulated in 4.57 b.y. and n-induced fission Xe from ^{235}U in case of n-irradiated samples marked 9: (∿ 2.3 x 10^{16} n/cm^2).

[9]n-irradiated (table 2) (second hand samples, courtesy Dr. Rambaldi), n-dose ∿ 2.3 x 10^{16} n/cm^2.

[10]Subject to error if spallation composition is unusual.

[11]Deduced from ^{128}Xe.

[12]Spallation composition 124:126:128: - :130:131:132=0.748:1.216:1.927: - :1.034:4.465:1.00.

[13]Remaining excess not accompanied by light spallation isotopes observed only for Guarena (^{131}Xe:1.1; ^{130}Xe:0.3) and Ambapur Nagla (^{130}Xe:0.9).

[14]Production rates from Cressy and Bogard (1976); ^{21}Ne as cited. In some cases, ^{38}Ar is also considered in order to deduce best estimate of exposure age, T.

[15]Srinivasan (1977).

[16]Kirsten and others (1963).

[17]Smith and Huneke (1975).

[18]Zähringer (1968a).

[19]Zähringer (1968b).

[20]Heymann (1967).

[21]Eberhardt (1966).

[22]Huneke (1972).

[23]Heymann (1965).

[24]Ganapathy and Anders (1969).

Table 2.--Xe results on phosphates from ordinary chondrites and whole rock Angra dos Reis

[Absolute concentrations refer to the mineral separates (for their purity, see table 1). Errors are ≤ 4 percent (absolute concentrations) and < 1.5 percent (isotopic ratios) unless marked: a (< 5 percent); b (5 - 10 percent); c (10 - 30 percent); or d (limit only). Errors include uncertainty of blank corrections and mass discrimination corrections. Listed are the sum of 700° C, 1500° C, and 1650° C extractions; main release always in 1500° C fraction. The bottom lines give the isotopic composition of Pu-fission-Xe, U-fission-Xe, trapped Xe, and spallation Xe used for component splitting (see table 1 for results.]

Meteorite	^{132}Xe (10^{-11}ccSTP/g)	Isotopic composition (^{132}Xe = 1000)								
		^{124}Xe	^{126}Xe	^{128}Xe	^{129}Xe	^{130}Xe	^{131}Xe	^{132}Xe	^{134}Xe	^{136}Xe
Menow[1]	51.5	c20	c28	b106	828	b120	733	= 1000	556	518
Nadiabondi	19.1	a50	a80	132	692	111	733	= 1000	765	773
Guarena	18.2	<10	<10	40	798	116	678	= 1000	680	652
Estacado	13.6	d∿5	d∿8	40	508	69	529	= 1000	749	769
Ambapur Nagla[1]	14.4	n.d.	c∿30	n.d.	440	126	522	= 1000	885	929
Peetz[1]	132.3	10	11	73	897	141	771	= 1000	460	404
Mocs[2]	7.91	c∿40	c∿60	110	429	60	598	= 1000	957	1020
Leedey[2]	30.2	n.d.	n.d.	b90	743	b120	673	= 1000	634	625
Alfianello[2]	20.5	c∿30	c∿50	b90	617	91	611	= 1000	874	931
Shaw	18.45	<20	<20	70	846	130	759	= 1000	529	520
Angra dos Reis (whole rock)	2.78	105	170	283	557	175	967	= 1000	789	821
Trapped Xe		3.6	3.3	71.4	983	151.5	788	= 1000	388	330
^{244}Pu-Fission[3]		-	-	-	55	-	282	= 1000	1057	1136
^{238}U-Fission		-	-	-	-	-	141	= 1000	1414	1724
Spallation[4]		700	1110	1744	1820	1033	4690	= 1000	89	0

[1]Preliminary data, computer calculations pending.

[2]Samples were subjected to thermal n-irradiation before analysis; n-induced ^{235}U-fission correction applied, always < 1 percent of total fission-^{136}Xe.

[3]Alexander and others (1971).

[4]Composition for (3Ba + 1 REE)-spallation (best ^{131}Xe-fit). Spallation ratios have been used only for iterative $^{132}Xe_C$-estimate from $^{126}Xe_C$, and for $^{129}Xe_C$. Otherwise, spallation ratios are determined from the experimental data for each sample.

The results of the component split are given in table 1 and illustrated in the three-isotope diagram shown in figure 1. The figure displays the relative proportions of the major Xe components for each sample. It is analogous to compositional diagrams in mineralogy. The $^{136}Xe_{Pu-F}/^{136}Xe_T$ ratios range from 0.36 (Peetz) to 35.4 (Mocs), whereas the spallogenic component is relatively small. The total spallogenic $^{126}Xe_C$ depends on the exposure age, T, and the Ba and REE concentrations. ^{21}Ne exposure ages taken from the literature are given in table 1. It is then possible to predict the target-element concentrations from the last column of table 1. One unit of 10^{-14}cc $^{126}Xe_C$(g-m.y.)$^{-1}$ corresponds to approximately 7 ppm Ba or 20 ppm REE. We conclude that the phosphate separates contain, within a factor of two, approximately 400 ppm REE and 150 ppm Ba. Menow must be enriched above the mean by about a factor of three.

In general, the component split leads to self-consistent partitioning of the isotopic pattern, except for ^{129}Xe excess (table 1) that indicates the presence of extinct ^{129}I in the phosphates and, thus, a geochemical affinity of iodine to the phosphates (especially in the case of Shaw, for which $^{129}Xe_{Ex}$ in phosphate is 10 times higher than in the bulk meteorite analyzed by us).

In two cases, Guarena and Ambapur Nagla, we also observed small amounts of excess ^{130}Xe (table 1).

Uranium data have been inferred from fission-track analysis both for whitlockites and apatites (table 1). The whitlockite/apatite partitioning among the phosphates was determined by microprobe and fission-track analysis. In addition, track analysis gave ratios $\alpha = (Pu/U)_{Wh}/(Pu/U)_{Ap}$, which are required to deduce $^{244}Pu/^{238}U$ ratios for whitlockite and apatite separately (table 3).

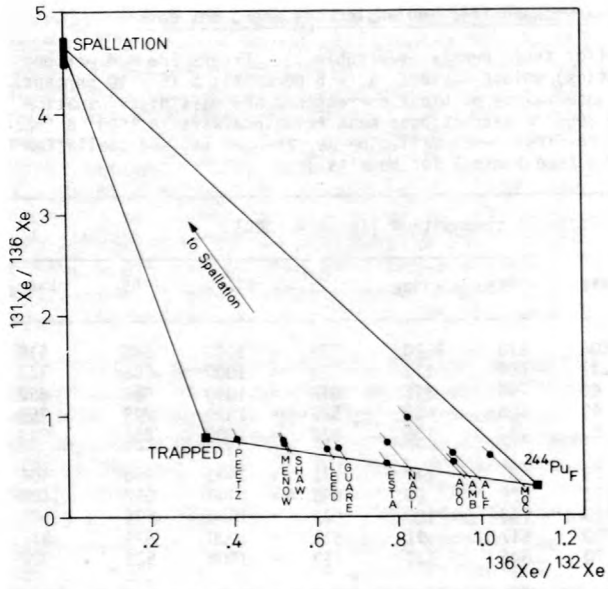

Figure 1.--Three-isotope plot for isotopic Xe composition of phosphate separates showing the relative proportion of Xe from ^{244}Pu-fission, spallogenic Xe_C, and trapped xenon for each sample.

The total ^{244}Pu quantities contained in the phosphates are calculated from $^{136}Xe_{Pu}$ and range from 8.77 ppb in Shaw to 27.8 ppb in Alfianello (table 1). They lead to $^{244}Pu/^{238}U$ ratios, at the onset of Xe retention $\sim$ 4.57 b.y. ago, ranging from 0.004 for Shaw to 0.120 for Nadiabondi. This variability is partly due to different whitlockite/apatite ratios because the data in table 3 shows that ^{244}Pu relative to U is highly enriched in whitlockite but depleted in apatite. Even the $^{244}Pu/U$ ratios in only the whitlockite are by no means uniform. The ratio in Shaw is 0.0115 but $\sim$ 0.120 in Nadiabondi, typical apatite ratios are $\sim$ 0.001 - 0.002. In conclusion, severe geochemical fractionations between U and Pu have taken place and the Pu/U ratio is by no means uniform for various parent bodies. Less variation is found for whitlockites from meteorites of the same parent body. For H6, whitlockite ratios fluctuate $\sim \pm$ 30 percent around the mean value. For 7 out of 10 chondrites analyzed, the bulk phosphate Pu/U ratios were only one- to two-thirds of the whole-rock ratio in the St. Severin Chondrite (0.0154; Podosek, 1972). This leads to the conclusion that the overall phosphate affinity of uranium is higher than that of Pu. The Pu-Xe data will also serve to deduce the cooling history of meteorite parent bodies, together with the Pu-fission track record in various detector minerals.

Table 3.--$^{244}Pu/^{238}U$ ratios in phosphates at time of Xe-retention $\sim$ 4.57 b.y. ago

Meteorite	$\alpha = \frac{(Pu/U)_{Wh.}}{(Pu/U)_A}$ [1]	$(^{244}Pu/^{238}U)_{4.57\ b.y.\ ago} \times 1000$ Phosphate[4]	Whitlockite	Apatite
Menow	[2]>15	[3](27.4)	[3](80± 5)	[3](2±1)
Nadiabondi	Not critical	120	116±14	
Guarena	44.6	5.13	36.9	0.83
Estacado	32.8	7.25	41.6	1.27
Ambapur Nagla	[5](38)	8.6	59	1.56
Peetz	To be determined	[3](14.2)	[3](14-58)	[3](<14)
Mocs	([6])	4.06	4-110	<4
Leedey	([6])	7.48	8-140	<7.5
Alfianello	([6])	9.58	10-170	<9.6
Shaw	5.8	4.07	11.5	1.98
Angra dos Reis		Whole Rock:8		

[1]Determined from track deduced ratio Pu_{Wh}/Pu_A.

[2]Assumption based on other H-chondrite data; determination pending.

[3]Rough estimates, U-analysis pending.

[4]Errors $\leq$ 15 percent.

[5]Mean estimated from Guarena and Estacado (H6).

[6]Shocked meteorites, track analysis impossible.

Alexander, E. C., Jr., Lewis, R. S., Reynolds, J. H., and others, 1971, Plutonium-244-confirmation as an extinct radioactivity: Science, v. 172, no. 3985, p. 837.

Cressy, P. J., Jr., and Bogard, D. D., 1976, On the calculation of cosmic-ray exposure ages of stone meteorites: Geochimica Cosmochimica Acta, v. 40, no. 7, p. 749.

Eberhardt, and others, 1966, Zeitschrift fur Naturforschung, v. 21a, p. 414.

Ganapathy, R., and Anders, E., 1969, Ages of calcium-rich achondrites-Part 2, Howardites, nakhlites, and the Angra dos Reis angrite: Geochimica Cosmochimica Acta, v. 33, no. 7, p. 775.

Heymann, Dieter, 1965, Cosmogenic and radiogenic helium, neon, and argon in amphoteric chondrites: Journal of Geophysical Research, v. 70, no. 15, p. 3735.

_____1967, On the origin of hypersthene chondrites: Ages and shock effects of black chondrites: Icarus, v. 6, p. 189.

Hohenberg, C. M., 1970, Xenon from the Angra dos Reis meteorite: Geochimica Cosmochimica Acta, v. 34, no. 2, p. 185.

Huneke, J. C., Podosek, F. A., Burnett, D. S., and Wasserburg, G. J., 1972, Rare gas studies of the galactic cosmic ray irradiation history of lunar rocks: Geochimica Cosmochimica Acta, v. 36, p. 269.

Kirsten, T., Krankowsky, D., and Zahringer, J., 1973, Edelgas-und Kalium-Bestimmungen an einer groberen Jahl von Steinmeteoriten: Geochimica Cosmochimica Acta, v. 27, p. 13.

Munk, M. N., 1967, Argon, krypton, and xenon in Angra dos Reis, Nuevo Laredo, and Norton County achondrites--the case for two types of fission xenon in achondrites: Earth and Planetary Science Letters, v. 3, no. 5, p. 457.

Podosek, F. A., 1972, Gas retention chronology of Petersburg and other meteorites: Geochimica Cosmochimica Acta, v. 36, no. 7, p. 755.

Smith, S. P., and Huneke, J. C., 1975, Cosmogenic neon produced from sodium in meteoritic minerals: Earth and Planetary Science Letters, v. 27, no. 2, p. 191.
Srinvasan, B., 1977, Noble gases in six ordinary chondrites: comparison of exposure ages from noble gases with ^{26}Al ages: Geochimica Cosmochimica Acta, v. 41, p. 977.
Tatsumoto, M., Knight, R. J., and Allegre, C. J., 1973, Time differences in the formation of meteorites as determined from the ratio of lead-207 to lead-206: Science, v. 180, no. 4092, p. 1279.
Zahringer, J., 1968a: Meteoritika, v. 27, p. 25.
_____1968b, Rare gases in stony meteorites: Geochimica Cosmochimica Acta, v. 32, p. 209.

INTRACRYSTALLINE SITE PREFERENCE OF HYDROGEN ISOTOPES IN THE WATER OF CRYSTALLIZATION OF COPPER SULFATE PENTAHYDRATE

By Itsuro Kita and Sadao Matsuo
Tokyo Institute of Technology, Tokyo, Japan

There are two types of water of crystallization in copper sulfate pentahydrate: The four water molecultes in the coordination sphere of the copper ion (site A) and the water molecule bonded to the sulfate ion through hydrogen bonding (site B). These sites are non-equivalent in terms of structure and energetics, and a site preference for oxygen and hydrogen isotopes is expected for the water of crystallization. In this study, the pentahydrate synthesized at 25°C was pulverized and fractionally dehydrated in a vacuum at 0° an 25°C to collect a series of water samples for D/H analysis. The method was basically the same as that given by Heinzinger (1969), Maiwald and Heinzinger (1972), and Heinzinger and Maiwald (1972). The site preference of hydrogen isotopes was estimated, based on the results of the D/H measurements for the fractionally collected samples.

The hydrogen isotopic ratio is represented by the usual δD expression. D/H of the mother liquor (the saturated) solution) for the synthesis of pentahydrate is taken as the standard:

$$\delta D \text{ (permil)} = \left\{\frac{(D/H)_{sample}}{(D/H)_{mother\ liquor}} - 1\right\} \times 10^3$$

The value of δD of the bulk water of crystallization is -21.1 permil, which agrees quite well with those given by Matsuo and others, (1972), and Maiwald and Heinzinger (1972).

In figure 1, the relationship between the dehydrated fraction (f) and the time (t) after the dehydration started at 0°C is shown. Three linear relationships are found in figure 1 in the range of f from 0.06 to ~0.23, 0.23 to ~0.46, and 0.46 to ~0.70, respectively. The fractional dehydration at 25°C gives a similar pattern. The dehydration proceeds as a zeroth-order rate process with three different rate constants.

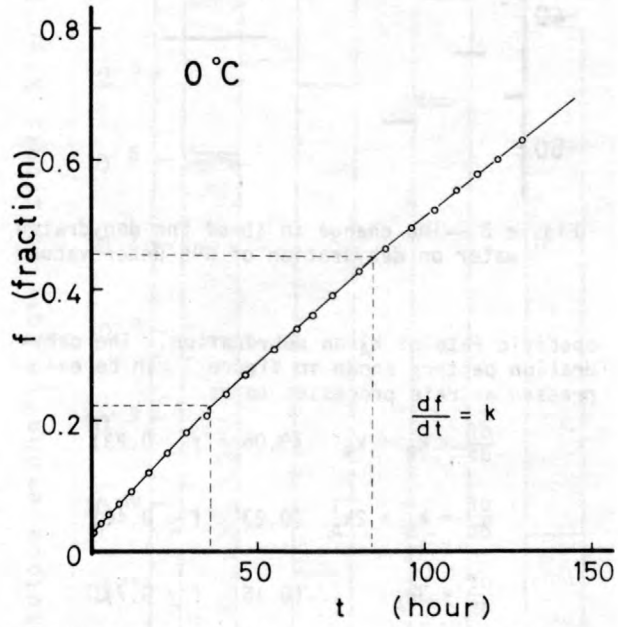

Figure 1.--Dehydration pattern of $CuSo_4 \cdot 5H_2O$ at 0°C under vacuum. The fraction refers to the fraction of water dehydrated.

In figure 2, δD values of the water for each fraction are plotted against f (0°C). Two maxima are observed at f = 0.06 and 0.35. The change in the grain size of pentahydrate from 150 mesh to 270 mesh does not affect the isotopic pattern.

We postulate that the dehydration from site B, with the specific dehydration rate constant of k_B, takes place first to leave tetrahydrate. Then the dehydration of tetrahydrate (site A of pentahydrate) occurs, with the specific rate constant of k_A. The resulting trihydrate loses two water molecules simultaneously with the

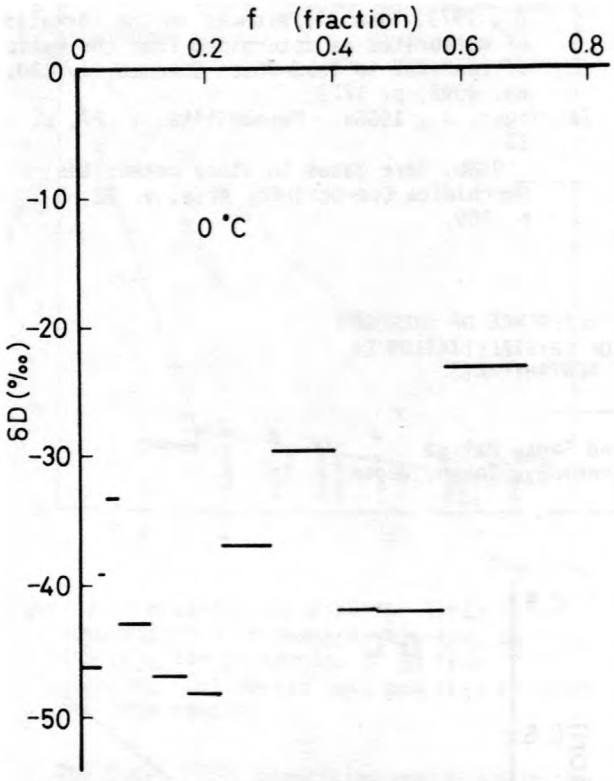

Figure 2.--The change in δD of the dehydrated water on dehydration of 0°C under vacuum.

specific rate of k_A' on dehydration. The dehydration pattern shown in figure 1 can be expressed as rate processes to be

$$\frac{df}{dt} = k_B + k_A \quad (0.06 \lesssim f \lesssim 0.23)$$

$$\frac{df}{dt} = k_A + 2k_A' \quad (0.23 \lesssim f \lesssim 0.46)$$

$$\frac{df}{dt} = 3k_A \quad (0.46 \lesssim f \lesssim 0.7)$$

We can solve these rate constants at 0°C from the experimental results to be 3.96×10^{-3}, 1.40×10^{-3}, and 1.75×10^{-3} fraction/hour for k_B, k_A, and k_A', respectively. The ratios of k_B/k_A and k_A'/k_A remain unchanged even when the grain size pentahydrate is changed. Combing the results of dehydration at 25°C, we get the activation energy for the dehydration to be 19.1, 18.1, and 19.6 Kcal/mol for E_{kB}, E_{kA}, and $E_{kA'}$, respectively. The low activation energy for dehydration, the dehydration process of zeroth-order rate, and the constancy of the ratio of rate constants together indicate that dislocations in crystal grains provide the bulk mechanism of dehydration. The dehydration rate is not controlled significantly by the surface area of crystal grains.

The occurrence of the maxima in δD of the dehydrated water (fig. 2) is due to the unsynchronized beginning of dehydration from two kinds of water with different δD values. For example, the maximum that appears at f = 0.06 can be interpreted to be the result of a combination of the earlier dehydration from site B and the retarded dehydration from site A. On this basis we can assign the dehydrated water up to f = 0.06 as the water derived exclusively from site B, and simultaneous dehydration takes place in the range of $0.06 \lesssim f \lesssim 0.23$.

We applied the Rayleigh distillation theory to water for $0 \lesssim f \lesssim 0.06$ to obtain δD^o_B (the initial δD value of water in site B) and α_B, the kinetic isotope fractionation factor

$$\delta D = \delta D^o + 10^3(1 - \alpha)\ln f_c^{\,r},$$

where δD is the integral mean value of δD of the dehydrated water ($\delta D = \Sigma f_i \cdot \delta D_i / \Sigma f_i$), f_c the remaining fraction of water in the crystal, and r is equal to $f_c/1 - f_c$. The result of the calculation for $0 \lesssim f \lesssim 0.06$ gives +8.2 permil for δD^o_B ($\alpha_B = 0.940$). Using the material balance equation

$$0.2\ \delta D^o_B + 0.8\ \delta D^o_A = -21.1,$$

we obtain -28.4 permil for δD^o_A.

In conclusion, the water of crystallization in the coordination sphere of the copper ion is depleted in deuterium as compared with the mother liquor, and the water bonded to the sulfate ion through hydrogen bonding is enriched slightly in deuterium relative to the mother liquor.

Heinzinger, K., 1969, Ein Wasserstoffisotopieeffekt im $CuSO_4 5H_2O$: Zeitschrift fur Naturforschung, v. 24a, 1052-1511.

Heinzinger, K., and Maiwald, B., 1972, Remarks on the crystallization and dehydration of copper sulfate pentahydrate: Chemical Society of Japan Bulletin, v. 45, p. 2237-2239.

Maiwald, B., and Heinzinger, K., 1972, Isotopieeffekte in den Hydratstrukturen von festem und gelostem Kupfersulfat: Zietschrift fur Naturforschung, v. 27a, 819-826.

Matsuo, S., Friedman, I., and Smith, G. I., 1972, Studies of Quaternary saline lakes - I. Hydrogen isotope fractionation in saline minerals: Geochimica Cosmochimica Acta, v. 36, p. 427-435.

D/H ISOTOPE EXCHANGE REACTION BETWEEN PETROLEUM AND WATER: A CONTRIBUTORY DETERMINANT FOR D/H-ISOTOPE RATIOS IN CRUDE OILS?

By M. Koepp
Federal Institute for Geosciences and Natural Recources
Hannover, West Germany

Uncatalyzed D/H isotope exchange reactions were carried out between a young Pleistocene oil from Louisiana, its chromatographically separated fractions (saturated hydrocarbons (SHC: 62 percent), aromatic hydrocarbons (AHC: 21 percent), and NSO bearing compounds (NSO: 11 percent)) and D_2O or D-enriched water. For comparison, low-molecular, pure hydrocarbons (PHC, Merck P.A. quality; n-hexane, cyclohexane, and toluene, Messer Griesheim 99.995 Vol percent; methane) were studied as well.

Reactants were sealed under high vacuum conditions in Pyrex tubes (for methane a stainless steel sample cylinder was used as reaction vessel). Reaction temperatures were 200° and 240°C and reaction times ranged from 25 to 2000 hours. Quantitative removal of D_2O after heat treating the samples was carried out by repeated intensive washing with small amounts of tap water.

The organic substances were prepared for precision mass spectrometric analysis on a VG-M 602 mass spectrometer, using advanced methods of well-known oxidation and reduction processes (Birkenfeld and others, 1969; Ehrenberger and Gorbach, 1973; Bigeleisen and others, 1952) in a special vacuum line. Detectable changes in the D-content of the organic material were as low as 5×10^{-5} atomic percent.

All exchange reactions were shown to be first order with respect to the water-hydrocarbon D-concentration difference.

$$\frac{dC_{D,HC}}{dt} = k\,(C_{D,H_2O} - C_{D,HC}) \qquad (1)$$

Methane, n-hexane, cyclohexane, and toluene have similar and very slow reaction rates; the first order reaction rate constants are in the range of $k = 10^{-6}$ to 10^{-5} yr^{-1} at 200°C and somewhat more than an order of magnitude faster at 240°C.

Calculated energies of activation (∿ 140 - 200 kJ $mole^{-1}$) lie between binding energies of C-H bonds (∿ 400 kJ $mole^{-1}$) and energies of activation found for metal catalyzed D/H-isotope exchange reactions (60 and 140 kJ $mole^{-1}$ (Metcalfe and Vickers, 1973)) as was to be expected. Evaluation of reaction rate constants from the data just mentioned for T = 100°C (typical reservoir temperatures) gives figures from $k_{100} = 10^{-11}$ up to some 10^{-10} yr^{-1}. This means that measurable δD-shifts at 100°C are not to be expected for the low molecular PHC's in less than 10^8 years for uncatalyzed exchange reactions under natural conditions.

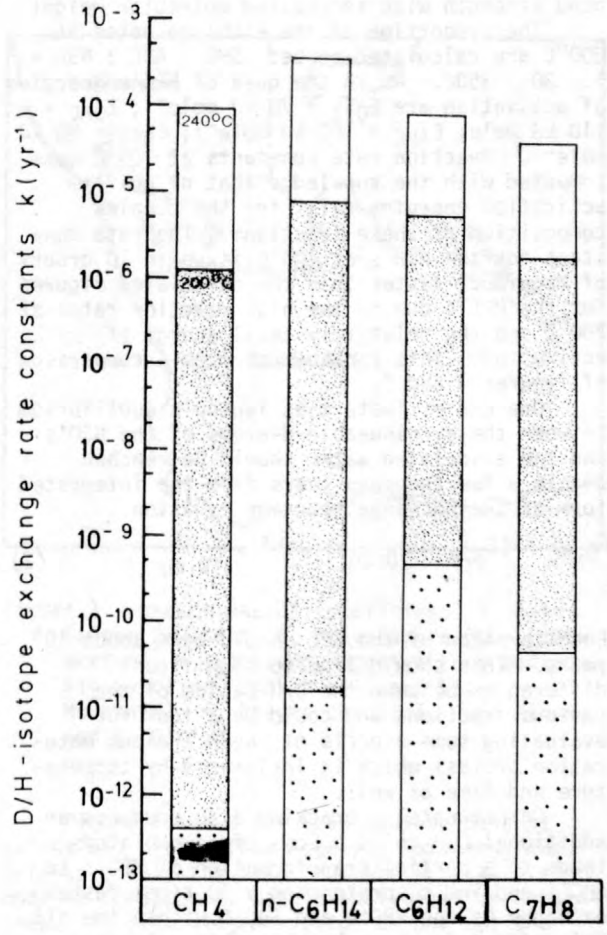

Figure 1.--Comparison of D/H-isotope reaction rate constants at three temperatures for methane, n-hexane, cyclohexane, and toluene. Rate constants for 200° and 240°C are experimental rate constants for 100°C are calculated. Methane figures for 100° and 240°C are estimated by using an energy of activation value from Watt and others (1966) for thermal D_2/CH_4 exchange.

The Pleistocene oil appears to be a factor of 10^4 more active at 200°C compared to the PHC's. Exchange reactions with its separated fractions revealed the NSO's to be the decisive factor for the exchange behavior of the whole oil. The reaction rate constants of these compounds reached k-values of 6×10^{-1} yr^{-1} at 200°C and 3 yr^{-1} at 240°C; the maximum experimental NSO enhancement in D concentration was 1.5 atomic percent. It is not known at the present if this is already the total amount of easily exchangeable H-atoms and whether there is a rigid boundary with "nonexchangeable" H-atoms. Reaction rate constants for the AHC's were found to be about 4×10^{-3} yr^{-1}, and 10^{-4} yr^{-1} for the SHC's at 200°C, the last figure being more than a factor of ten higher than that for the PHC's. This may be explained by the decrease in C-H bond strength with increasing molecular weight.

The proportion of the exchange rates at 200°C are calculated to be: SHC : AHC : NSO = 1 : 30 : 3500. As in the case of PHC's energies of activation are E_{Oil} = 70 kJ $mole^{-1}$; E_{SHC} = 110 kJ mole; E_{AHC} = 100 kJ $mole^{-1}$; E_{NSO} = 80 kJ $mole^{-1}$. Reaction rate constants at 100°C were computed with the knowledge that no uniform activation energies exist for the complex composition of these fractions. The rate constant for the NSO's at 100°C is up to 10 orders of magnitude faster than the calculated figures for the PHC's due to the high reaction rates at 200°C and the relatively small energy of activation. This can be seen from a comparison of figures 1 and 2.

One can estimate that isotopic equilibrium between the exchangeable H-atoms of the NSO's and the associated water should be reached within a few thousand years from the integrated form of the exchange reaction equation.

$$C_{D,HC} = (C_{D,o} - C_{D,eq}) e^{-kt} + C_{D,eq} \qquad (2)$$

Equilibration of the SHC should take about 10^8 years. This should lead to significant differences between the D/H-ratios of the various fractions and could be a tool for evaluating some aspects of the petroleum maturation process which is influenced by temperature and time as well.

Unfortunately, cracking also produces an additional D/H shift. Loss of hetero atoms leads to a partial transformation of NSO's to AHC's and SHC's, pretending a 30 times faster exchange of the AHC's and SHC's within the oil. This effect is shown by the split columns in figure 2. Further investigations are needed to explain this phenomenon.

Biegeleisen, J., Perlman, M. L., Prosser, H. C.: Anal. Chem. 24, 1356 (1952).

Birkenfeld, H., Haase, G., Zahn, H.: "Massenspektrometrische Isotopenanalyse" - Berlin 1969.

Ehrenberger, F., Gorbach, S.: "Methoden der organischen Elementar- und Spurenanalyse" - Weinheim/Germany 1973.

Metcalfe, A., Vickers, D. E.: J. Catal. 30, 250 (1973).

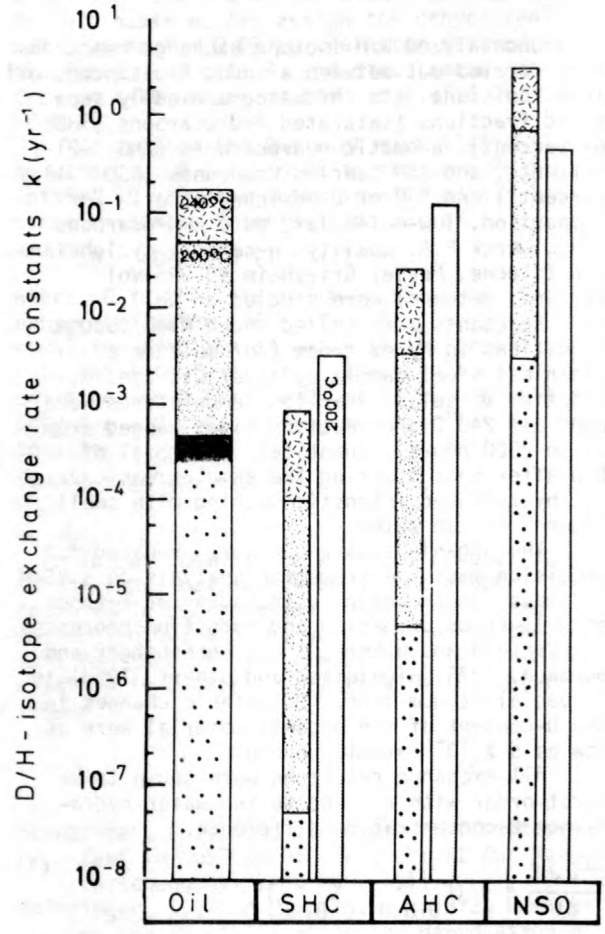

Figure 2.--Reaction rate constants (rrc) for D/H isotopic exchange between a Pleistocene oil, its fractions, and D_2O or D-enriched water. 200° and 240°C, experimental; 100°C, calculated. Paired columns: left part, comparison of rrc for separated fractions; right part, rrc for fractions in oil. Separation of oil after exchange reaction.

LEAD ISOTOPE STUDIES OF STRATIFORM ORE DEPOSITS OF NAMAQUALAND, NORTHWEST CAPE PROVINCE, SOUTH AFRICA, AND THEIR IMPLICATIONS ON THE AGE OF THE BUSHMANLAND SUPERGROUP

By Viktor Koeppel[1]
Bernard Price Institute of Geophysical Research
University of the Witwatersrand
Johannesburg 2001

[1]present address:
Laboratory for Isotope Geology and Mass Spectrometry
Swiss Federal Institute of Technology, Zurich

Nicolaysen and Burger (1965) recognized the existence of an extensive zone of metamorphic rocks in the Namaqualand yielding ages of about 1000 m.y. The question arose whether these rocks represent metamorphosed basement or whether, at least part of them, belonged to a sedimentary-volcanic sequence deposited after the consolidation of the Kaapvaal craton. This question is one of the major problems of South African geology and has received great attention since the discovery of large Cu, Pb, and Zn deposits during the late 1960s and early 1970s.

Based on structural correlations Joubert (1973) and Vajner (1974) postulated an age in excess of 2-5 b.y. for the rocks of the Namaqualand Metamorphic Complex. Paizes (1975) distinguished a so-called Bushmanland Supergroup from a basement within this complex. The supergroup may represent an equivalent of the Matsap-Waterberg Supergroup with an age of 1.8 - 2.1 b.y., or could have derived from the latter by erosion. It should be noted, however, that the distinction between a basement and a supergroup is not accepted by all investigators (Joubert, 1974). The Cu-Pb-Zn deposits at Aggenys and the Pb-Zn deposit at Gamsberg occur within the lowest formations of the Bushmanland Supergroup. The ore deposits are stratiform and occur in schists and quartzites, which are accompanied by barite and hematite or barite and magnetite layers. The ore and the host rocks are metamorphosed to the amphibolite facies. Metavolcanics do not play a conspicuous role at Aggenys and Gamsberg in contrast to the Prieska ore body at Copperton, which is located in metavolcanics of originally an andesitic to rhyolitic character (Cornell, 1975; Middleton, 1976).

The lead isotope model ages of syngenetic, stratiform to strata-bound sulfide deposits with lead as a major component normally agree reasonably well with the age of the ore and host rocks determined by other methods. Therefore, it appeared worthwhile to try to solve the problem by a regional study of the lead isotopes in ores of Namaqualand.

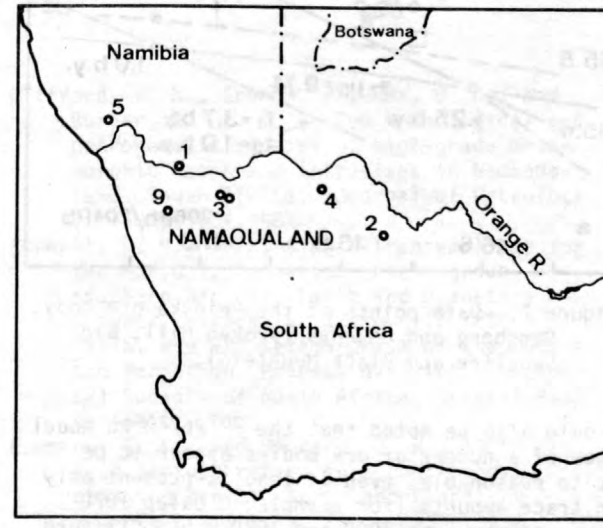

Figure 1.--Sketch map of localities: 1, Haib Copper Prospect; 2, Prieska ore body (Copperton); 3, Gamsberg, Aggenys (ore bodies--Big Syncline, Broken Hill and Black Mountain); 4, Rozynenbosch; 5, Rosh Pinah; and 9, O'Kiep.

Figure 2 shows the lead isotope data of galena and pyrite from Aggenys, Gamsberg, and Prieska. Only the lead from the Prieska ore body is homogeneous within analytical uncertainties. In both diagrams (fig. 2a and 2b) the data point lies close to the growth curves. The difference between the $^{207}Pb/^{206}Pb$ model age of 1305 m.y. and the $^{208}Pb/^{204}Pb$ model age of 1160 m.y. (Stacey and Kramers, 1975) or 1200 m.y. (Cumming and Richards, 1975) is somewhat large in comparison with the model ages of ore leads that were used to define the growth curves. The leads from the other deposits (fig. 4), except Rozynenbosch, show still larger differences. It

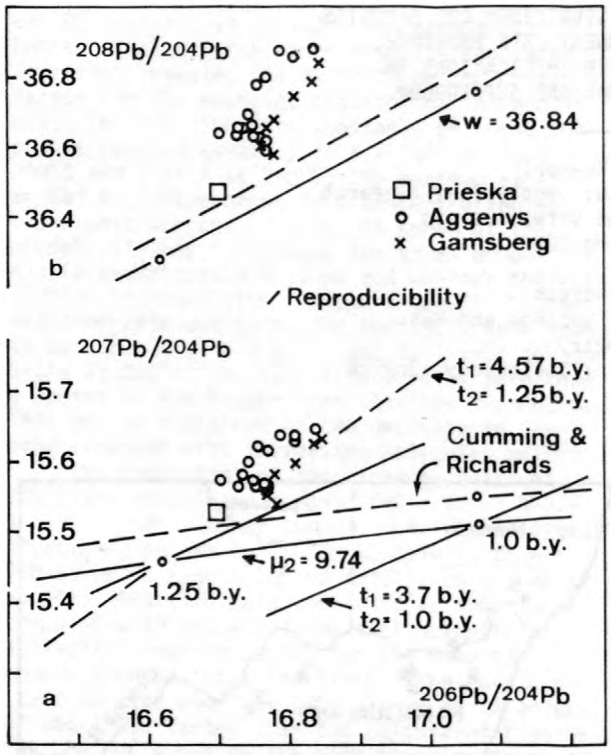

Figure 2.--Data points of the Prieska ore body, Gamsberg and Aggenys (Broken Hill, Big Syncline and Black Mountain).

should also be noted that the $^{207}Pb/^{206}Pb$ model ages of a number of ore bodies appear to be quite reasonable, even if lead is present only in trace amounts (for example, O'Okiep 1070 m.y., zircon ages 1000 and 1070 m.y., Clifford and others, 1975; Haib Copper Prospect 2135 m.y., Rb-Sr whole-rock 2000 m.y., Reid, 1975; Merensky Reef 1960 m.y., Rb-Sr whole rock 2095 m.y., Hamilton, 1977; Insizwa 50 m.y., post-Karoo). Thus, some confidence may be placed in the model age of 1305 m.y. for the Prieska ore body and its host rocks. An uncertainty of at least ± 100 m.y. should be assigned to this age. The $^{207}Pb/^{206}Pb$ model age agrees remarkably well with the age reported by Cornell (1975) on Rb-Sr whole-rock data from the metavolcanics of the foot and hanging walls of the ore body of 1312 ± 110 m.y. This age is considered to indicate the time of the early high-grade metamorphism. The initial $^{87}Sr/^{86}Sr$ of 0.7024 ± .0027 places an upper age limit of about 1500 m.y. on the deposition of the volcanics (Cornell, 1977).

The data points of Aggenys and Gamsberg scatter considerably. According to the favorite interpretation, these leads represent mixtures of at least three components, one of them being a Prieska-type lead. The major consequence of this interpretation is that it places an age on the lower portion of the Bushmanland Supergroup of 1300 ± 100 m.y. Additional evidence for the existence of comparatively young rocks within the Namaqualand Metamorphic Complex is indicated by the Rb-Sr data of Clifford and others (1975), which according to Cornell (1977) also suggests ages of the source rocks of less than 1600 m.y. Thus, evidence is gathering that a 1200 to 1600 m.y. old sedimentary-volcanic sequence does exist in South Africa.

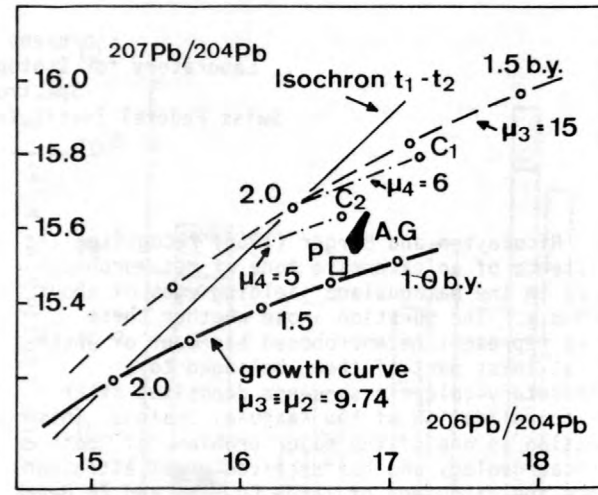

Figure 3.--Possible evolution path for the hypothetical components (C_1, C_2) which were incompletely mixed with a Prieska type lead (P) to produce the observed variations at Aggenys and Gamsberg (AG).

The mixing hypothesis explaining the lead isotopic pattern of Aggenys and Gamsberg requires, besides the Prieska-type lead, at least two further components (C_1 and C_2) with higher apparent μ and W values. The trend of the data points suggests that in spite of the high μ value the growth of the $^{206}Pb/^{204}Pb$ ratio was retarded. It appears, therefore, that these leads developed for some time in a high μ and W environment. This period of accelerated growth may have started as early as 3.7 b.y. ago and not later than 3.0 b.y. ago and reflects an upper crustal nature of the source rocks. Probably 2.5 to 2 b.y. ago the accelerated growth was drastically retarded by a major U loss of the source rocks. This change of the U/Pb ratio in the source rocks was most likely due to granulite facies conditions and thus signifies a change of the source rocks from upper crustal to lower crustal nature. Figure 3 illustrates a possible evolution path of these leads. The W value was probably not affected by the granulite facies event.

The presence of a lead component similar to the one found in the Prieska ore body associated with volcanic rocks and the presence of lead components indicative of a deep crustal origin argues for a deep seated origin of the metals in

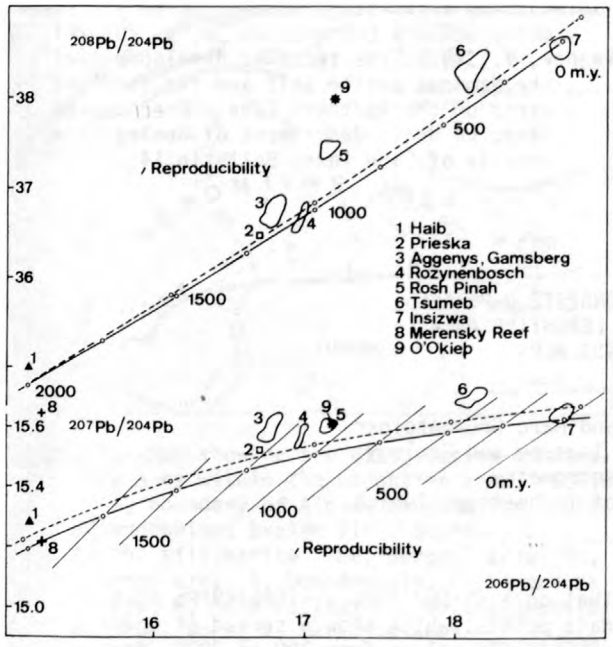

Figure 4.--Lead isotopic composition of sulfides from ore deposits in Southern Africa.

the ore-forming fluids and, thus, for a volcanogenic origin of the ore bodies.

Another possible interpretation of the lead isotope data would have to be based on the assumptions that the deposits are older and that the lead isotopic composition is therefore anomalously radiogenic. Such leads, however, are normally not observed in stratiform ore deposits with lead as a major component. Furthermore, where such leads do occur, normally in epigenetic deposits, they exhibit on a $^{207}Pb/^{204}Pb$ versus $^{206}Pb/^{204}Pb$ diagram a linear trend which often has the significance of an isochron and which allows one to draw conclusions with respect to the age of the source rocks. From the trend of the data points in figure 2a, it is obvious that the array cannot represent an isochron. One would therefore have to assume that the presently observed isotopic ratios were significantly modified during the subsequent regional metamorphism. Comparatively large amounts of lead would have to be introduced into the existing ore bodies during the regional metamorphism. Such a process seems rather unlikely to occur in nature.

Preliminary results from sulfides of magmatic deposits in basic rocks of mantle origin (Merensky Reef, Insizwa) indicate a distinctly different lead isotopic pattern. The data points in a $^{207}Pb/^{204}Pb$ - $^{206}Pb/^{204}Pb$ diagram plot close to the growth curves proposed by Stacey and Kramers (1975) or Cumming and Richards (1975) and in the $^{208}Pb/^{204}Pb$ - $^{206}Pb/^{204}Pb$ diagram close to or below the growth curves. It thus appears that the proposed lead growth curves for average crustal leads do not apply to South Africa. The lithosphere in southern Africa is characterized by higher μ, and possibly also be a higher W, value than those regions sampled for the lead growth curve.

In conclusion, one may therefore state that the Namaqualand Metamorphic Complex does contain supracrustal rocks deposited 1.2 to 1.5 b.y. ago. The lead in the ore bodies is mostly of crustal origin with a prolonged residence time in rocks of upper crustal nature which underwent a high grade metamorphism prior to supplying the lead into the ore bodies during a volcanic sedimentary cycle. A small portion of the lead may, however, be of mantle origin indicating the presence of a mantle component in the Namaqualand Metamorphic Complex, which was consolidated 1000 to 1200 m.y ago.

Clifford, T. N., Gronow, J., Rex, D. C., and Burger, A. J., 1975, Geochronological and petrogenetic studies of high-grade metamorphic rocks and intrusives in Namaqualand, South Africa: Journal of Petrology, v. 16, p. 154-188.

Cornell, D. H., 1977, A post-Transvaal age for the Marydale formation, Kheis group, southern Africa: Earth and Planetary Science Letters, v. 37, p. 117-123.

_____1975, Age and metamorphism of the Copperton formation, Prieska district: Geological Society of South Africa, Special Publication 4.

Cumming, G. L., and Richard, J. R., 1975, Ore lead isotope ratios in a continuously changing earth: Earth and Planetary Science Letters, v. 28, p. 155-171.

Hamilton, J., 1977, Isotope and trace element studies of the Great Dyke and Bushveld mafic phase and their relation to early Proterozoic magma genesis in Southern Africa: Journal of Petrology, v. 18, p. 24-52.

Jourbert, P., 1973, The development of the gneisses of part of the Namaqualand: Geological Society of South Africa Special Publication 3.

_____1974, The gneisses of Namaqualand and their deformation: Geological Society of South Africa Transactions, v. 77, p. 339-345.

Middleton, R. C., 1976, The geology of Prieska Copper Mines Ltd: Economic Geology, v. 71, p. 328-350.

Nicolaysen, L. O., and Burger, A. J., 1965, Note on an extensive zone of 1000 m.y. old metamorphic and igneous rocks in Southern Africa: Science de la Terre X, p. 497-516.

Paizes, P., 1975, The Geology of an area between Vaalkop and Aggenys, in the vicinity of Pofadder, Northwestern Cape Prov.: University of the Witwatersrand, M.Sc. thesis.

Reid, D. L., 1975, Radiometric age determinations in the Haib-Viools-drift region, lower Orange River: Precambrian Research Unit, University of Cape Town, 13th annual report, p. 49-60.

Stacey, J. S., and Kramers, J. D., 1975, Approximation of terrestrial lead isotope evolution by a two-stage model: Earth and Planetary Science Letters, v. 26, p. 207-221.

Vajner, V., 1974, The tectonic development of the Namaqua mobile belt and its foreland in parts of the Northern Cape: Precambrian Research Unit, Department of Geology, University of Cape Town, Bulletin 14.

THE SIGNIFICANCE OF MONAZITE U-Pb AGES; EXAMPLES FROM THE LEPONTINE AREA OF THE SWISS ALPS

By Viktor Koeppel and Marc Grünenfelder
Laboratory for Isotope and Geology and Mass Spectrometry
Swiss Federal Institute of Technology, Zurich

Within the Penninic realm of the central Alps, the Lepontine region is defined as the area where the thermal metamorphism of the Tertiary orogeny reached amphibolite facies conditions and where the structural discordancy between the pre-Upper Carboniferous crystalline rocks and the Mesozoic sedimentary cover disappears. Based on mineral parageneses as well as oxygen isotope fractionation between quartz-magnetite and quartz-ilmenite (Hoernes, oral commun.) temperatures of 600° to 700°C were reached in the central and eastern parts of the Lepontine area during the Alpine thermal event. The well-documented area is thus suitable for evaluating the significance of monazite U-Pb ages in metamorphic terranes.

The occurrence of monazite as an accessory rock-forming mineral is generally restricted to areas of medium to upper amphibolite facies metamorphism where it occurs predominantly in metasediments and metaigneous rocks of granodioritic to granitic composition. As already noted by Schwander and Wenk (1965), monazite is rare or absent in rocks containing minerals of the epidote group (orthite) and (or) sphene. Its distribution resembles closely that described by Overstreet (1967) from various parts of the world. Thin sections show monazite to be subhedral to euhedral with an isometric to platy habit. Thus, the distribution and the morphology indicate that the mineral was newly formed during the high-temperature metamorphism of the Alpine orogeny. The conclusion is supported by the monazite U-Pb ages--most of them are concordant at 20 to 30 m.y.

The truly concordant nature of the ages is, however, difficult to establish. The $^{207}Pb/^{206}Pb$ age is very sensitive to small changes in the lead isotopic composition and therefore fractionation effects, especially the common lead correction, play an important role. The best indication that the ages are concordant is that on a $^{207}Pb/^{204}Pb$ - $^{206}Pb/^{204}Pb$ plot the data points, which show a spread of their $^{206}Pb/^{204}Pb$ values from 200 to 2000, form a linear array with a slope corresponding to an age of 16 ± 10 m.y. (2σ). Compared with the apparent U-Pb ages, the mean $^{207}Pb/^{206}Pb$ age is somewhat low. This is most likely due to the presence of data points which require a significantly different common lead correction. It should be noted that one can find a reasonable common lead correction for every monazite sample such as to obtain a strictly concordant age pattern. The reproducibility of the $^{206}Pb/^{238}U$ age, the most reliable indicator of the true age, is ± 0.5 m.y. The few available Th-Pb ages indicate that the Th-Pb and the U-Pb systems behave identically and thereby support the contention that the ages are concordant.

The U-Pb age pattern of monazite shows regional variations (fig. 1), which are qualitatively similar to the Rb-Sr biotite age pattern (Jäger and others, 1967). The oldest ages are found in the Bergell area east of the Mera valley and along the root zone towards Domodossola. The youngest ages are found in the tectonically lowest units of the Lepontine area in the Leventina valley and the Verampio area.

Only in a few cases were discordant monazite ages found. Three samples from the central part of the Lepontine area yielded $^{206}Pb/^{238}U$ ages of 205 to 257 m.y., the coarse-grained fraction being less discordant than the finer fractions. Two size fractions of > 100 microns were obtained with almost concordant ages ($^{206}Pb/^{238}U$ = 255 m.y., $^{207}Pb/^{235}U$ = 257 m.y., and $^{207}Pb/^{206}Pb$ = 276 m.y.). Whether the monazite U-Pb system was opened during the metamorphism of the Alpine orogeny or whether the discordancy is due to the presence of two generations of monazites is as yet an unresolved question. A further example

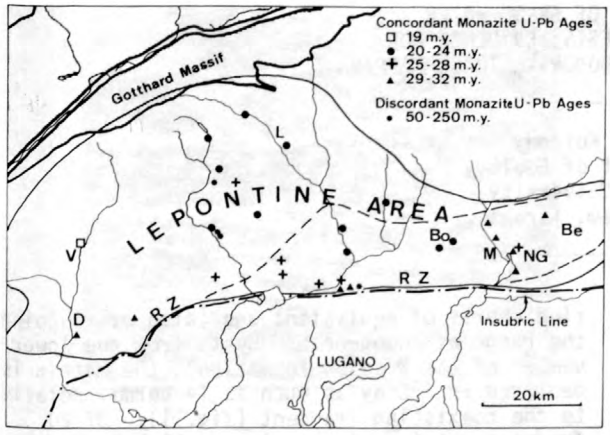

Figure 1.--Map showing the distribution of monazite ages within the Lepontine area. Solid line, boundary of Alpine amphibolite facies metamorphism; broken line, boundary of Alpine sillimanite. Be, Bergell area; Bo, Bodengo area; D, Domodossola; L, Leventina valley; M, Mera valley; NG, Novate granite; RZ, root zone; V, Verampio area.

was found in the so-called root zone. The degree of the discordancy is, however, considerably higher with apparent U-Pb ages of around 50 m.y. and a $^{207}Pb/^{206}Pb$ age of 250 m.y. These examples demonstrate that the U-Pb system of monazite is resistant to resetting at amphibolite facies conditions.

The U-Pb system of young monazites, which only witnessed the last thermal event of the Alpine orogeny, may perhaps be even more stable. Monazites from the Alpine Novate granite yielded ages of 25 m.y., whereas monazites from xenoliths within the granite yielded ages of 29 to 30.5 m.y. similar to the ages obtained from monazites of the surrounding country rocks (31 to 31.5 m.y.).

Hänny and others (1975) reported monazite ages from the Bodengo area, which agree within the analytical uncertainties with Rb-Sr whole-rock isochron ages of 22 ± 4 m.y. Such an Sr isotope equilibration probably requires the presence of a fluid phase. As the banded gneisses do not show any signs of retrograde metamorphism, the authors concluded that prograde conditions prevailed until 22 m.y. ago.

These examples demonstrate that the monazite ages record the end of the high-grade metamorphism of the Alpine orogeny and that the U-Pb systems of monazites are stable at temperatures as high as 600 to 650°C. Monazite is thus the only mineral yielding ages that directly record the time of amphibolite facies metamorphism.

The monazite ages from the Lepontine area have an important bearing on the cooling history of the central part of the Alps. Werner and others (1976) published cooling models with a time dependent uplift rate for selected areas where monazite ages and reliable Rb-Sr muscovite and biotite ages were available assuming temperatures of 600° to 650°C, 500°C, and 300° C, respectively, at the recorded times. Furthermore, initial depths of burial of 20 to 25 km and an appropriate initial temperature-depth distribution were assumed. The calculations demonstrate that it is possible to cool rocks from 500° to 300°C within 4 m.y. with a maximum uplift and erosion rate of 4 mm yr^{-1} during a short time span.

Hänny, R., Grauert, B., and Soptrajanova, G., 1975, Paleozoic migmatites affected by high grade Tertiary metamorphism in the Central Alps (Valley Bodengo, Italy): Contributions to Mineralogy and Petrology, v. 51, p. 173-196.

Jäger, E., Niggli, E., and Wenk, E., 1967, Rb-Sr Altersbestimmungen an Glimmern der Zentralalpen: Beiträge Geologioche Karte Schweiz.

Overstreet, W. C., 1967, The geological occurrence of monazites: U.S. Geological Survey Professional Paper 530.

Schwander, H., and Wenk, E., 1965, Monazit als Kern pleochroitischer Höfe in Biotiten der Tessiner Gneisse: Schweizerische Mineralogische und Petrographische Mitteilungen, v. 45, no. 2, p. 797-806.

Werner, D., Köppel, V., Hänny, R., and Rybach, L., 1976, Cooling models for the Lepontine area (Central Swiss Alps). Schweizerische Mineralogische und Petrographische Mitteilungen, v. 56, no. 3, p. 661-667.

PARTICIPATION OF FRESH WATER IN CHERT DIAGENESIS; EVIDENCE FOR OXYGEN ISOTOPES AND BORON--α TRACK MAPPING

By Y. Kolodny
Department of Geology
Hebrew University
Jerusalem, Israel

A typical component of the Brecciated Chert Member of the Cretaceous Mishash Formation in Israel are heterogeneous cherts, outstanding among them being chert breccias. In these rocks at least two silicification events can be seen--the first forming "fragments" and the second silicifying the "matrix," which shows definite indications of being mechanically incompetent after the first silicification stage. The matrix which contains calcite, clays, and apatite, is considerably less pure in chert than the fragments. Accordingly, chemical analysis shows the matrix to be strongly enriched in Ca, Al, Mg, Na, K, Sr, and Li (table 1).

Steinitz (in press) showed convincing petrographic evidence that rare but widely distributed relicts of evaporites occur in these rocks, indicating an intermittently hypersaline environment.

Oxygen isotopic analysis of separated fragments and matrix cherts show that whereas fragments have a compositional range of normal marine cherts of equivalent age (also overlapping the range of homogeneous cherts from the lower member of the Mishash Formation), the matrix is depleted in ^{18}O by as much as 14 permil relative to the coexisting fragment (fig. 1). Of 20 fragment-matrix pairs analyzed all but one showed a significant depletion in ^{18}O in the matrix (fig. 2).

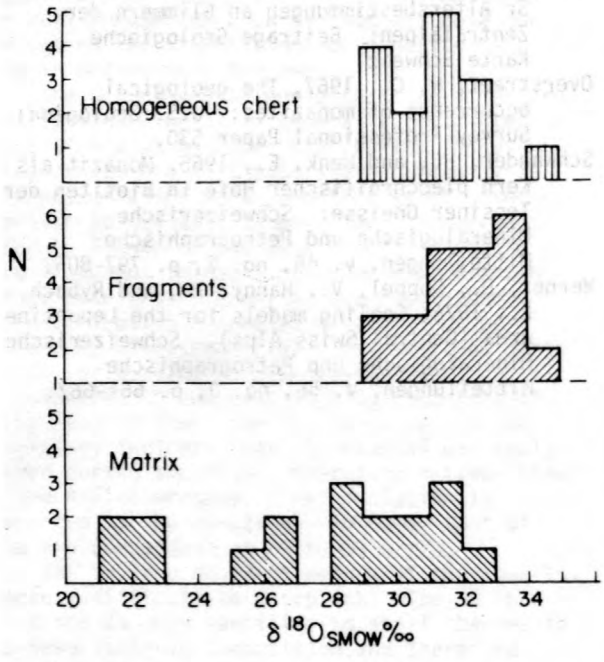

Figure 1.--Histogram of $\delta^{18}O$ in homogeneous chert, fragments, and matrix separates.

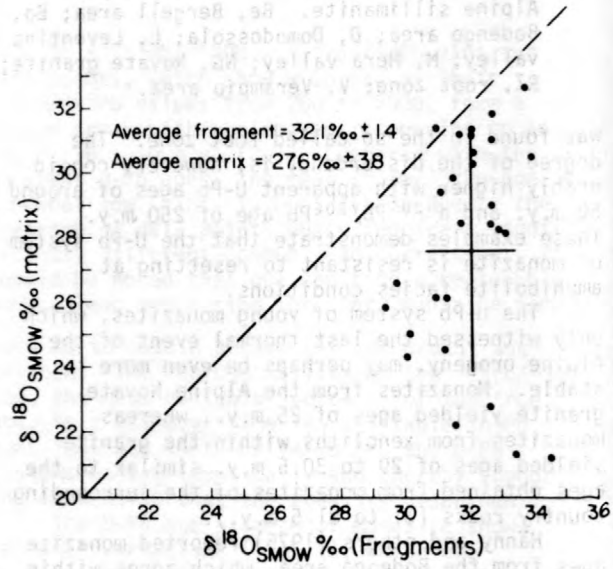

Figure 2.--$\delta^{18}O$ in corresponding fragments and matrix from cherts of the Mishash Formation.

This contrasting isotopic composition is interpreted to reflect fresh water participation in the second stage diagenetic silicification event. Thus, the environment of deposition and diagenesis of the Mishash Formation was a schizohaline environment, not unlike the one favored by Folk (1973, and in Folk and McBride, 1976) for the Caballos Novaculite.

The schizohaline nature of chert breccias in the Mishash Formation is confirmed by analysis of boron in matrix and fragments. This analysis is most convincingly performed by mapping on cellulose nitrate α tracks resulting from the ^{10}B (n, α) ^{7}Li reaction (fig. 3). Again, boron is significantly depleted in the matrix, this

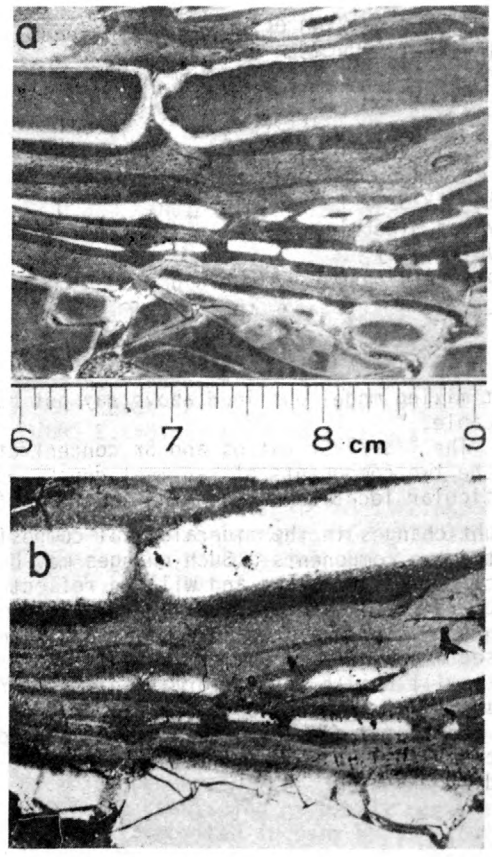

Figure 3.--Polished section of a chert breccia (a) and boron map of same (b) (sample no. MK302). Cellulose nitrate was used as a "negative" in a photographic enlarger. Areas of high-track density scatter light, and show up bright on the map. $\delta^{18}O$ values for this sample: 21 permil in matrix; 33.3 permil in fragments. Boron: 13 ppm in matrix, 70 ppm in fragments.

effect being most pronounced in the samples where the matrix is most ^{18}O depleted.

The samples which show the strongest depletion in ^{18}O and B in the matrix also show the strongest preferred orientation fabric of quartz in the matrix (Wenk and Kolodny, 1968; Kolodny, 1969).

The possibility exists that this preferred orientation is caused by a sharp change in the thixotropic properties of the siliceous sediment when the strong electrolyte sea-water solution was replaced by the diagenetic fresh-water aqueous phase.

Isotopic analyses of oxygen combined with boron alpha-track mapping are efficient indicators of schizohaline environments.

Table 1.--Comparison of chemical composition of "matrix" and "fragments" in five chert samples (results in parts per million)

Sample no. and type	Element							
	Ca	Al	Mg	Na	K	Sr	Li	B
MK 302, frag-----	1247	217	40	866	105	10.2	0.7	70
MK 302, matrix---	12220	1480	178	404	545	86.9	11.9	13
KF 94, frag-----	493	206	129	266	133	7.0	1.5	100
KF 94, matrix---	3497	729	91	181	256	24.1	14.7	5
MK 300, frag-----	1056	318	291	180	127	14.6	1.1	
MK 300, matrix---	4017	853	357	277	331	33.3	4.8	
KS 13, frag-----	6996	50	187	141	316	39.6	0.6	
KS 13, matrix---	153600	776	849	390	248	23.2	7.3	
MK 301, frag-----	1257	183	72	176	99.7	10.2	0.8	
MK 301, matrix---	7072	1035	125	390	410	59.8	11.6	

Folk, R. L., 1973, Evidence for peritidal deposition of Devonian Caballos Novaculite, Marathon basin, Texas: American Association of Petroleum Geologists Bull., v. 57, p. 702-725.

_____and McBride, E. F., 1976, The Caballos Novaculite revisited--Part 1; Origin of Novaculite Members: Journal of Sedimentary Petrology, v. 46, p. 659-669.

Kolodny, Y., 1969, Petrology of siliceous rocks in the Mishash Formation (Negev, Israel): Journal of Sedimentary Petrology, v. 39, p. 166-175.

Steinitz, G. (in press), Evaporite chert associations in Senonian bedded cherts, Israel.

Wenk, H. R., and Kolodny, Y., 1968, Preferred orientation of quartz in a chert breccia: U. S. National Academy of Science Proceedings, v. 59, p. 1061-1066.

USE OF STRONTIUM ISOTOPES TO STUDY MIXING OF SEDIMENT DERIVED FROM DIFFERENT SOURCES: THE ROSS SEA, ANTARCTICA

By Jack Kovach[1] and G. Faure[2]
[1]Department of Geology, Muskingum College
New Concord, Ohio 43762
[2]Department of Geology and Mineralogy
The Ohio State University
Columbus, Ohio 43210

The terrigenous sediment deposited in certain marine and nonmarine basins, existing now or in the geologic past, can be treated as mixtures of two components which are: 1) Weathering products of continental sialic rocks that are enriched in radiogenic ^{87}Sr depending on their ages and Rb/Sr ratios, and 2) Weathering products of volcanic rocks and volcanic ash, commonly of basaltic or andesitic composition, containing high concentrations of nonradiogenic Sr. Favorable conditions for mixing of two such components exist in areas where volcanic rocks occur on or along the margins of continents. The Red Sea is one of the few modern basins in which mixing of sediment derived from continental and volcanic sources has been studied by means of Sr isotopes (Boger and Faure, 1974, 1976). These studies are an extension of the pioneering work of Dasch (1969) and Biscaye and Dasch (1971) on the $^{87}Sr/^{86}Sr$ ratios of noncarbonate fractions of sediment in the Atlantic Ocean.

Sediment samples which are mixtures of two components fit straight lines in coordinates of $^{87}Sr/^{86}Sr$ and the reciprocal of the Sr concentration, provided the following conditions are satisfied: 1) Authigenic mineral phases are either removed prior to analysis or have negligibly low abundances; 2) The $^{87}Sr/^{86}Sr$ ratios and Sr concentrations of the two components deposited at a particular place in the basin remained constant throughout the period of deposition; 3) The composition of the sediment is not significantly altered after deposition; and 4) A correction is made for decay of ^{87}Rb since deposition.

Calcium carbonate is probably the most common authigenic phase and is easily removed by leaching with dilute acid. The presence of authigenic minerals low in Sr, such as biogenic opal and oxides of iron and manganese, does not alter the $^{87}Sr/^{86}Sr$ ratio of the sediment appreciably but does lower the Sr concentration. This problem can be corrected by removing excess silica or oxide components from appropriate chemical analyses and by recalculating the Sr concentrations. Zeolites, phosphates, authigenic clay minerals, and other Sr-bearing phases are more difficult to remove. Where such phases contribute significantly to the concentration and isotopic composition of Sr, the two-component mixing model outlined above may not be applicable.

The $^{87}Sr/^{86}Sr$ ratios and Sr concentrations of the two components of sediment deposited at a particular location may vary as a result of slight changes in the mineralogical composition of the two components. Such changes may be due to climatic variations and will be reflected by scattering of sediment data-points on the mixing diagram. More profound and persistent changes, caused by changes in the provenance of the sediment, will result in the formation of separate mixing lines. Postdepositional alteration of the sediment and in-situ decay of ^{87}Rb need to be considered only when lithified sediment is studied.

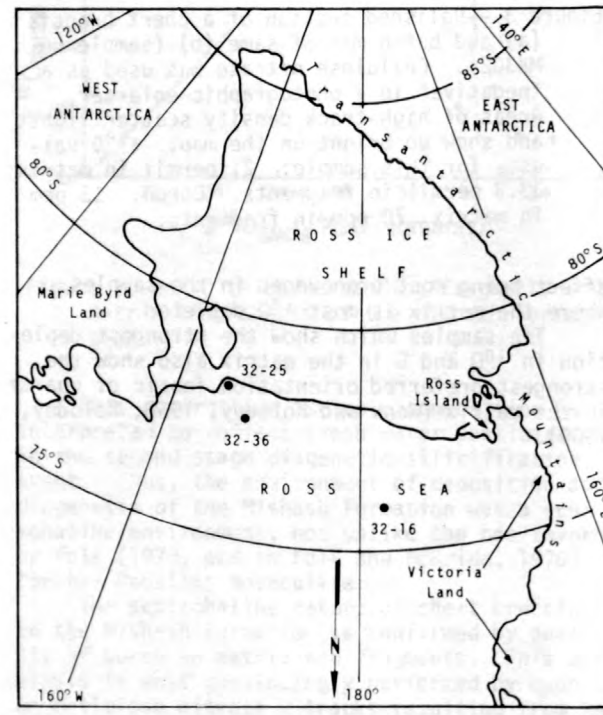

Figure 1.--Location of piston cores in the Ross Sea of Antarctica.

The sediment deposited in the Ross Sea since late Pliocene time satisifies the conditions outlined above. Shaffer and Faure (1976) demonstrated that the noncarbonate fractions of core-top sediment recovered from the Ross Sea can be regarded as mixtures of volcanogenic detritus derived from the basaltic rocks of the McMurdo Volcanic Group (Goldich and others, 1975; Kyle and Rankin, 1976) and of weathering products of the sialic rocks of East and West Antarctica. They concluded that the volcanogenic component contained 567 ± 143 ppm Sr and originated primarily from Ross Island and Victoria Land.

We report here data for the less-than 150 micrometer noncarbonate fractions of sediment from piston cores 32-16, 32-36 and 32-25 (raised by the USNS Eltanin) shown in figure 1. $^{87}Sr/^{86}Sr$ ratios were corrected for fractionation relative to $^{86}Sr/^{88}Sr = 0.1194$. The Eimer and Amend $SrCO_3$ standard was analyzed 13 times and has an average $^{87}Sr/^{86}Sr$ ratio of 0.70803 ± 0.00021 (1σ). The reproducibility of unknowns is ± 0.00035 (1σ), based on seven duplicate analyses. Strontium and rubidium concentrations were measured by X-ray fluorescence with a reproducibility of ± 1.8 ppm for each element. The concentrations of quartz, feldspar, and clay minerals were estimated from X-ray diffraction patterns based on calibrations using weighted mixtures of these minerals.

The cores penetrate from 3 to almost 5 meters of sediment consisting of pebbly mud that was presumably deposited in part by floating ice. The sediment at the tops of the three cores (upper 20 centimeters) is of Holocene age and is underlain by sediment that was deposited during the Pliocene Epoch prior to about 2.4 million years ago, based on paleomagnetic and micropaleontological data of Fillon (1975). The samples of older sediment from all three cores fit a straight line in coordinates of $^{87}Sr/^{86}Sr$ and 1/Sr (fig. 2). The goodness of fit indicates that the sediment in these cores may consist of mixtures of the same two components whose compositions remained essentially constant during the period of deposition represented by these samples. The equation of the hypothetical mixing line calculated from the data, is:

$$\frac{^{87}Sr}{^{86}Sr} = \frac{3.1783}{Sr} + 0.6944$$

This mixing equation can be used to estimate the Sr concentrations of the two components of the sediment. It is reasonable to assume that the sialic component has an $^{87}Sr/^{86}Sr$ ratio of 0.730 ± 0.005. The corresponding Sr content calculated from the mixing equation is 91 ± 13 ppm. This value is in good agreement with Sr = 82 ± 3 ppm obtained by Shaffer and Faure (1976) for the sialic component of Holocene sediment in the Ross Sea. The Sr content of the volcanic component is 318 ppm, assuming that its $^{87}Sr/^{86}Sr$ ratio is 0.704. This value is significantly less than that obtained by Shaffer and Faure (1976) and is too low to be compatible with the high Sr concentrations of alkali-olivine basalts of the McMurdo Volcanic Group. This result suggests that the volcanic component of the older sediment has a different provenance than that of the Holocene sediment studied by Shaffer and Faure (1976).

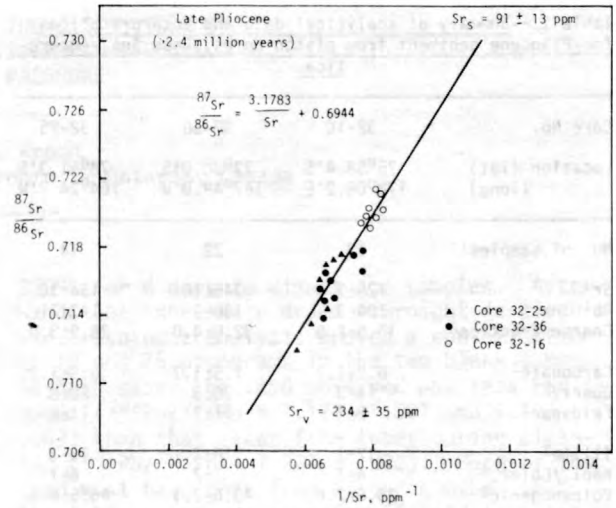

Figure 2.--Plot of $^{87}Sr/^{86}Sr$ ratios and reciprocals of the Sr concentrations of the < 150-micrometer noncarbonate fractions of sediment in the Ross Sea. The line was fitted by least-squares and is interpreted as a mixing line.

An analysis of ice-flow directions by Hughes (1975) indicates that West Antarctica is the dominant source of the Ross Ice Shelf. Therefore, the volcanic component in the piston cores may have originated from Mesozoic volcanics in West Antarctica described by LeMasurier and Wade (1977). These rocks are known from widely distributed exposures and are believed to be regionally significant. They are generally felsic in composition and have lower Sr concentrations (202 to 368 ppm) but higher $^{87}Sr/^{86}Sr$ ratios (0.7070 to 0.7102) than do the alkalic basalts of Cenozoic age in Marie Byrd Land and Victoria Land. An estimate of 0.708 ± 0.002 for the $^{87}Sr/^{86}Sr$ ratio of the volcanic component in the three piston cores yields a Sr concentration of 234 ± 35 ppm. This value if compatible with the Sr concentrations of the Mesozoic felsites from West Antarctica.

Additional supportive evidence for a West Antarctica source of the sediment is given in table 1. It includes increases in the average concentrations of Rb and Sr, and of quartz, feldspar, and clay minerals from core 32-16 to core 32-25 in the direction toward West Antarctica. The abundance of volcanogenic detritus (calculated from the Sr-data) rises from 25.6 ±

Table 1.--Summary of analytical data and interpretations for Pliocene sediment from piston cores, Ross Sea, Antarctica

Core No.	32-16	32-36	32-25
Location (lat)	75°58.4'S	77°38.0'S	78°31.3'S
(long)	178°08.2'E	167°49.0'W	164°24.7'W
No. of samples	17	22	14
Sr[1]	125±3	145±10	154±10
Rb[1]	104±3	130±3	143±11
Coarse fraction[2]	15.5±2.8	32.0±4.0	28.9±3.8
Carbonate[2]	6.8±1.2	7.5±1.7	6.9±1.2
Quartz[2]	14±3	20±3	20±3
Feldspar[2]	8±1	11±2	11±2
Illite[2]	12±1	16±2	15±3
Kaol./Chlor.[2]	4±1	7±2	6±1
Volcanogenic[2]	25.6±2.6	40.6±7.1	45.5±6.9

[1]In parts per million.

[2]In percent.

Note.--The concentrations of Rb, Sr, quartz, feldspar illite, kaolinite/chlorite, and of volcanogenic detritus refer to the < 150-micrometer, noncarbonate fraction. The carbonate concentration is for the < 150-micrometer fraction and the abundance of the coarse (> 150-micrometer) fraction is relative to the total dry sediment.

2.6 percent in core 32-16 to 45.5 ± 6.9 percent in core 32-25, which is closest to West Antarctica.

These results illustrate the use of Sr isotopic data to derive information regarding the provenance of sediment and to study systematic regional changes in lithofacies.

The cores were raised by the USNS Eltanin under the auspices of the National Science Foundation and were made available to us by D. S. Cassidy, Curator, Antarctic Research Facility, Department of Geology, Florida State University. This research was supported by NSF Grant DPP76-11871. This is Contribution No. 45, Laboratory for Isotope Geology and Geochemistry, The Ohio State University.

Biscaye, P. E. and Dasch, E. J., 1971, The rubidium, strontium, strontium-isotope system in deep-sea sediments: Argentine basin: Journal of Geophysical Research, v. 76, p. 5087-5096.

Boger, P. D. and Faure, G., 1974, Strontium-isotope stratigraphy of a Red Sea core: Geology, v. 2, p. 81-83.

Boger, P. D. and Faure, G., 1976, Systematic Variations of sialic and volcanic detritus in piston cores from the Red Sea: Geochimica et Cosmochimica Acta, v. 40, p. 731-742.

Dasch, E. J., 1969, Strontium isotopes in weathering profiles, deep sea sediments, and sedimentary rocks: Geochemica et Cosmochimica Acta, v. 33, p. 1521-1552.

Fillon, R. H., 1975, Late Cenozoic paleo-oceanography of the Ross Sea, Antarctica: Geological Society America Bulletin, v. 86, p. 839-845.

Goldich, S. S., Treves, S. B., Suhr, N. H., and Stuckless, J. S., 1975, Geochemistry of the Cenozoic volcanic rocks of Ross Island and vicinity, Antarctica: Journal of Geology, v. 83, p. 415-435.

Hughes, T., 1975, The West Anrarctic ice sheet; Instability, disintegration, and initiation of ice ages: Review of Geophysics Space Phys. v. 13, p. 502-526.

Kyle, P. R. and Rankin, P. C., 1976, Rare earth element geochemistry of Late Cenozoic lavas of the McMurdo Volcanic Group, Antarctica: Geochimica et Cosmochimica Acta, v. 40, p. 1497-1507.

LeMasurier, W. E. and Wade, F. A., 1977, Volcanic history in Marie Byrd Land: Implications with regard to southern hemisphere tectonic reconstruction: Proceedings of "Andean and Antarctic Volcanology Problems", Santiago Chile, Sept. 1974, p. 398-424.

Shaffer, N. R., and Faure, G., 1976, Regional variation of $^{87}Sr/^{86}Sr$ ratios and mineral compositions of sediment from the Ross Sea, Antarctica: Geological Society of America Bulleting, v. 87, p. 1491-1500.

VAPOUR TRANSFER FOR THE DISSOLUTION OF ZIRCONS IN A MULTI-SAMPLE CAPSULE, AT HIGH PRESSURE

By T. E. Krogh
Royal Ontario Museum, Toronto 5, Ontario, Canada

An ultra-clean method for the dissolution and loading of up to about 10 milligrams of zircon, using a vapour-transfer technique, with a blank between 7 and 25 picograms, has been developed. Although the new method is both easier and less time-consuming, the blank is well below the .1 to 5 nanograms usually achieved in the method of Krogh (1973). The new blanks include a loading blank which varies from between 3 to 8 picograms Pb. The method has no possibility of memory since disposable teflon tubes are used and although up to 12 samples can be dissolved simultaneously in one large capsule, detailed testing has shown no transfer of Pb or U through the vapour phase.

Teflon tubes about 5 mm in diameter are placed on a teflon rod, with the tube extending approximately 4 mm beyond the rounded end. The tube is taken to the gel point, closed, and then inserted into a rounded hole in a teflon block (in a fume hood). With practice, a mini test tube is produced but leak testing is necessary. A simple squeeze closure is used on caps. Plans for commercial production are underway.

Tubes are cleaned in soap and water in an ultrasonic tank, rinsed and emersed in clean aqua regia and HF, then rinsed and emersed in new acid again. In each cycle the tubes, loose in a large teflon bomb, are put into an oven at 220°C for about 2 days. For final cleaning, tubes are filled with HF, covered with their loose- or snug-fitting caps, and placed in a large teflon bomb in holes drilled in a puck sitting within the bomb. About 10 cc of HF, with 10 cc of water and a few drops of HNO_3 are placed below the puck in the bottom of the large bomb, and the bomb is held at 220°C for about one week.

In a recent test, the liquid from the final cleaning of 7 tubes was combined, spiked with about 0.5 ng ^{208}Pb, and dried in a clean capsule. Lead extracted was 0.057 ng per tube with a $^{206}Pb/^{207}Pb$ ratio of 1.221 ± .003. The cleaned tubes were rinsed with clean acetone, dried in clean air, and weighed amounts of ^{208}Pb (0.3 to 0.5 ng) were placed in two tubes while 1 to 7 milligrams of zircon were placed in three others. One zircon sample had a $^{206}Pb/^{207}Pb$ ratio greater than 4.0 (HF 0.2 gm) was added to each tube, caps were applied (one snug and one loose on blank tubes) and the tubes were placed in the puck over 10 cc HF (with a few drops of HNO_3), inside a large teflon vessel. The bomb was placed in a monel jacket and was held at 220°C for 6 days to digest the samples. Afterwards the tubes were dried overnight in clean air. Isotopic analysis proved a contamination of 19 and 25 picograms in the two blank tubes. In both cases the lead observed was less radiogenic ($^{206}Pb/^{207}Pb$ = 1.127 ± .001 and 1.193 ± .003) than that taken from tubes during cleaning ($^{206}Pb/^{207}Pb$ = 1.221 ± .003). Much of the lead must have come from a source other than the tube and vapour transfer of lead from the zircon sitting only one cm from the blank tubes was non-existent. A similar test from another batch of tubes gave blanks of 7 and 13 picograms, (including loading blanks). An early test using reagent grade HF for dissolution and reagent grade 3.1N for conversion to the chloride (see below) gave blanks ranging from 0.4 to 0.5 ng for 4 tubes. In this case, only water was added to the tubes and this was acidified by the vapour of the mineral acid. The high blank indicates either that the tubes were not clean, or a small amount of dirty acid became airborne during boiling in the initial heating. Preheating at 100°C could probably reduce such an effect. For a further test, 10 mg of zircon was placed in the reservoir below the tube and only common lead was found in the tube, after a 6-day dissolution time. A similar test over HCl containing dissolved zircon again showed no radiogenic transfer in the chloride. Data for one sample dissolved both in a tube and in a separate bomb agree within analytical uncertainties. Further comparative tests are under way.

A zircon can be dissolved in the vapour of 48 percent HF in a tube with nothing added, provided a pin hole or other access allows vapour in. As the zircon dissolves, water is taken from the vapour to make a solution. If the HF contains about 10 percent NaCl, or other salt, the vapour attack proceeds but in a dry state, due to the reduced activity of water. A zircon dissolved as a fluoride can be converted to a chloride by replacing the HF below by about 30 cc 3.1N HCl. Equilibration takes place through the vapour phase at 220°C and mass balance puts most of the fluoride in the reservoir below. This method eliminates drying samples down prior to column chemistry. If a dry sample is required, samples can be placed over a strong solution (say 10 percent NaCl in HF) and the water goes to dilute the salt at 220°C in the bomb. Some tests suggest that too much water may be taken in by the dissolving zircon, in which case about one gram of salt

per 30 cc of HF is effective and a liquid volume proportional to sample size can be achieved. For the tests noted above with 7 to 25 picogram blanks, snug lids were used, and the sample tubes did not overfill during dissolution.

Similar principles could be applied for the ultra-clean dissolution of other silicates and refractory minerals. Zircon samples can be dissolved over HF in the small regular bomb if all possibility of memory must be eliminated.

Krogh, T. E., 1973, A low-contamination method for hydrothermal decomposition of zircon and extraction of U and Pb for isotopic age determinations: Geochimica Cosmochimica Acta, v. 37, p. 485-494.

EXPERIMENTAL OXYGEN ISOTOPE FRACTIONATION BETWEEN KAOLINITE AND WATER

By Jean B. Kulla and T. F. Anderson
Department of Geology, University of Illinois-Urbana

The clay mineral kaolinite is widely found intimately associated in numerous geologic environments with quartz, feldspar, and other clay minerals. Information on the chemical and thermodynamic parameters governing the formation of this mineral aids in the understanding of such geochemical problems as: (1) authigenic mineral formation in diagenetic systems, (2) mineral transformations in diagenetic and hydrothermal systems, and (3) temperature gradients and their influence on fluid convective systems. Adequate evaluation of the above geochemical situations involves detailed knowledge of their respective thermal regime, which can be most adequately determined from stable isotope fractionation between co-existing minerals. In this paper we report the oxygen isotope fractionation factors determined experimentally for kaolinite and water at temperatures up to 320°C.

Experimentally, the clay was grown from an amorphous glass with a stoichiometric kaolinite composition in contact with water of known isotopic composition. Approximately 50 mg of glass and 150 mg of water were sealed in gold tubes and run in cold seal bombs at 2 kb pressure from 10 to 90 days. Under these conditions, the rate of kaolinite crystallization from glasses is relatively slow necessitating long run times. This synthesis technique was used rather than "true" exchange between kaolinite and water which is prohibitively slow (O'Neil and Kharaka, 1976). At each temperature two runs were conducted for the same duration in waters either markedly enriched or depleted in O^{18} relative to the glass in order to bracket the equilibrium fractionation. All samples were X-rayed, washed in HCl and NaOH to remove any amorphous material and analyzed on a ratio mass spectrometer after oxygen extraction with BrF_5. Kaolinite was the only crystalline phase observed.

The experimental results are given in table 1. The difference in isotopic composition between the glass and the initial water is reported as $10^3 \ln\alpha_i$, $\alpha_i = (O^{18}/O^{16}_{glass}) / (O^{18}/O^{16}_{water})$. Isotopic fractionation between kaolinite and water for a specific run is reported as $10^3 \ln\alpha_f$ determined from a mass balance calculation utilizing the measured isotopic ratio of the clay. The results indicate that isotopic equilibrium was closely approached (given the initial "distance" from equilibrium) but not attained in these experiments. Equilibrium fractionation $10^3 \ln\alpha_f$ and the fractional approach to equilibrium -1/B, were estimated using the partial exchange extrapolation technique of Northrop and Clayton (1966). Although the use of this technique is questionable in experimental systems that are not strictly "true" exchange reactions, the experimental evidence from the synthesis of muscovite (O'Neil and Taylor, 1969) and of feldspar (O'Neil and Taylor, 1967) indicates its reliable applicability.

Table 1.--Experimental results

Run[1]	Time (days)	Temp. (°C)	$10^3 \ln\alpha_i$	$10^3 \ln\alpha_f$	$10^3 \ln\alpha_E$	-100/B
K_1-D_1-8	90	172	27.92	7.64	6.46	94
K_1-H_1-2	90	172	-68.69	2.32		
K_1-D_1-14	81	222	27.92	5.87	4.57	94
K_1-H_1-5	81	222	-68.69	0.49		
K_2-D_1-12	30	271	20.01	4.10	3.20	95
K_1-H_1-7	30	271	-68.69	-0.66		
K_1-D_1-11	10	319	27.92	2.64	1.89	97
K_1-H_1-6	10	319	-68.69	-0.14		

[1]K is glass; D and H are water.

The fractionation factors are plotted as $10^3 \ln\alpha$ versus T^{-2} in figure 1. All the equilibrium data points fit a straight line

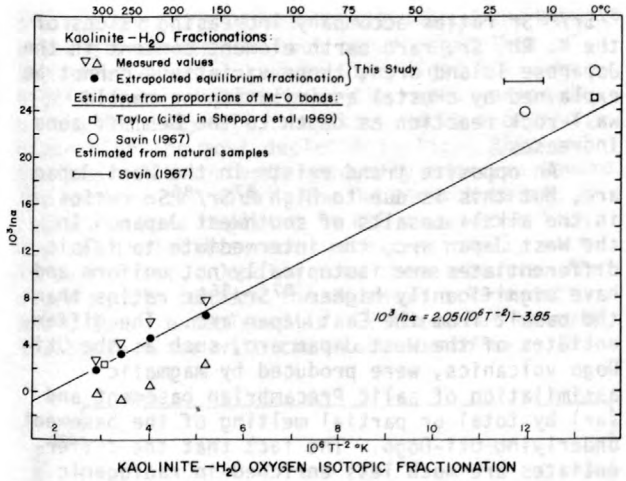

Figure 1.--Kaolinite-water isotopic fractionation as a function of temperature. Triangles represent experimental fractionations and point toward the direction of approach to equilibrium.

relationship, as predicted from theoretical arguments and from other experimental results.

$$10^3 \ln\alpha = 2.05 (10^6 T^{-2}) - 3.85$$

The experimental results essentially coincide with the kaolinite-water fractionation factor at 300°C estimated from "bond-type" calculation by H. P. Taylor, Jr. (in Sheppard and others, 1969). Extrapolating the line to low temperatures yields equilibrium fractionations in good agreement with Taylor's estimate and in fair agreement with independent estimates by Savin (1967). However, fractionations estimated by the isotopic composition of kaolinite from weathering zones by Savin and Epstein (1970) are about 5 permil more positive than predicted from our results. Uncertainty in the isotopic composition of waters equilibrated with these naturally occurring kaolinite or contamination of the samples by impurities may account for some of this discrepancy.

Northrop, D. A., and Clayton, R. N., 1966, Oxygen-isotope fractionations in systems containing dolomite: Journal of Geology, v. 74, p. 174-196.

O'Neil, James R., and Kharaka, Yousif K., 1976, Hydrogen and oxygen isotope exchange reactions between clay minerals and water: Geochimica Cosmochimica Acta, v. 40, no. 2, p. 241-246.

O'Neil, James R., and Taylor, H. P., Jr., 1967, The oxygen isotope and cation exchange chemistry of feldspars: American Mineralogist, v. 52, p. 1414-1437.

_____1969, Oxygen isotope equilibrium between muscovite and water: Journal of Geophysical Research, v. 74, p. 6012-6022.

Savin, S. M., 1967, Oxygen and hydrogen isotope ratios in sedimentary rocks and minerals: California Institute of Technology, Ph.D. Thesis.

Savin, S. M., and Epstein, S., 1970, The oxygen and hydrogen isotope geochemistry of clay minerals: Geochimica Cosmochimica Acta, v. 34, p. 25-42.

Sheppard, S. M. F., Nielsen, R. L., and Taylor, H. P., Jr., 1969, Oxygen and hydrogen isotope ratios of clay minerals from porphyry copper deposits: Economic Geology, v. 64, p. 755-777.

STRONTIUM ISOTOPES AND RARE EARTH ELEMENTS OF THE VOLCANIC ROCKS FROM THE JAPANESE ISLAND ARCS

By Hajime Kurasawa
Geochemical Research Section
Geological Survey of Japan
Kawasaki, Japan

Three petrographic provinces have been recognized in the Japanese islands, provinces which are arranged parallel to the island arcs and contain, from the ocean side to the continental side, low-alkali tholeiite, high-alkali tholeiite (high-alumina basalt), and alkali basalt. Figure 1 shows the relationship between the $^{87}Sr/^{86}Sr$ ratios and the volcanoes of three island arcs in the Japanese Islands. In the Kurile arc in Hokkaido, northern Japan, the rocks from Atosanupuri volcano on the ocean side have higher $^{87}Sr/^{86}Sr$ ratios than those of the alkali basalt from Rishiri volcano on the continental side. This relationship is again observed in the East Japan arc between the Yotei, Niseko, and Towada volcanoes on the ocean side

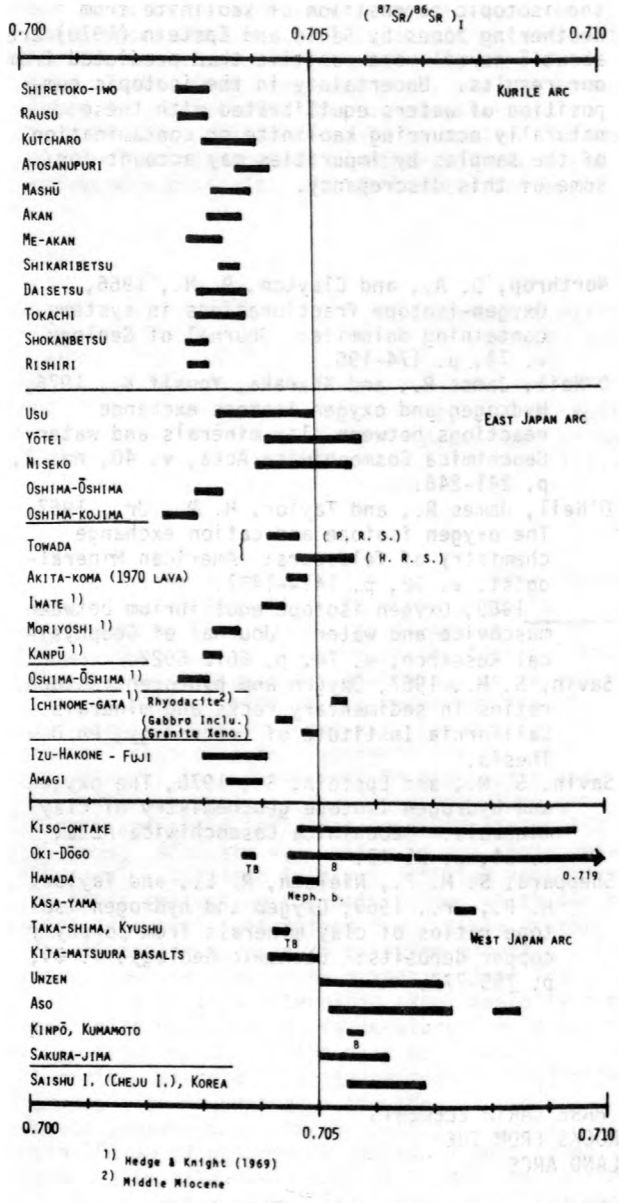

Figure 1.--$^{87}Sr/^{86}Sr$ ratios of volcanic rocks from the Japanese Island arcs.

and the Oshima-Oshima volcano on the continental side. Other geochemical contrasts can also be drawn between the low-alkali tholeiite on the ocean side, with its low Sr content of 150 - 250 ppm and K/Rb ratio higher than 1000, and the basalts of the continental side in the East Japan arc.

In the East Japan arc, the relationship of Sr content to the distance from the trench is extremely good. There is a positive correlation between the Rb/Sr and $^{87}Sr/^{86}Sr$ ratios in the East Japan arc suite, and a decrease in the $^{87}Sr/^{86}Sr$ ratios with increasing distance from the trench in the arc. Because the decreasing $^{87}Sr/^{86}Sr$ ratios accompany increasing values of the K, Rb, Sr, rare earth element content in the Japanese Island arcs, these variations cannot be explained by crustal assimilation or mantle wall-rock reaction as depth to the Benioff zone increases.

An opposite trend exists in the West Japan arc, but this is due to high $^{87}Sr/^{86}Sr$ ratios in the alkali basalts of southwest Japan. In the West Japan arc, the intermediate to felsic differentiates are isotopically not uniform and have significantly higher $^{87}Sr/^{86}Sr$ ratios than the basalt from the East Japan arc. The differentiates of the West Japan arc, such as the Oki-Dogo volcanics, were produced by magmatic assimilation of salic Precambrian basement and (or) by total or partial melting of the basement underlying Oki-Dogo. The fact that the differentiates are much less enriched in radiogenic lead isotopes supports this conclusion (Kurasawa, 1968). The Oki-Dogo suite is not appropriate for the rock of the continental side of a typical island arc traverse. It is questionable to consider the isotopic data of the Oki-Dogo suite as evidence for an assimilation model of subducting ocean floor under an island arc.

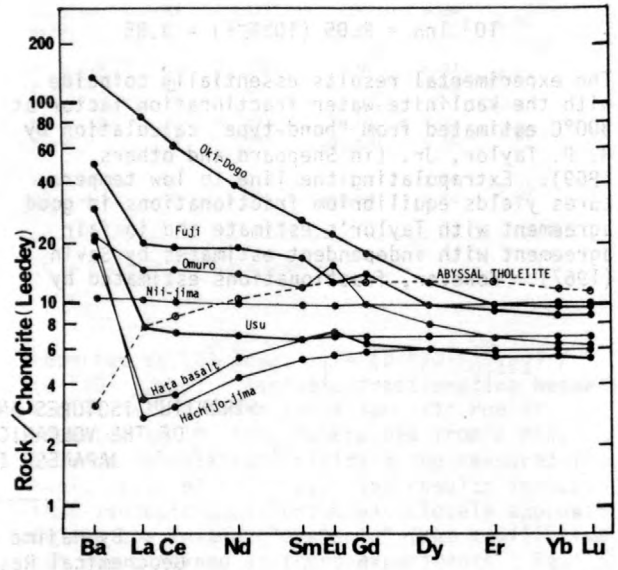

Figure 2.--Chondrite-normalized REE patterns for basaltic rocks from the Japanese Island arcs.

The chondrite-normalized REE pattern of the basaltic rocks in the Japanese Island arcs are shown in figure 2. Rare earth concentrations in the low-alkali tholeiite bear a strong resemblance to those in the abyssal tholeiite. However, some of the tholeiite show an even greater depletion in the light rare earth elements than is characteristic of the abyssal tholeiite. The heavy rare earth element contents in the basal-

tic rocks of the Japanese Island arcs are surprisingly similar to each other regardless of the rock series. However, the light REE vary significantly depending on the rocks series or on the locality of the rocks. Rocks from the ocean side are most depleted in light REE, and the light REE contents gradually increase toward the continental side. The Japanese basaltic rocks are more depleted in REE as a whole than abyssal tholeiites, and are exceptionally rich in Ba content. Judging from these results, the upper mantle beneath the Japanese Island arcs would be more depleted in REE than that beneath the ocean floor with the exception of Ba. It can be concluded that REE content in the mantle beneath the Japanese Island arcs may be homogeneous horizontally but heterogeneous vertically.

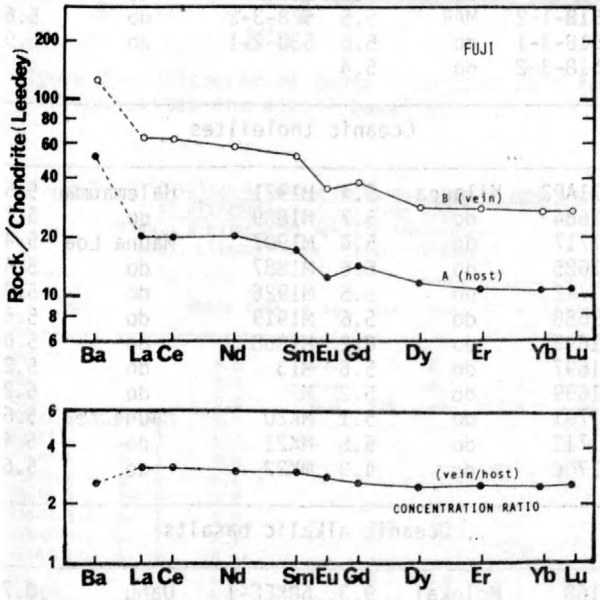

Figure 3.--Chondrite-normalized patterns and concentration ratio of REE for the host lava and segregation vein of the Mishima flow, Fuji volcano.

In the case of the in situ differentiation of a lava flow from Fuji volcano, the chondrite-normalized REE pattern for the segregation vein lies above and nearly parallel to that for the host basalt lava (fig. 3). However, concentration ratios show that the light REE have been more enriched than the heavy REE. No distinct difference in the size of the Eu anomaly can be detected.

REE contents in andesitic rocks from some of the volcanoes are higher than those in their associated basaltic rocks. REE patterns for the andesitic rocks from the volcanoes lie above and nearly parallel to those for the associated basaltic rocks. Consequently, both tholeiitic andesite and calc-alkali andesite can be explained by simple fractional crystallization from their associated basalt. Some of the calc-alkaline andesitic and dacitic rocks from the West Japan arc show intersections in the middle part of their REE patterns like a seesaw. These characteristics are extremely different from those of the REE patterns that arise from simple fractional crystallization of basalt.

Kurasawa, H., 1968, Isotopic composition of lead and concentrations of uranium, thorium and lead in volcanic rocks from Dogo of the Oki Islands, Japan: Geochemical Journal, v. 2, p. 11-28.

Hedge, C. E., and Knight, R. J., 1969, Lead and strontium isotopes in volcanic rocks from northern Honshu, Japan: Geochemical Journal, v. 3, p. 15-24.

OXYGEN ISOTOPE RELATIONS AMONG OCEANIC THOLEIITES, ALKALI BASALTS, AND ULTRAMAFIC NODULES

By T. Kurtis Kyser[1] and James R. O'Neil[2]
[1]University of California
Berkeley, California 94720
[2]U.S. Geological Survey
Menlo Park, California 94025

Many workers have demonstrated that there are differences in Sr, Nd, and Pb isotopic compositions between tholeiites and most alkali basalts. Any model for the generation of basalts must take into account not only these isotopic and other chemical differences, but

must also explain variations in the isotopic composition of oxygen, the most abundant element in the rocks.

Previous oxygen isotope studies have concentrated on ocean ridge basalts. Pineau and others (1976) examined 27 tholeiitic deep-sea basalts and three alkali basalts from seamounts. Although many of the tholeiites and all three basalts had high H_2O contents suggesting alteration, they were able to conclude that at least some fresh tholeiites and alkali basalts have the same oxygen isotope composition. On the basis of a correlation between $\delta^{18}O$ and percent total water of the basalts they examined, Muehlenbachs and Clayton (1972) also concluded that there was no difference in oxygen isotope composition between alkalic and tholeiitic basalts. In both of these studies, enrichment of ^{18}O in alkali basalts relative to tholeiites was attributed to the presence of alteration minerals. Moore (1970) has suggested that alkali basalts contain more original water than tholeiites so that conclusions based on a comparison between $\delta^{18}O$ and H_2O contents may not be firmly established.

Anderson and others (1971) measured the oxygen isotopic composition of several oceanic island basalts and found that $\delta^{18}O$ = 5.3 to 5.8 for tholeiites from Hawaii, whereas $\delta^{18}O$ = 5.8 to 7.3 for alkali basalts from Hawaii, Tristan da Cunha, and Tahiti. Taylor (1968) reported $\delta^{18}O$ values of 5.7 to 6.0 for alkali basalts from Hawaii, the Canary Islands, and Easter Island. Garlick (1966) measured $\delta^{18}O$ values of 6.0 to 6.3 for sodic trachytes from Gough and Flores. It seemed reasonable to us that Hawaii and the mid-ocean ridges are ideal areas to sample for a detailed study of the ^{18}O relations among tholeiites, alkali basalts, and ultramafic nodules because there one can obtain young samples that have a minimum amount of contamination and alteration minerals.

$\delta^{18}O$ values for whole-rock samples are given in table 1. Except for sample 1695 and the EPR tholeiites, most tholeiites have $\delta^{18}O < 5.8$, whereas the alkali basalts are more ^{18}O-rich. Figure 1 is a histogram of our analyses of tholeiites and our and others' analyses of alkali basalts. The oxygen isotope distinction between fresh alkali basalts and tholeiites is clear.

Chemical differentiation can affect the oxygen isotope compositions of basalts by preferential removal or concentration of relatively ^{18}O-rich phases. This may account in part for the higher ^{18}O content of the EPR basalts, which, according to Moore (1977), are more differentiated than their MAR counterparts. Carmichael and others (1970) have shown that tholeiites have a higher a_{SiO_2} than alkali basalts and, accordingly, should thus be richer in ^{18}O. However, this is in contradiction to the measurements reported here and we conclude that if isotopic equilibrium is maintained during melting, alkali basalts and tholeiites are derived from different sources.

Table 1.--Oxygen isotopic compositions of oceanic tholeiites and alkalic basalts

[All values ±.1 permil. MAR, EPR, Kilauea, and Mauna Kea samples supplied by J. G. Moore. Molokai samples supplied by M. H. Beeson.]

Sample	Location	$\delta^{18}O$	Sample	Location	$\delta^{18}O$
MOR tholeiites					
9A2	EPR	6.0	519-2-2	MAR	5.5
11A2	do	6.0	519-4-2a	do	5.5
6B2	do	5.8	519-2-3	do	5.5
10A2	do	6.2	528-1	do	5.5
518-1-2	MAR	5.5	528-3-2	do	5.6
518-3-1	do	5.6	530-2-1	do	5.9
518-3-2	do	5.4			
Oceanic tholeiites					
71AP3	Kilauea	5.4	H1971	Halemaumau	5.5
1684	do	5.7	H1889	do	5.7
1717	do	5.4	M1907	Mauna Loa	5.4
1685	do	5.6	M1887	do	5.4
1742	do	5.5	M1926	do	5.3
1688	do	5.6	M1919	do	5.5
1695	do	6.2	M1868	do	5.6
1697	do	5.6	M13	do	5.2
1699	do	5.2	M7	do	5.2
1701	do	5.1	MK20	Mauna Kea	5.6
1712	do	5.8	MK21	do	5.4
1706	do	4.9	MK22	do	5.6
Oceanic alkalic basalts					
16B	Molokai	9.3	68KEE-1	Oahu	10.7
33	do	7.4	77-EM1	Maui	5.9
3	do	7.7	H-1	Hualalai	6.3
28	do	7.5	H-7	do	5.9
5A	do	6.7	H-7A	do	7.4
9A	do	6.1	Hal-1	Haleakala	5.8
2	do	5.6			
27	do	5.9			

$\delta^{18}O$ values for whole rocks and mineral separates of ultramafic nodules from Hawaii are given in table 2, and a histogram of the whole-rock values is presented in figure 2. Comparison of these data indicates a possible genetic relationship between some of the nodules and alkali basalts but not to the tholeiites. This relationship is complicated by several oxygen isotope anomalies in the mineral data. The most common anomaly is the enrichment of ^{18}O in olivine relative to coexisting minerals in the nodule. The anomalies are not removed by etching the olivine. The origin of these effects

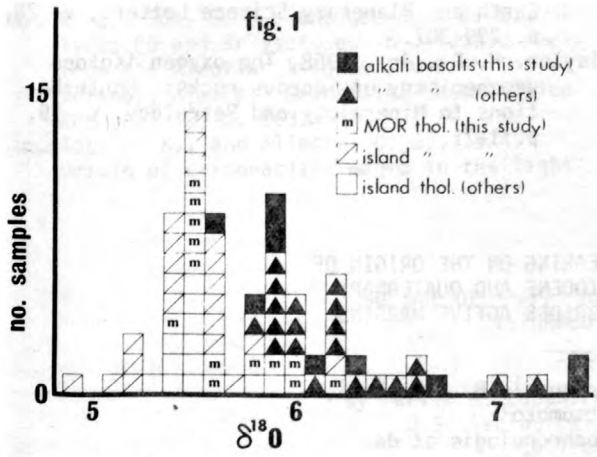

Figure 1.--Histogram of oxygen isotopic data for tholeiites and alkali basalts.

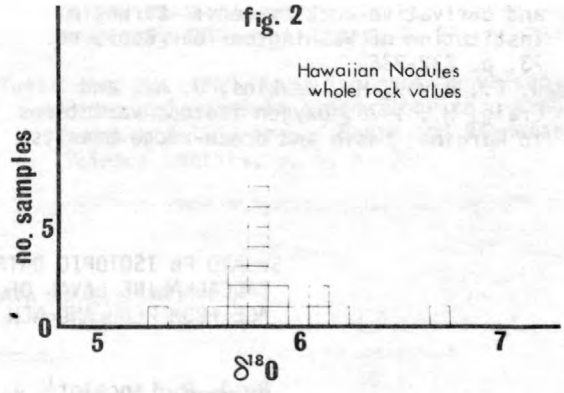

Figure 2.--Histogram of oxygen isotopic data for whole rocks and minerals of ultramafic nodules from Hawaii.

Table 2.--$\delta^{18}O$ values of whole rocks and mineral separates of ultramafic nodules from Hawaii
[Plag., plagioclase; opx., orthopyroxene; cpx., clinopyroxene; oliv., olivine.]

Sample	Whole rock	Plag.	Opx.	Cpx.	Oliv.	Spinel
H9	6.0	---	6.0	6.1	---	---
H5	5.9	---	---	6.1	5.7	---
H10	5.8	6.0	5.6	---	7.8	---
70KAP-1 (Dunite)	6.7	---	---	---	---	---
70KAP-2 (do)	5.3	---	---	---	---	---
75KAP-5 (do)	5.8	---	---	---	---	---
75KAP-6 (do)	6.2	---	---	---	---	---
75KAP-7 (do)	5.8	---	---	---	---	---
75KAP-8 (do)	5.8	---	---	---	---	---
75KAP-9 (do)	6.1	---	---	---	---	---
75KAP-10(do)	5.6	---	---	---	---	---
SLC 11	5.8	---	5.7	6.0	---	---
SLC 26	5.7	---	5.8	5.8	5.1	---
SLC 12	6.1	---	5.8	6.0	5.8	6.8
SLC 13	5.8	---	5.8	6.5	6.2	5.1
SLC 14	5.8	---	5.9	5.8	5.5	4.5
SLC 18	5.9	---	6.0	5.9	6.2	5.5
SLC 20	5.7	---	6.0	5.6	5.5	5.7

is not well-understood. Muehlenbachs and Kushiro (1974) suggested that oxygen isotope fractionation factors for melt-solid systems might undergo a "crossover" phenomenon at high temperatures such that liquids would be depleted in ^{18}O relative to residual solids. They used this suggestion to explain the bimodal oxygen isotope compositions of eclogites from kimberlites, the ^{18}O-depleted liquids having crystallized to ^{18}O-depleted eclogites. If tholeiites are generated at a higher temperature from a similar source as alkali basalts, the oxygen isotope distributions observed may be explained. There is no theoretical reason, however, that such isotopic reversals should occur in basalts within the temperature range of their history. Experiments are now in progress in our laboratory to help elucidate the oxygen isotope properties of minerals and liquids at high temperatures.

The various models for the generation of tholeiitic and alkalic basalts must now be constrained by the oxygen-isotope evidence. The enrichment of ^{18}O in alkali basalts relative to tholeiites suggests that isotopically distinct sources are involved. The isotopic anomalies found in ultramafic nodules also support the contention that processes in the upper mantle are complicated by "metamorphic" events that affect some minerals more than others. Their high $\delta^{18}O$-values indicate a genetic relation to their hosts rather than to tholeiites.

Anderson, T., Jr., Clayton, R. N., and Mayeda, T. K., 1971, Oxygen isotope thermometry of mafic igneous rocks: The Journal of Geology, v. 79, no. 6, p. 715-729.

Carmichael, I. S. E., Nicholls, J., and Smith, A. L., 1970, Silica activity in igneous rocks: American Mineralogist, v. 55, p. 246-263.

Garlick, G. D., 1966, Oxygen isotope fractionation in igneous rocks: Earth and Planetary Science Letters, v. 1, p. 361-368.

Moore, J. G., 1970, Water content of basalt erupted on the ocean floor: Contributions to Mineralogy and Petrology, v. 28, p. 272-299.

_____ 1977, Petrology of basalt from the East Pacific Rise near 21° north latitude: U.S. Geological Survey Journal of Research, v. 5, no. 6, p. 753-759.

Muehlenbachs, K., and Clayton, R. N., 1972, Oxygen isotope studies of fresh and weathered submarine basalts: Canadian Journal of Earth Sciences, v. 9, p. 172-184.

Muehlenbachs, K., and Kushiro, I., 1974, Oxygen isotope exchange and equilibrium of silicates with CO_2 or O_2, in Geophysical Laboratory; Igneous Petrology, experimental and field studies; Volatiles in ultrabasic

and derivative rock systems: Carnegie Institution of Washington Year Book, no. 73, p. 232-236.
Pineau, F., Javoy, M., Hawkins, J. W., and Craig, H., 1976, Oxygen isotope variations in marginal basin and ocean-ridge basalts: Earth and Planetary Science Letters, v. 28, p. 299-307.
Taylor, H. P., Jr., 1968, The oxygen isotope geochemistry of igneous rocks: Contributions to Mineralogy and Petrology, v. 19, p. 1-71.

Sr AND Pb ISOTOPIC DATA BEARING ON THE ORIGIN OF CALCALKALINE LAVAS OF PLIOCENE AND QUATERNARY AGE FROM PERU AND NEW HEBRIDES ACTIVE MARGINS

By J. R. Lancelot[1], L. Briqueu[1], B. Westphal[1], and M. Tatsumoto[2]
[1]Laboratoire de Géochronologie et de Geochimie Isotopique
C.G.G.M., U.S.T.L.
Place E. Bataillon
34060 Montpellier Cedex
France
[2]U.S. Geological Survey
Denver, Colorado, U.S.A.

Sr and Pb isotope analyses were performed on Pliocene and Quaternary calcalkaline lavas of two active margins where an oceanic slab is being subducted under another oceanic slab in New Hebrides, and under the South American place, where the Moho discontinuity is 50 - 60 km in depth in Southern Peru. In New Hebrides, Pb isotopic compositions of calcalkaline lavas (mostly andesites) fall in the M.O.R.B. field defined by Pacific and Atlantic samples. Spilitized M.O.R.B. (samples D1335 and D5334, dredged samples of the Fiji oceanic crust) fall in the same field. Sr isotope analyses ($^{87}Sr/^{86}Sr = 0.70238 \pm 0.00020$) are homogeneous for these calcalkaline lavas and in agreement with previous results obtained for same rocks of subduction zones where a continental crust is not involved. An anomalous $^{87}Sr/^{86}Sr$ value of 0.70453 has been measured for M.O.R.B. sample D1334, but leaching experiments clearly indicate that Sr exchange occurred between this rock and sea water. Pb and Sr ratios and trace-element data suggest that calcalkaline rocks of this island arc derived by partial melting of altered M.O.R.B. from the subducted oceanic slab. Furthermore, these data give support to the incorporation of sediments (1 - 2 percent) during this episode of partial melting (Tatsumoto, 1969; Kay and others, 1978), but the Pb isotopic data for this young island arc system appear to limit possible source materials of these sediments to the arc itself.

In Southern Peru, the Barrosso and Arequipa volcanic fields have been studied (andesite, dacite, rhyolite). Measured $^{87}Sr/^{86}Sr$ of 0.70511 to 0.70735 are in agreement with previous results of James and others (1976), but a plot of $^{87}Sr/^{86}Sr$ versus $1/(Sr^{86})$ as proposed for Pb by Lancelot and Allegre (1974) indicates that enrichment of radiogenic ^{87}Sr occurred during the fractional crystallization of the calcalkaline liquid. Similar trends have been observed by James and others (1976) in $^{87}Sr/^{86}Sr$ versus Rb/Sr diagrams, who interpreted them as apparent isochrons resulting from inhomogeneities in the source region. For us, an interpretation involving contamination by radiogenic Sr issued from the continental crust is more satisfactory, but the proposed binary mixing model does not involve a simple mass-mixing of the two components. This model is confirmed by Sm/Nd studies (DePaola and Wasserburg, 1977; Ben Othman and others, in press) and anomalous Pb isotopic compositions, both tracors clearly indicate the influence of an old continental material on the calcalkaline magma.

Ben Othman, D., Allegre, C. J., Polve, M., and Richard, P., (in press), Nd-Sr isotope correlation in mantle material and geodynamics: Earth and Planetary Science Letters.
DePaolo, D. J., and Wasserburg, G. J., 1977, The sources of island arcs as indicated by Nd and Sr isotopic studies: Geophysical Research Letters, v. 4, p. 465.
James, D. E., Brooks, C., and Cuyubamba, A., 1976, Andean Cenozoic volcanism; Magma genesis in the light of strontium isotopic composition and trace-element geochemistry: Geological Society of America Bulletin, v. 87, p. 592.

Kay, R. W., Sun, S. S., and Lee-Hu, C. N., 1978, Pb and Sr isotopes in volcanic rocks from the Aleutian Islands and Pribilof Islands, Alaska: Geochimica Cosmochimica Acta, v. 42, p. 263.

Lancelot, J. R., and Allegre, C. J., 1974, Origin of carbonatitic magma in the light of the Pb-U-Th isotope system: Earth and Planetary Science Letters, v. 22, p. 233.

Tatsumoto, M., 1969, Lead isotopes in volcanic rocks and possible ocean-floor thrusting beneath island arcs: Earth and Planetary Science Letters, v. 6, p. 369.

THE USE OF $^{40}Ar/^{39}Ar$ DATA IN EVALUATION OF DISTURBED K-Ar SYSTEMS

By Marvin A. Lanphere and G. Brent Dalrymple
U.S. Geological Survey, Menlo Park,
California 94025

The $^{40}Ar/^{39}Ar$ technique is being used extensively to supplement conventional K-Ar studies or to provide information that cannot be obtained with the conventional technique. In principle, the data from incremental heating of irradiated material can be used to distinguish disturbed from undisturbed samples, identify the presence of excess argon, and recover the age of crystallization or reheating for samples that have been thermally or chemically overprinted provided argon loss is less than about 15 - 20 percent.

In an ideal K-Ar system, each increment of gas released will have the same apparent age and the result will be a horizontal age spectrum. Age spectra for samples known to be undisturbed are reasonably consistent with this model (Dalrymple and Lanphere, 1974). The $^{40}Ar/^{36}Ar$ versus $^{39}Ar/^{36}Ar$ isochron for an undisturbed sample is concordant with the age-spectrum plateau age, whereas disturbed samples generally show neither a good plateau nor a well-fitted isochron.

An $^{40}Ar/^{39}Ar$ isochron is mathematically analogous to a $^{87}Sr/^{86}Sr$ versus $^{87}Rb/^{86}Sr$ isochron, but there are important differences that preclude drawing simple analogies between the isotopic systematics of these different parent-daughter systems. The most important difference is that the argon gas fractions in an incremental heating experiment are produced in the laboratory by diffusion after irradiation with high doses of fast neutrons, whereas Rb/Sr data represent separate analyses of discrete mineral or rock phases. Thus, there is potential for producing experimental artifacts during incremental heating that have no geological meaning.

Unless $^{40}Ar/^{39}Ar$ data for disturbed systems meet certain minimum criteria, it is probably not possible to extract a geologically meaningful age. A corollary of this is that meeting or failing to meet these criteria can be used to differentiate undisturbed from disturbed systems. The minimum criteria for a meaningful $^{40}Ar/^{39}Ar$ incremental heating age are:

1. Well-defined high-temperature plateau for more than 50 percent of the ^{39}Ar released.
2. Well-defined isochron for the plateau gas fractions.
3. Concordant plateau and isochron ages.
4. $^{40}Ar/^{36}Ar$ intercept not significantly different from 295.5.

The application of these criteria is illustrated in figure 1, A and B, by two hypothetical samples with a crystallization age of 100 m.y. One sample is undisturbed but the other was reheated or altered at some time between 50 m.y. ago and the present. For both samples the argon was extracted in five increments of equal size. Amounts of atmospheric argon ($^{40}Ar/^{30}Ar$ = 295.5) in each increment were assigned arbitrarily but were identical for disturbed and undisturbed cases. Various parameters for the age spectra and isochrons are given in table 1. The isochrons (fig. 1B) were fitted using York's (1969) cubic fit with correlated errors where a correlation coefficient of 0.8 was assumed for each datum.

The disturbed sample fits all of the criteria defined previously. The goodness of fit of the isochron as expressed by the quantity $[SUMS/(n-2)]^{\frac{1}{2}}$ (York, 1969), is excellent and R, the correlation between x and y values, is essentially 1.0.

For the disturbed sample, three of the criteria for acceptability are not satisfied. The quantity $[SUMS/(n-2)]^{\frac{1}{2}}$ is too large and the intercept is significantly lower than 295.5. Note that the intercept for this hypothetical sample is purely a consequence of $^{40}Ar_{rad}$ loss in the lower temperature steps and has no geologic meaning. Even though the sample is obviously disturbed the value of R is greater than 0.99, indicating that R is a very poor parameter for goodness of fit. Misleading information about the age of the disturbed sample is conveyed by a noncritical fitting of an

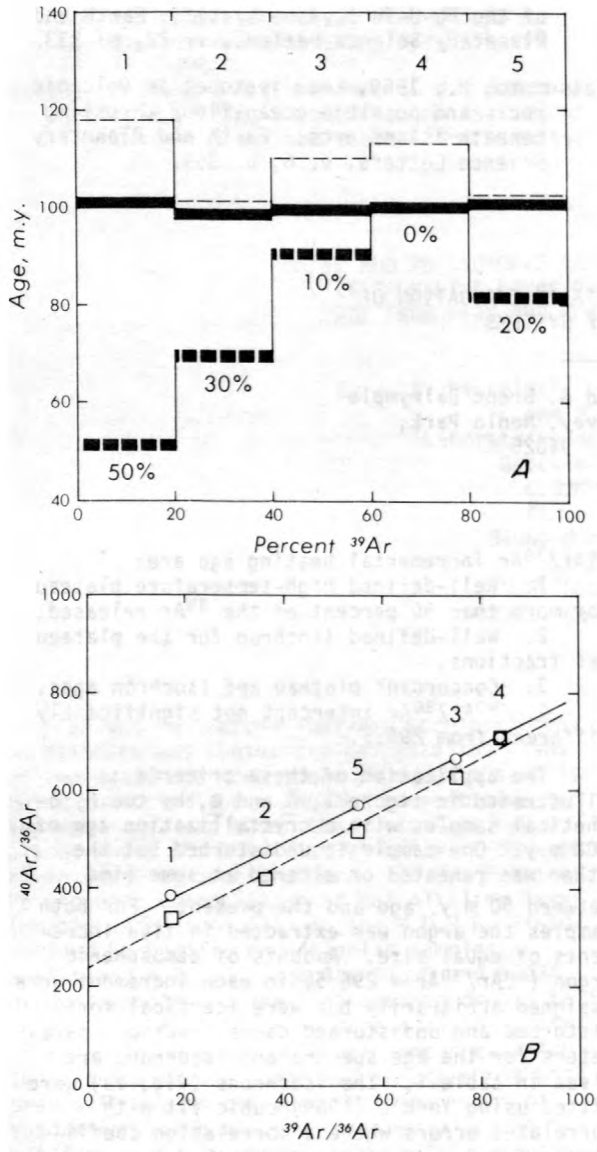

Figure 1.--A, Hypothetical $^{40}Ar/^{39}Ar$ spectra for two samples with a crystallization age of 100 m.y. Solid bars represent results from the undisturbed sample; heavy dashed bars represent results from the same sample after $^{40}Ar_{rad}$ loss from each gas increment as shown by the percentage figures. Thin dashed lines represent results from the disturbed sample recalculated using a $^{40}Ar/^{36}Ar$ intercept of 238.5. B, Isochrons diagrams for hypothetical samples in figure 1. Circles, undisturbed sample; squares, disturbed sample.

isochron to the data. Although the total fusion age of the disturbed sample is 78.4 m.y., the slope of an isochron fitted to the data points yields an age of 106.3 m.y. Some workers (for example, Jessberger, 1977; and Saito and Ozima, 1977) have argued that it is appropriate to recalculate ages using the intercept of the isochron for the $^{40}Ar/^{36}Ar$ ratio of nonradiogenic argon in a sample. We disagree. Using this procedure for the disturbed sample where the $^{40}Ar/^{36}Ar$ intercept = 238.5, simply forces the total-fusion age to agree with the invalid isochron age. The result is an age of 107.8 m.y. which apparently agrees with the isochron but is incorrect. Thus, any isochron should be considered suspect if the intercept is not the same as atmospheric argon within analytical uncertainty.

Application of these criteria to analyses of basalts from seamounts in the Pacific Ocean has provided an effective way to distinguish undisturbed from disturbed samples. The undisturbed samples meet all of the criteria defined above. For the disturbed samples, however, age spectra characteristically have no plateau and the apparent ages decrease markedly in medium- and high-temperature increments (Dalrymple and others, 1977). The data often show no linear

Table 1.--Parameters for the age spectra and isochrons of figure 1

	Undisturbed	Disturbed	Recalculated
Total fusion (m.y.) --	99.9	78.4	107.8
Plateau (m.y.) -------	99.9	--	--
Isochron (m.y.) ------	99.5±0.9	106.3± 6.7	--
Intercept ------------	296.5±2.4	238.5±17.1	--
$[SUMS/(n-2)]^{\frac{1}{2}}$ --------	0.7	5.4	--
R ---------------------	0.9999	0.994	--

correlation on an isochron diagram. Even when the data fit an isochron reasonably well, the $^{40}Ar/^{36}Ar$ intercept is different than the atmospheric value. Total fusion $^{40}Ar/^{39}Ar$ ages generally are considerably older than conventional K-Ar ages on the same samples, but the total fusion ages are still too young.

The four criteria defined in this paper provide a systematic way to distinguish disturbed from undisturbed samples using $^{40}Ar/^{39}Ar$ incremental-heating data. It may be difficult or impossible to extract geologically meaningful information from the age spectrum of a disturbed sample. But, the recognition that a sample is disturbed places important constraints on a geological situation.

Dalrymple, G. B., Clague, D. A., and Lanphere, M. A., 1977, Revised age for Midway volcano, Hawaiian volcanic chain: Earth and Planetary Science Letters, v. 37, p. 107-116.

Dalrymple, G. B., and Lanphere, M. A., 1974, $^{40}Ar/^{39}Ar$ age spectra of some undisturbed terrestrial samples: Geochimica Cosmochimica Acta, v. 38, p. 715-738.

Jessberger, E. K., 1977, Comment on "Identifi-

cation of excess ^{40}Ar by the $^{40}Ar/^{30}Ar$ age spectrum technique" by M. A. Lanphere and G. B. Dalrymple: Earth and Planetary Science Letters, v. 31, p. 167-168.

Saito, K., and Ozima, M., 1977, ^{40}Ar-^{39}Ar geochronological studies of submarine rocks from the western Pacific area: Earth and Planetary Science Letters, v. 33, p. 353-369.

York, D., 1969, Least squares fitting of straight line with correlated errors: Earth and Planetary Science Letters, v. 5, p. 320-324.

Rb/Sr ISOTOPIC STUDIES OF PRECAMBRIAN SUPRACRUSTAL ROCKS AT THE SOUTHERN MARGIN OF THE ARCHEAN CRATON OF SOUTH-WEST GREENLAND

By Ole Larsen, Institut of Petrology,
University of Copenhagen, Copenhagen, Denmark

The Precambrian basement of southern Greenland is composed of an Archean craton limited to the north and south by Proterozoic metamorphic belts. The southern margin of the Archean craton was mapped in West Greenland during the late 1950's (Berthelsen and Henriksen, 1975) and in East Greenland during the early 1970's (Andrews and others, 1973).

In East Greenland reconnaissance mapping was followed by U-Pb dating of zircons (Gulson and Krogh, 1972, 1975) and Rb/Sr whole-rock dating (Pedersen and others, 1974). The high-grade Archean gneisses bordering the younger Proterozoic belt yielded a U-Pb diffusion age of approximately 2800 m.y. The border zone itself shows field evidence of a complex metamorphic history comprising deposition of supracrustal rocks, deformation and granitization dated at 2620 m.y., and the later intrusion of basic dikes. South of the border zone, within the Ketilidian mobile belt, deformation and metamorphism around 1800 m.y. was followed by a period of late- to post-tectonic plutonic activity extending to about 1740 m.y. In East Greenland the border zone between the Archean basement complex and the Ketilidian mobile belt is very narrow. In West Greenland, in the region around the former mining town of Ivigtut, the transition zone is wider, so that the effects of the Ketilidian activity on older rocks may be studied in more detail.

Until recently a number of K-Ar mineral ages were the only geochronological data available to support the interpretations based on field work. Recent Rb-Sr whole-rock dating, mainly on supracrustal rocks deposited on or folded into the basement gneisses, has given further information about the time of the metamorphism in the border zone of the Ketilidian mobile belt. However, it has also emphasized the problem of whether or not the Ketilidian metamorphism and plutonic activity were superimposed on an already existing belt of supracrustal sediments and derived gneisses welded onto the southern edge of the Archean craton in early Proterozoic time.

The Ketilidian supracrustal suite of sediments (Vallen Group) and volcanics (Sortis Group) occurring in Graenseland (Bondesen, 1970) and on Midternaes (Higgins, 1970) appear to have been subjected to deformation and low-grade metamorphism at 1790 m.y. (using the $1.42 \times 10^{11}\ Yr^{-1}$ decay constant). This substantiates the conclusions of both Van Breemen and others (1974) and Gulson and Krogh (1975) that the final peak of regional Ketilidian metamorphism was close to 1800 m.y. According to the same authors, plutonic activity continued to about 1740 m.y. This is the age obtained by Van Breemen and others (1974) on the late Ketilidian Julianehaab granite (recalc. to $1.42 \times 10^{11}\ yr^{-1}$ constant) and is in agreement with a new Rb-Sr whole-rock date of a granitic intrusion, the Kerne granite, at Qornoq, South of Ivigtut.

In Graenseland the Ketilidian metasediments were deposited directly onto gneisses that are considered to be of Archean age. On Midternaes a similar sedimentary sequence was deposited on a basement consisting of a folded greenschist belt and derived gneisses. The unconformity appears to be an original autochthonous feature. Folded greenschists similar to those in the basement gneisses on Midternaes are found along both shores of Sermiligârssuk fjord. These schists have been regarded as tectonically separated parts of the same supracrustal rock sequence and are named the Tartoq Group. (Higgins and Bondesen, 1966). The deformation and metamorphism of the Tartoq supracrustal rocks is definitely pre-Ketilidian. It is doubtful however, whether they may be considered an integral part of the Archean basement. Rb-Sr isotope work on a band of micaceous quartz-talc schists interlayered and folded with the greenstones provides evidence against an Archean age (2800 - 2600 m.y. for the rocks. The isotopic data forms a

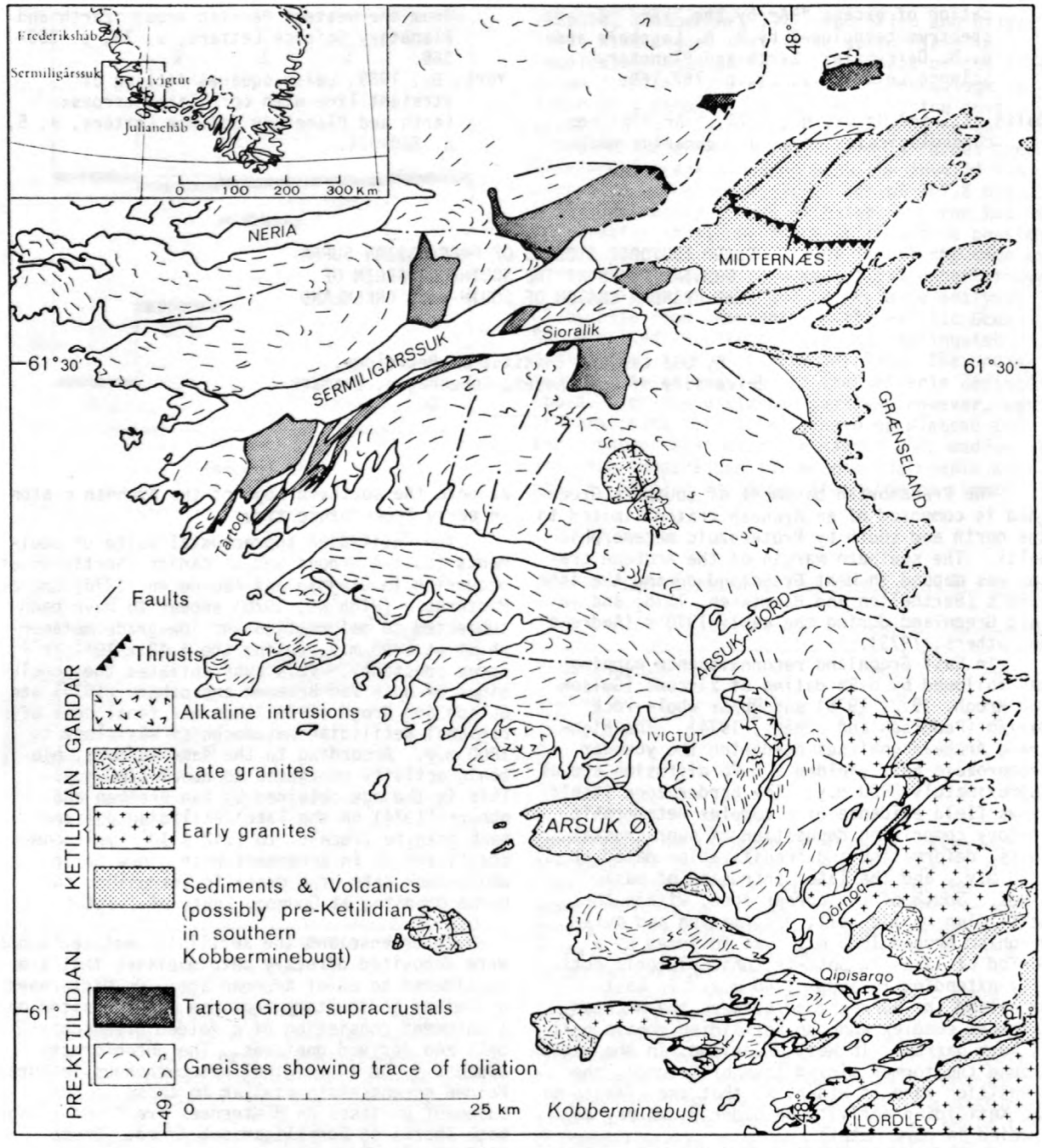

Figure 1.--Map of the Ivigtut region, southwest Greenland

scattered plot which seems to favor a metamorphism around 2250 m.y. followed by a disturbance of the isotopic systems close to 1800 m.y., as a result of Ketilidian shear movements in the supracrustal rocks of the Tartoq Group.

In a recent paper on the importance of major geological boundaries in Greenland, Bridgwater and others (1973) suggest from field evidence that a suite of volcanic rocks, the Ilordleq Group (Watterson, 1965), which outcrop in Kobberminebugt 35 - 40 km SSE of Ivigtut, were also metamorphosed before the deposition of the Ketilidian supracrustal rocks on Midternaes and in Graenseland. Supracrustal rocks outcrop in several places in Kobberminebugt and outcrops may be followed further northward along the shores of

Qornoq fjord. K-Ar mineral ages on metasediments in Qornoq fjord (Larsen, 1970) clearly reflect Ketilidian metamorphism, but the Sr-isotopes suggest that the schists might have had a more complex geological history than the Ketilidian sediments of Graenseland with which they have been correlated.

These preliminary Sr-isotope investigations of the supracrustal rocks in the Ivigtut region suggest, but as yet provide no proof, that supracrustal rocks were deformed and metamorphosed in post-Archean/pre-Ketilidian time. Such rocks may in fact be more wide-spread than hitherto supposed. To repeat the conclusion of Bridgwater and others (1973), it seems that the southern margin of the Archean craton remained tectonically active for a very long period of time, finally to be the site of intrusion of major dike swarms and alkali-igneous complexes emplaced from 1330 m.y. to 1150 m.y. (Blaxland and others, 1978) ago.

Andrews, J. R., Bridgwater, D., Gormsen, K., Gulson, B., Keto, L., and Watterson, J., 1973, The Precambrian of South-East Greenland, in Park, R. G., and Tarney, J., eds., The early Precambrian of Scotland and related rocks of Greenland: Newcastle, England, University of Keele, p. 143-156.

Bethelsen, A. and Henriksen, N., 1975, Descriptive text to Geological map of Greenland, 1:100.000, Ivigtut, 61 V 1 Syd. Meddr. Groenland v. 186, no. 1, p. 169.

Blaxland, A. B., Van Breemen, O., Emeleus, C. H., and Anderson, J. G., 1978, Age and origin of the major syenite centers in the Gardar province of South Greenland: Rb-Sr studies: Geological Society of America Bulletin, v. 89, p. 231-244.

Bondesen, E., 1970, The stratigraphy and deformation of the Precambrian rocks of the Graenseland area, South-West Greenland: Meddr. Groenland 185, 1 (Bull. Groenlands Geol. Unders. 86) p. 210.

Bridgwater, D., Escher, A. and Watterson, J., 1973, Dyke swarms and the persistence of major geological boundaries in Greenland, in Park, R. G. and Tarney, J., eds., The early Precambrian of Scotland and related rocks of Greenland. Newcastle, England, University of Keele, p. 137-141.

Gulson, B. L. and Krogh, T. E., 1972, U/Pb zircon studies on the age and origin of post-tectonic intrusions from South Greenland: Rapp. Groenland Geol. Unders., v. 45, p. 48-53.

_____, 1975, Evidence of multiple intrusion, resetting (of U-Pb ages) and possible new crystallization of zircons in the post-tectonic intrusions ("rapakivi granites") and gneisses from South Greenland: Geochimica cosmochimica Acta, v. 39, p. 65-82.

Higgins, A. K., 1970, The stratigraphy and structure of the Ketilidian rocks of Midternaes, South-West Greenland: Meddr. Groenland 189, 2 (also: Bull. Groenlands Geol. Unders. 87) 96 p.

Higgins, A. K., and Bondesen, E., 1966, Supracrustals of pre-Ketilidian age (the Tartoq Group) and their relationship with Ketilidian supracrustals in the Ivigtut region, South-West Greenland. Rapp. Groenland Geol. Unders., v. 8, 21 p.

Larsen, O., 1970, Preliminary report on K/Ar dating in the south-eastern part of the Ivigtut region: Rapp. Groenland Geol. Unders., v. 35, p. 49-52.

Pedersen, S., Larsen, O., Bridgwater, D., and Watterson, J., 1974, Rb/Sr whole-rock isochron age determinations on metamorphosed acid volcanic rocks and granitic gneisses from the Ketilidian mobile belt, South-East Greenland. Rapp. Groenland Geol. Unders., v. 66, p. 12-20.

Van Breemen, O., Aftalion, M., and Allaart, J.H., 1974, Isotopic and geochronologic studies on granites from the Ketilidian mobile belt of South Greenland: Geological Society of America Bulletin, v. 85, p. 403-412.

Watterson, J., 1965, Plutonic development of the Ilordleq area, South Greenland. I. Chronology, and the occurrence and recognition of metamorphosed basic dikes: Meddr. Groenland 172,7: Bull. Groenland Geol. Unders. 51, 147 p.

ON THE APPARENT CONFLICT BETWEEN THE TIME SCALES INFERRED FROM THE COSMOCHRONOMETERS ^{129}I, ^{244}PU, AND ^{26}AL

By Typhoon Lee[1], David N. Schramm[1], John P. Wefel[1], and J. Bernard Blake[2]
[1]Enrico Fermi Institute, University of Chicago
[2]The Aerospace Corporation, Los Angeles

The time interval Δ between the last nucleosynthetic event which contributed material to the solar system and the onset of condensation in the solar system has been estimated to be $\sim 10^8$ years from the chronometers ^{129}I ($t_{1/2} = 1.6 \times 10^7$ yr) and ^{244}Pu ($t_{1/2} \sim 8.3 \times 10^7$ yr) (Schramm and Wasserburg, 1970). However, the presence of significant amounts of ^{26}Al ($t_{1/2} \sim 7.3 \times 10^5$ yr) in the early solar system requires a $\Delta \sim 10^6$ years, about two orders of magnitude shorter than the previous estimate (Lee and others, 1977). The production of ^{129}I and ^{244}Pu are conventionally attributed to the r-process nucleosynthesis (rapid neutron captures on a time scale much faster than the beta-decay life time) whereas ^{26}Al is thought to be produced in either high-temperature hydrostatic or explosive-carbon burning (Arnett and Wefel, 1978). Therefore, one obvious solution to the apparent conflict was to assume that the ^{26}Al-producing event did not produce r-process material; 10^8 years is the time scale for the last r-process event and 10^6 years dates perhaps the last carbon burning in a massive star.

The above solution ran into difficulty with the newly discovered FUN anomalies, which seems to suggest that some r-process material might have been associated with the ^{26}Al. The FUN anomalies are a suite of isotopic anomalies found in two rare Allende inclusions characterized by extremely large mass fractionation effects and many unknown nuclear effects (and, hence, the abbreviation "FUN" for Fractionation and Unknown Nuclear). FUN anomalies are undoubtedly a very complicated phenomenon and no comprehensive interpretation is yet available. However, there is a systematic trend in the heavy part of the FUN anomalies. Among the isotopes of Ba, Nd, and Sm, those that are not shielded on the neutron-rich side always have anomalous abundances. This suggests that the nucleosynthesis responsible for this part of FUN anomalies has taken place in a neutron-rich environment. For this reason, classical r-process has been suggested to be the source of these anomalies (McCulloch and Wasserburg, 1978; Clayton, 1978; Lugmair and others, 1978).

Table 1 demonstrates this conclusion for the Allende inclusion EK1. In the first row we present the published values for ε (the fractional deviation), sometimes with a slightly different normalization procedure. The second row is the ε calculated from the solar system "r-process" pattern, which is obtained by subtracting the s-process contribution from the solar system abundance. The close resemblance between these two sets of values demonstrates that r-process may be responsible for the observed anomalies. Because it is difficult to envisage how this r-like material could have stayed unmixed if it was made 10^8 years prior to the formation of these inclusions, it seems more plausible to assume that the material was produced much more recently, perhaps at the same time as the ^{26}Al-event. This association of ^{26}Al with the r-like material is consistent with the new observation that inclusion C1, which is depleted in this r-like material, has a very low, if not zero, ^{26}Al-abundance (Esat and others, 1978). The ^{244}Pu and ^{129}I abundances in inclusion EK1 have been estimated from the Xe-isotope measurements (Papanastassiou and others, 1978) to be very close to those found previously in other meteorites and would imply the same $\Delta \sim 10^8$ years. Therefore, one is facing the same problem of conflicting estimates of Δ but can no longer resolve the dilemma by assuming that the r-process and ^{26}Al-events were independent if the r-like material was from a classical r-process.

Table 1.--R-process-like isotopic anomalies

[Entry is fractional excess ε of the isotope $\varepsilon \equiv (N^*/N_0) \times 10^4$ where N^* is the number of atoms from the peculiar component and N_0 is the number of atoms in the normal component. → indicates the abundance of this isotope has been normalized to the value shown for the purpose of removing mass fractionation effect of the entire pattern. ≡, set equal to.]

Row[1]	^{147}Sm	^{148}Sm	^{149}Sm	^{150}Sm	^{152}Sm	^{154}Sm
One ----	34.9	≡0	36.6	→ 0	28.0	37.6
Two ----	31.6	0	32.8	0	44.3	≡37.6
Three --	10.5	0	1.5	0	5.4	≡37.6
Four ---	242.0	0	184.0	0	29.9	≡37.6

	^{142}Nd	^{143}Nd	^{144}Nd	^{145}Nd	^{146}Nd	^{148}Nd	^{150}Nd
One ----	≡0	13.6	17.9	24.5	13.5	33.1	→33.6
Two ----	0	16.5	11.0	24.6	13.5	33.6	≡33.6
Three --	0	6.8	0.7	6.4	8.0	52.3	≡33.6
Four ---	0	14.9	8.7	26.6	8.3	8.1	≡33.6

	^{134}Ba	^{135}Ba	^{136}Ba	^{137}Ba	^{138}Ba
One ----	≡0	13.2	→0	13.7	1.6
Two ----	0	≡13.2	0	5.3	1.0
Three --	0	≡13.2	0	2.8	5.8
Four ---	0	≡13.2	0	7.7	0.7

[1]Row one is the observed values. Rows two, three, and four are calculated values by assuming that the isotopic pattern of the source is solar system r-process (see text), n-process in explosive ^{12}C burning (Blake and others, 1978), and calculated r-process (E. Norman, oral commun., 1978), respectively

Fortunately, the classical r-process is not the only place where the r-like material can be produced. One possible place is the explosive burning of carbon, itself, which is thought to be a promising source for the ^{26}Al production. We have recently examined the effect of exposing pre-existing heavy nuclei seed to the neutrons released in an explosive carbon burning (Blake and others, 1978). The neutron reactions were followed by using a general n-process computer program (Blake and Schramm, 1976) with seed composition and the neutron density-temperature profile generated from an explosive carbon burning calculation as input. Preliminary results show that this n-process is a possible source for the r-like material. The third row of table 1 shows the calculated ε based on a resulting isotopic pattern from our n-process with a temperature 2.1 x 10^9°K, density $\sim 10^5$ g/cc and an initial solar system seed composition. Qualitatively, this explains why the anomalies only occur on the unshielded isotopes. Quantitatively, the fit to the observed ε is not as good as the solar system r-process. However, the calculation of nucleosynthesis in the high atomic number region and away from the beta stability valley is notoriously imprecise and replete with uncertain nuclear parameters which are not measurable in the laboratory. In fact, there have been no r-process calculations that can reproduce the solar system r-process pattern in detail. To demonstrate this, the fourth row in table 1 shows the calculated ε based on a calculated r-process pattern which fits the solar system extraordinarily well (E. Norman, oral commun., 1978). It can be seen that the calculated r-process also occasionally fail to fit some isotopes by more than a factor of 5, similar to the n-process result. We have not yet finished exploring the possible range of conditions. The case presented in table 1 is merely an example to demonstrate that n-process during an explosive carbon burning is a promising source of the r-like material.

An important qualitative feature of the n-process during the explosive carbon burning is that the resulting abundance of the less stable nuclei are much lower than the classical r-process. This is because in the n-process the neutrons are exhausted when the explosive carbon zone is still at very high temperature. Thus, the rapid (γ, n) reactions tend to destroy loosely bound nuclei. Almost all the nuclei beyond Bi, including ^{244}Pu, are totally destroyed so that the production of ^{244}Pu in this case is zero. The iodine region (both ^{127}I and ^{129}I) is similarly depleted. For example, the $^{129}I/^{135}Ba$ production ratio in the n-process is about factor 10 lower than that in the classical r-process. Therefore, the n-process during the explosive carbon burning produces almost no ^{129}I and ^{244}Pu. This allows us to have a more coherent interpretation of Δ: the last r-process event took place $\sim 10^8$ years before the solar system formed, perhaps associated with the last passage of the density wave, while the r-like material observed in FUN samples were produced with ^{26}Al in the same zone of a supernova, which exploded $\sim 10^6$ years before the solar system formed.

This research is supported by NASA grant NSG-7212. The author gratefully acknowledges the support provided by the Robert R. McCormick Foundation.

Arnett, W. D., and Wefel, J. P., 1978, submitted to Astrophysical Journal Lett.

Blake, J. B., Lee, T., Schramm, D. N., and Wefel, J. P., 1978, submitted to Astrophysical Journal.

Blake, J. B., and Schramm, D. H., 1976: Astrophysical Journal, v. 209, p. 846.

Clayton, D. D., 1978: Astrophysical Journal (in press).

Esat, T. M., Lee, T., Papanastassiou, D. A., and Wasserburg, G. J.: (This conference).

Lee, T., Papanastassiou, D. A., and Wasserburg, G. J., 1977: Astrophysical Journal, v. 211, p. L107.

Lugmair, G. W., Marti, K., and Scheinin, N. B., 1978: Lunar Science IX, p. 672.

McCulloch, M. T., and Wasserburg, G. J., 1978: Astrophysical Journal, v. 220, p. L15.

Papanastassiou, D. A., Huneke, J. C., Esat, T. M., and Wasserburg, G. J., 1978: Lunar Science IX, p. 859.

Schramm, D. N., and Wasserburg, G. J., 1970: Astrophysical Journal, v. 162, p. 57.

CARBON-13 AS CLIMATE INDICATOR; FACTORS CONTROLLING STABLE CARBON ISOTOPE RATIOS IN TREE RINGS

By Juan Carlos Lerman and Austin Long
Laboratory of Isotope Geochemistry
Department of Geosciences, University of Arizona, Tucson, Arizona 85721

During the last few years several laboratories, including ours, have been concerned with whether cellulose in tree rings retains retrievable information about the local climate during the growth period of each tree ring. Particular attention was accorded to the relative abundances of the heavy isotopes of hydrogen, oxygen, and carbon. Since proposed by Urey (1947), this has seemed to be a potentially useful approach to paleoclimate research. Several authors concluded that variations in the isotope ratios H/D, $^{18}O/^{16}O$, and $^{13}C/^{12}C$ occur in tree rings and that they carry climatic information (see, for example, Epstein and Yapp, 1976; Epstein and others, 1976; Gray and Thompson, 1976; Libby and others, 1976; Long and Lerman, 1976; Pearman and others, 1976; Ferhi and others, 1977; Wilson and Grinsted, 1977a, b; Yapp and Eqstein, 1977; Mazany and others, 1978). However, some of these results appeared to be contradictory.

In our research group we are attempting, by performing several experiments, to understand the climatic and environmental factors which control the carbon ratios $^{13}C/^{12}C$. Two of the experiments are described at this conference: one on recent juniper twigs (Arnold, 1978), and one on prehistoric tree rings (Mazany, 1978). In both experiments, the stable carbon isotope ratio proved to respond to climate as shown by the high correlation between the carbon-13 abundance in juniper twigs and the temperature-precipitation factor (Arnold, 1978) in one experiment and in the other by the significant correlation between the carbon-13 contents of tree rings and the regional tree-ring index (Mazany, 1978). Other experiments, on bristlecone pine and ponderosa pine, are in progress and strongly indicate that these also contain climatic information, although the relationships appear to be more complex.

What are the links between environment, climate, and abundance of carbon-13 in tree rings? We advance here the hypothesis that a large part of the observed variations is a direct consequence of changes in the isotope composition of the atmospheric CO_2. The isotope response is directly related to the regional biomass activity. An increase in biomass productivity through increased plant respiration produces an atmosphere depleted in carbon-13, and, consequently, the carbon fixed in the cellulose during that period of time is also depleted or is composed of lighter carbon. For this model, which is up to the present in a qualitative stage, we assume: (a) that the isotope fractionation in the photosynthetic reactions, which assure the fixation of atmospheric CO_2, is independent of temperature as experimentally shown by Troughton and others (1974), and that the discrimination against ^{13}C is about 20 permil in the case of trees (plants of the C-3 photosynthetic type) (Lerman, 1975); (b) that the CO_2 respired by the trees and other vegetation in the environment has essentially the same $^{13}C/^{12}C$ ratio as cellulose (Park and Epstein, 1960). The local atmosphere, therefore, acquires a higher concentration of CO_2 which has a lower abundance of carbon-13 than before the productivity increased. This higher concentration is later reduced and the carbon-13 abundance increased (Lerman, 1974, 1975) by two processes--re-use of the CO_2 by photosynthesis as observed in the canopy of forests (Bolin, 1970) and mixing of that CO_2 with the "free atmosphere CO_2" by wind, eddy diffusion, thermal convection, and so forth. As the second mechanism becomes active only after the early morning photosynthesis begins, the vegetation would "see" and integrate a depleted or lighter than average "free atmosphere CO_2."

What then are the climatic changes that the carbon isotope ratios might have recorded? This question is equivalent to the following: what climatic changes produce a lighter local atmosphere? From the preceding paragraphs the answer appears to be those climate changes that favor plant growth. Naturally these conditions depend on the geographical area, but we may assume that in areas where precipitation limits growth, they would include a combination of (a) more precipitation, (b) lower temperature (which would decrease the evapotranspiration), and (c) less wind (which would also decrease the evapotranspiration). Then, more plant growth and more plant respiration would produce an increase in the respired CO_2 available for photosynthesis in the early morning. Denser vegetation would decrease the wind velocity and the diffusion and convection, thus contributing to the confinement of the "local CO_2" and making it lighter than average. This model is consistent with the following: (1) measurements of atmosphere CO_2 by Keeling (1961a), Lerman and

Raynal (1972), and ourselves (this communication); (2) atmosphere-enrichment model by Keeling (1961b); (3) height effect (Keeling, 1961b); (4) "juvenile" effect (Craig, 1954; Jansen, 1962); (5) intra-ring variations (Freyer and Wiesberg, 1975; Mazany and others, 1978, and a more complete article in preparation); (6) highly carbon-13 depleted undergrowth in dense forests (Lerman and Raynal, 1972; Raynal and Lerman, in preparation, as described by Lerman, 1974, 1975). This model might also explain the seasonal temperature coefficient of +0.2 permil reported by Wilson and Grinsted (1977a, b).

That the carbon isotope variations observed are not artifacts of tree-ring growth as hypothesized by Wigley, Gray, and Kelly (1978) has been proved by observations that the isotope abundance in the tree rings of the two specimens from Chaco Canyon (Mazany, 1978; Mazany and others, 1978) correlate with the regional tree-ring widths and not with the widths measured on the same specimens (the correlation factors are, referred to the regional indices, -0.65 and -0.80, while referred to the specimens they are only -0.26 and -0.07); the relationship seems to be the same for the juniper twigs (Arnold, 1978).

Concluding, we believe that apart from a useful paleoclimate retrieval tool, stable carbon ratios might also become a useful tool to follow the carbon cycle in ecosystems.

Acknowledgments: This research was funded by NSF Grant ATM77-06790 and the State of Arizona.

Arnold, L. D., 1978, The climatic response in the $\delta^{13}C$ values of juniper trees from the American Southwest (this conference).

Bolin, B., 1970, The carbon cycle: Scientific American, v. 223, no. 3, p. 125-132.

Craig, H., 1954, Carbon-13 variations in sequoia rings and the atmosphere: Science, v. 119, p. 141-143.

Epstein, S., and Yapp, C. J., 1976, Climatic implications of the D/H ratio of hydrogen in C-H groups in tree cellulose: Earth and Planetary Science Letters, v. 30, p. 252-261.

Epstein, S., Yapp, C. J., and Hall, J. H., 1976, The determination of the D/H ratio of non-exchangeable hydrogen in cellulose extracted from aquatic and land plants: Earth and Planetary Science Letters, v. 30, p. 241-251.

Epstein, S., Thompson, P., and Yapp, C. J., 1977, Oxygen and hydrogen isotopic ratios in plant cellulose: Science, v. 198, no. 4323, p. 1209-1215.

Ferhi, A. M., Long, A., and Lerman, J. C., 1977, Stable isotopes of oxygen in plants: a possible paleohygrometer: Hydrology and Water Resources in Arizona and the Southwest, v. 7, p. 191-198.

Freyer, H. D., and Wiesberg, L., 1975, Anthropogenic carbon-13 decrease in atmospheric carbon dioxide as recorded in modern wood, in, Isotope ratios as pollutant source and behaviour indicators: International Atomic Energy Agency, Vienna, IAEA-SM-191/10, p. 49-62.

Gray, J., and Thompson, P., 1976, Climatic information from $^{18}O/^{16}O$ ratios of cellulose in tree rings: Nature, v. 262, p. 481-482.

Jansen, H. S., 1962, Depletion of carbon-13 in a young Kauri tree: Nature, v. 196, p. 84-85.

Keeling, C. D., 1961a, The concentration and isotopic abundances of carbon dioxide in rural and marine air: Geochimica and Cosmochimica Acta, v. 24, p. 277-298.

_____1961b, A mechanism for cyclic enrichment of carbon-12 by terrestrial plants: Geochimica and Cosmochimica Acta, v. 24, p. 299-313.

Lerman, J. C., 1974, Isotope "paleothermometers" on continental matter; assessment: Paris, Colloques Internationaux du Centre National dela Recherche Scientifique, no. 219, p. 163-181.

_____1975, How to interpret variations in the carbon isotope ratio of plants; biologic and environmental effects, in, Environmental and biological control of photosynthesis, Marcelle, R., ed., The Hague, Jung, W., p. 323-335.

Lerman, J. C., and Raynal, J., 1972, La teneur en isotopes stables du carbone chez les Cyperacees; sa valeur taxonomique: Paris, Academic des Sciences, Comptes Rendus, ser. D, v. 275, p. 1391-1394.

Libby, L. M., Pandolfi, L. J., Payton, P. H., Marshall, J. III, Becker, B., and Giertz-Sienbenlist, V., 1976, Isotopic tree thermometers: Nature, v. 261, p. 284-288.

Long, A., and Lerman, J. C., 1976, Potential use of carbon isotope variations of CAM plants in paleoecological studies, in, What is new in plant physiology, Fritz, G., ed., Gainesville, Florida, v. 8, no. 5, p. 1-5.

Mazany, T., 1978, Isotope dendrochronology: Natural stable carbon isotope analyses of tree rings from an archeological site (this conference).

Mazany, T., Lerman, J. C., and Long, A., 1978, Climatic sensitivity in $^{13}C/^{12}C$ values in tree rings from Chaco Canyon: American Association for the Advancement of Science, Poster Session, Feb. 12-17, 1978, Washington, D.C.

Park, R., and Epstein, S., 1960, Carbon isotope fractionation during photosynthesis: Geochimica and Cosmochimica Acta, v. 21, p. 110-126.

Pearman, G. I., Francey, R. J., and Fraser, P. J. B., 1976, Climatic implications of stable carbon isotopes in tree rings: Nature, v. 260, p. 771-773.

Raynal, J., and Lerman, J. C., in prep., Local atmospheric CO_2 measured in $\delta^{13}C$ in dense forests.

Troughton, J. H., Card, K. A., and Bjorkman, O., 1974, Temperature effects on the carbon isotope ratio of C_3, C_4, and CAM plants: Carnegie Institute of Washington Year Book 73, p. 780-783.

Urey, H. C., 1947, The thermodynamic properties of isotopic substances: American Chemical Society Journal, v. 1947, p. 562-581.

Wigley, T. M. L., Gray, B. M., and Kelly, P. M., 1978, Climatic interpretation of $\delta^{18}O$ and δD in tree rings: Nature, v. 271, p. 92-93.

Wilson, A. T., and Grinsted, M. J., 1977a, $^{12}C/^{13}C$ in cellulose and lignin as palaeothermometers: Nature, v. 265, p. 133-135.

_____1977b, The possibilities of deriving past climate information from stable isotope studies on tree rings, in, International Conference on Stable Isotopes, 3rd, Proc.: Royal Society of New Zealand.

Yapp, C. J., and Epstein, S., 1977, Climatic implications of D/H ratios of meteoric water over North America (9500-22,000 B.P.) as inferred from ancient wood cellulose C-H hydrogen: Earth and Planetary Science Letters, v. 34, p. 333-350.

PRECAMBRIAN GEOCHRONOLOGY OF ARGENTINA[1]

By Enrique Linares[2] and Juan C. Turner[3]

[1]Contribution Ner. 34 of the Instituto de Geocronología y Geología Isotópica (INGEIS), Argentina National Research Council (CONICET), Pabellón 2, Ciudad Universitaria, Buenos Aires

[2]INGEIS and Department of Geological Sciences, University of Buenos Aires, Argentina

[3]Department of Geological Sciences, University of Buenos Aires, Argentina

INTRODUCTION

In this report a summary of the radiometric ages from different areas of Argentina with supposed Precambrian rocks, is presented.

Until 1972 the number of available radiometric data for all of the country was only for 200-250 samples. Most of them were analyzed in foreign laboratories. Since 1972 and after the beginning of the investigations by the INGEIS, some 2000 samples were dated by the K-Ar and Rb-Sr methods. This large amount of data in the last several years has added greatly to the geological and geochronological knowledge of Argentina, especially of the distribution of the Precambrian rocks.

Before the middle of the last decade, most Argentinian geologists assigned to the western and southern extension of the Precambrian Brazilian Shield had recognized several geostructural units of Argentina: (1) The Traspampean Ranges of the northwest in Catamarca and La Rioja provinces; (2) The Pampean Ranges of Santiago del Estero, Córdoba and San Luis provinces, located in the central part of the country; (3) The Sierras Septentrionales of the Buenos Aires province (Tandilia System); and (4) The small outcrops located near the Precordillera of La Rioja, San Juan and Mendoza provinces, near the Andean belt. Terranes not related with the Brazilian Shield were also postulated to contain Precambrian rocks; (5) The High Puna of Salta and Jujuy provinces; (6) The Nor-patagonian Massif of Río Negro and Chubut provinces; (7) The Deseado Shield of Santa Cruz in SE Patagonia; (8) The crystalline basement of the Sierras Australes of the Buenos Aires province; and (9) A small outcrop of metamorphic and granitic rocks on Cabo Belgrano (Cape Meredith) in the Islas Malvinas (Falkland Islands).

The radiometric dating of these supposed Precambrian rocks of Argentina is still inadequate for the large areas covered by these rocks, but the available data collected in the last five years show that the outcrops with ages ranging from 2200 to 1800 m.y. occupy only very restricted areas, which are smaller than previously thought. A major portion of the terranes contains metamorphic and igneous rocks of late Precambrian age (1800 to 570 m.y.), and larger areas yet correspond to Paleozoic rocks.

With the radiometric ages obtained up to the present a general scheme for the Precambrian rocks of Argentina can be sketched, although it will change in the future as the geochronological research continues. For the description of the different units that belong to

this era, the geochronological division of the Precambrian postulated by Harrington (1975) is as follows.

AREAS OF ARGENTINA WITH PRECAMBRIAN ROCKS

Lower Precambrian

Guriano Cycle (more than 2200 m.y.)

Until today samples with ages older than 2200 m.y. have not been analyzed for Argentina.

Transamazonian Cycle (2200 to 1800 m.y.)

The rocks of the basement of the Sierras Septentrionales of the Buenos Aires province are the oldest known in Argentina. The ages obtained range between 2200 and 1800 m.y. (Hart, 1966; Cazeneuve, 1967; Stipanicic and Linares, 1969; Halpern and Linares, 1970; Halpern, Umpierre and Linares, 1970; Teruggi, Kilmurray and Dalla Salda, 1973, 1974).

The rocks cropping out in the small island of Martín García, located near Buenos Aires city, belong to the same cycle which is related with the Tandilia System and with basement rocks of Uruguay. Linares and Latorre (1969), obtained an age of 1950 ± 200 m.y. for amphibolites from this island. These are the only outcrops known in Argentina with rocks of early Precambrian age.

Upper Precambrian

Espinhaciano Cycle (1800 to 1300 m.y.)

Some outcrops located in the Sierras Septentrionales of Buenos Aires correspond to this cycle (Cazeneuve, 1967; Teruggi, Kilmurray and Dalla Salda, 1973, 1974).

Uruacuano Cycle (1300 to 900 m.y.)

This cycle is represented by the metamorphic and granitic rocks cropping out in the Islas Malvinas. Recently Cingolani and Varela (1975a) obtained an age of approximately 1000 m.y. for the small outcrop on Cabo Belgrano (Cape Meredith). It is interesting to remark that this is the only place known in Argentina where ages of 1000 m.y. occur, and, based on this result and on the stratigraphic sequence superimposed on the basement rocks, the authors cited above correlated them with similar ones in Eastern South Africa.

Small areas in the Sierras Septentrionales of Buenos Aires have ages belonging to an earlier stage of this cycle (Linares and Latorre, 1969). Also, it is probable that in some areas covered by the metamorphic rocks of the Pampean Ranges (see below), remanents of rocks with ages corresponding to this cycle (Cingolani and Varela, 1975a,b; Linares and Cordani, 1975) could exist.

Brazilian Cycle (900 to 700 m.y.)

There are only sporadic results indicative of this cycle in some areas of the Pampean Ranges (Linares and Cordani, 1975; Cingolani and Varela, 1975 a,b; Ramos, 1977), and also in the Sierras Septentrionales of Buenos Aires (Teruggi and others, 1974).

Panamerican Cycle (700 to 500 m.y.)

This cycle is the best represented in Argentina and the rocks corresponding to it cover large areas in different parts of the country.

The major part of the high grade metamorphic rocks of the Cordillera Oriental of northern Argentina correspond to the Panamerican Cycle, in that some granitic intrusions in them were dated between 600 and 500 m.y. (Halpern and Latorre, 1973). The same authors found ages of 600 m.y. for granitic rocks of the Valles Calchaquíes (Salta province) and in the northern part of the Traspampean Ranges.

The great majority of metamorphic rocks of the Traspampean and Pampean Ranges correspond to this cycle according to geochronological research conducted in the last few years (Cingolani and Varela, 1975 a,b; Linares and Aparicio, 1975; Linares and Cordani, 1975; Halpern, Linares and Latorre, 1970; Linares and Latorre, 1970, 1973). The ages obtained for these rocks using the K-Ar and Rb-Sr methods range from 570-700 m.y., but isochron plots by the Rb-Sr method gave a more uniform age of 620-640 m.y.

Recently Linares and others (1977) showed that the outcrops of the Pampean Ranges continue to the south, and described metamorphic and granitic rocks of the same age in different places of the La Pampa province as far as the Colorado River, the limit of the so-called Patagonia.

It is necessary to remark that the granitic rocks that intrude the metamorphics of the Traspampean and Pampean Ranges, which were thought before to be Precambrian in age may, in fact, be earliest Paleozoic. Recent studies show that they were intruded in Paleozoic time and belong at least to three different magmatic cycles (Linares and Latorre, 1970, 1973; González and Toselli, 1973).

In the Sierras Australes of the Buenos Aires province, the granitic rocks that lie below the Grupo Curamalal (Silurian), belong to this cycle according to radiometric data obtained on them (Cazeneuve, 1967; Halpern, Umpierre and Linares, 1970; Cingolani and Varrela, 1972). The mean age for these rocks is 540 ± 10 m.y.

With regard to the Nor-patagonian Massif and the Deseado Shield that were also thought to be Precambrian, the radiometric ages obtained up to the present do not confirm this age. For the Nor-patagonian Massif Halpern, Umpierre and Linares (1970) gave a Permian age for granitic rocks that crop out near Gastre, Chubut, and also near the iron deposit of Sierra Grande, Río Negro. However, these rocks intrude metamorphic rocks that are supposed to belong to the Precambrian. It is necessary to carry out more detailed research in order to clarify the problem.

For the Deseado Shield, recent age determinations show the presence of two different generations of granitic rocks. The older one is Devonian with an age of 400 m.y. (Chebli, Gebhard and Menzel, 1975), and the other one with an age of 190 m.y. is Triassic (Stipanicic and Linares, 1969; Halpern, Umpierre and Linares, 1970; Chebli, Gebhard and Menzel, 1975).

CONCLUSIONS

With the geochronological knowledge obtained up to the present, it is possible to point out:

A. The areas covered by Precambrian rocks in Argentina, especially those related to the Brazilian Shield, are smaller than previously thought.

B. It is possible that small outcrops of Precambrian rocks can exist in several areas of Argentina, especially near the lower Paleozoic belts of the western part of the country, and also in some places of the Patagonia.

Cazeneuve, H., 1967, Edades isotópicas del basamento de la provincia de Buenos Aires: Buenos Aires, Rev. Ameghiniana, v. 1, p. 3-10.

Chebli, G. A., Gebhard, J., and Menzel, M., 1975, Estratigrafía y magmatismo en la zona de la estancia La Juanita y alrededores (Departamento Deseado, provincia de Santa Cruz): Actas VI Cong. Geol. Arg. (Bahía Blanca). I., p. 357-373. Buenos Aires.

Cingolani, C. A., and Varela, R., 1972, Examen geocronológico por el método rubidio-estroncio de las rocas ígneas de las Sierras Australes bonaerenses: Actas V Cong. Geol. Arg. (Córdoba). I, p. 349-371. Buenos Aires.

_____1975a, Investigaciones geológicas y geocronológicas en el extremo sur de la isla Gran Malvina, sector Cabo Belgrano (Cabo Meredith), Islas Malvinas: Actas VI Cong. Geol. Arg. (Bahía Blanca). I. Buenos Aires.

_____1975b, Geocronología rubidio-estroncio de las rocas ígneas y metamórficas de las Sierra Chica y Grande de Córdoba, República Argentina: II Cong. Iberoamericano de Geolog. Ecónomica. I, p. 9-33. Buenos Aires.

Gonzalez, R. R., and Toselli, A., 1973, Radiometric dating of igneous rocks from Sierras Pampeanas: Rev. Bras. Geocienc. IV (3), p. 137-141, San Pablo, Brazil.

Halpern, M., and Latorre, C. O., 1973, Estudio geocronológico inicial por el método rubidio-estroncio de rocas cristalinas del NO de la República Argentina: Rev. Asoc. Geol. Arg. XXVIII (2), p. 195-205. Buenos Aires.

Halpern, M., and Linares, E., 1970, Edad rubidio-estroncio de las rocas graníticas del basamento cristalino del área de Olavarría: Rev. Asoc. Geol. Arg. XXV (3), p. 303-306. Buenos Aires.

Halpern, M., Linares, E., and Latorre, C. O., 1970, Estudio preliminar por el método rubidio-estroncio de rocas metamórficas y graníticas de la provincia de San Luis: Rev. Asoc. Geol. Arg. XXV (3), p. 293-302. Buenos Aires.

Halpern, M., Umpierre, M., and Linares, E., 1970, Radiometric age of the Crystalline rocks from South America as related to Gondwana and Andean Geological provinces: Actas Conf. Problemas de la Tierra Sólida, II, p. 345-356. Buenos Aires.

Harrington, H. J., 1975, South America, in Fairbridge, R. W., ed., Encyclopedia of earth sciences, VIII, The encyclopedia of world regional geology: New York, Reinhold Book Corp.

Hart, S. R., 1966, A geochronological approach to the continental drift hypothesis: Carnegie Institute of Washington Yearbook 1965, p. 57-59.

Linares, E., and Aparicio, E. P., 1975, Edades potasio-argón de las Sierras Pampeanas de San Juan (Sierra de Pié de Palo, cerro Valdivia y Cerrillos de Barbosa), República Argentina: Actas VI Cong. Geol. Arg. (Bahía Blanca). I. Buenos Aires.

Linares, E., and Cordani, U. G., 1975, Edades potasio-argón de anfibolitas de la provincia de Córdoba, República Argentina: Actas VI Cong. Geol. Arg. (Bahía Blanca). I. Buenos Aires.

Linares, E., and Latorre, C. O., 1969, Datación por el método potasio-argón de algunas rocas ígneas argentinas: CNEA. Buenos Aires (unpublished).

_____1970, Edades potasio-argón y plomoalfa de rocas graníticas de las provincias de Córdoba y San Luis: Actas IV Jorn. Geol. Arg. (Com. Rivadavia). II, p. 195-204. Buenos Aires.

_____1973, Nuevas edades radimétricas por el método potasio-argón de rocas graníticas de Córdoba y San Luis: Actas V Cong. Geol. Arg. (Córdoba). I, p. 405-410. Buenos Aires.

Linares, E., Llambias, and Latorre, C. O., 1977

Ramos, A., 1977, Gneises y rocas básicas de la comarca de río Grande, departamento Calamuchita, provincia de Córdoba. Trabajo Final Licenciatura: Fac. Cienc. Exactas y Nat., UBA. Buenos Aires (unpublished).

Stipanicic, P. N., and Linares, E., 1969, Edades radimétricas determinadas para la República Argentina y su significado geologico: Acad. Nac. Cienc. Repub. Argent., Bol., v. 47, no. 1, p. 51-96.

Teruggi, M., Kilmurray, J., and Dalla Salda, L. H., 1973, Diques básicos en las sierras de Tandil: Rev. Asoc. Geol. Arg. XXIX (1), p. 41-60. Buenos Aires.

_____1974, Los dominios tectónicos de la región de Balcarce: Rev. Asoc. Geol. Arg. XXIX (3), p. 265-276. Buenos Aires.

OXYGEN-18 IN TREE RINGS: PALEOTHERMOMETERS OR PALEOHYGROMETERS?

By Austin Long[1], Juan Carlos Lerman[1], and André Ferhi[2]
[1]Laboratory of Isotope Geochemistry
Department of Geosciences
University of Arizona
Tucson, Arizona 85721
[2]U.E.R. Sciences de la Terre
Universite Pierre et Marie Curie
Paris 75230 France

It is reasonable to expect that the distributions of the ratios $^{18}O/^{16}O$ and D/H (expressed in the usual convention, $\delta^{18}O$ and δD with respect to the SMOW reference) in plant tissue or cellulose should be a function of the fixation temperature. At low temperature, phase changes, both equilibrium and non-equilibrium, involve isotope fractionation. Moreover, isotope ratios in precipitation--the source of at least some of the O and H in plants--are a function of precipitation temperature. Thus, even though the biochemical steps leading to the production of plant tissue are complex, several lines of reasoning lead to a probable temperature versus δD or $\delta^{18}O$ relationship.

Several studies from naturally growing trees have produced just such relationships (Schiegl, 1974; Gray and Thompson, 1976; Libby and others, 1976; Wilson and Grinsted, 1975). Some authors have been more cautious (Epstein and others, 1977; Friedman, 1975, written commun.; Ferhi and others, 1977; Grinsted and others, 1977), allowing for the complexity of plant photosynthetic processes in natural systems. There is no general agreement on which climatic variables control which isotopes, or the extent of their effect. Growth chamber experiments, carefully controlling the environmental variables seem to be a fruitful approach to resolving some apparent contradictions.

We have attempted to reconcile some recent growth-chamber experiments (Ferhi and others, 1977) with field studies, and to point out some of the problems found when trying a simple temperature interpretation of $\delta^{18}O$ variations in tree rings.

Ferhi and others measured $\delta^{18}O$ in dried bean-plant tissue (about 90 percent cellulose) which were grown under three different sets of conditions in which only one parameter was varied at a time: (1) relative humidity 90 to 100 percent, $\delta^{18}O_{SMOW}$ of irrigation water = -7.6 permil, temperature at 16, 21, 25, and 30°C; (2) relative humidity at 18 to 22, 40 to 60, 80 to 85, and 95 to 100 percent, $\delta^{18}O_{SMOW}$ of irrigation water = -7.4 permil, temperature = 21.5 ± 0.5°C; (3) relative humidity about 45 percent, $\delta^{18}O_{SMOW}$ of irrigation water = -14 permil, -9 permil, +12 permil, and +21 permil, temperature about 21°C. The plants were grown hydroponically with a film of oil to minimize evaporation from the water surface. Their $\delta^{18}O$ (plant tissue) results showed a striking linear effect with relative humidity; about 2 permil increase for every 10 percent decrease in relative humidity. As expected, the $\delta^{18}O$ depended also on the irrigation water, but only +0.15 permil plant tissue per permil water. The variable temperature experiments indicated little or no temperature effect.

More recently, we have repeated the experiments using soil (with an evaporation-suppressing membrane) rather than hydroponics, with similar results, but less humidity effect. The results of these experiments indicate three features of the behavior of oxygen isotopes in bean plants, which probably represent C_3-type plants in general: (1) no temperature effect; (2) a significant humidity effect; and (3) the irrigation water controls only 15 percent of the oxygen in plant tissue. The other 85 percent must derive from the atmospheric CO_2. Other studies (Gonfiantini and others, 1965; Wershaw and others, 1966; Dongmann, 1973; Lesaint and others, 1974; Strain, 1977; Epstein and others, 1977), have shown that leaf water evidently undergoes isotopic enrichment from kinetic evaporation (transpiration) from the leaves. The humidity effect that we observed is consistent with these observations.

If the humidity effect is so pronounced for oxygen isotopes, it must also affect the hydrogen isotopes. Since the non-exchangeable hydrogen in plants can only have derived from irrigation water, the influence of precipitation is at least as important in hydrogen isotopes. Epstein and others (1977) have discussed these points, and emphasized the desirability of measuring hydrogen as well as oxygen isotopes in tree rings for better understanding of past conditions.

A limited sampling of plants along a latitudinal gradient from Finland to the Ivory Coast illustrates the humidity and irrigation water effects combined. The high-latitude samples are relatively depleted in ^{18}O because of isotopically light precipitation and low transpiration. Mid-latitudes show highest val-

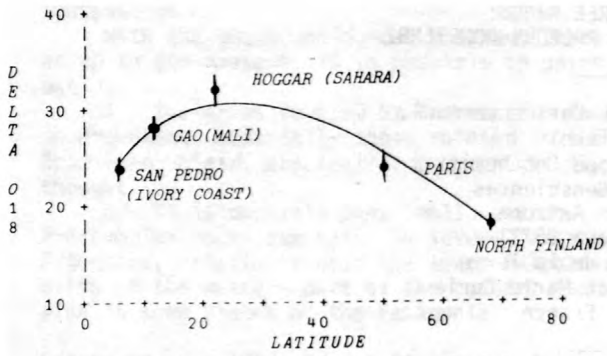

Figure 1.--$\delta^{18}O$ of plant tissue from plants grown at different latitudes.

ues due to both isotopically heavier precipitation and enrichment by transpiration. Lower values at equatorial latitudes (at least in coastal areas) illustrate the dominating effect of higher humidity, even though this area has the isotopically heaviest precipitation.

This modest study and preliminary results re-emphasize the potential value of the stable isotopes of all three of the major component elements in dendro-climatological studies, when used concurrently, and the need for further overlay of laboratory and field studies. The fact that each set of isotopes depends to a different degree on the climatic factors will eventually lead us to more quantitative reconstruction of past climates.

Plant cellulose $\delta^{18}O$ depends mostly on humidity and somewhat on irrigation water $\delta^{18}O$ which, in turn, is a function of temperature as shown by this study and by Epstein and others, (1977). Nonexchangeable cellulose δD depends on both of the above but in a different proportion (Epstein and others, 1977). Plant cellulose $\delta^{13}C$ depends on both temperature and precipitation (Arnold, 1978; Mazany and others, written commun.). When sufficient basic data are available, we should be able to construct numerical models which, with a few assumptions, will use the δ values and will result in paleoclimate data.

This work was sponsored in the United States by National Science Foundation Grant ATM77-06790 and the State of Arizona, and in France by the Centre National de la Recherche Scientifique and the Pierre and Marie Curie University.

Arnold, L. D., 1978, The climatic response in the $\delta^{13}C$ values of juniper trees from the American Southwest: (this conference).

Dongmann, G., 1973, Die $H_2{}^{18}O$-Anreicherung in den blättern transpirierender Pflanzen und ihre Bedeutung für die stationäre ^{18}O-Überhöhung in der Atmosphäre: RWTH Aachen, Germany, Ph.D. thesis.

Epstein, S., Thompson, P., and Yapp, C. J., 1977, Oxygen and hydrogen isotopic ratios in plant cellulose: Science, v. 198, no. 4323, p. 1209-1215.

Ferhi, A. M., Long, A., and Lerman, J. C., 1977, Stable isotopes of oxygen in plants--a possible paleohygrometer: Hydrology and Water Resources in Arizona and the Southwest, v. 7, p. 191-198.

Gonfiantini, R., Gratziu, S., and Tongiorgi, E., 1965, Oxygen isotopic composition of water in leaves, in Symposium on the use of isotopes and radiation in soil-plant nutrition studies: International Atomic Energy Agency, p. 405-410.

Gray, J., and Thompson, P., 1976, Climatic information from $^{18}O/^{16}O$ ratios of cellulose in tree rings: Nature, v. 262, p. 481-482.

Grinsted, J. J., 1977, A study of the relationships between climate and stable isotope ratios in tree rings: Hamilton, New Zealand, University of Waikato, Ph.D. thesis.

Lesaint, C., Merlivat, L., Bricout, J., Fontes, J. C., and Gautheret, R., 1974, Sur la composition en isotopes stables de l'eau de la tomate et du mais: Paris, Academie des Sciences, Compte Rendus, Series D, v. 278, p. 2925-2930.

Libby, L. M., Pandolfi, L. J., Payton, P. H., Marshall III, J., Becker, B., and Giertz-Sienbenlist, V., 1976, Isotopic tree thermometers: Nature, v. 261, p. 284-288.

Schiegl, W. E., 1974, Climatic significance of deuterium abundance in growth rings of Picea: Nature, v. 251, p. 582-584.

Strain, B. R., 1977, Diurnal enrichment of naturally occurring heavy water ($H_2{}^{18}O$) in plant leaves and its possible contribution to the isotopic composition of the global atmosphere: Bulletin of the Ecological Society of America, v. 58, no. 2, p. 34.

Wershaw, R. L., Friedman, I., and Heller, S. J., 1966, Hydrogen isotopic fractionation of water passing through trees, in Hobson, G. D., and Speers, G. C., eds., Advances in Organic Geochemistry: Oxford, Pergamon Press, p. 55-67.

Wilson, A. T., and Grinsted, M. J., 1975, Paleotemperatures from tree rings and the D/H ratio of cellulose as a biochemical thermometer: Nature, v. 257, p. 387-388.

THE OXYGEN ISOTOPE GEOCHEMISTRY OF ARCHEAN ROCKS FROM THE SUPERIOR PROVINCE

By Frederick J. Longstaffe[1], Henry P. Schwarcz[2], and Robert H. McNutt[2]
[1]Department of Geology, University of Alberta Edmonton, Alberta, Canada
[2]Department of Geology, McMaster University, Hamilton, Ontario, Canada

The oxygen isotope compositions have been measured for plutonic granitoids, metavolcanic rocks, clastic metasedimentary rocks, and granitoid gneisses from the Archean Superior Province of northern Ontario.

The greenschist facies volcanogenic metasedimentary rocks range in $\delta^{18}O$ from 8.0 to 13.3 permil; the relatively low values emphasize the immaturity of these clastic units. In some areas, however, a small but significant enrichment in ^{18}O can be shown to accompany increasing sediment maturity.

The felsic metavolcanic rocks range in $\delta^{18}O$ from 7.5 to 13.0 permil; oxygen isotope compositions, therefore, cannot be used alone to discriminate between Archean metamorphosed volcanogenic sedimentary rocks and felsic (including pyroclastic) metavolcanic rocks. Most of the felsic metavolcanic rocks with anomalously high $\delta^{18}O$ values occur within the Burditt Lake metavolcanic sequence; ultramfic rocks ($\delta^{18}O$ of 5.3 to 6.8 permil and mafic metavolcanic rocks ($\delta^{18}O$ of 7.0 to 9.2 permil in this volcanic pile have also been isotopically altered. The isotopic history of the Burditt Lake felsic metavolcanic rocks was further complicated by the intrusion of the Burditt Lake granodiorite; felsic metavolcanic rocks near the pluton have been depleted in $\delta^{18}O$, probably by pluton-derived magmatic fluids.

$\delta^{18}O$ values measured for twenty greenschist to amphibolite facies mafic metavolcanic rocks range from 4.4 to 9.4 permil. However, no consistent relationships between $\delta^{18}O$ and K, Rb, Sr and Ba were observed. Greenschist facies samples, however, are the most enriched in ^{18}O; only amphibolite facies samples have $\delta^{18}O$ values less than 7.0 permil.

Most of the $\delta^{18}O$ values for the plutonic granitoids fall within Taylor's (1968) I to H_2 categories for granitic rocks, and no values higher than 9.3 permil were measured (fig. 1); most of the $\delta^{18}O$ values of the metaigneous Footprint, Kenora, Cedar Lake, and Clay Lake. Gneisses also lie within this group (fig. 2). Thus, as Taylor (1977) has noted for other Archean granitoids, these rocks are less enriched in ^{18}O than most Phanerozoic granitoids. This may reflect their derivation from more primitive, less ^{18}O-rich sources than were involved in the formation of Phanerozoic batholiths.

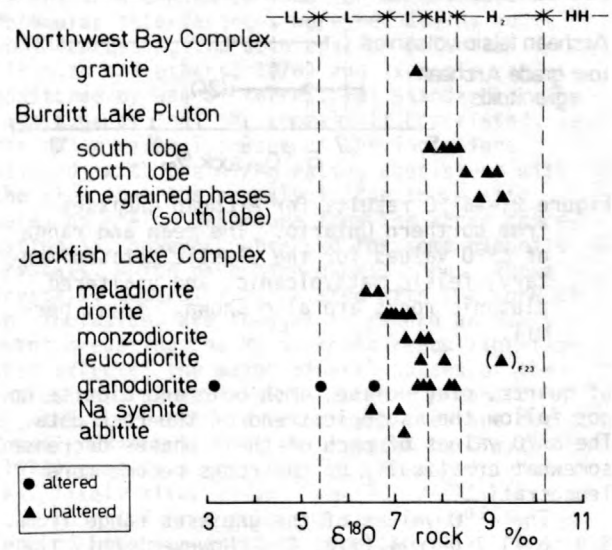

Figure 1.--$\delta^{18}O$ results for Archean plutonic rocks from northern Ontario. The classification scheme (LL, L, I, H_1, H_2, HH) is from Taylor (1968). °/₀₀, permil.

The anomalously low $\delta^{18}O$ values of some granodiorites of the Jackfish Lake Complex (fig. 1) are due to fault-related alteration. Mineral phases from the altered zone are grossly out of oxygen isotopic equilibrium; microcline, for example, has a $\delta^{18}O$ value of 3.93 permil, lower than coexisting hornblende (4.70 permil). The isotopic depletions are accompanied by chemical and mineralogical alteration. Interaction with ancient meteoric fluids is the most likely explanation of these data.

The $\delta^{18}O$ values of unaltered Jackfish Lake Complex rock types range from 6.4 to 9.2 permil (fig. 1) and generally increase as the rocks become more leucocratic. This reflects the mineralogical evolution of the suite from rock types containing up to 70 modal percent amphibole ($\delta^{18}O$ of 4.4 to 6.4 permil) to less voluminous felsic rocks containing less than 5 modal percent amphibole. Only the Na-syenite and albitite do not follow this trend; they may have exchanged isotopically with surrounding mafic metavolcanic rocks. Curiously, the $\delta^{18}O$ values

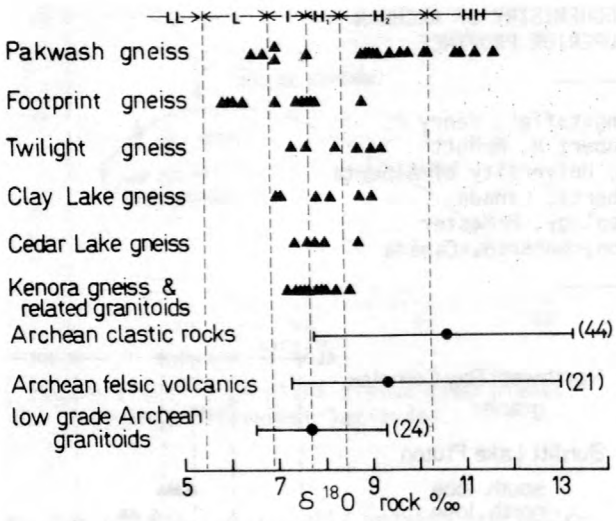

Figure 2.--$\delta^{18}O$ results for Archean gneisses from northern Ontario. The mean and range of $\delta^{18}O$ values for the clastic metasedimentary, felsic metavolcanic, and unaltered plutonic rocks are also shown. °/₀₀, permil.

of quartz, plagioclase, amphibole and biotite do not follow the isotopic trend of the rock data. The $\delta^{18}O$ values of each of these phases decrease somewhat erratically as the rocks become more leucocratic.

The $\delta^{18}O$ values of the gneisses range from 5.9 to 11.7 permil (fig. 2). However, only the Pakwash Gneiss has a $\delta^{18}O$ values higher than those measured for the plutonic granitoids. The Pakwash Gneiss is a middle to upper amphibolite-facies migmatized sequence of interlayered metagreywacke, shaley metagreywacke and meta-argillite (Beakhouse, 1977). In the least migmatized portions of the gneiss, the metagreywacke layers have been unaffected by melting and have $\delta^{18}O$ values of 8.8 to 11.7 permil. These values overlap the isotopic range of the greenschist-facies metagreywackes (fig. 2) and are consistent with a volcanogenic sedimentary protolith for these rocks. More highly migmatized portions of the gneiss are characterized by the abundant development of felsic leucosome in pelitic layers and the injection of leucosome into the metagreywacke units. These metagreywacke layers have low $\delta^{18}O$ values (6.5 to 7.0 permil) (fig. 2). Mineral phases from these samples are also depleted in ^{18}O but are not grossly out of oxygen isotopic equilibrium.

A similar pattern occurs in the tonalitic to granitic Footprint Gneiss. Unmigmatized portions have $\delta^{18}O$ values compatible with a plutonic granitoid protolith, but more deformed and highly migmatized samples are depleted in ^{18}O (5.9 to 7.0 permil). Thus, high temperature isotopic exchange with a low ^{18}O reservoir (6 permil) seems to have accompanied the partial melting of the Pakwash and Footprint Gneisses. This hypothetical reservoir is capable of producing final isotopic compositions in the gneisses of 6 to 7 permil, regardless of their initial values. Underlying basalt is one possible candidate for such a reservoir.

Up to the onset of partial melting, the $\delta^{18}O$ values of Archean granitoid gneisses reflect the nature of their protoliths. At higher metamorphic grades, accompanied by partial melting, the oxygen isotope composition of Archean gneisses cannot be relied upon to reflect the true isotopic compositions of their parent rock types.

Beakhouse, G. P., 1977, A subdivision of the western English River sub-province: Canadian Journal of Earth Sciences, v. 14, p. 1481-1489.

Taylor, H. P., Jr., 1977, Water/rock interactions and the origin of H_2O in granitic batholiths: Geological Society of London Quaternary Journal, v. 133, p. 509-558.

_____1968, The oxygen isotope geochemistry of igneous rocks. Contributions to Mineralogy and Petrology, v. 19, p. 1-71.

RADIOGENIC ^{26}MG FINE-SCALE DISTRIBUTION IN CA-AL INCLUSIONS OF THE ALLENDE AND LEOVILLE METEORITES

By Jean-Claude Lorin and Mireille Christophe Michel-Lévy
Laboratoire de Minéralogie, Université Pierre et Marie Curie, Paris, France, and
Laboratoire de Géochimie, Université Paris VII, Paris, France

It has been verified by ion-microprobe analysis (Hutcheon and others, 1977; Bradley and others, 1978; Steele and others, 1978) that the correlation between excess ^{26}Mg and the Al/Mg ratio observed by Lee and others (1977) in separated mineral phases of Ca-Al inclusions of the Allende meteorite also holds on a much finer scale, inside single mineral grains. It has been further demonstrated by the same technique (Lorin and others, 1977; Lorin and Christophe, 1978) that the ^{26}Mg anomaly is by no means restricted to the Allende meteorite but is a general feature of CV meteorites, in which Al is largely concentrated in refractory inclusions. Results of the study of one Allende and two Leoville inclusions are reported in table 1 and illustrated in figures 1-4. Analyses were performed on a CAMECA IMS 300 ion microscope. Molecular interferences were reduced by suitably depressing the acceleration potential (Shimizu and others, 1978) and isotopic ratios monitored by use of terrestrial standards. The magnitude of the ^{26}Mg anomaly is correlated, in the major mineral phases of the inclusions studied, with the Al/Mg ratio, consistent with the view that the anomaly is due to in situ decay of ^{26}Al. Departure from the above correlation is, however, observed for some hibonite crystals, which have high excess ^{26}Mg. These crystals, generally associated with the core of the inclusion, are thought to record an early event predating the Mg isotopic reequilibration that affected the major mineral phases of the inclusions, as well as rim-forming hibonite crystals. That these inhomogeneities are due to fossil radiogenic ^{26}Mg as proposed by Clayton (1975) remains a possible but, in our opinion, less likely alternative. The ^{26}Al/^{27}Al ratio of c.a. 10^{-3} inferred from the radiogenic ^{26}Mg content of hibonite crystals from Leoville L $\neq$ 4 inclusion constitutes a lower limit to the initial value. This ratio is so close to the expected production ratio in explosive carbon burning (Truran and Cameron, 1978) that it implies that solar system formation closely followed supernova explosion, and suggests the existence of a causal relationship between the two events, as proposed by Cameron and Truran (1978). The small amount of dilution of freshly

Table 1.--Magnesium isotopic composition and ^{27}Al/^{24}Mg ratio for one Allende and two Leoville inclusions

[HV, accelerating potential, in volts]

Mineral	HV	^{25}Mg/^{24}Mg	^{26}Mg/^{24}Mg	^{27}Al/^{24}Mg (IMPA)[1]
Allende inclusion 3529-42				
Hibonite 2 ---	4400	0.1287±20	0.1452±19	50
Hibonite 1 ---	4400	0.1278±11	0.1473±18	18
Hibonite 3 ---	4400	0.1273±21	0.1461±21	91
Hibonite 5 ---	4400	0.1282±26	0.1414±23	25
Melilite 1 ---	4400	0.1286±19	0.1436±17	37
Melilite 2 ---	4400	0.1277±27	0.1488±56	50
Spinel 2 -----	4350	0.1278±18	0.1415±51	2.5
Spinel 3 -----	4400	0.1270±8	0.1400±29	2.5
Leoville inclusion L 1				
Anorthite 1 --	4407	0.1290±37	0.1586±35	250
Anorthite 2 --	4400	0.1272±22	0.1450±42	50
Anorthite 3 --	4400	0.1277±50	0.1542±63	280
Anorthite 4 --	4400	0.1277±20	0.1525±41	300
Anorthite 5 --	4400	0.1254±93	0.1558±89	350
Melilite 1 ---	4360	0.1265±23	0.1395±33	2.5
Leoville inclusion L#4				
Hibonite 1 ---	4320	0.1281±38	0.1626±35	22
Melilite 1 ---	4400	0.1256±13	0.1405±23	35
Phase 1 ------	4350	0.1276±23	0.1401±17	0.2

[1]IMPA, Ion microprobe analysis.

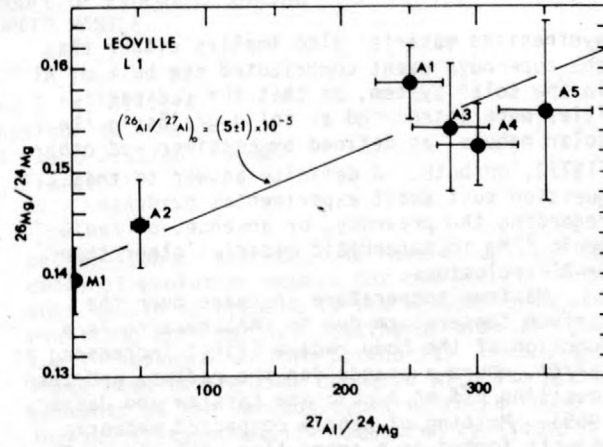

Figure 1.--^{27}Al/^{24}Mg versus ^{26}Mg/^{24}Mg diagram for Leoville L1.

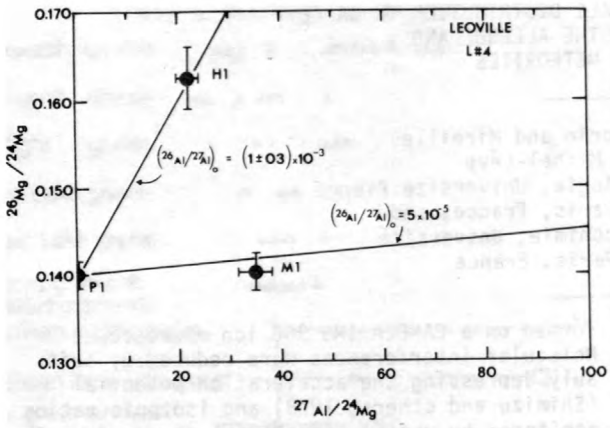

Figure 2.--$^{27}Al/^{24}Mg$ versus $^{26}Mg/^{24}Mg$ diagram for Leoville L#4.

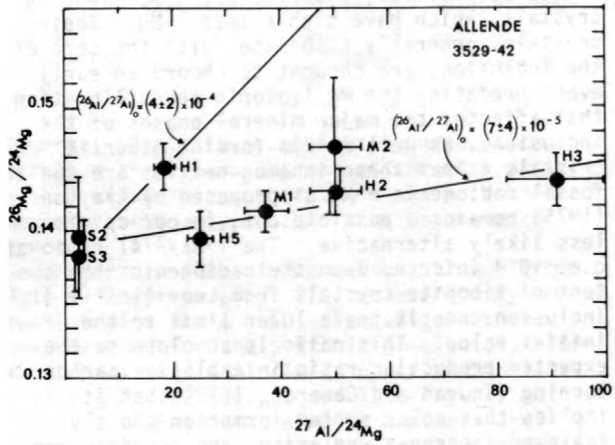

Figure 3.--$^{27}Al/^{24}Mg$ versus $^{26}Mg/^{24}Mg$ diagram for Allende 3529-42.

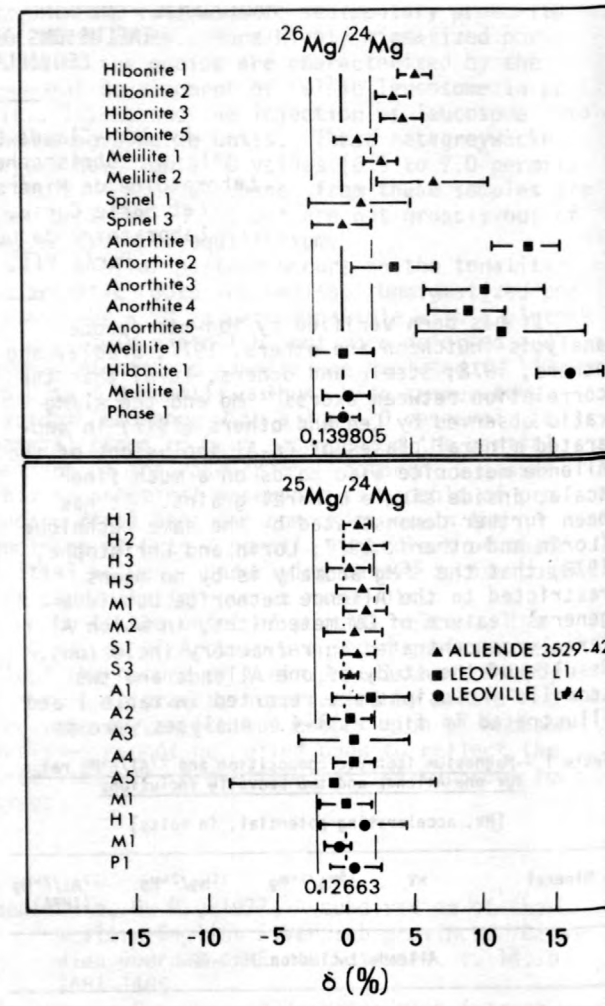

Figure 4.--Summary diagram of $^{26}Mg/^{24}Mg$ and $^{25}Mg/^{24}Mg$ ratios in Allende 3529-42, Leoville L1, and Leoville L#4.

synthesized material also implies either that the supernova event contributed the bulk of Al in the solar system, or that the radioactivities were introduced as solid grains in the solar nebula, as defined by Lattimer and others (1977), or both. A definite answer to this question must await experimental evidence regarding the presence, or absence, of radiogenic ^{26}Mg in meteoritic material other than Ca-Al inclusions.

Maximum temperature increase over the surface temperature due to ^{26}Al heating is a function of the body radius (first increasing as $Aa^2/6K$, where a stands for the radius, and then levelling off at $A/\rho c\lambda$; see Carslaw and Jaeger, 1959). Melting of poorly compacted meteoric objects formed on a short time scale by rapid accumulation of refractory dust material and followed by quasi-instantaneous cooling due to the ensuing drastic changes in the material thermal properties may provide a mechanism for the formation of the parent rocks of Ca-Al inclusions. Discovery of ^{26}Al leads to a revival of many of the ideas expressed by Fish and others (1960). As proposed by these authors, superheating in growing planetesimals may induce quasi-volcanic eruptions. Superheating may also provoke catastrophic disruptions, as in small bodies where internal gas and vapor pressure will be balanced uniquely by the tensile strength of the overlying material. Fate of the meteorite parent bodies (survival, differentiation, and so forth) will depend critically upon the accretion rate, which, in turn, is expected to be a function of heliocentric distance (Safronov, 1972). If the Mg isotopic-reequilibration event which affected many Ca-Al inclusions is contemporaneous with

the accretion of the inclusions onto planetary objects, the accretion rate of the CV parent body should not have exceeded 0.5 cm yr^{-1} in order to account for the low peak temperatures experienced by the bulk CV material. This would imply a growth time of a million years for this planetary object, which contrasts with the apparent sharp isochronism of Mg isotopic-reequilibration in the Ca-Al inclusions. A search in unmetamorphosed carbonaceous material for the effects of 2×10^{17} photons of 1.8 MeV and 8×10^{15} photons of 1.13 MeV emitted per gram of Ca-Al inclusion (corresponding to a total dose of about 7×10^{9} rads) could possibly shed some light upon this apparent discrepancy.

Bradley, J. G., Huneke, J. C., and Wasserburg, G. J., 1978, Ion microprobe evidence for the presence of excess ^{26}Mg in an Allende anorthite crystal: Journal of Geophysical Research, v. 183, p. 244-254.

Cameron, A. G. W., and Truran, J. W., 1977, The supernova trigger for formation of the solar system: Icarus, v. 40, p. 447-461.

Carslaw, H. S., and Jaeger, J. C., 1959, Conduction of heat in solids: London, Oxford University Press, 2nd ed.

Clayton, D. D., 1975, ^{22}Na, Ne-E extinct radioactive anomalies and unsupported ^{40}Ar: Nature, v. 257, p. 36-37.

Fish, R. A., Goles, G. G., and Anders, E., 1960, The record in the meteorites-III; On the development of meteorites in asteroides bodies: Astrophysics I, v. 132, p. 243-258.

Hutcheon, I. D., Steele, I. M., Solberg, T. N., Clayton, R. N., and Smith, J. V., 1977, Ion microprobe measurements of excess ^{26}Mg in Allende inclusions [abs.]: Meteoritics, v. 12, p. 262.

Lattimer, I. M., Schramm, D. N., and Grossman, L., 1977, Supernovae, grains, and the formation of the solar system: Nature, v. 269, p. 116-118.

Lee, T., Papanastassiou, D. A., and Wasserburg, G. J., 1977, Aluminum 26 in the early solar system; fossil or fuel?: Astrophysics I, v. 211, p. L107-L110.

Lorin, J. C., and Christophe, Michel-Levy M., 1978, Heavy rare metals and magnesium isotopic anomalies studies in Allende and Leoville calcium-aluminum rich inclusions, in, Lunar and Planetary Science IX: Houston, The Lunar and Planetary Institute, p. 660-662.

Lorin, J. C., Shimizu, N., Christophe Michel-Levy, M., and Allegre, C. J., 1977, The Mg isotope anomaly in carbonaceous chondrites; an ion-probe study [abs.]: Meteoritics, v. 12, p. 299-300.

Safronov, V. S., 1972, Evolution of the protoplanetary cloud and formation of the Earth and planets: Israel Program for Scientific Translations, Jerusalem.

Shimizu, N., Semet, M., and Allegre, C. J., (in press), Geochemical application of quantitative ion-microprobe analysis: Geochimica Cosmochimica Acta.

Steele, I. M., Smith, J. V., Hutcheon, I. D., and Clayton, R. N., 1978, Allende inclusions; cathodoluminescence petrography; anorthite and spinel chemistry; Mg isotopes, in, Lunar and Planetary Science IX: Houston, The Lunar and Planetary Institute, p. 1104-1106.

Truran, W., and Cameron, A. G. W., 1978, ^{26}Al production in explosive carbon burning: Astrophysics I., v. 219, p. 226-229.

REE GEOCHEMISTRY OF UPPER MANTLE REPRESENTATIVE BODIES--THE LHERZOLITE-TYPE ALPINE PERIDOTITE MASSIFS--CONSECUTIVE MODEL OF EVOLUTION OF THE EARTH'S UPPER MANTLE

By M. Loubet and C. J. Allegre
Institut de Physique du Globe
Universite Paris 6, 4 Place Jussieu, 75230
Paris, France

Various authors have deduced from studies made on materials representative of the upper mantle (lherzolite-type peridotite massifs and nodules) that the composition of the peridotites, which constitute the most important part of these materials, corresponds to that of an originally uniform upper mantle later subjected to one or more partial melting processes. The relationship of such a model to the nature of the upper mantle can be tested using a set of elements with variable sensitivities to the melts, such as the REE. We have calculated theoritical evolution models for the REE contents that should be present in the various products resulting from partial melting of a mantle originally having a uniform peridotitic composition. These results are then compared with the REE contents of the various types of rocks found in lherzolite-type massifs (measured by isotopic dilution technique). Our studies were carried out on various massifs: Beni-Bouchera (Morocco), Lanzo (Alps), Lherz, and Freychinede

(French Pyrenees). Associated with the common lherzolites in these massifs are layers displaying a mean pyroxenic composition, the origin of which gives rise to controversial interpretations. The origin of these layers is discussed on the basis of the models developed.

The most noticeable conclusions of the models are apparent in figure 1, in which one specific percentage of partial melting has only been considered. The primary peridotitic upper mantle (CO) is assumed to have a constant chondrite normalized REE pattern. Two different types of partial melting processes giving rise to two different residual peridotite trends were studied: (1) an equilibrated type partial melting process (batch melting) (curve Re) and (2) a fractionated type partial melting process (curve Rf). The melts Me and Mf produced by these processes are those in equilibrium with the peridotites Re and Rf, respectively. These melts further evolve after their formation through a fractional crystallization process giving rise to various cumulates (respectively Ce and Cf)

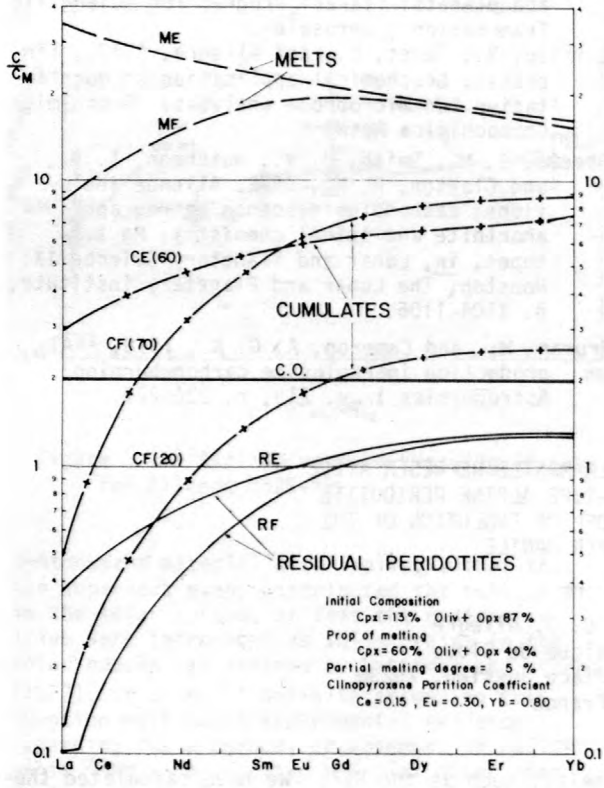

Fig. 1.--Model of evolution of the REE in a peridotitic upper mantle affected by a 4 percent partial melting process in a chondrite normalized representation. Residual peridotites, Melts produced, and Cumulates crystallized from the melts are represented. See terminology in Text. Clinopyroxene partition coefficients from Tanaka and Nishizawa (1975).

that we have characterized by their clinopyroxene content (number in parentheses). Garnet is absent in all the rock facies. As a consequence, the fractionation of the REE appears to be controlled mainly by the clinopyroxene phase throughout the various events. The most important conclusions are:

1. The residual peridotites resulting from a low degree partial melting present typical light REE depleted patterns. Considering a set of residual peridotites, we should expect large variations of their light REE contents (the content depending on the degree and the type of the partial melting process) and relatively low variations of their heavy REE contents.

2. The melts produced present REE patterns characterized by a large variety of light REE fractionations relative to the heavy REE.

3. The cumulates as well as the melts, can display REE patterns having a large variety of light REE versus heavy REE fractionations. As a consequence of the major role of clinopyroxene, the cumulates crystallized from the same melt, but displaying various mineralogical compositions, should present parallel REE patterns. These patterns should also be parallel to that of the residual peridotite which gave rise to the melt.

In figure 2 are plotted the REE contents of common lherzolites obtained from various lherzolite-type massifs analyzed either by us or by others. These peridotites, which comprise the most important part of these massifs, present the characteristics that according to our model we can expect for residual peridotites (Loubet and others, 1975). Additional data and, in par-

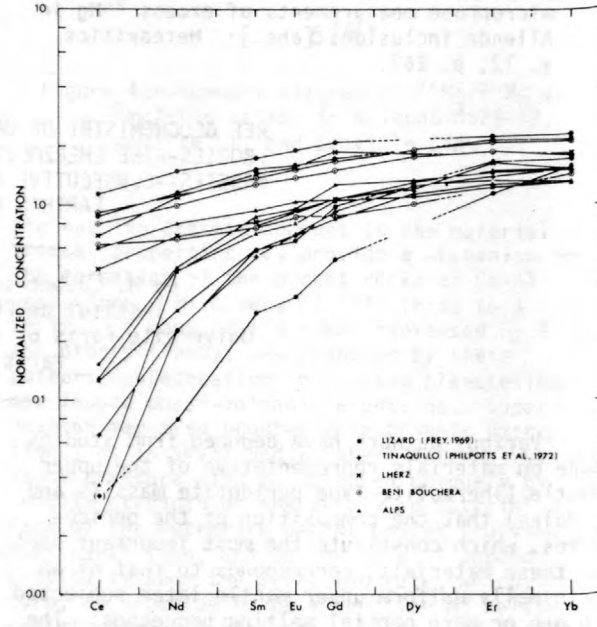

Fig. 2.--Chondrite normalized REE contents of peridotites from lherzolite-type massifs.

ticular, Ni contents (Henry Bougault analysis) have given further support to this interpretation. The Ni contents of these peridotites lie in a narrow range which does not exceed 20 percent of the mean value. Taking into account possible variations of the mineralogical composition of the samples, this is the range of concentration expected for such an element having great affinities of the solid phases in a residual set of rocks of originally uniform composition.

The same agreement with the model was found between the REE contents of the pyroxenite layers and those of the "cumulates". The cumulate nature of these layers has been confirmed by analyzing elements highly attracted by the solid phases, such as the Ni. In figure 3 and 4 are shown, as examples, various pyroxenite layers we analyzed in the Lherz and in the Freychinede massifs. We notice a large variety of light REE /heavy REE fractionation patterns in these rocks (most of them are light REE depleted but some are light REE enriched) as expected for cumulates derived from melts produced by a partial melting process. A set of pyroxenite layers sampled in one particular locality of the Freychinede massif presents some very interesting features. The REE patterns of these layers are highly light REE depleted and characteristically approximately parallel one to another. Such parallelism between rocks presenting very different petrological compositions can be explained if these rocks crystallized from the same type of melt and if the clinopyroxene controlled the fractionation of the REE during the crystallization process. A comparison of the REE patterns of this set of layers with that of the common peridotite permits one to conclude that the original melt of these layers could not have been in equilibrium with the common peridotite of this massif. This is a normal feature in a mantle evolving by partial melting processes but which is not permissible in a model forming such massifs by the crystallization of a huge magma (Conquere, 1977).

In general, a good concordancy is observed with the conclusions of the model represented in figure 1; however, some discrepancies are apparent. They concern specifically the light REE content of some garnet pyroxenite layers, which is too low. The primary clinopyroxene content of this type of rock is fairly high (perhaps the highest of all the rocks from these massifs). According to this model, we should expect the light REE content of this rock to be several times higher than that of the common peridotites. In figure 4, one can see that the garnet clinopyroxenite from Lherz (70 - 291) presents light REE contents 10 times lower than we should expect. We explain such discrepancies by the occurrence in these massifs of a second selective partial melting process, that is one which affected the most differentiated layers. The arguments supporting this interpretation are the following: (1) such discrepancies are mainly noticed in the garnet clinopyroxenite layers which are the most differentiated layers, that is, the ones which crystallized last; (2) some

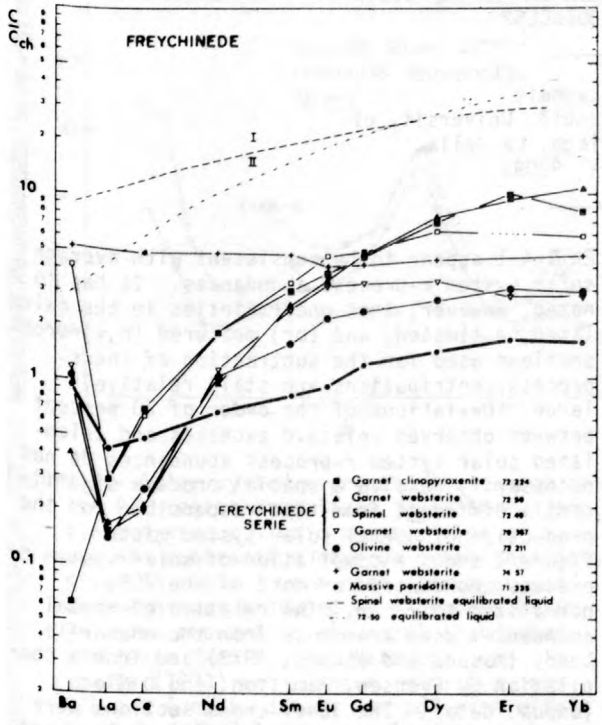

Fig. 3.--Chondrite normalized REE contents of pyroxenite layers from Freychinede massif (French Pyrenees).

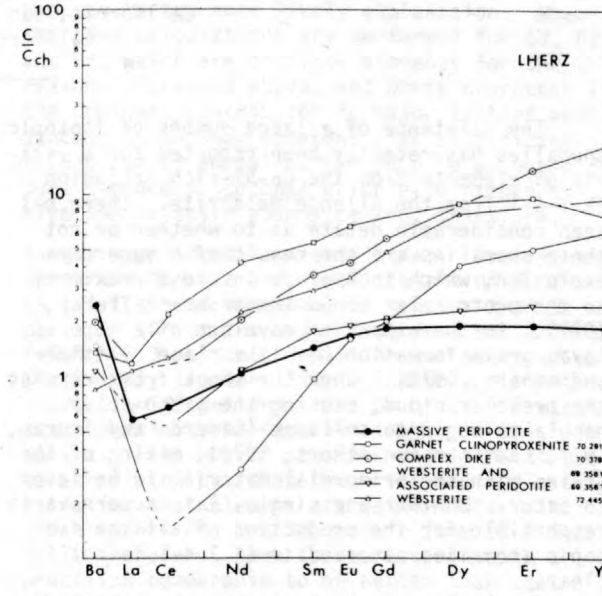

Fig. 4.--Chondrite normalized REE contents of pyroxenite layers from Lherz massif (French Pyrenees).

massifs mark such a late partial melting event in the form of dikes cutting the peridotitic massif; and (3) Rb-Sr isotope studies performed on these rocks allow the same interpretation (M. Polve and C. J. Allegre, unpublished data).

The final picture resulting from our studies is one of an upper mantle, originally uniform, affected by successive partial melting processes. In the massifs we studied, at least two successive partial melting events were detected. The first event affected the massive peridotites giving rise to the pyroxenite layers, which represent various cumulates crystallized from the melts produced. The actual lherzolites represent the residual solid left either after this event or after a series of partial (2 to 5 percent) melting events, the last event invariably masking the effects of the earlier ones. The second partial melting event detected was of lower intensity than the first one. It selectively affected the pryoxenite layers in some massifs (Lherz, Freychinede, Beni-Bouchera massifs), but elsewhere included the peridotites, as in the Lanzo massif. In this case, a sort of reequilibration process of the pyroxenite layers with the common peridotites is observed.

From a geodynamical point of view these successive partial melting events can be allocated to successive uprising processes of the upper mantle through convection, orogenic events, etc. From a petrological point of view, we should expect that the various partial melting events affected different types of rocks and gave rise to various volcanic rock-types. Our conclusions should also help to clarify the apparent isotopic heterogeneities of the upper mantle, which is seen in the analysis of oceanic volcanic rocks.

Conquere, F., 1977, Petrologie des roches litees dans les complexes ultramafiques de l'Ariege, France: Bulletin de la Societe Francaise de Mineralogie et de Cristallographie, p. 101.

Loubet, M., Shimizu, N., and Allegre, C. J., 1975, Rare earth elements in alpine peridotites: Contributions to Mineralogy and Petrology, v. 53, p. 1-12.

Philpott, J. A., Schnetzler, C. C., Thomas, H. H., 1972, Petrogenetic implications of some new geochemical data on eclogitic and ultrabasic inclusions: Geochimica Cosmochimica, Acta, v. 36, p. 1131-1166.

Tanaka, T., and Nishizawa, O., 1975, Partitioning of REE, Ba, and Sr between crystal and liquie phases for a natural silicate system at 20 kb pressure: Geochemical Journal, v. 9, no. 3, p. 161-166.

REE ISOTOPIC ANOMALIES IN EK 1-4-1: TRUTH AND CONSEQUENCES?

By G. W. Lugmair
Chemistry Department, B-017, University of California, San Diego, La Jolla, California 92093

The existence of a large number of isotopic anomalies has recently been reported for a variety of elements from the Ca-Al-rich inclusion EK 1-4-1 from the Allende meteorite. There has been considerable debate as to whether or not these anomalies are the result of a supernova explosion, which took place in close proximity to the proto-solar cloud (Cameron and Truran, 1977). In the expanding envelope of a supernova, grain formation may take place (Lattimer and others, 1978). When the shock front reaches the presolar cloud, causing the proto-solar nebula to begin to collapse (Cameron and Truran, 1977; Lattimer and others, 1978), mixing of the grains with the primordial material is believed to occur. Whether one single, late supernova is responsible for the production of all the isotopic anomalies observed in EK 1-4-1 is not clear.

One important constraint can be obtained from the isotopic data of the REE. Lugmair and others (1978) have discussed the fact that the isotopic excesses obtained for Sm and Nd from EK 1-4-1 appear to be consistent with average solar system r-process abundances. It has to be noted, however, that uncertainties in the calculated, estimated, and (or) measured (n,γ)-cross sections used for the subtraction of the s-process contributions are still relatively large. Deviations of the order of 20 percent between observed relative excesses and calculated solar system r-process abundances do not necessarily resolve a special process significantly different from that responsible for the production of normal solar system matter. Figure 1 shows a compilation of solar system r-process abundances for most of the REE, normalized to ^{154}Sm. The relative elemental abundances used are those from the chondrite Leedy (Masuda and others, 1973) and from a compilation by Evensen, Hamilton, and O'Nions (unpub. data). The 30keV cross sections were taken from Allen and others (1971), Holmes and others (1976), and Cullen and others (1976) and are given in table 1. The square symbols indicate r-only isotopes. There exist two curves:

one for the even-mass nuclides and the other for the odd-mass nuclides. The difference between odd- and even-mass yields in the region between Nd and Gd appears to be on the order of 25 to 40 percent. This relative difference becomes significantly smaller in the region of the "REE-peak" from Tb through Er. It has been suggested that this "REE-peak" is partly due to spontaneous fission of nuclei with A ≈260 to 280 (Cameron, 1957; Schramm and Fowler, 1971). More recently, extensive calculations by Steinberg and Wilkins (unpub. data) have shown that extension of the r-process to neutron numbers near 200 could indeed account for the high REE abundances in the region around A = 164. Fission-yield curves are known to be a smooth function with mass number. Therefore, addition of fission products to a constant or slowly decreasing odd-even pattern throughout the region between A = 160 and 170 could account for the decrease in the relative odd-even effect in the total r-process yield. Estimates obtained from Xe measurements in EK 1-4-1 (Papanastassiou and others, 1978; Marti, oral commun.) show that the abundance of ^{244}Pu in this inclusion was very similar to that observed in other solar system materials at 4.56 b.y. ago. If most of the r-process component in this inclusion has indeed its origin in a very recent supernova event, then either Xe was lost by diffusion or ^{244}Pu was not produced in the same event. Hence, if the latter is true, heavier nuclei

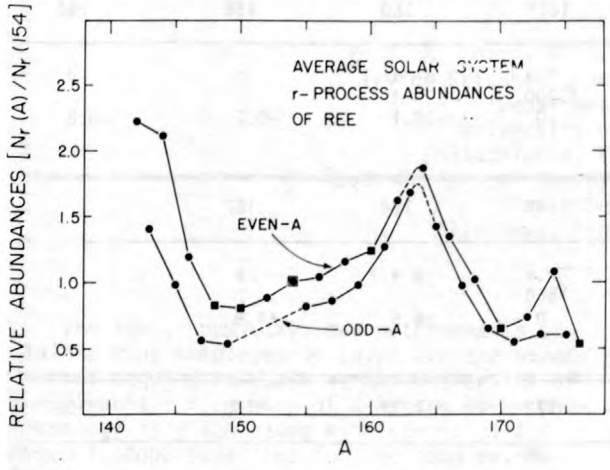

Figure 1.--Solar system r-process abundances in the REE region normalized to ^{154}Sm = 1 are plotted versus atomic number. For s-process subtraction neutron cross sections given in table 1 were used. Squares indicate isotopes produced by r-process only. Relative chondritic elemental abundances are taken from Masuda, Nakamura, and Tanaka (1973) and Evensen, Hamilton, and O'Nions (unpub. data). An odd-even effect appears to be clearly resolved throughout the REE region and is indicated by the two parallel curves.

with neutron numbers above 184 could also not have been produced. Therefore, if the fission hypothesis is correct, large negative anomalies should be detectable in the region around A = 164. On the other hand, if the relative excesses in REE heavier than Sm are similar to those found in Nd and Sm, then either the fission hypothesis is incorrect and a special characteristic of the nuclear structure is responsible for the "REE-peak" (for example, Burbidge and others, 1957) or they are the result of incomplete mixing of "ancient" classical (r + p) and s-process products.

In table 1, we show the calculated (labelled "expected") relative anomalies ε (in parts in 10^4) of all REE having more than four isotopes for the case of normal r-process addition (or s-process depletion). The r-process excess ε = 37.6, as obtained for ^{154}Sm, has been used for all elements and no fractionation between r- and p-products has been assumed (Lugmair and others, 1978). All values are calculated in a manner such that normalization and fractionation correction procedures for the "expected" EK 1-4-1 mass spectrometric data are the same as those typically employed for terrestrial normals. For illustration, the measured Sm and Nd isotopic anomalies, as obtained by us, are compared with the calculated values before special correction and normalization procedures, such as discussed by Lugmair and others (1978), are applied. It can be seen from table 1 that isotopic anomalies of a few permil caused by r-process excesses can be readily resolved for these two elements on normally treated data. Also, the calculated and the measured ε-values are in remarkably good agreement, at least for the major isotopes, which led us to suggest earlier that excess of normal solar system r-process is the most likely explanation. When the same calculations are performed for Gd, Dy, and Er, which are critical elements for the reasons discussed above, and where r-process is the dominant contributor to major isotope abundances, it becomes apparent that significant resolution of anomalies can only be expected for pure s-process isotopes which also happen to have low relative abundance and, therefore, larger experimental uncertainties. Preliminary measurements on a very small sample of Dy from EK 1-4-1 showed no anomalies greater than 9 parts in 10^4 on the major isotopes, but a large (-0.6 ± 0.3 percent) depletion was observed on the s- only isotope ^{160}Dy. The only element where significant anomalies on a major isotope can potentially be resolved is Yb (^{176}Yb). Yb, however, lies beyond the "REE-peak" and it has to be pointed out that the cross-section estimates for this element are rather uncertain. The elements Gd, Dy, Er, and Yb from EK 1-4-1 will, therefore, have to be measured with a precision comparable to or better than that obtained for Sm, if isotopic anomalies due to classical r-process excess should be resolved. If significantly different results from those

Table 1.--Measured and expected relative REE isotopic anomalies ε (in parts in ten thousand) in EK 1-4-1

[Asterisk, *, indicates isotopes used for normalization or fractionation correction. p.o.p., process of production. σ, (n, γ) cross sections at 30keV in mb.]

Element	Isotopes						
Nd	150	148*	146	145	144*	[1]143	142
p.o.p. ------	r	r	s,r	r,s	s,r	r,s	s,(p)
σ ----------			[2]102	[3]600	[3]100	[3]425	[2]76
Expected --	-7.1	0	-12.2	+3.8	0	+11.2	[4]-16.3
Measured --	-6.9±1.1	0	-12.3±1.4	+2.7±1.6	0	+13.3±1.6	-9.6±1.6
$N_s\sigma$ interpolated between $N_s\sigma$ (148-Sm) and $N_s\sigma$ (142-Nd) as smooth function of mass.							
Sm	154	152*	150	149	148	147*	144
p.o.p. ------	r	r,s	s	r,s	s	r,s	p
σ ----------		[3]450	[3]370	[3]1620	[3]260	[3]1150	
Expected --	+10.5	0	-29.4	+3.0	-30.5	0	+4.5
Measured --	+12.4±1.2	0	-30.7±1.6	+4.4±0.9	-33.4±1.6	0	-8.4±5.8
Gd	160*	158	157	156*	155	154	152
p.o.p. ------	r	r,s	r,s	r,s	r,s	s	s,p
σ ----------		[2]302	[3]2070	[2]520	[3]2280	[3]520	
Expected --	0	-4.6	+1.7	0	+3.8	-31.6	[5]+8.0
$N_s\sigma$(154) was used.							
Dy	164*	163	162	161*	160	158	156
p.o.p. ------	r,s	r,s	r,s	r,s	s	p	p
σ ----------	[6]820	[3]1600	[3]470	[3]2800	?		
Expected --	0	+0.3	-2.0	0	-37.1	-0.2	-0.8
$N_s\sigma$(154-Gd) was used.							
Er	170*	168	167	166*	164	162	
p.o.p. ------	r	r,s	r,s	r,s	p + ?	p	
σ ----------		[3]400	[3]2000	[3]560			
Expected --	0	-3.6	+1.0	0	+4.5	+4.9	
$N_s\sigma$(170-Yb) = $N_s\sigma$(154-Gd) was used.							
Yb	176	174*	173	172	171*	170	168
p.o.p. ------	r	r,s	r,s	r,s	r,s	s	p
σ ----------		[3]275	[3]990	[3]380	[3]1320	[3]510	
Expected --	+13.9	0	+1.8	-2.7	0	-35.6	-0.7
$N_s\sigma$(170-Yb) was used.							

[1]Corrected for α-decay from ^{147}Sm.
[2]Holmes and others (1976).
[3]Allen and others (1971).
[4]Calculated without p-process contribution.
[5]Upper limit if s-branch is ignored.
[6]Cullen and others (1976).

indicated in table 1 are obtained for Dy or its neighboring even-Z elements, then an exotic r-processlike contribution could be the explanation.

Allen, B. J., Gibbons, J. H., and Macklin, R. L., 1971, Nucleosynthesis and neutron-capture cross sections: Advances in Nuclear Physics, v. 4, p. 205-259.

Burbidge, E. M., Burbidge, G. R., Fowler, W. A., and Hoyle, F., 1957, Synthesis of the elements in stars: Revue of Modern Physics, v. 103, p. 547-650.

Cameron, A. G. W., 1957, Nuclear reactions in stars and nucleogenesis: Astronomical Society of the Pacific Publications, v. 69, p. 201.

Cameron, A. G. W., and Truran, J. W., 1976, The supernova trigger for formation of the solar system: Icarus, v. 30, p. 447-461.

Cullen, D. E., Howerton, R. J., MacGregor, M. H., and Perkins, S. T., 1976, Major neutron-induced interactions (Z755), in An integrated system for production of neutronics and photonics calculational constants: University of California Radiation Laboratory, UCRL-50400, 7B, Revision 1.

Holmes, J. A., Woosley, S. E., Fowler, W. A., and Zimmerman, B. A., 1976, Tables of thermonuclear-reaction-rate data for neutron-induced reactions on heavy nuclei: Atomic Data and Nuclear Data Tables, v. 18, no. 4, p. 305-412.

Lattimer, J. M., Schramm, D. N., and Grossman, L., 1978, Condensation in supernova ejecta and isotopic anomalies in meteorites: Astrophysical Journal, v. 219, no. 1, p. 230.

Lugmair, G. W., Marti, K., and Scheinin, N. B., 1978, Incomplete mixing of products from r-, p-, and s-process nucleosynthesis; Sm-Nd systematics in Allende inclusion EK 1-04-1: Lunar Science IX, p. 672.

Masuda, A., Nakamura, N., and Tanaka, T., 1973, Fine structures of mutually normalized rare-earth patterns of chondrites: Geochimica Cosmochimica Acta, v. 37, p. 239.

Papanastassiou, D. A., Huneke, J. C., Esat, T. M., and Wasserburg, G. J., 1978, Pandora's box of the nuclides: Lunar Science IX, p. 859-861.

Schramm, D. N., and Fowler, W. A., 1971, Synthesis of superheavy elements in the r-process: Nature, v. 231, p. 103-106.

AGES OF EGYPTIAN ALKALINE COMPLEXES AND Sr AND O ISOTOPE RELATIONS AT THE ABU KHRUQ COMPLEX

By T. M. Lutz[1], K. A. Foland[1], Henry Faul[1], Irving Friedman[2], and C. McC. Serencsits[3]

[1]Department of Geology
University of Pennsylvania
Philadelphia, Pennsylvania 19104

[2]U.S. Geological Survey, Denver, Colorado 80225

[3]Muhlenberg College
Allentown, Pennsylvania 18104

The ages, chemistry, and petrogenesis of alkaline ring complexes in Egypt are the objectives of ongoing research at the University of Pennsylvania. A summary of K-Ar and Rb-Sr geochronology is given along with strontium and oxygen isotope relations for one complex, Abu Khruq.

The alkaline complexes in Egypt intrude the Precambrian basement between the Red Sea and the Nile River along ring fractures. The complexes typically consist of nepheline or quartz-bearing syenites, or both, together with associated alkaline volcanics, essexite gabbros, and carbonatites (El Ramly and others, 1971). They are confined to the exposed basement bordering the Red Sea, but in Sudan similar complexes extend further to the west.

The ages of nine complexes in Egypt are presented in table 1. They are believed to indicate times of emplacement because there is general concordance between K-Ar and Rb-Sr systems. Their chronologic distribution may correlate with groups of ages for ring complexes observed in Sudan (Vail, 1976), but no such rocks reliably dated younger than Cambrian have been found in Saudi Arabia. Alkaline activity has continued intermittently along a zone west of the present Red Sea trough since the Cambrian. The long history of alkaline activity, its temporal and spatial distribution, and the apparent absence of counterparts east of the Red Sea in Saudi Arabia do not support the hypothesis that these rocks are associated with the early stages of rift tectonics in a simple manner. However, the positions at which the ring complexes intruded may be influenced by zones of weakness in the basement as postulated by Garson and Krs (1976). The low initial $^{87}Sr/^{86}Sr$ ratios ($\sim$0.703) of some complexes are consistent with a mantle origin, but Sr and O iso-

Table 1.--Ages of Egyptian alkaline complexes
[K-Ar data from Serencsits and others, 1978. Relevant isotopic constants from Steiger and Jäger, 1977]

Complex	Lat (°N.), long (°E.)	K-Ar age[1] (m.y.)		Rb-Sr age[1] (m.y.)	
Abu Khruq---	24.65, 34.27	89±2	2b	87	b
				89	R,a,f,b
				91	f,p
El Kahfa----	24.13, 34.65	91±4	6b,2h	92	2b
Nigrub El Fogani----	22.85, 34.95	139±5	3b	141	b
Mishbeh-----	22.72, 34.68	142±3	2b	145	2b
El Naga-----	22.70, 34.47	146±3	6b	144	b
El Gezira---	22.33, 33.67	229±5	b		
Tarbtie North-----	23.88, 33.57	351±7	h	336	3R,h
Zargat Naam-	23.75, 34.68	404±8	h	424	4R,h
Wadi Dib----	27.58, 32.93	554±12	3b		

[1]b = biotite, h = amphibole, a = analcite, f = alkali feldspar, p = pyroxene, R = whole-rock, preceding number is number of samples.

tope data for some localities indicate that interaction with crustal materials has clearly played a role.

The Abu Khruq Complex is emplaced in granitic country rock and is well exposed. It consists of a central stock of nepheline syenite, several incomplete rings of alkali and quartz syenite, separated masses of essexite gabbro, and down-faulted blocks of alkaline trachyte. Field relations indicate the intrusive sequence gabbro to syenite, quartz syenite to nepheline syenite. In thin section these rocks show, to varying extents, clouded feldspars, myrmekitic textures, and effects of alkali metasomatism, such as albite overgrowths.

A strontium development diagram, figure 1, clearly shows the isotopically heterogeneous nature of the whole-rock samples. No single rock unit satisfies an isochron. The dashed line is a least-squares fit to the data and, for purposes of comparison has a slope equivalent to an age of 96 m.y. The solid line is based upon an 89 m.y. age, constrained by K-Ar and Rb-Sr mineral data, and $^{87}Sr/^{86}Sr$ ratios in high-Sr rocks and represents the expected development line. It appears that the array of points has been rotated upward by addition of radiogenic Sr.

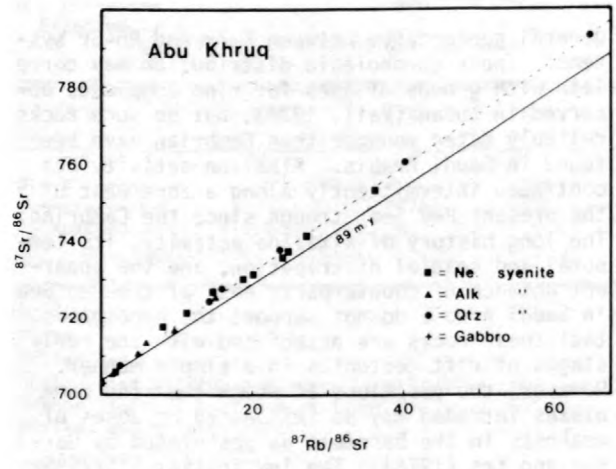

Figure 1.--Strontium development diagram for whole-rock data from the Abu Khruq Complex.

Many of the Abu Khruq rocks show ^{18}O depletion. Whole-rock $\delta^{18}O$ values show a progressive increase throughout the intrusive sequence. Because of the concentric pattern of intrusion, this is expressed as a gross geographic zoning of oxygen isotopes, with $\delta^{18}O$ increasing toward the center of the complex. Average values are: essexite gabbros, 3.5 permil; quartz syenites, 4.5 permil; alkali syenites, 5.5 permil; and nepheline syenites, 7.5 permil.

Some samples have equilibrated with respect to both strontium and oxygen isotopes.

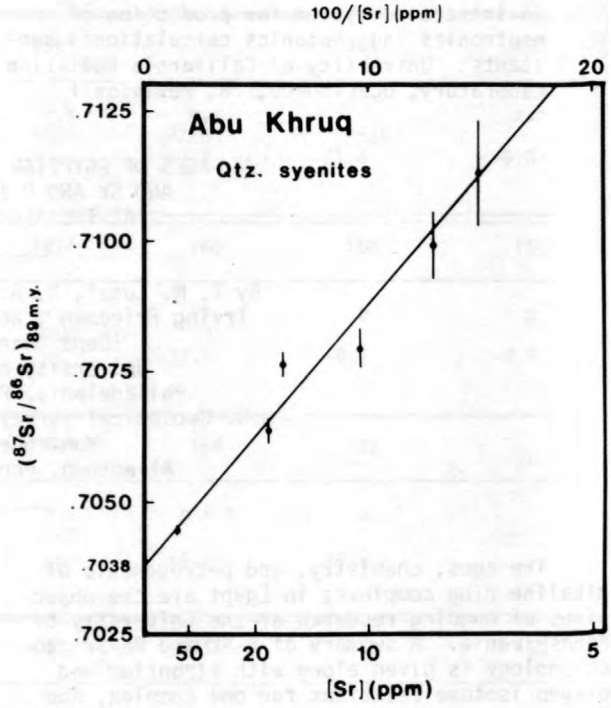

Figure 2.--Whole-rock $(^{87}Sr/^{86}Sr)_0$ versus Sr^{-1} for quartz syenites of the Abu Khrug Complex.

Mineral and whole-rock data are consistent with the 89 m.y. age. The high initial $^{87}Sr/^{86}Sr$ ratios of these isochrons demonstrate that addition of radiogenic strontium must have occurred at sufficiently high temperatures for equilibration to take place among major minerals. Furthermore, ^{18}O fractionations between minerals are generally consistent and indicate high temperatures of equilibration.

Quartz-feldspar fractionations of about 1 permil suggest that exchange of oxygen was restricted to high temperatures, at least in the quartz-bearing rocks. The nepheline syenites show a positive correlation of whole-rock $\delta^{18}O$ with $(^{87}Sr/^{86}Sr)_o$. The quartz and alkali syenites do not show simple trends in this respect.

In general, syenites with lower strontium concentrations have higher initial $^{87}Sr/^{86}Sr$ ratios. This relationship is particularly well-developed for the quartz syenite unit, and the data may be described by a mixing line as illustrated in figure 2. Petrographic characteristics of the rocks also change along this line. Samples lying close to the lower end contain low concentrations of quartz ($\sim$ 5 percent) in large blocky grains, whereas those lying toward the upper end have large ($\sim$ 35 percent) amounts of quartz, much of it replacing alkali feldspar in myrmekitic intergrowths. The net effect is that rocks with high initial ratios and low strontium concentrations are enriched in silica and depleted in alkalis with respect to those near the lower end.

A consistent explanation of the quartz-syenite genesis could involve depletion in ^{18}O, alkalis, alumina, and strontium, with an increase in the $^{87}Sr/^{86}Sr$ ratio and silica as a result of inward-migrating water. The country rock could act as a source of radiogenic strontium and silica, and meteoric waters could provide a medium of transport with low $\delta^{18}O$. Alkalis removed from the quartz syenites may have been concentrated in the metasomatic fluids affecting the inner syenites.

El Ramly, M. F., Budanov, V. I., and Hussein, A. A., 1971, The alkaline rocks of south-eastern Egypt: Geological Survey of Egypt Paper no. 53.

Garson, M. S., and Krs, M., 1976, Geophysical and geological evidence of the relationship of Red Sea transverse tectonics to ancient fractures: Geological Society of America Bulletin, v. 87, p. 169-181.

Serencsits, C. McC., El Ramly, M. F., Faul, H., Foland, K. A., and Hussein, A. A., (in press), Alkaline ring complexes in Egypt; their ages and relationship to tectonic development of the Red Sea: Geological Survey of Egypt Annals.

Steiger, R. H., and Jäger, E., 1977, Subcommission on geochronology; Convention on the use of decay constants in geo- and cosmochronology: Earth and Planetary Science Letters, v. 36, p. 359-362.

Vail, J. R., 1976, Location and geochronology of igneous ring complexes and related rocks in northeast Africa: Geologisches Jahrbuch, v. 20, p. 97-114.

URANIUM EXCHANGE IN ALTERING OCEANIC BASALTS: ISOTOPIC EVIDENCE

By J. D. MacDougall, R. Finkel, and J. Carlson
Scripps Institution of Oceanography
La Jolla, California 92093

INTRODUCTION

During low-temperature sea-floor alteration, oceanic basalts undergo a number of changes in chemical composition. Uranium, in particular, is strongly affected; highly altered tholeiites frequently contain more uranium than their fresh counterparts. Aumento (1971) documented a general increase in whole rock uranium contents as a function of distance from the mid-Atlantic Ridge for a series of dredged tholeiites, and argued that basalts continuously gain uranium at a rate of about 1 ppm per 10 m.y. However, MacDougall (1977), in a study of uranium distribution in Deep Sea Drilling Project (PSDP) basalts, found generally lower uranium concentrations for highly altered rocks than those reported by Aumento, and also noted considerable variability, even within single samples. In order to examine more closely the nature and chronology of the exchange process for uranium, we report here isotope activity ratios ($^{234}U/^{238}U$, denoted R) and uranium contents for a set of basalts, and separated phases therefrom, chosen to exemplify varying degrees of alteration. We have also begun an examination of DSDP core basalts in order to investigate the depth to which exchange extends, and its influence on the marine budget of uranium.

In seawater, the activity ratio $^{234}U/^{238}U$ has a value of 1.14 $\pm$ 0.03 (Ku and others, 1977). Since the indigenous uranium in freshly erupted basalts is expected to be in secular equilibrium (R = 1.00), the addition of seawater uranium to basalts will result in R values > 1.00. In a closed system, R will return toward equilibrium with a half time of 2.48×10^5 yr, and thus acts both as a simple tracer for seawater uranium and as a chronometer to monitor the time scale over which uranium exchange occurs.

Samples which we have examined include fresh young ridge basalts (glass and interior); a set of progressively altered basalts and manganese crusts dredged along a traverse across the mid-Indian Ocean Ridge (MIOR); and heavily altered old (> 30 x 10^6 yr) DSDP basalts.

ANALYTICAL

Whole-rock samples were sawed pieces of uniform-appearing interior portions of the rock. Glass, palagonite, and manganese crust samples were hand scraped and picked. After chemical separation of uranium, samples were electroplated and counted by alpha particle spectrometry.

RESULTS AND DISCUSSION

Uranium contents and isotope ratios, for all samples measured, are shown in table 1. Quoted errors are one standard deviation, based on counting statistics. The data are discussed below in three sections dealing with fresh basalts, the MIOR traverse, and old DSDP basalts.

Table 1.--Data

Sample		Age (m.y.)	U (ppb)	$^{234}U/^{238}U$ (activity)
Young basalts				
AMPH 3D (glass)		< 1	69	1.02±0.03
DS5-6 (interior)		< 1.5	93	0.97±0.02
MIOR				
Interior:	D115	3	68±2	0.98±0.03
	D114	12	157±3	1.20±0.03
	D143	13	68±2	1.03±0.04
	D113	23	601±9	1.14±0.02
Palagonite:	D115	--	493±13	0.99±0.04
	D114	--	515±27	--
	D143	--	468±11	0.84±0.03
	D113	--	713±14	0.93±0.02
Mn Crust:	D143	--	5100±100	1.04±0.02
	D113	--	8300±100	1.05±0.01
DSDP				
Site 213:	154 m	57	380±15	0.96±0.05
	165 m	57	620±10	0.99±0.02
Site 238:	517 m	30	170±6	1.00±0.04
	527 m	30	570±25	1.07±0.02

Fresh young basalts

Two East Pacific Rise samples, AMPH-3D (fresh glass, $< 10^6$ yr) and DS5-6 (interior, $< 1.6 \times 10^6$ yr) have low uranium concentrations and $^{234}U/^{238}U$ activity ratios consistent with little or no addition of seawater uranium. Neither exhibit even incipient palagonitization of glassy margins, although DS5-6 has a relatively thick manganese encrustation. Induced fission-track determination of uranium in the glassy margin from DS5-6 gave an identical value to that reported here for an interior sample, a further indication that little seawater uranium has been added.

MIOR traverse

Sample locations for these four rocks are shown in figure 1. Ages (table 1), which are based on the magnetic anomaly sequence in this area (Fisher and others, 1971), range from 3 x 10^6 yr for D115 to 23 x 10^6 yr for D113. There is a corresponding general progression of degree of alteration observable in the samples. In addition to measurements of the interior crystalline portions, palagonite and manganese crust analyses were made for some of these samples.

Interior samples from D115 and D143 both have low total uranium, in the range of the expected original concentrations. For both, R = 1.00 within the experimental uncertainty. Apparently the measured samples have experienced little exchange with seawater. In contrast, the D114 interior sample has high uranium and a large ^{234}U activity excess. The same is true for the D113 interior sample. This limited set of data does not allow a distinction to be made between continuous exchange and recent pick up.

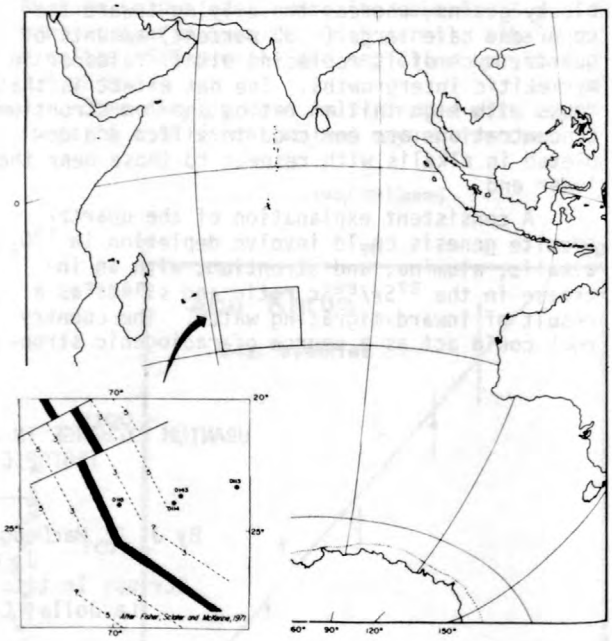

Figure 1.--Sample locations from the mid-Indian Ocean Ridge (MIOR) traverse.

Sample D114 is particularly interesting. Assuming its initial (at crystallization) uranium content was close to that of D115 and D143, it has acquired an approximately equal component of uranium during alteration. If the initial uranium is at equilibrium the added component must have $^{234}U/^{238}U \geq 1.40$. Such a high value is well outside the seawater range and difficult to explain. High values have also been observed for East Pacific Rise sediments (Veeh and Bostrom, 1971). It is conceivable that high $^{234}U/^{238}U$ source fluids are created by preferential leaching of ^{234}U from under-

lying basalts. Measurements of R in submarine hydrothermal fluids might help to solve this problem.

The palagonite and manganese crust measurements for some of these same rocks provide an interesting contrast to the interior samples. A typical case is illustrated in table 2 for D113. All palagonite rims have high uranium, almost an order of magnitude higher than probable initial values. While palagonite from the youngest sample is at equilibrium, the older samples have lower R values. Low values are common in continental rocks where radiogenic ^{234}U is preferentially leached. A similar process may occur in the palagonite. For a constant rate of palagonite formation, with all added uranium having R = 1.14 and no leaching, a total palagonite layer would exhibit ratios as a function of age as shown in figure 2. Although preferential leaching of ^{234}U would reduce R values, this model for the continuous formation of palagonite could be tested by measuring R as a function depth in individual palagonite layers.

Table 2.--MIOR Basalt D113

Phase	U (ppb)	$^{234}U/^{238}U$ (activity)
Crystalline interior	601±9	1.14±0.02
Palagonite	713±14	0.93±0.02
Mn crust	8300±100	1.05±0.01

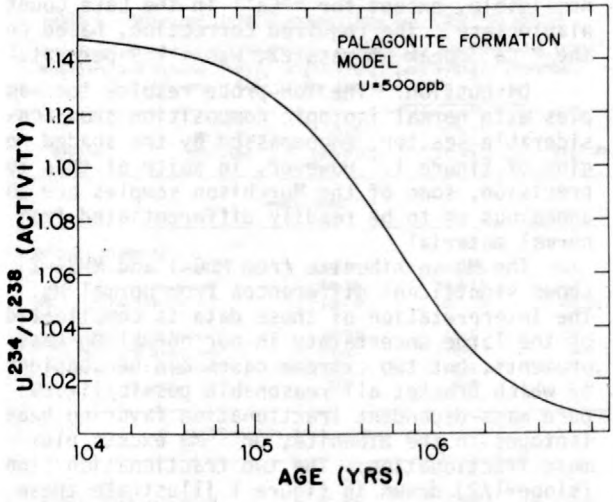

Figure 2.--$^{234}U/^{238}U$ activity ratios as a function of age for a constant rate of palagonite formation.

For two of the MIOR basalts, manganese crust samples were also measured. Both exhibit very high uranium concentrations, relative to the basalt and palagonite. Both also have R value > 1.00, suggesting either recent interaction with seawater, or recent crust formation.

DSDP basalt

A pair of samples from different depths within each of two DSDP cores were also analyzed. All four samples are visibly highly altered. Three have R values at equilibrium within the experimental uncertainty. However, a fourth has R = 1.07 ± 0.02. This ratio implies that seawater-basalt interaction has occurred recently at a depth of ∿ 0.5 km beneath the seawater-sediment interface. Further detailed work on this core will be equired to analyze the pattern of interaction.

CONCLUSION

1. Uptake of uranium by altering oceanic basalts is a common occurrence. Uranium isotope ratios demonstrate that manganese crusts, palagonite rims, and the fine-grained alteration products of the crystalline interior all behave differently with respect to uranium uptake. For the oldest MIOR samples, none of the three exhibit equilibrium $^{234}U/^{238}U$ activity.

2. The data are consistent with continuous palagonite growth and incorporation of seawater uranium combined with preferential leaching of in situ radiogenic ^{234}U.

3. Continuing interaction with seawater uranium may be more common for exposed basalts than for those buried by thick sediment cover.

4. A single altered basalt interior contained uranium from a source with R much greater than the seawater value. This may be the effect of recent addition of uranium leached from the oceanic crust.

Aumento, F., 1971, Uranium content of mid-ocean basalts: Earth and Planetary Science Letters, v. 11, p. 90-94.

Fisher, R. L., Sclater, J. G., and McKenzie, D. P., 1971, Evolution of the Central Indian Ridge, Western Indian Ocean: Geological Society of America Bulletin, v. 82, p. 553-562.

Ku, T., Knauss, K., and Mathieu, G., 1977, Uranium in the open ocean-concentration and isotopic composition: Deep Sea Research, v. 24, p. 1005-1017.

MacDougall, J. D., 1977, Uranium in marine basalts-concentration, distribution and implications: Earth and Planetary Science Letters, v. 35, p. 65-70.

Veeh, H., and Bostrom, K., 1971, Anomalous $^{234}U/^{238}U$ on the East Pacific Rise: Earth and Planetary Science Letters, v. 10, p. 372-374.

FRACTIONATED MAGNESIUM ISOTOPES IN MURCHISON REFRACTORY INCLUSIONS

By J. D. Macdougall[1] and D. Phinney[2],
[1]Scripps Institution of Oceanography,
La Jolla, California
[2]Lockheed Electronics, Johnson Space Center,
Houston, Texas

Although refractory-element-rich inclusions in C3 meteorites, particularly Allende, have been the object of intense study, their counterparts in C2's have received much less attention. Fuchs and others (1973) first described a hibonite-rich variety from Murchison; these have subsequently been studied in greater detail (Macdougall and Carlson, 1978; J. D. Macdougall, unpub. data). Here we report ion-probe measurements of magnesium isotope compositions for selected phases from several of these hibonite-bearing inclusions.

Typical examples of these inclusions are small (generally less than 1 mm in maximum dimension), fine grained, and relatively simple mineralogically. The major phase is frequently very pure spinel (FeO < 0.5 percent; Cr_2O_3 < 0.2 percent), sometimes containing rounded blebs of perovskite. Bright-blue hibonite occurs as patches and stringers. The chemical composition is variable, even within single inclusions, but falls within the range reported by Keil and Fuchs (1971) for hibonite from Allende and Leoville. Some inclusions also contain small amounts of titanium-rich pyroxenes (fassaites) with compositions similar to the Ti-rich pyroxenes of Allende Type-B inclusions as defined by Grossman (1975). Most inclusions also exhibit a thin ($\leq$ 5 μm) diopside outer rim in contact with matrix.

A variety of other rarely occurring refractory-element-rich types has also been observed. One type consists almost exclusively of hibonite. These are coarser grained than the spinel-bearing types; there also appears to be less void space. SEM observations of crystals from one such inclusion revealed perovskite blebs (up to 2 μm) within the hibonite, in contrast to the spinel bearing inclusions where the perovskite seems to be included only in the spinel.

Analytical Results: Grains from four separate inclusions have been analyzed by ion probe. These include two coarse-grained hibonite inclusions (MG8A-2 and MHG-1), and two typical spinel-plus-hibonite inclusions (MH4-1 and MH-10). In addition, we have analyzed several samples expected to have normal Mg isotopic composition--an olivine from the Murchison matrix (MH4-Oℓ) adjacent to inclusion MH4; terrestrial spinel (TS); and terrestrial plagioclase (Lake County, L.C.).

Only hibonite was analyzed from MHG-1 and MH8A-2. A large Ti-rich pyroxene was analyzed from MH-10. Very fine grain size and intergrown phases in MH4 precluded analyses of single grains, and hibonite-rich (∿ 90 percent hibonite, MH4-H) and spinel-rich (∿ 70 percent spinel, MH4-S) areas were measured. In addition, a single large forsteritic olivine (MH4-Oℓ) from the matrix near the inclusion was measured in the MH4 section.

Results are listed in table 1 and shown graphically in figure 1. The δ-values are given relative to the terrestrial values of Catanzaro and others (1967). No corrections have been applied for instrumental mass discrimination. All data are mean values of repeated measurements and uncertainties are ±2σ mean. Uncertainties due to counting statistics alone were always $\leq$ 1 percent. The $^{27}Al/^{24}Mg$ ratios were calculated from mass 27 and mass 24 peak heights, and are valid within ± 15 percent.

For these analyses, a 16.6 KeV $^{16}O^-$ sputtering-beam with spot diameter of ∿ 20 μm was used. Mass peaks in the Mg region have flat tops at the mass resolution used (250 for run No. 2 on MH8A-2 --100 for all others). Possible interferences in the Mg region due to Ca^{++}, Ti^{++}, and hydrocarbons, and due to specular reflection (from Na, Al, Si) were carefully checked. The Al-interference varies smoothly across the magnesium mass-24 peak and the correction was made by background subtraction. All other interferences examined were negligible, except for $^{48}Ca^{++}$ in the Lake County plagioclase. The required correction, based on the $^{44}Ca^{++}$ peak at mass 22, was < 1.2 percent.

Discussion: The ion-probe results for samples with normal isotopic composition show considerable scatter, encompassed by the shaded region of figure 1. However, in spite of this low precision, some of the Murchison samples are so anomalous as to be readily differentiated from normal material.

The Mg in hibonite from MHG-1 and MH8A-2 shows significant differences from normal Mg. The interpretation of these data is complicated by the large uncertainty in our normal Mg measurements, but two extreme cases can be considered which bracket all reasonable possibilities: pure mass-dependent fractionation favoring heavy isotopes in the hibonite, or ^{26}Mg excess plus mass fractionation. The two fractionation lines (slope=1/2) drawn in figure 1 illustrate these cases. The lower line is drawn through the most extreme data point on the low end of our normal Mg measurements and provides a reasonable fit to

the MHG-1 and MH8A-2 data. The upper line passes through the extreme point on the upper end of normal Mg measurements and would require excess ^{26}Mg in MHG-1 and MH8A-2. The MHG-1 data would require ~ 6 percent excess ^{26}Mg (relative to ^{24}Mg) and no fractionation, while the MH8A-2 would require 7.2 percent excess ^{26}Mg. Upper limits for the initial $^{26}Al/^{27}Al$ would be 2.7×10^{-3} and 7×10^{-4}, respectively. However, the presence or absence of a ^{26}Mg-excess cannot be conclusively demonstrated with the present data. Nevertheless, it is clear that a large degree of fractionation must be involved in any reasonable explanation of the Mg in MH8A-2.

In contrast, the hibonite from MH4, as well as the spinel-rich area, the adjacent MH4-olivine, and the MH10-pyroxene all lie within uncertainty of normal Mg. The large uncertainties in normal Mg may obscure small differences (2-3 percent) in $\delta^{(24)}_{26}$ for these samples, as is suggested by the displacement in δ_{26} between MH4-Ol and the MH4 hibonite and spinel points.

The presence of large mass-dependent fractionation in the Mg from MH8A-2, and possibly MHG-1, hibonite, coupled with its absence in MH4 hibonite, in spite of their chemical similarity, suggests that the hibonite in these two different types of inclusions may have formed from different batches of Mg--one fractionated and one normal. Alternatively, different formation processes could have been involved. In either case the difference could represent temporal or spatial variations in formation, in spite of the present close association of the inclusions in Murchison.

In addition to the present observations, large isotope fractionation has been documented for oxygen (Clayton and Mayeda, 1977) and magnesium (Wasserburg and others, 1977) in two Allende inclusions. Possible mechanisms for production

Table 1.--Magnesium isotopic compositions and $^{27}Al/^{24}Mg$ ratios

[δ-values calculated using $^{25}Mg/^{26}Mg = 0.12663$ and $^{26}Mg/^{24}Mg = 0.13932$ (Cantanzaro and others, 1967), $\delta^{(x)} = [(R^{(x)}$ sample$/R^{(x)}$ reference$) - 1] \times 10^3$, where $R^{(x)}$ is the isotopic ratio x/y]

Sample	No. of analyses	$\delta^{(24)}_{25}$ (permil)	$\delta^{(24)}_{26}$ (permil)	$^{27}Al/^{24}Mg$
Murchison				
MH8A-2, hibonite:				
Run 1	8	98±14	183±20	103
Run 2	7	74±16	149±23	---
MHG-1, hibonite	2	33±12	82±13	23
MH4-1:				
Hibonite-rich area	7	38±23	15±5	19
Spinel-rich area	6	23±4	16±2	4.0
Adjacent olivine	5	35±2	-16±6	0.01
MH10, Ti-pyroxene	6	2±4	6±4	5.0
Terrestrial standards				
Lake County, plagioclase	8	44±27	22±28	---
Spinel:				
Run 1	5	29±4	0.8±3.4	2.1
Run 2	3	35±32	2±15	---
Run 3	2	1±6	5±9	2.6

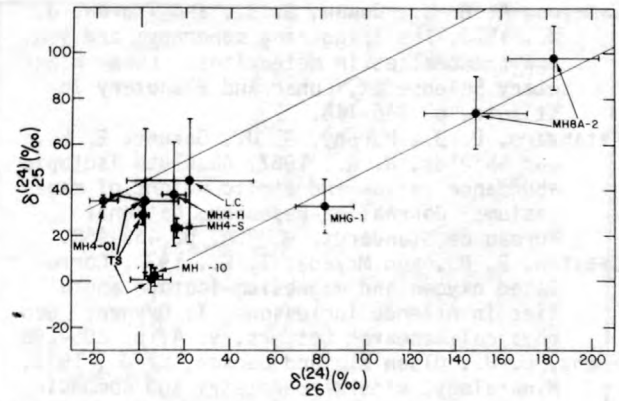

Figure 1.--Magnesium isotopic composition given as δ-values relative to the terrestrial values of Catanzaro and others (1967).

of such fractionation in the early solar system have been reviewed recently by Arrhenius (1978). These include kinetic isotope effects, equilibrium fractionation at low kinetic temperatures and electrodynamic separation processes. The presence of large mass-dependent fractionation in some, but not all, Murchison hibonite, and the lack of such effects in hibonite from Allende and Leoville (Lorin and Michel-Lévy, 1978), suggest that the fractionation is not characteristic of the final reaction step leading to the formation of hibonite. Similarly, for the two Allende inclusions mentioned above (Wasserburg and others, 1977), Mg shows large and uniform mass-fractionation effects in different phases, an indication that the source material from which the different minerals formed was mass-fractionated. As is the case for Murchison, the phases are chemically similar to those in inclusions not exhibiting such effects. Unfortunately, for the Murchison mass-fractionated inclusions there are no other phases associated with the hibonite that can be investigated.

The question of whether these observed isotopic abundances were produced by chemical or electrodynamic effects, or by an alternative mechanism--for example, nuclear effect simulating mass fractionation (Cameron and others, 1978)--cannot be answered conclusively with the present data. However, taken together, the Allende and Murchison data suggest that the ultimate reaction steps accompanying the formation of a particular phase were not responsible. Assuming that the inclusions formed by condensation processes, there must have existed reservoirs in the solar nebula with highly fractionated Mg isotope abundances, relative to normal solar system values.

Arrhenius, G., (in press), Chemical aspects of the formation of the solar system, in Dermott, S. F., ed., Proceedings of the Symposium on origin of solar system, Newcastle, 1976.

Cameron, A. G. W., Cowan, J. J., and Truran, J. W., 1978, The triggering supernova and isotopic anomalies in meteorites: Lunar Planetary Science IX, Lunar and Planetary Institute, p. 146-148.

Catanzaro, E. J., Murphy, G. J., Garner, E. L., and Shields, W. R., 1967, Absolute isotopic abundance ratios and atomic weight of magnesium: Journal of Research, National Bureau of Standards, v. 70A, p. 453-458.

Clayton, R. N., and Mayeda, T. K., 1977, Correlated oxygen and magnesium isotope anomalies in Allende inclusions, I; Oxygen: Geophysical Research Letters, v. 4, p. 295-298.

Fuchs, L. H., Olsen E., and Jensen, K. J., 1973, Mineralogy, mineral-chemistry and composition of the Murchison (C2) meteorite: Smithsonian Contributions to the Earth Sciences, v. 10, 39 p.

Grossman, L., 1975, Petrography and mineral chemistry of Ca-rich inclusions in the Allende meteorite: Geochimica Cosmochimica Acta, v. 39, p. 433-454.

Keil, K., and Fuchs, L. H., 1971, Hibonite [$Ca_2(Al,Ti)_{24}O_{38}$] from the Leoville and Allende chondritic meteorites: Earth and Planetary Science Letters, v. 12, p. 184-190.

Lorin, J. C., and Michel-Levy, M. Cristophe, 1978, Heavy rare metals and magnesium isotopic anomalies studies in Allende and Leoville calcium-aluminum rich inclusions: Lunar and Planetary Science IX, Lunar and Planetary Institute, p. 660-662.

Macdougall, J. D., and Carlson, J., 1978, Refractory element rich inclusions in C1 and C2 meteorites: Lunar and Planetary Science IX, Lunar and Planetary Institute, p. 683-685.

Wasserburg, G. J., Lee, T., and Papanastassiou, D. A., 1977, Correlated O and Mg isotopic anomalies in Allende inclusions, II; Magnesium: Geophysical Research Letters, v. 4, p. 299-302.

SIGNIFICANCE OF CARBONATITE AND KIMBERLITE AGE DETERMINATIONS

By Robert M. Macintyre
Scottish Universities Research and Reactor Centre
Scotland

Some intriguing age relationships appear to exist between carbonatite and kimberlite rocks. These magmatic rocks, derived from the asthenosphere, are often associated with deep crustal fractures, and the timing of events along these 'pipelines to the mantle' is regarded as fundamentally important.

The ages of Paleozoic and Precambrian carbonatites cluster around certain geochronologic peaks separated by intervals of approximately 230 m.y. The last few hundred m.y. seem to be characterized by an increased abundance of these rocks, and their emplacement seems to have accompanied major changes in the motions of the plates. Several examples of major occurrences of carbonatite and kimberlite are shown in figures 1-5.

An increased geochronologic effort is urged to test these correlations. As there are many ramifications--including possible relationships with convection, eustacy and epeirogeny, faunal extinction, galactic precession, geological time scale, glaciation and the greenhouse effect, magnetic field, mantle events, and uniformitarianism--these rocks appear to warrant much more detailed investigation by the methods of isotope geology.

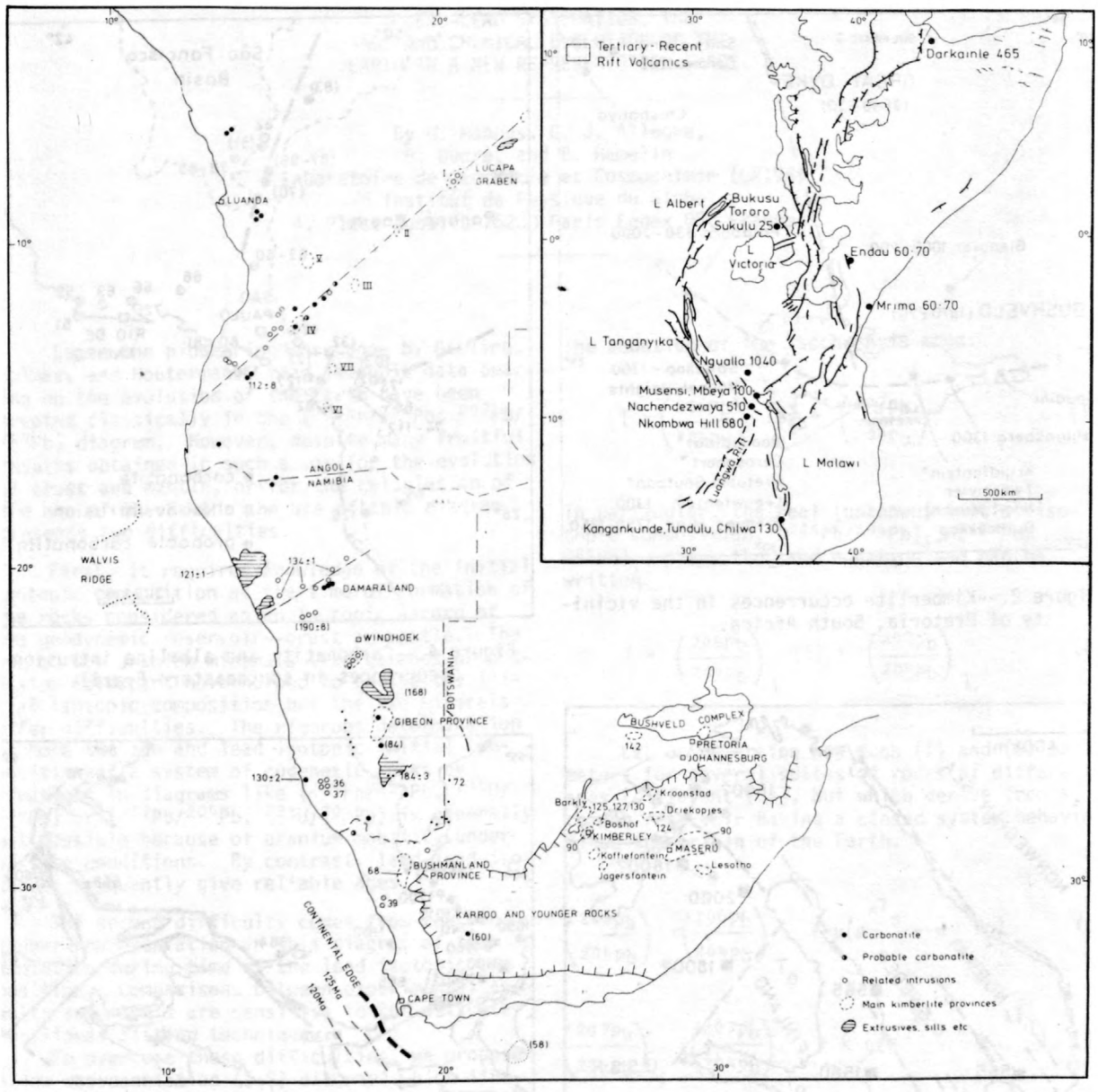

Figure 1.--Carbonatite and kimberlite occurrences in Africa.

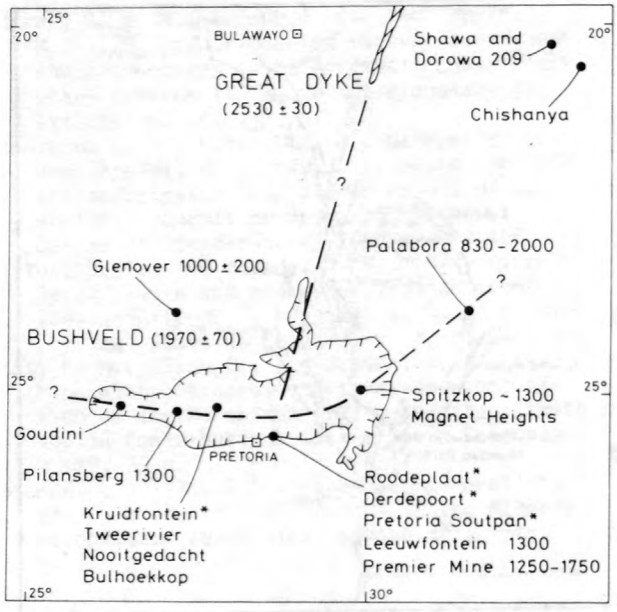

Figure 2.--Kimberlite occurrences in the vicinity of Pretoria, South Africa.

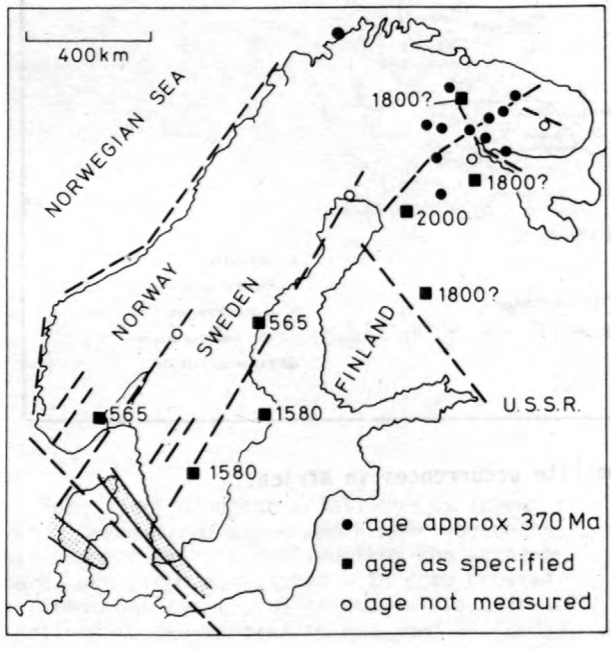

Figure 3.--Carbonatite and kimberlite occurrences in Scandinavia.

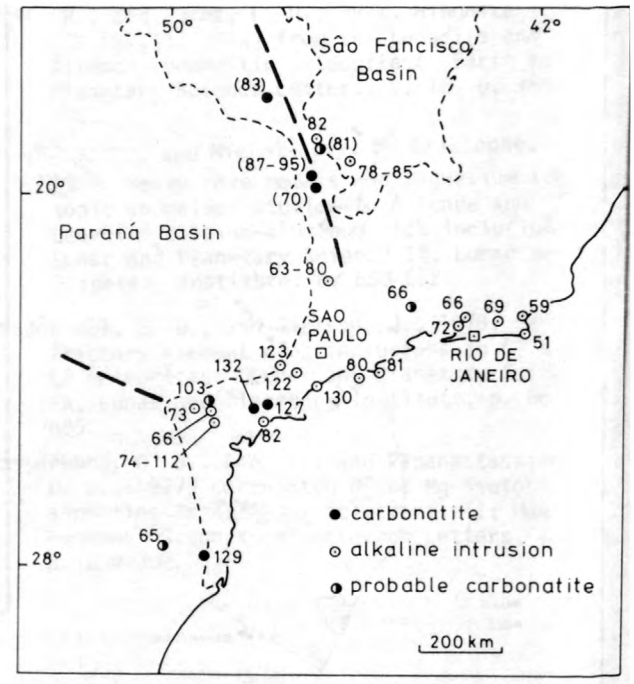

Figure 4.--Carbonatite and alkaline intrusion occurrences in southeastern Brazil.

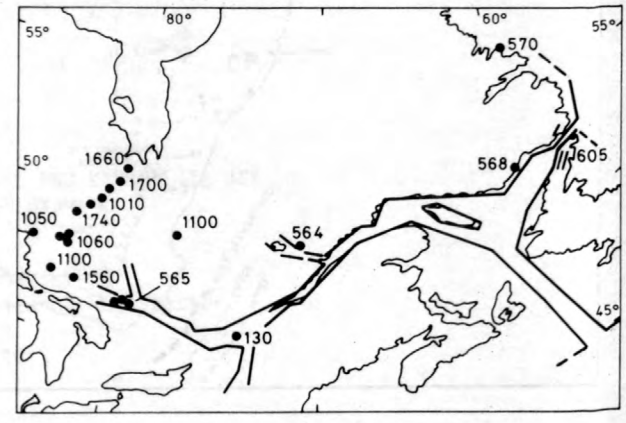

Figure 5.--Carbonatite occurrences in southeastern Canada.

Macintyre, R. M., 1971, Apparent periodicity of carbonatite emplacement in Canada: Nature, v. 230, p. 79-81.

_____1977, Anorogenic magmatism, plate motion and Atlantic evolution: Geological Society of London Journal, v. 133, p. 375-384.

LEAD-LEAD SYSTEMATICS, THE AGE AND CHEMICAL EVOLUTION OF THE EARTH IN A NEW REPRESENTATION SPACE

By G. Manhes, C. J. Allegre,
B. Dupre, and B. Hamelin
Laboratoire de Géochimie et Cosmochimie (LA196)
Institut de Physique du Globe
4, Place Jussieu-75230 Paris Cedex 05, France

Since the pioneering work done by Gerling, Holmes, and Houtermans, lead isotopic data bearing on the evolution of the Earth have been treated classically in the ($^{206}Pb/^{204}Pb$; $^{207}Pb/^{204}Pb$) diagram. However, despite many fruitful results obtained in such a way for the evolution of crust and mantle, or for the calculation of the age of the Earth, the use of this diagram presents two difficulties.

First, it requires knowledge of the initial isotopic composition at the time of formation of the rocks considered as an isotopic record of the geodynamic reservoir--crust or mantle. The use of low uranium minerals like galenas or potassium feldspars have helped to define the initial isotopic composition but the two minerals offer difficulties. The rigorous determination of both the age and lead isotopic initial composition of a system of cogenetic rocks by treatment in diagrams like ($^{206}Pb/^{204}Pb$, $^{238}U/^{204}Pb$) or ($^{207}Pb/^{204}Pb$, $^{235}U/^{204}Pb$) is generally not possible because of uranium mobility under surface conditions. By contrast, lead-lead isochrons frequently give reliable ages.

The second difficulty comes from the non-linear representation in this diagram of the evolution during time of the lead isotopic composition. Comparisons between experimental results and models are sensitive to the delicate non-linear fitting technique.

To overcome these difficulties, we propose a new representation (I,S) diagram, which linearizes the (α,β) diagram and which uses only the lead-lead isochron data with no need for "initial" isotopic composition.

The idea is to use, as a substitute parameter, the "initial" ratio ($^{207}Pb/^{204}Pb$), called (I), corresponding to the ($^{206}Pb/^{204}Pb$) = 0 in the ($^{207}Pb/^{204}Pb$; $^{206}Pb/^{204}Pb$) diagram. Let us consider in this diagram an isochron, representing a cogenetic suite of rocks of age Ti, whose slope, S, is time-related, as follows:

$$S = \frac{1}{137.8} \times \frac{e^{\lambda T_1} - 1}{e^{\lambda T_1} - 1}$$

λ = ^{235}U decay constant

λ = ^{238}U decay constant

The equation of the isochron is then:

$$I = \left(\frac{^{206}Pb}{^{204}Pb}\right) (S) + \left(\frac{^{207}Pb}{^{204}Pb}\right) \quad (1)$$

In particular, the real (unknown) initial isotopic composition, ($^{206}Pb/^{204}Pb)_i$, ($^{207}Pb/^{204}Pb)_i$, obeys the same equation and can be written:

$$I = \left(\frac{^{206}Pb}{^{204}Pb}\right)_i (S) + \left(\frac{^{207}Pb}{^{204}Pb}\right)_i \quad (2)$$

Let us determine now such (I) and (S) parameters for several suites of rocks of different ages [different (S)], but which derive from a common reservoir having a closed system behavior since the origin of the Earth.

$$\left(\frac{^{206}Pb}{^{204}Pb}\right)_i = \left(\frac{^{206}Pb}{^{204}Pb}\right)_{T_o} + \mu(e^{\lambda T_o} - e^{\lambda T_1}) \quad (3)$$

$$\left(\frac{^{207}Pb}{^{204}Pb}\right)_i = \left(\frac{^{207}Pb}{^{204}Pb}\right)_{T_o} + k\,\mu(e^{\lambda T_o} - e^{\lambda T_1}) \quad (4)$$

$(^{206}Pb/^{204}Pb)_{T_o}$ and $(^{207}Pb/^{204}Pb)_{T_o}$ are the initial isotopic composition of the Earth. T_o is the age of the Earth, T_1 is the age of the suite of rocks [determined by the ($^{206}Pb/^{204}Pb$), ($^{207}Pb/^{204}Pb$) diagram].

μ = ($^{238}U/^{204}Pb$) is the ratio of the closed system reservoir. k = 1/137.8 is the isotopic ratio of uranium today.

Then, replacing $(^{206}Pb/^{204}Pb)_i$ and $(^{207}Pb/^{204}Pb)_i$ in equation (2) by their values in (3), we obtain after an easy simplification:

$$I = -\left(\frac{^{206}Pb}{^{204}Pb}\right)_{T_o} + (e^{\lambda T_o} - 1)\,S + \left(\frac{^{207}Pb}{^{204}Pb}\right)_{T_o} + k\,(e^{\lambda T_o} - 1) \quad (5)$$

Then, representing each suite of rocks by a point in the (I,S) diagram, they plot on a straight line described by equation (4). The slope is equal to $(^{206}Pb/^{204}Pb)_{T_o} + \mu(e^{\lambda 238 T_o}-1)$ and the intercept is equal to $(^{207}Pb/^{204}Pb)_{T_o} + k\,\mu(e^{\lambda 235 T_o}-1)$.

Advantages of the (I,S) diagram are: (1) knowledge of the initial isotopic composition if the cogenetic system does work is not necessary, and only the lead-lead data need be used; and (2) closed system assumption can be tested by a linear least-square technique. Mapping between (α,β) and (I,S) diagram is shown in figures 1 and 2.

Using such formalism we will try to determine the age of the earth and examine the past evolution of the U-Th-Pb system in the Earth.

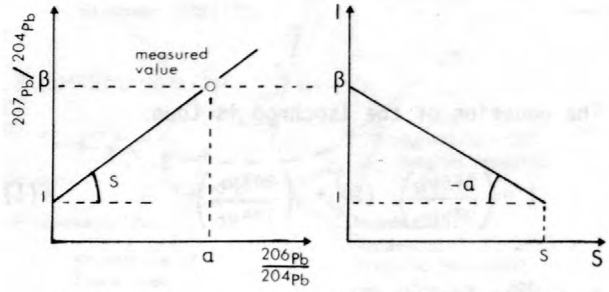

Figure 1.--Representation of the measured isotopic composition (α,β) are the measured isotopic ratios. The point (α,β) in the Holmes-Houtermans plot obeys the equation:

$$I = -\alpha S + \beta$$

and is represented by a straight line in the (I,S) diagram.

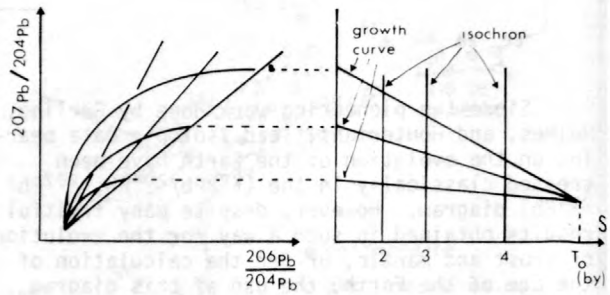

Figure 2.--Mapping between the (α,β) and the (I,S) diagram. The growth curves are straight lines passing through a common point (starting point is the "beginning" of the Earth). The isochrons are vertical straight lines. Time is expanded around the age of the Earth and collapsed around present day.

GEOTHERMAL ACTIVITY INDICATED BY OXYGEN AND HYDROGEN ISOTOPES OF ROCKS FROM A PALEOGENE CAULDRON, SOUTHWEST JAPAN

By Yukihiro Matsuhisa[1], Teruki Imaoka[2], and Nobuhide Murakami[3]
[1]Geological Survey of Japan, Kawasaki, Japan
[2]Hiroshima University, Hiroshima, Japan
[3]Yamaguchi University, Yamaguchi, Japan

Waters from present-day geothermal areas are sometimes enriched in ^{18}O as a result of isotopic exchange with heated rocks (Craig, 1963). Conversely, if geothermal water is meteoric in origin, rocks which have reacted with a considerable amount of water at elevated temperatures would be lowered in ^{18}O relative to the original rocks (Clayton and others, 1968; Taylor, 1971). In other words, a record of geothermal activity is preserved in isotopic compositions of rocks even after the activity has ceased. Detailed studies of oxygen and hydrogen isotopes of rocks from geothermal areas would provide us with information about extent of geothermal activity, relationship between geologic structure and geothermal activity, origin of geothermal water, and water-to-rock ratio in the area.

The Hamada cauldron, which is located on the Sea of Japan side of Honshu approximately 300 km west of Osaka, southwest Japan, is a well-exposed cauldron of Paleogene age, 10 km in diameter, consisting of andesitic to rhyolitic volcanic rocks and dioritic to granitic plutonic rocks (fig. 1). The cauldron was formed in Mesozoic volcanic and metamorphic rocks, and is circumscribed by faults. The east and west rims of the cauldron are intruded

by granitic and quartz dioritic plutons, respectively. Small stocks of quartz diorite are also seen inside the cauldron. The Kumoki granite pluton on the eastern rim of the cauldron, which seems to have been originally homogeneous in mineral assemblage and chemical composition, shows a concentric zoning of magnetite-to-biotite ratio in modal composition with a higher ratio in the outer zone of the pluton. Biotite in the granite is more or less chloritized. Iron content of biotite decreases as the magnetite content of rocks increases. Biotite was probably oxidized to produce magnetite after crystallization. Light-colored quartz-sericite rocks, which might have been heavily leached by hydrothermal water, are observed in the outer zone of the pluton. These facts suggest that extensive geothermal activity might have taken place in the cauldron, penetrating into the pluton from outside to produce the oxidizing condition.

In the present study, $^{18}O/^{16}O$ and D/H ratios were determined for whole-rock and mineral samples from the cauldron and from the basement rocks. The oxygen isotopic results for whole-rock samples are shown in figure 1 by approximate $\delta^{18}O$ contours. The whole-rock $\delta^{18}O$-values (relative to SMOW) range from -2.3 to +4.9 permil for volcanic rocks, and from -1.8 to +7.0 permil for plutonic rocks, The δD-values (relative to SMOW) of granites from the Kumoki pluton range from -101 to -88 permil. No correlation is seen between $\delta^{18}O$-value and silica content of rocks. These low $\delta^{18}O$-values of rocks suggest isotopic exchange reaction with ^{18}O-poor meteoric ground water at elevated temperatures--in other words, existence of geothermal activity in the past. The distribution of ubiquitous low-$\delta^{18}O$ rocks in the cauldron suggests that extent of the geothermal activity was as large as the entire area of the cauldron.

Concentric zoning of whole-rock $\delta^{18}O$ values is seen in the cauldron with the lowest value (-2.3 permil) in the midst of the cauldron. Since the original isotopic compositions of the rocks of the cauldron are presumed to have shown a narrow range, lower $\delta^{18}O$ values indicate higher water-to-rock ratio in the reaction or higher temperature at which the reaction took place. The pattern of $\delta^{18}O$-contours seems to correlate not to distribution of plutons which might be the heat source of the area, but to distribution of fracture zones in the cauldron. Hydrothermal water would have been preferentially percolated into the cauldron through the fracture zones, resulting in high water-to-rock ratio or low $\delta^{18}O$-values of rocks in the vicinity of the fracture zones. Low-$\delta^{18}O$ rocks, as low as -2.0 permil for schist, are also seen at the contact of the plutons and the country rocks. The boundaries between different rock bodies would provide easy access for hydrothermal water.

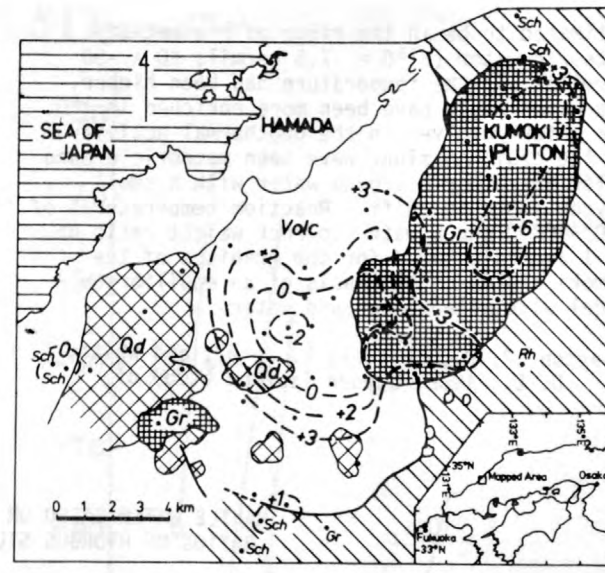

Figure 1.--Geologic map of the Hamada cauldron, southwest Japan, showing $\delta^{18}O$ contours of whole-rock samples. The lowest $\delta^{18}O$ values are observed in the midst of the cauldron, extending toward the southwest corner of the Kumoki pluton. Sampling localities are indicated by small dots. Gr (fine cross-hatched pattern), granite intrusions; Qd (coarse cross-hatched pattern), quartz-diorite intrusions. Basement rocks (diagonal pattern); Sch, green schist or pelitic schist; Rh, rhyolite; Gr, granite; Volc (no pattern) volcanic rocks of the cauldron, consisting of andesite, dacite, tuff, rhyolite, and rhyolite tuff.

Zoning of oxygen isotopic composition in the Kumoki pluton, being lower in $\delta^{18}O$-value in the outer zone of the pluton, accords with the zoned pattern of degree of oxidation of the rocks. Feldspar in the outer zone is much more depleted in ^{18}O than the coexisting quartz. Sericite in a hydrothermally altered rock has a $\delta^{18}O$ value of -2.8 permil and a δD value of -78 permil. In the core of the pluton is preserved a fresh original granite with a whole-rock $\delta^{18}O$ value of +7.0 permil. The quartz-alkali feldspar-magnetite assemblage in this rock shows oxygen isotopic equilibrium at a temperature of about 650°C (ΔQz-Mt = 6.8 permil; ΔAF-Mt = 6.4 permil). Water-to-rock ratio or reaction temperature of isotopic exchange was evidently higher in the outer part of the pluton. The effect of the fracture zone is again seen in the southwestern part of the pluton where the lowest $\delta^{18}O$ values are obtained.

The isotopic composition of the hydrothermal water, assuming the water to have been in equilibrium with sericite at 250°C, was

estimated to be in the range of present-day meteoric water ($\delta^{18}O$ = -7.5 permil; δD = -50 permil). If the temperature had been higher, the water could have been more enriched in ^{18}O. The water involved in the geothermal activity in the cauldron might have been meteoric ground water or meteoric ground water with a small oxygen isotopic shift. Reaction temperatures of 200°-400°C and a water-to-rock weight ratio up to 1 are calculated for the granites of the Kumoki pluton on the basis of an equilibrium model with meteoric ground water.

Clayton, R. N., Muffler, L. J. P., and White, D. E., 1968, Oxygen isotope study of calcite and silicates of the River Ranch No. 1 Well, Salton Sea geothermal field, California: American Journal of Science, v. 266, p. 968-979.

Craig, H., 1963, The isotopic geochemistry of water and carbon in geothermal areas; in Tongiorgi, E., ed., Nuclear geology on geothermal areas: Spoleto, p. 17-53.

Taylor, H. P., Jr., 1971, Oxygen isotope evidence for large-scale interaction between meteoric ground waters and Tertiary granodiorite intrusions, western Cascade Range, Oregon: Journal of Geophysical Research, v. 76, p. 7855-7874.

MANTLE WATER BASED ON THE HYDROGEN ISOTOPIC RATIOS OF HYDROUS SILICATES IN THE MANTLE

By Sadao Matsuo[1], Yoshimasu Kuroda[2], Tetsuro Suzuoki[3], Ken'ichiro Aoki[4], and Yu Hariya[5]
[1]Tokyo Institute of Technology
[2]Shinshu University
[3]Japan Meteorological Agency
[4]Tohoku University
[5]Hokkaido University

Suzuoki and Epstein (1976) found that the distribution of hydrogen isotopes between hydrous silicates and water depends on the chemical composition of the octahedral cation site in the hydrous silicates as well as the temperature of equilibration. They conducted experiments in the temperature range from 450° to 800°C and derived the following relationship for micas and amphiboles:

$$10^3 \ln\alpha = -22.4\,(10^6 T^{-2}) + 28.2 + (2X_{Al} - 4X_{Mg} - 68X_{Fe}) \quad (1)$$

where α is $(D/H)_{mineral}/(D/H)_{water}$, and X is the atomic fraction of the cations in the octahedral site. When we apply Suzuoki and Epstein's results to natural samples, a basic problem arises because their experiment is only valid for the "aqueous fluid"-hydrous silicates system(I). When a magma is undersaturated with water, however, hydrogen isotopic fractionation takes place in the "dissolved water"-hydrous silicates system(II). The energetics of water molecules are different for the aqueous fluid and the dissolved water systems, which implies that the pattern of hydrogen isotope fractionation is different for system(I) and system(II).

In a magma formed in the mantle, system(II), for which we have no systematic knowledge on hydrogen isotopic fractionation, would prevail. Kuroda and others (1975; Kuroda, Suzuoki, and Matsuo, 1977) reported δD values of coexisting phlogopite and potassic richterite from mica-rich nodules and a peridotite nodule in South African kimberlite, which are given in table 1 and figure 1. The most unusual aspect of their results is that δD values of the pairs are internally quite different although the pairs are inferred to be formed under high temperature and pressure condition (Aoki, 1974; Dawson and Smith, 1977).

Aoki (1974) suggested that the phlogopite had crystallized earlier than the richterite based on the observed texture of the nodules. The large difference in δD values of a pair should be attributed to the sequential crystallization of phlogopite and richterite under water-undersaturated condition. In such a case, "Rayleigh-distillation" may apply to the crystallization of hydrous silicates. When phlogopite crystallizes first, the change in hydrogen isotopic ratios can be expressed in the following way:

$$R_{phlo} = R^{\circ}_{d.w.} \frac{1 - f^{\alpha}}{1 - f} \quad (2)$$

and

$$R_{d.w.} = R^{\circ}_{d.w.} f^{\alpha - 1} \quad (3)$$

where R denotes D/H $(1 + 10^{-3}\delta D)$, f is the remaining fraction of the dissolved water (d.w.)

Table 1.--Analytical results on phlogopite-richterite pair

[$X_{Fe} \equiv Fe^{II}/Fe^{II} + Me^{II}$. $X_F \equiv F/F + OH$]

Sample no.	H_2O content (weight percent)	δD_{SMOW} (permil)	X_{Fe}	X_F
		Phlogopite		
[1]DU 1	3.66	- 43.2	0.097	0.16
[1]DU 2	3.44	- 65.1	0.11	0.19
[2]WE 3	3.13	- 77.4	0.20	0.13
[3]BF 3	4.37	- 36.2	0.06	0.10
		Richterite		
[1]DU 1	1.73	-103.1	0.06	0.29
[1]DU 2	1.74	-132.5	0.07	0.29
[2]WE 3	1.72	-120.6	0.15	0.23
[3]BF 3	2.34	- 79.5	0.04	0.14

[1]Mica nodule from Dutoitspan mine.
[2]Mica nodule from Weselton mine.
[3]Peridotite nodule from Benfontein.

and α is the isotopic fractionation factor in the system phlogopite-dissolved water. When the crystallization of phlogopite ends, the crystallization of richterite follows. In this case,

$$R_{richt.} = [R^{\circ}_{d.w.} f^{\alpha-1}] \frac{1 - F^{\beta}}{1 - F} \quad (4)$$

where F refers to the remaining fraction of the dissolved water after the crystallization of richterite has started and β is the isotope fractionation factor in the system richterite-dissolved water. In the above three equations, the unknowns are $R^{\circ}_{d.w.}$, α, β, f, and F. For simplicity, we assume that α and β are the same. We can estimate the rough volume ratios of phlogopite to richterite for our particular samples. This gives a rough relationship between f and F. Then we can calculate $R^{\circ}_{d.w.}$, $\alpha(\beta)$, and f(F) through iteration. The best-fit values for the four pairs are in the range, $1.035 < \alpha(\beta) < 1.05$, and -90 permil $< \delta^{\circ}_{d.w.} < -75$ permil for DUI, DU2, WE3 and -60 permil for BF3. The final fraction of dissolved water remaining after both minerals have crystallized out ranges from 0 to 13 percent.

It is to be noted that the range of -90 permil $< \delta^{\circ}_{d.w.} <$ -75 permil agrees well with that designated by Craig and Lupton (1976) and

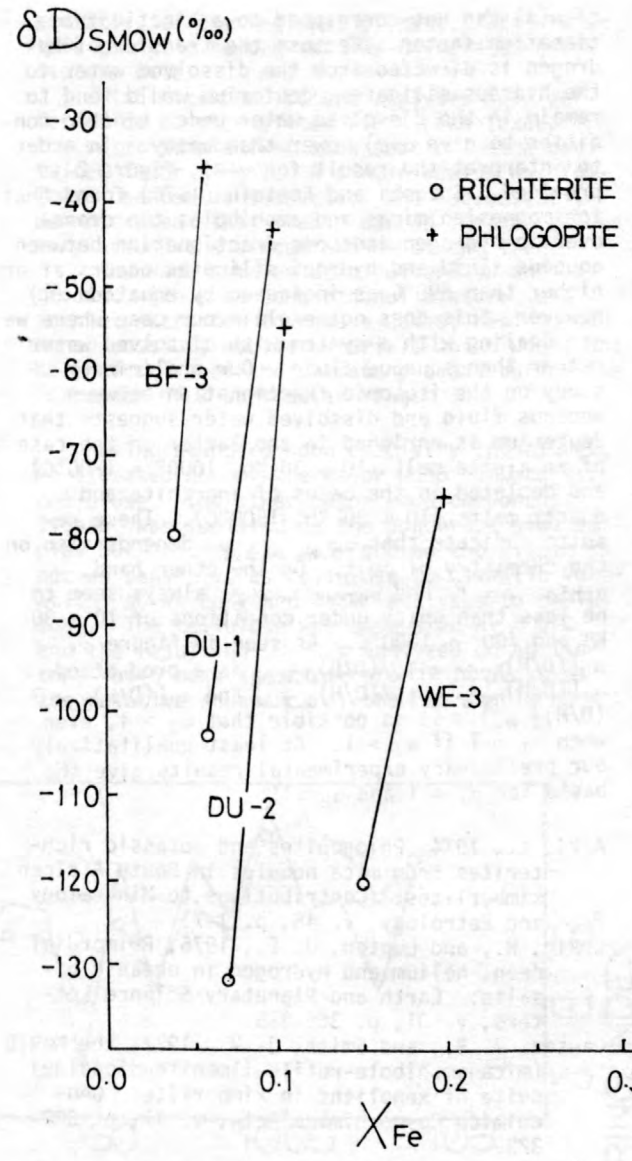

Figure 1.--δD versus X_{Fe} plot of phlogopite-richterite pair. X_{Fe}: $Fe^{II}/Fe^{II} + Mg^{II}$.

Kuroda and others (1977) for primordial water. The estimated value of -60 permil for BF3 apparently lies outside of this range. The BF3 pair was sampled from a peridotite nodule, while the other three pairs are taken from mica-rich nodules. The high value of $\delta^{\circ}_{d.w.}$ for BF3 may be a reflection of water contamination in the crust. This study would seem to offer supporting evidence that there still exists primordial water in mantle.

Another feature of our model study is that α or β must be significantly larger than unity. This is a strange situation at first glance because $\alpha(\beta)$ is supposed to be quite close to unity at elevated temperature. The estimated value

of $\alpha(\beta)$ can not correspond to a kinetic fractionation factor. Because the transfer of hydrogen is directed from the dissolved water to the hydrous silicates, deuterium would tend to remain in the dissolved water under kinetic condition to give $\alpha(\beta)$ lower than unity. In order to interpret the result for $\alpha(\beta)$, figure 2 is provided. Suzuoki and Epstein (1976) found that for magnesian micas and amphiboles the cross-over in hydrogen isotopic fractionation between aqueous fluid and hydrous silicates occurs at or higher than 690°C as indicated by equation (1). However, this does not explain our case where we are dealing with a system with dissolved water rather than aqueous fluid. Our preliminary study on the isotopic fractionation between aqueous fluid and dissolved water suggests that deuterium is enriched in the latter in the case of an albite melt (10 $\sim$ 30 Kb, 1000° $\sim$ 1200°C) and depleted in the cases of anorthite and quartz melts (10 $\sim$ 30 Kb, 1500°C). These results indicate that $\alpha_{d.w. - a.f.}$ depends also on the chemistry of melt. On the other hand, $\alpha_{phlo. - a.f.}$ and $\alpha_{amph. - a.f.}$ always seem to be less than unity under conditions of 10 $\sim$ 30 KB and 700° $\sim$ 1000°C. As seen in figure 2, $\alpha_3[(D/H)_{hydr.sil.}/(D/H)_{d.w.}]$ is a product of $\alpha_1[(D/H)_{hydr.sil.}/(D/H)_{a.f.}]$ and $\alpha_2[(D/H)_{a.f.}/(D/H)_{d.w.}]$. It is possible that $\alpha_3 > 1$, even when $\alpha_1 < 1$ if $\alpha_2 > 1$. At least qualitatively our preliminary experimental results give the basis for $\alpha_1 < 1$ and $\alpha_2 > 1$.

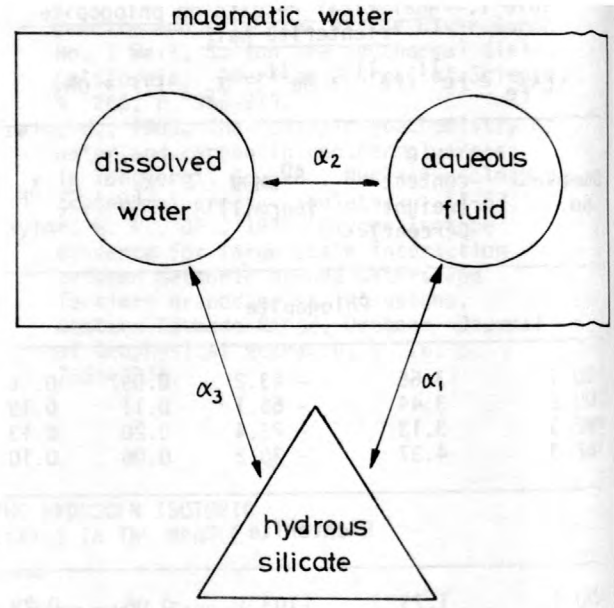

Figure 2.--Fractionation of hydrogen isotopes between various phases in magmatic processes.

Aoki, K., 1974, Phlogopites and potassic richterites from mica nodules in South African kimberlites: Contributions to Mineralogy and Petrology, v. 48, p. 1-7.

Craig, H., and Lupton, J. E., 1976, Primordial neon, helium and hydrogen in oceanic basalts: Earth and Planetary Science Letters, v. 31, p. 369-385.

Dawson, J. B., and Smith, J. V., 1977, the MARID (mica-amphibole-rutile-ilmenite-diopside) suite of xenoliths in kimberlite: Geochimica Cosmochimica Acta, v. 41, p. 309-323.

Kuroda, Y., Suzuoki, T., and Matsuo, S., 1977, Hydrogen isotope composition of deepseated water: Contributions to Mineralogy and Petrology, v. 60, p. 311-315.

Kuroda, Y., Suzuoki, T., Matsuo, S., and Aoki, K., 1975, D/H ratios of the coexisting phlogopite and richterite from mica nodules and a peridotite in South African kimberlites: Contributions to Mineralogy and Petrology, v. 52, p. 315-318.

Suzuoki, T., and Epstein, S., 1976, Hydrogen isotope fractionation between OH-bearing minerals and water: Geochimica Cosmochimica Acta, v. 40, p. 1224-1240

ISOTOPE DENDROCLIMATOLOGY: NATURAL STABLE CARBON ISOTOPE ANALYSIS OF TREE RINGS FROM AN ARCHAEOLOGICAL SITE

By Terry Mazany
Laboratory of Isotope Geochemistry
Department of Geosciences
University of Arizona, Tucson, Arizona 85721

Increasing interest in the Earth's climate has prompted an increasing amount of research designed to reconstruct past climate. This reconstruction will benefit disciplines such as archaeology and, from a more detailed reconstruction and understanding of the past climate, predictions will become more accurate. A portion of this research centers around the hypo-

thesis that relative abundances of certain stable isotopes (^{12}C and ^{13}C, ^{16}O and ^{18}O, H and D) are related to climatic variation (Lerman, 1974). Our present investigations, working with the stable carbon isotopes ^{13}C and ^{12}C in wood, are an attempt to verify a relationship between stable isotopes and climate and to determine various problems which must be recognized if useful data are producible.

For our isotope analyses, we selected dendrochronologically dated tree-ring sections from two species: ponderosa pine (Pinus ponderosa) dating from AD 810-1045, and white fir (Abies concolor) dating from AD 931-1047. These samples, provided by the Laboratory of Tree-Ring Research at the University of Arizona, were collected from Chetro Ketl, an archaeological site in Chaco Canyon, New Mexico. We used tree-ring samples because dendrochronology establishes an accurate time span (Bannister, 1969), and in the case of Chaco Canyon, a well-documented regional chronology provides a generalized record of climate derived from relative widths of individual rings: narrow rings indicate a warm and dry climate; wide rings, a wet and cool climate (Fritts, 1976; LaMarch, 1974). This chronology is composed of tree-ring width data from several trees so that it is representative of the regional climate. It is with this climatic record that we correlated our isotope data.

Stable carbon isotope analyses were performed on samples of ten rings each (excepting the outer sample from each section which contained fewer rings). A single radius was followed because we suspected, and subsequently demonstrated, that stable carbon isotope values vary around the circumference of the tree.

The wood samples were pulverized and extracted with a benzene-ethanol mixture in a Soxhlet extractor to remove waxes, resins, and other possibly mobile materials which would not be indicative of the climate present during the formation of a particular ring.

Using standard wood chemistry techniques, we isolated one of the major wood components: cellulose. The other major wood component, lignin, was isolated in the ponderosa pine samples but isotope analysis showed the lignin is not as sensitive as cellulose to climatic variation, so we confined later analyses to cellulose. The cellulose was combusted at 800°C, and the resulting CO_2 was analyzed on an isotope-ratio mass spectrometer. This measures the relative abundance of the two stable car-

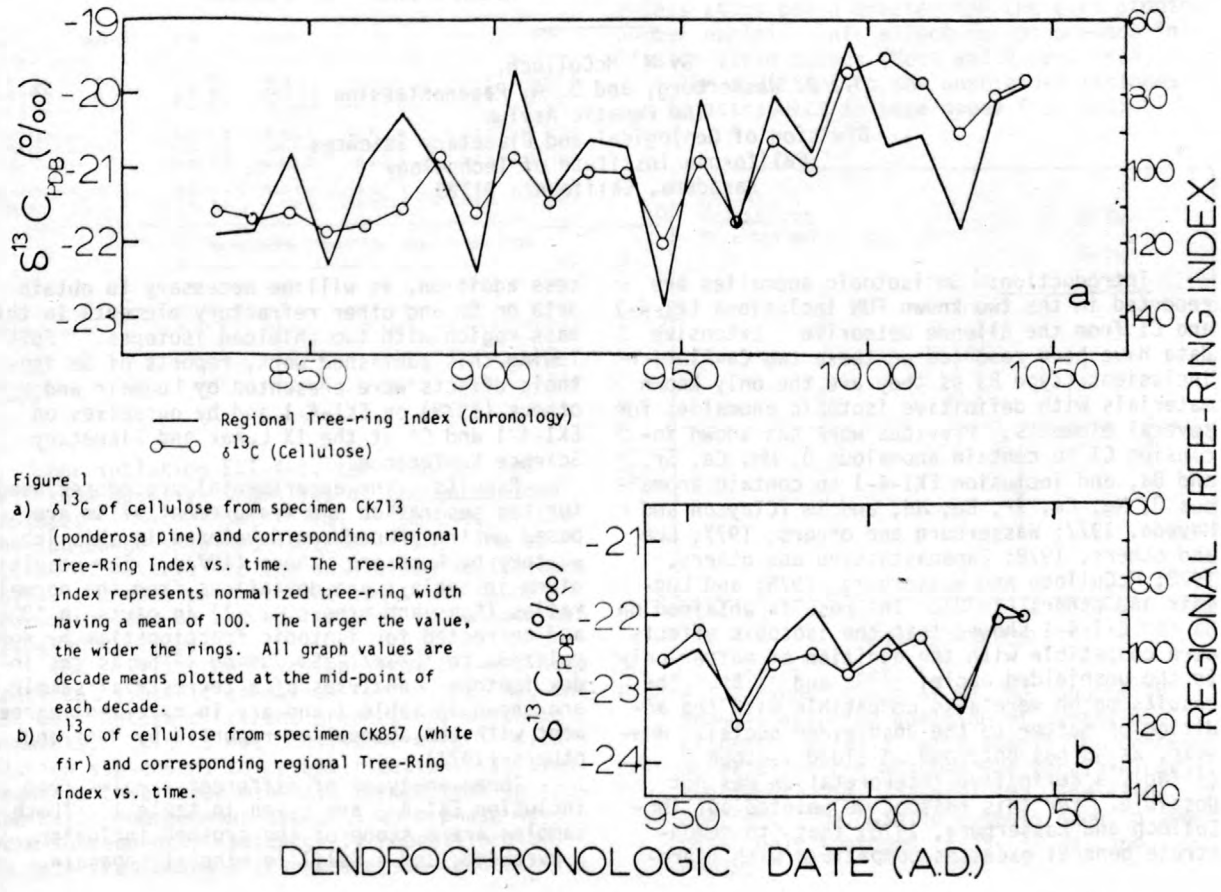

Figure 1

a) $\delta^{13}C$ of cellulose from specimen CK713 (ponderosa pine) and corresponding regional Tree-Ring Index vs. time. The Tree-Ring Index represents normalized tree-ring width having a mean of 100. The larger the value, the wider the rings. All graph values are decade means plotted at the mid-point of each decade.

b) $\delta^{13}C$ of cellulose from specimen CK857 (white fir) and corresponding regional Tree-Ring Index vs. time.

bon isotopes, relative to a standard, which is reported in the standard manner as δ^{13}PDB.

The data show a significant correlation with the regional tree-ring chronologies. The correlation coefficient (r) for δ^{13} of the ponderosa pine cellulose plotted against the tree-ring chronology for ponderosa pine is 0.65 (fig. 1a). For the white fir isotope values plotted against the white fir chronology, r = 0.80 (fig. 1b).

The results of this research are very promising. The significant correlation between isotope data and tree-ring chronologies suggests that stable carbon isotope values do record climatic variation. The value of stable carbon isotope analysis is that it might be used when tree-ring material is complacent (not sensitive to climatic variation, as when a tree has tapped a permanent supply of water). And, in addition, the isotope data from one tree are representative of a tree-ring chronology composed of the ring width measurements of several trees. This suggests that where sufficient trees are not available to form a representative tree-ring chronology, the isotope analysis from just one tree will be able to provide the needed data.

I thank William Robinson and Jeff Dean for providing samples and data; Gail Hennington and Jim LoFaro for chemical preparations. Thanks are also due Austin Long, Juan Carlos Lerman, Tom Harlan, Bryant Bannister, Paul Damon, Harold Fritts, and Sandy Harralson.

This research was funded by NSF Grant No. ATM77-06790 and the State of Arizona.

Bannister, B., 1969, Dendrochronology, in Brothwell, D., and Higgs, E., eds., Science in Archaeology: London, Thames and Hudson, 2nd edition, p. 191-205.

Fritts, H. C., 1976, Tree Rings and Climate: New York, Academic Press, 567 p.

LaMarche, V. C., Jr., 1974, Paleoclimatic inferences from long tree-ring records: Science, v. 183, p. 1043-1048.

Lerman, J. C., 1974, Isotope "paleothermometers" on continental matter; assessment: Paris, France, Centre National de la Recherche Scientifique Colloques Internationaux, no. 219, p. 163-181.

MORE MYSTERIES FROM PANDORA'S BOX

By M. McCulloch,
G. J. Wasserburg, and D. A. Papanastassiou
The Lunatic Asylum
Division of Geological and Planetary Sciences
California Institute of Technology
Pasadena, California 91125

Introduction: Sm isotopic anomalies are reported in the two known FUN inclusions Ek1-4-1 and C1 from the Allende meteorite. Extensive data have been reported on these two Ca-Al-rich inclusions (type B) as they are the only known materials with definitive isotopic anomalies for several elements. Previous work has shown inclusion C1 to contain anomalous O, Mg, Ca, Sr, and Ba, and inclusion EK1-4-1 to contain anomalous O, Mg, Ca, Sr, Ba, Nd, and Sm (Clayton and Mayeda, 1977; Wasserburg and others, 1977; Lee and others, 1978; Papanastassiou and others, 1978; McCulloch and Wasserburg, 1978; and Lugmair and others, 1978). The results obtained on Ba for EK1-4-1 showed that the isotopic effects were compatible with the addition of matter only to the unshielded nuclei ^{135}Ba and ^{137}Ba. The results on Nd were also compatible with the addition of matter to the unshielded nuclei. However, as Nd has only one shielded isotope (^{142}Nd), a definitive interpretation was not possible. For this reason, we pointed out (McCulloch and Wasserburg, 1978) that "to demonstrate general excesses compatible with r-process addition, it will be necessary to obtain data on Sm and other refractory elements in this mass region with two shielded isotopes." Following this published work, reports of Sm isotopic effects were presented by Lugmair and others (1978) on EK1-4-1 and by ourselves on EK1-4-1 and C1 at the IX Lunar and Planetary Science Conference.

Results: The experimental procedures used for the separation and measurement of Sm are based on the procedures developed in this laboratory by Russ and others (1971). The results given in table 1 are deviations from the normal ratios (Russ and others, 1971) in parts in 10^4 and corrected for isotopic fractionation by normalizing to ^{147}Sm/^{154}Sm, using ^{154}Sm as the index isotope. Analyses of a terrestrial sample are shown in table 1 and are in excellent agreement with the abundances reported by Russ and others (1971).

Three analyses of different samples from inclusion EK1-4-1 are given in table 1. These samples are a scoop of the crushed inclusion, a pyroxene, and a melilite mineral separate.

All samples show large deviations from normal which exceed the uncertainties by a factor of more than 10. The deviations for the different samples are identical within error with the exception of $^{144}Sm/^{154}Sm$-deviations for EK1-4-1 SC and EK1-4-1 PYX which are at the limit of the 2σ uncertainty. The larger uncertainties for the melilite analysis are a consequence of a factor of 10 smaller sample size (4-ng Sm). These isotopic effects are in agreement with a recent report by Lugmair and others (1978) on a pyroxene separate.

From inclusion C1, two different pyroxene separates and a split of the crushed inclusion were analyzed. These analyses all show an enrichment in only $^{144}Sm/^{154}Sm$ of 15 ± 5 parts in 10^4. All other isotopic ratios are identical within error to the terrestrial normal.

Discussion: To elucidate the effects in Sm, it is more appropriate to use the two shielded isotopes ^{150}Sm and ^{148}Sm to correct for fractionation with ^{148}Sm as an index isotope. The renormalized data for EK1-4-1, C1 and the terrestrial sample are also shown in table 1.

Table 1.--Samarium isotopic variations

[Errors are 2σ mean. Deviations in parts per ten thousand relative to our grand mean of six terrestrial normals. $^{144}Sm/^{154}Sm = 0.13516 \pm 1$; $^{148}Sm/^{154}Sm = 0.49419 \pm 2$; $^{149}Sm/^{154}Sm = 0.60750 \pm 2$; $^{150}Sm/^{154}Sm = 0.32440 \pm 2$; $^{152}Sm/^{154}Sm = 1.17537 \pm 4$; $^{147}Sm/^{154}Sm = 0.65918$. PYX, pyroxene; MEL, melilite; S1, SC, splits of crushed inclusion]

		Normalized to $^{147}Sm/^{154}Sm$, index isotope ^{154}Sm				
Sample	Sm(ppm)	ε144	ε148	ε149	ε150	ε152
EK1-4-1 SC-----	4.1	-17.0± 5.2	-36.2±2.2	-0.7±1.5	-35.1±2.2	-9.1±1.4
EK1-4-1 PYX----	5.3	- 5.2± 5.9	-38.2±2.6	+0.2±2.1	-33.9±3.1	-9.4±1.7
EK1-4-1 MEL----	1.4	- 7.4±13.0	-37.0±4.9	+0.2±4.1	-31.4±7.7	-6.5±3.7
C1 PYX (1)-----	4.9	+11.8± 4.0	-4.2±1.8	-0.8±1.8	- 3.1±2.2	+0.2±0.6
C1 PYX (2)-----	4.4	+17.0± 3.0	-0.6±1.0	-0.5±0.7	- 1.2±1.2	-0.6±0.5
C1 S1----------	--	+15.5± 5.9	-0.4±1.8	-0.2±1.5	- 1.2±1.5	-1.7±1.2
Terrestrial---- sample	20.0	0.0± 3.7 + 1.5± 3.0	-1.0±1.8 -0.4±0.6	-0.3±1.3 +0.8±1.0	-0.3±2.1 - 1.8±2.2	+0.6±0.8 +0.3±0.5

	Normalized to $^{150}Sm/^{148}Sm$, index isotope ^{148}Sm				
	ε144	ε147	ε149	ε152	ε154
EK1-4-1--------	+34.4±8.4	+38.5±3.3	+36.5±2.1	+24.1±4.0	+31.6±4.2
C1----------	+15.4±5.0	+ 0.4±1.6	+ 1.3±1.0	+ 2.0±2.1	+ 2.0±3.9
Terrestrial---- sample	+ 1.6±4.0	+ 0.4±1.6	+ 0.1±1.6	- 0.8±3.3	- 1.4±4.7

For inclusion EK1-4-1, the renormalized data show positive anomalies at the unshielded isotopes ^{154}Sm, ^{152}Sm, ^{149}Sm, ^{147}Sm and, at the low-abundance shielded isotope ^{144}Sm. The addition of material to the unshielded Sm isotopes is fully consistent with the additions found in the unshielded Ba and Nd isotopes (McCulloch and Wasserburg, 1978).

The melilite and pyroxene from EK1-4-1 have identical isotopic anomalies for Sr, Ba, Nd, and Sm, but contain different proportions of these elements. This is not consistent with in situ fission subsequent to crystallization. It also requires that these minerals formed from an isotopically homogeneous gas or liquid phase or were subsequently isotopically reequilibrated. Xe data from EK1-4-1 (Papanastassiou and others, 1978) are also not consistent with an origin of these anomalies by in situ fission. The Xe data are consistent with mixtures of ^{244}Pu fission Xe, air Xe, Xe from cosmic-ray-induced reactions on Ba, REE and I, and Xe from ^{129}I decay. There is no evidence for isotopic enrichments from any other sources (for example, Xe from an unknown origin in bulk acid insoluble residues; Lewis and others, 1975).

Assuming that the isotopic effects in Sm found in EK1-4-1 are due to the addition of excess nuclides to average solar-system material of cosmic abundances, the number of excess atoms (*) can be calculated. This gives (cosmic Si = 10^6 atoms) $^{144}Sm^* = 2.4 \times 10^{-5}$, $^{147}Sm^* = 1.4 \times 10^{-4}$, $^{149}Sm^* = 1.1 \times 10^{-4}$, $^{152}Sm^* = 1.5 \times 10^{-4}$, and $^{154}Sm = 1.6 \times 10^{-4}$ atoms. These excess atoms together with those calculated for Ba and Nd are plotted in figure 1. For Ba and Nd the normalizations are as described by McCulloch and Wasserburg (1978), although for Nd the arbitrary assignment of an excess to ^{144}Nd of +20 parts in 10^4 has been adjusted to +18 to produce a smooth curve between excess atoms of ^{150}Nd and ^{152}Sm. The main feature of the curve in figure 1 is the pronounced peak between Ba and Nd. Chemical fractionation between Ba* and the exotic rare-earth nuclei during formation of the inclusion, would modify this peak. A small odd-even effect is also apparent in Nd and Sm, with the excess atoms being greater for the even atomic number nuclei. This effect is not present in fission-yield curves (Meek and Rider, 1974).

The additions to the unshielded isotopes can be attributed to beta decay from unstable

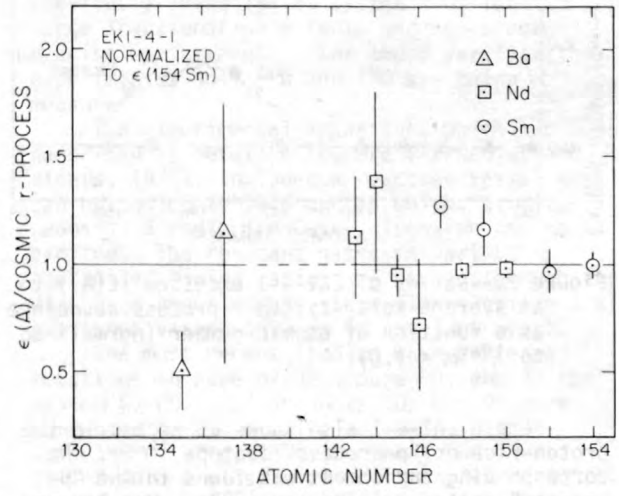

Figure 1.--Excess atoms of Ba, Nd, and Sm in EK1-4-1 assuming addition of exotic nuclides to material with cosmic abundances. No excesses are assumed for the shielded nuclides ^{150}Sm, ^{148}Sm, ^{142}Nd, and ^{134}Ba, and for ^{138}Ba. Solid symbols show "p-process" only isotopes ^{130}Ba, ^{132}Ba, and ^{144}Sm.

neutron-rich species. Isotopes produced by this general mechanism are often referred to as "r-process". To test whether the excess atoms shown in figure 1 are produced by an average "cosmic" r-process, we have calculated the ratios of excess atoms to "cosmic" r-process atoms (normalized to ^{154}Sm). This is shown in figure 2 as a function of atomic number. The isotopes ^{154}Sm, ^{150}Nd, and ^{148}Nd are produced only by the r-process. However, the other isotopes ^{152}Sm, ^{149}Sm, ^{147}Sm, ^{146}Nd, ^{145}Nd, ^{144}Nd, ^{143}Nd, ^{137}Ba, and ^{135}Ba also contain an s-process component which must be subtracted to obtain the cosmic r-process. The uncertainty in calculating the r-process contribution depends on the accuracy of the calculated s-process and the relative proportions of the s and r components. Figure 2 indicates that the excess atoms in EK1-4-1 are, in general, similar to the cosmic r-process distribution. However, the significant deviations at ^{149}Sm, ^{147}Sm, and ^{135}Ba show that the exotic material was not identical to the average solar system r-process, or that the additions were not made to material with an average solar-system isotopic composition.

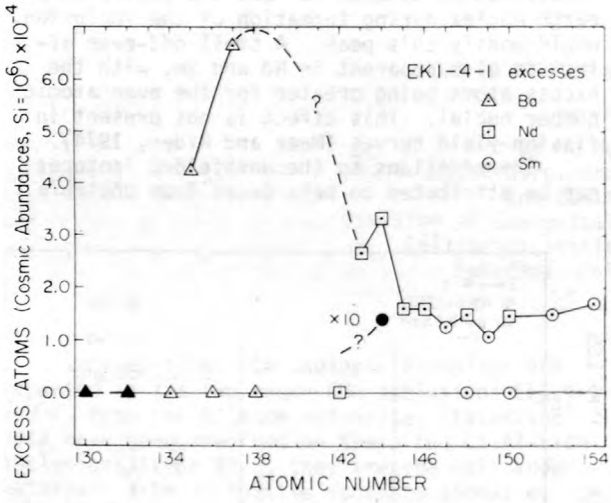

Figure 2.--Ratios of EK1-4-1 excesses (E(A)) to an average solar-system r-process abundance as a function of atomic number (normalized to ^{154}Sm = 1.0).

Sample EK1-4-1 also shows an excess in the proton-rich or "p-process" isotope ^{144}Sm. No corresponding enrichment was found in the "p-process" isotopes ^{132}Ba and ^{130}Ba. Woosley and Howard (1978) have indicated that the production of p-process nuclei by photo-disintegration reactions operating on r- and s-process seeds is temperature dependent. Using this model, it may be possible to overproduce ^{144}Sm relative to its cosmic abundance without corresponding additions to ^{132}Ba and ^{130}Ba.

In the other FUN sample C1, an excess in only the "p-process" isotope ^{144}Sm is present. All other isotopic ratios are normal. The presence of only a "p-process" addition to C1 is important as it shows that the "p-process" is not necessarily coupled to the r-process. This is in contrast to EK1-4-1 where both p- and r-process additions are present. The ^{144}Sm "p-process" excess in C1 is approximately a factor of two smaller than that in EK1-4-1. Although close to the limit of our resolution, no corresponding addition has been detected in the "p-process" isotopes ^{132}Ba and ^{130}Ba in C1 (McCulloch and Wasserburg, 1978). However, using the same arguments as discussed for EK1-4-1, this may not be unexpected. The normal Nd isotopic composition in C1 is in consonance with these results as it has no "p-process" only isotopes.

The discussion of Ba, Nd, and Sm data for EK1-4-1 and the Sm data for C1 has been based on the premise of addition of exotic materials to material with a normal solar-system isotopic composition. However, the presence of negative isotopic anomalies in other elements, ^{135}Ba and ^{48}Ca in C1 and ^{84}Sr and ^{26}Mg in EK1-4-1 and C1, suggests that this may not have been the case and materials which received these additions may have been depleted in some isotopes. This is particularly apparent in Sr (Papanastassiou and others, 1978) which shows anomalies in $^{84}Sr/^{88}Sr$ of -32 ± 2 and -9 ± 2 parts in 10^4 for EK1-4-1 and C1, respectively, when normalized to $^{86}Sr/^{88}Sr$ = 0.1194. These data are consistent with a deficiency in either the "p-process" ^{84}Sr or r-process ^{88}Sr. Alternatively, it may represent an excess in the s-process ^{86}Sr. As suggested by McCulloch and Wasserburg (1978), the negative ^{135}Ba anomaly may also imply that C1 represents precursor solar-system material before r-process addition. However, the depletions of ^{135}Ba in C1 and in EK1-4-1 could also be due to a holdup at ^{135}Cs, which is the progenitor for ^{135}Ba. If C1 and EK1-4-1 condensed before the more volatile ^{135}Cs ($\tau_{1/2}$ = 2.3 x 10^6 yr) decayed to ^{135}Ba, this could account for these discrepancies. It is apparent from the data presented here that there are probably many more mysteries left within Pandora's Box.

Clayton, R. N., and Mayeda, T. K., 1977, Correlated oxygen and magnesium isotope anomalies in Allende inclusions, I; Oxygen: Geophysical Research Letters, v. 4, p. 295-298.

Lee, T., Papanastassiou, D. A., and Wasserburg, G. J., 1978, Calcium isotopic anomalies in the Allende meteorite: Astrophysical Journal Letters, v. 220, p. L21-L25.

Lewis, R. S., Scrinivasan, B., and Anders, E., 1975, Host phase of a strange xenon component in Allende: Science, v. 190, p. 1251-1262.

Lugmair, G. W., Marti, K., and Scheinin, N. B., 1978, Incomplete mixing of products from r-, p-, and s-process nucleosynthesis; Sm-

Nd systematics in Allende inclusion EK1-4-1 (abs.): Lunar and Planetary Science IX, p. 672-674.

McCulloch, M. T., and Wasserburg, G. J., 1978, Barium and neodymium isotopic anomalies in the Allende meteorite: Astrophysical Journal Letters, v. 220, p. L15-L19.

Meek, M. E., and Rider, B. F., 1974, Compilation of fission product yields: Pleasanton, California, Vallecitos Nuclear Center.

Papanastassiou, D. A., Huneke, J. C., Esat Tezer, M., and Wasserburg, G. J., 1978, Pandora's box of the nuclides (abs.): Lunar and Planetary Science IX, p. 859-861.

Russ, G. P., III, Burnett, D. S., Lingenfelter, R. E., and Wasserburg, G. J., 1971, Neutron capture on ^{149}Sm in lunar samples: Earth and Planetary Science Letters, v. 13, p. 53-60.

Wasserburg, G. J., Lee, T., and Papanastassiou, D. A., 1977, Correlated O and Mg isotopic anomalies in the Allende inclusions, II; Magnesium: Geophysical Research Letters, v. 4, p. 299-302.

Woosley, S. E., and Howard, W. M., 1978, The p-process in supernovae: Astrophysical Journal Supplementary, v. 36, p. 285-304.

CHEMICAL ISOTOPE FRACTIONATION IN INTERSTELLAR CLOUD CONDENSATES - SOME MODEL EXPERIMENTS

By J. L. McCrumb, S. Markus, R. Fitzgerald, J. Killingley, and G. Arrhenius
Scripps Institution of Oceanography
La Jolla, California 92093

Distinction of chemical isotope effects from nucleosynthetic effects is crucial for interpretation of the evolutionary record in meteorites. Furthermore, the chemical, kinetic, and equilibrium effects can provide significant information on the state of excitation of the cloud medium in which they are now observed, and in the presumably similar medium from which meteorite solids formed. Non linear effects in three-isotope systems, such as oxygen, have, in the past, been interpreted as nucleosynthetic in origin (Clayton and others, 1973; Clayton and others, 1976) because such effects were unknown in equilibrated geological materials studied on Earth (although known from kinetic laboratory studies of organic reactions, Melander, 1960). The significance of such effects in meteorites is suggested by the very large chemical isotope effects observed by microwave spectroscopy in two-isotope systems in dark interstellar clouds (see references in Arrhenius, 1976).

The investigations reported on here aim at experimental modeling of some of the isotope effects observed in the interstellar cloud medium. Initial measurements were undertaken on nitrogen in reactions with oxygen in plasmas with low-kinetic temperature, and demonstrate enrichment of the heavy isotope ^{15}N up to 42 percent (Arrhenius and others, 1978). Present and planned experiments concern the oxygen isotope fractionation in molecules of importance in condensation from the source-cloud medium such as CO, CO_2, H_2O, OH, HCO, O_2, MgO, SiO, CaO, AlO, and others.

The ultimate purpose of the studies involving oxygen compounds is to measure the kinetic-fractionation effects on the three stable isotopes of this nuclide. Because of the low relative abundance of ^{17}O we try first to identify specific reactions which, as in the previously investigated system N-O, lead to large fractionation effects and hence permit precise measurements. For these verification experiments, only ^{16}O and ^{18}O are being measured.

The experimental apparatus, which has been described in detail elsewhere (Arrhenius and others, 1978), includes a reaction vessel that can be cooled to 77 K and in which, simultaneously, a radio frequency discharge can be excited. The reactant gases in various controlled-mixing ratios are passed through the discharge under steady-state-flow conditions at pressures varied between 50 and 1000 mtorr.

The most recent studies have concerned reactions in pure oxygen, pure CO, and in the system O_2-CO. The products CO_2 and O_3 were condensed onto the walls of the reaction vessel and, after the experiment, were distilled into a glass vial and transferred to the mass spectrometer for isotopic analysis.

In a pure oxygen discharge we have intestigated $\delta^{18}O$ in the ozone product, which was found not to exceed 1.5 percent over a wide range of experimental conditions. In contrast, carbon dioxide resulting from oxidation of carbon monoxide in pure CO and CO-O_2 discharge shows marked enrichment of ^{16}O (and ^{12}C) in the product CO_2.

These results are shown in figure 1 for a series of experiments carried out at a reaction-vessel pressure of 300 mtorr and a flow rate of about 70 torr cc sec^{-1}. The enrichment curves for ^{13}C and ^{18}O, which depend strongly on the composition of the reactant mixture, both give a maximum at an oxygen mole fraction of 0.02. For ^{18}O, however, this maximum corresponds to zero enrichment relative to the reactant gas, whereas a maximum depletion of 30 permil occurs at an oxygen mole fraction of 0.15.

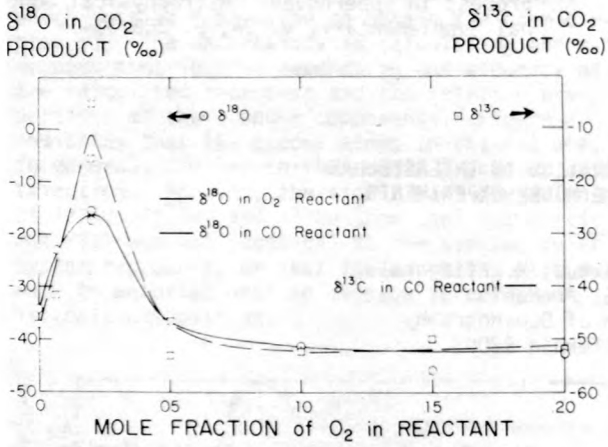

Figure 1.--Isotopic fractionations of ^{13}C and ^{18}O (relative to a PDB CO_2 standard) in product CO_2 formed in an O_2/CO discharge at a temperature of 77 K and a pressure of 300 millitorr.

For ^{13}C a maximum enrichment of 30 permil occurs at an O_2 mole fraction of 0.02 and a maximum depletion of 10 permil at an O_2 mole fraction of 0.10.

Variation of the pressure and flow rate were found to affect the observed fractionation; higher pressures and flow rates gave larger depletion in product ^{13}C and ^{18}O. These effects, however, were on the order of ± 2 permil, - small compared to the changes with O_2 mole fraction shown in figure 1.

In addition to the volatile products CO_2 and O_3, a nonvolatile brown deposit of C_3O_2 was observed to form on the walls of the reaction vessel. The polymetric tricarbon dioxide, a substance often observed in CO discharges (Rudolph and Lind, 1960), was removed by oxidation with a pure O_2 discharge. Current experiments are aimed at determining the chemical and isotopic composition of this deposit.

The manner in which the various products were deposited on the wall is also of interest. The volatile CO_2 and O_3 products were deposited uniformly over the surface of the vessel, while the tricarbon dioxide polymer formed in a ring clearly defined by the shape of the r.f. discharge coils. This suggests the possibility that CO_2 and O_3 are formed by a neutral mechanism and thus spatially unaffected by the r.f. field of the discharge, and that the polymer is formed by an ionic mechanism, the ions being strongly affected by the field leading to the well defined deposit.

The mechanism leading to the formation of the fractionated carbon dioxide can be generalized as:

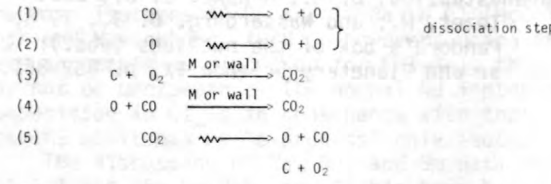

As written, this procedure allows for several different pathways leading from reactants to the CO_2 product. The exact path cannot be specified at the present time, but according to this procedure, it is certainly a strong function of experimental conditions. For example, in the dissociation steps 1 and 2 the relative amount of CO and O_2 dissociated is a function of the O_2 mole fraction. Likewise, in the combination steps the O_2 mole fraction, as well as the pressure, will determine the rates and relative importance of reactions 3 and 4.

Comparison of these results with those from the N_2/O_2 discharge experiments (Arrhenius and others, 1978) allows some general speculation as to the chemical mechanisms responsible for the fractionation. The most striking difference in the two sets of results is the fact that the product N_2O was enriched in the heavier isotope, whereas the CO_2 product from oxidation of carbon is enriched in the lighter isotope relative to the reactants. Possible mechanisms were suggested to explain the effect observed in the product N_2O in the N_2/O_2 system. The product molecule may, in this case, be partially redissociated by a predissociation from an excited vibrational level. The light isotope having a higher vibrational frequency would have a higher probability for dissociation, leaving the remaining product enriched in the heavier isotope. In the present experiment, resulting in a light CO_2 product, such a mechanism would require that the critical predissociation occurs in the dissociation of one or both of the parent molecules CO and O_2.

Arrhenius, G., 1976, North Atlantic Treaty Organization Cont. Origin Solar System, Newcastle, England, April 1976; in The origin of the solar system, Dermott, S. F., ed., Wiley, N. Y., 1978.

Arrhenius, G., Fitzgerald, R., Markus, S., and Simpson, C., 1978, Isotope fractionation under simulated space conditions: Astrophysics and Space Science (in press).

Clayton, R. N., Grossman, L., and Mayeda, T. K., 1973, Science, v. 182, p. 485-488.

Clayton, R. N., Onuma, N., and Mayeda, T. K., 1976, Earth and Planetary Science Letters, v. 30, p. 10-18.

Melander, L., 1960, Isotope Effects on Reaction Rates, Ronald Press, New York.

Rudolph, P. S., and Lind, S. C., 1960, Journal of Chemical Physics, v. 33, p. 705.

REVISION OF THE GEOMAGNETIC POLARITY TIME SCALE FOR THE LAST 5 M.Y.

By Ian McDougall, Research School of Earth Sciences, Australian National University, Canberra, A.C.T., Australia

The geomagnetic-polarity time scale for the last 4 m.y. was developed by combining paleomagnetic and K-Ar age data from subaerial volcanic rocks. Recently the IUGS Subcommission on Geochronology recommended the adoption of more precise and accurate ^{40}K decay constants based upon those given by Beckinsale and Gale (1969), adjusted to the ^{40}K abundance determined by Garner and others (1975). The recommended values are: $\lambda_e + \lambda_e' = 0.581 \times 10^{-10}y^{-1}$, $\lambda_\beta = 4.962 \times 10^{-10}y^{-1}$, and $^{40}K/K = 1.167 \times 10^{-4}$ (Steiger and Jäger, 1977). Use of these values requires that the K-Ar ages on which the polarity time scale is based be increased by 2.67 percent, compared with the ages previously reported. A revised polarity time scale, based upon the recalculated ages, and taking into account many new data published since the last comprehensive review of the time scale (Dalrymple, 1972), is given in figure 1.

The revised age for the boundary between the Brunhes and Matuyama epochs is 0.72 m.y., probably with an uncertainty of about 0.02 m.y. As the age of this boundary has assumed considerable importance in the interpolation of ages in deep-sea sedimentary cores, particularly in respect to the detailed interpretation of paleoclimates from oxygen isotope data, it is desirable to determine the age with as much precision as possible. For this to be accomplished it is probably necessary to locate a continuous succession of fresh subaerial lavas in which the polarity transition is recorded so that appropriate detailed age measurements can be made.

The boundary between the Matuyama and Gauss epochs is well controlled at 2.47 m.y., based upon the K-Ar dating and paleomagnetic measurements given by McDougall and Aziz-ur-Rahman (1972) on lavas from Norfolk Island in the South Pacific, where normal polarity lavas of the Gauss epoch are overlain by reversed polarity lavas of the Matuyama epoch. The Gauss-Gilbert boundary, estimated to have an age of 3.41 m.y., is controlled by measurements from diverse localities, and an independent estimate of its age at 3.36 m.y. is given from polarity-age data for a continuous sequence of lavas in Iceland (McDougall and others, 1977). For the Gilbert-epoch 5 boundary the density of age and polarity data is such that its estimated age of 5.44 m.y. probably has an uncertainty of about 0.15 m.y.

The situation regarding the age limits for the shorter intervals (events) of opposite polarity within the epochs is rather less satisfactory, although the Jaramillo event in the Matuyama epoch and the Kaena and Mammoth events within the Gauss epoch are relatively well dated. With the possible exception of the reversed polarity Laschamp event, dated at about 30,000 years, there is insufficient evidence that other postulated events within the Brunhes epoch reflect behaviour of the geomagnetic field on a global scale. Considerable uncertainty still exists as to the number, age, and duration of normal polarity events in the early part of the Matuyama reversed epoch. It is not yet clear whether the Gilsá and Olduvai normal events within the age span 1.6-1.95 m.y. are separate entities or one and the same, and this probably will be resolved only by detailed study of a continuous section of volcanics covering the time interval in question. A normal polarity event of short duration and dated at 2.07 m.y. is well-documented from a lava sequence in Réunion. Magnetic polarity measurements on deep-sea sedimentary cores and marine magnetic-anomaly data indicate that four normal polarity events occur within the Gilbert reversed epoch, but the age and duration of these events is not as well-controlled as those of the younger events.

The polarity time scale for the last 3.3 m.y., compiled from measurements on subaerially erupted volcanic rocks, was correlated with the pattern of linear marine magnetic anomalies, and by extrapolation a predicted time scale extend-

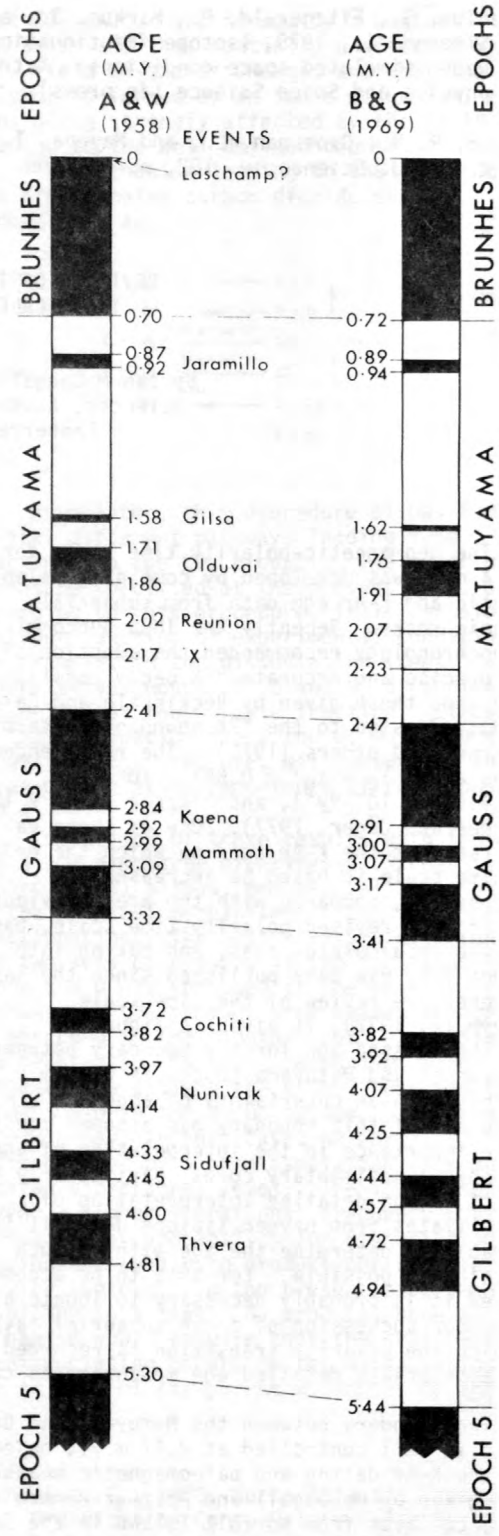

Figure 1.--Revised geomagnetic polarity time scale based mainly upon K-Ar and paleomagnetic data from volcanic rocks, after McDougall (1977). The time scale on the left is derived using K-Ar ages calculated using ^{40}K decay constants proposed by Aldrich and Wetherill (1958). The time scale on the right is adjusted to the recently recommended decay constants for ^{40}K (Steiger and Jäger, 1977). Black represents normal polarity, white represents reversed polarity.

ing to about 80 m.y. ago was derived (Heirtzler and others, 1968; La Brecque and others, 1977). Use of the recently recommended ^{40}K decay constants requires that the age of each polarity inversion be increased. Due to the exponential nature of radioactive decay and the involvement of two partial decay constants in the calculation of a K-Ar age, the increase in age ranges from 2.66 percent at 5 m.y., to 2.62 percent at 25 m.y., to 2.52 percent at 80 m.y. For all practical purposes the correction to be applied to the previous time scales decreases linearly with increasing age for the last 80 m.y., and thus, modified versions can be readily calculated.

Because of the extensive use of the polarity time scale in geological studies it is of some importance to test the validity of the extrapolations required to obtain this predicted time scale covering the last 80 m.y. of geological time. Lack of resolution in the K-Ar dating means that direct testing is difficult for times earlier than about 5 m.y. ago by measurement of individual volcanic units that are not in known stratigraphic relation to one another. However, detailed paleomagnetic and K-Ar age measurements on thick sequences of basaltic lavas in Iceland demonstrate that a reasonably precise polarity time scale can be determined directly in the time interval between 4 and 13 m.y. (McDougall and others, 1976; 1977). Results presently available indicate that at an age of 10 m.y. the predicted polarity time scale from the marine magnetic anomaly data is correct to within about 3 percent.

Aldrich, L. T., and Wetherill, G. W., 1958, Geochronology by radioactive decay: Annual Review of Nuclear Science, v. 8, p. 257-298.

Beckinsale, R. D., and Gale, N. H., 1969, A reappraisal of the decay constants and branching ratio of ^{40}K: Earth and Planetary Science Letters, v. 6., p. 289-294.

Dalrymple, G. B., 1972, Potassium-argon dating of geomagnetic reversals and North American glaciations, in, Calibration of Hominid

Evolution, Bishop, W. W., and Miller, J. A., eds., Edinburgh, Scottish Academic Press, p. 107-134.

Garner, E. L., Murphy, T. J., Gramlich, H. W., Paulsen, P. J., and Barnes, I. L., 1975, Absolute isotopic abundance ratios and the atomic weight of a reference sample of potassium: U. S. National Bureau of Standards, Journal of Research, v. 79A, p. 713-725.

Heirtzler, J. R., Dickson, G. O., Herron, E. M., Pitman, W. C. III, and Le Pichon, X., 1968, Marine magnetic anomalies, geomagnetic field reversals, and motions of the ocean floor and continents: Journal of Geophysical Research, v. 73, p. 2119-2136.

La Brecque, J. L., Kent, D. V., and Cande, S. C., 1977, Revised magnetic polarity time scale for Late Cretaceous and Cenozoic time: Geology, v. 5, p. 330-335.

McDougall, I., 1977, The present status of the geomagnetic time scale: Australian National University, Research School of Earth Sciences, Publication 1288, 34 p.

McDougall, I., and Aziz-ur-Rahman, 1972, Age of the Gauss-Matuyama boundary and the Kaena and Mammoth events: Earth and Planetary Science Letters, V. 14, p. 367-380.

McDougall, I., Saemundsson, K., Johannesson, H., Watkins, N. D., and Kristjansson, L., 1977, Extension of the geomagnetic polarity time scale to 6.5 m.y. - K-Ar dating, geological, and paleomagnetic study of a 3,500-m lava succession in western Iceland: Geological Society of America Bulletin, v. 88, p. 1-15.

McDougall, I., Watkins, N. D., Walker, G. P. L., and Kristjansson, L., 1976, Potassium-argon and paleomagnetic analysis of Icelandic lava flows - Limits on the age of anomaly 5: Journal of Geophysical Research, v. 81, p. 1505-1512.

Steiger, R. H., and Jäger, E., 1977, Subcommission on Geochronology - Convention on the use of decay constants in geo- and cosmochronology: Earth and Planetary Science Letters, v. 36, p. 359-362.

AGE AND STRONTIUM ISOTOPE CHEMISTRY OF THE SIERRA MADRE OCCIDENTAL VOLCANIC PROVINCE, WESTERN MEXICO

By F. W. McDowell[1], T. W. Duex[1], C. D. Henry[2], and L. E. Long[1]
[1]Department of Geological Sciences,
[2]Bureau of Economic Geology
The University of Texas at Austin
Austin, Texas 78712

Western Mexico has experienced repeated episodes of igneous activity since the end of the Paleozoic (McDowell and Clabaugh, 1978). The oldest igneous rocks are nearly everywhere covered by younger rocks formed during two major periods of magmatism. The first of these occurred during Late Cretaceous and early Tertiary time (100 to 45 m.y. ago) in the Sierra Madre Occidental and on the Mexican coastal plain adjacent to the Gulf of California (Henry, 1975). It produced a vast complex of ignimbrites, lavas, and composite batholiths, called the "lower volcanic complex" by McDowell and Keizer (1977). In middle Tertiary time, following a distinct hiatus in magmatic activity, the entire Sierra Madre Occidental was blanketed by a sequence of ignimbrites with interlayered lava flows and tuffaceous sediments, the "upper volcanic supergroup" of McDowell and Keizer (1977). The 200,000 km^2 continuous expanse of these rocks delineates the Sierra Madre Occidental volcanic province (zone I of fig. 1). These same volcanic rocks continue to the east and west of the Sierra in block-faulted mountain ranges, and through eastern Chihuahua (zone II, fig. 1) they connect with the alkalic volcanic province of Trans-Pecos Texas (zone III, fig. 1). Less extensive post-mid-Tertiary igneous activity formed alkali basalts of Miocene age associated with Basin and Range style faulting, and widespread basalts of late Tertiary and Quaternary age. Little is known about the distribution and tectonic significance of these youngest igneous rocks.

This discussion concerns only the rocks of the upper volcanic supergroup within the Sierra Madre Occidental volcanic province. They have been studied in detail near latitude 24°N between Mazatlán and Durango City, where continuous mapped areas extend across the Sierra, and near latitude 28°N west of Chihuahua City where several separated areas have been mapped (fig. 1). Stratigraphic sections typically indicate more than 500 m of moderately to densely welded, rhyo-

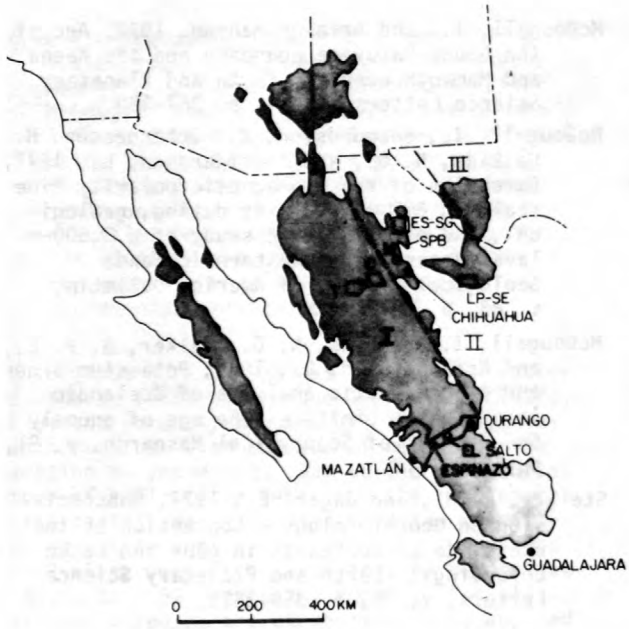

Figure 1.--Generalized distribution of volcanic rocks of middle Tertiary age in western Mexico and adjacent United States. Zone I, Sierra Madre Occidental volcanic province; Zone II, eastern Chihuahua; Zone III, Trans-Pecos Texas volcanic field. Mapped areas are outlined in black. T, Tomóchic; C, Cuauhtémoc; localities in zone II not relevant to this report.

dacitic to rhyolitic ignimbrites and associated lava flows and tuffs. Subordinate amounts of mafic rock commonly are present, mostly at or near the top of the section. Mapping has revealed numerous large calderas associated with these rocks (Swanson and others, 1978). The distribution of calderas is probably similar to that in the San Juan volcanic field, Colorado (Steven and Lipman, 1976).

Major-element chemical analyses of rocks from these well-studied sequences indicate that the upper volcanic supergroup is calc-alkalic and the rocks are quartz normative. Felsic rocks dominate, intermediate rocks are strikingly absent, and mafic rocks are widespread though subordinate. The genetic relationship between the mafic and felsic rocks poses an interesting problem for trace-element and isotope study.

Of the 76 available potassium-argon ages from the upper volcanic supergroup (fig. 2), 67 are from carefully controlled stratigraphic sections in areas of detailed mapping. The ages were determined on feldspar and biotite phenocrysts from felsic tuffs and flows, and on plagioclase separates and total-rock samples of mafic rocks. In each area nearly all of the volcanic rocks were emplaced within a short interval, typically 3 - 5 m.y., and K-Ar ages generally agree with stratigraphic position. Most of the activity took place between 34 and 27 m.y. ago (fig. 2). The westernmost sequence of rocks along the Durango-Mazatlán traverse was emplaced rapidly 23 m.y. ago. They appear to belong to a single source or a closely related group of sources. Volcanic rocks of this age are evidently less common than those 34 to 27 m.y. old elsewhere.

Initial $^{87}Sr/^{86}Sr$ ratios from feldspar separates and whole rocks vary from 0.7033 to 0.7062 and cluster about a value of 0.7045 (table 1). Initial ratios were determined from present-day ratios using Rb and Sr concentrations and the K-Ar age. Three average values of

Table 1.--Strontium isotope ratios from the upper volcanic supergroup of the Sierra Madre Occidental volcanic province

Sample	Rb/Sr	$^{87}Sr/^{86}Sr_p$	$^{87}Sr/^{86}Sr_I \pm 2\sigma$
Durango-Mazatlán			
West (El Salto), 23.3 m.y.:			
3-71-4, plagioclase	0.013	0.7058	0.7058±.0002
3-71-3, sanidine	0.102	0.7034	0.7033±.0002
3-71-7, plagioclase	0.011	0.7050	0.7050±.0004
3-71-8, sanidine	0.307	0.7045	0.7042±.0006
3-71-9, plagioclase	0.018	0.7062	0.7062±.0002
4-22-71, plagioclase	0.024	0.7046	0.7046±.0002
East (Durango), ~30 m.y.:			
2-71-2, sanidine	0.109	0.7048	0.7047±.0003
2-71-1, sanidine	0.321	0.7065	0.7061±.0003
Chihuahua (Cuauhtémoc) ~30 m.y.; whole-rock			
D69C	1.596	0.7065	0.7046±.0003
D76A[1]	0.029	0.7047	0.7047±.0006
D53D[1]	0.035	0.7043	0.7043±.0004

[1]Basalt; all samples are rhyolite.

0.7047, 0.7047, and 0.7049 have been reported by Cameron and others (1977). Apparently little or no radiogenic crustal material was involved in generating magmas that produced the upper volcanic supergroup. A similar range and distribution of initial values was found by Henry (unpublished data) for batholithic rocks from the lower volcanic complex in western Mexico. Initial ratios for andesites of the Trans-Mexico volcanic belt range from 0.7036 to 0.7043 (Moorbath and others, 1978).

Igneous rocks in western Mexico are similar in strontium isotope chemistry to those of the Andes (McNutt and others, 1975; Klerkx and others, 1977; Francis and others, 1977). We do not find the complicated trend toward higher initial ratios typical for the Central Andes that has been interpreted as a progression both inland and toward younger age by McNutt and others (1975), and as due to crustal contamination by Klerkx and others (1977) and Francis and others (1977).

Because the upper volcanic supergroup occurs at the continental edge, is calc-alkalic in com-

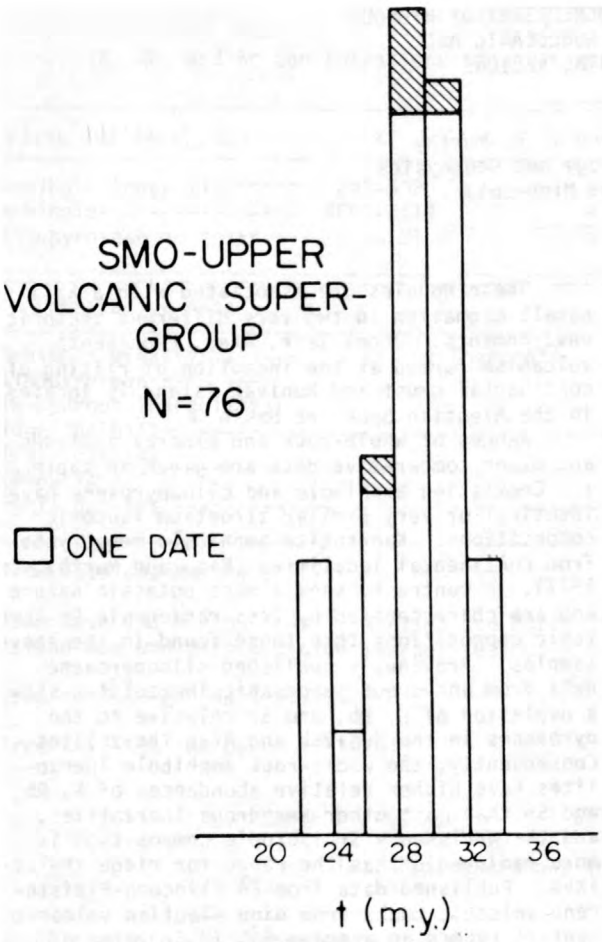

Figure 2.--Histogram of K-Ar ages from the upper volcanic supergroup. Diagonally ruled analyses are those not made at the University of Texas at Austin.

position, and is Tertiary in age, it is most simply interpreted as a classic continental-margin igneous arc related to subduction of the Farallon plate beneath the North American plate. The strontium isotope ratios and the age range of the rocks support this idea. Slackening of magmatic activity 27 m.y. ago fits the timing of collision of the east-Pacific spreading system with North America proposed by Atwater (1970) and the timing of a 26 m.y. reorientation of the east-Pacific spreading system (Handschumacher, 1976). However, no known event in east-Pacific spreading history coincides with the abrupt onset of volcanism 34 m.y. ago in the Sierra Madre Occidental. In fact, the extreme brevity of activity and the bimodal chemistry are atypical of continental margin magmatism.

Atwater, T., 1970, Implications of plate tectonics for the Cenozoic tectonic evolution of western North America: Geological Society of America Bulletin, v. 81, p. 3513-3536.

Cameron, M., Bagby, W. C., Cameron, K. L., and Lanphere, M. A., 1977, Geochemistry and mineralogy of mid-Tertiary rhyolites and related volcanics, Sierra Madre Occidental, Chihuahua, Mexico: Transactions of the American Geophysical Union, v. 58, no. 12, p. 1246.

Francis, P. W., Moorbath, S., and Thorpe, R. S., 1977, Strontium isotope data for recent andesites in Ecuador and north Chile: Earth and Planetary Science Letters, v. 37, p. 197-202.

Handschumacher, D. W., 1976, Post-Eocene plate tectonics of the eastern Pacific: American Geophysical Union Monograph, v. 19, p. 177-204.

Henry, C. D., 1975, Geology and geochronology of the granitic batholithic complex, Sinaloa, Mexico: Geological Society of America Abstract with Programs, v. 7, no. 2, p. 172.

Klerkx, J., Deutsch, S., Pichler, H., and Zeil, W., 1977, Strontium isotopic composition and trace-element data bearing on the origin of Cenozoic volcanic rocks of the Central and Southern Andes: Journal of Volcanology Geothermal Research, v. 2, p. 49-71.

McDowell, F. W., and Clabaugh, S. E., (in press), Ignimbrites of the Sierra Madre Occidental and their relation to the tectonic history of western Mexico: Geological Society of America Memoir.

McDowell, F. W., and Keizer, R. P., 1977, Timing of mid-Tertiary volcanism in the Sierra Madre Occidental between Durango City and Mazatlán, Mexico: Geological Society of America Bulletin, v. 88, p. 1479-1487.

McNutt, R. H., Crocket, J. H., Clark, A. H., Caelles, J. C., Farrar, E., Haynes, S. J., and Zentilli, M., 1975, Initial $^{87}Sr/^{86}Sr$ ratios of plutonic and volcanic rocks of the Central Andes between latitudes 26° and 29° south: Earth and Planetary Science Letters, v. 27, p. 305-313.

Moorbath, S., Thorpe, R. S., and Gibson, I. L., 1978, Strontium isotope evidence for petrogenesis of Mexican andesites: Nature, v. 271, p. 437-439.

Steven, T. A., and Lipman, P. W., 1976, Calderas of the San Juan volcanic field, southwestern Colorado: U. S. Geological Survey Professional Paper 958, 85 p.

Swanson, E. R., Keizer, R. P., Lyons, J. I., and Clabaugh, S. E., 1978, Tertiary volcanism and caldera development in the Durango City area, Sierra Madre Occidental, Mexico: Geological Society of America Bulletin, v. 89.

STRONTIUM ISOTOPE GEOCHEMISTRY OF HYDROUS LITHOSPHERE IN SUBOCEANIC AND SUBCONTINENTAL REGIONS

By M. Menzies and V. R. Murthy
Department of Geology and Geophysics
University of Minnesota

INTRODUCTION

Studies of spinel and garnet lherzolites from suboceanic (Varne and Graham, 1971; Francis, 1976) and subcontinental mantle (for example, Best, 1974; Lloyd and Bailey, 1975) reveal localized metasomatic events caused by the infiltration of alkali-rich fluids. Such pervasive episodes of "alteration" radically change the chemistry of the host peridotite. Prior to metasomatism the mantle lherzolites are essentially anhydrous and are fertile with respect to their major element chemistry (see summary by Maaloe and Aoki, 1977). However, they lack sufficient quantities of vital trace elements (K, Rb, Sr, rare-earth elements (REE) and so forth) that are necessary if tholeiitic and alkali basaltic melts are to be extracted upon partial melting. Metasomatism introduces these elements as either an intergranular or hydrous phase in the anhydrous parent thus producing "modified" mantle, sometimes termed alkali peridotite. Occasionally the host rock is radically changed, as is the case in some subcontinental regions (Lloyd and Bailey, 1975); but in the case of suboceanic peridotite, a hydrous lherzolite is generated (Varne and Graham, 1971; Francis, 1976).

These metasomatic events may closely parallel the "enrichment events" invoked by Kay (1977) and by Carter and others (1978). Such events are required to enrich source regions in K, Rb, Sr, and light REE prior to, or synchronous with, the eruption of LIL element enriched magmas. Sm/Nd studies reveal that prior to the introduction of such elements the source regions are light REE depleted (Carter and others, 1978). It can be similarly shown that suboceanic (and perhaps subcontinental) mantle has chondritic or light REE depleted characteristics and that metasomatism introduces light REE enriched hydrous (Varne and Graham, 1971) or intergranular phases (Frey and Green, 1974).

SUBOCEANIC HYDROUD MANTLE

Amphibole lherzolites (for example Talbot and others, 1963; Varne and Graham, 1971; Francis, 1976) are volumetrically insignificant, in suboceanic regions, relative to anhydrous lherzolite. Samples from the Jebel Tair volcano located in the Red Sea, and from Nunivak Island, Alaska have been studied for K, Rb, Sr, and $^{87}Sr/^{86}Sr$. The techniques used in these analyses remain essentially those described earlier (Murthy and others, 1971).

These nodules are associated with alkali basalt magmatism in two very different tectonic environments. Jebel Tair, Ataq, represents volcanism formed at the inception of rifting of continental crust and Nunivak Island is located in the Aleutian back-arc basin.

Ranges of whole-rock and mineral analyses and other comparative data are given in table 1. Coexisting amphibole and clinopyroxene have identical or very similar strontium isotopic compositions. Kaersutite amphibole megacrysts from continental localities (Basu and Murthy, 1977), in contrast, show a more potassic nature and are characterized by less radiogenic Sr-isotopic compositions than those found in the above samples. Previously published clinopyroxene data from anhydrous suboceanic lherzolites show a depletion of K, Rb, and Sr relative to the pyroxenes in the Nunivak and Ataq lherzolites. Consequently, the whole-rock amphibole lherzolites have higher relative abundances of K, Rb, and Sr than most other anhydrous lherzolites, and the whole-rock Sr isotopic composition is more radiogenic than the range for ridge tholeiites. Published data from 24 Pliocene-Pleistocene volcanic rocks from nine Aleutian volcanic centers record an average $^{87}Sr/^{86}Sr$ value of 0.70322 ± 8 (Kay and others, 1978). This value is identical to that obtained from a Nunivak lherzolite nodule. If the amphibole lherzolite analyzed here is typical of the suboceanic mantle involved in the genesis of alkali basalts, a source content of about 400-600 ppm of K is indicated. This compares favorably with several other independent estimates for the K content of the suboceanic mantle (for example, Hofmann and Hart, 1978).

SUBCONTINENTAL MANTLE

Subcontinental peridotite nodules found in kimberlite pipes are frequently phlogopite bearing (Carswell, 1975), while those occurring in alkali basalt flows contain small veins or dispersed phlogopite or amphibole not generally exceeding 1 percent by mode (Best, 1974). Examples from both eruptive types are under investigation, but here we report data of ten garnet lherzolites from Bultfontein and Kimberley, South Africa. Clinopyroxene, garnet, and phlogopite were analyzed for K, Rb, Sr, and $^{87}Sr/^{86}Sr$ ratios. The whole-rock lherzolites were not analyzed because of the unacceptable degree of alteration. Studies of minerals as opposed to whole-rock peridotites has already been demon-

Table 1.--Suboceanic amphibole lherzolite

[K, Rb, and Sr concentrations in parts per million unless otherwise indicated.]

Nunivak and Jebel Tair	K	Rb	Sr	$^{87}Sr/^{86}Sr$
Amphibole lherzolite	242-532	0.30-1.85	79-95	0.70312±9 - 0.70358±10
Amphibole	4003-6114	4.37-8.41	805-1434	0.70337±8 - 0.70347±11
Clinopyroxene	16.8-101.4	0.01-0.18	160-1072	0.70323±6 - 0.70340±9

Comparative data	K	Rb	Sr	$^{87}Sr/^{86}Sr$
Amphibole megacrysts[1]	1.26-2.2 (percent)	4.4-16.2	463-769	0.70266 - 0.70290
Clinopyroxene (anhydrous lherzolite)[2]	8-38	0.01-0.14	1.61-124.16	0.70196 - 0.70316
Ridge tholeiites[3]				0.7025 - 0.7035
Alkali basalts (Aleutians)[4]				0.70322±8
Alkali basalts[3]				0.7027 - 0.7070

[1]From Basu and Murthy (1977).

[2]From Basu and Murthy (1977); Menzies and Murthy (1978); and unpublished data on Guadalupe island and whole-rock alpine lherzolites.

[3]From Hoffman and Hart (1978).

[4]From Kay, Sun and Lee Hui (1978).

Table 2.--Subcontinental phlogopite-garnet lherzolites

[All concentrations in parts per million]

Bultfontein and Kimberley		K	Rb	Sr	$^{87}Sr/^{86}Sr$
Clinopyroxenes:	Clear	66-296	0.11-80	141-340	0.70465± 8 - 0.70752± 7
	Cloudy	199-546	2.46-3.10	283-441	0.70585± 5 - 0.70702± 5
Garnets:	Untreated	160-678	.33-1.84	2.5-6.4	0.70473±12 - 0.70657± 8
	Treated	5.3-27.9	.015-.083	.24-1.72	----
Phlogopite		52631	148	22	0.70966± 6
		65710	163	115	0.72521±10

Comparative Data	K	Rb	Sr	$^{87}Sr/^{86}Sr$
Clinopyroxenes[1]	110-673	0.015-1.78	89-903	0.70342 - 0.7075
Garnets[1]	1.7	0.006	0.98	----

[1]From Shimizu (1972), and Barret (1975).

strated to be a valid approach (Menzies and Murthy, 1978).

Diopsides

Clinopyroxenes are classified as clear or cloudy in table 2. The cloudy pyroxenes have higher relative abundances of K and Rb, but Sr is similar in clear and cloudy samples. A linear relationship exists between K and Rb and the possibility that the cloudy and (or) clear clinopyroxenes have been subject to the introduction of these alkalis is under investigation by mild leaching studies. Previous studies have shown that K and Rb are highly mobile because they coat internal fractures within the crystals. The analyzed pyroxenes display a considerable range in isotopic composition ($^{87}Sr/^{86}Sr$ = 0.70465 ± 8 - 0.70752 ± 7) (table 2) similar to that reported from other kimberlite peridotite nodules.

Garnets

Garnets were analyzed from seven lherzolites and four of these garnets were analyzed before and after acid washing. Relative-abundance data change dramatically (table 2) lessening the K and Rb by approximately 90 percent and the Sr between 50-90 percent in the washed samples. The treated garnets have extremely low contents of Rb and Sr but slightly higher K than has been previously reported (table 2). The strontium isotopic composition of the garnets ($^{87}Sr/^{86}Sr$ = 0.70473 ± 12 - 0.70657 ± 8) and coexisting diopsides are very similar (table 2).

Phlogopites

The analyzed peridotites contain primary and secondary phlogopites that are compositionally different (Carswell, 1975). The phlogopites analyzed to date have high concentrations of K, Rb, and Sr and a range of $^{87}Sr/^{86}Sr$ = 0.70966 ± 8 - 0.72521 ± 10. The relative-abundance data indicates that less than 0.01 percent mica on internal fractures within the garnets could account for much of the labile K and Rb. The Sr-isotopic data of phlogopites suggest that they were formed ≈ 70 m.y. ago, indicating their origin at the time of kimberlite forming event. This is compatible with the petrographic data of Carswell (1975).

CONCLUSION

Petrographic and chemical studies of amphibole-bearing suboceanic lithosphere indicate that the introduction of amphibole and the genesis of associated alkali basalts are genetically related events. It is interesting to note that (a) the lherzolite and recent alkalic volcanics in the Aleutian arc have identical Sr isotopic compositions, and (b) Na/Na+K ratios of the Nunivak lavas and the amphibole are very similar (Francis, 1976). Perhaps the "enrichment event" in the anhydrous suboceanic mantle, necessary for the genesis of alkali basalts, produced the amphibole. Further studies of Nunivak and Ataq lavas are in progress to help evaluate this question.

Previous studies of subcontinental mantle contend that it is grossly heterogeneous fertile garnet peridotite. The present data on clinopyroxenes from garnet lherzolites support the contention that the subcontinental mantle below the Bultfontein and Kimberley pipes is isotopically heterogeneous. If, as we show here, the phlogopite in the nodules is secondary, the relative abundance levels of several trace elements in the subcontinental mantle, as indicated by these granular lherzolite nodules, may indeed be low and approximate the levels of the suboceanic anhydrous mantle. Thus, the general problem of providing a satisfactory explanation of the trace-element and isotopic chemistry of basalts may also apply to the subcontinental mantle. The suggestion of about 1 percent phlogopite as a primary constituent of the subcontinental mantle as indicated in several petrologic studies (Carswell, 1975; Lloyd and Bailey, 1975) may be debated, but it may be necessary to account for the trace-element chemistry of basalts.

Barret, D. R., 1975, The genesis of kimberlites and associated rocks, strontium isotopic evidence, in Ahrens, L. H., Dawson, J. B., Duncan, A. R., and Erlank, A. J., eds: Physics and Chemistry of the Earth, v. 9, p. 637-653.

Basu, A., and Murthy, V. R., 1977, Ancient lithospheric lherzolite xenolith in alkali basalt from Baja California, Earth and Planetary Science Letters, v. 35, p. 239-246.

_____1977, Kaersutites, suboceanic low velocity zone and the origin of mid-ocean ridge basalts: Geology, v. 5, p. 365-368.

Best, M. G., 1974, Mantle-derived amphibole within inclusions in alkalic-basaltic lavas, Journal of Geophysical Research, v. 79, p. 2107-2113.

Carswell, D. A., 1975, Primary and secondary phlogopites and clino-pyroxenes in garnet lherzolite xenoliths, in Ahrens, L. H., Dawson, J. B., Duncan, A. R., and Erlank, A. J., eds.: Physics and Chemistry of the Earth, p. 417.

Carter, S. R., Evensen, N. M., Hamilton, P. J., O'Nions, R. K., 1978, Continental volcanics derived from enriched and depleted source regions: Nd and Sr isotope evidence: Earth and Planetary Science Letters, v. 37, p. 401-409.

Francis, J. M., 1976, The origin of amphibole in lherzolite xenoliths from Nunivak Island, Alaska: Journal of Petrology, v. 17, p. 357-378.

Frey, F. A., and Green, D. H., 1974, The mineralogy, geochemistry, and origin of lherzolite inclusions in Victorian basanites: Geochimca et Cosmochimica Acta, v. 38, p. 1023-1059.

Hoffman, A. W., and Hart, S. R., 1978, An assessment of local and regional isotopic equilibrium in the mantle: Earth and Planetary Science Letters, v. 38, p. 44-62.

Kay, R. W., 1977, Geochemical constraints on the origin of Aleutian magmas, in Talwani, M., and Pitman II, W. C., eds.: Island Arcs, Deep Sea Trenches and Back-Arc Basins, Maurice Ewing Series 1, p. 229-242.

Kay, R. W., Sun, S. S., and Lee Hui, C. N., 1978, Pb and Sr isotopes in volcanic rocks from the Aleutian Islands and Pribilof Island, Alaska: Geochimica Cosmochimica Acta., v. 42, no. 3, p. 263-274.

Lloyd, F. E., and Bailey, D. K., 1975, Light element metasomatism of the continental mantle: the evidence and the consequences,

in Ahrens, L. H., Dawson, J. B., Duncan, A. R., and Erlank, A. J., eds.: Physics and Chemistry of the Earth, v. 9, p. 389-416.

Maaloe, S., and Aoki, K., 1977, The major element composition of the upper mantle estimated from the composition of lherzolites, Contributions to Mineralogy and Petrology, v. 63, p. 161-173.

Menzies, M., and Murthy, V. R., 1978, Strontium isotope geochemistry of alpine tectonite lherzolites: data compatible with a mantle origin: Earth and Planetary Science Letters, v. 38, p. 346-354.

Murthy, V. R., Evensen, N. M., Jahn, B. M., and Coscio, M. R., 1971, Rb-Sr ages and elemental abundances of K, Rb, Sr, and Ba in samples from the Ocean of Storms: Geochimica Cosmochimica Acta, v. 34, p. 1139-1153.

Shimizu, N., 1972, Trace element contents of clinopyroxenes from garnet lherzolites in Kimberlites, Department of Terrestrial Magnetism Annual Report, 1973-1973, p. 272.

Talbot, J. L., Hobbs, B. E., Wilshire, H. G., and Sweatman, T. R., 1963, Xenoliths and xenocrysts from lavas of the Kerguelen archipelago: American Mineral, v. 48, p. 159-179.

Varne, R., and Graham, A. L., 1971, Rare earth abundances in hornblende and clinopyroxene of hornblende lherzolite xenoliths: implications for upper mantle fractionation processes, Earth and Planetary Science Letters, v. 13, p. 11-18.

A HIGH SENSITIVITY THERMAL IONIZATION MASS SPECTROMETER INCORPORATING DOUBLE COLLECTION AND AUTOMATION

By T. O. Merren, R. C. Haines, E. Hall, and G. P. Wells
VG-Isotopes Limited
Winsford, Cheshire, U. K.

The objectives which were laid down and have been achieved in the design of the Micromass 54E were: (1) improved sensitivity; (2) improved precision on low abundance nuclides and on difficult samples; and (3) automated operation.

Sensitivity: High sensitivity has been achieved by a high transmission analyzer and more efficient source arrangements. The most significant improvement is the use of ion optics (Cross, 1951) which give focussing in the direction perpendicular to the plane of the ion beam and also enable wider source slits to be used for the same resolution. The sensitivity is shown by the following results:

Sample size: 0.56 μgm strontium.
Time to run: 9.5 hours.
Integrated beam current: 1.7×10^{-6} coulombs.
Atoms per ion: < 300.

Similar sensitivities have been achieved on lead and neodymium.

These results were obtained with thorough preconditioning of the loaded bead, but a subsequent run with a similar sample and no preconditioning at all gave a sensitivity of 650 atoms per ion.

Precision: The precision achieved on a clean standard may not be achieved on a real sample. The double collector will give between 2 and 10 times better precision in such practical cases. The double collector will also obtain more data from a small sample because adequate precision will be obtained when the intensities are rising and falling.

The results in table 1 show the type of improvement that is obtained. The sequence of peaks is chosen so that the ratios of 86/88 and 87/86 can be calculated from single-collector data and the 87/86 from double-collector operation--that is, during part of sequence the two beams were being collected and integrated simultaneously. The last line is the double collector result. The results were made early in the measurement with a large sample for test purposes and the surface conditions had not stabilized. It can be seen that the precision within this run (0.087 permil) is improved by the double-collector method. The last column in the table is the expected error in the ratio, and is calculated from amplifier noise value and ion statistics combined. The value can be compared with the value obtained, and it can be seen that even with some instability in the beam the expected value of precision is reached. For single-collector measurements, there are other nonrandom errors presumably due to fluctuating or drifting beam intensities.

Abundance sensitivity: With the high precision which modern measuring circuits attain, the tail contribution of major peaks to minor peaks becomes significant. The use of correction factors is simple when a data system is

Table 1.--Single and double collector precisions

Ratio	Collector	No. of cycles	Standard deviation (permil)	
			Observed	Calculated
86/88	Single	9	0.143	0.049
87/86	Single	9	.119	.075
86/88	Single	9	.089	.049
87/86	Single	9	.193	.075
87/86	Double	10	.087	.085

used, but sometimes the tails of the major peak may vary with sample history--that is, with time. On conventional 30-cm single focussing mass spectrometers, the contribution of a major peak to an adjacent peak one mass number away can be 20 ppm or more even though the instrument can achieve 3 ppm with a clean standard and low source pressures.

The tails of the peak that give this contribution are due to ions that have collided with gas molecules in the analyzer or source. The majority of such ions will have lost energy by collision and the rejection of these ions by retarding grids has been used. Grids, however, are not very practical because they collect material, and then become charged with consequent deterioration in peak shape and also a loss of sensitivity.

The energy filter is advantageous in that it transmits all of the ions of the ion beam because there are no restricting baffles to ions of the correct energy and mass.

The Micromass 54E is fitted with energy filters consisting of curved parallel plates (electric sectors). These are relatively small electric sectors fitted at the collector end and give abundance sensitivities in the 1 ppm to 3 ppm range (table 2).

Automation: Thermal ionization mass spectrometry has always been operator-intensive. The first step to routine acquisition of data was the replacement of chart recorders by peak jumping with integrating digital voltmeters. The use of calculators or minicomputers simplified the processing of data, but the operator had still to locate and focus the beam, control the buildup of its intensity, and monitor the progress of the run. The Micromass 54E incorporates the necessary hardware, interfacing, and

Table 2.--Abundance sensitivities using an energy filter (ppm of major beam U238)

[Sample is NBS U005]

Mass	234.5	236.5	237	238.5	239.5
Mass difference	- 3.5	- 1.5	- 1	+ 0.5	+ 1.5
Very high source pressure (10^{-7} torr)	0.3	2	3	4	2
Normal operating source pressure (5×10^{-8} torr)	0.2	1	2.5	3.5	1.5
Normal operating source pressure (10^{-8} torr)	<0.1	<0.5	<1.0	<1.0	<0.5

software to allow a calculator (such as a Hewlett Packard HP 9831) or computer (such as a PDP8A) to carry out the following functions:

1. Locate and center the appropriate ion beams.
2. Step-up filament currents in a predetermined sequence or until certain intensities are reached (also control heating).
3. Adjust focus voltages, optimize intensity, check peak shape. .
4. Monitor the instrument's condition--that is, pressure and HT.
5. Select Faraday or multiplier according to need.
6. Move to next sample.

The measurement of strontium isotopic ratios is particularly tedious because typically 100 cycles must be made to get sufficient precision. The data system runs the sample and checks the beam centering and focus parameters, which improves the reproducibility of the results. The addition of a double-collector system does not complicate the operation of the mass spectrometer, as all the controls and tests are done on one beam only; for normal running, the calculation of the double-collector ratio would make the data reduction exceptionally simple.

Isotope dilution on rare-earth elements is another complex analysis. Of the 55 isotopes, 27 need to be measured in numerous combinations and corrections for possible interferences are frequently necessary, even with chemical separation into three groups. The use of an automated system is described more fully in Merren and Pankhurst (1977).

Cross, W. G., 1951, Two-directional focusing of charged particles with a sector-shaped uniform magnetic field: Review of Scientific Instruments, v. 22, no. 10, p. 717.

Merren, T. O., and Pankhurst, R. J., 1977: Fifth Colloquium of Geochronology Cosmochronology and Isotope Geology, September, 1977.

FISSION TRACK AGES ON APATITE, SPHENE AND ZIRCON OF BERGELL ROCKS FROM CENTRAL ALPS AND OF BERGELL BOULDERS IN OLIGOCENE SEDIMENTS

By Donald S. Miller, Günther A. Wagner
and Emilie Jäger
Max-Planck-Institut für Kernphysik
Heidelberg, Germany

The Bergell region, central Alps, is an area of high-grade alpine metamorphism. This region cooled earlier than other central Alp regions resulting in older fission track, Rb-Sr, and K-Ar ages. It was intruded 30 m.y. ago by the Bergell granodiorite body as shown by uranium-lead analysis of zircon and monazite (Gulson and Krogh, 1973).

Previous studies using fission track analysis to reveal the uplift history of the central Alps indicated that the Bergell region had a decreasing rate of uplift in contrast to other regions (Wagner and others, 1977). The purpose of this study was to analyze more apatites and additional minerals such as sphene and zircon. A suite of samples was available from a range of elevations between 265 and 2340 meters. Three samples of the boulders postulated to be from the Bergell intrusive, but found in upper Oligocene sediments of the Po-plain Molasse, were available for analysis.

Nearly pure mineral separates were obtained using normal mineral separation techniques. One of the two identical aliquots of each mineral concentrate was annealed (apatite 450°C, 14h; sphene 750°C, 4h; zircon 850°C, 5h) and sent to the reactor for thermal neutron bombardment; the other aliquot was retained for determining the fossil fission-track density. Both aliquots were mounted separately, polished, and then etched simultaneously: the apatite with 5 percent HNO_3 at 23°C for 45 seconds, the sphene with a solution consisting of concentrated HF, HNO_3, H_2SO_4 and H_2O (in volume ratio of 2:1:1:6) at 23°C for 5 or 6 minutes, and the zircon with the eutectic mixture of NaOH and KOH at 200°C for 70 hours. All samples (both aliquots) were counted a minimum of five times and each sample was analyzed at least twice by two different persons. It was possible to determine track densities for all the minerals using population counting because of the homogeneous distribution of uranium in the apatite, sphene, and zircon. The neutron dose was established through the analysis of the standard glasses "Trebic 2" (moldavite, Heidelberg laboratory) and NBS standard 962 (38 ppm U, using the Au calibration, Carpenter and Reimer, 1974). The dose value determined by both glasses are in very good agreement. The constants used for age calculations are 137.88 for $^{238}U/^{235}U$, 580.2 barns for the fission cross section of ^{235}U, and 8.46×10^{-17} yr^{-1} for the spontaneous fission decay constant recommended by Wagner and others (1975).

The data for the Bergell region (table 1 and fig. 1) are a combination of newly obtained results and previous analyses (Wagner and others, 1977). Those points plotted as squares have not been included to determine the uplift rate on the basis of geologic and (or) geographic information (fig. 2). The Engadin fault and the Insubric line separate the early uplifted intrusives and nearby rocks from the surrounding rocks, which were uplifted later through the 120°C isotherm. The uplift rates shown in figure 1 are in good agreement with those obtained previously for the Bergell granodiorite (Wagner and others, 1977).

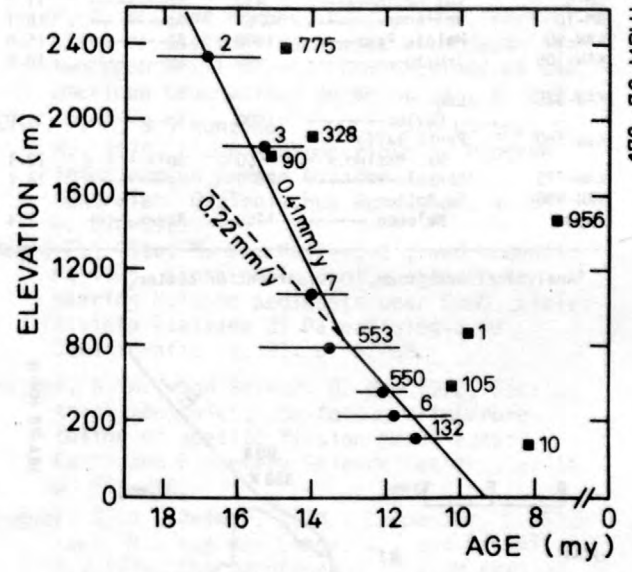

Figure 1.--Uplift rate using apatite fission track ages.

Analysis of sphene and zircon (table 1) suggests the possibility of determining the cooling history from 27 m.y. to 14 m.y.; however, the annealing data available for sphene and zircon are not as complete as for apatite so that the assumed apparent retention temperatures are not as precisely known. The choice of 350°C for sphene was made based upon data obtained using 90°C HCl as an etchant (Naeser and Faul, 1969). An appropriate temperature for zircon is more difficult to choose because of the lack of suitable data. Our choice of 350°C

Table 1.--Fission track ages, Bergell region and the Bergell boulders from the Molasse

[Ap, apatite; Sph, sphene; Zir, zircon]

Sample No.	Locality	Elevation (meters)	Mineral	Age (m.y.)[1]
	Bergell intrusive rocks			
BM-2	Val Bondasca----	2340	Ap--------	16.8
BM-3	Val Bondasca----	1860	Ap--------	15.3
BM-7	Val Masino------	430	Ap--------	11.8
			Sph-------	27.0
			Zir-------	26.2
KAW-132	Novate/Mezzolo--	310	Ap--------	11.2
KAW-553	Codera----------	800	Ap--------	13.5
	Bergell boulders from the Molasse			
KAW-1003	Pedrinate--------------		Ap--------	23.4
KAW-1004	Pedrinate--------------		Ap--------	24.1
KAW-1005	Pedrinate--------------		Ap--------	25.9
	Preintrusive rocks			
BM-1	Promontogno-----	850	Ap--------	9.7
BM-6	Val Masino------	430	Ap--------	11.8
BM-10	Val Adda--------	265	Ap--------	8.1
KAW-90	Maloja Pass-----	1800	Ap--------	15.0
KAW-105	Truzzo----------	590	Ap--------	10.2
KAW-328	Lago di Cavloc--------	1900	Ap--------	14.0
Kaw-550	Ponte Baffo Val Masino.---	560	Ap--------	12.1
KAW-775	Fextal----------	2370	Ap--------	14.7
KAW-956	Ca Rotte Malenco.------	1450	Ap--------	7.4

[1]Analytical precision, ± 10 percent or better.

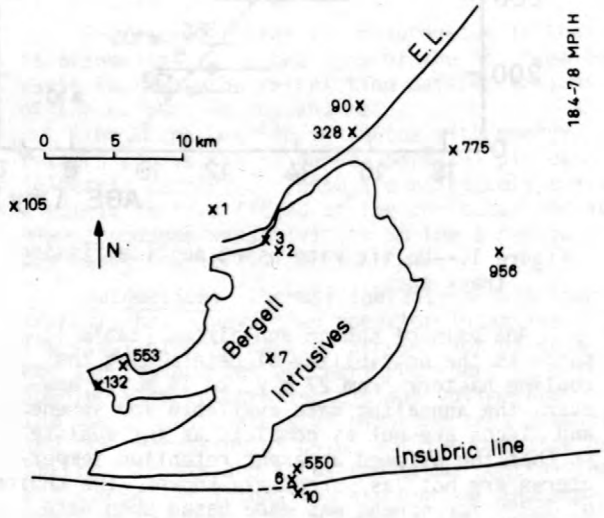

Figure 2.--Map showing sample locations and simple geology.

for both zircon and sphene apparent-retention temperatures is not to be considered as definite because the estimate is based upon limited data. The 120°C apparent-retention temperature for apatite fission tracks is well-documented (Wagner and Reimer, 1972; Naeser and Forbes, 1976).

The cooling history of the Bergell intrusive is illustrated in figure 3. The very early cooling history is derived from data on the boulders. Uranium-lead ages of zircons are 30 m.y. and the K-Ar ages of biotites are 29 m.y. (Gulson and Krogh, 1973); zircon data indicate the crystallization time at which the temperature is at least 650°C for the granite and the K-Ar age indicates the time at which 300°C was reached. This gives a cooling rate of more than 100°C per m.y., taking into account the error limits. Biotite Rb-Sr and apatite fission track ages show cooling from 300°C at 29 m.y. to 120°C at 25 m.y., giving a value of 50°C per m.y. From 26 m.y. to 14 m.y., a cooling rate of 18°C per m.y. is given by sample BM-7; during the last 14 m.y. a lower cooling rate of 6°C per m.y. is reached.

Uplift rates can be calculated by using the apatite ages versus elevation data (fig. 1) and by using fission track ages of apatite, sphene, and zircon as indicators of the time when specific temperatures were reached (fig. 3). These two independent methods result in a very consistent picture of the uplift history of the Bergell region. During the early stages of cooling, from the time of intrusion at 30 m.y. to about 25 m.y. ago, cooling occurs by two processes: cooling of the initially hot intrusive rock by loss of heat to the country rocks and cooling by regional uplift and erosion. Around 25 m.y. ago, the granites and country rocks reached the same temperature, as indicated by Rb-Sr biotite data. An uplift rate of 0.6 mm yr^{-1} is found from 26 to about 17 m.y.; a rate of 0.4 mm yr^{-1} from 17 to about 13 m.y.; and a rate of 0.2 mm yr^{-1} during the last 13 m.y. Thus, a decreasing rate of uplift is shown for the Bergell intrusion.

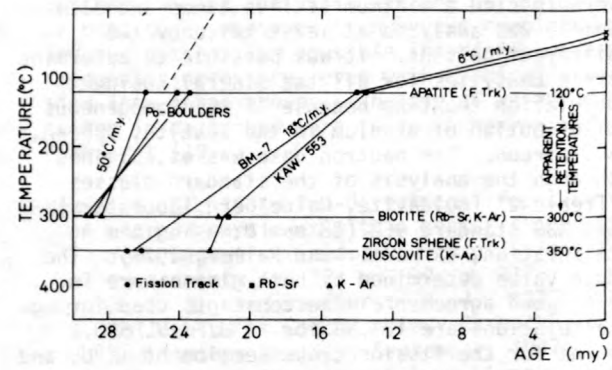

Figure 3.--Cooling history of the Bergell.

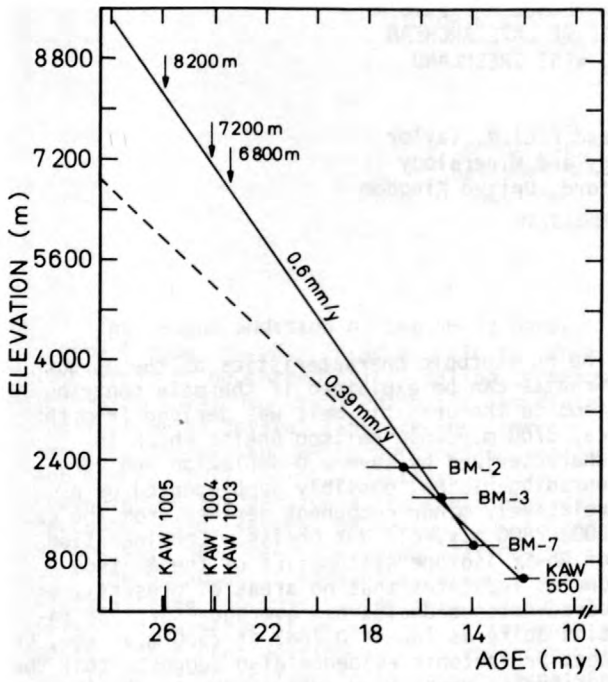

Figure 4.--Elevation determination of boulders from the Molasse.

An interesting use of the preceding information is consideration of the origin of the boulders found in the Molasse of the Po-plain, which are considered to have been derived from the Bergell intrusive (Longo, 1968). Because these boulders occur in Oligocene sediments (> 22 m.y., Odin and others, 1975), the boulders had to be available for erosion relatively soon after the Bergell emplacement 30 m.y. ago. Consequently, the apatite fission track ages should be older than the Oligocene sediments in which they are imbedded and younger than the Bergell intrusion. The ages range from 23.4 to 25.9 m.y., which is consistent with the hypothesis that the boulders are from the Bergell intrusive. According to the apatite fission track ages of the boulders (and excluding effect of erosion) their original position in the intrusion would be between 6800 and 8200 meters (fig. 4). Because the boulders are found imbedded in sediments of equal age, the paleo-relief of the Bergell intrusive was at least on the order of 1400 m during Oligocene time.

The 23.4 m.y. fission track age of the boulder which occurs in the stratigraphically controlled Molasse (between the NP 24 and NP 25 zones, Rögl and others, 1975) of the Po-plain gives an upper limit to the Oligocene-Miocene boundary. This age is an upper limit because after 23.4 m.y. the rocks must cool from 120°C to surface temperatures while being uplifted and eroded, then transported and embedded in the Oligocene sediments.

Carpenter, B. S., and Reimer, G. M., 1974, Standard reference material: Calibrated glass standards for fission track use: National Bureau of Standards Publication, p. 260-49.

Gulson, B. L., and Krogh, T. E., 1973, Old lead components in the young Bergell Massif, south-east Swiss Alps: Contributions to Mineralogy and Petrology, v. 40, p. 239-252.

Longo, V., 1968, Geologie und Stratigraphie des Gebietes zwischen Chiasso und Varese, Dissertation ETH, Zürich.

Naeser, C. W., and Faul, H., 1969, Fission track annealing in apatite and sphene: Journal of Geophysical Research, v. 74, p. 705-710.

Naeser, C. W., and Forbes, R. B., 1976, Variation of fission track ages with depth in two deep drill holes: Transactions of the American Geophysical Union, v. 57, p. 353.

Odin, P. G. S., Hunziker, J. C., and Lorenz, C. R., 1975, L'age radiometrique du Miocene inferieur en Europe Occidentale et Centrale: Geologisches Rundschau, v. 64, p. 570-592.

Rögl, F., Cita, M. B., Müller, C., and Hochuli, P, 1975, Biochronology of conglomerate bearing Molasse sediments near Como, Italy: Rivista Italiana di Paleontologia -e Stratigrafia, v. 81, p. 57-88.

Wagner, G. A., and Reimer, G. M., 1972, Fission track tectonics; The tectonic interpretation of apatite fission track ages: Earth and Planetary Science Letters, v. 14, p. 263-268.

Wagner, G. A., Reimer, G. M., Carpenter, B. S., Faul, H., van der Linde, R., and Gijbels, R., 1975, The spontaneous fission rate of U-238 and fission track dating: Geochimica Cosmochimica Acta, v. 39, p. 1279-1286.

Wagner, G. A., Reimer, G. M., and Jäger, E., 1977, Cooling ages derived by apatite fission-track, Mica Rb-Sr and K-Ar dating; The uplift and cooling history of the Central Alps: Mem. Ist. Geol. Min. Univ. Padova, Vol. XXX.

ISOTOPIC EVIDENCE FOR THE AGE AND ORIGIN OF THE QÔRQUT GRANITE OF LATE ARCHEAN AGE, GODTHAAB AREA, WEST GREENLAND

By Stephen Moorbath and Paul N. Taylor
Department of Geology and Mineralogy
Oxford University, Oxford, United Kingdom

The last major rock-forming event in the Archean of West Greenland was the emplacement of the Qôrqut Granite. It occupies an area of about 1000 km^2 to the east and northeast of the Godthaab region. Large areas in the central part of the pluton consist of homogeneous granite, but elsewhere there are complex migmatites containing numerous partly granitized rafts and inclusions of country rocks. The granite has a fairly restricted range of composition, with approximately equal amounts of quartz, plagioclase and microcline, and minor amounts of biotite.

A single 22-point Rb-Sr whole-rock isochron on the main body of the granite and on marginal offshoots (dykes) yields an age of 2498 ± 16 m.y. ($\lambda = 1.42 \times 10^{-11}$ yr^{-1}) and initial $^{87}Sr/^{86}Sr$ ratio of 0.7083 ± 0.0004 (errors at 2 sigma). A 23-point Pb/Pb whole-rock isochron yields an age of 2580 ± 65 m.y. ($\lambda_{238} = 1.55125 \times 10^{-10}$ yr^{-1}; $\lambda_{235} = 9.8485 \times 10^{-10}$ yr^{-1}).

The very unradiogenic Pb isotopic compositions of some samples of Qôrqut Granite rule out a simple two-stage model for the Pb isotopic evolution in this intrusion. The Qôrqut Granite Pb/Pb isochron line plots well below theoretical isochron lines for rocks of the same age derived from primitive-mantle source regions. This feature, together with the unradiogenic Pb isotopic compositions and the high initial $^{87}Sr/^{86}Sr$ ratio of 0.7083 ± 0.0004 of the Qôrqut Granite, suggests that the granitic magma was derived from partial melting of ancient continental crust, which agrees with field evidence concerning the relationship between the Qôrqut Granite and the country rock.

The Pb isotopic characteristics of the Qôrqut Granite can be explained if the main contribution to the granitic melt was derived from the ca. 3700 m.y.-old Amîtsoq Gneiss which is characterized by severe U-depletion and very unradiogenic Pb, possibly supplemented by a relatively minor component derived from the ca. 3000-2800 m.y.-old NûK Gneiss. Consideration of Rb-Sr isotope systematics of the Amîtsoq Gneiss indicates that no areas of presently exposed Amîtsoq Gneiss had average $^{87}Sr/^{86}Sr$ ratios quite as low as 0.7083 at 2500 m.y. ago, so that Sr isotopic evidence also suggests that the NûK Gneiss might have contributed to the formation of the Qôrqut Granite magma.

The initial Pb isotopic composition of the Qôrqut Granite still has to be satisfactorily established in order to thoroughly test the model outlined above for the origin of the granite. However, we emphasize that the initial Pb is less radiogenic than suggested by Gancarz and Wasserburg (1977), since several granite samples have present-day Pb isotopic compositions markedly less radiogenic than the feldspar sample which they analyzed. Our least radiogenic Pb comes from a single K-feldspar crystal from a pegmatite in the Qôrqut Granite. Its isotopic composition is only slightly more radiogenic than average Amîtsoq Gneiss Pb ca. 2500 m.y. ago.

Gancarz, A. J., and Wasserburg, G. J., 1977, Initial Pb of the Amîtsoq Gneiss, West Greenland, and implications for the age of the earth: Geochimica et Cosmochimica Acta, v. 41, p. 1283-1301.

ISOTOPIC FRACTIONATION PHENOMENA AND HIGH PRECISION NEODYMIUM ANALYSES

By Larry J. Moore
Center for Analytical Chemistry,
National Measurement Laboratory,
National Bureau of Standards,
Washington, D.C. 20234

The recent addition of the Sm-Nd decay scheme [$^{147}Sm \longrightarrow {}^{143}Nd + \alpha$ ($t_{1/2}$ = 1.06 x 10^{11} yrs)] to geochronological dating techniques (Lugmair, 1974) has resulted in its immediate application by several laboratories (for example, DePaolo and Wasserburg, 1976; Hamilton and others, 1977; Unruh and others, 1977). Depending on the particular isotopic analysis technique used, several neodymium isotope ratio values have been used for normalization.

The purposes of this paper are: (1) to discuss these isotopic procedures; (2) to correlate in-house relative isotope ratio measurements with recent developments in research involving isotopic fractionation phenomena; and (3) to suggest a "best absolute" neodymium normalizing ratio for interlaboratory comparisons.

Subsequent to the partially successful assignment of "square root of atomic mass" fractionation effects to the single filament isotopic analysis of selected alkali elements (Eberhardt and others, 1964), it has become obvious to some investigators that this model is inadequate to explain many "anomalous" fractionation effects. Investigations by Kanno (1971), and more recently Moore, Heald, and Filliben (1976), have resulted in the construction of an isotopic fractionation model for the multiple filament thermal ion source (MFTIS). The model is based on the vaporization of molecules [α = fractionation factor = $(^{h}MX/^{l}MX)^{\frac{1}{2}}$] as well as atoms [$\alpha = (^{h}M/^{l}M)^{\frac{1}{2}}$] in the MFTIS (fig. 1), and can be used to explain many "anomalous" fractionation effects observed with the MFTIS (Moore and others, 1976).

An experimental evaluation of the model versus several "classic" NBS (National Bureau of Standards) absolute measurements is summarized in figure 2. Because only a small part of the sample is actually consumed for isotopic analysis, the first few percent define an isotopic fractionation bracket to be used for comparison with the "absolute" isotope ratios. The model is further buttressed by evidence from: (1) high temperature Knudsen cell mass spectrometric characterization of vaporizing species; (2) equilibrium thermodynamic calculations of vaporizing species expected from sample filaments under mass spectrometer conditions (Heald, 1977) and (3) computation of mass fragments attached to the vaporizing metal species (Moore and others, 1976).

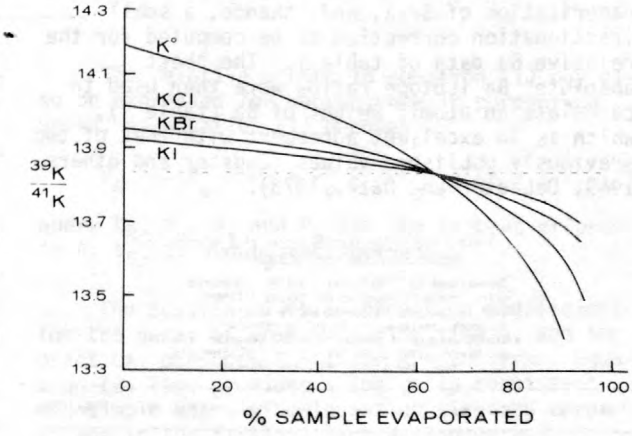

Figure 1.--Typical fractionation curves; calculated assuming vaporization of different molecular species.

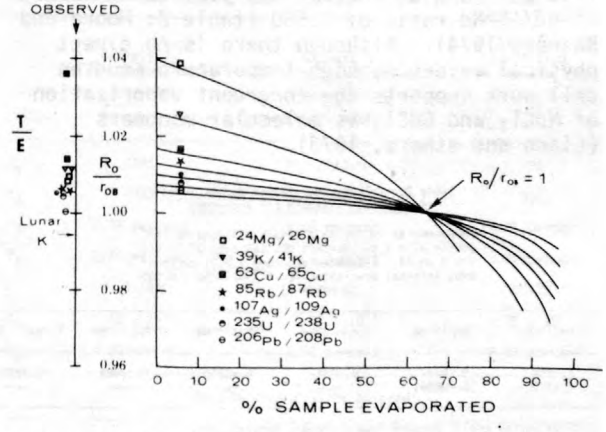

Figure 2.--Comparison of R_0/r_{ob} curves calculated on the basis of atomic vaporization with observed T/E values for various elements.

The alkaline earth group is a good example of "family" fractionation behavior. The MFTIS isotopic analysis techniques and fractionation characteristics of Ca, Ba, and Sr are nearly identical. Physical evidence supporting their vaporization characteristics include: (1) in-house identification by electron diffraction of

$Ca_3Re_2O_9$ and $CaReO_4$ on the Re filament material (Moore and others, 1976); (2) Knudsen cell vaporization studies of $Ba(ReO_4)_2$ (S) ——> Ba $(ReO_4)_2$ (g), supporting congruent vaporization of barium perrhenates in an appropriate temperature range (Semenov and others, 1973); and (3) the recently completed absolute abundance measurement at NBS of the $^{86}Sr/^{88}Sr$ ratio (which agrees within 5 parts in 10^4 with Nier's (1938) value of 0.11940). The collective consideration of these data and evidence permit the calculation of a mass fragment, X, for the vaporization of Sr-X, and, thence, a small fractionation correction to be computed for the relative Ba data of table 1. The "best absolute" Ba isotope ratios were then used to calculate an atomic weight of Ba (table 1), which is in excellent agreement with that of two previously published values (Eugster and others, 1969; DeLaeter and Date, 1973).

Table 1.--Relative isotope ratios of a natural barium shelf standard (6 analyses)

[Normalized to $^{138}Ba/^{136}Ba$ = 9.1300. Measured using triple filament Re and triple filament with Ta ionizing filament, and Re sample filament, analagous to Ca and Sr procedures. Atomic weights of barium: 137.327 (Eugster and others, 1969); 137.327 ± 0.005 (DeLaeter and Date, 1973); 137.330 (this paper)]

$^{138}Ba/^{136}Ba$	$^{137}Ba/^{136}Ba$	$^{135}Ba/^{136}Ba$	$^{134}Ba/^{136}Ba$	$^{132}Ba/^{136}Ba$	$^{130}Ba/^{136}Ba$
9.1300	1.4288	0.83919	0.30779	0.01289	0.01350
9.1300	0.0003	0.00026	0.00018	0.00001	0.00003

The isotopic analysis of Nd, from a 2-percent (V/V) HCl solution, using a triple filament rhenium source, has yielded an average $^{142}Nd/^{146}Nd$ ratio of 1.580 (table 2; Moore and Baines, 1974). Although there is no direct physical evidence, high-temperature Knudsen cell work supports the congruent vaporization of $NdCl_3$ and $GdCl_3$ as molecular monomers (Ciach and others, 1973).

Table 2.--Relative Nd isotope ratios for a Nd_2O_3 shelf standard (12 analyses)

[Measured as Nd^+ using a triple filament Re ion source with a two percent HCl solution of Nd and ~ 0.5 µg Nd. Estimated accuracy ± 0.01 percent/amu; internal precisions for $^{143}Nd/^{146}Nd$ < 0.005 percent]

$^{142}Nd/^{146}Nd$	$^{143}Nd/^{146}Nd$	$^{144}Nd/^{146}Nd$	$^{145}Nd/^{146}Nd$	$^{148}Nd/^{146}Nd$	$^{150}Nd/^{146}Nd$
1.5800	0.70737	1.38442	0.48249	0.33484	0.32787
1.5800	(0.70849) [1]	-----	-----	-----	-----

[1]High-purity shelf standard from different manufacturer.

Based on these data, observations, and several years' experience with absolute-abundance measurements, an upper limit of 1.580 can be placed on the "absolute" $^{142}Nd/^{146}Nd$ ratio. A "best absolute" value of ~ 1.570 is calculated on the basis of $NdCl_3$(g) vaporization, which should approximate the "absolute" value. It is suggested that these observations and calculations be considered for the selection of a value for interlaboratory comparisons.

Ciach, S., Nicholson, A. J. C., Swingler, D. L., and Thistlethwaite, P. J., 1973, Mass spectrometric study of the vapor phase over neodymium chloride and gadolinium chloride: Inorganic Chemistry, v. 12, p. 2072.

DeLaeter, J. R., and Date, R., 1973, The isotopic composition of Ba: International Journal of Mass Spectrometry and Ion Physics 12, p. 455.

DePaolo, D. J., and Wasserburg, G. J., 1976, Nd isotopic variations and petrogenetic models: Geophysical Research Letters, v. 3, p. 249.

Eberhardt, A., Delwiche, R., and Geiss, J., 1964: Zeitschrift fur Naturforschung, Teil A, v. 19, p. 736.

Eugster, O., Tera, F., and Wasserburg, G. J., 1969, Isotopic analyses of barium in meteorites and in terrestrial samples: Journal of Geophysical Research, v. 74, p. 3897.

Hamilton, P. J., O'Nions, R. K., and Evensen, N. M., 1977, Sm-Nd dating of Archaean basic and ultrabasic volcanics: Earth and Planetary Science Letters, v. 36, p. 263.

Heald, E. F., 1977, Computer calculations of equilibrium components in a thermal ionization mass spectrometer: Annual Conference on Mass Spectrometry and Allied Topics, 25th, Washington, D.C., 1977.

Kanno, H., 1971, Isotopic fractionation in a thermal ion source: Chemical Society of Japan Bulletin, v. 44, p. 1808.

Lugmair, G. W., 1974, Sm-Nd ages; A new dating method [abs.]: Meteoritics, v. 9, p. 369.

Moore, L. J., and Barnes, I. L., 1974, A general approach to fractionation corrections for isotopic analyses of the polynuclidic elements: International Conference on Geochronology, Cosmochronology and Isotope Geology, 3rd, Paris, France, 1974.

Moore, L. J., Heald, E. F., Filliben, J. J., 1976, An isotopic fractionation model for the multiple filament thermal ion source: Advances in mass spectrometry, v. 7, International Mass Spectrometry Conference, 7th, Florence, Italy, 1976, Proceedings.

Nier, A. O., 1938, The isotopic constitution of strontium, barium, bismuth, thallium and mercury: The Physical Review, v. 5, p. 275-278.

Semenov, G. A., Nikolaev, E. N., and Opendak, I. G., 1973, Mass-spectrometric investigation of the vaporization of barium and magnesium per-rhenates: Russian Journal of Inorganic Chemistry, v. 17, p. 943.

Unruh, D. M., Nakamura, N., and Tatsumoto, M., Earth and Planetary Science Letters, v. 37, p. 1.

A PRACTICAL METHOD OF ESTIMATING STANDARD ERROR OF AGE IN THE FISSION-TRACK DATING METHOD

By C. W. Naeser[1], Noye M. Johnson[2], and Victor E. McGee[2]
[1]U. S. Geological Survey
Denver, Colorado 80225
[2]Dartmouth College
Hanover, New Hampshire 03755

A rigorous treatment of the stochastic elements in a fission-track dating model has been described recently by McGee and Johnson (1978). A computer program (named FISSION) was developed in this work to calculate the propagated error for any given case of fission-track dating. As a practical matter, however, the use of FISSION requires access to a computer and a nontrivial amount of computer time, so that it is useful to look for alternate ways of implementing the model. The purpose of this paper is twofold: (1) to develop useful approximations for the determination of error variance (or standard error) of age, and (2) to describe experimental practices which will help keep the standard error of age to a minimum.

Our first objective is to derive an approximate expression for the variance of the age (A) specifically for the fission-track age equation. The assumptions that we consider consistent with normal fission-track dating practice include: (1) the errors in determining the neutrons dose ϕ ($t\phi$ = tracks counted in standard) are statistically independent from the errors in determining the fossil (t_s) and induced counts (t_i); (2) t_s and t_i are correlated by crystal uranium content; and (3) A is a constant, supplied by standard fission-track age equation. Given these assumptions, we may adapt the Kendall and Stuart (1963, p. 232) approximation for variance to the age equation, to yield

$$\frac{\sigma_A}{A} = C\left[\left(\frac{\sigma_s}{t_s}\right)^2 + \left(\frac{\sigma_i}{t_i}\right)^2 + \left(\frac{\sigma_\phi}{t_\phi}\right)^2 - 2r\left(\frac{\sigma_s}{t_s}\right)\left(\frac{\sigma_i}{t_i}\right)\right]^{1/2} \quad (1)$$

where σ_A = standard error of A

σ_s = standard error of t_s (tracks counted)

σ_i = standard error of t_i (tracks counted)

σ_ϕ = standard error of t_ϕ (tracks counted)

r = correlation between t_s and t_i, and

$$C = \frac{\lambda_D}{A}\left(1 - e^{-A/\lambda_D}\right)$$

λ_D = total decay constant ^{238}U

The relative errors in equation (1) may also be expressed for convenience in percentage units, so equation (1) becomes

$$P_A = C(P_s^2 + P_i^2 + P_\phi^2 - 2rP_sP_i)^{1/2} \quad (2)$$

where P_A, P_s, P_i and P_ϕ are the percent errors in A, t_s, t_i and t_ϕ respectively.

The constant C is a correction coefficient for the decay of uranium during time A, and for practical purposes C = 1 for A < 10^8 yrs. Equation (2) thus provides a logically consistent and simple means of calculating standard error of age in the fission-track dating method. Table 1 compares the results from equation (2) with those from FISSION (McGee and Johnson, 1978) for three separate dating attempts.

Table 1.--Comparisons of computer (FISSION) and approximation results (equation (4)) for standard error of some zircon fission-track ages

	Example 1 (Fish Canyon Tuff)	Example 2 (Pike's Peak Granite)	Example 3 (Tuff from San Pedro Valley)
	Experimental data		
t_s	1145	2313	90
t_i	1325	361	937
P_s	2.96 percent	2.08 percent	10.31 percent
P_i	2.75 percent	5.26 percent	3.27 percent
r	0.891	0.940	0.930
ϕ	1.10×10^{15}	5.52×10^{15}	1.06×10^{15}
P_ϕ	3.00 percent	3.00 percent	3.00 percent
	Results from FISSION program		
A	29.09 m.y.	1004 m.y.	3.11 m.y.
P_A	±3.30 percent	±4.18 percent	±8.04 percent
	Results from equation (2)		
P_A	3.29 percent	4.19 percent	7.95 percent

Table 1 shows that equation (2) closely approximates the results from the full theory behind FISSION for a variety of experimental conditions. The differences may be attributed partly to the skewness of the age distribution which is not accounted for in equation (2). For

practical purposes, however, equation (2) provides a reliable working tool in the practice of fission-track dating. Its simplicity obviates the need for a digital computer. The arithmetic operations, functions, and even the calculation of the correlation coefficient, can be handled by modern pocket calculators.

It must be emphasized that equations (1) and (2) are quite general and will operate regardless of how the errors in t_s, t_i, and ϕ are actually estimated. We prefer to make the assumption that fission tracks are spatially distributed in a Poisson manner, so that $\sigma_s^2 = t_s$ and $\sigma_i^2 = t_i$. This relationship is supported by our experience and that of others (Gold and others, 1968).

A complete error analysis requires consideration of the correlation between the fossil and induced track counts. A compilation of the experimentally determined correlation of fossil and induced tracks in the 68 zircon samples dated with the external detector method shows that correlations of greater than 0.90 were found in 72 percent of the cases. A correlation of less than 0.70 was found in only 12 percent of its samples. A low correlation was found in those cases where there was a mixed population of grains (detrital and pyrogenic) or where the fossil-track densities were very low. If a set of data on six or more grains has a correlation of less than 0.7, there may well be something wrong with the sample, and a careful appraisal of the sample and data is necessary.

The data in table 2 can be used to illustrate some advantages of the statistical method outlined in the previous paragraphs. This table shows the results of nine separate age determinations of a standard zircon concentrate performed over a 5-year period. The error of the age as calculated by a previous method (Lindsay and others, 1975) is also shown for comparison. The Lindsay and others method assumes that the fossil and induced counts are independent variables. It is readily seen that the correlation term has a marked effect on reducing the standard error of the age.

Table 2.--Fission-track data of zircons from the Fish Canyon Tuff, San Juan Mountains, Colorado, as determined by C. W. Naeser

[λ_f = 6.85 x 10^{-17} yr^{-1}. Mean age, 27.0; standard deviation, ±1.1; standard error of mean, ±0.35]

Sample No.	t_s	t_i	t_ϕ	ϕ x10^{15} n/cm^2	Correlation (r)	T x10^6 yr	σ x10^6 yr[1]	σ x10^6 yr[2]
5-24-72	687	831	616	1.01	0.99	25.5	1.3	1.0
6-02-72	994	1364	710	1.16	0.95	25.9	1.1	1.0
8-24-72	1145	1325	696	1.10	0.89	29.1	1.2	1.2
6-07-74	1215	1306	2275	0.950	0.98	27.1	1.1	0.6
8-04-75	1035	1100	2065	0.927	0.99	26.7	1.2	0.6
8-15-75	1726	1618	1880	0.844	0.72	27.5	1.0	0.8
11-25-75	1142	1434	2481	1.11	0.98	27.1	1.1	0.7
12-27-76	1140	964	1727	0.819	0.99	28.0	1.2	0.7
1-16-78	1061	1237	2213	1.00	0.99	26.2	1.1	0.6

[1]Lindsay and others (1978).

[2]This work.

An inspection of equation (2) shows that a minimum in age error occurs at the point where P_s and P_i are about equal. To the extent that P_s and P_i are related to the number of tracks counted, it would seem advantageous to employ a neutron dose that will produce an induced track density identical to the spontaneous track density. In actual practice, however, it is not always possible to obtain reasonable experimental data and still have the fossil and induced counts approximately equal. This problem arises when the fossil-track density is either very low $< 5 \times 10^5$ tracks cm^{-2} or very high $> 1 \times 10^7$ tracks cm^{-2}.

Conclusions: The statistical model presented here shows that the age error in the fission-track dating method can be reduced considerably. A crucial parameter in establishing age error is the correlation between spontaneous and induced track density.

The model described here can only deal with the stochastic properties of a carefully defined situation. It must be emphasized that correct statistical practice will not compensate for errors associated with crystal selection, thermal annealing effects, blunders in track counting, incorrect fission constants, counting geometry, and the like. Such errors pertain to the overall validity of the results, and not to the experimental resolution of the results. Given any set of values for σ_s, σ_i, σ_ϕ, however obtained, the equations given here will correctly propagate them through the age equation, and specify the statistical uncertainty of the age.

Gold, Raymond, Armani, R. J., and Roberts, J. H., 1968, Absolute fission-rate measurements with solid-state track recorders: Nuclear Science and Engineering, v. 34, p. 13-32.

Kendall, M. G., and Stuart, A., 1963, The advanced theory of statistics: v. 1, London, Charles Griffin and Co., Ltd.

Lindsay, D. A., Naeser, C. W., and Shawe, D. R., 1975, Age of volcanism, intrusion, and mineralization in the Thomas Range, Key Mountain and Desert Mountain, Western Utah: U. S. Geological Survey, Journal of Research, v. 3, p. 597-604.

McGee, V. E., and Johnson, N. M., (in press), Statistical treatment of experimental errors in the fission-track dating method: Math. Geol.

THE YOUNG MAGMATIC EVENT IN THE NAKHLA ACHONDRITE PARENT BODY

By N. Nakamura[1], D. M. Unruh, and M. Tatsumoto
U.S. Geological Survey
Denver, Colorado 80225
[1]Present address: Kobe University
Kobe, Japan

The Nakhlitic are unique among meteorites in their fractionate REE patterns and their young K-Ar (or Ar-Ar), Rb-Sr, and Sm-Nd ages of ∿ 1.3 b.y. (Podosek, 1973; Papanastassiou and Wasserburg, 1974; Gale and others, 1975; Nakamura and others, 1977). A magmatic origin for these meteorites has been proposed by many workers using independent evidence (for example, Schmitt and Smith, 1963; Bunch and Reid, 1975) and the similarity in ages obtained among the various radiometric clocks suggests that the ∿ 1.3 b.y. ages date the magmatic event that formed the Nakhla meteorite (Nakamura and others, 1977). Papanstassiou and Wasserburg (1974), on the other hand, have proposed that the ∿ 1.3 b.y. Rb-Sr age represents partial resetting on the Rb-Sr system during metamorphism. These authors did conclude, however, that Nakhla is younger than 3.6 b.y.

Accumulated U-Pb data provide only qualitative information regarding the evolution of Nakhla because at least the near surface area and the fusion crust contain significant amounts (at least 50 percent) of terrestrial Pb contamination. Pb isotopic data, on what is believed to be the least contaminated portion yet analyzed, indicate that Nakhla meteorite has undergone net enrichment of U relative to Pb. The U-Pb data, when plotted on concordia, also show enrichment of U relative to Pb (the data plot below the concordia curve). Based on the little information known about U and Pb during crystal-liquid partitioning, we would predict Pb enrichment relative to U to occur during the formation of a basaltic cumulate, unless the cumulate were formed by a large degree of fractional crystallization from a liquid that represented a small degree of partial melting of the original source. Alternatively, Pb depletion relative to U could occur during a post-crystallization thermal event that caused volatile loss from the system. Similarly, if Nakhla was produced by fractional crystallization of either an impact melt, or a liquid produced at shallow depth in the Nakhlite parent body, then one might also expect volatile (Pb) loss to have occurred. Thus, the U-Pb data could be compatible with a simple two-stage evolution model. The 1.27 ± 0.06 b.y. Sm-Nd internal isochron age (Nakamura and others, 1977) and the 5.3 b.y. Sm-Nd whole-rock model age (assuming an initial $^{143}Nd/^{144}Nd$ ratio equal to that of the Moore County initial value) also indicate that Nakhla was derived by at least two distinct stages of evolution.

If we attempt to fit the Sm-Nd data to a two-stage evolution model, then we calculate an initial Sm/Nd ratio for the Nakhla source of 0.363 (chondrite normalized Sm/Nd ratio = 1.18), assuming a 4.56 b.y. age for the source and an initial $^{143}Nd/^{144}Nd$ ratio of 0.50674 at 4.56 b.y. ago (the Sm/Nd ratio of 1.18 is a lower limit). Thus, Nakhla could not have been derived by a single episode of differentiation from a 4.56 b.y. chondritic source.

In an attempt to more precisely constrain evolution models for the meteorite, we have analyzed the REE abundances in olivine, pyroxene, and plagioclase mineral separates from Nakhla. The clinopyroxene, which has a cumulate texture, has a relatively flat REE pattern (La 3.3X, Lu 1.05 x chondrite: with no Eu anomaly). The whole rock has a much more fractionated REE pattern (La 7X, Lu 1.6 x chondrite).

To test the 4.56 b.y. model source with an initial Sm/Nd ratio = 1.18, we first employed a fractional-crystallization model. Using available crystal/liquid partion coefficients, it is possible to estimate the REE pattern of the melt that might have equilibrated with the Nakhla pyroxene. However, the Nakhla pyroxene (augite) contains an extremely high iron content (FeO ∿ 14 percent). Thus, it appears that there is no safe choice of the REE partition coefficients among available data because coefficients strongly depend on the major chemistry of the minerals. Examination of published clinopyroxene liquid partition coefficients from both natural phenocryst-matrix pairs (Schnetzler and Philpotts, 1970) and experimental systems (Onauma and others, 1968), suggests a rather good correlation between the REE partition coefficients and the Fe content of the pyroxene. Employing such a relationship, we have obtained what we believe to be a "best estimate" for the REE partition coefficients in the Nakhla system.

Using the estimated partition coefficients, we have calculated an REE pattern for a liquid in equilibrium with Nakhla and for the Nakhla parent liquid (assuming Nakhla represents ∿ 100 percent pyroxene that was produced at ∿ 85 - 90 percent fractional crystallization from this liquid). The REE pattern for the calculated source material thus obtained, has a slightly

concave shape (similar Sm/Nd ratio estimated for source from Sm-Nd systematics) and REE abundances of 2 - 3 x chondrites.

A partial-melting model has also been examined to reconcile the Nakhla whole-rock REE data. We find that if Nakhla represents a small degree of partial melting ($\lesssim$ 15 percent), then the calculated source has an REE abundance pattern virtually identical to that calculated from the fractional-crystallization model above.

These calculations, when viewed together, suggest that Nakhla is a cumulate containing a significant amount of trapped liquid, and that the trapped liquid dominates the whole-rock REE pattern. The trace element concentration data support this hypothesis in that the olivine and pyroxene mineral separates have REE, U, and Th abundances much lower than those found in the whole-rock, even though Nakhla contains $\sim$ 80 percent clinopyroxene and $\sim$ 15 percent olivine. Nakhla does contain interstitial/intercumulae phases, such as the alteration product "iddingsite"(?), olivine, and K-feldspar (Bunch and Reid, 1975). Analysis of a 2.6 g cm^{-3} < ρ < 2.8 g cm^{-3} density fraction has produced an extremely fractionated REE pattern (La $\sim$ 45 x and Lu $\sim$ 3 x chondrites). This fraction probably contains plagioclase, K-feldspar, and some interstitial material (a very late-stage trapped liquid?). The addition of $\sim$ 10 percent of this material to the olivine and pyroxene data can account for the REE pattern of the whole rock.

We tentatively conclude that Nakhla represents material produced at a relatively advanced stage of fractional crystallization 1.3 b.y. ago, plus some late-stage residual liquid. The REE abundances in the calculated parent liquid suggest that this liquid may have been produced by partial melting of pre-existing cumulates which were produced during the primary differentiation of the Nakhlite parent body $\sim$ 4.56 b.y. ago. The mechanism that triggered the partial-melting event was probably a meteorite or an asteroidal collision.

Bunch, T. E., and Reid, A. M., 1975, The Nakhlites Part I - Petrography and mineral chemistry: Meteoritics, v. 10, p. 303-314.

Gale, N. H., Arden, J. W., and Hutchison, R., 1975, The chronology of the Nakhla achondritic meteorite: Earth and Planetary Science Letters, v. 26, p. 195-206.

Nakamura, N., Unruh, D. M., Tatsumoto, M., and Hutchison, R., 1977, Nakhla - Further evidence for a young crystallization age: Meteoritics, v. 12, p. 324-325.

Onuma, N., Higuchi, H., Wakita, H., and Nagasawa, H., 1968, Trace element partition between two pyroxenes and the host lava: Earth and Planetary Science Letters, v. 5, p. 47-51.

Papanastassiou, D. A., and Wasserburg, G. J., 1974, Evidence for late formation and young metamorphism in the achondrite Nakhla: Geophysical Research Letters, v. 1, p. 23-26.

Podosek, F. A., 1973, Thermal history of the Nakhlites by the ^{40}Ar-^{39}Ar method: Earth and Planetary Science Letters, v. 19, p. 135-144.

Schmitt, R. A., and Smith, R. H., 1963, Implications of similarity in REE fractionation of Nakhlitic meteorites and terrestrial basalts: Nature, v. 199, p. 550-551.

Schnetzler, C. C., and Philpotts, J. A., 1970, Partition coefficients of REE between igneous matrix material and rock forming mineral phenocrysts-II: Geochimica Cosmochimica Acta, v. 34, p. 331-340.

ON THE VALUE OF THE DECAY CONSTANT FOR SPONTANEOUS FISSION OF URANIUM-238

By Susumu Nishimura
Institute of Earth Science
Faculty of General Education
Kyoto University
Kyoto, Japan 606

Since the 3rd International Conference for Geochronology, Cosmochronology and Isotope Geology, several experiments were carried out to obtain the most reliable value of the decay constant for spontaneous fission of 238-uranium. The fission sources used were prepared by the self-electrodeposition of natural uranium on an aluminium plate. The determination of the amount of fissionable material on the plate was carried out by alpha-spectrometry. Homogeneity of the distribution of fissionable materials was checked by the fission-track technique. The fission sources were divided into three parts, upon which polycarbonate or muscovite sheets as a track detector were firmly attached with adhesive tape.

One of the samples was then exposed to neutrons in the reactor. The instrument used for neutron bombardment was the heavy water facility of KUR-1 and its flux was determined by the Au-foil and the fission track methods. The neutron detectors were firmly attached to the turntable with a motor (60 rpm) on the front of the bismuth plug. The neutron flux of this experiment was $3.9 \pm 0.3 \times 10^{13}$ cm^{-2} for the fission-track method and $3.8 \pm 0.2 \times 10^{13}$ cm^{-2} for the Au-foil method (Hashimoto and others, 1969; Kanda and others, 1969).

The other parts were left alone for 3.11, 6.07, 5.40 and 3.96 years, respectively. Then the polycarbonate and muscovite sheets were etched. The fission-track density was calculated from photographs taken through an optical microscope.

If the fission-track age, T (yr), is smaller than 10^9 years, T can be represented by the following equation:

$$T = \frac{1}{\lambda_f} \frac{\sigma\phi}{\eta} \frac{\rho_s}{\rho_i},$$

where λ_f is the decay constant for spontaneous fission of uranium-238 (yr^{-1}), ρ_s the spontaneous fission-track density (cm^{-2}), ρ_i the induced fission-track density (cm^{-2}) by bombardment with a thermal neutron dose ϕ (cm^{-2}), σ the thermal neutron cross section of uranium-235 (cm^2), and η is the isotope ratio of $^{238}U/^{235}U$.

The values used in these experiments were:

$\sigma = 5.77 \times 10^{-22}$ cm^2 (Goldman, 1965),
$\phi = 3.8 \pm 0.2 \times 10^{13}$ cm^{-2},
$\eta = 138$ (Lederer and others, 1967),
and $\rho_i = 5.79 \times 10^7$ cm^{-2} (counts: 23148), (Nishimura, 1975).

The results are shown in table 1. These values are in good agreement with the values obtained by Fleischer and Price (1964), Robert and others (1968), Leme and others (1971), and Kleeman and Lovering (1971).

As an additional experiment, glass containing natural uranium was stored in a refrigerator for 4.78 years to prevent fading.

For $Cos^2\theta_c = 0.65$ (θ_c: critical angle),
range of length of track = 10 μm,
specific weight = 1.5,
number of atoms in glass = 2.78 cm^{-3},
and $\rho_s = 64.0$ cm^{-2} (128 counts),
we get $\lambda_f = 7.4 \pm 0.7 \times 10^{-17}$ yr^{-1}.

Table 1.--Value of the decay constant for spontaneous fission of uranium-238

T (yr)	Spontaneous fission track		λ_f (x 10^{-17} yr^{-1})
	Density (cm^{-2})	Counts	
3.11 (May 23, '68-July 3, '71)	79.5	318	7.0±0.6
6.07 (May 23, '68-March 10, '74)	157	314	7.1±0.6
5.40 (July 3, '71-Nov. 25, '76)	141	282	7.2±0.6
3.96 (March 11, '74-March 6, '78)	101	202	7.0±0.7

This value is in good agreement with the values obtained by the sandwich method.

Fleischer, R. L. and Price, P. B., 1964, Decay constant for spontaneous fission of U^{238}: The Physical Review, v. 133, p. 63-64.

Goldman, D. T., 1965, Chart of the Nucleides: General Electric Company, Schenectady, New York.

Hashimoto, T., Iwata, S., Nishimura, S., Nakanishi, T., and Sakanoue, M., 1969, Measurements of reactor neutron flux by fission track method: Proceedings of the 9th Japanese Conference on Radioisotopes, p. 133-134.

Kanda, K., Nanjo, T., Kobayashi, K., Nakagome, Y., Kozuka, T., Tsukaguchi, K., Kimura, I., and Shibata, T., 1969, Measurements of neutron flux and spectrum at KUR irradiation facilities: KURRI-TR-60.

Kleeman, J. D. and Lovering, J. F., 1971, A determination of the decay constant for spontaneous fission of natural uranium using fission track accumulation: Geochimica Cosmochimica Acta, v. 35, no. 6, p. 637-640.

Leme, M. P. T., Renner, C., and Cattani, M., 1971, Determination of the decay constant for spontaneous fission ^{238}U: Nuclear Instruments and Methods, v. 91, p. 577-579.

Nishimura, S., 1975, On the value of the decay constant for spontaneous fission of uranium-238: Kyoto University Faculty of Science Memoirs, Geology and Mineralogy Series, v. 41, no. 2, p. 15-19.

Roberts, J. H., Gold, R., and Armani, R. J., 1968, Spontaneous-fission decay constant of ^{238}U: The Physical Review, v. 174, p. 1482-1484.

ISOTOPIC COMPOSITION OF METEORITIC CHROMIUM

By O. Nitoh, M. Kamata, and M. Honda
University of Tokyo
Institute for Solid State Physics
Roppongi, Minatoku, Tokyo

Recently, several outstanding reports have been published concerning isotopic anomalies produced by unknown nuclear effects (Lee and others, 1977, 1978; Lugmair and others, 1978; McCulloch and Wasserburg, 1978). It seems quite possible that nuclear processes giving rise to detectable anomalies affected some elements just before the formation of the solar system or in its early stages, and that the fossil records have been preserved in some primitive products.

Mn-53 and its daughter Cr-53 were possibly formed in this manner and might be observed in primitive fractions of unequilibrated chondrites. Iron is one of the most abundant elements, and Mn and Cr isotopes are readily produced from neighboring elements in a manner similar to Al-26 and Mg-26. In fact, in high temperature minerals Mn could not be found as a major constituent. On the other hand, the half-life of Mn-53, 3.7 x 10^6 years, is favourable for detection if it were present in the earliest stage. In iron meteorites, Mn-53 and Cr-53 have been determined extensively (Shima and others, 1966). However, no contribution from cosmic-ray irradiations in the earlier stages of the solar system has been illustrated so far.

Chromium isotopes as galactic cosmic-ray products were studied in our previous work. An extension of these measurements has now been made by employing techniques of solid source mass spectrometry. In this paper we report some preliminary results obtained from several fractions separated from the Allende chondrite and other samples. As stated above, fractions having a high Mn/Cr or a high Fe/Cr ratio are useful samples.

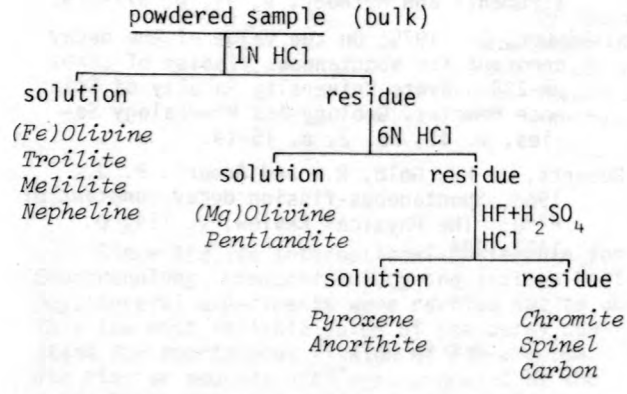

Figure 1.--Stepwise dissolution scheme.

The stepwise dissolution method was used to separate phases of the Allende chondrite. The powdered bulk sample (∿one gram) was leached with 1N HCl to dissolve Fe-rich olivine, troilite, melilite, and nepheline; it was then leached again with 6N HCl to dissolve the remainder of the olivine (Mg-rich), and pentlandite. The insoluble materials, pyroxene, anorthite, etc., were decomposed with HF + H_2SO_4. Finally, the residue composed of chromite, spinel, and carbon was fused with Na_2CO_3. The highest Fe/Cr ratios (∿2100) and the highest Mn/Cr ratios (∿11) were found in the 1N HCl fraction (fig. 2).

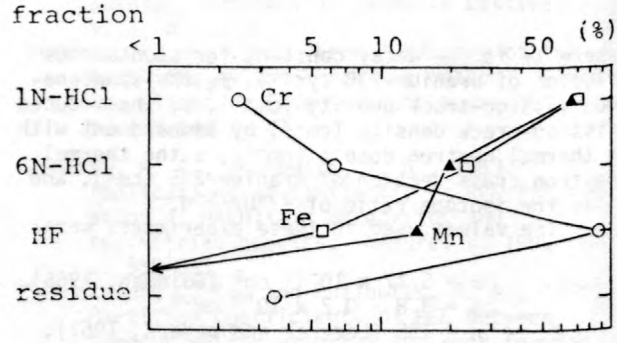

	Mn/Cr	Fe/Cr
1N-HCl	11.4	2100
6N-HCl	1.3	270
HF	0.07	4.5
residue	0.002	0.4
(bulk)	0.38	64

Figure 2.--Composition of fractions.

Iron in the individual fractions was extracted from 8N HCl solution with isopropyl ether, and the aqueous phase, containing Cr, was evaporated to dryness and fused with Na_2CO_3 in a platinum crucible to oxidize Cr (III) to Cr (VI). From a dilute H_2SO_4 solution, chromium (VI) was extracted into isoamyl alcohol with diphenyl carbazide. The organic phase was decomposed with HNO_3, H_2SO_4, and H_2O_2, and the residue was dissolved in dilute HCl for the mass spectrometry.

About one microgram of chromium sample was loaded on a rhenium single filament with silica

gel. When the samples were contaminated with a trace of sodium salts after the chemical treatments, a substantial chromium and sodium ion beam was observed at a filament temperature far below the optimum measuring condition for chromium. The iron beam, which could disturb the M/e=54 peak, disappeared just before the optimum emission of chromium ions. Although CaO^+ was sometimes observed at M/e=56 in the later stage of a run, an iron beam did not appear again at higher filament temperature. About 10^{-13} amperes of $^{52}Cr^+$ were observed for several hours. The beam was amplified by a 17-stage electron multiplier with a gain of 10^5 to 10^6. Runs of a reference sample of reagent chromium were repeated between sample runs. Abundance ratios given by National Bureau of Standards (Shields and others, 1966) were used for normalization. In a single run, 5 to 10 groups of 30 to 50 sets each of four chromium peaks were taken under different conditions of filament current, focusing, multiplier gain, etc. The peak height ratios observed in natural chromium were compared with those from previous studies, and the agreement seemed to be reasonably good except for small systematic deviations and run-to-run errors in a series of the measurements extending more than one year.

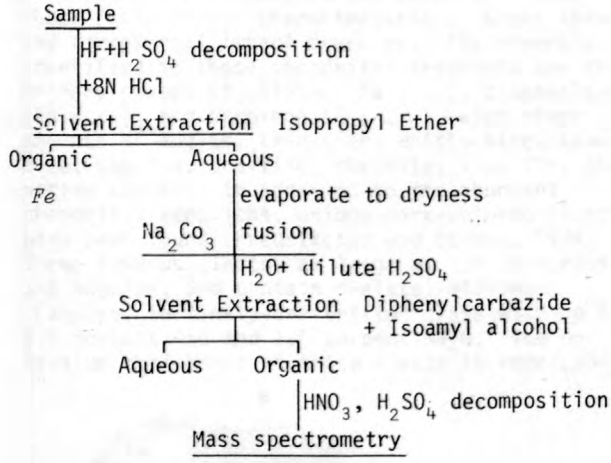

Figure 3.--Chemical extraction for chromium.

Some preliminary data are tabulated in table 1 in terms of delta Cr-53 in parts per ten thousand--a measure of the difference in Cr-53 abundance with respect to the reagent Cr. Poor precision could be attributed partly to lower beam intensities of $\leq 10^{-14}$ amperes caused by chemical recoveries and the presence of impurities, as described above; another cause of poor precision in later runs is lower multiplier gains. The applied voltages were 1.7 to 2 kV in the earlier runs, but in later runs it was necessary to raise them to 2.5 to 3 kV.

Table 1.--Some preliminary data of mass spectrometry

Sample	$\Delta^{53}Cr$ ($\times 10^4$)
Allende	
reference	± 4**
1N HCl	- 10± 6
residue	- 3± 7
HF	+ 5± 7
reference	± 5
6N HCl	- 5± 6
HF	- 4± 8
reference	± 3
residue	- 5± 5
reference	± 4
1N HCl	+ 11±12
inclusion	+ 13±18
Henbury* (iron meteorite)	-129±10

$\Delta^{53}Cr=\{(^{53}Cr/^{52}Cr)_{sample}/(^{53}Cr/^{52}Cr)_{reference}\}^{-1}$

Mass fractionation has been corrected by a normalization using $^{54}Cr/^{52}Cr=0.028222$. The variation reached up to 0.1 percent/mass.

*About 30 ppm Cr. The enrichment of ^{54}Cr reflects on apparent deficiency in ^{53}Cr. About 100 ppb of cosmic ray produced ^{53}Cr and the same content of ^{54}Cr could be estimated.

**reproducibility: $\pm 2\varepsilon = 2\sqrt{\Sigma\Delta^2/n(n-1)}$, n: set No.

In this preliminary study, no visible enrichment or depletion of Cr-53 beyond ± 0.1 percent, relative to the other isotopes, has been observed in the fractions of the Allende meteorite. The method could be applied for the inclusions hand-picked from unequilibrated chondrites. This method could also be applied to the determinations of the cosmic-ray, galactic-, and solar-produced nuclides. In previous work (Shima and others, 1966), even with ordinary iron meteorites, some difficulties have been found in the determination of ppb level products of Cr-54 and Cr-53 in the presence of higher than 10 ppm of natural chromium found in most meteorites.

Gensho, R., Nitoh, O., Makino, T., and Honda, M., (in press), Some long-lived and stable nuclides produced by nuclear reactions: Proceedings of IAGC 2nd Symposium on the Origin and Distribution of the Element, Paris.

Lee, T., Papanastassiou, D. A., and Wasserburg, G. J., 1977, Aluminum-26 in the early solar system: fossil or fuel?: Astro-

physics Journal, v. 211, p. L107-L110.
_____ (in press), Calcium isotopic anomalies in the Allende meteorite: Astrophysics Journal.

Lugmair, G. W., Marti, K., and Scheinin, N. J., 1978, Incomplete mixing of products from r-, p- and s-process nucleosynthesis: Sm-Nd systematics in Allende inclusion EK 1-04-1: 9th Lunar and Planetary Science Conference, p. 672-674.

McCulloch, M. T., and Wasserburg, G. J., (in press), Barium and neodynium isotopic anomalies in the Allende meteorite: Astrophysics Journal.

Shields, W. R., Murphy, T. J., Catanzaro, E. J., and Garner, E. L., 1966, Absolute isotopic abundance ratios and the atomic weight of a reference sample of chromium: National Bureau of Standards Journal of Research (Physics and Chemistry), v. 70A, no. 2, p. 193-197.

Shima, M., and Honda, M., 1966, Distribution of spallation produced chromium between alloys in iron meteorites: Earth and Planetary Science Letters, v. 1, no. 2, p. 65-74.

PETROLOGIC AND ISOTOPIC CONSTRAINTS ON THE ORIGIN OF BHOLA CHONDRITE

By A. F. Noonan[1], R. S. Rajan[2], J. A. Nelen[1] and K. Fredriksson[1]
[1]Department of Mineral Sciences
Smithsonian Institution, Washington, D.C. 20560
[2]Department of Terrestrial Magnetism
Carnegie Institution, Washington, D.C. 20015

Petrologic studies of the Bhola amphoterite show it to be a unique impact breccia containing rounded to angular chondritic and igneous clasts that range in size from less than a millimeter to at least 1.4 cm across (fig. 1). Chondritic inclusions vary texturally from fragments with close-packed, well-defined chondrules (LL4), to the more abundant, often shock-blackened chondritic inclusions containing relict chondrules (LL5-6), to relatively coarse-grained recrystallized clasts (LL7?). These inclusions were shock altered prior to their incorporation into the meteorite, as indicated by mechanical abrasion, shock-blackening, crystal deformation, metal and sulfide veining, and recrystallization of troilite, plagioclase, and chromite. Many of these features are characteristic of known lunar and terrestrial impact breccias. The minerals identified in these chondritic fragments are the primary phases of olivine (Fa_{27-30}), plagioclase (An_{10-12}), and pyroxene (Fs_{10-26}), with minor amounts of augite, tridymite, whitlockite, kamacite, taenite, troilite, chromite, ilmenite, and native copper. In addition to the abundant chondritic xenoliths, unique dark-colored clasts have been found (Fredriksson and others, 1974). These igneous clasts, as large as 1.4 cm across, are angular, and contain skeletal olivines (Fa_{28-29}) in finely-devitrified glass with up to 4.5 percent K_2O and 1.5 percent Na_2O. The potassium enrichment of these clasts is remarkably similar to the dark portion of the Krahenberg amphoterite (Kempe and Muller, 1969). Our studies imply the existence of new rock types and/or extreme fractionation processes occurring on the parent body of amphoterites.

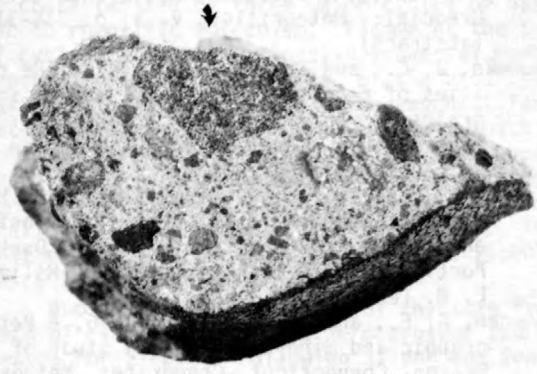

Figure 1.--The cut surface shows the extreme brecciation of the Bhola stone and angularity of included dark clasts. Arrow indicates the location of the large, K-rich (1.3 percent K_2O) fragment. Cut surface is approximately 4 cm across.

We have performed ^{40}Ar-^{39}Ar dating on a sample of the K-rich devitrified-glass clast weighing ~ 10 mg (Rajan, Huneke, Smith and Wasserburg, unpublished data). The resulting age spectrum is highly anomalous, as shown in fig. 2. The K-Ar age from the integrated Ar release is 3.65 b.y., which is a lower limit to the gas-retention age of the glass. Since the clast contains skeletal and euhedral olivines embedded in the fine-grained K-rich glass, it is possible that ^{39}Ar recoil effects are important. Indeed, Huneke and Smith (1976) were able to produce thermal-release patterns similar to that obtained in Bhola from simulated glass-olivine mixtures. In spite of the recoil problem, it is possible that the nominal plateau around ~ 4.3 b.y. may have some age significance. In any case, the formation of K-rich Bhola glass took place at $\geq$ 3.65 b.y. ago.

The light-colored Bhola host material contains fragments and chondrule silicates that are essentially identical in composition to minerals in the xenoliths. As with other xenolithic chondrites, the host contains less than 10 percent intact and broken chondrules, the bulk of the matrix silicates apparently being the crushed or fine-grained equivalents of the xenoliths. Fine-grained recrystallized plagioclase appears to be a matrix-bonding material in some parts of Bhola and may account, at least in part, for the white to gray matrix coloring. The presence of small amounts of primary glass in the matrix (both fragmental and chondritic), as well as one relatively high-iron-matrix olivine crystal (Fa_{18}), shows that there has not been significant thermal metamorphism of the meteorite subsequent to its final agglomeration.

A lithium-tetraborate glass-bead analysis (Noonan and Nelen, 1976) of ~ 1 gram of Bhola host material is probably representative of the major-element chemistry of the bulk meteorite (table 1.). A comparison of the above analysis with that of a coarsely chondritic clast (LL4) suggests that there is no difference in major-element composition between most xenoliths and matrix, with the one important exception of to-

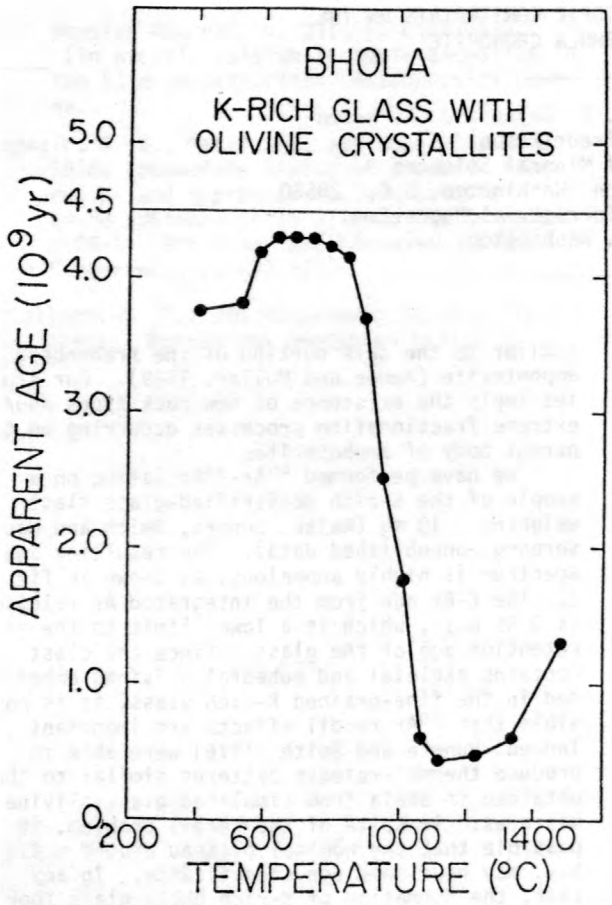

Figure 2.--Apparent age spectrum obtained from the analysis of a devitrified, K-rich glass clast from the Bhola chondrite. The ages are plotted as a function of extraction temperature, which should better reflect the physical processes yielding the anomalous pattern. The Bhola pattern shows evidence of low-temperature ^{40}Ar losses. The apparent age increases to a maximum at 4.30 AE, then decreases precipitously to 0.46 AE. The anomalous pattern is almost certainly due to the recoil transfer of ^{39}Ar into the olivine from surrounding K-rich phases and its retention by the olivine to high temperatures.

tal iron which is attributed to varying amounts of metal in selected samples.

The uniformity in composition of the major silicates in Bhola cannot be attributed to thermal metamorphic equilibration, although this process may, in part, account for the constant

Table 1.--Chemical Composition of Components in the Bhola Amphoterite (USNM 1806)

	Bhola[1] Host	Bhola LL4[1] Xenolith	Bhola dark[1] K-rich clast	K-Rich glass[2] in clast	Krahenberg[3] dark material
SiO_2	38.76	38.55	43.66	59.51	41.3
Al_2O_3	2.08	2.08	2.30	8.41	1.59
FeO (all Fe)	24.34	28.73	21.26	10.48	24.52
MgO	24.92	24.00	26.26	5.85	25.0
CaO	1.75	1.73	2.12	8.96	2.02
Na_2O	1.04	0.91	0.42	1.63	2.35
K_2O	0.09	0.15	1.30	4.34	1.45
TiO_2	0.15	0.14	0.20	0.44	0.3
P_2O_5	0.17	0.18	--	--	--
MnO	0.46	0.34	0.44	0.27	0.36
Cr_2O_3	0.56	0.60	0.70	--	0.3
C	0.01	0.04	--	--	--

[1]These measurements were made using a lithium tetraborate glass bead technique.
[2]These measurements are the average of four broad-beam analyses using the ARL-SEMQ electron probe.
[3]Analyses by Kempe and Muller, 1969.

compositions of the silicates in the LL6 clasts. The occurrence of equilibrated silicates in Bhola, and other chondrites which contain primitive glassy material (Fredriksson and others, 1975), argues against simple metamorphic equilibration of these chondrites. It is equally apparent that Bhola and other xenolithic chondrites cannot be assigned a unique petrologic grade using the Van Schmus - Wood classification. On the basis of the various petrologic grades recognized in Bhola, it can perhaps be classified as an LL4-6 breccia. This is a recurring paradox of the Van Schmus - Wood System, which emphasizes the need for expanding the traditional schemes or establishing a more useful classification.

Fredriksson, K., Dube, A., Jarosewich, E., Nelen, J. A., and Noonan, A. F., 1975, The Pulsora anomaly - A case against metamorphic equilibration in chondrites: Contributions to Earth Sciences, v. 14, p. 41-53.

Fredriksson, K., Noonan, A. F., and Nelen, J. A., 1974, The Bhola Stone - A True Polymict Breccia?: Meteoritics, v. 9, p. 338-339 (abstract).

Huneke, J. C., and Smith, S. P., 1976, The realities of recoil - ^{39}Ar recoil out of small grains and anomalous age patterns in ^{39}Ar-^{40}Ar dating: Lunar Science Conference 7th, Proceedings, 1987-2008.

Kempe, W., and Muller, O., 1969, The Stony Meteorite Krahenberg. Its Chemical Composition and the Rb-Sr Age of the Light and Dark Portions: in Meteorite Research, Millman, P. M. (ed.), p. 418-428.

Noonan, A. F., and Nelen, J. A., 1976, A Petrographic and Mineral Chemistry Study of the Weston, Connecticut, Chondrite: Meteoritics, v. 11, p. 111-130.

EVOLUTION OF A SINGLE GREENSTONE BELT OVER 220 MILLION YEARS--A ZIRCON STUDY OF THE UCHI LAKE AREA, NORTHWESTERN ONTARIO

By. P. D. Nunes[1] and P. C. Thurston[2]
[1]Royal Ontario Museum
Toronto, Ontario, Canada
[2]Ontario Geological Survey
Toronto, Ontario, Canada

Greenstone belts separated from each other by extensive gneissic terrains and intruded by granitic batholiths are known in shield areas the world over. Detailed mapping of Superior Province Canadian Shield greenstone belts by the Ontario Geological Survey has revealed extensive stratigraphic records of Archean crustal development in Ontario. Prominent mineral deposits in these volcanic terrains provide additional incentive to document as accurately as possible their geologic evolution. Precise absolute age measurements are essential to decipher geological histories. Accordingly, the Ontario Geological Survey is sponsoring an ongoing geochronology research program with these primary goals: (1) to accurately document time intervals involved in the development of major greenstone belts and associated rocks in Ontario, and (2) to determine the extent to which geochronology can be used as a time-stratigraphic correlation tool.

Attempts by other workers to decipher greenstone belt histories using the Rb-Sr technique (for example, Jahn and Murthy, 1975; Jahn and Condie, 1976; Hawkesworth and others, 1975) have yielded questionable success owing to large age-measurement errors.

In this paper, we present preliminary zircon age determinations of three rhyolites from the Uchi Lake greenstone belt, northwestern Ontario. The volcanic sequence (Thurston, 1978) is characterized by three major cycles of basaltic to rhyolitic volcanism. Fiammé at the top of cycle 2 attest to a locally subaerial mode of deposition in contrast to all of the other submarine volcanic units. Lower greenschist facies metamorphism predominates. Two $\sim$ 50 m-thick units of carbonate separate cycle 1 from cycle 2 and cycle 2 from cycle 3. These carbonate horizons, in part stromatolitic, are suggestive of shallow, stable, shelf-type environments. The entire stratigraphic sequence is about 11,000 m thick in the area sampled.

About one hundred pounds of rhyolite from each of cycles 1, 2, and 3 were crushed and processed for zircon. Following Silver and Deutsch (1963), different size and magnetic separates of each zircon population were analyzed separately in order to produce discordia lines which enable us to extrapolate back to concordant (that is, closed-system) ages. Preliminary zircon ages and precision error estimates are shown in figure 1: 2959 ± 3 m.y. for cycle 1 rhyolite, 2800 ± 12 m.y. for cycle 2 rhyolite, and 2738 ± 5 m.y. for cycle 3 rhyolite. The internal consistency of the concordia-intercept ages and stratigraphy, and the lack of physical evidence for more than one generation of zircon growth indicate that the ages are best interpreted as the times of extrusion of the rhyolites.

The 2959 m.y. age for the cycle 1 rhyolite is the oldest yet determined from a greenstone belt in the Superior Province of the Canadian Shield. Its antiquity stresses the fact that greenstone assemblages > 2950 m.y. old exist in the Canadian Shield and weakens the conclusion drawn by Baragar and McGlynn (1976) that granitic rocks clearly existed prior to the formation of the greenstone belts. Our data indicate that volcanism and intermittent supracrustal sedimentation in the Uchi area proceeded for at least 221 ± 8 m.y. Such a long period of apparent crustal stability contrasts sharply with the rapid development of modern volcanic piles and emphasizes the apparent significance of chemical sediments (in this case carbonates) as representing paraconformities.

These data clearly illustrate the usefulness of zircon geochronology which, within the limits of reproducibility, will assist in geological unit correlations and significantly advance our understanding of the evolution of Archean greenstone belts. Additional detailed studies such as this are underway, and will greatly enhance our ability to more precisely determine the regional geologic history of the Canadian Shield.

Approximately 100-pound rock samples were crushed in a jaw crusher and pulverized in a hammer mill. Standard density and magnetic separation techniques were used prior to hand-picking of zircon concentrates to > 99.9 percent purity.

Zircon-digestion procedures were those of Krogh (1973). Samples were totally spiked with a mixed ^{205}Pb-^{235}U spike. The ^{205}Pb spike was a portion of that prepared and described by Krogh and Davis (1975). For most samples, lead was isolated on a 0.012-cc resin column with a miniaturized version of a single-column HBr-technique (Nunes, 1975). U passed through the HBr column and was isolated with HCl on a 0.4-cc column (Krogh, 1973).

Isotopic compositions were determined with

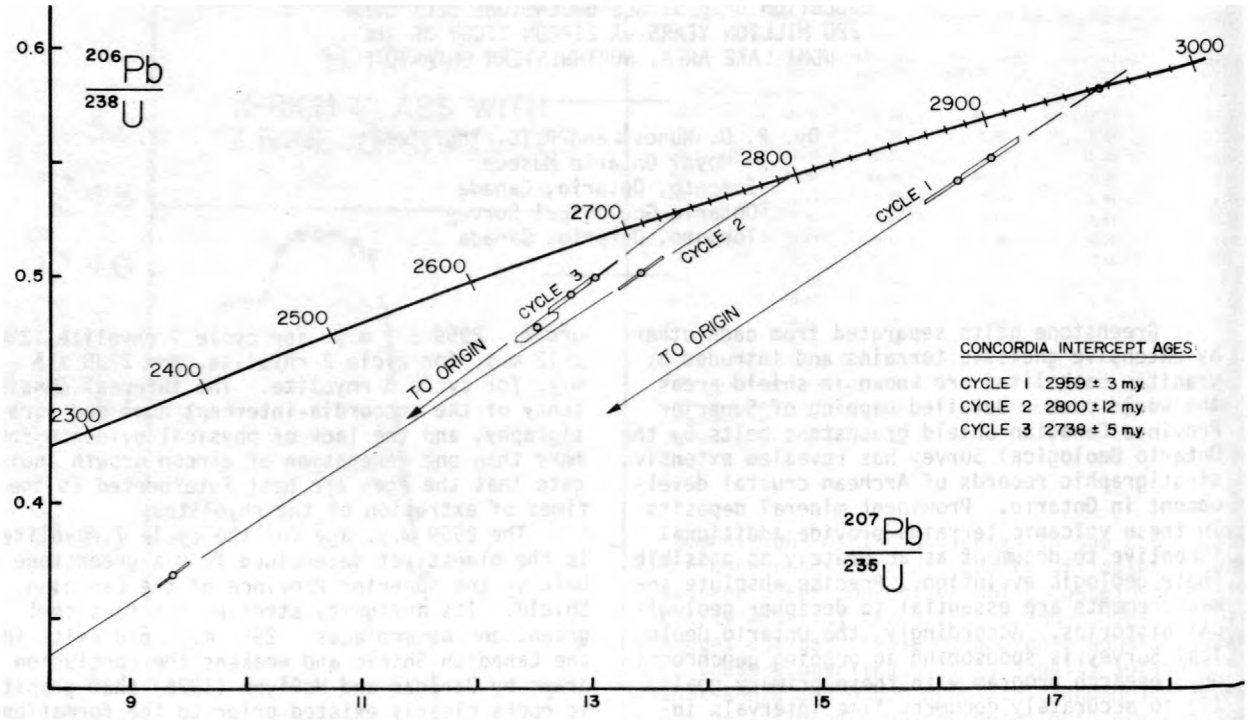

Figure 1.--Concordia diagram with 3 cycle 1, 2 cycle 2, and 3 cycle 3 zircon analyses of varying size and magnetic susceptibilities. Decay constants: $\lambda_{238} = 0.155126 \times 10^{-9}$ yr^{-1} and $\lambda_{235} = 0.98485 \times 10^{-9}$ yr^{-1}. Total-chemistry Pb-blanks ranged from 2.5 ng (earliest data) to 0.2 ng (most recent data). Sample size, 2.3 - 0.76 mg. Current lead blanks, 7 - 11 pg. (9 loading blanks); 21 - 26 pg. (2 HBr column-blanks); and 44 - 300 pg (15 teflon-bomb digestion blanks). Radiogenic lead memory of reused digestion bombs detected at levels of $\sim$ 0 - 220 pg. Monitored to insure negligible cross-contamination of samples. Initial Pb subtracted from data calculated using parameters of Stacey and Kramers (1975). $^{206}Pb/^{204}Pb$ values corrected for mass fractionation and blanks ranged from > 20,000 (cycle 1, least magnetic zircon-population) to 401 (cycle 2, most magnetic-zircon population). $^{207}Pb/^{206}Pb$-errors compiled with error-propagation program that quadratically adds $\pm 2\sigma_m$ mass spectrometric isotope-ratio erros, ± 0.03 percent/a.m.u. mass fractionation error (Faraday Cup Cary detector); ± 0.1 percent/a.m.u. mass fractionation error (Daly Knob photomultiplier detector); and estimated ± 50 percent Pb-blank uncertainty. Estimated U/Pb errors of ± 1.5 percent reflect concentration uncertainties in the mixed- ^{205}Pb-^{235}U-spike. Concordia-intercept ages for cycles 1 and 3 are negligibly affected by the U/Pb uncertainties because these data all lie on lines passing through the origin of the concordia diagram.

a Micromass 30 cm radius mass spectrometer. Lead was analyzed on 20-mil filaments with the silica-gel technique. U was analyzed with a single-filament Ta_2O_5 technique.

Publication authorized by the Director, Ontario Geological Survey.

Baragar, W. R. A., and McGlynn, J. C., 1976, Early Archean basement in the Canadian Shield; a review of the evidence: Special Paper of the Geological Association of Canada, v. 76-14, p. 1-21.

Hawkesworth, C. J., Moorbath, S., and O'nions, R. K., 1975, Age relationships between greenstone belts and "granites" in the Rhodesian Archaean craton: Earth and Planetary Science Letters, v. 25, p. 251-262.

Jahn, Bor-Ming, and Condie, Kent C., 1976, On the age of Rhodesian greenstone belts: Contributions to Mineralogy and Petrology, v. 57, p. 317-330.

Jahn, Bor-Ming, and Murthy, V. Rama, 1975, Rb-Sr ages of the Archean rocks from the Vermilion district, northeastern Minnesota: Geochimica Cosmochimica Acta, v. 39, p. 1679-1690.

Krogh, T. E., 1973, A low contamination method for hydrothermal decomposition of zircon and extraction of U and Pb for isotopic age determinations: Geochimica Cosmochimica Acta, v. 37, p. 485-494.

Krogh, T. E., and Davis, G. L., 1975, The production and preparation of ^{205}Pb for use as a tracer for isotope dilution analyses:

Carnegie Institution of Washington Year Book, v. 74, p. 416-417.
Nunes, P. D., 1975, Pb loss from Apollo 17 glassy samples and Apollo 16 revisited: Proceedings of the Lunar Science Conference 6th, p. 1491-1499.
Silver, L. T., and Deutsch, S., 1963, U-Pb isotopic variations in zircon--a case study: Journal of Geology, v. 71, p. 721-758.
Stacey, J. S., and Kramers, J. D., 1975, approximation of terrestrial lead isotope evolution by a two-stage model: Earth and Planetary Science Letters, v. 26, p. 207-221.
Thurston, P. C., 1978, Geology of the Earngey-Costello area, district of Kenora: Ontario Geological Survey OFR 5240, 120 p.

Rb-Sr AND Sm-Nd CHRONOLOGY OF THE SHERGOTTY ACHONDRITE

By L. E. Nyquist[1], C. Y. Shih[2], B. M. Bansal[2], J. Wooden[2], H. Wiesmann[2], and G. McKay[3]
[1]NASA Johnson Space Center
[2]Lockheed Electronics Co., Inc.
[3]National Research Council
All in Houston, Texas 77058

A chronological study of the Shergotty achondrite by the $^{40}Ar/^{39}Ar$, Rb-Sr, and Sm-Nd methods has been undertaken. $^{40}Ar/^{39}Ar$ results are reported in the companion paper by Bogard and Husain (1978) and the first Rb-Sr results were reported by Nyquist and others (1978). Additional Rb-Sr data and the first Sm-Nd data are reported here.

The Rb-Sr and Sm-Nd data are shown in figures 1 and 2, respectively. The Rb-Sr data for maskelynite (CG1,2), pyroxene (PX1,2) and whole-rock (WR1,2,3) samples lie on or near an isochron corresponding to an age T = 167 ± 14 m.y. and initial $^{87}Sr/^{86}Sr$ = 0.72260 ± 0.00014. As previously discussed (Nyquist and others, 1978), some of the data (CG2, WR2, WR3) lie off this isochron by $\lesssim 4\ \sigma_m$ (σ_m = standard deviation of the mean for about 150 $^{87}Sr/^{86}Sr$ measurements). Because Sr in Shergotty is so radiogenic the deviations from the isochron are $\lesssim 1$ percent of the enrichment in $^{87}Sr/^{86}Sr$ relative to BABI (Basaltic Achondrite Best Initial, Papanastassiou and Wasserburg, 1969). The deviations from the isochron are interpreted to be due to an incomplete resetting of the Rb-Sr system due to only local exchange of Rb and Sr between mineral grains.

The Sm-Nd data are not consistent with the young Rb-Sr age (fig. 2). Data obtained to date define an isochron corresponding to an age T_S = 1.13 ± 0.19 b.y. and initial $^{143}Nd/^{144}Nd$ (I_{Nd}) = 0.50975 ± 0.00029 (normalized to $^{148}Nd/^{144}Nd$ = 0.24308). Bogard and Husain (1978) found an $^{40}Ar/^{39}Ar$ age of 250 m.y. for separated maskelynite and apparent ages for individual gas fractions of up to 640 m.y. for a whole rock sample. Thus, the three radiometric dating methods yield different apparent ages for Shergotty. This finding reflects a relatively complex history for the meteorite and poses difficulties in identifying the apparent ages with real events.

There have been at least two major events in the history of this meteorite, which could have affected the isotopic systems. The first was its solidification from a melt and the second was its involvement in an energetic collision, which resulted in the shock metamorphism of plagioclase to maskelynite (compare Duke, 1968). It is plausible to identify the youngest age as most closely approximating the time of occurrence of the last event. The Rb-Sr age is the youngest and presumably reflects resetting of the Rb-Sr system by shock metamorphism. The mechanism by which the Rb-Sr system was reset cannot be completely characterized at this time. Postshock temperatures of ~300°C are expected to accompany the shock

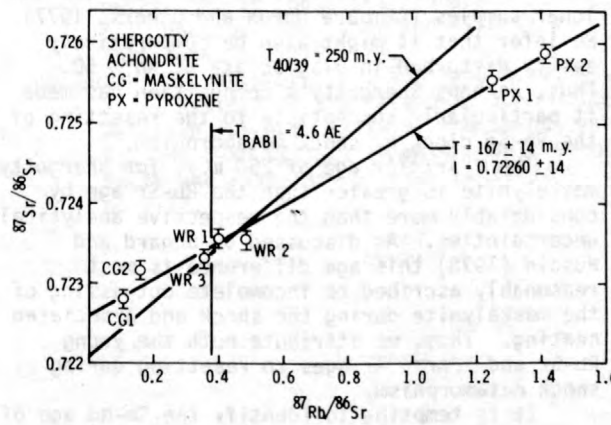

Figure 1.--$^{87}Pb/^{86}Sr$ versus $^{87}Sr/^{86}Sr$ diagram for Shergotty achondrite.

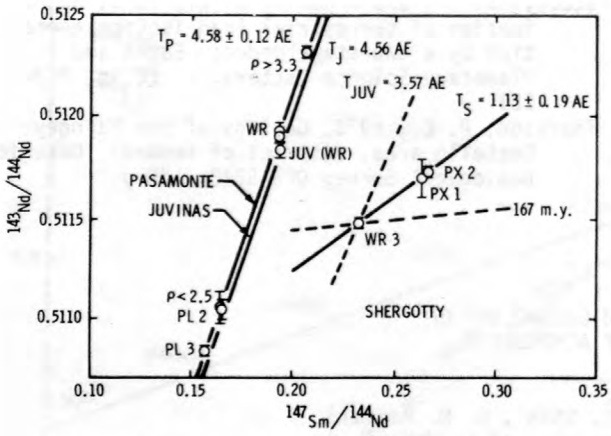

Figure 2.--$^{147}Sm/^{144}Nd$ versus $^{143}Nd/^{144}Nd$ diagram for Shergotty achondrite.

pressures of ∿ 350 kb required for shock metamorphism of plagioclase to maskelynite (Stöffler, 1974). Duke (1968) limits the post-shock thermal history of Shergotty to less than a few minutes at temperatures > 400°C. Literature values of Sr diffusion coefficients (for example, Hart and others, 1968) require long diffusion times for Sr migration over millimeter-distances at these low temperatures. This, in turn, requires considerable thermal blanketing implying deep burial on "Proto-Shergotty". Shock mobilization of trace elements accompanied by enhanced post shock diffusion may facilitate resetting the Rb-Sr clock. Jeanloz and Ahrens (1976) demonstrated a dramatic enhancement in Na mobility following shock metamorphism of plagioclase to maskelynite. The effect is pronounced for plagioclase of composition An ∿ 50 but vanishes for An $\gtrsim$ 80. Shergotty contains ∿ 20 percent plagioclase (An 40-60) and ∿ 75 percent pyroxene by volume. The Rb-Sr system seems to be comparatively easily disturbed in the pyroxenes of some eucrites and lunar samples (compare Unruh and others, 1977). We infer that it might also be comparatively easily disturbed in plagioclase of An ∿ 50. Thus, perhaps Shergotty's composition has made it particularly susceptible to the resetting of the Rb-Sr clock by shock metamorphism.

The $^{40}Ar/^{39}Ar$ age of 250 m.y. for Shergotty maskelynite is greater than the Rb-Sr age by considerably more than the respective analytical uncertainties. As discussed by Bogard and Husain (1978) this age difference is most reasonably ascribed to incomplete outgassing of the maskelynite during the shock and associated heating. Thus, we attribute both the young Rb-Sr and $^{40}Ar/^{39}Ar$ ages to resetting during shock metamorphism.

It is tempting to identify the Sm-Nd age of ∿ 1.1 b.y. with the solidification age of Shergotty. It is, of course, possible that this "age" only reflects incomplete resetting of the Sm-Nd system during shock metamorphism. However, there are several reasons for believing that this may not be the case. First, the Sm-Nd system has been shown to be relatively insensitive to secondary disturbances. For example, a primary Sm-Nd age of 4.58 b.y. was preserved in the Pasamonte meteorite although the Rb-Sr system was disturbed subsequent to 3.4 b.y. ago (Unruh and others, 1977). As discussed above, the near total resetting of the Rb-Sr system for Shergotty may reflect the comparative ease with which that system may be disturbed for mineral compositions such as those found in Shergotty. It need not imply that the secondary event was particularly severe from a Sm-Nd viewpoint. Secondly, the solidification age of Shergotty should be bracketed by the maximum $^{40}Ar/^{39}Ar$ "age" of the whole rock sample (0.64 b.y.) as a lower limit and the Rb-Sr and Sm-Nd model ages (∿ 4.6 b.y. and ∿ 3.6 b.y., respectively) as upper limits. The solidification age should thus lie within the range 0.6-3.6 b.y. The Sm-Nd age satisfies this criteria. Finally, it is difficult to reconcile the Sm-Nd data with a solidification age significantly in excess of 1.1 b.y. accompanied by partial resetting at ∿ 0.2 b.y. ago. This is best illustrated with the aid of a (T, I_{Nd}) - diagram (fig. 3).

The Shergotty (T, I_{Nd}) parameters obtained from the pyroxene-whole rock isochron (fig. 2) are shown in figure 3. They plot significantly below the Juvinas evolution line. ε_T^{CHUR} (T) = -13 ± 3 in the terminology of De Paolo and Wasserburg (1976). Thus, the Shergotty source region must have had a low $^{147}Sm/^{144}Nd$ ratio (Sm/Nd is proportional to the slope of evolution lines in fig. 3). An upper limit to $^{147}Sm/^{144}Nd$ in the source is given by the single-stage evolution line between the (T, I_{Nd}) parameters of Juvinas (Lugmair and others, 1976) and those for Shergotty. A lower limit to $(Sm/Nd)_2/(Sm/Nd)_1 = R$ is $R \geq 1.4$ where $(Sm/Nd)_2$ = ratio in Shergotty and $(Sm/Nd)_1$ = ratio in the source. It is difficult to increase the Sm/Nd

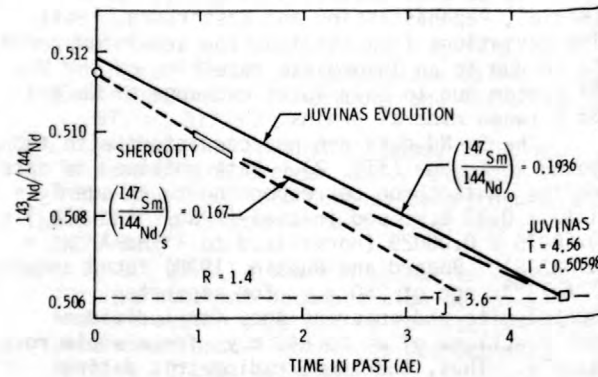

Figure 3.--$^{143}Nd/^{144}Nd$ evolution diagram for Shergotty achondrite.

ratio by this much igneous processes. Among the major minerals the pyroxenes are the most effective in fractionating light REE during igneous processes but can only change Sm/Nd by $\lesssim$ 50 percent. Thus, we expect R $\lesssim$ 1.5 which limits the solidification age to T $\lesssim$ 1.6 b.y.

Stolper and McSween (1978) propose a model in which Shergotty is envisioned to have formed from ∿ 30 percent cumulus pyroxene and ∿ 70 percent intercumulus liquid. Such a model would produce only ∿ 5 percent increase of the Sm/Nd ratio relative to that in the liquid. The parental liquid suggested for the Shergottites by Stolper and McSween (1978) is not plagioclase saturated, implying the absence of plagioclase from the source residue. The parental liquid would thus be expected to have a lower Sm/Nd ratio than the source, and it is difficult to account for the large increase of Sm/Nd in Shergotty relative to the source unless the ratio of cumulus pyroxenes to intercumulus liquid is higher than that envisioned by Stolper and McSween (1978) or unless light REE-enriched residual liquid is removed from the system at a late stage of crystallization.

The low single-stage Sm/Nd ratio calculated for the Shergotty source could reflect either a nonchondritic relative abundance of the REE for the Shergotty parent body or an early stage of igneous differentiation in which an originally chondritic Sm/Nd ratio was decreased by ∿ 16 percent. The numerical values for some of these Sm-Nd constraints may change with the acquisition of more data, but it is unlikely that the qualitative interpretations will change drastically. One need only compare the Shergotty data in figure 2 to that of Pasamonte (Unruh and others, 1977) and Juvinas (Lugmair and others, 1976) to see that Shergotty's evolution has been significantly different from that of the eucrites. It is interesting to note that for Shergotty the ICE-age (Lugmair and others, 1976) it yet to come.

Bogard, D. D., and Husain, L., 1978, ^{40}Ar-^{39}Ar dating of shock events in the Shergotty achondrite and the Plainview chondrite: (this conference).

De Paolo, D. J., and Wasserburg, G. J., 1976, Nd isotopic variations and petrogenetic models: Geophysical Research Letters, v. 3, p. 249-252.

Duke, M. B., 1968, The Shergotty meteorite: magmatic and shock metamorphic features, in Shock metamorphism of natural materials: eds., French, B. M., and Short, N. M., p. 613-621. Baltimore, Mono Book Corporation.

Hart, S. R., Davis, G. L., Steiger, R. H., and Tilton, G. R., 1968, A comparison of the isotopic mineral age variations and petrologic changes induced by contact metamorphism, in Radiometric Dating for Geologists: Interscience Publishers, p. 73-110.

Jeanloz, R., and Ahrens, T. J., 1976, Alkali mobility in shocked basalt: in Proceedings of the Lunar Science Conference, 7th, Pergamon Press, p. 1623-1632.

Lugmair, G. W., Marti, K., Kurtz, J. P., and Scheinin, N. B., 1976, History and genesis of lunar troctolite 76535 or, How old is old?, in Proceedings of the Lunar Science Conference 7th: Pergamon Press, p. 2009-2033.

McSween, H. Y., and Stolper, E., 1978, Shergottite meteorites, I; Mineralogy and petrography, in Lunar and Planetary Science IX: p. 732-734, Houston, Lunar and Planetary Science Institute.

Nyquist, L. E., Wooden, J., Bansal, B., and Wiesmann, H., 1978, A shocking Rb-Sr age for the Shergotty achondrite, in Lunar and Planetary Science IX: Houston, The Lunar and Planetary Institute, p. 820-821.

Papanastassiou, D. A., and Wasserburg, G. J., 1969, Initial strontium isotopic abundances and the resolution of small time differences in the formation of planetary objects: Earth and Planetary Science Letters, v. 5, p. 361-376.

Stöffler, D., 1974, Ries meteorite crater, Germany II: Fortschritte der Mineralogie, v. 52, p. 103-122.

Stolper, E., and McSween, H. Y., 1978, Shergottite meteorites, II; Experimental petrology, in Lunar and Planetary Science IX: Houston, The Lunar and Planetary Institute, p. 1119-1121.

Unruh, D. M., Nakamura, N., and Tatsumoto, M., 1977, History of the Pasamonte achondrite; Relative susceptibility of the Sm-Nd, Rb-Sr, and U-Pb systems to metamorphic events: Earth and Planetary Science Letters, v. 37, p. 1-12.

COMPARISON BETWEEN RADIOMETRIC AGES OF GLAUCONITES AND OF HIGH-TEMPERATURE MINERALS AND ROCKS AND THEIR IMPLICATIONS FOR THE NUMERIC TIME SCALE

By G. S. Odin[1] and J. C. Hunziker[2]
[1]University of P. and M. Curie
2 Place Jussieu
75230 Paris Cedex 05
[2]Universitat Bern
Sahlistr. 6
3000 Bern, Switzerland

The time scale of the Mesozoic and Tertiary, as revealed mainly by K-Ar isotopes, is discussed in this paper. First, a comparison is drawn between the quality of the different chronometers. Then, comparisons between sedimentary sequences of probable equal age are discussed and the establishment of fixed time points is stressed.

COMPARISON OF QUALITIES AND UNCERTAINTIES

If a geochronometer does not show the exact age of formation, there are evidently reasons for its discrepant behavior. We will try to show that it is possible to predict with good probability before an isotopic analysis why things can go wrong. Three sorts of uncertainties--analytical, genetical, and stratigraphical--can be distinguished. No absolute approach can be established to overcome these uncertainties, but every case has a particular solution, beginning with field work, and followed by petrographic and laboratory work.

1. The analytical uncertainty comes from the K analysis, the Ar analysis, and the homogeneity and representativeness of the sample with respect to the rock from which it was extracted. The error on the K determination should be equal to or smaller than ± 1 percent. Only the abundant use of standards assert a high accuracy of the Ar analysis. For glauconites, the backing of the line should not exceed 150°C.

Homogeneity and representativeness of a sample depend on the type of chronometer used. One critical point is the original sample size. This size can become very large in the case of an igneous rock (Obradovich and Cobban, 1975) and should not be smaller than 1 kg, even for a sediment rich in glauconite. The degree of representativeness of a sample further depends on a careful splitting and on a skillful separation giving comparable aliquots even over the long term. Experience shows that glauconite grains with the highest evolution, rich in K, are the most homogenous (Odin, 1978a). The sum of these uncertainties rarely is smaller than 3 percent (2σ) and is of the same order for the different chronometers, if adequately prepared.

A further uncertainty is added by the differences in argon retention between the genesis of a mineral and its analysis. Evidently, the low formation temperature of glauconites renders them more sensitive to temperature changes due to burial and tectonic deformation. From nature and experiments (Odin, Velde and Bonhomme, 1977), it is clear that a petrographic and field analysis should enable one to exclude most of the dubious samples that have suffered severe tectonization and (or) burial of over 2000 m.y. Avoiding such material and choosing the most evolved glauconites, richest in potassium, the correct age should be found. It is clear that such ideal glauconites are found only in epicontinental basins with weak subsidence.

Glauconite and biotite show equivalent behavior after rinsing. A biotite with less than 5 percent K shows scattered ages (Obradovich and Cobban, 1975). In the case of glauconite, it is necessary to select the sample with the highest K content; in other words, with the lowest amount of expandable layers--the capacity of cationic exchange being directly a function of the amount of expandable layers (Cimbalnikova, 1971c). Experience with natural and artificial rinsing shows that, at least for highly evoluted glauconites, a moderate rinsing does not affect the K-Ar and Rb-Sr ages (Odin and Hunziker, 1974; Pasteels and others, 1976). The ages are lowered only after the departure of 10 to 15 percent of the K. This type of alteration does produce important systematic effects in volcanic ashes deposited into water, volcanic rocks altered to bentonites, or even weathered basaltic rocks. In these cases, the mineral richest in potassium should also be chosen for analysis.

2. The genetic uncertainty depends on the time gap between crystallization and closure of the isotopic system under consideration, and the anomaly and uncertainty of the initial composition of this isotopic system. The fast closure of high-temperature volcanic minerals is ideal. In this respect glauconites are very imperfect and plutonic minerals show a variable response. The response of a volcanic mineral is well known. A glauconite, on the other hand, shows a late closure, often contemporaneous to the covering sediment. The glauconite age, therefore, represents the time of the fauna

covering the green strata and is not coincident with the age of the fauna deposited together with the evolving glauconite grains. Therefore, only a detailed sedimentological work will lead to the correct interpretations of the measured age.

The initial isotopic composition of an igneous rock can sometimes be anomalous. Measuring different cogenetic minerals of such a rock may lead to useful corrections, but uncertainties may also exist, as in the case of sanidine in volcanic ashes (Obradovich and Cobban, 1975). No such corrections can be applied for glauconites. Here the uncertainties come from an inheritance of radiogenic argon during the process of recrystallization of the evolving glauconite pellets, both in nature and in the experiment (Odin and others, 1977; Odin, 1978a). The importance of the inheritance of radiogenic argon decreases with increasing evolution of the glauconite. This, again, shows that the oldest glauconite age of a stratigraphic horizon is not always the most representative.

3. The stratigraphic uncertainty for a glauconite sample in a reference sequence is small. In some cases, as revealed by sedimentological studies, the formation of the green grains corresponds to a sedimentation gap of significant duration. For igneous rocks this problem may be of primary importance. Bentonites sometimes are difficult to place precisely in a reference sequence but are

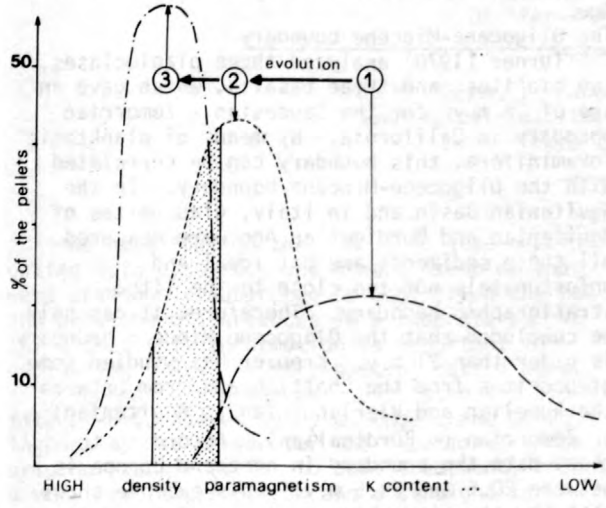

Figure 1.--Principles for choosing the presumably best green pellets of a sediment. Growing evolution of a glauconite tends to give more honogeneous populations. The separation using various properties (x axis) permits the selection of the most evolved grains. For the case of a partially evolved glauconite (2) the stippled part is chosen.

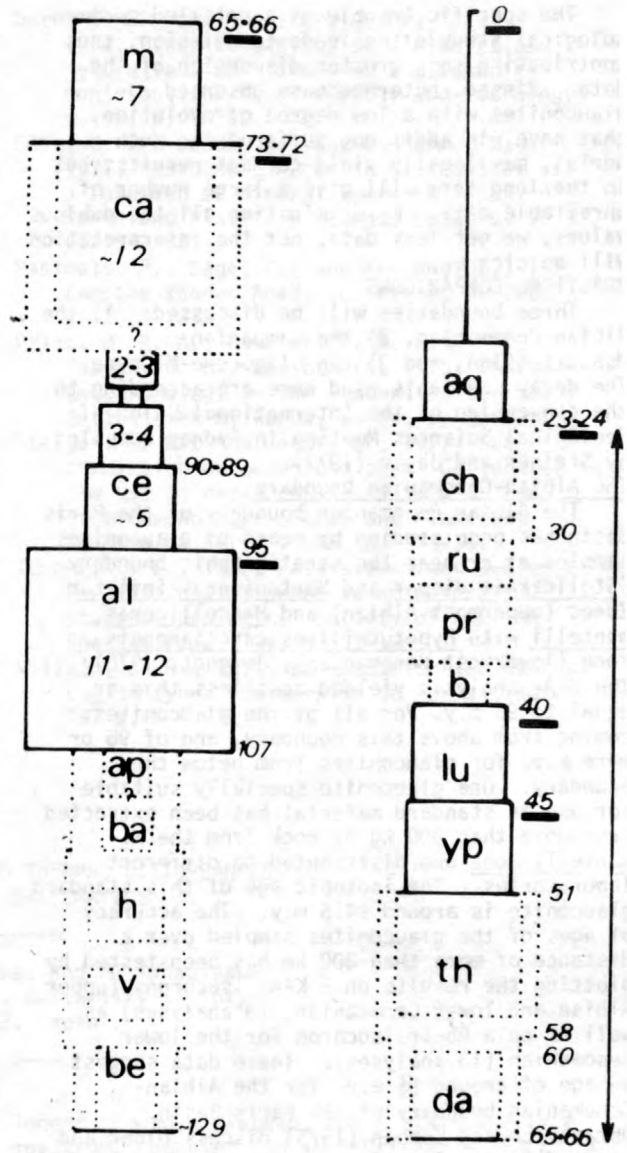

Figure 2.--Duration and probably boundaries of Cretaceous and Palaeogene stages in Europe. All numbers in millions of years (ICC). Underlined are the safe limits; stippled, the limits to be worked on.

preferred chronometers for establishing regional time scales. Continental volcanic strata and plutons only occasionally provide useful data because of the uncertainty of their cooling rate with respect to the life of the interbedded fauna. These two last uncertainties, genetic and stratigraphic, are difficult to quantify and are, therefore, often not taken into consideration in a great number of syntheses (Odin, 1978b). They nevertheless become decisive in a detailed sedimentological investigation.

The specific trouble of a detailed sedimentological study often leads to omission, thus contributing to a greater dispersion of the data. Rinsed, heterogenous, unsorted glauconites with a low degree of evolution, that have, in addition, suffered too much burial, may locally yield correct results, but in the long term will give a large number of unreliable data. By eliminating all the dubious values, we get less data, but the interpretation will be clearer.

PRACTICAL COMPARISONS

Three boundaries will be discussed: 1) the Albian-Cenomanian, 2) the Campanian-Maastrichtian, and 3) the Oligocene-Miocene. The decay constants used here are according to the convention of the International Union of Geological Sciences Meeting in Sydney compiled by Steiger and Jäger (1977).

The Albian-Cenomanian boundary

The Albian Cenomanian boundary of the Paris Basin has been studied by means of glauconites sampled at or near the stratigraphic boundary (Stoliczkaia dispar and Mortoniceras inflatum Zones (uppermost Albian) and Mantelliceras mantelli with Hypoturrilites carcitanencis Zone (lowermost Cenomanian), Juignet, 1970). The K-Ar analysis yielded ages less than or equal to 95 m.y. for all of the glauconites coming from above this boundary, and of 96 or more m.y. for glauconites from below the boundary. One glauconite specially suitable for use as standard material has been extracted from more than 300 kg of rock from the M. mantelli Zone and distributed to different laboratories. The isotopic age of this standard glauconite is around 94.5 m.y. The accuracy of ages of the glauconites sampled over a distance of more than 300 km has been tested by plotting the results on 2 K-Ar isochrons (upper Albian and lower Cenomanian, 19 analyses) as well as on a Rb-Sr isochron for the lower Cenomanian (13 analyses). These data suggest an age of around 95 m.y. for the Albian-Cenomanian boundary of the Paris Basin. Obradovich and Cobban (1975) discuss older and newer data on minerals extracted from bentonites from the western United States. These authors also compare their ammonite fauna with the European fauna. In Cretaceous times the Atlantic Ocean already provided a barrier for the macropelagic and benthic fauna, thereby making such comparisons difficult. Nevertheless, Obradovich and Cobban (1975) propose an age of 96 m.y. for the Albian-Cenomanian boundary. Allowing for the palaeontologic uncertainty, the concordance is striking and demonstrates that both types of chronometers are comparable.

The Campanian-Maastrichtian boundary

This boundary presents severe biostratigraphic problems. According to Cobban it can vary in North America between two extremes including 10 thin ammonite biozones. The adapted biostratigraphic boundary according to Cobban is around 72 m.y., as dated by means of minerals extracted from bentonites. The Maastrichtian includes the equivalent of 10 biozones and the Campanian 20 biozones of ammonites.

In the Limburg region, Priem and others, (1975) have published glauconite data from the Campanian-Maastrichtian boundary. According to the authors, the lithostratigraphic limits in this small basin are variable. A recent micropalaeontological study by Vilain (1974) discusses these variations. Today, a broader definition than that of the stratotype of earlier workers is suggested. At the base of the Maastrichtian a hardground occurs in this small basin. Here the sedimentologic gap seemed rather important and allowed the glauconites to develop. All of the glauconites analyzed in this work were not of optimum quality. Nevertheless, the stratigraphic limit is bracketed by two good glauconites representative of the lower Maastrichtian yielding 71.6 and 72.6 m.y. and two glauconites from the upper Campanian giving 74.2 and 75.2 m.y. This places the boundary near 73 m.y. disregarding the pecularity of the basin.

In Bern we have worked on glauconites sampled from Danian sands with Globorotalia globigerini found above the Maastrichtian in the region of Kurfs and along the Albert Channel. The micropalaeontologic study of the samples shows reworking of various Maastrichtian foraminifera. The glauconite is all very fresh and rich in K, pointing to a massive reworking. The K-Ar age of around 72 m.y. shows that the glauconites have preserved their Maastrichtian Age.

The Oligocene-Miocene boundary

Turner (1970) analyzed three plagioclases, two biotites, and three basalts, which gave an age of 23 m.y. for the Saucesian - Zemorrian boundary in California. By means of planktonic foraminifera, this boundary can be correlated with the Oligocene-Miocene boundary. In the Aquitanian Basin and in Italy, glauconites of Aquitanian and Burdigalian Age were measured. All these sediments are not ideal and unfortunately not too close to the lithostratigraphic boundary. Therefore, it can only be concluded that the Oligocene-Miocene boundary is older than 21 m.y. Kreuzer has studied some glauconites from the Chattian and from between the Rupelian and Vierlanderian (≈ Aquitanian) or Zemorrian (≈ Burdigalian). According to these data the boundary in northern Europe is between 20.5 and 24.5 m.y. This example shows that the stratigraphic problems and the dating by means of igneous rocks are more nearly resolved than are the problems of the genesis of the glauconites.

CONCLUSIONS

The recent progress allows a closer correlation between data on igneous rocks and on sedimentary rocks. Knowledge of the geochemistry of sediments has advanced considerably in the last years permitting a more rigorous

selection and a better interpretation of the data. Hopefully, the combined chronometers of igneous rocks and of sedimentary rocks will help to establish a consistent world-wide time scale.

Cimbalnikova, A., 1971, Index of refraction and density of glauconites: Casopis pro

Folinsbee, R. E., and others, 1966: Alberta Society of Petroleum Geologists, p. 162-174.

Juignet, P., 1970, Precisions stratigraphiques et sedimentologiques sur le Cenomanien du Pays de Caux entre Saint-Jouin-Bruneval et el cap d'Antifer (Seine-Maritime): Bulletin du Bureau de Recherches Geologiques et Minieres, v. 2, no. 1, p. 11-15.

Obradovich, J. D., and Cobban, W. A., 1975, A time-scale for the late Cretaceous of the Western Interior of North America: Special Paper of the Geological Society of Canada, v. 13, p. 31-54.

Odin, G. S., (in press), Results of dating Cretaceous and Palaeogene sediments of Europe: American Association of Petroleum Geologists Bulletin.

_____ ,(in press), Isotopic dates for a Palaeogene time scale: American Association of Petroleum Geologists Bulletin.

Mineralogii a Geologii, v. 15, no. 4, p. 335-345.

Odin, G. S., and Hunziker, J. C., 1974, Etude isotopique de l'alteration naturelle d'une formation a glauconie: Contributions to Mineralogy and Petrology, v. 48, p. 9-22.

Odin, G. S., Velde, B., and Bonhomme, M., 1977, Radiogenic Argon in Glauconites as a Function of Mineral Recrystallization: Earth and Planetary Science Letters, v. 37, p. 154-158.

Pasteels, P., Laga, P., and Keppens, E., 1976, Comptes-rendus Acad. Sc. Paris, v. 282, p. 2029-2032.

Priem, H. N. A., Boerlerijk, N. A. I. M., Hebeda, E. H., and others, 1975, Isotope geochronology in the Indonesian tin belt: Geologie en Mijnbouw, v. 54, p. 205-207.

Steiger, R. H., and Jäger, E., 1977, Sub-commission on Geochronology: Convention on the use of decay constants in geo- and cosmochronology: Earth and Planetary Science Letters, v. 36, p. 359-362.

Turner, D. L., 1970, Potassium-argon dating of Pacific Coast Miocene foraminiferal stages: Geological Society of America Special Paper 124, p. 91-129.

Villain, J. P., 1974, Le Maastrichtien dans sa region type: Universite de Paris, Thèse, 197 p.

EFFECTS OF PRESSURE AND THERMAL DISTURBANCES ON ^{40}Ar-^{39}Ar SYSTEMATICS

By M. Ozima, I. Kaneoka, and M. Yanagisawa
Geophysical Institute, University of Tokyo
Tokyo 113, Japan

We have applied the ^{40}Ar-^{39}Ar step-heating dating method to rock and mineral samples that were previously subjected to controlled thermal and pressure disturbances in a laboratory. We think that this information is important in evaluating ^{40}Ar-^{39}Ar step-heating dating ages.

Thermal disturbances: USGS standard biotite LP-6 (prepared by J. C. Engels and C. O. Ingamells) was chosen for the experiment. The original sample (prior to heat treatment) showed a very flat age spectrum and a straight isochron. Both the plateau and isochron ages agree perfectly with a total-fusion age. The sample was then subjected to various heat treatments, both in air and in a vacuum. The heat treated samples were then analyzed by the ^{40}Ar-^{39}Ar step-heating dating method. The results are shown in table 1.

After one hour of heating in air at 700°C, we observed that a total-fusion age was reduced by about 20 percent and an age spectrum no longer showed a plateau, but a staircase-type spectrum. However, in an $^{40}Ar/^{36}Ar$ - $^{39}Ar/^{36}Ar$ plot, data still formed a nice straight correlation line, which gave the same isochron age as the original undisturbed age, although the intercept with the y-axis (a value of $(^{40}Ar/^{36}Ar)_0$) was considerably reduced.

Heating in air at a higher temperature (850°C) caused more distortion, both in the age spectrum and the isochron plot. The total-fusion age was reduced by more than 25 percent. In this case, neither an age plateau nor an isochron age could be defined.

The results of heat treatment in air can be explained as partial loss of Ar (^{40}Ar and ^{36}Ar) from the samples. Reduction in the total age can be easily explained as loss of radiogenic $(^{40}Ar)^*$ from the sample. The staircase-type age spectrum then reflects loss of $(^{40}Ar)^*$ preferentially from lower temperature sites. If the amount of the partial Ar loss due to the

Table 1.--Effect of heat treatment of LP6-biotite samples on ^{40}Ar-^{39}Ar systematics
[USGS standard sample prepared by J. C. Engels and C. O. Ingamells]

Heat treatment	$(^{40}Ar/^{36}Ar)_o$[1]	Total age (m.y.)	Isochron age (m.y.)	Age spectrum
(Original)	309.5±10.4	124.5	125	Flat
Heated in air, at 700°C, 1 hour	235.1± 6.15	105.7	124.6±2.5	Staircase
Heated in air, at 860°C, 1 hour	(~100)	102	---	Staircase
Heated in vacuum ($P=1x10^{-3}$), at 700°C, 1 hour	317.2±9.15	127.9	125.4±2.4	Inverse staircase

[1]Intercept value in an $^{40}Ar/^{36}Ar$-$^{39}Ar/^{36}Ar$ isochron plot.

disturbances was assumed to be proportional to the amount of Ar that should be released at each respective temperature during a normal step-heating process and the proportional constant for the loss is assumed to be dependent only on temperature, then

$$\Delta^i Ar = k(T) \cdot {}^i Ar, \quad i = 36, 40$$

$\Delta^i Ar$: Argon partially lost from a sample by disturbances

${}^i Ar$: Argon released at T on stepheating

k : proportional constant.

We can show that the effect of such Ar loss is simply to displace the original isochron horizontally without greatly disturbing its gradient and linearity. It is then easy to see that even after the partial Ar loss, data points in an $^{40}Ar/^{36}Ar$ - $^{39}Ar/^{36}Ar$ plot still retain approximate linearity with a reduced intercept value of $(^{40}Ar/^{36}Ar)_o$.

Heat treatment in vacuum resulted in less disturbance in ^{40}Ar-^{39}Ar systematics. A total-fusion age agrees well with an isochron age. However, the age spectrum was distorted to show an inverse staircase type (higher ages for lower temperature fractions). The intercept value $(^{40}Ar/^{36}Ar)_o$ was increased, which is contrary to the case for air heating. We conclude that in the case of vacuum heating, there was no total loss of Ar from the sample, but Ar (mostly radiogenic $(^{40}Ar)^*$) was partially reequilibrated within the sample, resulting in an apparent trapped Ar of higher $(^{40}Ar/^{36}Ar)_o$ than that of the original trapped Ar. Less severe disturbances during vacuum heating suggest that the air heating resulted in oxidation, whereas the vacuum heating resulted only in mechanical disturbances of the samples.

Pressure disturbances: One Cretaceous granite and one Cretaceous basalt were studied. Samples were drill cores with a 20-mm diameter and a 8.15-mm length. Before applying pressure, the granite sample was first kept in a vacuum chamber and then dropped in a water bath that was also placed in the vacuum chamber. The sample was then quickly covered with plastic glue to prevent water evaporation, thus providing a water-saturated sample. We thought that pressure applied to a water-saturated sample would simulate actual tectonic disturbances more closely. The water-saturated sample was then subjected to pressure by using a piston cylinder.

Experimental results are shown in table 2. The original granite sample showed a flat age spectrum and straight isochron on an $^{40}Ar/^{36}Ar$ - $^{39}Ar/^{36}Ar$ plot. Both the plateau and isochron ages agree well with the total-fusion age. After the application of a uniaxial compression of 1650 bar, we observed about a 10 percent reduction in the total age, and a disturbed age spectrum showing a staircase pattern, but preserving a linear correlation on an $^{40}Ar/^{36}Ar$ - $^{39}Ar/^{36}Ar$ plot, with a significantly reduced intercept value $(^{40}Ar/^{36}Ar)_o$. In the case of the basalt sample, no water-saturation treatment was applied. Pressure was applied to the basalt sample in a dry condition. After the pressure disturbance, we observed trends similar to those for the granite: that is, a reduction of a total-fusion age, a reduction in the intercept value, $(^{40}Ar/^{36}Ar)_o$, and practically no change in the isochron age. The effect of the pressure disturbance on ^{40}Ar-^{39}Ar systematics can be understood as partial loss of Ar from the samples, as in the case of thermal disturbances.

In summary, the effect of the thermal and pressure disturbances on ^{40}Ar-^{39}Ar systematics can generally be explained as partial loss of Ar from the samples. Symptomatically, the partial loss of Ar results in reduction of the total-fusion age, distortion of the age spectrum, retention of linearity and the original isochron age on an $^{40}Ar/^{36}Ar$ - $^{39}Ar/^{36}Ar$ plot, and reduction of the $(^{40}Ar/^{36}Ar)_o$ intercept value. Such characteristics can be explained if we assume that the amount of the partial Ar loss is

Table 2.--Effects of compaction of samples on ^{40}Ar-^{39}Ar systematics

Sample	Pressure treatment	$(^{40}Ar/^{36}Ar)_o$[1]	Total age (m.y.)	Isochron age (m.y.)	Age spectrum
Inada Granite	(Original)	293.3 ± 2.3	59.85	59.93±0.6	Flat
	1400 bars, with H_2O[2]	210.5 ±108.5	55.8	60.92±1.2	Staircase
Niizuki Basalt	(Original)	307.95± 2.8	123.5	107.2 ±2.5	Ragged
	1650 bars	301.5 ± 2.8	116.0	107.5 ±2.5	Ragged

[1]An intercept value in an $^{40}Ar/^{36}Ar$-$^{39}Ar/^{36}Ar$ diagram.
[2]Samples were previously water-saturated and the surface was sealed with plastic glue.

proportional to that of Ar released from the sample at each respective temperature in the step-heating process and the proportionality constant depends only upon temperature.

Finally we would like to emphasize that the above thermal and pressure disturbances hardly affected the isochron age, although the age spectrum was significantly distorted. These experimental results may suggest that, in some cases, we can still derive meaningful geological ages from an ^{40}Ar-^{39}Ar isochron even though the age spectrum does not show a plateau.

RESPONSE OF U-Pb ZIRCON AND Rb-Sr TOTAL ROCK AND MINERAL SYSTEMS TO LOW-GRADE REGIONAL METAMORPHISM IN PROTEROZOIC IGNEOUS ROCKS, MOUNT ISA, AUSTRALIA

By Rodney W. Page
Bureau of Mineral Resources
Canberra, A.C.T., Australia

A detailed Rb-Sr total-rock and mineral and U-Pb zircon study has been made on a number of suites of Proterozoic acid volcanic rocks and granitic intrusions near Mount Isa, northwest Queensland. Stratigraphic relationships (fig. 1) within and between each of these igneous units are well known, and provide the ultimate criteria for interpretation of the isotopic results.

Precise dating of primary igneous crystallizational events has been achieved through the use of U-Pb systematics in zircons (figs. 2 and 3). Stratigraphically consistent U-Pb zircon ages within the basement igneous rocks show that the oldest recognized crustal development was the outpouring of acid volcanics (Leichhardt Metamorphics) 1865 + 3 m.y. ago, which are intruded by coeval epizonal granites, and granodiorites (Kalkadoon Granite) whose pooled U-Pb age is 1862 $\pm^{27}_{21}$ m.y. A younger rhyolitic suite (Argylla Formation) within the basement succession has an age of 1777 ± 7 m.y., and a third acid volcanic unit (Carters Bore Rhyolite), much higher in the sequence, crystallized 1678 ± 1 m.y. ago.

All of these rocks are altered in various degrees by low-grade events, and in at least one area these events were accompanied by, and can be partly related to, emplacement of a syntectonic, foliated granitic batholith (Wonga Granite) between 1670 and 1625 m.y. ago. Rocks which significantly predate this earliest recognized metamorphism, have had their primary

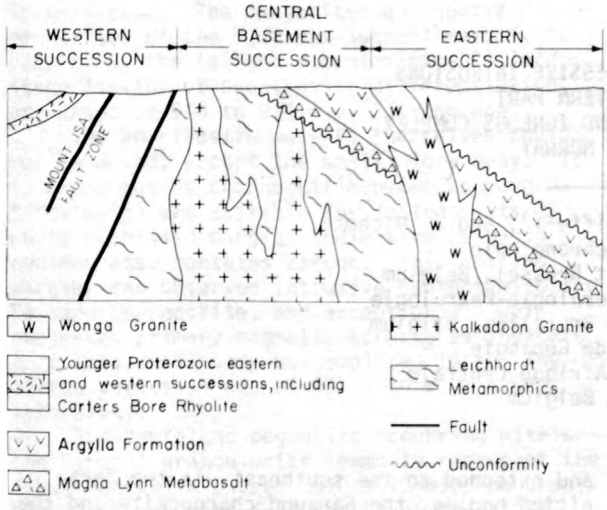

Figure 1.--Stratigraphic relationships among several suites of Proterozoic acid volcanic rocks and granitic intrusions near Mount Isa, northwest Queensland.

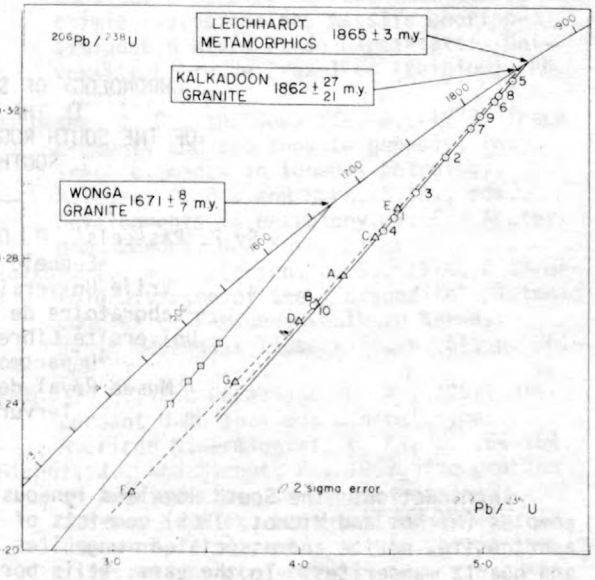

Figure 2.--Concordia diagram for plutonic and metamorphic rocks.

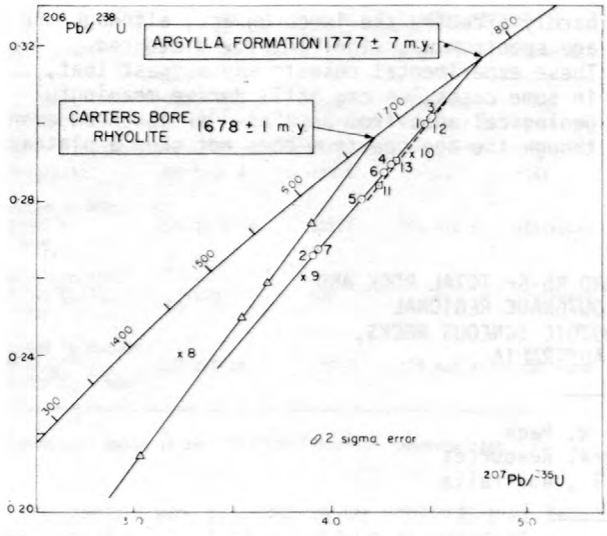

Figure 3.--Concordia diagram for volcanic rocks.

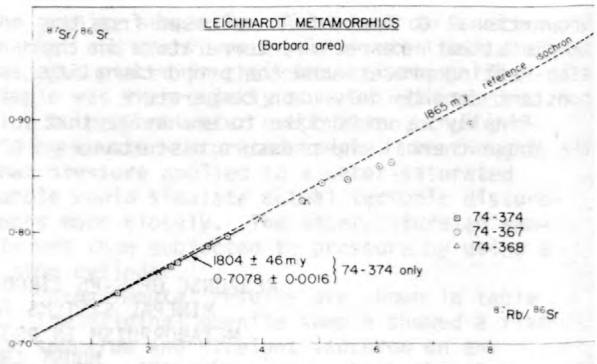

Figure 4.--Rb-Sr isochron diagram for the Leichhardt Metamorphics (Barbara area).

Rb-Sr total-rock systematics profoundly disturbed, as evidenced by a 10 to 15 percent lowering of most Rb-Sr isochron ages, and a general grouping of many of the lowered ages (some of which are in conflict with unequivocal geological relationships) within the 1600 to 1700 m.y. interval. Such isochrons possess anomalously high indicated initial $^{87}Sr/^{86}Sr$ ratios (fig. 4), and some show a slighly curved array of isotopic data points. This isotopic redistribution is considered to be part of a more pervasive element mobility, especially prevalent in the volcanic pile, during the period of alteration. Disturbance of the Rb-Sr total-rock ages is attributed primarily to the loss of Sr, which is relatively enriched in ^{87}Sr in Sr-poor (high Rb/Sr) rocks compared to Sr-rich rocks. Isotopic perturbations between total rocks in the predominantly submarine volcanic succession were probably initiated during diagenesis by the leaching action of circulating aqueous solutions that enhanced elemental migration during incipient breakdown of the minerals. This process was on-going, but in some areas was overridden when the prevailing P-T conditions became such that a definite greenschist facies imprint (in the interval of from 1670 to 1625 m.y.) was imposed. A second period of tectonism and low-grade metamorphism post-dates deposition of the Mount Isa Group, and is constrained by geologic and isotopic evidence to within the age limits of from 1620 to 1490 m.y.

CHRONOLOGY OF SUCCESSIVE INTRUSIONS IN THE EASTERN PART OF THE SOUTH ROGALAND IGNEOUS COMPLEX, SOUTHERN NORWAY

By P. Pasteels[1], D. Demaiffe[2,3], and J. Michot[2]
[1]Eenheid Geochronologie
Vrije Universiteit Brussel, Belgium
[2]Laboratoire de Mineralogie-Petrologie
Université Libre de Bruxelles, Belgium
[3]Département de Géologie
Musée Royal de l'Afrique Centrale
Tervuren, Belgium

Introduction: The South Rogaland igneous complex (Michot and Michot, 1969) consists of anorthosite, norite and associated mangerites, and quartz mangerites. To the east, it is bordered by two outliers of anorthosite and leuconorite (the Hidra and the Garsaknatt bodies) and extended to the southeast via two "granitic" bodies, the Farsund charnockite and the Lyngdal granodiorite, formerly mapped as a single unit called the "Farsundite" (Falkum and Petersen, 1974). Recent REE and other geochemical investigations (Duchesne and Demaiffe,

1978) have cast some light on the possible origin of the rocks associated with anorthosite--derivation from the same parent magma or by anatectic processes. Simultaneously, a geochronologic reinvestigation of the case has been carried out with considerably improved analytical methods compared to the early work of Pasteels, Michot, and Lavreau (1970). All geochronologic data here mentioned are calculated with the decay constants recommended by the IGCP-IUGS Subcommission for Geochronology (Steiger and Jaeger, 1977). With few exceptions, the new data are compatible with the observed field relations concerning the timing of intrusion, and with other geochemical data concerning the probable origin of the different rock types. Additional information on this latter subject is provided by the strontium initial ratios and the presence or absence of inherited zircon. The above mentioned exceptions are two whole-rock Rb-Sr isochrons yielding, seemingly, too low ages, for reasons which remain to be determined.

Timing of intrusion as deduced from the U-Pb data: Since the Rb-Sr isochron method gives obviously spurious ages in two cases, a geochronology of the successive phases of emplacement has been established solely on the basis of U-Pb data on uraniferous accessories (mainly zircon).

The highest age recorded, 955 ± 10 m.y., would correspond to the emplacement of the layered norites of the Bjerkrem-Sogndal lopolith (concordant ages of a monazite from the gneiss at the contact). The Lyngdal granodiorite yields an age of 950 ± 5 m.y. (zircon upper intercept confirmed by data on sphene). The geologically younger anatectic Farsund charnockite gives results of 920 to 940 m.y. The presence of an inherited component makes a precise age assignment impossible for the zircon in this case. The mangerites and quartz mangerites of the Bjerkrem-Sogndal massif, representing the (slightly contaminated?) late stage liquids of anorthosite differentiation, are dated at 910 to 930 m.y. (zircon age).

The anorthosite massifs themselves could not be dated, except the small Hidra body. It is cross-cut by charnockitic dykes and pegmatites which are suitable for dating. Its noritic chilled margin, indicative of rapid cooling also contains zircon. This chilled margin, the observed intrusive contact with the Farsund charnockite, and exceptionally well preserved primary magmatic structures indicate that this small body was emplaced late. The zircon yields an age of 931 ± 10 m.y. (upper intercept).

The Rymteland pegmatite occurring within the Lyngdal granodiorite seems to represent the final intrusive phase: 910 ± 10 m.y. on uraninite (compare with Kulp and Eckelmann, 1957).

Rb-Sr isotope geochemistry: A "reasonable" agreement is observed between the above mentioned U-Pb ages and Rb-Sr isochron ages in two cases: the Lyngdal granodiorite (Pedersen and Falkum, 1975) and the charnockitic dykes and pegmatites at Hidra (this study). Respectively, 912 ± 36 m.y. and 892 ± 25 m.y. have been obtained, which, compared to the U-Pb data, is on the low side. The initial strontium ratio for the first rock is 0.7054 ± 0.0005, and for the second 0.7085 ± 0.0007. These figures are to be compared with the 0.7035 to 0.7065 ratios measured on the anorthosites from the same region (Demaiffe, 1977). The Lyngdal granodiorite seems genetically related to the anorthosites because of its low initial ratio and negative Eu anomaly. Concerning the charnockitic dykes at Hidra, which are clearly comagmatic with the adjacent anorthosites, on the base of geochemistry one may assume that strontium isotope migration has occurred after cooling or else that the residual magma has been contaminated in order to explain the rather high initial ratio.

Pedersen and Falkum (1975) mention a 839 ± 21 m.y. Rb-Sr total-rock isochron age for the Farsund charnockite, with an initial strontium ratio, Ri, of 0.7128 ± 0.0009. We have obtained 857 ± 21 m.y., Ri = 0.7107 ± 0.0004 for the Bjerkrem-Sogndal mangerites, which is practically the same as 842 ± 29 m.y., Ri = 0.7121 ± 0.0012 reported by Versteeve (1975). Those two isochrons have been obtained independently in different laboratories, thirty-seven samples being analyzed in total. Little doubt is left in this case on the reality of strontium isotope migration after the rock emplacement and cooling, in the absence of observable metamorphism.

This work is part of the programme of the Belgian Centre for Geochronology.

Demaiffe, D., 1977, De l'origine des anorthosites--Pétrologie, Géochimie et Géochimie isotopique des massifs anorthositiques d'Hidra et de Garsaknatt: Université Libre de Bruxelles [Belgium], Ph.D. Thesis, 363 p.

Duchesne, J. C., and Demaiffe, D., 1978, Trace elements and anorthosite genesis, in, Trace elements in igneous petrology, Allegre, C. J., and Hart, S. R., eds., Developments in petrology, v. 5: Amsterdam, London, New York, Elsevier.

Falkum, T., and Petersen, J. S., 1974, A threefold division of the "Farsundite" plutonic complex at Farsund, southern Norway: Norsk Geologisk Tidssrkift, v. 54, p. 361-366.

Kulp, J. L., and Eckelmann, W. R., 1957, Discordant U-Pb ages and mineral type: American Mineralogist, v. 42, p. 154-164.

Michot, J., and Michot, P., 1969, The problem of anorthosites; The South-Rogaland igneous complex, southwestern Norway, in, Isachsen, Y. W., ed., Origin of anorthosites and related rocks: New York State Museum and Science Service Memoir 18, p. 399-410.

Pasteels, P., Michot, J., and Lavreau, J., 1970, Le complexe éruptif du Rogaland méridional (Norvège); Signification pétrogénétique de la farsundite et de la mangérite quartzique des unités orientales--arguments géochronologiques et isotopiques: Annales Societé Géologique Belgique, v. 93, p. 453-476.

Pedersen, S., and Falkum, T., 1975, Rb-Sr isochrons for the granitic plutons around Farsund, southern Norway: Chemical Geology, v. 15, p. 97-101.

Steiger, R. H., and Jaeger, E., 1977, Subcommission on Geochronology; convention on the use of decay constants in geo- and cosmochronology: Earth and Planetary Science Letters, v. 36, p. 359-362.

Versteeve, A., 1975, Isotope geochronology in the high grade metamorphic precambrian of southwestern Norway: Norges Geologiske Undersökelse, v. 318, p. 1-50.

ANTHROPOGENIC PERTURBATIONS OF THE NATURAL BIOGEOCHEMISTRY OF LEAD

By C. C. Patterson
Division of Geological and Planetary Sciences
California Institute of Technology
Pasadena, California 91125

The body burdens of lead in people in the United States and the United Kingdom have been elevated by industrial lead pollution more than 100-fold above natural levels that existed in their prehistoric ancestors. Three different kinds of studies show that this is so. First, analyses of lead in bones of people known to have lived before metallurgy was practiced, show lead concentrations of < 0.1 ppm dry weight compared to 20 ppm dry weight in the bones of the average American today. Second, the food eaten by Americans is polluted many orders of magnitude above natural prehistoric levels of lead. For example, the concentration of lead in canned tuna is 20,000-fold above prehistoric natural levels. Third, lead was biodepleted 1000-fold relative to calcium in going from rock to carnivore in prehistoric food chains, but lead is biodepleted only two-fold relative to calcium in going from rock to the average American today.

On a worldwide basis the annual industrial production of lead greatly exceeds the prehistoric natural reservoirs of lead in the biosphere, atmosphere, and hydrosphere. The Pb/Si ratio in the earth's troposphere is 100-fold above crustal values except in urban regions where it ranges up to 10,000-fold above crustal values. Surface waters in shelf and nearshore regions of the oceans of the northern hemisphere have been polluted two-fold to ten-fold above prehistoric natural concentrations with industrial lead, while surface waters in the central North Pacific have been polluted ten-fold with such lead, which originates mainly from lead alkyls and is transported to the oceans via the atmosphere.

The concentration of lead in the Earth's total marine biomass has been elevated about ten-fold, mainly by sorption of dissolved sea water lead on algal surfaces. The concentration of lead in the Earth's total living terrestrial biomass has also been elevated about ten-fold by the deposition of industrial lead-rich aerosols on plant foliage and bark, and by the accumulation of industrial lead in soil humus. The total amount of soil lead participating each year in the Earth's biomass production is considerably less than 1 percent of the total annual production of industrial lead.

Erroneous lead analyses have for decades obscured the true magnitudes of industrial lead pollution of people, foods, and the Earth's atmosphere, hydrosphere, and biosphere. Reported erroneous lead concentrations 100-fold to 1000-fold higher than true values prevail in the literature and support the erroneous view that lead concentrations in the average American are "normal" and similar to prehistoric values, and that man has not substantially altered the natural biogeochemistry of lead on a worldwide scale. Cities and towns in the US and UK are vast cesspools of industrial lead where the average person is subjected to severe chronic lead insult; the effects probably lead to significant reductions in mental acuity, increases in mental irrationality, reduction in resistance to malignancies and infectious diseases, and damages to germ plasm.

TRITIUM IN THE WATERS OF YELLOWSTONE NATIONAL PARK

By F. J. Pearson, Jr.[1], and A. H. Truesdell[2]
[1]U.S. Geological Survey, Reston, Virginia
[2]U.S. Geological Survey, Menlo Park, California

Relatively little is known of the local and regional ground-water system of which the hot springs and geysers of Yellowstone National Park are the surface expression. Conventional ground-water investigations require more bore holes for water level measurements and pump tests than would be appropriate within the Park. Even measurements of hot water discharges are sparse because to make them properly would require disturbing the delicate deposits around many of the springs and geysers. In the absence of conventional hydrologic data, the tritium content of both hot and cold waters in the Park can be used to infer something of the ground-water system feeding some hot springs and geysers.

Tritium (^3H) is radioactive and decays with a 12.3 year half-life to helium-3. Concentrations are reported in tritium units (TU) which equal a $^3H/H$ ratio of 10^{-18}, about 3 picocuries per liter. Although tritium is formed by cosmic ray interactions with the upper atmosphere, most tritium now in the hydrosphere is from atmospheric testing of thermonuclear devices between 1953 and 1963. Tritium levels in precipitation in the Park before testing were probably about 10 TU. In 1963, following the last large atmospheric tests, the concentration reached 7000 TU in the Park region. It has since been declining, but the average 1977 tritium was still about 50 TU.

The tritium content of the output of a ground-water system depends on that of the input, and on the residence time and type of flow of water in the system. If the ground water moves by piston flow, the tritium content (T) at any point within it will be related to the tritium level of the input (T°) and the transit time or age (t) of the sampled water by: $T = T°e^{-\lambda t}$, where the decay constant $\lambda = \ln 2/\text{half-life}$.

A piston-flow model does not account for hydrodynamic-dispersive mixing within the ground-water system, nor for the likely possibility that there are many points of input to the system. At the opposite extreme to the piston-flow model is the well-mixed reservoir model. For such a reservoir, with constant volume V and input (= output) of Q (per year):

$$\frac{dT}{dt} = T° \frac{Q}{V} - T \frac{Q}{V} - \lambda T$$

where T, T°, λ, and t are as above. The tritium content of such a reservoir at t will be the integral of this expression from time = 0 to t. The ratio of volume to input or output (V/Q) is the turn-over time of the system. Bolin and Rodhe (1973) have shown that this turn-over time is identical to the average transit time or average age of particles leaving the reservoir, which they prefer to term "residence time".

Figure 1 compares the tritium content of waters of varying residence times in piston-flow and mixed-reservoir systems. The input used was the monthly concentration of tritium in precipitation in Yellowstone Park as measured there and as estimated from correlations between the Park records and longer precipitation records at Salt Lake City, UT, Bismarck, ND, and Ottawa, Canada. The curve for piston flow reflects the variation in atmospheric tritium resulting from the various thermonuclear-test series beginning in 1953. The other curve shows how the tritium content of a reservoir of long residence time is increased by a small amount of relatively recent high-tritium input.

Measurements from a small stream, a major river with a large natural reservoir (Yellow-

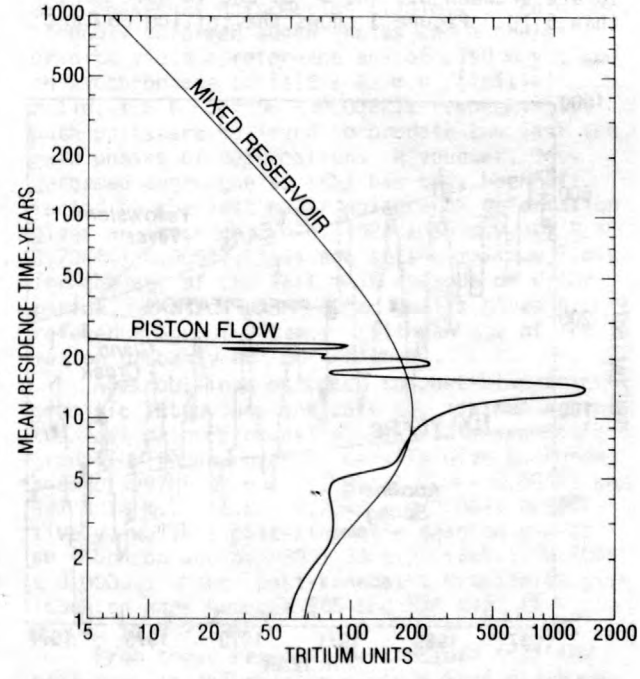

Figure 1.--Tritium content of water leaving piston flow and well mixed ground-water systems in Yellowtone Park.

stone Lake), and a cold spring are shown in figure 2, with monthly precipitation values and the concentrations to be expected in well-mixed reservoirs of 10 and 100 year residence times. Tritium in Glenn Creek varies with time, but is close to that of precipitation. The residence time of the combined surface runoff and groundwater reservoir drained by Glenn Creek must thus be short (on the order of a few months).

The Yellowstone River has considerably higher tritium than contemporaneous precipitation. Its late 1976 tritium content of about 200 TU is that of a reservoir of 10 years residence time (fig. 1), and its tritium variation with time is also about that of such a reservoir. The physical reservoir in this case is Yellowstone Lake.

Tritium in Apollinaris Spring was about 55 TU in late 1976, about that of precipitation or of either piston flow or mixed ground water of one year or less residence time (fig. 1). 55 TU also is that of a 100 year residence time mixed reservoir, but from the 1975 to 1977 data alone, one can choose neither the type of flow nor the residence time in the system feeding Apollinaris. The 1971 sample (fig. 2) has less tritium than expected from a short residence time piston-flow or mixed-reservoir system, but, with the later samples, describes a line close to that expected from a 100 year mixed-reservoir system.

Of the 37 hot springs and geysers analyzed, 8 have less than 0.5 TU (the detection limit), 16 are between 0.5 and 5 TU, and 13 have more than 5 TU. Figure 3 shows the tritium content

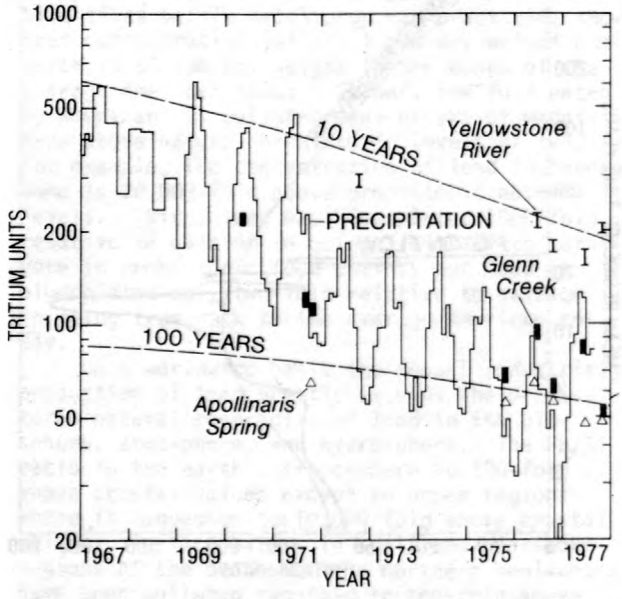

Figure 2.--Tritium in precipitation, mixed reservoirs, and cold waters of Yellowstone Park.

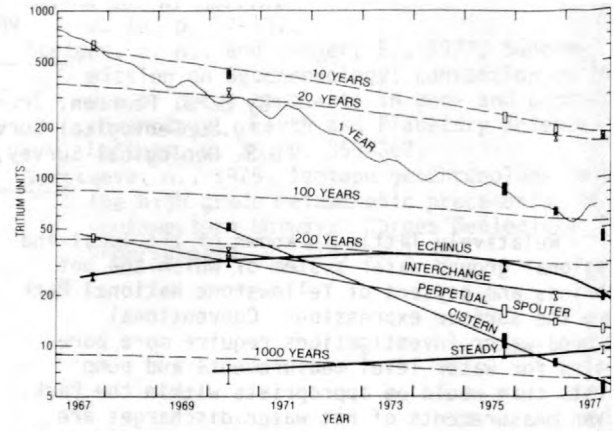

Figure 3.--Tritium in mixed reservoirs and hot waters of Yellowstone Park.

of 5 of the higher tritium sites that have been measured several times.

Because of their late 1976 tritium contents of between 6 and 30 TU, these hot waters could all come from mixed reservoirs with residence times of between 200 and 1000 years (fig. 1). However, it is evident from figure 3 that the decrease in tritium with time in all of the hot waters is more rapid than it would be from reservoirs of such long residence times. The thermal systems appear, rather, to be mixtures of two waters - one from an open, well-mixed reservoir of relatively short residence time (presumably cold and at shallow depth), the other containing little or no tritium (presumably hot and deeper).

For example, the change in tritium content with time in Perpetual Spouter is at the rate expected from a 10 year reservoir, yet its tritium in late 1976 was only about 14 TU, rather than the 200 TU expected at that time from such a reservoir (fig. 1). Perpetual Spouter, then, would be a mixture of 7 percent water from a mixed 10 year residence time reservoir with 93 percent zero tritium water. Similarly, Cistern contains 12 percent one year mixed water and 88 percent tritium free water while Interchange is 11 percent 20 year mixed and 89 percent zero tritium water.

These proportions were used to calculate the tritium contents of the mixed-reservoir components of these thermal features at the times they were sampled. The calculated values are the upper set of symbols on figure 3. Interchange and Perpetual Spouter agree well with the calculated tritium contents of reservoirs for the residence times assumed, suggesting that neither the mixing ratios nor the hydrologic systems feeding them have changed significantly during the period over which samples are available. The constant chemistry of these features over the same period supports this hypothesis.

The agreement between the points for Cis-

tern and the line for a one year reservoir is poorer. This could be due to unmodeled variations in the tritium-bearing reservoir, which would not be unexpected in one with such a short residence time. It could also result from varying ratios of mixing between the tritium-bearing and tritium-free reservoirs. The chemistry of Cistern has varied with time, but the relationships between the chemical and tritium variations and their implications on changes in the mixing ratios have not yet been fully explored.

The tritium contents of Echinus and Steady Geysers (fig. 3) change with time in a way which cannot be explained with the simple model just discussed. By adding additional mixing, or time delays between mixing and the arrival of the mixture at the surface, curves of almost any shape could be generated.

Bolin, Bert, and Rodhe, Henning, 1973, A note on the concepts of age distribution and transit time in natural reservoirs: Tellus, v. 25, p. 58-62.

Rb/Sr-DATING OF THE PLUTONIC AND TECTONIC EVOLUTION OF THE SVECONORWEGIAN PROVINCE, SOUTHERN NORWAY

By S. Pedersen[1], A. Berthelsen[1], T. Falkum[2], O. Graversen[1], B. Hageskov[1], S. Maaløe[3], J. S. Petersen[2], L. Skjernaa[1], and J. R. Wilson[2]
[1]Institut for almen Geologi
Øster Voldgade 10, DK-1350 Copenhagen K, Denmark
[2]Laboratorium for endogen Geologi
Århus Universitet, Universitetsparken, DK-8000 Århus C, Denmark
[3]Geologisk Institut, avdeling A
Bergen Universitet, N-5014 Bergen, Norway

The Precambrian of southern Norway has recently attracted considerable interest in connection with attempts to reconstruct the trans-Atlantic continuation of the Grenville belt and to define the Proterozoic plate borders (for example, Davies and Windley, 1976; Torske, 1977). This paper presents some factual data obtained in connection with the Norwegian Geological Survey's systematic mapping in the Agder-Rogaland and the Østfold regions (fig. 1), together with recent Rb-Sr age determinations of various granitoids from these regions.

The geologic maps of both the Agder-Rogaland and the Østfold regions are dominated by complex large-scale interference patterns that evolved as a result of several major episodes of deformation. Both regions were metamorphosed under conditions corresponding to granulite and (or) amphibolite facies. Published K-Ar dates for Agder-Rogaland and Østfold cluster between 1100 and 800 m.y. (Broch, 1964), and Rb-Sr and U-Pb ages from neighboring regions of southwestern Norway range from 1500 to 850 m.y. (Pasteels and Michot, 1975; Versteeve, 1975).

The general lithology and chronology of the two key regions mapped, together with the results from the Rb-Sr age studies are shown in tables 1 and 2.

In the Agder-Rogaland region, a number of granitic rock units have been dated that have demonstrable age relations to the two latest main phases of deformation (table 1). An older, strongly deformed augen gneiss and a gneissic granite yield a reference age of 1350 m.y., and an isochron age of 1112 ± 42 m.y. (initial ratio, I.R.: 0.7066 ± 0.0022), respectively; both units are believed to predate the last two main phases of deformation. A younger, less deformed augen gneiss that has only been affected by the last major episode of deformation gives an isochron age of 1024 ± 53 m.y. (I.R.: 0.7044 ± 0.0004); this age sets a maximum limit for the age of the last main episode of deformation. Another young augen gneiss gives a reference age of 980 m.y. (with an age of formation probably not much higher).

Ages obtained on late- to post-kinematic granitic intrusions indicate the minimum age of the last main deformation. Two late-kinematic granodiorite and granite massifs give isochron ages of 997 ± 57 m.y. (I.R.: 0.7044 ± 0.0002) and 997 ± 14 m.y. (I.R.: 0.7043 ± 0.0006), respectively, while a post-kinematic granite yields an isochron age of 980 ± 33 m.y. (I.R.: 0.7045 ± 0.0003). Other post-kinematic granitoids give isochron ages between 945 and 834 m.y. (I.R.: 0.7040 to 0.7128).

From these results, we conclude that the next-to-last deformation episode in Agder-Rogaland may have occurred around 1100 m.y. ago, and the last main phase of deformation culminated 1000 - 990 m.y. ago. Initial Sr-isotope

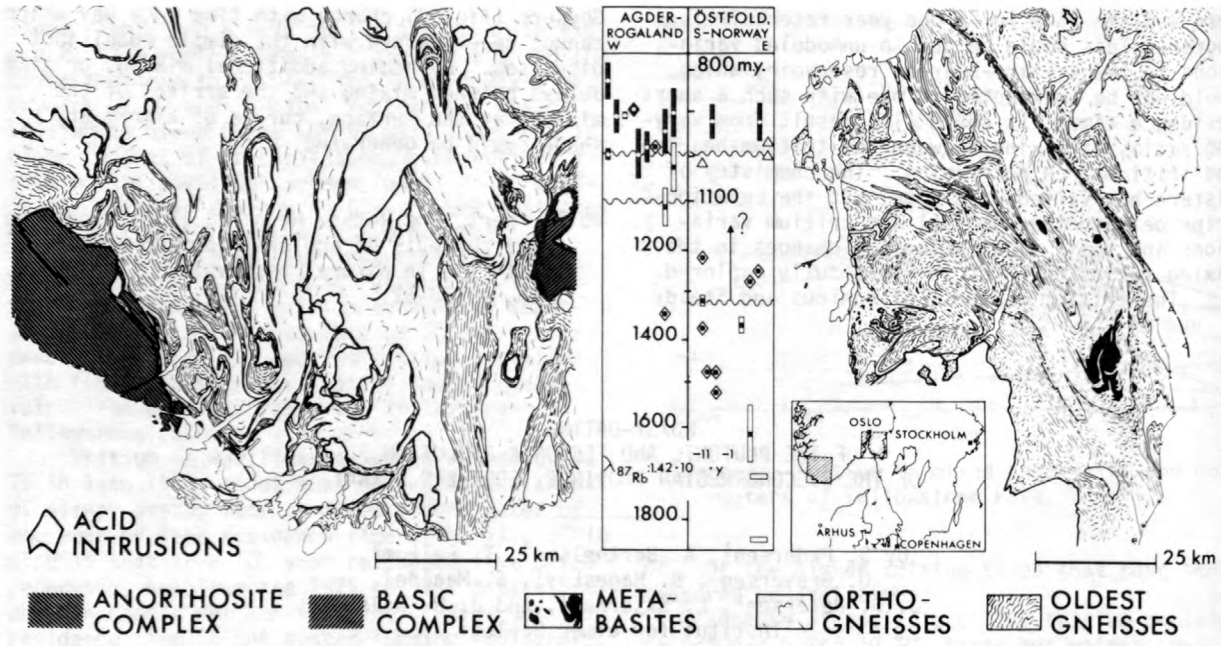

Figure 1.--Provisional sketch maps of the Agder-Rogaland region (compiled by T. Falkum) and the Östfold region (compiled by A. Berthelsen). In the central chronological column vertical bars indicate isochron ages, rhombs reference ages, horizontal bars model ages. Solid symbols, late- to post-kinematic intrusives; triangles indicate metamorphic ages.

ratios suggest that none of the granitoids arose by simple anatexis of significantly older crustal rocks.

Data for similar rocks from Östfold showed that the last main episode of deformation there was more or less contemporaneous with that in Agder-Rogaland; in both regions this deformation gave rise to roughly north-south oriented structures.

Orthogneisses from Östfold that yield an isochron age of 1320 ± 12 m.y. (age of intrusion) gave a reference age of 1015 m.y. when sampling was confined to a single locality where new leucosome formed during the last deformation. In northeastern Östfold, a series of samples from a single locality in a ca. 1710 m.y. augen gneiss (see below) give reference ages of 1000 and 970 m.y., which reflect the last homogenization of the isotope systems on a cm-scale. Two granitic massifs intruded after the last main deformation yield isochron ages of 923 ± 38 m.y. (I.R.: 0.7053 ± 0.0030) and 924 ± 42 m.y. (I.R.: 0.7105 ± 0.0020).

The plutonic activity that preceded the last main deformation in Östfold apparently both started and ended earlier than the early plutonism in Agder-Rogaland (fig. 1; tables 1 and 2).

The oldest reliable age from Östfold is an isochron age of 1616 ± 63 m.y. (I.R.: 0.7028 ± 0.0004) from a gneissified quartz-diorite, which was sampled regionally in an area where it is incorporated in large fold structures formed during the next-to-last major deformational episode in Östfold. Farther south, where this meta-quartz-diorite was also affected by the younger north-south folding, it has yielded a similar age of 1616 ± 63 m.y., which is considered an intrusive age.

From the extreme northeastern Östfold, augen gneisses that, from field evidence, are reckoned to be older than the 1616 m.y.-old quartz-diorite give model ages of 1850 and 1710 m.y. (assumed I.R.: 0.703). It is not known whether these rocks were deformed prior to the intrusion of the 1616 m.y.-old quartz-diorite. At other localities in Östfold, different types of quartz-dioritic gneisses have yielded reference ages of 1525, 1485, and 1480 m.y. and an isochron age of 1375 ± 18 m.y. (I.R.: 0.7042 ± 0.0002), all probably representing intrusion ages.

The youngest meta-plutonic rocks in Östfold are granitic orthogneisses that yield an isochron age of 1320 ± 12 m.y. (I.R.: 0.7174 ± 0.0010), and reference ages of 1380, 1285, 1255, and 1225 m.y.

These data imply repeated intrusive activity in Östfold from at least 1616 m.y. to 1320 m.y. (or ?1225 m.y.). The next-to-last folding in the Östfold region affected most, if not all, of these intrusives, and it was succeeded by widespread intrusion of basic rocks before the onset of the 1000 - 900 m.y. deformation. We consider it premature and probably incorrect to correlate the next-to-last folding in Östfold

Table 1.--General lithology and chronology of the Agder-Rogaland region (ages in m.y.) compiled by T. Falkum, S. Pedersen, J. S. Petersen, and J. R. Wilson

WNW-ESE-trending dolerite dikes.
Common pegmatites and large massifs of granite, granodiorite, anorthosite, mangerite, and charnockite (980-834 m.y.).
Last major deformational episode (1000-990 m.y.) causing large-scale folds with N-S axes and axial planes.
Megacryst granites (1024 m.y.), anorthositic and basic complexes.
Deformational episode (ca. 1100 m.y.) causing large-scale tight- to isoclinal structures.
Granitic intrusions. Rare basic dikes. Granodiorites and granites, often with megacrysts.
Formation of early foliation and isoclinal folds.
Older rocks: Banded gneisses with intermediate and felsic gneisses, amphibolites and pyribolites. Local intercalations of garnet-cordierite-sillimanite gneisses. Rare marble and calc-silicate layers. The oldest rocks make up around 20 percent of the region.

Table 2.--General lithology and chronology of the Östfold region (ages in m.y.), compiled by A. Berthelsen, O. Graversen, B. Hageskov, S. Maaløe, S. Pedersen, and L. Skjernaa

WNW-ESE-trending dolerite dikes.
Swarms of pegmatite and local massifs of granodiorite and granite (924, 923 m.y.).
Last major deformational episode (1000-990 m.y.) causing open- to closed-folds with N-S- to NW-SE-trending axes, and thrusting of folded deep-level rocks towards east.
Intrusion of basic dikes, sheets, and minor massifs.
Next-to-last deformational episode causing open to overturned and thrust folds with more or less E-W-trending axes; general vergence southerly.
Intrusion of basic dikes, sheets, and gabbro massifs.
Several generations (1616-1320 m.y. (?1225 m.y.)) of quartz-diorites, granodiorites, and granites (occasionally with megacrysts).
An old deformational episode ? Augen gneisses (1850, 1710 m.y.).
Oldest rocks: Oldest metaplutonics and still older semipelitic gneisses with accessory graphite, pelitic intercalations, and calc-silicate "inclusions". The oldest rocks make up around 60 percent of the region.

with the next-to-last deformation that affected Agder-Rogaland around 1100 m.y. ago, cf. fig. 1. As in Agder Rogaland, the initial Sr isotope ratios from Östfold are, in general, low, suggesting that anatexis of sialic crust was not the main source of the magmas.

Broch, O. A., 1964, Age determinations of Norwegian minerals up to March 1964: Norges Geologiske Undersokelse, v. 228, p. 84-113.

Davies, F. B., and Windley, B. F., 1976, Significance of major Proterozoic high grade linear belts in continental evolution: Nature, v. 263, p. 383-385.

Pasteels, P., and Michot, J., 1975, Geochronologic investigations of the metamorphic terrain of southwestern Norway: Norsk Geologisk Tidsskrift, v. 55, p. 111-134.

Torske, T., 1977, The South Norway Precambrian Region--a Proterozoic cordilleran-type orogenic segment: Norsk Geologisk Tidsskrift, v. 57, p. 97-120.

Versteeve, A., 1975, Isotope geochronology in the high-grade metamorphic Precambrian of southwestern Norway: Norges Geologisk Undersokelse, v. 318, p. 1-50.

GNEISS OF EARLY ARCHEAN AGE IN NORTHERN MICHIGAN, U.S.A.

By Zell E. Peterman, Robert E. Zartman, and P. K. Sims
U.S. Geological Survey, Denver, Colorado 80225

Precambrian rocks of the Lake Superior region (Minnesota, Michigan, and Wisconsin) represent the southernmost exposure of the Canadian Shield and contain more than three billion years of earth history. The Archean rocks themselves record at least a billion years of history, but the record is fragmentary and difficult to decipher because of younger tectonothermal events. Gneisses of early Archean age in the Minnesota River Valley that are 3500 to 3800 m.y. old have been studied by S. S. Goldich and colleagues (Goldich and other, 1970; Goldich and Hedge, 1974). These gneisses are distinctly older and differ in lithologic character from the upper Archean greenstone-granite complexes of the northern part of the region, which developed over a narrow span time between 2600 and 2700 m. y. ago (Goldich, 1972). A second occurrence of gneiss of early Archean age has recently been discovered near Watersmeet in northern Michigan.

The Marenisco-Watersmeet area in the western part of northern Michigan, mapped earlier by Fritts (1969), contains both Archean greenstone and gneiss terranes (Morey and Sims, 1976). In the north, greenstone and granite (Puritan Quartz Monzonite) is overlain by sedimentary and volcanic rocks of the Marquette Range Supergroup (approximately equivalent to the Animikie Group of Minnesota). In the southern part of the area, these supracrustal rocks surround elliptical bodies of older tonalitic gneiss (gneiss at Watersmeet) and are intensely folded and metamorphosed. A narrow belt of gneiss and granite called "granite near Thayer" intervenes between the tonalitic gneiss and the greenstone-granite terrane. The Puritan Quartz Monzonite previously was dated by Rb-Sr at 2650 ± 140 m.y. (Sims and others, 1977), an age in agreement with those of greenstone-granite terranes of northern Minnesota and western Ontario.

The gneiss at Watersmeet and the granite near Thayer have been cataclastically deformed and recrystallized, and geochronologic data reflect the effects of severe tectonic and thermal events in the early Proterozoic. Both whole-rock and mineral Rb-Sr data define secondary isochrons of 1750 m.y. (figs. 1 and 2). An older age for the gneiss at Watersmeet is indicated by high initial $^{86}Sr/^{86}Sr$ ratios of the secondary isochrons (fig. 1). Redistribution of radiogenic ^{87}Sr occurred on a local scale in the sheared and recrystallized facies but not on a regional scale as shown by parallel secondary isochrons having different initial-Sr ratios. Less sheared phases of the gneiss (locality 3, fig. 1) do not show equilibration at 1750 m.y. on a very small scale, nor do the systems retain the systematics of an older age.

U-Th-Pb studies of zircon have successfully penetrated the effects of the 1750 m.y. event and have shown that the gneiss at Watersmeet is at least 3400 m.y. old, and possibly much older (fig. 3). However, systematics in the zircon data indicate multiple younger events, and a single episode of lead loss cannot explain the discordance patterns. A highly cataclasized phase of the gneiss at Watersmeet yielded abundant zircon with concordant ages of 1755 m.y. (point 4, fig. 3). We interpret this zircon to be of metamorphic origin and to have formed during the episode of cataclasis and recrystallization; Rb-Sr whole-rock and mineral data from this locality also give a 1750 m.y. age (fig. 1).

Size and magnetic fractions of zircon from relatively unsheared phases of the gneiss give much older ages, with one sample having a $^{207}Pb/$

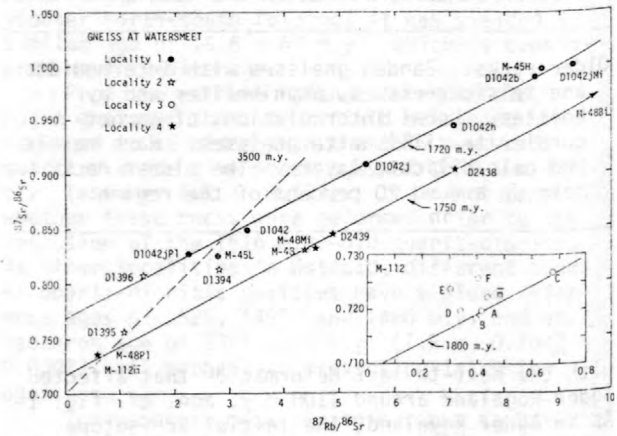

Figure 1.--Whole-rock and mineral Rb-Sr data for the gneiss at Watersmeet, including results published previously by Sims and Peterman (1976). Localities represent sampled areas or outcrops within the gneiss. Data points represent whole-rock samples unless indicated by Pl (plagioclase), Mi (microcline), or Bi (biotite). Inset shows the results from small slabs taken across a 25-cm-width of a banded gneiss of alternating layers of biotite-hornblende gneiss and leucocratic quartz-plagioclase layers.

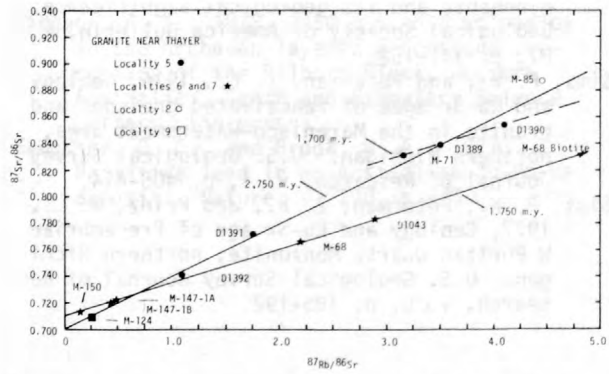

Figure 2.--Whole-rock and mineral Rb-Sr data for the granite near Thayer. Data points represent whole-rock samples except for Bi (biotite). Reference isochron of 2750 m.y. is based on the zircon ages.

^{206}Pb age of 3410 m.y. (1a, 1b, 1c, 2a, 2e, and 2f, fig. 3). In an attempt to better understand the discordance patterns, and with the hope of identifying a component with a greater $^{207}Pb/^{206}Pb$ ratio, a simple leaching experiment was done on sample 2a (fig. 3). Leaching in 6N HCl followed by 6N HNO_3 removed a high common lead component that was mainly surficial (2b, fig. 3--the two points represent modern lead and 3400 m.y. lead corrections). Approximately 64 percent of the zircon dissolved in HF at atmospheric pressure (2c, fig. 3). The residue (2d, fig. 3) showed slight reverse discordance, but elemental fractionation may well have been induced by the experiment. The leaching experiment did not identify older and younger components but, rather, produced surprisingly consistent $^{207}Pb/^{206}Pb$ ratios among the fractions. However, the nonlinearity of the data for the three size and magnetic fractions of zircon from this sample (2a, 2e, and 2f, fig. 3) shows the presence of $^{207}Pb/^{206}Pb$ variability, and we do not preclude the possibility that the zircons are substantially older than 3400 m.y.

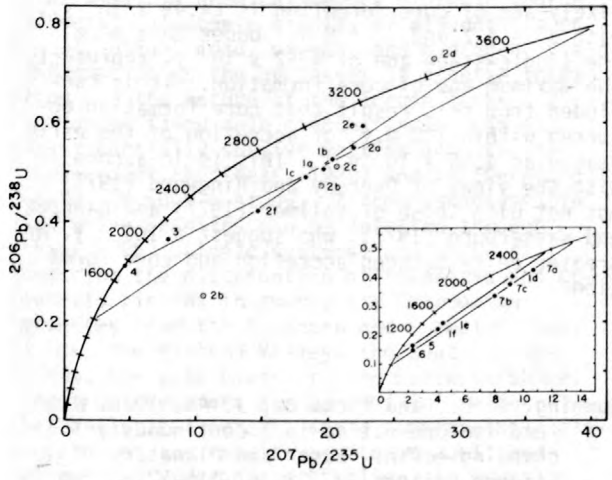

Figure 3.--U-Pb data for zircons from gneiss at Watersmeet (main diagram) and from granite near Thayer and leucogranite dikes (inset diagram). Numbers refer to individual samples and suffix letters represent size and (or) magnetic splits. Open circles are results of leaching experiment described in text.

The tonalitic phase of the gneiss at Watersmeet is intruded by leucogranite dikes that were also involved in the early Proterozoic tectonism. Three size fractions of zircon from a single sample (1d, 1e, and 1f, fig. 3) suggest provisionally that these dikes were emplaced about 2600 m.y. ago. The two highly discordant fractions contain much more uranium than zircons from the tonalitic gneiss, and the systematics include lead loss much more recently than 1750 m.y. ago.

Two high-uranium zircons from granitic phases of the granite near Thayer (5 and 6, fig. 3) are highly discordant. Zircon from a tonalitic phase provides data (7a, 7b, and 7c, fig. 3) that establish an age of 2750 m.y. for the unit and also indicate lead loss in the late Proterozoic. In view of these results, the complex discordancy patterns shown by zircon from the gneiss at Watersmeet are not surprising. These zircons were clearly affected by the 1750 m.y. event; probably, additional lead loss occurred at a later time, as indicated by the systematics for the leucogranite and granite near Thayer. Discordancy may have also resulted from the 2700 m.y. event, but the results have been obscured by the younger episodes of lead loss.

The minimum age of 3400 m.y. for the gneiss at Watersmeet extends the known occurrences of gneisses of early Archean age in the Lake Superior region. Very likely more occurrences will be found as methods capable of penetrating the effects of subsequent orogenic events are applied. Probably, both the granite near Thayer and the leucogranite dikes are related to plutonic activity associated with the development of the greenstone-granite terrane immediately to the north. The data suggest that the two Archean crustal blocks were in juxtaposition at 2600 to 2700 m.y. ago, and subsequently formed a continuous and coherent basement to the early Proterozoic sedimentary basins. During the early Proterozoic Penokean orogeny, the ancient gneisses were reactivated to form domical uplifts within the supracrustal sequences.

Fritts, C. E., 1969, Bedrock geologic map of the Marenisco-Watersmeet area, Gogebic and Ontonagon Counties, Michigan: U.S. Geological Survey Miscellaneous Geologic Investigations Map I-576.

Goldich, S. S., 1972, Geochronology in Minnesota, in Sims, P. K., and Morey, G. B., eds., Geology of Minnesota--A centennial volume: Minnesota Geological Survey, p. 27-37.
Goldich, S. S., and Hedge, C. E., 1974, 3800 Myr granitic gneiss in southwestern Minnesota: Nature, v. 252, p. 467-468.
Goldich, S. S., Hedge, C. E., and Stern, T. W., 1970, Age of the Morton and Montevideo Gneisses and related rocks, southwestern Minnesota: Geological Society of America Bulletin, v. 81, p. 3671-3696.
Morey, G. B., and Sims, P. K., 1976, Boundary between two lower Precambrian terranes in Minnesota and its geological significance: Geological Society of America Bulletin, v. 87, p. 141-152.
Sims, P. K., and Peterman, Z. E., 1976, Geology and Rb-Sr ages of reactivated gneisses and granite in the Marenisco-Watersmeet area, northern Michigan: U.S. Geological Survey Journal of Research, v. 4, p. 405-414.
Sims, P. K., Peterman, Z. E., and Prinz, W. C., 1977, Geology and Rb-Sr age of Precambrian W Puritan Quartz Monzonite, northern Michigan: U.S. Geological Survey Journal of Research, v. 5, p. 185-192.

BIG STUBBY AND THE EARLY HISTORY OF THE EARTH

By R. T. Pidgeon
Research School of Earth Sciences,
Australian National University
Canberra, Australia

A conformable lead deposit known as Big Stubby occurs in the Duffer Formation of the Warrawoona Group in the Archaean Layered Greenstone Succession of the Pilbara Block, Western Australia. Lead from Big Stubby is the least radiogenic ore lead reported to date (Sangster and Brook, 1977); only feldspar lead from the Amitsoq Gneiss from West Greenland is less radiogenic (Gancarz and Wasserburg, 1977).

The age of the Duffer Formation, and therefore the lead deposit, has been determined as 3453 ± 16 m.y. (Pidgeon, 1978) on the basis of a slightly discordant zircon population from a dacite from within the formation. This situation, of an excpetionally well dated, Archaean, conformable lead is unique and provides the most favourable opportunity yet recognized for estimating the 'age of the earth' using terrestrial material.

Isotopic analyses of Big Stubby lead have also been made at the Australian National University. These results differ slightly but significantly from those reported by Sangster and Brook (1977). Using the Australian National University measurements the model lead ages of Big Stubby are 3.37 x 10^9 y. according to the "two stage" model of Stacey and Kramers (1975) and 3.48 x 10^9 y. according to the continuous linearly increasing μ model of Cumming and Richards (1975). These model ages, in particular the Cumming and Richard's age, are in close agreement with the zircon age.

Using Canyon Diablo troilite lead as the primordial isotopic composition, the calculated single stage "age of the earth" based on Big Stubby lead is 4.52 x 10^9 y. This is slightly younger than the 4.55 x 10^9 y. age of chondrites and could indicate that the earth accreted a little later than the chondrites did. Big Stubby lead can also be interpreted in terms of two-stage evolutionary model based on the expected change in μ during formation of earth's core (Oversby and Ringwood, 1971). Applying the two-stage model for Oversby and Ringwood (1971) and Vollmer (1977) to Big Stubby lead, the most likely age of core formation is c4.49 x 10^9 y., with μ_1 = 4.2 and μ_2 = 8.4. Under this model the single-stage age of 4.52 x 10^9 y. represents the maximum age of core formation. It is concluded from this result that core formation occurred within 100 m.y. of accretion of the earth (taken as 4.55 x 10^9 y.). This is in accord with the views of Oversby and Ringwood (1971) but not with those of Vollmer (1977) and Gancarz and Wasserburg (1977), who suggest a 100 m.y. or greater delay between accretion and core formation.

Cumming, G. L., and Richards, J. A., 1975, Ore lead isotope ratios in a continuously changing earth: Earth and Planetary Science Letters, v. 28, p. 155-171.
Gancarz, A. J. and Wasserburg, G. J., 1977, Initial Pb of the Armitsoq gneiss, West Greenland and implications for the age of the Earth: Geochimica Cosmochimia Acta, v. 41, p. 1283-1301.
Oversby, V. M., and Ringwood, A. E., 1971, Time of formation of the Earth's core: Nature, v. 234, p. 463-465.

Pidgeon, R. T., 1978, 3450 m.y.-old volcanics in the Archaean layered greenstone succession of the Pilbara Block, Western Australia: Earth and Planetary Science Letters, (in press).

Sangster, D. F., and Brook, W. A., 1977, Primitive lead in an Australian Zu-Pb-Ba deposit: Nature, v. 270, p. 423.

Stacey, J. S. and Kramers, J. D., 1975, Approximation of terrestrial lead isotope evolution by a two-stage model: Earth and Planetary Science Letters, v. 26, p. 207-221.

Vollmer, R., 1977, Terrestrial lead isotopic evolution and formation of the Earth's core: Nature, v. 270, p. 144-147.

INHERITED ZIRCON U-Pb SYSTEMS AS INDICATORS OF GRANITE SOURCE ROCKS IN THE BRITISH CALEDONIDES

By R. T. Pidgeon[1] and M. Aftalion[2]
Research School of Earth Sciences,
Australian National University,
Canberra, Australia
Isotope Geology Unit, Scottish Universities
Research and Reactor Centre,
East Kilbride, Scotland

Most of the granites of the British Caledonides were emplaced in Late Silurian to Early Devonian time although granite episodes are known to span much of the history of the Caledonian orogeny. Despite their differentiated and possibly contaminated character, the granites retain a chemical memory of their source material. Isotopic studies of elements, such as strontium, lead, oxygen, and hydrogen, yield information on the processes of granite formation and the nature of the soruce rocks. Zircon under favourable circumstances, can at least partially survive melting and granite emplacement (Pasteels, 1964) and is therefore useful in such a study. Zircon xenocrysts in intrusive granites can be detected through their U-Pb isotopic systems, and we briefly describe the distribution of inherited and cogenetic zircons in twenty-six Caledonian granites from the Northern and Grampian Highlands, the Midland Valley, the Southern Uplands, the Lake District, and Leicestershire, and from Connemara and Donegal in Ireland. The analytical details and a comprehensive discussion of the results are to be published elsewhere (Pidgeon and Aftalion, in press).

Zircons from pretectonic granites from the Grampian and Northern Highlands, including the Carn Chuinneag (Pidgeon and Johnson, 1974) and Ben Vuirich granites (Pankhurst and Pidgeon, 1976), the Ardgour granite gneiss, and the granite at Vagastie Bridge, have complex U-Pb systems that indicate the presence of a significant component of ca. 1600 m.y. old zircon. Zircon U-Pb systems from most of the more recent granites (400 ± 10 m.y. old) from the Grampian and Northern Highlands and the Donegal granite also indicate the presence of inherited "Proterozoic" zircon (fig. 1).

None of the granites investigated from the Midland Valley, the Southern Uplands, the Lake District (except the Eskdale Granite), and Leicestershire and Galway (Pidgeon, 1969) show isotopic evidence of inherited zircons. This suggests either that these granites formed under different conditions from those to the north whereby all zircon xenocrysts were dissolved, or that older zircon xenocrysts were not present in the source rocks of these granites, which were derived from new Palaeozoic crust. We favour the second explanation and tentatively mark the Highland Boundary Fault as the fundamental structure separating a dominantly "Proterozoic" basement to the north from a mainly middle Palaeozoic basement to the south.

Age determinations based on the present zircon U-Pb results indicate a common age for the Ardgour granite gneiss and the Carn Chuinneag granite. They also support previous views that the main Grampian metamorphism in the Highlands was completed 475 m.y. ago and that the major influx of newer granites occurred 400 ± 10 m.y. ago, (Pankhurst, 1974). The c 405 m.y. ago for the foliated granite at Vagastie Bridge presents a problem because this is in apparent conflict with previous conclusions on the age of the regional D_2 deformation in part of the Moines (Soper, 1971).

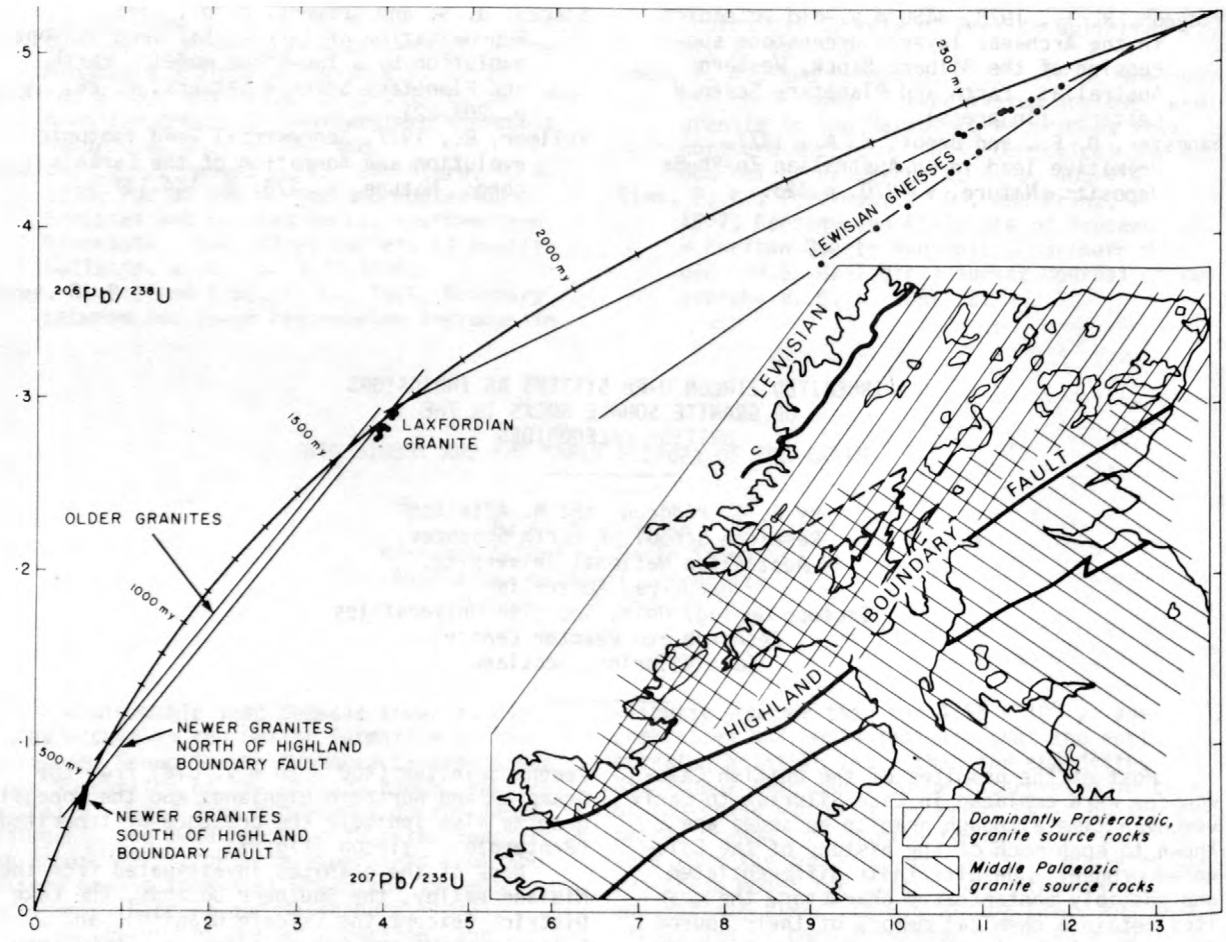

Figure 1.--Concordia plot showing the generalized distribution of zircon U-Pb systems from granites of the British Caledonides. Older granites (c 560 m.y.) and newer granites (400 ± 10 m.y.) from north of the Highland Boundary Fault define two "reverse discordia" which give a "Laxfordian age" intersection with concordia. Newer granites south of the Highland Boundary Fault have no inherited zircon component (except for the Eskdale Granite). The inset shows the indicated distribution of Proterozoic and Paleozoic crustal rocks beneath northern England and Scotland before dextral movement on the Great Glen Fault (Brown and Hughes, 1973).

Brown, G. C., and Hughes, D. J., 1973, Great Glen Fault and timing of granite intrusion on the Proto-Atlantic continental margins: Nature, Physical Science, v. 244, p. 129-132.

Pankhurst, R. J., 1974, Rb-Sr whole-rock chronology of Caledonian events in Northeast Scotland: Geological Society of America Bulletin, v. 85, p. 345-350.

Pankhurst, R. J., and Pidgeon, R. T., 1976, Inherited isotope systems and the source region pre-history of early Caledonian Granites in the Dalradian Series of Scotland: Earth and Planetary Science Letters, v. 31, p. 55-68.

Pasteels, P., 1964, Measures d'âges sur les zircons de quelques roches des Alpes: Bulletin Suisse de Minéralogie et Petrographie, v. 44, p. 519-541.

Pidgeon, R. T., 1969, Zircon U-Pb ages from the Galway granite and the Dalradian, Connemara, Ireland: Scottish Journal of Geology, v. 5, p. 375-392.

Pidgeon, R. T. and Johnson, M. R. W., 1974, A comparison of zircon U-Pb and whole-rock Rb-Sr systems in three phases of the Carn Chuinneag granite, northern Scotland: Earth and Planetary Science Letters, v. 24, p. 105-112.

Pidgeon, R. T. and Aftalion, M., (in press), Cogenetic and inherited zircon U-Pb systems in Palaeozoic granites from Scotland and England: Geological Journal Special Issue.

Soper, N. J., 1971, The earliest Caledonian structures in Moine thrust belt: Scottish Journal of Geology, v. 7, p. 241-253.

U/Pb EVIDENCES OF BIMODAL MAGMATISM OF EARLY PALEOZOIC AGE IN THE MASSIF CENTRAL (FRANCE); THE LEPTYNO-AMPHIBOLITIC GROUP

By C. Pin and J. R. Lancelot,
Laboratoire de Geochronologie et de
Géochimie Isotopique, C.G.G., U.S.T.L.,
34060 Montpellier Cedex, France.

Metamorphic rocks in the basement of the Massif Central can be subdivided into two parts (Burg, 1977). On the one hand, mica schists and quartzo-feldspathic gneisses, and on the other hand, the leptyno-amphibolite group (L.A.G.). Usually this latter group is composed of catazonal metasedimentary rocks (paragneisses, mica schists, marbles) including metamorphosed igneous bodies of acid composition (leptynites and augen gneisses) or mafic and ultramafic composition (amphibolites, metagabbros, eclogites, pyrigarnites). In Variscan Europe, this group is extensively developed from Galicia to the Bohemian Massif (Moldanubicum). The age, metamorphic evolution, and geodynamic significance of this L.A.G. are much debated questions.

Several rocks from the southern Massif Central have been studied by the U-Pb method, with 7 to 10 zircon fractions for each sample. For two L.A.G. meta-igneous rocks, we obtain 478 ± 7 m.y. on one leptynite and 487 ± 12 m.y. on one metagabbro. In one L.A.G. amphibole gneiss of volcano-sedimentary origin, two zircon populations have been separated and provide, respectively, 482 ± 8 m.y. and 815 ± 14 m.y. ages. One L.A.G. overlying paragneiss presents highly discordant experimental points for inherited zircons, which indicate old ages of 1700 - 2000 m.y. One metaquartzo-diorite, which intruded underlying mica schists and quartzo-feldspathic gneisses has been dated at 540 ± 15 m.y. Using the episodic lead-loss model of Wetherill (1956) all the lower intercepts fall between 300 and 350 m.y. in a concordia diagram.

Actually, available geological and geochemical data indicate that the great extent of this bimodal igneous activity is of early Paleozoic age (480 ± 15 m.y.); and do not lend support to the hypothesis of a Precambrian igneous or metamorphic event for the L.A.G. rocks. Furthermore, in Variscan Europe, "Caledonian" radiometric ages have been reported previously but without real geologic evidence of an orogeny (Schmidt, 1976, 1977). In agreement with recent work by Den Tex and collaborators in Galicia, we explain this early Paleozoic thermal event in terms of crustal thinning, which gave rise to important bimodal igneous activity extending throughout Europe. This evolution may be comparable to that occurring in the Basin and Range during Cenozoic times (Christiansen and others, 1972; Lipman and others, 1972). At depth, granulite metamorphism may be related to this thermal event (Jäger and Wacznauer, 1969; Arnold and Scharbert, 1973; Grauert and others, 1974). However, an alternative model may be proposed: a supracrustal series laid down during early Proterozoic times was subjected later to conditions of HP-HT metamorphism which would be an early manifestation of the Variscan tectogenesis and crustal thickening.

Arnold, L., and Scharbert, A.H.G., 1973, Rb-Sr Alterbestimmungen an Granuliten der Südlichen Böhmischen Massiv in Österreich: Schweizerische Mineralogische und Petrographische Mi Heilungen, v. 63, p. 61.

Burg, J. P., 1977, Tectonique et microtectonique des series crystallophylliennes du Haut-Allier et de la Vallie de la Truyère: Université Montpellier, Th. 3e cycle, 79 p.

Grauert, B., Hänny, R., and Soptrajanova, G., 1974, Geochronology of a polymetamorphic and anatectic gneiss region; the Moldanubicum of the area Lam-Deggendorf Eastern Bavaria (Germany): Contributions to Mineralogy and Petrology, v. 45, p. 37-63.

Jäger, E., and Wacznauer, A., 1969, Einige Rb-Sr Datierungen an Granuliten des Achsischen Granulitgebirges: Deutsche Akadamie der Wissenschaften zu Berlin, Monatsberichte, v. 11, p. 420-426.

Lipman, P. W., Prostka, H. J., and Christiansen, R. L., 1972, Cenozoic volcanism and plate tectonic evolution of the Western United States, I; Early and Middle Cenozoic: Royal Society of London Philosophical Transactions, v. 271, p. 217-284.

Schmidt, K. K., 1976, Das "Kaledonische Ereugnis in Mittel und Südwestliche Europa": Nova Acta Leopoldina, v. 45, p. 381-402.

Schmidt, K. K., 1977, Der Altpaläeozoïsche Magmatismus und seine Spellung in der Tektonischen Geschichte der Mittel und Südwestliche Europa: Zeitsohrift Deutschen Geologischer Gesohichte, v. 128, p. 121-141.

Wetherill, G. W., 1956, Discordant Uranium-Lead ages: Transactions of the American Geophysical Union, v. 37, p. 320-326.

Sr-Nd ISOTOPE SYSTEMATICS IN OROGENIC LHERZOLITES

By M. Polve, P. Richard, and C. J. Allegre
Laboratoire de Géochimie et Cosmochimie - LA 196
Institut de Physique du Globe et Département des Sciences de la Terre - Universités de Paris VI et VII - 4, Place Jussieu 75230 Paris Cedex 05

The coupled Sr and Nd isotopic ratios are a very good petrogenetic tracer (De Paolo and Wasserburg, 1976; Richard and others, 1976; O'nions and others, 1977), recently developed for terrestrial samples. Earlier results on basaltic rocks show a correlation line which can be explained by different models of partial melting and mixing processes (Allegre and others, unpublished data).

Systematic studies of Nd-Sr isotopes on orogenic lherzolite bodies have been made to better understand the systematic correlation for other types of mantle materials.

The orogenic lherzolites have been extensively studied petrographically and by trace-element geochemistry and it is suggested that these bodies are mainly composed of a massive lherzolite and pyroxenite veins and have undergone multiple events of partial melting and crystallization--the last one having occurred possibly during the tectonic emplacement in orogenic zones (Loubet and others, 1975; Loubet, 1976; Loubet and others, 1978; Loubet and Allegre, unpublished data).

Samples from different massifs were studied: Baldissero and Lanzo (Alps), Beni Bousera (Morocco), and Lherz (French Pyrénees).

As shown in figure 1, all of the lherzolites lie on or near the correlation line, in the field of the mid-ocean ridge tholeiites. Note that no age corrections have been made for these lherzolites. However, the similarity of Sr-Nd systematics between orogenic lherzolites and MOR basalts is consistent with the residual character of the lherzolites, demonstrated by rare earth systematic studies (Loubet and others, 1978) and suggests that the mantle source of MOR basalts may have geochemical characteristics similar to the orogenic lherzolites. Note that a large isotopic variation exists within a single massif (for instance, the Beni Bousera massif shows ε_{Nd} ranging from +2.1 to +11.7).

The model ages calculated from the two-stage Nd isotopic evolution with the measured Sm/Nd ratios are about 1 b.y., much older than the emplacement ages inferred from geologic data.

The age of fractionation of the different lherzolites is currently being determined by Sm-Nd whole-rock and mineral isochrons.

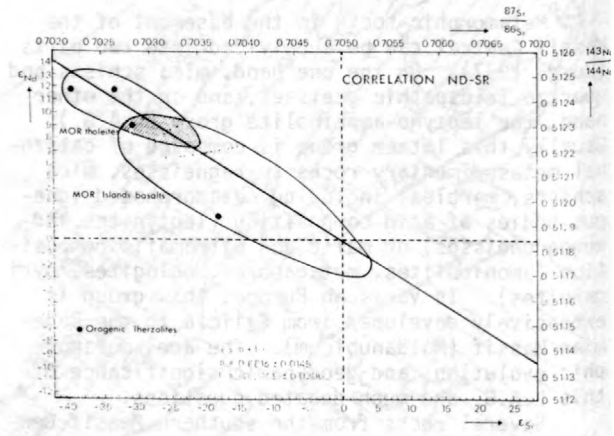

Figure 1.--Position of the orogenic lherzolites on the correlation line defined by oceanic basalts.

De Paolo, D. J., and Wasserburg, G. J., 1976, Interferences about magma-sources and mantle structure from variations of $^{143}Nd/^{144}Nd$: Geophysical Research Letters, v. 3, no. 12, p. 743-746.

Loubet, M., Shimizu, N., and Allegre, C. J., 1975, Rare earth elements in Alpine peridotites: Contributions to Mineralogy and Petrology, v. 53, p. 1-12.

Loubet, M., 1976, Géochimie des Terres Rares dans les massifs de péridotites dits de haute température--Evolution du manteau terrestre: Paris, Thèse de Doctorat, 357 p.

Loubet, M., Polve, M., Richard, P., and Allegre, C. J., 1978, Trace elements, strontium, and neodymium isotopes in orogenic lherzolites, International Symposium on Basic Ultra Mafic Association, Grenoble 1977 à paraître: edition CNRS.

O'Nions, R. K., Hamilton, P. J., and Evensen, N. M., 1977, Variations in $^{143}Nd/^{144}Nd$ and $^{87}Sr/^{86}Sr$ ratios in oceanic islands: Earth and Planetary Science Letters, v. 34, p. 13-22.

Richard, P., Shimizu, N., and Allegre, C. J., 1976, $^{143}Nd/^{144}Nd$ a natural tracer--an application to oceanic basalts: Earth and Planetary Science Letters, v. 31, p. 269-278.

ON THE FISSION-TRACK PLATEAU AGES OF MINERALS

By G. Poupeau, Ph. Romary, and P. Toulhoat
Centre des Faibles Radioactivités (C.N.R.S.-C.E.A.), 91190 Gif sur Yvette, France

One of the most interesting properties of the fission-track dating method is its high sensitivity to thermal events, which makes it a unique tool in dating mild metamorphisms and uplift rates. As a counterpart, fission-track ages are often hybrid ages when spontaneous fission tracks are partially annealed since the last major thermal event. Significant geologic ages can then be obtained only if one can evaluate the degree of annealing of the fossil tracks. Various correction methods have been proposed, based on the reduction of the etchable track length with annealing, or, in the plateau method, on the correlative reduction of etchable track densities for fossil and neutron-induced tracks with annealing (see Fleischer and others, 1975).

In volcanic glasses and tektites, both correction methods give satisfactory results, producing corrected fission-track ages concordant with K-Ar ages (Storzer and Poupeau, 1973). In minerals, however, the applicability of these age-correction methods has been questioned on the basis of differences between corrected fission-track ages of the Cerro de Mercado apatites and their age deduced from K-Ar data (Naeser and Fleischer, 1975).

The purpose of this article is to present a further investigation of plateau ages on micas (phlogopite, muscovite) and apatites. The micas used in this work were previously fission-track dated by Maurette and others (1964). They were selected because they presented anomalously young ages, presumably due to track annealing.

EXPERIMENTAL PROCEDURES

The micas were prepared as freshly cleaved sheets and etched under controlled temperature conditions in 40 percent HF. The phlogopites were etched at various temperatures between -20°C and +35°C, for times from 15 seconds up to 240 minutes. It was noted that, for fossil tracks, a saturation value for the etched track density was reached after an etching time varying from 80 minutes at -20°C to $\sim$ 8 minutes at 20°C. The saturation density value is the same at 20°C and at higher temperatures. Induced fission-tracks need only 2 minutes to reach a saturation value at 20°C. All fission-track ages were subsequently measured on tracks etched at 20°C. The muscovite was etched for times varying between 60 and 450 minutes. For plateau age measurements, standard etching times of 8 minutes and 6 hours were used for the phlogopites and the muscovite, respectively. The apatites were mounted in epoxy and polished before etching for 50 seconds at 20°C in 7 percent HNO_3.

The induced fission-tracks were counted in samples annealed for 2 hours before thermal neutron irradiation at 850°C for the micas and 500°C for the apatites. The neutron doses were measured with the NBS glass standard 963 and the ^{60}Co activity induced in a cobalt disc placed adjacent to the samples during the irradiation. The thermal neutron doses as deduced from fission tracks in the glass standard and the ^{60}Co activity agree to within 5 percent. Track density counts were performed with an optical microscope for muscovite; with a Scanning Electron Microscope (SEM) for apatites; and using a combination of both for phlogopites.

For the determination of plateau ages, pairs of samples with fossil and induced tracks, respectively, are annealed together at increasing temperatures up to the point where--the fossil and induced tracks being reduced to the same degree of annealing--they behave similarly with increasing annealing and the resulting age reaches a plateau value. In the present case, the temperatures were, at most, 380°C for apatite, 500°C for phlogopite, and 640°C for muscovite. In the case of apatite and muscovite, these maximum temperatures correspond to total-track annealing; and for phlogopites, to the point where the development of corrosion figures during etching in the irradiated samples prevents fission-track counting. The above temperatures are given to within ±20°C.

RESULTS AND COMMENTS

The results are presented in table 1. For each sample, two ages are given. The first one is the apparent age obtained by etching the fossil and induced fission tracks up to a saturation value; the second is the plateau age.

Phlogopites

For the three phlogopites studied, the apparent age and the plateau age are indistinguishable. The notably lower fisshion-track age values obtained previously by Maurette and others (1964) for these phlogopites (table 1, column 4) was due to incomplete etching of the fossil tracks. In effect, fossil tracks need etching times 4 to 5 times longer than induced tracks to reach a saturation density value.

The plateau ages were obtained by using a series of up to 5 annealing steps (1 hour each) between 300°C and 500°C. It was noted that, in this temperature interval, while the etchable fossil and induced track densities were similarly affected, the calculated ages remained constant. For instance, in the Madagascar phlogopite, the fossil track density decreases from 5.2×10^4 cm^{-2} at 300°C down to 3.2×10^4 cm^{-2} at 500°C, while the age calculated for five

Table 1.--Analytical results

Sample locality	Fission-track ages x 10^6 yr[1] Apparent age	Plateau age	Other authors	Age (and method) of last reheating x 10^6 yr
		Phlogopite		
Madagascar, --- 12 267.	420±8	415±8	[2]190 232	440-460 (Rb-Sr biotites).
Ceylan, ------- 103 794.	620±22	620±20	[2]338	450-500 650-700 (Rb-Sr, K-Ar).
New York, ----- 55 250.	319±22	326±16	[2]193	360-400 (Rb-Sr, K-Ar).
		Muscovite		
Ivory Coast, -- 108 314.	1075±150	1480±150	[2]400 [3]207	1800-2000 (Rb-Sr, K-Ar). 1500 (K-Ar on K-feldspars).
		Apatites		
Anglès --------	180±5	265±7		283 (Rb-Sr internal isochron[4]).

[1] $\lambda_f = 6.85 \times 10^{-17}$ yr^{-1}.
[2] Maurette and others (1964).
[3] Brito (1972).
[4] Hamet and Allegre (1976).

temperatures in this interval fall between 410 m.y. and 420 m.y.

The fission-track ages of the phlogopites appear to be slightly lower than the age of the last dated reheating (table 1, last column; and Romary and Poupeau, unpub. data). Although this difference may partly result from an experimental effect (overevaluation of the induced track density due to the presence of short corrosion figures mostly developed in the irradiated samples), we rather believe that it reflects the lower closing temperature of phlogopites for fission-track retention. In the latter case, the lower fission-track age would merely reflect a cooling history.

Muscovite

The muscovite presents an interesting situation with an apparent age of 1075 m.y., significantly lower than the plateau age of 1480 m.y. (table 1). Both ages, however, are much older than those obtained earlier by Maurette and others (1964) of 400 m.y. and Brito (1972) with 207 m.y. The apparent age was obtained after an etching time of 4 hours and remains constant thereafter. The plateau age of 1480 m.y. was obtained for annealing temperatures above 580°C, corresponding to a reduction in the fossil- and induced-track densities of more than 40 percent and 60 percent, respectively. This muscovite comes from the well dated 1800 - 2000 m.y.-old Precambrian shield of the Ivory Coast. To our knowledge, the only younger radiometric ages obtained for this province are a few K-Ar measurements of 1500 m.y. on K-feldspars (Maluski, 1973), a phase highly sensitive to thermal events. The concordancy between this age and our own fission-track age measurements suggests that a mild thermal event occurred in the Ivory Coast Precambrian shield some 1500 m.y. ago.

Apatites

The dated apatites come from a granite in the Hercynian province of the Massif Central (France). As in muscovites, their apparent age is much lower than their plateau age. The latter is reached at a temperature of 320°C. The fission-track plateau age of 266 ± 7 m.y. appear to be significantly younger than the Rb-Sr internal isochron age of 283 m.y. The latter corresponds to the final phase of uplift of the Massif Central and the younger fission-track age of the apatites here also is interpreted as a cooling age (Toulhoat and Poupeau, unpub. data).

CONCLUSION

The results obtained in this study are very encouraging. They show that the plateau method is able to produce gelogically significant ages in minerals in which the spontaneous fission tracks are partially annealed. Further tests are now needed in order to define the range of applicability of the method. It appears, however, that Precambrian studies with the fission-track method will be made easier and will allow a finer approach in the dating of mild thermal events and cooling histories.

Brito, U. P., 1972, Effacement thermique des traces de fission dans le mica muscovite: Université Paris 11, Thèse d'Etat.

Fleischer, R. L., Price, P. B., and Walker, R. M., 1975, Nuclear tracks in solids: The University of California Press, 605 p.

Hamet, J., and Allegre, C. J., 1976, Hercynian orogeny in the Montagne Noire (France): Application of ^{87}Rb-^{87}Sr systematics: Geological Society of America Bulletin, v. 87, p. 1429-1442.

Maluski, H., 1973, Datation par la méthode K-Ar des granites précambriens du Centre de la Côte d'Ivoire [abs.]: Réunion Annuelle des Sciences de la Terre, Ed. Soc. Geol. France, p. 284.

Maurette, M., Pellas, P., and Walker, R. M., 1964, Etude des traces de fission fossiles dans le mica: Bulletin de la Societe Francaise de Mineralogie et de Cristallographie, v. 87, p. 6-17.

Naeser, C. W., and Fleischer, R. L., 1975, The age of the apatite at Cerro de Mercado, Mexico; A problem for fission-track annealing corrections: Geophysical Research Letters, v. 2, p. 67-70.

Storzer, D., and Poupeau, G., 1973, Ages-plateaux de minéraux et verres par la méthode des traces de fission: Academy of Science, Paris, Comptes, Rendus, v. 276, p. 137-139.

HOW OLD ARE THE SUPPOSEDLY ARCHEAN CHARNOCKITIC GRANULITES IN THE GUIANA SHIELD BASEMENT OF WESTERN SURINAME (SOUTH AMERICA)?

By H. N. A. Priem, N. A. I. M. Boelrijk,
E. H. Hebeda, R. P. Kuijper, E. W. F. de Roever,
E. A. Th. Verdurmen, R. H. Verschure, and
J. B. W. Wielens
Z.W.O. Laboratorium voor Isotopen-Geologie
Amsterdam, The Netherlands

The charnockitic granulites of the Bakhuys Mountains in western Suriname form part of a belt of high-grade metamorphic rocks stretching over at least 1000 km through the Guiana Shield from northernmost Brazil to near Paramaribo in Suriname (Kroonenberg, 1976). This catazonal belt is surrounded by Trans-Amazonian granitoid-acid volcanic suites, metavolcanic-metasedimentary sequences, and minor gabbroic-ultramafic plugs (ages between about 2000 and 1850 m.y., Priem and others, 1971, 1977; Z.W.O. Laboratory, unpub. data). Recently, Gaudette and others (1977) claimed an age of 2760 m.y. (recalculated with the Rb decay constant 1.42×10^{-11} yr^{-1}) and initial $^{87}Sr/^{86}Sr$ of 0.7013 for the charnockitic granulites in the Bakhuys Mountains, on the basis of the linear arrangement of the Rb-Sr data points four samples. Two samples of basement gneisses in the Supamo Complex in Venezuela (a distance of some 600 km from the Bakhuys Mountains) are also included in the isochron. Data points of samples with $^{87}Rb/^{86}Sr$ above 0.4 fall below this linear array and were omitted. A pre-Trans-Amazonian age of the charnockitic granulites in the Bakhuys Mountains is indeed probable in view of the geological relationships. However, earlier Rb-Sr investigations of 15 charnockitic and enderbitic samples in our laboratory did not reveal any linear correlation, and certainly did not give an isochron age as high as 2750 to 2800 m.y. In order to solve this discrepancy, 13 additional samples were collected in 1977 for further Rb-Sr and zircon U-Pb investigation. Figure 1 shows the locations of all investigated samples; also the four samples analyzed by Gaudette and others (1977).

Geology and Petrology: The high-grade metamorphic terrain of the Bakhuys Mountains occupies a northeast elongate area approximately 125 by 35 km in extent (fig. 1). It is essentially composed of charnockitic granulites with minor occurrences of various high-grade gneisses and mafites (de Roever, 1973, 1975, de Roever and Bosma, 1975). A few dolerite dikes (1660 ± 25 m.y., Hebeda and others, 1972; Z.W.O. Laboratory, unpub. data) and Trans-Amazonian granitic and gabbroic-ultramafic bodies have invaded this high-grade crustal segment. Like the whole of western Suriname, the charnockitic area has been affected by the low-grade Nickerie Metamorphic Episode (greenschist facies) about 1250 m.y. ago, as reflected in the pattern of Rb-Sr and K-Ar mica ages (Priem and others, 1971, 1977; Z.W.O. Laboratory, unpub. data) and mylonitic phenomena.

The charnockitic granulites are banded, granoblastic rocks. Part of the banding is a relict sedimentary bedding (intercalations of impure quartzites, calc-silicate rocks, and graphite-bearing layers), accentuated by metamorphic differentiation and incipient migmatization. Essentially, the charnockitic granulites are characterized by the assemblage or-

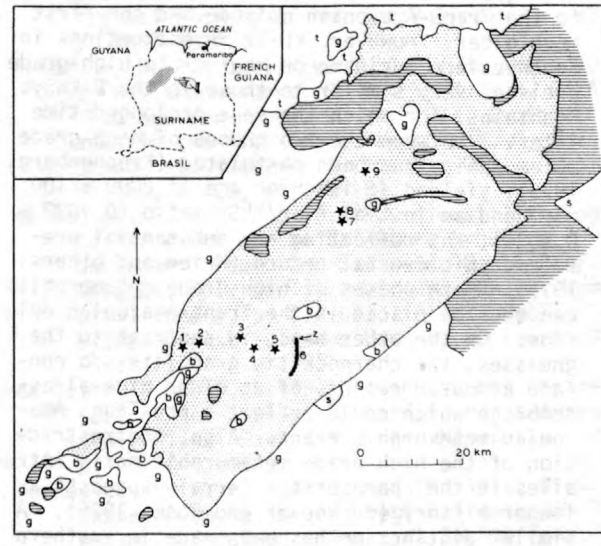

Figure 1.--Geologic sketch map of the charnockitic terrain in the Bakhuys Mountains, western Suriname (modified from Bosma and others, 1978). Stippled, charnockitic-enderbitic suites; horizontal shading, high- and medium-grade gneisses; Trans-Amazonian rocks--g, various granites, s, schists, and b, gabbroic-ultramafic intrusions; t, Tertiary sands; 1-9, sites of samples used for whole-rock Rb-Sr analysis; Z, sampling site of Sur 408, also used for zircon U-Pb analysis. Four samples investigated by Gaudette and others (1977), come from our locations 2, 3, 9, and Z.

thopyroxene + plagioclase (An_{60}-An_{15}) ± clinopyroxene ± hornblende ± biotite ± perthite ± quartz, formed under conditions of the lower pressure granulite facies. The paragenesis developed roughly contemporaneous with the migmatization and a phase of isoclinal folding. Relicts of an older assemblage, kinked biotite and undulous hornblende, occur within undeformed pyroxene crystals. A younger phase of higher pressure granulite facies conditions is reflected by symplectitic reaction rims of garnet, clinopyroxene, quartz, and albite-oligoclase surrounding the orthopyroxene and hornblende. A similar metamorphic evolution, but without the armoured relicts of the oldest assemblage, can be observed in the high-grade gneisses (sillimanite gneisses ± cordierite ± garnite ± biotite, and biotite gneisses ± orthopyroxene). The mafites (granulite facies metadolerite dikes, bodies of garnet-bearing metanorite, and a small body of calcic anorthosite) are exclusively found in the charnockitic terrain, being conspicuously absent in the areas underlain by the gneisses.

It was originally speculated (de Roever, 1973, 1975) that there should have been a prolonged time interval between the two phases of high-grade metamorphism, the second belonging to the Trans-Amazonian episode and the first much older. However, Rb-Sr investigations in southwestern Suriname on medium- to high-grade gneisses very similar to those in the Bakhuys Mountains, for which the same prolonged time interval between the two phases of high-grade metamorphism had been postulated (Kroonenberg, 1975), yielded an isochron age of 2000 ± 100 m.y. and an initial $^{87}Sr/^{86}Sr$ ratio (0.7027 ± 0.0039), not reflecting any substantial pre-metamorphic crustal record (Priem and others, 1977). Both phases of high-grade metamorphism can thus be placed in the Trans-Amazonian episode. On the other hand, in contrast to the gneisses, the charnockitic granulites do contain armoured relicts of an older mineral assemblage which could reflect a pre-Trans-Amazonian metamorphic event. Also, the restriction of the high-grade metamorphic mafic intrusives to the charnockitic terrain suggests a longer history (de Roever and Bosma 1975). A similar distinction has been made in southern Guyana between the older Kanuku Granulites and their cover of high-grade paragneisses (Berrange, 1977). The zircons in the charnockitic granites are round or oval-shaped (a shape typical for granulite facies rocks) with some zoning and containing few inclusions. Cores of a possibly older zircon generation are common.

Isotopic investigations: Rb-Sr whole-rock measurements were made on 28 charnockitic and enderbitic samples (fig. 1). Four size fractions of the zircon separated from one enderbite sample (Sur 408) were analyzed according to the U-Pb method. Standard procedures were used for chemical treatment, and mass spectrometric and X-ray fluorescence analysis. The age calculations are based upon the constants

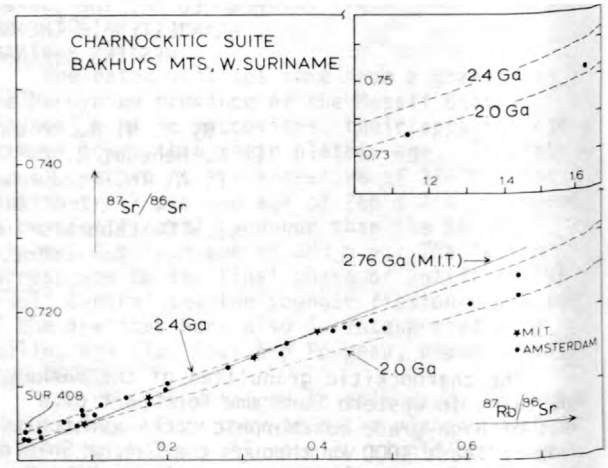

Figure 2.--Plot of Rb-Sr data.

recommended by Steiger and Jäger (1977). The Rb-Sr data points scatter and do not show any linear correlation (fig. 2). At best, the points may be interpreted as lying within an envelope, with the lower and upper boundary lines corresponding to ages of 2.0 b.y. and 2.4 b.y. respectively. The four samples analyzed by Gaudette and others (1977) are also plotted and fall perfectly within the envelope; the apparent linear relationship of these samples, corresponding to an age of 2760 m.y. is fortuitous in view of the overall scatter of the data points. The scatter of Rb-Sr data points could reflect variations in initial $^{87}Sr/^{86}Sr$ through the sedimentary sequence and incomplete homogenization during Trans-Amazonian high-grade metamorphism. It is also feasible to interpret the Rb-Sr systematics in terms of a prolonged pre-Trans-Amazonian Rb-Sr history and varying degrees of metamorphic resetting of the Rb-Sr systems about 2.0. b.y. ago. However, no age higher than about 2.4 b.y. can possibly be deduced from the Rb-Sr data points. Whether this upper boundary line approximates the age of an older phase of metamorphism or is only a minimum age remains a matter of speculation. The initial $^{87}Sr/^{86}Sr$ ratio lies between 0.7023 and 0.7035, more probable values than the very low ratio of 0.7013 according to Gaudette and others (1977).

Regarding the zircon U-Pb systematics of enderbite Sur 408, the age of 2026 ± 20 m.y. (2σ) deduced from the discordia plot (fig. 3) corresponds very well with the 2035 m.y. line defined by the lowest Rb-Sr data-points. This age agrees with the age of Trans-Amazonian high-grade metamorphism in southwestern Suriname (2000 ± 100 m.y., Priem and others, 1977).

Conclusions: Our whole-rock Rb-Sr and zircon U-Pb results point to an age of about 2030 m.y. (Trans-Amazonian) for the high-grade metamorphism in the Bakhuys Mountains. A prolonged pre-Trans-Amazonian history may be deduced for the charnockitic granulites from the Rb-Sr systematics of many samples, but there is no evi-

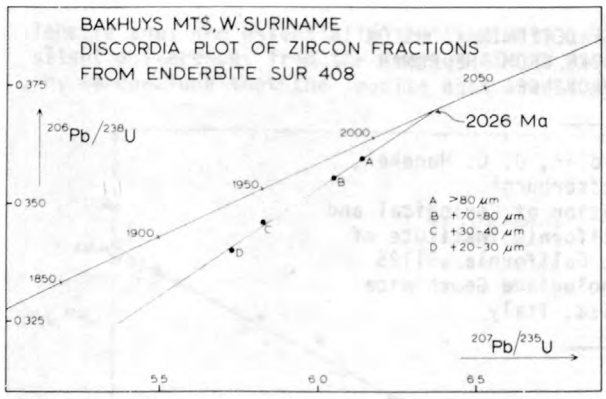

Figure 3.--Plot of U-Pb data in a Concordia diagram.

dence whatsoever for an age older than about 2400 m.y. The charnockitic suite may be correlated on the basis of structural, petrographic, and stratigraphic similarities with the Imataca Series in Venezuela with an age in excess of 3100 m.y. and successively affected by the Guriense orogeny (2800 to 2700 m.y. ago) and the Trans-Amazonian orogeny (Hurley and others, 1976), but in the Bakhuys Mountains this possibly very old history has at best only partially been preserved in the isotopic record. The age of 2760 m.y. claimed by Gaudette and others (1977) results from a fortuitous linear arrangement of four samples.

If we are indeed dealing with ancient rocks, the charnockitic granulites should thus have retained parts of their pre-Trans-Amazonian Rb-Sr record, whereas the zircon U-Pb systems were wholly reset during Trans-Amazonian granulite facies metamorphism. It may be noteworthy that we have observed a similar pattern in the Sveconorwegian charnockitic granulites of southwestern Norway (Versteeve 1975). Finally, it should be stressed that apparently excellent Rb-Sr "isochrons" in metamorphic terrains based upon a few samples can easily be misleading .

Berrangé, J. P., 1977, The geology of southern Guyana, South America: Overseas Mem. Inst. Geol. Sci., no. 4, 112 p.

Bosma, W., Kroonenberg, S. B., van Lissa, R. W., Maas, K., and de Roever, E. W. F., (in press), Geological Map of Suriname (1:500.000), with Explanatory Note: Geol. Mijnb. Dienst Suriname.

Gaudette, H. E., Hurley, P. M., Fairbairn, H. W., Espejo, A., and Dahlberg, E. H., 1977, Older Guiana basement south of the Imataca Complex in Venezuela and in Suriname: 24th Progress Report 1974/1976, M. I. T. Geochronology Laboratory, R. M. 54-1122, p. 26-34.

Hebeda, E. H., Boelrijk, N. A. I. M., Priem, H. N. A., Verdurmen, E. A. Th., and Verschure, R. H., 1972, Excess radiogenic argon-in the Precambrian Avanavero Dolerite in western Suriname (South America): Earth and Planet. Science Letters, v. 20, p. 189-200.

Hurley, P. M., Fairbairn, H. W., and Gaudette, H. E., 1976, Progress report on Early Archean rocks in Liberia, Sierra Leone and Guyayana, and their general stratigraphic setting, in, Windley, B. F., ed., The early history of the Earth: New York, John Wiley, p. 511-521.

Kroonenberg, S. B., 1975, Polymetamorphism in pelitic gneisses and amphibolites of the Coeroeni Group, S. W. Suriname: Anais da Decima Conference on Geology, Inter-Guinas, Belém, Pará, Brasil, v. 1, p. 414-429.

Kroonenberg, S. B., (in press), Amphibolite-facies and granulite-facies metamorphism in the Coeroeni-Lucie area, southwestern Suriname: University of Amsterdam, Ph.D. thesis. Also; Geol. Mijnb. Dienst Suriname Meded., v. 25.

Priem, H. N. A., Boelrijk, N. A. I. M., Hebeda, E. H., Verdurmen, E. A. Th., and Verschure, R. H., 1971, Isotopic ages of the Trans-Amazonian acidic magmatism and the Nickerie Metamorphic Episode in the Precambrian basement of Suriname, South America: Geological Society of America Bulletin, v. 82, p. 1667-1679.

Priem, H. N. A., Boelrijk, N. A. I. M., Hebeda, E. H., Kroonenberg, S. B., Verdurmen, E. A. Th., and Verschure, R. H., 1977, Isotopic ages in the high-grade metamorphic Coeroeni Group, southwestern Suriname: Geol. Mijnb., v. 56, p. 155-160.

de Roever, E. W. F., 1973, Provisional lithologic framework of the Falawatra Group, W. Suriname: Paper 2nd Latin-Am. Geol. Conf. Caracas, Bol. Geol., publ. esp. Nr. 7, Memoria, tomo 2, p. 637-647. Also: Geol. Mijnb. Dienst Suriname Meded., v. 23, p. 34-44.

de Rover, E. W. F., 1975, Geology of the central part of the Bakhuys Mountains, W. Suriname: Geol. Mijnb. Dienst Suriname Meded., v. 23, p. 65-101.

de Roever, E. W. F., and Bosma, W., 1975, Precambrian magmatism and regional metamorphism in Suriname: Anais da Decima Conf. Geol. Inter-Guianas, Belém, Pará, Brasil, v. 1, p. 123-163.

Steiger, R. H., and Jager, E., 1977, Subcommission on Geochronology: Convention on the use of decay constants in geo- and cosmochronology: Earth and Planetary Science Letters, v. 36, p. 359-362.

Versteeve, A., 1975, Isotope geochronology in the high-grade metamorphic Precambrian of southwestern Norway: Norges geologiske Undersokelse, v. 318, p. 1-50.

^{39}Ar-^{40}Ar AND Rb-Sr AGE DETERMINATIONS ON QUATERNARY VOLCANIC ROCKS FROM THE ROMAN VOLCANIC PROVINCE

By F. Radicati di Brozolo[1,2], J. C. Huneke[1], and G. J. Wasserburg[1]
[1]The Lunatic Asylum, Division of Geological and Planetary Sciences, California Institute of Technology, Pasadena, California 91125
[2]Laboratorio di Geocronologia e Geochimica Isotopica, Pisa, Italy

We report ^{39}Ar-^{40}Ar and Rb-Sr analyses performed on mineral separates from very young ($\sim$ 350,000 yr) tuffs from the potassic Roman volcanic province to establish the feasibility of age measurements on potassic minerals with the high precision necessary for good stratigraphic definition. Several outcrops of the Villa Senni tuff in the Albano volcanic complex were sampled. The tuff contains fresh leucite and biotite crystals 0.1 - 1 cm in size and minor amounts of amphibole. Leucite and biotite separates were irradiated for the ^{39}Ar-^{40}Ar analyses with a fast neutron fluence of $\sim$ 7 x 10^{14} n cm^2 in the TRIGA reactor facility at the University of California, Berkeley. The Be 4 M standard muscovite (Steiger, 1964; Lanphere and Dalrymple, 1965) was used as the irradiation monitor. Neutron fluence inhomogeneities were monitored by measuring the ^{58}Co γ activity induced in Ni wires that were placed in known positions. The monitor $^{40}Ar/K$ ratio is reported with an uncertainty of $\sim$ 4 percent, which affects the absolute ages of our samples. The errors in the relative ages from the mass spectrometric analyses and the fluence normalizations amount to approximately 8000 years (2σ). We have analyzed the samples for Ar using the stepwise heating technique. Typically we used eight steps plus a high-temperature ($\sim$ 1650°C) re-extraction step which was never noticeably above the blank level. The first observation to be made is that the bulk $^{40}Ar/^{36}Ar$ ratios of leucites are much higher than those of biotites (leucites $\sim$ 5,000; biotites $\sim$ 360).

In figure 1 we plot the $^{36}Ar/^{40}Ar$ ratios versus the $^{39}Ar/^{40}Ar$ ratios for samples VS-6 leucite and biotite and VS-5 leucite and biotite. K-derived Ar plots on the abcissa. Trapped Ar (not derived from in situ decay of ^{40}K) plots on the ordinate. A linear data array indicates mixtures of two well-defined end members in different proportions. The abcissa intercept of the line passing through the data points defines the age. The leucites yield well-defined and distinctly different linear arrays. They contain very small amounts of trapped argon and plot close to the $^{39}Ar/^{40}Ar$ axis, whereas biotites, with a high amount of nonradiogenic argon and an uncertainty in the composition of trapped components, plot close to the $^{36}Ar/^{40}Ar$ axis. The difference in age of the two leucites is insensitive to the composition of the trapped component. The apparent age versus ^{39}Ar fractional release of the VS-5 and VS-6 leucites is shown on the left side of figure 2; the results for biotites VS-6 and VS-5 are shown on the right side of figure 2. The data are corrected for trapped Ar with air composition. All of the leucites studied exhibit extremely well-defined age plateaus over the entire ^{39}Ar release. There is no evidence for ^{40}Ar loss, and the plateau ages are indistinguishable from the ^{39}Ar-^{40}Ar ages calculated from the integrated Ar release. The biotites show a very irregular pattern of apparent ages that does not define a plateau. Only the bulk ^{39}Ar-^{40}Ar age can be calculated for the biotites. The plateau ages of leucites and bulk K-Ar ages calculated from the integrated Ar release from the biotites are reported in table 1.

In no case do the biotite and leucite ages agree; the biotite ages are much more variable and, with one exception, are older. Because (1) the leucites yield extremely well-defined ^{40}Ar-^{39}Ar age plateaus, (2) very small trapped ^{40}Ar corrections are required, and (3) the

Table 1.--Ages of biotites and leucites

Sample no.	Leucites Plateau age±2σ (yr)	Biotites K-Ar age±2σ (yr)
VS-3	345,900±9,300	437,400±13,800
VS-4A	347,900±9,700	368,500± 9,600
VS-5	338,900±7,500	433,200±14,500
VS-6	353,600±9,100	332,500±43,400
VS-7	356,600±8,400	366,700± 9,000
VS-8	[1]$\sim$330,000	
VS-10	[1]$\sim$340,000	

[1]Preliminary calculations on leucites VS-8 and VS-10 show that their plateau ages are not significantly different from the other leucites.

leucite ages are essentially the same with only slight differences from the average of 348,000 yr, we conclude that the leucite ages are valid.

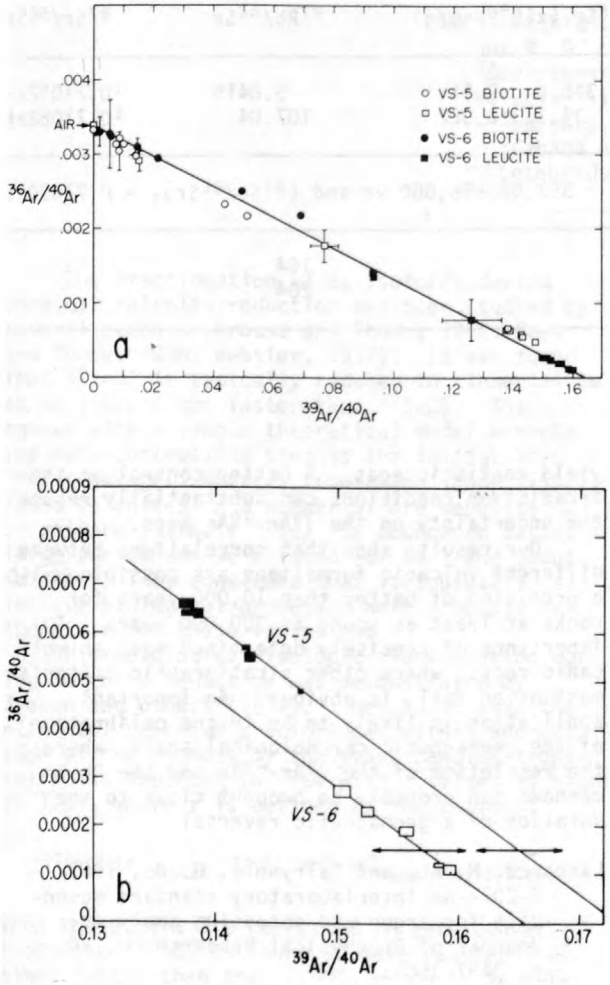

Figure 1.--a, $^{36}Ar/^{40}Ar$ versus $^{39}Ar/^{40}Ar$ correlation diagram for Ar extracted from the VS-6 and VS-5 leucite and biotite. K-derived Ar plots on the abcissa, trapped Ar on the ordinate. Mixtures of two components lie along the line connecting the two end-member compositions. Boxes and error bars represent the 2σ uncertainty from the mass spectrometric analyses only. The line is drawn from trapped Ar of air composition through the VS-6 leucite points. Abcissa intercept of the line defines the age. b, Enlargement of the lower right-hand corner of the previous diagram. The boxes represent the most radiogenic Ar extracted from VS-5 leucite and VS-6 leucite and lie on two different lines. Horizontal arrows indicate the 2σ uncertainty on the correlation lines introduced by the uncertainty on the relative fluences for the two samples.

The resolution obtainable in our laboratory for the measurements of $^{87}Sr/^{86}Sr$ ratios allows the determination of a Rb-Sr age on geologic material less than 10^5 yr old, with Rb/Sr values of ∿ 300 (Papanastassiou and Wasserburg, 1969). In consideration of the very high K and Rb contents of our samples, it was evident that a search for suitable minerals could be profitable.

Several leucite-biotite pairs were carefully handpicked under the microscope and were analyzed for Rb and Sr concentrations to determine if sufficient enrichment in $^{87}Sr/^{86}Sr$ ratios could be expected. The biotites have constant concentration of Rb (∿ 550 ppm) and Sr (∿ 300 ppm) corresponding to a $^{87}Rb/^{86}Sr$ ratio of approximately 5. Leucites have constant Rb (∿ 1000 ppm) but variable Sr contents, from 16 to 40 ppm giving $^{87}Rb/^{86}Sr$ ratios from 80 to 200. For an expected age of 300,000 yr such values yield increases of 3 x 10^{-4} to 9.5 x 10^{-4} in the $^{87}Sr/^{86}Sr$ of the leucites over the biotites, which are well resolvable with the precision of our mass spectrometers (∿ 3 x 10^{-5}).

In figure 3 and table 2, we report the results of our measurement on the leucite-biotite pair from sample VS-8. The elemental concentrations for two other leucites are also reported in table 2. The two-point isochron defines an age of 353,000 ± 56,000 yr which agrees with the preliminary ^{39}Ar-^{40}Ar age of the leucite (∿ 330,000). The initial $^{87}Sr/^{86}Sr$ is 0.71030 ± 0.00006, which is higher than the less precise value of 0.70947 ± 0.00010 reported by Vollmer (1976) for a rock from the same volcanic complex. We are currently investigating the problem of whether or not our samples are characterized by a unique initial $^{87}Sr/^{86}Sr$.

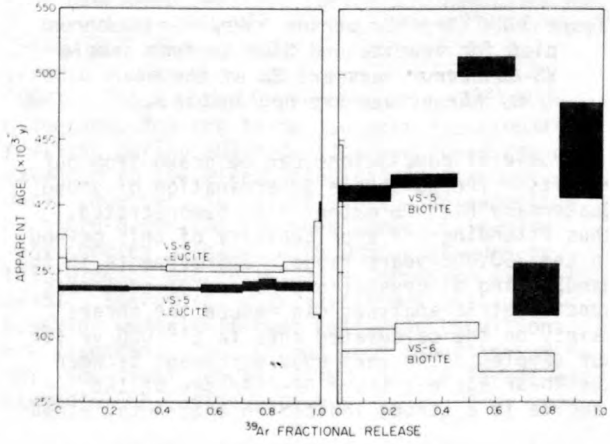

Figure 2.--Apparent age versus ^{39}Ar fractional release for leucites VS-6 and VS-5 and biotites VS-6 and VS-5. The data are corrected for trapped Ar of atmospheric composition. Errors shown are 2σ of the mean for mass spectrometric analyses only.

Table 2.--Analytical results

Sample no.	Rb (ppm)	Sr (ppm)	^{88}Sr (x10^{-8} nm/g)	$^{87}Rb/^{86}Sr$	$^{87}Sr/^{86}Sr$
VS-8, Biotite ----	628		340.0 ±0.11	5.0415	[1]0.71032±5
Leucite ----	1348		34.353±0.022	107.04	[1]0.71082±6
Age = 353,000±56,000 yr and $(^{87}Sr/^{86}Sr)_I$ = 0.71030±6					
VS-6, Leucite[2] ---	1236	34		104	
VS-3, Leucite[2] ---	1119	16		204	

[1]Errors are 2σ of the mean.
[2]Preliminary results.

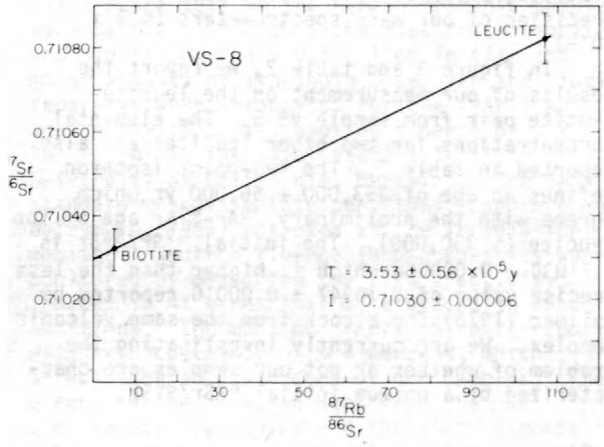

Figure 3.--$^{87}Sr/^{86}Sr$ versus $^{87}Rb/^{86}Sr$ isochron plot for leucite and biotite from sample VS-8. Error bars are 2σ of the mean. $^{87}Rb/^{86}Sr$ errors are negligible.

Several conclusions can be drawn from our results. The Rb-Sr age determination of young Quaternary high-Rb material is demonstrated, thus extending the applicability of this method to the 300,000-years range. Improvements in the handpicking of crystal grains and careful mass spectrometric analyses can reduce the uncertainty on the calculated ages to ±15,000 yr for our samples. The very good agreement between the Rb-Sr age and the ^{39}Ar-^{40}Ar age of the leucite is a strong indication that both methods yield realistic ages. A better control on the irradiation conditions can substantially reduce the uncertainty on the ^{39}Ar-^{40}Ar ages.

Our results show that correlations between different volcanic formations are possible, with a precision of better than 10,000 years for rocks at least as young as 300,000 years. The importance of precisely determined ages on volcanic rocks, where other stratigraphic criteria most often fail, is obvious. An important application is likely to be in the calibration of the geomagnetic chronological scale, where the resolution of the ^{39}Ar-^{40}Ar and the Rb-Sr methods can probably be brought close to the duration of a geomagnetic reversal.

Lanphere, M. A., and Dalrymple, G. B., 1965, P-207--An interlaboratory standard muscovite for argon and potassium analyses: Journal of Geophysical Research, v. 70, p. 3497-3503.

Papanastassiou, D. A., and Wasserburg, G. J., 1969, Initial strontium isotopic abundances and the resolution of small time differences in the formation of planetary objects: Earth and Planetary Science Letters, v. 5, no. 6, p. 361-376.

Steiger, R. H., 1964, Dating of orogenic phases in the Central Alps by K-Ar ages of hornblende: Journal of Geophysical Research, v. 69, no. 24, p. 5407-5421.

Vollmer, R., 1976, Rb-Sr and U-Th-Pb systematics of alkaline rocks; the alkaline rocks from Italy: Geochimica Cosmochimica Acta, v. 40, p. 283-295.

SELENIUM ISOTOPE FRACTIONATION DURING BACTERIAL SELENITE REDUCTION

By K. Rashid[1], H. R. Krouse[1], and R. G. L. McCready[2]
[1]Department of Physics
The University of Calgary
Calgary, Alberta
[2]Canada Agriculture
Lethbridge, Alberta

The fractionation of Se isotopes during chemical selenite reduction has been studied by several authors (Krouse and Thode, 1962; Rees and Thode, 1966; Webster, 1972). It was found that $^{76}SeO_3^=$ is typically reduced to elemental Se about 1.016 times faster than $^{82}SeO_3^=$. This agrees with a simple theoretical model whereby the rate-controlling step is the initial Se-O bond cleavage. Whereas Krouse and Thode (1962) found selenites in a number of ore deposits to be uniform in their $^{82}Se/^{76}Se$ abundance ratio, large variations were found for soil and plant samples. They concluded that isotopically selective biological processes were probably responsible for these variations.

Microbiological isotopic fractionation during selenite reduction was demonstrated by Zyakun and others (1974). They found that the elemental selenium precipitated within and outside of the biomass by the yeast Candida tropicalis was depleted in ^{82}Se with r values as high as 1.04, where r is defined as the ratio of

$$[^{76}Se/^{82}Se]_{biomass} \text{ to } [^{76}Se/^{82}Se]_{remaining\ solution}.$$

When these data are corrected to zero conversion, the $^{76}SeO_3^=$ is found to have reacted 1.02 times faster than the $^{82}SeO_3^=$, which is in agreement with data of the chemical reduction experiments. Reshetnikova (1975) found r values of 1.04 for the selenite reduction by Pseudomonas aeruginosa-71, Bacillus cereus-525, and Candida guilliermondii-2. Since the extent of conversion was not reported in this latter work, the ratio of the isotopic rate constants cannot be evaluated. In these studies the source of ions was $AgSeO_3$ heated above 200°C to release SeO_2, with measurements being performed on the SeO_2^+ species. The error of ± 0.01 quoted for r is quite large and resulted from the use of a single collector and the lack of a rapid standard-unknown comparison.

Despite difficulties in preparation, SeF_6 is preferable for analyses. Since fluorine has only one stable isotope, a number of selenium isotopes can be examined to ascertain the mass dependence of the conversion. We measured the most abundant SeF_5^+ species using a multiple collector. δ values are defined in terms of ^{76}Se, for example

$$\delta^{82}Se = \left\{ \frac{[^{82}Se/^{76}Se]_{Se\ product}}{[^{82}Se/^{76}Se]_{INITIAL\ SeO_3^=}} - 1 \right\} \times 10^3$$

Errors in the δ values are typically ± 0.5 permil standard deviation.

Six different Salmonella sp. were found to reduce $^{76}SeO_3^=$ faster with $\delta^{82}Se$ values ranging from -5 to -40 permil. The less negative values probably correspond to a step with negligible isotopic selectivity competing with the initial Se-O bond cleavage for rate control. An analogous argument was used by Harrison and Thode (1958) in connection with microbiological sulphate reduction studies. On the other hand, it appears that the microbiological isotopic selectivity can be greater than that identified with the initial Se-O bond rupture. The results are not surprising in that similar observations are noted with sulphur isotopes during $SO_3^=$ reduction. Whereas κ_{32}/κ_{34}, the ratio of rate constants identified with S-O bond rupture, is 1.022 (Harrison and Thode, 1957), values up to 1.05 have been realized during $SO_3^=$ reduction by S. cerevisiae (Kaplan and Rittenberg, 1964; McCready and others, 1974) and Salmonella spp. (Krouse and others, 1967; Krouse and Sasaki, 1968). These authors proposed a number of explanations for the large isotopic fractionations realized during $SO_3^=$ reduction and these can be extended to the microbiological $SeO_3^=$ reduction data. However, in recent years, $SO_3^=$ reduction by micro-organisms has been shown to involve very complex pathways with processes such as thiosulphate and trithionate formation (Siegel, 1975). Therefore, wide variations in isotopic behavior under different culturing conditions are expected. The $SO_3^=$ and $SeO_3^=$ reductions differ; the final product is H_2S in the former and elemental Se in the latter.

Preliminary data in our laboratory also show that Clostridium pasteurianum favors the lighter selenium isotopes during $SeO_3^=$ reduction. Therefore, the point has been reached where selenium isotope selectivity during $SeO_3^=$ reduction has been demonstrated for numerous organisms in the laboratory and presumably this fractionation occurs in nature.

Harrison, A. G., and Thode, H. G., 1957, The kinetic isotope effect in the chemical reduction of sulphate: Faraday Society Transactions, v. 53, p. 1648-1651.

_____1958, Mechanism of bacterial reduction of sulphate from isotope fractionation studies: Faraday Society Transactions, v. 54, p. 84-92.

Kaplan, I. R., and Rittenberg, S. C., 1964, Microbiological fractionation of sulfur isotopes: Journal of General Microbiology, v. 34, p. 195-212.

Krouse, H. R., and Thode, H. G., 1962, Thermodynamic properties and geochemistry of isotopic compounds of selenium: Canadian Journal of Chemistry, v. 40, p. 367-375.

Krouse, H. R., McCready, R. G. L., Husain, S. A., and Campbell, J. N., 1967, Sulfur isotope fractionation by Salmonella sp.: Canadian Journal of Microbiology, v. 13, p. 21-25.

Krouse, H. R., and Sasaki, A., 1968, Sulphur and carbon isotope fractionation by Salmonella heidelberg during anaerobic sulphite reduction in trypticase soy broth medium: Canadian Journal of Microbiology, v. 14, p. 417-422.

McCready, R. G. L., Kaplan, I. R., and Din, G. A., 1974, Fractionation of sulfur isotopes by the yeast Saccharomyces cervisiae: Geochimica Cosmochimica Acta, v. 38, p. 1239-1253.

Rees, C. E., and Thode, H. G., 1966, Selenium isotope effects in the reduction of sodium selenite and of sodium selenate: Canadian Journal of Chemistry, v. 44, p. 419-427.

Reshetnikova, I. A., 1975, Fractionation of selenium isotopes by bacteria and yeasts: Vestnik Moskovskoga Universiteta Biologija, v. 30, no. 3, p. 119-120.

Siegel, L. M., 1975, Biochemistry of the sulfur cycle, in Greenberg, P. M., ed., Metabolic pathways VII--metabolism of sulfur compounds: New York, Academic Press, p. 217-286.

Webster, Jr., C. L., 1972, Selenium isotope analysis and geochemical applications: Colorado State University, Ph.D. thesis.

Zyakun, A. M., Reshetnikova, I. A., Matrosov, A. G., and Eroshin, V. K., 1974, Fractionation of selenium isotopes by the yeast Candida tropicalis: Dokl. An. SSSR 215, no. 2, p. 478-482.

HYDROGEN AND CARBON ISOTOPES IN COALS AND KEROGENS

By C. Redding
Federal Institute for Geosciences and Natural Resources, Hannover, Germany

The range of carbon isotope ratios in coals and kerogens, and to some extent the processes affecting their isotope fractionations, has long been established. However, very little work has been done on the hydrogen isotope ratios. In the present study, 24 coals of various origins and a similar number of kerogens have been analyzed for both carbon and hydrogen isotope ratios in an attempt to determine the role of hydrogen isotope fractionation in ancient organic matter. The coals were prepared by heating them to 100°C for 12 hours at a pressure of 100 torr to remove adsorbed water. The kerogens were treated in both hydrochloric and hydrofluoric acid baths to remove calcite and silicate minerals and the organic material was further separated from the inorganic material by heavy liquid techniques.

All samples were oxidized at 1000°C in a stream of oxygen and passed over copper oxide at 850°C to assure complete combustion. Plots of D/H isotope ratios with wetness and ash contents show that the measured isotope ratios are not due to adsorbed or to structural water. All values are reported in the usual form where

$$\delta^{13}C = \left(\frac{^{13}C/^{12}C\ (\text{sample})}{^{13}C/^{12}C\ (\text{standard})} - 1\right) \times 1000$$

and

$$\delta D = \left(\frac{D/H\ (\text{sample})}{D/H\ (\text{standard})} - 1\right) \times 1000$$

All carbon isotope results are compared to PDB (Craig, 1957) and all hydrogen results to SMOW (Craig, 1961). Reproducibility (1σ) of double oxidations is greater than 0.2 permil (kerogens) and 0.4 permil (coals) for carbon and 2.2 permil (kerogens) and 3.7 permil (coals) for hydrogen.

The measured isotope values are:

Kerogens

$\delta^{13}C_{PDB}$ -23.2 to -30.4 permil

δD_{SMOW} -58.7 to -111.6 permil

Coals

$\delta^{13}C_{PDB}$ -23.2 to -27.1 permil

δD_{SMOW} -65.2 to -153.8 permil

The kerogens are all low-maturity samples (R_o = 0.3 percent) and were taken from drill samples at depths of less than 60 m. They were sampled at different distances from the paleocoast and, therefore, should be a sample series that grades from a terrestrial into a progressively marine milieu. This is true for the n-alkane distribution of the extractable material; however, the kerogens are composed almost exclusively of terrestrial organic material (P. Flekken, written commun.) and are not intimately related to their extracts.

The coal samples are of different ranks (R_o = 0.25 to 4.8 percent) and of different origin. Six samples came from an open pit mine from northeastern West Germany (Meissner) and were sampled at distances of a few cm to somewhat less than 5 m from a basalt sill. Previous work has shown that no correlation exists between $^{13}C/^{12}C$ isotope ratios and either age or maturity (Degens, 1969; Wickman, 1953, 1956). However, mass balance calculations indicate that thermally produced hydrogen isotope fractionation should be detectable, if present, due to the much smaller size of the hydrogen reservoir and its more rapid depletion. A Rayleigh fractionation calculation using a fractionation of 308 permil (Chung, 1976; W. M. Sackett, written commun.) for methane cracked from coal shows a hydrogen isotope fractionation of approximately 24 permil for the highest rank of coal investigated (R_o = 4.8 percent). The fractionation factor was determined at 500°C to be 147.9 permil using the data of Chung (1976) and measurements from BGR laboratories. This value was extrapolated to 100°C using W. M. Sackett's (written commun.) data for n-octadecane at 400° and 500°C and assuming that the fractionation for n-octadecane also applies to coals and that the fractionation observed between 400° and 500°C can be linearly extrapolated. This fractionation factor is only a rough estimate and are not meant to be taken as a precise value. If this fractionation factor is approximately correct, then catalysis accounts for a small part of the isotopic fractionation observed in coals. This is in agreement with the Meissner and other published data (Simoneit and others, in press); although the Meissner data indicates that the fractionation factor for coals should be somewhat larger than 308 permil. Furthermore, these data indicate a very inhomogeneous hydrogen composition for coals samples over short distances and presumably having the same original composition. This tends to rule out ground water exchange.

The kerogen data have hydrogen isotope ratios that are comparable to the humic acid fraction of plants using the Calvin Photosynthetic Cycle (Nissenbaum, 1973). This is also partially true of the coal data, although the hydrogen isotope ratios of these samples are more negative than previously published humic acid data (Nissenbaum, 1973). The carbon isotope data tends to be more scattered and to resemble soil acids. These data, when combined with the lack of a positive correlation between carbon and hydrogen isotope ratios, demonstrate that the carbon and hydrogen fractionation pathways, although not well understood, are probably different.

Chung, M., 1976, Isotope fractionation during the maturation of organic matter: Texas A. and M. University, Ph.D. thesis.

Craig, H., 1957, Isotopic standards for carbon and oxygen and correction factors for mass-spectrometric analysis of carbon dioxide: Geochimica Cosmochimica Acta, v. 12, p. 133-149.

_____1961, Standard for reporting concentrations of deuterium and oxygen-18 in natural waters: Science, v. 133, no. 3467, p. 1833-1834.

Degens, E. T., 1969, Biogeochemistry of stable carbon isotopes; in Eglington, G., and Murphy, M. T. J., Organic Geochemistry: Berlin, Springer Verlag, Heidelberg.

Nissenbaum, A., 1973, The organic geochemistry of marine and terrestrial humic substances -Implication of carbon and hydrogen isotope studies: Actes du 6e Congres International de Geochimie Organique.

Simoneit, B. R. T., Brenner, S., Peters, K. E. and Kaplan, I. R., in press, Thermal alteration of Cretaceous black shale by basaltic intrusion at Deep Sea Drilling Project Site 41-368 in the Eastern Atlantic Ocean: American Association of Petroleum Geologists Bulletin.

Wickman, F., 1953, Wird das Haufigkeitsverhaltnis der Kohlenstoffisotopen bei der Inkohlung verändert?: Geochimica Cosmochimica, Acta, v. 3, p. 244-252.

_____1956, The cycle of carbon and the stable carbon isotopes: Geochimica et Cosmochimica Acta; v. 9, p. 136-153.

Nd AND Sr SYSTEMATICS IN OPHIOLITES

By P. Richard, D. Rousseau, and C. J. Allegre
Laboratoire de Géochimie et Cosmochimie - LA 196
Institut de Physique du Globe et Département des
Sciences de la Terre - Universités de Paris VI
et VII - 4, Place Jussieu 75230 Paris Cedex 05

INTRODUCTION

We have used Nd and Sr isotopic ratios in an attempt to understand the origin of ophiolite complexes.

These complexes, which are composed of pillow-lavas, dolerites, gabbros, ultramafic cumulates, and tectonized harzburgites, are generally supposed to have an oceanic origin. However, the geologic setting of their place of origin is unclear. It could be either typical ocean floor, or marginal seas and island arcs, or even intracontinental rift zones.

The Nd isotopic ratio, which has recently gained wide use in the study of terrestrial rocks, is a very good petrogenetic tracer, especially when used with the Sr isotopic ratio (De Paolo and Wasserburg, 1976 a,b; Richard and others, 1976; O'Nions and others, 1977; Hawkesworth and others, 1977; Carter and others, 1978).

EXPERIMENTAL PROCEDURE

For Nd analyses the chemical technique has been previously described in Richard and others, 1976. For mass spectrometery we are now running neodynium with the triple-filament technique--the sample is loaded in a chloride form onto tantalum lateral filaments and ionized by a rhenium central filament. Following the method of De Paolo and Wasserburg, we normalize the $^{143}Nd/^{144}Nd$ ratio using $^{146}Nd/^{144}Nd = 0.724118$ as reference.

RESULTS AND DISCUSSION

Ophiolite Complexes

We have studied different complexes: the Papua-New Guinea series, the Insecca series (Corsica), the well-known Vourinos complex (Greece), the Pindos series, the Oman ophiolites, the Newfoundland ophiolites, the Troodos complex (Cyprus), and the Permian Toba complex (Japan).

For these massifs we have chosen to study only the gabbroic members of the ophiolite series because gabbros are the least contaminated by seawater and the least transformed by metamorphism. Analytical data are presented in figure 1.

All the gabbros give positive ε_{Nd}. Systematic compilation of available data on different types of oceanic rocks (De Paolo and Wasserburg, 1976; O'Nions and others, 1977; Allegre and others, unpublished data) indicated (fig. 1) that Newfoundland ophiolite-gabbro can be compared to MOR tholeiites (but its low ε_{Nd} is also due to the radioactive decay of Sm since its emplacement, 480 m.y. ago). By contrast, the Vourinos complex does not have a tholeiitic ε_{Nd}. Between these two extremes the other complexes have no clear character, and can be compared to any kind of basalt--MOR tholeiite, oceanic island basalts, or island arc basalts. We, therefore, assume that ophiolites may have been created in different oceanic zones. This is in agreement with the trace element study of Noiret and others (unpublished data), and studies of microfabrics and stress.

In the (ε_{Nd}, ε_{Sr}) diagram illustrated in figure 1, the ophiolitic gabbros generally lie off the correlation line. We suppose that ε_{Sr} is too high compared with ε_{Nd} and we explain this by isotopic equilibration of the Sr between the ophiolite complex and seawater.

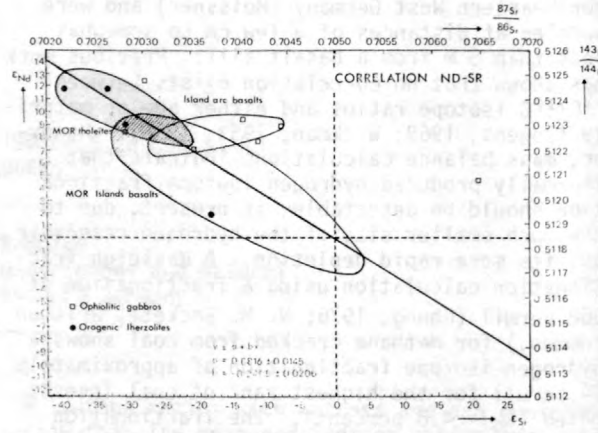

Figure 1.--Position of the ophiolitic gabbros in the Nd-Sr correlation diagram.

Carter, S. R., Evensen, N. M., Hamilton, P. J., and O'Nions, R. K., 1978, Continental volcanics derived from enriched and depleted source regions. Nd and Sr isotopes evidence: Earth and Planetary Science Letters, v. 37, p. 401-408.

De Paolo, D. J., and Wasserburg, G. J., 1976a, Nd isotopic variations and petrogenetic models: Geophysical Research Letters, v. 13, no. 5, p. 249-252.

_____1976b, Inferences about magma sources and mantle structure from variations of $^{143}Nd/^{144}Nd$: Geophysical Research Letters, v. 3, no. 12, p. 743-746.

Hawkesworth, C. J., O'Nions, R. K., Pankhurst, R. J., Hamilton, P. J., and Evensen, N. M., 1977, A geochemical study of island arc- and back-arc tholeiites from the Scotia Sea: Earth and Planetary Science Letters, v. 36, p. 253-262.

O'Nions, R. K., Hamilton, P. J., and Evensen, N. M., 1977, Variations in $^{143}Nd/^{144}Nd$ and $^{87}Sr/^{86}Sr$ ratios in oceanic islands: Earth and Planetary Science Letters, v. 34, p. 13-22.

Richard, P., Shimizu, N., and Allegre, C. J., 1976, $^{143}Nd/^{146}Nd$ a natural tracer--an application to oceanic basalts: Earth and Planetary Science Letters, v. 31, p. 269-278.

THE LENGTH OF THE DEVONIAN PERIOD

By John R. Richards
Research School of Earth Sciences
Australian National University
PO Box 4, CANBERRA, A.C.T.

Current estimates for the base of the Devonian (Armstrong's computer fit) are in reasonable accord with a 409 ± 3 m.y. K-Ar age on a rock which intrudes sediments reasonably accorded a Ludlovian Age, and is overlain by sediments containing a good middle Siegenian fauna.

However, Armstrong's upper boundary should be extended upwards, possibly to as young as 350 m.y. Older estimates for this boundary seem to depend heavily on the allocation of the Victorian Cerberean Volcanics to the very Late Devonian. The present estimate by Victorian palaeontologists is that the relevant fish (Bothryolepus ?), for which the latest K-Ar measurements give an age of 367 m.y., should be ascribed to somewhere in the Frasnian. Therefore, other estimates for the age of the upper Famennian should take precedence.

GRANITOID AGES IN A PALAEOZOIC BACK-ARC BASIN

By J. R. Richards[1] and O. P. Singleton[2]
[1]Research School of Earth Sciences
Australian National University
Canberra
[2]Department of Geology
University of Melbourne

The Palaeozoic stratigraphic section of Victoria, Australia, is dominated by a thick sequence of shallow marine sedimentary rocks, which, in the central portion of the State, are shown to be of Ordovician age by a very well-developed graptolite sequence (Douglas and Ferguson, 1976). The absence of graptolites to the west suggests a possible Cambrian age. Precambrian continental craton lies further west, in South Australia. The eastern margin of the present continent is distinguished by a meridional sequence of granitoid intrusions of dominantly Silurian - Devonian age. These igneous rocks are well developed to the north in New South Wales and are considered to represent a mid-Palaeozoic island arc system, which continues southward into eastern Victoria.

Development of this arc was accompanied by regional metamorphism of the already existing Ordovician sediments, and by tectonic deformation in the back-arc basin further west. The deformation resulted in a central trough (the Melbourne Trough) in which sedimentation continued at least until the Middle Devonian, and in a series of narrow meridional ridges in which underlying shallow-water, Cambrian, basalts are exposed. No exposure of older basement rocks is known in Victoria.

Granitoid intrusions occur throughout the whole State. There is some stratigraphic

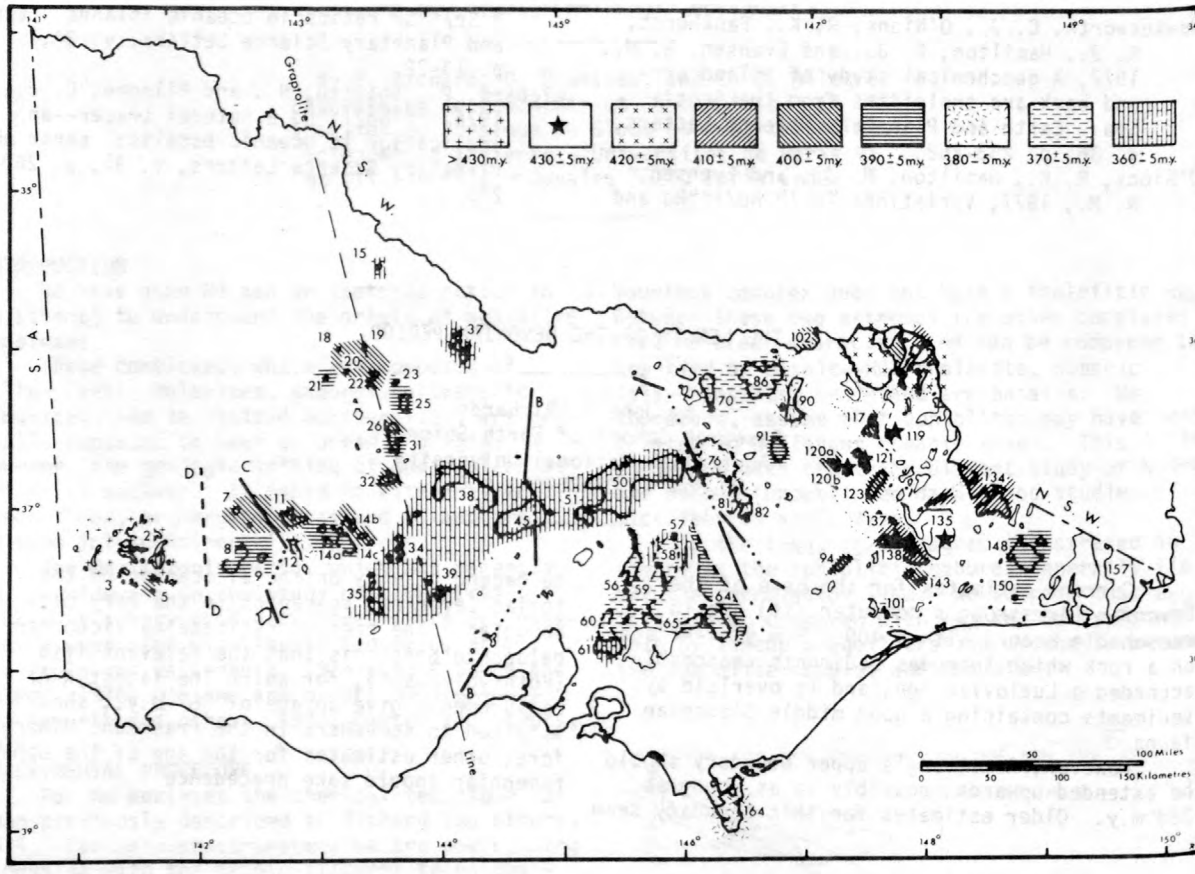

Figure 1.--Results of a K-Ar dating survey in Victoria, Australia.

control on ages in central and eastern Victoria, enough to predict that the intrusions should range in age from post-Middle Ordovician pre-Middle Silurian right through to Late Devonian. Some of the latter, in central Victoria, are associated with felsic volcanic cauldrons. The only control in the west is that the granitoids intrude the lower Palaeozoic sediments, and are overlain in some areas by Cainozoic sediments.

The results of a K-Ar dating survey are summarized in figure 1. Two generations of argon spike have been employed. The data on central and eastern Victoria were obtained with an old Berkeley spike preparation system and carry 95-percent confidence limits of approximately ± 16 m.y. Those to the west were dated with spikes prepared by gas pipette, with 95-percent confidence limits around ± 6 m.y. The very marked age pattern in western Victoria has been confirmed by Rb-Sr dating on whole rocks and separated micas from eight selected sites. All dates have been calculated according to the new decay constant convention.

The lack of any age discordance between the two methods suggests a simplicity in the tectonic history within the basin, and that the actual intrusive ages are being displayed, at least in the western half of the State. The pattern in the east is distinctly more complicated. In the west, it would seem that consolidation and granitoid intrusion takes place in blocks which succeed each other in the same sense as the advancing front of sedimentation, but after an interval of at least 100 m.y. following deposition.

Major-element content and petrographic character, when examined from the viewpoint of White and Chappell (1977), suggest that some but not all of these granitoids could have been derived by partial melting of parent material similar to the intruded sediments (S magma-type); others, of I magma-type, would seem to have other derivation. It seems significant that the empirical chemical function of Shaw (1972) provides evidence suggesting presence of paragneiss only in the vicinity of the regional metamorphic zone of eastern Victoria.

Acknowledgements are due to I. McDougall and W. Compston for access to calibrated spikes and equipment. Some of the measurements in central Victoria were made by I. McDougall.

Douglas, J. G., and Ferguson, J. A., eds., 1976, Geology of Victoria: Geological Society of Australia, Special Publication 5, 528 p., plus map.
Shaw, D. M., 1972, The origin of the Apsley Gneiss, Ontario: Canadian Journal of Earth Sciences, v. 9, p. 18-35.
White, A. J. R., and Chappell, B. W., 1977, Ultrametamorphism and granitoid genesis: Tectonophysics, v. 43, p. 7-22.

APPLICATION OF GEOCHRONOLOGIC DATING TECHNIQUES IN FAULT INVESTIGATIONS FOR NUCLEAR POWER PLANTS

By Gary A. Robbins and Richard W. Turnbull
Office of Standards Development
U. S. Nuclear Regulatory Commission
Washington, D.C. 20553

Geochronologic dating is employed in two phases of the geologic site evaluation for nuclear power plants. First, it is used as an aid in the unraveling of the tectonic history of a region and in the correlation of site geology with the regional tectonic framework. Second, geochronologic dating is used in the assessment of the age of movement on a particular fault. Both of these applications are important in the evaluation of the safety significance of faults found in the vicinity of a site.

In the United States, geologic and seismic investigations that are required for nuclear power plant site evaluations are listed in the U.S. Nuclear Regulatory Commission's Regulation, Appendix A to 10 CFR Part 100, "Seismic and Geologic Siting Criteria for Nuclear Power Plants." In the regulation the term "capable fault" is defined to provide a standard for assessing the activity, safety significance, and design impact of faults with respect to ground rupture and the localization of earthquakes. Two of the criteria that characterize a capable fault and depend upon geochronologic dating are: (1) the fault has exhibited movement at least once in the past 35,000 years; and (2) the fault has exhibited movement of a recurring nature within the past 500,000 years.

The ages specified in the regulation were based on the age ranges of radiometric-dating techniques. The 35,000 years represented the upper limit of radiocarbon dating; the 500,000 years represented the lower limit of potassium-argon dating. The ages are not based conclusively on geological observation, hypothesis, or theory that can be used to discriminate active from inactive faults, and in light of existing data the rates of fault activity seem extremely low (fig. 2, Slemmons, 1977).

"Absolute" dating techniques are employed when stratigraphic, paleontologic, or regional tectonic controls establishing the age of last fault movement are absent or tenuous. Ages are obtained either from material in a fault zone or from material immediately adjacent to a fault. Situations are encountered that do not permit the standard application of dating techniques because of the nature of the materials and the limitations in the techniques themselves. In some instances we permit the use of novel age-dating techniques; in others we permit the use of techniques that must be extended to their limit of reliability. The use of fluid-inclusion data obtained from undeformed minerals in fault zones, along with estimates of rates of

Table 1.--Geochronologic methods used in dating faults in the geologic investigations of nuclear power plant sites

Method	Number of sites[1] employed
1. Potassium-Argon	20
2. Radiocarbon	11
3. Pedogenic soil development	9
4. Weathering rates	7
5. Saprolite development	7
6. Erosion (denudation) rates	6
7. Fluid inclusion analysis	6
8. Paleomagnetism	6
9. Rubidium-Strontium	5
10. Amino acid	4
11. Uranium series	2
12. Sedimentation rates	2
13. Fission track	2
14. Tephrochronology	1
15. Lead isotopes	1

[1]Sites refers to locations which may contain one or more plants. The location of faults investigated ranges from the immediate vicinity of sites to tens of kilometers away.

uplift, rates of denudation, and pressure-temperature conditions, is an example of a novel age-dating technique. The dating of zeolites with the potassium-argon method is an example of extending a technique to its limit of reliability. In situations where novel approaches are applied or standard techniques are extended to their limit of reliability, the "absolute" ages that are obtained are not considered conclusive without other corroborative data: the consistency of the ages with those derived from other data, as well as with ages obtained using other dating methods.

Information has been examined from 44 nuclear power plant sites which faults were investigated. For 32 of the 44 sites, "absolute" dating methods were employed to date fault movement; relative-dating techniques were employed at the remaining sites. For 21 sites, two or more "absolute" age methods were used. Table 1 lists the dating techniques that were used to try to establish the "absolute" age of fault movement. Potassium-argon dating followed by radiocarbon dating are the two conventional techniques most often used. Substantial use has also been made of age estimates based on geologic and chemical rate processes. At all sites in which "absolute" techniques were employed, the assessment of the age of last fault movement included consideration of other information, such as stratigraphic correlations, structural relationships, and regional tectonic history.

In order to assure that the best approaches are brought to bear on this important aspect of the geologic evaluation of nuclear power plant sites, the Office of Standards Development of the USNRC is sponsoring the preparation of a state-of-the-art report on approximately 18 dating techniques. Based on the report and experience gained in the licensing of nuclear power plants, a regulatory guide will be developed which describes generally acceptable dating methods for determining the age of movement on faults. The regulatory guide is scheduled for completion in November 1979.

Slemmons, D. B., 1977, Faults and earthquake magnitude, Report 6 of State-of-the-art for assessing earthquake hazards in the United States: U.S. Army Corps of Engineers, Waterways Experiment Station Miscellaneous Paper S-73-1.

SULPHATE-WATER AND -H_2S ISOTOPIC THERMOMETRY IN THE NEW ZEALAND GEOTHERMAL SYSTEMS

By Brian W. Robinson
Institute of Nuclear Sciences, Department of Scientific and Industrial Research,
Lower Hutt, New Zealand

Sulphate (and bisulphate) ions occurring in geothermal discharges can be analyzed for both their sulphur and oxygen isotopic compositions. Isotopic equilibration with the H_2S and H_2O of the fluids produces temperature-dependent fractionations which make two geothermometers, sulphate-H_2S and sulphate-water, practicable.

Laboratory calibrations of oxygen isotope fractionation between sulphate and water have been executed in the hydrothermal temperature range (fig. 1; Kusakabe, 1974). These experiments were chiefly conducted in the acid pH range but geothermal fluids are normally close to neutral. Sakai (1977) preferred to use the $BaSO_4$-H_2O isotope calibration curve to approximate the $SO_4^{=}$-H_2O system in geothermal fluids. This study, however, uses the HSO_4^{-}-H_2O calibration curve shown in figure 1.

The experimentally determined sulphur isotopic fractionation factors for sulphate-H_2S are shown in figure 2 (see also Robinson, 1978). The best-fit line through all the data points is used to obtain the equation used here.

The calibration curves can be more rigorously applied to natural systems if the

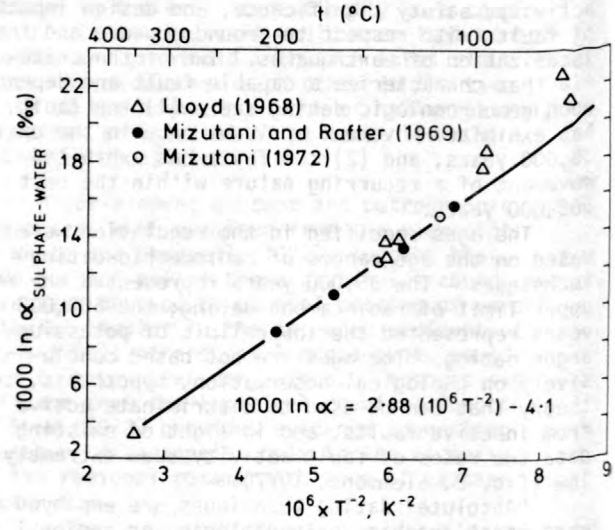

Figure 1.--Oxygen isotope fractionation between sulphate and water as a function of temperature.

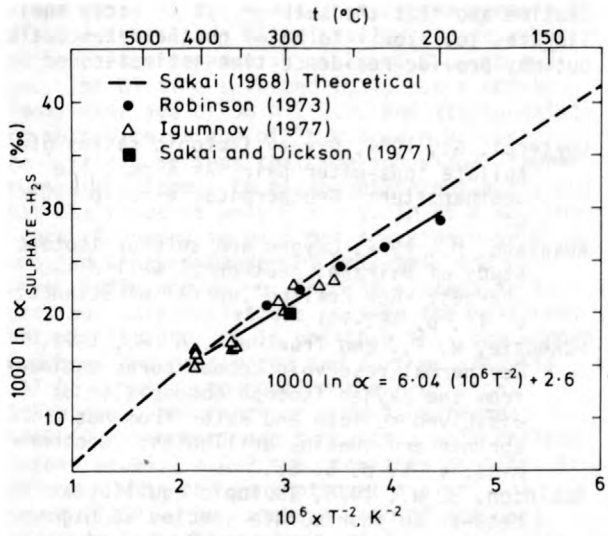

Figure 2.--Sulphur isotope fractionation between sulphate and H_2S as a function of temperature.

kinetics of the isotope exchange reactions are also known. The rate of oxygen isotope exchange between sulphate and water is both pH and temperature dependent (Cortecci, 1974). At pH 6, 97 percent equilibrium (5 x $t_{\frac{1}{2}}$) is achieved in about 0.5 years at 300°C and in about 4 years at 200°C. Exchange is exceedingly slow at lower temperatures and higher pH values. Sulphur isotope exchange between sulphate and H_2S is also a function of pH and temperature, as well as the ΣS concentration in the fluids (Robinson, 1978). The reaction rates are slower than those for the oxygen exchange; at pH 6 and ΣS 10^{-4} mol kg^{-1}, 97 percent equilibrium requires about 5 years at 300°C and 5 x 10^5 years at 200°C.

The first applications of sulphur and oxygen isotope thermometry to geothermal fluids were made on the New Zealand geothermal systems of the Taupo volcanic zone and the Ngawha hot springs, 400 km to the northwest. Following worldwide applications (Cortecci, 1974; McKenzie and Truesdell, 1977; Sakai, 1977), the New Zealand systems are now being more extensively investigated. Table 1 shows typical analyses for samples from the active volcanic environment (Giggenbach and Robinson, written commun.). Because of the high sulphate and hydrogen ion concentrations, isotopic exchange is very rapid and the sulphate $\delta^{18}O$ values can represent equilibrium with the water down to about 100°C. In addition, the Ruapehu and White Island samples have also very positive $\delta^{34}S$ values, indicating a movement towards equilibrium with reduced sulphur. The Ketetahi $\delta^{34}S$ values are identical to those for the H_2S and represent sulphate formation by complete oxidation of H_2S at the surface.

The most recent isotopic analyses for the Wairakei system (Kusakabe, 1974; M. K. Stewart, oral commun.) are shown, as averages, in table 2 for the low, intermediate, and high enthalpy wells representing conditions of steam loss, deep chloride water, and steam gain, respectively. The oxygen isotope temperatures (error ±20°C) are close to the measured downhole temperatures of around 260°C. However, the higher sulphur isotope temperatures reflect either a lack of equilibrium or hotter conditions at greater depth. For the deep chemical conditions (ΣS 5 x 10^{-4} mol kg^{-1}, pH 6.5, 260°C) the oxygen isotopes would equilibrate in about 1 year, but the sulphur species would take about 10^3 years to reach the 70 percent equilibrium observed at 260°C from a common sulphur origin.

Table 1.--Average isotopic analyses (permil relative to CDT for S and SMOW for O) from Ruapehu crater lake and hot springs of White Island and Ketetahi

	pH	Sulphate			Water
		g/kg	$\delta^{34}S$	$\delta^{18}O$	$\delta^{18}O$
Ruapehu ---	∿1.1	5-10	+18.3	+19.6	+2.0
White Island --	∿1.4	6-10	+ 6.6 to +20.4	+11.4 to +21.9	+2.9 to +8.2
Ketetahi --	∿3.6	0.6	+ 3.3	+ 8.1	+4.2

Table 2.--Average isotopic analyses for the Wairakei system

Well Enthalpy	H_2S	Sulphate			Deep H_2O	Temp. (°C)	
	$\delta^{34}S$	$\delta^{34}S$	mg/kg	$\delta^{18}O$	$\delta^{18}O$	Sulphur	Oxygen
Low -----	+4.6	+23.3	∿30	-1.3	-5.7	340	310
Medium --	+5.2	+22.1	∿30	-1.5	-5.7	380	320
High ----	+4.8	+14.8	∿10	-0.8	-5.7	500	290

Analyses from the Broadlands-Ohaki region (table 3) give lower oxygen isotope temperatures than the measured downhole temperatures of around 270°C. In the intermediate enthalpy wells the sulphate content is higher than at Wairakei and addition of near-surface sulphate may occur. For the high enthalpy wells, with high H_2S and low $SO_4^{=}$ contents, any near-surface and surface sampling contamination by H_2S oxidation is more critical and lower indicated temperatures occur. Moreover, the $\delta^{34}S$ sulphate values are lower than those for the H_2S, indicating a kinetic isotope effect during sulphate formation. The intermediate enthalpy wells only display about 3 percent sulphur isotopic equilibrium. For the deep chemical conditions (ΣS 4 x 10^{-3} mol kg^{-1}, pH 6, 270°C) this would have been achieved in about 1 year, after which time

Table 3.--Average isotopic analyses for the Broadlands-Ohaki system

Well Enthalpy	H_2S	Sulphate			Deep H_2O	Oxygen
	$\delta^{34}S$	$\delta^{34}S$	mg/kg	$\delta^{18}O$	$\delta^{18}O$	T(°C)
Inter-mediate --	+5.8	+6.5	∿60	+3.0	-4.0	240
High -------	+5.5	+0.7	∿ 5	+9.6	-4.0	120

the oxygen isotopes would be over 97 percent equilibrated. The shorter indicated residence times probably reflect the fact that the Broadlands wells draw above the boiling zone compared to those at Wairakei which draw below this zone.

The Ngawha hot spring samples (table 4) show a complete lack of sulphur isotopic equilibrium in the pools and a shallow well, but samples from Bore 1 indicate a temperature of 300 ± 10°C compared to a measured downhole temperature of 240°C at 590 m. Also, the $\delta^{18}O$ sulphate values would indicate temperatures in excess of 300°C, but the high sulphate concentrations suggest near-surface contamination and spurious results.

Further sampling is being made at the Kawerau and Waiotapu geothermal areas. It is, however, apparent that the oxygen isotope geothermometer must be applied with great caution and that the sulphur system often equilibrates too slowly to be of geothermetric value but may provide residence time estimates.

Table 4.--Average isotopic analyses from Ngawha

	H_2S	Sulphate			Water	Sulphur
	$\delta^{34}S$	$\delta^{34}S$	mg/kg	$\delta^{18}O$	$\delta^{18}O$	T(°C)
Warm pools --	+2.4	+ 3.1	~300	+1.8	-1.5	-
Hot well ----	+2.2	+ 4.0	100	+2.6	+2.2	-
Bore 1 ------	-1.0	+20.0	30	-	-	300

Cortecci, G., 1974, Oxygen isotopic ratios of sulfate ions-water pairs as a possible geothermeter: Geothermics, v. 3, p. 60-64.

Kusakabe, M., 1974, Oxygen and sulphur isotope study of Wairakei geothermal well discharges: New Zealand Journal of Science, v. 17, p. 183-191.

McKenzie, W. F., and Truesdell, A. H., 1977, Geothermal reservoir temperatures estimated from the oxygen isotope composition of dissolved sulfate and water from hot springs and shallow drillholes: Geothermics, v. 5, p. 51-61.

Robinson, B. W., 1978, Isotopic equilibria between sulphur solute species at high temperature, in Robinson, B. W., ed., Stable Isotopes in the Earth Sciences: New Zealand Department of Scientific and Industrial Research Bulletin, v. 220, p. 203-206.

Sakai, H., 1977, Sulfate-water isotope thermometry applied to geothermal systems: Geothermics, v. 5, p. 67-74.

^{40}Ar-^{39}Ar DATA ON THE DISTRIBUTION OF ARGON IN BIOTITES WITH EXCESS ARGON

By J. C. Roddick
Department of Earth Sciences
University of Leeds, Leeds, England

One of the potential uses proposed for the ^{40}Ar-^{39}Ar age spectrum technique was the identification and correction for excess ^{40}Ar in rocks and minerals. However, a study by Lanphere and Dalrymple (1976) has shown that the application of ^{40}Ar-^{39}Ar dating is not able to resolve completely the excess argon from the radiogenic component. Saddle-shaped age spectra were obtained while isochron plots produced a scatter of data points. Recently, however, Roddick (1978) has indicated that the isochron data points of Lanphere and Dalrymple (1976) were probably contaminated with extraction-system argon and the scatter could be the result of this contamination.

Consider a simple model of crystallization where, as a mineral becomes closed to argon diffusion, it incorporates any excess ^{40}Ar and also any ^{36}Ar present in the environment. This initial argon will be in isotopic equilibrium and the ^{40}Ar and ^{36}Ar will occupy identical sites. Subsequent step-heating should result in the evolution of mixtures, in various proportions, of two components - the initial argon and the radiogenic component. An isochron plot of an irradiated sample would produce a linear array with an intercept of initial-argon composition and slope proportional to age.

One of the most critical requirements of the isochron treatment is the control of and correction for extraction-system atmospheric argon (Hayatsu and Carmichael, 1977; Roddick, 1978). Two large samples (0.3 gms) of biotite containing excess argon have been analyzed by ^{40}Ar-^{39}Ar step-heating in a low-blank (~ 1 x 10^{-9}cc ^{40}Ar) extraction furnace. The results do not show saddle-shaped spectra, nor do they indicate a simple mixture of two argon components.

The first sample is a metamorphic biotite from the Eastern Alps, previously analyzed by

Brewer (1969). He showed that over a large area of the Austroalpine Altkristallin excess argon had been incorporated in micas at 80 - 65 m.y. ago. The biotite selected (L61) has a conventional K-Ar age of 98 ± 1 m.y. and its co-existing muscovite an age of 78.9 ± .8 m.y. In figure 1 it may be seen that the individual temperature steps appear to define different ages, but that the range is only 0.7 m.y. in 99 m.y. The errors (2 sigma) in each gas fraction have been computed as recommended by Dalrymple and Lanphere (1971) and do not include systematic errors, but only analytic errors in the measured isotopic ratios. It is possible that the errors have been underestimated and further analysis will be required to confirm the precision. In either case, the range of ages is extremely small (0.7 percent) and suggests a well-defined plateau at 99.7 ± 0.2 m.y. for this biotite, in agreement with the conventional analysis of Brewer (1969). An isochron plot of the data, corrected for system blank, yields a well-fitting isochron with the same age.

The second biotite (3520), from a granite gneiss of the Eastern Tauern Window, Austrian Alps, was suspected to contain excess argon, because the conventional K-Ar age is 19.2 m.y. but the co-existing muscovite has an age of 16.5 m.y. - a reverse of the usual metamorphic cooling-age pattern. In addition, biotites within 1 km have Rb-Sr ages of 17 m.y. Figure 2 indicates that the pattern is approximately flat, with the ages ranging from 19.1 m.y. to 19.5 m.y. for 95 percent of the gas. However, there is a slight systematic increase in the age with increasing temperature--a pattern similar to that resulting from a high degree of diffusion loss of radiogenic ^{40}Ar (Turner, 1968). An isochron plot yields an age of 19.2 m.y., with some scatter in the data, but an arbitrary selection of the six high-temperature points yields a 'minimum age of 18.0 m.y. with an initial $^{36}Ar/^{40}Ar$ ratio of about 700.

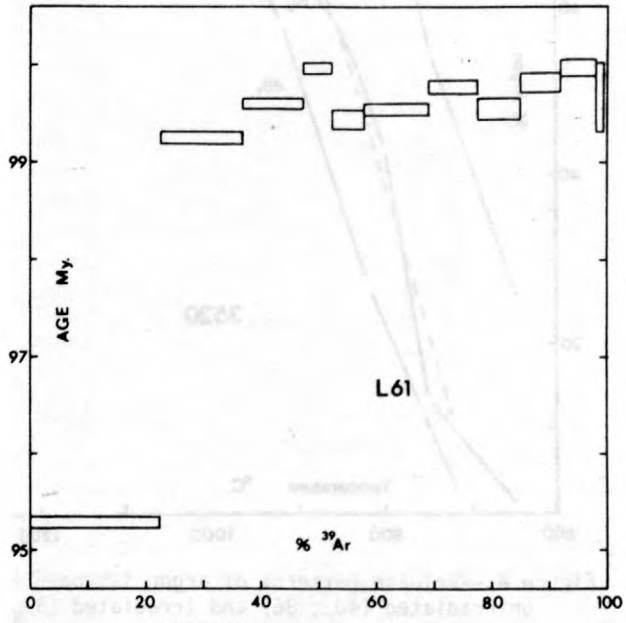

Figure 1.--^{40}Ar-^{39}Ar age-spectrum plot of sample L61 biotite. Rectangles are ± 2 sigma analytic error limits.

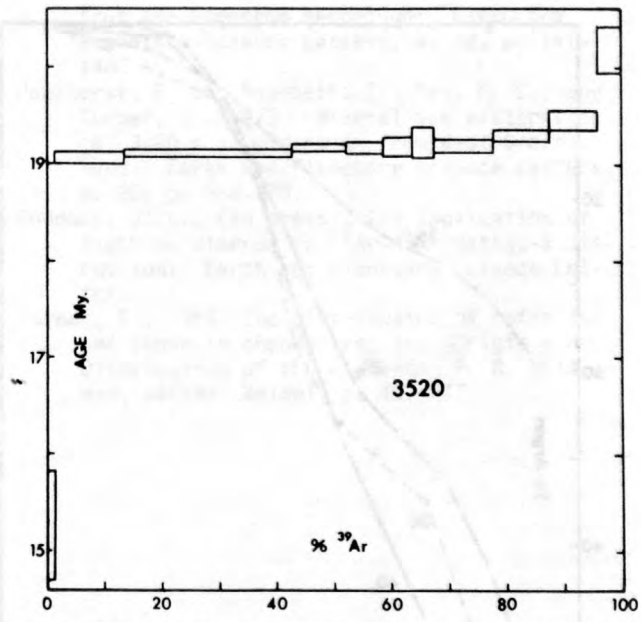

Figure 2.--^{40}Ar age-spectrum plot of sample 3520 biotite. Rectangles are ± 2 sigma analytic error limits.

These two biotites in no way support a model of mixing between an initial argon component of anomalous composition and a pure radiogenic component. The spectrum of L61 closely resembles the analyses of Greenland biotites containing large amounts of excess ^{40}Ar (Pankhurst and others, 1973). In both cases the radiogenic and excess ^{40}Ar are closely associated and the ratio of these two components must be the same in the various heating steps to yield constant though anomalous ages in different gas fractions.

Pankhurst and others (1973) suggested that all the argon in a biotite lattice may be effectively homogenized during reactor irradiation or during argon extraction. Figures 3 and 4 indicate that the irradiation does have a marked effect on the ^{36}Ar component within these two biotites. The fraction of argon isotopes in both irradiated and unirradiated samples are plotted as a function of heating temperature. The evolution of radiogenic ^{40}Ar in an unirradiated sample and ^{39}Ar (equivalent to radiogenic ^{40}Ar because the ages are essentially constant in all steps) in an irradiated sample closely parallel each other. The evolution of ^{36}Ar, however, is notably different, with about 75 percent of the isotope evolving by 800°C in an irradiated sam-

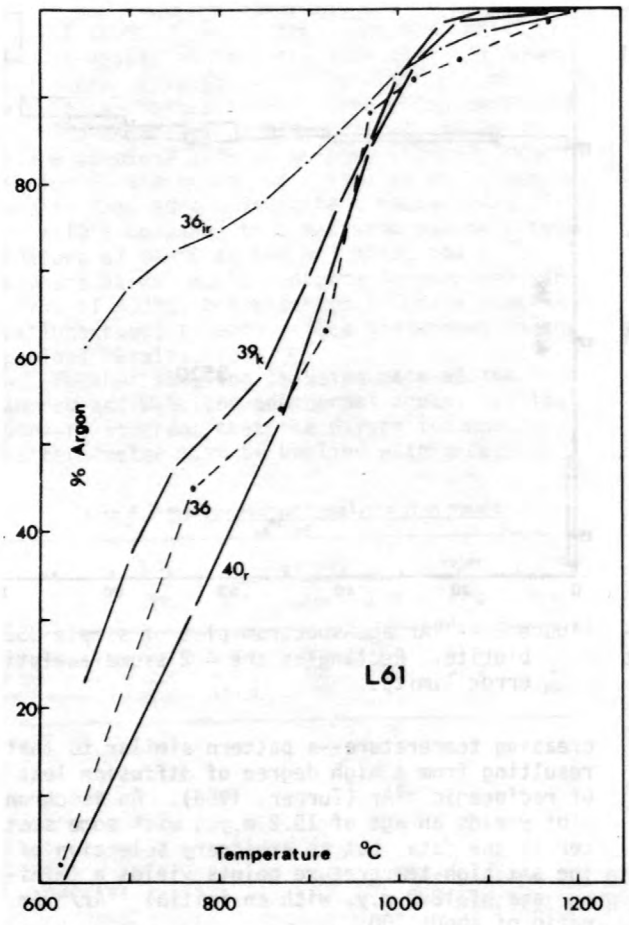

Figure 3.--Release patterns of argon isotopes in unirradiated (40_r, 36) and irradiated (39_k, 36_{ir}) samples of biotite L61.

ple, but in an unirradiated biotite less than 50 percent is evolved by this temperature. These data suggest that ^{36}Ar and presumably its associated initial ^{40}Ar component are more sensitive to neutron irradiation than radiogenic ^{40}Ar. Irradiation displaces this initial component to less retentive sites and during step-heating this initial argon is evolved in the low-temperature fractions. The present data suggests that any loss of ^{36}Ar from biotite during irradiation is small (< 10 percent). This process of low-temperature evolution of ^{36}Ar may be a general feature of irradiated minerals and could explain the observation that ^{40}Ar-^{39}Ar step-heating usually results in lower fractional amounts of 'atmospheric' argon than conventional analyses.

The failure of the simple two-component model may be related to the neutron-induced effect on the initial-argon component. However, the two age spectra presented are fundamentally different from those of Lanphere and Dalrymple (1976) and may relate to the history of the minerals. The four minerals analyzed by Lanphere and Dalrymple are from plutonic rocks undisturbed since their emplacement; the Alpine biotites and the biotites of Pankhurst and others (1973) are from metamorphic terranes.

^{40}Ar-^{39}Ar data, to date, suggests that in the geologically undisturbed environment, excess argon is closely associated with the initial ^{36}Ar and step-heating of these minerals may yet yield isochrons as proposed in the simple model. Within a metamorphic environment the excess ^{40}Ar may represent a third component that, at least after irradiation, is closely associated with the radiogenic argon and thus results in flat age patterns with anomalously old ages. The initial argon appears to be unaffected by metamorphism, but is more sensitive to neutron irradiation.

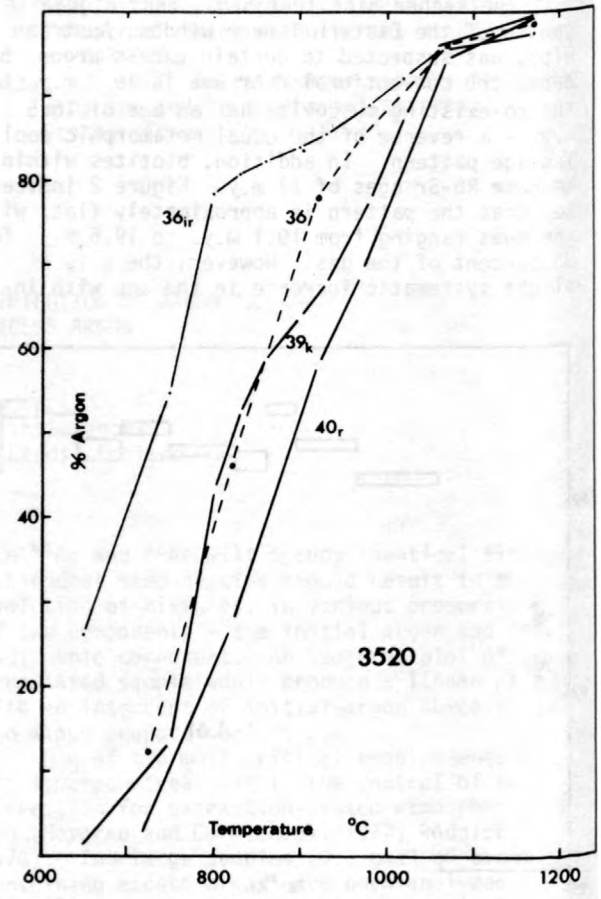

Figure 4.--Release patterns of argon isotopes in unirradiated (40_r, 36) and irradiated (39_k, 36_{ir}) samples of biotite 3520.

Brewer, M. S., 1969, Excess radiogenic argon in metamorphic micas from the Eastern Alps, Austria: Earth and Planetary Science Letters, v. 6, p. 321-331.

Dalrymple, G. B., and Lanphere, M. A., 1971, $^{40}Ar/^{39}Ar$ technique of K-Ar dating-a comparison with the conventional technique: Earth and Planetary Science Letters, v. 12, p. 300-308.

Hayatsu, A., and Carmichael, C. M., 1977, Removal of atmospheric argon contamination and the use and misuse of the K-Ar isochron method: Canadian Journal of Earth Science, v. 14, p. 337-345.

Lanphere, M. A., and Dalrymple, G. B., 1976, Identification of excess ^{40}Ar by the $^{40}Ar/^{39}Ar$ age spectrum technique: Earth and Planetary Science Letters, v. 32, p. 141-148.

Pankhurst, R. J., Moorbath, S., Rex, D. C., and Turner, G., 1973. Mineral age patterns in ca. 3700 m.y. old rocks from West Greenland: Earth and Planetary Science Letters, v. 20, p. 157-170.

Roddick, J. C., (in press), The application of isochron diagram in ^{40}Ar-^{39}Ar dating-a discussion: Earth and Planetary Science Letter.

Turner, G., 1968, The distribution of potassium and argon in chondrites, in: Origin and Distribution of the Elements, P. M. Millman, editor, Reidel, p. 407-417.

URANIUM-TREND DATING OF ALLUVIAL DEPOSITS

By John N. Rosholt
U.S. Geological Survey, Denver, Colorado

Radioactive disequilibrium studies of the ^{238}U-^{234}U-^{230}Th system in soil samples have been used to estimate the time required for soil development (Hansen and Stout, 1968) and to describe the evolution of uranium and thorium isotopic fractionation (Rosholt and others, 1966). A new concept in uranium-series dating called uranium-trend dating has been tested extensively over the past year to determine the reliability of this technique in estimating the time of deposition of alluvial deposits over the range from 2,000 years ago to about 800,000 years ago.

$$\text{U-trend slope} = \frac{C_1 e^{-\lambda_0 t} - C_2 e^{-\lambda_2 t}}{C_3 e^{-\lambda_0 t} + C_4 e^{-\lambda_2 t} + C_5 e^{-\lambda_3 t}}$$

$$\lambda_0 = \frac{\ln 2}{\text{half period of } F_{(0)}} \qquad \lambda_2 = \frac{\ln 2}{247{,}000 \text{ yr}} \qquad \lambda_3 = \frac{\ln 2}{75{,}200 \text{ yr}}$$

$$C_1 = -\frac{\lambda_0 \lambda_2}{\lambda_2 - \lambda_0} \qquad C_2 = \frac{\lambda_2 \lambda_2}{\lambda_2 - \lambda_0} - \lambda_2$$

$$C_3 = -\frac{3 \lambda_0 \lambda_2 \lambda_3}{(\lambda_2 - \lambda_0)(\lambda_3 - \lambda_0)} + \frac{\lambda_0 \lambda_2}{\lambda_2 - \lambda_0}$$

$$C_4 = -\frac{3 \lambda_2 \lambda_2 \lambda_3}{(\lambda_0 - \lambda_2)(\lambda_3 - \lambda_2)} + 2\lambda_2 - \frac{\lambda_2 \lambda_2}{\lambda_2 - \lambda_0}$$

$$C_5 = -\frac{3 \lambda_2 \lambda_3 \lambda_3}{(\lambda_0 - \lambda_3)(\lambda_2 - \lambda_3)} - \lambda_3$$

Figure 1.--Empirical equation for U-trend dating.

Studies of the long-lived isotopes in the ^{238}U decay series in soil samples and in deeply buried granite suggest an important mechanism of uranium-isotope fractionation that may be useful in characterizing the degree and length of time during which uranium mobility has occurred in porous zones of hard rocks and sediments. As ^{238}U and ^{234}U atoms, dissolved in water, decay by alpha disintegration, recoiling nuclides of ^{230}Th, ^{234}Th, ^{234}Pa, and ^{234}U produced with beta recoil are adsorbed or driven into particles at their interface with uranium-bearing water. After sufficient time, this mechanism (uranium emplacement) results in porous material that has $^{234}U/^{238}U$ and $^{230}Th/^{238}U$ ratios significantly higher than material that was not exposed to uranium-bearing water. A complimentary mechanism (uranium displacement) exists where ^{234}U is preferentially leached from available sites in minerals caused by alpha recoil following ^{238}U disintegration in solid phases. The uranium-displacement mechanism has been studied extensively and these studies have been summarized by Osmond and Cowart (1976). Similar processes may occur in sedimentary stratigraphy, and this is the basis for investigating the possibilities of uranium-trend dating in soil profiles useful for estimating the time of deposition of alluvial deposits.

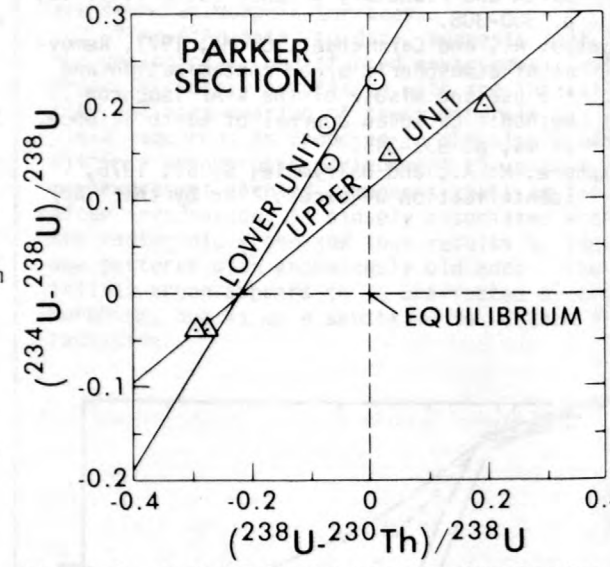

Figure 2.--U-trend isochrons of Parker Section units.
○ Represent upper unit samples.
△ Represent lower unit samples.

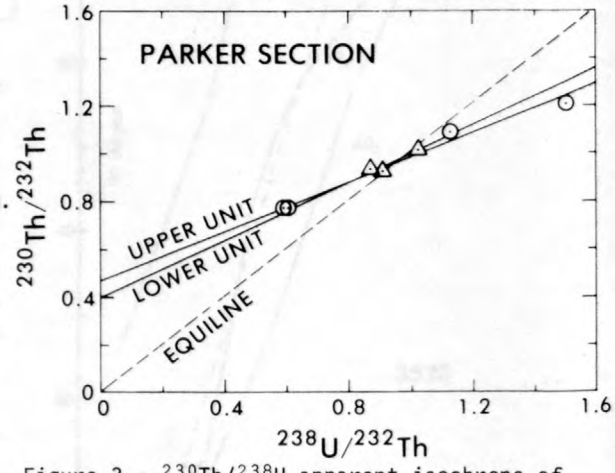

Figure 3.--$^{230}Th/^{238}U$ apparent isochrons of Parker Section Units.
△ Represents upper unit samples.
○ Represents lower unit samples.

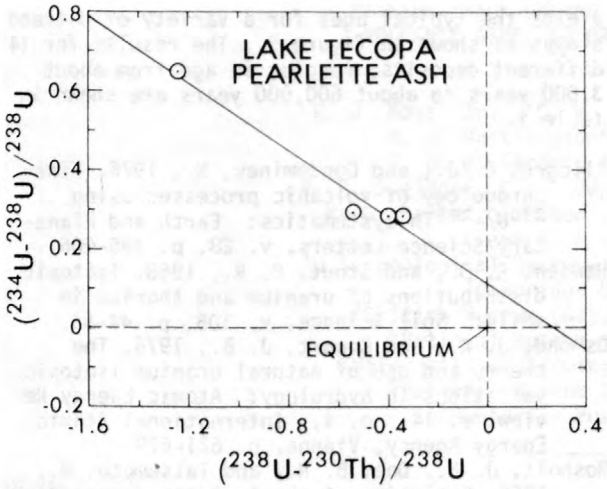

Figure 4.--Uranium-trend isochron for Lake Tecopa altered ash.

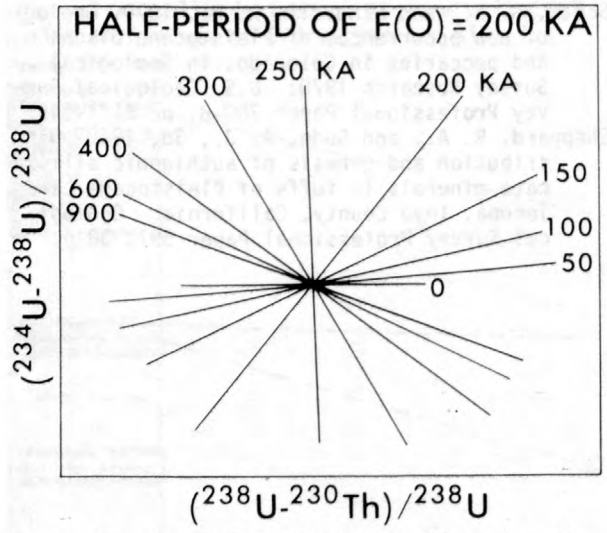

Figure 5.--Variation of U-trend slope with age of alluvium deposition.

Table 1.--Uranium-trend ages for alluvium, eolian, and marine deposits

Type of deposit	U-trend slope	X-intercept ^{232}Th index	Half-period of $F_{(0)}$ ($\times 10^3$)	Age ($\times 10^3$)
Piney Creek Alluvium, Colo.	+0.139	-4.9	10	3
Alluvium of Corral Creek, Colo.	+ .453	-2.3	24	18
Loess of late Wisconsin age, Minn.	+ .145	+1.9[1]	30	8
Loess of late Wisconsin age, Minn.	+ .167	+1.0[1]	57	17
Till of Wisconsin age, Minn.	+ .216	-0.35	170	65
Marine terrace, Cabrillo Beach, San Pedro, Calif.	+ .225	+ .26	220	85
Marine terrace Palos Verdes No. 2, Calif.	+ .313	+ .07[1]	260	125
Marine terrace Palos Verdes No. 12, Calif.	- .461	- .03	610	650
Parker Section, Colo. (upper unit)	+ .516	- .42	140	97
Parker Section, Colo. (lower unit)	+1.036	- .37[1]	160	140
Bull Lake end moraine, W. Yellowstone, Wyo.	+ .120	- .02[1]	625	140
Late Riverbank Terrace r3 Soil, Calif.	+ .140	- .12[1]	540	140
Middle Riverbank Terrace r2 Soil, Calif.	+ .377	- .03	610	260
Golden fault section, Colo., (upper unit)	-2.52	-2.6	240	260
Golden fault section, Colo., (lower unit)	- .763	- .26	240	350
Lake Tecopa, Calif., altered type O Pearlette Ash	- .422	+ .033[1]	435	600

[1]Data used for calibration to determine half period of $F_{(0)}$.

The dating technique consists of determining an isochron from analyses of several samples covering the various soil horizons in a given alluvial unit; from four to nine samples of each alluvial unit are analyzed. In each sample an accurate determination of the abundances of ^{238}U, ^{234}U, ^{230}Th, and ^{232}Th is required. Except for the most resistant minerals, such as zircon and magnetite, the sample is decomposed by dissolution in a mixture of HNO_3, $HClO_4$ and HF. Uranium and thorium are separated and purified for alpha-spectrometry measurements, using the techniques described by Rosholt and others (1966). Spikes of ^{236}U and ^{229}Th are used in the radioisotope-dilution technique to determine the concentrations of uranium and thorium.

The results of these analyses are plotted where $(^{238}U-^{230}Th)/^{238}U$ vs. $(^{234}U-^{238}U)/^{238}U$ ideally yields a linear relationship in which the resulting slope, $\Delta(^{234}U-^{238}U)/\Delta(^{238}U-^{230}Th)$, increases with the increasing age of the alluvium for a given half-period of the flux controlling the migration of uranium in the alluvial environment. An empirical model compensates for different climatic and environmental regimes and the model has primary-time calibrations at 11,000 years, 140,000 years (Bull Lake), and 600,000 years (type-O Pearlette ash). Calibrations have been made based on correlations with similar material that has been dated by radiocarbon and K-Ar.

An empirical mathematical model using the first derivatives of Bateman's equations describing the growth and decay of ^{234}U and ^{230}Th requires a variable factor called the half-period of flux controlling uranium migration (fig. 1). The value of this factor, $F_{(0)}$, is determined as a function of the intercept of the U-trend isochron on the X-axis (Y-axis = 0 in fig. 2) and a $^{230}Th/^{238}U$ apparent isochron calculated in the same manner as that for ionium dating of volcanic rocks (Allegre and Condomines, 1976) where $^{238}U/^{232}Th$ and $^{230}Th/^{232}Th$ ratios of the samples are plotted as shown in figure 3. The value of the slope of the $^{230}Th/^{238}U$ apparent isochron is a rough approximation to the relative age of the alluvial unit; this value is called the ^{232}Th index. Analytical data from alluvium of known age are used to calibrate the variation of the half-period of the flux factor, $F_{(0)}$, with the numerical value of (X-intercept)/(^{232}Th index). The values of these two factors in 16 analyzed deposits are shown in columns 3 and 4 of table 1. Examples of the isochron plots of a alluvium of Bull Lake age buried by a younger deposit at the Parker Section, described by Scott and Lindvall (1970), are shown in figures 2 and 3. An example of the isochron plot of altered tuff from Lake Tecopa, locality 6, described by Sheppard and Gude (1968), is shown in figure 4.

The solution of the empirical equation shown in figure 1, using a half-period of 200,000 years for the flux factor as an example, yields the typical ages for a variety of U-trend slopes as shown in figure 5. The results for 14 different deposits, ranging in age from about 3,000 years to about 600,000 years are shown in table 1.

Allegre, C. J., and Condomines, M., 1976, Fine chronology of volcanic processes using $^{238}U/^{230}Th$ systematics: Earth and Planetary Science Letters, v. 28, p. 395-406.

Hansen, R. O., and Stout, P. R., 1968, Isotopic distributions of uranium and thorium in soils: Soil Science, v. 105, p. 44-50.

Osmond, J. K., and Cowart, J. B., 1976, The theory and use of natural uranium isotopic variations in hydrology: Atomic Energy Review, v. 14, no. 4, International Atomic Energy Agency, Vienna, p. 621-679.

Rosholt, J. N., Doe, B. R., and Tatsumoto, M., 1966, Evolution of the isotopic composition of uranium and thorium in soil profiles: Geological Society of America Bulletin, v. 77, p. 987-1004.

Scott, G. R., and Lindvall, R. M., 1970, Geology of new occurrences of Pleistocene bisons and peccaries in Colorado; in Geological Survey Research 1970: U.S. Geological Survey Professional Paper 700-B, p. B141-149.

Sheppard, R. A., and Gude, A. J., 3d, 1968, Distribution and genesis of authigenic silicate minerals in tuffs of Pleistocene Lake Tecopa, Inyo County, California: Geological Survey Professional Paper 597, 38 p.

FISSION-TRACK DATING OF LOWER PALEOZOIC VOLCANIC ASHES IN BRITISH STRATOTYPES

R. J. Ross, Jr.[1], C. W. Naeser[1], G. A. Izett[1],
H. B. Whittington[2], C. P. Hughes[2],
R. B. Rickards[2], Jan Zalasiewicz[2],
P. R. Sheldon[2], C. J. Jenkins[2], L. R. M. Cocks[3],
M. G. Bassett[4], Peter Toghill[5], W. T. Dean[6],
and J. K. Ingham[7]
[1]U.S. Geological Survey, Denver, Colorado 80225
[2]Cambridge University
[3]British Museum (Natural History) London
[4]National Museum of Wales, Cardiff
[5]University of Birmingham, Church Stretton
[6]National Museum of Wales, Cardiff
[7]Hunterian Museum, Glasgow

INTRODUCTION

In order to establish a radiometric geochronology based on lower Paleozoic British stratotypes, 41 collections of bentonites and other volcanically derived rocks were collected in five main areas of Ordovician and Silurian outcrops in Wales, England, and Scotland in September 1976 (fig. 1). These are the areas studied by Sedgwick, Murchison, and Lapworth in establishing the lower Paleozoic systems on which our modern work is based (Ross and others, 1977).

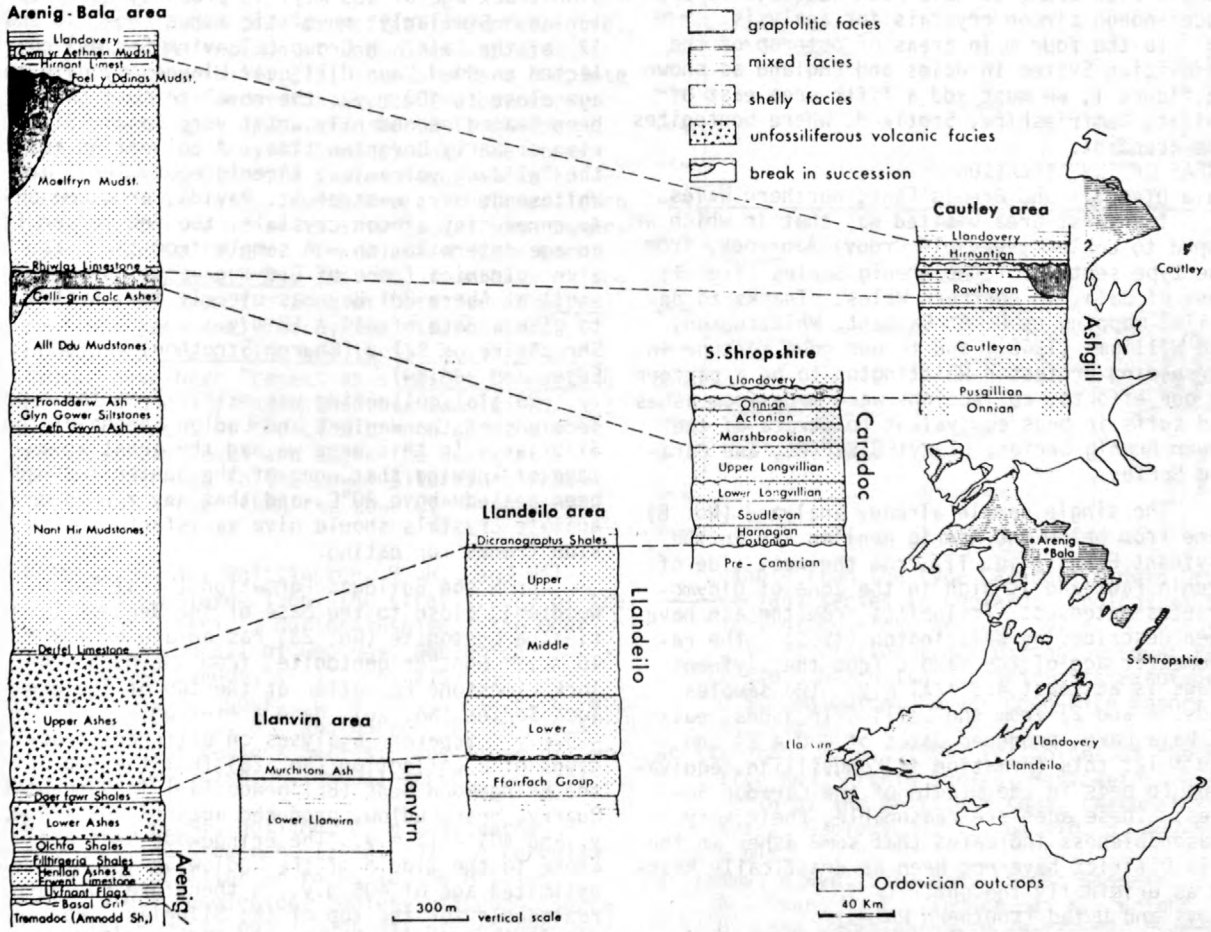

Figure 1.--Biofacies and correlation of stratotype sections of the Ordovician of England and Wales (from Williams and others, 1972).

Although only 21 of the 41 samples collected have been analyzed, they have provided minimum ages for the Lower Arenig, Lowest Llandeilo, and upper Caradoc Series of the Ordovician System, and for the lower Wenlock, uppermost Wenlock, and middle Ludlow Series of the Silurian System. The project was undertaken under the auspices of the U.S. Geological Survey and the National Geographic Society.

It is our purpose to establish a radiometric geochronology of early Paleozoic time, particularly of the Ordovician, using the fission-track method of dating bentonites and other volcanically derived strata in the British stratotypes, against which all other lower Paleozoic biostratigraphic sections throughout the world are ultimately compared.

About 15 kg of rock constituted each sample, considerably less than we had originally planned; the logistics of gathering samples at the end of field work in southern Scotland for consolidated shipment by air freight from London to Denver dictated a reduction in the size of collections. With a few exceptions, the reduced sample size seems to have been adequate to produce enough zircon crystals for analysis.

To the four main areas of outcrop of the Ordovician System in Wales and England as shown in figure 1, we must add a fifth area east of Moffat, Dumfrieshire, Scotland, where bentonites are abundant.

AREAS OF INVESTIGATION

Bala District and Arenig Fawr, northern Wales

The first area visited was that in which we hoped to collect very old Ordovician rock, from the type section of the Arenig Series (fig. 1) west of Bala, in northern Wales. Thanks to detailed mapping by D. A. Bassett, Whittington, and Williams (1966), and to our good fortune in persuading Professor Whittington to be a partner in our efforts, collections were made from ashes and tuffs in beds equivalent to strata of the lower Arenig Series, Llanvirn Series, and Caradoc Series.

The single sample already analyzed (No. 8) came from below the Arenig Henllan ash in the Llyfnant Flags (fig. 1), from the west side of Arenig Fawr and is high in the zone of Didymograptus extensus. Trilobites from the ash have been described by Whittington (1966). The radiometric age of the sample from the Llyfnant Flags is at least 493 ± 11 m.y. Two samples (nos. 1 and 2) from the Gelli Grin ashes, east of Bala Lake, produced dates of 460 ± 14 and 469 ± 12; this formation is Longvillian, equivalent to beds in the middle of the Caradoc Series. These ages are reasonable; their very reasonableness indicates that some ashes in the Bala District have not been as drastically heated as originally thought.

Powys and Dyfed (southern Wales)

Twelve collections were made in southern Wales along the belt of outcrop from Llandrindod Wells to St. Davids (fig. 1). In this large region, C. P. Hughes discovered 19 different localities at which volcanic strata had been described. At two localities we were unable to find the reported ashes. At five other localities the rock seems so thoroughly indurated that separation of zircon crystals was deemed impractical. The four samples analyzed gave mixed results.

The most rewarding collection of the four (No. 13) was taken from a thin bentonite layer in shales bearing Glyptograptus teretiusculus, in a stream section east of Bach-y-graig, near Llandrindod Wells. We obtained an age of 477 ± 11 m.y. from the sample, which comes from the topmost Llanvirn or lowermost Llandielo Series. Two other samples indicated that the rock had been heated after deposition, which may be significant in delineating Silurian or later tectonism. In the upper reaches of Howey Brook, near Builth Wells, a bentonite (No. 12) is present in a section first described by Murchison in 1839; it lies beneath shales carrying Didymograptus murchisoni and might have given an age for the Llanvirn Series. Regrettably, the fission-track age of 433 m.y. is probably Early Silurian. Similarly, rhyolitic ashes (Nos. 16 and 17) of the Fairfach Group (Llanvirn Series) collected on Coed Duon Hill near Llandovery gave an age close to 400 m.y.; the rhyolite must have been heated secondarily until very latest Silurian or Early Devonian time. A collection from the Pwllevog volcanics, (Arenig equivalent) at Whitesands Bay, west of St. Davids, produced only three tiny zircon crystals, too few to permit an age determination. A sample from the Llanvirn volcanics (zone of Didymograptus murchisoni) at Abereiddi Bay has clearly been heated to give a date of 444 ± 12 m.y.

Shropshire or Salop (Church Stretton, Wenlock Edge, and Ludlow)

Initial collecting was mainly from the type sections of the Wenlock and Ludlow Series of the Silurian. In this area we had the great advantage of knowing that none of the bentonites had been heated above 80°C, and that any zircon or apatite crystals should give satisfactory fission tracks for dating.

From the Buildwas Formation (basal Sheinwoodian), close to the base of the Wenlock Series, a bentonite (No. 23) has an age of 422 ± 10 m.y. Another bentonite, from the Much Wenlock Limestone Formation at the top of the Wenlock Series (No. 26), gave a minimum age of 416 ± 9 m.y. Separate analyses on different fractions of a collection (No. 28) from the top of the Bringewood Beds (Bringewoodian) in Sunnyhill Quarry, near Ludlow, produced ages of 409 ± 9 m.y. and 404 ± 12 m.y. The Bringewood Beds are close to the middle of the Ludlow Series. An estimated age of 405 m.y. is therefore not unreasonable for the top of the Silurian. We might also guess that the time represented by the Ludlow Series was about 10 m.y. in length and the Wenlock about 6 m.y. Unfortunately, we

have obtained no samples from the type Llandovery Series suitable for fission-track dating.

The original locality in the Acton Scott beds, Caradoc Series, of the Ordovician System, on the south side of the Onny River, was resampled in the company of Dr. W. T. Dean, Geological Survey of Canada. A collection made by Ross in 1968, with Dean, was shown to have a minimum age of 451 ± 21 m.y. (Ross and others, 1976) based on fission tracks in apatite and using an old decay constant. The result using zircon crystals and the new constant from that early collection is 464 ± 21. The data for the Acton Scott beds based on 1976 samples from the same locality is 468 ± 12 m.y. This becomes the youngest Ordovician age we have been able to determine.

Cautley District (Sedbergh, Cumbria)

In the company of Ingham a search was made for Cautley volcanic rocks within the Ashgill Series containing zircon crystals. The search was not successful and the one sample (No. 36) could not be dated.

Moffat District, Dumfrieshire (Moffat Water, Dobs Linn)

East of the town of Moffat in Dumfrieshire, Scotland, the section at Dobs Linn was made famous by Lapworth in 1879; it exhibits a complete stratigraphic succession across the boundary from the topmost Ordovician Hartfell shales (equivalent to Ashgill Series) into the lowermost Silurian Birkhill Shales (equivalent to Llandovery Series). Furthermore, the transition from one to the other is interbedded with numerous bentonite layers. Three collections were made with Ingham. One (No. 40) from east of the Linn branch from the zone of Dicellograph<u>us</u> anceps has been analyzed by the fission-track method; the resulting age is 332 m.y. The tracks have been "reset" as a result of heating prior to 332 m.y. ago. Another sample (No. 41) was taken west of the Linn branch about 3 m above stream level and above the west fault. Thick bentonite in the Lower Silurian Birkhill Shale not higher than the zone of Monograph<u>us cyphus</u> has an age of 437 ± 11 m.y. This analysis at least indicates that the Ordovician-Silurian boundary is not younger than 437 ± 11 m.y. old.

For the first time radiometric dates have been obtained from bentonites interstratified within the type sections of two lower Paleozoic systems. The ages obtained, using the fission-track method, are mostly in the proper order and of reasonable magnitude.

Our preliminary results are shown graphically (ages in parentheses are estimated) and compared with fission-track dates on three formations in the central and southeastern United States:

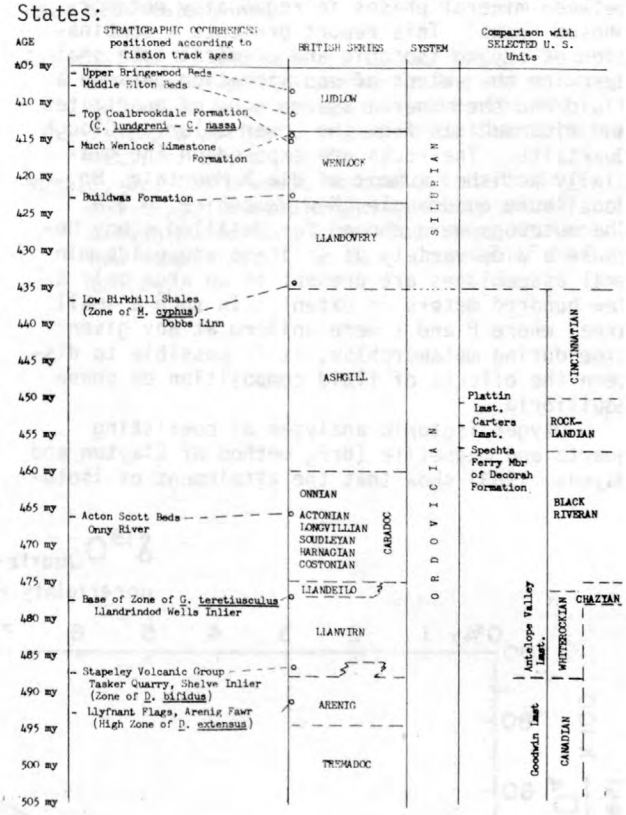

Bassett, D. A., Whittington, H. B., and Williams, Alwyn, 1966, The stratigraphy of the Bala District, Merionethshire: The Quarterly Journal of Geology, Geological Society of London, v. 122, p. 219-271.

Bassett, M. G., Cocks, L. R. M., Holland, C. H., Rickards, R. B., and Warren, P. T., 1975, The type Wenlock Series: Institute of Geological Sciences, Annual Report, no. 75/13, 19 p.

Cocks, L. R. M., Holland, C. H., Rickards, R. B., and Strachan, Isles, 1971, A correlation of Silurian rocks in the British Isles: Geological Society of London Special Report, no. 1, Journal of Geology, v. 127, p. 103-136.

Ross, R. J., Jr., Naeser, C. W., and Izett, G. A., 1976, Apatite fission-track dating of a sample from the type Caradoc (Middle Ordovician) Series in England: Geological Society of America, Geology, v. 4, p. 505-506.

_____1977, Fission track dating of Lower Paleozoic bentonites in British stratotypes: U.S. Geological Survey Open-File Report 77-348, 12 p.

Whittington, H. B., 1966, Trilobites of the Henllan Ash, Arenig Series, Merioneth: Bulletin of the British Museum, (Natural History), Geology, v. 11, no. 10, p. 489-505, 5 pls.

Williams, Alwyn; Strachan, Isles; Bassett, D. A., Dean, W. T., Ingham, J. K., Wright, A. D., and Whittington, H. B., 1972, A correlation of Ordovician rocks in the British Isles: Geological Society of London, Special Report, no. 3, 74 p.

OXYGEN ISOTOPIC AND CHEMICAL EQUILIBRIUM BETWEEN MINERAL ASSEMBLAGES AND THE FLUID PHASE OF METAMORPHISM

By Douglas Rumble, III and Thomas C. Hoering
Geophysical Laboratory
2801 Upton St., N.W.
Washington, D.C. 20008

A fluid phase is the chief agent aiding the attainment of chemical and isotopic equilibrium between mineral phases in regionally metamorphosed rocks. This report presents a combination of oxygen isotopic and chemical data that describe the extent of equilibration between a fluid and the mineral assemblages of quartzites and mica schists from the Lower Silurian Clough Quartzite. The rocks are exposed on the glacially polished summit of Black Mountain, Mt. Moosilauke quadrangle, New Hampshire, U.S.A. The outcrops were chosen for detailed study because a wide variety of silicate and oxide mineral assemblages are present in an area only a few hundred meters in extent. In such a small area, where P and T were uniform at any given time during metamorphism, it is possible to discern the effects of fluid composition on phase equilibria.

Oxygen isotopic analyses of coexisting quartz and magnetite (BrF_5 method of Clayton and Mayeda, 1963) show that the attainment of isotopic-exchange equilibrium was limited to single sedimentary beds. The slope of tie lines between minerals in figure 1 is dependent on the temperature of isotopic equilibration, since it is equal to $\Delta^{18}O$(quartz-magnetite). The relative positions of the tie lines are dependent on the bulk oxygen isotopic composition of each rock. The analyses plotted on figure 1 show mutually parallel tie lines within the uncertainty of measurement. Thus, the data are consistent with the attainment of isothermal isotopic exchange equilibrium between mineral pairs in single sedimentary beds. Equilibrium was not achieved, however, between minerals from rocks of different bulk isotopic composition.

Chemical analyses of coexisting minerals, using the electron microprobe analyzer, indicate that attainment of chemical equilibrium was limited to single sedimentary beds. Silicate and oxide minerals vary sympathetically in chemical composition from bed to bed: Fe-rich silicate assemblages occur with magnetite-ilmenite pairs

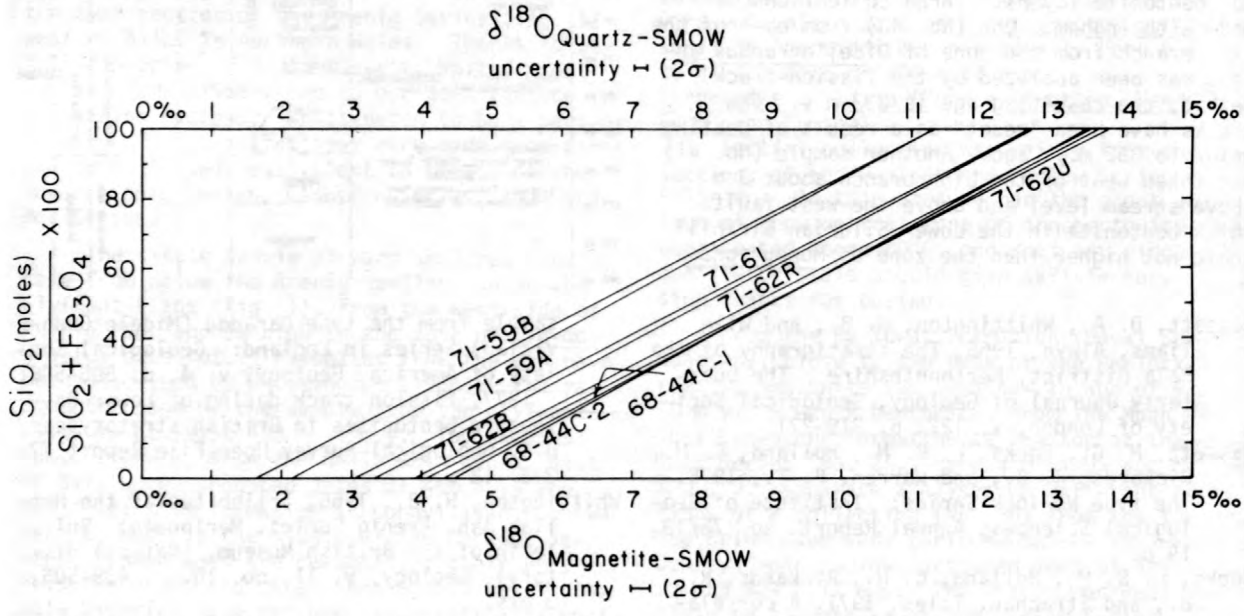

Figure 1.--Exchange-equilibrium diagram showing isotopic composition of analyzed quartz and magnetite (in permil). Tie lines connect quartz and magnetite from the same rock. Minerals were separated from rock volumes of 10-20 cm^3 in order to maintain a consistency of scale between the volume sampled for isotopic analysis and the area spanned by 2.5 cm diameter polished thin sections used for electron microprobe analysis.

in which ilmenite is poor in Fe_2O_3; Mg-rich silicates occur with oxide pairs in which ilmenite is rich in Fe_2O_3. Graphic and algebraic analysis of compositions of coexisting minerals in the system K_2O-Al_2O_3-SiO_2-H_2O-MgO-FeO-Fe_2O_3-TiO_2 demonstrates an absence of crossing tie lines between mineral assemblages from rocks of different bulk chemical content (Rumble, in press). Minor components such as Mn are partitioned systematically between minerals. These observations are consistent with the attainment of isothermal, isobaric chemical equilibrium between minerals in single sedimentary beds. Minerals from rocks of different bulk chemical composition, however, failed to attain equilibrium.

It is likely that fluid was present in the rocks of Black Mountain during metamorphism because these rocks contain concordant quartz segregations with fluid inclusions. Such a volatile phase could not have been homogeneous both in its isotopic and chemical composition and also in equilibrium with each mineral assemblage. The oxygen isotopic composition of an aqueous solution would have varied over a range of 2.5 permil in $\delta^{18}O$ if it were in equilibrium with each analyzed mineral pair. The sympathetic variation of silicate Fe/Mg and oxide Fe^{2+}/Fe^{3+}, described above, records variations in equilibrium fluid composition from a reduced composition containing 75 percent H_2O and 25 percent H_2 to an oxidized composition consisting of nearly pure H_2O.

The results of our study demonstrate that both isotopic and chemical equilibration were restricted to single sedimentary beds ranging in thickness from 1 cm to 1 m. Localized equilibration of this kind is probably indicative of low permeability in metamorphosed quartzites. Fluid flow was so low that both the isotopic and chemical compositions of the volatile phase was controlled by the inherent buffer capacity of each sedimentary bed.

Clayton, R. N. and Mayeda, T. K., 1963, The use of bromine pentafluoride in the extraction of oxygen from oxides and silicates for isotopic analysis: Geochimica Cosmochimica Acta, v. 27, p. 43-52.

Rumble, D., (in press), Mineralogy, petrology, and oxygen isotopic geochemistry of the Clough Formation, Black Mountain, Western New Hampshire, U. S. A.: Journal of Petrology.

RARE GASES IN MANTLE-DERIVED AMPHIBOLES

By K. Saito, E. C. Alexander, Jr., and
A. R. Basu
Department of Geology and Geophysics
University of Minnesota
Minneapolis, Minnesota 55455

It has recently been reemphasized that a knowledge of the isotopic and elemental composition of the rare gases in the Earth's interior would establish a powerful boundary condition for models of the evolutionary history of the atmosphere (Ozima, 1975; Ozima and Alexander, 1976). Several workers have successfully measured the rare gases in ultramafic xenoliths and (or) in minerals separated from such xenoliths (Hennecke and Manuel, 1975; Kaneoka and others, 1977; Rison and Kyser, 1977). In general, these mantle-derived samples contained very small amounts of gas whose abundance patterns differed from that of atmospheric rare gases.

We have recently shown (Saito and others, 1978) that a sample of a mantle-derived amphibole, kaersutite (from Kakanui, New Zealand), contains a high concentration of rare gases. The elemental abundance-pattern of the rare gases closely resembles the "planetary" primordial pattern. The sample's rare gases are characterized by excess ^{21}Ne and ^{3}He relative to atmospheric abundances and by an $^{40}Ar/^{36}Ar$ ratio of 400, which, when corrected for the in situ radiogenic component, may represent an initial value as low as 240.

Thompson and others (1978) recently reported an analysis of the rare gases from a mantle-derived kaersutite from Dish Hill, California. Their analysis also revealed a high concentration of rare gases, but the elemental pattern of those gases was distinctly different from the "planetary" pattern.

In an attempt to resolve this discrepency and to extend our data, we have analyzed four

Table 1.--Rare gases in kaersutites

[Leaders (---) indicate not measured]

Sample No.	Weight (mg)	Fusion Temp. (°C)	^{4}He (10^{-8}cc/g)	^{20}Ne (10^{-10}cc/g)	^{36}Ar (10^{-10}cc/g)	^{40}Ar (10^{-8}cc/g)	^{84}Kr (10^{-12}cc/g)	^{132}Xe (10^{-12}cc/g)	Reference
Kakanui, New Zealand									
	403.8	1400	381	33.8	140	560	436	307	Saito and others, (1978).
Dish Hill, California									
Ba 1-72	161.2	([1])	2.5	[2]230	197	598	288	42	Thompson and others, (1978).
Ba 1-72	103.6	1550	10.2±8.4	50.0±2.7	125±16	393±22	289±13	131±10	This work.
H-19	99.2	1400	3.6±2.7	2.8±1.1	[3](4.8)	29.7±5.9	32.2±3.2	13.1±3.2	Do.
H-13	150.7	1550	4.2±5.7	2.6±1.0	---	---	5.0±3.4	32.3±4.4	Do.
H-9	152.1	1550	[4] < 8	[4] < 0.7	[3](9.5)	14.8±7.2	2.5±3.1	[4] < 7.4	Do.
Spring Mountain, New South Wales, Australia									
	78.2	1550	2.5±7.4	0.31±1.00	([5])	159±16	[4] < 6.1	[4] < 0.024	This work.

[1] Rare gas amounts are the sums of 900° and 1600°C fraction.
[2] $^{20}Ne/^{22}Ne$ = 0.102 is assumed.
[3] The ^{36}Ar in these two samples were less than average blank. The values shown are calculated from the ^{40}Ar content assuming that $^{40}Ar/^{36}Ar$ = 314 - the value measured in Ba 1-72.
[4] Upper limit = sample $x(1+2\sigma_s)$ - blank $x(1-2\sigma_b)$.
[5] The ^{36}Ar was less than the average ^{36}Ar blank. The measured $^{40}Ar/^{36}Ar$ ratio was ~ 800.

samples of kaersutite from Dish Hill and one sample from Spring Mountain, New South Wales, Australia. All five samples were ∿ 100 mg, handpicked kaersutite separates and one sample, Ba 1-72, was separated from the same sample of Thompson and other's (1978)--but the two samples were not aliquots of one another. The only significant changes in our published procedure (Saito and others, 1978) are that four of the samples were fused at 1550°C, while sample H-19 was fused at 1400°C (as was the Kakanui sample), and that a double separation of Ar from the Kr fraction was not used. The higher blanks associated with the 1550°C fusion temperature proved to be equal to, and in some cases greater than, the gas contents of the low gas samples (see below).

Our results are shown in table 1 and figure 1. Samples H-9, H-13, and H-19 from Dish Hill, California, and the sample from Spring Mountain, New South Wales, proved to contain much less gas than sample Ba 1-72, or the Kakanui sample. In many of the analyses, those samples run at 1550°C yielded gas amounts smaller than the average blank signal. Sample H-19 from Dish Hill, which has a lower associated blank due to the lower fusion temperature, is the only gas-poor sample for which we obtained reasonably complete abundance measurements.

Our main conclusions are: (1) The two

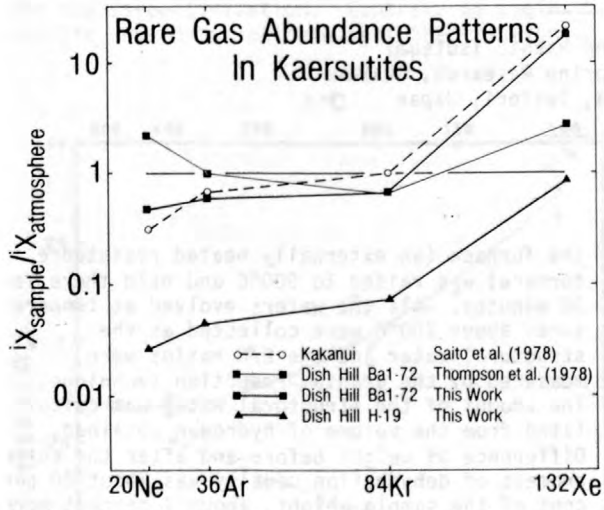

Figure 1.--The rare gas abundances in kaersutite samples normalized to the "atmosphere"--where "atmosphere" is defined as abundance of rare gases in the atmosphere divided by the mass of the entire Earth.

kaersutite samples, from which we obtained good abundance patterns, reproduce the "planetary" pattern reported by Saito and others (1978). The pattern evidently is not unique to the Kakanui sample; (2) large variations exist in the gas contents of kaersutite--even from the sample locality; (3) we confirm Thompson and others' (1978) report that sample Ba 1-72 from Dish Hill, California, is gas rich, but we do not confirm the abundance pattern they reported; and (4) low $^{40}Ar/^{36}Ar$ ratios and excess ^{21}Ne seem to be characteristic of the rare gases in mantle-derived kaersutites.

Our analyses of samples H-19 and Ba 1-72 from Dish Hill, California, yield very similar abundance patterns, despite the order-of-magnitude variation in gas content. Those patterns are remarkably similar to the pattern in the Kakanui, New Zealand, sample and closely resemble the "planetary" primordial pattern. Indeed, the $^{20}Ne/^{36}Ar$ and $^{132}Xe/^{36}Ar$ ratios in sample Ba 1-72 are a better fit to the "planetary" values than are the corresponding values in the Kakanui sample. Such patterns have, therefore, been demonstrated in mantle-derived kaersutites from two widely separated geographic locations. The reservoirs of rare gases in the regions of the mantle from which the kaersutites formed must be similar in at least two widely spaced locations. If the rare gases in kaersutite are trapped in the large empty "A" site (Saito and others, 1978), and the crystallizing kaersutite does not fractionate the rare gases in its environment, then there exist regions in the mantle containing "planetary" rare gases. On the other hand, if the rare gases in kaersutites are fractionated samples of the reservoirs from which they were trapped, then: (1) those reservoirs must still be identical in widely spaced regions of the mantle; (2) the fractionation process must produce the same elemental ratios independent of the fraction of gas trapped; and (3) this hypothetical reservoir and fractionation must accidentally mimic the "planetary" pattern. We believe that the former 'if' is more probably than is the latter.

As an alternative, we can postulate that the rare gases are not trapped in the crystal structure, but are contained in the liquid CO_2-filled inclusions which are known to occur in nodules from Kakanui (Roedder, 1965). In such a model, the variation in gas content from sample to sample could be attributed to a variation in the number of fluid inclusions. J. O'Neil (oral commun., 1977) observed that a large variation in the water content of kaersutites could be interpreted in such a context. The implication of the rare gas patterns would remain unaltered, however. There exist in the mantle rare gas reservoirs of "planetary" composition.

Although our analysis of kaersutite from Ba 1-72 confirms that this sample is rich in rare gas, the elemental pattern we obtained is different from the results of Thompson and others (1978). Because our respective samples of kaersutite from Ba 1-72 were not aliquots of the same mineral separate, we cannot rule out sample inhomogeneity as the cause of this difference. We are puzzled by the results, however, and have no good explanation for the

lack of interlaboratory reproducibility.

We agree with Thompson and others (1978) that Ba 1-72 contains Ar with an $^{40}Ar/^{36}Ar$ ratio similar to the atmospheric value. We also obtained a value of $^{21}Ne/^{20}Ne = (40.4 \pm 5.2) \times 10^{-3}$ from Ba 1-72. Although not as significant statistically as our result from the Kakanui sample, this value confirms the existence of excess ^{21}Ne in mantle-derived kaersutites.

Hennecke, E. W., and Manuel, O. K., 1975, Noble gas in an Hawaiian xenolith: Nature, v. 257, p. 778-780.

Kaneoka, I., Takaoka, N., and Aoki, K., 1977, Rare gases in a phlogopite nodule and a phlogopite-bearing peridotite in South African kimberlites: Earth and Planetary Science Letters, v. 36, p. 181-186.

Ozima, M., 1975, Ar isotopes and earth-atmosphere evolution models: Geochimica Cosmochimica Acta, v. 39, p. 1127-1134.

Ozima, M., and Alexander, E. C., Jr., 1976, Rare gas fractionation patterns in terrestrial samples and the earth-atmosphere evolution model, Reviews of Geophysics and Space Physics, v. 14, p. 385.

Rison, W., and Kyser, K., 1977, Rare gases, oxygen and hydrogen in Hawaiian xenoliths and basalts: EOS, Transactions of the American Geophysical Union, v. 58, p. 537.

Roedder, E., 1965, Liquid Co_2 inclusion in olivine-bearing nodules and phenocrysts from basalts: American Mineralogist, v. 50, p. 1746-1782.

Saito, K., Basu, R. A., and Alexander, E. C., Jr., 1978, Planetary type rare gases in an upper mantle-derived amphibole: Earth and Planetary Science Letters, (in press).

Thompson, D. P., Basu, A. R., Hennecke, E. W., and Manuel, O. K., 1978, Noble gases in the earth's mantle: Physics of the Earth and Planetary Interiors, (in press).

EXPERIMENTAL DETERMINATION OF THE D/H FRACTIONATION FACTORS BETWEEN SERPENTINE AND WATER AT 100° TO 500°C UNDER 2000 BARS WATER PRESSURE; SOME IMPLICATION TO THE D/H RATIOS OF NATURAL SERPENTINITES

By Hitoshi Sakai and Makoto Tsutsumi
Institute for Thermal Spring Research, Okayama University, Misasa, Tottori, Japan

Commercially obtained clinochrysotile asbestos was powdered to -200 mesh. About 100 mg of this powder (δD = -136.4 permil) was weighed into a silver capsule of 2.8 mm in outer diameter and 60 mm in length, together with about 200 mg of water of three different D/H ratios (+219.9, -46.8, and -171.1 permil SMOW). The three tubes of different water were heated together as a set in a cold-seal pressure vessel under 2000 bars water pressure at a desired temperature. After a designed period of reaction, both water and serpentine were analyzed for D/H ratios as described below and the equilibrium fractionation factors were calculated by the method of Northrop and Clayton (1966). Silver capsules which showed more than 1 mg weight-loss during reaction were discarded. Remaining capsules were kept under vacuum for 30 minutes and those which showed more than 0.1 mg weight-loss were also discarded.

The D/H ratios of water were measured by the conventional uranium-reduction technique. Serpentine samples were dried overnight in open air and then heated in vacuo for 2 hours to drive off adsorbed moisture. The temperature of the furnace (an externally heated resistance furnace) was raised to 900°C and held there for 30 minutes. All the waters evolved at temperatures above 200°C were collected as the structural water and the D/H ratios were measured by the uranium-reduction technique. The amount of the structural water was calculated from the volume of hydrogen obtained. Difference of weight before and after the entire process of dehydration usually was about 20 percent of the sample weight, about 7 percent more than expected from pure serpentine. In one experiment, all the water evolved below 200°C was measured for the amount and D/H ratio. We observed a 7.3 percent sample weight loss and a D/H ratio of -79.5 permil, which we attribute to adsorbed water in the asbestos. Experiments indicated that the absorbed water can be completely eliminated by 2 hours evacuation of the sample at 200°C.

The D/H ratios reported in this paper are relative to the International Atomic Energy Agency (IAEA) SMOW. The reproducibility and precision of the measurements for both water and serpentine are ±3 permil. Another IAEA standard

water, NBS-1A, was analyzed to be -181.5 permil, in good accord with other results compiled by IAEA (Gonfiantini, 1977).

Table 1 summarizes the experimental condition and the results obtained. In the calculation of the fractionation factors, the D/H ratios of the original waters were corrected for the absorbed water in the asbestos powder using the amount and D/H ratios previously mentioned. The equilibrium fractionation factors are plotted in figure 1 against the reciprocal of the absolute temperature. The solid line is the least-square fit to the data and is expressed by the following equation:

$$1000 \ln \alpha = 2.75 \times 10^7/T^2 - 7.69 \times 10^4/T + 40.8 \quad (1)$$

where T and α are the absolute temperature and equilibrium fractionation factor. The standard deviation of the observed data from equation (1) is ±6.1 permil. An equilibrium fractionation factor of -20 permil was measured at 400°C by Suzuoki and Epstein (1976), the only previous measurement made on serpentine-water system. The present results at 400°C are in accord with their result within the uncertainty cited above.

The dashed line in figure 1 is drawn through the empirical fractionation factors estimated by Wenner and Taylor (1973). Their estimation was based on the data point at 400°C by Suzuoki and Epstein (1976) and D/H ratios of certain natural serpentines and inferred fluids for the serpentinization. Contrary to their results, our data indicate that the fractionation factors become greater than unity above a "cross-over" temperature of 210°C. In many silicate-water systems, the mineral-water oxygen isotope fractionation factors are greater than unity at low temperature but decrease with temperature, crossing the unity line at some higher temperature. They then approach unity again with further increase of temperature. The "cross-over" of this type occurs because the reduced partition function ratios (r.p.f.r.) of water decrease with increasing temperature more slowly than that of silicates due to the high vibrational frequency of OH in water. Similarly in serpentine, OH ions are under the influence of the crystal field of serpentine. Vibrational and restricted rotational motions of the ions in the crystal field would overcome the intermolecular interaction of liquid water at low temperature and enrich D into serpentine. However, with increasing temperature, the contribution of these low frequency vibrations would decrease more rapidly than that of intermolecular interaction of liquid water. The "cross-over" at 210°C may be interpreted in this way.

Wenner and Taylor (1973) indicated that the D/H ratios of continental serpentinites are lower by about 40-60 permil than local meteoric water and therefore a correlation exists between latitude and δD. We have found that this correlation can be extended to the

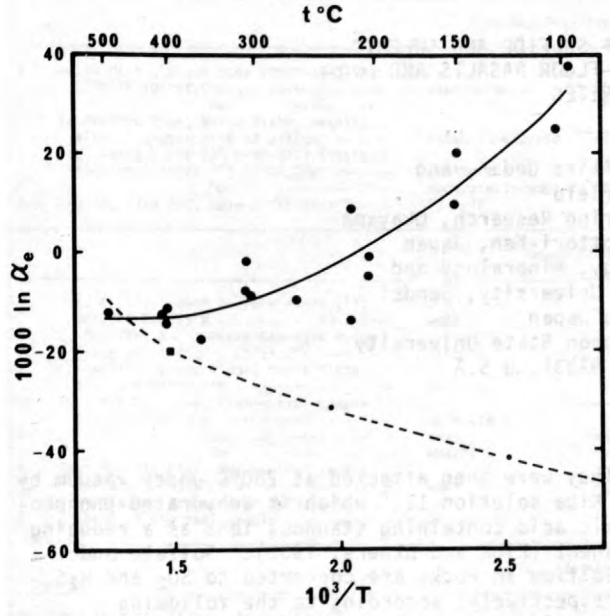

Figure 1.--Experimental fractionation factors between serpentine and water. Dashed line, empirical fractionation factors by Wenner and Taylor (1973). Solid line, least-square fit to the data points and expressed by equation (1) in text.

Table 1.--Experimental conditions and results of partial equilibrium runs

[Water pressure is 2000±100 bars except for run No. 1 (1000 bars), No. 2 (2500 bars), No. 14 (3800 bars), and No. 15 (1000 bars)]

Run no.	Temp. (°C)	Period (hours)	$10^3 \ln\alpha_e$ (permil)	Percent exchanged
1	98	1254	38.5	17.9
2	101	2880	25.9	24.5
3	152	1254	10.0	54.1
4	151	1807	20.8	45.4
5	204	3308	- 0.7	65.7
6	204	3308	- 4.5	69.0
7	217	730	8.7	69.2
8	217	1708	-13.4	78.4
9	262	156	- 9.3	77.0
10	306	122	- 8.7	85.8
11	308	163	- 1.6	87.0
12	308	163	- 8.3	83.7
13	359	161	-17.5	92.7
14	405	216	-11.4	92.4
15	405	384	-14.2	93.0
16	408	300	-12.5	90.6
17	494	192	-12.9	92.9

Japanese serpentinites (Sakai and Tsutsumi, unpub. data). According to the empirical fractionation factors of Wenner and Taylor (1973), the latitude-δD correlation can be explained by the assumption that the continental serpentinites formed by equilibrium serpentinization of ultramafic rocks by local meteoric hydrothermal solution under conditions of relatively high water/rock ratios. The present results indicate, however, that at no temperatures below 500°C and above 100°C can serpentine be lighter than fluids by more than 18 permil. At inferred temperatures for serpentinization (100°-200°C), the serpentine should be enriched in D compared to the fluids. Thus, the present results require some other mechanism(s) to interpret the latitude-δD correlation.

If the light water is consumed preferentially in serpentinization and if later exchange does not occur, the same latitude-δD correlation would be found as a result of the kinetic serpentinization under a high water/rock ratios. Our preliminary experiments at 200°C indicated that a kinetic isotope effect of the desired magnitude and direction do exist. However, it was not possible to suggest any effective means to protect the kinetic isotope effect from later exchange. Alkaline environments which would prevail in serpentinization of ultramafic rocks cannot slow down the exchange rate.

Oceanic serpentinites of lizardite-chrysotile also are 40-60 permil lower in D/H than seawater (Wenner and Taylor, 1973). The present results suggest two possible origins for the oceanic serpentinites; (1) the kinetic serpentinization of ultramafic rocks by seawater, implying a relatively shallow site of serpentinization in the ocean crusts or (2) equilibrium serpentinization by a 3 : 1 mixture of upper-mantle water (-70 permil) and seawater, suggesting a deeper site of serpentinization.

Gonfiantini, R., 1977, Consultant's meeting on stable isotope standards and intercalibration in hydrology and in geochemistry: International Atomic Energy Agency, IAEA 77-3977.

Suzuoki, T., and Epstein, S., 1976, Hydrogen isotope fractionation between OH-bearing minerals and water: Geochimica Cosmochimica Acta, v. 40, p. 1299.

Northrop, D. A., and Clayton, R. N., 1966, Oxygen isotope fractionation in systems containing dolomite: Journal of Geology, v. 74, p. 174.

Wenner, D. B., and Taylor, H. P., Jr., 1973, Oxygen and hydrogen isotope studies of the serpentinization of ultramafic rocks in oceanic environments and continental ophiolite complexes: American Journal of Science, v. 273, p. 207.

$\delta^{34}S$ AND CONCENTRATION OF SULFIDE AND SULFATE SULFURS IN SOME OCEAN-FLOOR BASALTS AND SERPENTINITES

By Hitoshi Sakai[1], Akira Ueda[2], and Cyrus W. Field[3]

[1]Institute for Thermal Spring Research, Okayama University, Misasa, Tottori-Ken, Japan

[2]Department of Petrology, Mineralogy and Economic Geology, Tohoku University, Sendai Miyagi-Ken, Japan

[3]Department of Geology, Oregon State University Corvallis, Oregon 97331, U.S.A.

Five basalts from the Nazca Plate, Bauer Deep (Deep Sea Drilling Project Leg 34), a basalt from Deep Sea Drilling Project Leg 46, 3 submarine basalts from western Oregon, and 8 basalts and 4 serpentinites from dredge-hauls at ocean ridges and a trench, were analyzed for the concentration and isotopic ratio of sulfur in sulfide and sulfate phases. Epigenetic pyrites separated from these basalts have been previously analyzed for $\delta^{34}S$ (Field and others, 1976). The basalt samples were carefully purified by removing any epigenetic pyrite veinlets. They were then attacked at 280°C under vacuum by "Kiba solution II," which is dehydrated phosphoric acid containing stannous ions as a reducing agent (Kiba and others, 1955). Sulfate and sulfide in rocks are converted to SO_2 and H_2S, respectively, according to the following reactions:

$$SO_4^{2-} + Sn^{4+} + 4H^+ \rightarrow SO_2 + Sn^{6+} + 2H_2O \quad (1)$$

and

$$S^{2-} + 2H^+ \rightarrow H_2S. \quad (2)$$

During the reaction time of about 2 hours, 5 to 10 percent of the sulfate also is reduced to H_2S:

$$SO_4^{2-} + Sn^{4+} + 10H^+ \rightarrow H_2S + 4Sn^{6+} + 4H_2O. \qquad (3)$$

The $\delta^{34}S$ value of this H_2S was found experimentally to be about 5 to 10 permil lower than the original sulfate value because of the kinetic isotope effect in the sulfate breakdown. However, because no SO_2 is formed from sulfide and because in basaltic rocks, sulfate/sulfide ratios are generally below unity (table 1), the concentration and $\delta^{34}S$ of both sulfate- and sulfide-sulfurs in rocks can be obtained separately (but simultaneously) from the volumes and $\delta^{34}S$ values of these SO_2 and H_2S after appropriate corrections are made for the hydrogen sulfide generation from sulfate.

Other major gaseous products of the reaction are carbon dioxide from carbonate, and hydrocarbons presumably from carbide. Graphite, another major carbon compound in igneous rocks, would not react with "Kiba solution II." SO_2, H_2S, CO_2, and hydrocarbons (C_nH_m) were collected in a liquid N_2-cooled trap. They were then released at the freezing temperature of trichloroethylene (-86°C) and passed through Cu_2O at 200°C. The H_2S was fixed in the Cu_2O as Cu_2S, and the other gases were collected into another liquid N_2-cooled trap. The Cu_2S was converted to SO_2 by raising the temperature of the furnace to 900°C, and the SO_2 was measured for volume and set aside for the isotopic-ratio measurements. The CO_2 in the second trap was distilled from the remaining gases at the freezing temperature of normal pentane (-130°C). The SO_2 and C_nH_m were then passed through Cu_2O at

Table 1.--Concentration and isotopic ratios of sulfur and carbon in oceanic basalts

[The concentration and $\delta^{34}S$ values were corrected for the generation of H_2S from SO_4^{2-}, assuming that 7.5 percent of the SO_4^{2-} was reduced to H_2S with the kinetic isotope effect of -4.5 permil. Epigenetic pyrite data from Field and others, 1976.]

	Sample number and locality	Alteration	Age	S (ppm)		$\delta^{34}S_{CD}$ (permil)			Epigenetic pyrite
				S^{2-}	SO_4^{2-}	S^{2-}	SO_4^{2-}	ΣS	
	Eocene submarine basalts, Western Oregon								
1	Western Oregon, Siletz River Volc.,								
2	Eocene Coast Range Mtns. ----------	moderate	Eocene	30	107	+0.3	-1.5	-1.1	-17.4
3	Do ----------	weak/moderate	Do	325	51	+17.4	+8.3	+12.7	+14.2
	Western Oregon, Lower Umpqua Formation, Eocene (altered) Coast Range Mtns. ---	intense	Do	280	24	-0.9	±0.0	-0.8	-2.5
	Deep Sea Drilling Project basalts								
4	Nazca Plate, Bauer Deep (DSDP-34-319A)								
5	13°01'S 101°31.5'W ----------	weak/moderate	16 m.y.	254	109	+1.9	-6.9	-0.7	-14.1
6	Do ----------	Do	16 m.y.	642	176	-0.5	-5.4	-1.6	+23.0
7	E. Pacific Rise, Nazca Plate; basalt; altered glassy rind of pillow? -------	intense/moderate	<5 m.y.	231	52	-2.2	+15.9	+1.1	--
8	East Nazca Plate (DSDP-34-321) (vesicle fillings) 12°01.3'S 81°54.2'W --------	unaltered	40 m.y.	1181	172	-12.7	-3.2	-11.4	+2.0
9	Do ----------	moderate/intense	40 m.y.	1022	136	-0.4	-0.2	-0.3	-1.1
	Leg 46, Site 396, Hole B (Atlantic) ----	18-1-7F	--	386	223	+4.3	+0.3	+2.8	--
	Ocean ridge basalts								
10	N.E. Pacific, Juan de Fuca Ridge (1X)								
11	44°20'N 129°55'W ----------	weak	<5 m.y.	190	32	-0.4	+8.8	+0.9	-5.6
12	E. Pacific, Nazca Plate Carnegie Ridge (altered) 1°45.7'S 85°54.2'W ---------	intense	8 m.y.	139	31	+0.3	-3.1	-0.3	-24.2
13	E. Pacific, Cocos Ridge, Cocos Plate 6°37.4'N 85°14.2'W ----------	weak	14 m.y.	198	97	-3.3	+5.2	-0.5	-15.5
14	East Pacific Rise, dredge-haul sample 32°34'S 109°19'W ----------	moderate	<5 m.y.	267	39	+5.4	+11.0	+6.1	-2.7
15	Do ----------	weak	<5 m.y.	706	67	+0.1	+3.0	+0.3	--
16	Do ----------	moderate	<5 m.y.	12	10	-2.7	+7.2	+5.0	-4.1
17	East Pacific Rise, dredge-haul sample 33°00.5'S 109°30.5'W ----------	weak	<5 m.y.	883	134	-0.2	+0.5	-0.0	--
18	Mid-Atlantic Ridge, near 30°N, Duplicates of the same sample ----------	unaltered	--	958	66	+0.6	+5.3	+0.8	--
			--	1045	67	+0.2	--	--	--
	Oceanic serpentinites								
19	Mid-Atlantic Ridge; ultramafic,								
20	altered to serpentinite ----------	serpentinite	<5 m.y.?	10	309	+2.2	+19.9	+19.3	--
21	Famous Area (fracture zone B) 36°34.5'N 33°31'W ----------	Do	<5 m.y.?	6	265	+2.0	+20.2	+19.7	--
22	Mid-Atlantic Ridge 30°06'N 42°08'W, 1460 m depth ----------	Do	--	147	250	+5.6	+15.4	+11.8	--
	Yap trench, 7150-7500 m deep, near shore slope 9°39.2'N 138°30.6'E ------	Do	--	12	254	--	+19.7	--	--

900°C in order to isotopically equilibrate the oxygen in the SO_2 with Cu_2O and combust the hydrocarbons to CO_2. The SO_2 and CO_2 were separated using normal pentane and each fraction was measured for volume and isotope ratios. All the procedures were carried out within a single vacuum line and no wet chemistry was involved. This enables us to handle very small quantities of sulfur and carbon compounds. A rock sample containing 50 micrograms of sulfur may be isotopically and chemically analyzed without difficulty.

The results of the present analyses and those of Field and others (1976) are summarized in table 1. Some preliminary conclusions and questions about the results may be summarized as follows:

1. The ocean-floor basalts studied show considerable scatter in both the concentration and $\delta^{34}S$ of the total sulfur. The unusually high $\delta^{34}S$ of sample no. 4 may be due to contamination by epigenetic pyrite in the sample. The unaltered to weakly altered basalts have $\delta^{34}S$ from -0.5 to 0.9 permil, except for 7, implying that their sulfurs are essentially of upper mantle origin. For the other samples, tests for any definite correlation among these data and the mode and extent of alteration are incomplete.

2. In all of the basalts studied, sulfate sulfur makes up approximately 10 percent or more of the total sulfur. In 11 of the 17 basalts, $\delta^{34}S$ of the sulfate is higher than that of sulfide, with the fractionation factors varying from near zero to 10 permil. Important questions are: in what form and where in what part of the rocks does the SO_4 exist? and what do the SO_4/S ratio and the fractionation factor imply?

3. Serpentinites from both the ocean ridges and the trench contain essentially no sulfide except for sample 21. They all contain about 300 ppm of sulfate sulfur of seawater origin. Grinienko and others (1975) reported similar results and concluded that the sulfate is adsorbed as ions from seawater. We have looked for other possibilities, such as barite and/or anhydrite, but so far have been unsuccessful.

4. Transfer of sulfur between seawater and ocean-floor basalts may have an important effect on the geochemical cycle of sulfur and sulfide mineralization on the ocean floor. Although no clear correlation exists between the sulfur content, sulfate/sulfide ratio, the $\delta^{34}S$ values, and the grade and degree of alteration, the data in table 1 strongly suggest that, in most cases, the altered basalts lost sulfur to varying extents, but the isotope fractionation in the leaching process is not large. The leached sulfur could have recrystallized within ocean-floor basalts as the epigenetic pyrite (Field and others, 1976). The $\delta^{34}S$ values for the majority of the epigenetic pyrite samples in table 1 and those determined by Krouse and others (1977) for pyrites in basalts from Deep Sea Drilling Project Leg 37, Holes 333A and 332B, are also negative. This would imply that the leached magmatic sulfur ($\delta^{34}S$ = 0 to 1 permil) is only partially retained in basalts and the rest may have been lost to seawater. However, net sulfur balance between seawater and the ocean floor depends on the extent to which bacterial reduction of sulfate at the sediment-ocean interface affect the sulfur balance.

Field, C. W., Dymond, J. R., Heath, G. R., Corliss, J. B., and Dasch, E. J., 1976, Sulfur isotope reconnaissance of epigenetic pyrite in ocean-floor basalts, Leg 34 and elsewhere: in Initial Reports of the Deep Sea Drilling Project, U.S. Government Printing Office, Washington, v. 34, p. 381-384.

Grinienko, V. A., Dmitriev, L. V., Migdisov, and Sharas'kin, A. Ya., 1975, Sulfur contents and isotopic composition of igneous and metamorphic rocks from Mid-Ocean Ridges: Geochemistry International, v. 12, p. 132-137.

Kiba, T., Takagi, T., Yoshimura, Y., and Kishi, I., 1955, Tin (II)-strong phosphoric acid. A new reagent for the determination of sulfate by reduction to hydrogen sulfide: Bulletin of the Chemical Society of Japan, v. 28, p. 641-644.

Krouse, H. R., Brown, H. M., and Farqubarson, R. B., 1977, Sulfur isotope compositions of sulphides and sulphates, Deep Sea Drilling Project Leg 37: Canadian Journal of Earth Sciences, v. 14, p. 787-793.

PRELIMINARY REPORT ON INITIAL LEAD AND STRONTIUM ISOTOPES FROM OPHIOLITIC AND BATHOLITHIC ROCKS SOUTHWESTERN FOOTHILLS SIERRA NEVADA CALIFORNIA

By Jason Saleeby[1] and James H. Chen[2]
[1]Department of Geology and Geophysics
University of California
Berkeley, California 94720
[2]Department of Geological Sciences
University of California
Santa Barbara, California 93106

Initial lead and strontium isotopic ratios have been determined for three suites of gabbros from the mafic-ultramafic belt of the Kings and Kaweah Rivers in the southwest Sierra Nevada foothills. Geochronological control is derived from zircon studies on the same suites (Saleeby and Sharp, 1978). The oldest suite of gabbro is from the metamorphosed Kings-Kaweah ophiolite belt whose petrogenetic age is 250 to 300 m.y. The second suite is a 169 m.y. (Middle Jurassic) syntectonic gabbrodiorite complex which intrudes the ophiolite. The third suite is a posttectonic suite of voluminous olivine-hornblende gabbros, which are intimately related to norites, pyroxene diorites, and quartz diorites, all yielding ages from 115 to 125 m.y. (Early Cretaceous). The Jurassic and Cretaceous gabbros constitute the mafic members of the composite Sierra Nevada batholith. The ophiolitic gabbros are part of an allocthonous terrane, which forms part of the western metamorphic wall of the batholith.

The isotopic compositions of lead from the ophiolitic suite range from 17.90 to 17.95 for $^{206}Pb/^{204}Pb$, and from 15.45 to 15.52 for $^{207}Pb/^{204}Pb$. The Jurassic suite yields a more radiogenic lead of 18.47 for $^{206}Pb/^{204}Pb$ and 15.60 for $^{207}Pb/^{204}Pb$. The Cretaceous olivine gabbros yield ratios similar to the ophiolitic gabbros. In a $^{206}Pb/^{204}Pb$ - $^{207}Pb/^{204}Pb$ diagram, the ophiolitic and Cretaceous gabbros plot within the ocean ridge basalt field. The Jurassic gabbro lies within the field of Sierran granitoids (Chen and Tilton, 1978).

Initial $^{87}Sr/^{86}Sr$ value on a gabbro from the ophiolitic suite is 0.7026. Initial $^{87}Sr/^{86}Sr$ values determined on the Cretaceous suite range from 0.7031 to 0.7039, and for the Jurassic suite a value of 0.7032 was determined. These data are in agreement with the values measured on other batholithic rocks of the western Sierra by Kistler and Peterman (1973). Lead and strontium isotopic studies on other fractions of the Kings-Kaweah mafic-ultramafic belt are in progress.

Several significant conclusions can be drawn from this study.

1. The ophiolitic and Cretaceous suites bear some of the least radiogenic leads on the west coast. They are less radiogenic than the oceanic-affinity volcanic rocks of the Franciscan assemblage to the west (Sinha and Davis, 1971), and they are comparable to leads measured on the eastern Taiwan ophiolite (Chen, unpub. data) and on Mid-Atlantic ridge basalts (Tatsumoto, 1978).

2. The ophiolitic and Cretaceous suites were derived from a source that had the characteristics of oceanic upper mantle. Geologic relations indicate that in the case of the ophiolitic suite petrogenesis was in the oceanic realm far removed from the Sierran region, whereas the Cretaceous suite was generated beneath its present position.

3. When compared with the more radiogenic initial lead and strontium values measured on batholithic rocks to the east (Kistler and Peterman, 1973; Chen and Tilton, 1978), these data support the notion that ophiolitic rocks of the Kings-Kaweah belt mark a fossil suture between oceanic and continental lithospheric plates (Saleeby, 1977). The fundamental nature of this suture has been masked by the Sierra Nevada batholith.

Chen, J. H., and Tilton, G. R., 1978, Lead and strontium isotopic studies of the southern Sierra Nevada batholith, California: Geological Society of America Abs. with Programs, v. 10, p. 99-100.

Kistler, R. W., and Peterman, Z. E., 1973, Variations in Sr, Rb, K, Na and initial Sr^{87}/Sr^{86} in Mesozoic granitic rocks and intruded wallrocks in Central California: Geological Society of America Bulletin, v. 84, p. 3489-3512.

Saleeby, J. B., Fracture zone tectonics, continental margin fragmentation, and emplacement of the Kings-Kaweah ophiolite belt, southwest Sierra Nevada, California, in, Coleman, R. G., and Irwin, W. P., eds., North American Ophiolite Volume: Portland, Oregon Department of Geology and Mineral Industries Bulletin, v. 95, p. 141-160.

Saleeby, J. B., and Sharp, W. D., 1978, Preliminary report on the behavior of U-Pb zircon and K-Ar systems in polymetamorphic ophiolitic rocks and batholithic rocks, southwestern Sierra Nevada foothills, California: (this conference).

Sinha, A. K., and Davis, T. E., 1971, Geochemistry of Franciscan volcanic and sedimentary rocks from California: Carnegie Institution of Washington Year Book 69, 1969-1970, p. 394-400.

Tatsumoto, M., 1978, Isotopic composition of lead in oceanic basalt and its implication to mantle evolution: Earth and Planetary Science Letters, v. 38, p. 63-87.

PRELIMINARY REPORT ON THE BEHAVIOR OF U-Pb ZIRCON AND K-Ar SYSTEMS IN POLYMETAMORPHOSED OPHIOLITIC ROCKS AND BATHOLITHIC ROCKS, SOUTHWESTERN SIERRA NEVADA FOOTHILLS, CALIFORNIA

By Jason Saleeby and Warren Sharp
Department of Geology and Geophysics
University of California
Berkeley, California 94720

Ophiolitic rocks of the southwest Sierra Nevada foothills form part of the western metamorphic wall of the Sierra Nevada batholith (fig. 1). Geochronological studies were undertaken to determine: (1) The igneous petrogenetic age of the ophiolite; (2) The age of a pre-batholith dynamic greenschist to amphibolite facies metamorphic event experienced by the ophiolite; and (3) The emplacement ages of the batholithic rocks. Geochronological work was interfaced with detailed structural and petrologic studies. A summary of the geochronological data is given in figure 2.

Zircon from four widely spaced leucocratic dikes within the ophiolite yield suites of internally consistent discordant U-Pb ages. Each zircon sample was split into size and magnetic fractions, which were analyzed separately. Each sample showed the same pattern of greater discordance with increase in U concentration and decrease in grain size. Zircon discordance is attributed to regional thermal metamorphism related to emplacement of the Sierra Nevada batholith. Metamorphism affected the hornblende hornfels facies, but one of the main factors which is believed to have affected the zircon is the intense metasomatic system, which was set up between the batholithic rocks and serpentinite that enclosed the ophiolitic blocks containing the sampled dikes.

Numerous concordant zircon ages measured on the cross-cutting batholithic rocks of gabbroic to granodioritic composition range from 100 to 125 m.y. Mafic metaigneous rocks of the ophiolite, which enclose the leucocratic-dike rocks, were sampled for K-Ar age determinations. The K-Ar ages were reset to ages which fall within the range of concordant batholithic-zircon ages. Concordia plots made for each of the discordant ophiolitic zircon populations yielded lower intercept ages, which are in agreement with the concordant batholithic-zircon ages and the reset ophiolitic K-Ar ages.

The intercept age ranges for each ophiolitic-zircon population are derived by fitting a family of lines through the error brackets of the discordant U-Pb points on a concordia plot, and noting the ranges over which these lines intercept concordia. The upper intercept falls around 300 m.y. and may represent an initial crystallization age for the ophiolitic-dike rocks. The oldest $^{206}Pb/^{238}U$ age obtained from the discordant populations is 247 m.y. $^{206}Pb/^{207}Pb$ ages for the discordant populations range back to 275 m.y. These data together suggest that the igneous ages of the ophiolitic-dike rocks are between 250 and 300 m.y. The dike rocks are an integral part of the ophiolite assemblage and thus this petrogenetic age range is assigned to the entire igneous assemblage of the ophiolite. The petrogenetic age is considered an oceanic spreading center age.

Mafic metamorphic tectonites of amphibolite facies were sampled from the ophiolite in domains of lowest textural and mineralogic contact metamorphic grade. K-Ar ages on amphibole represent a minimum age on the dynamic metamorphic event that was related to tectonic disruption of the ophiolite. The minimum ages range from 179 m.y. to 190 m.y. Where sampled adjacent to the batholith a similar mafic tectonite sample (not shown on fig. 2) had its K-Ar system reset to the batholithic-zircon age. Geological relations suggest that the dynamic metamorphic age should be close to the petrogenetic age of the ophiolite, and that this metamorphism occurred

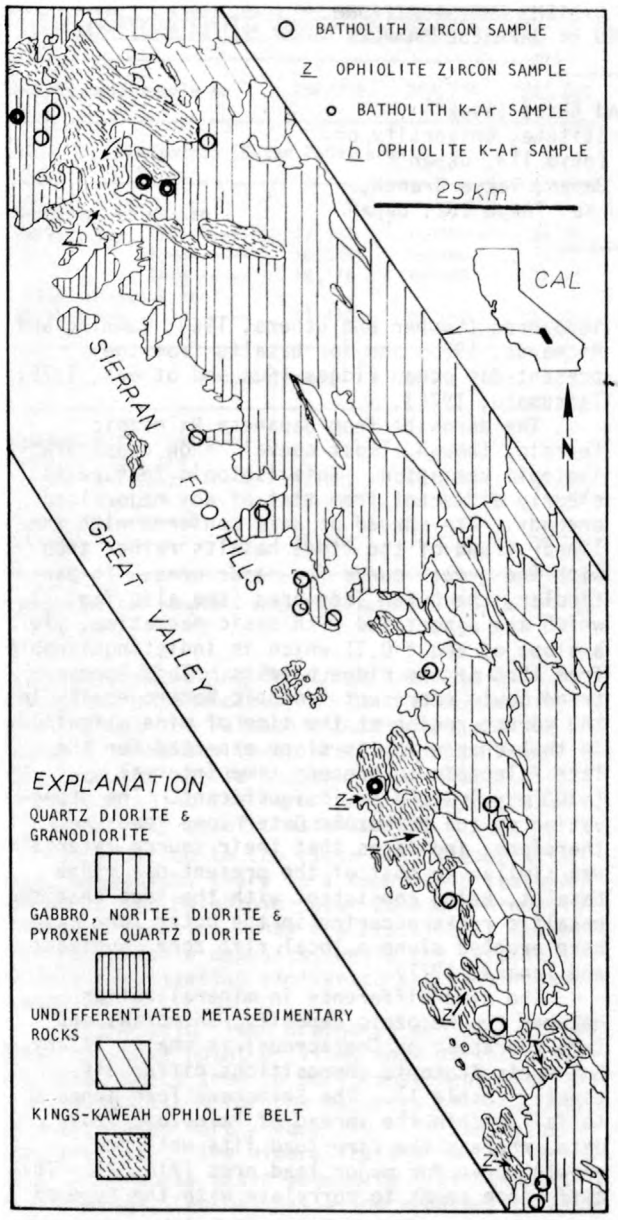

Fig. 1.--Generalized geologic map of part of the southwestern Sierra Nevada foothills showing locations of geochronological samples.

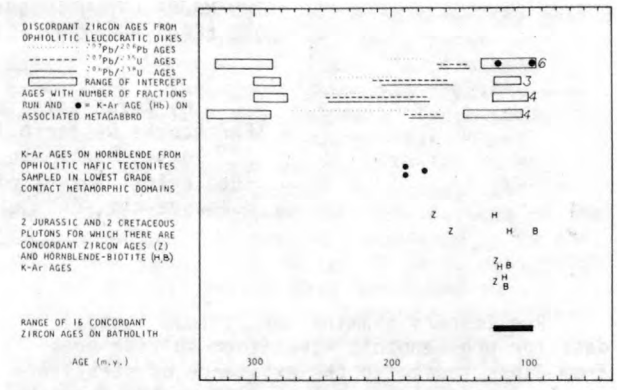

Fig. 2.--Plot of zircon U-Pb and K-Ar age data for ophiolitic and batholithic rocks. K-Ar data on two Cretaceous plutons after Evernden and Kistler (1970).

in the ocean domain (Saleeby, 1977).

An older deformed fraction of the batholith, which cuts the ophiolite near its northern end, yields concordant-zircon ages of 169 m.y. and 157 m.y. These older plutons, in addition to the ophiolite, are cut by the voluminous younger batholithic rocks. K-Ar systems on the older plutons have been reset to the age range of the younger batholithic rocks.

Concordant zircon ages of 121 m.y. and 120 m.y. were measured on two plutons along the western margin of the batholith for which Evernden and Kistler (1970) report hornblende-biotite K-Ar pairs of 121 to 113 m.y. and 115 to 114 m.y. The zircon ages are interpreted as crystallization ages whereas the K-Ar ages are interpreted as cooling ages. The close correspondence between the zircon and K-Ar ages, which is in contrast to the older batholithic rocks, is consistent with the plutons being young and located at the extreme western edge of the batholith.

The following conclusions can be drawn from this study:

1. Even though the ophiolite consists of a polymetamorphic assemblage of mafic and ultramafic rocks, its igneous petrogenesis can be placed between 250 m.y. and 300 m.y.

2. The first high-grade metamorphism of the ophiolite occurred prior to 190 m.y. This metamorphism may have occurred in the oceanic realm in conjunction with igneous petrogenesis.

3. Plutons of 169 m.y. and 157 m.y. ago intruded the disrupted ophiolite and then were deformed and later contact metamorphosed.

4. Voluminous plutons ranging in age from 125 m.y. to 100 m.y. intruded the ophiolite and older plutons and caused high-grade contact metamorphism, which is isotopically recorded in ophiolite zircon discordance and in partial to complete resetting of K-Ar systems in both the ophiolitic and the older plutonic rocks.

Evernden, V. F., and Kistler, R. W., 1970, Chronology of Emplacement of Mesozoic batholithic complexes in California and western Nevada: U.S. Geological Survey Professional Paper, 623, 42 p.

Saleeby, J. B., 1977, Fracture zone tectonics, continental margin fragmentation, and emplacement of the Kings-Kaweah ophiolite belt, southwest Sierra Nevada, California, in Coleman, R. G., and Irwin, W. P., eds., North American Ophiolite Volume: Oregon Department of Geology and Mineral Industries Bulletin, v. 95, p. 141-160.

TWO MAJOR EVOLUTIONARY SYSTEMS FOR STRATIFORM ORE LEADS AS EXEMPLIFIED BY JAPANESE SAMPLES

By Kazuo Sato[1] and Akira Sasaki[2]
[1]Earthquake Research Institute, University of Tokyo, Bunkyo-ku, Tokyo 113, Japan
[2]Geological Survey of Japan, Tokyo Branch, 8 Kawada-cho, Shinjuku-ku, Tokyo 162, Japan

Preliminary examination of lead isotopic data for pre-Cenozoic stratiform sulfide ores from Japan indicated the existence of stratiform ore leads that have evolved differently from the major conformable ore leads (Sato and Sasaki, 1976). The ores, mainly bedded cupriferous iron sulfide ("Besshi-type") deposits, occur in the late Paleozoic and Mesozoic terrains of the Japanese Islands. Locations of the deposits examined are shown in figure 1. New data given in table 1 and the previous results from Sato and Sasaki (1976) are plotted in figure 2 together with isotopic data available for major lead ores (Cooper and others, 1969; Cumming and Richards, 1975) and for basalts from the present-day ocean ridges (Sun and others, 1975; Tatsumoto, 1978).

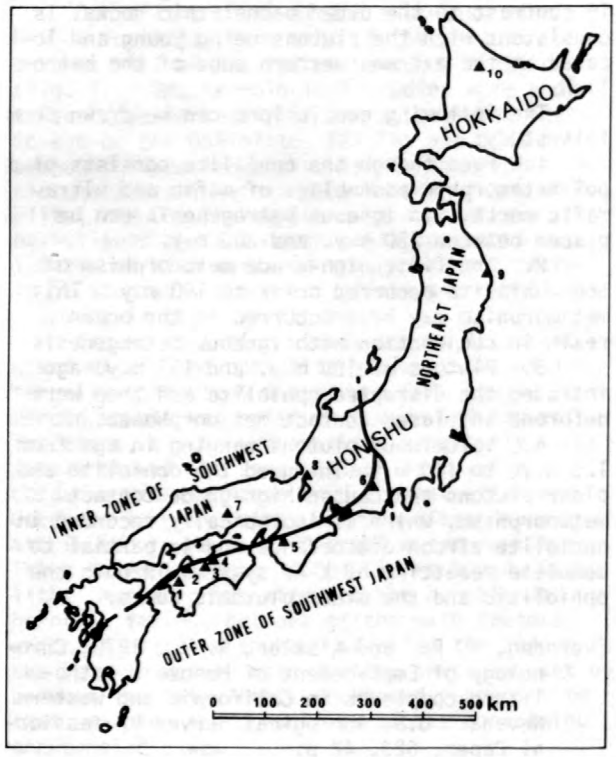

Figure 1.--Locations of the pre-Cenozoic stratiform deposits examined. Outer Zone deposits: 1, Okuki; 2, Chihara; 3, Shirataki; 4, Sazare; 5, Iimori; 6, Oi. Inner Zone deposits: 7, Yanahara; 8, Tsuchikura. Mesozoic deposits: 9, Taro; 10, Shimokawa.

The deposits from Japanese Paleozoic terrain, though almost coeval, show considerable isotopic variation. This isotopic feature is clearly different from that of any major lead orebody. The spread of data conforms with the linear trend of the ridge basalts rather than with the growth curve for major ores. In particular, the Outer Zone ores (see also fig. 1), which are associated with basic magmatism, yield a slope of about 0.11 which is indistinguishable from that of the ridge basalts. This linear trend could represent isotopic heterogeneity in the source region at the time of mineralization, in that change in its slope expected for the late Paleozoic to present time interval (≈300 m.y.) would be insignificant. The observation on the Paleozoic Outer Zone leads, therefore, indicates that their source material was similar to that of the present-day ridge basalts, being consistent with the idea that the basaltic rocks occuring in the Outer Zone may have erupted along a local rift zone (Sugisaki and Tanaka, 1971).

The time difference in mineralization between two Mesozoic deposits, Shimokawa and Taro (Jurassic or Cretaceous) is small, if any, but their isotopic compositions differ distinctly (table 1). The Shimokawa lead appears to fall within the spread of Paleozoic lead data, whereas the Taro lead fits well the growth curve for major lead ores (fig. 2). This difference seems to correlate with the type of

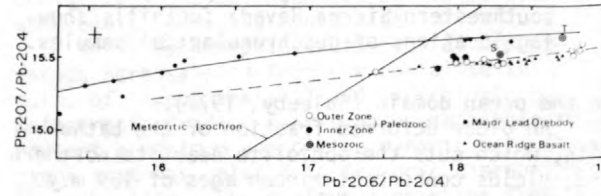

Figure 2.--$^{207}Pb/^{204}Pb$ versus $^{206}Pb/^{204}Pb$ plot for pre-Cenozoic stratiform deposits in Japan, major conformable orebodies, and ocean-ridge basalts. Meteoritic isochron (4.57 b.y.) and ore-lead growth curve are from Cumming and Richards (1975). S, Shimokawa; T, Taro.

Table 1.--Lead isotopic data for some pre-Cenozoic stratiform sulfide deposits in Japan

Locality and sample no.	206/204	207/204	208/204
Paleozoic (Outer Zone) ores			
Okuki mine, Ehime-ken:			
Pyritic ore 1201 -----	17.983	15.459	37.76
1308 -----	18.054	15.465	37.67
1414 -----	18.176	15.487	37.93
Oi mine, Shizuoka-ken:			
Pyritic ore 5 --------	17.444	15.399	37.18
Mesozoic ores			
Shimokawa mine, Hokkaido:			
Iron sulfides ore;			
1810 HCl-leach -----	18.281	15.509	38.30
Residue -------	18.282	15.523	38.29
Taro mine, Iwate-ken:			
Galena[1] ----------	18.706	15.630	38.68

[1]Average of two samples; data from Sato and Sasaki (1976).

associated magmatism for these two deposits, tholeiitic in Shimokawa and calc-alkaline in Taro. Thus, the Paleozoic Outer Zone and the Mesozoic Shimokawa leads are thought to have come from the mantle through ocean-floor magmatism, while the Taro lead, like the major ore leads, may be of crustal origin.

In addition to the close association with basic magmatism, there is a remarkable feature common to the Paleozoic Outer Zone and Mesozoic Shimokawa deposits--they are practically galena-free conformable deposits, while the Taro is a Pb-Zn mineralization similar to the major lead orebodies.

If the major lead orebodies are re-examined from the above point of view, some of the existing data, which seem to be inconsistent with the trend established for the majority of data, may be interpreted more adequately. Of the major lead orebodies, the mineralization in the terrains of Archean basic magmatism (for example, Manitouwadge, Canada) has a low apparent μ value as compared with Proterozoic to Phanerozoic deposits (Oversby, 1974), and is rather difficult to incorporate into a class of a single evolutionary system. These Archean deposits, which may be called "low μ type" orebodies, seem to be generally Pb-impoverished. These features could also suggest a mantle origin for the lead.

The mineralization of "low μ type" stratiform deposits in Japan--the Paleozoic Outer Zone and Mesozoic Shimokawa deposits--may belong to the tectonic regime of large-scale continental rifting and young ocean floors, which brings abundant mantle material to the surface. The environments for mineralization might have been somewhat similar to those of the Archean deposits occurring predominantly in the greenstone belts. On the other hand, many "high μ type" stratiform deposits are found in Proterozoic to Phanerozoic terrains of continental regions where sialic materials prevail. It appears that the major lead ores of this type may only be expected in such environments.

The view presented here would be consistent with the idea of three major tectonic regimes of the Earth crust evolution as first discussed by Engel and others (1974).

Cooper, J. A., Reynolds, P. H., and Richards, J. R., 1969, Double-spike calibration of the Broken Hill standard lead: Earth and Planetary Science Letters, v. 6, p. 467-478.

Cumming, G. L., and Richards, J. R., 1975, Ore lead isotope ratios in a continuously changing earth: Earth and Planetary Science Letters, v. 28, p. 155-171.

Engel, A. E. J., Itson, S. P., Engel, C. G., Stickney, D. M., and Cray, E. J., 1974, Crustal evolution and global tectonics; a petrogenic view: Geological Society of America Bulletin, v. 85, p. 843-858.

Oversby, V. M., 1974, New look at the lead isotope growth curve: Nature, v. 248, p. 132-133.

Sato, K., and Sasaki, A., 1976, Lead isotopic evidence on the genesis of pre-Cenozoic stratiform sulfide deposits in Japan: Geochemical Journal, v. 10, p. 197-203.

Sugisaki, R., and Tanaka, T., 1971, Magma types of volcanic rocks and crustal history in the Japanese pre-Cenozoic geosynclines: Tectonophysics, v. 12, p. 393-413.

Sun, S. S., Tatsumoto, M., and Schilling, J. G., 1975, Mantle plume mixing along the Reykjanes Ridge axis; lead isotope evidence: Science, v. 190, p. 143-147.

Tatsumoto, M., 1978, Isotopic composition of lead in oceanic basalt and its implication to mantle evolution: Earth and Planetary Science Letters, v. 38, p. 63-87.

ROCK DEFORMATION AND ZIRCON-SPHENE U-Pb DATING

By Urs Schaerer
Laboratory for Isotope Geology and Mass Spectrometry
Swiss Federal Institute of Technology
Zurich, Switzerland

Introduction: This paper presents data obtained from the allochthonous part of a nappe complex (Jotun nappe) in central south Norway (Tyin region). The aim of our work was to date the major events by studying the U-Pb-systematics of zircon and sphene from various rock types, which suffered a large scale overthrust under lower greenschist facies conditions.

Previous mapping of the area (Heim and others, 1971) showed that the nappe is composed of Precambrian basement rocks, mainly syenitic gneisses and gabbros, and probably Eocambrian to Cambrian sediments; for example, generally arkoses and sandstones. The gneisses and gabbros have remained almost unaffected by the Caledonian deformation, except some parts very close to the sediment contact. In contrast, the sediments and the adjacent basement parts have been penetratively deformed during the Caledonian orogeny.

The units are inverted and thrust on Lower Palaezoic schists and quartzites lying on the Precambrian shield. Within the nappe three samples from the upper part (unaffected in Caledonian time)--one epidote-biotite-gneiss, one biotite-gneiss, and one biotite-gabbro--have been collected as well as three samples from the lower penetratively deformed part: a cataclastic gabbro, a meta-arkose and a flinty quartzite. In addition, one quartz-diorite sample from north of the nappe area has been analyzed. A fault (Tyin-Gjende Fault) separates the two regions.

All samples, except the quartz-diorite, lie geologically close to each other, for example, only a few hundred meters apart ensuring, therefore, that they had equal temperature conditions during the major Caledonian metamorphism.

Sample description and U-Pb data: Both gneiss samples (fig. 1) show a strong pre-Caledonian deformation under lower amphibolite facies conditions with a zoisite-epidote-hornblende-biotite-K-feldspar-assemblage. The Caledonian influence is limited to fissures with newly grown chlorite. In both samples two morphologically different zircon types occur. One, the probably older generation, shows an euhedral prismatic habit with a length-to-width ratio varying from 2 to 3--the crystals being mostly translucent with corroded faces. The other generation, mostly clear and colorless grains, is euhedral, short prismatic, ranging in its length-to-width ration from 1 to 2. The grain morphology of all sphene fractions does not show any significant difference.

The gabbro (fig. 1) is metamorphosed and slightly deformed under lower amphibolite facies conditions, however, it has preserved about 70 percent of its igneous texture and mineral assemblage. The zircon fractions consist mainly of brown, clear to translucent, often broken, euhedral prisms with a length-to-width ratio between 1 and 6.

The mineral fractions have been sieved and magnetically separated. The Concordia diagram (fig. 1) shows the zircon and sphene data from the two gneiss samples as well as the zircon data from the gabbro. Nine zircon fractions extracted from the gneisses define a discordia (York regression line) with a lower intercept age of 909 m.y. and an upper intercept age of 1694 m.y., 3 sphene fractions from one gneiss lie within analytical error (0.3 percent for $^{206}Pb/^{238}U$, 0.6 percent for $^{207}Pb/^{235}U$, and 0.3 percent for $^{207}Pb/^{206}Pb$) on the curve giving concordant ages at 906 m.y. Thus, corresponding to the lower intercept of the zircon discordia line, 5 data points obtained from the gabbro

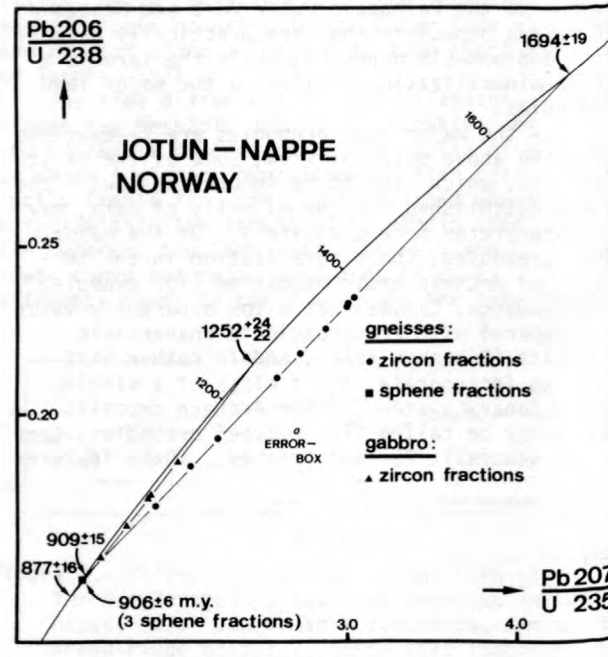

Figure 1.--Concordia diagram of zircon and sphene data obtained from rocks left undeformed during Caledonian time.

zircon plot on a discordia with a lower intercept of approximately 877 m.y. and an upper intercept of approximately 1252 m.y.

Based on structural and petrographic arguments, it can be shown that in the cataclastic gabbro the deformation occurred in Caledonian time. The previous mineral assemblage is converted to an extreme fine-grained matrix with fragments of pyroxenes and plagioclase. Most of the fissures contain newly grown chlorite.

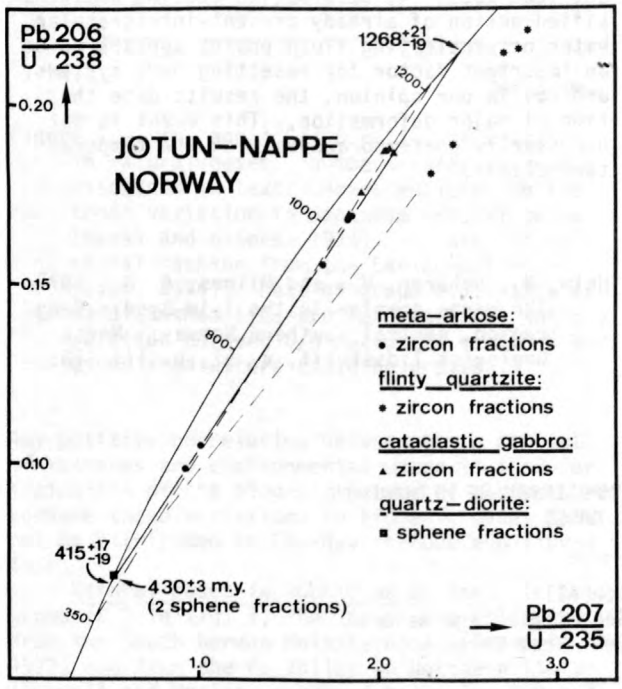

Figure 2.--Concordia diagram of zircon data from rocks deformed in Caledonian time under lower greenschist facies conditions and sphene data from a quartz-diorite intrusion.

Two very different populations of zircon are characteristic in all size and magnetic fractions. One with a length-to-width ratio of 1 to 5 is brown, often containing broken prisms of varying transparency. The second generation has grown in a "peanut-like" shape which seems to be an intergrowth of zircon globules.

The meta-arkose (Valdres-sparagmite) has been penetratively folded and metamorphosed under lower greenschist facies conditions during the Caledonian orogeny. Recrystallized quartz and the growth of sericite originate during this deformation. K-feldspar and plagioclase still show the old detrital shape.

The flinty quartzite (Mellsenn Group) consists of more than 90 percent quartz which recrystallized during the Caledonian deformation.

Zircons from both sediments are extremely heterogeneous, exhibiting a great variety in color and transparency. The shape ranges from euhedral, slightly rounded prisms to completely rounded grains.

The quartz-diorite from north of the studied nappe area is intrusive and only slightly deformed. Biotite seems to be, in part, a secondary mineral. Sphenes from the two separated size and magnetic fractions are transparent brown.

Zircon data from the sediments and from the cataclastic gabbro as well as the sphene data obtained from the quartz-diorite are plotted in figure 2.

The well-defined discordia line for the 5 zircon fractions extracted from the meta-arkose intercepts Concordia at 415 m.y and 1268 m.y. The sphene data from the quartz-diorite lie within analytical error on the Concordia curve, the corresponding age being 430 m.y.

The array of the zircon data from the cataclastic gabbro and from the flinty quartzite also show a significant Caledonian lead loss.

U-contents of the measured mineral fractions: The uranium content in all studied fractions is of the same order of magnitude and can be summarized as follows:

Rock type	Mineral	Number of measured fractions	U (ppm)
Epidote-biotite-gneiss	Zircon	5	357-692
	Sphene	3	332-350
Biotite-gneiss	Zircon	4	350-737
Gabbro (undeformed in Caledonian time)	Zircon	5	270-559
Cataclastic gabbro	Zircon	6	423-986
Meta-arkose	Zircon	5	283-1257
Flinty quartzite	Zircon	5	209-427
Quartz-diorite	Sphene	2	276-281

Interpretation of the results and conclusions: Based on petrographic and stratigraphic observations, structural and lithological mapping, grain morphologies of the zircon populations, and the U/Pb-data, we deduced the following geological development:

1713-1675 m.y.--Intrusion of syenitic magmas or anatexis of earlier material.

1276-1230 m.y.--Intrusion of large gabbroic bodies probably contemporaneous with the first deformation causing the gneissification of the syenites.

903-890 m.y.--Metamorphism and locally strong deformation under lower amphibolite facies conditions.

--Uplift and erosion

? -432 m.y.--Sedimentation of arkoses, sandstones and pelites derived from the basement rocks within the nappe.

432-396 m.y.--Metamorphism, deformation and thrusting under lower greenschist facies conditions.

--Uplift, erosion and faulting.

Despite the same heating conditions in Caledonian time and despite the same spread in U contents of the analyzed mineral fractions, the studied U-Pb systems show a very distinct behaviour. Taking these facts into account, we conclude: (1) Progressive metamorphism under greenschist facies conditions alone does not explain lead loss of zircon populations; (2) The uniform U content of the various zircon fractions makes it difficult to postulate the observed highly variable lead loss as being the result of different degrees of metamictization; (3) On the other hand it appears that there exists a positive correlation between deformation and lead loss; (4) Deformation causing an intensified action of already present intragranular water or penetrating fluid phases appears to be an important factor for resetting U-Pb systems; and (5) In our opinion, the results date the time of major deformation. This event is not necessarily contemporaneous with the temperature climax.

Heim, M., Schärer, U., and Milnes, A. G., 1977, The nappe complex in the Tyin-Bygdin-Vang region, central southern Norway: Norsk Geologisk Tidsskrift, v. 57, p. 171-178.

THE HYDROGEN ISOTOPIC COMPOSITION OF METHANE IN NATURAL GASES

By M. Schoell
Federal Institute for Geosciences and Natural Resources, Hannover, West Germany

The variations of the deuterium content in methanes occuring in nature are poorly known but may be of interest in helping to understand chemical and biological processes by which methane is formed in nature. Therefore, approximately 150 natural gases of various origins have been collected. The methanes were separated and analyzed for their D/H ratios. $^{13}C/^{12}C$ ratios are included in this report because the variations of carbon isotopes in the methane fraction of natural gases is comparatively well understood (Fuex, 1977; Stahl, 1977). The procedure has been described in detail (Kopp, 1978). The results are reported in the usual δ-notation:

$$\delta D = \frac{R\ (Sample) - R\ (Standard)}{R\ (Standard)} \times 1000\ (permil).$$

The standards are SMOW and PDB for hydrogen and carbon, respectively. The results are summarized in figure 1; already published data are also included (Nakai and others, 1974; Lyon, 1974; Schoell, 1977). The presentation of δD versus $\delta^{13}C$ values allows the differentiation of several groups which are discussed separately.

Glacial drift and marsh gases: These gases (group 1 in fig. 1) are of terrestrial biogenic origin and show a variation of approximately 50 permil in their δD values. The D/H ratios in these gases are correlated with the D/H ratios of environmental water in a manner roughly similar to Japanese natural gases of biogenic origin (Nakai and others, 1974). The few gases give the following relationship:

$$\delta D_{CH} = \delta D_{H_2O} - 180.$$

It is not known whether or not this will turn out to be a fundamental relationship between biogenic methane and water. Initial laboratory experiments with raw sewage and deuterated waters revealed the following relationship:

$$\delta D_{CH_4} = 0.4\ \delta D_{H_2O} - 312.$$

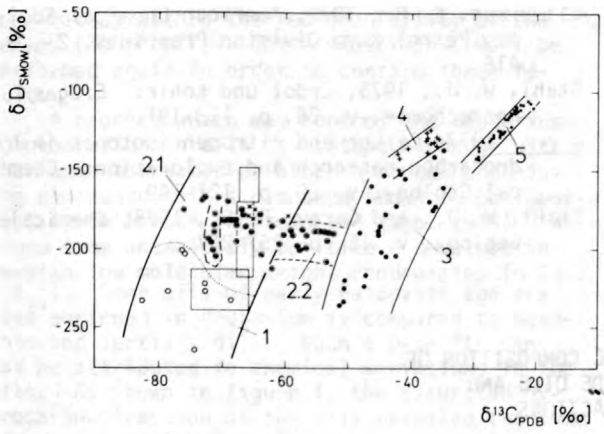

Figure 1.--D/H- and $^{13}C/^{12}C$ ratios of methanes in natural gases. Numbers refer to groups discussed in text. Boxes enclose the isotopic variation in Japanese natural gases (Nakai and others, 1974). X, data of bacterial methane from the Cariacho Trench (Lyon, 1974). Data of group 2.1 within area of dashed line are for gases for which a relation between D/H ratios of methanes and associated waters could be proved.

Any positive correlation between the D content of methanes and environmental water is therefore indicative of the biogenic nature of the methane because these variations in biogenic gases cannot be attributed to CH_4-H_2O isotope equilibration.

Natural gases in subalpine basins: In this group (2.1 in fig. 1) the gases were collected from the South German Molasse Basin (Schoell, 1977) and from the Po Valley in Northern Italy (Schoell and Neglia, unpub. data). The D/H and $^{13}C/^{12}C$-ratios of the methanes in these gases are similar in both areas and are close to young biogenic gases of marine environments (Lyon, 1974). A relationship between the D/H isotope ratios of methanes and associated waters could also be shown in some gases of late Tertiary age from the South German Molasse Basin. It is therefore assumed that the gases which plot in group 2 in figure 1 are of biogenic origin. It is argued in the literature (Schoell, 1977) that the ^{13}C-depletion in young sedimentary basins could be attributed to ^{13}C-isotope fractionation during migration in water wet sediments (Silverman, 1976; S. Neglia, oral commun., 1976). However, the D/H-fractionation in these gases argues for a biogenic origin.

These gases (group 2.2 in fig. 1) primarily occur at basal unconformities of Tertiary basins. The gases are characterized by relatively high ethane contents, which cannot be attributed to biogenic activity. Also, the ^{13}C-content in the methane increases with increasing C_2 content of the gases. This argues for an admixture of gases of thermocatalytic and of biogenic origin.

Gases which are closely associated with oils: These gases (group 3 in fig. 1) are derived from Mesozoic source rocks of various areas (North Sea, North Germany, South Germany, North Italy). The D/H-variations are large (δD: -140 to -230 permil) even in geographically small areas (South Germany). Gases with high C_{2+} content tend to be depleted in deuterium and carbon-13. The D/H fractionations are erratic in some areas and are not fully understood. Various processes should be considered, such as mixing, migration, or kinetic fractionation effects during thermocatalytic reactions in source rocks, as is observed in laboratory simulation experiments (Sackett, unpub. data).

Natural gases from marine source rocks: These are gases (group 4 in fig. 1) from the Delaware and Valverde Basins, Texas, for which a relationship between the ^{13}C-content and maturity of the source rocks has been established (Stahl and Carey, 1975). The D/H ratios vary between -120 and -170 permil. A weak correlation exists between $\delta^{13}C$ and δD values.

Natural gases from terrestrial source rocks: This group (5 in fig. 1) is represented by the NW-German Paleozoic gases, which originate from Upper Carboniferous coal measures. These gases are the most enriched in deuterium and have a D/H range between -105 and -145 permil; the δD and the $\delta^{13}C$ values are positively correlated: ($\delta D = 4.3\ \delta^{13}C - 14$). Marine and terrestrial source rocks can be differentiated by the ^{13}C-content of the thermocatalytic gases (Stahl, 1975). The type of the source rocks is, however, not reflected in the D/H variations of the gases, as can be seen by comparing groups 4 and 5 (fig. 1).

Several mechanisms which could cause the observed D/H variations in the group 4 and 5 gases must be considered: (1) Bond energy differences during the formation of CH_4 from precursor molecules, which is supported by the correlation of $\delta^{13}C$ and δD values; (2) C_{2+}-molecules are enriched in D and may contribute increasingly to the formation of methane, and (3) CH_4-H_2O equilibration around 200°C. The methane D-concentrations of some of the most D-enriched gases are near the CH_4-H_2O equilibrium values if a temperature of 200°C and a D/H ratio of -40 permil for the associated water is inferred. More work is necessary to determine which mechanism is correct.

Craig, H., 1957: Geochimica Cosmochimica Acta, v. 12, p. 133.

_____1961: Science, v. 133, p. 1833-1834.

Fuex, A. N., 1977, The use of stable carbon isotopes in hydrocarbon exploration: Journal of Geochemical Exploration, v. 7, p. 155-188.

Kopp, M., 1978, Unpub. Rep. Bundesanstalt für Geowissenschaften, Archiv no. 79, 894 p. 134-176.

Lyon, G. L., 1974, in, Natural Gases in marine sediments, Kaplan, I. R., ed., Plenum Press, p. 91-97.
Nakai, N., Yoshida, Y., Ando, N., 1974, Chikyakaga KU (Geochemistry) no. 1, p. 7-8.
Sackett, W. M., Unpubl. Rep. Bundesanstalt fur Geowissenschaften, Hannover, Archiv no. 79 894.
Schoell, M., 1977, Erdoel Erdgas Zeitschrift, v. 93, p. 311-322.
Silverman, S. R., 1976, American Chemical Society Petrol Chem Division Preprints, 21, 3, 416.
Stahl, W. J., 1975, Erdöl und Kohle: Erdgas Petrochemie, v. 28, p. 188-191.
_____1977, Carbon and nitrogen isotopes in hydrocarbon research and exploration: Chemical Geology, v. 20, p. 121-149.
Stahl, W. J., and Carey, B. D., 1975, Chemical Geology, v. 16, p. 257-267.

HYDROGEN ISOTOPIC COMPOSITION OF SELECTED CRUDE OILS AND THEIR FRACTIONS

By M. Schoell and C. Redding
Federal Institute for Geosciences and Natural Resources, Hannover, West Germany

The hydrogen isotopic composition of oils and oil fractions of various age and origin were determined. The samples were oxidized in a stream of dried oxygen over copper oxide at temperatures of 800 - 1000°C. The resulting water was transformed to hydrogen (Bigeleisen and others, 1952) and the D/H-ratios were determined with a Vacuum Generators MM 602 mass-spectrometer. The results are expressed in permil as follows:

$$\delta D = \left(\frac{D/H_{(sample)}}{D/H_{(standard)}} - 1\right) \times 1000 \text{ permil.}$$

The standard is SMOW (Craig, 1961). The overall reproducibility of the entire system is ± 2 permil or better.

The analyzed oils are late Tertiary to Ordovician in age and have already been described in geochemical studies (Welte and others, 1975; Stahl, 1978; Schoell, 1978). The δ D-values in the oils range between -90 and -160 permil (fig. 1). This corresponds to the range of δ D-values which have been reported for humic substances and lipids in young marine sediments (Hoering, 1974).

Oils are isotopically heterogeneous; that is, the D-content usually increases in the following manner:

$$\delta D_{\text{saturate hydrocarbon}} < \delta D_{\text{aromatic hydrocarbon}} < \delta D_{\text{NSO bearing compounds.}}$$

This isotopic discrimination may reflect roughly the primary discrimination in precursors; that is, lipids (depleted in D) and humic acids (enriched in D). Alternatively, transformation processes may have caused the hydrogen isotopic variability as it is assumed to explain the ^{13}C discrimination in oils (Silverman, 1971). A positive correlation of $\delta\ ^{13}C$ and δ D-values in oils may only reflect chemical variations of the oils.

The 26 investigated crude oils (and their fractions) did not reveal positively correlated $^{13}C/^{12}C$ and D/H-ratios. This indicates that the known primary and secondary effects that cause $^{13}C/^{12}C$ variations do not similarily affect D/H ratios. For example, a Tertiary crude oil and its fractions from California are highly enriched in ^{13}C ($\delta\ ^{13}C$: -23 to -25 permil) and are among the most depleted in deuterium. A Tertiary crude oil from South Germany which has undergone bacterial degradation showed no change in D/H ratios when compared to other genetically related unaltered oils. Initial laboratory bacterial degradation experiments using aerobic bacteria also show no change in hydrogen iso-

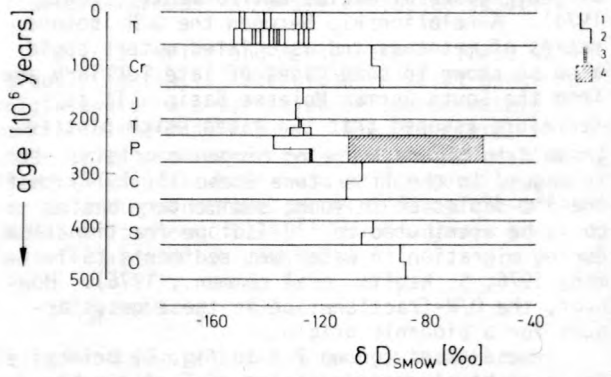

Figure 1.--D/H ratios in crude oils of various age and origins. Vertical lines represent one sample. 1, whole crude (C_{15+}); 2, saturated hydrocarbons; 3, aromatic hydrocarbons; 4, Zechstein condensates, northwest Germany.

tope ratios within the reproducibility of the series (10 permil). These experiments will be performed again in order to confirm these results.

A process which may control the deuterium concentration in oils is isotope exchange with environmental water or other hydrogen containing compounds. This has been shown to be important in cellulose (Epstein and Yapp, 1976). We found some anomalously positive δ D-values in Permian low molecular weight condensates ($\sim C_9 - C_{14}$). Some oils of early Paleozoic age are also enriched in deuterium as compared to Mesozoic and Tertiary oils. Both δ D-shifts cannot be attributed to chemical variations in the oils. As shown in figure 1, the saturated hydrocarbon fraction of the oils revealed the same trend of D-enrichment; the condensates also contain nearly only saturated HC. We have to consider D/H-isotope exchange with oil field brines as one possible explanation. In a parallel experimental study (Köpp, 1978) deuterium shifts have been demonstrated in organic compounds which were in contact with deuterated waters. The observed D-enrichment in the crude oils with increasing age may therefore be the result of exchange reactions of hydrocarbon molecules with oil field brines. This effect is presently being studied in more detail.

Although the genetic interpretation of D/H-ratios in oils is presently not well understood, D/H-variations can be used in combination with $^{13}C/^{12}C$-variations for oil-oil correlation purposes. One example is given in figure 2. The oils are derived from the South German subalpine foredeep in which two independent basins, a western and an eastern basin, produce oils. In the eastern basin the oils are all derived from different Tertiary basal sandstone reservoirs. In the western basin, the oils occur in Triassic sandstones and in upper Tertiary reservoir rocks. The oils cannot be clearly grouped by their chemical composition, because bacterial degradation and water-washing have changed the chemical compositions. Also, the $\delta\ ^{13}C$-values do not allow one to differentiate between the two basins. However, a combined $\delta^{13}C/\delta D$-plot shows the Tertiary oils from both basins to be easily differentiatable. Furthermore, the Triassic oils from the western basin are isotopically identical with oils from one of the reservoirs of the eastern basin.

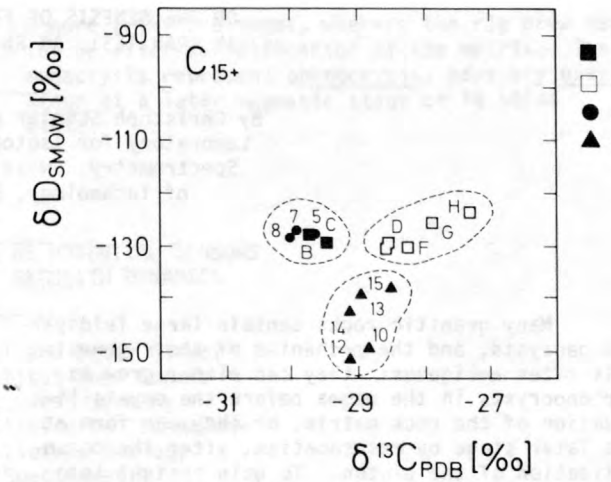

Figure 2.--Example of crude oil correlation (C_{15+}) in a $\delta^{13}C/\delta D$-plot. 1, Tertiary sandstone P; eastern basin; 2, Tertiary sandstone A, eastern basin; 3, Triassic reservoirs, western basin; 4, Tertiary reservoirs, western basin.

The authors are indebted for sample material to the following companies: Amoco Production Company, Chevron Oil Field Research Company, Companie Francaise du Petrole, Deutsche Schachtbau und Tiefbohrgesellschaft mbH, Deutsche Texaco AG, Institut Francais du Petrole, Gewerkschaften Brigitta and Elwerath, Preussag AG, Wintershall AG.

Bigeleisen, J., Perlman, M. L., and Prosser, H. C., 1952: Analytical Chemistry, 24, p. 1356.

Craig, H., 1961: Science, v. 133, p. 1833-1834.

Epstein, S., and Yapp, J., 1976: International Conference on Stable Isotopes, Lower Hutt.

Hoering, T. C., 1974: Annual Report of the Geophysical Laboratory, Carnegie Institute, No. 1655, p. 590-595.

Köpp, M., 1978: Unpub. Rep. Bundesanstalt für Geowissenschaften und Rohstoffe, Archiv-NR. 79894.

Schoell, M., (in press), Erdöl, Erdgas Zeitschrift.

Silverman, S. R., 1971: Proceedings of the 8th World Petroleum Congress, v. 2, p. 47-54.

Stahl, W. J., (in press): Geochemica Cosmochimica Acta.

Welte, D. H., Hagemann, H. W., Hollerbach, A., and Leythaeuser, D., 1975: Proceedings of the 9th World Petroleum Congress Panel Discussion 3, Tokyo, p. 179-191.

ON THE GENESIS OF FELDSPAR MEGACRYSTS IN GRANITES: AN Rb-Sr ISOTOPIC STUDY

By Christoph Schuler and Rudolf H. Steiger
Laboratory for Isotope Geology and Mass Spectrometry, Swiss Federal Institute of Technology, CH-8092 Zurich

Many granitic rocks contain large feldspar megacrysts, and the mechanism of their genesis is often ambiguous: they can either grow as phenocrysts in the magma before the crystallization of the rock matrix, or they can form at a later stage by metasomatism, after the consolidation of the pluton. To gain insight into this problem, megacrysts of the Albtal granite from Black Forest, Germany, are being investigated. This Variscan granite was not subjected to any metamorphism subsequent to its intrusion. The mostly idiomorphic megacrysts are perthitic orthoclases with sizes up to 3 x 6 x 6 cm, the thin-section showing zonal growth with minerals such as biotite and albite included.

The purpose of this study was to decode the history of megacryst development using Sr isotopes as petrogenetic tracers. The following technique was used: Out of a 40 kg block of granite, a large megacryst was removed and cut into the various zones recognized in the thin-section. From the remaining block, a representative whole-rock sample (WR) of the groundmass was prepared and the minerals potassium feldspar (KF) and biotite (BI) were separated. The analytical results are shown in figure 1. The reference isochron that was determined corresponds to an age of 326 ± 2 m.y. with an initial $^{87}Sr/^{86}Sr$ of .7088 ± .0001.

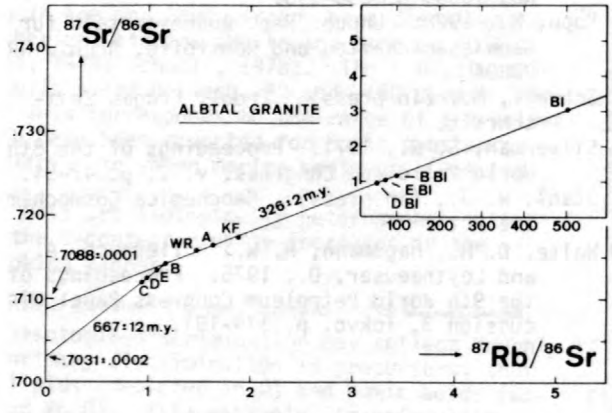

Figure 1.--Sr-evolution diagram showing the mineral isochron of the Albtal granite and data points (A for the rim, B, C, D, and E for the core) for the analyzed zones of the feldspar megacryst.

The results for the zones of the K-feldspar megacrysts are also presented in figure 1. The zones close to the core of the megacryst (C, D, and E) show a low Rb/Sr ratio and low $^{87}Sr/^{86}Sr$ ratio, the data points plotting significantly below the 326 ± 2 m.y. mineral isochron of the host rock. Because the points C, D, E, and B form a linear array, an isochron can be calculated yielding an "age" of 667 ± 12 m.y. and an initial $^{87}Sr/^{86}Sr$ ratio of .7031 ± .0002. The data point of zone A lies on the mineral isochron and is therefore clearly influenced by the matrix. It was possible to separate and analyze the biotite included in three zones of the megacryst. The resulting data points are indicated by D BI, E BI, and B BI. They do not lie on the 667 m.y. isochron of the megacryst zones, because they have lost their radiogenic Sr to the megacryst without significantly affecting its isotopic ratio.

The concentration diagram (fig. 2) indicates that the Rb-content of the feldspar (KF) and the megacryst zones differ only slightly. The Sr-content, on the contrary, is highly variable. Only the Rb and Sr concentration in zone A approaches that of the groundmass potassium feldspar from the granite.

The previous investigation of a K-feldspar megacryst gave quite similar results, the isochron through the inner zones pointing to 509 ±

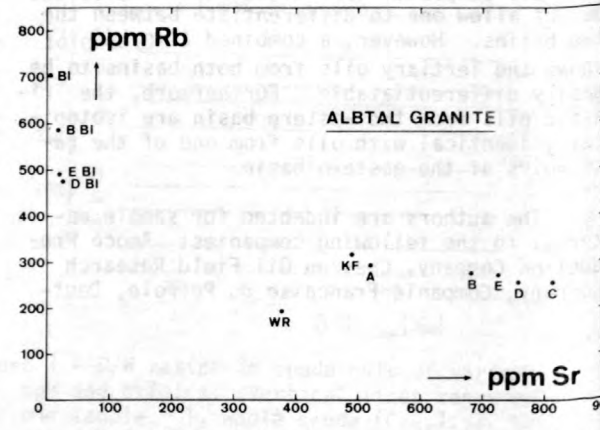

Figure 2.--Rb/Sr-concentrations of the Albtal granite and the different feldspar megacryst zones.

38 m.y. with an initial $^{87}Sr/^{86}Sr$ of .7053 ± .0006.

Therefore, the following conclusions can be drawn: The K-feldspar megacrysts display a two-stage history, the core having crystallized from a more primitive magma, whereas the rim grew during or after solidification of the matrix. The megacrysts represent phenocrysts, possibly overgrown at a later magmatic stage or in solid state.

GAS-RICH METEORITES AS POTENTIAL SENSORS FOR PARENT-BODY REGOLITH DYNAMICS

By Ludolf Schultz[1] and Peter Signer[2]
[1]Max-Planck-Institut Fuer Chemie
D-6500 Mainz, West Germany
[2]Swiss Federal Institute of Technology
Laboratory for Isotope Geology
and Mass Spectrometry
CH-8092 Zurich, Switzerland

Introduction: Noble gas investigations of matrix and individual xenoliths separated from brecciated chondrites with trapped solar gases revealed some interesting disparities. Apparently, there is some resemblance between meteoritic gas-rich breccias and low-grade lunar breccias. This is taken as strong indication that such meteorites originate from regolith-like surface layers of their parent-bodies. The comparison of gas-rich meteorites and lunar surface material may therefore contribute to answering questions such as: (1) What are the time scales of the various processes determining the regolith dynamics on a meteorite parent-body?; and (2) Are the trapped solar gases in gas-rich meteorites evidence of a very ancient solar irradiation or have the solar gases been acquired shortly before ejection of the meteorite from its parent body?

Here we summarize results on the gas-rich meteorites Weston (Schultz and others, 1972), St. Mesmin (Schultz and Signer, 1977) and Djermaia. Meteorite exposure ages, duration of the irradiation of regolith components, time of compaction, and implication to gardening will be discussed in relation to the above questions.

Meteorite exposure ages and pre-irradiation of clasts: In Weston, St. Mesmin, and Djermaia we determined He, Ne, and Ar concentrations and isotope abundances in the matrix as well as in several xenoliths. The matrix contains large amounts of trapped solar gases, which, in most cases, mask the spallogenic and radiogenic gases. The xenoliths, comparable in a sense to rock fragments in the lunar regolith, contain little or no trapped gases. Therefore, they reveal the exposure history of the parent-body regolith to the galactic cosmic radiation. This irradiation effect is superimposed by the cosmic-ray exposure of the material as a meteoroid. Shielding effects within the meteoroid produce variations in the concentration of spallogenic noble gases in different parts of one meteorite. However, investigations of meteorites with galactic cosmic ray exposure only as a meteoroid (Wright and others, 1973; Schultz and Signer, 1976) allow these effects to be eliminated. The basis for this is illustrated in figure 1. For the St. Mesmin meteorite, as an example, figure 2 shows how, from the off-line position of the data point from one clast, D5, an additional exposure must be postulated.

Table 1 summarizes the exposure ages of three polymict chondritic breccias investigated. In each meteorite, one or more clasts are anomalous and have exposure ages which are higher than those of the majority of the clasts. The trapped solar gases in the matrix of all

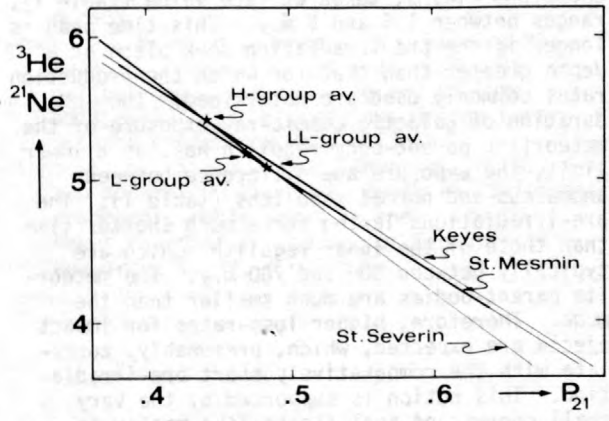

Figure 1.--The spallogenic $^3He/^{21}Ne$ ratio as a function of the production rate P_{21} of ^{21}Ne in the chondrites Keyes, St. Mesmin and St. Severin. Observed correlation is normalized to average values of the respective meteorite class.

Table 1.--Summary of exposure ages

	Exposure age (m.y.)	K-Ar Retention age (b.y.)
Weston		
Mean of 5 clasts-------	23.3±1.3	
Anomalous clast (L3)---	27.3±2.0	
Matrix-----------------	28.2±1.2	
St. Mesmin		
Mean of 12 clasts------	10.3±0.3	4.33±0.26
Anomalous clast (D5)---	11.8±0.5	
H-group xenolith----------		1.36±0.06
Djermaia		
Mean of 5 clasts ------	12.9±0.3	
4 anomalous clasts-----	16 -18	
Matrix-----------------	14.1±0.4	
Exposure age deduced from track studies[1]--	8 -18	

[1]J. C. Lorin and P. Pellas (oral commun.).

three meteorites show that the material of these objects was, at one time, exposed to the solar irradiation in a finely dispersed, that is a regolith-like, state. This observation goes together with evidence from track studies (Lal and Rajan, 1969; Pellas and others, 1969) and the observation of microcraters on meteoritical grains (Brownlee and Rajan, 1973). The exceptionally high exposure ages of some of the meteoritic clasts are therefore taken as indication of an exposure while they were still part of the parent-body regolith.

The duration of the pre-irradiation of the anomalous clasts, taken at face value (table 1), ranges between 1.5 and 5 m.y. This time span is longer if the pre-irradiation took place at a depth greater than that for which the production rates commonly used are determined. The duration of galactic cosmic-ray exposure of the meteoritic parent-body regolith has, as a lower limit, the exposure age difference between anomalous and normal xenoliths (table 1). The pre-irradiations lasted for a much shorter time than those of the lunar regolith, which are typically between 300 and 700 m.y. The meteorite parent-bodies are much smaller than the moon. Therefore, higher loss-rates for impact ejecta are expected, which, presumably, correlate with the comparatively short pre-irradiation. This notion is supported by the very small content of agglutinate-like matter in meteorites (Rajan and others, 1974), by the low concentrations of trapped gases, by track-rich grains in gas-rich meteorites when compared to lunar soils, and by model calculations (Housen and others, 1978).

At what time did the regolith exist and when were the regolithic meteorites compacted?: With respect to these questions, the H-group xenolith found in St. Mesmin is of great importance. This xenolith has concordant K-Ar and U-Th-He gas-retention ages of 1.36 b.y. Recently, a $^{40}Ar/^{39}Ar$ age on the clast of 1.40 b.y. has been reported (G. Turner, oral commun.). The concordance of the gas retention ages indicates a rather intense event, thermal or mechanical, as cause for the low ages. The matter in which this clast is embedded is, however, unaffected by this event. This shows that the degassing event took place before compaction of the material now called "St. Mesmin". Therefore, at least St. Mesmin is known to have been compacted from its parent-body regolith less than 1.4 b.y. ago. One possibility is that the compaction event was identical with the event that caused St. Mesmin to be ejected from its parent body. This event took place less than or at most 10.3 m.y. ago. In this case the regolith on the parent-body is likely to still exist and the trapped solar gases in St. Mesmin may have been acquired, at least in part, quite recently. If, on the other hand, the compaction event took place earlier, then it had to bury the parent-matter of St. Mesmin to a depth great enough to shield it efficiently from the galactic cosmic radiation. There "St. Mesmin" rested until the ejection event unburied it and threw it into space, about 10.3 m.y. ago. Again in this case, the regolith may still exist. Furthermore, it must have been not only buried to a depth on the order of meters, but it must also have been "dormant" at the burial site from the time of the burial event until the time of the ejection event.

Gardening: The short residence times of material in the top layers of its parent-body

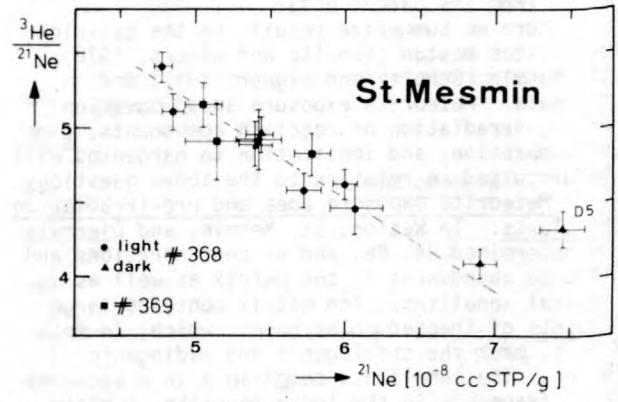

Figure 2.--Observed ^{21}Ne-concentrations in different clasts of the St. Mesmin chondrite. Note that clast D5 has a higher concentration than expected from a one-stage irradiation. This is taken as indication that clast D5 was irradiated before compaction of the breccia.

regolith have implications with respect to the question of the cause for the grain-size dependent concentration of trapped gases in lunar soils. Criswell (1975) interpreted this dependance, detected in lunar soils, as proof for the saturation of the grain surfaces with trapped gases. Becker (1977) criticized this view on the basis of the applicability of the Rosiwal principle to the lunar regolith. Signer and others (1977), on the other hand, found no evidence for saturation. Trapped gas studies in grain-size separates from Khor Temiki (Eberhardt and others, 1965) and Weston (Schultz and others, 1975) also show, in spite of much lower concentrations, an increase of trapped gas concentrations with decreasing grain size. This not only casts additional doubts on Criswell's interpretation, but also gives evidence for basically similar dynamic processes active on the lunar and meteoritic regoliths.

Summary: In summary, one notes many similarities in the exposure history of the lunar regolith and of material from gas-rich brecciated chondrites. It appears likely that the gas-rich meteorites acquired their trapped gases not just in the very early times of the solar system. Concerning the regolith dynamics, it is clear that the mean residence time of material in the parent-body regolith is much shorter than that of material in the lunar regolith because of the higher loss rates and (or) different gardening. More quantitative comparisons of regolith dynamics may become possible when gas-rich meteorites are studied thoroughly and comprehensively with the approaches developed for lunar soil investigations.

Becker, R. H., 1977, Does application of the Rosiwal principle to lunar soils require that concentrations of solar-wind-implanted species be grain-size independent?: Earth and Planetary Science Letters, v. 34, p. 136-140.

Brownlee, D. E., and Rajan, R. S., 1973, Micrometeorite craters discovered on chondrule-like objects from Kapoeta meteorite: Science, v. 182, p. 1341.

Criswell, D. R., 1975, The Rosiwal principle and the regolithic distribution of solar-wind elements: Proceedings of the Lunar Science Conference 6th, 1967.

Eberhardt, P., Geiss, J., and Grögler, N., 1965, Further evidence on the origin of trapped gases in the meteorite Khor Temiki: Journal of Geophysical Research, v. 70, p. 4375.

Housen, K., Wilkening, L. L., Greenberg, R., and Chapman, C. R., 1978, Regolith evolution on small bodies, in "Lunar and Planetary Science IX", p. 546.

Lal, D., and Rajan, R. S., 1969, Observations on space irradiation of individual crystals of gas-rich meteorites: Nature, v. 223, p. 269.

Pellas, P., Poupeau, G., Lorin, J. C., Reeves, H., and Adouze, J., 1969, Primitive low-energy particle irradiation of meteorite crystals: Nature, v. 223, p. 272.

Rajan, R. S., Brownlee, D. E., Heiken, G. H., and McKay, D. S., 1974, Glassy agglutinate-like objects in the Bununu howardite: Meteoritics, v. 9, p. 394.

Schultz, L., Frick, U., and Signer, P., 1975, Noble gases in grain size fractions of Weston; A comparison with lunar soil data: Meteoritics, v. 10, p. 483.

Schultz, L., and Signer, P., 1976, Depth dependence of spallogenic helium, neon, and argon in the St. Severin chondrite: Earth and Planetary Science Letters, v. 30, p. 191.

_____, 1977, Noble gases in the St. Mesmin chondrite; Implications to the irradiation history of a brecciated meteorite: Earth and Planetary Science Letters, v. 36, p. 363.

Schultz, L., Signer, P., Lorin, J. C., and Pellas, P., 1972, Complex irradiation history of the Weston chondrite: Earth and Planetary Science Letters, v. 15, p. 403.

Signer, P., Baur, H., Derksen, U., Etique, Ph., Funk, H., Horn, P., and Wieler, R., 1977, Helium, neon, and argon record of lunar soil evolution: Proceedings of the Lunar Science Conference 8th, p. 3657.

Wright, R. H., Simms, L. A., Reynolds, M. A., and Bogard, D. D., 1973, Depth variation of cosmogenic noble gases in the ∿ 120-kg Keyes chondrite: Journal of Geophysical Research, v. 78, p. 1308.

FISSION-TRACK, K-Ar and Pb-U MINERAL AGES FROM DANTA MICA MINE PEGMATITE (BHUNAS), CENTRAL RAJASTHAN, INDIA--A COMPARISON

By Kewal K. Sharma[1], and K. K. Nagpaul[2]
[1]Wadia Institute of Himilayan Geology,
Dehradum 248001, India
[2]Department of Physics, Kurukshetra University,
Kurukshetra 132119, India

Danta Mica Mine pegmatite (Bhunas, fig. 1) in central Rajasthan is a unique occurrence of pegmatitic uraninite in India and has produced a large tonnage of uraninite, beryl and commercial mica. It was emplaced into the rocks of the Precambrian Aravalli Group, metamorphosed to the upper amphibolite facies, and now occurs as a crescent-shaped complex pegmatite body. A thick hanging-wall zone rich in ruby-colored muscovite is followed by an intermediate zone of blocky microcline and a central quartz core, superimposed upon which is an albite-rich replacement zone. The pegmatite has systematically been mined down to the 18th level for sheet mica for more than 45 years and is, at present, the deepest (165 m) mica mine in Rajasthan. The dating of various minerals from this pegmatite has been attempted using different radiometric techniques. The uraninite collected from the superimposed replacement zone was dated by the Pb-U method (Chaudari and others, 1967) and apatite from the same zone by the fission-track method. Muscovite and garnet collected from the hanging-wall zone of this pegmatite were also dated by the K-Ar (Mehta, 1976) and fission-track (Sharma and others, 1975; Nand Lal and others, 1976) methods, respectively. A comparison of radiometric data on a variety of minerals from the same pegmatite using different methods has been attempted in the present paper.

Garnet, muscovite, and apatite from the pegmatite were dated by the fission-track method using the following etching conditions (table 1).

Table 1.--Etching conditions for fission track counts

Mineral	Solution	Temperature	Time
Garnet--	50 N NaOH	150°C	10-30 Min.
Muscovite	48 percent HF	70°C	30 Min.
Apatite--	5 percent HNO_3	27°C	10-30 Min.

The samples were irradiated with 10^{16} to 10^{17} n/cm^2 of thermal neutrons at the CIRUS reactor, Bhabha Atomic Research Centre, Bombay. Because of low uranium content (8.95 g/g x 10^{-8}) in the garnet, four to six thin sections of 6.25 cm^2-area each were scanned for fossil-track density calculations. Total number of fossil tracks counted were more than 140, whereas total number of induced tracks were greater than 1000. A glass dosimeter of known uranium concentration was also irradiated along with each run of the sample in order to determine the thermal neutron dose. The decay constant (λF) used in calculating the ages in this study was 7.03 x 10^{-17}yr^{-1}. The corrected fission track ages are given in table 2.

Table 2.--Fission track ages from Danta Mica Mine pegmatite

Mineral	Age in m.y. corrected fission-track
Garnet---	990 ± 110
Muscovite	812 ± 25
Apatite--	556 ± 100

The age of the separated mineral fraction of uraninite, collected from the replacement zone of the Danta Mica Mine pegmatite, was determined by Chaudari and others (1967) in the Laboratory of the Centre de Researches radiogeologiques, Nancy, France. The apparent age of the uraninite calculated on the basis of total lead content uncorrected for the presence of primary lead and for alteration effects is:

$$t = 7600 \frac{Pb}{U + 0.36\ Th} \times 10^6 = 1008 \text{ m.y.},$$

or, on the basis of the following formula

$$t = \frac{\lg(U+0.36Th + 1.155Pb) - \lg(U+0.36TH)}{6.6 \times 10^{-5}} = 937 \text{ m.y.}$$

Chaudari and others (1967) also attempted to determine the age of the uraninite on the basis of its Pb isotope composition using an "Atlas" type CH_4 Mass Spectrometer with tungsten filament. Various ages determined are as follows:

$$\frac{^{207}Pb}{^{206}Pb} = 930 \pm 71 \text{ m.y.}$$

$$\frac{^{206}Pb}{^{238}U} = 896 \pm 2 \text{ m.y.}$$

$$\frac{^{207}Pb}{^{235}U} = 906 \pm 20 \text{ m.y.}$$

The above ages should have been concordant had the samples remained a closed system throughout their history, but small losses or gains of pertinent nuclides are bound to occur. According to the authors (Chaudari and others, 1967) the age of 906 ± 20 m.y. determined from the $^{207}Pb/^{235}U$ relationship corresponds to the time of uraninite formation in the pegmatite.

Recently, K-Ar ages of muscovite from the Danta Mica Mine pegmatite were reported by Mehta (1976). The analyses were carried out in the Geochronological Laboratory of the Department of Earth Sciences, University of Leeds (U.K.). Potassium was determined by an EEL flame photometer and the argon measured on a modified AEI MS10 Mass-Spectrometer, using ^{38}Ar as spike.

The ages quoted below (table 3) are the average of three determinations on each sample. The average of the two muscovite dates from the Danta Mica Mine pegmatite is 1024 ± 40 m.y.

The fission-track age of the garnet is more or less concordant with the K-Ar age of muscovite

Table 3.--K-Ar ages of muscovite from Danta Mica Mine pegmatite

Mineral	K (in percent)	Vol of ^{40}Ar radiogenic sec $gm^{-1} \times 10^{-4}$	^{40}Ar radiogenic (in percent)	Age in million years[1]
Muscovite	8.70	4.8725	97.3	1042±42
Muscovite	8.66	4.5931	96.9	1006±40

[1]Constants used: $\lambda e = 0.584 \times 10\text{-}10\ yr^{-1}$
$\lambda b = 4.72 \times 10\text{-}10\ yr^{-1}$
40 K/K (atomic) = 0.0119 percent.

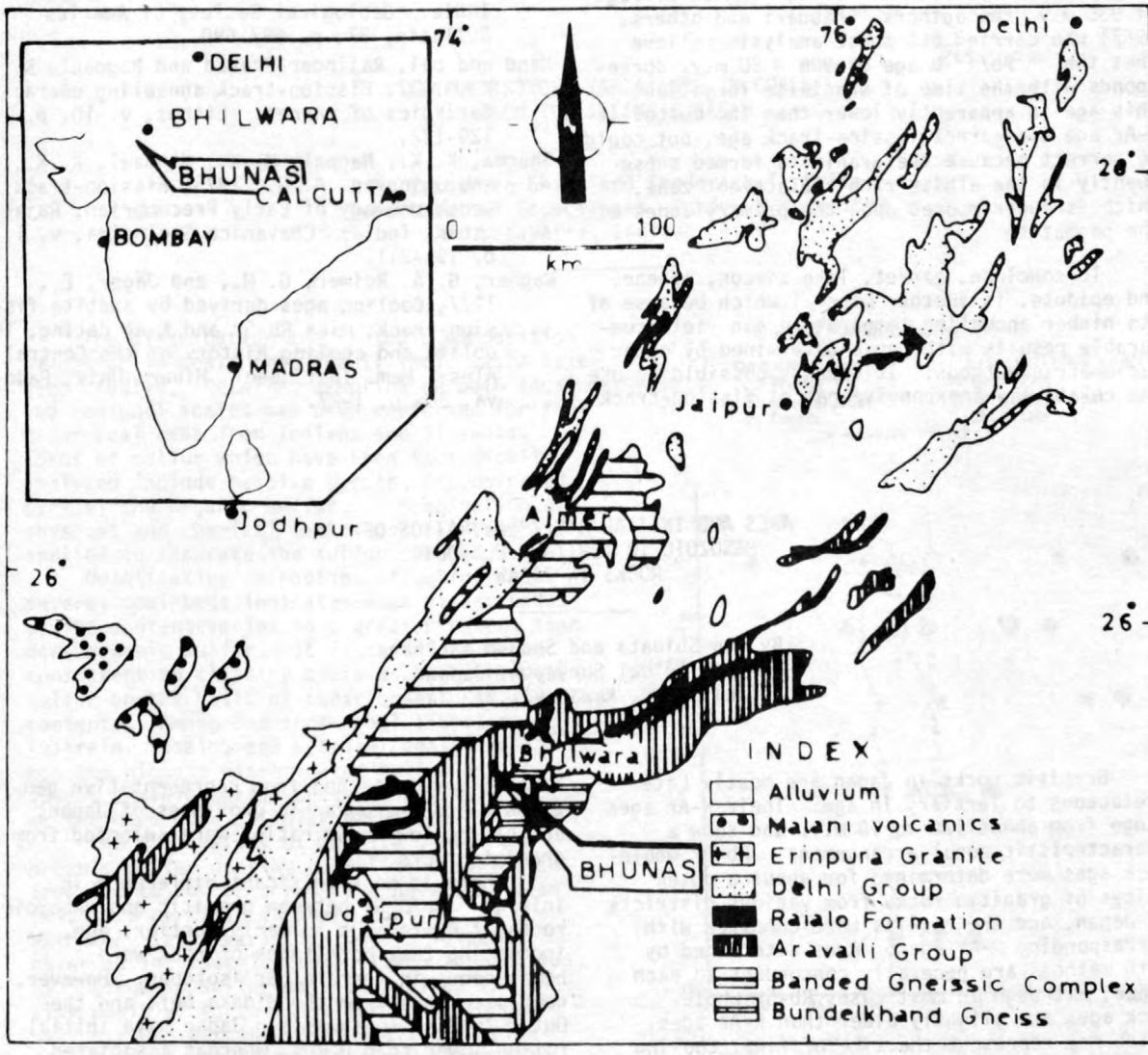

Figure 1.--Geological sketch map of Rajasthan showing location of Danta Mica Mine pegmatite, Bhunas (Modified from Heron, 1935).

collected from the same unit (that is, the hanging wall zone) of the pegmatite, in agreement with the fact that the "blocking temperatures" for both minerals are nearly identical--310°-350°C (Nand Lal and others, 1977, Wagner and others, 1977). By "blocking temperature" we mean the temperature at which the radiometric clock is reset and, in case of fission-tracks it is the maximum temperature at which at least half of the tracks in that mineral remain stable if the mineral is held at temperature for longer than 10^3 m.y. The difference in the fission-track ages of garnet, muscovite, and apatite from the same pegmatite is attributed to the differences in their annealing characteristics.

Although the Pb-U ages of the uraninite vary between 896 and 1008 m.y., with an average of 935 m.y. the authors (Chaudari and others, 1967) who carried out these analysis believe that the $^{207}Pb/^{235}U$ age of 906 ± 20 m.y. corresponds with the time of uraninite formation. This age is apparently lower than the muscovite K-Ar age and garnet fission-track age, but could be correct because the uraninite formed subsequently in the albite-rich replacement zone, which is superimposed upon the primary zones of the pegmatite.

To conclude, garnet, like zircon, sphene, and epidote, is another mineral which because of its higher annealing temperature can yield comparable results with those determined by other radiometric methods. It appears possible to use the relatively inexpensive garnet fission-track ages in conjunction with other radiometric data for correlation of metamorphic and magmatic episodes.

Chaudari, R., Kosztolanyi, C., and Coppens, R., 1967, Uraninite de la pegmatite de Rajasthan, Ind.: Bull. Soc. Miner., Cristallogra, 90, p. 77-81.

Heron, A. M., 1935, Synopsis of the Pre-Vindhyan Geology of Rajputana: Trans. Nat. Inst. Sci. India, v. 1., p. 17-33.

Mehta, P. K., 1976, Potassium-Argon ages of micas from the pegmatites of Bhilwara, Rajasthan, India: Current Science, 45, p. 454-455.

Nand Lal, Nagpaul, K. K., and Sharma, K. K., 1976, Fission-track ages and uranium concentration in garnets from Rajasthan, India: Geological Society of America Bulletin, 87, p. 687-690.

Nand and Lal, Rajinder Prasad and Nagpaul, K. K., 1977, Fission-track annealing characteristics of garnet: Lithos, v. 10, p. 129-132.

Sharma, K. K., Nagpal, M. K., Nagpaul, K. K., and Jhingran, A. G., 1975, Fission-track Geochronology of Early Precambrian, Rajasthan, India: Chayanica Geologica, v. 1, p. 196-211.

Wagner, G. A. Reimer, G. M., and Jäger, E., 1977, Cooling ages derived by apatite fission-track, mica Rb-Sr and K-Ar dating; The uplift and cooling history of the Central Alps: Mem. Inst. Geol. Miner. Univ. Padova, 30, p. 1-27.

AGES AND INITIAL $^{87}Sr/^{86}Sr$ RATIOS OF MESOZOIC TO TERTIARY PLUTONIC ROCKS IN JAPAN

By Ken Shibata and Shunso Ishihara
Geological Survey of Japan
Takatsu-ku, Kawasaki, 213 Japan

Granitic rocks in Japan are mostly Late Cretaceous to Tertiary in age. Their K-Ar ages range from about 120 to 10 m.y. and show a characteristic zonal arrangement. Rb-Sr whole-rock ages were determined for about a dozen suites of granitic rocks from various districts of Japan, and the results were compared with corresponding K-Ar ages. Ages determined by both methods are generally concordant to each other, although in most cases Rb-Sr whole-rock ages are slightly older than K-Ar ages, which may represent the time of final cooling for the granitic masses.

Initial $^{87}Sr/^{86}Sr$ ratios were determined for more than 80 granitic and gabbroic rocks. Samples were selected from representative geographic and petrographic provinces of Japan, and having low Rb-Sr ratios were selected from granitic rocks.

There is no significant difference in initial $^{87}Sr/^{86}Sr$ between granitic and gabbroic rocks of Cretaceous to early Tertiary age, indicating that both types of rock were homogeneous in terms of Sr isotopes. However, gabbroic rocks from the Hidaka belt and the Outer Zone of southwestern Japan have initial ratios lower than 0.704, whereas associated granitic rocks from these areas have higher initial ratios. In particular, all Neogene granitic rocks from the Outer Zone have ratios

higher than 0.706, implying that they have a different origin than that of the gabbroic rocks.

Initial $^{87}Sr/^{86}Sr$ ratios of granitic rocks range from 0.704 to 0.712, and show a remarkable regional variation determined by the geotectonic provinces. The ratios are generally low (< 0.706) in northeastern Japan and high (> 0.706) in southwestern Japan, divided by the Tanakura Tectonic Line. However, ratios lower than 0.706 are also found in the Sanin and northern Kyushu districts, which lie in southwestern Japan. Granitic rocks of the Green Tuff, Kitakami, and Hidaka belts have the lowest values (around 0.7045) and it is concluded that granitic magmas in these belts were derived from the mantle and had little contribution from crustal material. Granitic rocks from the Abukuma, Sanin, and northern Kyushu belts have initial $^{87}Sr/^{86}Sr$ ratios of 0.7055, indicating a slight contribution from crustal material.

Initial $^{87}Sr/^{86}Sr$ ratios for granitic rocks in the Ryoke belt are generally higher than those in other areas; values over 0.710 are found in central Japan, where the continental crust is the thickest in the Japanese Islands. Together with the geochronological evidence for the existence of Precambrian rocks in this area, it is suggested that granitic magmas in the Ryoke belt were partly derived from the continental crust, although a simple anatectic model is ruled out.

Granitic rocks show no clear correlation between initial $^{87}Sr/^{86}Sr$ and age, nor between initial $^{87}Sr/^{86}Sr$ and Rb/Sr. Initial $^{87}Sr/^{86}Sr$ ratios are generally low for the magnetite-series granitic rocks but high for the ilmenite-series rocks.

SULFUR ISOTOPE VARIATIONS IN COALS FROM THE ILLINOIS BASIN

By Yuch-Ning Shieh and Frederick T. Price
Department of Geosciences, Purdue University,
W. Lafayette, Indiana 47907

The distribution and isotopic composition of sulfur in coals from the Illinois Basin have been studied. Detailed sampling on both local and regional scales has been performed for five major coal beds from Indiana and Illinois. Forms of sulfur which have been isotopically analyzed include massive pyrite, disseminated pyrite, and organic sulfur. A combination of physical and chemical techniques has been applied to separate the sulfur compounds.

Quantitative extraction of sulfur from several coal beds indicates that disseminated pyrite content varies to a greater extent than does organic sulfur. It is therefore more consistent to classify coals as high or low sulfur on the basis of their organic sulfur contents. Among the three coal lithotypes (vitrain, fusain, and attrital coal), fusain has the highest disseminated pyrite and the lowest organic sulfur content, possibly because of the more open cellular structure.

The δS^{34}-values of massive pyrite and organic sulfur display very little variation from top to bottom across a single coal seam (within 5 permil), in sharp contrast to the extremely large variation (up to 40 permil) observed in disseminated pyrite. In addition, ΔS^{34} (organic sulfur-massive pyrite) is generally positive for high-sulfur coals (organic sulfur > 0.8 percent) and negative for low-sulfur coals (organic sulfur < 0.8 percent). Figures 1 and 2 illustrate the δS^{34} variation for coals V and VII from two Indiana mines.

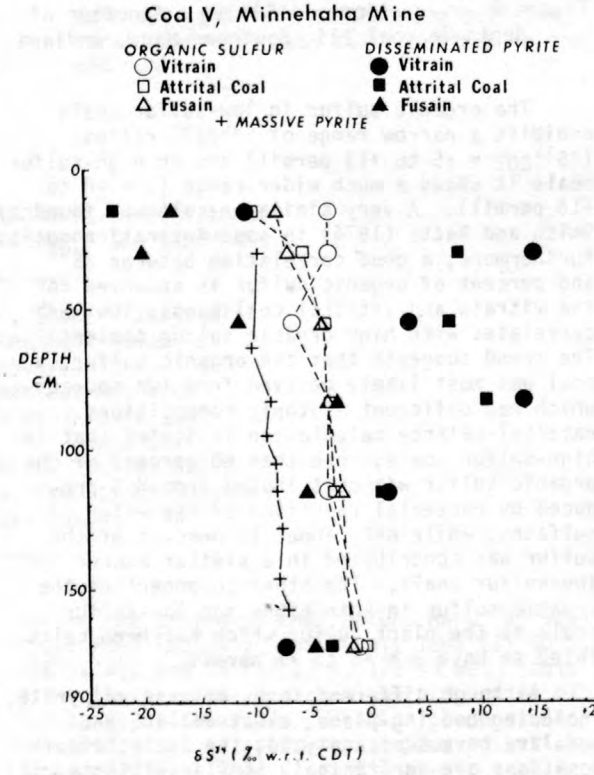

Figure 1.--Variation of δS^{34} as a function of depth in coal V, Minnehaha Mine, Indiana.

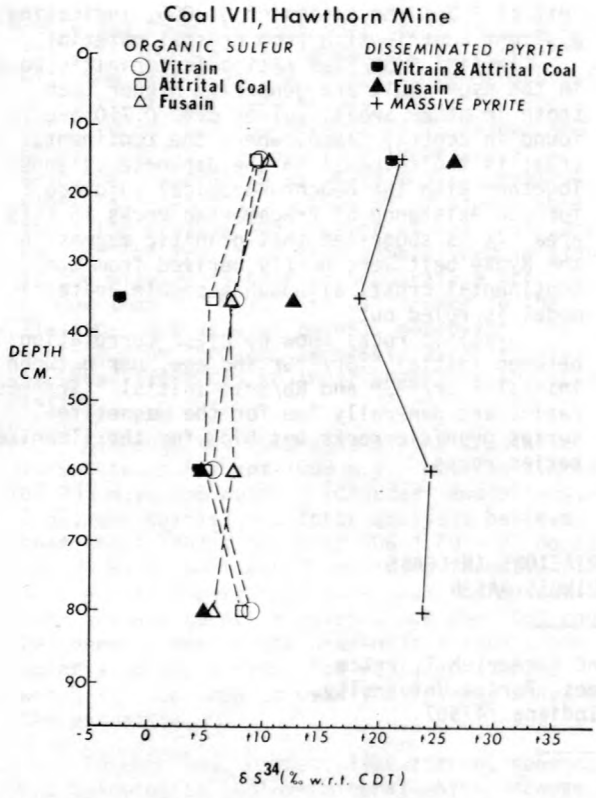

Figure 2.--Variation of δS^{34} as a function of depth in coal VII, Hawthorn Mine, Indiana.

The organic sulfur in low-sulfur coals exhibits a narrow range of S^{34}/S^{32} ratios (δS^{34}_{CDT} = +5 to +13 permil) and in high-sulfur coals it shows a much wider range (δ = -8 to +15 permil). A very similar result was found by Smith and Batts (1974) in some Australian coals. Furthermore, a good correlation between δS^{34} and percent of organic sulfur is observed for the vitrain and attrital coal bands; low δS^{34} correlates with high organic sulfur content. The trend suggests that the organic sulfur in coal was most likely derived from two sources which had different isotopic compositions. Material-balance calculation indicates that in high-sulfur coals, more than 60 percent of the organic sulfur was contributed from H_2S produced by bacterial reduction of sea water sulfates, while only about 15 percent of the sulfur was contributed in a similar manner for low-sulfur coals. The other component of the organic sulfur in both high- and low-sulfur coals is the plant sulfur which has been calculated to have δ = +5 to +7 permil.

Although different forms of massive pyrite, including bedding-plane, cleat-filling and nodular, have been analyzed, the isotopic compositions are surprisingly similar within a coal bed. However, they may differ considerably from bed to bed within a coal mine.

In high-sulfur coals, the average δS^{34}-value of massive pyrite in a coal column correlates well with the average δS^{34}-value of organic sulfur (r = 0.96). No such correlation is obvious in the low-sulfur coals (fig. 3). This and other evidence suggest that an isotopically homogeneous H_2S, which was derived from bacterial reduction of sea water sulfate has, in part, been incorporated into the organic sulfur and, in part, into the massive pyrite.

The relatively constant and characteristic δS^{34}-values observed in massive pyrite and organic sulfur in a coal section as shown in figures 1 and 2 suggest that it may be possible to use sulfur isotopes as a stratigraphic indicator in coal-bearing formations. To explore this possibility, the variations of δS^{34} in massive pyrite and in organic sulfur from five important coal beds in Indiana and Illinois, covering a distance of 250 km have been investigated. The result is summarized in figure 4. In certain places, such as between the Minnehaha and the Hawthorn mines, coals V, VI, and VII are clearly distinguishable by their isotopic compositions. Coal V is isotopically lighter than coals VI and VII, while coal VI and coal VII have opposite relationships between δ-values for

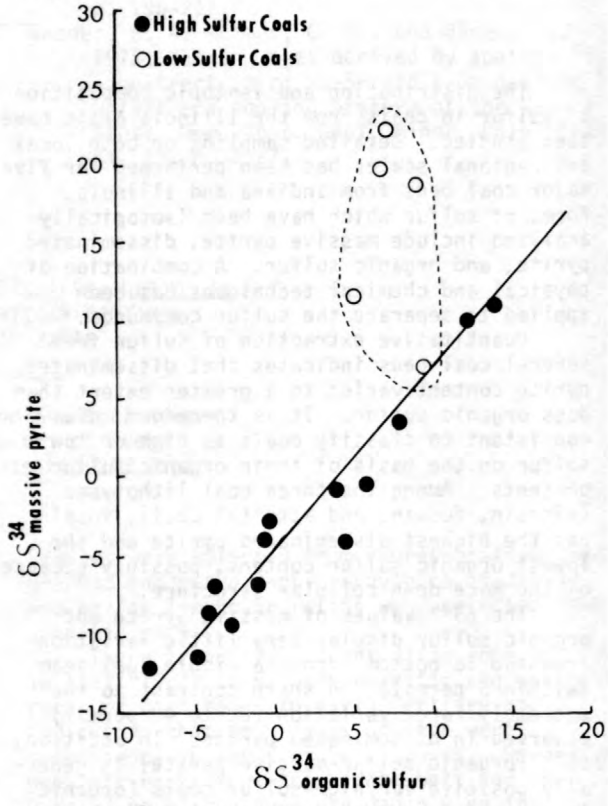

Figure 3.--Plot of average δS^{34} of organic sulfur versus δS^{34} of massive pyrite for all analyzed coal samples from Indiana and Illinois.

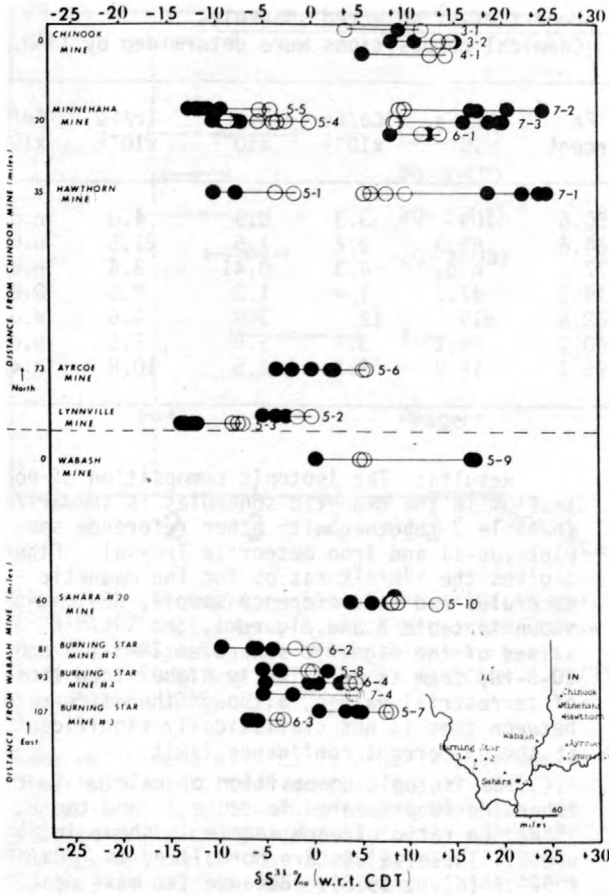

organic sulfur and massive pyrite. The application of sulfur isotopes to problems of stratigraphic correlation of coal beds may prove to be extremely useful when the results from other methods of correlation are ambiguous or obscure.

Smith, J. W., and Batts, B. D., 1974, The distribution and isotopic composition of sulfur in coal: Geochimica Cosmochimica Acta, v. 38, p. 121-133.

Figure 4.--δS^{34} variations for organic sulfur (open circles) and massive pyrite (solid circles) from different coal beds in Indiana and Illinois. Horizontal lines join data points from the same coal bed. First number in each column refers to coal bed number.

POTASSIUM AND CALCIUM ISOTOPIC COMPOSITIONS IN MAGNETIC SPHERULES FROM DEEP SEA SEDIMENTS

By Tadashi Shimamura[1], Shohei Yanagita[1], Kazuo Yamakoshi[1], Ken'ichi Nogami[2], and Koichi Kobayashi[3]

[1]Institute for Cosmic Ray Research
Univ. of Tokyo, Tanashi Tokyo 188

[2]Department of Physics, Dkkyo Univ.
School of Medicine, Mibu, Tochigi 321-02

[3]Department of Physics, Faculty of Science
Kyushu University, Fukuoka 812

In an earlier study it was reported that the cosmogenic nuclide ^{40}K was detected in some magnetic spherules from deep sea sediments (Shimamura and Kobayashi, 1977). We report here the isotopic compositions of potassium and calcium in magnetic spherules, together with their chemical compositions.

Spherule samples: The magnetic spherules were collected from red clay, which was sampled during the cruise of the "Hakuho Maru" at stations 20-3 (35°04'S, 139°39'W), 12-2 (11°00'S, 146°02'W), and 35 (17°17'N, 176°18'W). Table 1 gives the physical and chemical properties of the selected spherules. Chemical composition was determined by instrumental neutron-activation analysis (INAA). Ir, Ni, and Co were detected in all of the sample spherules. Therefore, these spherules are expected to be of

Table 1.--Physical and chemical properties of selected spherules
[Weight was determined by a Cahn Electrobalance. Chemical compositions were determined by INAA.]

Sample No.	Diameter (μm)	Weight (μg)	Density (g/cm^3)	Fe percent	Mn/Fe x10^{-6}	Co/Fe x10^{-3}	Ni/Fe x10^{-2}	Ir/Fe x10^{-6}	Au/Fe x10^{-6}
35-(7)	450	331	6.5	50.6	109	3.3	5.9	4.0	n.d.
12-2- (3)	350	126	5.6	64.6	65.3	2.2	1.5	21.5	n.d.
20-3- (7)	420x380	146	4.4	77.6	n.d.	4.3	0.41	3.4	n.d.
20-3- (8)	310	61	3.9	49.3	47.7	1.4	1.3	2.8	0.87
20-3-(12)	310	128	8.2	38.8	619	12	3.9	4.6	n.d.
20-3-(13)	370	201	7.6	40.9	36.2	3.7	8.8	9.8	n.d.
20-3-(14)	320	135	7.9	25.1	15.9	3.2	2.5	10.8	n.d.

extraterrestrial origin.

Chemical preparation and mass spectrometry: Chemical preparation and mass spectrometry were done in the same way as reported in our previous work (Shimamura and Kobayashi, 1977). For sensitive ion-current detection, an ion-counting method was applied (Kobayashi and Shimamura, 1975). At the first stage, potassium isotopes were measured at lower temperature and subsequently calcium isotopes were measured at higher temperature. No interference by ^{40}Ca ions was observed in the measurements of potassium.

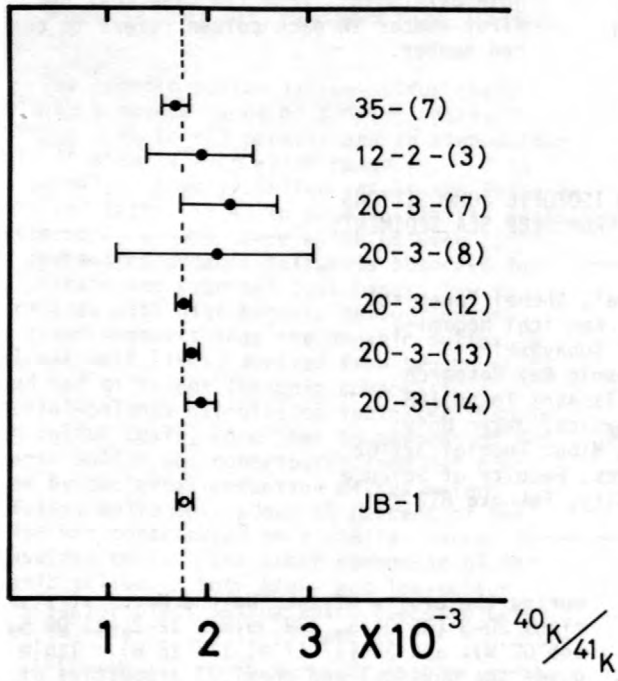

Figure 1.--Isotopic ratios of $^{40}K/^{41}K$ in the individual spherule and the standard rock JB-1. The broken line expresses the literature value of $^{40}K/^{41}K$ = 0.00173 (Kendall, 1960).

Results: The isotopic composition of potassium in the magnetic spherules is summarized in table 2 together with other reference samples (JB-1) and iron meteorite Treysa). Figure 1 gives the $^{40}K/^{41}K$ ratios for the magnetic spherules and the reference sample, JB-1. As shown in table 2 and figure 1, the $^{40}K/^{41}K$ values of the magnetic spherules 20-3-(7) and 20-3-(8) seem to be slightly higher than those of terrestrial values, although the difference between them is not statistically significant at the 95 percent confidence limit.

The isotopic composition of calcium in the spherules is presented in table 3, and the $^{46}Ca/^{48}Ca$ ratio of each sample is shown in figure 2. These values are normalized to $^{40}Ca/^{48}Ca$ = 524.2 (Nier, 1938). Because the mass peak of m/e = 43 was disturbed by hydrocarbon in the measurement, the $^{43}Ca/^{48}Ca$ ratios are not reliable for the spherules. Titanium ions, which interfere with mass peaks 46 and 48, do not appear at all. It is clear that ^{46}Ca of the spherule 20-3-(13) is significantly enriched.

Table 2.--Isotopic composition of potassium in the magnetic spherules and other reference samples
[Errors are twice that of the statistical counting errors.]

Sample No.	$^{39}K/^{41}K$	$^{40}K/^{41}K$
35-(7)	14.000±0.03	0.00167±0.00014
12-2- (3)	13.450±0.08	0.00193±0.00054
20-3- (7)	13.820±0.09	0.00221±0.00050
20-3- (8)	13.550±0.18	0.00207±0.00098
20-3-(12)	13.717±0.022	0.00176±0.00008
20-3-(13)	13.797±0.024	0.00184±0.00008
20-3-(14)	13.590±0.044	0.00193±0.00016
Treysa	12.470±0.11	0.05490±0.0021
JB-1	13.891±0.019	0.00176±0.00007

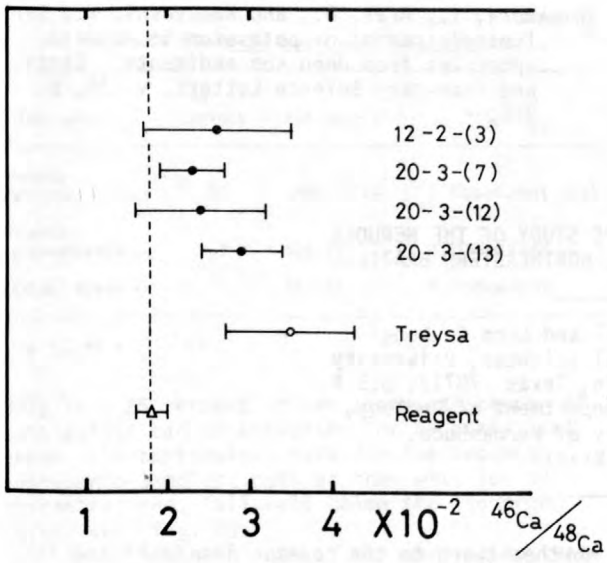

Figure 2.--Isotopic ratios of $^{46}Ca/^{48}Ca$ in the individual spherule, iron meteorite Treysa and reagent. The broken line expresses the literature value of $^{46}Ca/^{48}Ca$ = 0.0178 (Nier, 1938).

Some enrichment of ^{46}Ca is usually observed in other spherules, such as 12-2-(3), 20-3-(7), and 20-3-(12), although the enrichment is not statistically significant at the 95 percent confidence limit. For 20-3-(7), 35-(7), and 20-3-(14), calcium isotopic compositions were not determined because of very weak calcium ion currents. Table 4 gives the amount of excess in the isotopic ratios of $^{42}Ca/^{48}Ca$ and $^{46}Ca/^{48}Ca$ relative to the excess in $^{44}Ca/^{48}Ca$ observed in the spherules and the iron meteorite Treysa.

Discussions: The amounts of excess ^{42}Ca, ^{44}Ca, and ^{46}Ca observed in the spherules show quite good agreement with the relative yield of spallogenic calcium isotopes observed in the iron meteorite, as shown in table 4. This fact clearly shows that the excess in the calcium isotopes is caused by cosmic-ray irradiation in outer space. An extraterrestrial origin for the spherules is also supported by the detection of Ir, Ni, and Co in all of the spherules.

Table 3.--Isotopic composition of calcium in the magnetic spherules and reference samples

[Normalized to $^{40}Ca/^{48}Ca$ of Nier's value (1938). The errors are twice that of the statistical counting errors.]

Sample No.	$^{40}Ca/^{48}Ca$	$^{42}Ca/^{48}Ca$	$^{43}Ca/^{48}Ca$	$^{44}Ca/^{48}Ca$	$^{46}Ca/^{48}Ca$
12-2- (3)	524.2	3.700±0.20	1.3100±0.09	11.450±0.6	0.02600±0.009
20-3- (7)	524.2	3.670±0.10	1.1800±0.04	11.420±0.3	0.02300±0.004
20-3-(12)	524.2	3.560±0.15	1.0500±0.06	11.400±0.4	0.02400±0.008
20-3-(13)	524.2	3.680±0.10	2.0900±0.06	11.740±0.3	0.02900±0.005
Treysa	524.2	3.900±0.16	2.1600±0.10	11.780±0.4	0.03500±0.008
Reagent	524.2	3.590±0.11	0.7610±0.03	11.370±0.3	0.01800±0.002
Nier ('38)	524.2	3.459	0.7838	11.135	0.01784

Significant excess in ^{40}K could be expected for the spherules if the Ir potassium and calcium contents are similar to those in iron meteorites. Unfortunately, the content of potassium and calcium in the spherules was not determined in our experiment. No excess ^{40}K was observed in our experiment, including spherule 20-3-(13), which shows the significant excess in ^{46}Ca. This apparent discrepancy may be explained by the following scenario. When the spherule enters the Earth's atmosphere (as a spherule itself or an ablation droplet of a meteorite), the volatile element potassium probably evaporates. Therefore, most of the potassium may have been lost from the spherule, and contamination from the terrestrial environment, though very small, will almost certainly mask the isotopic anomaly. The refractory element calcium will be retained in the spherule during its entrance into the atmosphere, and it is easy to detect the cosmogenic calcium nuclide. Thus, it is possible to determine the cosmic-ray irradiation age of magnetic spherules by their calcium rather than their potassium isotopes--by assuming the production rate of calcium isotopes by cosmic-ray spallation reactions and determining the absolute content of calcium in the magnetic spherules.

Kendall, B. R. F., 1960, Isotopic composition of potassium: Nature, v. 186, p. 225.

Kobayashi, K., Arai, O., and Shimamura, T., 1975, An ion counting method with multichannel pulse height analyzer for highly sensitive mass spectrometry: Japanese Journal of Applied Physics, v. 14, p. 1368.

Nier, A. O., 1938, The isotopic constitution of calcium, titanium, sulphur, and argon: Physics Review, v. 53, p. 282.

Table 4.--Relative enrichments of calcium isotopes in the magnetic spherules

[Δ_i is defined as: $\Delta_i = \left(\frac{^{i}Ca}{^{48}Ca}\right)$ sample - $\left(\frac{^{i}Ca}{^{48}Ca}\right)$ Nier]

Sample No.	Δ_{42}/Δ_{44}	Δ_{46}/Δ_{44}
12-2- (3)	0.770±0.77	0.025±0.027
20-3- (7)	0.750±0.38	0.017±0.011
20-3-(12)	0.370±0.29	0.022±0.023
20-3-(13)	0.380±0.12	0.018±0.006
Treysa	0.690±0.25	0.027±0.003
Grant A-350[1]	0.690±0.036	0.017±0.002
Grant I-110[1]	0.768±0.120	0.021±0.004

[1]Shima and others, 1968.

Shima, M., Imamura, M., and Honda, M., 1968, Determination of cosmic-ray-produced potassium and calcium in iron meteorites [in Japanese]: Mass Spectroscopy, v. 16, p. 277.

Shimamura, T., Arai, O., and Kabayashi, K., 1977 Isotopic ratios of potassium in magnetic spherules from deep sea sediments: Earth and Planetary Science Letters, v. 36, p. 317.

Rb-Sr AND OXYGEN ISOTOPE STUDY OF THE MERUOCA AND MOCAMBO GRANITES, NORTHEASTERN BRAZIL

By Alcides N. Sial[1,2] and Leon E. Long[1]
[1]Department of Geological Sciences, University of Texas at Austin, Austin, Texas 78712, U.S.A.
[2]Permanent address: Department of Geology, Federal University of Pernambuco, Recife, Brazil

The geology of shield rocks in the northeastern corner of Brazil is of special interest, not only for its own sake but for the excellent opportunity that it provides for making a precontinental-drift correlation with Africa. Throughout a vast exposure of some 630,000 km^2, the unfoliated Meruoca and Mocambo granites, 240 km west of Fortaleza (fig. 1), are the only known major granitic bodies whose field relationships point indisputably to an igneous origin. Both plutons are truncated on the east by a prominent fault system that continues northeastward to the coast. The fault and its associated sedimentary-volcanic trough are presumably the Brazilian counterpart to a similar system in eastern Ghana.

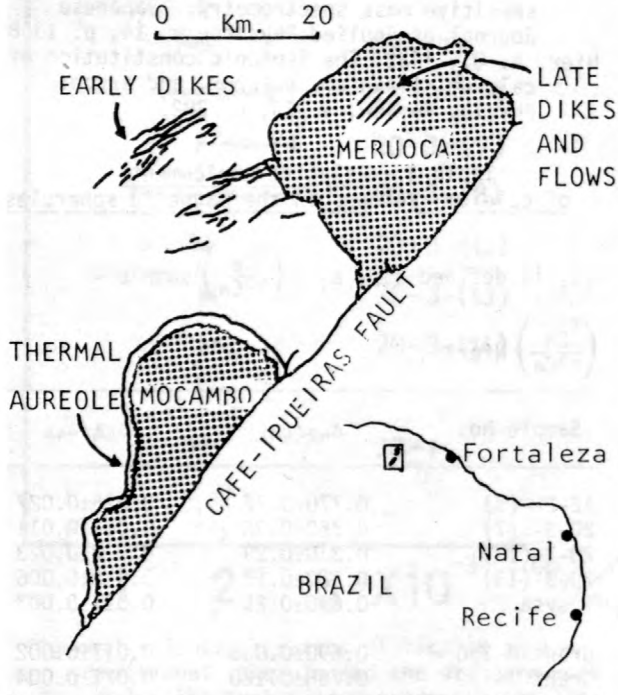

Figure 1.--Index map and simplified geologic map of the Meruoca and Mocambo plutons and associated dikes.

Meruoca, the northern intrusion, stands as a high massif exhumed by erosion but with granite-roof facies yet well preserved. It is an alkalic to peralkalic, coarse- to fine-grained granite containing biotite and hornblende. Fluorite is an abundant accessory mineral. Graphic and granophyric intergrowths, and drusy miarolitic cavities are common, and so are large areas of rock containing turbid brick-red feldspar. These characteristics strongly imply that the granite was a high-level intrusion that experienced alteration. The southern, Mocambo, pluton is a porphyritic monzonite to granodiorite containing hornblende and biotite, but lacking granophyre. Brick-red feldspar occurs in a few places. Xenoliths and autoliths are locally abundant. The autoliths suggest that the Mocambo body is dioritic to gabbroic at greater depth. Where not bounded by faults, both plutons cut the host rock discordantly and have well-developed contact aureoles.

The host metasedimentary rock (Bambui Group) was probably deposited about 1 billion years ago. Emplaced into it are numerous east-northeast trending diorite to rhyolite dikes, which are in turn crosscut by the Meruoca granite (fig. 1). A later set of tholeiite dikes and flows in large volume is preserved in the roof of the northern part of the Meruoca body. This area is also the site of a strong positive magnetic anomaly.

We interpret K-Ar ages of about 430 m.y. on feldspar and biotite (Vandoros, 1967) at Meruoca as indicating the time of final regional cooling. Whole-rock Rb-Sr isochrons were determined separately for the Meruoca granite, the Mocambo granodiorite, and the early set of dikes (table 1, fig. 2). The age (485 ± 14 m.y.) and initial $^{87}Sr/^{86}Sr$ ratio (0.7096 ± 0.0016) for the Meruoca body must be viewed with caution.

Table 1.--Rb-Sr isochron calculations

Rock unit	No. of points	Age (m.y.)[1]	$^{87}Sr/^{86}Sr)_o$
Meruoca granite -------	10	485±14 (1σ)	0.7096±0.0016 (1σ)
Mocambo granodiorite --	6	544±15	0.7106±0.0008
Earlier dikes --	7	562±19	0.7066±0.0009

[1] $\lambda_{Rb} = 1.42 \times 10^{-11}$/yr.

Only 20 - 25 percent of the observed scatter of data points can be accounted for by analytical error. In particular, data for the two most radiogenic samples, both of them with low Sr concentrations, fall well below the isochron (asterisks, fig. 2).

Rb-Sr isochron ages of the early dike swarm (assumed to comprise a single system) and the Mocambo granodiorite are similar within analytical error at about 550 m.y. These rocks appear to be less disturbed although they exhibit a slight excessive scatter of data points. The age is typical for the Brazilian event--a regional metamorphism that profoundly influenced all of the northeastern part of Brazil and corresponding parts of Africa. The initial ratio (0.7106) for the Mocambo body is rather high, suggesting that some ancient continental crust may have contributed to the magma.

Oxygen isotope data on whole-rock granite samples from the Meruoca body reveal a crudely concentric pattern (fig. 3) centered at the

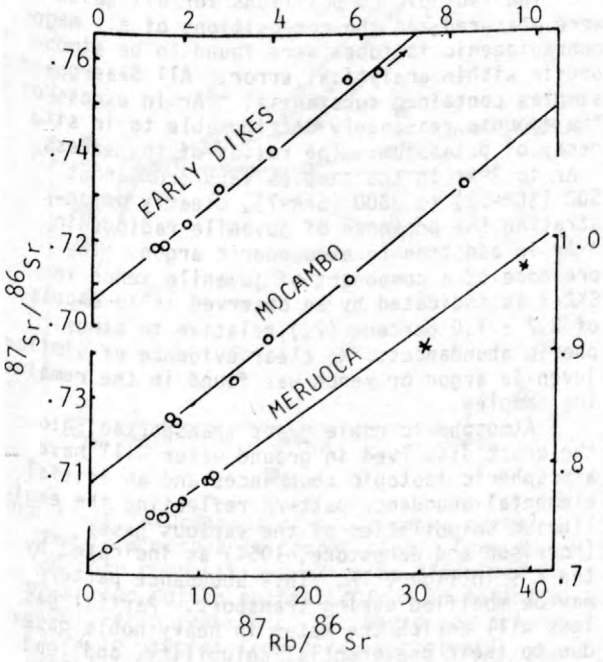

Figure 2.--Rb-Sr whole-rock isochrons.

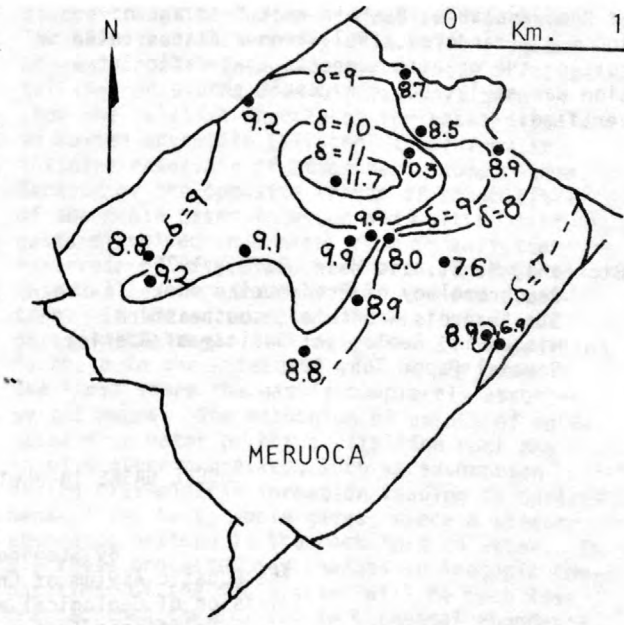

Figure 3.--Map of Meruoca granite body showing localities and $\delta^{18}O$ for 17 whole-rock samples.

location of the basalt dikes and flows. The value of $\delta^{18}O$ approaches 12 permil at the center, diminishing toward the periphery to more "normal" granitic values (δ = +7 to +8). (This pattern, where $\delta^{18}O$ is highest in the center, is just the opposite of that observed by Forester and Taylor (1977) at the Tertiary igneous complex in the Isle of Skye.) Analyses of separated quartz and feldspar show that some of the mineral pairs are not in isotopic equilibrium (Δqtz-feld is negative).

We postulate that the Meruoca granite was subjected to a prolonged, low-temperature interaction with meteoric water producing brick-red feldspar with exceptionally high $\delta^{18}O$, and that the heat necessary to drive the process was supplied by the later basaltic intrusions. In many respects the situation at Meruoca appears identical to that in the St. Francois Mountains, Missouri, where Bickford and Mose (1975) have determined Rb-Sr and U-Pb ages, and Wenner and Taylor (1976) have studied the stable oxygen and hydrogen isotopic relationships. As in Missouri, the whole-rock Rb-Sr isochron at Meruoca has been too disturbed to give a reliable age of granite emplacement. If the isochron has been systematically rotated clockwise somewhat, the indicated age is too low and the initial ratio is spuriously high.

An important question is the timing of hydrothermal alteration. This alteration may have occured at a relatively ancient time during major faulting and widespread volcanism at the close of the Brazilian orogeny--an interpretation supported by the 485 m.y. Rb-Sr isochron--or else much later during the Mesozoic breakup

of Gondwanaland. A whole-rock K-Ar age of 400 m.y. (Vandoros, 1967) from a diabase dike cutting the granite suggests that mafic intrusion was early, but the result should be verified.

Bickford, M. E., and Mose, D. G., 1975, Geochronology of Precambrian rocks in the St. Francois Mountains, southeastern Missouri: Geological Society of America Special Paper 165, 48 p.

Forester, R. W., and Taylor, H. P., Jr., 1977, $^{18}O/^{16}O$, D/H, and $^{13}C/^{12}C$ studies of the Tertiary igneous complex of Skye, Scotland: American Journal of Science, v. 277, p. 136-177.

Vandoros, P., 1967, Sôbre o granito da Serra Meruoca-Rosário, intrusivo na formacão Jaibara, Ceará: Ciência e Cultura, v. 19, no. 2, p. 255, 256.

Wenner, D. B., and Taylor, H. P., Jr., 1976, Oxygen and hydrogen isotope studies of a Precambrian granite-rhyolite terrane, St. Francois Mountains, southeastern Missouri: Geological Society of America Bulletin, v. 87, p. 1587-1598.

NOBLE GASES IN PLUTONIC IGNEOUS ROCKS

By Stephen P. Smith
The Lunatic Asylum of Charles Arms Laboratory,
Division of Geological and Planetary Sciences,
California Institute of Technology,
Pasadena, California 91125

This paper reports neon, argon, krypton, and xenon measurements made on a number of plutonic igneous rocks, including samples from the Skaergaard intrusion and the Southern California batholith, a peridotite nodule, and a gabbro from the Romanche trench. Plutonic rocks were selected for study because the higher crystallization pressures of these rocks should favor the incorporation of ambient noble gases compared with magmas crystallizing at the Earth's surface. This study also presents evidence that plutonic rocks may incorporate atmospheric noble gases transported into the continental and oceanic crusts by groundwater. Several samples were found to contain juvenile magmatic noble gases. We show that subduction into the upper mantle of gases in crustal rocks and subsequent incorporation of these gases in magma reascending to the crust may be an important transport cycle that must be considered when trying to determine the origins of gases measured in igneous rocks.

Concentrations of noble gases measured in the samples are listed in table 1. All concentrations are variable, possibly due to factors such as gas pressure during crystallization, subsequent degassing, interaction with gas-charged groundwater, or mineralogy of gas-bearing phases. The concentrations of neon, argon, and krypton are consistently lower than the whole-Earth "atmospheric" concentrations (atmospheric abundance divided by mass of the Earth) given in the last line in table 1. Xenon is lower than or about equal to "atmospheric" value. Because the atmosphere is generally thought to have originated by degassing of the earth, the average gas contents of the material from which the earth formed must have been at least as high as the "atmospheric" concentrations. It is clear that the gases in none of the samples, including the upper-mantle peridotite nodule, can be directly representative of this original material. All samples have at least undergone extensive degassing.

The isotopic compositions for all gases were measured and the compositions of all major nonradiogenic isotopes were found to be atmospheric within analytical error. All Skaergaard samples contained substantial ^{40}Ar in excess of the amounts reasonably attributable to in situ decay of potassium. The ratios of the excess ^{40}Ar to ^{36}Ar in the samples vary from about 500 (SKR-12) to 3800 (SKR-7), clearly demonstrating the presence of juvenile radiogenic ^{40}Ar in addition to atmospheric argon. The presence of a component of juvenile xenon in SKR-7 is indicated by an observed ^{129}Xe excess of 3.7 ± 1.0 percent (2σ) relative to atmospheric abundances. No clear evidence of similar juvenile argon or xenon was found in the remaining samples.

Atmospheric noble gases transported into the crust dissolved in ground water will have atmospheric isotopic abundances and an initial elemental abundance pattern reflecting the equilibrium solubilities of the various gases (Morrison and Johnstone, 1954) as indicated by the x's in figure 1A. This abundance pattern may be modified during transport. Partial gas loss will enrich the water in heavy noble gases due to their preferential solubility, and lead to abundance patterns in the water that are

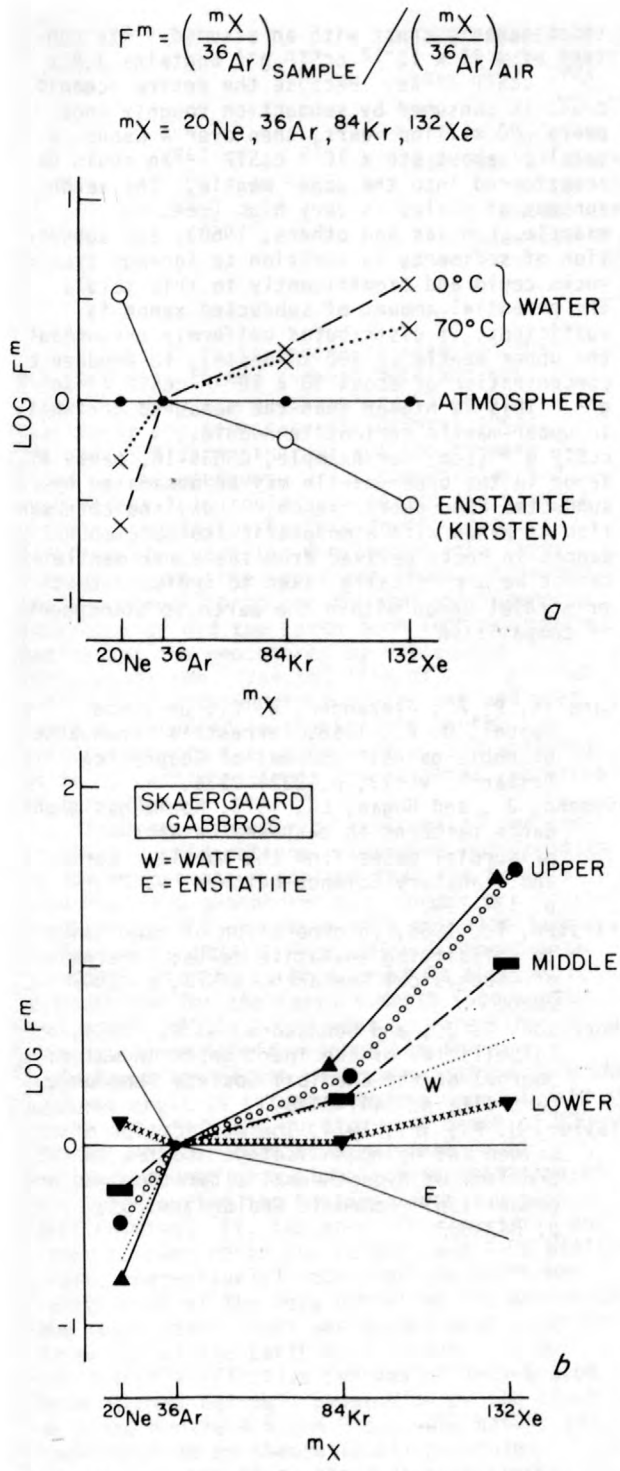

Figure 1.--A, Abundances of noble gases normalized to atmospheric composition. Curves indicate compositions of gases dissolved in water and molten enstatite from an infinite atmospheric reservoir. B, Abundance patterns in gabbros from different stratigraphic horizons of the layered series of the Skaergaard igneous intrusion.

steeper than the "water" curves in figure 1A. The abundance pattern may also shift if gases are exchanged between water and magma or crystalline rock. The open circles in figure 1A show the relative abundances for gases dissolved in molten enstatite (Kirsten, 1968) from an infinite reservoir of atmospheric composition. Because of the opposite trends of solubilities of the noble gases in water and molten silicate, gases dissolved in a magma from an infinite reservoir of water saturated with atmospheric gases will show a roughly flat abundance pattern. If the water reservoir is finite, the gases in the magma will be closer in composition to those in the water and will be the same in the limit where the gas is completely absorbed by the magma. The mechanism of uptake of noble gases from water by hot crystalline rock may involve other processes, such as adsorption during clay-mineral formation leading to enrichment of the heavy noble gases, hence a steeper abundance pattern in the rock than in water. In all these processes any changes in isotopic compositions of the noble gases will be much less drastic than the changes in elemental abundance patterns.

Elemental abundance patterns for the noble gases in four gabbros from the Skaergaard intrusion are shown in figure 1B. The patterns shift regularly from an approximately flat pattern in a sample (SKR-7) from the lower zone of the layered series to steep patterns in two samples (G263, SKR-12) from the upper zone. This trend is paralleled by a decrease in the $^{40}Ar/^{36}Ar$ ratio (corrected for in situ decay of ^{40}K) from a value of 3800 in SKR-7 to about 500 in SKR-12 (table 1). The high $^{40}Ar/^{36}Ar$ ratio in SKR-7 as well as the ^{129}Xe excess in this sample demonstrate the presence of a juvenile component of noble gases in the Skaergaard samples. The patterns in figure 1B suggest that this component is characterized by an elemental abundance pattern that is relatively flat. Mixed with the juvenile component, and masking it in the samples from the upper zone, is a second component with a very steep abundance pattern, containing xenon of atmospheric isotopic compo-

Table 1.--Noble gas content of plutonic rocks

[All concentrations in 10^{-12}cc/g. Absolute uncertainty ≤ 15 percent.]

Sample no. and type	^{20}Ne	^{36}Ar	^{84}Kr	^{132}Xe	$^{40}Ar/^{36}Ar$[6]
SKR-12, gabbro UZ[1]------	215	2380	133	53	520
G263, gabbro UZ[1] -------	150	790	40	20	~1100
SKR-8, gabbro MZ[1] ------	350	1200	45	10	2300
SKR-7, gabbro LZ[1] ------	3420	4820	108	6.3	3800
SCB-13, tonalite[2] ------	235	715	44	14	-
SCB-4, gabbro[2] ---------	190	435	17	2.7	-
CSQ35-1A, peridotite[3] --	125	70	2.3	0.4	-
110753/82, gabbro[4] -----	-	-	-	18	-
Atmospheric[5] -----------	10800	21200	440	16	-

[1]Skaergaard UZ, MZ, LZ = upper, middle, and lower zones of layered series.
[2]Southern California batholith.
[3]San Quintin, Baja California.
[4]Romanche Trench.
[5]Atmospheric abundance divided by the mass of the Earth.
[6]^{40}Ar corrected for in situ decay of K.

sition, and argon of near-atmospheric composition. It has been demonstrated from the oxygen isotope systematics of the Skaergaard (Taylor, 1974) that, in general, as one moves higher in the section, rocks have been more thoroughly exchanged with meteoric water. We conclude that the second component of noble gases is most probably atmospheric noble gases transported into the cooling intrusion by the circulating ground water. The steep abundance curve may reflect gas-loss from the water or adsorption during exchange with the intrusion, as discussed above.

The Skaergaard results illustrate the incorporation by plutonic rocks of atmospheric noble gases transported into the crust by ground water. Similar circulation of gas-bearing seawater takes place in the cooling oceanic crust near a spreading ridge and can lead to the incorporation of atmospheric noble gases in oceanic crustal rocks. Subduction of the oceanic crust provides a means of mixing these atmospheric gases into the upper mantle. There they may form a reservoir of atmospheric gases accessible to rising magmas generated in the mantle, and thus may be cycled back to the Earth's surface. Radiogenic ^{40}Ar generated in the oceanic crust and sediments may be similarly cycled through the mantle by subduction, giving rise to juvenile ^{40}Ar observed in mid-ocean ridge basalts and plutonic rocks. Unlike juvenile ^{40}Ar, juvenile ^{3}He and ^{129}Xe observed in mantle-derived samples require an additional reservoir of noble gases, possibly lower in the mantle, which has never been fully exchanged with the atmosphere because these isotopes are not presently being generated in the crust and, thus, could not be replenished by subduction.

As an example of the potential importance of the subduction of noble gases, the gas contents of oceanic crustal rocks allow all the nonradiogenic xenon observed in mantle-derived samples to have been mixed into the upper mantle from the atmosphere. The atmospheric xenon content of a gabbro from the Romanche trench is 18×10^{-12} ccSTP ^{132}Xe g^{-1} (table 1). Two samples of diabase from the mid-Atlantic ridge contain 43×10^{-12} and 52×10^{-12} ccSTP ^{132}Xe g^{-1} (Dymond and Hogan, 1973). A seven-kilometer thick oceanic crust with an assumed ^{132}Xe content of $\sim 35 \times 10^{-12}$ ccSTP g^{-1} contains 2.8×10^{-14} ccSTP ^{132}Xe. Because the entire oceanic crust is consumed by subduction roughly once every 200 million years, then over 4 aeons, a total of about 5.6×10^{15} ccSTP ^{132}Xe could be transferred into the upper mantle. The xenon content of shales is very high (see, for example, Canalas and others, 1968), and subduction of sediments in addition to igneous crustal rocks could add significantly to this total. The potential amount of subducted xenon is sufficient, if distributed uniformly throughout the upper mantle ($\leq$ 400 km depth), to produce a concentration of about 10×10^{-12} ccSTP ^{132}Xe g^{-1}. This is higher than the measured contents in upper-mantle peridotite nodules, $\leq 10^{-12}$ ccSTP g^{-1} (see, for example, CSQ35-1A, table 1). Xenon in the upper mantle may be dominated by subducted atmospheric xenon. Thus, the observation of xenon with atmospheric isotopic abundances in rocks derived from the upper mantle cannot be uncritically taken to indicate that primordial xenon within the earth is atmospheric in composition.

Canalas, R. A., Alexander, E. C., Jr., and Manuel, O. K., 1968, Terrestrial abundance of noble gases: Journal of Geophysical Research, v. 73, p. 3331-3334.

Dymond, J., and Hogan, L., 1973, Noble gas abundance patterns in deep-sea basalts--primordial gases from the mantle: Earth and Planetary Science Letters, v. 20, p. 131-139.

Kirsten, T., 1968, Incorporation of rare gases in solidifying enstatite melts: Journal of Geophysical Research, v. 73, p. 2807-2810.

Morrison, T. J., and Johnstone, N. B., 1954, Solubilities of the inert gases in water: Journal of the Chemical Society (London), part III, p. 3441-3446.

Taylor, H. P., Jr., 1974, The application of oxygen and hydrogen isotope studies to problems of hydrothermal alteration and ore deposition: Economic Geology, v. 69, p. 843-883.

ON THE PROBLEM OF HETEROGENEITY OF THE PRIMARY MATTER OF THE EARTH

By E. V. Sobotovich
Institute of Geochemistry and Physics
of Minerals
Novobelichanskaya 34
Kiev-68, PR, Palladina 34
USSR

At present it is generally accepted that the Earth was formed through dust and gas accretion from a protoplanetary cloud at relatively low temperatures (Anders, 1964). The question is whether or not the primary cloud was homogeneous in its composition and what effect this could have had on the element distribution in the Earth's forming body. Particularly, were the geospheres (the inner and outer core, the upper and lower mantle and the protocrust) produced through heterogeneous accretion or did the Earth form from homogeneous matter and the geospheres by subsequent differentiation. The solution of this problem will allow us to understand what can and what can't be expected in the Earth's depth, particularly in the upper mantle, and will help us to correctly estimate the material resources of our planet.

There are a number of geochemical and geophysical considerations preventing confirmation of the conservative concept that the Earth's division into geospheres was caused by differentiation processes of a magmatic type (Sobotovich, 1974). That which is known with certainty for the Earth's crust is impossible to extrapolate for the Earth's depth (Sobotovich and Rudnik, 1971). And what is more, the energy source itself responsible for the transformation of the protocrust matter into the present crust is situated in the upper levels of the Earth (from the surface to a depth of 200-300 km), rather than at very great depth.

The concept of a global differentiation of the Earth during its history meets two main difficulties: (1) The ages of terrestrial and lunar surface rocks (up to 4000 and 4600 million years, respectively) show that the Earth was rather cold at the very outset of its existence, and the Earth's crust was formed soon after the formation of the Earth as a planet; (2) No sufficiently effective process of deep-seated heat removal exists. Separation of the crust from the mantle 4.5 - 4.0 b.y.-ago hasn't yet been shown to be theoretically possible.

At the same time, there is much cosmochemical evidence that the Earth's geospheres could have formed during accretion from heterogeneous material of the protoplanetary nebula. This evidence is based not only on theoretical constructions but also on experimental data (the regularities of element distribution in meteorites of different types and in lunar and terrestrial rocks; data derived from the isotopic composition of a number of elements).

The first heralds of genetic heterogeneity of the protoplanetary nebula matter were the lead isotopic data for iron meteorites (Starik and others, 1960). It appeared that iron meteorites could be divided into two approximately equal groups differing distinctly in the isotopic composition of the lead which they contain. At the same time different mineral fractions of the same meteorite were also shown to contain the different types of lead. Detailed consideration of these and accompanying data lead to the assumption that one of these types of lead doesn't belong to our solar system (Starik and others, 1960). Most likely, some of these meteorite groups are "relict" relative to the solar system (Sobotovich, 1968). It was noted that the lead or iron meteorites of "Starik's" type have a small excess of ^{207}Pb in comparison with terrestrial lead (Murthy, 1964). Accordingly, it was supposed that the uranium isotopic composition of different meteorite fragments was different, too (Sobotovich, 1968, 1970). Actually, Arden (1977) did later measure $^{238}U/^{235}U$ ratios in meteorite extracts that were lower than in a terrestrial standard. This finding contradicts accepted nucleosynthesis theory unless the nucleosynthesis time-value (4.7 b.y.) is not decreased for 100 - 200 million years. There is also other evidence for heterogeneity in meteoritic matter, including the argon age data (Müller and Zäringer, 1966), the helium age values (Levsky and Komarov, 1975), oxygen isotope ratios of the light inclusions of Allende (Clayton and others, 1975), and others. For more than 10 years variations in lithium and boron isotopic composition have been known, but they were completely attributed to cosmic ray effects. Now primary heterogeneity may be considered as responsible for this effect, too. Apart from these direct evidences for the protoplanetary cloud heterogeneity, there are indirect ones based on some element abundances in meteorites and lunar samples.

The fixed heterogeneity may be caused by two main reasons: (1) The protoplanetary cloud is a mixture of matter of at least two generations--for example, as a result of the influence of supernova plasma on the primary nebula "relict" matter, which stimulated the solar system

formation (Sobotovich, 1970; Sobotovich and Rudnik, 1971); (2) The heterogeneity is caused by physical-chemical fractionation processes (Lavrukhina, 1972; Clark and others, 1976; Clayton and others, 1975)--but these processes in some cases can't explain the isotopic anomalies observed). The heterogeneity thus is likely to be caused by the first reason, and the second one is of minor importance.

It is proposed that the Earth was formed during heterogeneous accretion and the geospheres result from successive absorbtion of protoplanetary material of different origin, chemical composition, and phase state by the growing Earth. The large iron fragments served as a condensation center (the inner core) for future Earth. As the core increased in size the gravitational potential energy (GPE) of the infalling bodies increased the surface temperature probably up to the melting point ("plastic" core). After the large bodies were exhausting, the GPE decreased again. At this stage, mainly accretion of stony material took place. The top of the upper mantle (protocrust) was formed by the finest dust and gas component and, thus, from the very beginning surface material was enriched in the volatiles and radioactive elements (the last supernova substances initiated during formation of the solar system 4.7 b.y. ago). Thus, the radio-

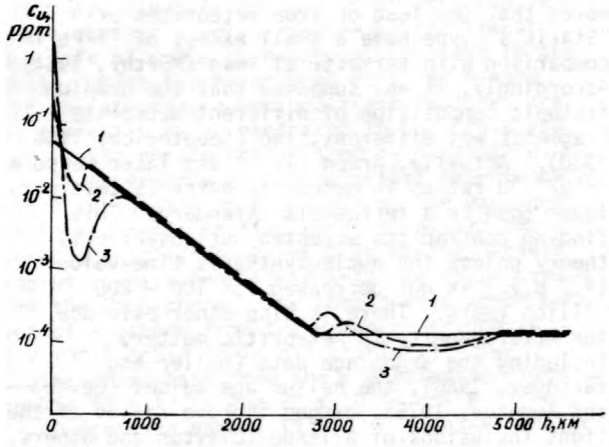

Figure 1.--Uranium distribution in the Earth with depth down to the boundary between the inner and outer core. 1, Primary distribution before existence of crust (4.5 - 4.6 b.y. ago); uranium content of Earth's surface is assumed to be 8×10^{-2} ppm (conforms to that of achondrites). 2, Distribution at the time when basic global magmatism (4.2 - 3.7 b.y. ago) reached depth up to 300 - 400 km; plastic core differentiation led to enrichment of its peripheral parts with sialic components (discompression) as well as with U, Th, and K. 3, Present distribution.

Table 1.--Chemical composition of geospheres, in (mass percent)

[Numbers in parentheses represent percentage of crust, mantle, and core]

Element	Whole Earth	Crust (0.4)[1]	Mantle			Core	
			whole (67.2)	upper (26.2)	lower (41)	outer (30.6)	inner (1.8)
Fe---	35.87	4.89	9.86	6.22	12.19	88.2	90.24
O---	28.50	46.90	21.37	44.27	39.52	--	--
Si---	14.34	26.97	20.80	21.00	20.67	--	--
Mg---	13.21	2.48	20.93	23.40	19.35	--	--
Ni---	2.04	0.0075	0.54	0.20	0.76	4.73	9.06
Ca---	1.93	4.61	2.79	2.32	3.09	--	--
S----	1.84	0.039	0.53	0.40	0.61	4.75	0.01
Al---	1.77	8.14	2.54	1.85	2.98	--	--
Cr---	0.48	0.01	0.14	0.28	0.051	1.23	--
P----	0.215	0.098	0.063	0.04	0.078	0.55	0.19
Na---	0.16	2.29	0.22	0.21	0.23	--	--
Ti---	0.103	0.49	0.044	0.054	0.038	--	--
Co---	0.094	0.0025	0.024	0.017	0.028	0.22	0.54
Mn---	0.059	0.091	0.085	0.085	0.085	--	--
C----	0.035	0.47	0.0095	0.009	0.009	0.085	0.013
K----	0.017	1.66	0.016	0.029	0.008	--	--
H----	0.0078	0.85	0.0063	0.006	0.006	--	--
Cu---	0.0057	0.0055	0.0011	0.001	0.001	0.0097	0.11
U 10^{-7}	18	1800	16.0	39.5	1.0	0.1	0.01

[1]Each geosphere mass relative to the whole Earth's mass is noted in parentheses.

active-element content of the Earth increased as the Earth grew and reached a maximum in the protocrust (fig. 1).

If we accept such a model of Earth formation, the chemical composition of the main structural subdividions since the end of its formation as a planet may be evaluated. Table 1 is composed on the basis of the data by Ganapathy and Anders (1974), Ronov and Yaroshevsky (1971), Hutchisson (1974), Sobotovich and others (1977), and others.

Further evolution of the Earth, including both pre-geological history (4.5 - 4.0 b.y. ago) and geological history (from 4.0 b.y. to the present) could not change to any significant degree the composition of each geosphere. Considerable changes took place only on the borders of geospheres, particularly between the outer "plastic" core and mantle and within the protocrust (the sharp division between solid and gas phases was made possible by the existence of energetic sources, such as radiogenic heat).

Taking into account the "poured" character of the protocrust (a good heat-insulating cover) and the periodic energy associated with the last stage of infalling bodies against a background of increased radiogenic heat generation, the local magmatic differentiation of the protocrust may have begun already in the first dozens or hundreds of million years of the Earth's existence as a result of near surface melting. As more time passed, deeper magmatism was initiated until reaching today the bottom boundary of the upper mantle. This principle, particularly, is confirmed by the circumstance that the ancient rocks were usually formed at lesser depth than younger ones. The lower mantle and the core wouldn't be significantly heated on such a time scale. The plastic core thickness will decrease until the radioactivity of the transition zone reaches a value that compensates for the heat loss due to heat conductivity of higher and lower layers.

Anders, E., 1964, Origin, age, and composition of meteorites: Space Science Reviews, v. 3, p. 5.
Arden, Y. W., 1977, Isotopic composition of uranium in chondritic meteorites: Nature, v. 269, no. 5631, p. 788.
Clark, and others, 1976, A model of the early history of the Earth, in Robertston, Iu., ed., The nature of the solid Earth. Ed. by Mir Publishers, p. 9-23.
Clayton, and others, 1975, Non-uniformity in the solar system, in Cosmic-chemistry of the moon and planets: Moscow, Nauka Publishers, p. 620-623.
Ganapathy, R., and Anders, E., 1974, Bulk composition of the Moon and Earth estimated from meteorites: Geochimica Cosmochimica Acta, Supplement , v. 5, p. 1181-1206.
Hutchisson, R., 1974, The formation of the Earth: Nature, v. 250, no. 5467, p. 556-558.
Lavrukhina, A. K., 1972, Nuclear reactions in cosmic bodies: Moscow, Nauka Publishers.
Levsky, L. K., and Komarov, A. N., 1975, He, Ne and Ar isotopes in inclusions of some iron meteorites: Geochimica Cosmochimica Acta, v. 39, p. 275.
Müller, O., and Zäringer, J., 1966, K/Ar-Alterbestimmungen, III--Kalium und Argon Bestimmungen: Geochimica Cosmochimica Acta, v. 30, p. 1075.
Murthy, R., 1964, in Isotopic and cosmic chemistry: Amsterdam, North Holland Publishing Company.
Ronov, and Yaroshevsky, 1971, The Chemical Structure of the Earth's Crust, in The link between surface structures of the Earth's crust and deep ones: Kiev, p. 192-207.
Sobotovich, E. V., 1968, Uranium Cosmochronology: Meteoritics, v. 28, p. 30.
_____, 1970, Lead Isotopes in geo- and space chemistry: Moscow, Atomic Publishers.
_____, 1974, Isotope space-chemistry: Moscow, Atomic Publishers.
Sobotovich, E. V., and Rudnik, V. A., 1971, Cosmo-geological aspects of the Earth's formation, in Problems of space chemistry and meteoritics: Kiev, Naukova Dumka Publishers, p. 51-117.
Sobotovich, E. V., and others, 1977, An attempt at reconstructing the composition of the Earth's mantle and nucleus, in Space environment and the Earth: Kiev, Naukova Dumka Publishers, p. 31-45.
Starik, and others, 1960, Lead and its isotope composition in iron meteorites: Reports of the Academy of Sciences, USSR, v. 134, p. 555.

USE OF THE PETROGEOCHEMICAL AND LEAD-ISOTOPIC DATA FOR THE CORRELATION AND DIVISION OF PRECAMBRIAN EVENTS

By E. V. Sobotovich and V. A. Rudnik
Institute of Geochemistry and
Physics of Minerals
An Uk. SSR,
Pr. Palladina 34,
Kiev 68 Uk., USSR

Geological methods for the correlation and division of Precambrian events frequently yield discrepant results, especially when stratigraphic analysis is applied to complexes of deep and repeatedly metamorphosed rocks. The data on element distribution regularities in basaltoids and metamorphic strata--in crystalline schists of metabasaltoid nature--make an essential contribution to the solution of this problem. The typomorphic role of the basaltoids is clearly defined in that their chemical composition is the least subjected to change in the process of regional metamorphism (Yakovleva, 1974), and in that the petrochemical criteria for rejection of rock samples affected by the granitization processes is worked out only for the basaltoids (Velikoslavinsky, 1976). Basaltoids and metabasaltoids, as well as marbles, are the rocks that allow us to correlate events for the stratigraphic units under consideration on the basis of geochronological interpretation of the lead, uranium, and thorium isotopes distribution data (Rudnik and others, 1970).

The methodology of petrogeochemical and lead-isotope study is given for the Aldan-Stanovoy shield as an example. Within its limits the following series and complexes from the oldest to the youngest unit analyzed in this work are recognized: Ijengra Complex, including the Upper-Aldan Series (Upper-Aldan Suite) and Fyodorov's Series (Fyodorov's Suite); Kurulta-Gonam Complex, including the Gonam and Kurulta Series (Zvyerev's Suite); Olekma Series (Hoyko Suite); Timpton-Jeltula Complex, including Timpton Series (Kyurikan Suite) and Jeltula

Series (Sutam Suite); Stanovoy Complex (Uda-Maya Series); and Ungra complex. The Precambrian complexes of other East Siberia regions, the Soviet part of the Pacific Mobile Belt (PMB), and Enderbyland in Antarctica are also attractive for correlation according to petrochemical data. The computer analysis results of data on 22 petrogenic and trace elements contents of 350 metabasaltoids samples (Velikoslavinsky, 1977) form the basis of the rocks petrogeochemical typization. As the basis of division of events the lead isotopic composition for 56 rock samples, 25 fractions of 4 rock types subjected to fractional lead sublimation, and uranium and lead distribution obtained by means of isotope dilution in 22 rock samples were considered (Iskanderova and others, 1977; Sobotovich and others, 1977a, 1977b).

Crystalline schists modified by granitizing processes were excluded by only using analyzed rocks with silica content near 51 weight percent or less. The metabasaltoid nature of crystalline schists was established on the basis of: (1) similarity in composition to magmatic rocks, which is revealed by means both of direct comparison of bulk composition and of reconstructional petrochemical diagrams; (2) similarity of their geochemical associations to those of basalts; (3) passing of their lead-lead isochrons through the point of modern lead (PML) and coordination of lead-lead ratios with lead-thorium ratios (Rudnik and others, 1970); (4) agreement of their substantial compositional changes to the magmatic differentiation laws.

Analysis of the variation diagrams, constructed according to the silicate analysis data using "oxide-differentiation degree index" as coordinates reveals distinct trends in the change of composition, which agrees with the element's behavior in the process of ordinary basalt differentiation. The differentiation trends established differ significantly for the metabasalts of the Upper-Aldan and Fyodorov's Series and for the Timpton-Jeltula Complex, for which two petrochemical series are displayed. On the one hand, these patterns confirm the magmatic nature of the crystalline schists under investigation, and, on the other, they indicate the genetic type difference between the petrogenetic series revealed. Application of the basalts normative classification principles for the metabasalts under consideration allows us to attribute "basic" crystalline schists of the Upper-Aldan Series to the tholeiitic basalts, of the Fyodorov's Series to alkalic basalts, and, limits, of the Timpton-Jeltula Complex to both tholeiitic and alkalic basalts. All these metabasalts differ significantly in contents of both major and trace elements. These differences are confirmed also by discriminant analysis results with probability more than 90 - 95 percent, even for a single sample.

Application of the major-components method of factor analysis allowed identification of the first major component direction with the differentiation process, and revealed the individuality of magmatic differentiation trends of metabasalts from the cited stratigraphic subdivisions. Interpretation of established trends for crystallization differentiation allowed S. D. Velikoslavinsky to calculate the normative mineral removal, which caused the observed changes in chemical components content and provided an estimation of magma-formation depth on the basis of comparison with the results of experimental study of basalts differentiation processes (Green and Ringwood, 1967; Green, 1973). On the basis of titanium, calcium, phosphorus, zirconium, and strontium contents as criteria for division of oceanic and continental basalt types (Pearce and Cann, 1973; Pearce and others, 1975), the metabasalts of the Upper-Aldan Series may be attributed to oceanic, and that of the Fyodorov's Series and the Timpton-Jeltula Complex to continental type.

Apart from metabasalts, the marbles also can be used for determination of the radiologic age of Precambrian stratigraphic subdivisions (Gerling and Iskanderova, 1976). The most informative dating methods are the lead-uranium-thorium isochron methods for the whole rock (Rudnik and others, 1970). A necessary condition for the correspondence of radiologic age to the rock's formation time rather than to its subsequent transformation time is passing of their lead-lead isochrons through PML. Another condition is the coincidence of lead-lead and lead-thorium isochron ages (Rudnik and others, 1970) through the methods of coordinated differences (Sobotovich, 1970) or internal isochrons constructed both from accessory and rock-forming minerals and from fractional sublimation (Sobotovich and others, 1974; Sobotovich and Komaristy, 1976). Sampling was carried out from the natural exposures within stratotype regions of corresponding series and suites development. Sampling from the central parts of metabasaltoid strata, if their thickness is not less than 2 - 3 m, is one of the most important conditions for ensuring the absence of changes in the lead isotopic composition of metabasaltoids, especially in the case of their occurrence within granitoid and migmatite strata as a result of repeated but ancient regional metamorphism.

The lead-isotope data confirm the earlier work that confined different types of metabasalts to different stratigraphical subdivisions of the Aldan-Stanovoy shield, whose formation was significantly separated in time and later metamorphism (Rudnik, 1973, 1975; Rudnik and Sobotovich, 1971, 1973). These data may be taken as a basis for the correlation of other regions of East Siberia and PMB metamorphic complexes. Such correlation is based on determining (a) whether the metabasalts belong to tholeiitic or alkaline basaltic petrochemical series; and (b) depth of magma formation derived

from the regularity of differentiation processes. Together with lead-isotopic data the results of such correlation allow us to better understand the evolution of basaltoid volcanism during the early stages of the Earth's development as well as to outline the following sequences of Precambrian events for East Siberia and PMB. From the study areas we note the following stratigraphic subdivisions, which display various stages (pro-, proto-, and geosyncline) of tectonomagmatic cycles:

1. Upper-Aldan Series and Sutam Complex of the Aldan-Stanovoy shield, Kan Series of the Yenisey ridge, rocks of the Daldyn Series of the Anabara and Upper-Maya uplift within the Okhota crystalline massif, Neipir Complex of Enderbyland in Antarctica (nearly 4 b.y.-old, tholeiitic metabasalts, depth of magma formation - $p_1 \approx 1 - 9$ kbars).

2. Kurulta Series of Aldan-Stanovoy shield (more than 3.5 b.y.-old, tholeiitic oceanic metabasalts - $p_1 < 9$ kbars).

3. Fyodorov's Series of the Aldan-Stanovoy shield, Upper-Aldan Series of the Anabara massif, rocks of the Taigonoss and Omolon massifs, and probably the bottom and middle strata of the Okhota-Kukhtuy uplift within the Okhota crystalline massif (more than 3 b.y.-old, alkalic continental metabasalts - $p_1 \approx 9$ kbars).

4. Olekma Series of the Aldan-Stanovoy shield (nearly 3 b.y.-old, tholeiitic - p_1 = 15 - 20 and $p_2 \approx 9$ kbars - and alkaline-basaltic - $p_1 \approx 15$ kbars - petrochemical series of continental type).

5. Timpton-Jeltula (2.3 ± 0.1 b.y.), Stanovoy (2.5 ± 0.2 b.y.) and Ungra (2.7 ± 0.13 b.y.) Complexes of the Aldan-Stanovoy shield (tholeiitic - p_1 = 15 - 20 and $p_2 \approx 9$ kbars - and alkaline-basaltic - $p_1 \approx 15$ kbars - petrochemical series of continental type).

Gerling, E. K., and Iskanderova, A. D., 1976, Lead-isochronic dating of carbonate rock and its application for ascertaining the early stages of metamorphosis: in Real questions of modern geochronology, Moscow, "Nauka" Publishers, p. 224.

Green, D. H., 1973, The composition of basaltic magma as a criterion of their appearance during oceanic volcanism: in Petrology of igneous and metamorphic rock at the bottom of the ocean, Moscow, Mir Publishers, p. 242-258.

Green, D. H., and Ringwood, A. E., 1967, The origin of basaltic magma: in Petrology of the upper mantle, Moscow, Mir Publishers, p. 132-227.

Iskanderova, A. D., and others, 1973, New information on the geochronology of the Aldansk Pre-Cambrian: in Geologic interpretation of geochronological data, Irkutsk, p. 6-7.

Pearce, I. A., and Cann, I. R., 1973, Tectonic setting of basic volcanic rocks, determined using trace elements analyses: Earth and Planetary Science Letters, v. 19, p. 290-300.

Pearce, T. H., Gorman, B. S., Birkett, T. C., 1975, The TiO_2-K_2O-P_2O_5 diagram: a method of discriminating between oceanic and non-oceanic basalts: Earth and Planetary Science Letters, v. 24, p. 419-426.

Rudnik, A. V., 1973, Succession of geologic events in the Pre-Cambrian of Eastern Siberia from radiologic data: in Geochronology of the USSR - Volume I - the Pre-Cambrian, Leningrad, Nedra Publishers, p. 228-254.

Rudnik, V. A., 1975, Granite-formation and the forming of the Earth's crust in the Pre-Cambrian, Leningrad, Nedra Publishers, 416 p.

Rudnik, V. A., and Sobotovich, E. V., 1971, A lead-isochronic method of stratigraphic analysis (in the Example of the Aldansk Shield): Reports of the Academy of Sciences of the USSR, v. 193, p. 897-900.

Rudnik, V. A., and Sobotovich, E. V., 1973, The early history of the Earth: Leningrad, Nedra Publishers, 24 p.

Rudnik, V. A., and others, 1970, The lead-isochronic relationship as a basis of Precambrian periodization: Bulletin of the Academy of Sciences of the USSR - Geology, no. 11, p. 44-55.

Sobotovich, E. V., 1970, Lead isotopes in geochemistry and space-chemistry: Moscow, Atomic Press, 352 p.

Sobotovich, E. V., and Komaristyi, A. A., 1976, Fractional sublimation in lead-isochronic dating of mountain rock: Geochemistry, no. 2, p. 211-216.

Sobotovich, E. V., and others, 1974, Ancient rocks of Antarctica (Enderbyland): Bulletin of the Academy of Sciences of the USSR - Geology, no. 11, p. 30-50.

Sobotovich, E. V., and others, 1977a, The Early-Archean Age of rocks of the Taigonossk and Omolonsk Massives of the Pacific Ocean Migratory Zone: in Geological Interpretation of geochronological data, Irkutsk, p. 10-11.

Sobotovich, E. V., and others, 1977b, The lead-isochronic age of the Early-Precambrian crystalline shale of the Stanovaia Folded Zone: in Geological interpretation of geochronological data, Irkutsk, p. 14-15.

Velikoslavinsky, S. D., 1976, Features of the Early-Archean basic volcanism of the central part of the Aldansk Shield: Notes of the All-Union Minerological Society, Part 105, issue 1, p. 48-58.

Velikoslavinsky, S. D., 1977, Geochemical Specialization of Metabasaltic Complexes of the Central Part of the Aldansk Sheet:

in Materials of the third young people's geological conference of the VSEGEI, Leningrad, Leningrad University Press, p. 25-92.

Yakovleva, S. Z., 1974, The abundance and the rules of abundance of K and Rb in basic rocks: Leningrad, Leningrad University Press, 23 p.

OXYGEN AND CARBON ISOTOPE INTERNAL THERMOMETRY USING BENTHIC CALCITE AND ARAGONITE FORAMINIFERA PAIRS

By Michael A. Sommer II[1] and Danny M. Rye[2]
[1]Department of Geological Sciences
Brown University, Providence, Rhode Island 02912
[2]Department of Geology and Geophysics
Yale University, New Haven, Connecticut 06520

Introduction: In 1947 Urey presented a paper concerning the thermodynamics of isotopic systems and suggested that variations in precipitation temperatures of $CaCO_3$ from water should lead to measurable variations in the $^{18}O/^{16}O$ ratio of calcium carbonate. This work led directly to the paleotemperature equation (Epstein and others, 1951, 1953; Craig, 1965), an empirical relationship between the variation in the oxygen isotopic composition of shell material and its growth temperature. The most recent inorganic calcite-water equation of O'Neil and others (1969), is $T^{\circ}C = 16.80 - 4.40(\delta^{18}O_c - \delta^{18}O_w) + 0.1(\delta^{18}O_c - \delta^{18}O_w)^2$

where: $\delta^{18}O_c$ is $\delta^{18}O$ value of CO_2 produced from H_3PO_4 treatment at 25°C relative to PDB CO_2 produced from H_3PO_4 treatment at 25°C.

$\delta^{18}O_w$ is $\delta^{18}O$ value of CO_2 equilibrated with H_2O at 25°C relative to PDB CO_2.

A vast amount of important work has evolved from paleotemperature studies (Lowenstam and Epstein, 1954; Emiliani, 1966; Shakleton, 1967). However, this work continues to be plagued by the unknown ^{18}O content of the water in which the shell material grew. Only the ^{18}O content of the carbonate can be measured using fossil material and we must assume the ^{18}O content of the water. An example of how severely this assumption can effect paleotemperature determinations is seen in the $\delta^{18}O$ variations observed in fossil material from Pleistocene deep-sea cores. Shackleton and Opdyke (1973), have shown that two-thirds of the total observed isotopic variations ($\sim$ 1.0 permil) observed in some Pleistocene cores are due to variations in the $\delta^{18}O$ content of the water.

In principle, there exists an approach to circumvent this type of problem. If two minerals precipitated in equilibrium with one another, then calibration-fractionation curves can be worked out for each mineral pair. Barring coincident slopes, in an assemblage of n-phases we can obtain n - 1 unique and independent temperature determinations (Epstein and Taylor, 1967). The question is, can we employ this method of internal thermometry to a low-temperature biologic system where equilibrium fractionation may not have occurred.

Experimental Results and Discussion: We have investigated the fractionation of ^{18}O and ^{13}C between low-Mg calcite and aragonite benthic-foraminiferal pairs with the intent of calibrating an internal-isotopic thermometer. We collected contemporaneous low-Mg calcite foraminifera (Uvigernia) and aragonite foraminifera (Hoeglundina) from supposed core tops distributed throughout the ocean basins. Table 1 summarizes the core designation, the interval sampled in the core (cm), the core location, the core depth (m), the species analyzed, the $\delta^{18}O$ and $\delta^{13}C$ measurements of the foraminifera and duplicates relative to PDB, the in situ temperatures, $\Delta^{18}O$ (aragonite-calcite) and $\Delta^{13}C$ (aragonite-calcite) of the foraminiferal pairs, and the reference for each core.

The $\delta^{18}O$ and $\delta^{13}C$ values were obtained on CO_2 gas produced by reacting the samples with 100 percent ortho-phosphoric acid at 50°C. Measurements were made on a VG Micromass 602C mass spectrometer. The kinetic isotope effects for calcite and aragonite were assumed to be equal (Tarutani and others, 1969). Samples varied in size utilizing between 3 and 10 Uvigerina specimens and 1 to 5 Hoeglundina specimens per analysis. All values are reported relative to PDB CO_2 gas. Analytical precision for replicate-standard powder is 0.06 permil (1σ) for $\delta^{18}O$ and 0.05 permil (1σ) for $\delta^{13}C$. Duplicate-sample precision is about 0.1 permil for both $\delta^{18}O$ and $\delta^{13}C$.

A temperature range of from 1° to 20°C was obtained for 9 pairs of organisms and duplicates. The $\Delta^{18}O$ values for aragonite-calcite pairs vary between +0.45 to +1.53 permil. The $\Delta^{13}C$ values for aragonite-calcite pairs vary between +1.58 and +2.60 permil. Figure 1 is a plot of the $\Delta^{18}O$ and $\Delta^{13}C$ aragonite-calcite versus temperature. The least squares fit to

the data yields lines where $\Delta^{18}O = 1.37 - 0.037T$ (correlation factor R = 0.81) and $\Delta^{13}C = 2.56 - 0.065T$ (correlation factor R = 0.91). The inorganic point of Tarutani and others (1969), ($25^{\circ}C$ = +0.6 permil), is within 0.2 permil of the oxygen line.

There is clearly some scatter in the observed data. This scatter is probably attributable to sedimentological processes. Differential mixing of the foraminifera during bioturbation or during the piston-coring process could introduce spurious specimens to the core top.

Clayton (oral commun.) has suggested that the slope of the oxygen aragonite-calcite curve is in the predicted direction, but the magnitude of the observed fractionations may be larger than those predicted from statistical mechanics. However, we must point out that the aragonite vibrational data is poorly known. The magnitude of the oxygen fractionation may, if Clayton is correct, be the result of a vital effect in the aragonite organism. Most certainly the carbon fractionation curve represents nonequilibrium conditions. We must, therefore, view our fractionation curves as an empirical relationship between calcite and aragonite produced by biological systems in sea water. However, comparison of the Tarutani and others (1969) experimental aragonite oxygen point indicates that equilibrium may have been approached.

Conclusions: By collecting both aragonite and calcite-benthic foraminifera from piston-core tops over a wide range of temperatures and measuring the $\delta^{18}O$ and $\delta^{13}C$ values of both aragonite and calcite, we have established an empirical relationship between the isotopic fractionation of aragonite-calcite and the temperature. We, therefore, propose that the empirical equation $\Delta^{18}O$ (aragonite-calcite) = 1.37 - 0.37T is a valid first approximation to the aragonite-calcite oxygen-isotope fractionation between 0° and $25^{\circ}C$. This approach may have great potential for determining paleotemperatures and salinities.

Craig, H., 1965, The measurement of oxygen isotope paleotemperatures: Spoleto Conference on stable isotopes in oceanographic studies and paleotemperatures, 3rd, Proc.

Emiliani, C., 1966, Paleotemperature analysis of Caribbean core P6304-8 and P6304-9 and

Table 1.--Summary of aragonite-calcite isotope and piston-core hydrographic data
[Hoegl. Hoeglundina; Uvig., Uvigernia]

Core	Interval (cm)	Location	Depth (m)	Species[1]	T°C	$\delta^{18}O$ [2]	$\delta^{13}C$[2]	$\Delta^{18}O$	$\Delta^{13}C$	Ref.[3]
E49-2	0-1	47°15'S-100°8'E	2897	Hoegl.	1.2	4.86	2.09	1.31	2.43	(1)
				Uvig.		3.55	- .34			
V29-135	0-1	19°42'S-8°53'E	2675	Hoegl.	2.2	4.89	1.98	1.08	2.48	(2)
				Uvig.		3.81	- .50			
V29-143	0-1	00°45'S-7°15'E	2756	Hoegl.	2.7	4.73	1.94	1.13	2.18	(2)
				Uvig.		3.60	- .24			
TR121-37	0-2	37°25'N-25°54'W	2310	Hoegl.	3.0	5.33	2.52	1.27	2.60	(3)
						5.19	2.60			
				Uvig.		3.99	- .04			
TR126-19	0-1	19°59'N-96°13'W	710	Hoegl.	6.2	4.08	2.26	0.98	2.59	(4)
				Uvig.		3.10	- .33			
				Hoegl.		4.53	1.76	1.25	2.08	
				Uvig.		3.28	- .32			
TR126-13	0-1	21°36'N-96°55'W	560	Hoegl.	8.0	4.97	1.89	1.53	1.91	(4)
				Uvig.		3.26	0.01			
						3.44	0.05			
TR171-11	0-2	38°10'N-11°13'E	640	Hoegl.	13.5	3.32	1.76	0.98	1.54	(5)
				Uvig.		2.34	0.22			
V3-54	0-1	23°18'N-89°31'W	201	Hoegl.	16.3	5.08	1.30	0.81	1.23	(4)
				Uvig.		4.27	0.07			
V3-78	0-1	23°01'N-88°53'W	155	Hoegl.	19.7	3.23	1.78	0.45	1.58	(4)
				Uvig.		2.78	0.20			

[1]Hoegl., Hoeglundina; Uvig., Uvigernia.
[2]Relative to PDB (subject to revision).
[3](1) Gordon and Molinelli, 1975; (2) Fuglister, 1960; (3) Wust, 1933; (4) Mclellan and Nowlin, 1962; (5) Miller and others, 1970.

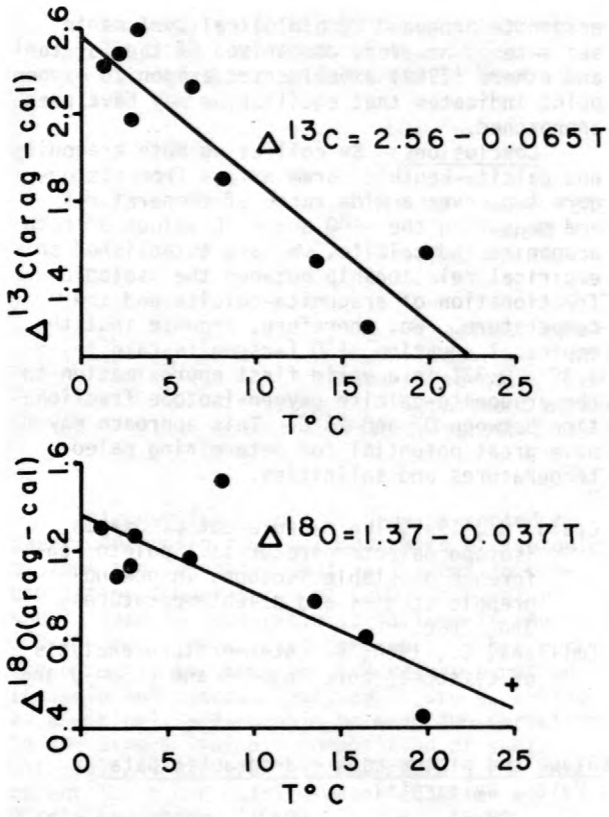

Figure 1.--A plot of the oxygen and carbon isotopic fractionation curves of aragonite-calcite for foraminiferal pairs versus the temperature. + is the inorganic aragonite data point of Tarutani and others, 1969.

a generalized temperature curve for the past 425,000 years: Journal of Geology, v. 74, no. 2, p. 109-126.

Epstein, S., Buchsbaum, R., Lowenstam, H., and Urey, H. C., 1951, Carbonate-water isotopic temperature scale: Geological Society of America Bulletin, v. 62, p. 417-426.

_____1953, Revised carbonate-water isotopic temperature scale: Geological Society of America Bulletin, v. 64, p. 1315-1326.

Epstein, S., and Taylor, H. P., Jr., 1967, Variation of $^{18}O/^{16}O$ in minerals and rocks, in Abelson, P. H., ed., Researches in Geochemistry: New York-London, John Wiley and Sons, v. 2, p. 29-62.

Fuglister, F. C., 1960, Atlantic Ocean atlas: Woods Hole Oceanographic Institution, Woods Hole, Mass., 209 p.

Gordon, A. L., and Molinelli, E., 1975, U.S. N. S. Eltanin Southern ocean oceanographic atlas: Lamont-Dohery Geological Observatory, Palisades, New York, 91 p.

Lowenstam, H., and Epstein, S., 1954, Paleotemperatures of the post-Aptian Cretaceous as determined by the oxygen isotope method: Geology, v. 62, p. 207-248.

McLellan, H. J., and Nowlin, W. D., 1962, The waters of the Gulf of Mexico observed in February and March 1962: A and M Project 286, reference 62-16D, The A and M College of Texas.

Miller, A. R., Tchernia, P., Charnock, H., and McGil, D. A., 1970, Mediterranean Sea Atlas: Woods Hole Oceanographic Institution, Woods Hole, Mass., 190 p.

O'Neil, J. R., Clayton, R. N., and Mayeda, T. K., 1969, Oxygen isotope fractionation in divalent metal carbonates: Journal of Chemical Physics, v. 51, p. 5547-5558.

Shackleton, N., 1967, Oxygen isotope analysis and Pleistocene temperatures re-assessed: Nature, v. 215, no. 5096, p. 15-17.

Shackleton, N. J., and Opdyke, N. O., 1973, Oxygen isotope and Paleomagnetic stratigraphy of equatorial Pacific core V28-238 - Oxygen isotope temperatures and ice volumes on a 10^5 and 10^6 near scale: in CLIMAP Program, Quarterly Research (Washington University Quarterly Research Cent.), v. 3, no. 1, p. 39-55.

Tarutani, T., Clayton, R. N., and Mayeda, T. K., 1969, The effect of polymorphism and magnesium substitution on oxygen isotope fractionation between calcium carbonate and water: Geochimica Cosmochimica Acta, v. 33, p. 487-496.

Urey, H. C., 1947, The thermodynamic properties of isotopic substances: Journal Chemical Society, p. 562-581.

Wust, G., 1933, Das Bodenwasser und die Gliederung der Atlantischen Tiefsee: Wiss. Ergeb. Deut. Atl. Exped. Meteor, 1925-1927, v. 6 (1), p. 1-126.

A COMPUTER-CONTROLLED, FIVE-COLLECTOR MASS SPECTROMETER FOR PRECISION MEASUREMENT OF ARGON ISOTOPE RATIOS

By J. S. Stacey[1], N. D. Sherill[2], G. B. Dalrymple[2], M. A. Lanphere[2] and N. V. Carpenter[1]

[1]U.S. Geological Survey, Denver, Colorado 80225

[2]U.S. Geological Survey, Menlo Park, California 94025

Introduction: Argon isotopic analyses for potassium-argon dating studies are usually made with the analyzer of the mass spectrometer isolated from the vacuum pumps, that is, in the "static" mode of operation. Such a closed-system method provides the required sensitivity for the analysis of small samples, and avoids the use of an electron multiplier for ion detection. Static analysis of rare gases, however, has the disadvantage that the composition of the sample gas changes continuously during an analysis, a phenomenon known as "memory". In addition to the adsorption onto, and subsequent release of gas molecules from the internal surfaces of the instrument, memory seems to be caused by two other related effects. One effect results in a gradual decrease in the ion currents with time, and is probably caused by the burial of a fraction of the high-energy ions in the surfaces of the source and collector electrodes. The other is a form of contamination caused when the ions bombarding the electrode surfaces release some of those ions implanted from previously analyzed samples (Reynolds, 1956). Most often, memory results in a small, approximately linear change in gas composition as the analysis proceeds. Thus, in order to estimate the true sample composition, it becomes necessary to extrapolate the data taken during an analysis to some time, "t_0", a few seconds after the sample is admitted to the analyzer. The uncertainty in the t_0-intercept increases rapidly with extrapolation time. In single-collector instruments reduction of the extrapolation time is limited by the time taken to measure each peak of the spectrum in turn. Even with very rapid magnet switching (Wasserburg and others, 1969) a cyclic scan of several isotopes may take many seconds. Using single collector instruments, ion current intercepts at t_0, as determined by a linear least-squares fit, have standard deviations of ± 0.1 to ± 0.2 percent for ion currents larger than about 5×10^{-11} amps. In such instruments that use peak hopping rather than scanning, these uncertainties are considerably decreased. However, one of our primary goals for the new mass spectrometer was to decrease the uncertainties in the t_0-intercepts as far as possible, and thus to eliminate those factors as significant sources of error.

Because multiple collectors permit simultaneous measurement of the ion currents, they would obviously help to reduce the memory problem. A further advantage is that simultaneous ion-current measurement also minimizes errors due to ion beam instability. Although dual collectors were first suggested by Aston (1930), the concept was not applied until 1941 (Strauss, 1941). Since the work of Nier and others (1947) dual collection systems have become standard practice in stable isotope studies, but in the various systems used, the collectors have seldom been alined on the focal plane, and most systems have used a null method for comparison of ion currents. Contemporaneously with our own work, however, the Varian MAT Corporation has produced a triple-collector instrument with all three collectors on the focal plane. In that instrument the ions enter and exit from the 90° sector magnetic field at the same oblique angle of 26.5°. This has the effect of doubling the beam separation at the collectors as well as of focussing the beams in both the "r" and "z" directions (Cross, 1951; Ezoe, 1967).

We have designed and constructed a first-order direction focussing static mass spectrometer, with five independent Faraday cup collectors alined on the focal plane. All ion beams have some fringe field focussing in the z-direction that results from their oblique (85°) intersection with the magnetic field boundaries. The five collectors permit either conventional isotope dilution measurements (^{36}Ar, ^{38}Ar, ^{40}Ar) or neutron irradiation measurements (^{36}Ar, ^{37}Ar, ^{39}Ar, ^{40}Ar) to be made. Each collector has its own electrometer amplifier and data channel. The mass spectrometer is controlled by a PDP8/e minicomputer (Digital Equipment Corporation) that also takes data simultaneously from each collector channel as well as from an elapsed time clock. With these facilities all the ion currents may be measured together, starting as soon as the sample is admitted to the spectrometer. Although the instrument was designed specifically for argon analyses, the concept is easily adaptable to other elements where precise isotopic data are required.

Design Considerations: Sensitivity in argon analyses for geochronology is not generally a problem. Typical gas samples range from 10^{-11} to 10^{-9} moles total argon ($\sim 2 \times 10^{-7}$ to 10^{-5} cc STP) with individual ion currents from 10^{-9} to 10^{-13} amps. We required ion-beam counting sta-

tistics of ± 0.1 percent for an ion current of 10^{-12} amps when using an integration time of 1 second. The ion detector and data channels need a dynamic range of at least 1 x 10^5; an ion current sensitivity (defined as twice the total background noise current) of 1 x 10^{-14} amperes or better, and the instrument must have an absolute ion current transfer function of about 3 amperes/mole Ar.

Choice of a sector angle of 90° for the flight tube helped to maintain sensitivity by reducing the total volume and, with a radius of 23 cm, sufficient dispersion was provided for the required mass range. In addition, an angle of 80 degrees between the boundaries of the magnetic field gives some focussing in the z-direction for all of the ion beams. The resulting central ray focal length is 25 cm with a dispersion at mass 38 of 6.6 mm.

Five separate but identical collector assemblies were constructed. Each employs a Faraday cup 32 mm deep, a grounded guard ring and shield, an electron-suppressor electrode and two grounded electrodes with a 1.27-mm entry slits, one electrode placed 8 mm behind the other. The purpose of the two entry slits is to limit the acceptance angle for each collector and so avoid spurious baseline signals during scanning.

The five units are mounted in a "staircase" arrangement along the focal plane of the instrument. This is designed so that a beam will encounter the edge of only one electrode when it is scanned between any pair of adjacent collector slits. Ions reflected from that edge could cause spurious signals but the limited acceptance angle for the collectors ensures that there is no line of sight between each reflecting edge and the adjacent Faraday cup.

A fairly conventional Nier-type electron bombardment source was provided for the instrument with a source magnet external to the vacuum envelope. The whole analyzer assembly was designed to be bakeable to 400°C.

The signal from each collector is fed to its own data channel that comprises an electrometer amplifier, a voltage-to-frequency converter and two cascade-connected 12-bit counters. Each counter is gated and read independently by the PDP8 computer via its own interface. Timing is provided by a nonprogrammable quartz crystal clock. The 5 kH_z output from the clock is fed directly to the computer bus where it is available to the software for timing of integration times.

Simultaneously, the computer can read the integrated signals from all five data channels and the elapsed time clock in less than 1 millisecond. Integration times can be varied from 0.02 to 8.4 seconds, but a value of 1 second is generally used.

Changes in the magnetic field of the mass spectrometer are made under software control from the computer. The computer signals the required field increment via a 12-bit digital-to-analog converter, and at the input of the magnet power supply that signal is compared with the output of a high resolution gaussmeter to adjust the field accordingly. In this manner, 4096 increments are available for a maximum of 300-gauss change in field above the base operating value of 1565 gauss. Good transient response for the system has been obtained so that the total time for a 100-gauss step change in field is one second. Temperature stability is 8 ppm/°C to 30°C.

Analyses are performed under complete program control and are divided into four sequences of 2 minutes duration. These are: Monitoring background peaks before sample inlet; measurement of peaks immediately after the sample is admitted; baseline measurement; and an interchannel calibration procedure.

Performance Characteristics: The instrument has been in operation since May 1977 and the following analysis is based partly on the results from more than 400 argon analyses made between May and November, 1977.

The principle characteristics of an argon ion beam in the center collector are tabulated in table 1 for a magnetic field of 1565 gauss and an accelerating potential of 2000 volts. For the 0.3-mm source slit and the 1.27-mm collector slit, we find a beam width for 99.9 percent of the ions of 0.63 mm. The peak top is flat to ± 1 x 10^{-4} for a change in magnetic field of 1.7 gauss that corresponds to a beam translation of 0.31 mm.

Interference between beams (tailing) is not detectable to better than 1 part in 50,000 at 0.2-mass units from the beam centers. We have checked for spurious signals due to ion scattering by reflection from plate edges in the multiple collector assembly. This was done by scanning a high intensity ion beam across three adjacent collectors in magnetic field increments of 0.15 gauss. The three adjacent data channels

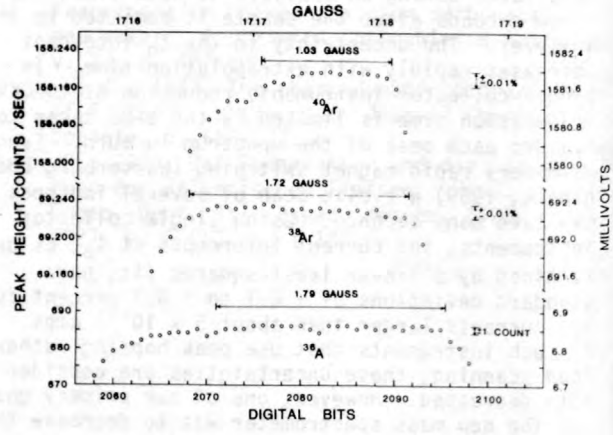

Figure 1.--Peak top data obtained simultaneously from the ^{36}Ar, ^{38}Ar, and ^{40}Ar data channels as the ion beams are scanned across their collector slits. The "all in" peak width (± 0.01 percent) is limited to 1.03 gauss.

Table 1.--Ion beam characteristics for the center collector
[Magnetic field 1565 gauss; ion accelerating potential 2000 volts. Tailing << 2×10^{-5} at 0.2 mass units from peak center.]

	mm	Corresponding magnetic field change in gauss
Source slit	0.305	-
Collector slit	1.270	4.1
Beam width (99.9 percent)	0.63	2.1
Dispersion (per mass unit)	6.31	20.6
Drift during an analysis	<0.02	<0.07
Peak top flat to $\pm 1 \times 10^{-4}$	0.31-0.53	1.0-1.7

were read at each value of magnetic field. No spurious signals were detected in any of the channels.

Of critical importance to a multiple-collector instrument is the magnetic field increment over which all of the ion beams are in their proper collectors. Figure 1 shows the relative positions of the beams for ^{40}Ar, ^{38}Ar and ^{36}Ar in their respective collectors. In this case the "all in width" (for peak tops flat to ± 0.01 percent) is limited by the width of the ^{40}Ar peak top to 1.03 gauss, or 0.31 mm. With magnetic field stability of ± 0.07 gauss (± 0.02 mm) during an analysis, this figure is more than adequate. We have found that sometimes when we make small adjustments in the collector spacings of 0.025 to 0.075 mm, based on calculations from ion beam data, the adjustments may be effectively cancelled by the following bakeout at 300°C. This problem of precise relative positioning of the collectors could presumably be overcome by making them externally adjustable, but the mechanism necessary for this might be quite complicated.

The sensitivity of the instrument has proved to be about twice the design goal, with a transfer function of 6.8 amperes/mole of argon, using a 5×10^9 ohms input resistor. This provides an input voltage to the voltage-to-frequency converters of 0.34 V for 1×10^{-11} moles of a sample argon isotope ($\sim 2.2 \times 10^{-7}$ cc STP) and a digital count of 34,000 for a 1-second integration. The signal voltage could be greatly increased by increasing the input resistor, but for our work we have found this to be unnecessary.

Figure 2 shows some of the data obtained during a typical argon analysis. The ion current for an individual isotope reaches a maximum value within 12 to 15 seconds, and the isotope ratios stabilize within 7 to 9 seconds after admitting the sample to the analyzer. The change in ion current per unit time is similar to that observed under good conditions in our single collector instrument, but it is invariably linear and shows little contamination from previous samples. The ion current varies typically a maximum of ± 0.02 percent about the least-squares line, and the 95 percent confidence interval for the t_0-intercept of the ^{40}Ar-data of figure 2 is ± 0.0097 percent (33.3 counts out of 342,000 for 135 data points, each with a 1-second integration time.) This precision is typical for data of comparable ion-current intensity. The 95-percent confidence interval for the t_0-intercept with 125 data

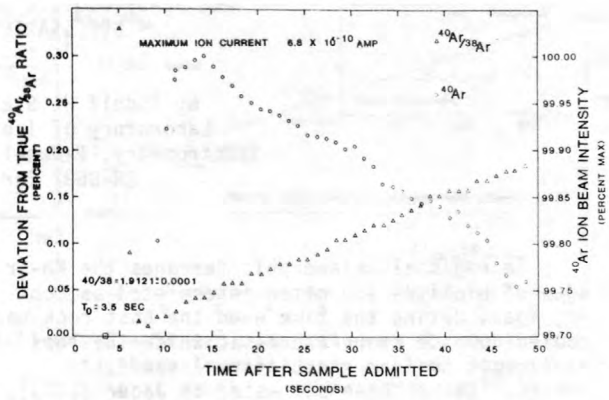

Figure 2.--Data from typical argon analysis showing time required for ion beam and ratio stabilization, and change in ratio (R) and ion beam current (I) as functions of time. Each point represents data from a one-second integration. T_0 is selected 3.5 seconds after gas sample is admitted to analyzer, at which time the ^{40}Ar-ion beam current is about 80 percent of maximum. Data are from an analysis of the standard muscovite P-207; only the first 50 seconds of data are shown.

points is typically 0.01 percent for input signals larger than 500 mV (10^{-11} amps with a 5×10^9 ohm resistor), but rises logarithmically to about 1 percent for an input of 0.5 mV.

Aston, F. W., 1930, The photometry of mass spectra and the atomic weights of krypton, xenon, and mercury: Proceedings of the Royal Society of London, v. A126, p. 511-525.

Cross, W. G., 1951, Two-directional focussing of charged particles with a sector shaped, uniform magnetic field: Review of Scientific Instruments, v. 22, p. 717-722.

Ezoe, H., 1967, Two directional beam convergence by sector shaped uniform magnetic field: Review of Scientific Instruments, v. 38, p. 390-394.

Nier, A. O., Ney, E. P., and Inghram, M. G., 1947, A null method for the comparison of two ion currents in a mass spectrometer: Review of Scientific Instruments, v. 18, p. 294-297.

Reynolds, J. H., 1956, High sensitivity mass spectrometer for noble gas analysis: Review of Scientific Instruments, v. 27, p. 928-934.

Strauss, H. A., 1941, A new mass spectrograph and the isotopic composition of nickel: The Physical Review, v. 59, p. 430-433.

Wasserburg, G. J., Papanastassiou, Ninow, E. V., and Bauman, C. A., 1969, A programmable magnetic field mass spectrometer with on-line data processing: Review of Scientific Instruments, v. 40, p. 288-295.

ARE Rb-Sr BIOTITE AGES IN THE CENTRAL ALPS NECESSARILY COOLING AGES?

By Rudolf H. Steiger and Irene Bucher
Laboratory of Isotope Geology and Mass Spectrometry, Federal Institute of Technology, CH-8092 Zurich, Switzerland

In regional metamorphic terranes the Rb-Sr ages of biotites are often interpreted as cooling ages, dating the time when the host rock has cooled down to temperatures at which the loss of radiogenic Sr from the biotite essentially ceases. It has been suggested by Jäger (1973), that the blocking temperature for the biotite Rb-Sr system corresponds to some 300 ± 50°C. On this basis the impressive body of young biotite Rb-Sr ages in the Central Alps has been interpreted by our Berne colleagues as representing the time of uplift after the last metamorphism.

Petrofabric and petrologic studies of the last decades, however, have revealed that the Alpine metamorphism in the Central Alps consists of several phases, or pulses, of metamorphism. In a study combining petrofabric analyses with isotopic age determinations (Steiger, 1964), it was demonstrated that rocks in the northern region of Alpine metamorphism were subjected to three distinct constructive phases of Alpine metamorphism, the last of which involved the formation of coarse-grained, cross-cutting biotites. These crossbiotites grew in a girdle oblique to the lineation of the host rock and contain elongated inclusions of host-rock minerals (in particular, quartz), which are oriented parallel to the lineation of the host rock. This clearly proves crossbiotite growth after the lineation-forming event.

In order to test the hypothesis that the Rb-Sr age of the crossbiotites possibly reflects the age of formation and not just a cooling age, we analyzed three crossbiotite-bearing specimens of metasedimentary rock from outcrops along the transition zone between Alpine amphibolite- and greenschist-facies metamorphism. To this end we adopted a special mineral separation procedure; cubes of 27 cm^3, or drill cores of similar volume, were roughly separated into their major mineral constituents after careful removal of all crossbiotites. From a split of the cube a representative whole-rock sample was prepared. One portion of the crossbiotite was thoroughly cleaned from contiguous mineral grains and from the majority of the inclusions by grinding the flakes under alcohol, the other portion of the crossbiotites was analyzed without further purification, that is, including the impurities.

We assume that if the crossbiotites indicate the time of formation, all phases involved in the reaction would have to homogenize their Sr-isotopic composition. The data pattern on the Sr-evolution diagram should then correspond to that shown in figure 1a, with all phases falling on a straight line whose slope defines the concluding time of equilibration. If the crossbiotites indicate a cooling age, on the other hand, one would expect to see the following data pattern (fig. 1b)--the mineral phases in close contact with the crossbiotite should act as a receptacle for the radiogenic ^{87}Sr expelled in the time span between the formation of the biotite and the closure of its Rb-Sr system. The data points for the clean crossbiotite, and for the impurities removed

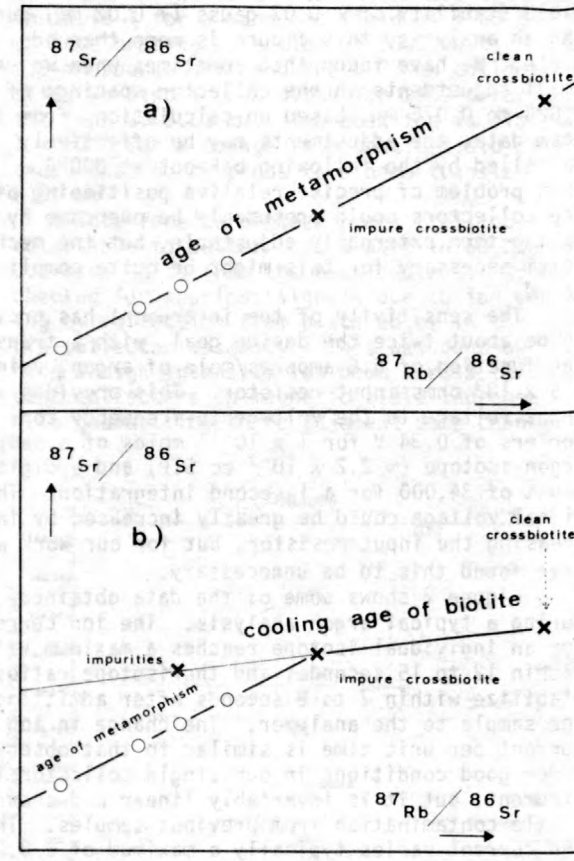

Figure 1.--Sr-evolution diagram with data pattern expected for (a) crossbiotites symbol = X) showing age of metamorphism, and (b) crossbiotites (symbol = X) showing cooling age while minerals with low Rb/Sr ratios (symbol = O) retain age of metamorphism.

from it, should plot on a new line of lesser slope, while the impure crossbiotite, which remained a closed system, should act as a hinge for the "cooling age" isochron.

The analytical results obtained for all three of the rocks show a pattern similar to that of figure 1a. As an example, the data for a rock from the southern Tremola series are presented in figure 2. This rock is essentially a white mica-crossbiotite-plagioclase-quartz gneiss with xenoblastic porphyroblasts of hornblende, garnet, kyanite, and staurolite. Minor phases comprise chlorite, epidote, tourmaline, apatite, and carbonate. The microstructural relationships clearly show that the crossbiotites were the last prograde mineral to be formed in the rock. From the array of the data in figure 2 it follows that essentially all minerals analyzed so far were equilibrated, within limits of analytical error, some 15.24 ± .13 m.y. ago. Isochrons calculated separately for both of the minerals with low Rb/Sr ratios, and for the biotites, are indistinguishable within their respective limits of error. This observation appears to indicate that we are indeed dating the time when the exchange and migration of ^{87}Sr-bearing fluids came to a close after the last metamorphic phase. We have determined, therefore, that the time when the minerals participating in the formation of the crossbiotites were last in equilibrium within the given volume of the rock cube.

To clarify whether this age corresponds to the peak of the metamorphism, or to some later stage during the cooling, we have to consider the possible metamorphic reactions leading to the formation of the crossbiotite. In the rocks investigated, any formation of new biotite will involve the dehydration breakdown of white mica. According to Jäger (1973), white mica forming at temperatures below 500°C will retain a closed Rb-Sr system and therefore date the time of formation. If we assume this to be valid also for white mica having participated in a dehydration reaction, which led to the homogenization of the Sr isotopic composition, then the mineral isochron of figure 2 will approximately determine the time when this metamorphic reaction took place.

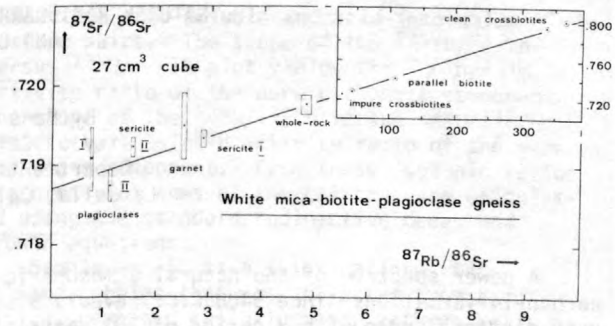

Figure 2.--Sr-evolution diagram for rock from southern Tremola series. The slope of the mineral isochron corresponds to 15.24 ± .13 m.y. (York, 1966), the initial $^{87}Sr/^{86}Sr$ ratio to .71872 ± .00005. The estimated error in the $^{87}Rb/^{86}Sr$ is ± 2 percent, the $^{87}Sr/^{86}Sr$ error represents the 95 percent confidence limit.

We tentatively conclude from this preliminary investigation that the Rb-Sr mineral isochrons for the crossbiotite-bearing rocks date the phase of metamorphism which induced the growth of the crossbiotites in the respective localities. In other words, it seems likely that the Rb-Sr ages for coarse-grained crossbiotites, if properly corrected for common Sr, do represent the age of formation and not cooling ages to some 300°C.

Experiments currently underway on progressively larger sample volumes may yield insight into the extent and time of Sr migration during the earlier phases of Alpine metamorphism.

Jäger, E., 1973, Die alpine Orogenese im Lichte der radio-metrischen Altersbestimmung: Eclogae Geologicae Helvetiae, v. 66, no. 1, p. 11-22.

Steiger, R. H., 1964, Dating of orogenic phases in the central Alps by K-Ar ages of hornblende: Journal of Geophysical Research, v. 69, no. 24, p. 5407.

York, Derek, 1966, LcasD-squares filting of a straight line: Canadian Journal of Physics, v. 44, p. 1079-1086.

NATURAL RADIOCARBON, SOLAR ACTIVITY, AND CLIMATE

By Hans E. Suess
University of California, San Diego
Department of Chemistry
La Jolla, California 92093

A power spectrum of the natural atmospheric carbon-14 variations since 5400 B.C. reveals a very distinct cycle with a period of 203 years. This period was particularly pronounced during sub-Atlantic times since about 800 B.C. It is also very marked for the time prior to 3400 B.C., the so-called Atlantic period. The time of the Subboreal shows a markedly different power spectrum, indicating a correlation between carbon-14 variations and climate. During sub-Atlantic and Atlantic times, the 200 year cycle is in phase and is so regular that the clock governing this periodicity can be assumed to be in the sun.

DATING CALICHES FROM SOUTHERN NEVADA BY $^{230}Th/^{232}Th$ VERSUS $^{234}U/^{232}Th$ AND $^{234}U/^{232}Th$ VERSUS $^{238}U/^{232}Th$ ISOCHRON-PLOT METHOD

By Barney J. Szabo[1] and Horst Sterr[2]
[1]U.S. Geological Survey
Denver Federal Center
Denver, Colorado 80225
[2]University of Colorado
Boulder, Colorado 80304

Caliches are widespread components in most of the world's dry zones. Dating these deposits is important because it would help to assess paleoclimatic conditions, it would allow us to understand the geomorphic processes affecting pediments and river terraces, and it would play a significant role in studies of Quaternary faulting.

Inorganically precipitated carbonates, such as caliches, may be dated by the uranium-series method, provided that the samples initially had uranium but no thorium isotopes and that the samples were free of post-depositional migration of uranium and its long-lived daughter isotope ^{230}Th. The major problem with dating caliches is that they always contain large amounts of detrital materials that cannot be separated from the carbonate fraction by simple physical means.

Because of the difficulties involved, there are few published data on dating caliches. Ku (oral commun., 1975) and Ku and others (1977) reported on dating on soil caliches. They leached the samples with dilute hydrochloric acid and analyzed both soluble and insoluble fractions. Ages were calculated from the results of the soluble fraction after correcting for chemical fractionations. Rosholt (1976) dated caliche rinds and travertines. The samples were ashed to CaO and the soluble and insoluble fractions of individual aliquots were separated by means of dilute acetic, nitric and hydrochloric acids. The ages were calculated using $^{230}Th/^{232}Th$ versus $^{234}U/^{232}Th$ plots of the soluble and insoluble fractions. It was shown that the use of dilute nitric acid produced the least chemical fractionation. Szabo and Butzer (in press) analyzed caliches from playa deposits. They dissolved and analyzed an aliquot of the total sample; then another aliquot was leached by dilute acetic acid and the acid insoluble residue was also analyzed. Ages were calculated from the $^{230}Th/^{234}U$ versus $^{232}Th/^{234}U$ and $^{234}U/^{238}U$ versus $^{232}Th/^{238}U$ plots.

Samples for this study were crushed, ground to a fine powder, then ashed for a period of about eight hours at 900°C to convert all $CaCO_3$ to CaO. Each sample was added to a dilute solution of nitric acid (0.1-0.5 N HNO_3) in very small portions so that at no time was the solution allowed to turn basic. The final acidity of the solution, with the slurry of the detrital acid-insoluble component, was set to about pH 1. The liquid and solid fractions were separated by centrifuge and the solid fraction was dried and weighed. Both fractions were then spiked by a combined solution of ^{236}U, ^{229}Th, and ^{228}Th.

The acid-insoluble residue was totally dissolved by repeated addition of concentrated $HClO_4$, HNO_3 and HF mixtures. The uranium and thorium in the acid-soluble fraction were coprecipitated with iron and aluminum hydroxides by the addition of concentrated NH_4OH. The precipitate was separated by centrifuge, dissolved in 6N HNO_3, and loaded on an anion-exchange resin column in NO_3^- form. Further steps of purification and separation were described previously by Szabo and Rosholt (1969). The uranium and thorium concentrations, $^{234}U/^{238}U$, $^{230}Th/^{232}Th$ and $^{230}Th/^{234}U$ were determined by alpha-spectrometry (Rosholt and others, 1966).

Results of the analyses and calculated ages of six caliche samples (both soluble and insoluble fractions) from southern Nevada localities are shown in table 1. Ages are calculated by means of isochron plots of the respective acid-soluble and acid-insoluble residue pairs. The slope of the $^{230}Th/^{232}Th$ versus $^{234}U/^{232}Th$ plot yields the $^{230}Th/^{234}U$ activity ratio of the pure carbonate component. The slope of the $^{234}U/^{232}Th$ versus $^{238}U/^{232}Th$ yields the $^{234}U/^{238}U$ activity ratio of the pure carbonate component. From these isotopic ratios isochron-plot ages of the caliches are calculated using the standard radioactive decay and growth equations.

Sample no. 60 is a thick caliche rind between cobbles that was collected from a caliche-cemented colluvium near Lathrop Wells by W. J. Carr. Dating this sample is particularly interesting because the deposit is directly overlain by a basalt flow dated 250,000 ± 50,000 years by whole-rock K-Ar method. (W. J. Carr, U.S.G.S., written commun.). Sample no. 60-A is the inner laminated, dense zone.

Table 1.--Uranium-series data and isochron-plot ages of caliche samples

[SOLN, acid soluble solution; RES, acid insoluble residue.]

Sample No.	Fraction	U (ppm)	$\frac{^{230}Th}{^{232}Th}$	$\frac{^{234}U}{^{238}U}$	$\frac{^{230}Th}{^{234}U}$	U-series isochron-plot age (years)
60-A[1]	SOLN	5.32±0.08	6.98±0.28	1.23±0.02	1.05±0.04	$345{,}000^{+180{,}000}_{-70{,}000}$
	RES	3.73±0.06	1.46±0.06	1.06±0.02	1.14±0.05	--
60-B[2]	SOLN	5.37±0.08	5.62±0.22	1.20±0.02	1.03±0.04	∿ 400,000
	RES	6.11±0.09	1.62±0.06	1.10±0.02	1.04±0.04	--
50[3]	SOLN	6.21±0.09	11.2 ±0.2	1.37±0.02	0.242±0.010	24,000±3,000
	RES	4.36±0.07	4.56±0.18	1.34±0.02	0.279±0.011	--
51[4]	SOLN	4.77±0.07	1.62±0.65	1.37±0.02	0.164±0.007	8,000±2,000
	RES	3.50±0.05	1.07±0.04	1.20±0.02	0.587±0.023	--
HOV-1[5]	SOLN	6.51±0.10	2.95±0.12	1.21±0.02	0.877±0.035	128,000±20,000
	RES	4.09±0.06	1.37±0.05	1.10±0.02	1.18 ±0.05	--
HOV-2[6]	SOLN	16.8 ±0.3	2.90±0.15	1.34±0.02	0.0806±0.0032	4,000±2,000
	RES	11.4 ±0.2	1.82±0.09	1.35±0.02	0.331 ±0.013	--

[1] The inner part of the hard and dense caliche rind growing on cobbles from caliche-cemented colluvium near Lathrop Wells; collected by W. J. Carr.

[2] The softer and porous outer part of the same caliche rind as [1].

[3] Poorly cemented, porous caliche filling along recent fault; collected at the Oak Spring area by W. J. Carr.

[4] Strongly cemented, porous caliche in Cca horizon; collected at the Oak Spring area by W. J. Carr.

[5] Soft, powdery caliche collected at the base of a trench in pediment gravel at Syncline Ridge area; collected by D. Hoover and A. Fernard.

[6] Hard caliche layer from the upper part of the same trench as [5].

Sample no. 60-B is the outer, softer, and porous part of the same caliche rind. The isochron-plot age of sample no. 60-A is 345,000 $\pm^{180,000}_{70,000}$ years, and is in good agreement with the limiting K-Ar age of the basalt flow. It appears from the isotopic data of sample no. 60-B that some extraneous ^{230}Th was taken up by this sample late in its geologic history, probably while the old colluvium was being down-cut by modern drainage. The approximate age estimate for this sample is 400,000 years or about the same age as sample no. 60-A, as expected.

Sample no. 50 and no. 51 were collected at the Oak Springs area by W. J. Carr. The poorly cemented, porous caliche is filling along recent fault. The well-cemented but porous caliche sample no. 51, from the Cca horizon is judged on topographic and morphologic considerations to be relatively young in age. The isochron-plot ages of samples no. 50 and no. 51 are 24,000 ± 3000 and 8000 ± 2000 years, respectively.

Samples no. Hov-1 and no. Hov-2 are from a trench in pediment gravel overlying the Eleana Formation of Mississippian age in the Syncline Ridge area. The trench was sampled and mapped by D. Hoover and A. Fernard, U.S.G.S. Sample no. Hov-1 is from a soft, powdery caliche layer at the base of the trench. The isochron-plot age of this sample is 128,000 ± 20,000 years and the pediment gravel must be at least that old. Sample no. Hov-2 is from a hard caliche layer at the upper part of the trench. This hard caliche shows evidence of redeposition, therefore the isochron-plot age of 4000 ± 2000 years is probably a minimum-age estimate only.

Ku, T. L., Bull, W. B., Freeman, S. T., and Knauss, K. G., 1977, Th^{230}/U^{234} dating of pedogenic carbonates in desert soils: Geological Society of America Abstracts with Programs, v. 9, no. 7, p. 1061.

Rosholt, J. N., 1976, $^{230}Th/^{234}U$ dating of travertine and caliche rinds: Geological Society of America Abstracts with Programs, v. 8, no. 6, p. 1076.

Rosholt, J. N., Doe, B. R., and Tatsumoto, M., 1966, Evolution of the isotopic composition of uranium and thorium in soil profiles: Geological Society of America Bulletin, v. 77, no. 9, p. 987-1004.

Szabo, B. J., and Butzer, K. W., (in press), Uranium-series dating of lacustrine limestones from pan deposits with final Acheulian assemblage at Rooidam, Kimberley District, South Africa.

Szabo, B. J., and Rosholt, J. N., 1969, Uranium-series dating of Pleistocene molluscan shells from southern California - An open system model: Journal of Geophysical Research, v. 74, no. 12, p. 3253-3260.

RARE GAS ELEMENTAL ABUNDANCES AND ISOTOPIC COMPOSITIONS IN DIAMONDS

By N. Takaoka[1] and M. Ozima[2]
[1]Department of Physics, Osaka University
Toyonaka 560, Japan
[2]Geophysical Institute, University of Tokyo
Tokyo 113, Japan

The rare gases have been extracted from natural diamonds in a three-step heating program, at 800°C, 2000°C and 2100°C. Elemental abundances and isotopic compositions of the extracted rare gases were studied using a mass spectrometer.

Samples: Experiments have been conducted in two phases. For the first phase, about 6 grams of industrial diamonds were purchased. Two years later, about 5 grams of industrial diamonds were purchased from the same dealer. We were told by the dealer that both groups of diamonds came from the Kimberley Mines, South Africa. There seemed no visible difference between the two groups of diamonds. They are about 4 mm in size, some have visible black inclusions, and some are nearly inclusion-free.

In the first phase of the experiment, diamonds were divided by eye into two batches (the nearly inclusion-free and the inclusion-rich) purely on the basis of the amount of inclusions. To facilitate degassing, both batches of diamonds were crushed in a stainless steel mortar with a stainless steel burin and a hammer. The crushed sample ranged from a few hundred micrometers to a few millimeters. No attempt was made to separate the inclusions from the crushed diamonds. Rare gas extraction was made on the crushed samples.

In the second phase of the experiment, diamonds were first crushed to less than a few hundred microns. The crushed samples were then divided into two batches (the nearly inclusion-free and the inclusion-rich). The nearly inclusion-free sample was kept in hot HNO_3 overnight to remove any inclusions and contaminations that

were still present. After the acid-washing, the weight of the diamonds was reduced by about 5 percent. We believe that separation of the inclusions was more thorough in the second phase experiment. Hence, rare gases in the nearly inclusion-free diamonds in the second phase experiment would be more representative of the genuine trapped rare gases in the diamond.

Experiments: The experimental techniques used for rare gas measurements are essentially the same as described in Takaoka (1976). The mass discrimination for the $^3He/^4He$ ratio was calibrated using a known $^3He/^4He$ ratio in Bruderheim standard. The mass spectrometer has a mass resolution of about 600, which is sufficient to separate ^3He from ^3H and HD, ^{38}Ar and ^{40}Ar from C_3H_2 and C_3H_4, and Kr and Xe from hydrocarbon peaks. The contribution from ^3H and HD at ^3He was less than 1 percent.

Results: A preliminary degassing experiment was made on about 1 gram of the inclusion-rich diamonds. From this study, we learned that 1500°C heating in a vacuum for one hour did not cause graphitization at all, but 2000°C heating for one hour in a vacuum completely converted diamond to graphite, that most of the degassing occurred during the graphitization process, and that only a negligible amount of rare gases were degassed (less than a few percent) from the graphite above 2000°C.

Amounts of rare gases degassed from the diamonds were of a similar order of magnitude as are commonly found in volcanic rocks and ordinary chondrites. The inclusion-rich diamonds had considerably larger amounts of rare gases than the nearly inclusion-free samples.

Elemental abundance patterns of the rare gases in diamonds are characterized by a large deficiency in Ne and an enrichment in Xe relative to the atmospheric composition. However, not much difference was observed in the elemental abundance patterns between the nearly inclusion-free and inclusion-rich diamonds.

Except for $^3He/^4He$, $^{40}Ar/^{36}Ar$ and possibly $^{129}Xe/^{132}Xe$, other isotopic ratios were indistinguishable from the atmospheric values. Be-

Table 1.--Elemental abundances and isotopic compositions of rare gases in diamond sample 1 (Phase 1)

Sample	Nearly inclusion-free			Blank	Inclusion-rich			Blank
Weight (grams)		2.61				1.98		
Temperature (°C)	800	2000	2100	2000	800	2000	2100	2000
Time of heating (min.)	30	60	60	60	30	60	5	60
$^3He \times 10^{-13}$ cm^{3}g^{-1}(STP)	<10	179	<10	<20	< 3	286	<10	<20
$^4He \times 10^{-9}$	1.57	918	0.37	2	1.36	3480	0.09	1.1
$^{20}Ne \times 10^{-12}$	2.1	10.2	< 0.1	20	6.3	20.7	< 0.1	20
$^{36}Ar \times 10^{-11}$	1.54	9.37	1.90	2	3.35	36.7	10	2.4
$^{84}Kr \times 10^{-12}$	1.0	2.9	0.26	0.8	1.8	3.6	< 0.02	0.6
$^{132}Xe \times 10^{-13}$	4.4	7.3	1.0	2	3.5	9.1	< 2	2
$^3He/^4He$		$(1.95\pm0.07) \times 10^{-5}$			$< 2 \times 10^{-4}$	$(8.23\pm0.35) \times 10^{-6}$		
$^{40}Ar/^{36}Ar$	574±14	1121±8			359±2	436±2		
$^{128}Xe/^{132}Xe$		0.0718±0.0037				0.0754±0.0011		
$^{129}Xe/^{132}Xe$		0.978 ±0.004				0.996 ±0.019		
$^{130}Xe/^{132}Xe$		0.149 ±0.006				0.161 ±0.007		
$^{131}Xe/^{132}Xe$		0.779 ±0.014				0.786 ±0.023		
$^{134}Xe/^{132}Xe$		0.386 ±0.009				0.391 ±0.012		
$^{136}Xe/^{132}Xe$		0.318 ±0.018				0.328 ±0.012		

Table 2.--Elemental abundances and isotopic compositions of rare gases in diamond sample 2 (Phase 2)

Sample	Nearly inclusion-free			Blank	Inclusion-rich			Blank
Weight (grams)		2.078		24.7 mg of Al foil		2.278		25.0 mg of Al foil
Temperature (°C)	800	2000	2100	2000	800	2000	2100	2000
Time of heating (min.)	30	60	60	60	30	60	60	60
$^3He \times 10^{-13}$ cm^{3}g^{-1}(STP)	<10	204	[1]	<10	<10	147	[1]	<10
$^4He \times 10^{-9}$	1.08	958	0.224	0.62	1.77	1540	0.303	0.63
$^{20}Ne \times 10^{-12}$	--	5.5	[1]	11	9.2	7.5	[1]	1.3
$^{36}Ar \times 10^{-11}$	1.51	4.33	[1]	5.3	3.75	4.21	[1]	5.1
$^{84}Kr \times 10^{-12}$	0.69	2.5	[1]	0.74	2.3	4.3	[1]	1.1
$^{132}Xe \times 10^{-13}$	2.4	2.9	[1]	2.6	15.4	10.9	[1]	4.0
$^3He/^4He$	--	$(2.13\pm0.13) \times 10^{-5}$			--	$(9.53\pm0.67) \times 10^{-6}$		
$^{40}Ar/^{36}Ar$	338±6	2441±206			581±9	4096±203		
$^{128}Xe/^{132}Xe$	0.071±0.006	0.070±0.005			0.0711±0.0038	0.0725±0.0027		
$^{129}Xe/^{132}Xe$	0.985±0.020	0.992±0.035			0.991 ±0.027	0.988 ±0.029		
$^{130}Xe/^{132}Xe$	0.147±0.007	0.145±0.013			0.150 ±0.005	0.151 ±0.009		
$^{131}Xe/^{132}Xe$	0.776±0.025	0.789±0.031			0.781 ±0.018	0.789 ±0.018		
$^{134}Xe/^{132}Xe$	0.387±0.012	0.392±0.024			0.382 ±0.014	0.387 ±0.009		
$^{136}Xe/^{132}Xe$	0.323±0.019	0.349±0.015			0.323 ±0.007	0.335 ±0.009		

[1]less than the blank (2100°C).

cause there may be some in-situ decayed radiogenic ^4He, the ratio must be a minimum of the primary trapped He. $^{40}Ar/^{36}Ar$ is also much higher than the atmospheric value. However, because the inclusion-rich samples show a higher $^{40}Ar/^{36}Ar$ ratio than the nearly inclusion-free diamonds do, we suspect that the high $^{40}Ar/^{36}Ar$ ratio is partly due to in-situ decayed radiogenic ^{40}Ar. Hence, the $^{40}Ar/^{36}Ar$ isotopic ratio found in the diamonds would be only a maximum value of the primary trapped Ar. The $^{129}Xe/^{132}Xe$ ratio seems to be slightly higher than the atmospheric value. However, it would be premature to firmly draw such a conclusion owing to the large experimental uncertainty.

Discussion: Among mantle derived materials, diamond seems to be very unique in its inertness to any known chemicals and in its high temperature stability. Trapped rare gases in diamonds must be the most faithful representation of rare gases in the mantle source region where diamonds were formed. Although rare gas elemental compositions are approximately similar between the inclusion-free and inclusion-rich diamonds, differences in some isotopic ratios and elemental abundances are evident. We assumed that the rare gases trapped in the inclusion-free diamonds represented more closely the genuine rare gas composition in the source mantle. Therefore the mantle source region for diamonds is characterized by high $^3He/^4He$ and $^{40}Ar/^{36}Ar$ ratios relative to the atmospheric ratios.

The $^3He/^4He$ ratio in the inclusion-free diamonds is even higher than the ratio generally found in oceanic-ridge basalts ($^3He/^4He \sim 1.4 \times 10^{-5}$), which is supposed to represent an upper mantle source region where the oceanic-ridge basalts were formed (Craig and Lupton, 1976). The high $^3He/^4He$ ratio may suggest that diamonds were derived from a mantle source region different from the upper-mantle source region for oceanic-ridge basalts, most likely from the deeper regions in the mantle. It is interesting to note that similar high $^3He/^4He$ ratios of $\gtrsim 2 \times 10^{-5}$ (Craig and Lupton, 1976, Kaneoka and others, 1978) were observed in Hawaiian volcanic rocks, which may be derived from deeper mantle through a hot spot.

The $^{40}Ar/^{36}Ar$ ratio in the diamonds is definitely higher than the atmospheric ratio. However, it appears to be smaller than the value assumed for the upper-mantle source region for oceanic-ridge basalts, which is likely to be more than 5000 (Hamano and Ozima, 1978).

In summary, the mantle source region for diamonds appears to be characterized by smaller $^{40}Ar/^{36}Ar$ and higher $^3He/^4He$ ratios than are those for the oceanic-ridge basalts, though both of these ratios are considerably higher than the atmospheric ratios.

Craig, H., and Lupton, J. E., 1976, Primordial neon, helium and hydrogen in oceanic basalts: Earth and Planetary Science Letters, v. 31, p. 369-385.

Hamano, Y., and Ozima, M., (in press), Earth-atmosphere evolution model based on Ar isotope data, in Alexander, E. C. and Ozima, M., eds., Terr. Rare Gases: Japan Scientific Society Press, Tokyo.

Kaneoka, I., Takaoka, N., and Aoki, K., (in press), Rare gases in mantle derived rocks and minerals, in Alexander, E. C., and Ozima, M., eds., Terr. Rare Gases: Japan Scientific Society Press, Tokyo.

Takaoka, N., 1976, A low-blank, metal system for rare-gas analysis, Mass Spectrometry, v. 24, p. 73-86.

LEAD ISOTOPIC COMPOSITION OF THE VOLCANIC SEQUENCE IN THE CRESCENT FORMATION FROM WASHINGTON

By Mitsunobu Tatsumoto, Daniel M. Unruh, and Wallace M. Cady
U.S. Geological Survey
Denver, Colorado 80225

There are many examples of oceanic plates being subducted or obducted at continental margins. Many studies involving Pb (for example, Tatsumoto, 1969; Oversbey and Ewart, 1972; Kay and others, 1978), Sr (for example, Meijer, 1976), and Nd (for example, DePaolo and Wasserburg, 1978) isotopes having been undertaken to determine if basalts or andesites erupted near continental margins can be related to the subducting oceanic place. However, the Crescent Formation, on the Olympic Peninsula in Washington, is unique. This formation, which contains both sedimentary rocks and volcanics, apparently represents an early to middle Eocene volcanic island (and surrounding sediments) near the eastern margin of the oceanic plate that, with the adjoining continent to the east, was sliced off from the oceanic plate and thrust

westward over the main oceanic plate (Cady, 1975). The Crescent Formation consists of an apparently unbroken volcanic sequence of ∿ 15 km of lower Tertiary tholeiite exposed in river valleys on the Olympic Peninsula. The sequence has a near-vertical dip with the top to the east.

Basalts of the Olympic Peninsula are chiefly oceanic tholeiites as indicated by their low contents of K_2O (< 0.5 percent), TiO_2 (< 2.0 percent), and P_2O_5 (< 0.36 percent), but the compositions do range to alkali basalts. Cady (1975) thus concluded that the basalts did not emerge at an active ridge crest, but instead were extruded on the eastern flank of the Juan de Fuca Ridge.

The $^{207}Pb/^{204}Pb$ versus $^{206}Pb/^{204}Pb$ ratios from basalts of the Olympic Peninsula and mid-ocean ridge (MOR) basalts and seamounts from near the Juan De Fuca ridge are shown in figure 1. Those from the Olympic Peninsula fall

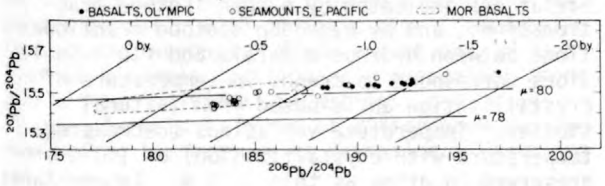

Figure 1.--$^{207}Pb/^{204}Pb$ versus $^{206}Pb/^{204}Pb$ plot for basalts from the Olympic Peninsula (solid circles) and from seamounts samples near Gorde-Juan de Fuca (open circles). Field of Pb-data from MOR basalts is shown by a dashed line.

approximately on the trend of the MOR basalt data. The slope of this trend yields a two-stage model age of ∿ 1.5 b.y. The Pb isotopic compositions of basalts from the Olympic Peninsula are more radiogenic than those in MOR basalts from the Gorda-Juan De Fuca Ridges. For example, $^{206}Pb/^{204}Pb$ of those from the Olympic Peninsula ranges from 18.8 to 19.7, whereas this ratio for MOR basalts ranges from 18.2 to 18.8. The isotopic values in some seamount basalts (Union, Dellwood) reported by Church and Tatsumoto (1975) fall in the range as those of the Olympic Peninsula.

The $^{232}Th/^{238}U$ (κ)-ratios of abyssal tholeiites are distinctly lower (< 3) than those of alkali basalts ($\gtrsim$ 3.5), and seamount basalts generally have intermediate κ-values. For the basalts of the Olympic Peninsula, κ ranges, from 0.54 to 5.7, which are similar values to those (0.53 - 4.9) reported for seamounts near the Juan De Fuca Ridge (Church and Tatsumoto, 1975). The κ-values and radiogenic characters of the basalts are not clearly related; neither parameter increases systematically within the erupted sequence. The apparent ∿ 1.5 b.y. trend, therefore, probably does not define a real source age, but is simply a mixing line between alkali basalt and tholeiite. We believe that these U-Th-Pb results clearly support Cady's (1975) conclusion that the basalts erupted on the flank of a ridge instead of at an active ridge crest.

The Pb-isotopic data indicate that the basalt source regions are isotopically heterogeneous, but the data do form a linear array indicating that the heterogenieties in the mantle are not completely random. The fact that all oceanic basalt data fall to the right of the Geochron (0-b.y. isochron) indicates that U-enrichment relative to Pb has occurred in the source regions; that is, the mantle has been an open system.

It is widely concluded that the source for oceanic alkali basalt is the deeper, fertile mantle and that the source for tholeiite it is depleted low-velocity zone (LVZ) because oceanic alkali basalt Pb (and Sr) is more radiogenic than that of tholeiite Pb (although among alkali basalts there is often a negative correlation between Pb and Sr radiogenic enrichment. Therefore, Pb in the oceanic alkali basalt wource hasevolved under a higher U-Pb environment than that of oceanic tholeiites. Based on what is known about U- and Pb- partitioning during igneous processes, the U/Pb ratio of the deeper mantle should be lower than that of the upper mantle (assuming the mantle can be explained by core-mantle segregation (for example, see Vollmer, 1977) and subsequent lack of chemical and Pb isotopic homogenization in the differentiated mantle. Alternatively, LIL-element segregation in the alkali basalt source may account for the more radiogenic character of these basalts as proposed in the dynamic model of Church and Tatsumoto (1975).

Cady, W. M., 1975, Tectonic setting of the Tertiary volcanic rocks of the Olympic Peninsula, Washington: U.S. Geological Survey Journal of Research, v. 3, p. 573.

Church, S. E., and Tatsumoto, M., 1975, Lead isotopic relations in oceanic ridge basalts from the Juan de Fuca-Gorda Ridge agea, N.E. Pacific Ocean: Contributions to Mineralogy and Petrology, v. 53, p. 253.

DePaolo, D. J., and Wasserburg, G. J., 1977, The course of island arcs is indicated by Nd and Sr isotopic studies: Geophysical Research Letters, v. 4, p. 465.

Kay, R. W., Sun, S. S., and Lee-Hu, C. N., 1978, Pb and Sr isotopes in volcanic rocks from the Aleutian Islands and Probilof Island, Alaska: Geochimica Cosmochimica Acta, v. 42, p. 263.

Meijer, A., 1976, Pb and Sr isotopic data bearing on the origin of volcanic rocks from the Mariana island-arc system: Geological Society of America Bulletin, v. 87, p. 1358.

Oversby, V. M., and Ewart, A., 1972, Lead isotopic composition of Tonga-Kermadec volcanics and their petrogenetic significance: Contributions to Mineralogy and Petrology, v. 37, p. 181.
Tatsumoto, M., 1969, Lead isotopes in volcanic rocks and possible ocean floor thrusting beneath island arcs: Earth and Planetary Science Letters, v. 6, p. 369.
Vollmer, R., 1977, Terrestrial lead isotopic evolution and formation time of the Earth's core: Nature, v. 270, p. 144.

STABLE ISOTOPE STUDIES OF GRANITIC PEGMATITES

By B. E. Taylor[1] and H. Friedrichsen[2]
[1]Department of Geology
University of California
Davis, California 95616
[2]Mineralogisches Institut
Universität Tübingen, 7400 Tübingen
Federal Republic of Germany

Oxygen, carbon, and hydrogen isotope compositions of minerals, whole rocks, and fluid inclusions were determined for granitic pegmatites and associated wall rocks of Precambrian to Late Cretaceous age from North America and Scandinavia. Most of the pegmatites studied were complex, and included those of the Evje region, Norway; the Tanco pegmatite, Manitoba; the Harding pegmatite, New Mexico; and the pegmatite-aplite dikes of the San Diego County area, southern California. These complex pegmatites are characterized by their economic concentrations of rare-earth elements and other elements such as lithium. Some of the pegmatites, for example, those from southern California and the Evje district of Norway, are also noted for their yields of gem-quality minerals (tourmaline, beryl, topaz, and aventurine feldspar). Other pegmatites, such as the Kiawa pegmatites of the Petaca district, northern New Mexico, (Jahns, 1974) are noted more for mica than for rare-earth elements or gems, and were studied for comparison with other pegmatites. The pegmatites studied are variable in form: some are dike-like, others are lens shaped with respect to wall-rock structures; some dikes are essentially concordant, while others are discordant; some were emplaced along pre-existing fractures.

Oxygen isotope fractionations between constituent minerals (quartz, feldspar, muscovite, biotite, and magnetite) record evidence of supersolidus pegmatite formation at "magmatic" temperatures of 580° to 750°C. Subsolidus hydrothermal crystallization appears to have been largely complete for many dikes by about 500°C, with minor crystallization continuing to lower temperatures. For individual bodies, the temperature range of supersolidus crystallization tends to be narrower than 580 to 750°C, in keeping with experimental data (Jahns and Burnham, 1969; Vaughan, 1963) on natural pegmatites. In zones, pegmatite-aplite dikes, temperature variations indicated by oxygen isotope fractionations, and by hydrogen isotope fractionations between hydrous minerals and fluid inclusions correspond to trends in temperature of crystallization anticipated from textural studies. Temperature variations (decreasing temperature with crystallization) of 110°C are preserved in dikes as thin as 1 m. Temperatures significantly below about 550°C for aplitic and pegmatitic zones of the Kiawa pegmatites indicate an over-all history more complex than simple magmatic crystallization.

Except for appropriate geologic situations, such as in the contact-metamorphic aureole at Crestmore, California, or subsequent structural deformation of still-hot pegmatites, we find no evidence in the oxygen isotope data for large-scale influx into the pegmatites of meteoric water during the main magmatic and hydrothermal stages of pegmatite formation. The isotopic data support the model of genesis described by Jahns and Burnham (1969), in which P_{H_2O} increases with time in the pegmatite system, particularly near the end of pegmatite crystallization. P_{H_2O} may be greater within than external to the pegmatites, especially in dikes emplaced close to the Earth's surface.

The range of $\delta^{18}O$ of quartz is $\sim$ +8.2 to $\sim$ +11.2 permil among the dikes studied, and this range of values is also reflected in other pegmatite minerals. Because similar oxygen isotope fractionations are observed between the same constituent minerals in different pegmatites, the above variation in $\delta^{18}O$ reflects variation in the oxygen isotope compositions of the pegmatite melts prior to crystallization. Pegmatite dikes in southern California, although probably having the same initial oxygen isotope composition, exchanged oxygen to various degrees with wall rock (primarily gabbroic; $\delta^{18}O \simeq +7.4$ permil) prior to crystallization of the dikes; a range in $\delta^{18}O$ of the final products resulted.

Similar $\delta^{18}O$ values are found for minerals in the Harding and Tanco pegmatites, which are associated with amphibolite wall rocks. No model involving fractional and isotopic fractionation, or other such process, offers as simple or as attractive an explanation for the range and ^{18}O enriched nature of the pegmatites studied as does isotopic exchange between the pegmatites and wall rocks.

The hydrogen isotope compositions of primary hydrous minerals, from the various pegmatites studied, fall within the range of -35 to -80 permil, but only within a very narrow range for any particular pegmatite or pegmatite district. When oxygen isotope formation temperatures and chemical compositions of the minerals are taken into account, the hydrogen isotope compositions of pegmatite muscovite and biotite indicate a very restricted range for δD of water exsolved from the pegmatites during later stages of crystallization ($\delta D_{H_2O} = 50 \pm 5$ permil). This value is strongly supported by isotopic analyses of fluid inclusions. No variation has been observed for the hydrogen isotope composition of pegmatite water with geologic time (Precambrian to Late Cretaceous). Minor variations in δD of hydrous minerals (particularly muscovite) among and within individual pegmatites, can be explained largely in terms of differences and variations in temperature of formation. Variation in chemical complexity of the pegmatite fluid, involving possible hydrogen isotope fractionations between water and species such as HF and LiH, may have been important locally.

The carbon isotope compositions of CO_2 released from primary fluid inclusions in most pegmatite minerals fall close to an average value of $\delta^{13}C = -7.9$ permil. More negative values of $\delta^{13}C$ for CO_2 suggest incorporation by the pegmatite of a more ^{13}C-depleted source of carbon. Where $\delta^{13}C$ values more negative than ~ -8.0 permil are found, other isotopic data also suggest more extensive isotopic exchange with wall rocks.

Jahns, R. H., 1974, Structural and petrogenetic relationships of pegmatites in the Petaca district, New Mexico: New Mexico Geological Society Guidebook, 25th Field Conference, p. 371-375.

Jahns, R. H., and Burnham, C. W., 1969, Experimental studies of pegmatite genesis - I. A model for the derivation and crystallization of granitic pegmatites: Economic Geology, v. 64, p. 843-864.

Vaughan, D. E. W., 1963, The crystallization ranges of the Spruce Pine and Harding pegmatites: The Pennsylvania State University, unpublished M.S. thesis, 66 p.

OXYGEN ISOTOPE RELATIONSHIPS IN PLUTONIC IGNEOUS ROCKS OF THE PENINSULAR RANGES BATHOLITH, SOUTHERN AND BAJA CALIFORNIA

By Hugh P. Taylor and Leon T. Silver
Division of Geological and Planetary Sciences
California Institute of Technology
Pasadena, California 91125

Whole-rock $\delta^{18}O$ values have been determined for 155 samples from approximately 140 plutons in the northern 600 km of the Peninsular Ranges batholith (fig. 1). Analyses of tonalites, granodiorites, gabbros and a few quartz monzonites are represented in crude proportion to the abundance of these rocks in the batholith. Most samples have been studied also for U-Pb zircon geochronology (Banks and Silver, 1968; Silver and others, 1968); K-Rb-Sr isotope and trace element systematics (Early and Silver, 1973); and rare earth element distributions (Gromet and Silver, 1977). All of these parameters display striking geographic regularities and profound transverse asymmetries related to the NNW-trending plutonic arc (Silver and others, 1975; Silver and Early, 1977).

The major conclusions of this study are as follows:

1. The $\delta^{18}O$ values of the various plutons change systematically from west to east across the batholith, and these differences persist along the length of the batholith for at least 600 km (fig. 1). Except for the gabbros, the $\delta^{18}O$ variations are purely geographic and essentially independent of rock type; the primary $\delta^{18}O$ values of the tonalites and granodiorites systematically increase from about 6.0 to 7.0 in the west to values as high as 12.8 in the east.

2. These $^{18}O/^{16}O$ relationships are virtually identical with the systematic west-to-east $^{87}Sr/^{86}Sr$ variations found in the batholith by Early and Silver (1973); both effects must be a result of the same basic process, as evidenced by the correlation in fig. 2.

3. The $^{18}O/^{16}O$ data show one feature not visible in the $^{87}Sr/^{86}Sr$ results, namely a $\delta^{18}O$ step separating the western and eastern

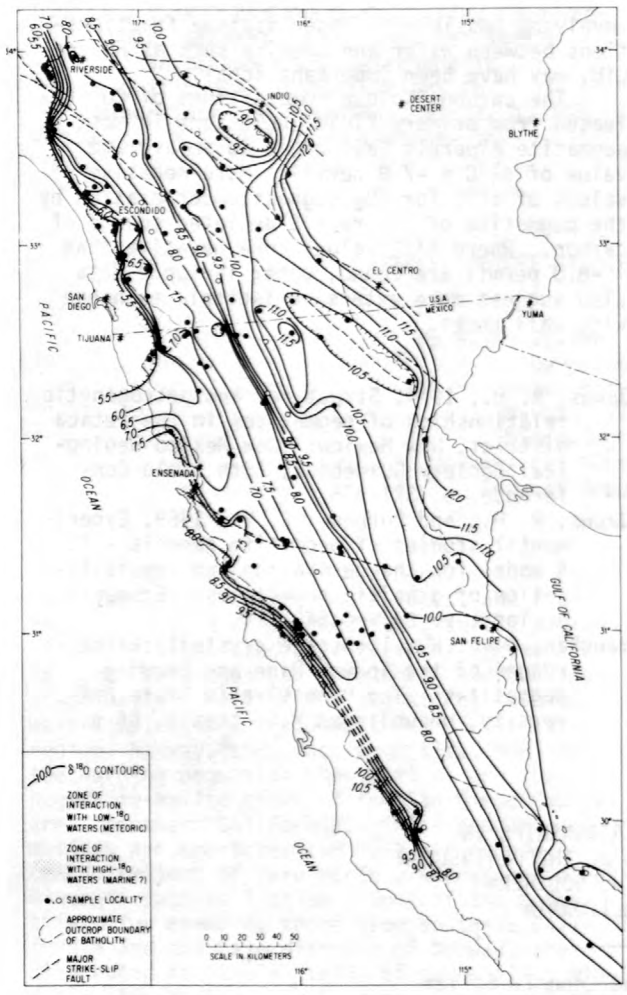

Figure 1.--Sample localities and whole-rock $\delta^{18}O$ contours of plutonic granitic rocks, Peninsular Ranges batholith. Open circles indicate gabbros with $\delta^{18}O$ values 1.0 to 2.5 permil lower than the adjacent granitic plutons.

portions of the batholith. This $\delta^{18}O$ step is shown in figure 1 by the close spacing of the $\delta^{18}O$ = 8.5 and 9.0 contours, and it is apparent as a "gap" on figure 2. This remarkably straight ^{18}O discontinuity extends the entire length of the batholith.

4. The ^{18}O boundary approximately coincides with a major geologic boundary which divides the batholith into an epizonal to mesozonal western half characterized by abundant gabbro, inclusion-rich tonalites, and high SiO_2 granodiorites (for example, Woodson Mtn. type, > 70 weight-percent SiO_2), and a more deep-seated eastern half dominated by sphene-rich tonalites and low-K granodiorites (Larsen, 1948; Gastil, 1975). The discontinuity is also an age boundary, as U-Pb zircon ages range from 105 to 130 m.y. in the west, whereas in the east they range from 80 to 103 m.y. (Silver and others, 1975). Gabbros are sparse and in small masses in the eastern half, which is the locus of the most abundant and largest tonalitic plutons. Because of greater depths of erosion and a thicker crust, the original volume of batholithic rocks in the high-^{18}O eastern zone must have far exceeded the volume of lower ^{18}O rocks in the western zone.

5. The gabbros also show a progressive enrichment in ^{18}O from west-to-east, but to a lesser degree than the quartz-rich rocks, ranging from values as low as 5.3 in the west to values as high as 8.3 in the east. The gabbros also fit the $^{18}O/^{16}O$-$^{87}Sr/^{86}Sr$ correlation pattern, but all of the gabbros plot in the field of the western granitic rocks on Figure 2.

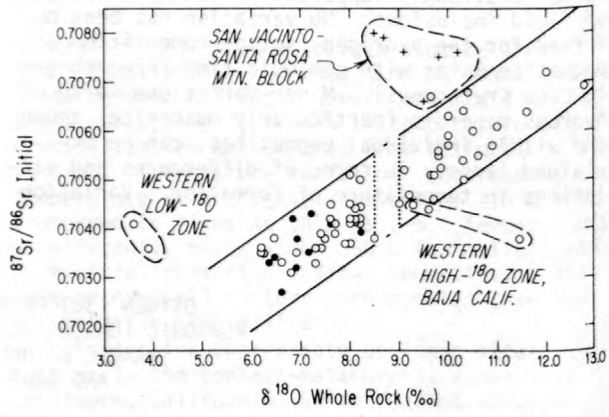

Figure 2.--Plot of whole-rock $\delta^{18}O$ versus initial $^{87}Sr/^{86}Sr$ for plutonic igneous rocks, Peninsular Ranges batholith. Solid circles indicate gabbros. The $\delta^{18}O$ "gap" at 8.5 to 9.0 divides the western group of granodiorites and tonalites from the eastern group.

6. Except along a strip at the extreme western edge of the batholith, the $\Delta^{18}O$ quartz-feldspar fractionations in the granitic rocks all have "normal" values of 1.1 to 2.3, indicating little or no postcrystallization alteration. However, the epizonal, commonly granophyric plutons found along the entire western edge of the batholith suggest that this zone was close to the roof of the batholith in the Early Cretaceous. All along this zone, we find exceedingly heterogeneous whole-rock $\delta^{18}O$ values and abnormal $\Delta^{18}O$ quartz-feldspar values. This is clearly the result of strong interactions with convectively circulating hydrothermal fluids in the roof zone of the batholith. However, at least two kinds of H_2O are indicated , a low-^{18}O meteoric ground water in the north and a high-^{18}O (marine?) pore fluid in the

south. In the strip extending from Ensenada north to Riverside, the whole-rock $\delta^{18}O$ values vary by more than 10 permil, from $\delta^{18}O = -5.0$ to $\delta^{18}O = 6.5$, and the more susceptible feldspar has typically been depleted in ^{18}O to a much greater degree than the coexisting quartz. Heterogeneous ^{18}O variations are also characteristic of the altered country rocks around these plutons. South of Ensenada the alteration produced ^{18}O enrichment in the feldspars, and no evidence was found for the above type of low-^{18}O meteoric hydrothermal alteration. Previous studies (Silver and others, 1963; 1975) have suggested that the batholith is the deeper extension of a volcanic arc which extended from a continental margin in southern California into an oceanic island arc in Baja California. The contrasting nature of the $\delta^{18}O$ values in the two types of hydrothermal fluids is compatible with such a transition. The heterogeneous isotopic effects described above do not, however, extend any appreciable distance eastward into the main part of the batholith, indicating that the major ^{18}O variations in the batholith are primary characteristics of the original magmas. This is in sharp contrast to the pronounced meteoric-hydrothermal $^{18}O/^{16}O$ and D/H effects observed within the interiors of the more northerly Cordilleran batholiths in Idaho and British Columbia (for example, see Taylor, 1978). This difference can be ascribed to the less complicated intrusive and tectonic history of the Peninsular Ranges batholith, which formed totally in the Cretaceous, whereas the northerly batholiths exhibit a complex multi-episode history extending from the Triassic well into the Tertiary. The slight upturn in the initial $^{87}Sr/^{86}Sr$ ratio found by Early and Silver (1973) along the western edge of the Peninsular Ranges batholith conceivably might reflect such peripheral hydrothermal alteration effects (see fig. 2).

7. As far as primary $\delta^{18}O$ variations are concerned, the only geographic unit of the batholith that clearly deviates from the regional east-west patterns is the San Jacinto-Santa Rosa Mtns. block that lies just northeast of the San Jacinto fault. The tonalite and granodiorite samples in this part of the batholith form a separate population on figure 2, indicating derivation from a distinctive source rock at depth, presumably from a parent material that was slightly lower in ^{18}O and higher in $^{87}Sr/^{86}Sr$ than that which dominated most of the eastern half of the batholith. This "reversal" in $\delta^{18}O$ to the northeast might be attributed to involvement of the extreme southwest edge of crystalline basement of the North American craton in the fusion process that produced these magmas. Such an older, high-rank metamorphic complex might be expected to contain more radiogenic strontium and to exhibit $\delta^{18}O$ values of about +10 or lower. There is some other evidence that supports this concept, namely slightly higher K-feldspar contents in the granodiorites and the occasional appearance of traces of inherited zircons in a few plutons (L. T. Silver, unpublished data).

8. The simplest explanation of the patterns shown in figures 1 and 2 is that the source materials of the Peninsular Ranges batholith were dominated by two end-members, one with $\delta^{18}O \approx +6.0$ and $^{87}Sr/^{86}Sr \approx .703$, and the other with $\delta^{18}O \approx 13.0$, or higher, and $^{87}Sr/^{86}Sr \approx 0.708$, or higher. Evidence for a less important, third end-member, is present in the rocks northeast of the San Jacinto fault. The low-^{18}O, low ^{87}Sr end-member that dominates the western part of the batholith appears to be derived from melting of the upper mantle, although it is also possible that this may have involved a two-stage process in which oceanic lithosphere was re-melted in the orogenic environment, perhaps as a consequence of the subduction process. The uniformly low $^{87}Sr/^{86}Sr$ and $\delta^{18}O$ values of all the western plutonic rocks, from gabbro to high-SiO_2 granodiorite, clearly imply that the parent magmas of all these rocks were derived from fundamentally the same source material. An important corollary of this statement is that less than a one permil change in $\delta^{18}O$ takes place during "differentiation" of hydrous plutonic granitic magmas in the batholithic environment. This has never before been so clearly demonstrated (for example, see Taylor, 1978).

9. The nature of the high-^{18}O, high ^{87}Sr end-member(s) is much more problematical. The important contribution of the $^{18}O/^{16}O$ data to this problem is that up to the present time, large reservoirs of rock with such high $\delta^{18}O$ values have been identified only in materials which once resided on or very near the earth's surface (that is, either sedimentary rocks or possibly volcanic rocks that have been intensively altered at very low temperatures). In terms of the ^{18}O results alone, the most likely end-member would be a thick section of sedimentary or metasedimentary rocks, as this is the only sufficiently abundant type of rock on Earth with the requisite high $\delta^{18}O$ values. Several samples of the batholithic country rocks were analyzed. Except for one sample of volcanoclastic sediment with $\delta^{18}O = 7.9$, the $\delta^{18}O$ values range from +10.9 to +20.2, the highest values being recorded in the northwest part of the batholith in the Bedford Canyon and French Valley Formations. Thus, the low-^{18}O plutons in the western belt are surrounded by extremely high-^{18}O metasedimentary rocks, indicating that ^{18}O exchange with the adjacent country rocks is not a significant factor in determining the $\delta^{18}O$ values of the plutons. Furthermore, mechanisms involving partial melting of such country rocks do not satisfy some major chemical constraints because these rocks are much too aluminous and potassic to provide the characteristic calcic to calkalkaline plutons of the batholith. A possibly more favorable rock type might be a Franciscan-type graywacke, which has extremely

uniform $\delta^{18}O$ values of +11 to +14 (Magaritz and Taylor, 1976). However, in order for this type of sedimentary section to satisfy the chemical constraints on magma genesis it would have to contain appreciable amounts of intermixed basaltic greenstones and (or) limestones, and there would have to be remarkably complete chemical homogenization during the melting process. Because of the complexities involved, without further sampling and more chemical data, we cannot at this time more specifically identify the high ^{18}O end-member.

In summary, during the Early Cretaceous the western part of the batholith was generated dominantly from a primitive source material apparently derived from the upper mantle. Eastward migration of the axis of magmatism involved increasing access to heavy ^{18}O reservoirs, probably involving assimilation from or exchange with a thick pile of metasedimentary rocks, or with the extensively altered upper portions of an ancient oceanic lithospheric slab. The principal source of heat energy to drive this gigantic mixing process was probably contributed by mantle-derived magmas analogous to the western series of plutons, because the isotopic contribution of the low-^{18}O end-member is observed throughout the eastern side of the batholith (fig. 2).

Banks, P. O., Silver, L. T., 1968, Uranium lead U-Pb isotope analyses of zircons from Cretaceous plutons of the Peninsular and Traverse Ranges, Southern California, Prog. with abstracts, 1968 Annual Meeting, p. 17-18. Mexico City Meeting.

Early, T. O., and Silver, L. T., 1973, Rb-Sr isotopic systematics in the Peninsular Ranges batholith of southern and Baja California: EOS Transactions, American Geophysical Union, v. 54, p. 494.

Gastil, R. G., 1975, Plutonic zones in the Peninsular Ranges of southern California and northern Baja California: Geology, v. 3, p. 361-363.

Gromet, L. P., and Silver, L. T., Geographic variations of rare earth fractionations in plutonic rock across the Peninsular Ranges batholith, Southern California: in EOS Transactions, American Geophysical Union, v. 58, no. 6, p. 532, 1977.

Larsen, E. S., 1948, Batholith and associated rocks of the Corona, Elsinore, and San Luis Rey quadrangles, southern California: Geological Society of America Memoir, v. 29, p. 1-182.

Magaritz, M., and Taylor, H. P., 1976, Oxygen, Hydrogen, and carbon isotope studies of the Franciscan formation, Coast Ranges California: Geochimica Cosmochimica Acta, v. 40, p. 215-234.

Silver, L. T., Stehli, F. G., and Allen, C. R., 1963, Lower Cretaceous pre-batholithic rocks of northern Baja California, Mexico: American Association of Petroleum Geologists Bulletin, v. 47, p. 2054-2059.

Silver, L. T., Allen, C. R., Stehli, F. G., Geological and Geochronological observations on a portion of the Peninsular Ranges batholith of northwestern Baja California, Mexico. Geological Society of America, 1968, Annual Meetings, p. 279-280. Mexico City Meeting, 1968.

Silver, L. T., Early, T. O., 1977, Rubidium-strontium fractionation domains in the Peninsular Ranges batholith and their implications for magmatic arc evolution, EOS Transactions, American Geophysical Union, v. 58, no. 6, p. 532.

Silver, L. T., Early, T. O., and Anderson, T. H., 1975, Petrological, geochemical, and geochronological asymmetries of the Peninsular Ranges batholith: Geological Society of America, Abstracts with Programs v. 7, no. 3, p. 375-376.

Taylor, H. P., 1978, Oxygen and hydrogen isotope studies of plutonic granitic rocks: Earth and Planetary Science Letters, v. 38, p. 177-210.

Pb AND Sr ISOTOPIC REGIMES WITHIN THE 3000-2800 M.Y.-OLD GNEISSES OF WEST GREENLAND: THEIR REGIONAL AND PETROGENETIC SIGNIFICANCE

By Paul N. Taylor and Stephen Moorbath
Department of Geology and Mineralogy
Oxford University, Oxford, United Kingdom

Pb and Sr isotopic data have been used to determine whether ca. 3700 m.y.-old sialic crust contributed to the production of the immense amounts of sial formed ca. 3000-2800 m.y. ago in the Archean of West Greenland.

Two isotopically distinct regimes of ca. 3000-2800 m.y.-old gneisses and associated anorthosites have been found. In areas lying to the north and south of the Isua-Godthaab-Buksefjord region, whole-rock Pb isotopic analyses give straightforward $^{207}Pb/^{204}Pb$ vs. $^{206}Pb/^{204}Pb$ isochrons yielding rock-formation

ages and indicating derivation from a laterally extensive, homogeneous source region with $^{238}U/^{204}Pb$ (μ_1) of ≈ 7.3, if two-stage Pb isotopic evolution is assumed.

In contrast, within the centrally situated Isua-Godthaab-Buksefjord region, Pb isotopic compositions in the ca. 3000-2800 m.y.-old NûK Gneiss and associated layered anorthosites exhibit a very complex pattern. Nearly all samples from this region show modification of initial magmatic Pb isotopic composition by assimilation of unradiogenic Pb derived from ancient uranium-depleted rocks such as the ca. 3700 m.y. -old Amîtsoq Gneiss. In some cases, where several samples of a single homogeneous intrusive body have been analysed, Pb/Pb isochron ages are in good agreement with Rb-Sr isochron ages but yield anomalously low μ_1 values if two-stage Pb isotopic evolution is assumed. In other cases, especially where NûK Gneiss has been sampled in close proximity to Amîtsoq Gneiss, Pb isotopic data do not yield meaningful isochrons but exhibit severe scatter below the appropriate reference isochron for a μ_1 value of 7.3.

Neither Pb nor Sr isotopic data support the view that the NûK Gneiss represent reworked ancient sialic crust similar to the Amitsoq Gneiss. Nor is such a view supported by other geochemical data. No NûK Gneiss Pb has yet been found that plots on or below the reference isochrons calculated for hypothetically remelted Amîtsoq Gneiss between 3000 and 2800 m.y. ago, whilst the average $^{87}Sr/^{86}Sr$ of exposed Amîtsoq Gneiss between 3000 and 2800 m.y. ago was far more radiogenic than initial $^{87}Sr/^{86}Sr$ ratios for NûK Gneiss.

Thus the incorporation of ancient unradiogenic crustal Pb in NûK Gneiss of the Isua-Godthaab-Buksefjord region is regarded not as resulting from bulk melting or assimilation of Amîtsoq Gneiss, but as due to selective contamination of magmas with Pb (and probably other trace elements) during ascent and emplacement. The mechanism of this contamination is indicated by comparison of measured Pb isotopic compositions with Pb contents for individual rock samples. Preliminary indications are that processes such as scavenging and zone-refining are more probable than isotopic exchange reactions.

The boundaries between the two isotopic regimes are, not surprisingly, closely linked to the known occurrences of Amîtsoq Gneiss. The fact that NûK Gneiss with measurable Pb are not found far beyond the known occurrences of Amîtsoq Gneiss suggests that early Archean crust does not occur either at the surface or at depth in areas beyond the Isua-Godthaab-Buksefjord region.

ANOMALOUS $^{40}Ar/^{39}Ar$ RELEASE SPECTRA FOR BIOTITES FROM THE BERRIDALE BATHOLITH, NEW SOUTH WALES, AUSTRALIA

By Neil Tetley and Ian McDougall
Research School of Earth Sciences
The Australian National University
Canberra, A.C.T., Australia

To further test the $^{40}Ar/^{39}Ar$ step-heating technique on areas which have had a simple geological history, we have chosen to study biotite and hornblende (where available) from the lower Paleozoic Berridale batholith of southern New South Wales, Australia. The batholith consists of a number of granitoid plutons that have been thoroughly mapped (White and others, 1977; White and others, in press), and evidence indicates that since their emplacement there has not been any significant geological disturbance, such as regional metamorphism. These authors have distinguished two distinct granite types, the S-type and the I-type, which are thought to represent the partial melting of sedimentary and igneous source material. Isotopic dating by the Rb-Sr method (Williams and others, 1976) and the K-Ar conventional technique on separated biotites from eight of the plutons, suggest that emplacement and cooling occurred over a time span of ∿ 10 m.y., beginning about 420 m.y. ago.

The excellent agreement of the Rb-Sr, K-Ar, $^{40}Ar/^{39}Ar$ total-fusion and incremental total-fusion ages (the latter obtained by summing the data from all steps of a step-heating experiment) measured on biotites separated from eight granitoids in the Berridale batholith, indicates that each of these techniques is recording the same geological event (table 1). However, it appears that the $^{40}Ar/^{39}Ar$ plateau ages form two very distinct groups. The first group comprises results which have a classical "flat plateau" over the majority of the ^{39}Ar released, yielding a plateau age concordant with the other ages; an example of this type of release pattern is shown in figure 1. The second group gives plateau ages which are several percent higher than the ages determined by the other techniques. These high apparent plateau ages

Table 1.--Summary of biotite ages on samples used for $^{40}Ar/^{39}Ar$ age spectra experiments

Pluton	Sample no.	Magma source	Rb-Sr[1,5] age	K-Ar age[1,2]	Total-fusion age[1,2,4]	Incremental total-fusion Age[1]	Plateau Age[1,2,3]
"Ideal" plateaux							
Wullye	BB- 62	I	414.6	411.2±2.4	409.0±3.7	409.1	412.2±1.2
Maffra	BB- 21	I	413.9	412.9±2.4	413.3±3.7	413.4	414.2±1.1
Dalgety	BB- 9	S	415.4	410.3±2.3	416.7±3.7	417.6	421.6±1.1
Cootralantra	BB- 19	S	421.2	417.2±2.0	420.0±3.8	420.1	422.1±1.1
"Anomalous" plateaux							
Tara	BB- 15	I	414.3	415.5±3.4	412.1±3.7	412.6	420.5±1.2
Buckleys Lake	BB- 10	I	416.9	412.9±2.4	414.6±3.7	418.7	421.9±1.4
Numbla Vale	BB- 2	S	417.5	422.2±2.4	424.4±3.8	423.4	429.1±1.2
Finister	BB-163	I	415.9	420.1±2.9	421.3±3.8	421.5	430.7±1.2

[1]Ages are in million years and have been calculated using the decay constants recommended by Steiger and Jäger (1977).
[2]Errors are in million years and are given at the level of one standard deviation.
[3]Errors have been calculated by a weighted mean.
[4]Total-fusion analyses were performed on a ¼-split of the sample used for the step-heating experiments.
[5]Data from Williams and others (1976).

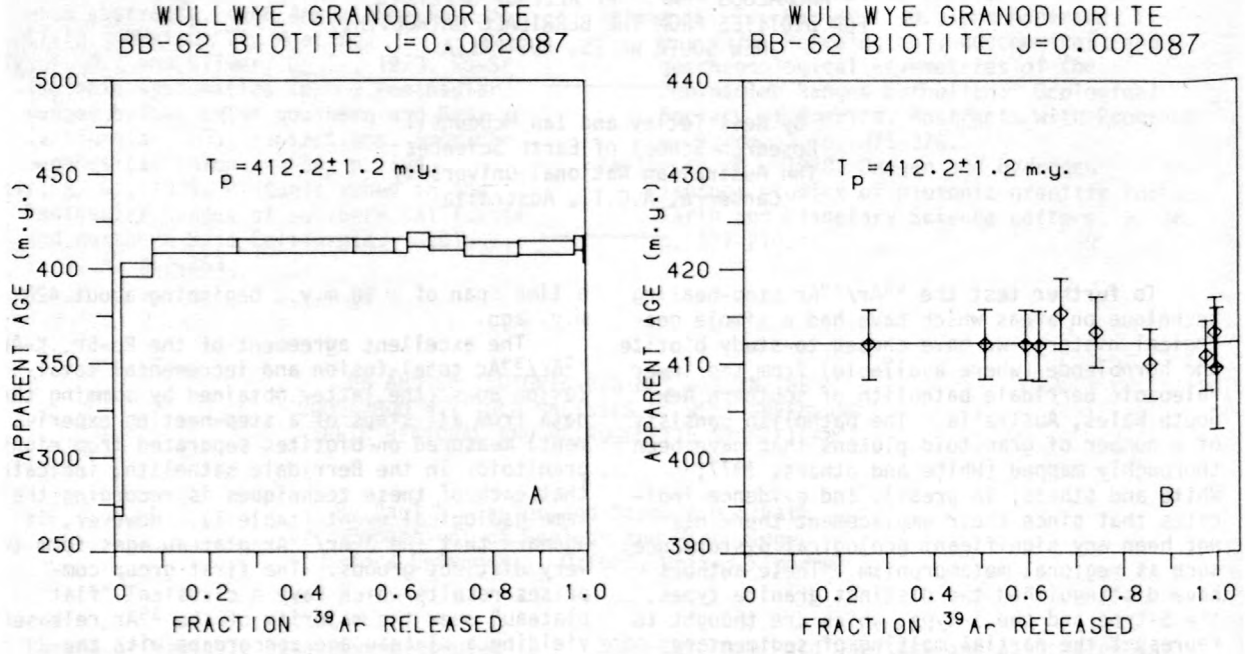

Figure 1.--Ideal $^{40}Ar/^{39}Ar$ release spectrum for biotite from the Wullwye Granodiorite, Berridale batholith, New South Wales, Australia. Plat A shows a bar diagram with all steps included (temperature interval 50°C.), whereas plot B shows only those points used in the calculation of the plateau age. Error bars are given at the level of one standard deviation.

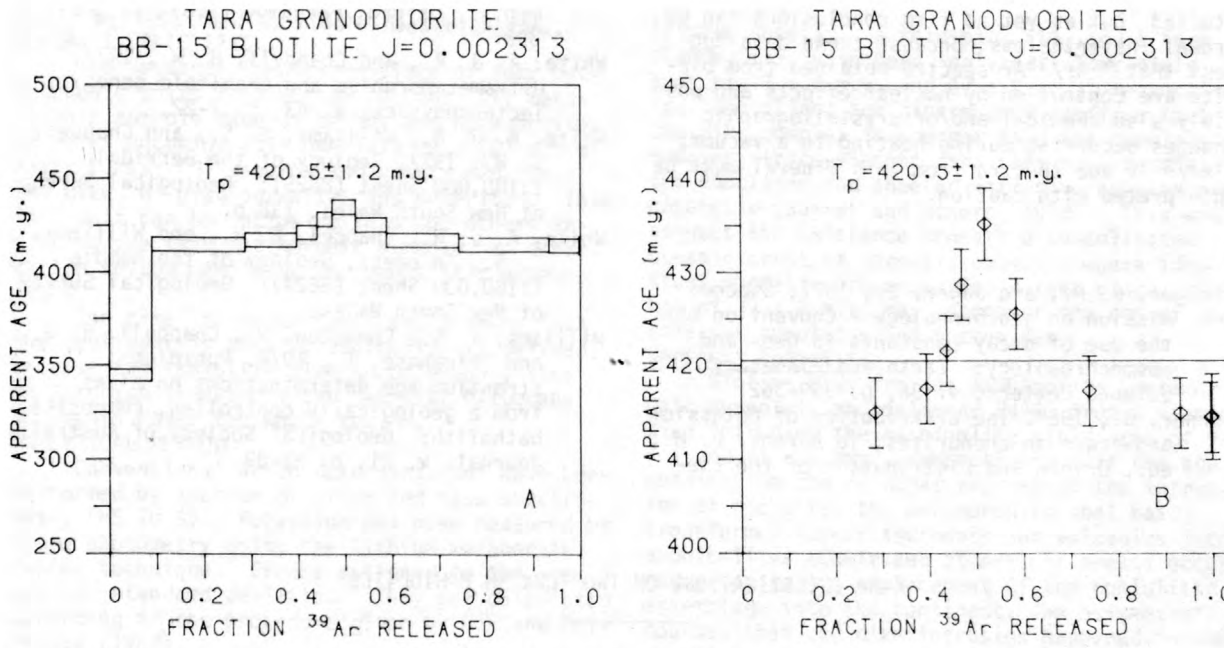

Figure 2.--Anomalous $^{40}Ar/^{39}Ar$ release spectrum for biotite from the Tara Granodiorite, Berridale batholith, New South Wales, Australia. Plot A shows a bar diagram with all steps included (temperature interval 50°C.), whereas plot B shows only those points used in the calculation of the plateau age. Error bars are given at the level of one standard deviation.

are caused by a few data points with high apparent ages, centering around 50 to 60 percent of ^{39}Ar released, as shown in figure 2. Hornblende from the same sample of the Tara Granodiorite yields a flat plateau over the majority of the ^{39}Ar released. These anomalous spectra for biotite are highly reproducible on the same sample and for other samples of biotite from the same pluton. The spectra for biotite cannot be changed simply by changes in the heating schedule (50°C. versus 100°C. steps), and are found in samples from both S- and I-type plutons.

All biotites analyzed by the step-heating technique are characterized by low initial ages at the start of the heating schedule. The model of Turner (1968) would suggest that each biotite has lost a small amount of radiogenic argon ($^{40}Ar^*$). An alternative view is that these low apparent ages are caused by disproportionate release of loosely bound ^{39}Ar held in lattice defects caused by recoil effects. However, recoil effects seem unable to account for the two different release patterns found in biotite. Because the incremental total-fusion ages agree with the conventional K-Ar ages, it is suggested that in the case of the "flat plateaux", the proportionate amount of $^{40}Ar^*$ that was not released in the initial steps with the ^{39}Ar, is being released over the entire plateau after annealing of the biotite. In the case of the anomalous spectra, we suggest that this same amount of $^{40}Ar^*$ is being released disproportionately, between ~ 750° and 950°C. It has been shown that the processes of dehydroxylation and delamination of the biotite and oxidation of Fe^{++} to Fe^{+++}, resulting in the formation of oxybiotite, are operative within the temperature range of interest (750° to 950°C). The disproportionate release of $^{40}Ar^*$ over a particular temperature range may indicate that, in addition to nuclear effects, the release is controlled by the physical and/or chemical processes just described.

Three of the four plutons which have complex spectra are probably reset by later intrusions in regard to their biotite age. However, the Tara Granodiorite does not fit in this category, because it is one of the youngest intrusives. Tara is unusual in that it contains very large quantities of restite, a material relict from the source region where partial melting has occurred to produce the more felsic granitic magma. The restite is believed by White and Chappell (1977) to be metamorphic in character. The metamorphism experienced by these biotites may have caused chemical and/or crystallographic changes to their structure, indirectly resulting in a disproportionate release of the argon isotopes over the spectrum and thereby the anomalous plateaux.

To further understand the difference between the two groups of biotites, their chemistry and crystal structure is currently being

studied, but as yet no firm conclusions can be drawn. Nevertheless, because these data suggest that $^{40}Ar/^{39}Ar$ spectra obtained from biotite are controlled by nuclear effects and possibly also chemical and/or crystallographic changes occurring during heating in a vacuum, $^{40}Ar/^{39}Ar$ age spectra from this mineral must be interpreted with caution.

Steiger, R. H., and Jäger, E., 1977, Subcommission on geochronology - Convention on the use of decay constants in geo- and cosmochronology: Earth and Planetary Science Letters, v. 36, p. 359-362.

Turner, G., 1968, The distribution of potassium and argon in chondrites, in Ahrens, L. H., ed., Origin and Distribution of the Elements: Oxford, Pergamon Press, p. 387-398.

White, A. J. R., and Chappell, B. W., 1977, Ultrametamorphism and granitoid genesis: Tectonophysics, v. 43, p. 7-22.

White, A. J. R., Williams, I. S., and Chappell, B. W., 1977, Geology of the Berridale 1:100,000 Sheet (8625): Geological Survey of New South Wales, 138 p.

White, A. J. R., Chappel, B. W., and Williams, I. S., in press, Geology of the Numbla 1:100,000 Sheet (8624): Geological Survey of New South Wales.

Williams, I. S., Compston, W., Chappell, B. W., and Shirahase, T., 1976, Rubidium-strontium age determinations on micas from a geologically controlled, composite batholith: Geological Society of Australia Journal, v. 21, p. 81-89.

K-Ar INVESTIGATIONS ON TWO TURKISH OPHIOLITES

By Robert Thuizat[1], Raymond Montigny[1], Uner Cakir[2], and Thierry Juteau[2]

[1]Laboratoire de Paleomagnetisme
Institut de Physique du Globe
5, Rue Descartes, 67084
Strasbourg, France

[2]Laboratoire de Mineralogie-Petrologie
I, Rue Blessig, 67084
Strasbourg, France

It has been suggested that the ophiolite complexes are slices of the sub-oceanic lithosphere, tectonically emplaced on the continent (Dietz, 1963); Coleman, 1971). The ophiolitic rocks are, therefore, allochthonous and have been affected by several episodes of deformation and faulting. All sequences of ophiolitic rocks show evidence of water-rock interaction, such as spilitization of basalts and serpentinization of peridotites. These alterations have occurred either in the submarine environment or during the tectonic emplacement.

The aim of this work is to decipher the past history of two ophiolitic assemblages--Antalya (southwestern Turkey) and Kersanti (southern Turkey)--by providing estimates of time intervals elapsed between their genesis and their tectonic emplacement. Alpine tectonics and water-rock interactions do not favor the use of the conventional K-Ar method to obtain geochronological information on ophiolites. To circumvent these two serious obstacles we have analyzed minerals known for their good argon retention, such as fresh plagioclase and hornblende, that have been separated from undeformed samples.

ANTALYA OPHIOLITES

The description of the Antalya complex is based on Juteau's (1975) works. The complex can be generally divided into the following units, which form a superposed sequence from bottom to top: (1) metamorphic aureole consisting of amphibolites unconformably overlain by; (2) ultramafic tectonites; (3) cumulate materials composed of ultramafics, gabbros, and quartz diorites; (4) dolerites occurring either as individual dikes intruding both tectonites and cumulates or within sheeted dike complexes on the top of the assemblages; and (5) lavas of alkaline nature resting unconformably on the other units. They are either interbedded with Triassic sediments or occur as individual sills within sediments of unknown age.

The sheeted dike complexes, the gabbros, and the ultramafic cumulates are interpreted to be the result of fractional crystallization within a magma that originated from a partially molten lherzolite. The ultramafic tectonites would be residua of this fused lherzolite. The alkali lavas, on petrological grounds, cannot be cogenetic with the other terms of the series. Dewey and others (1973), however, attributed a Triassic age for the whole ophiolitic assemblage because some of these lavas are interbedded with Triassic sediments. The age of the tectonic emplacement into the continent is stratigraphi-

cally well-defined as middle Maestrichtian.

KERSANTI OPHIOLITES

The Kersanti complex consists of four petrographic units from bottom to top: (1) metamorphic aureole made of ortho- and para-derivated rocks unconformably overlain by; (2) ultramafic rocks; (3) gabbros and quartz diorites; (4) dikes of plagiogranites and dolerites. This last unit can be intrusive into the others including the thin metamorphic aureole, an observation seldom mentioned for ophiolitic assemblages.

The time of the tectonic emplacement into the continent is stratigraphically ill-defined, because the ophiolite slab unconformably lies on Turonian limestones and detrital Oligocene sediments cover the whole region.

ANALYTICAL METHOD

Conventional argon determinations have been performed by isotope dilution and mass spectrometry (MS 10 S). Potassium has been measured by flame photometry using the lithium-metaborate fusion technique. Errors assigned to the ages are one standard deviation. They are calculated according to the procedure given by Cox and Dalrymple (1967).

RESULTS (TABLE 1) AND DISCUSSION

Antalya Ophiolites

Three feldspars and one amphibole have been analyzed. Feldspar T7 separated from a dolerite sill occurring within sedimentary pelites yields an age of 81 ± 3 m.y., different from the age given by fossils in sediments interbedded with lava flows of similar mineralogical composition. However, one cannot say whether there are several generations of alkaline lavas or not.

Table 1.--Potassium-argon ages on mineral separates

[s.d. = standard deviation]

Sample no.[1]	K_2O (weight percent)	$^{40}Ar_{rad}$ (10^{-11} mol/g)	$\frac{100\ ^{40}Ar_{rad}}{^{40}Ar_{total}}$	Calculated age (m.y.) ±1 s.d.
T7	0.233	2.869	19	81±3
T14	0.182	2.176	30.5	79±2
T15	0.178	1.796	28.3	67±2
D261	0.361	3.276	53	61±2
U496	0.220	2.354	16.5	71±3
U19	7.69	107.3	90	92±1
U12b	2.60	33.45	81	85±1

[1]Antalya ophiolite-T7 feldspar; T14 feldspar; T15 hornblende; D261 feldspar. Kersanti ophiolite-U496 feldspar; U19 biotite; U12b feldspar.

Feldspar D 261 separated out of a gabbro gives an age of 61 ± 2 m.y. This value corresponds to a major tectonic event subsequent to the emplacement of the ophiolites into the continental area.

Sample T14, a quartz diorite, and sample T15, a dolerite, were taken from the same outcrop--quartz diorite intruded by a sheeted intrusive complex. A feldspar, T14, and a hornblende, T15, have been analyzed. They yield ages of 79 ± 2 m.y. and 67 ± 2 m.y., respectively. The slight age discrepancy confirms that the dike complex is younger than the cumulates. However, trace-element data seem to show that the cumulates and sheeted intrusive complex are cogenetic (Noiret and others, 1978). This would suggest the existence beneath a consolidated oceanic crust of magmatic chambers where identical magmatic processes would take place. The age of 79 ± 2 m.y. may represent the age of genesis for cumulates and tectonites.

Kersanti Ophiolites

Biotite U19, from an amphibolite (metamorphic aureole), and feldspar U496, from a diabase dike intruding the amphibolite yield ages of 92 ± 1 and 71 ± 3 m.y., respectively. If the age obtained on the feldspar represents the intrusion of the dike, the metamorphism that has transformed former sediments and volcanics into amphibolites (Cakir and others, in press) occurred prior to the emplacement of the ophiolitic assemblage into the continent. We assume, of course, that the dike intrusion happened in the oceanic environment. These preliminary results would seem to corroborate the suggestion (Parrot and Whitechurch, 1978) that the metamorphism giving rise to metamorphic aureoles occurred during the slicing process of the oceanic crust, that is, before emplacement. An age of genesis for the ophiolites older than 92 m.y. is, therefore, expected. This prediction fails, though, to be confirmed because feldspar U12b from plagiogranite intruding the upper part of the cumulates and regarded as a residual liquid of magmatic differentiation gives an age of 85 m.y. This value is too low and can be explained in one of two ways. Either the suggestion made by Parrot and Whitechurch (1978) is not correct, or the volcanic feldspar has lost part of its radiogenic argon. It has, indeed, been observed that volcanic feldspars with potassium concentrations higher than 1 percent may not completely retain their radiogenic argon (Evernden and James, 1964).

CONCLUSION

It is not unreasonable to assume that age of emplacement of the Kersanti massif is also middle Maestrichtian. Then, the minimum estimates for the time intervals elapsed between genesis and emplacement are 12 and 18 m.y. for the Antalya and Kersanti ophiolites, respectively. If confirmed on other ophiolitic assemblages, these low values would suggest that the Turkish ophiolites originated in small ocean basins rather than in a large ocean.

Cakir, U., Juteau, T., and Whitechurch, H., in press, Une nouvelle preuve de l'écaillage intra-océanique précoce des ophiolites téthysiennes; les roches métamorphiques infra-péridotitiques du massif de Pozanti-Kersanti (Turquie): Bulletin de la Societe Geologique de France.

Coleman, R. G., 1971, Plate tectonic emplacement of upper mantle peridotities along continental edges: Journal of Geophysical Research, v. 76, p. 1212-1222.
Cox, A., and Dalrymple, G. B., 1967, Statistical analysis of geomagnetic reversal data and the precision of potassium-argon dating: Journal of Geophysical Research, v. 72, p. 2603-2614.
Dewey, J. F., Pitman, III, W. C., Ryan, W. B. F., and Bonnin, J., 1973, Plate tectonics and the evolution of the alpine system: Geological Society of America Bulletin, v. 84, p. 3137-3180.
Dietz, R. S., 1963, Alpine serpentinites as oceanic rind fragments: Geological Society of America Bulletin, v. 74, p. 947-952.
Evernden, J. F., and James, G. T., 1964, Potassium-argon dates and the Tertiary floras of North America: American Journal of Science, v. 262, p. 945-974.
Juteau, T. 1975, Les ophiolites des nappes d' Antalya (Taurides occidentales); Pétrologie d'un fragment de l'ancienne croûte téthysienne: Science de la Terre, 692 p.
Noiret, G., Allègre, C. J., and Montigny, R., 1978, Géochimie des éléments en trace des nappes d'Antalya, 6 R.A.S.T.
Parrot, J. F., and Whitechurch, H., in press, Subductions antérieures au charriage nord-sud de la croûte téthysienne; facteurs de métamorphisme de séries sédimentaires et volcaniques, liées aux assemblages ophiolitiques syro-turcs, en schistes verts et amphibolites: Revue de Géographie Physique et de Géologie Dynamique.

GEOCHEMICAL INVESTIGATIONS OF ANDEAN HYDROTHERMAL ORE DEPOSITS AND ASSOCIATED IGNEOUS ROCKS

By G. R. Tilton[1], A. H. Clark[2], and S. E. Church[3]
[1]Department of Geological Sciences
University of California
Santa Barbara, California 93106
[2]Department of Geological Sciences
Queen's University
Kingston, Ontario K7L 3N6, Canada
[3]Applied Research Laboratories
Sunland, California 91040

Lead isotopic compositions were measured for chalcopyrite, pyrite, and galena samples of hydrothermal ore deposits from southern Peru, northern Chile, northwestern Argentina, and the northern Bolivian tin belt. Additional lead isotope data were obtained for 14 andesitic rocks from northern Chile. In $^{207}Pb/^{204}Pb$-$^{206}Pb/^{204}Pb$ and $^{208}Pb/^{204}Pb$-$^{206}Pb/^{204}Pb$ diagrams the andesite leads plot distinctly above the regression line determined by oceanic volcanic rocks (Church and Tatsumoto, 1975). The andesite data also plot slightly above the field of sediments from the Nazca plate. The $^{87}Sr/^{86}Sr$ ratios of the andesites are $\sim$ 0.707 (C. E. Hedge, in Pichler and Zeil, 1972). The andesite isotope data suggest substantial contributions from the thick sialic crust to the magmas.

The ore data include two general traverses: a northern one from southern Peru to western Bolivia and one from northern Chile to northwestern Argentina. Precambrian basement rocks (up to 2 X 10^9 yr. old) are exposed in the northern traverse; in the south basement rocks are of Mesozoic to Cenozoic age. In addition, two separate ore sequences, an older one of Triassic-Jurassic age and a younger one of Oligocene-Miocene age, were sampled in the Bolivian tin belt. In general, the northern Chile, northwestern Argentina, and Tertiary Bolivian ores contain lead whose isotopic composition is very similar to that in the andesites. The Mesozoic Bolivian ores differ from the Tertiary ores in that they tend to show higher values of μ in a $^{207}Pb/^{204}Pb$-$^{206}Pb/^{204}Pb$ diagram. The similarity in isotopic composition of lead in the ores and the volcanic rocks indicates that the origin of lead in the lavas can be explained by the same mechanisms.

A comparison of the data from the two traverses reveals no correlation with the presence of exposed Precambrian basement, suggesting that upper crustal rocks do not exert a controlling influence on lead isotopes. We are unable to say from present data whether lead isotopic compositions correlate with distance inland from the Chile trench, as has been reported for Sr from northern Chile and northwestern Argentina (McNutt and others,

1975). The sources of lead appear to be in the lower continental crust, the underlying continental lithosphere, or both. Nazca plate sediments do not play a significant role in the production of lavas and ores. By extrapolation, models for the origin of the ore lead are assumed to apply to other chalcophillic elements such as Cu.

A review of various data in the literature indicates that, although there are local exceptions, the isotopic composition of Sr and Pb in calc-alkaline lavas correlates with crustal thickness in any given locality. A thicker crust yields higher $^{87}Sr/^{86}Sr$ ratios and higher μ values for lead in the lavas. Rogers and Novitsky-Evans (1977) also note an increasing potassium content with an increase in crustal thickness. These observations suggest that crustal thickness either exerts a controlling influence on, or is indicative of, some process that determines the geochemical characteristics of the lava sources.

Church, S. E., and Tatsumoto, M., 1975, Lead isotope relations in oceanic ridge basalts from the Juan-de-Fuca-Gorda Ridge area, N. E. Pacific Ocean: Contributions to Mineralogy and Petrology, v. 53, p. 253-279.

McNutt, R. H., Crocket, J. H., Clark, A. H., Caelles, J. C., Rarrar, E., Haynes, S. J., and Zentilli, M., 1975, Initial $^{87}Sr/^{86}Sr$ ratios of plutonic and volcanic rocks of the central Andes between latitudes 26° and 29° south: Earth and Planetary Science Letters, v. 27, p. 305-313.

Pichler, H., and Zeil, W., 1972, The Cenozoic rhyolite-andesite association of the Chilean Andes: Bulletin Volcanologique, v. 35, p. 424-452.

Rogers, J. J. W., and Novitsky-Evans, J. M., 1977, The Clarno formation of central Oregon, U.S.A. - volcanism on a thin continental margin: Earth and Planetary Science Letters, v. 34, p. 56-66.

ISOTOPIC ANOMALIES AND OLD COSMOCHRONOMETERS

By B. M. P. Trivedi
Institute of Geophysics and Planetary Physics
University of California, Los Angeles
Los Angeles, California 90024

Cosmochronology models have been developed on the assumption that long-lived chronometers (^{232}Th, ^{238}U, ^{235}U) and short-lived chronometers (^{129}I and ^{244}Pu) could be coupled together to give a consistent picture of the chemical evolution of the solar system and possibly the galaxy. In view of the recently discovered anomaly in ^{26}Mg and its association with ^{26}Al (Lee and others, 1977) it becomes necessary to investigate whether the source material which contributed to ^{26}Al and possibly to some other short-lived nuclides, disturbed the ^{129}I and ^{244}Pu (from the previous contributions) abundance significantly so that the old assumptions do not hold. This point is significant because Cameron and Truran (1977) have pointed out that all the ^{129}I and ^{244}Pu was injected by a nearby supernova at the time of collapse of the presolar cloud and hence these nuclides cannot be used as cosmochronometers. The following discussion will be somewhat model-dependent but even one or two orders of magnitude error in calculations will not change our conclusion that both ^{129}I and ^{244}Pu are good cosmochronometers.

Let us briefly discuss a possible mechanism for the accretion of heavy elements by a gas cloud, which will be a key to the following discussion. Astronomical observations indicate that in spiral galaxies, like ours, the supernovae of type II, which presumably synthesize the heavy elements, occur in the spiral arms (Maza and van den Bergh, 1976, and references therein). Based on this simple observation, Trivedi (1977) argued that a gas cloud could get its share of heavy elements from supernovae while passing through the galactic arms. During its passage through the inter-arm region, the radioactive nuclides decay freely. The passage time between the arms is about 150×10^6 yr so that nuclides with half-lives less than about 15×10^6 yr could not survive this passage.

Where do short-lived nuclides like ^{26}Al (half-life of 7×10^5 yr) fit into this picture and what will be their implication? Certainly they had to be accreted within a few million years to have survived at the time of their incorporation into minerals and subsequent retention of their decay products. From the supernova frequency in our galaxy of one per 50 - 200 yr (Tammann, 1974; Clark and Culhane, 1976) and the normal mixing period of supernova ejecta with the interstellar medium of about 10^6 yr (Reeves, 1972) we find that nuclides similar to ^{26}Al could be accreted by the presolar cloud during its collapsing stage. From the arguments that the star formation takes place in a narrow region of the galactic arm (Roberts, 1969), we conclude that the amount of new material collected during this period would be rather small as compared to the full passage through the arm.

We can make an estimate, within an order of magnitude, of the relative amounts of ^{129}I and ^{244}Pu during the collapsing period of the cloud as follows. A gas cloud can accrete appreciable amount of heavy elements as long as it presents a large surface area to the incoming flux of heavy elements. Thus, a good estimate of this accretion period would be the hydrodynamic collapsing period of the cloud given by

$$t_c = R^{3/2} / (2 G m)^{1/2}$$

where R is the radius, m is the mass of the cloud, and G is the gravitational constant. For a Cameron and Pine (1973) type of nebula, $R \approx 100$ AU and $m \approx 2 m_\odot$ so that $t_c \approx 80$ yr. It will be found that even a factor of a thousand error in this estimate will not affect our conclusions. A passage through the spiral arm takes $\sim 10^7$ yr, which gives about 2 percent increase in the yeavy element abundance of the cloud (Trivedi, 1977). Hence, the fractional increase in the r-process elements of the cloud during the collapsing period would be,

$$\Delta Z_r \approx (2/100) \times (80/10^7) = 1.6 \times 10^{-7}$$

Now let us consider the specific cases of ^{129}I and ^{244}Pu. ^{127}I in a supernova ejecta would be present from all the previous contributions whereas ^{129}I would be mostly freshly formed. Therefore, the $(^{129}I/^{127}I)$ in the ejecta would be given by,

$$(^{129}I/^{127}I)_{ejecta} < 1.5$$

where 1.5 is the production rate ratio (P_{129}/P_{127}) (Fowler, 1972). Hence the material collected during the last stage would increase the $(^{129}I/^{127}I)$ ratio of the cloud by,

$$\Delta (^{129}I/^{127}I) < 2.4 \times 10^{-7}$$

On the other hand, the $(^{129}I/^{127}I)$ ratio in the meteorites is $\sim 10^{-4}$, which is about three orders of magnitude larger than the value calculated above.

Similar calculations can be done for ^{244}Pu and the result is,

$$\Delta (^{244}Pu/^{238}U) < 1.4 \times 10^{-7}$$

which is about five orders of magnitude smaller than the average meteoritic value (0.013). We conclude that the last accreted ^{129}I and ^{244}Pu did not change significantly the abundance of these isotopes already present in the solar system. Hence both of these isotopes are good cosmochronometers.

We now present an astrophysical argument to support the above conclusion. Let us consider ^{244}Pu. This nuclide has a half-life of 82×10^6 yr. If all of this isotope was accreted during the collapsing stage only, then this would imply that the presolar cloud was isolated from the galactic activity for at least 10^9 yr (10 half-lives). This will be highly unreasonable because the mixing period in the galaxy is 100 - 200×10^6 yr, equal to the rotation period of the galaxy (Reeves, 1972).

We reemphasize the validity of ^{129}I and ^{244}Pu as good cosmochronometers. Isotopic anomalies in meteorites could have been induced by the small amount of matter collected during the collapsing stage of the cloud in the arm of the galaxy. This has been treated in detail in another paper (Trivedi, 1978).

Cameron, A. G. W., and Pine, M. R., 1973, Accumulation processes in the primitive solar nebula: Icarus, v. 18, p. 407.

Cameron, A. G. W., and Truran, J. W., 1977, The supernova trigger for formation of the solar system: Icarus, v. 30, no. 3, p. 447-461.

Clark, D. H., and Culhane, J. L., 1976: Monthly Notices of the Royal Astronomical Society, v. 175, p. 573.

Fowler, W. A., 1972, in Reines, F., ed., Cosmology, fusion, and other matters, Chapter 7: Boulder, University of Colorado press.

Lee, T., Papanastassiou, D. A., and Wasserburg, G. J., 1977: Astophysical Journal, v. 211, p. L107.

Maza, J., and van den Bergh, S., 1976: Astrophysical Journal, v. 204, p. 519.

Reeves, H., 1972: Astronomy and Astrophysics, v. 19, p. 215.

Roberts, W. W., 1969, Large-scale shock formation in spiral galaxies and its implications on star formation: Astrophysical Journal, v. 158, p. 213.

Tammann, G. A., 1974, in Cosmovici, C. B., ed., Supernovae and supernova remanants: D. Reidel Publishing Company, Holland, p. 155.

Trivedi, B. M. P., 1977: Astrophysical Journal, v. 215, p. 877.

_____1978, preprint (submitted to Astrophysical Journal).

SULFATE CHEMICAL AND ISOTOPIC PATTERNS IN THERMAL WATERS OF YELLOWSTONE PARK, WYOMING

By A. H. Truesdell[1], R. O. Rye[2]
J. F. Whelan[2], and J. M. Thompson[1]
[1]U. S. Geological Survey, Menlo Park California, [2]U. S. Geological Survey
Denver, Colorado 80225

Sulfate and chloride in thermal waters from Norris, Upper, and Lower Geyser Basins, Yellowstone have a distinctive pattern of scattered maximum sulfate contents but sharply defined minimum sulfate contents that do not extrapolate to zero sulfate at zero chloride (fig. 1). This pattern is interpreted to indicate subsurface mixing (dilution) of deep thermal water containing chloride, sulfate ("deep sulfate"), and H_2S with shallow, cold, aerated ground water containing essentially no chloride or sulfate. During this dilution, reaction of excess H_2S carried in the thermal water with the limited amount of atmospheric oxygen dissolved in the cold, diluting water produces about 13 mg of "dilution" sulfate per kg of diluting water. This subsurface mixing and reaction produces the well-defined minimum sulfate contents of Yellowstone thermal waters, but additional "surface" sulfate produced by surface oxidation of H_2S (with unlimited availability of oxygen) produces their variable maximum sulfate contents.

Previous studies (Truesdell and others, 1977; Fournier and others, 1976; Truesdell and Fournier, 1976) have shown that geothermometer temperatures and chloride and deuterium contents of most Yellowstone thermal waters can be explained by steam loss during adiabatic cooling of mixtures of a single deep thermal water (360°C and 310 ppm Cl) with shallow, cold, diluting waters local to each geyser basin. Undiluted deep thermal water reaches the surface (after boiling) only in a few high-chloride springs in Norris Geyser Basin; all other Park waters are more or less mixed.

The sulfate and chloride contents of the high-chloride Norris springs are about 24 and 675 ppm which result from concentration by steam loss during adiabatic cooling of the original 11 ppm SO_4 and 310 ppm Cl in the deep water (point DW in fig. 1). Cold ground waters local to the geyser basins infiltrate at about 2,500 m altitude and 5°C and carry in solution 9 ppm atmospheric O_2 which produces 13 mg SO_4 per liter of cold water when these waters mix in the subsurface with H_2S-bearing thermal waters. Calculated compositions before boiling of mixtures of deep thermal water with cold diluting waters and the calculated surface compositions of these waters after boiling and steam loss are shown in figure 1. Agreement with observed minimum sulfate contents is reasonable although a few low chloride (< 20 ppm), slightly thermal waters contain much less sulfate, possibly because H_2S was not in excess at these high dilutions.

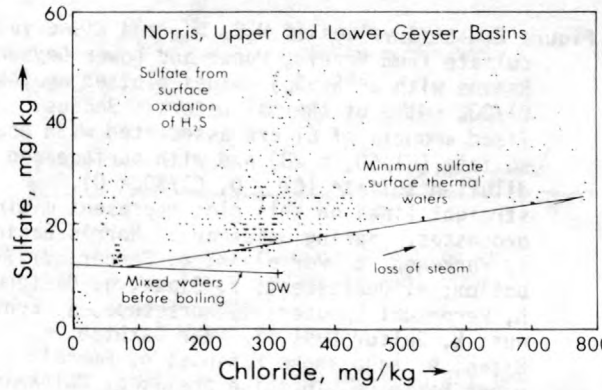

Figure 1.--Sulfate and chloride contents of analyzed thermal waters of Norris, Upper and Lower Geyser Basins, from Rowe and others, (1973); Thompson and others, (1975), and unpublished data. Lines show the surface minimum sulfate contents and the compositions of mixed subsurface thermal waters before boiling. Chloride composition (310 ppm) and temperature (360°C) of deep thermal end-member (DW) have been chosen to agree with earlier studies. Only one of the family of steam-loss lines is shown. Mixed waters with less than 80 ppm Cl have temperatures below 93°C after mixing and do not lose steam during ascent to surface.

This model of sulfate chemistry at Yellowstone is supported by isotope analyses. Oxygen in deep and dilution sulfates was found to equilibrate isotopically with water oxygen at high temperatures ($\delta^{18}O(SO_4)$ = -9 to -13 permil) while surface sulfate-oxygen isotope compositions are influenced by atmospheric oxygen ($\delta^{18}O(SO_4)$ > -5 permil; McKenzie and Truesdell, (1976).

Sulfur isotope compositions (fig. 2) distinguish deep sulfate from sulfate produced by oxidation of H_2S (surface and dilution sulfate). Sulfates from waters with high Cl/SO_4 ratios

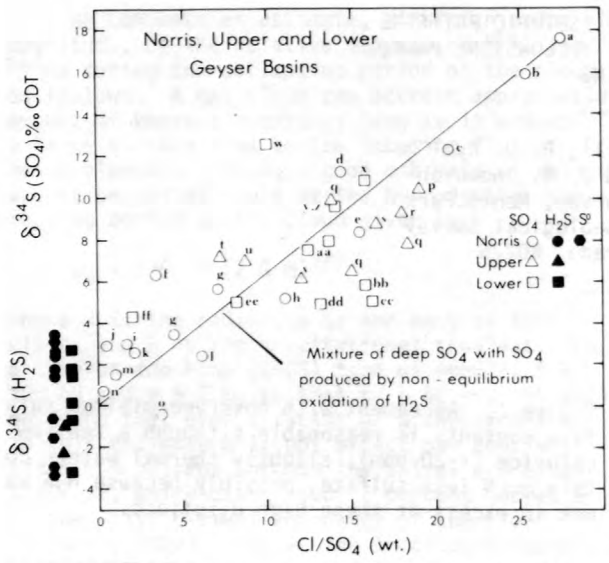

Figure 2.--$\delta^{34}S$ values of H_2S, S^o, and dissolved sulfate from Norris, Upper and Lower Geyser Basins with $\delta^{34}S(SO_4)$ values plotted against Cl/SO_4 ratio of thermal waters. Because fixed amounts of Cl are associated with deep sulfate (Cl/SO_4 = 28) and with surface and dilution sulfate (Cl = 0, Cl/SO_4= 0), straight lines on this plot represent mixing processes. Spring names are: Norris Basin: a, Porkchop; b, Porcelain; c, Fenner; d, Y12 bottom; e, Opalescent; f, Black; g, Cistern; h, Perpetual Spouter; i, Horseshoe; j, Echinus; k, Sulfur Dust; l, near Bathtub; m, Bijah; n, seep above Echinus; o, Emerald. Upper Basin: p, Tortoise Shell; q, Chinaman; r, Miriad; s, Ear; t, Hillside; u, Sapphire; v, Interchange. Lower Basin: w, Spray; x, Snort; y, near Y13; z, Steep Cone; aa, Ojo Caliente; bb, Midway; cc, Shelf; dd, Excelsior; ee, Perch; ff, Firehole Lake.

(largely deep sulfate) have high $\delta^{34}S$ values (as much as +18 permil), and sulfates from waters with low Cl/SO_4 ratios have low $\delta^{34}S$ values similar to those of Yellowstone H_2S. An isotope-mixing relation is apparent in figure 2 with deep thermal sulfate (Cl/SO_4 = 28, $\delta^{34}S$ = +18 permil) mixing with surface and dilution sulfate (Cl/SO_4 = 0, $\delta^{34}S$ = 0 permil). We interpret the sulfur isotope relations to indicate that the $\delta^{34}S$-value of H_2S in the deep thermal aquifer is near 0 permil and that deep sulfate has equilibrated with this H_2S at about 360°C with a fractionation of +18 permil (Rye and Ohimoto, unpublished data). All sulfate produced at lower temperatures by oxidation of H_2S (surface and dilution sulfate) appears to have formed out of isotopic equilibrium and has the same sulfur-isotope composition as the reacting H_2S. If diluting or surface sulfates had formed in equilibrium with H_2S of constant isotopic composition near 0 permil, the $\delta^{34}S$ values of these sulfates would be more positive than that of deep sulfate. Alternatively, if the supply of H_2S were limited and sulfate formed at equilibrium, then the $\delta^{34}S$-values of the remaining H_2S would become extremely negative. The analyses do not agree with either of these mechanisms.

The observed $\delta^{34}S$ values of H_2S and S^o (formed at the surface from H_2S without fractionation; Schoen and Rye, 1970) range from +4 to -4 permil. This range probably results from alteration of H_2S during ascent from the deep aquifer. The deep H_2S-sulfur isotope composition is probably near $\delta^{34}S$ = 0 permil but it is fractionated during boiling and steam loss with isotopically light H_2S separating into the vapor and issuing in the fumarolic areas of the eastern Park ($\delta^{34}S$ (H_2S) to -5.5 permil; Schoen and Rye, 1970) and residual, isotopically heavy H_2S issuing with the hot spring waters of the western Park (fig. 2). H_2S of Upper and Lower geyser basins may be lighter than that of Norris because the Norris waters contain less HCO_3 so that CO_2 loss during boiling produces less increase in pH and less near-surface deposition of isotopically heavy pyrite.

Fournier, R. O., White, D. E., and Truesdell, A. H., 1976, Convective heat flow in Yellowstone National Park: Proceedings of the 2nd United Nations Symposium on Geothermal Energy, San Francisco, 1975, p. 731-739.

McKenzie, W. F., and Truesdell, A. H., 1976, Geothermal reservoir temperatures estimated from the oxygen isotope compositions of dissolved sulfate and water from hot springs and shallow drillholes: Geothermics, v. 5, p. 51-61.

Rowe, J. J., Fournier, R. O., and Morey, G. W., 1973, Chemical analysis of thermal waters in Yellowstone National Park, Wyoming, 196065: U. S. Geological Survey Bulletin 1303, 31 p.

Schoen, R., and Rye, R. O., 1970, Sulfur isotope distribution in solfataras, Yellowstone National Park: Science, v. 170, p. 1082-1084.

Thompson, J. M., Presser, T. S., Barnes, R. B., and Bird, D. B., 1975, Chemical analysis of the waters of Yellowstone National Park, Wyoming from 1965 to 1973: U. S. Geological Survey Open-File Report 75-25, 59 p.

Truesdell, A. H., and Fournier, R. O., 1976, Conditions in the deeper parts of the hot spring systems of Yellowstone National Park, Wyoming: U. S. Geological Survey Open-File Report 76-428, 29 p.

Truesdell, A. H., Nathenson, Manuel, and Rye, R. O., 1977, The effects of subsurface boiling and dilution on the isotopic compositions of Yellowstone thermal waters: Journal of Geophysical Research, v. 82, p. 3694-3704.

SOME EXAMPLES OF DATING METAMORPHIC ROCKS BY THE Pb-U METHOD

By A. I. Tugarinov[1] and
E. V. Bibikova[2]
[1]Deceased
[2]Vernadsky Institute, Moscow, USSR

One of the most complicated problems in geochronology is the dating of metamorphic rocks. The interpretation of data obtained by the Pb-U method on accessory zircons from such rocks is not always obvious.

Most promising has been the construction of an internal isochron on a Concordia diagram for different zircon fractions from a single rock--the upper interception corresponding to the premetamorphic age of the rock, and lower interception corresponding to the time of metamorphic influence. The internal-isochron method proved to be satisfactory for solving age problems in Phanerozoic time, but attempted application of the method to Precambrian tertain with polymetamorphic history was not as successful. The false linearity on a Concordia plot for zircon fractions from Precambrian metamorphic rocks may be due to the proportional disturbance in the Pb-U isotopic system during repeated metamorphic episodes. As a consequence, the interceptions with Concordia need not correspond to any real events.

We will present here two examples of dating Precambrian metasedimentary and metaigneous rocks by the Pb-U method. The first example concerns the metasedimentary succession of the Ladoga region in the southeastern part of the Baltic Shield. The Ladoga Formation, developed in synclinal zones mantling granite gneiss domes, is represented by terrigenous flusch. The intensity of metamorphism increases from greenstone grade in the NNE through amphibolite to granulite grade in the SSW. The granite gneiss domes have also undergone post-Ladoga metamorphism.

Radiometric age determinations were carried out for zircons from granite gneisses, quartzites, and gneisses from different metamorphic zones of the Ladoga Formation. A mineralogical investigation shows that accessory zircons from the granite gneisses are present as a terrigenous constituent in rocks of the Ladoga Formation. Only the granulite zone is characterized by newly formed grains--the content of the terrigeneous constituents being no more than 10 percent. Our attempt to date the zircons using the internal-isochron method for size and magnetic fractions failed. We can see on figure 1 that discordia lines for two samples with the same metamorphic history gave quite different interceptions with the Concordia curve.

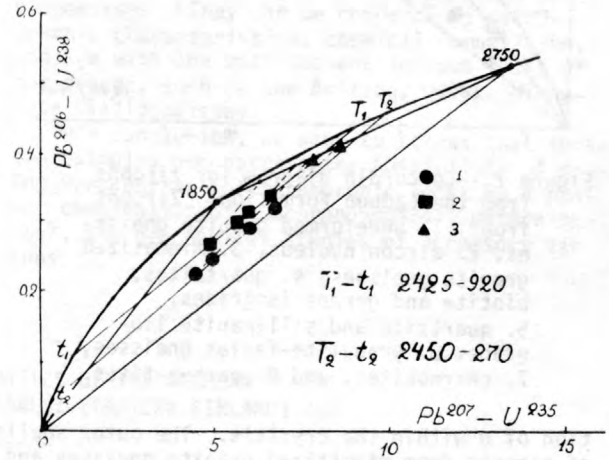

Figure 1.--Internal isochron for size and magnetic fractions of zircons from the Ladoga Formation.

On figure 2 all data obtained for the zircons from the Ladoga region are plotted. The zircon points from undeformed granite gneisses of the domes determine an isochron passing through 2750 m.y. and zero, thus dating the pre-Ladoga basement rocks. Another isochron also passing through zero cuts the Concordia curve at 1870 m.y. It is constructed of zircons from the granulite zone and dates the time of post-Ladoga metamorphism. All other data points for zircons from different metamorphic zones lie inside the triangle bordered by these two lines and point to a two-stage disturbance of the Pb-U isotopic system. A strict regularity in point position is observed--zircons from higher grade metamorphic zones lie closer to the 1870 m.y. isochron. Only one sample, representing a zircon nucleus, lies directly on the 2750-1870 m.y. line, indicating that its isotopic system was not disturbed in recent time.

The regular increase in U content in zircon from low-grade to high-grade metamorphic zones suggests the possibility of U enrichment during post-Ladoga metamorphism as a region for Pb-U isotopic disturbance. Proof of this process was confirmed by fission-track investigations. The zircons from the undeformed granite gneisses are characterized by a low and homogeneous distribu-

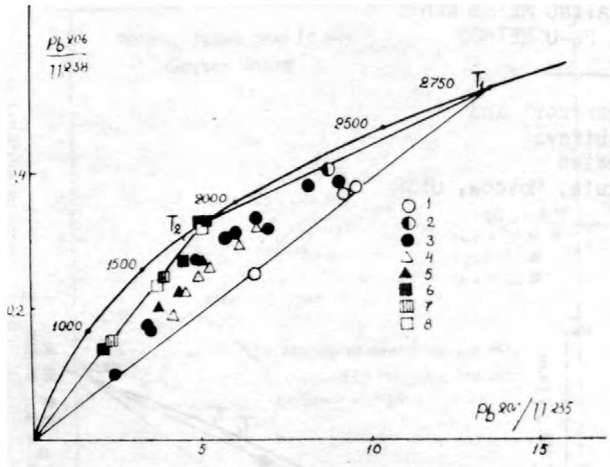

Figure 2.--Concordia diagram for zircons from the Ladoga Formation. Zircons from: 1. undeformed granite gneisses, 2. zircon nucleus, 3. migmatized granite gneisses, 4. quartzites, biotite and garnet isograde, 5. quartzite and sillimanite isograde, 6. granulite-facies gneisses, 7. charnokites, and 8. carbonatites.

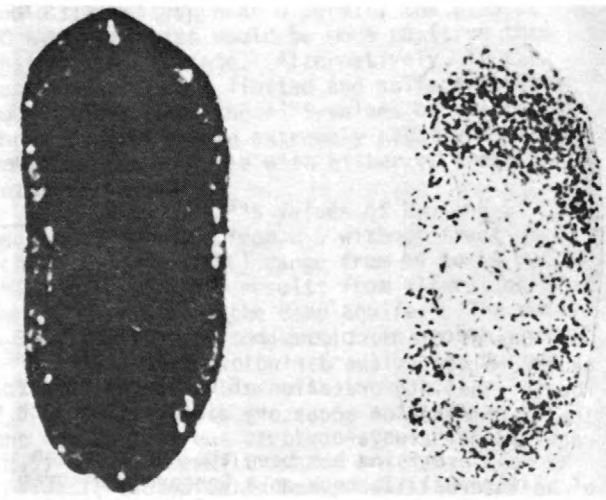

Figure 3.--Fission-track distribution in zircon from migmatized granite gneisses.

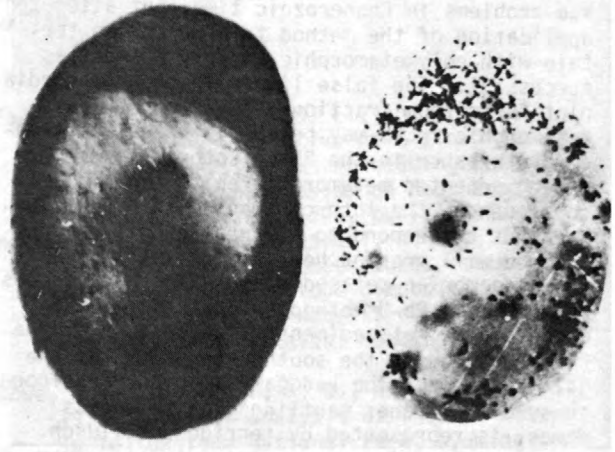

Figure 4.--Fission-track distribution in zircon from quartzites of the Ladoga Formation.

tion of U within the crystals. The outer shells of zircons from migmatized granite gneisses and the very surface of zircon grains from quartzites of the Ladoga Formation are enriched in U (figs. 3 and 4). These newly formed zones or phases enriched in U eventually represent the most vulnerable parts of zircons because they lose radiogenic lead more easily under the influence of surface agents. The correlation of these two processes--the addition of U and the ability to lose radiogenic lead--is obvious. The proportionality leads to an appearance of false linearity on the Concordia diagram, as was demonstrated earlier. The complex of investigations permit us to date two geological events--the age of the pre-Ladoga basement (2750 m.y. ago) and the time of post-Ladoga metamorphism (1870 m.y. ago).

The second example refers to the metamorphic rocks of the Omolon massif--the crystalline basement of a Mesozoic geosyncline in the northeasternmost USSR. The rock investigated was a leucocratic plagiogneiss with granulitic structure. The accessory zircon in this rock was not homogeneous. About 80 percent of the zircon population had a eudral, long, prismatic appearance, 10 percent consisted of extremely irregular, corroded grains and about 5 percent was isometric, "faceted", transparent crystals with brilliant luster.

Improvement in the chemical procedure permitted us to carry out Pb-U isotopic determinations on 5 to 15 mg samples for separate fractions and morphological types of zircons. Isotopic composition of lead was determined with high precision on a CAMECA mass spectrometer TSN-206. $^{207}Pb/^{206}Pb$ ages for all zircon fractions, excluding the isometric grains, proved to be about 3200 m.y. The isometric grains representing newly formed metamorphic crystals have $^{207}Pb/^{206}Pb$ ages of 2750 m.y. On a Concordia diagram (fig. 5) all size and magnetic fractions determine a discordia line $y = (0.01997 \pm 0.00422 \times +0.15213$, giving interceptions with the Concordia curve at 3400 and 1100 m.y. and demonstrating again false linearity.

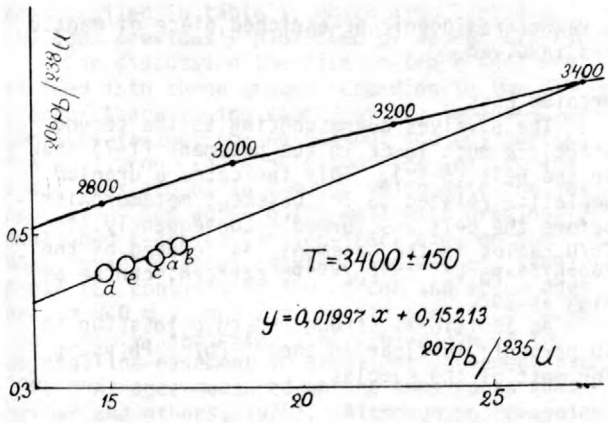

Figure 5.--Concordia diagram for zircon fractions from the Omolon plagiogneiss. Constants used: $\lambda_{238U} = 1.55125 \times 10^{-9}\ yr^{-1}$, $\lambda_{235U} = 9.8485 \times 10^{-9}\ yr^{-1}$, $^{238}U/^{235}U = 137.88$.

There were undoubtedly at least two isotopic disturbances in the Pb-U isotopic system of zircons during their existence--2750 m.y. ago when newly formed isometric grains appeared and later in Mesozoic time by reactivation of the old basement. The influence of the last event on the zircons was proved by infrared examination of the zircons. If we adopt a two-stage disturbance model for the Pb-U isotopic system of these zircons, the premetamorphic age of this mineral is more than 3400 m.y. The prevalence of euhedral, long, prismatic zircon grains points to a primary igneous origon of the plagiogneisses. They can be compared by petrographic characteristics, chemical composition, and age with the most ancient igneous rocks of our planet, such as the Amitsoq, Uivak, Minnesota plagiogneisses.

In conclusion, we want to stress that these two examples demonstrate the possibility of dating Precambrian polymetamorphic rocks by a proper combination of geochronological, mineralogical, and geochemical studies of accessory zircons.

Pb-Pb AND Rb-Sr SYSTEMATICS OF THE ARCHEAN GREENSTONE BELT OF SUOMUSSALMI (EASTERN FINLAND)·

By Philippe Vidal[1] and George R. Tilton
Department of Geological Sciences, University of California, Santa Barbara, California 93106
[1]Permanent address: Centre Armoricain d'Etude Structurale des Socles, Institut de Geologie, BP 25A, 35031, Rennes, Cedex, France

The Archean greenstone belt of Suomussalmi is a typical example of a greenstone belt development in Finland. It consists of a lower volcanic cycle of komatiitic and tholeiitic composition, a middle unit of sediments, and an upper volcanic cycle that is mainly andesitic in composition. This series has been folded and then intruded by granodioritic plutons and, after a new phase of folding, by tonalitic and leucogranodioritic plutons. The metamorphism corresponds to the upper greenschist facies or lower garnet amphibolite facies; it started with phase 1 and reached a maximum during phase 2.

The surrounding basement is composed mainly of migmatitic gneisses which have undergone a complex tectonometamorphic history.

In order to understand the relationships between the basement and the belt, we applied the Pb-Pb (whole-rock, K-feldspar) and Rb-Sr (whole-rock, biotite) methods on both basement and belt. The main results are as follows.

Age Relationships:

1. Whole-Rock. A Pb-Pb secondary isochron including 6 basement samples and 6 belt samples give an age of 2.6 ± 0.03 b.y. ($\lambda_{238} = 0.1551 \times 10^{-9}yr^{-1}$, $\lambda_{235} = 0.9849 \times 10^{-9}yr^{-1}$). A whole-rock Rb-Sr isochron on the basement, with an age of 2.61 ± 0.06 b.y. ($\lambda^{87}Rb = 1.42 \times 10^{-11}yr^{-1}$) fits well with the Pb-Pb age.

   These results suggest that the large number of geologic events observed within the basement and until the last magmatic episodes of the belt, occurred in a very restricted time span (∿ 50 m.y.). It implies geodynamic mechanisms in Archean time which must have been very fast.

   Rb-Sr data on the belt (volcanites) and plutonites) are very scattered and give model ages between 2 and 3 b.y. This pattern is attributed to whole-rock opening during a subsequent metamorphism, as indicated by mineral ages.

2. Minerals. Biotite Rb-Sr ages in the belt range between 1.6 and 1.8 b.y. They are related to the thermal influences of the Svecokarelian orogeny.

   Pb-Pb systematics for K-feldspars also display a strong disturbance, proba-

bly connected with the same subsequent thermal episode.

Origin:

The lead secondary isochrons pass through a Suomussalmi greenstone belt galena, which was previously analyzed by Kouvo (α = 13.60, β = 14.80). The model age of this galena is close to that of the secondary isochron (2.61 b.y.). The μ corresponding to the first stage is 8.1. These data strongly support the hypothesis that all the basement and the belt rocks are derived from the mantle and that the involvement of some hypothetical older rocks was negligible or nonexistent. This interpretation disagrees with the rather high initial $^{87}Sr/^{86}Sr$ ratio of the basement (0.7033), however, unless a rather radiogenic Sr-enriched piece of mantle was involved.

Uranium Loss:

The μ valves corresponding to the second stage are much lower in the basement (1→7) than in the belt (6→18). This indicates a uranium depletion related to the basement metamorphism before the belt was formed. Consequently, the Th/U ratios in the basement, as deduced by the $^{208}Pb/^{204}Pb$ vs. $^{206}Pb/^{204}Pb$ pattern, can be as high as 20.

An additional strong modern U loss (up to 60 percent) is clear in the $^{206}Pb/^{204}Pb$ vs. μ for most of the samples.

COOLING HISTORY OF ROCKS IN THE RIES CRATER REVEALED IN FISSION-TRACK ANALYSIS

By Günther A. Wagner and Donald S. Miller[1]
Max-Planck-Institut für Kernphysik
Heidelberg, West Germany
[1]On leave from Rensselaer Polytechnic Institute
Troy, New York

Detailed information on the thermal history of rocks can be obtained by fission-track analysis. The Nördlinger Ries crater structure (southern Germany) can be effectively used to demonstrate this type of application of fission-track dating. About 15 m.y. ago, the Paleozoic crystalline basement and the overlying Mesozoic sediments were intensely disturbed by a giant meteorite impact, forming the Ries crater. The high temperatures (and pressures) during and after the impact caused fission-track fading in the minerals, in addition to many other effects. From the various degrees of track fading in different minerals, the thermal history and the age of the rocks can be inferred.

Most of the samples analyzed were derived from a research drill core (FBN 73) in the crater basin. In the uppermost 314 m, the drill core penetrates sedimentary crater filling of post-impact age (fig. 1). Underneath are highly shocked suevite breccias with crystalline inclusions. At a depth of 602 m, crystalline rocks are reached that probably represent the crater floor (Chao, 1977). Samples for fission-track analysis were taken from the suevite (377 m), from crystalline inclusions (401.5, 503, 553, 571, 585, and 600.5 m) and from the crystalline rocks at and below the crater floor (603, 637 and 1201 m). Additional samples, collected from the surface, include crystalline breccias (Langenmühle, Leopold-Meyers-Keller) and granitic inclusions from the suevite ejecta blanket (Otting).

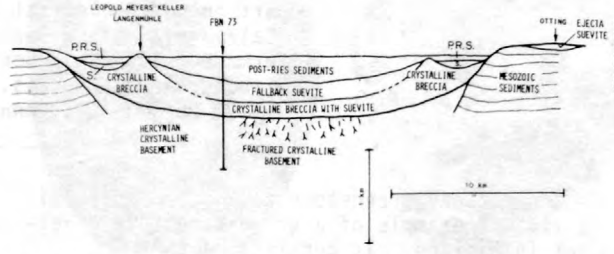

Figure 1.--Schematic cross-section through Ries Crater.

Apatites, sphenes, and zircons were separated from the crushed rocks by using common laboratory techniques. Aliquots of the apatite, sphene, and zircon (603 m) concentrates were annealed to produce complete erasing of fossil tracks and irradiated with thermal neutrons. The experimental procedures of annealing, neutron-dose determination, and etching were the same as those described by Miller and others, (this conference). The polished zircons (553 m), etched for 70 hours in a eutectic mixture of NaOH and KOH at 217° C (Gleadow and others, 1976), were irradiated together with external muscovite detectors (etched for 10 minutes in 48 percent HF at 23°C). The induced-track densities in muscovite were doubled. The fission-track ages were calculated using the decay constant of 8.46 x $10^{-17}y^{-1}$ (Galliker and others, 1970; Wagner and others, 1975). The age results

are compiled in table 1, which also includes the ages previously published by Wagner (1977).

For discussion the fission-track ages are divided into three groups according to the degree of track fading caused by the impact: (a) complete fading; (b) no fading; and (c) partial fading. Group (a) consists of the apatite and spene ages around 14.7 m.y., which date the impact event and agree quite well with previously published K-Ar and fission-track ages on the Ries impact glasses (Gentner and Wagner, 1969). Group (b) consists of the zircon and spene ages around 310 m.y. and the apatite age of 151 m.y. The 310 m.y. indicates a Hercynian age of the crystalline basement in excellent agreement with ^{39}Ar-^{40}Ar ages measured on the same rocks (Jessberger and others, 1978). Although no Hercynian ages were found for apatite, it is believed that the 151 m.y. age is representative for the apatite fission-track age of the crystalline basement that was undisturbed by the Ries impact. This conclusion is based on data from other parts of Hercynian orogenic rocks where apatite fission-track ages were on the order of 100 m.y. (Wagner, 1968). These low ages are believed to be caused by Mesozoic subsidence. Group (c) consists of mixed ages due to partial track fading caused by the impact. The various degrees of track fading in group (c) are calculated by comparing the measured ages with those of group (b) (table 1).

There are two possible causes for the fission-track fading connected with the impact: the shock-wave itself (extremely brief, but with high-peak pressures and temperatures) and the residual temperatures which the rocks retain after the shock wave has passed. Because no simple correlation between the shock-wave intensity and the degree of track fading was observed for the Ries rocks, it is assumed that most of the heating is due to the residual heat that became uniformly distributed throughout each rock unit. Thus, the cooling history can be inferred from the track-fading data.

To determine the initial equilibrium temperature (T_{EQ}), a cooling model must be assumed. A conductive-cooling model is realistic but complex. Therefore, a step-function model is discussed that gives upper and lower limits of the initial equilibrium temperature (fig. 2). In a conductive-cooling model the actual temperature follows the exponential curve from T_{EQ} to the temperature of full-track retention (T_{FTR}). In a step-function cooling model T_{LL} is the temperature required to produce an observed amount of track fading over the time t_{FTR}. This temperature is a lower limit of T_{EQ} because the continually decreasing conductive-cooling temperature has to produce the same amount of fading as T_{LL} during the time t_{FTR}. In the second model of step-function cooling the time used is the time required to obtain temperature equilibration within a rock unit, t_{EQ}. The temperature required to produce the observed amount of track fading over the time t_{EQ} is T_{UL}. This temperature, T_{UL}, is an upper limit for T_{EQ} because the

Table 1.--Fission-track ages of minerals from the Ries crater

Depth (m)	Rock	Mineral	Age (m.y.)	Percent of track fading
	Research Drill Core Nördlingen (FBN 73)			
377	Suevite	Apatite	14.8	100
		Sphene	100	70
401.5	Amphibolite inclusion in Suevite	Apatite	14.8	100
503	Gneiss inclusion in Suevite	Apatite	14.2	100
553	Amphibolite block	Zircon	52	87
571	Amphibolite injected with Suevite	Apatite	15.1	100
585	Amphibolite block	Apatite	73	57
600.5	Gneiss inclusion in Suevite	Apatite	76	56
603	Amphibolite	Apatite	60	67
		Zircon	310	0
637	Amphibolite	Apatite	65	63
		Sphene	300	0
1201	Gneiss	Apatite	129	16
	Otting crystalline inclusion in Suevite			
0	Granitic inclusion from Suevite ejecta blanket	Apatite	14.7	100
		Sphene	14.8	100
	Leopold-Meyers-Keller (Nördlingen) hornblende-gneiss			
0	Breccia	Apatite	31	88
	Langenmühle Granite			
0	Breccia	Apatite	151	0

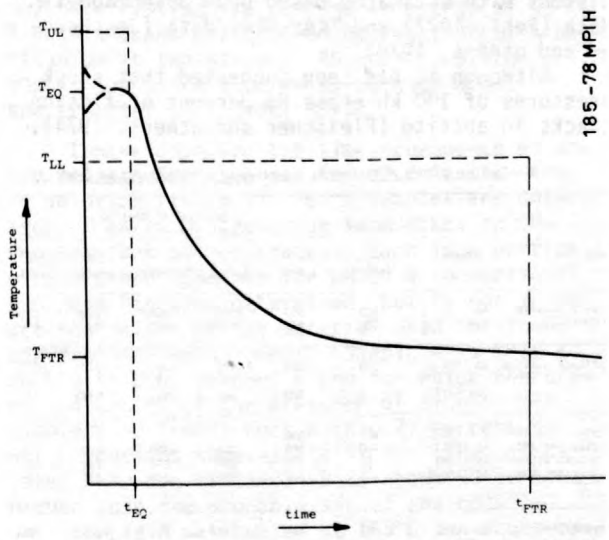

Figure 2.--Temperature-time models for fission-track fading.

track fading due to the conductive cooling is not included.

Table 2 represents the analytical data along with temperature data obtained by using a step-function cooling model in combination with experimental annealing data for apatite (Wagner and Reimer, 1972), sphene (Naeser and Faul, 1969) and zircon (Nishida and Takashima, 1975). Estimated duration of cooling for the rock units in the Ries crater range up to a few thousand years (Pohl, 1977). The times chosen for illustrating the effects are one hour, three days, one year, 100 years and 1000 years.

Ages of group (a), completely reset (100 percent annealed), give minimum temperatures for the rock units. Ages of group (b), not reset (0 percent annealed), give maximum temperatures. Ages of group (c) give the approximate temperature.

The upper portion of the fallback suevites was at a high temperature. T_{LL}, the lower limit of T_{EQ}, is 445°C assuming 1000 years for t_{FTR}. The upper limit of T_{EQ}, T_{UL}, is 560°C assuming three days for T_{EQ}. Both these temperatures are based on the sphene data (377). This is compatible with the apatite information (401.5, 503). Crystalline blocks occurring in the lower portion of the fallback suevite were at a lower temperature of about 200 to ∿ 300°C, based upon the apatite data. The crater floor experienced similar temperatures of around 200 to 250°C. In these two cases, a t_{EQ} of one year is used for the large crystalline inclusions, rather than three days as used for the fine-grained suevite. The ejecta suevite unit was subjected to the highest temperatures. Due to the faster cooling of the ejecta blanket (Pohl, 1977), 10 years is used for t_{FTR} to determine the lower temperature limit T_{LL} of 520°C. Because of the complete track annealing, no upper limit can be estimated. These temperature estimates are consistent with estimates based upon paleomagnetic data (Pohl, 1977) and ^{40}Ar-^{39}Ar data (Jessberger and others, 1978).

Although it has been suggested that shock pressures of 100 kb erase 96 percent of fission tracks in apatite (Fleischer and others, 1974), sample 600.5 still retains 50 percent of its tracks, although it was subjected to shock pressures in excess of 100 kb (Horn, personal commun.).

It should be noted that, in addition to being able to decipher much of the complicated thermal history of the Ries crater, it has been possible to date the impact event at 14.7 m.y. and to establish a Hercynian 310 m.y. age for the basement rocks.

Table 2.--Cooling history of Ries rocks according to the step-function model

Rock	Mineral	Percent of track fading	Duration of heating				
			1 hour	3 days	1 year	100 years	1000 years
Ejecta suevite (Otting)	Ap	100	>360	>320	>285	>250	>235
	Sph	100	>640	>585	>540	>500	>475
Fallback suevite (FBN 73)	Ap (401.5, 503)	100	>360	>320	>285	>250	>235
	Sph (377)	70	620	560	510	470	445
Crystalline inclusions and blocks within suevite (FBN 73)	Zir (553)	87	800				
	Ap (571)	100	>360	>320	>285	>250	>235
	Ap (585)	57	335	280	245	210	195
	Ap (600.5)	56	335	280	245	210	195
Crystalline rocks of crater floor (FBN 73)	Ap (603, 637)	65	340	290	255	215	200
	Sph (637)	0	<560	<470	<400	<340	<310
	Zir (603)	0	<550				

Chao, E. C. T., 1977, The Ries crater of southern Germany, a model for large basins on planetary surfaces: Geologisches Jahrbuch A , v. 43, p. 3-81.

Fleischer, R. L., Woods, R. T., Hart, H. R., Jr., Price, P. B., and Short, N. M., 1974, Effect of shocks on fission-track dating of apatite and sphene from the Hardhat and Sedan underground nuclear explosions: Journal of Geophysical Research, v. 79, p. 339-442.

Galliker, D., Hugentobler, E., and Hahn, B., 1970, Spontane Kernspaltung von 238-U and 241-Am: Helvetica Physica Acta, v. 43, p. 593-606.

Gentner, W., and Wagner, G. A., 1969, Altersbetimmung an Riesgläsern und Moldaviten: Geologica Bavarica, v. 61, p. 296-303.

Gleadow, A. J. W., Hurford, A. J., and Quaife, R. D., 1976, Fission-track dating of zircon-improved etching techniques: Earth and Planetary Science Letters, v. 33, p. 273-276.

Jessberger, E. K., Staudacher, Th., Dominik, B., Kirsten, T., and Schaeffer, O. A., 1978, Limited response of the K-Ar system to the Nörlinger Ries giant meteorite impact: Nature, v. 271, p. 338-339.

Naeser, C. W., and Faul, H., 1969, Fission-track annealing in apatite and spene: Journal of Geophysical Research, v. 74, p. 705-710.

Nishida, T., and Takashima, Y., 1975, Annealing of fission tracks in zircons: Earth Planetary Science Letters, v. 27, p. 257-264.

Pohl, J., 1977, Paläomagnetische und gesteinsmagnetische Untersuchungen an den Kernen der Forschungsbohrung Nördlingen 1973: Geologica Bavarica, v. 75, p. 329-348.

Wagner, G. A., 1968, Fission-track dating of apatites: Earth and Planetary Science Letters, v. 4, p. 411-415.

———1977, Spaltspurendatierung an Apatit und Titanit aus dem Ries-Ein Beitrag zum Alter und zur Wärmegeschichte: Geologica Bavarica, v. 75, p. 349-354.

Wagner, G. A., and Reimer, G. M., 1972, Fission-track tectonics--the tectonic interpretation of fission-track apatite ages: Earth Planetary Science Letters, v. 14, p. 263-268.

Wagner, G. A., Reimer, G. M., Carpenter, B. S., Faul, H., Van der Linden, R., and Gijbels, R., 1975, The spontaneous fission rate of U-238 and fission-track dating: Geochimica Cosmochimica Acta, v. 39, p. 1279-1286.

A COMPARISON OF CHEMICAL AND THERMAL METHODS FOR INCREMENTAL RELEASE OF ARGON

By J. M. Wampler
School of Geophysical Sciences
Georgia Institute of Technology,
Atlanta, Georgia

I have described a procedure for purification and mass spectrometric analysis of argon released by chemical reaction in aqueous solution (Wampler, 1977). With this procedure, the argon that accumulates within a reaction vessel during an interval of time may conveniently be analyzed at the end of the interval. Among a number of potential applications of this procedure in potassium-argon studies is the use of chemical release of argon in $^{40}Ar/^{39}Ar$ work to obtain information about the distribution of potassium and radiogenic argon within heterogeneous materials. Incremental release of argon by stepwise heating has been established as an excellent procedure for identifying samples which have undisturbed potassium-argon relationships (Dalrymple and Lanphere, 1974), but the interpretation of incremental release spectra for samples which have internal variations in the ratio of radiogenic argon to potassium is a subject which still needs considerable development (Lanphere and Dalrymple, 1977). I expect that chemical release of argon from irradiated samples will play an important role in the interpretation of discordant $^{40}Ar/^{39}Ar$-age spectra, because the type of information obtainable by chemical release is generally different from that obtained by thermal release.

The most obvious way in which a chemical release technique may yield $^{40}Ar/^{39}Ar$-information which differs from that obtainable by stepwise heating is by complete destruction of one (or more) constituent(s) with little effect on other constituents. Because the reaction may be carried out at a temperature sufficiently low that there is no diffusive loss from, nor diffusive mixing within, the remaining constituents, chemical release should provide a degree of resolution of the relationship between argon isotope ratios and mineral type which is not generally obtainable from age spectra obtained by thermal release of argon.

A second way in which I expect the chemical release procedure to be important in $^{40}Ar/^{39}Ar$-work is that is provides a possible way to remove all atmospheric contamination (as opposed to initial atmospheric argon) at a temperature low enough so that there can be no diffusive mixing. Elimination of contamination is essential to argon isochron studies (Hayatsu and Carmichael, 1977), and should be possible if all surfaces that have been exposed to air can be etched by an aqueous solution.

As our understanding of the mechanism of thermal release of argon grows, there are many ways in which the chemical-release procedure can supplement thermal-release studies. For example, chemical destruction of a more refractory component before thermal release begins would allow one to follow the high-temperature release from a less refractory constituent without interference. No information would be lost in preparation for the thermal study, if the argon released by the chemical reaction is measured.

I will now describe some preliminary experiments that I have carried out to examine the argon released by partial destruction of mafic igneous rock in acid solution. The procedure begins with preparation of an argon-free solution of a suitable acid of low volatility, into which a sample may be dropped to begin the chemical reaction. Temperature of the solution is controlled in the range 0 - 100°C by fixing the vapor pressure of water in the reactor via a reflux condenser. The argon released by the chemical reaction is allowed to accumulate in the reactor for an interval of time, then released via a capillary tube into a purification system. Water vapor is removed in a cold trap at 161 K. Carbon dioxide and certain other volatiles that may have evolved are removed in a trap at 90 K. Reactive gases are removed by reaction with hot titanium in two stages. Abundances of the argon isotopes are then measured with a mass spectrometer (AEI Model MS-10).

I have observed the time-dependence of argon release from two samples of dolerite in acid solution (table 1). Both samples are dolerites of early Mesozoic age from dikes in the southeastern United States. Each is a portion of a crushed specimen for which a conventional K-Ar age has been determined, but is not an exact equivalent of the material used for the conventional measurement. Sample A is from a rock with 0.65 percent K and for which there is no indication of the presence of excess ^{40}Ar. Sample B is from a rock with 0.21 percent K which contains some excess ^{40}Ar. (The calculated K-Ar age of sample B is about 50 percent higher than the probable age of the rock.)

Sample A was heated at 155°C in vacuum before being dropped into a 5N H_2SO_4 solution. Table 1 gives the temperature and duration of

Table 1.--Rates of release of radiogenic argon from dolerite samples by reaction in aqueous acid solution

[Data for successive increments of argon released from each sample are given in order downward from line on which sample is indicated]

Temperature (°C)	Elapsed time (hours)	Radiogenic Argon[1] (percent)	Radiogenic Argon[1] (pl/g)	Average release rate (pl/g-hr)
		Sample A[2]		
0	1	43	82	82
15	1.7	56	29	17
25	17	47	244	14
25	5	42	28	5.6
25	24	38	84	3.5
25	46	39	80	1.7
25	30	45	31	1.0
25	20	50	20	1.0
25	20	47	14	0.7
		Sample B[3]		
0	1	26	36	36
25	1	21	22	22
25	18	22	79	4.4
25	1	30	19	19
55	1	29	51	51
25	20	13	11	0.5
100	1	29	109	109
100	2	29	74	37
25	114	19	10	0.1
100	3	34	53	18

[1]Percentage of radiogenic argon is based on conventional model which considers all non-radiogenic argon to be equivalent to modern atmospheric argon. Amounts are in picoliters (standard temperature and pressure) per gram of sample.

[2]2.25 g of dolerite containing about 0.6 percent K and no excess argon.

[3]0.49 g of a dolerite (irradiated) containing about 0.2 percent K and having some excess argon.

each interval of argon accumulation. Mechanical stirring was used only at the end of each interval to aid the escape of argon from the liquid. The total of the radiogenic argon released during the experiment is about 15 percent of that originally in the sample. Sample B was preheated at only 50°C (for four days) before being dropped into a 0.2N $HClO_4$ solution (which also contained Na, Ca, and Al perchlorates, each 0.2N). Mechanical stirring was used throughout the shorter reaction intervals but not during the overnight or longer periods. It may be seen that stirring has a considerable influence on the argon release-rate. The total of the apparent radiogenic argon released during this experiment is neary 20 percent of that originally in the sample.

At a fixed temperature the release of argon is rapid at first, and then decreases. The change in release rate as a function of time is not that of a first-order reaction, but rather the fractional change in release rate (per unit time) becomes smaller as time advances. Modest increases in temperature produce the large increases in argon release-rate that one would expect for a chemical reaction whose rate is controlled by a specification activation energy (as opposed to mere increased mobility of the reactants).

Examination of the residual solids after these reactions showed that the ferromagnesian constituents were preferentially dissolved by the acid, but that plagioclase was also affected. Some of the crystals remaining have smoothly rounded surfaces characteristic of a simple but incomplete process of solution. Other fragments have highly complex surfaces indicative of preferential solution (etching) of portions of the material. In these preliminary experiments there was a wide range of partical size (about 0.05 - 1 mm) in the original sample, a possible complication due to mechanical attrition during stirring, and no attempt to examine the solid residue at different stages of the dissolution process. Thus, it would be premature to say much more than that the acid reaction affected the ferromagnesian constituents much more than the plagioclase. But, it is tempting to speculate that those fragments that were etched to a complicated form by the acid represent portions of the original rock that were mechanically or chemically disturbed during the late stages of crystallization and cooling of the rock. Such disturbed portions (such as microfractures, microtubes, deuterically altered crystals) are likely to have incorporated argon if a significant argon pressure existed in the cooling environment, and may be sites of high concentration of initial argon within a dolerite.

Sample B was used in an attempt to determine the character of the $^{40}Ar/^{39}Ar$ ratio in argon released chemically from a dolerite containing excess ^{40}Ar. The sample had been irradiated in the Georgia Institute of Technology research reactor long enough to produce a small, but measurable, amount of ^{39}Ar. The data on ^{39}Ar released during the chemical treatment of sample B are not of accuracy adequate for publication, but the $^{40}Ar/^{39}Ar$ ratio appeared to be rather constant and 2 - 3 times greater than the $^{40}Ar/^{39}Ar$ ratio of an undisturbed dolerite of similar age which had been irradiated with sample B. The preliminary results suggest, then, that a large percentage of the excess ^{40}Ar of the sample was released by the acid reaction.

Experiments in progess should show definitely how much of the excess ^{40}Ar may typically be removed from a dolerite by reaction in acid solution. Argon will be released from the residual solids by stepwise heating so that the effect of the chemical reaction on the entire

age spectrum can be determined. I expect that the combination of information from chemically released argon and thermally released argon will contribute much to our understanding of the problem of excess argon in dolerites. I further expect that, by development of reactions which are considerably more sophisticated than simple treatment by strong acid, the chemical release technique will become of importance in $^{40}Ar/^{39}Ar$-studies involving disturbed samples of many types.

Dalrymple, G. P., and Lanphere, M. A., 1974, $^{40}Ar/^{39}Ar$ age spectra of some undisturbed terrestrial samples: Geochimica Cosmochimica Acta, v. 39, p. 715-738.

Hayatsu, A., and Carmichael, C. M., 1977, Removal of atmospheric argon contamination and the use and misuse of the K-Ar isochron method: Canadian Journal of Earth Sciences, v. 12, p. 337-345.

Lanphere, M. A., and Dalrymple, G. P., 1977, Identification of excess ^{40}Ar by the $^{40}Ar/^{39}Ar$ age spectrum technique: Earth and Planetary Science Letters, v. 32, p. 141-148.

Wampler, J. M., 1977, Release of argon by chemical reaction: An alternative method for incremental release of argon for isotopic analysis (abs.): EOS, Transactions of the American Geophysical Union, v. 58, p. 537.

AMINO-ACID RACEMIZATION DATING OF QUATERNARY MOLLUSKS, PACIFIC COAST UNITED STATES

J. F. Wehmiller[1], K. R. Lajoie[2], A. M. Sarna-Wojcicki[2], R. F. Yerkes[2], G. L. Kennedy[3], T. A. Stephens[4], and R. F. Kohl[5]
[1]University of Delaware
Newark, Delaware 19711, USA
[2]U.S. Geological Survey
Menlo Park, California 94025, USA
[3]Los Angeles County Museum of Natural History
Los Angeles, California 90007, USA
[4]U. S. Geological Survey
Eureka, California 95501, USA
[5]Humboldt State University
Arcata, California 95521, USA

Enantiomeric ratios (D/L) of amino acids in fossil mollusks yield relative and absolute age estimates of Quaternary marine terraces and stratigraphic sequences along the Pacific Coast of the United States (Wehmiller and others, 1977). Virtually all biological processes produce only L enantiomers that, upon death of an organism, convert to D enantiomers by a spontaneous and reversible process called racemization. In living organisms D/L = 0 and in fossil organisms at racemic equilibrium D/L = 1. Amino acids in fossil mollusks buried at shallow depths along the Pacific Coast reach racemic equilibrium in one to three million years. At present, there is no theoretical model describing the racemization process in mollusks and the physical and chemical factors controlling rates of racemization are poorly understood. Field and laboratory data indicate that crystalline matrix, temperature, and chemical environment are dominant controlling factors. It is virtually impossible to evaluate these factors independently. Interpretation of amino-acid enantiomeric ratios for geochronological purposes involves three complex elements: (1) an understanding of the systematic generic effects on rates of racemization (King and Neville, 1977; Wehmiller and others, 1977); (2) an empirically derived and calibrated kinetic model (Wehmiller and others, 1977; Wehmiller and Belknap, 1978); and (3) a means of estimating effective burial temperatures.

Well-preserved pelecypods with thick aragonitic shells yield the most reproducible (± 3 percent for leucine) and geologically meaningful results. Analyses of coexisting pelecypod genera from several Pacific Coast localities indicate racemization rates increase systematically from Protothaca to Saxidomus to Macoma. The kinetic model for racemization in mollusks is based on leucine data from Protothaca (fig. 1) (Wehmiller and others, 1977). Where Protothaca does not occur, Saxidomus and Macoma leucine values are converted to equivalent Protothaca values. The conversion factors are derived by regression analysis of data from 16 sample pairs each of coexisting Saxidomus - Protothaca and Macoma - Protothaca.

S D/L leucine = 0.983 (P D/L leucine) + 0.048; r = 0.992

M D/L leucine = 1.103 (P D/L leucine) + 0.076; r = 0.967

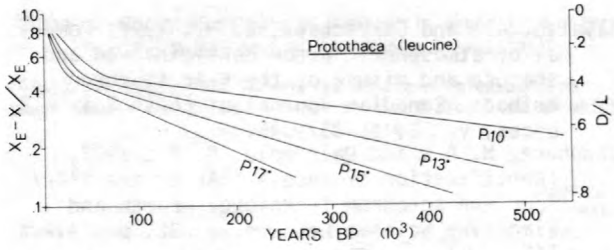

Figure 1.--Kinetic model for racemization of leucine in Protothaca, derived from deep-sea foraminifera data at 3° ± 1°C Wehmiller and Hare, 1971) and extrapolated to effective diagenetic ground temperature in the 10° - 17°C range (Wehmiller and others, 1977; Wehmiller and Belknap, 1978). The Protothaca-leucine model is calibrated by data from two California localities with U-series ages on corals: Point Loma, 121,000 ± 7,000 years and Cayucos, 124,000 ± 27,000 years (Ku and Kern, 1974); and two Washington localities with ^{14}C ages on mollusks: Orcas Island, 12,350 ± 400 years (Easterbrook, 1969) and Bainbridge Island, 3,260 ± 80 years (Gower, 1977, written commun.). Shown are D/L ratios and equivalent $(X_E - X)/X_E$ versus time. X = leucine $D/(D + L)$ at any time and $X_E = D/(D + L)$ at equilibrium. For leucine $X_E = 0.50$.

High-temperature kinetic experiments yield activation energies of racemization (Mitterer, 1975; Schroeder and Bada, 1976). However, direct extrapolation of laboratory-derived kinetic data to ambient conditions yields ambiguous estimates of age and effective burial temperatures for late Quaternary mollusks (Wehmiller and Belknap, 1978). Amino-acid data on mollusks from independently dated localities along the Pacific Coast best fit a non-linear kinetic model derived empirically from data on deep-sea foraminifera at 3° ± 1°C (Wehmiller and Hare, 1971) and extrapolated to ambient temperatures in the 10° - 20°C range (Wehmiller and others, 1977; Wehmiller and Belknap, 1978). The Protothaca-leucine kinetic model (fig. 1) is calibrated using data from two localities in California dated by U-series ages on corals and from two localities in Washington dated by ^{14}C (fig. 2). Data from the two California localities yield estimates of effective diagenetic temperatures 2° - 3°C cooler than modern effective ground temperatures (Wehmiller and others, 1977). Effective diagenetic temperatures for other localities are estimated by extrapolation of these temperatures using the temperature-latitude gradient of present-day mean annual air temperatures. Imprecise determination of effective diagenetic temperature is the main source of uncertainty in amino-acid age estimates of mollusks and probably will remain the limiting factor in application of the technique.

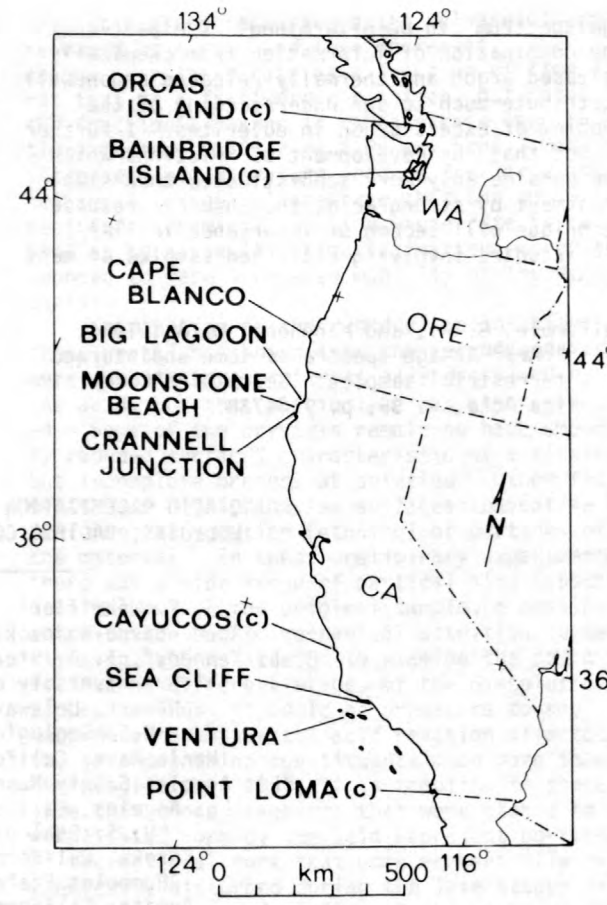

Figure 2.--Sample localities along the Pacific Coast of the United States. (C), calibration locality.

To illustrate the range and accuracy of the technique, we present amino-acid age estimates of mollusks from several Pacific Coast localities with some independent age control (table 1, fig. 2). Considering the limitations of the technique and the uncertainties of independent age control for most of these localities, the agreements are quite good over a range from a few thousand years to about one million years. Resolution of the technique decreases markedly past about 400 thousand years; therefore, relative ages among the four old samples from northern California and southern Oregon probably are more significant than the absolute age estimates.

Results from marine terrace deposits and a thick stratigraphic sequence on the south limb of the Ventura Avenue anticline near Ventura, California (fig. 3) are particularly important for evaluating the kinetic model. Samples from the four horizons in the San Pedro Formation yield age estimates (200 - 400 thousand years) that are stratigraphically consistent and are reasonable within constraints imposed by the

Table 1.--Amino-acid kinetic model age estimates and independent age data for comparison

[LACM, Los Angeles County Museum of Natural History, California; HSU, Humboldt State University, Arcata, California; M, U. S. Geological Survey, Menlo Park, California; (M), Macoma; (S), Saxidomus; (P), Protothaca, (N) or (R), Normal or Reversed paleomagnetic orientation. Fossil localities not directly analyzed but stratigraphically or geologically related to analyzed localities.]

Locality (fig. 2)	Locality number	Amino-acid age estimate (10^3 years)	Independent age control (10^3 years)
Cape Blanco, Oregon (Elk River Beds)	LACM-3960	500±100 (M)	<700 (N)
Big Lagoon, California	LACM-5003	900±150 (S)	>700 (R)
Moonstone Beach, California	HSU-1360	710±100 (S)	>700 (R)
Crannell Junction, California	HSU-197	470±100 (P,S,M)	<700 (N)
Sea Cliff, California (fig. 4):			
(1st terrace)	M7228	<5 (P)	[1]5 [2]2.1±0.08
(2nd terrace)	M7230 M7229 M7249	45±5 (P,S,M)	[3]50
Ventura, California (fig. 3):			
Marine Terrace deposit	M7241 M7237	80±10 (P,M) 80±10 (P,M)	
San Pedro Formation	M7238 M7240 M7239 M7243	205±25 (M) 275±30 (M) 335±40 (M) 395±50 (M)	[4]<<700

[1]U-series age from published mollusk data (sample 892, Kaufman and others, 1971).

[2]C-14 data on mollusks, this study.

[3]U-series age from published mollusk data (samples 849C, 849F, and 849G, Kaufman and others, 1971) from our M7230 locality.

[4]Age of Bishop(?) ash, lower in section. Trace element correlation with dated locality.

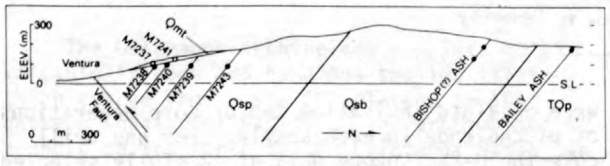

Figure 3.--Stratigraphic cross-section of the southern limb of the Ventura Avenue anticline north of Ventura, California. (Qmt) Marine terrace deposit, (Qsp) San Pedro Formation, (Qsb) Santa Barbara Formation, and (TQp) Pico Formation. The age of the Bishop(?) ash is 0.7 m.y. by trace-element correlation to dated locality (Sarna-Wojcicki, unpub. data). The age of the Bailey ash is 1.2 m.y. (Izett and others, 1974). Locality numbers as in table 1.

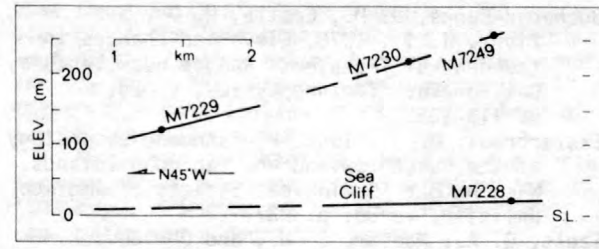

Figure 4.--Longitudinal profiles of marine terraces at Sea Cliff, California. These terraces lie on the westward plunging axis of the Ventura Avenue anticline 12 km NW of Ventura, California. Locality numbers as in table 1.

ages of volcanic ashes (0.7 - 1.2 m.y.) lower in the section. Two samples from a marine terrace deposit unconformably overlying the upper part of the San Pedro Formation yield consistent and reasonable age estimates of 80,000 years. Samples close to the Bishop(?) ash are being analyzed to evaluate the effects of the geothermal gradient.

The four localities at Sea Cliff, California (fig. 4) provide an opportunity to evaluate amino-acid age estimates for late Pleistocene and Holocene molluscan samples. Samples from three isolated remnants of a tectonically deformed marine terrace (2nd) yield identical age estimates of 45,000 years that agree with the 50,000 year age derived from published U-series data on mollusks (Kaufman and others, 1971). The cool-water molluscan fauna from this terrace supports its mid-Wisconsin age estimate. The < 5,000 year amino-acid age estimate of samples from the lower terrace (1st) at Sea Cliff agrees with the 5,000 year age derived from published U-series data (Kaufman and others, 1971) and a 2100 ± 80 year ^{14}C date on mollusks (this study). The anomalously high tectonic uplift rates ($\geq$ 7.6 mm yr^{-1} and $\geq$ 6.5 mm yr^{-1}) derived from the ages and elevations of these two terraces are similar and are consistent with the local tectonic uplift rate ($\geq$ 10 mm yr^{-1}) derived from geodetic data (Buchanan-Banks and others, 1975). No other known uplift rate in central or southern California exceeds 1 mm yr^{-1} (Wehmiller and others, 1977).

Though amino-acid dating of mollusks is still in the experimental stage, data from localities with independent age control such as those presented here indicate the technique is already an extremely valuable chronological tool for Quaternary studies in temperate coastal regions.

Buchanan-Banks, J. M., Castle, R. O., and Ziony, J. I., 1975, Elevation changes in the central Transverse Ranges near Ventura, California: Tectonophysics, v. 29, p. 113-125.

Easterbrook, D. J., 1969, Pleistocene chronology of the Puget lowland and San Juan Islands, Washington: Geological Society of America Bulletin, v. 80, p. 2273-2286.

Izett, G. A., Naeser, C. W., and Obradovich, J. D., 1974, Fission-track age of zircons from an ash bed in the Pico Formation (Pliocene and Pleistocene) near Ventura, California: Geological Society of America Abstracts with Programs, v. 6, p. 197.

Kaufman, A., Broecker, W. S., Ku, T. L., and Thurber, D. L., 1971, The status of U-series methods of mollusk dating: Geochimica Cosmochimica Acta, v. 35, p. 1155-1183.

King, K., and Neville, C., 1977, Isoleucine epimerization for dating marine sediments--importance of analyzing monospecific foraminiferal samples: Science, v. 195, p. 1333-1335.

Ku, T. L., and Kern, J. P., 1974, Uranium-series age of the Upper Pleistocene Nestor Terrace, San Diego, California: Geological Society of America Bulletin, v. 85, p. 1713-1716.

Mitterer, R. M., 1975, Ages and diagenetic temperatures of Pleistocene deposits of Florida based on isoleucine epimerization in Mercenaria: Earth and Planetary Science Letters, v. 28, p. 275-282.

Schroeder, R. A., and Bada, J. L., 1976, A review of the geochemical applications of the amino acid racemization reaction: Earth Science Reviews, v. 12, p. 347-391.

Wehmiller, J. F., and Hare, P. E., 1971, Racemization of amino acids in marine sediments: Science, v. 173, p. 907-911.

Wehmiller, J. F., and Balknap, D. F., 1978, Alternative kinetic models for the interpretation of amino acid enantiomeric ratios in Pleistocene mollusks--examples from California, Washington, and Florida: Quaternary Research, v. 9.

Wehmiller, J. F., Lajoie, K. R., Kvenvolden, K. A., Peterson, E., Belknap, D. F., Kennedy, G. L., Addicott, W. O., Vedder, J. G., and Wright, R. W., 1977, Correlation and chronology of the Pacific coast marine terrace deposits of continental United States by fossil amino acid stereochemistry--technique evaluation, relative ages, kinetic model ages, and geologic implications: U.S. Geological Survey Open-file Report 77-680, 106 p.

RADIOMETRIC AGE DETERMINATION ON SAMPLES OF KEY LAKE URANIUM DEPOSIT

I. Wendt, A. Hohndorf, H. Lenz, and V. Voultsidis
Bundesanstalt fuer Geowissenschaften und Rohstoffe
Stilleweg 2
3000 Hannover 51, W. Germany

The Key Lake uranium deposit was discovered within the Northern Saskatchewan Joint Venture Program in July, 1975, at the southeastern margin of the Athabaska basin. The geologic setting of the Key Lake uranium deposit shows great similarities to that of the Rabbit Lake deposit, which occurs in lower Proterozoic metasediments below a major unconformity overlain by middle Proterozoic sandstone (Knipping, 1974). The metasediments were deformed and metamorphosed during the Hudsonian orogeny about 1800 m.y. ago. After peneplanation of the Hudsonian orogenic surface, weathering created a porous and permeable regolith that was later covered by sandstone.

In order to obtain information about time of deposition and genesis of the uranium mineralization, U/Pb age determinations were carried out on 14 pitchblende samples from three drill cores. For all samples, discordant U/Pb ages were obtained indicating two or more generations of pitchblende in each sample. For one drill core the U-Pb isotope data of carefully selected samples of the oldest pitchblende generation yielded a straight line on the concordia plot corresponding to an upper-intersection age of about 1200 m.y. for the initial uranium mineralization and a lower-intersection age of about 100 m.y. The isotope data of samples from the other drill cores also fit on straight lines on the concordia plot (fig. 1), indicating three generations of pitchblende with the ages 1200 m.y., 918 m.y., and about 270 m.y. From these data we can deduce that uranium emplacement at Key Lake started about 500 to 600 m.y. after the Hudsonian orogeny, followed by several phases of uranium deposition or remobilization and redeposition, until about 100 m.y. ago.

A galena was found in close vicinity to the uranium ore body. Isotope data, however, showed

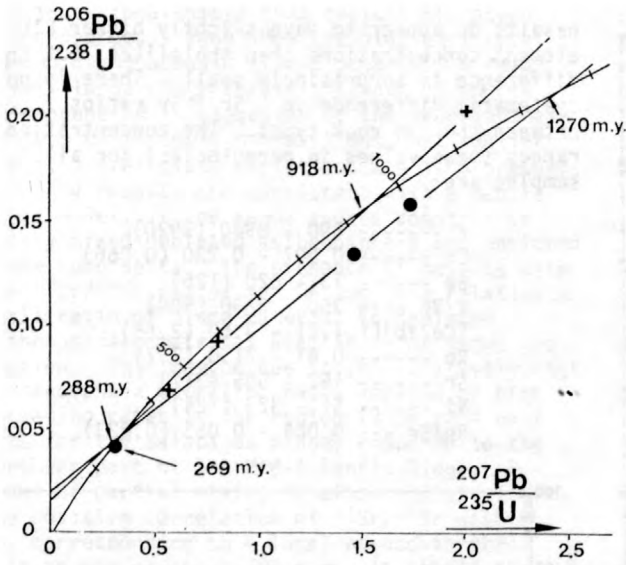

Figure 1.--Concordia diagram for the pitchblende samples of 2 drill cores from Key Lake uranium deposit.

that the lead is highly radiogenic. The possible age of the lead mineralization was calculated from the isotope ratios to range between 450 and 975 m.y. This galena sample shows that there was a mobilization of radiogenic lead after the initial uranium deposition.

Rb-Sr and K-Ar biotite ages from two fresh samples of the basement gave concordant ages of 1700 m.y., reflecting a cooling below $\sim 350^{o}C$ soon after the Hudsonian orogeny.

Knipping, H. D., 1974, The concepts of supergene versus hypogene emplacement of uranium at Rabbit Lake, Saskatchewan, Canada, in: Formation or Uranium deposits, Proc. Symp. held at Athens 6-10 May 1974, IAEA, Vienna.

ISOTOPE AND LIL ELEMENT GEOCHEMISTRY OF THE GALAPAGOS ISLANDS

By W. M. White[1], A. W. Hofmann[1], and Craig S. Bow[2]
[1]Carnegie Institution of Washington, Department of Terrestrial Magnetism, 5241 Broad Branch Rd. NW, Washington, D.C. 20015
[2]Center for Volcanology, University of Oregon, Eugene, Oregon 97403

The Galapagos archipelago consists of 15 volcanic islands and numerous smaller islets which emerge from a shallow plateau in the eastern equatorial Pacific. The archipelago is bounded on the north by the Galapagos Ridge, an active spreading center, which extends from the East Pacific Rise to the Peru-Chile trench and forms the boundary between the Cocos and Nazca plates. The Galapagos have been interpreted as the surface manifestation of a deep mantle plume (Morgan, 1971) on the basis of structural, geophysical, and geochemical evidence (for example, Johnson and others, 1976; Case and others, 1973; Schilling and others, 1976). There have been several petrological studies of the Galapagos since Darwin first visited the islands, the most complete of which is McBirney and Williams (1969). Of particular interest to us is the fact that these islands are among the relatively few oceanic islands with abundant tholeiites as well as alkali basalts.

In an attempt to test geochemical models for the origin of oceanic islands and mid-ocean ridges, we have so far determined $^{87}Sr/^{86}Sr$ ratios and K, Rb, Cs, Sr, Ba, and Ni abundances in 23 samples from 9 islands. In seven samples we have also determined rare-earth abundances. Most of the samples were kindly provided by A. R. McBirney, and major-element analyses and petrographic descriptions of these samples are given in McBirney and Williams (1969). We used isotope dilution analysis for all element abundances except Sr and Ni, which were determined by X-ray fluorescence. $^{87}Sr/^{86}Sr$ ratios were normalized to $^{86}Sr/^{88}Sr = 0.11940$ and are reported relative to a value of 0.70800 for the E&A standard. Precision is ±0.00007 (±2 sigma) or better.

Figure 1 shows the average $^{87}Sr/^{86}Sr$ ratio of each island. In contrast with some other oceanic islands or island groups, the isotope ratios are surprisingly variable. Individual values from the island of Santa Cruz range from 0.70263 to 0.70399. This is also the maximum

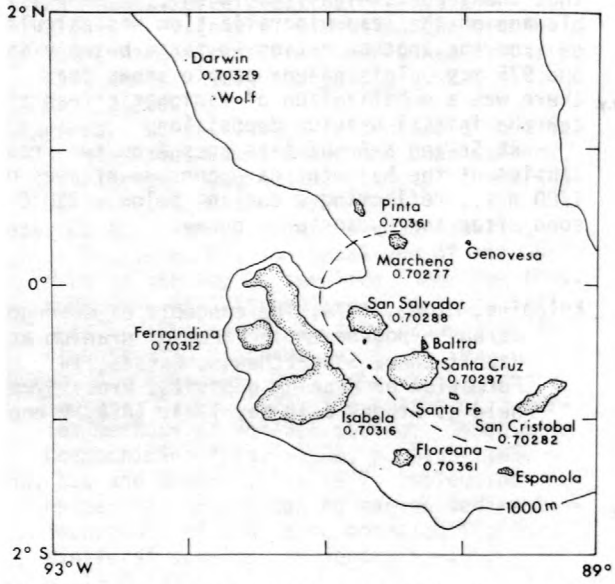

Figure 1.--Map of the Galapagos Islands. 1000-meter bathymetric contour outlines the Galapagos Plateau. Average $^{87}Sr/^{86}Sr$ for each island is given below island name. Dashed line separates islands with average $^{87}Sr/^{86}Sr$ ratios greater than 0.7030 from islands with average ratios less than 0.7030.

range for the entire Galapagos group. Nevertheless, such extreme local variation is the exception rather than the rule. For example, four of the five Santa Cruz samples have $^{87}Sr/^{86}Sr$ ratios between 0.70263 and 0.70289, and three of the four tholeiites from Isabela range from 0.70327 to 0.70331 (the fourth sample has a ratio of 0.70278). We do not know whether these local consistencies reflect an unknown sampling bias, but the geographical pattern of the average isotopic ratios shown in figure 1 indicates that the consistencies may be real. The four islands with $^{87}Sr/^{86}Sr$ averages less than 0.7030 may be separated geographically from the five islands with averages greater than 0.7030 by a simple contour line. Significantly, the islands with low $^{87}Sr/^{86}Sr$ ratios all occur in the east-central portion of the archipelago, while the islands with higher ratios occur on the western, northern, and southern edges of the archipelago.

The large-ion-lithophile (LIL) element abundances of the Galapagos basalts are low when compared to most other oceanic islands. Especially striking are the low LIL element abundances in most of the alkali basalts (thus defined if nepheline normative). For example, an alkali basalt from San Salvador (E-24) has 1190 ppm K, 1.39 ppm Rb, 0.010 ppm Cs, 242 ppm Sr, and 25 ppm Ba. Except for Sr, these concentrations are within the mid-ocean ridge basalt range. When the effects of fractional crystallization are taken into consideration, alkali basalts do appear to have slightly higher LIL element concentrations than tholeiites, but the difference is surprisingly small. There is no systematic difference in $^{87}Sr/^{86}Sr$ ratios between the two rock types. The concentration ranges (mean values in parentheses) for all samples are:

K ------- 690 - 8940 (3920)
Cs ------ 0.007 - 0.230 (0.066)
Ba ------ 13 - 620 (126)
K/Rb ---- 350 - 2130 (508)
[Ce/Yb]EF 1.21 - 3.69 (2.68)
Rb ------ 0.61 - 21.0 (7.7)
Sr ------ 192 - 505 (317)
Ni ------ 51 - 323 (124)
Rb/Sr --- 0.004 - 0.055 (0.023)

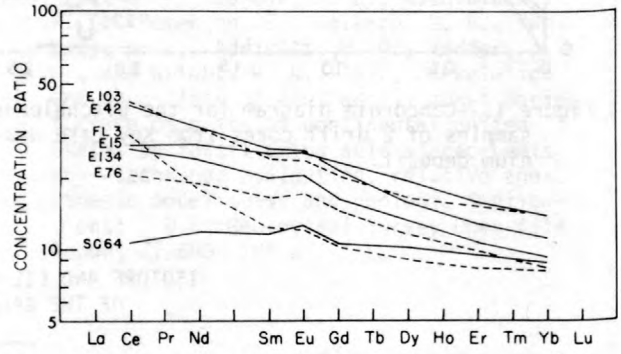

Figure 2.--Chondrite-normalized rare-earth abundance patterns of Galapagos Islands basalts. Solid lines, tholeiites; dashed lines, alkali basalts. Sample numbers beginning with 'E' are described by McBirney and Williams (1969). Samples SC-64 and FL-3 are from the islands of Santa Cruz and Floreana, respectively.

Rare-earth abundance patterns are shown in figure 2. Most of the samples have a modest light rare earth enrichment, again with little difference between tholeiites and alkali basalts. Sample SC-64 (tholeiite from Santa Cruz) has a rare-earth pattern similar to that of mid-ocean ridge basalts. This sample also has other LIL element characteristics of mid-ocean ridge basalts (690 ppm K, 0.61 ppm Rb, 0.010 ppm Cs, 236 ppm Sr, 13.6 ppm Ba, K/Rb = 1138, $^{87}Sr/^{86}Sr$ = 0.70289). All samples show a slight positive Eu anomaly, a feature also characteristic of basalts from the Azores Islands (White, 1977). The Eu anomaly could reflect source chemistry or peculiarities of magma genesis in the area.

The variability of the trace-element abundances and Sr isotope ratios clearly indicates that the mantle source of these magmas is inhomogeneous. On the average, the magma sources are more depleted in character than are those of most other oceanic islands, and some

are indistinguishable from typical mid-ocean ridge sources. None show the high enrichment common among oceanic island basalts. A relatively large characteristic length of source heterogeneity is suggested by the geographical pattern of isotopic compositions, but smaller scale, intra-island variations are also present.

The results are consistent with a mantle plume model, if the magma source consists of poorly mixed depleted asthenosphere and enriched plume components. The presence of basalts with low $^{87}Sr/^{86}Sr$ ratios may be due to a relatively small ratio of plume material to depleted asthenosphere material available for magma production. This may be due to the relatively high asthenosphere upwelling rates implied by high spreading rates in the region (3 cm yr^{-1} half rate for the Galapagos Ridge) compared to the northern part of the Mid-Atlantic Ridge. A model of partial mixing is also consistent with the positive correlation of $^{87}Sr/^{86}Sr$ with Rb/Sr, corresponding to a local pseudo-isochron with an age of about 500 m.y. It should be noted, however, that the geographical pattern observed for the $^{87}Sr/^{86}Sr$ ratios is not consistent with Schilling's (1976) simple model of plume-asthenosphere mixing based on the variation of La/Sm ratios along the Galapagos Ridge, because the apparent center of the plume contains a large proportion of depleted asthenosphere component.

The average $^{87}Sr/^{86}Sr$ and Rb/Sr ratios of all 12 tholeiites analyzed fall within the field of oceanic tholeiites defining the 1.6 b.y. mantle isochron described by Brooks and others (1976). In this respect, the Galapagos are similar to Samoa and Kerguelen in that although they fit the 1.6 b.y. oceanic mantle isochron, the data also define a much younger local isochron. We consider the present data to be a test of the world-wide nature of that oceanic mantle isochron, because the plot shown by Brooks and others (1976) contained no data from the Galapagos Islands.

Brooks, C., Hart, S. R., Hofmann, A. W., and James, D. E., 1976, Rb-Sr mantle isochrons from oceanic regions: Earth and Planetary Science Letters, v. 32, p. 51-61.

Case, J. E., Ryland, S. L., Simkin, T., and Howard, K. A., 1973, Gravitational evidence for a low density mass beneath the Galapagos Islands: Science, v. 181, p. 1040-1042.

Johnson, G. L., Vogt, P. R., Hey, R., Campsie, J., and Lowrie, A., 1976, Morphology and structure of the Galapagos Rise: Marine Geology, v. 21, p. 81-120.

McBirney, A. R., and Williams, H., 1969, Geology and petrology of the Galapagos Islands: Geological Society of America Memoir 118, 197 p.

Morgan, W. J., 1971, Convection plumes in the lower mantle: Nature, v. 230, p. 42-43.

Schilling, J. G., 1976, Galapagos mantle plume: geochemical evidence: EOS: Transactions, American Geophysical Union, v. 57, p. 343.

Schilling, J. G., Anderson, R. N., and Vogt, P. R., 1976, Rare earth, Fe, and Ti variations along the Galapagos spreading center, and their relationship to the Galapagos mantle plume: Nature, v. 261, p. 108-113.

White, W. M., 1977, Geochemistry of igneous rocks from the Central North Atlantic, the Azores, and the Mid-Atlantic Ridge: Kingston, Rhode Island University, Ph. D. Thesis, 287 p.

ORIGIN OF THE NINETYEAST RIDGE-- Sr ISOTOPE AND TRACE-ELEMENT EVIDENCE

By D. J. Whitford[1], and R. A. Duncan[2]
[1]Department of Terrestrial Magnetism
Carnegie Institution of Washington
Washington, D. C. 20015
[2]School of Oceanography
Oregon State University
Corvallis, Oregon 97330

The Ninetyeast Ridge is located in the eastern Indian Ocean, along the 90° E meridian from ~ 31° S to 9° N. It is elevated about 2 km above the surrounding ocean floor and varies in width from 100 - 200 km. There have been numerour theories about the origin of this enigmatic aseismic ridge. It has been variously interpreted as an extinct spreading center, an extinct island arc, a horst structure, a "leaky" transform fault, and a "hot-spot" trace (Luyendyk and Rennick, 1977). Drilling has shown that basal sediments overlying the basalt crust of the ridge became progressively younger from north to south, and recent K-Ar geochronological studies (Duncan, 1978) have demonstrated a corresponding decrease in age of the underlying basement. Together with palaeomagnetic and geological arguments, Duncan (1978) interpreted

these results to indicate that the Ninetyeast Ridge manifests the northward movement of the Indian Plate over a hot-spot, presently situated beneath Heard Island, located on the Kerguelen Plateau in the southern Indian Ocean.

In an attempt to test this model, we have determined $^{87}Sr/^{86}Sr$ ratios together with LIL-element (K, Rb, Cs, Ba, Sr) abundances in a range of basalts from the ridge. Trace-element abundances have been determined by isotope dilution. Trace-element abundances and measured $^{87}Sr/^{86}Sr$ ratios in the basalts dated by Duncan (1978) are listed in table 1 together with White and Bryan's (1977) estimate of the average MORB from the Atlantic Ocean.

Table 1.--Sr isotope and trace-element results

[All trace-element data as ppm. Tr, total rock analysis; L, residue after leaching with HCl. Ages and Tr K-concentrations from Duncan (1978). $^{87}Sr/^{86}Sr$ ratios normalized to $^{86}Sr/^{88}Sr = 0.1194$, relative to E and A $SrCO_3$ $^{87}Sr/^{86}Sr = 0.70800$.]

DSDP site[1]		K	Rb	Cs	Ba	Sr	$^{87}Sr/^{86}Sr$ (±2σ)	Age (m.y.)
214:	Tr------	13500	34.1	0.49	278	333	0.70492± 6	58
	L-------	15300	41.3	0.52	291	196	0.70493± 7	
215:	Tr------	7440	11.2	0.23	276	268	0.70448± 6	61
	L-------	7340	9.5	0.21	327	112	0.70454±10	
216:	Tr------	6230	11.2	0.18	94	143	0.70557± 6	81
	L-------	3240	1.7	0.13	103	86	0.70548± 6	
253:	Tr------	1170	1.6	0.052	15	90	0.70554± 8	46
	L-------	880	0.74	0.0018	15	41	--	
254:	Tr------	3320	6.0	0.030	88	169	0.70470± 8	38
	L-------	3430	7.2	0.018	82	111	0.70472±11	
MORB----------		855	0.87	0.012	8.3	103	0.70266	

[1]Samples: 214-48-1, 147-150 m
215-19-2
216-38-3, 135-138 m
253-58-cc, 140-143 m
254-35-3, 26-28 m

Abundances of K, Rb, Cs, Ba, and Sr are significantly greater than those in MORB and resemble more closely those found in basalts from oceanic islands. $^{87}Sr/^{86}Sr$ ratios show a similar effect.

Despite the retention of age information, all samples have suffered some degree of low-grade alteration. In order to test whether the measured $^{87}Sr/^{86}Sr$ ratios are the result of alteration and contamination with seawater-Sr, samples were also leached in hot 6N HCl and the residue subsequently analyzed (O'Nions and Pankhurst, 1976). The close similarity between $^{87}Sr/^{86}Sr$ ratios measured in leached and unleached samples suggests that the high ratios of up to 0.7055 are primary. In both cases, calculated initial ratios are only slightly lower (typically $\leq$ 0.0005) than the measured ratios--a consequence of low ages together with low Rb/Sr ratios. In most cases, leached samples are characterized by lower abundances of Sr and higher Ba relative to the unleached rocks. K, Rb, and Cs show no consistent pattern.

The results listed in table 1 allow us to draw the following conclusions:

1. The analyzed lavas do not resemble MORB but show closer geochemical affinities with oceanic island basalts. This similarity with island basalts argues against the hypothesis that the Ninetyeast Ridge represents an old spreading center, or, perhaps more realistically, a leaky transform fault.

2. Basalts from the Ninetyeast Ridge are isotopically heterogeneous, which implies a heterogeneous mantle source. Considerable caution is therefore required when attempting to relate rock-types from different locations by simple processes such as fractional crystallization (see, for example, Ludden and others, 1977).

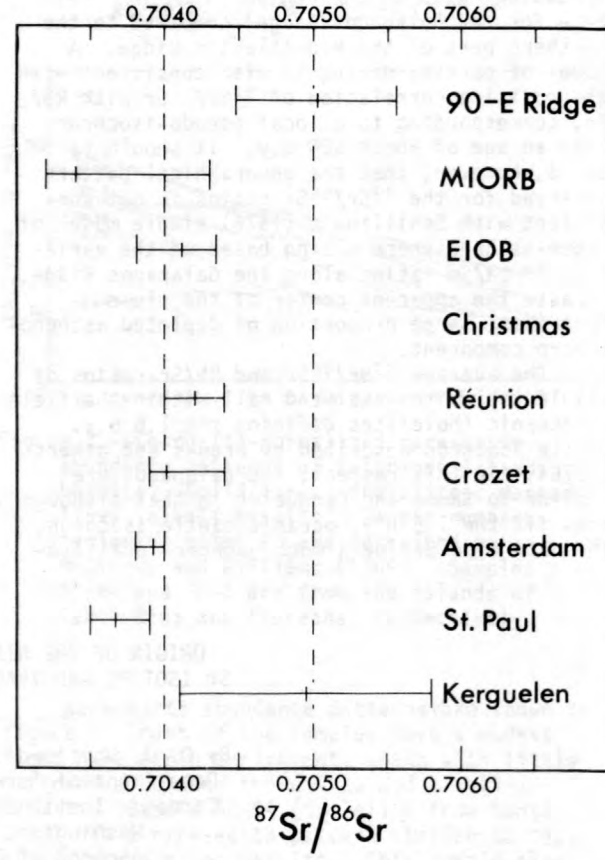

Figure 1.--Comparison of measured $^{87}Sr/^{86}Sr$ ratios in basalts from the Ninetyeast Ridge with those from the mid-Indian Ocean ridge (MIORB), the eastern Indian Ocean (EIOB (altered), and various islands in the Indian Ocean. Ranges and average $^{87}Sr/^{86}Sr$ ratios are shown. Data sources: Hedge and others (1973); Subbarao and Hedge (1973); Whitford (1975; and unpub. data results).

3. From figure 1, it can be seen that among analyzed basalts from islands in the Indian Ocean, only those from Kerguelen have $^{87}Sr/^{86}Sr$ ratios higher than 0.7044. With respect to both

the range of $^{87}Sr/^{86}Sr$ and the average ratio, there is a close similarity between rocks from the Ninetyeast Ridge and those from Kerguelen. Therefore, if the Ninetyeast Ridge does represent an older trace from a presently active hot-spot, only that which produced the Kerguelen basalts and subsequently migrated south, has the appropriate geochemical characteristics.

Although this does not prove the model, it is not inconsistent with such a scheme. It may be significant that basalts from Amsterdam and St. Paul Islands are characterized by much lower $^{87}Sr/^{86}Sr$ ratios than those observed along the Ninetyeast Ridge (fig. 1). It seems less likely, therefore, that these islands represent the location of the hot-spot which produced the Ninetyeast Ridge (Luyendyk and Rennick, 1977).

Ken Burrhus and Mark Feigenson provided valuable expertise in all phases of the analytical work.

Duncan, R. A., (in press), Geochronology of basalts from the Ninetyeast Ridge and continental dispersion in the eastern Indian Ocean: Journal of Volcanology and Geothermal Research.

Hedge, C. E., Watkins, N. D., Hildreth, R. A., and Doering, W. P., 1973, $^{87}Sr/^{86}Sr$ ratios in basalts from islands in the Indian Ocean: Earth and Planetary Science Letters, v. 21, p. 29-34.

Ludden, J. N., Thompson, G., Bryan, W. B., and Frey, F. A., 1977, An evaluation of fractional crystallization and the origin of lavas from the 90° E Ridge, eastern Indian Ocean: Geological Society of America Abstracts with Programs, v. 9, p. 1077-1078.

Luyendyk, B. P., and Rennick, W., 1977, Tectonic history of aseismic ridges in the eastern Indian Ocean: Geological Society of America Bulletin, v. 88, p. 1347-1356.

O'Nions, R. K., and Pankhurst, R. J., 1976, Sr isotope and rare earth element geochemistry of DSDP Leg 37 basalts: Earth and Planetary Science Letters, v. 31, p. 255-261.

Subbarao, K. V., and Hedge, C. E., 1973, K, Rb, Sr, and $^{87}Sr/^{86}Sr$ in rocks from the mid-Indian Oceanic ridge: Earth and Planetary Science Letters, v. 18, p. 223-228.

White, W. M., and Bryan, W. B., 1977, Sr isotope, K, Rb, Cs, Sr, Ba and rare-earth geochemistry of basalts from the FAMOUS area: Geological Society of America Bulletin, v. 88, p. 571-576.

Whitford, D. J., 1975, Strontium isotopic studies of the volcanic rocks of the Sunda arc, Indonesia, and their petrogenetic implications: Geochimica Cosmochimica Acta, v. 39, p. 1287-1302.

CIRCULATION IN A FOSSIL GEOTHERMAL AREA--$\delta^{18}O$ STUDY

By Alan E. Williams
Department of Geological Sciences, Brown University, Providence, Rhode Island 02912

The Alamosa River stock, in the San Juan mountains of Colorado, has been shown to have undergone extensive hydrothermal circulation and isotopic exchange with large quantities of meteoric water (Taylor, 1974; Williams and Sommer, 1977). It may therefore be considered a "fossil geothermal area" and information about its circulation and thermal history may be important to the understanding and modeling of similar areas.

Inhomogeneous Flow: Analysis of whole-rock $\delta^{18}O$ values for samples from the Alamosa River stock and its surrounding volcanics show several important effects. The contouring of isotopic values in the volcanics (fig. 1) shows an obvious asymmetry in the distribution of oxygen isotopic depletion. This asymmetry is correlative with a high degree of inhomogeneity in the hydrothermal circulation system. The extreme elongation of the isotopic contours toward the northeast extends the oxygen-exchange aureole at least 10 km from the boundary of the stock. This effect seems to be explainable by the presence of the Cornwall fault zone (Lipman, 1975), the southern boundary fault of the Summitville caldera (fig. 2), in that orientation. A similar effect may be shown by the southeastward "bulge" in the isotopic contours of figure 1. The platoro fault system (Lipman, 1975) passes directly through that area with a generally northwest orientation. It seems probable that the fault zones serve as high permeability conduits, and as such, dominate the circulation in their vicinities.

In the field, it can be seen that these major fault trends tended to influence not only the isotopic depletion, but also the intrusive activity itself, and the low temperature hydrothermal alteration and mineralization which seems to overprint much of this geothermal system.

Figure 3 shows a slightly more localized

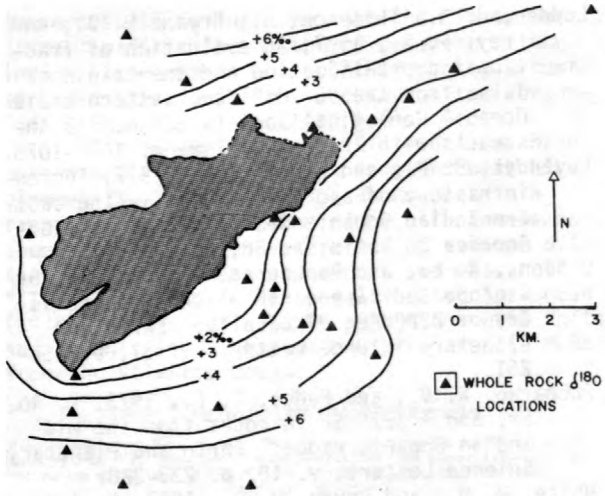

Figure 1.--Map of the Alamosa River stock. Isotopic data in the surrounding volcanics contoured in $\delta^{18}O$ (relative to SMOW).

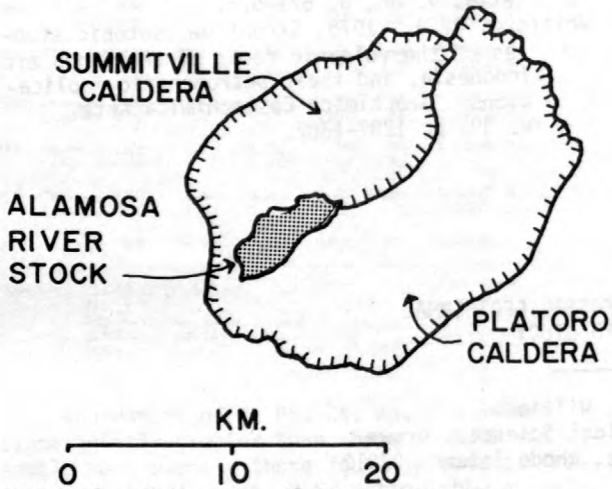

Figure 2.--Map of the Alamosa River stock showing relationship to Platoro and Summitville calderas.

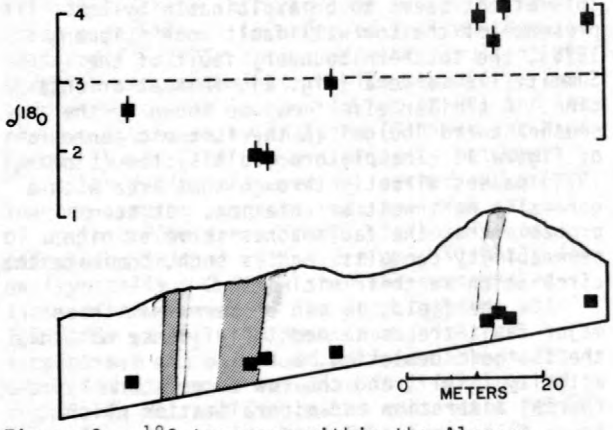

Figure 3.--^{18}O traverse within the Alamosa River stock. Darkness of tone indicates degree of alteration.

example of this fracture domination of fluid flow and isotopic depletion. A suite of samples was collected in an 80-meter traverse that was perpendicular to and inclusive of several minor fractures of the Platoro fault system. The isotopic data shown in the upper part of the diagram show a distinct increase in isotopic depletion (lower $\delta^{18}O$) toward the larger, more altered (darker pattern) fracture zone, shown in the lower part of the diagram. Little added isotopic effect, however, is seen near the less altered zone.

The whole-rock samples near the large fracture zone, as those near major faults, seem to have been able to exchange oxygen more efficiently with the circulating meteoric waters. This is most probably due to easier access of the water to those areas, allowing a greater flux of water near the more highly permeable fracture zones (a greater local water-rock ratio).

Although changes in other circulation parameters could cause similar effects, continuing studies of smaller-scale fractures (millimeter-size) could give a good idea of the mechanism and degree of inhomogeneous circulation in such a geothermal system.

Multiple Circulation: At this point it should be noted that although alteration and mineralization have been used as convenient indicators of highly permeable zones, preliminary data in the Alamosa River stock seems to show that this low-temperature alteration may have been produced by a subsequent circulation event, totally different from that producing the isotopic depletions.

In many areas of the Alamosa River stock, unaltered samples have undergone significant exchange of oxygen with the circulating water, while in other areas fairly altered samples show no isotopic depletion. In the Alamosa area at least two formations, the latite porphyry of South Mountain and the Alum Creek Porphyry, exhibit extensive (even economic) mineralization and alteration but give only igneous isotopic values. Although local high-temperature circulation without isotopic depletion is feasible, as well as low-temperature isotopic enrichment during alteration, it seems fortuitous that all samples would achieve "igneous" isotopic values. At this point it appears that these formations postdate the high-temperature geothermal circulation event but predate the lower-temperature event producing the alteration and mineralization. Research on this complication in geothermal systems is proceeding at Brown University.

Forester, R. W., and Taylor, H. P., 1972, Oxygen and hydrogen isotope data on the interaction of meteoric groundwater with a gabbro-diorite stock, San Juan Mountains, Colorado: International Geological Congress, Proceedings, v. 24, sect. 10, p. 254-263.

Lipman, P. W., 1975, Evolution of the Platoro Caldera complex and related volcanic rocks, southeastern San Juan Mountains, Colorado: U.S. Geological Survey Professional Paper 852, 128 p.

Taylor, H. P., 1974, Oxygen and hydrogen isotope evidence for large-scale circulation and interaction between groundwaters and igneous intrusions, with particular reference to the San Juan Volcanic Field, Colorado: Geochemical Transport and Kinetics, Carnegie Institution of Washington Publication, p. 299-323.

Williams, A. E., and Sommer, M. A., 1977, ^{18}O study of the Alamosa River Stock, a fossil geothermal area [abs.]: Transactions of the American Geophysical Union, v. 58, p. 540.

U-Pb EVIDENCE FOR THE PRE-EMPLACEMENT HISTORY OF GRANITIC MAGMAS, BERRIDALE BATHOLITH, SOUTHEASTERN AUSTRALIA

By Ian S. Williams
Research School of Earth Sciences, ANU, Canberra
Present Address: Division of Geological and Planetary Sciences, California Institute of Technology, Pasadena, California 91125
(Division Constribution Number 3073)

The Berridale batholith is one of many mid-Paleozoic granitic batholiths which comprise a large part of the southeastern corner of the Australian continent. For the past decade, the geology and geochemistry of the batholith have been studied in detail (White and others, 1974; Chappell and White, 1974; White and others, 1977; 1978), and more recently by O'Neil and Chappell (1977). As a result of these studies:

1. Twenty principal granitoids have been identified and mapped.
2. Chemical, isotopic, and petrographic characteristics of each granitoid have been determined.
3. Groups of granitoids with characteristics in common have been recognized.
4. An intrusive sequence has been deduced from field relationships.

The detail in which the Berridale batholith is already known makes it an ideal locality for studying the interaction between different techniques of granitoid geochronology.

A study of mica Rb-Sr ages by Williams and others (1976), revealed small but significant age differences between the granitoids; differences which were consistent with the known intrusive sequence. Williams and others (1976) argued that in at least some cases, the mica Rb-Sr age was a close approximation of the crystallization age of the granitoid.

The purpose of the present paper is to summarize the findings of a zircon and monazite U-Pb study of the Berridale batholith. The data are calculated using the decay constants and isotopic abundances recommended for conventional use (Steiger and Jäger, 1977) and the uncertainties assigned are two standard errors.

Before a comparison can be made between ages measured using different isotopic techniques, the effects of inaccuracies in the decay constants must be assessed. A study of the geochronology of the Myalla Road Syenite by N. W. Tetley and others (written commun., 1978), in which the ages obtained were 173.8 ± 3.9 m.y. (plagioclase, total-rock, K-feldspar Rb-Sr isochron), 172.8 ± 1.6 m.y. (biotite Rb-Sr), 173.1 ± 1.4 m.y. (biotite K-Ar), and 173.2 ± 1.7 m.y. (U-Pb zircon), suggests that the systematic bias between techniques is smaller than can be detected at this level of precision.

A feature of the zircon U-Pb data from the Berridale batholith is the strong discordance commonly obtained when analyses of several fractions from the same sample are plotted on a concordia diagram. In addition, different sorts of discordance patterns are characteristic of the different granitoids.

In the Maffra Adamellite, one of the youngest granitoids in the batholith, the biotite Rb-Sr age (412.8 ± 1.9 m.y.), the muscovite Rb-Sr age (413.6 ± 3.7 m.y.), and the U-Pb concordant age of monazite (412.2 ± 2.3 m.y.) are in mutual agreement. The zircon discordia for the granitoid is unusual in that a straight line fitted to the data intersects the $^{207}Pb/^{235}U$ axis to the right of the origin. Its intersection with the concordia is at 438.6 $\pm {}^{9.2}_{10.8}$ m.y. Several interpretations of the data are possible including: 1) The common Pb in the zircon may have had a higher $^{207}Pb/^{206}Pb$ than was assumed. 2) The zircon may be a mixture of zircon approximately 440 m.y. old with very highly discordant, much older zircon. 3) Long-term leakage of ^{222}Rn may have caused zircon approximately 410 m.y. old to have become differentially depleted in ^{206}Pb. The example of the Maffra Adamellite shows that there are granitoids in the Berridale batholith for which the zircon apparent ages may be interpreted so as to be consistent with ages measured

independently by other techniques.

The Tara Granodiorite is another of the younger granitoids in the batholith. The zircon discordance pattern for the Tara differs considerably from that of the Maffra in that the fractions analyzed have $^{207}Pb/^{206}Pb$ ages as high as 817 ± 50 m.y. This is far older than stratigraphic limits permit for the age of the Tara pluton. The high ages are attributable to an older zircon component mixed with the magmatic zircons. The older component may be derived by the assimilation of wall rock, but chemical constraints require that the amount of assimilation be very small. The older component alternatively may be cognate.

Examination of a mafic xenolith which is considered to be residual from the granitoid's source (in accordance with the genetic model of Chappell, 1966), from the Tara revealed that the older component is partially or possibly totally absent from it. The oldest $^{206}Pb/^{238}U$ age measured on the xenolith zircon was 442 ± 4 m.y. and, in retrospect, there is no unequivocal evidence for the crystallization of zircon in the xenolith of in the granitoid magma after that time. If all the zircon in the Tara is cognate, these data suggest that the oldest component in the granitoid's source must be at least 817 m.y. old, that the zircon in the source was probably unequally distributed, and that there was a major episode of zircon crystallization at least as early as 442 m.y. If the older zircon component is not cognate, less can be said of the source age of the granitoid but, unless the xenolith also has been contaminated, zircon crystallization at least as early as 442 m.y. must still be postulated. These zircon apparent ages contrast with the biotite Rb-Sr ages measured both on the granitoid and on its contact aureole, which suggest strongly that the Tara was not emplaced until 412.3 ± 1.3 m.y. ago. The Tara Granodiorite is only one of three granitoids studies in which a case can be made for the granitoid magma having contained cognate zircon that must have crystallized before the granitoid was finally emplaced.

Discordance patterns akin to those in the Maffra and the Tara are found in only about a half of the granitoids of the Berridale batholith. For the remainder, the patterns are characterized by:

1.1. A discordia which intersects the concordia twice, once at an age of the same order as that expected for the emplacement age and once at an age far older than stratigraphic limits permit for the age of the pluton.

2.1. An imperfect fit of the data to a straight line.

3.1. An invariable pattern in which successively higher ages are recorded by the discordia's lower intersection with the concordia, by biotite Rb-Sr, and by monazite.

This type of discordance pattern is explained by the presence in the magma of an older detrital zircon component. Similar large components of old Pb have been found both in a biotite-cordierite xenolith from one of the granitoids and in a very felsic granitoid which is free of xenoliths. The older component is therefore considered to be an integral part of the magmas' source material. All the granitoids which contain the large components of older Pb are S-type granitoids as defined by Chappell and White (1974).

Evidence found in one granitoid, the Dalgety Granodiorite, indicates that the effects of Pb loss with respect to U, as well as multicomponent mixing, must be considered when the zircon discordance patterns are interpreted. Pb loss is considered to be the reason for the zircon lower intersection ages consistently being less than the biotite Rb-Sr ages. The likelihood that Pb loss has occurred places the geological significance of the zircon upper intersection ages in doubt.

Whether monazite U-Pb or biotite Rb-Sr has recorded the age of emplacement of the granitoids has not yet been established. It is possible that the monazites record emplacement and that some of the biotite ages have been reset subsequently in such a way that the differences in biotite ages which still can be detected are consistent with the intrusive sequence. The alternative interpretation is that biotite Rb-Sr has recorded the age of emplacement and that some of the monazite U-Pb systems have closed prior to the final intrusion of the magmas. If that is so, the data suggest that the crustal history of granitic magmas may be an extended one.

Chappell, B. W., 1966, Petrogenesis of the granites at Moonbi, New South Wales: Australian National University, Ph. D. Thesis.

Chappell, B. W., and White, A. J. R., 1974, Two contrasting granitic types: Pacific Geology, v. 8, p. 173-174.

O'Neil, J. R., and Chappell, B. W., 1977, Oxygen and hydrogen isotope relations in the Berridale Batholith: Journal of the Geological Society of London, v. 133, p. 559-571.

Steiger, R. H., and Jäger, E., 1977, Subcommission on Geochronology--Convention on the use of decay constants in geo- and cosmochronology: Earth and Planetary Science Letters, v. 36, p. 359-362.

White, A. J. R., Chappell, B. W., and Cleary, J. R., 1974, Geologic setting and emplacement of some Australian Paleozoic batholiths and implications for intrusive mechanisms: Pacific Geology, v. 8, p. 159-171.

White, A. J. R., Williams, I. S., and Chappell, B. W., 1977, Geology of the Berridale 1:100,000 Sheet (8625): Geological Survey of New South Wales.

White, A. J. R., Chappell, B. W., and Williams, I. S., 1978, Geology of the Numbla 1:100,000 Sheet (8624): Geological Survey of New South Wales (in press).
Williams, I. S., Compston, W., Chappell, B. W., and Shirahase, T., 1976, Rubidium-strontium age determinations on micas from a geologically controlled, composite batholith: Geological Society of Australia Journal, v. 22, p. 497-505.

ISOTOPE FRACTIONATION BY MARINE DIATOMS AND PALEOCLIMATOLOGICAL IMPLICATIONS

By William W. L. Wong and William M. Sackett
Texas A&M University
College Station, Texas 77843

The apparent dependence of the stable carbon isotope compositions of plankton on the temperature of their environmental water forms the basis for a potential paleoclimatological tool for the study of deep sea sediments. However, the reasons for the 15 permil range in carbon-13 compositions of natural oceanic phytoplankton populations are not completely understood, with variations being attributed directly to temperature (Sackett and others, 1965), to a temperature associated CO_2 pool effect (Degens and others, 1968), and to a temperature associated species effect (Sackett and others, 1973). In the work described below several of the ten species of marine diatoms are shown to exhibit significantly different and characteristic stable carbon isotope fractionations. For this study, the design of the culture system was extremely important and, as it turned out, rather simple. The various species of phytoplankton had to be exposed to identical conditions so that only the species effect was observed. Also, the experimentally determined carbon isotope fractionation for a particular species had to be reproducible to within a small fraction of the differences in isotopic composition observed between various species. Both of these requirements were realized.

Unialgal cultures of marine diatoms were cultured in 1-liter aliquots of an autoclaved artificial sea water media with a final bicarbonate concentration about ten times the 2 millimoles found in natural sea water. This excess bicarbonate minimized isotopic changes due to substrate depletion but did not adversely affect phytoplankton viability. The pH of the culture media was adjusted to 7.6 at the beginning and remained with $\pm$ 0.2 units for the duration of the experiments. The culture vessels consisted of 2-liter Erlenmeyer flasks with stoppers containing two sections of small-diameter glass tubing: one was a screw-cap tube to provide easy access to the cultures and the other was connected to an ascarite absorption tube which prevented exchange of CO_2 between the outside and inside atmospheres. The culture chamber was kept at 18°C and a constant illumination of approximately 60 microeinsteins m^{-2} sec^{-1} was provided by two 15-W cool white fluorescent tubes mounted on a reflector. Only healthy cultures, as determined by examination under a light microscope, were used for the experiments. The algae, together with the culture media, were withdrawn from the culture vessels at different intervals after visible growth was established. The algae were separated from the media by filtration through two Gelman type A-E glass fiber filters. Organic carbon in algal cells was converted to CO_2 by combustion at 800 to 900°C over cupric oxide in an oxygen atmosphere (Craig, 1953), whereas bicarbonate in the filtrates was converted to CO_2 by the addition of 85 percent phosphoric acid after the evacuation of atmospheric gases from the reaction vessels. The purified CO_2 was analyzed with an isotope-ratio mass spectrometer. The results are expressed in $\delta^{13}C$ values which are defined as follows:

$$\delta^{13}C \text{ (permil)} = \left[\frac{(^{13}C/^{12}C) \text{ sample}}{(^{13}C/^{12}C) \text{ standard}} - 1 \right] \times 10^3$$

where the standard is the Chicago PDB sample (Craig, 1953). Corrections were made in the manner prescribed by Craig (1957). The working standards for inorganic and organic samples were NBS-Solenhofen limestone #20 ($\delta^{13}C_{PDB}$ = -1.1 permil) and Norit, a powdered charcoal sample ($\delta^{13}C_{PDB}$ = -24.8 permil), respectively.

Data were treated as illustrated by Coscinodiscus asteromphalus in figure 1 which shows a plot between the $\delta^{13}C$ values of cells of Coscinodiscus and the corresponding $\delta^{13}C$ values for the dissolved bicarbonate in the filtrates. As shown by this figure, the isotopic composition of algal cells and filtrates become isotopically heavier and heavier in time. In order to avoid the problem of the time functionality of $\delta^{13}C$ values of the algae, the initial fractionations ($\Delta^{13}C$ values) were calculated. This value, characteristic of each organism under the specific culture conditions,

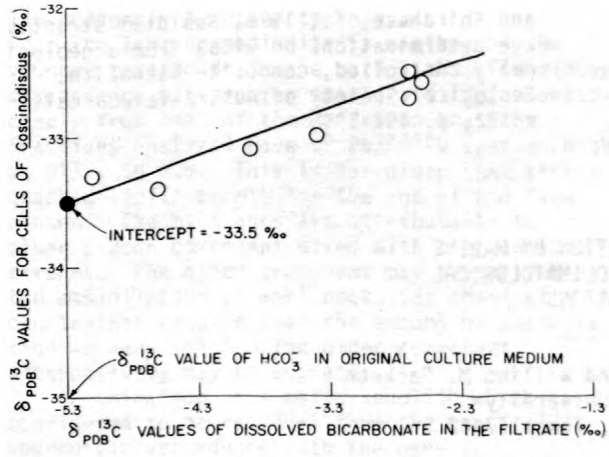

Figure 1.--A plot of the $\delta^{13}C$ values of the cells of Coscinodiscus asteromphalus versus the corresponding $\delta^{13}C$ values for the dissolved bicarbonate in the filtrates. The algae were cultured in an artificial sea water medium with a salinity of 26 permil, at a temperature of 18°C and under a constant illumination of 60 micro-einsteins m^{-2} sec.

is the difference between the initial isotopic composition of each organism and the appropriate isotopic composition of bicarbonate in the original culture media. The initial isotopic compositions of algae are the intercepts from linear-regression analyses between the $\delta^{13}C$ values of algal cells and the corresponding $\delta^{13}C$ values of filtrates as illustrated in figure 1. The intercept for Coscinodiscus asteromphalus is -33.5 permil and so the $\Delta^{13}C$ value is equal to -33.5 minus -5.3 or -28.2 permil. The value, -5.3 permil, is the isotopic composition of the bicarbonate in the original culture medium of Coscinodiscus. Based on the results ($\Delta^{13}C$ values) of six replicate experiments: 1. -29.1, -28.8; 2. -31.9, -31.1; 3. -29.7, -28.3; 4. -30.4, -29.8; 5. -29.1, -29.5; and 6. -34.8, -34.2; the standard deviation for a given experiment of 0.4 permil.

One point that should be made here is that dissolved CO_2 is probably the active species of CO_2 assimilated by diatoms during photosynthesis. In our experiments it is assumed that chemical and isotopic equilibria are rapidly established relative to cellular uptake. As all experiments were conducted at 18°C, the CO_2 vs HCO_3^- fractionation is taken as -9.1 permil (Wendt, 1968). Rather than using a calculated value, we chose to use the actual measured $\delta^{13}C$ value of total inorganic carbon in reporting our experiments.

The overall results are summarized in table 1. $\Delta^{13}C$ values vary from species to species and cover a range of 7.8 permil. Skeletonema costatum shows the largest fractionation of 29.9 permil and Nitzschia closterium shows the least fractionation of -22.1 permil. Metabolic fractionation of carbon isotopes by two species of marine centric diatoms, Cyclotella nana (transferred to Thalassiosira by Hasle and Heimdal, 1970) and Skeletonema costatum, has been examined by Degens and others, (1968). Their results indicate that $\Delta^{13}C$ values vary from -12.3 to -28.0 permil depending on the algae and the culture conditions. Even though the $\Delta^{13}C$ value for the Thalassiosira pseudonana reported in table 1 (-26.7 permil) agrees very well with that of the T. pseudonana cultured by Degens and others (1968) at 20°C with ten times excess bicarbonate ($\Delta^{13}C$ = -26.0 permil), our results are not directly comparable because of the differences between our culture systems.

Organism	Code[1]	Isotope Fractionation (permil)	
		Intercept[2]	°C[3]
Centric Diatoms:			
Skeletonema costatum	F22a	-34.7	-29.9
Chaetoceros didymus	F57	-34.3	-29.0
Chaetoceros lorenzianus	F29b	-32.1	-26.7
Thalassiosira subtilis	F50b	-34.9	-29.3
Thalassiosira pseudonana	F43a	-32.1	-26.7
Coscinodiscus asteromphalus	F71	-33.5	-28.2
Cyclotella sp.	F59a	-30.7	-25.4
Pennate Diatoms:			
Nitzschia closterium	F56ud	-27.3	-22.1
Nitzschia frustulum	IUCC 2042	-29.7	-24.2
Nitzschia curvilineata	IUCC 2033	-31.1	-26.0

[1] Designations: F = Fryxell cultures; IUCC = Indiana University Culture Collection
[2] Intercept = Initial isotopic composition of algae
[3] $\delta^{13}C$ = $\delta^{13}C$ value of alga versus HCO_3^-

Of the few plausible reasons for species-related differences in isotope fractionation, the variability in growth rates is an obvious first possibility. All isotope-fractionating processes show decreasing apparent fractionations in the total accumulated product versus the reactant as a particular reaction approaches completion. Thus a fast-growing, efficient utilizer will show a smaller apparent fractionation relative to a slow-grower if they both have the same mechanisms, for example, diffusion of CO_2 across a membrane followed by enzymatic fixation of the transferred CO_2. In view of this rationale, growth rates were determined by measuring particulate organic carbon as a function of time for aliquots of each of the ten cultures. Although there were marked differences in growth rates, there appeared to be no correlation between the slopes of the experimental curves and the measured fractionations. Accordingly, growth rates do not appear to affect carbon isotope fractionation in our cultures of marine diatoms.

Another plausible explanation for species-related differences in isotope fractionation is the presence of different enzymatic fixation and /or other metabolic mechanisms in one group relative to another group of marine phytoplankton. In this regard, our experimental data present an interesting correlation with one parameter. Of the ten species of diatoms tested, the four that have been shown by Lewin (1963), to grow heterotrophically on glucose or lactate in the dark, the pennate diatoms Nitzschia closterium, N. frustulum and N. curvilineata (3 of 12 species found by Lewin)

and the centric diatom Cyclotella sp. (the only one of 15 species of centric diatoms capable of heterotrophic growth), show the smallest fractionations. Thus the property of a cell that allows for heterotrophic growth apparently is related to the property that results in a smaller overall discrimination against carbon-13 during photosynthesis.

The species cultured in this study are those that grow in moderately warm environments in the sea. Presumably, those species common to polar environments would show a similar variability in their fractionation capabilities. Thus, it would appear that the pool effect (Degens and others, 1968) and the species effect reported here can easily account for the 15 permil range in the stable carbon isotope composition of oceanic plankton populations. The gross mean differences of about 7 permil between polar ($\delta_{PDB}^{13}C \simeq -27$ permil) and tropical ($\delta_{PDB}^{13}C \simeq -20$ permil) types may still be used to advantage in paleoclimatic studies on sediments deposited in environments far removed from continentally derived land-plant debris and recycled kerogen.

We thank G. A. Fryxell for providing the diatom cultures. Financial support was provided by NSF grant OCE-75-13299-A01.

Craig, H., 1953, The geochemistry of the stable carbon isotopes: Geochimica et Cosmochimica Acta, v. 3, p. 53-92.

Craig, H., 1957, Isotopic standards for carbon and oxygen and correction factors for mass-spectrometric analysis of carbon dioxide: Geochimica et Cosmochimica Acta, v. 12, p. 133-149.

Degens, E. T., Guillard, R. R. L., Sackett, W. M., and Hellebust, J. A., 1968, Metabolic fractionation of carbon isotopes in marine plankton-I, Temperature and respiration experiments: Deep-Sea Research, v. 15, p. 1-9.

Hasle, G. R., and Heimdal, B. R., 1970, Some species of the centric diatom genus Thalassiosira studied in the light and electron microscopes: Beihefte zur Nova Hedwigia, v. 31, p. 559-590.

Lewin, J. C., 1963, Heterotrophy in marine diatoms, in Oppenheimer, C. H., ed., on marine microbiology: Springfield, Illinois, C. C. Thomas, p. 229-235.

Sackett, W. M., Eadie, B. J., and Exner, M. E., 1973, Stable isotope composition of organic carbon in recent Antarctic sediments, in Advances in organic geochemistry, edited by Technip, p. 661-671.

Sackett, W. M., Eckelmann, W. R., Bender, M. L., and Be, A. W. H., 1965, Temperature dependence of carbon isotope composition in marine plankton and sediments: Science, v. 148, p. 235-237.

Wendt, I., 1968, Fractionation of carbon isotopes and its temperature dependence in the system CO_2-gas-CO_2 in solution and HCO_3-CO_2 in solution: Earth and Planetary Science Letters, v. 4, p. 64-68.

MAJOR AND TRACE ELEMENT DISEQUILIBRIUM DURING PARTIAL MELTING

By B. J. Wood and R. F. Heming
Department of Geology, University of Manchester, Manchester M13 9PL, England

There have been a number of recent publications in which the possibility of isotopic and trace element disequilibrium during partial melting has been discussed. These discussions resulted, in part, from the observation that the constituent minerals of some ultramafic xenoliths are not in isotopic equilibrium with one another (Paul, 1971; Stueber and Ikramuddin, 1974). O'Nions and Pankhurst (1974) suggested that such isotopic disequilibrium could persist during partial melting in the mantle and that the isotopic ratios and trace element contents of the melts produced depended on the proportions of the phases concerned during the melting process. With one or two exceptions (Beswick, 1976), more recent studies have tended to discount the disequilibrium-melting hypothesis. Hofmann and Hart (1978) pointed out that, although disequilibrium might persist for long periods in a melt-free mantle, the relatively rapid diffusion of Sr, REE, and such, through silicate melts will tend to speed up equilibration once the grain boundaries are coated with melt. Nelson and Dasch (1976) suggest that isotopic disequilibrium between crystals and melt could not persist for longer than from 10^4 to 10^6 years, a period which they consider to be short with respect to the residence times of melts in the mantle.

The present study arose from the authors' belief that disequilibrium melting had been too readily dismissed on the basis of inadequate data. We have attempted to obtain information on the rates of equilibration of major and trace elements in the simple system $CaMgSi_2O_6$-$CaAl_2Si_2O_8$-Mg_2SiO_4 and its Co-Mg analogue. These data were then used to model partial-melting events in the mantle. It will be shown that the con-

tinuous, rather than the discontinuous, nature of partial melting must have considerable effect on the compositions of product melts. The rate of melt production is itself dependent on major element diffusion coefficients; trace element partitioning is, in some cases, strongly coupled to major element diffusion.

Preliminary crystallization experiments were performed on a glass of composition $diopside_{70}anorthite_{21.5}forsterite_{8.5}$ spiked with a total of 80 ppm Sm, of which about 1 percent was radioactive ^{151}Sm. Each run was taken to 1380°C (at 1 atmosphere) to remelt the charge. The temperature was then dropped to 1280°C over a period of 10 minutes and the experiment was performed at the latter temperature. On quenching in water, products were clinopyroxene, olivine, and glass. Melting experiments were performed on the same composition and on $diopside_{68}anorthite_{22}(Co_2SiO_4)_{10}$. For melting experiments, the bulk compositions were mixed from crystalline diopside, forsterite, anorthite, and Co_2SiO_4 olivine. The diopside (pure $CaMgSi_2O_6$) and olivine crystals were sieved to sizes of 23 - 58 μ. The starting materials in this case also contained 80 ppm Sm, all of which resided in the anorthite phase. Melting experiments were brought up in temperature to 1280°C and held at this temperature until quenching.

Crystallization experiments of less than 2 hours duration yielded only olivine and glass, despite the bulk composition lying in the clinopyroxene field (Schairer and Osborn, 1952). Clinopyroxene crystallized in runs of between 2 and 4.5 hours duration. Longer runs produced apparent marked recrystallization of the clinopyroxene with concomitant decrease of $K_{D_{Sm}}$ (Sm pyroxene/Sm melt) and of the alumina content of the pyroxene (figs. 1 and 2). Melting experiments on the same bulk compositions containing 23 - 58 μ crystals of pure diopside (Sm-free) demonstrated the slow approach to Al_2O_3 and Sm contents of the pyroxene to the equilibrium values (figs. 1 and 2). Calculated diffusion coefficients for Al and Sm in the clinopyroxene at 1280°C and 1 atmosphere based on these data are $D_{Sm} \simeq 5 \times 10^{-13}$ cm^2 sec^{-1} and $D_{Al} \simeq 2 \times 10^{-13}$ cm^2 sec^{-1} (assuming spherical crystals of 40 μ diameter). The similarity of these values strongly suggests that Sm diffusion (at trace concentration) is coupled to Al diffusion in the clinopyroxene and that Sm substitution takes place via Ca Si ↔ Sm Al replacement. It should be noted, however, that this does not constitute a measurement of the Sm tracer diffusion coefficients--the latter may be substantially greater than the value of D_{Sm} given above.

Melting experiments (at 1280°C) on the mixture of diopside, Co_2SiO_4 olivine and anorthite demonstrated that Co-Mg exchange is much more rapid for the olivine than for the clinopyroxene (fig. 3). Estimated values of Co-Mg interdiffusion coefficients at 1280°C are $D^{ol}_{CoMg} \simeq 4 \times 10^{-11}$ cm^2 sec^{-1} and $D^{cpx}_{CoMg} \simeq 4 \times 10^{-13}$ cm^2 sec^{-1}. The former is in good agreement with

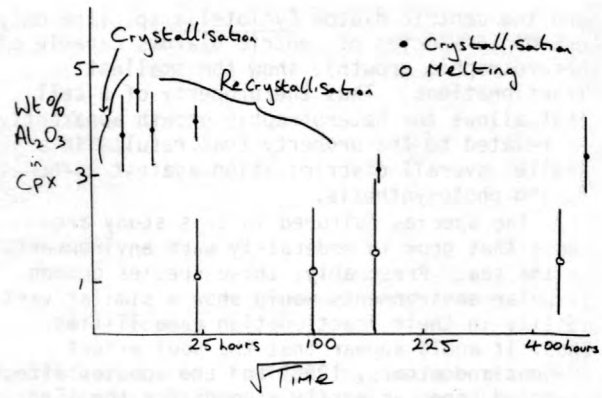

Figure 1.--Al_2O_3 content of clinopyroxene as a function of time-crystallization experiments at 1280°C.

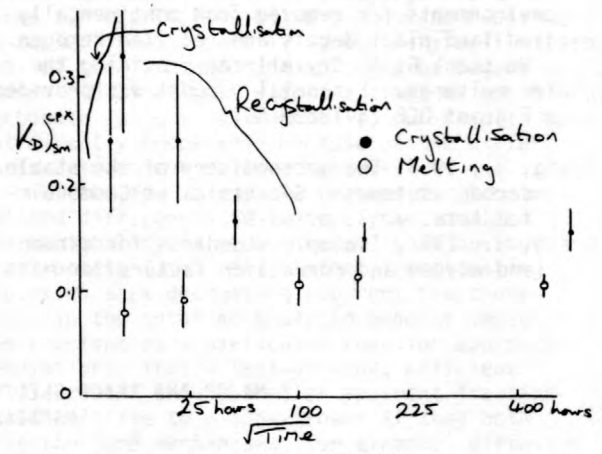

Figure 2.--K_D (= Sm^{cpx}/Sm^{liquid}) as a function of time in crystallization experiments.

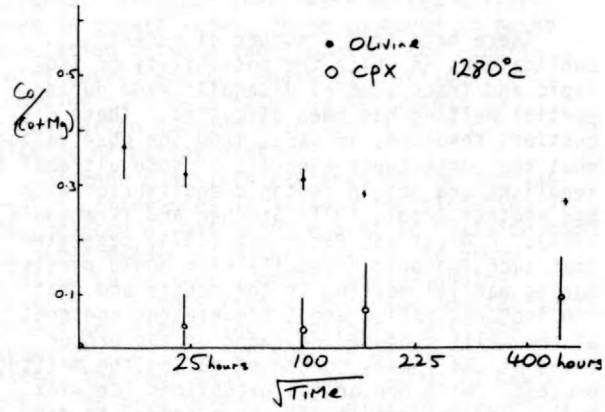

Figure 3.--Co/Co + Mg ratios of olivine and clinopyroxene as a function of time in melting experiments.

values of Co self-diffusion in Co_2SiO_4 olivine and Fe-Mg interdiffusion in olivine at 1280°C. These results demonstrate that Fe-Mg equilibrium between crystals and liquid in the mantle will be much more rapidly achieved for olivine than for clinopyroxene crystals.

There are, of course, important thermal constraints on the rate at which melt is produced in the mantle. As a "packet" of initially melt-free mantle moves upwards into the melting zone, the rate of melt production will depend on (assuming chemical equilibrium): the rate of rise, the solidus P-T curve and the liquidus-solidus interval, and the latent heat of fusion.

If the fertile mantle is ascending at 1-10 cm yr^{-1}, then a time on the order of 10^3 - 10^4 years will be necessary to produce 1 percent melting after the solidus is crossed, given a solidus P-T slope of about 4°C km^{-1}. The rate of melt production, as melting begins, also depends on the rates of diffusion of species in the solid phases present. This is because the melt differs in composition from any possible combination of the solid phases, particularly with respect to the (Fe/Fe + Mg) ratio. Thus, the very first melt produced (which must be in chemical equilibrium with the solid phases) necessitates diffusion of Fe and probably of Al through the residual silicate minerals. In order for the melt to be in equilibrium with the residual phases, the rate of melting must be sufficiently slow for the solids to remain essentially homogeneous. Combined dissolution and diffusion have been investigated numerically in a manner similar to that described by Albarede and Bottinga (1972). Figure 4 illustrates an example of the apparent value of K_D (concentration in solid/concentration in liquid) plotted as a function of Log (D/VL) where D = solid diffusion coefficient, V = velocity of the crystal-liquid interface, and L is the initial half-width of the crystal. It can be seen that, in order for crystals and liquids to remain in equilibrium, D/VL must be on the order of 10 - 50.

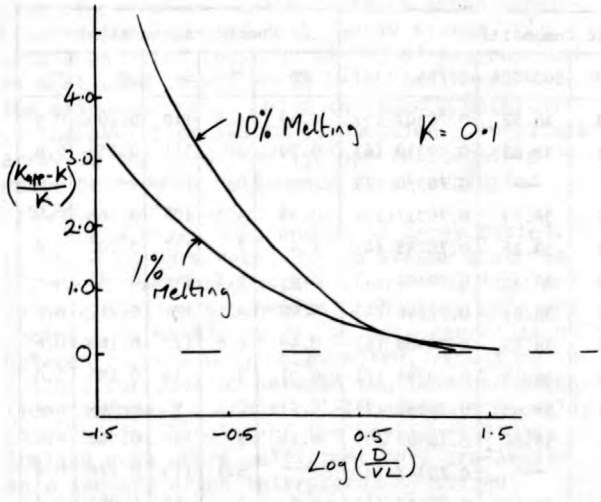

Figure 4.--The dependence of apparent K_D on D/VL for an equilibrium K_D of 0.1.

The Fe-Mg interdiffusion coefficient for olivine decreases with increasing pressure and with decreasing temperature (Misener, 1974). Thus, with a beginning of melting near 1200°C at 10 - 20 kb, the Fe-Mg interdiffusion coefficient could be expected to be on the order of 10^{-11} -10^{-12} cm^2 sec^{-1}. If Fe diffusion in olivine controls the rate of melting at the solidus, then 1 percent melting would take about 10^2 years, given L = 0.2 cm, V = 10^{-12} cm sec^{-1}, and $D_{FeMg} \simeq 5 \times 10^{-12}$ cm^2 sec^{-1}. At the solidus, however, the melt composition is constrained to be exactly in equilibrium with the crystals so that it is more likely that the slowest diffusing major species controls the rate of melt formation. For aluminous diffusion in clinopyroxene, given that $D_{Al}^{cpx} \simeq 0.01\ D_{FeMg}^{ol}$, 1 percent melt formation would take on the order of 10^4 years as long, or longer than it would take from thermal considerations. It is unlikely, therefore, that the initial melt can exhibit any major or trace-element disequilibrium because of the diffusional control on melt formation.

As the extent of melting increases, the diffusional constraint is progressively relaxed because the melt can exhibit an increasing amount of disequilibrium. Under these circumstandes, the likelihood of trace-element disequilibrium increases. If, as seems likely, REE diffusion is coupled to Al diffusion in pyroxene, then REE abundance patterns should decouple from the major element composition as the extent of melting increases. More detailed modeling of this phenomenon is currently in progress.

It was mentioned in the introduction that contact of a melt with residual minerals will tend to remove disequilibrium due to diffusion. Previous studies have tended to treat this as a problem of static melt in contact with crystals. In practice, however, the solids recrystallize in the presence of a melt so that all liquid-solid interfaces are moving. The rate of recrystallization of the experimentally produced clinopyroxenes has been extrapolated to mantle conditions by assuming that the driving force is proportional to the surface area per unit volume and that the rate of recrystallization is proportional to this force. Interface velocities on the order of 10^{-12} cm sec^{-1} are obtained. Under such circumstances the liquid approaches trace element equilibrium much more slowly than in the static case.

Albarede, F., and Bottinga, Y., 1972, Kinetic disequilibrium in trace element partitioning between phenocrysts and host lava: Geochimica Cosmochimica Acta, v. 36.

Beswick, A. E., 1976, K and Rb relations in basalts and other mantle derived minerals.

Is phlogopite the key? Geochimica Cosmochimica Acta, v. 40, p. 1167.
Hofmann, A. W., and Hart, S. R., 1978, An assessment of local and regional isotopic equilibrium in the mantle: Earth and Planetary Science Letters, v. 38, p. 44.
Misener, D. J., 1974, Cationic diffusion in olivine to 1400°C and 35 kbar in Hofmann, Giletti, Yoder, and Yund, eds.: Geochemical transport and kinetics, Carnegie Institution of Washington Publication, v. 634, p. 117.
Nelson, D. O., and Dasch, E. J., 1976, Disequilibrium of strontium isotopes between mineral phases of parental rocks during magma genesis--a discussion: Journal of Volcanology and Geothermal Research, v. 1, p. 183.
O'Nions, R. K., and Pankhurst, R. J., 1974, Petrogenetic significance of isotope and trace element variations in volcanic rocks from the mid-Atlantic: Journal of petrology, v. 15, p. 603.
Paul, D. K., 1971, Strontium isotope studies on ultramafic inclusions from Dreiser Weiher, Eifel, Germany: Contributions to Mineralogy and Petrology, v. 34, p. 22.
Schairer and Osborn, 1952.
Stueber, A. M., and Ikramuddin, M., 1974, Rubidium, strontium, and the isotopic composition of strontium in ultramafic nodule minerals and host basalts: Geochimica Cosmochimica Acta, v. 38, p. 207.

A MULTI-STAGE EVOLUTION MODEL INTERPRETATION OF THE MANTLE BY LEAD AND STRONTIUM ISOTOPIC COMPOSITION IN BASALTIC ROCKS

By Masaru Yamaguchi
Department of Geology, Kyushu University,
Fukuoka 812, Japan

Lead and strontium isotopic composition and concentration of Rb, Sr, U, and Th determined on low alkali tholeiitic basalts recovered from DSDP Leg 37 cores (Yamaguchi and others, 1977; Yamaguchi, Armstrong, and others, 1977; Cumming, 1976; Gray and others, 1977) were integrated and reexamined. Many of these rocks were altered and the isotopic compositions give a wide spread, which is probably due to exchange of isotopes with sea water.

Degrees of alteration were estimated by thin section under the microscope, and the isotopic compositions were selected for fresh and slightly altered samples. The results are

Table 1. Isotopic composition and concentration of lead and strontium for fresh and slightly altered basalts, DSDP Leg 37

[Compiled from Yamaguchi, Russell, and Slawson (1977); Yamaguchi, Armstrong and others (1977); Gray, Cumming, and Lambert (1977); Cumming (1976). Strontium isotopic compositions are corrected to average values of NBS standard (SRM987 = 0.71014, E and A = 0.70794.]

No.	Sample				Isotopic Composition				Concentration (ppm)				
	Hole	Core-Section	Interval in cm	Piece No.	206/204	207/204	208/204	87/86 (1σ)	Pb	Rb	Sr	U	Th
2	332A	8-1	98-100	11	18.86	15.59	38.52	0.70307 (5)	0.69	6.8	118	0.205	0.4
3	332A	12-1	123	12D	18.85	15.68	38.81	0.70310 (6)	0.59	2	111	0.158	0.6
3'	332A	12-1	123	12D	—	—	—	0.70330 (7)	—	5	120	—	—
5	332A	21-1	57-59	4	18.90	15.64	38.73	0.70317(10)	0.58	4.3	108	0.166	0.9
6	332A	26-1	43-45	2	19.26	15.74	39.15	0.70285 (4)	7.4	7	117	0.202	0.8
7	332A	28-1	34-36	4	18.74	15.60	38.45	0.70307 (4)	n.d.	5.2	116	0.285	0.6
8	332A	28-2	57-59	9	18.83	15.66	38.67	0.70296 (4)	0.90	4	121	0.212	0.7
9	332A	29-1	37-39	5	18.72	15.58	38.46	0.70308 (6)	0.49	6.6	112	0.169	0.6
10	332A	32-1	106-108	14B	18.48	15.52	38.14	0.70296 (7)	(~6.0)	3	114	0.185	1.0
11	332A	40-3	37-39	4B	18.93	15.63	38.63	0.70297 (7)	0.41	2.1	95	0.064	n.d.
12	332B	2-5	103-106	10	18.88	15.60	38.54	0.70302 (3)	0.95	1	97	0.048	n.d.
13	332B	6-1	100-	11A	—	—	—	0.70342 (7)	—	8.1	115	0.276	0.4
16	332B	21-1	27-30	1B	18.75	15.62	38.47	0.70317 (2)	n.d.	3	62	0.082	n.d.
17	332B	27-2	56-58	6	18.41	15.55	37.75	0.70300 (4)	0.74	3	118	0.252	0.4

given in table 1. Only eight samples were found sufficiently fresh among twenty-four samples analyzed.

The validity of either an evolution or a mixing model to interpret the linear array of the lead isotope data for Leg 37 was tested in various ways. The relationship between strontium and lead isotopic composition was examined, and it was possible to distinguish two groups--one making a straight line and the other making a curve when only fresh samples were considered (fig. 1). The curve may be interpreted as a mixing line.

It is possible to interpret the straight line as arising either by mixing or evolution. Straight-line mixing occurs only when the ratio of ^{204}Pb concentrations in the two end members is equal to the ratio of ^{86}Sr concentration in the same end members. Straight-line evolution relationship, on the other hand, will be formed when the r/μ ratio remains constant ($r = {}^{87}Rb/{}^{86}Sr$, $\mu = {}^{238}U/{}^{204}Pb$).

Microscopic examination of basalts from Leg 37 indicates crystal fractionation in the magma reservoir at shallow depth. Therefore, concentration of U, Pb, Rb, and Sr in each lava will be different from their initial magma. However, a loose correlation was observed between the $^{207}Pb/^{206}Pb$ ratio and 1/Pb concentration, and $^{87}Sr/^{86}Sr$ ratio and 1/Sr concentration for the group, which results in a curved relation in figure 1. It is possible to interpret this group as having been produced by mixing in the source region of the basalt magma. In contrast, it was found to be difficult to interpret another group showing a straight-line relationship in the same diagram (not shown) in terms of mixing. Because lead and strontium do not have the same substitution tendency, it is unlikely that a straight-line mixing relation (fig. 1) could be maintained between the two end members.

I interpret the straight line as a special case of evolution, which could be established between the U-Pb and Rb-Sr decay system. It should be noted that the mixing of a group such as mentioned above, would be a local process--the main end member being the source material of the evolution system in question. The linear array in the lead-lead isotope relationship would be largely determined by an evolution system.

For a given U-Pb and Rb-Sr decay system, it is not always necessary to assume that the r/μ ratio remains constant. However, if U and Rb have similar geochemical behaviors when entering into mantle rocks, a loose correlation between r and μ will be expected, resulting in a loose correlation between the lead and strontium isotopes. Such a relationship is actually observed for basalts of the Reykjanes Ridge-Iceland area where sufficient data are available and are often interpreted by mixing.

Assuming that the linear array in the lead isotopic relation results from mantle evolution,

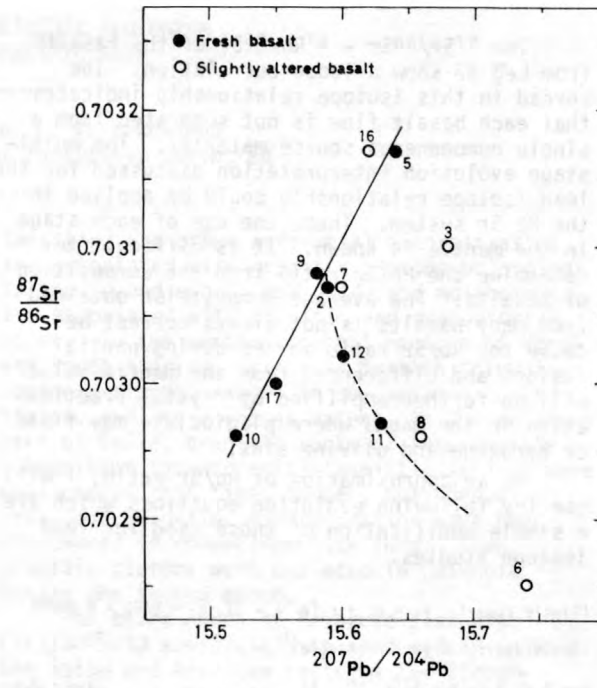

Figure 1.--Relationship between strontium and lead isotopic composition from basalts of DSDP Leg 37. Dashed curve indicates a probable mixing line; solid line indicates a probable constant time, constant $^{87}Rb/^{86}Sr/^{235}U$ ^{204}Pb line.

the lead isotopic composition of basalts reported in the literature was examined. Data from altered basalts and some unusual compositions compared to the general linear array were omitted. It is noted that the regression lines determined on each area from the Pacific (Japanese tholeiitic basalts - 3.7 b.y., alkali-basalt $\sim$ 4.5 b.y., Hawaiian islands - 0.94 b.y., Mariana arc - 2.3 b.y., Nazca Plate - 1.7 b.y.) intercept in a very narrow area along the meteorite isochrons, indicating a two-stage evolution developed from a similar (or single) source ($\mu_1 = 8.25$). The age of the geochron could then be calculated. On the other hand, the regression lines of Leg 37 (2.6 b.y.) and basalts of the Reykjanes Ridge-Iceland area (1.5 b.y.) intercept at the left of, but close to, the above geochron. The extension of the Reykjanes Ridge to the site of Leg 37 in the Mid-Atlantic Ridge is interrupted by the Gibbs fracture zone, and the mantle (or plate) at each area may be different. If it is admitted that the two plates are genetically related, the point of intercept could be the end point of the second stage and the basalts of Leg 37 and Reykjanes Ridge-Iceland can be explained as a three-stage evolution. The second-stage mantle began 3.1 b.y. ago and had a μ_2 value of 8.0.

The $^{87}Sr/^{86}Sr$ - $^{87}Rb/^{86}Sr$ of the basalts from Leg 37 show a loose correlation. The spread in this isotope relationship indicates that each basalt flow is not separated from a single homogeneous source material. The multi-stage evolution interpretation discussed for the lead isotope relationship could be applied to the Rb-Sr system. Thus, the age of each stage in the mantle is known. It is difficult to determine the Rb/Sr ratio from the composition of basalts. The average composition obtained from many basalts is not always correct because the Rb/Sr ratio varies during partial fusion, and differences from the mantle value will be further amplified by crystal fractionation in the magma where plagioclase may float or pyroxene and olivine sink.

As an approximation of Rb/Sr ratio, I will use the following evolution equations which are a simple modification of those used for lead isotope studies.

(Single stage): $y_1 = a_1 + r_1(e^{\lambda t_1} - 1)$, $a_1 = BABI = 0.69899$

(Two stage): $y_2 = a_1 + r_1(e^{\lambda t_1} - e^{\lambda t_2}) + k\, r_1(e^{\lambda t_2} - 1)$

$y_{2m} = y_1 + r_1(k - 1)(e^{\lambda t_{2m}} - 1)$

$y_{2n} = y_1 + r_1(k - 1)(e^{\lambda t_{2n}} - 1)$

$$r_1(k - 1) = \frac{y_{2m} - y_{2n}}{e^{\lambda t_{2m}} - e^{\lambda t_{2n}}}$$

(Three stage):

$y_3 = a_1 + r_1(e^{\lambda t_1} - e^{\lambda t_2}) + j\, r_1(e^{\lambda t_2} - e^{\lambda t_3}) + h\, j\, r_1(e^{\lambda t_3} - 1)$

$a_2 = a_1 + r_1(e^{\lambda t_1} - e^{\lambda t_2})$; $\quad a_3 = a_2 + j\, r_1(e^{\lambda t_2} - e^{\lambda t_3})$

$y_3 = y_2 + j\, r_1(h - 1)(e^{\lambda t_3} - 1)$; $\quad j\, r_1(h - 1) = \dfrac{y_{3p} - y_{3q}}{e^{\lambda t_{3p}} - e^{\lambda t_{3q}}}$

Suffixes 1, 2, 3 denote stage; m, n, p, q denote each local area; t denotes age of each mantle area; $y = {}^{87}Sr/{}^{86}Sr$ ratio; $r_1 = {}^{87}Rb/{}^{86}Sr$ of the single-stage mantle; $a_1, {}_2, {}_3$, = initial $^{87}Sr/^{86}Sr$ ratio of each stage; and h, j, k = concentration factors.

In these equations, concentration factors are used to make the equation simple. It is assumed that similar types of basalt in two areas are produced from a similar mantle with respect to the present $^{87}Rb/^{86}Sr$ ratio for the same degree of partial fusion. Using the ages obtained from the lead-lead isochrons and observed mean $^{87}Sr/^{86}Sr$ ratios of each type of basalts in two areas, we can calculate the initial ratio, concentration factors, and, finally, Rb/Sr ratio of each stage of the mantle. A strontium isotope evolution diagram of the mantle is then constructed.

The coincidence of 3.7 - 2.6 b.y. ages in the Pacific and Atlantic areas (tholeiitic basalt of Japan which probably related to the Philippine plate - 3.7 b.y.; separation of the second-stage mantle of Leg 37-Reykjanes Ridge-Iceland - 3.1 b.y., and 3.7 - 2.7 b.y. old rocks found in Greenland and Canada) should be noted.

It is possible that the age around 3.7 b.y. indicates a global event, the time of formation of the early Eurasian-North American continent, and the second-stage mantle which existed or may exist beneath the Mid-Atlantic area reflects a reduction in the Rb/Sr and U/Pb ratios by the formation of the continental crust. The third-stage mantle in the north Mid-Atlantic later again enriched, while it is still depleted when compared to the second-stage mantle in the Pacific area. In conclusion, the mantle which is the source of basalt magma has experienced repeated and episodic events in the long span of the Earth both in the Pacific and Atlantic area. The observed isotope variation will be due largely to the difference in the isotopic evolution of each mantle area.

Cumming, G. L., 1976, Lead isotope ratios in Deep Sea Drilling Project Leg 37 basalts: Earth and Planetary Science Letters, v. 31, p. 179-183.

Gray, J., Cumming, G. L., and Lambert, R. St. J., 1977, Oxygen and strontium isotopic compositions and thorium and uranium contents of basalts from Deep Sea Drilling Project 37 cores, in, Aumento, F., Mellson, W. G., and others, Initial reports of the Deep Sea Drilling Project, v. 37: U.S. Government Printing Office, Washington, p. 607-611.

Yamaguchi, M., Armstrong, R. L., Russell, R. D., and Slawson, W. F., 1977, Strontium and lead isotopic investigations of igneous rocks from the Mid-Atlantic Ridge: Deep Sea Drilling Project Leg 37, in Aumento, F., Melson, W. G., and others, Initial Report of the Deep Sea Drilling Project, v. 37: U.S. Government Printing Office, Washington, p. 613-616.

Yamaguchi, M., Russell, R. D., and Slawson, W. F., 1977, Concentration and composition of lead in Deep Sea Drilling Project Leg 37 cores: Canadian Journal of Earth Sciences, v. 14, p. 785-786.

THE MAIN EPOCHS OF MESOZOIC PLUTONISM IN THE CIRCUM-PACIFIC AREA

By I. A. Zagruzina and L. V. Yakovleva
USSR All-Union Geological Institute, Leningrad

Mesozoic plutonism has occurred on a very large scale in the Circum-Pacific area. Most abundant are linear belts of granitoid plutons, which border the Pacific Ocean almost as a complete ring. The association of numerous mineral deposits with Mesozoic granitic rocks gives an impetus to their petrologic and radiometric investigation. A vast amount of radiometric information has been accumulated as a result of numerous investigations in different countries. These analytical data permit us to characterize the succession and duration of Mesozoic granitoid plutonism and related ore mineralization.

Statistical generalization based on more than 10 thousand radiometric data enabled the authors to postulate four main widespread epochs of Mesozoic granitoid plutonism in the Circum-Pacific area (Zagruzina and Yakovleva, 1977). Only plutonic rocks are considered; the ages of volcanic and hypabysall intrusive rocks are beyond the scope of this paper.

The first epoch falls at 200 ± 10 m.y. and is revealed most intensively in the eastern peripheral regions of Asia. A great number of tinbearing granitic plutons of the Burma-Malayan and the North Vietnamese orogenic zones were emplaced at this time. Included also are many granitoid plutons of eastern Mongolia, central and western Zabaikal, the Bureinskii massif, and those in northwestern and southeastern China, which, in a number of cases, are associated with tin, tungsten, and other rare-metal mineralization. Granitic rocks of this age are also found in Japan (Funatsu group), New Zealand (the Bay Fovo area), and Australia (New South Wales, Victoria).

Rocks of the first epoch are much less abundant along the western coast of North and South America. Some dioritic, granodioritic, and tonalitic inclusions are present in Alaska, British Columbia, the eastern part of the Sierra Nevada batholith, and southern Chile. Some copper-molybdenum, iron, and lead-zinc mineralization is associated with them. Granitic plutons belonging to the first epoch are known in Bolivia and Columbia.

The second epoch of Mesozoic plutonism, at 150 ± 15 m.y., includes emplacement of numerous and various types of granitic plutons in eastern, central, and western Zabaikal, eastern Mongolia, the Bureinskii massif, the Stanovoi region, and North Korea. It is intensively manifested in the Yano-Kolimskii orogenic system and Burma-Malayan zone, in Japan, and in southern and southeastern China. In the Asian part of the Circum-Pacific area, mainly tin, tungsten, and other rare-metal mineralization are associated with granitic plutons belonging to the second epoch, and gold, and molybdenum, are associated with dioritic and granodiorite rocks. In the western coastal regions of North and South America, mainly in British Columbia, southern Alaska, ranges in the western United States, and, to a lesser extent, in the southern part of Chile, granitic rocks of intermediate composition (granodiorite-tonalitic series) were emplaced at this time; copper, molybdenum, iron, and lead-zinc mineralization have been discovered in connection with them. Some granitic plutons were emplaced in Columbia during the second epoch.

The third epoch of Mesozoic plutonism (at 100 ± 10 m.y.), is displayed widely in both the Asian and American parts of the Circum-Pacific area. Granitic rocks of this age are particularly widespread in northeastern USSR (in the Mesozoic Yano-Kolimskii and Chucotskii orogenic zones and the Ochotsko-Chucotskii volcanic belt), North Sichote-Alin, the Stanovoi region, and Japan. They are also widely distributed in Korea, southeastern China, the Bureinskii massif, Australia, Tasmania and New Zealand.

A large number of granitic rocks belonging to the third epoch were developed within extended batholithic belts along the entire western coast of North and South America. They retain the general metallogenic character and the petrological and geochemical features of the granitic rocks of the previous epoch.

The fourth epoch (at 70 ± 10 m.y.), like the previous one, is broadly distributed in the whole Circum-Pacific area. At this time many granitic rocks containing tin tungsten, and rare metals were emplaced in the Yano-Kolimskii, Chucotskii, and Sichote-Alinskii orogenic zones, the northern part of Vietnam, southeastern China, and the Bureinskii massif (Tomson and Kravtsov, 1975). The granitic rocks belonging to the fourth epoch are widespread in Ochotsko-Chucotskii and Sichote-Alinskii volcanic belts, Japan, the eastern part of Australia, Tasmania, and New Zealand. During this epoch, granitic plutonism also occurred on a large scale along the entire western coast of North and South America, where copper, copper-molybdenum, iron, and lead-zinc ores are associated with dioritic, granodioritic and tonalitic intrusions, similar to the previous epochs (White, 1968).

The above-mentioned four main epochs of Mesozoic plutonism have a well defined, discrete character; they are separated by periods of relative quiescence. Their discrete character

is clearly displayed by systematization of the concordant radiometric data, obtained by the various radiometric methods on two or more coexisting minerals (Lanphere and Reed, 1973). Artificial prolongation of the age range for plutonic complexes and individual granitic plutons, which veils the time gaps between culminations of intrusive epochs, cannot be used as an argument that the discrete intrusive epochs in the Circum-Pacific area are lacking (Zagruzina, 1977). The intrusive activity appears to be not continuous, but episodic.

During each of the four above-mentioned intrusive epochs, co-magmatic series or compound plutons were emplaced; their composition varies to a large degree-mainly from diorite and tonalite to granodiorite, quartz monzonite, and alaskite. The duration of all the epochs was within 20 - 30 m.y.

Many of the large Mesozoic batholiths consist of intrusive bodies of various ages, genesis, composition, size, and morphology. Some comparatively small granitic plutons included in such batholiths are dissociated in space by metamorphic rock screens, xenolith-blocks, numerous dikes, and fractures.

This type of batholith is found in the Sierra-Nevada, Inyo, Southern California, North America (Baddington, 1963; Bateman, 1965), the Andes (Pitcher, 1974; Myers, 1975), and northeastern USSR, especially in the East Chukotka region (Zagruzina, 1977).

The complex history of the formation of similar batholiths is made particularly evident by their large range of available radiometric data, where ages sometimes span up to several tens of million of years. For example, the age range of the Andean batholith is between 265 and 30 m.y. (Pitcher, 1974; Myers, 1975), and for the Sierra Nevada batholith between 210 and 79 m.y. (Bateman, 1965). However, the radiometric data for comparatively small and more homogeneous plutons in northeastern (Zagurzina, 1977) and far eastern USSR (Bondarenko, 1971) usually ranges not more than 10 - 20 m.y. New, recently obtained data affirms the fact that the true duration of the emplacement of granitic plutons of homogeneous composition and comparatively simple structure does not exceed one million years (Dobretsov and Popov, 1974). An emplacement duration of about the same time interval (2 - 4 m.y.) was established for some metasomatic ore-formation processes (Zagurzina, 1971; Rusinov and Volkov, 1977).

In all cases it is necessary to take into account the fact that the range of radiometric data is dependent not only on the true age of crystallization of the granitic rocks, but also on the various transformations that take place later (the time of tectonic uplift subsequent to crystallization, repeated progressive metamorphism, metasomatism, and mylonitization). Also the influence of analytical errors cannot be excluded (about 3 - 5 percent for most laboratories). Since modern standards for analytical determination of mother and daughter isotopic species is sufficiently high, the various geological processes that disturb radioactive equilibrium are the main causes of radiometric data dispersion and age distortion in comparison with experimental errors.

No geological object is a really closed system in respect to radioactive elements or daughter decay products. The age ranges obtained for them, which span up to tens of millions of years, reflect the combined influence of all possible geological factors, and also analytical errors. They are a function of many independent variable quantities, and it is impossible at present to form a correct quantitative estimate of each of them. The true duration of emplacement of geological objects cannot exceed the range in value of the radiometric data. One should bear this in mind when one interprets geochronological data.

Bateman, P. C., 1965, Geology and tungsten mineralization of the Bishop District, California: U.S. Geological Survey Professional Paper 470, 270 p.

Bondarenko, E. I., 1971, On the age of some magmatic complexes and the mineralization of the Sikhote-Alinsk Folded Region using radiological data: in Problems of geology and mineral ore in the far east, Khabarovsk, p. 26-31.

Buddington, A. F., 1963, The formation of granite bodies: Moscow, 145 p.

Dobretsov, N. A., and Popov, N. B., 1974, On the length of the formation of granitoid plutons: Geology and Geophysics, no. 1, p. 50-60.

Lanphere, M. A., Reed, B. L., 1973, Timing of Mesozoic and Cenozoic plutonic events in circum-Pacific North America: Geological Society of America Bulletin, v. 84, no. 12, p. 3773-3782.

Myers, J. S., 1975, Cauldron subsidence and fluidization: mechanisms of intrusion of the Coastal Batholith of Peru into its own volcanic ejecta: Geological Society of America Bulletin, v. 86, no. 9, p. 1209-1220.

Pitcher, W. S., 1974, The Mesozoic and Cenozoic batholiths of Peru: Pacific Geology, no. 8, p. 51-62.

Rusinov, V. L., and Volkov, V. N., 1977, The argon-potassium age of near-ore metasomatites of the Okhotsko-Chukotsk and Sikhote-Alinsk volcanic zones: in Geological interpretation of geochronological information, Irkutsk, p. 49-51.

Tomson, I. N., and Kravtsov, V. S., 1975, The stages and cycles of tin mineralization in the Pacific Ocean Ore Belt: in Ore provinces and genetic types of tin and tungsten deposits, Novosibirsk, p. 65-70.

White, W. M., Harakal, I. E., Carter, N. S., 1968, Potassium-argon ages of some ore deposits in British Columbia: Canadian Mining and Metallurgical Bulletin, v. 61, no. 679, p. 1326-1334.

Zagruzina, I. A., 1971, Absolute dating of gold ore formations and gold-bearing magmatic complexes of the North-East USSR: in Basic problems of metallogeny of the Pacific Ocean Zone, Vladivostok, p. 109-112.

Zagruzina, I. A., 1977, Geochronology of Mesozoic granitoids of the North-East USSR: Nauka, Moscow, 278 p.

Zagruzina, I. A., and Yakovleva, L. V., 1977, The main periods of Mesozoic magmatism in the Pacific Ocean Belt and their metalliferousness: in Geological interpretation of geochronological information, Irkutsk, p. 46-48.

A NEW APPROACH TO THE STUDY OF FISSION TRACK FADING

By Robert Allen Zimmerman[1], and Alan M. Gaines[2]
[1]University of Pennsylvania, Philadelphia Pennsylvania
[2]National Science Foundation, Washington, D.C.

Detailed fission-track fading data were obtained for a natural fluorapatite (from the Winnipesaukee quartz diorite). Splits of this sample were annealed at three temperatures, 300, 325, and 348°C. The fractional reduction of fission-track density (ρ/ρ_0) was determined for serially removed samples at each temperature. A least-squares regression was performed on the data for a fit to the relationship

$$\rho/\rho_0 = c - k \times \ln(t)$$

where c and k are regression constants. This is one possible analytical expression for the apparent linear relationship interpreted from a plot of ρ/ρ_0 versus the logarithm of annealing time. Reasonably good correlations result but systematic deviations from this function are evident, particularly where $\rho/\rho_0 < 0.2$. Better fits are obtained for the relationship

$$\rho/\rho_0 = \exp(\alpha \times t)$$

appropriate to first-order reaction kinetics, and for a more complex function corresponding to the kinetics of the radial diffusion in a cylinder. These functions provide not only better empirical fit (the sole criterion of previous studies) but also correspond to kinetic equations of reasonable controlling mechanisms of track fading. Because the differences in correlation of our data with these two models is not significant, the simple exponential function is adopted as an improved approximation to the actual kinetics of track fading. Where analysis of data from previous studies of track fading in apatite was possible (Naeser, 1967; Reimer, 1972), equal or better correlation is obtained for the exponential as compared to the logarithmic function. In an earlier study Märk and others (1973) proposed an exponential fading relationship.

Several factors contribute to the difficulty in differentiating between the logarithmic and exponential kinetic functions. In figure 1 the fading data for the 348°C isothermal run and the regression curves for the logarithmic and exponential functions are plotted with a linear time scale. The two functions can be assumed to be noticeably different only where they differ by greater than twice the relative uncertainty (~ 10 percent for one standard deviation) of a datum at that point, a criterion appropriate for

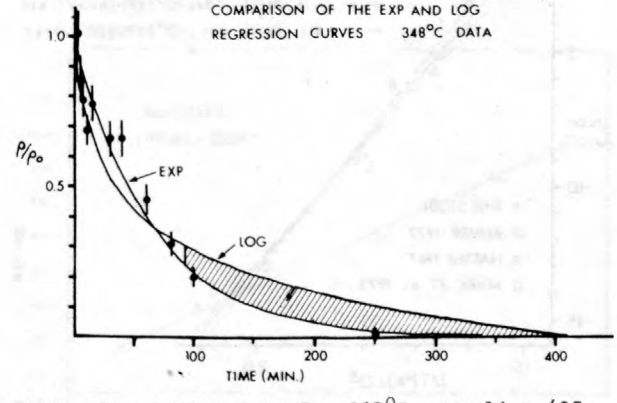

Figure 1.--Fading data for 348°C annealing (95-percent confidence limits are shown) appear with regression curves for logarithmic (LOG) and exponential (EXP) functions. Striped region is the only region where a critical choice between the two functions is likely.

visual curve-fitting employed in most studies. It is seen that the functions differ significantly only for small values of ρ/ρ_0 (the striped region in fig. 1) and that the two data points in this region appear to follow the exponential function. It is in this critical region where few data are obtained in most studies because of the progressively longer experimental runs required, particularly at lower temperatures. Unequal weight is also given to shorter annealing times by designing the annealing intervals to accommodate an expected logarithmic time relationship. Lack of agreement of data at short annealing times with the logarithmic function is usually discounted with the ad hoc assumption of a "prefading" or induction period. These data can be accommodated in a continuous manner by the exponential function.

A modified Arrhenius diagram plotting ln t versus 1/T, where t is the annealing time and T is the absolute temperature of the isothermal run, can be constructed for the exponential kinetic model. A family of parallel straight lines corresponding to selected amounts of track fading results rather than the fan of lines with its paradoxical point of convergence that results with the logarithmic model. While this approach allows an adequate interpretation of the time constants involved in track fading, a more powerful analysis is possible by plotting the logarithm of α (which is shown to be the isothermal rate constant) versus 1/T. On this Arrhenius diagram (fig. 2) fourteen data points from this and other similarly analyzed studies of fading in fluorapatites (Naeser, 1967; Reimer, 1972; and Märk and others, 1973) statistically fall on a single straight line (coefficient of determination 0.98). This is contrary to the conclusion reached by Märk and others (1973). The line is expressed by the equation

$$\alpha(T) = 10^{(14.49 \pm 1.63)} \times \exp\left[(2.00 \pm 0.19\ \text{eV})/kT\right]$$

where the 95-percent confidence intervals are indicated. Both the value of the pre-exponential term ($\sim 10^{14}$ min-1) and the activation energy (2.00eV) are reasonable for a process controlled by solid state diffusion.

With the demonstration that track fading can be described by first order kinetics, the analysis developed by Dodson (1973) for the interpretation of the effective closure temperature can be applied to the apatite fission-track age system. Using the fading parameters developed above, closure temperatures were calculated corresponding to a number of sample cooling rates. In the range 0.1°C to 100°C cooling per million years closure temperatures vary from 85° to 126°C. The relationship between apatite fission-track age and temperature (depth) in deep boreholes such as reported by Naeser and Forbes (1976) can provide geologically calibrated values of the closure temperatures.

Their Alaskan borehole data indicate a closure temperature of $\sim$ 105°C for a steadily maintained regional cooling rate of $\sim$ 1°C/m.y. A closure temperature of 98°C is predicted by the fading model developed here, in close agreement with the geological value and decidedly more accurate than estimates based on other theoretical models and interpretations of experimental data.

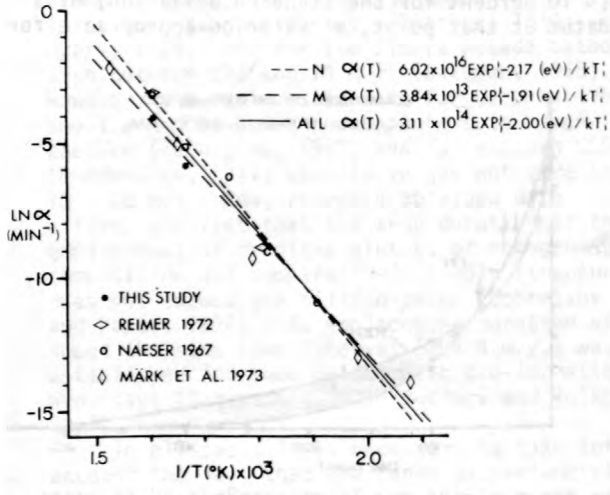

Figure 2.--Rate constants derived from the exponential kinetic function for data of this fading study as well as that of Reimer (1972), Naeser (1967), and Märk and others (1973) plot on a single straight line on this Arrhenius diagram (lnα vs. 1/T°K).

Dodson, M. H., 1973, Closure temperature in cooling geochronological and petrological systems: Contributions to Mineralogy and Petrology, v. 40, p. 259-274.

Märk, E., Pahl, M., Purtsheller, F., and Märk, T. D., 1973, Thermische Ausheilung von Uranspaltspuren in Apatiten, Alterskorrekturen und Beitrage zur Geothermochronologie: Tschermaks Mineralogische und Petrographische Mitteilungen, v. 20, p. 131-154.

Naeser, C. W., 1967, Fission track age relationships in a contact zone, Eldora, Colorado: Southern Methodist University, Ph.D. thesis.

Naeser, C. W., and Forbes, R. B., 1976, Variations of fission-track ages depth in two deep drill holes: EOS, Transactions of the American Geophysical Union, v. 57, p. 353.

Reimer, G. M., 1972, Fission track geochronology; Method for tectonic interpretation of apatite studies with examples from the central and southern Alps: University of Pennsylvania, Ph.D. thesis.

Nd AND Sr ISOTOPE DATA FROM KOMATIITIC AND THOLEIITIC ROCKS OF MUNROW TOWNSHIP, ONTARIO

by Alan Zindler[1], Chris Brooks[2], N. T. Arndt[3], and Stan Hart[1]
[1]Center for Geoalchemy, Department of Earth and Planetary Sciences, M.I.T., Cambridge Massachusetts 02139
[2]Department de Géologie, Universite de Montréal, Montreal, Canada
[3]Department of Geological Sciences, University of Saskatchewan, Saskatoon, Saskatchewan, Canada

Nd and Sr isotopic compositions have been measured in komatiitic and tholeiitic rocks, which occur as flows and hypabyssal sills in Munro Township (Abitibe belt, Superior Province, Canada). The samples come from: (1) the Munro-Warden sill, a tholeiitic layered sill which is differentiated from dunitic peridotite to leuco-gabbro (MacRae, 1969); (2) Fred's Flow, a komatiitic layered flow, differentiated from dunite to gabbro and containing spinifex-textured pyroxene and olivine (Arndt and others, 1977); (3) Pike Hill complex, a series of peridotitic komatiite flows (Arndt and others, 1977); (4) Theo's Flow, a tholeiitic layered sill differentiated from peridotite to gabbro (Arndt and others, 1977). All rocks are metamorphosed to prehnite-pumpellyite to lower greenschist facies, and, while clinopyroexene tends to remain unaltered, olivine is serpentinized and plagioclase in the grabbroic rocks is highly saussuritized.

Results from Nd: The nine samples analyzed for Nd Isotopes come from the Munro-Warden sill (samples MW-1, MW-2, MW-3, MW-4, MW-6) and from Fred's Flow (105, 106, 167, 197). The results of the analyses are shown in table 1 and are plotted on an isochron diagram in figure 1. With three exceptions, all analyses fall on the isochron within experimental error and yield an age of 2765 ± 42 m.y. (1σ), with an initial ratio of 0.50911 ± 7. This age was obtained from a regression analysis which excluded MW-2 and MW-4, whose significant deviations from the trend are thought to be the result of secondary alteration (MW-2 is a leuco-gabrro with completely saussuritized plagioclase and MW-4 is a very friable, coarse-grained pyroxenite). The 2765 m.y. age is in good agreement with other published ages from the Abitibi belt obtained from the U-Pb system (Krogh and Davis, 1971).

Results from Sr: The 9 new analyses for Sr isotopes come from samples of Fred's Flow (503, 507, 159), Theo's Flow (60, 163, 164, 165) and the Pike Hill complex (157, 156); the results are shown in table 2 and are plotted on an isochron diagram in figure 2. Also plotted on figure 2 are analyses of clinopyroxene separates from the Abitibi belt (from Hart and Brooks, 1977). Together the points define an errorchron for which a regression analysis yields an age of 3120 ± 78 m.y. (1σ) with an initial ratio of 0.70117 ± 15. Given the scatter in the data and the difference between this age and the known age of the Abitibi belt, the data probably do not document any particular event in time but rather are an indication of the degree of alteration of these rocks.

Table 1.--Nd isotope analyses

Sample No.	$^{147}Sm/^{144}Nd$	$^{143}Nd/^{144}Nd$ (± 2σ)
MW-1	0.1729	0.512253 ± 22
MW-2	.1883	.512395 ± 21
MW-3	.1991	.512486 ± 18
MW-4	.1833	.512822 ± 14
MW-6	.2097	.512916 ± 24
105	.2225	.513168 ± 37
106	.2268	.513262 ± 36
107	.2376	.513445 ± 20
167	.2325	.513361 ± 30

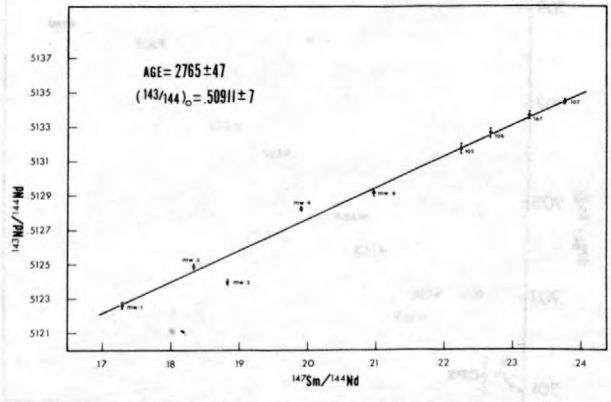

Figure 1.--$^{143}Nd/^{144}Nd$ - $^{147}Sm/^{144}Nd$ isochron diagram. Error bars represent 2 standard errors of the mean from run statistics. $^{143}Nd/^{144}Nd$ values are normalized to $^{146}Nd/^{144}Nd$ = 0.72190.

Table 2.--Sr isotope analyses

Sample No.	$^{87}Rb/^{86}Sr$	$^{87}Sr/^{86}Sr$ ($2\sigma \simeq .00010$)
60	0.0261	0.70302
156	.0376	.70305
165	.0434	.70257
163	.0608	.70395
164	.0695	.70469
157	.1013	.70597
503	.1216	.70652
507	.1534	.70824
159	.1911	.70821

Table 3.--$(Nd/Sm)_n$ values

Sample No.	Locality	Rock type	$(Nd/Sm)_n$
MW-1	Munro-Warden sill--	Gabbro----------	1.12
MW-2	--------do.--------	----------do.----------	1.03
MW-3	--------do.--------	----------do.----------	1.06
MW-4	--------do.--------	Pyroxenite----------	0.97
MW-6	--------do.--------	----------do.----------	0.92
105	Fred's Flow--------	Gabbro textured lava------	0.89
106	--------do.--------	----------do.----------	0.86
107	--------do.--------	Pyroxene, spinafex-textured lava--------	0.85
167	--------do.--------	Olivine, spinafex-textured lava	0.84
A-2	Pyke Hill complex	----------do.----------	0.71
130	Munro Township flow	Peridotitic komatiite flow	0.98
185	--------do.--------	Pyroxenitic komatiite flow	0.89
131	--------do.--------	Basaltic komatiite flow---	1.05
158	Theo's Flow--------	Aphanitic pyroxenite------	1.08
195	Munro Township flow	Tholeiitic basalt flow----	1.11

Rare Earth Elements: The REE data in figure 3 represent analyses of Munro Township rocks from Whitford and Arndt (1977) (samples 105, 106, 107, 167), and from Arth, Arndt and Naldrett (1977) (samples 158, 195, 131, 185, 130, A-2). Sample localities are given in table 3 along with $(Nd/Sm)_n$ ratios, as an indication of the degree of light REE fractionation. We chose Nd/Sm so that we could compare light REE fractionation in these rocks to that in rocks from the Munro-Warden sill for which complete REE analyses are not yet available. This choice was justified because when $(Nd/Sm)_n$ is plotted against $(Ce/Sm)_n$ for rocks in figure 3, a very good linear correlation is observed.

The initial $^{143}Nd/^{144}Nd$ ratio of 0.50911, at 2765 m.y., obtained from the Sm/Nd isochron diagram, falls precisely on a chondritic evolution line for the earth, defined by primordial Nd in the basaltic achondrite Juvinas (Lugmair and others, 1975). The two additional Sm/Nd isochron ages and initial $^{143}Nd/^{144}Nd$ values which are available to date also plot directly on this chondrite evolution line. One point, at 2640 m.y., represents samples from several Rhodesian greenstone belts (Hamilton and others, 1977), and the other at 3770 m.y. comes from the Isua Series, Greenland (O'Nions and others, 1978). Although these points represent only three individual times and places within the mantle, one may still reasonably conclude that, prior to 2.6 b.y. ago, the mantle was chondritic with respect to REE. However, the Munro Township rocks show significant fractionation of the light REE (table 3, fig. 3), and conventional melting models would suggest that the rocks are mimicking the chondrite-normalized rare-earth patterns of their source regions within the mantle.

Two end-member-type models are considered capable of explaining this apparent discrepancy: (1) heterogeneities, with respect to REE, were

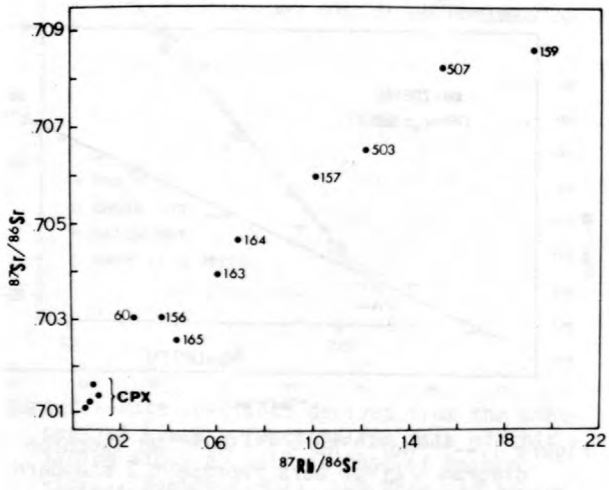

Figure 2.--$^{87}Sr/^{86}Sr$ - $^{87}Rb/^{86}Sr$ isochron diagram. Two sigma errors are within points on diagram.

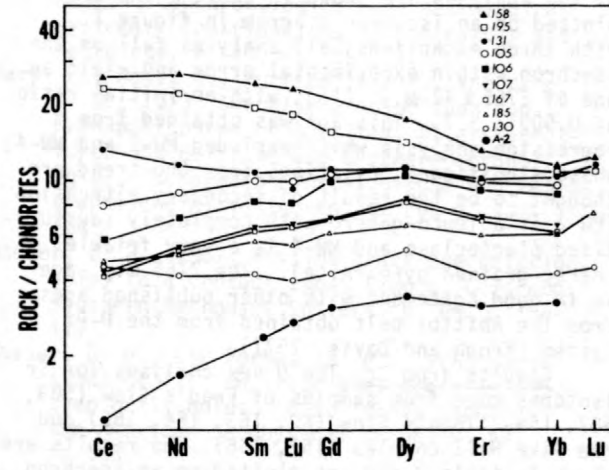

Figure 3.--Chondrite-normalized rare-earth element diagram. Data for 105, 106, 107, and 167 from Whitford and Arndt; (1977); data for 158, 195, 131, 185, 130, and A-2 from Arth, Arndt, and Naldrett (1977).

created within the mantle source-region immediately prior to the melting event that produced the Munro Township liquids, not allowing enough time for $^{143}Nd/^{144}Nd$ to respond to the new Sm/Nd ratios, or (2) the chondrite-normalized REE patterns in the Munro Township rocks do not reflect those of their mantle source regions and primary liquids are chemically affected by some process prior to their extrusion. One such process capable of producing a light REE enriched liquid would involve the fractional crystallization of clinopyroxene. In such a process, an erupted liquid would be light REE enriched and the residual liquid + cumulate would be light REE depleted, relative to chondrites, Because the tholeiitic and komatiitic rocks in Munro Township tend to be light REE enriched and light REE depleted, respectively, this model would suggest a comagmatic relationship for the two chemical suites. The tholeiites would be expected to make up the first eruptive phase, followed by the komatiites, which formed by the accumulation of ol + cpx by the residual liquid. This interpretation is consistent with the observed stratigraphy of the Munro Township lavas.

Arndt, N. T., Naldrett, A. J., and Pyke, D. R., 1977, Komatiitic and iron-rich tholeiitic lavas of Munro Township, Northeast Ontario: Journal of Petrology, v. 18, p. 319-369.

Arth, J. G., Arndt, N. T., and Naldrett, A. J., 1977, Genesis of Archaean komatiites from Munro Township, Ontario; trace-element evidence: Geology, v. 5, p. 590-594.

Hamilton, P. J., O'Nions, R. K., and Evensen, N. M., 1977, Sm-Nd dating of Archaean basic and ultrabasic volcanics: Earth and Planetary Science Letters, v. 36, p. 263-268.

Hamilton, Pl J., O'Nions, R. K., Evensen, N. M., Bridgewater, D., and Allaart, J. H., 1978, Sm-Nd isotope systematics of Isua Supracrustals, West Greenland: Nature, v. 272, p. 41.

Hart, S. R., and Brooks, C., 1977, The geochemistry and evolution of the early Precambrian mantle: Contributions to Mineralogy and Petrology, v. 61, p. 109-128.

Krogh, T. E., and Davis, G. L., 1971, Zircon U-Pb ages of Archean metavolcanic rocks in the Canadian Shield: Carnegie Institution of Washington Year Book, v. 70, p. 241-242.

Lugmair, G. W., Scheinin, N. B., and Marti, K., 1975, Search for extinct ^{146}Sm, 1. The isotopic abundance of ^{142}Nd in the Juvinas meteorite: Earth and Planetary Science Letters, v. 27, p. 79-84.

MacRae, N. D., 1969, Ultramafic intrusions of the Abitibi area, Ontario: Canadian Journal of Earth Science, v. 6, p. 281-303.

O'Nions, R. K. Hamilton, P. J., and Evensen, N. M., (in press), Sm-Nd dating of Isua Series, Greenland [not exact title]: Nature.

Whitford, D., and Arndt, N. T., 1977, Rare-earth elements in a thick, layered komatiite lava flow: Carnegie Institution of Washington Year Book, v. 76, p. 594-598.

AUTHOR INDEX

☆ U.S. GOVERNMENT PRINTING OFFICE:1978—778-718 / 37